

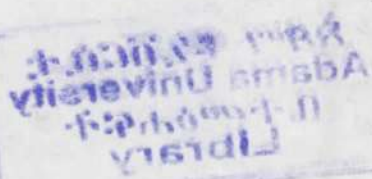
621.8
GHO
1998 C-7

Not to be taken out side
the Library

037633

THEORY OF MECHANISMS AND MACHINES

THIRD EDITION



Amitabha Ghosh

Director

Indian Institute of Technology

Kharagpur

Asok Kumar Mallik

Professor of Mechanical Engineering

Indian Institute of Technology

Kanpur



Affiliated East-West Press Private Limited
NEW DELHI

830580

TO OUR PARENTS

Not to be
sold or
distributed
by third
parties

THEORY OF MECHANISMS AND MACHINES

written by



Reprint 2005

© 1998, 1988, 1976 Affiliated East-West Press Private Limited

No reproduction in any form of this book, in whole or in part (except for brief quotations in critical articles or reviews), may be made without written permission of the publishers.

*Third Edition First Published 1998
Reprinted 1999, 2000, 2001, 2002 (twice), 2003,
2004 (twice), 2005*

Printed at Rekha Printers Pvt Ltd, New Delhi 110 020
Published by Affiliated East-West Press Private Limited
105 Nirmal Tower, 26 Barakhamba Road, New Delhi 110 001
e-mail: affiliat@nda.vsnl.net.in
www.aewpress.com

Price: Rs 295

ISBN 81-85938-93-8

Contents

Preface

vii

1 INTRODUCTION	1
1.1 INTRODUCTION	1
1.2 MECHANISMS AND MACHINES	3
1.3 KINEMATIC PAIRS	4
1.4 PLANE AND SPACE MECHANISMS	7
1.5 KINEMATIC CHAINS AND THEIR CLASSIFICATION	7
1.6 KINEMATIC DIAGRAMS, LIMIT AND DISGUISE OF REVOLUTE PAIRS	9
1.7 KINEMATIC INVERSION	12
1.8 EQUIVALENT LINKAGES	17
1.9 FOUR-LINK PLANAR MECHANISMS	21
1.10 MOBILITY AND RANGE OF MOVEMENT	24
1.11 PROBLEMS	39
2 KINEMATIC ANALYSIS OF PLANE MECHANISMS	45
2.1 INTRODUCTION	45
2.2 DISPLACEMENT ANALYSIS	45
2.3 GENERAL PLANE MOTION	66
2.4 INSTANTANEOUS CENTRE OF VELOCITY	71
2.5 ARONHOLD-KENNEDY THEOREM OF THREE CENTRES	72
2.6 VELOCITY AND ACCELERATION IMAGES	73
2.7 VELOCITY AND ACCELERATION ANALYSIS (GRAPHICAL)	75
2.8 ACCELERATION ANALYSIS OF COMPLEX MECHANISMS	88
2.9 VELOCITY AND ACCELERATION ANALYSIS (ANALYTICAL)	106
2.10 PROBLEMS	107
3 DIMENSIONAL SYNTHESIS OF LINKAGES	119
3.1 INTRODUCTION	119
3.2 GRAPHICAL METHOD (THREE POSITIONS)	122
3.3 FOUR-POSITION SYNTHESIS (POINT-POSITION REDUCTION)	141
3.4 DEAD-CENTRE PROBLEMS	144
3.5 ANALYTICAL METHODS	147
3.6 BRANCH AND ORDER DEFECTS	158

3.7	SPECIAL STRAIGHT-LINE MECHANISMS	158
3.8	PROBLEMS	161
4	DYNAMIC FORCE AND MOTION ANALYSIS OF PLANE MECHANISMS	167
4.1	INTRODUCTION	167
4.2	MOTION OF A RIGID BODY SUBJECTED TO A SYSTEM OF FORCES	167
4.3	PRINCIPLE OF VIRTUAL WORK	168
4.4	D'ALEMBERT'S PRINCIPLE AND DYNAMIC EQUILIBRIUM	168
4.5	DYNAMIC FORCE ANALYSIS (GRAPHICAL METHOD)	169
4.6	DYNAMIC FORCE ANALYSIS (ANALYTICAL METHOD)	173
4.7	STRESSES IN MOVING MEMBERS	178
4.8	DYNAMIC MOTION ANALYSIS	179
4.9	DYNAMICS OF SLIDER-CRANK MECHANISM	185
4.10	TURNING MOMENT ON CRANKSHAFT AND TURNING-MOMENT DIAGRAM	188
4.11	FLUCTUATION OF CRANKSHAFT SPEED	197
4.12	FLYWHEEL (AN APPROXIMATE ANALYSIS)	198
4.13	FLYWHEEL IN PUNCHING PRESS	203
4.14	DESIGN OF RIM-TYPE FLYWHEEL	205
4.15	WITTENBAUER'S METHOD OF FLYWHEEL ANALYSIS	206
4.16	DYNAMICS OF MECHANISMS WITH ELASTIC LINKS	211
4.17	PROBLEMS	214
5	KINEMATICS OF SPATIAL CHAINS	221
5.1	INTRODUCTION	221
5.2	MATRIX METHOD	223
5.3	LOOP-CLOSURE EQUATION	230
5.4	KINEMATICS OF OPEN CHAINS	233
5.5	PROBLEMS	242
6	GOVERNOR MECHANISMS	247
6.1	INTRODUCTION	247
6.2	TYPES OF GOVERNORS	249
6.3	CHARACTERISTICS OF CENTRIFUGAL GOVERNORS	249
6.4	GRAVITY-CONTROLLED CENTRIFUGAL GOVERNORS	251
6.5	SPRING-CONTROLLED CENTRIFUGAL GOVERNORS	260
6.6	HUNTING OF CENTRIFUGAL GOVERNORS	265
6.7	APPROXIMATE ANALYSIS OF SPEED-LOAD CHARACTERISTICS OF AN ENGINE	267
6.8	INERTIA GOVERNORS	269
6.9	OTHER GOVERNOR MECHANISMS	272
6.10	PROBLEMS	274
7	BALANCING OF INERTIA FORCES AND MOMENTS IN MACHINES	277
7.1	INTRODUCTION	277
7.2	BALANCING OF ROTATING MASSES	277
7.3	TWO-PLANE BALANCING	280

7.4 DETERMINATION OF BALANCING MASSES	281
7.5 BALANCING OF ROTORS	287
7.6 BALANCING OF INTERNAL-COMBUSTION ENGINES (APPROXIMATE ANALYSIS)	298
7.7 BALANCING OF INTERNAL-COMBUSTION ENGINES (GENERALIZED APPROACH)	321
7.8 LANCHESTER TECHNIQUE OF ENGINE BALANCING	326
7.9 BALANCING OF PLANAR LINKAGES	329
7.10 PROBLEMS	333
8 CAMS	341
8.1 INTRODUCTION	341
8.2 CLASSIFICATION OF FOLLOWERS AND CAMS	341
8.3 RADIAL CAM NOMENCLATURE	343
8.4 DESCRIPTION OF FOLLOWER MOVEMENT	345
8.5 ANALYSIS OF FOLLOWER MOTION	349
8.6 DETERMINATION OF BASIC DIMENSIONS	351
8.7 SYNTHESIS OF CAM PROFILE (GRAPHICAL APPROACH)	362
8.8 SYNTHESIS OF CAM PROFILE (ANALYTICAL APPROACH)	367
8.9 CAMS WITH SPECIFIED CONTOURS	378
8.10 DYNAMIC ANALYSIS OF CAMS	382
8.11 SPATIAL CAM-FOLLOWER MECHANISMS	390
8.12 PROBLEMS	396
9 GEARS	401
9.1 INTRODUCTION	401
9.2 GEARING ACTION, FUNDAMENTAL LAW OF GEARING, AND INVOLUTE SPUR GEARS	403
9.3 PROPERTIES OF THE INVOLUTE OF A CIRCLE	406
9.4 CHARACTERISTICS OF INVOLUTE ACTION	406
9.5 SYNTHESIS OF CONJUGATE TOOTH PROFILES FOR CIRCULAR SPUR GEARS	412
9.6 HELICAL, SPIRAL, BEVEL, AND WORM GEARS	419
9.7 GEAR TRAINS	423
9.8 TORQUES IN EPICYCLIC GEAR TRAINS	430
9.9 PROBLEMS	432
10 GYROSCOPIC ACTION IN MACHINES	435
10.1 INTRODUCTION	435
10.2 MOTION OF A RIGID BODY IN THREE DIMENSIONS	435
10.3 RIGID BODIES IN SPHERIC MOTION	437
10.4 EULER'S EQUATION OF MOTION	439
10.5 SIMPLE PRECESSION OF A SYMMETRICAL ROTOR	441
10.6 GYRODYNAMICS	447
10.7 GYROSCOPIC EFFECTS IN MACHINES	454
10.8 PROBLEMS	459

11 VIBRATIONS IN MECHANICAL SYSTEMS	463
11.1 INTRODUCTION	463
11.2 BASIC FEATURES OF VIBRATORY SYSTEMS	463
11.3 SINGLE-DEGREE-OF-FREEDOM SYSTEMS	466
11.4 SYSTEMS WITH TWO DEGREES OF FREEDOM	526
11.5 SYSTEMS WITH MULTIDEGREES OF FREEDOM	533
11.6 CONTINUOUS SYSTEMS	548
11.7 APPROXIMATE METHODS	557
11.8 VIBRATION MEASURING INSTRUMENTS	563
11.9 PROBLEMS	572
12 DYNAMICS OF ROTATING SHAFTS	581
12.1 INTRODUCTION	581
12.2 SHAFT WITH AN UNBALANCED DISC AT THE MIDSPAN	583
12.3 EFFECT OF INTERNAL FRICTION	589
12.4 EFFECT OF EXTERNAL FRICTION	596
12.5 GYROSCOPIC EFFECT ON CRITICAL SPEED	596
12.6 EFFECT OF THE GRAVITATIONAL FIELD (SECONDARY CRITICAL SPEED)	598
12.7 EFFECT OF BEARING STIFFNESS	600
12.8 EFFECT OF VARIABLE SHAFT STIFFNESS	603
12.9 EFFECT OF OIL FILM IN BEARINGS	605
12.10 ROTATING SHAFTS WITH SEVERAL DISCS	610
12.11 WHIRLING OF SHAFTS WITH DISTRIBUTED MASS	613
FURTHER READING	619
ANSWERS TO SELECTED PROBLEMS	621
INDEX	625

PREFACE

This new edition continues to provide a comprehensive, balanced treatment of the theory of mechanisms and machines for the undergraduate in mechanical engineering. Keeping in view the requirements of machine design, the chapters covering the basics of kinematic analysis and synthesis of planar linkages (Chapters 1-3) have been thoroughly revised and extended. Many more solved and exercise problems, highlighting the practical aspects of kinematic design of linkages, have been added. A new, short chapter on kinematics of spatial linkages is included in this edition. This will introduce the readers to the special techniques required for the study of kinematics of robot manipulators. The treatment of the synthesis of cam-follower mechanisms has been reoriented with a new design perspective. Some new sections have also been incorporated which outline the treatment of three-dimensional cam-follower mechanisms.

Extra care has been taken to emphasize the fundamental concepts in almost all chapters of the previous edition. The inclusion of the advanced topics will ensure that the text retains its usefulness for advanced undergraduate and postgraduate courses. To restrict the length of the book, a conscious decision has been made to delete certain rather advanced sections. These, in our opinion, were difficult to treat through classroom lectures.

The entire text has been reset using L^AT_EX. So there are bound to be some misprints which have eluded our scrutiny. We shall be grateful if the readers take the trouble of pointing out mistakes (for correction in future reprints) and also offer suggestions for further improvements. We thank Ms. Sandhya for typing the entire text. We are indebted to Messrs Goutam Chakraborty and Arun Kumar Saha for their help during the preparation of the final manuscript. Finally, we acknowledge the support and understanding of our families during the preparation of this edition.

AMITABHA GHOSH
ASOK KUMAR MALLIK



Chapter 1

INTRODUCTION

1.1 INTRODUCTION

The importance of mechanisms and machines is well recognized by all sections of human society and the subject forms an integral part of the mechanical engineering curricula in all universities. However, as in many other branches of science and technology, the actual developments have been need-oriented and not been derived from logical considerations based on a well-founded theory.

From the ancient times, man has always tried to invent contrivances for augmenting human abilities and that has led to the development of mechanisms and machines. Initially, the primary engineering activities were related to construction, which required the shifting and lifting of heavy objects. This, in turn, gradually led to the development of lever mechanisms, wedges, and pulley systems. As more and more new activities like mining, irrigation, and water supply started, pumping of water in large quantities became a never-ending task. The use of wind and water power for running pumps and many other activities became more prevalent in the medieval age. As a result, the ideas and concepts emerged for transferring and transforming motion and power (from one form to another) by using different types of mechanisms and machines.

The need to augment human abilities with the help of mechanical artefacts was not only for generating large forces but also for generating high-speed rotation (for drilling, fire making, etc.), creating geometric perfection, achieving precision and accuracy, etc. In many cases, the forces involved were not large. Many contrivances were for measurements, some were simply for generating geometric motions. The development of clocks, textile looms, and printing machines played a very important role in the history of mechanisms and machines. The emergence of machine tools for cutting screws and boring cannons and finally the onset of industrial revolution resulted in a tremendous growth of mechanisms and machines. Of course, one must not imagine that the minds of the clever persons of the antiquity were always busy in inventing useful mechanisms. Many times mechanisms and machines were developed for demonstrating magical effects in places of worship to impress (and fool) the common man.

A vast number of mechanical devices came into existence, but till the recent centuries there was no well-founded subject which could scientifically handle all such systems. Following a true Aristotelian style, scientists believed that all machines were composed of five simple components—lever, windlass, screw, wedge, and pulley. It was Franz Reuleaux who first proposed in the second half of the last century that kinematic pairs (a pair of contacting surfaces) are the true building blocks of all mechanical devices.

2 THEORY OF MECHANISMS AND MACHINES

The basic principles of mechanics were established by Newton while Euler and Huygens further sharpened the ideas about the geometrical aspects of motion and force-mass interaction. With engines, machines, locomotives, and ships coming into existence, the application of the principles of Newtonian mechanics in their design became essential. As can be seen from very old books on theory of machines, the subject primarily revolved around the design and development of engines. The application of the scientific principles of mechanisms in the design of complex machinery is a relatively recent phenomenon.

The true beginning of the science of mechanisms (in its modern perspective) started with James Watt when he used a four-link mechanism for guiding a point along an approximate straight line. Most mechanical engineering activities revolve around a mechanical system whose function depends on the relative movements among its various members. The design of a mechanical system needs a proper understanding of (i) the geometrical aspects of motion, and (ii) the various forces involved in motion. The subject which deals only with the geometric aspects of motion, without any consideration of the forces involved or the system inertia, is referred to as *kinematics* (derived from the Greek word *kinema*, meaning motion). When the system inertia and the involved forces are also considered, the subject is called *dynamics*. When the system is in equilibrium under the influence of the externally applied forces, the concerned branch of mechanics is termed *statics*, and if the system is in motion, it is called *kinetics*. Though there is no generalized theory which can handle all mechanisms yet a substantial number of systems can be understood with the existing theories. The appearance of high-speed computers has also made many previously unsolvable problems amenable to design and analysis.

Once the scientific principles behind the behavioural characteristics of all machines and mechanisms are well understood, rigorous design methods can be developed. The mechanisms and machines of the modern times with unbelievable high speed and accuracy have become possible only because of the subject *theory of mechanisms and machines*. More advanced systems, e.g., robots and intelligent machines, are emerging on the scene. To ensure *optimal result*, the design of such systems must be as accurate as possible which only the computers can achieve.

The major objectives of the subject *theory of mechanisms and machines* are to provide the engineers the necessary tools to systematically synthesize a system which means scientifically arriving at the critical shapes and dimensions of the bodies constituting the system. However, it is rarely possible to obtain a closed-form solution and the optimal design almost always requires an iterative procedure. Thus, the analysis of a synthesized system to evaluate its performance is necessary, and the techniques of *kinematic and dynamic analysis* must be learned to make an optimal *synthesis*. The synthesis can be either purely of kinematic nature or can also incorporate the dynamical aspects of the system.

The design of mechanisms to satisfy certain prescribed kinematic specifications is generally termed *kinematic synthesis*, and there are numerous situations covered by it. One such is the design of a cam profile to generate a prescribed motion of the follower. Another pertains to the shape of pitch curves and tooth profiles of two mating gears in order to obtain a prescribed rotational relationship. Both examples relate to the higher-pair group of mechanisms and are discussed separately in Chapters 8 and 9, respectively. In this chapter, and in Chapter 3 we shall restrict our discussion mainly to the kinematic synthesis of planar linkages. In fact, there are so many different problems in the kinematic synthesis of linkages that this topic forms a separate field of study by itself. Our objective here is to provide a brief introduction to the subject.

There are three different phases in the solution of problems of kinematic synthesis: type synthesis, number synthesis, and dimensional synthesis. In the first phase, we have to choose the type of mechanisms, e.g., gears, cams, and linkages, to be used for satisfying the motion specifications. This

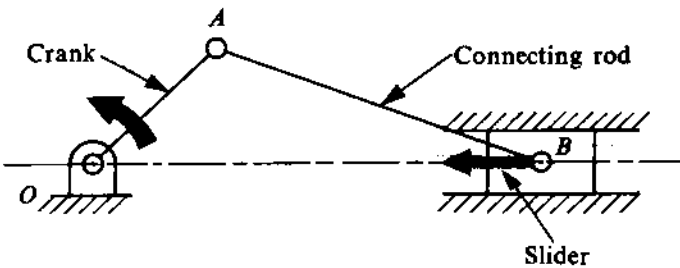


FIGURE 1.1

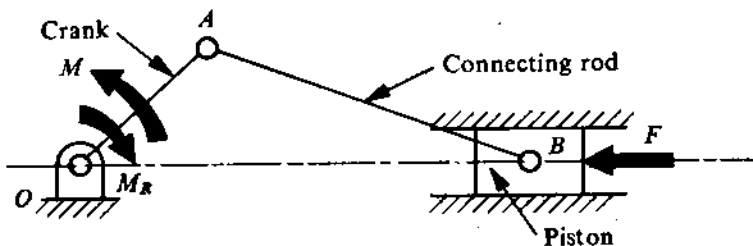


FIGURE 1.2

decision, in most cases, is beyond the field of kinematics and is guided by other design criteria, such as space limitations and the relationship of the mechanism with other elements in the assembly. Thus, the first phase is excluded from our discussion.

Since mechanisms and machines are at the centre of mechanical engineering activity, it is essential to start with simplified definitions of these terms.

1.2 MECHANISMS AND MACHINES

Mechanism

A mechanism is a combination of rigid or restraining bodies so shaped and connected that they move upon each other with definite relative motion. A simple example is the slider-crank mechanism (Fig. 1.1), used in internal-combustion engine or reciprocating air compressor, where the rotary movement of the crank is converted through the connecting rod into the reciprocating motion of the slider, or vice versa.

Machine

A machine is a mechanism or a collection of mechanisms which transmits force from the source of power to the resistance (load) to be overcome, and thus performs useful mechanical work. A simple example is the one in the internal-combustion engine (Fig. 1.2), where the force, F , available at the piston is transmitted to the crank in the form of driving torque, M , to overcome the resistance M_R at the crankshaft. Obviously, a system can be defined as a *mechanism* or a *machine* on the basis of its primary objective. When the objective is only to transfer and transform the motion (without consideration of the forces involved), the system is said to be a *mechanism*. On the other hand, if the system is used with the objective of transferring mechanical energy, then it is called a *machine*.

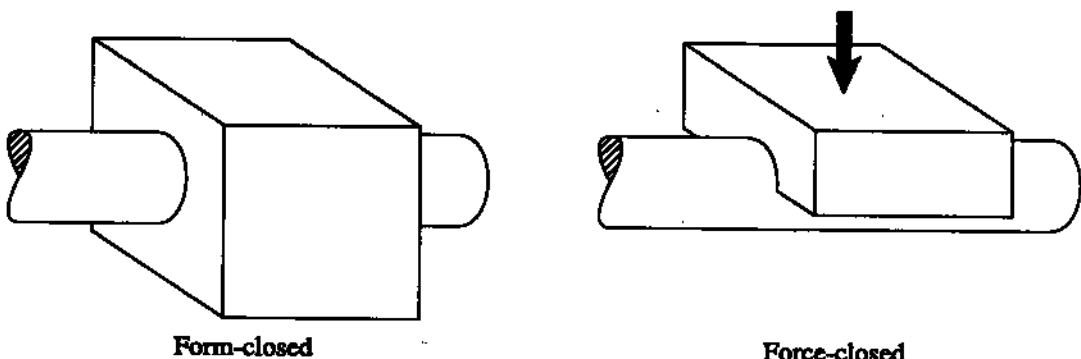


FIGURE 1.3

As mechanical work is always associated with movement, every machine has to transmit motion. Therefore, every machine is a mechanism, but not vice versa. More rigorous and comprehensive definitions will follow when the reader becomes conversant with the basic constituent elements of mechanisms and machines.

1.3 KINEMATIC PAIRS

A mechanism has been defined as a combination of bodies so connected that each moves with respect to another. A clue to the behaviour of the mechanism lies in the nature of the connections, commonly known as *kinematic pairs*, and in the type of relative motions they permit. The *degree of freedom* of a kinematic pair is given by the number of independent coordinates required to completely specify the relative movement. These coordinates are commonly known as *pair variables*. Broadly, kinematic pairs can be classified as lower, higher, and wrapping pairs. The contact between two bodies can be maintained either by geometrically enclosing one body in the other or with the help of an externally applied force. In the first case, the pairs are referred to as *form-closed* and in the second as *force-closed*. Figure 1.3 shows two examples.

Lower Pairs

A pair is said to be a lower pair when the connection between two elements is through the area of contact. A description of six commonly-used lower pairs follows.

Revolute or Turning Pair (Hinged Joint)

A revolute pair is shown in Fig. 1.4a. It is seen that this connection allows only a relative rotation between elements 1 and 2, which can be expressed by a single coordinate θ . Thus, a revolute pair has a single degree of freedom.

Prismatic Pair

As shown in Fig. 1.4b, a prismatic pair allows only a relative translation between elements 1 and 2, which can be expressed by a single coordinate S , and thus it possesses one degree of freedom. It

should be noted that in such a pair it is only the direction of relative motion which is important. The location of a prismatic pair has no relevance to the kinematics of a system.

Screw Pair

As shown in Fig. 1.4c, a screw pair also has one degree of freedom since the relative movement between elements 1 and 2 can be expressed by a single coordinate θ or S . These two coordinates are related, that is,

$$\frac{\Delta\theta}{2\pi} = \frac{\Delta S}{L},$$

where L is the lead of the thread.

Cylindrical Pair

As shown in Fig. 1.4d, a cylindrical pair has two degrees of freedom because it allows both rotation and translation, parallel to the axis of rotation, between the connected elements. These relative movements can be expressed by two independent coordinates θ and S , respectively.

Spheric Pair

A ball-and-socket joint, as shown in Fig. 1.4e, forms a spheric pair. This connection has three degrees of freedom since the complete description of the relative movement between the connected elements needs three independent coordinates. Two of these coordinates α and β are required to specify the position of the axis OA and the third coordinate θ describes the rotation about the axis OA .

Planar Pair

A planar pair, shown in Fig. 1.4f, has three degrees of freedom. Two coordinates x and y describe the relative translation in the xy -plane and the third θ describes the relative rotation about the z -axis.

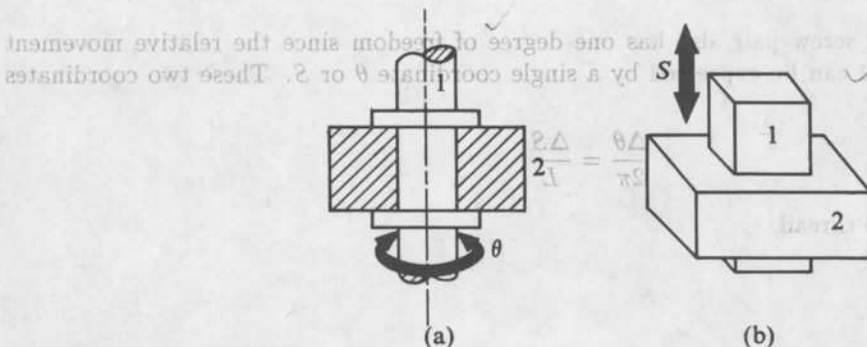
Higher Pairs

A higher pair is defined as one in which the connection between two elements has only a point or line contact. A point contact takes place in ball bearings or between the teeth of skew-helical gears. A line contact is observed in roller bearings, between the teeth of most gears, and in cam-follower elements. Figure 1.5 shows point contact and line contact in higher pairs.

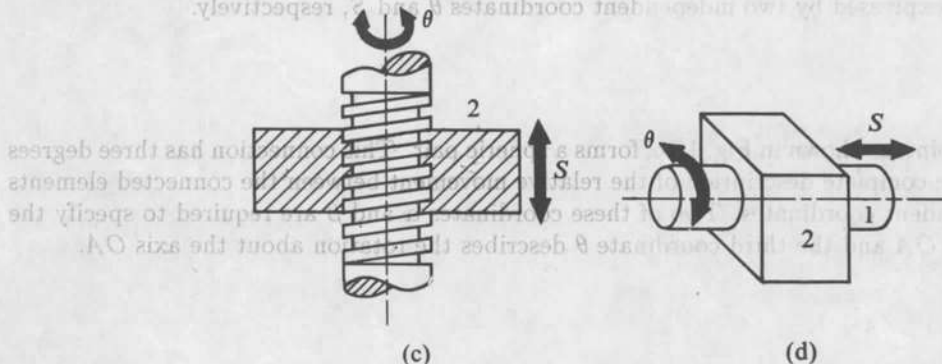
Wrapping Pairs

Wrapping pairs comprise belts, chains, and such other devices. Figure 1.6 shows a belt-driven pulley arrangement. In this text, we shall discuss the mechanisms consisting only of lower and higher pairs.

The position of a linkage with respect to the direction of relative motion is important.



Y-axis shows the two degrees of freedom because it allows both rotation and translation. The connecting rod 2 rotates about its pivot. The slider 1 moves vertically as the connecting rod 2 rotates.



A horizontal force S describes the relative motion of the slider 1 about the axis Oy. The connecting rod 2 rotates about its pivot. The slider 1 moves vertically as the connecting rod 2 rotates.

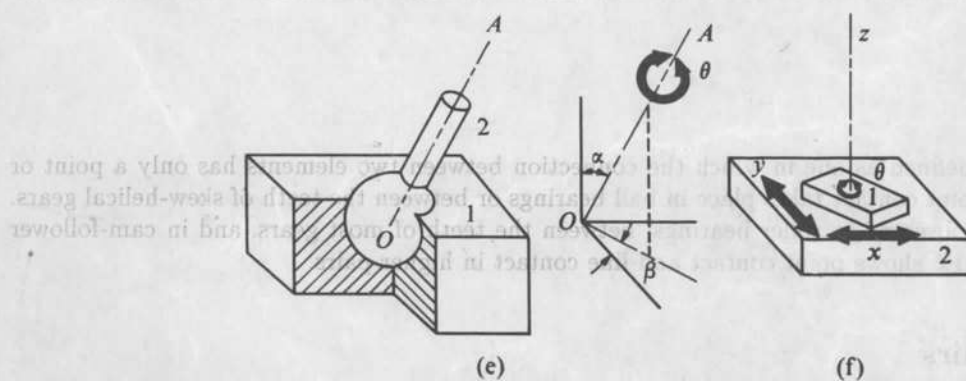


Figure 1.4 shows a pull-follower device. The follower 1 moves only in the direction of the pull-pusher base.

FIGURE 1.4

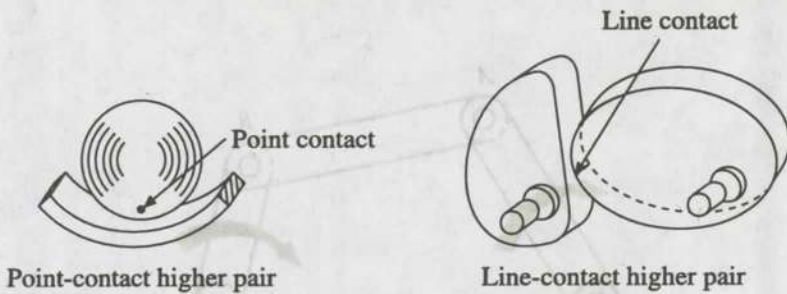


FIGURE 1.5

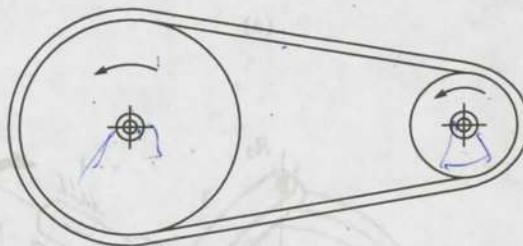


FIGURE 1.6

1.4 PLANE AND SPACE MECHANISMS

If all points of a mechanism move in parallel planes, then it is defined as a *plane mechanism*. A simple plane mechanism is shown in Fig. 1.7a, where all points move in parallel planes. A *space mechanism* is one in which all points of the mechanism do not move in parallel planes. A very common example of a space mechanism, known as Hooke's joint, is shown in Fig. 1.7b. The major part of this book will be devoted to a study of the characteristics of only the plane mechanisms.

1.5 KINEMATIC CHAINS AND THEIR CLASSIFICATION

To rigorously define a mechanism, we must first formally define the basic elements which comprise a mechanism.

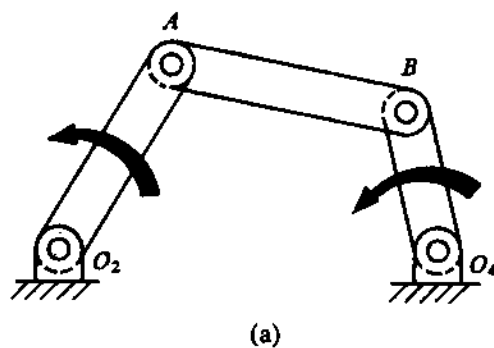
Link

A material body which is common to two or more kinematic pairs is called a *link*. Figure 1.8 shows two revolute pairs. Link 1 is common to the pairs formed by elements 1 and 2, and elements 1 and 3.

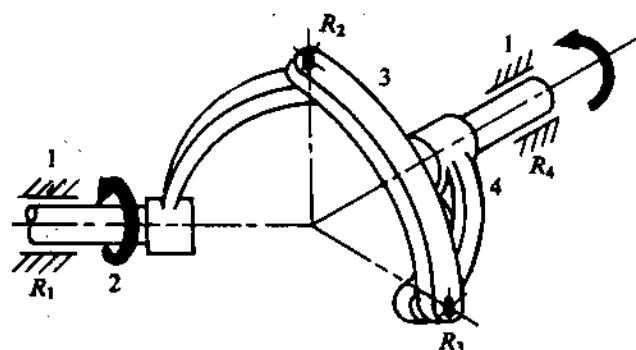
Kinematic Chain

A *kinematic chain* is a series of links connected by kinematic pairs. The chain is said to be *closed* if every link is connected to at least two other links, otherwise it is termed an *open chain*.

A link which is connected to only one other link is known as a *singular link*. If it is connected to two other links, it is called a *binary link*. Similarly, if a link is connected to three other links, it is



(a)



(b)

FIGURE 1.7

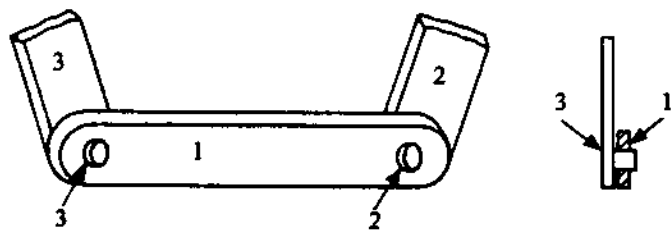


FIGURE 1.8

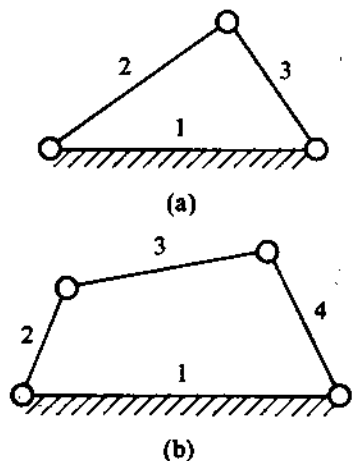


FIGURE 1.9

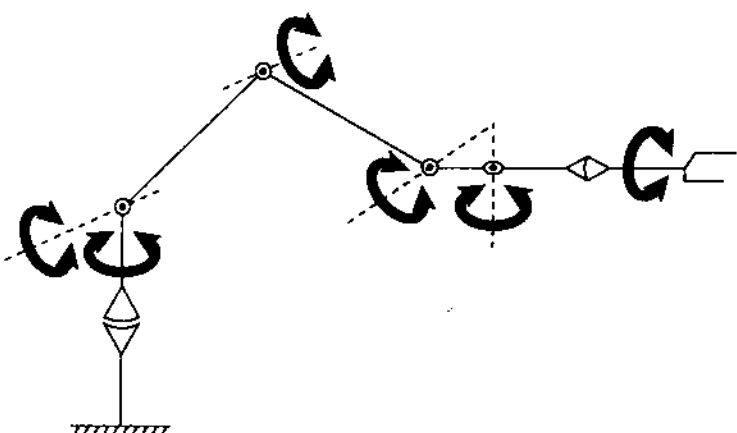


FIGURE 1.10

referred to as a *ternary link*, and so on. By definition, a closed chain cannot contain a singular link. A chain which consists only of binary links is termed a *simple chain*.

A very important type of kinematic chain is one with *constrained motion*, which means that a definite motion of any link produces unique relative motion of all other links. In other words, the relative position of any one link uniquely defines the relative position of any point on any other link. Thus, a *constrained kinematic chain* has a single degree of freedom.

At this stage, a *mechanism* can be defined more rigorously as a closed kinematic chain in which one link is fixed.

Before going into the general theory of mechanisms, it may be observed that to form a simple closed chain we need at least three links with three kinematic pairs. However, if one of these three links is fixed (Fig. 1.9a), there cannot be any relative movement, and so the closed chain does not form a mechanism. Such an arrangement is referred to as a *structure* which is completely rigid. Thus, the simplest mechanism consists of four binary links, each connected by a kinematic pair of the revolute type, and is known as a *four-bar mechanism* (Fig. 1.9b). According to many kinematicians, a mechanism consisting of only the lower pairs may be called a *linkage*. However, the term linkage has been widely used as a synonym for the word mechanism. For obvious reasons, the emphasis, so far, has been only on closed kinematic chains. But due to the recent emergence of robot technologies, a considerable amount of interest in open chains has been generated. This is mainly because, in most cases, the robot manipulator arm is kinematically an open spatial chain as indicated in Fig. 1.10.

1.6 KINEMATIC DIAGRAMS, LIMIT AND DISGUISE OF REVOLUTE PAIRS

To facilitate the study of a real-life mechanism, it is generally represented by a *kinematic diagram*. Such a diagram depicts the essential kinematic features of the mechanism. The conventions followed to illustrate these features are explained in Fig. 1.11.

A prismatic pair can always be thought of as the limit of a revolute pair. To demonstrate this, let us consider the two mechanisms shown in Figs. 1.12a and 1.12b. The curved slider (the connection between links 1 and 4) in Fig. 1.12b remains a revolute pair, as the pair variable (to describe relative

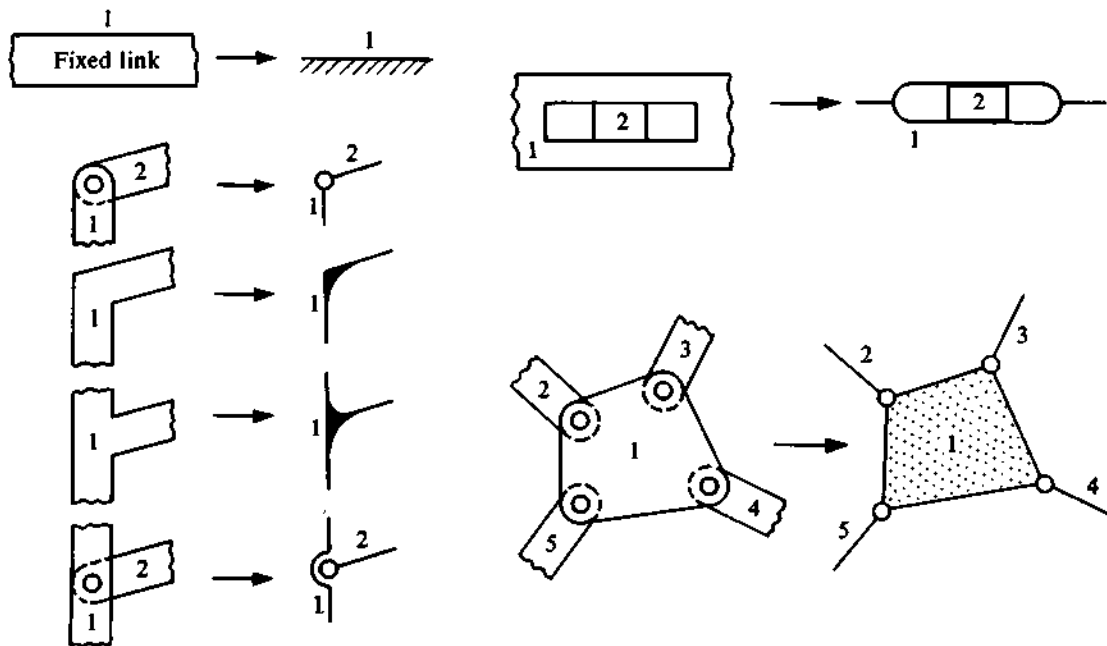


FIGURE 1.11

motion) is still represented by an angular movement. If the radius of curvature ρ of the curved slider shown in Fig. 1.12b becomes infinitely large, the pair variable transforms to linear displacement (from angular movement) and the revolute pair R_4 transforms to a prismatic pair. As explained in Figs. 1.13a and 1.13b, we can see that a slider-crank mechanism is obtained as a *limit* of the four-bar linkage in which one hinge point goes to infinity, thus transforming one revolute pair to a prismatic pair.

In some cases, the true character of a revolute pair is not apparent. This *disguise* results from some practical considerations such as strength and space limitations. Figures 1.14a and 1.14b show the same slider-crank mechanism; the crank in Fig. 1.14a has been replaced by an eccentric in Fig. 1.14b.

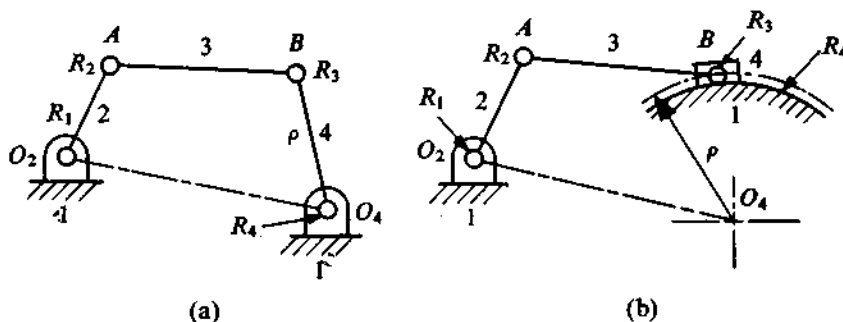


FIGURE 1.12

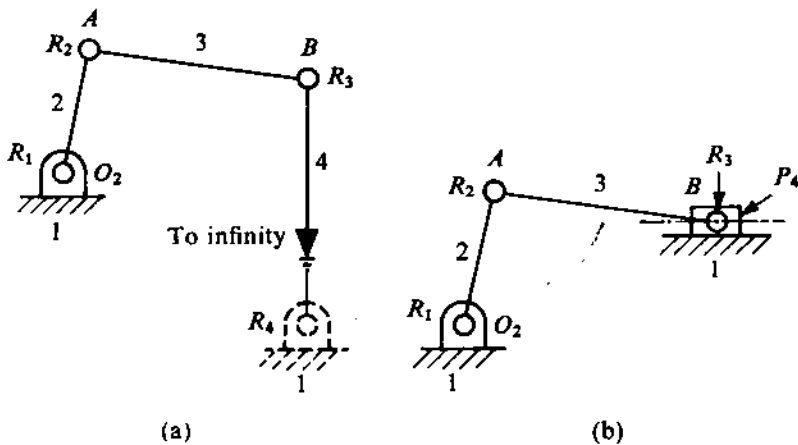


FIGURE 1.13

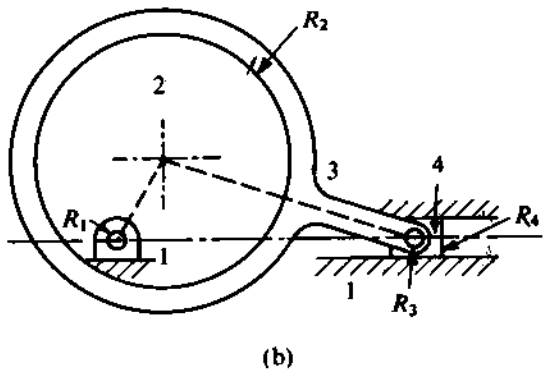
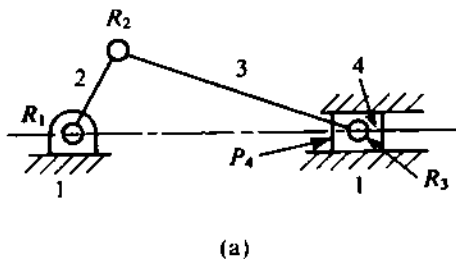


FIGURE 1.14

The reader should note that the number and the types of links and connections alone do not give the true description of a mechanism. For example, all four binary links of both plane and space mechanisms, shown in Figs. 1.7a and 1.7b, are connected by revolute pairs. The difference between them is that the axes of all revolute joints are parallel in the former mechanism, which is not so in the latter.

PROBLEM 1.1

Figure 1.15 shows a drafting mechanism with the help of which the two scales *A* and *B* (at right angles to each other) execute a purely translatory motion. Draw the kinematic diagram considering the scales (i) clamped, and (ii) unclamped.

SOLUTION

The system is easily identified as two parallelogram linkages in series as shown in Fig. 1.16a. When the scales are clamped, these form parts of the same link 7. On the other hand, in the unclamped condition, the scales form a separate link 8 which is hinged to 7 (shown in Fig. 1.16b).

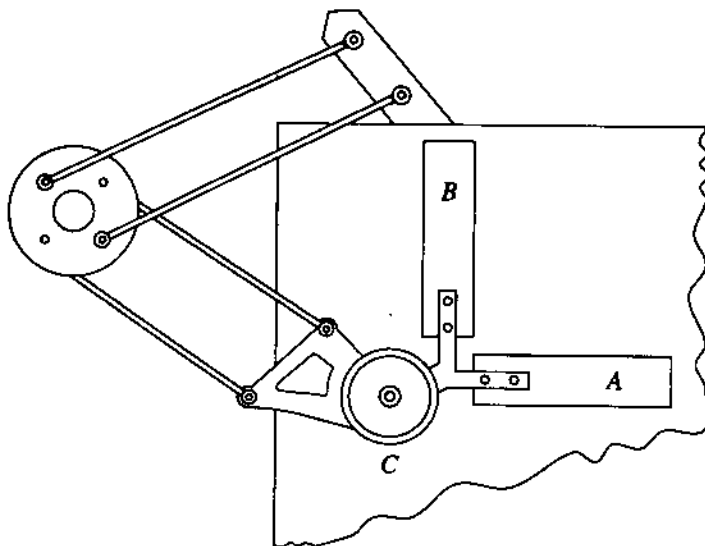


FIGURE 1.15

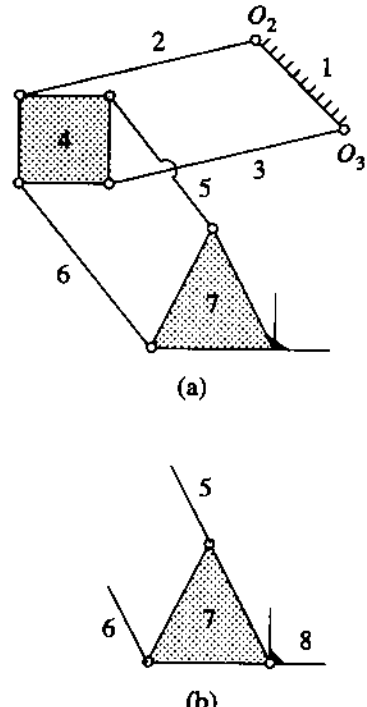


FIGURE 1.16

PROBLEM 1.2

Figure 1.17 shows a V-twin internal-combustion engine with articulated connecting rod. Draw the kinematic diagram.

SOLUTION

Figure 1.18 shows the kinematic diagram. The crank (along with the counter-balancing mass) is termed as link 2 which is hinged to the ground link 1 at O_2 . The connecting rod of the cylinder A is a ternary link numbered 3 whereas that of the cylinder B is a binary link numbered 4. The cylinders are fixed with the frame and, therefore, the pistons (5 and 6) are sliding members connected to the ground link 1 through prismatic pairs as shown.

1.7 KINEMATIC INVERSION

From the definition of mechanism given in Section 1.5, it is seen that by fixing the links of a closed chain one at a time, we get as many different mechanisms as the number of links in the chain. This process of fixing different links of the same kinematic chain to produce distinct mechanisms is called *kinematic inversion*. In this process, the relative motions of the links of the mechanisms produced remain unchanged.

First, let us consider the simplest kinematic chain, i.e., a chain consisting of four binary links and four revolute pairs (see Fig. 1.19a). The four dissimilar mechanisms that can be obtained by the

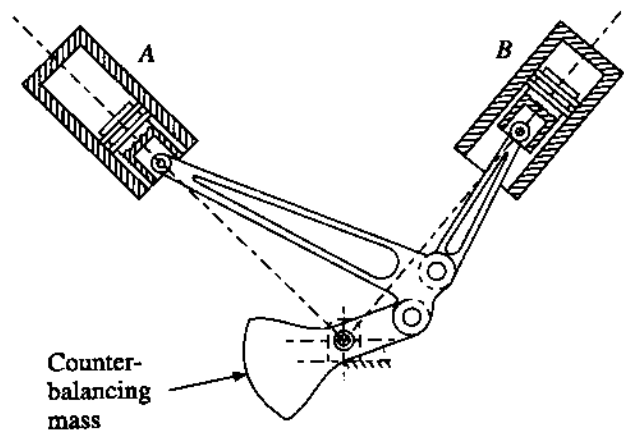


FIGURE 1.17

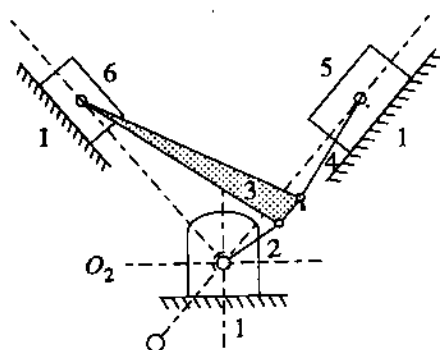


FIGURE 1.18

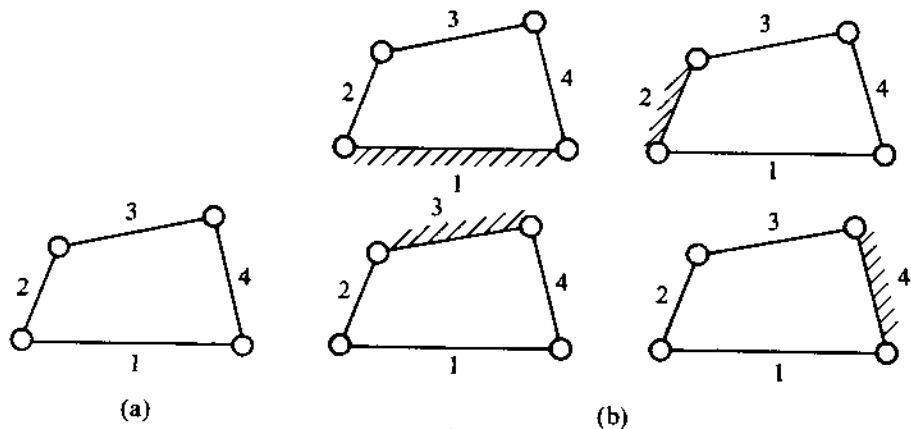


FIGURE 1.19

four different inversions of the chain are shown in Fig. 1.19b. Though each resulting mechanism is a four-bar linkage, the movability characteristics of the mechanisms, as we shall see in Section 1.10, are diverse.

Next, let us consider a kinematic chain with four binary links, three revolute pairs, and one prismatic pair (Fig. 1.20a). Fixing links 1, 2, and 3 in turn, we get three different mechanisms shown in Fig. 1.20b. The reader is advised to complete the fourth inversion by fixing link 4 and to satisfy himself that the mechanism so produced is the mechanism used in a hand pump where the connecting rod acts as the driving member. It should be noted that a kinematic inversion may change the appearance of a mechanism.

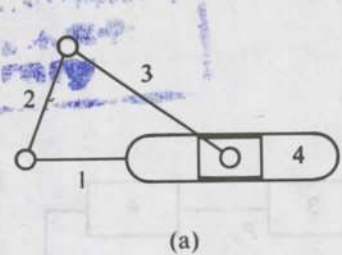
Let us again consider a kinematic chain, this time with four binary links and two revolute and two prismatic pairs placed in the order stated (see Fig. 1.21). As can be noted, the ordering of the four pairs here, unlike in the foregoing two situations, must be specified so as to uniquely describe the kinematic chain. In this kinematic chain, the constant rotation of crank 2 produces a harmonic translation of yoke 4. Such a mechanism is known as *scotch yoke*. Its four binary links are

$1 \rightarrow$ fixed link, $2 \rightarrow$ crank, $3 \rightarrow$ sliding block, $4 \rightarrow$ yoke, and four kinematic pairs are
 $R_1 \rightarrow$ revolute pair (between links 1 and 2), $R_2 \rightarrow$ revolute pair (between links 2 and 3).
 $P_3 \rightarrow$ prismatic pair (between links 3 and 4), $P_4 \rightarrow$ prismatic pair (between links 4 and 1).

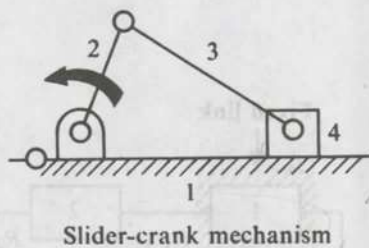
Link 1 has two elements, one forming a revolute pair with link 2 and the other forming a prismatic pair with link 4. Link 2 has two elements, both forming revolute pairs, one with link 1 and the other with link 3. Link 3 has two elements, one forming a revolute pair with link 2 and the other a prismatic pair with link 4. Link 4 also has two elements, both forming prismatic pairs, one with link 3 and the other with link 1. This arrangement is schematically shown in Fig. 1.22.

If in the chain shown in Fig. 1.22 link 2 is fixed, we obtain a mechanism, known as *Oldham's coupling*, used for transmitting constant angular velocity between two parallel but eccentric shafts (Fig. 1.23). The representative kinematic scheme for this mechanism is shown in Fig. 1.24. It should be noted that Figs. 1.22 and 1.24 are the same but for the fixed link.

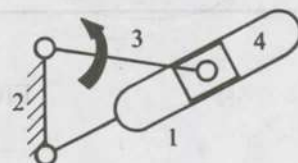
An inversion of the same chain yields yet another common mechanism called *elliptic trammel*, shown in Fig. 1.25, in which link 4 is fixed. Any point D on link 2 describes an ellipse as it moves.



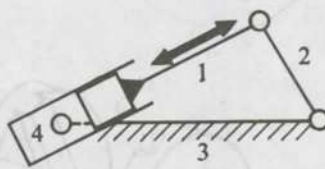
(a)



Slider-crank mechanism



Quick-return mechanism



Oscillating-cylinder engine mechanism

(b)

FIGURE 1.20

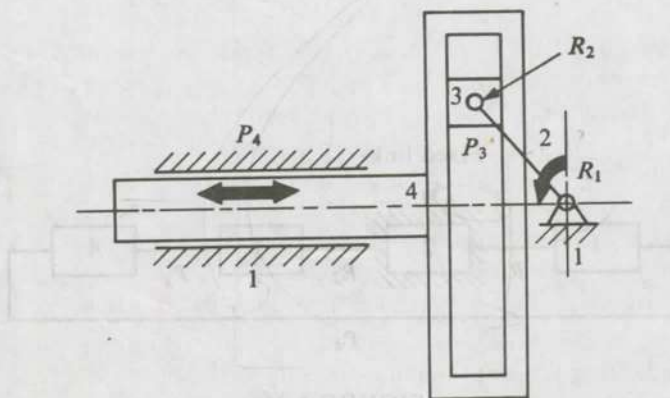


FIGURE 1.21

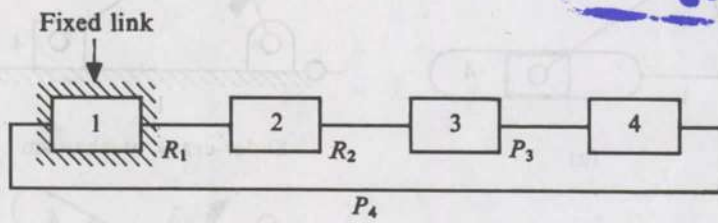


FIGURE 1.22

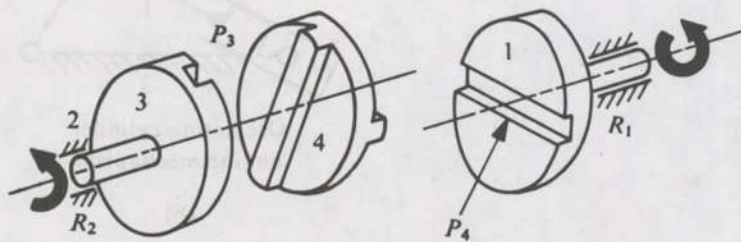


FIGURE 1.23

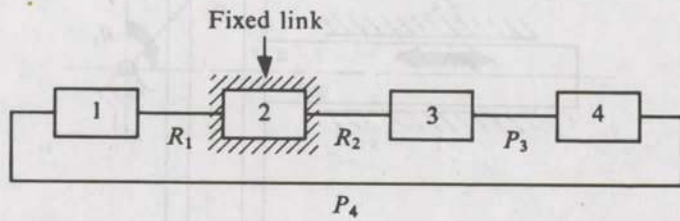


FIGURE 1.24

Adama University
A research
Library

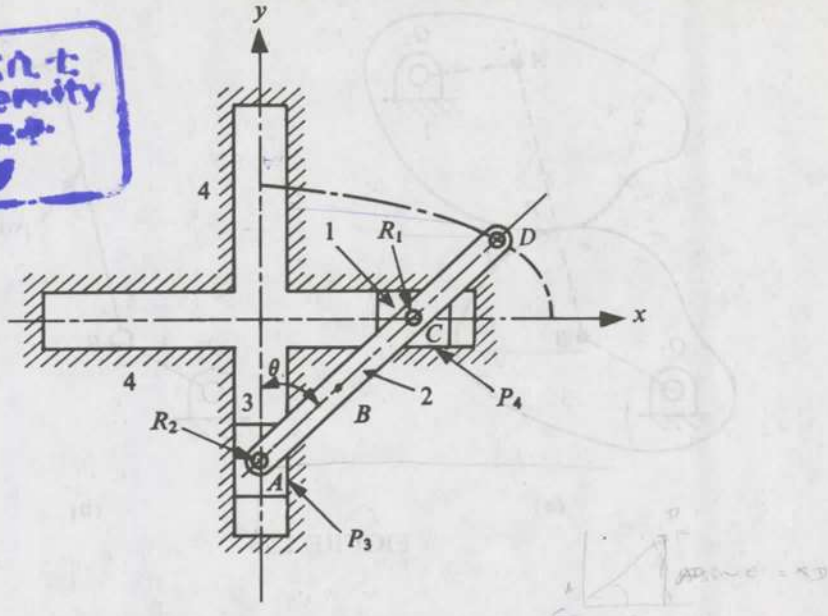


FIGURE 1.25

This can be proved by considering the coordinates of the point D in the xy -system, which are

$$x_D = AD \sin \theta, \quad \sin \theta = x_D/AD, \quad (1.1)$$

$$y_D = CD \cos \theta, \quad \cos \theta = y_D/CD. \quad (1.2)$$

Squaring and adding (1.1) and (1.2), we get

$$\left(\frac{x_D}{AD}\right)^2 + \left(\frac{y_D}{CD}\right)^2 = 1 \quad (1.3)$$

which is the equation for an ellipse. The midpoint B of AC will obviously describe a circle. The reader is advised to check from Fig. 1.25 that the kinematic chain remains the same, and also to obtain the fourth inversion from the same chain.¹

1.8 EQUIVALENT LINKAGES

Very often a mechanism with higher pairs can be replaced by an *equivalent mechanism* with lower pairs. This equivalence is valid for studying only the instantaneous characteristics. The equivalent lower-pair mechanism facilitates analysis as a certain amount of sliding takes place between connected links in a higher-pair mechanism. Referring to Fig. 1.26a, links 2 and 3 are connected to the fixed link by revolute pairs at O_2 and O_3 , respectively. These links are connected to each other at P , thus forming a higher pair. The relative motion between links 2 and 3 consists of rolling, coupled with a certain amount of sliding. A and B are the centres of curvature of surfaces 2 and 3, respectively, at the point P . The instantaneous equivalent lower-pair mechanism shown in Fig. 1.26b calls for an additional link AB , and the higher pair is replaced by two revolute pairs at A and B . Another

¹See Bevan, T., *The Theory of Machines*, Longmans Green, London, 1962.

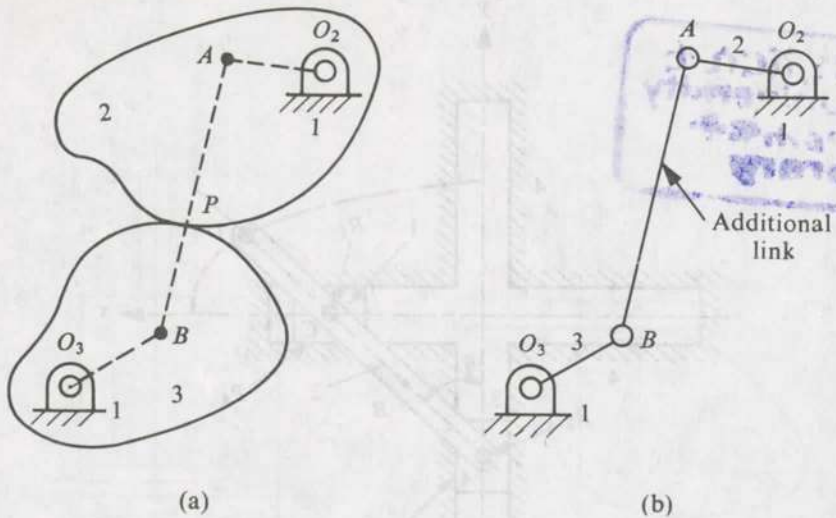


FIGURE 1.26

example of an equivalent lower-pair mechanism for a cam-follower system is shown in Fig. 1.27. The sliding block 4 is the additional link and the higher pair is replaced by two lower pairs, one revolute and the other prismatic. C is the centre of curvature of the cam surface at the point of contact between the cam and the follower. The centre of curvature of the follower surface at the same point is at infinity, and that is why one of the additional lower pairs becomes prismatic. It should be noted that an equivalent mechanism with lower pairs, representing a mechanism with higher pair(s), is not unique. Instead, an infinite number of equivalent mechanisms are possible for a given mechanism with higher pair(s). If A be a point on body 2, then its path can be traced on a plane rigidly attached to body 3 as shown in Fig. 1.28a. If B be the centre of curvature of this path at location A , then the equivalent mechanism will be $O_2 A B O_3$ as shown in Fig. 1.28b. Since there are an infinite number of choices possible for A , infinite possibilities exist for the equivalent mechanism. However, it must be remembered that the determination of the path of A on body 3 is normally not a simple task.

PROBLEM 1.3

Figure 1.29 shows a generalized cam mechanism. Find out an equivalent mechanism with lower pairs only.

SOLUTION

Since nothing is mentioned, it will be best to find out the simplest solution. Let the point A be the centre of curvature of the profile of 3 at the point of contact P with follower 5. At P , follower 5 has an infinite radius of curvature. Therefore, the additional link 6 is hinged to 3 at A and has a prismatic pair with 5. The direction of the prismatic pair is parallel to the flat follower surface. If the profile of link 3 is circular, then the kinematic equivalence remains valid for all instants. This is shown in Fig. 1.30.

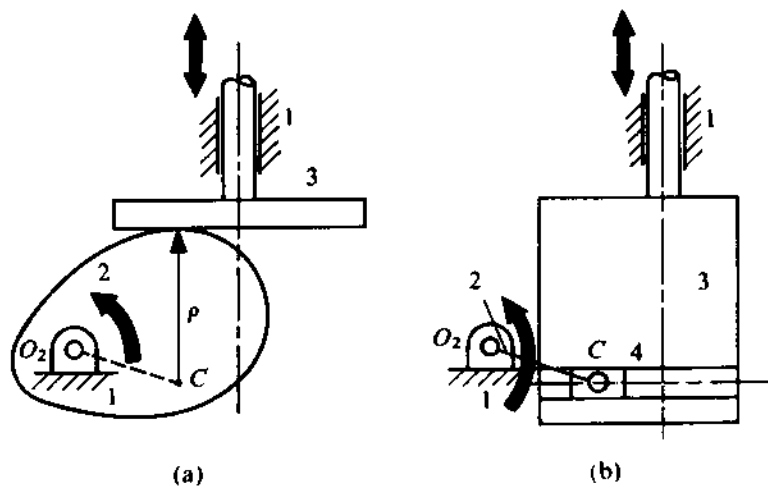


FIGURE 1.27

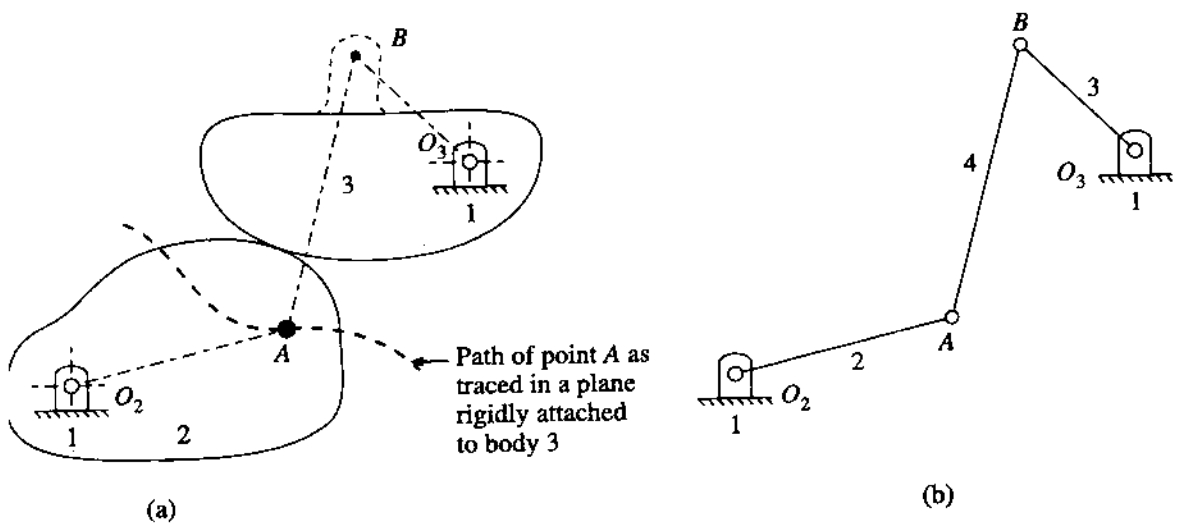


FIGURE 1.28

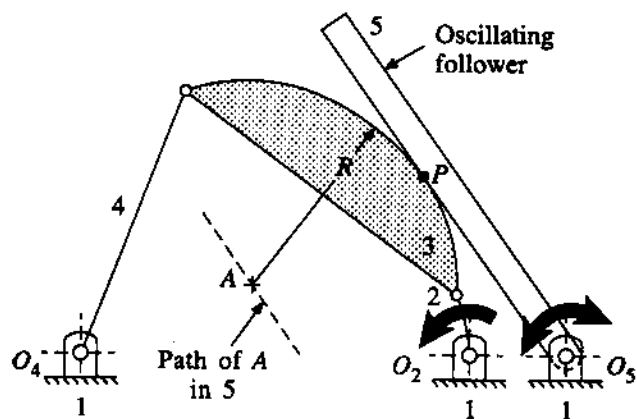


FIGURE 1.29

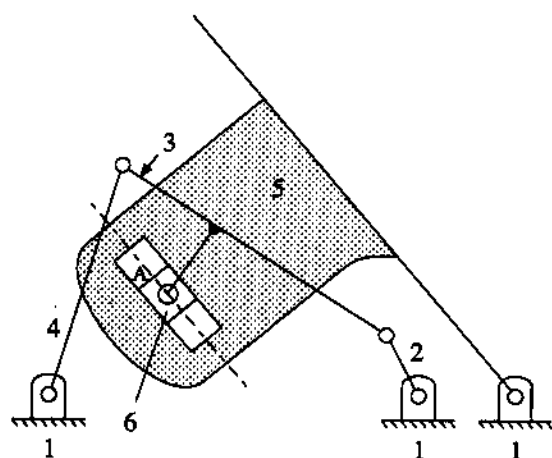


FIGURE 1.30

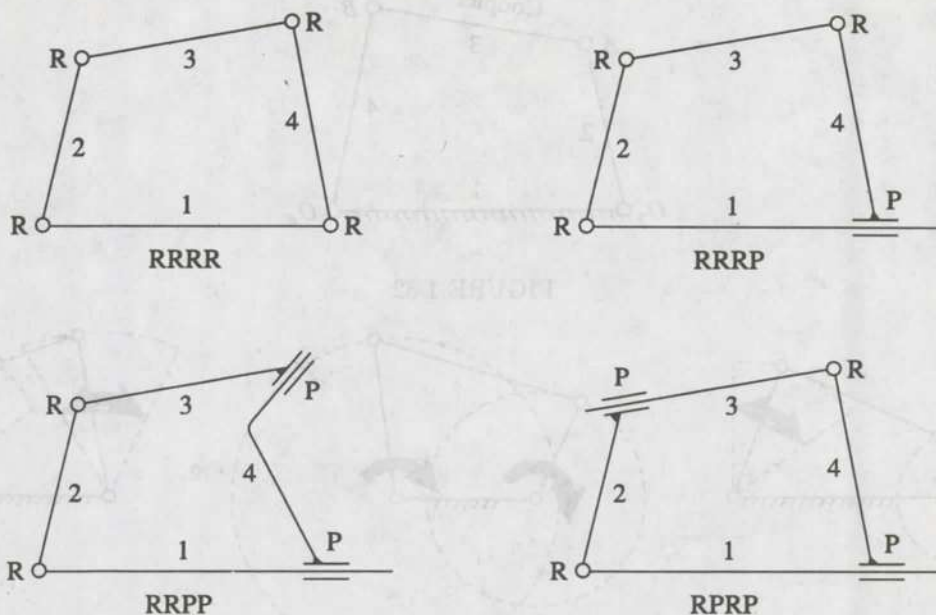


FIGURE 1.31

1.9 FOUR-LINK PLANAR MECHANISMS

Four-link planar mechanisms are the simplest of all mechanisms. However, their use and application in machines and mechanical devices are so extensive that a brief introduction to these mechanisms is desirable. This will also familiarize the reader with many commonly-used terms and ideas related to mechanisms. Furthermore, it can be also appreciated, after this introduction, that a large variety of motions is possible even with only four links (in fact, three moving links) with different combinations of kinematic pairs and with different inversions of the chain.

Four lower pairs are required to connect the four links in a 4-link mechanism. Since there are two types of kinematic pairs in plane kinematic chains – revolute pairs (R) and prismatic pairs (P) – the possible topologically different combinations are as follows: (i) RRRR, (ii) RRRP, (iii) RRPP, and (iv) RPRP. Figure 1.31 shows these possible situations. There are four possible inversions for each kinematic chain, resulting in a wide variety of mechanisms.

4R Mechanisms: It may appear at the first sight that all inversions of a 4R kinematic chain lead to similar mechanisms (commonly known as four-bar mechanisms). But it will be seen that the geometric motion characteristics can be different for mechanisms resulting from different inversions. When one of the links of a 4R chain is grounded (say, link 1), two hinges (R pairs) are grounded. These are called *fixed or ground hinges*, denoted by O_2 and O_4 in Fig. 1.32. The other two hinges, A and B, are called *moving hinges*. The points A and B are also termed as *motion-transfer points*. Links 2 and 4 execute a pure rotary motion, being hinged to the frame, and link 3 executes a generalized plane motion, being composed of both translation and rotation. Such a link is termed as a *floating link*. When a link hinged to the frame can make a complete rotation, it is called a *crank*, and it is called a *rocker* when such a link can execute only an oscillatory motion. Usually, one of the links hinged to the frame is chosen as the *input link* and the other as the *output link* or the *follower*.

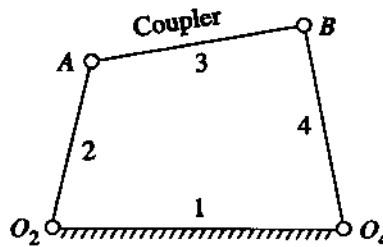
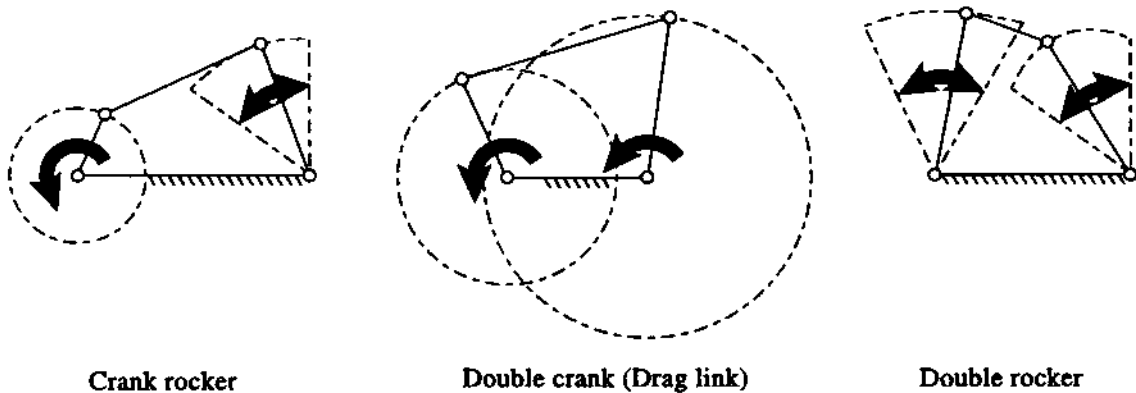


FIGURE 1.32



Double crank (Drag link)

Double rocker

FIGURE 1.33

The connecting link (AB in Fig. 1.32) is called the *coupler*.

Three different geometric motion characteristics are possible for a 4R mechanism. One of the links hinged to the frame makes a complete rotation whereas the other one rocks. This type of mechanism is called a *crank rocker*. When both the links hinged to the frame make a complete rotation, the mechanism is called a *double-crank* or a *drag-link* mechanism. In the remaining case, when both the links hinged to the ground execute only oscillatory motions, the mechanism is called a *double rocker*. Figure 1.33 shows the three types of mechanisms. Since most machines are driven by electric motors, the input link in such cases has to be a crank. In a large number of cases, the follower is the other link with a ground hinge though there are special situations when the output motion is provided by the coupler. The conditions which lead to different types of 4R mechanisms will be discussed in the next section.

3R-1P Mechanisms: The different inversions of a 3R-1P kinematic chain lead to four different types of mechanism. Figure 1.34 shows these mechanisms along with the associated applications. It must be mentioned that these are only a few of the applications of such mechanisms. Out of all the cases, the first one, obtained by fixing link 1, is by far the most important and the mechanism is popularly known as *slider-crank* mechanism. All engines, compressors, presses are based on this mechanism. In the general configuration of a slider crank (known as *offset slider crank*), the path of the motion-transfer point on the slider does not pass through the fixed hinge of the crank. In most cases, however, the *offset*, e (Fig. 1.34), is equal to zero as shown in Fig. 1.20.

2R-2P Mechanisms: With this chain, three distinct possibilities exist. The link between the revolute pairs can be grounded, and one such mechanism based on this inversion is Oldham's coupling shown in Fig. 1.23. When the link with one revolute pair and one prismatic pair is grounded, the

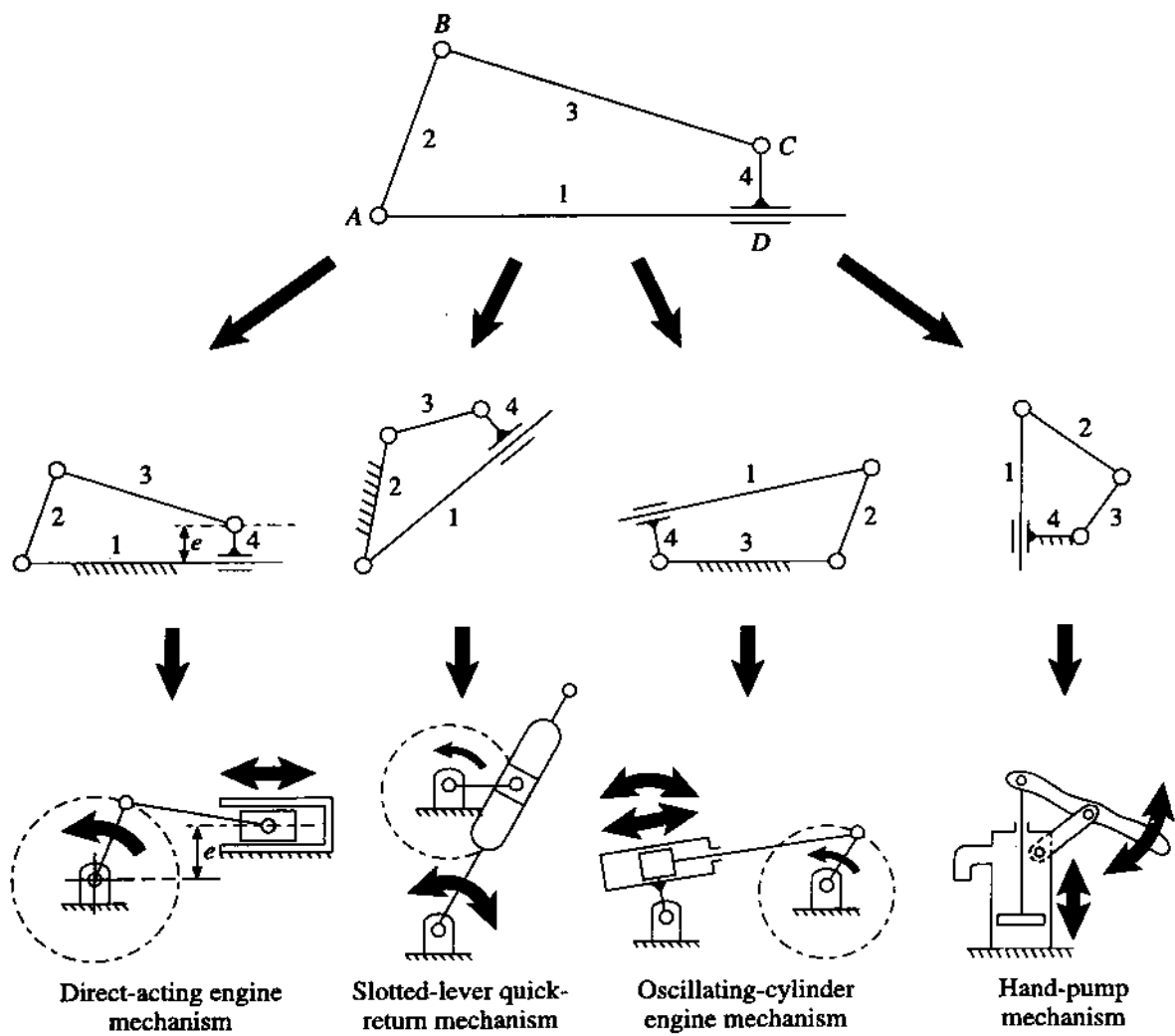


FIGURE 1.34

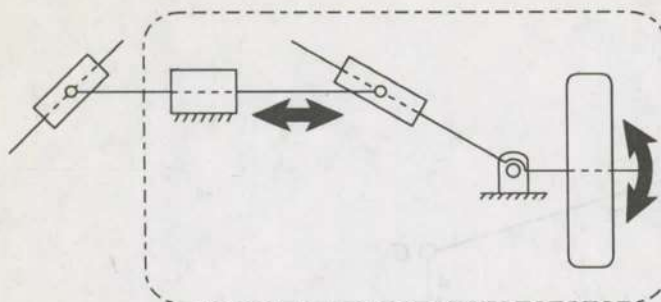


FIGURE 1.35

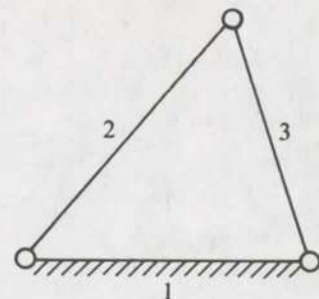


FIGURE 1.36

inversion yields a scotch-yoke mechanism (Fig. 1.21), and for the last case (i.e., when the link with two prismatic pairs is grounded), an example is the elliptic trammel shown in Fig. 1.25.

RPRP Mechanisms: There are not many mechanisms derived from this chain. Figure 1.35 shows a part (indicated by the circumscribing dashed lines) of the *Davis automobile steering gear* which can be easily identified as an inversion of RPRP chain.

A 3P-1R chain is not meaningful as no relative rotation can take place among the links. When all the four lower pairs are prismatic pairs, the derived system is not a constrained mechanism. However, the reader should note that when three links are connected by three prismatic pairs, a constrained chain is obtained as discussed in more details in the next section.

1.10 MOBILITY AND RANGE OF MOVEMENT

It must be remembered that an arbitrary number of links connected by a number of kinematic pairs do not result in a mechanism. Some conditions must be satisfied for a system of interconnected links to serve as a useful mechanism. The foremost thing which has to be investigated is the mobility of a mechanism in terms of the number of *degrees of freedom F*, which is equal to the number of independent coordinates required to specify its configuration, i.e., the relative positions of all the links. In this section, we shall first try to express the number of degrees of freedom of a mechanism in terms of the number of links and the number of pair connections of a given type. This is known as *number synthesis*.

★ Kutzbach Equation and Grübler's Criterion

Let n be the number of links in a mechanism, out of which one is fixed, and let j be the number of simple hinges (i.e., those which connect two links). Now, as the $(n - 1)$ links move in a plane, in the absence of any connections, each has three degrees of freedom; two coordinates are required to specify the location of any reference point of this rigid link (e.g., centre of gravity) and one more coordinate is required to define the orientation of the link. Once we connect two links by a hinge, there cannot be any relative translation between them and only one coordinate is necessary to specify their relative orientation. Thus, two degrees of freedom (translational) are lost at every hinge and only one degree of freedom (rotational) remains. So, the number of degrees of freedom of the mechanism is given by the following equation known as the Kutzbach equation:

$$F = 3(n - 1) - 2j. \quad (1.4)$$

If $F = 0$, we call the mechanism a *structure* and there is no relative motion between the links. If $F = 1$, the mechanism is said to be *constrained*. As only one coordinate is sufficient in this case, one input gives a unique output. With $F = 2$, obviously it needs two inputs to produce a unique output. Most mechanisms used in machinery are constrained; for this condition, putting $F = 1$ in (1.4), we have

$$2j - 3n + 4 = 0. \quad (1.5)$$

The simple estimate of constrained movement expressed by (1.5) is known as *Grübler's criterion* for plane mechanisms.

To have a closed chain with simple hinges, we must have a minimum of three links with three hinges (Fig. 1.36). Using (1.4), we get

$$F = 3(3 - 1) - 2 \times 3 = 0.$$

It will be observed from Fig. 1.36 that there cannot be any relative movement between the links. A prismatic pair (which is the limit of a hinged joint) also has one degree of freedom; so j in (1.4) and (1.5) may also include prismatic pairs.

If a mechanism includes higher-order hinges, j in (1.4) and (1.5) should be replaced by

$$j = j_1 + 2j_2 + 3j_3 + 4j_4 + \dots + ij_i, \quad (1.6)$$

where j_i is the number of hinges connecting $i + 1$ links. The reason for this is that each hinge in the category j_2 is equivalent to two simple hinges, and so on.

A higher pair has two degrees of freedom. Following the same argument as before, the degrees of freedom of a mechanism having higher pairs can also be written as

$$F = 3(n - 1) - 2j - h; \quad (1.7a)$$

where h is the number of higher pairs. An equation, equivalent to (1.7a), can be derived by replacing a higher pair with an additional link and two hinged joints as explained in Section 1.8.

Quite often, one or more links of a mechanism may have a redundant degree of freedom. If a link can be moved without causing any movement in the rest of the mechanism, then the link is said to have a redundant degree of freedom. For example, consider the mechanisms shown in Figs. 1.37a and 1.37b. Rod 3 in Fig. 1.37a and roller 3 in Fig. 1.37b can, respectively, slide and rotate without causing any movement in the rest of the mechanism, and thus each represents one redundant degree of freedom. If link 3 in Fig. 1.37a is bent as shown in Fig. 1.37c, obviously then the redundant degree of freedom of the link gets eliminated. The effective degrees of freedom of a mechanism can be expressed as

$$F_e = 3(n - 1) - 2j - h - F_r, \quad (1.7b)$$

where F_r is the number of redundant degrees of freedom. It is thus interesting to note that the mechanism in Fig. 1.37a is a locked system since its effective degree of freedom is zero, whereas that in Fig. 1.37c is capable of movement, its effective degree of freedom being one.

A system may possess one or more links which do not introduce any extra constraint. Such links are redundant. For example, consider the mechanism shown in Fig. 1.37d. A little examination of the system reveals that the functions of the links AB and CD are identical, and therefore each of the links leads to the same constraint. Thus, when determining the degrees of freedom of the system, only one of these two constraints should be counted. Similarly, some of the constraints may not be independent and should not be counted. For instance, in Fig. 1.37e, the prismatic pair connecting

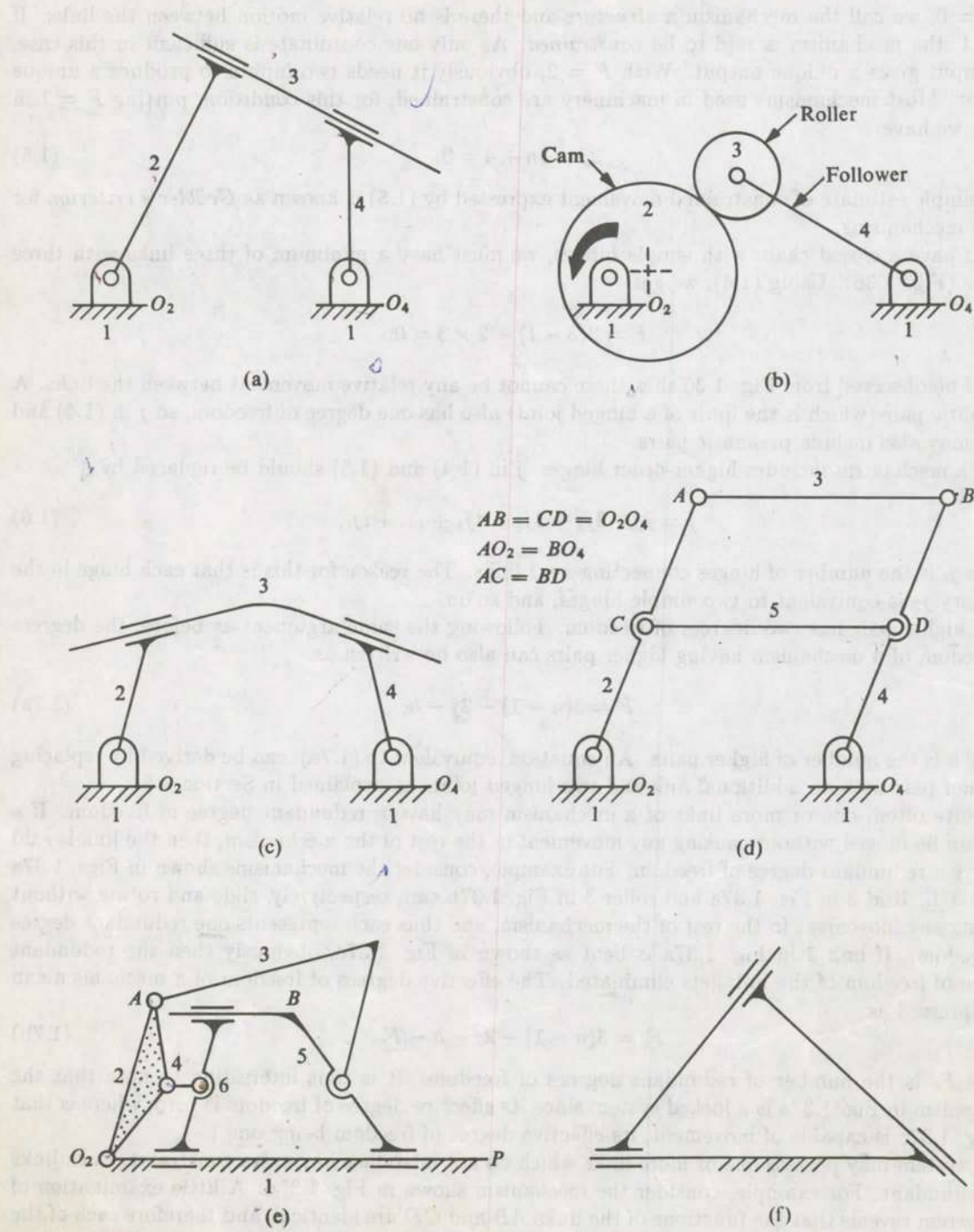


FIGURE 1.37

links 5 and 6 should not be taken into consideration because the relative motion between these two links is determined by the prismatic pairs between 1 and 6 and 1 and 5. In other words, the prismatic pair connecting links 5 and 6 is not imposing any independent constraint. Thus, finally, if a plane mechanism has redundant links and redundant kinematic pairs, (1.7b) gets modified as

$$F_e = 3(n - n_r - 1) - 2(j - j_r) - h - F_r, \quad (1.7c)$$

where n_r is the number of redundant links and j_r is the number of redundant pairs.

Another mechanism where the direct application of Grübler's criterion gives a wrong result is shown in Fig. 1.37f. In this mechanism, the relative (unique) movement between the various links, as can be easily seen, is possible, whereas, according to Grübler's criterion, the mobility is zero. Therefore, care should be exercised when deciding the mobility of a mechanism consisting of a closed loop with only three prismatic pairs.

In what follows, we shall use Grübler's criterion (1.5) to derive some useful results for a mechanism with simple hinges.

Minimum Number of Binary Links in a Constrained Mechanism with Simple Hinges

In a mechanism, there cannot be any singular link. Let

- n_2 = number of binary links,
- n_3 = number of ternary links,
- n_4 = number of quaternary links,
- and so on.

Then, the total number of links is

$$n = n_2 + n_3 + n_4 + \dots + n_i. \quad (1.8)$$

Each simple hinge consists of two elements as shown in Fig. 1.38a (1^+ and 1^- or 2^+ and 2^-). Thus, the total number of elements in the mechanism is

$$e = 2j, \quad (1.9)$$

where j is the number of simple hinges. From Fig. 1.38a, it is seen that a binary link has two elements (1^+ and 2^+). Similarly, a ternary link will have three elements, and so on. Thus,

$$e = 2n_2 + 3n_3 + \dots + in_i$$

or, using (1.9), we get

$$2j = 2n_2 + 3n_3 + \dots + in_i. \quad (1.10)$$

To satisfy Grübler's criterion (1.5), using (1.8) and (1.10), we have

$$2n_2 + 3n_3 + \dots + in_i - 3(n_2 + n_3 + \dots + in_i) + 4 = 0,$$

$$n_2 = 4 + n_4 + 2n_5 + \dots + (i-3)n_i = 4 + \sum_{4}^{i} (i-3)n_i. \quad (1.11)$$

So, the minimum number of binary links is four, i.e., the four-bar linkage is the simplest mechanism.

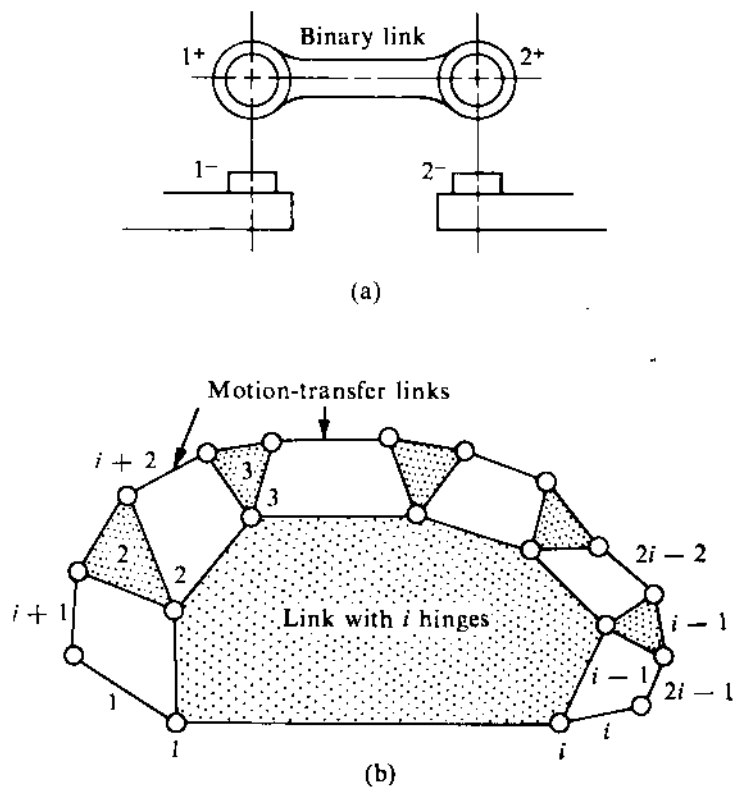


FIGURE 1.38

Maximum Number of Hinges on One Link in a Constrained Mechanism with n Links

Here again, we assume all hinges to be simple. Let us approach the problem in an indirect manner, i.e., to find the minimum number of links n required for closure when one link has i hinges. The mechanism shown in Fig. 1.38b has one such link with i hinges. To each of these i hinges, we connect a link denoted by 1, 2, 3, ..., i . To transfer motion from one of the i links to the next, the number of motion-transfer links to be added will be $(i - 1)$, which are numbered $(i + 1), (i + 2), (i + 3), \dots, (2i - 1)$. Thus, the closure is obtained with a total number of $2i$ links, i.e.,

$$\begin{aligned} n &= i + (i - 1) + 1 \quad (\text{i.e., the link with } i \text{ hinges}) \\ &= 2i. \end{aligned}$$

In other words, the maximum number of hinges which a link can possess is

$$i_{\max} = n/2. \quad (1.12)$$

Now, let us check for constrained motion using (1.5). If the total number of links n is $2i$, the total number of simple hinges will be

$$j = i + 2 + 2(i - 2) = 3i - 2.$$

From (1.5), we have

$$2j - 3n + 4 = 2(3i - 2) - 3(2i) + 4 = 0.$$

Constrained Motion of a Kinematic Chain of n Links with Simple Hinges

From Grübler's criterion for constrained movement, we see that $3n = 2j + 4$. So, the number of links n must be even. We have already seen that the minimum number of binary links is 4, i.e., the four-bar linkage is the simplest mechanism. The next higher-order mechanism starts with $n = 6$. From (1.12), we get $i_{\max} = n/2 = 3$, i.e., the highest order of the links will be ternary. So, from (1.8), we have

$$n_2 + n_3 = 6. \quad (a)$$

From (1.5), we get

$$2j = 3n - 4, \quad j = \frac{(3 \times 6) - 4}{2} = 7.$$

Using (1.10), we get

$$14 = 2n_2 + 3n_3. \quad (b)$$

Solving (a) and (b), $n_2 = 4$ and $n_3 = 2$. Thus, in a six-link mechanism with constrained movement, there will be four binary links and two ternary links, the number of simple hinges being seven. Two possible arrangements are shown in Figs. 1.39a and 1.39b. In Fig. 1.39a, two ternary links are connected directly, whereas in the alternative arrangement, two ternary links are connected by means of binary links. Figure 1.39a is the kinematic representation of Watt's mechanism shown in Fig. 1.40a (in both cases, link 1 refers to the fixed link). Note that one simple hinge has been replaced by a prismatic pair. Figure 1.39b is the kinematic representation of Watt's walking-beam mechanism shown in Fig. 2.58. Again, link 1 refers to the fixed link, and a hinged joint has been

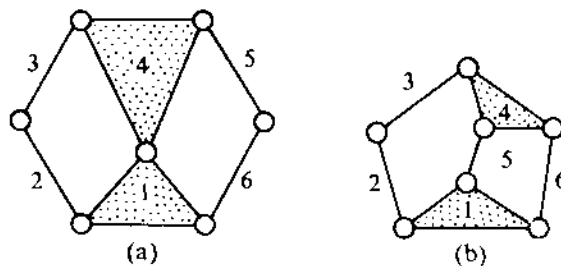


FIGURE 1.39

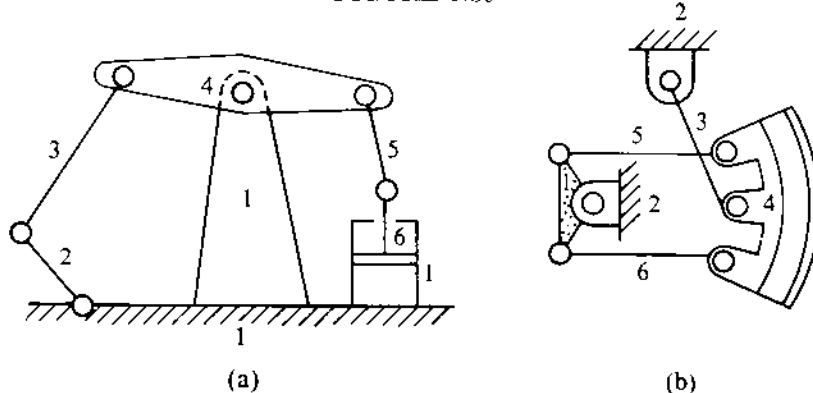


FIGURE 1.40

replaced by a prismatic pair. A kinematic inversion of the arrangement, shown in Fig. 1.39b with link 2 as the fixed link, is the kinematic representation of the Stephenson link used in valve gears (shown in Fig. 1.40b).

Let us now consider the movability of an eight-link chain. From (1.12), we have

$$i_{\max} = n/2 = 8/2 = 4,$$

i.e., the highest-order link will be quaternary. From (1.8), we get

$$8 = n = n_2 + n_3 + n_4. \quad (c)$$

From (1.5), we get

$$2j = 3n - 4 = 20, \quad j = 10 \quad (\text{i.e., the number of simple hinges is } 10).$$

Using (1.10), we get

$$20 = 2n_2 + 3n_3 + 4n_4. \quad (d)$$

It is seen that there cannot be a unique solution to the two equations (c) and (d) as three unknowns are involved. Although at first it appears that there are infinite number of solutions, but this is not so. The reason is that n_2 , n_3 , and n_4 are non-negative integers, and $(n_2)_{\min}$ is 4. So, the only possible solutions, when $n_2 = 4$, are

$$n_3 + n_4 = 4 \quad [\text{from (c)}],$$

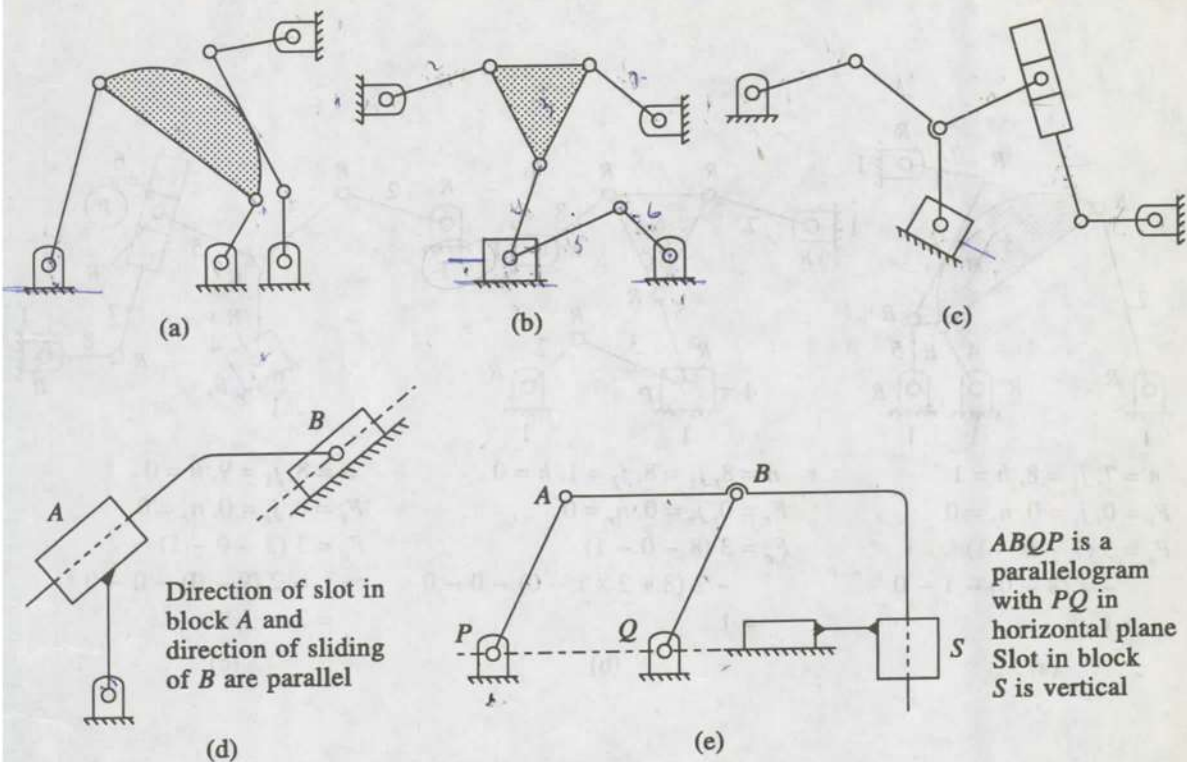


FIGURE 1.41

$$3n_3 + 4n_4 = 12 \quad [\text{from (d)}].$$

From these, we get $n_3 = 4$ and $n_4 = 0$. Similarly, with $n_2 = 5$, we get $n_3 = 2$ and $n_4 = 1$, and with $n_2 = 6$, we have $n_3 = 0$ and $n_4 = 2$. The different arrangements possible with each of these three combinations are left as an exercise for the reader.

PROBLEM 1.4

Determine the effective degrees of freedom for the mechanisms shown in Fig. 1.41.

SOLUTION

First, the links are numbered, and the simple and higher-order lower pairs, the higher pairs, the redundant degrees of freedom, and the redundancies in the constraints are identified. These are shown in Fig. 1.42. Next, the effective degrees of freedom are determined using (1.7c). Simple hinges are denoted by R , second-order hinges by R^2 , prismatic pairs by P , and higher pairs by H .

The results indicate that systems (a), (b), and (e) are constrained mechanisms as the effective degree of freedom in each case is equal to 1. Since in the mechanism shown in Fig. 1.42e $PABQ$ is a parallelogram, link 3 is in pure translation with respect to link 1. Links 1, 5, and 3 are also in pure translation with respect to one another because of prismatic pairs. Thus, links 2 and 4 together provide the same constraint (on link 3) as link 5. Hence, link 5 (along with its 2 P-pairs) can be considered as redundant. Thus, in effect, $n = 4$, $j_1 = 4$ when $F_e = 1$. Alternatively, due to the

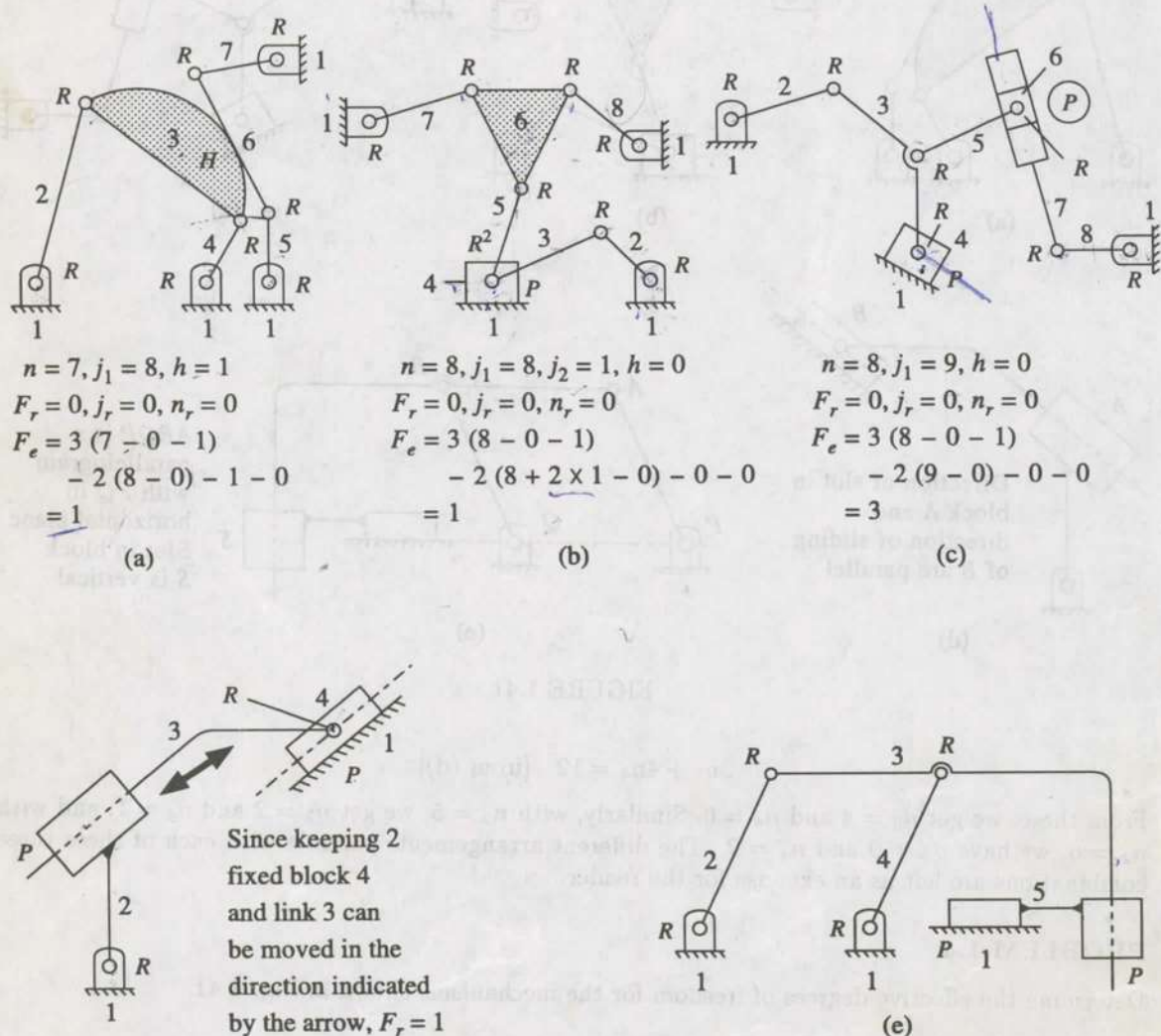


FIGURE 1.42

parallelogram $PABQ$, AB remains horizontal. Therefore, the axis of the P-pair between links 3 and 5 always remains vertical. Consequently, link 5 remains horizontal and the P-pair between links 1 and 5 can be replaced by a higher pair. Thus, we have $n = 5$, $j_1 = 5$, and $h = 1$, yielding $F = 1$. This is an example where no kinematic pair is totally redundant (i.e., $j_r = 0$), but a lower pair can be equivalently replaced by a higher pair. In cases (c) and (d), that is equal to 3 and 0, respectively. In the mechanism shown in Fig. 1.42d, keeping 2 fixed, block 4 and link 3 can be moved in the direction indicated by the arrow. Hence, $F_r = 1$. The reader should note that care should be taken in identifying the links and the higher-order hinges. Cases (b) and (c) are good examples in this direction. In case (e), a peculiar situation arises which has already been explained in details.

Ranges of Motion of a Four-bar Linkage (Grashof's Criterion)

The discussion so far helps only to identify the effective degrees of freedom of a mechanism but tells nothing about the possible ranges of movements of the links. However, to a designer, this information is extremely important. The problem is not easy and a comprehensive formulation is possible only in the case of four-link mechanisms.

The approach here is to arrive at the movability of a four-bar linkage from the relative dimensions of the links and from the considerations that govern the choice of the link which represents the frame (or is taken to be fixed). In a four-bar linkage, the link not connected to the frame is called the coupler, whereas the two links hinged to the frame are called the crank and follower. (Normally, the driving member is referred to as the crank and the other as the follower.) The three different kinds of mechanisms that can be obtained from a four-bar linkage are

- (i) the *double-crank or drag-link mechanism*, in which both the crank and the follower make a complete rotation,
- (ii) the *crank-rocker mechanism*, in which the complete rotation of one link (crank) causes an oscillation of the other (rocker), and
- (iii) the *double-rocker mechanism*, in which both the driver and driven links only oscillate (as none of these two links can make a complete rotation).

Let

l = length of the longest link,
 s = length of the shortest link,
 p, q = length of the other two links.

We shall consider the following three distinct situations:

(i) $(l + s) < (p + q)$ In this situation, the linkage is known as *Grashof's linkage*. Its inversion leads to the three aforementioned mechanisms, namely,

- (a) a double-crank mechanism when s is the frame,
- (b) two different crank-rocker mechanisms when s is the crank and any one of the adjacent links is the frame, and
- (c) one double-rocker mechanism when s is the coupler (opposite to the frame).

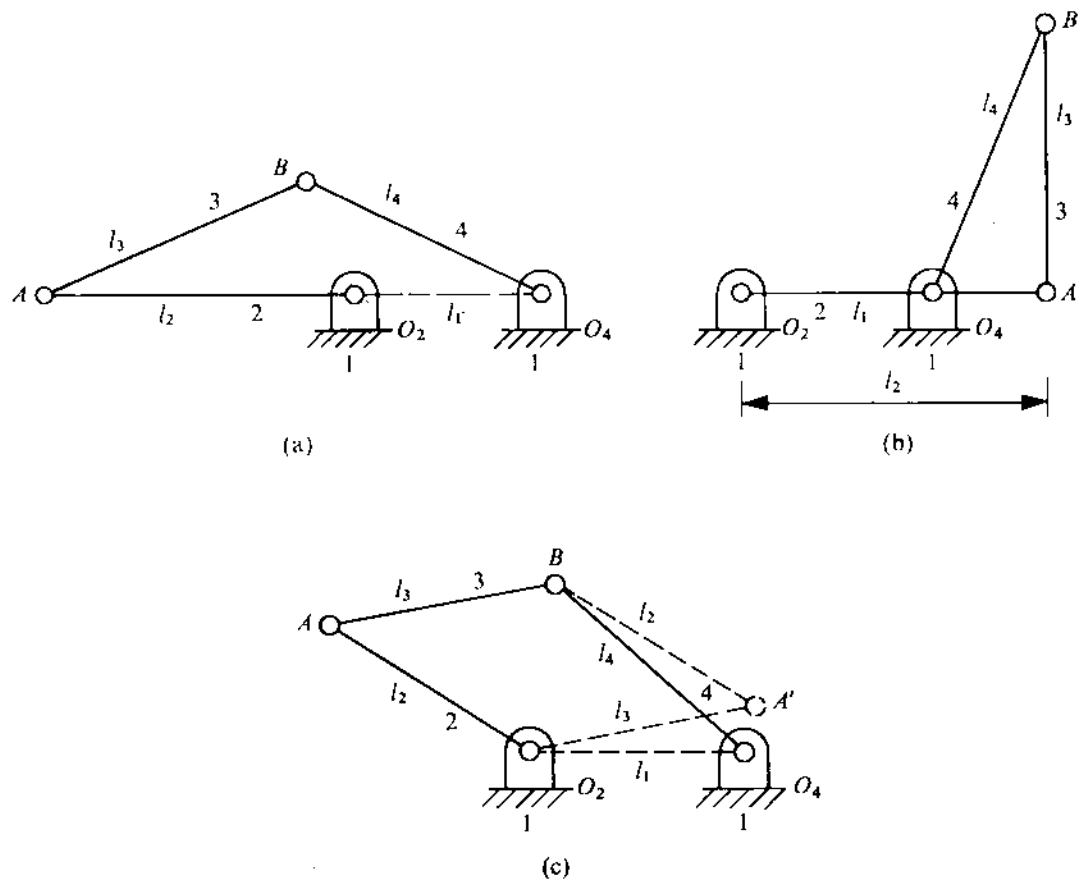


FIGURE 1.43

We shall now prove these statements.

Consider a four-bar mechanism with sides l_1 , l_2 , l_3 , and l_4 , the link l_1 being fixed. If link 2 (assuming $l_2 > l_1$) has to make a complete rotation, obviously then it must be able to attain the two extreme positions shown in Figs. 1.43a and 1.43b. This implies that the presence of links 3 and 4 should not prevent the maximum and minimum separations attained between the points O_4 and A . Thus, for ΔO_4AB to exist in both the extreme situations, the conditions the link lengths should satisfy are

$$l_1 + l_2 < l_3 + l_4, \quad l_4 < l_3 + (l_2 - l_1), \quad l_3 < l_4 + (l_2 - l_1).$$

These inequalities can be rewritten as

$$l_1 + l_2 < l_3 + l_4, \quad (1.13a)$$

$$l_1 + l_4 < l_3 + l_2, \quad (1.13b)$$

$$l_1 + l_3 < l_4 + l_2. \quad (1.13c)$$

So, when these conditions are met, link 2 will be capable of making a complete rotation about its hinge point O_2 . If link 4 has to make a complete rotation about O_4 , the necessary conditions are obtained by interchanging l_2 and l_4 in (1.13). In this process, it is easy to see, equations (1.13) remain unchanged. To prove that (1.13) also constitute the conditions for a complete rotation of link 3, we proceed as follows. Construct a four-bar mechanism $O_2A'B'O_4$ by interchanging l_2 and l_3 as shown in Fig. 1.43c. Then, we find the conditions for a complete rotation of the link O_2A' are again the same as (1.13). Overlapping the given mechanism with the same fixed hinges O_2 and O_4 (Fig. 1.43c), we get a six-bar linkage, where AB and O_2A' are always parallel (since $O_2A'BA$ is a parallelogram). Therefore, a complete rotation of O_2A' implies a complete rotation of AB .

Hence, (1.13) give the conditions for the complete rotational capability of all the three links, namely, 2, 3, and 4. Adding any two inequalities in (1.13) at a time, it can be easily shown that

$$l_1 < l_2, \quad l_1 < l_3, \quad l_1 < l_4.$$

Thus, l_1 is the shortest link, i.e., s . Further, it can be verified that the sum of l_1 (or s) and the largest link length l (any one of l_2 , l_3 , and l_4) is smaller than the sum of the remaining two link lengths. If link 3 has to make a complete rotation with respect to either link 2 or link 4, the angle $\angle O_2AB$ or $\angle ABO_4$ has to exceed 180° . But such a situation under conditions (1.13) is not permitted in Grashof's linkage. This is so because the triangles $O_2(A)BO_4$ and $O_2A(B)O_4$ cannot exist since one of the sides in each of these triangles is the shortest link. For the inversion we are considering with l_1 fixed, we get a double-crank mechanism as both l_2 and l_4 make a complete rotation. If one of the two links l_2 and l_4 is fixed, link 1 will make a complete rotation (as an inversion does not change the relative movements among the links), whereas link 3 will oscillate, thus constituting a crank-rocker mechanism. When l_3 is fixed, l_1 will make a complete rotation, whereas both l_2 and l_4 will oscillate, thus resulting in a double-rocker mechanism.

(ii) $(l + s) > (p + q)$ In this situation, all four inversions result in a double-rocker mechanism.

(iii) $(l + s) = (p + q)$ Here, in general, the four inversions result in mechanisms similar to those obtained when $(l + s) < (p + q)$, the only difference being that there will be instances here when the links become collinear. This situation is commonly referred to as the uncertainty configuration. To overcome this, the links must be guided in the proper direction (done automatically by the inertia of the links).

The situation $(l + s) = (p + q)$ is also true when a linkage has two pairs of equal link lengths. This results in two special mechanisms, namely:

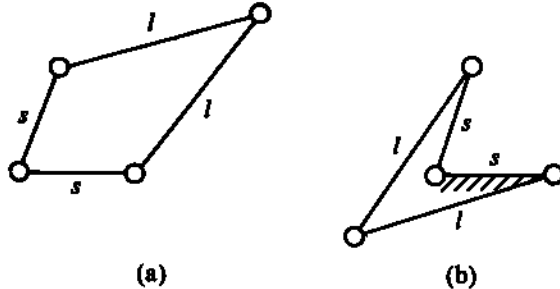


FIGURE 1.44

- (a) The *parallelogram linkage* [in which the equal links are not adjacent]. All four inversions of this linkage yield double-crank mechanisms if the linkage is properly controlled at the uncertainty configurations.
- (b) The *deltoid linkage* [in which the equal links are adjacent (Fig. 1.44a)]. Here, when any of the longer links l is fixed, two crank-rocker mechanisms are obtained. On the other hand, when any of the shorter links s is fixed, two double-crank mechanisms result. In this situation, one revolution of the longer link causes two revolutions of the other shorter link, and for the mechanism in Fig. 1.44a, one rotation of the shorter link s (the other link s acting as the frame) will yield the configuration shown in Fig. 1.44b. This is known as the *Galloway mechanism*.

The movability characteristics, i.e., the ranges of motion, of a general-four-link mechanism with revolute and prismatic pairs are summarized in Fig. 1.45. The reader is advised to derive the results by considering the prismatic pairs as the limiting case of a revolute pair as shown in Fig. 1.13.

PROBLEM 1.5

Prove that the rocker of a Grashof linkage can never cross the line of frame.

SOLUTION

If the rocker has to cross the line of frame, it is essential for the mechanism to attain at least one of the configurations indicated in Fig. 1.46. l_1 is the length of the frame and l_4 is that of the rocker.

The following conditions have to be satisfied if the configurations are to be attained: (a) $l_3 < l_2 + (l_1 - l_4)$, (b) $l_3 < l_2 + (l_4 - l_1)$, (c) $l_1 + l_4 < l_2 + l_3$. But since l_2 is the crank, it has to be the shortest link. So the sum of l_2 and the length of any other link has to be less than the sum of the two other links. But all the above conditions can be written as

$$l_2 + l_i > l' + l'', \quad i = 1, 3, 4.$$

This violates the Grashof condition.

PROBLEM 1.6

The offset slider crank mechanism shown in Fig. 1.45 is required to have a stroke length of 200 mm with the connecting rod 150 mm long. Determine the maximum possible length of the crank.

AT LEAST ONE LINK ROTARY				ALL LINKS OSCILLATORY			
$l_{\max} + l_{\min} < l' + l''$		$l_{\max} + l_{\min} > l' + l''$		$l_{\min} + e < l'$		$l_{\min} + e > l'$	
Double crank	Crank rocker	Double rocker	Double rocker both inward	Double rocker both outward	Double rocker inward-outward	Double rocker both outward	Double rocker both outward
$l_{\min} = l_1$	$l_{\min} = l_2$	$l_{\min} = l_3$	$l_{\max} = l_1$	$l_{\max} = l_2$	$l_{\max} = l_3$	$l_{\max} = l_1$	$l_{\max} = l_3$
Inverted slider crank	Inverted slider rocker	Slider crank	Slider rocker	Inverted slider rocker	Slider rocker	Inverted slider rocker	Slider rocker
$l_{\min} = l_1$	$l_{\min} = l_2$	$l_{\min} = l_2$	$l_{\min} = l_3$	$l_{\min} = l_3$	$l_{\min} = l_3$	$l_{\min} = l_3$	$l_{\min} = l_3$
Inverted double slider	Scotch yoke	Double slider	R-P-R-P	Double slider	R-P-R-P	Double slider	R-P-R-P
$l_{\min} = l_1$	$l_{\min} = l_2$	$l_{\min} = l_2$	$l_{\min} = l_3$	$l_{\min} = l_3$	$l_{\min} = l_3$	$l_{\min} = l_3$	$l_{\min} = l_3$

FIGURE 1.45 (e, e_1 , e_2 offset; l_{\max} , longest link length; l' , l'' , other link lengths)

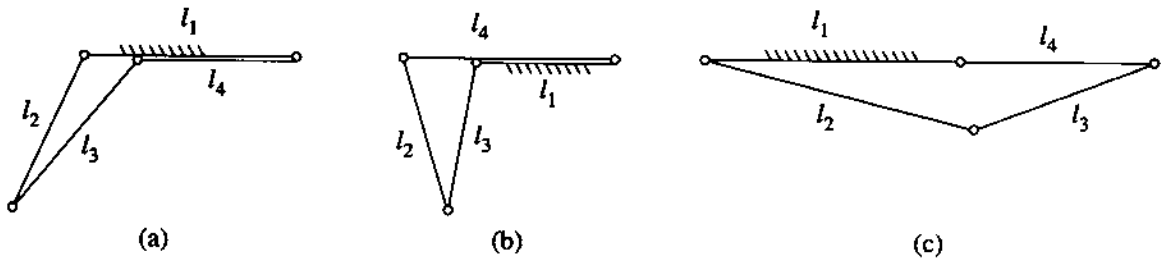


FIGURE 1.46

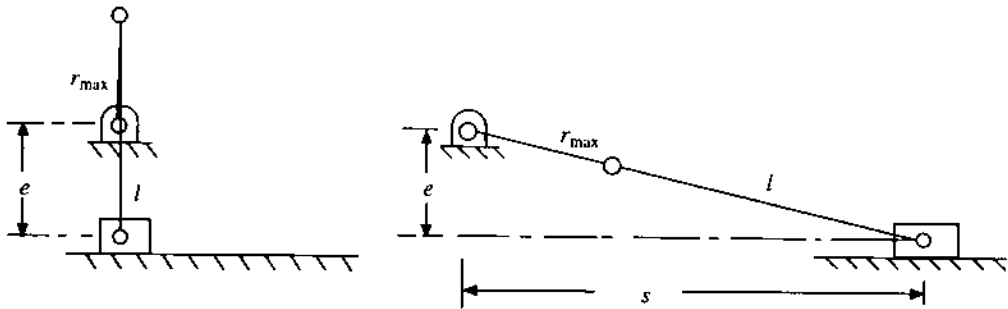


FIGURE 1.47

SOLUTION

A slider crank has to be a Grashofian chain and the condition to be satisfied is (see Fig. 1.45)

$$l_{\min} + e < l',$$

where e is the amount of offset. Furthermore, l_{\min} should represent the length of the crank in case of slider-crank mechanisms. So, in the extreme situation,

$$r_{\max} + e = l, \quad (a)$$

where r_{\max} is the maximum crank radius and l is the connecting-rod length. From the two extreme positions shown in Fig. 1.47, we find

$$(l + r)^2 - e^2 = s^2, \quad (b)$$

where s is the stroke length.

Using (a) in (b) and after algebraic manipulation, we get

$$4lr_{\max} = s^2$$

or

$$r_{\max} = s^2 / (4l).$$

Substituting the values of s and l , we obtain

$$r_{\max} = 66.7 \text{ mm.}$$

The mobility and ranges of motion are two very important aspects that must be considered while designing mechanisms in a systematic manner as will be evident when the synthesis of mechanisms is discussed in Chapter 3.

1.11 PROBLEMS

- 1.7 Figure 1.48 shows (i) a device to draw the indicator diagrams of an engine (Fig. 1.48a), (ii) a linkage used in an electric typewriter (Fig. 1.48b), (iii) a pair of vice grip pliers (Fig. 1.48c), and (iv) a pair of parallel-jaw pliers (Fig. 1.48d). Following the conventions described in Fig. 1.11, draw the kinematic diagram corresponding to each of the four mechanisms. (In the first case, draw the diagram only for the mechanism required to move the pen tip.)
- 1.8 For each mechanism shown in Fig. 1.49, draw the equivalent mechanism with lower pairs. Then, identify the mechanisms where the equivalence holds good for all instants of time. (It should be noted that it is possible to physically realize such a permanent equivalence.)
- 1.9 Two plates cut to have involute profiles are hinged to the frame at O_1 and O_2 and are in contact with each other as shown in Fig. 1.50. The point of contact P always lies on the common tangent to the circles k_1 and k_2 which are the generating circles for the involutes. Show that the dimensions and the configuration of the equivalent mechanism are the same for all positions of the plates (so long as they are in contact with each other).
- 1.10 Figure 1.51 schematically shows a Rapson's slide used in marine steering gear. Show that this mechanism and the Davis automobile steering gear schematically shown in Fig. 1.35 are inversions of the same kinematic chain.
- 1.11 Determine the degrees of freedom of the Peaucellier mechanism (Fig. 3.28), and of the planar mechanisms shown in Fig. 1.52.
- 1.12 Prove that both the systems shown in Fig. 1.53 are constrained mechanisms.
- 1.13 An assortment of five links of lengths 5 cm, 8 cm, 15 cm, 19 cm, and 28 cm is available for constructing a crank-rocker mechanism. Sketch the crank-rocker mechanism, indicating the crank and showing all the link lengths.
- 1.14 Find out the cases shown in Fig. 1.54 where the input link can make a complete rotation. The numbers indicate link lengths.
- 1.15 Figure 2.48 shows a crossed-slider trammel where $OB = AB = BC$. Determine the degree of freedom of this mechanism. *Hint:* Consider the elliptic trammel shown in Fig. 1.25. Join the centre of the cross (O) with the point B by a rigid link OB with R-pairs at O and B . Now make a kinematic inversion with OB as the fixed link.

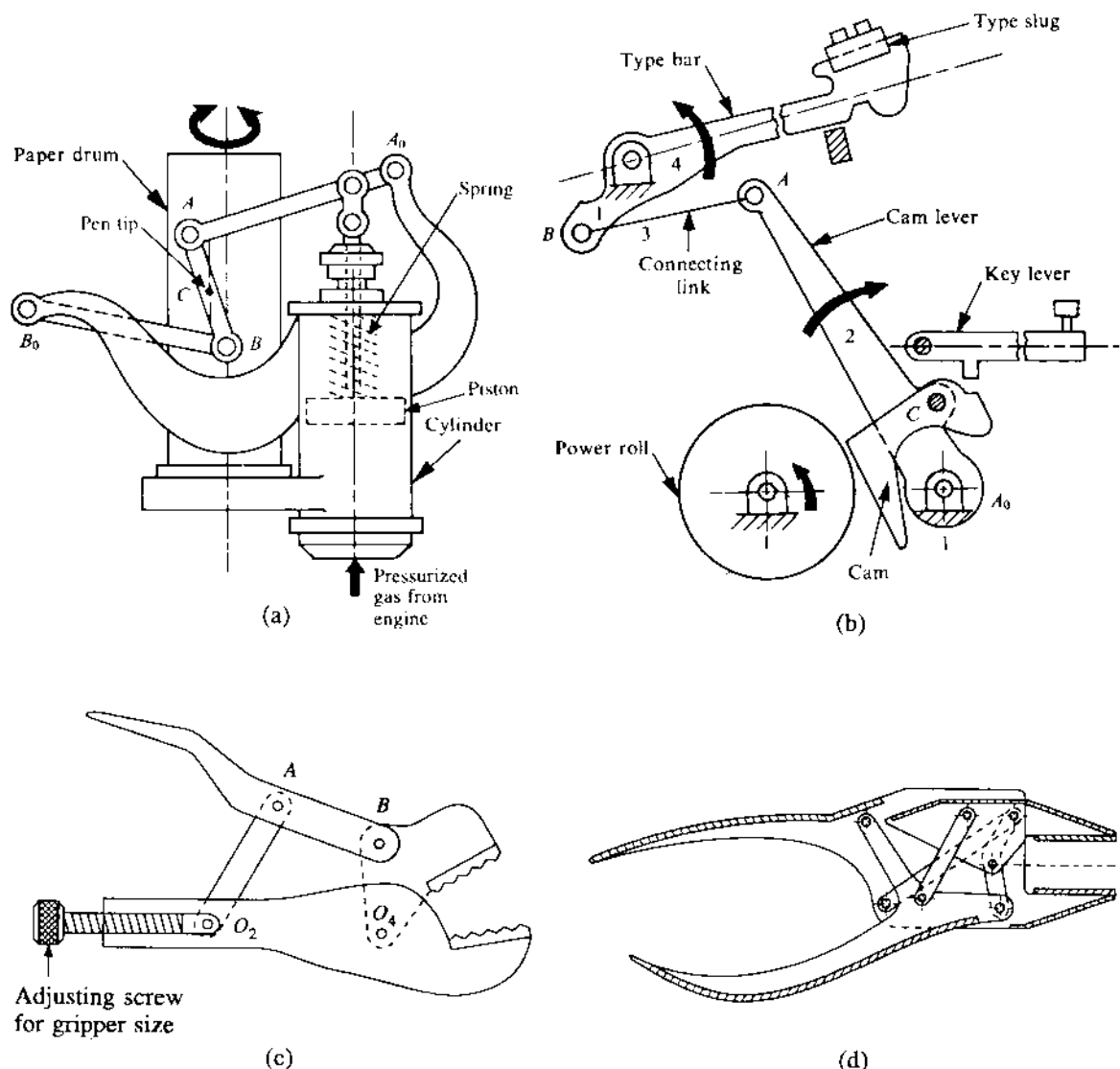


FIGURE 1.48

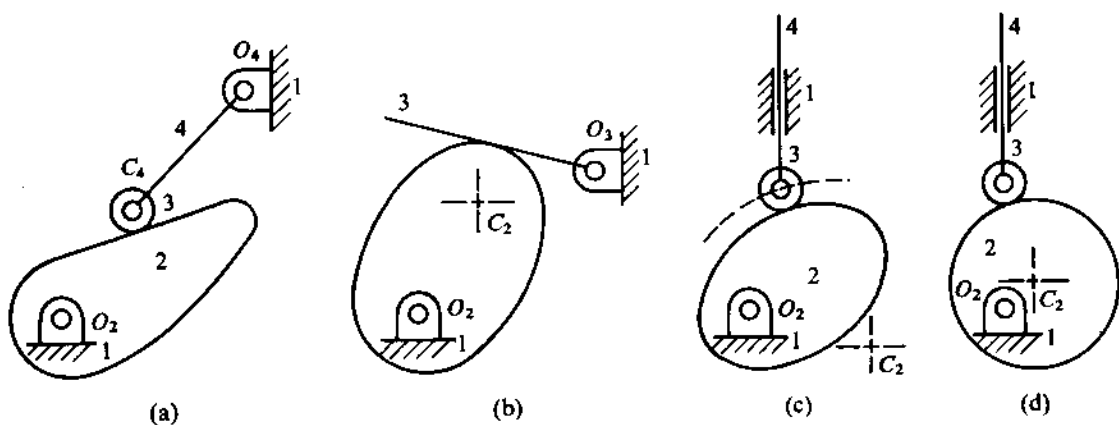


FIGURE 1.49

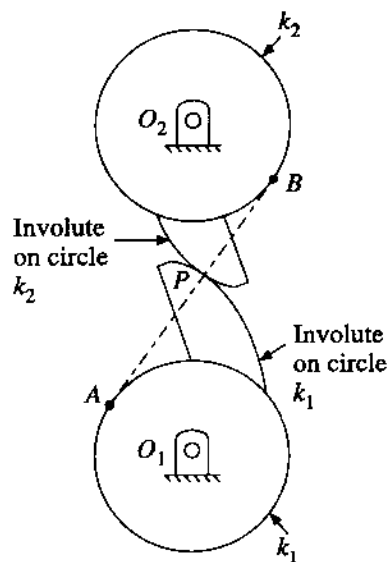


FIGURE 1.50

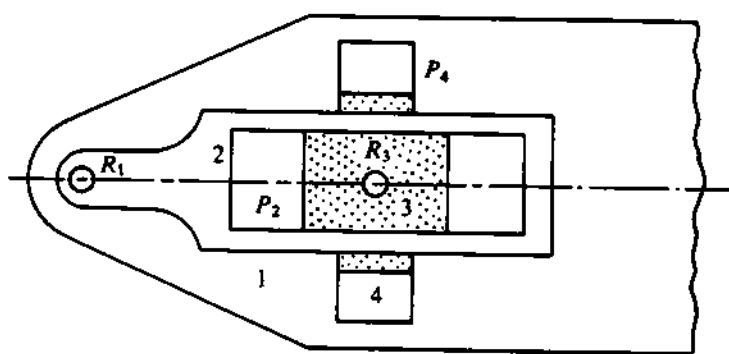


FIGURE 1.51

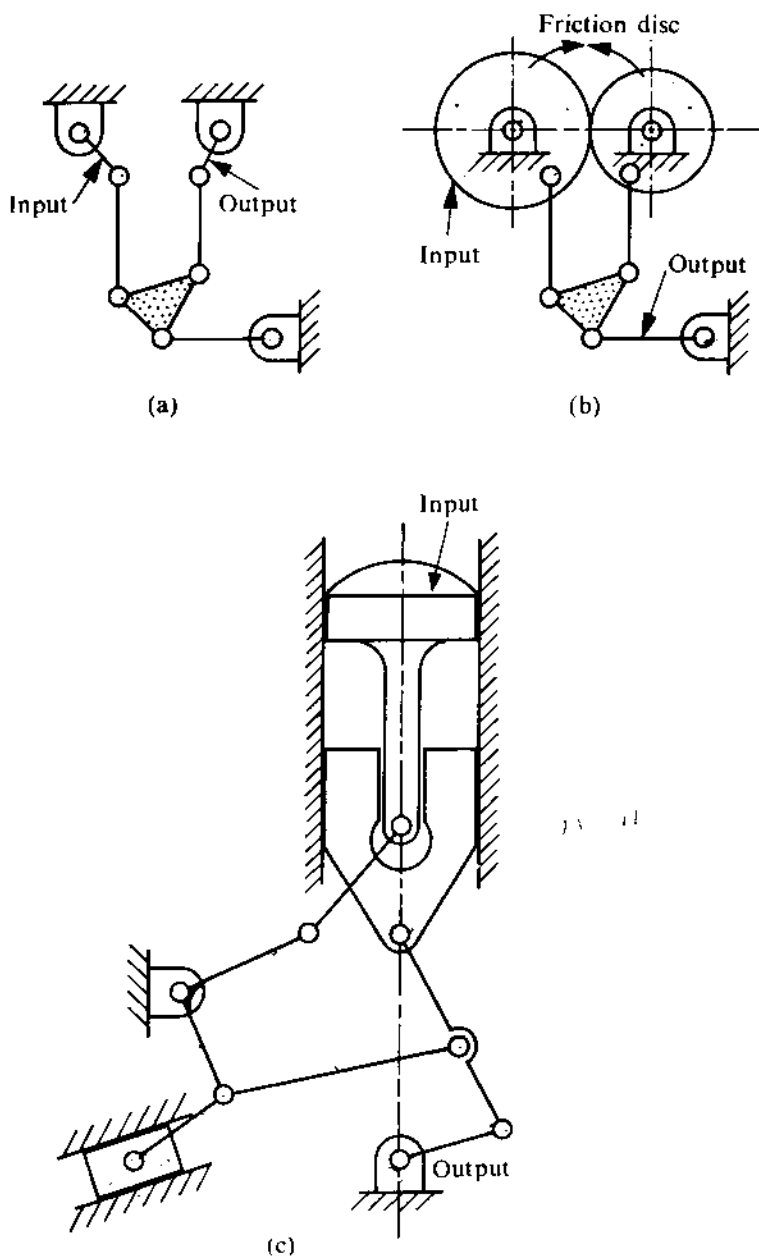


FIGURE 1.52

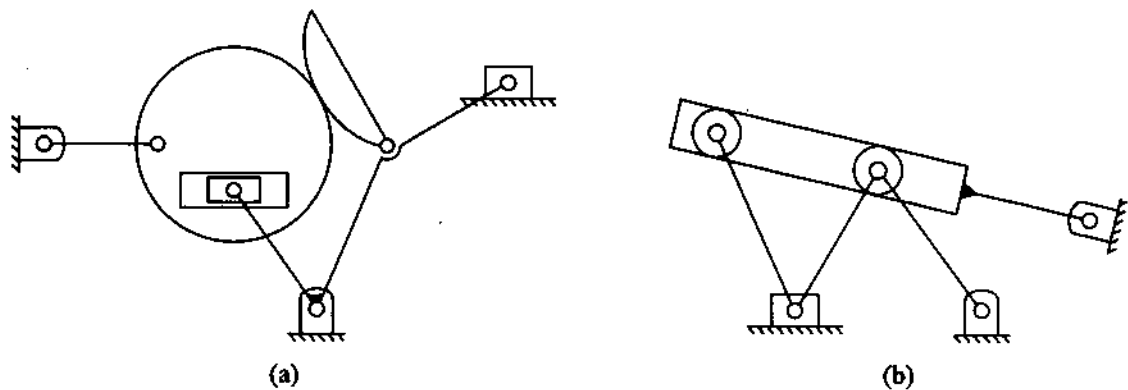


FIGURE 1.53

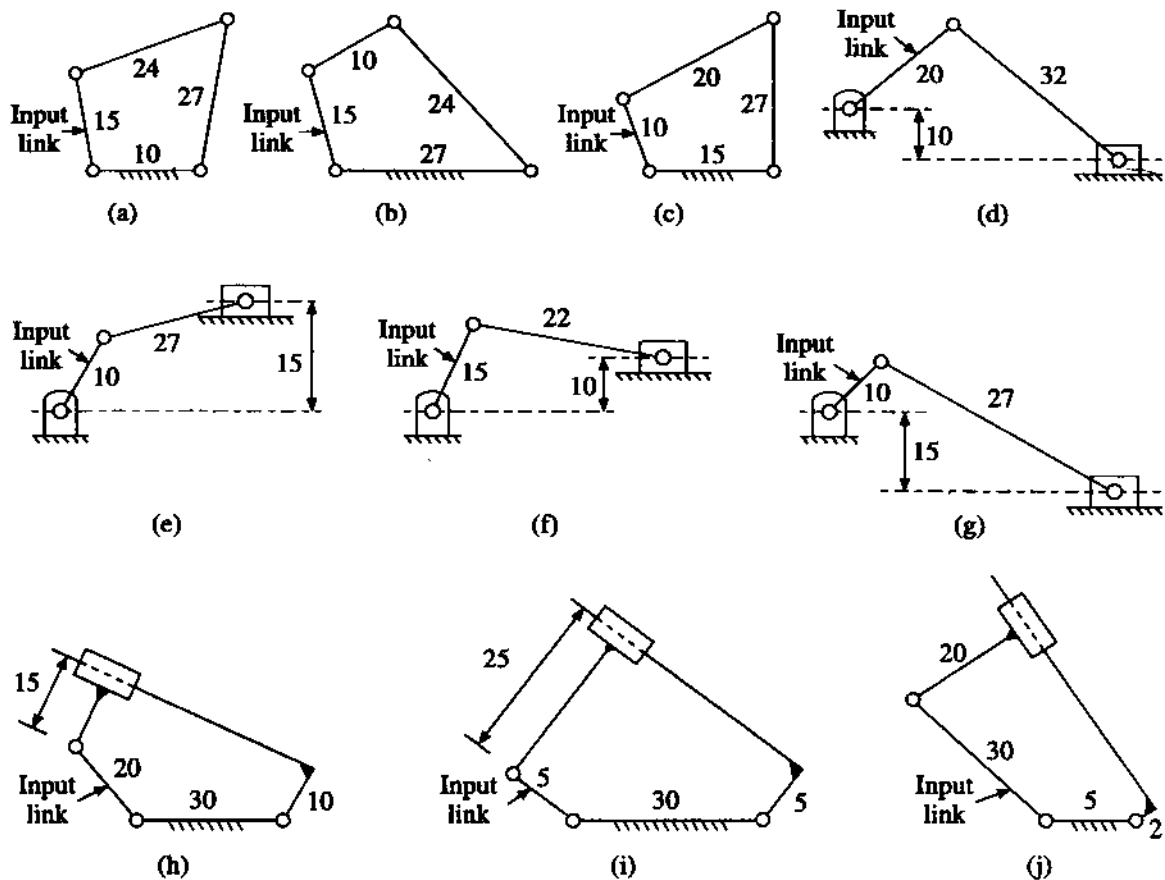


FIGURE 1.54

Chapter 2

KINEMATIC ANALYSIS OF PLANE MECHANISMS

2.1 INTRODUCTION

The objective of kinematic analysis is to determine the kinematic quantities such as displacements, velocities, and accelerations of the elements in a mechanism when the input motion is given. Conversely, the objective may be to determine the input motion required to produce a specified motion of another element. In short, kinematic analysis establishes the relationship between the motion of the various components or links of a mechanism. In this chapter, we shall consider only the mechanisms with lower pairs. The kinematic analysis of a higher-pair mechanism can also be carried out. This may be done by converting the mechanism into an equivalent mechanism consisting of only the lower pairs. Both the graphical and analytical methods can be used for kinematic analysis. With the advent of digital computers, lately analytical methods are being widely used, especially with the help of computer-aided graphics. However, the graphical methods, providing better insight and visualization, still occupy a prominent place in planar kinematics. Unlike in an analytical method, the accuracy of the solution provided by a graphical method is often limited.

2.2 DISPLACEMENT ANALYSIS

When the kinematic dimensions and the configuration(s) of the input link(s) of a mechanism are prescribed, the configurations (linear and angular) of all the other links are determined by displacement analysis.

Graphical Method

In a graphical method of displacement analysis, the mechanism is drawn to a convenient scale and the desired unknown quantities are determined through suitable geometrical constructions and calculations. No generalized approach can be discussed so far as the graphical methods are concerned; the solution technique will vary from problem to problem. We shall demonstrate the basic features of the methods through a few examples. Some of these features which play a major role in displacement analysis are as follows:

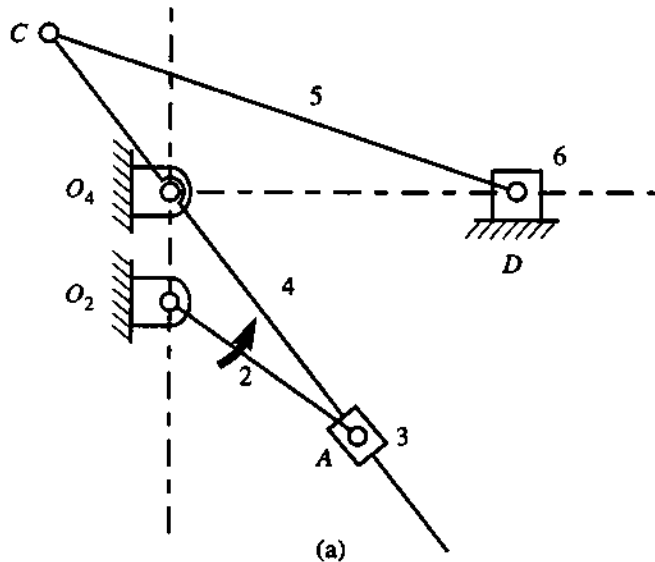


FIGURE 2.1 (cont.)

- (i) The configuration of a rigid body in plane motion is completely defined by the locations of any two points on it.
- (ii) Two intersecting circles have two points of intersection and one has to be careful, when necessary, to choose the correct point for the purpose in hand.
- (iii) The use of a tracing paper, as an overlay, is very convenient and very often provides an unambiguous and quick solution.
- (iv) The graphical method of displacement analysis fails if no closed loop with four links exists in the mechanism.

PROBLEM 2.1

Figure 2.1a shows a six-link, Whitworth quick-return mechanism used in slotting machines. Link 2 ($= O_2 A$) rotates with a constant angular speed in the counter-clockwise (CCW) direction. The sliding link 6 represents the cutting tool whose cutting motion is to the left and the return (idle) motion is to the right. Determine the quick-return ratio which is defined as the ratio of the time intervals taken by the tool to complete its cutting and idle motions, respectively.

SOLUTION

Referring to Fig. 2.1b, the circles k_A and k_C are the paths of the points A and C, respectively. The centres of these circles are at O_2 and O_4 and their radii are $O_2 A$ and $O_4 C$, respectively. The tool occupies its extreme right and extreme left positions (D_R and D_L) when links 4 and 5 become collinear as indicated in the figure, i.e., $O_4 C_R D_R$ and $O_4 C_L D_L$. The distance $D_R D_L$ is the stroke of the tool ($= 2.O_4 C$). Since the points A, O_4 , and C always remain collinear (on link 4), the locations of A (on k_A) corresponding to the extreme positions are now easily obtained as A_R and A_L , respectively. Thus, the rotations of link 2 corresponding to the forward and return motions of

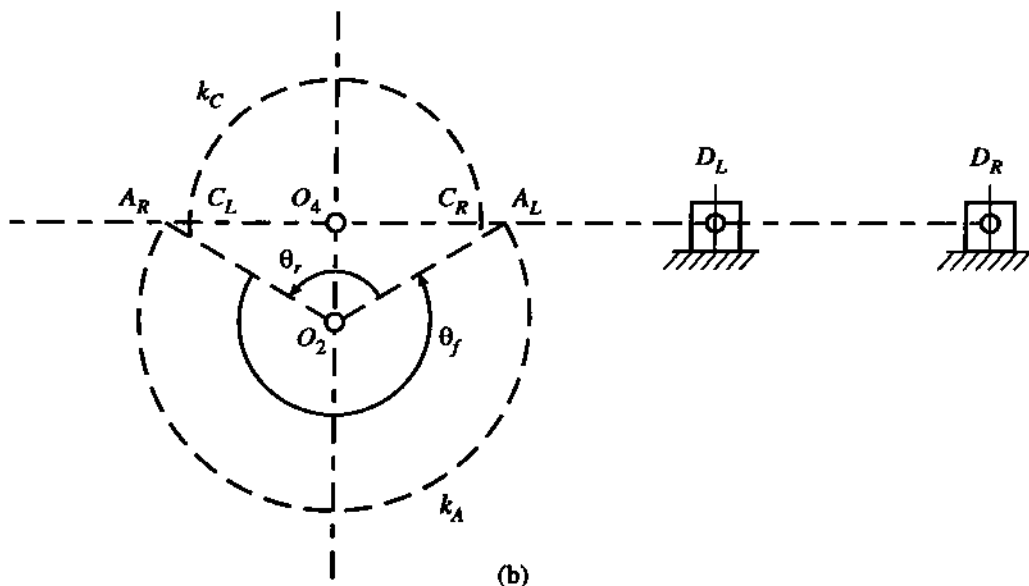


FIGURE 2.1

the tool are obtained as θ_f and θ_r , respectively. From measurement, $\theta_f = 239^\circ$. Since link 2 rotates at a constant angular speed, the quick-return ratio (qrr) is obtained as

$$qrr = \frac{\theta_f}{\theta_r} = \frac{\theta_f}{360 - \theta_f} = \frac{239}{121} = 1.975.$$

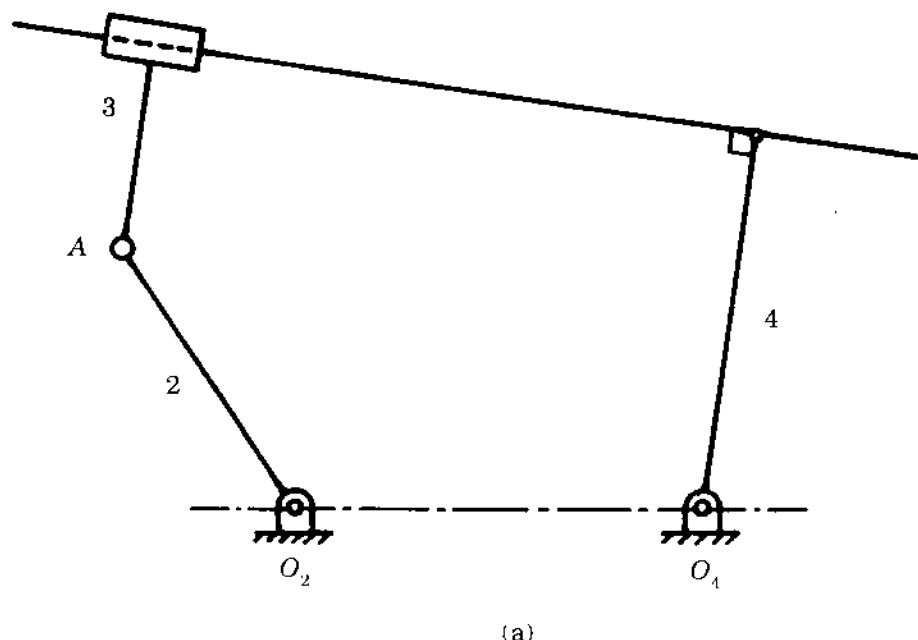
PROBLEM 2.2

Figure 2.2a shows a 3R-1P mechanism. Verify, using Grashof's criterion, that no link can make a complete rotation. Also, obtain the extreme positions of links 2 and 4.

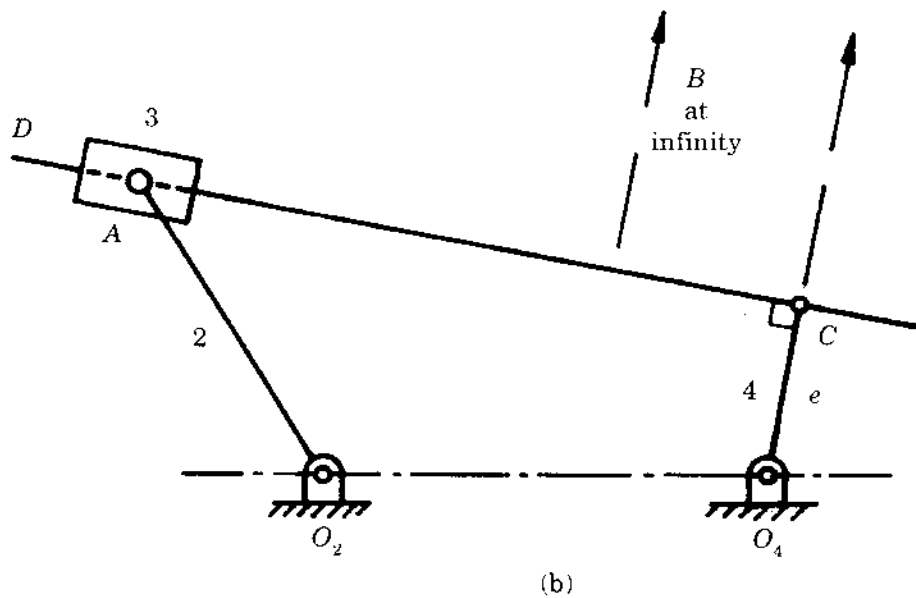
SOLUTION

Since, for a prismatic pair, only the direction (and not its location) is of significance, we can draw the kinematic diagram of the given mechanism, as shown in Fig. 2.2b, with three kinematic dimensions, viz., O_2A , O_2O_4 , and O_4C . The minimum link length is ($l_2 = O_2A$), the other link length is ($l_1 = O_2O_4$) and the offset is ($e = O_4C$). Since, by measurement, we can see $l_2 + e > l_1$, using Grashof's criterion, it can be concluded that no link can make a complete rotation.

To determine the extreme positions of links 2 and 4, it may be convenient to consider the equivalent 4R mechanism where the prismatic pair (between 3 and 4) is replaced by an R-pair which is at infinity (B) in the direction perpendicular to the axis of the prismatic pair, i.e., along O_4C (see Section 1.6). This has also been indicated in Fig. 2.2b. So, we finally have a 4R linkage with $l_1 = O_2O_4$, $l_2 = O_2A$ and both l_3 and l_4 are infinity with $|l_3 - l_4| = e$. It is easy to visualize that in the 4R linkage O_2ABO_4 , link 4 (i.e., O_4B) reaches its extreme position when links 2 and 3 (i.e., O_2A and AB) become collinear. And similarly, link 2 (i.e., O_2A) reaches its extreme positions when links 3 and 4 (i.e., O_4B and AB) become collinear. Since the point B (at infinity) is always along O_4C ,



(a)



(b)

FIGURE 2.2 (cont.)

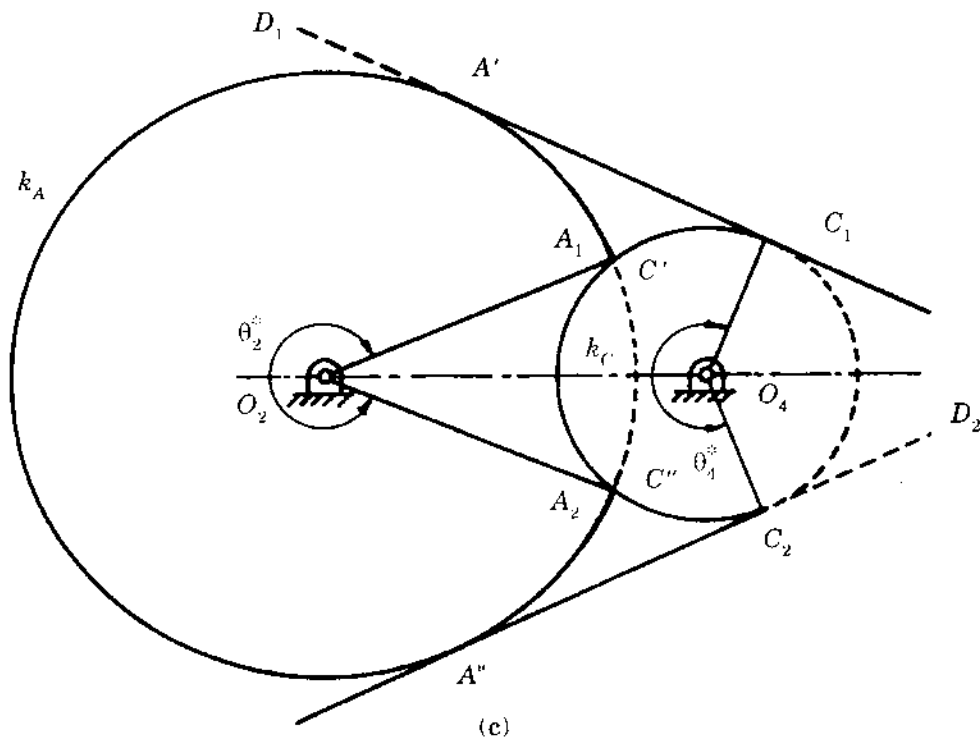


FIGURE 2.2

the lines O_2A and AB become collinear when O_2A and O_4C become parallel. The points A and C move on circles (k_A and k_C) with centres at O_2 and O_4 and with radii O_2A and O_4C , respectively. Therefore, O_2A and O_4C will become parallel when the line CAD becomes the common tangent to k_A and k_C (Fig. 2.2c). Consequently, the extreme positions of link 4 are determined as O_4C_1 and O_4C_2 , with a swing angle θ_4^* . Similarly, at the extreme positions of link 2, O_4CB and AB become collinear and obviously these occur when the point A lies at the intersection of k_A and k_C . Thus, the extreme positions of links 2 and 4 are determined as O_2A_1 and O_2A_2 (Fig. 2.2c), with a swing angle θ_2^* . The students are advised to verify for themselves the extreme positions of the input and output links of various mechanisms indicated in Fig. 1.45.

PROBLEM 2.3

Figure 2.3a shows an earth-moving machine with two degrees of freedom. There are nine links and two hydraulic actuators Z_1 and Z_2 . The scale of the diagram is also indicated.

- Determine the rotation of the bin (link 9) and the movements of the actuators Z_1 and Z_2 when the point D moves to D' .
- Assume O_2A is held constant in the configuration shown. If now Z_2 is retracted so that O_7F is reduced to $3/4$ th of its value indicated in Fig. 2.3a, what is the rotation of the bin?

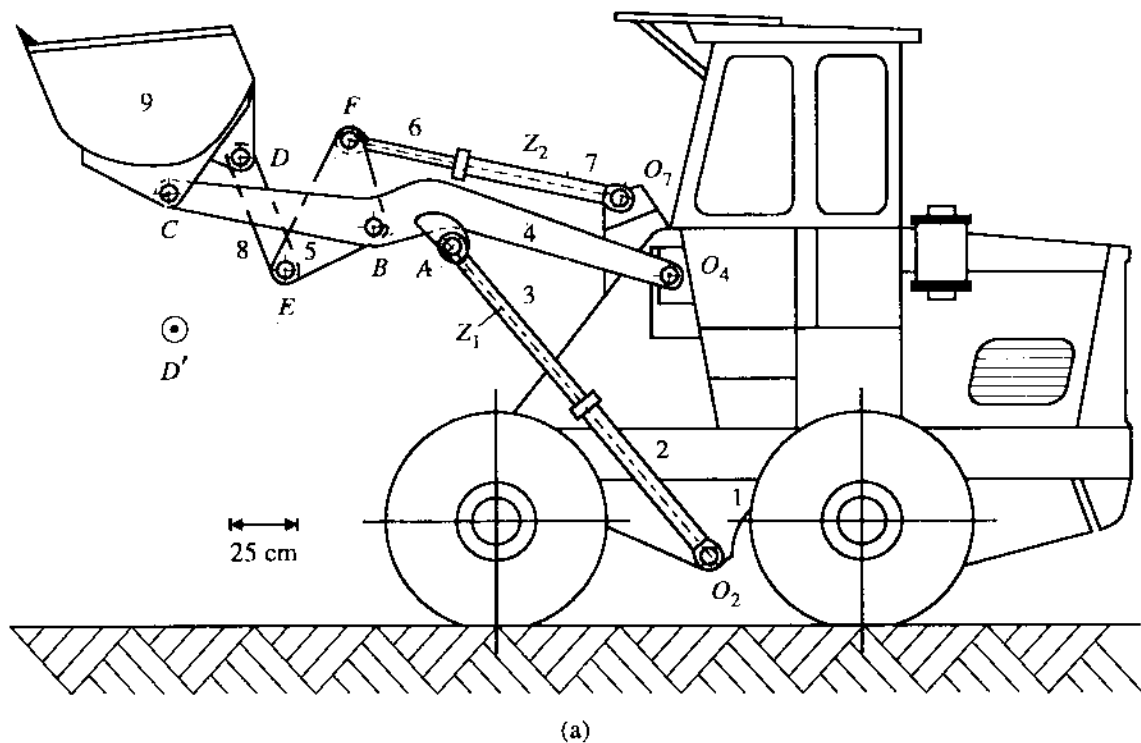


FIGURE 2.3 (cont.)

SOLUTION

- (a) First, the locations of all the R-pairs shown in Fig. 2.3a are reproduced in Fig. 2.3b. The point C moves on the circle k_C with centre at O_4 and radius O_4C . Again, the length DC remains constant. So, the new location C' is determined on k_C with $D'C' = DC$. Note that the correct solution out of the possible two solutions has to be chosen. With two points, viz., O_4 and C' , on link 4 now known, the locations of two other points A and B on link 4 are easily determined as A' and B' , respectively. One may use a tracing paper for this purpose. Mark O_4 , A , B , and C on the tracing paper. Now move the tracing paper on Fig. 2.3b so that O_4 and C coincide with O_4 and C' , respectively. The locations of A and B on the tracing paper are marked as A' and B' , respectively, in Fig. 2.3b. Then the point E' is located using the fact $DE = D'E'$ and $BE = B'E'$. With B' and E' located, the point F' on link 5 is easily determined, since $\Delta BEF \cong \Delta B'E'F'$. The entire linkage in the primed configuration is indicated in Fig. 2.3b. Using the scale of the diagram, we get retraction in the actuator $Z_1 = O_2A - O_2A' = 28.75$ cm and expansion in the actuator $Z_2 = O_7F' - O_7F = 7.5$ cm. The rotation of link 9, $\theta = 53^\circ$ (CCW) (from measurement in Fig. 2.3b).
- (b) With O_2A held constant, one should first realize that, since O_4A is also constant, links 2, 3, and 4 become immovable. Consequently, links 5, 6, 7, 8, 9 and (4 \equiv 1) constitute a six-link constrained mechanism where link 9 (i.e., the bin) rotates about the fixed point C .

First, the points O_7 , B , C , D , E , and F shown in Fig. 2.3a are reproduced in Fig. 2.3c. The point F' is located with $O_7F' = (3/4)O_7F$ and $BF' = BF$. Now the point E' can be easily located since $\Delta BEF = \Delta BE'F'$ (link 5 rotates about the point B). Next, D' is located using the fact $CD = CD'$ and $E'D' = ED$. Thus, the rotation of link 9 is obtained, from measurement, as $\phi = 77^\circ$.

Analytical Method

An analytical method of displacement analysis, amenable to computer programming, is preferred whenever (i) a high level of accuracy is desired, (ii) a large number of configurations have to be solved or (iii) the graphical methods fail. In this method, every link length and slider displacement (from a suitable reference point) are represented by two-dimensional vectors expressed through complex exponential notation. Considering each independent closed loop in the mechanism, a vector equation (complex) is established. Separating the real and imaginary parts of all these vector equations, a sufficient number of nonlinear algebraic equations are obtained to solve for the unknown quantities. Generally, these nonlinear equations can be solved numerically using a computer. However, for some simple and useful mechanisms, the nonlinear equations can be solved analytically in closed form. In what follows, we shall demonstrate the method for a 4R mechanism and obtain some very useful results.

Let us consider a 4R linkage (Fig. 2.4) of given link lengths, viz., l_i , $i = 1, 2, 3$, and 4. The configuration of the input link (2) is also prescribed by the angle θ_2 , and we have to determine the configurations of the other two links, namely, the coupler and the follower, expressed by the angles θ_3 and θ_4 .

Referring to Fig. 2.4, all links are denoted as vectors, viz., l_1 , l_2 , l_3 , and l_4 . All angles are measured CCW from the X -axis which is along the fixed vector l_1 , rendering $\theta_1 = 0$. Considering the closed loop $O_2O_4BAO_2$, we can write

$$l_1 + l_4 + l_3 - l_2 = 0. \quad (2.1)$$

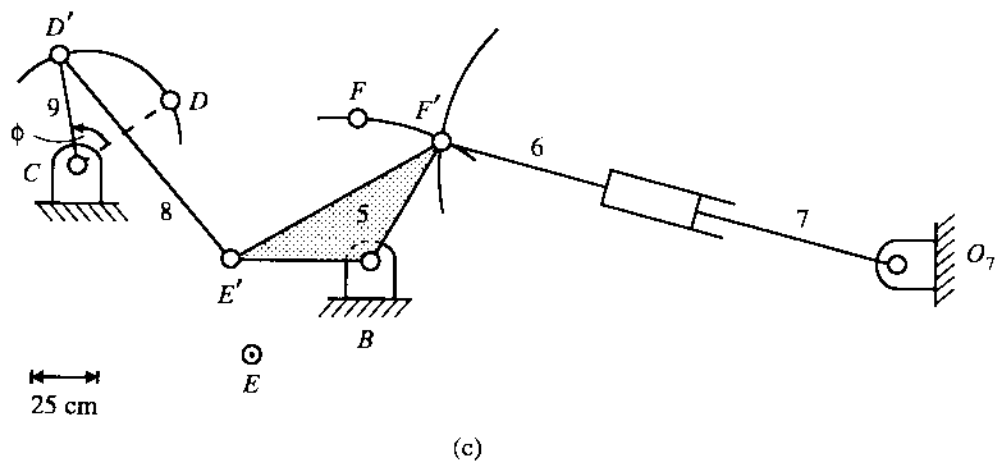
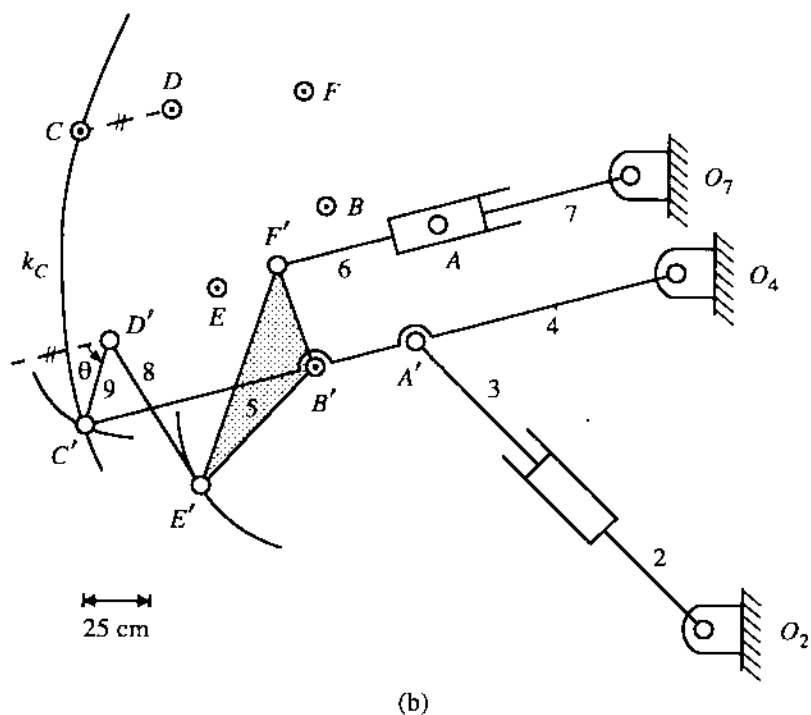


FIGURE 2.3

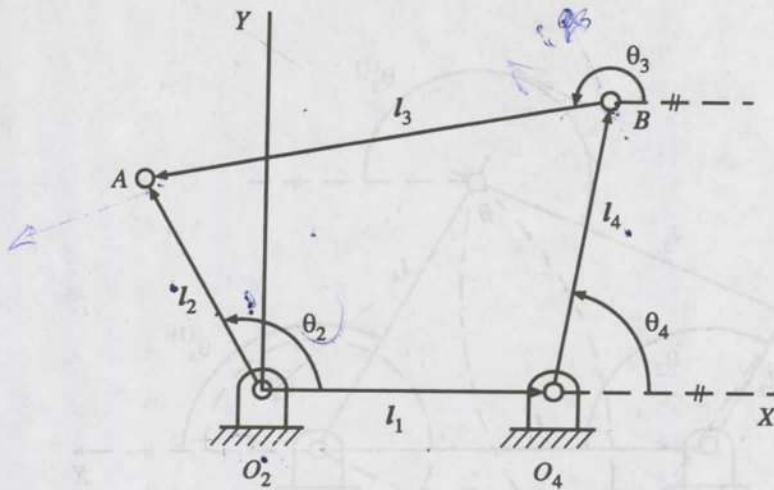


FIGURE 2.4

Using complex exponential notation with $\theta_1 = 0$, (2.1) can be written as

$$l_1 + l_4 e^{i\theta_4} + l_3 e^{i\theta_3} - l_2 e^{i\theta_2} = 0.$$

Equating the real and imaginary parts of this equation separately to zero, we get

$$l_1 + l_4 \cos \theta_4 + l_3 \cos \theta_3 - l_2 \cos \theta_2 = 0, \quad (2.2a)$$

$$l_4 \sin \theta_4 + l_3 \sin \theta_3 - l_2 \sin \theta_2 = 0. \quad (2.2b)$$

Thus, the two unknowns, namely, θ_3 and θ_4 , can be solved from the two equations (2.2a) and (2.2b) as now explained.

Rearranging (2.2a) and (2.2b), we get

$$l_3 \cos \theta_3 = l_2 \cos \theta_2 - (l_1 + l_4 \cos \theta_4),$$

$$l_3 \sin \theta_3 = l_2 \sin \theta_2 - l_4 \sin \theta_4.$$

Squaring both sides of these two equations and adding, we obtain

$$l_3^2 = l_2^2 + l_1^2 + l_4^2 - 2l_4 \sin \theta_4 (l_2 \sin \theta_2) - 2l_1 l_2 \cos \theta_2 - 2l_4 \cos \theta_4 (l_2 \cos \theta_2 - l_1)$$

or

$$a \sin \theta_4 + b \cos \theta_4 = c, \quad (2.3)$$

where

$$a = \sin \theta_2, \quad b = \cos \theta_2 - \frac{l_1}{l_2},$$

$$c = -(l_1/l_4) \cos \theta_2 + [(l_1^2 + l_2^2 + l_4^2 - l_3^2)/(2l_2 l_4)].$$

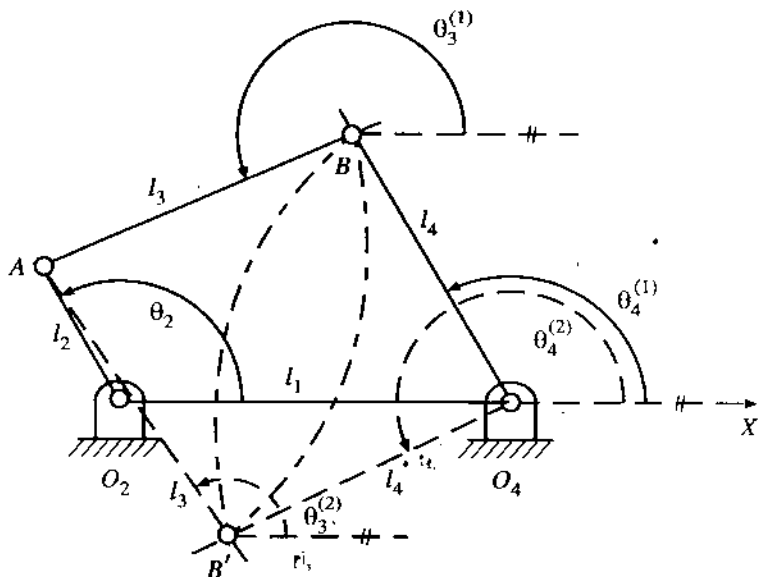


FIGURE 2.5

It may be noted that with the prescribed data (i.e., link lengths and θ_2), the coefficients a , b , and c of (2.3) are known. To solve for θ_4 , from (2.3), without ambiguity of quadrant, it is better to substitute

$$\sin \theta_4 = 2 \tan (\theta_4/2) / [1 + \tan^2 (\theta_4/2)],$$

$$\cos \theta_4 = [1 - \tan^2 (\theta_4/2)] / [1 + \tan^2 (\theta_4/2)]$$

in (2.3) to yield

$$(b + c) \tan^2 (\theta_4/2) - 2a \tan (\theta_4/2) + (c - b) = 0$$

which gives

$$\tan (\theta_4/2) = (a \pm \sqrt{a^2 + b^2 - c^2}) / (b + c).$$

Thus, for a given position of the input link, two different values of θ_4 are obtained as follows:¹

$$\theta_4^{(1)} = 2 \tan^{-1} [(a - \sqrt{a^2 + b^2 - c^2}) / (b + c)], \quad (2.4a)$$

$$\theta_4^{(2)} = 2 \tan^{-1} [(a + \sqrt{a^2 + b^2 - c^2}) / (b + c)]. \quad (2.4b)$$

These two values correspond to the two different ways in which the 4R mechanism can be formed for any given value of θ_2 , as explained in Fig. 2.5 where the same problem has been solved by a graphical method.

To solve for the coupler orientation θ_3 , we can eliminate θ_4 from (2.2a) and (2.2b) to get

$$\theta_3^{(1)} = 2 \tan^{-1} [(a + \sqrt{a^2 + b^2 - c'^2}) / (b + c')], \quad (2.5a)$$

¹To avoid the ambiguity of quadrant, in a Fortran program use ATAN2 function.

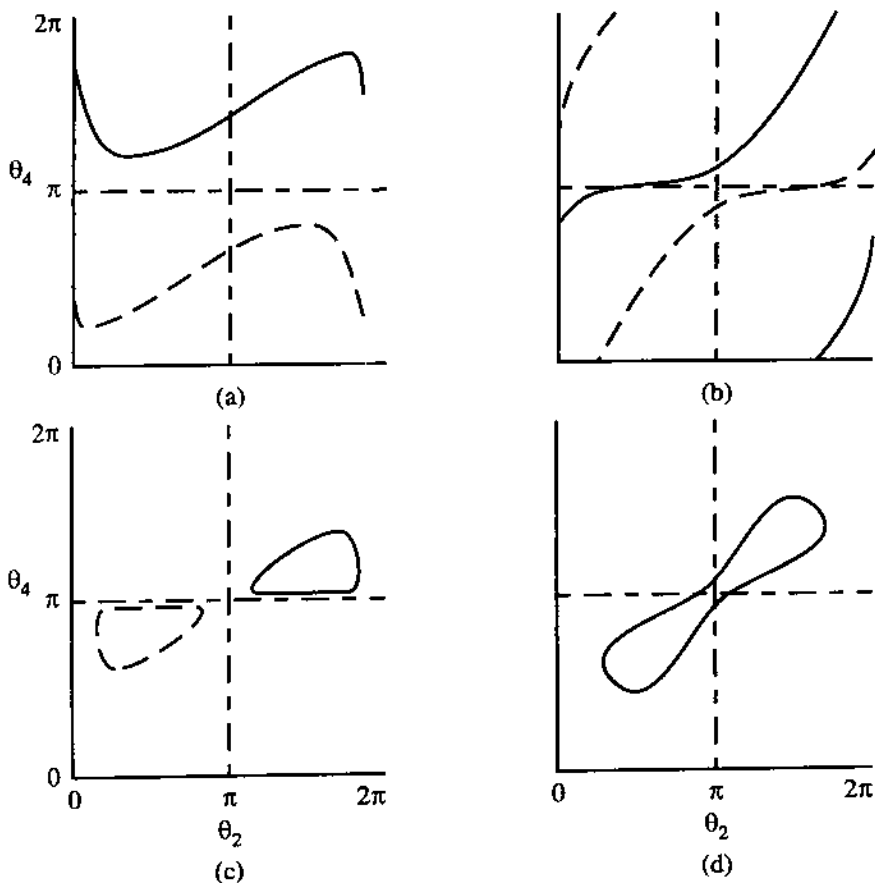


FIGURE 2.6

$$\theta_3^{(2)} = 2 \tan^{-1} [(a - \sqrt{a^2 + b^2 - c'^2})/(b + c')], \quad (2.5b)$$

where

$$c' = -(l_1/l_3) \cos \theta_2 + [(l_1^2 + l_2^2 + l_3^2 - l_4^2)/(2l_2l_3)].$$

It is quite obvious that we can get c' from the expression for c by interchanging l_3 and l_4 but attention may be drawn to the roots of θ_3 and θ_4 which pertain to the same configuration.

Since the 4R linkages are very useful in practice, it is instructive to go into further details of the output-input (i.e., plots of θ_4 vs. θ_2) relationship of these linkages. The typical nature of this relationship for various types of 4R linkages is indicated in Figs. 2.6a-d. For crank-rocker and double-crank mechanisms, the output-input characteristics are as shown in Figs. 2.6a and 2.6b, respectively. The same characteristics for double-rocker mechanisms are like those shown in Fig. 2.6c or Fig. 2.6d, depending on whether the linkage is Grashof type or non-Grashof type. The following distinctive features of various plots shown in Fig. 2.6 should be noted:

- (i) For all Grashof-type linkages, there are two disconnected branches, each corresponding to one mode of assembly. The assembly modes are mirror image of each other, with the mirror placed along the fixed link. The linkage shown in Fig. 2.5 is a crank rocker, therefore the dashed configuration can never be obtained from the configuration O_2ABO_4 . The dashed

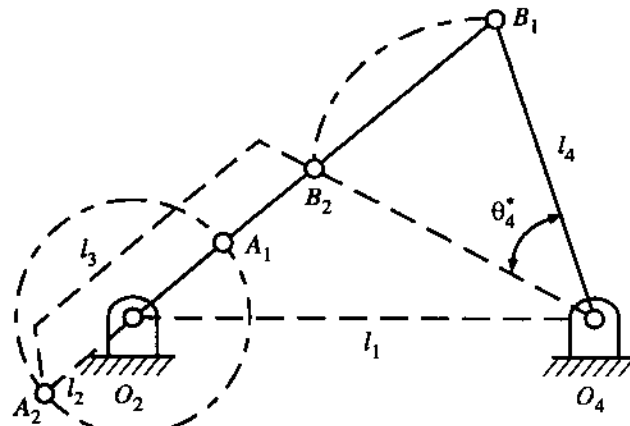


FIGURE 2.7

configuration will be obtained if initially the mechanism is assembled as the mirror image of O_2ABO_4 and link 2 then driven so as to coincide with O_2A .

- (ii) For a non-Grashof linkage, the plot of θ_4 vs. θ_2 is a single closed loop, implying that, once assembled, it can take up the mirror image configuration without being dismantled.
- (iii) Except at the ends of the swing, all rocking links pass through the same position twice with different orientations of the other link connected to the frame.

Of all the possible variations of a 4R mechanism, crank rocker is most commonly used in practice. In general, for a uniform angular speed of the crank, the rocker takes a different time interval during its forward and return motions. It is useful (at this stage) to note the relationship between the link lengths that ensures equal time for the forward and return strokes of the rocker. If the rotation of the crank has to be exactly equal to π corresponding to both forward and return strokes of the rocker, then the link lengths should be such that the outer and inner dead-centre configurations are like those shown in Fig. 2.7, where the points A_1 , A_2 , B_1 , B_2 , and O_2 are all collinear. From the triangles $O_2O_4B_1$ and $O_2O_4B_2$, we can write

$$l_4^2 = l_1^2 + (l_3 + l_2)^2 - 2l_1(l_3 + l_2) \cos \angle B_1O_2O_4,$$

$$l_4^2 = l_1^2 + (l_3 - l_2)^2 - 2l_1(l_3 - l_2) \cos \angle B_2O_2O_4.$$

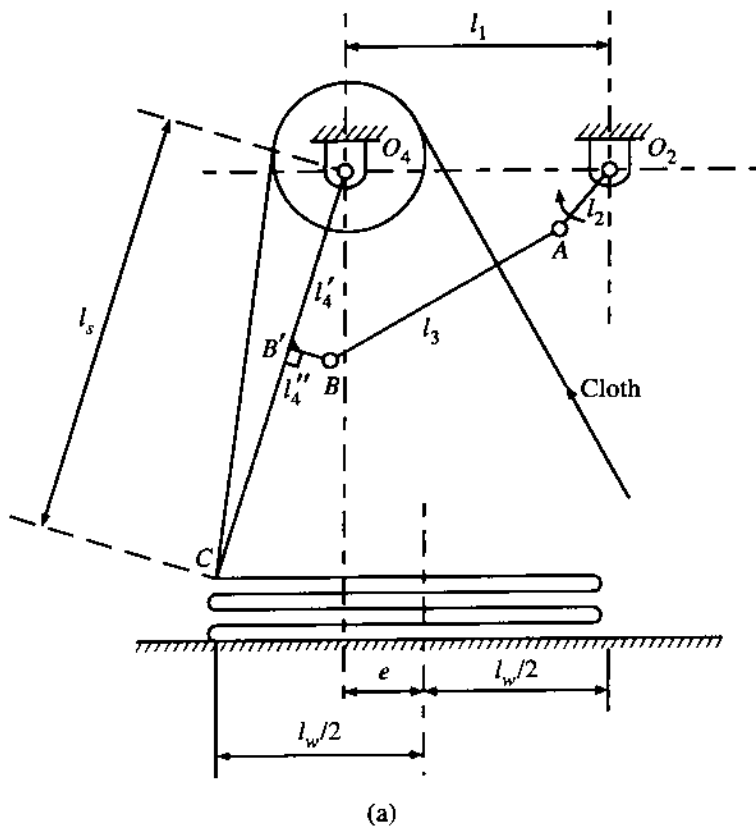
These two equations, after simplification, result in

$$l_1^2 + l_2^2 = l_3^2 + l_4^2, \quad (2.6)$$

where l_1 , l_2 , l_3 , and l_4 are the lengths of frame, crank, coupler, and follower, respectively.

Thus, (2.6) constitutes the condition required for equal time interval during the forward and return motions of the follower (link 4) when the crank (link 2) rotates with a constant angular speed. Furthermore, we should note, from Fig. 2.7, that for such a 4R mechanism without quick return,

$$B_1B_2 = 2l_2 = 2l_4 \sin(\theta_4^*/2)$$



(a)

FIGURE 2.8 (cont.)

or

$$l_2 = l_4 \sin (\theta_4^*/2), \quad (2.7)$$

where θ_4^* is the swing angle of the rocker. Now onwards, such a 4R linkage will be designated as one without the quick-return effect.

PROBLEM 2.4

Figure 2.8a schematically shows the output section of a textile mill, where the mechanism is laying the woven cloth. In this mechanism, the crank (link 2) O_2A rotates at a constant speed and the different dimensions are $l_1 = O_2O_4 = 550$ mm, $l_2 = O_2A = 170$ mm, $l_3 = AB = 550$ mm, $l_4' = O_4B' = 400$ mm, $l_4'' = BB' = 80$ mm, and the swing-arm length $l_s = 900$ mm.

- (a) Determine the width of the layer (l_w) being laid, the eccentricity (e), defined as the distance between the vertical line through O_4 and the centre of the laid layers, and the ratio of the time intervals (t_f/t_b) of the forward and backward motions of the swing arm.
- (b) It is desired to have $l_w = 1000$ mm, with $e = 0$ and a further requirement of equal time for the forward and return motions of the swing arm is to be also satisfied. Determine the required values of l_3 , l_4' , and l_4'' with all the other dimensions remaining unchanged.

SOLUTION

(a) First, the given mechanism is drawn to a scale (Fig. 2.8b) for the extreme positions of the swing arm, i.e., when O_2A and AB are collinear. It may be noted that

$$l_4 (\equiv O_4B) = \sqrt{l'_4{}^2 + l''_4{}^2} \approx 408 \text{ mm}$$

with $O_2B_1 = l_2 + l_3 = 720 \text{ mm}$ and $O_2B_2 = l_3 - l_2 = 380 \text{ mm}$. Thus, the extreme positions of B are located as B_1 and B_2 after choosing O_2 and O_4 with $O_2O_4 = 550 \text{ mm}$ and taking $O_2B_1 = 720 \text{ mm}$, $O_4B_1 = 408 \text{ mm}$, $O_2B_2 = 380 \text{ mm}$, and $O_4B_2 = 408 \text{ mm}$. Thereafter, the corresponding locations of the crank pin (A) are located on k_A (circle with radius l_2 and centre at O_2) as A_1 and A_2 using the fact that O_2 , B_1 , and A_1 are collinear and so are O_2 , B_2 , and A_2 .

The extreme positions of the swing arm (O_4C_1 and O_4C_2) are obtained by locating B'_1 and B'_2 using the lengths l'_4 and l''_4 .

The horizontal distance between the points C_1 and C_2 is the width of the laid layer $l_w = 780 \text{ mm}$ (by measurement). It may be noted that

$$l_w = l_s(\sin \theta'_4 + \sin \theta''_4), \quad (a)$$

where the total swing angle $\theta_4^* = \theta'_4 + \theta''_4$.

From measurement, we also get

$$\text{the time ratio } \frac{t_f}{t_b} = \frac{\theta_f}{\theta_b} = \frac{193^\circ}{167^\circ} = 1.156$$

and the eccentricity $e = 125 \text{ mm}$.

(b) It is easy to visualize that, with $e = 0$,

$$l_w = 2l_s \sin (\theta_4^*/2)$$

(since, in this case, $\theta'_4 = \theta''_4 = \theta_4^*/2$ in equation (a)). So, for $l_w = 1000 \text{ mm}$ and $l_s = 900 \text{ mm}$, we get

$$\sin (\theta_4^*/2) = \frac{1000}{1800} = \frac{5}{9}$$

or

$$\theta_4^*/2 = 33.75^\circ.$$

From (2.7) with $l_2 = 170 \text{ mm}$, we obtain

$$l_4 = \frac{170}{5/9} = 306 \text{ mm.}$$

From (2.6), we get

$$l_3^2 = l_1^2 + l_2^2 - l_4^2 = (550)^2 + (170)^2 - (306)^2$$

or

$$l_3 \approx 487 \text{ mm.}$$

Now, with the link lengths determined, we can construct the extreme configuration $O_4O_2A_1B_1$ of this linkage with $O_2O_4 = 550 \text{ mm}$, $O_4B_1 = 306 \text{ mm}$, and $O_2B_1 = l_2 + l_3 = 170 + 487 = 657$

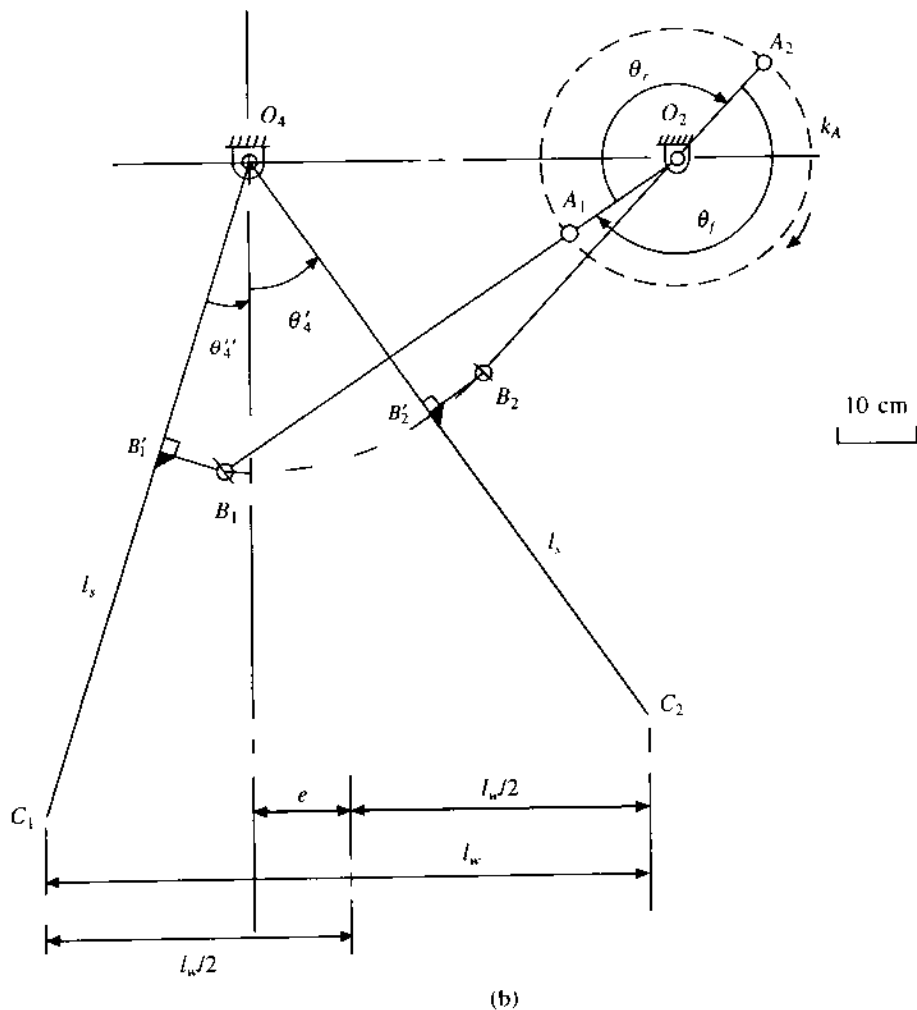


FIGURE 2.8 (cont.)

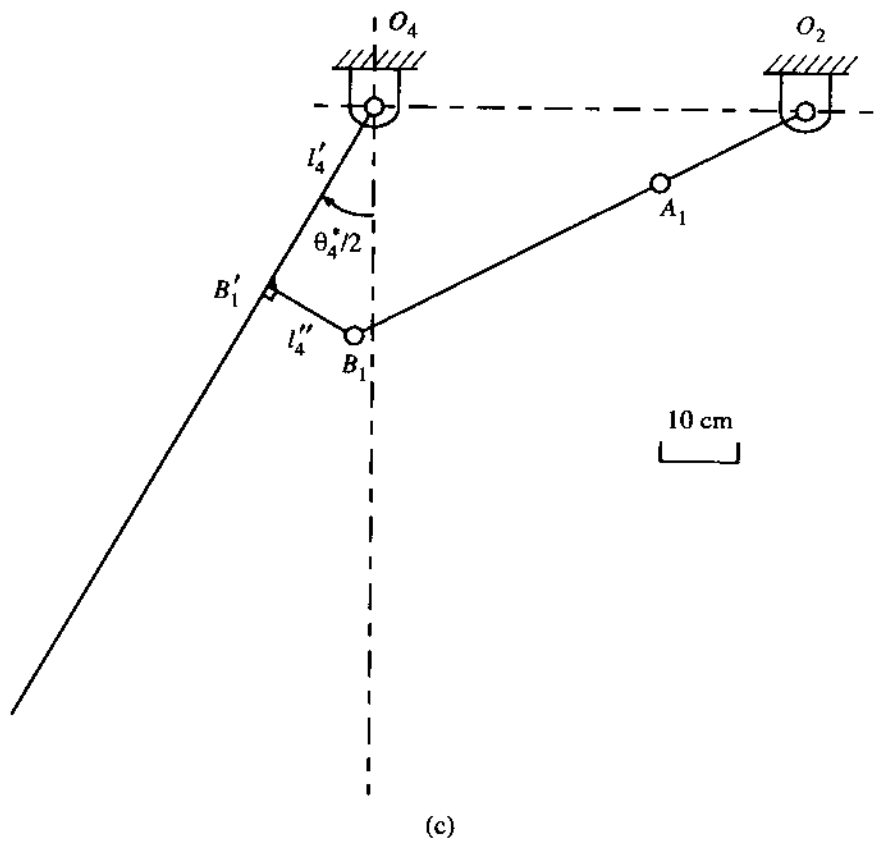


FIGURE 2.8

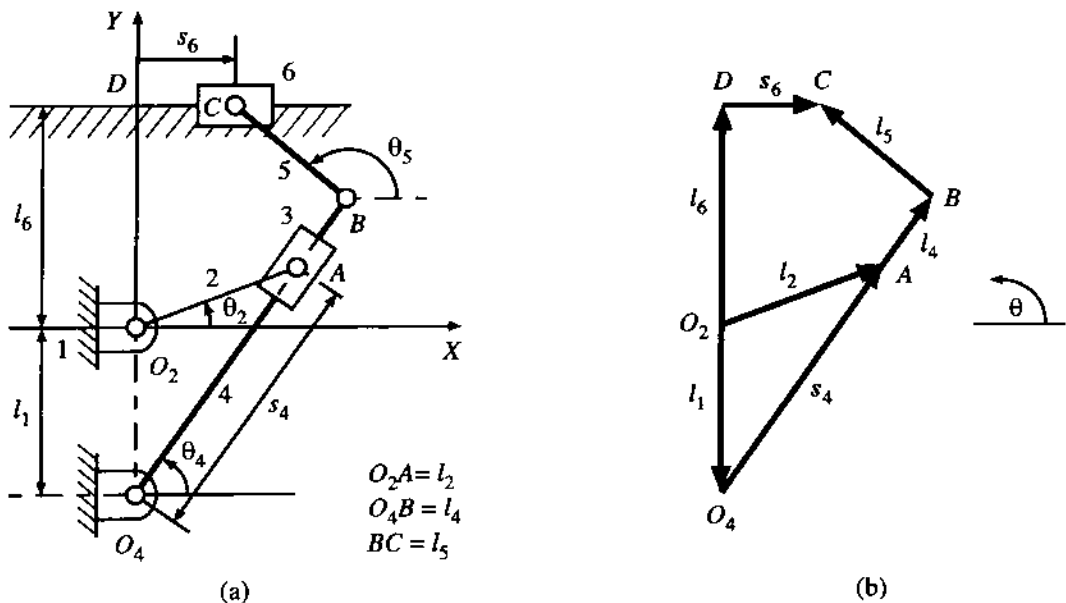


FIGURE 2.9

mm (Fig. 2.8c). Also, draw the corresponding extreme position of the swing arm at an angle $\theta_4^*/2$ ($= 33.75^\circ$) from the vertical line through O_4 . Dropping a perpendicular from B_1 on to l_s , we get (from measurement)

$$l'_4 = 270 \text{ mm}, \quad l''_4 = 145 \text{ mm}.$$

To illustrate the use of analytical method of displacement analysis for a mechanism having prismatic pair(s) and multiple closed loops, let us consider the slotted-lever quick-return mechanism (used in shapers) shown in Fig. 2.9a. In this mechanism, link 2 (the crank) rotates at a constant angular speed and slider 6 represents the cutting tool. The link lengths, the coordinate axes, and the slider displacements are also indicated in the same figure. The corresponding vector diagram, after representing the link lengths and slider displacements as two-dimensional vectors, shown in Fig. 2.9b, indicates two independent closed loops. Considering $O_2O_4AO_2$ and O_2ABCDO_2 as the two independent loops, the loop-closure equations are

$$\begin{aligned} l_1 + s_4 &= l_2, \\ l_2 + (l_4 - s_4) + l_5 &= l_6 + s_6. \end{aligned}$$

In complex exponential notation, these two equations can be written as

$$l_1 e^{i(3\pi/2)} + s_4 e^{i\theta_4} - l_2 e^{i\theta_2} = 0, \quad (2.8)$$

$$l_2 e^{i\theta_2} + (l_4 - s_4) e^{i\theta_4} + l_5 e^{i\theta_5} - l_6 e^{i\pi/2} - s_6 e^{i0} = 0. \quad (2.9)$$

For the given link lengths and the input link orientation (θ_2), the four real unknowns, viz., θ_4 , θ_5 , s_4 , and s_6 , can be solved from two nonlinear complex equations (2.8) and (2.9). Thus, the configuration of the entire mechanism is obtained as now detailed.

First, equating the real and imaginary parts of (2.8) separately to zero and solving, we obtain

$$s_4 = (l_1^2 + l_2^2 + 2l_1 l_2 \sin \theta_2)^{1/2}, \quad (2.10)$$

$$\theta_4 = \tan^{-1} [(l_1 + l_2 \sin \theta_2)/(l_2 \cos \theta_2)]. \quad (2.11)$$

It may be mentioned again that the quadrant in which θ_4 lies can be determined from the signs of the numerator and denominator of the argument of \tan^{-1} in (2.11) (just as in ATAN2 function in Fortran).

Once s_4 and θ_4 are determined, θ_5 and s_6 can be obtained from (2.9). The details of the algebra are left out as an exercise for the reader with the comment that, just as in the case of a 4R linkage, two roots of θ_5 and s_6 will be obtained. The complex roots imply that the linkage cannot be assembled with the prescribed link lengths at the given value of θ_2 . Two real roots imply that the linkage can be assembled in two different ways.

PROBLEM 2.5

A plagiograph (copying) mechanism, shown in Fig. 2.10, has two degrees of freedom. In this mechanism, O_2ABC is a parallelogram and the triangles ADB (link 5) and CBE (link 4) are similar. This mechanism can be used to reproduce a figure, traced by the point D , at E to a different scale ($= L/l$) at a different orientation ($= \sigma$). Determine the values of this scale factor and σ .

SOLUTION

Let the locations of the points D and E with respect to the fixed point O_2 at any instant be represented by two vectors \mathbf{X} and \mathbf{Y} , respectively (Fig. 2.10). It is easy to see

$$\mathbf{X} = O_2\mathbf{A} + \mathbf{AD}, \quad (a)$$

$$\mathbf{Y} = O_2\mathbf{C} + \mathbf{CE}. \quad (b)$$

Since O_2ABC always remains a parallelogram, we can write

$$O_2\mathbf{C} = \mathbf{AB} = (AB/AD)\mathbf{AD}e^{i\alpha}, \quad (c)$$

$$\mathbf{CE} = (CE/CB)O_2\mathbf{A}e^{i\alpha} = (AB/AD)O_2\mathbf{A}e^{i\alpha}, \quad (d)$$

because, from similar triangles, $(CE/CB) = (AB/AD)$. Using (c) and (d) in (b), we get

$$\mathbf{Y} = (O_2\mathbf{A} + \mathbf{AD})e^{i\alpha} \cdot (AB/AD). \quad (e)$$

Substituting (a) in (e), we have

$$\mathbf{Y} = \mathbf{X} \cdot (AB/AD)e^{i\alpha}.$$

Hence,

$$d\mathbf{Y} = (AB/AD)e^{i\alpha} d\mathbf{X}, \quad (f)$$

where $d\mathbf{Y}$ and $d\mathbf{X}$ represent displacements of the points E and D , respectively. Since $(AB/AD)e^{i\alpha}$ is a constant, the movements at E and D are similar, with the scale factor $L/l = AB/AD$ and the relative orientation $\sigma = \alpha$.

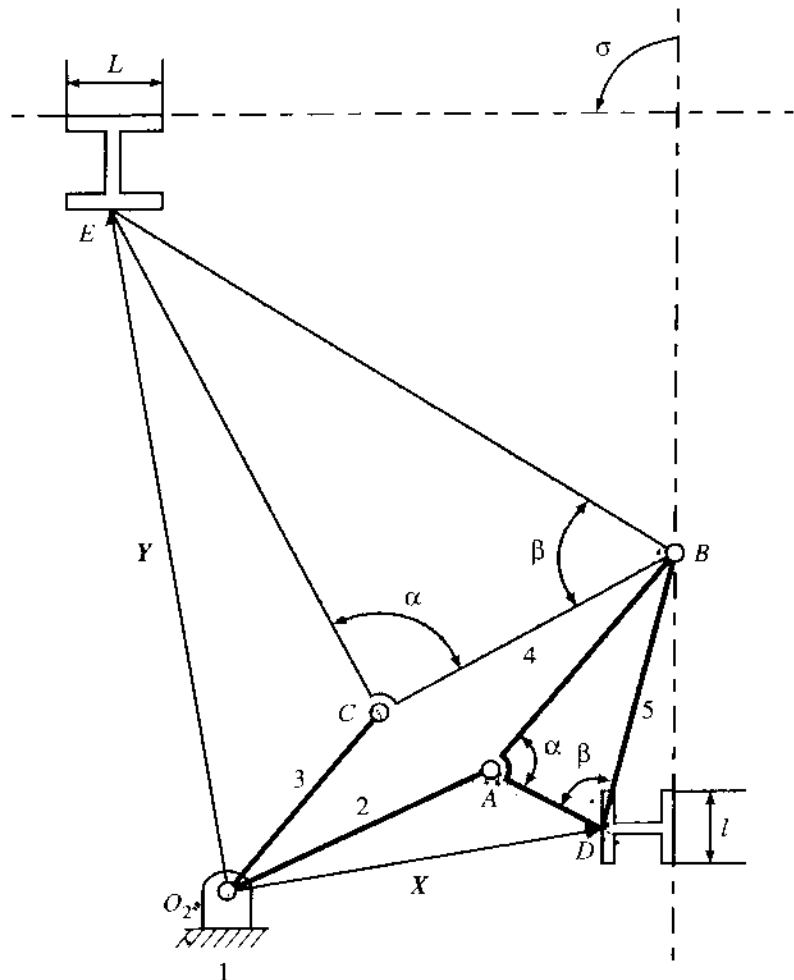


FIGURE 2.10

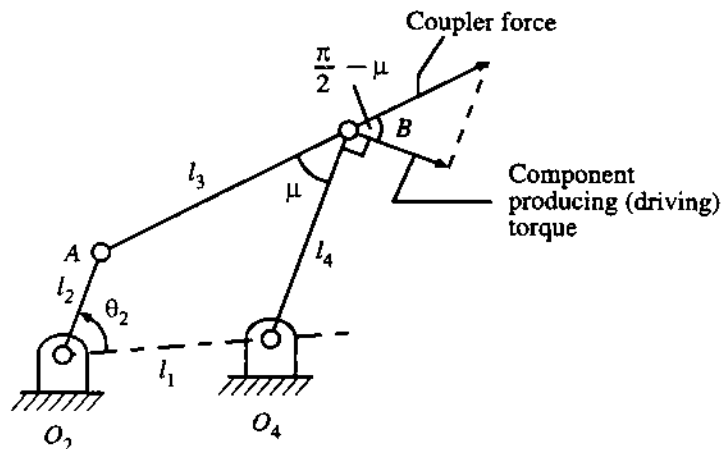


FIGURE 2.11

Transmission Angle

A mechanism, in practice, besides satisfying kinematic requirements, should also move freely. A complete dynamic force analysis, including gravity, inertia, and friction effects, is necessary to check this free-running quality. However, even at the stage of kinematic design, we should ensure that the output member receives, along its direction of movement, a large component of the force (or torque) from the member driving it. Assuming all binary links as two-force members (i.e., neglecting gravity, inertia, and frictional effects), we can express the free-running quality of simple mechanisms (like 4R or slider-crank mechanisms) through an index known as the transmission angle.

For a 4R linkage, the transmission angle (μ) is defined as the acute angle between the coupler (AB) and the follower (O_4B), as indicated in Fig. 2.11. If $\angle ABO_4$ is acute (Fig. 2.11), then $\mu = \angle ABO_4$. On the other hand, if $\angle ABO_4$ is obtuse, then $\mu = \pi - \angle ABO_4$. As explained in this figure, if $\mu = \pi/2$, then the entire coupler force is utilized to drive the follower. For good transmission quality, the minimum value of μ (μ_{\min}) $> 30^\circ$. For a crank-rocker mechanism, the minimum value of μ occurs when the crank becomes collinear with the frame, i.e., $\theta_2 = 0^\circ$ (if $l_3^2 + l_4^2 \geq l_1^2 + l_2^2$) or 180° (if $l_3^2 + l_4^2 \leq l_1^2 + l_2^2$). It is not at all difficult to prove the last assertion. The reader may tackle this as a small challenge. If the swing angle (θ_4^*) of the rocker is increased, maintaining the same quick-return ratio, then the maximum possible value of μ_{\min} decreases. If the forward and return strokes of the rocker take equal time, then $(\mu_{\min})_{\max}$ is restricted to $(\pi - \theta_4^*)/2$ (see Problem 2.6). Therefore, such a crank rocker will have a poor transmission quality if $\theta_4^* > 120^\circ$.

PROBLEM 2.6

A crank-rocker 4R linkage without the quick-return effect has to have a swing angle θ_4^* and a minimum transmission angle μ_{\min} . Determine the link-length ratios l_2/l_1 , l_3/l_1 , and l_4/l_1 .

SOLUTION

From (2.6) and (2.7), for such a linkage, we have

$$l_1^2 + l_2^2 = l_3^2 + l_4^2, \quad (a)$$

$$l_2 = l_4 \sin (\theta_4^*/2). \quad (b)$$

Considering the configuration $\theta_2 = 0$ in Fig. 2.11, when $\angle ABO_4 = \mu_{\min}$, we can write

$$O_4A^2 = (l_1 - l_2)^2 = l_3^2 + l_4^2 - 2l_3l_4 \cos \mu_{\min}. \quad (c)$$

Equations (a), (b), (c) are rewritten, respectively, as

$$1 + \left(\frac{l_2}{l_1}\right)^2 = \left(\frac{l_3}{l_1}\right)^2 + \left(\frac{l_4}{l_1}\right)^2, \quad (d)$$

$$\frac{l_2}{l_1} = \frac{l_4}{l_1} \sin (\theta_4^*/2), \quad (e)$$

$$1 + \left(\frac{l_2}{l_1}\right)^2 - 2\frac{l_2}{l_1} = \left(\frac{l_3}{l_1}\right)^2 + \left(\frac{l_4}{l_1}\right)^2 - 2\frac{l_3}{l_1}\frac{l_4}{l_1} \cos \mu_{\min}. \quad (f)$$

Using (d) in (f), we get

$$\frac{l_2}{l_1} = \frac{l_3}{l_1} \frac{l_4}{l_1} \cos \mu_{\min}. \quad (g)$$

Using (e) in (g), we obtain

$$\frac{l_3}{l_1} = \sin (\theta_4^*/2) / \cos \mu_{\min}. \quad (h)$$

Using (d), (g), and (h), it is easy to show that

$$\frac{l_4}{l_1} = \left[\left\{ 1 - \left(\frac{l_3}{l_1}\right)^2 \right\} / \left\{ 1 - \sin^2 (\theta_4^*/2) \right\} \right]^{1/2}, \quad (i)$$

$$\frac{l_2}{l_1} = \left[(l_3/l_1)^2 + (l_4/l_1)^2 - 1 \right]^{1/2} \quad (j)$$

It is obvious from (i) that $l_3/l_1 \leq 1$, and then, from (h), we get

$$\cos \mu_{\min} \geq \sin (\theta_4^*/2)$$

or

$$\cos \mu_{\min} \geq \cos [(\pi - \theta_4^*)/2]$$

or

$$(\mu_{\min})_{\max} \leq (\pi - \theta_4^*)/2.$$

For a slider-crank mechanism, the transmission angle is defined as the acute angle between the connecting rod and the normal to the slider movement as indicated in Fig. 2.12. The reader can easily prove that the minimum transmission angle in this case is given by

$$\mu_{\min} = \cos^{-1} [(l_2 + e)/l_3]. \quad (2.12)$$

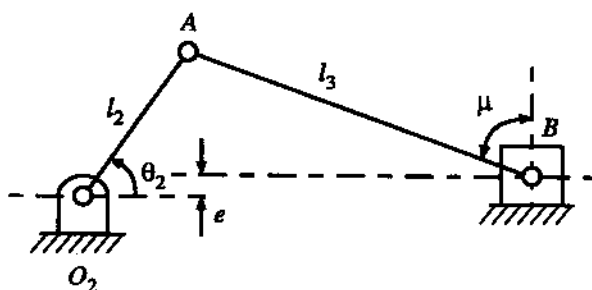


FIGURE 2.12

2.3 GENERAL PLANE MOTION

Before going into the details of various methods of velocity and acceleration analysis of plane mechanisms (i.e., a series of interconnected rigid bodies), let us briefly recapitulate the fundamentals of the velocity and acceleration of a particle and a rigid body in plane motion.

Plane Motion of a Particle

The path of a particle moving in a plane is shown in Fig. 2.13a. The positions and velocities of the particle at the instants t and $(t + \delta t)$ have been indicated. Also, the radius and centre of curvature corresponding to these instants have been shown. As depicted in Fig. 2.13b, the change in velocity δV can be resolved into two mutually perpendicular components δV^n and δV^t . When $\delta t \rightarrow 0$, the direction of the tangential component δV^t coincides with that of V , and the normal component δV^n will be directed towards the centre of curvature.

Obviously, the magnitude of the velocity of the particle at the time t can be expressed as

$$V = \lim_{\delta t \rightarrow 0} \frac{\delta s}{\delta t} = \lim_{\delta t \rightarrow 0} \rho \frac{\delta \theta}{\delta t} = \rho \dot{\theta} = \rho \omega, \quad (2.13)$$

where θ is the inclination [with respect to a reference line (see Fig. 2.13a)] and ω is the magnitude of the angular velocity of the radius of curvature. The velocity vector V is always tangential to the path and its direction is obtained by rotating ρ through 90° in the sense of ω . In vector notation,

$$\mathbf{V} = \boldsymbol{\omega} \times \boldsymbol{\rho}.$$

The normal and tangential components of acceleration can be derived as follows. The normal component of acceleration is

$$a^n = \lim_{\delta t \rightarrow 0} \frac{\delta V^n}{\delta t}.$$

From Fig. 2.13b, the magnitude of δV^n is

$$\delta V^n = V \delta \theta.$$

So,

$$a^n = \lim_{\delta t \rightarrow 0} \frac{V \delta \theta}{\delta t} = V \dot{\theta}.$$

Using (2.13) in this relation, we obtain

$$a^n = V^2/\rho = \rho\dot{\theta}^2 = \rho\omega^2. \quad (2.14)$$

The normal component of acceleration is always directed towards the centre of curvature. In vector notation,

$$\mathbf{a}^n = \boldsymbol{\omega} \times (\boldsymbol{\omega} \times \boldsymbol{\rho}).$$

The magnitude of the tangential component of acceleration is

$$a^t = \lim_{\delta t \rightarrow 0} \frac{\delta V^t}{\delta t} = \frac{dV^t}{dt} = \dot{V}.$$

Using (2.13), we find the final expression for a^t becomes

$$a^t = \rho\dot{\theta} + \rho\ddot{\theta} = \rho\omega + \rho\alpha, \quad (2.15)$$

where α is the magnitude of the angular acceleration of the radius vector.

Plane Motion of a Rigid Body

The position of a rigid body in plane motion is completely defined by specifying either the positions of any two points on the body or the position of a point and the orientation of a line fixed on the rigid body.

Similarly, the velocity (of all points) of a rigid body in plane motion is completely defined by specifying the velocity of any point on the body along with the angular velocity ω of the body. If the rigid body is in pure translation (without rotation), then the motion of all points on it is identical. The difference in velocity of two points A and B (Fig. 2.13c) is entirely due to ω and this difference is expressed as (Fig. 2.13d)

$$\mathbf{V}_{BA} = \mathbf{V}_B - \mathbf{V}_A = \boldsymbol{\omega} \times \mathbf{AB}.$$

It is easy to identify that the difference in the motions of B and A , due to ω , is a circular motion of B about A since AB remains constant, i.e., ρ in (2.13)-(2.15) is constant and replaced by AB .

For the velocity analysis of a mechanism, the following form of the foregoing equation is used:

$$\mathbf{V}_B = \mathbf{V}_A + \mathbf{V}_{BA} = \mathbf{V}_A + \boldsymbol{\omega} \times \mathbf{AB}. \quad (2.16)$$

It should be noted that for this equation to be valid, A and B must be on the same rigid body and ω must be the angular velocity of the body.

The acceleration of a rigid body is defined by specifying either the accelerations of any two points on it or the acceleration of any point on it and its angular acceleration α (assuming that the angular velocity of the body is already known). The acceleration of a point B on a rigid body can be expressed in terms of the acceleration of a point A and the angular velocity and acceleration of the body. The difference in acceleration is given by

$$\mathbf{a}_{BA} = \mathbf{a}_B - \mathbf{a}_A = \mathbf{a}_{BA}^n + \mathbf{a}_{BA}^t.$$

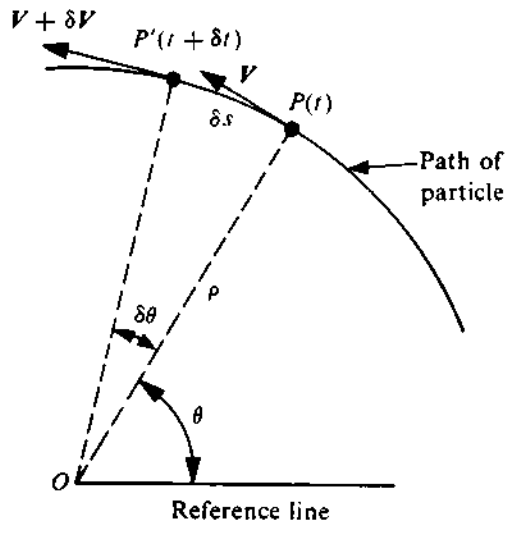
From (2.14) and (2.15), with $\rho = AB = \text{constant}$,

$$a_{BA}^n = AB\omega^2 \quad [\text{written in vector notation as } \mathbf{a}_{BA}^n = \boldsymbol{\omega} \times (\boldsymbol{\omega} \times \mathbf{AB})],$$

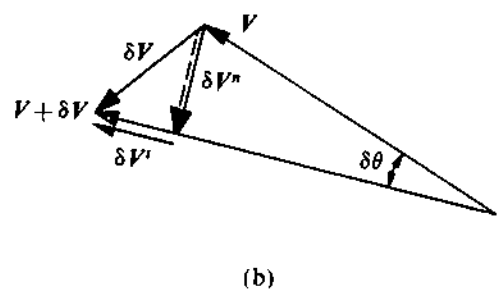
$$a_{BA}^t = AB\alpha \quad [\text{written in vector notation as } \mathbf{a}_{BA}^t = \boldsymbol{\alpha} \times \mathbf{AB}].$$

The normal component is always along BA and the tangential component is perpendicular to AB in the sense of α . The commonly-used form of the acceleration relation is

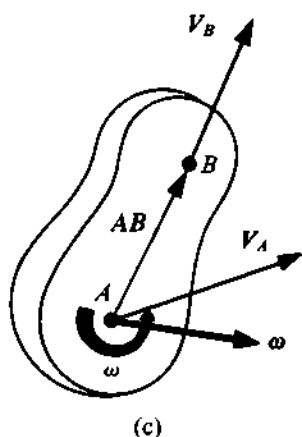
$$\mathbf{a}_B = \mathbf{a}_A + \mathbf{a}_{BA}^n + \mathbf{a}_{BA}^t. \quad (2.17)$$



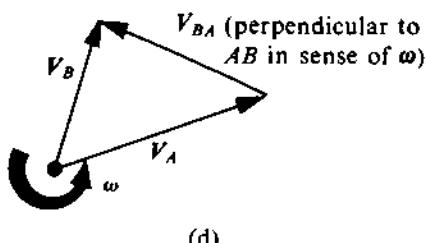
(a)



(b)



(c)



(d)

FIGURE 2.13

Motion Difference between Two Instantaneously Coincident Points

In a mechanism, a link is quite often guided along a prescribed path in another moving link. For the velocity and acceleration analyses of such a mechanism, the differences in the velocities and accelerations of two instantaneously coincident points belonging to the two links have to be determined. In this section, we shall derive the expressions for these quantities.

Figure 2.14a shows a rotating rigid link (labelled 2) on which link 3 is moving along a straight line. The configurations at the instants t and $(t + \delta t)$ are, respectively, shown by the symbols without and with a prime. Further, P_2 and P_3 represent two points on links 2 and 3, respectively, coincident at the instant t . The displacement of P_3 can be written as

$$\delta P_3 = P_3 P'_3 = P_2 P'_2 + P'_2 P'_3 = \delta P_2 + \delta P_{3/2},$$

where δP_2 ($= \delta P_2$) represents the displacement of P_2 and $\delta P_{3/2}$ ($= \delta P_{3/2}$) represents the displacement of P_3 with respect to link 2. Dividing both sides of the foregoing equation by δt and taking the limit $\delta t \rightarrow 0$, we get

$$V_{P_3} = V_{P_2} + V_{P_{3/2}}, \quad (2.18)$$

where $V_{P_{3/2}}$ is the velocity of P_3 as seen by an observer attached to link 2. The direction of $V_{P_{3/2}}$ is tangential to the path of P_3 in link 2.

From (2.18), it may appear that the absolute acceleration of P_3 can also be obtained from an equation similar to it, i.e., $a_{P_3} = a_{P_2} + a_{P_{3/2}}$, where $a_{P_{3/2}}$ is the acceleration of P_3 as seen by an observer on link 2. However, this is incorrect since an extra term has to be added to the right-hand side of this equation, as now explained.

From Fig. 2.14b, we see that the block has moved through an additional transverse distance AP'_3 because of the rotation of link 2 and the radial motion of link 3 with respect to link 2. When $\delta t \rightarrow 0$,

$$AP'_3 = P'_2 P'_3 \cdot \delta\theta_2 = V_{P_{3/2}} \cdot \delta t \cdot \omega_2 \cdot \delta t = V_{P_{3/2}} \cdot \omega_2 \cdot \delta t^2.$$

From this equation, we observe that the additional displacement term is proportional to the square of the time elapsed. Therefore, this displacement must be due to an additional acceleration of P_3 in the transverse direction. If the magnitude of this additional acceleration is a_c , then

$$\frac{1}{2} a_c \delta t^2 = V_{P_{3/2}} \cdot \omega_2 \cdot \delta t^2$$

or

$$a_c = 2V_{P_{3/2}} \cdot \omega_2. \quad (2.19)$$

In vector notation, (2.19) is written as

$$\mathbf{a}_c = 2\omega_2 \times \mathbf{V}_{P_{3/2}}.$$

This extra transverse component of acceleration is known as the Coriolis component. The final expression for \mathbf{a}_{P_3} will then be

$$\mathbf{a}_{P_3} = \mathbf{a}_{P_2} + \mathbf{a}_{P_{3/2}} + \mathbf{a}_c. \quad (2.20)$$

It should be noted that the direction \mathbf{a}_c is obtained by rotating $\mathbf{V}_{P_{3/2}}$ through 90° in the sense of ω_2 . For a straight-line path of P_3 on link 2, the direction of $\mathbf{a}_{P_{3/2}}$ is along the straight line.

When link 3 moves along a curvilinear path on the rotating link 2 (see Fig. 2.14c), equation (2.20) can be written in terms of the components of $\mathbf{a}_{P_{3/2}}$ as

$$\mathbf{a}_{P_3} = \mathbf{a}_{P_2} + \mathbf{a}_{P_{3/2}}^n + \mathbf{a}_{P_{3/2}}^t + \mathbf{a}_c. \quad (2.21)$$

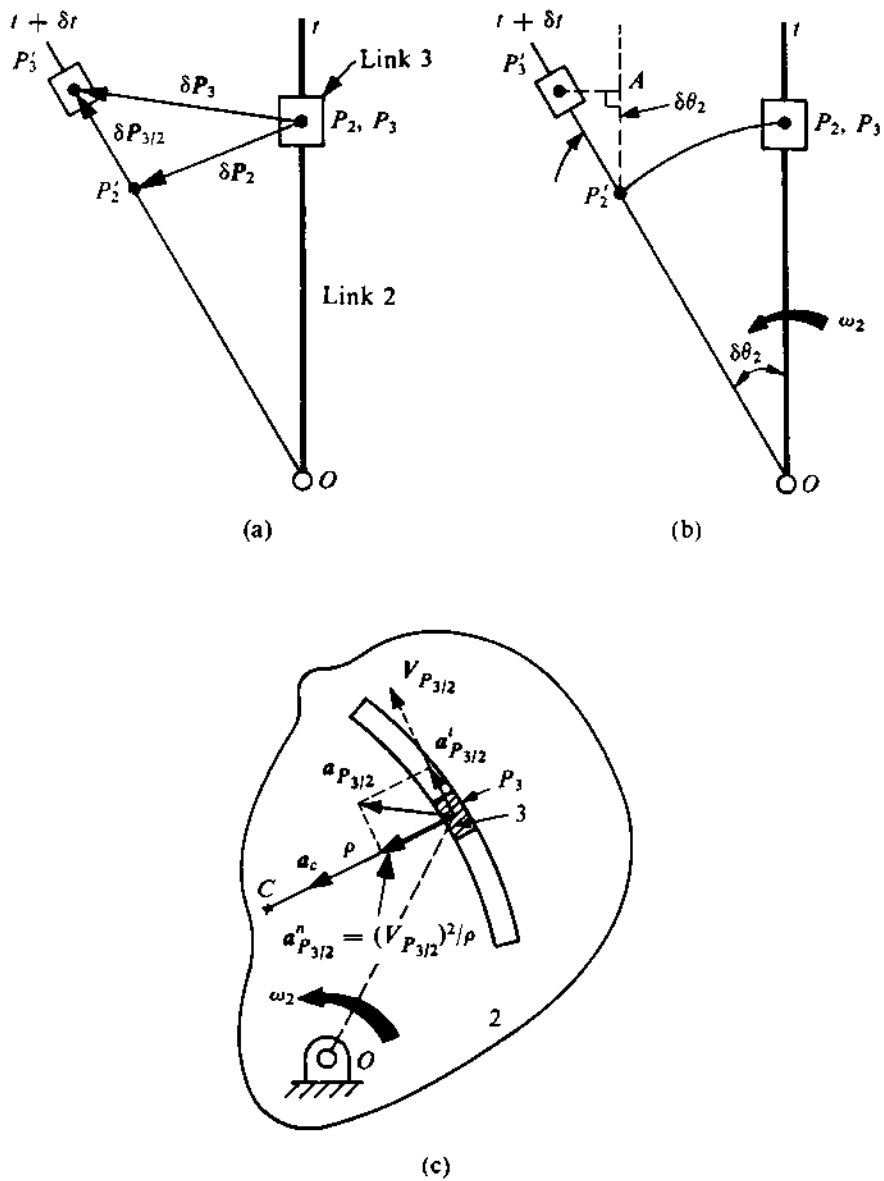


FIGURE 2.14

It may be noted that the magnitude of $a_{P_{3/2}}^n$ is equal to $(V_{P_{3/2}})^2/\rho$, where ρ is the radius of curvature of the path of P_3 on link 2. The direction of $V_{P_{3/2}}$ is obviously tangential to this path. For a straight-line path of P_3 on link 2, ρ becomes infinite and $a_{P_{3/2}}^n = 0$.

It may be pointed out that for (2.18) and (2.21) to be valid, P_2 and P_3 need not belong to two adjacent links. We can use these relations for two coincident points, P_i and P_j , belonging to the i -th and j -th links, respectively. The important point is that the path of P_j in the i -th link should be known (generally, the path of P_i in the j -th link is not the same as this one) and we can write

$$\mathbf{V}_{P_j} = \mathbf{V}_{P_i} + \mathbf{V}_{P_{j/i}}, \quad (2.22)$$

$$\mathbf{a}_{P_j} = \mathbf{a}_{P_i} + \mathbf{a}_{P_{j/i}}^n + \mathbf{a}_{P_{j/i}}^t + \mathbf{a}_c \quad (2.23)$$

with

$$\mathbf{a}_c = 2\omega_i \times \mathbf{V}_{P_{j/i}}. \quad (2.24)$$

To identify the path of P_j in the i -th link, it is advisable to consider a kinematic inversion of the mechanism keeping the i -th link fixed.

2.4 INSTANTANEOUS CENTRE OF VELOCITY

In Fig. 2.15, a rigid body 2 is shown to be in plane motion with respect to the fixed link 1. The velocities of two points A and B of the rigid link 2 are shown by \mathbf{V}_A and \mathbf{V}_B , respectively. Two lines drawn through A and B in directions perpendicular to \mathbf{V}_A and \mathbf{V}_B meet at P . Let $PA = r_1$ and $PB = r_2$. The velocity of the point B in the direction of AB is $V_B \cos \phi$, and that of the point A in the same direction is $V_A \cos \theta$. As the length of AB is fixed, the component of \mathbf{V}_{BA} in the direction of AB is zero. Thus, $V_B \cos \phi = V_A \cos \theta$. From the triangle PAB , we have

$$\frac{PA}{\sin(90^\circ - \phi)} = \frac{PB}{\sin(90^\circ - \theta)}, \quad \frac{r_1}{r_2} = \frac{PA}{PB} = \frac{\cos \phi}{\cos \theta} = \frac{V_A}{V_B},$$

$$\frac{V_A}{r_1} = \frac{V_B}{r_2} = \omega \quad (\text{angular velocity of link 2}).$$

Thus, the velocities of the points A and B are proportional and perpendicular to PA and PB , respectively. So, instantaneously, the rigid body can be thought of as being momentarily in pure rotation about the point P . The velocity of any point C on the body at this instant is given by $V_C = PC \cdot V_B / r_2$ in a direction perpendicular to PC . This point P is called the *instantaneous centre of velocity*, and its instantaneous velocity is zero. So, alternatively, the instantaneous centre of velocity can be defined as a point which has no velocity with respect to the fixed link.

If both links 1 and 2 are in motion, in a similar manner, we can define a *relative instantaneous centre* P_{12} (sometimes called *centro*) to be a point on 2 having zero relative velocity (i.e., the same absolute velocity) with respect to a coincident point on 1. Consequently, the relative motion of 2 with respect to 1 appears to be pure rotation (for the instant) about P_{12} . It is evident that P_{12} and P_{21} are identical. Thus, if a mechanism has N links, the number of relative instantaneous centres is $N(N - 1)/2$. The *absolute instantaneous centre of velocity* of a link is the relative instantaneous centre of velocity with respect to the fixed link. Note carefully that the instantaneous centres can lie outside the physical boundary of the links and anywhere in the plane of motion. However, they are considered to be integral points of the concerned two links (imagined to be extended). In certain cases, the relative instantaneous centres are easily identified by inspection of the geometry of motion. Examples of such situations are as follows:

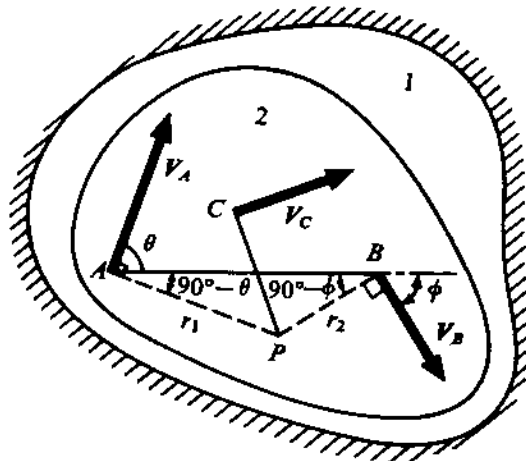


FIGURE 2.15

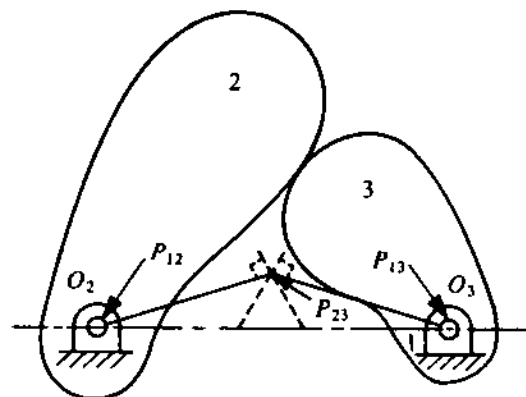


FIGURE 2.16

- If two links have a hinged joint, the location of the hinge is the relative instantaneous centre because one link is in pure rotation with respect to the other about that hinge.
- If the relative motion between two links is pure sliding, the relative instantaneous centre lies at infinity on a line perpendicular to the direction of sliding.
- If one link is rolling (without slipping) over another, the point of contact is the relative instantaneous centre.
- If a link is sliding over a curved element, the centre of curvature is the relative instantaneous centre. (Remember the curved slider and the equivalent hinge cited in Section 1.6.)
- If the relative motion between two links is both rolling and sliding, the relative instantaneous centre lies on the common normal to the surfaces of these links passing through the point of contact. The determination of its exact location requires some more information.

The instantaneous centre of acceleration is defined as a point on a link having zero relative acceleration with respect to a coincident point on the other link, and in general is different from the instantaneous centre of velocity. Being of little use in the analysis of mechanisms, it will not be discussed here.

2.5 ARONHOLD-KENNEDY THEOREM OF THREE CENTRES

The Aronhold-Kennedy theorem states that *if three bodies are in relative motion with respect to one another, the three relative instantaneous centres of velocity are collinear*.

The proof of the theorem is as follows. Figure 2.16 shows three links 1, 2, and 3 in relative motion with respect to one another. Since we are interested only in the relative motion, without any loss of generalities we can assume one of the three links, say, link 1, is fixed. $P_{12}(O_2)$ and $P_{13}(O_3)$ are the points about which links 2 and 3 are rotating. If P_{23} is not on the line joining $P_{12}P_{13}$, let it be somewhere else as shown in the figure. Considering P_{23} as a point on link 2, its velocity must be in a direction perpendicular to $P_{12}P_{23}$. If P_{23} is taken as a point on link 3, its velocity must be in a direction perpendicular to $P_{13}P_{23}$. By definition, P_{23} must have the same velocity whether it

is considered to be on link 2 or 3. This cannot be so unless P_{23} is on the line $P_{12}P_{13}$, otherwise the directions will be different as has been shown in the figure.

This theorem will be used very often for determining the relative instantaneous centres of a mechanism.

2.6 VELOCITY AND ACCELERATION IMAGES

The concepts of velocity and acceleration images are used extensively in the kinematic analysis of mechanisms having ternary, quaternary, and higher-order links. If the velocities and accelerations of any two points on a link are known, then, with the help of images, the velocity and acceleration of any other point on the link can be easily determined. An example to illustrate this concept follows. The method used will be better appreciated when the kinematic analysis of complex mechanisms is considered later in this chapter.

A rigid link $BCDE$ having four hinges is shown in Fig. 2.17a. Let the angular velocity and acceleration of this link be ω and α (CCW). The absolute velocity vectors of the points E , B , C , and D are shown in Fig. 2.17b as \mathbf{V}_E , \mathbf{V}_B , \mathbf{V}_C , and \mathbf{V}_D , respectively. The velocity difference vectors are

$$\mathbf{eb} = \mathbf{V}_{BE}, \quad \mathbf{bc} = \mathbf{V}_{CB}, \quad \mathbf{ec} = \mathbf{V}_{CE}, \quad \mathbf{bd} = \mathbf{V}_{DB},$$

and their magnitudes are, respectively,

$$EB\omega, \quad BC\omega, \quad EC\omega, \quad BD\omega.$$

So,

$$\frac{\mathbf{eb}}{EB} = \frac{\mathbf{bc}}{BC} = \frac{\mathbf{ec}}{EC} = \frac{\mathbf{bd}}{BD} = \omega.$$

Hence, the velocity diagram $bcd e$ is a scale drawing of the link $BCDE$. The figure $bcd e$ (formed by the tip of the absolute velocity vectors) is called the *velocity image* of the link $BCDE$. The velocity image is rotated through 90° in the direction ω , as all the velocity difference vectors are perpendicular to the corresponding lines. The scale of the image is determined by ω , and therefore the scale will be different for each link of a mechanism. The letters identifying the end points of the image are in the same sequence as that in the link diagram $BCDE$. The absolute velocity of any point X on the link is obtained by joining the image of $X(x)$ with the pole of the velocity diagram ω .

The absolute acceleration vectors of the points E , B , C , D are shown in Fig. 2.17c as \mathbf{a}_E , \mathbf{a}_B , \mathbf{a}_C , \mathbf{a}_D , respectively. The acceleration difference vectors are

$$\mathbf{eb} = \mathbf{a}_{BE}, \quad \mathbf{bc} = \mathbf{a}_{CB}, \quad \mathbf{ec} = \mathbf{a}_{CE}, \quad \mathbf{bd} = \mathbf{a}_{DB},$$

$$\mathbf{a}_{BE} = \mathbf{a}_{BE}^n + \mathbf{a}_{BE}^t, \quad a_{BE}^n = BE\omega^2 = eb_1, \quad a_{BE}^t = BE\alpha = b_1b.$$

Thus,

$$eb = (eb_1^2 + b_1b^2)^{1/2} = BE(\omega^4 + \alpha^2)^{1/2}.$$

Similarly,

$$cb = BC(\omega^4 + \alpha^2)^{1/2}, \quad ec = CE(\omega^4 + \alpha^2)^{1/2}, \quad bd = DB(\omega^4 + \alpha^2)^{1/2}.$$

So, the figure $ebcd$ (formed by the tip of the absolute acceleration vectors) is a scale drawing of the link $EBCD$ and is called the *acceleration image*. The scale will be different for each link of

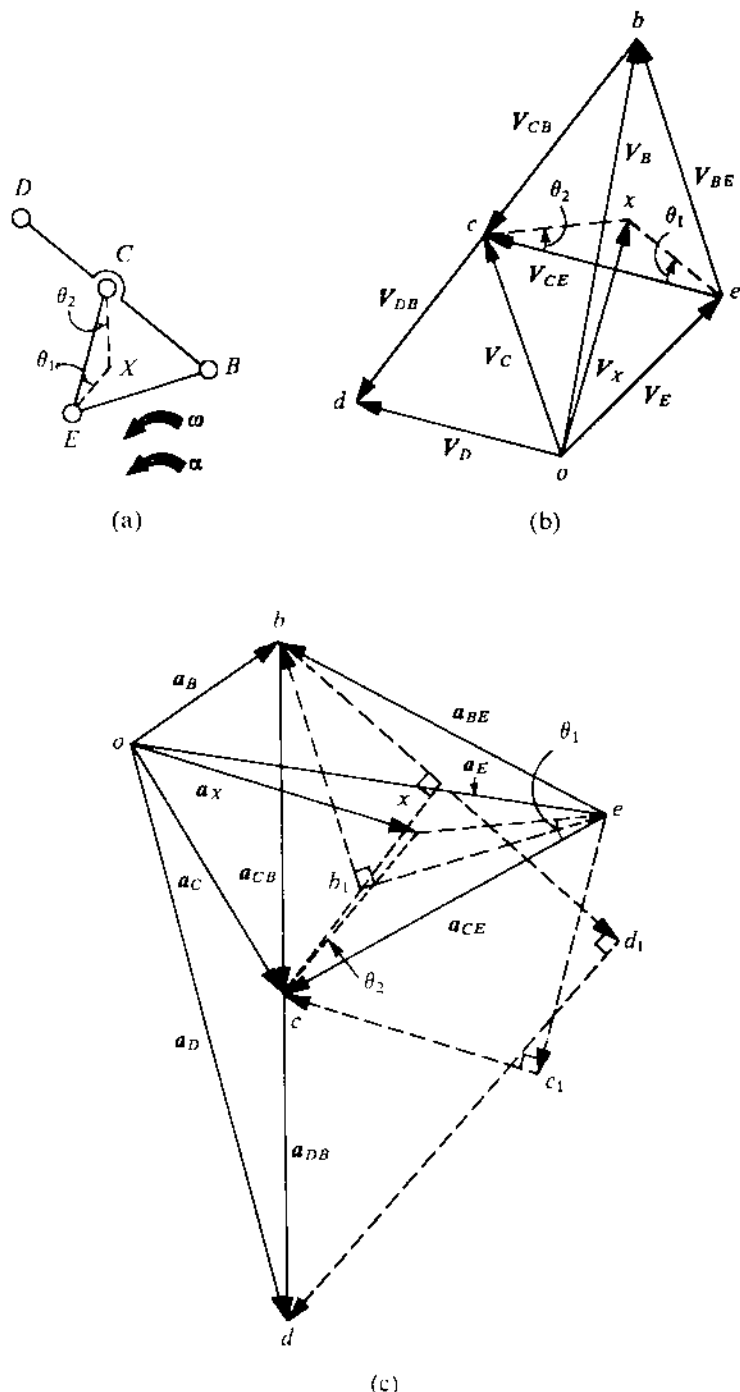


FIGURE 2.17

a mechanism. The letters identifying the end points of the image are in the same sequence as that in the link diagram $BCDE$. The absolute acceleration of any point X on the link can be obtained by joining the image of $X(x)$ with the pole of the acceleration diagram o . The orientation of the acceleration image from the link diagram is $(180^\circ - \theta)$ in the counter-clockwise direction, where $\theta = \tan^{-1} [bb_1/(b_1e)] = \tan^{-1} (\alpha/\omega^2)$, with α positive in the CCW sense (as explained in Fig. 2.17c). It should be noted that once the absolute velocities and accelerations of any two points (e.g., E and C) of a rigid link are known, those of any other point on the link (such as X , B , and D) can be determined just by drawing the respective images.

2.7 VELOCITY AND ACCELERATION ANALYSIS (GRAPHICAL)

The velocity and acceleration analysis of most of the simple mechanisms can be carried out graphically using the concepts developed in Sections 2.3-2.6. In this section, we shall illustrate this through a number of examples. The kinematic (especially the acceleration) analysis of complex mechanisms will be considered in the next section whereas the analytical method following loop-closure equations will be discussed in Section 2.9.

Velocity Analysis Using Instantaneous Centres

The velocity analysis using instantaneous centres involves almost no computations; it can be carried out graphically. Sometimes, this method can be used in conjunction with other methods of velocity analysis. If the velocity of a particular link in a mechanism is to be determined, the efficiency of the method depends on the choice of the relative instantaneous centres to be used. This idea will be clarified in Problem 2.8 in which there are two different choices. The method is also sometimes useful for the velocity analysis of complex mechanisms considered in Section 2.8.

PROBLEM 2.7

The angular velocity of link 2 of the four-bar linkage shown in Fig. 2.18 is given. Determine the velocities of the points E and F .

SOLUTION

There are six instantaneous centres, namely,

$$\begin{array}{ccc} \overset{x}{P_{12}} & P_{13} & \overset{x}{P_{14}} \\ & \overset{x}{P_{23}} & P_{24} \\ & & \overset{x}{P_{34}} \end{array}$$

of which four (indicated by the cross mark) are easily determined as the hinge points (by definition). The other two, P_{13} and P_{24} , are determined by the Aronhold-Kennedy theorem. P_{13} lies on the line joining P_{14} and P_{34} ; it also lies on the line joining P_{12} and P_{23} . So, P_{13} is determined by the intersection of lines $P_{14}P_{34}$ and $P_{12}P_{23}$. Similarly, P_{24} is determined by the intersection of lines

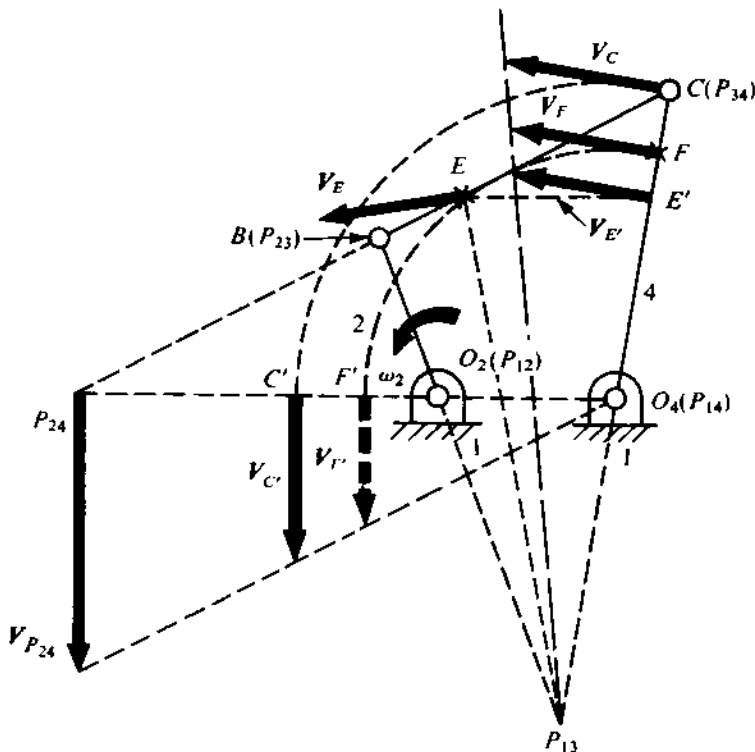


FIGURE 2.18

$P_{12}P_{14}$ and $P_{23}P_{34}$.² Considering P_{24} to be a point on link 2, $\mathbf{V}_{P_{24}}$ ($= \omega_2 \times \mathbf{O}_2 P_{24}$) is laid out to some scale. Now, consider P_{24} to be a point on link 4 which is rotating about the fixed point $P_{14}(O_4)$. F' is an auxiliary point on link 4 such that $O_4F = O_4F'$. So, $V_F = V_{F'}$, and $\mathbf{V}_{F'}$ is determined graphically (see the figure) as

$$\mathbf{V}_{P_{24}} = \omega_4 \cdot \mathbf{O}_4 P_{24}, \quad \mathbf{V}_{F'} = \omega_4 \cdot \mathbf{O}_4 F',$$

$$\frac{\mathbf{V}_{P_{24}}}{\mathbf{V}_{F'}} = \frac{\mathbf{O}_4 P_{24}}{\mathbf{O}_4 F'} \quad (\text{as seen from the similar triangles}).$$

The direction of \mathbf{V}_F is perpendicular to O_4F . Thus, \mathbf{V}_F is determined completely. \mathbf{V}_C , shown in the figure, is determined completely in a similar fashion, considering C to be a point on link 4. Now, this point C has the same velocity on link 3 which is rotating with respect to the fixed link 1 about P_{13} . E' is an auxiliary point on link 4 such that $P_{13}E = P_{13}E'$. So, $V_E = V_{E'}$, and $\mathbf{V}_{E'}$ is determined graphically, using the relation

$$\frac{\mathbf{V}_{E'}}{P_{13}E'} = \frac{\mathbf{V}_C}{P_{13}C} = \omega_3.$$

The direction of \mathbf{V}_E is perpendicular to $P_{13}E$. Thus, \mathbf{V}_E is determined completely. It should be noted that the auxiliary points (say, F') are taken on the line joining the absolute instantaneous centre of the corresponding link (O_4) with a point on the link, of which the velocity is known (P_{24}).

²For complicated mechanisms, wastage of time and confusion can be avoided if the instantaneous centres are determined in a systematic manner. In the next problem, a method for this has been explained.

PROBLEM 2.8

In the Whitworth quick-return mechanism shown in Fig. 2.19a, ω_2 is given. Determine the velocity of the slider at D. Given $O_2A = 8 \text{ cm}$, $O_4C = 6 \text{ cm}$, $O_2O_4 = 4 \text{ cm}$, and $CD = 20 \text{ cm}$.

SOLUTION

The mechanism has six links, so it has $6 \times (6 - 1)/2$, i.e., fifteen instantaneous centres. For convenience, if we denote the centre P_{12} as 12, and so on, these instantaneous centres are

\times	\checkmark	\times	\checkmark	\times
12	13	14	15	16
\times	\checkmark	\checkmark	\checkmark	
23	24	25	26	
\times	\checkmark			
34	35	36		
\times				
45	46			
\times				
56				

Of these, seven (indicated by the cross mark) can be easily identified and are

$$O_2 \rightarrow 12, \quad O_4 \rightarrow 14, \quad A \rightarrow 23, \quad C \rightarrow 45, \quad D \rightarrow 56,$$

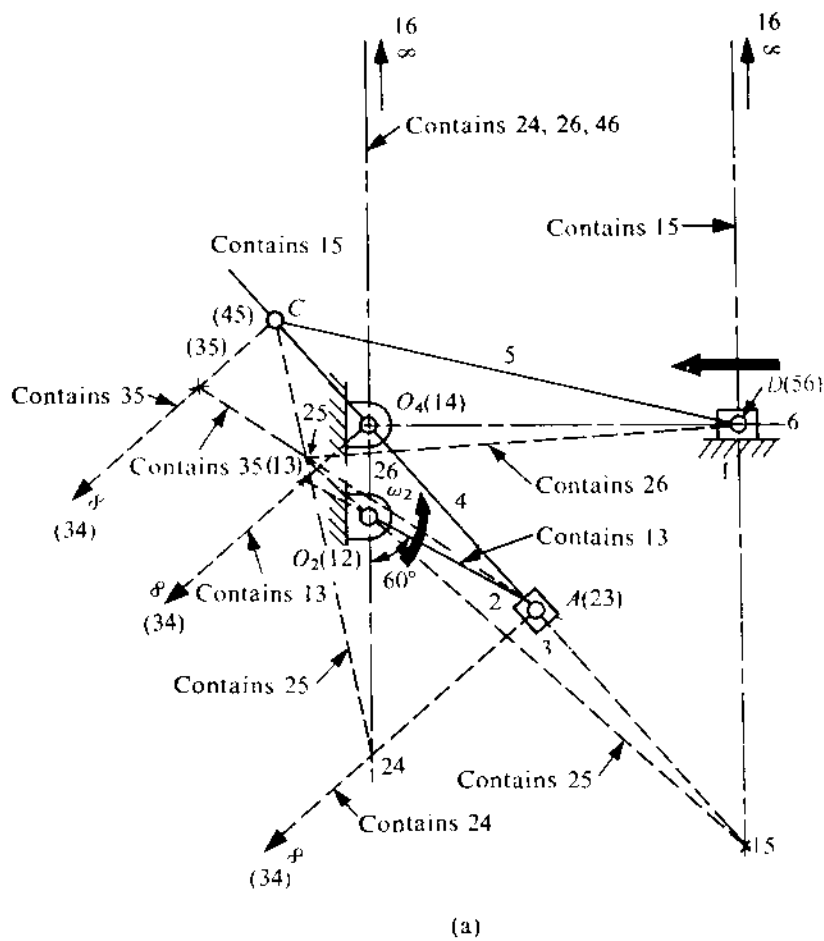
16 at infinity on a vertical line (link 6 is sliding horizontally on 1),

34 at infinity on a line perpendicular to O_4A (link 3 is sliding on 4 along O_4A).

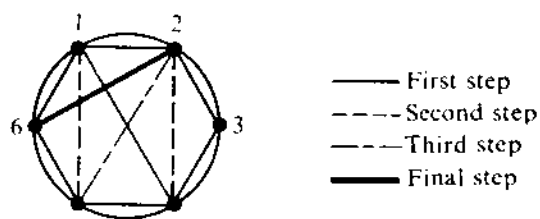
Of the remaining, those with a tick mark (\checkmark) are determined using the Aronhold-Kennedy theorem as explained in the figure.

The instantaneous centres can be determined in a systematic manner by using the *circle diagram*. At first, all the readily available instantaneous centres are determined by observation. In the present problem, the directly obtainable centres are P_{12} , P_{23} , P_{34} , P_{45} , P_{56} , P_{16} , and P_{14} . Now, a circle is drawn and all the links are represented by equally-spaced points on the circumference of the circle as shown in Fig. 2.19b. There are six links, so the points lie on the vertices of a regular hexagon. Let the lines joining two points represent the relative instantaneous centres of the two links. The lines representing the known instantaneous centres are drawn first. Since the motion of link 2 is given and that of link 6 has to be ascertained, it is necessary to find P_{26} which has been shown by the thick line in Fig. 2.19b. If the line representing an unknown instantaneous centre happens to be the common side of two triangles, all the other sides of the triangles being shown by solid lines (i.e., representing known or determined instantaneous centres), the unknown instantaneous centre can be obtained by the Aronhold-Kennedy theorem. So, to find P_{26} , we must first determine P_{25} . Then, 26 becomes the common side of the two triangles 126 and 256. If P_{36} is known, then also P_{26} can be found from triangles 126 and 236. Now, P_{24} and P_{15} can be determined as these are represented by the common sides of triangles 234 and 124 and triangles 145 and 165, respectively. P_{25} can then be found from triangles 125 and 245, with 25 as the common side.

Consider D to be a point on 6. Since ω_2 is given, $\mathbf{V}_{26} = \omega_2 \times \mathbf{O}_2\mathbf{P}_{26}$ (because O_2 is 12 and P_{26} is a point on 2) towards left and in the horizontal direction. Then, considering 26 to be a point on



(a)



(b)

FIGURE 2.19

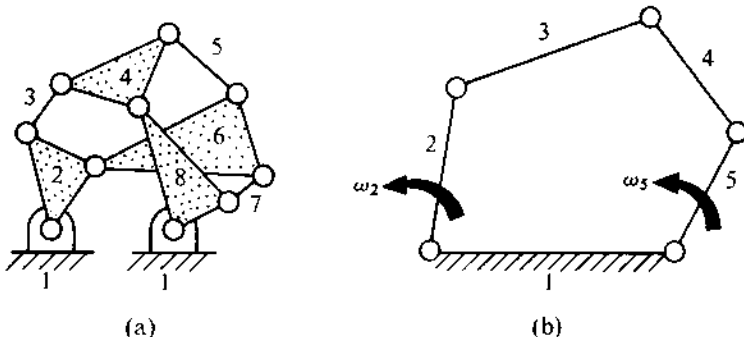


FIGURE 2.20

link 6, $V_D = V_{26}$, as link 6 is in pure translation with respect to the fixed link, i.e., all the points on 6 have the same absolute velocity.

Alternative Approach

Consider D to be a point on link 5. The instantaneous centre 35 is determined by the Aronhold-Kennedy theorem. Now, considering A to be on link 2, $V_A = \omega_2 \cdot O_2 A$, and then taking A to be a point on link 3 ($A \rightarrow 23$, so that it has the same velocity on links 2 and 3), we can find ω_3 and then V_{35} as we have already determined 13.

Consider 35 to be a point on link 5. As 15 is known, the velocity of any point on link 5, and so of point D , can be determined by a similar procedure.

The reader is advised to locate centres 36 and 46, and confirm that V_D , for a given value of ω_2 , obtained by these two alternative methods is the same.

It is not always possible to find out all the relative instantaneous centres by a graphical procedure. For example, for the constrained linkage shown in Fig. 2.20a, the reader can try and satisfy him(her)self that all the relative instantaneous centres cannot be determined geometrically. Similarly, for a mechanism with more than one input (such as the one shown in Fig. 2.20b), all the instantaneous centres cannot be found out graphically.

Velocity and Acceleration Diagrams

The general principle for carrying out the kinematic analysis of most problems is to construct the velocity and acceleration diagrams starting from the input link. In these diagrams, the fixed link is represented by a point. Such a point is called the pole of the velocity diagram or the acceleration diagram. In what follows, we shall work out a few problems to explain the method of constructing velocity and acceleration diagrams using equations (2.16)-(2.21).

PROBLEM 2.9

In the slider-crank mechanism shown in Fig. 2.21a, the crank $O_2 A$ rotates at a constant speed of 1000 rpm in the clockwise direction. Determine the velocity and acceleration of the slider when $\theta_2 = 45^\circ$, given that the crank length $O_2 A = 6$ cm and the connecting-rod length $AB = 16$ cm.

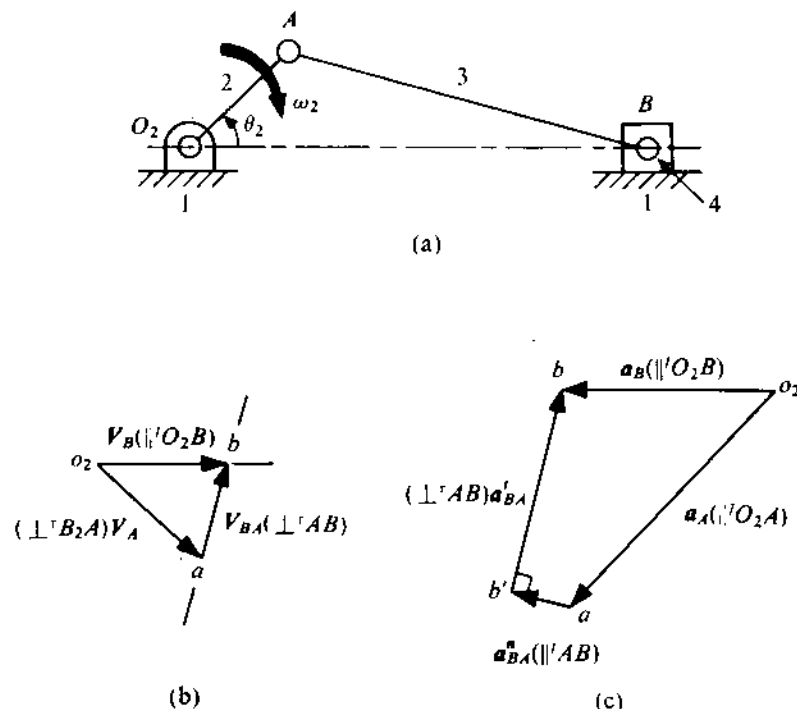


FIGURE 2.21

SOLUTION

The angular velocity of link 2 is³

$$\omega_2 = 1000 \times (2\pi/60) = 105 \text{ rad/s (CW)}.$$

Velocity Analysis (Fig. 2.21b)

The fixed link is represented by the velocity-diagram pole o_2 which also represents the fixed point O_2 on link 2. As A and O_2 are the points on the same rigid body, using (2.16), we have

$$\mathbf{V}_A = \mathbf{V}_{O_2} + \omega_2 \times \mathbf{O}_2 A = \omega_2 \times \mathbf{O}_2 A.$$

The magnitude of \mathbf{V}_A turns out to be $V_A = 630 \text{ cm/s}$ and \mathbf{V}_A is perpendicular to $O_2 A$ in the sense of ω_2 . Hence, \mathbf{V}_A is represented by o_2a . Now, considering B and A as the two points on the rigid link 3, we can write

$$\mathbf{V}_B = \mathbf{V}_A + \omega_3 \times \mathbf{AB}.$$

The direction of \mathbf{V}_B is horizontal and $(\omega_3 \times \mathbf{AB})$ is a vector perpendicular to the connecting rod AB . Since \mathbf{V}_A is completely known, the velocity diagram o_2ab is completed as done in Fig. 2.21b. Using the scale of this diagram, we obtain $V_B = 574 \text{ cm/s}$ (towards right) and, since

$$\omega_3 \times \mathbf{AB} = ab,$$

³The abbreviation CW stands for the clockwise direction.

$$\omega_3 = 27.5 \text{ rad/s (CCW).}$$

Acceleration Analysis (Fig. 2.21c)

The acceleration of point A we have, using (2.17), is $\mathbf{a}_A = \mathbf{a}_{O_2} + \mathbf{a}_{AO_2}^n + \mathbf{a}_{AO_2}^t$. The magnitude of each \mathbf{a}_{O_2} and $\mathbf{a}_{AO_2}^t$ is zero (since ω_2 is constant), whereas that of $\mathbf{a}_{AO_2}^n$ is equal to $\omega_2^2 \cdot O_2A$ and is represented by o_2a in the figure. As before, we write

$$\mathbf{a}_B = \mathbf{a}_A + \mathbf{a}_{BA}^n + \mathbf{a}_{BA}^t,$$

where the magnitude of \mathbf{a}_{BA}^n is

$$a_{BA}^n = \omega_3^2 \cdot AB$$

and its direction is along BA . The direction of \mathbf{a}_B is also known to be horizontal and the acceleration diagram is completed (Fig. 2.21c). Using the scale of the diagram, we have

$$a_B = 46,000 \text{ cm/s}^2 \text{ (towards left).}$$

Since $a_{BA}^t = \alpha_3 \cdot AB$, the angular acceleration of the connecting rod is

$$\alpha_3 = 2845 \text{ rad/s}^2 \text{ (CCW).}$$

PROBLEM 2.10

In the slotted-lever quick-return mechanism shown in Fig. 2.22a, the crank O_2A rotates at a constant speed of 30 rev/min (CCW). For the position shown, determine the velocity and acceleration of the ram (i.e., of the point C). Given $O_2A = 12 \text{ cm}$, $O_2O_4 = 30 \text{ cm}$, $O_4B = 60 \text{ cm}$, and $BC = 15 \text{ cm}$. The line of movement of C is 30 cm above the point O_2 .

SOLUTION

The magnitude of the angular velocity of link 2 is

$$\omega_2 = 2\pi \times (30/60) = 3.14 \text{ rad/s (CCW).}$$

Velocity Analysis (Fig. 2.22b)

The fixed points O_2 and O_4 of the mechanism are represented by the velocity-diagram pole $o_2 (\equiv o_4)$.

Let us consider three coincident points A_2 , A_3 , and A_4 (Fig. 2.22a) belonging to links 2, 3, and 4, respectively. The points A_2 and A_3 always remain coincident, i.e., $\mathbf{V}_{A_3} = \mathbf{V}_{A_2}$. As ω_2 is prescribed, we can write

$$\mathbf{V}_{A_2} = \mathbf{V}_{O_2} + \mathbf{V}_{A_2O_2} = \omega_2 \times \mathbf{O}_2A_2.$$

Thus, in Fig. 2.22b, the vector o_2a_2 has been drawn (to some scale) to represent $\mathbf{V}_{A_2} (\equiv \mathbf{V}_{A_3})$. Now, using (2.18), we can write

$$\mathbf{V}_{A_3} = \mathbf{V}_{A_4} + \mathbf{V}_{A_3A_4},$$

where \mathbf{V}_{A_3} is completely known and the directions of \mathbf{V}_{A_4} (\perp^r to O_4A_4) and $\mathbf{V}_{A_3A_4}$ (\parallel^t to O_4A_4 , i.e., along the slot centreline) are also known.⁴ Hence, the triangle $o_2a_4a_3$ is drawn satisfying the foregoing equation.

⁴The symbols \parallel^t and \perp^r stand for parallel and perpendicular, respectively.

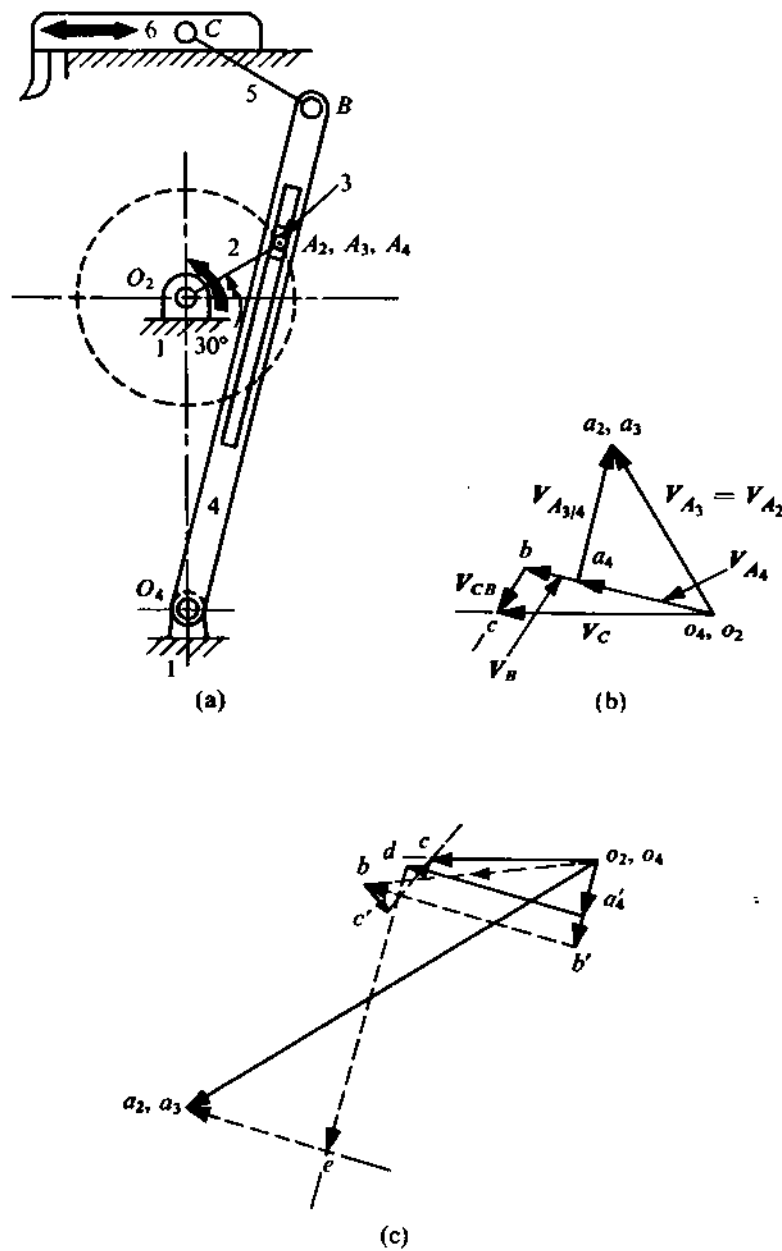


FIGURE 2.22

As $\omega_4 \alpha_4 = V_{A_4} = \omega_4 \times O_4 A_4$, using the scale of the velocity diagram and measuring the length $O_4 A_4$ from Fig. 2.22a, we get

$$\omega_4 = 0.603 \text{ rad/s (CCW).}$$

Again, from Fig. 2.22b, $V_{A_{3/4}} = 27 \text{ cm/s}$. Now, considering the two points B and O_4 on link 4, we determine

$$V_B = V_{O_4} + V_{B_4 O_4} = \omega_4 \times O_4 B_4$$

represented by $\omega_4 b$. Then, considering C and B , we can write

$$V_C = V_B + V_{CB} = V_B + \omega_5 \times BC,$$

where the directions of V_C (horizontal) and V_{CB} (\perp^r to BC) are known and V_B has already been completely determined. The velocity triangle $\omega_4 bc$ has been so drawn that it satisfies the foregoing equation, and V_C , as determined from the velocity diagram, is

$$V_C = 40 \text{ cm/s (towards left).}$$

The angular velocity of link 5 is determined from $V_{CB} (\equiv bc)$ as

$$\omega_5 = 0.667 \text{ rad/s (CCW).}$$

Acceleration Analysis (Fig. 2.22c)

The acceleration of the points A_2 and A_3 is the same (as these always remain coincident), i.e., $a_{A_2} = a_{A_3}$. Now a_{A_2} can be determined from (2.17) as

$$a_{A_2} = a_{O_2} + a_{A_2 O_2}^n + a_{A_2 O_2}^t,$$

where each of a_{O_2} and $a_{A_2 O_2}^t$ is zero and $a_{A_2 O_2}^n$ is parallel to $A_2 O_2$ and has a magnitude $\omega_2^2 \cdot O_2 A_2$. Thus, $a_{A_2} (\equiv a_{A_3})$ is represented by $\omega_2 a_2 (\equiv \omega_2 a_3)$ to some scale in Fig. 2.22c. Using (2.20), we can write

$$\begin{aligned} a_{A_3} &= a_{A_4} + a_{A_{3/4}} + a_c = a_{A_4 O_4} + a_{A_{3/4}} + 2\omega_4 \times V_{A_{3/4}} \\ &= a_{A_4 O_4}^n + a_{A_4 O_4}^t + a_{A_{3/4}} + 2\omega_4 \times V_{A_{3/4}}. \end{aligned}$$

In these equations, the vectors a_{A_3} , $a_{A_4 O_4}^n$, a_c can be completely determined (using the results obtained in the velocity analysis) and the directions of the other two vectors are known. So, the acceleration polygon $\omega_4 a'_4 d e_3$ is completed and it satisfies the foregoing equations. In this diagram,

$$\omega_4 a'_4 = a_{A_4 O_4}^n \quad \text{with} \quad a_{A_4 O_4}^n = \omega_4^2 \cdot O_4 A_4,$$

$$a'_4 d = a_c,$$

$$d e = a_{A_{3/4}},$$

$$e a_3 = a_{A_4 O_4}^t = \alpha_4 \times O_4 A_4.$$

So, from $e a_3$, the angular acceleration α_4 of link 4 is 0.897 rad/s^2 (CCW).

We can now determine the acceleration of the point B as

$$\mathbf{a}_B = \mathbf{a}_{BO_4} = \mathbf{a}_{BO_4}^n + \mathbf{a}_{BO_4}^t = \omega_4 \times (\boldsymbol{\omega}_4 \times \mathbf{O}_4B) + \boldsymbol{\alpha}_4 \times \mathbf{O}_4B.$$

This is represented in Fig. 2.22c by

$$\mathbf{o}_4b = \mathbf{o}_4b' + \mathbf{b}'\mathbf{b} = \mathbf{a}_{BO_4}^n + \mathbf{a}_{BO_4}^t.$$

Finally, considering C and B as two points on link 5, we can write

$$\mathbf{a}_C = \mathbf{a}_B + \mathbf{a}_{CB}^n + \mathbf{a}_{CB}^t,$$

where $\mathbf{a}_{CB} [= \boldsymbol{\omega}_5 \times (\boldsymbol{\omega}_5 \times BC)]$ and \mathbf{a}_B are completely known and the directions of \mathbf{a}_C (horizontal) and \mathbf{a}_{CB}^t (\perp to BC) are known. So, the acceleration polygon $\mathbf{o}_4bc'c$ can be completed, where $\mathbf{bc}' = \mathbf{a}_{CB}^n$. Hence, \mathbf{a}_C is determined as

$$\mathbf{a}_C = 43.8 \text{ cm/s}^2 \text{ (towards left).}$$

It may again be emphasized that $\mathbf{a}_{A_3A_4} \neq \mathbf{a}_{A_{3/4}}$. From (2.20), we see that

$$\mathbf{a}_{A_3A_4} = \mathbf{a}_{A_3} - \mathbf{a}_{A_4} = \mathbf{a}_{A_{3/4}} + \mathbf{a}_c.$$

This is given by $d\mathbf{e} + \mathbf{a}'_4d = \mathbf{a}'_4\mathbf{e}$ in Fig. 2.22c.

From the two foregoing examples, it should be noted that two scalar unknowns can be found from a vector equation. In other words, from a vector equation, two magnitudes or two directions or a magnitude and a direction can be determined.

PROBLEM 2.11

An RPRP linkage is shown in Fig. 2.23a. At the configuration indicated in the figure, $\omega_2 = 2 \text{ rad/s}$ (CCW) and $\boldsymbol{\alpha}_2 = 4 \text{ rad/s}^2$ (CW). Determine the velocity and acceleration of slider 4 at this instant.

SOLUTION

Consider the three instantaneously coincident points P_2 , P_3 , and P_4 as indicated in Fig. 2.23a. It is obvious that $P_3 \equiv P_4$. The path of P_3 (i.e., also of P_4) in link 2 is a straight line parallel to O_2A . This path can be easily visualized by holding 2 fixed (and making link 1 free). The prismatic pair between 2 and 3 allows P_3 to move only parallel to O_2A (the direction of the prismatic pair).

Velocity Analysis (Fig. 2.23b)

From (2.18), we can write

$$\mathbf{V}_{P_4} = \mathbf{V}_{P_2} + \mathbf{V}_{P_{4/2}},$$

where $\mathbf{V}_{P_2} = \omega_2 \cdot O_2P_2 = 10 \text{ cm/s}$ in the vertically upward direction. $\mathbf{V}_{P_{4/2}}$ is also vertical (along the path of P_4 on 2 which has already been identified as vertical) and \mathbf{V}_{P_4} is horizontal (due to the horizontal prismatic pair between 1 and 4). Since both the vectors on the right-hand side of the above equation are vertical, the conclusion is $\mathbf{V}_{P_4} = 0$ and $\mathbf{V}_{P_{4/2}} = 10 \text{ cm/s}$ in the vertically downward direction. Slider 4 is momentarily at rest. (The students are advised to reach the same conclusion by using the method of instantaneous centres.)

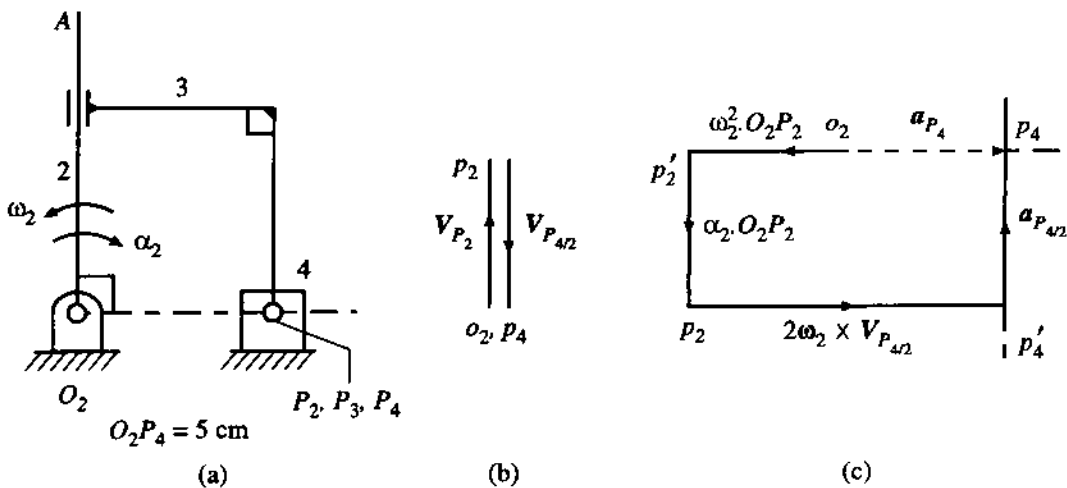


FIGURE 2.23

Acceleration Analysis (Fig. 2.23c)

From (2.21), we can write

$$a_{p_4} = a_{p_2} + a_{p_{4/2}}^n + a_{p_{4/2}}^t + 2\omega_2 \times V_{p_{4/2}}, \quad (\text{a})$$

where \$a_{p_2} = a_{p_2}^n + a_{p_2}^t\$ is completely known with \$a_{p_2}^n = \omega_2^2 O_2 p_2 (= 20 \text{ cm/s}^2)\$ in the direction \$P_2 O_2\$ and is represented by \$o_2 p'_2\$ in Fig. 2.23c. Similarly, \$a_{p_{4/2}}^t = \alpha_2 O_2 p_{4/2} (= 20 \text{ cm/s}^2)\$ in the vertically downward direction and is represented by \$p'_2 p_2\$ in Fig. 2.23c. Then the Coriolis component \$2\omega_2 \times V_{p_{4/2}} (= 40 \text{ cm/s}^2)\$ in the horizontal (towards right) direction is represented by \$p_2 p'_4\$ in Fig. 2.23c.

Now \$a_{p_{4/2}}^n = 0\$ (because of the straight-line path of \$P_4\$ in link 2). Therefore, \$a_{p_{4/2}} = a_{p_{4/2}}^t\$, the direction of which is known to be vertical.

Further, the direction of \$a_{p_4}\$ is known to be horizontal. Thus, the acceleration diagram, shown in Fig. 2.23c, satisfies equation (a). It is now readily seen that \$a_{p_4} = 20 \text{ cm/s}^2\$ horizontally to the right.

PROBLEM 2.12

Consider Problem 2.9 again. Determine the point on the connecting rod which has zero acceleration at this instant.

SOLUTION

The mechanism is redrawn in Fig. 2.24a and the acceleration of two points (\$A\$ and \$B\$) of the connecting rod is reproduced (from Fig. 2.21c) as \$o_2a\$ and \$o_2b\$ in Fig. 2.24b. The points \$a\$ and \$b\$ are the images of \$A\$ and \$B\$. The image of the point \$(O_{13})\$ on the connecting rod which has zero acceleration is the pole of the acceleration diagram \$o_2\$. The point \$O_{13}\$ is located in Fig. 2.24a using the fact that the triangles \$O_{13}AB\$ and \$o_2ab\$ are similar as explained in Figs. 2.24a and 2.24b. We

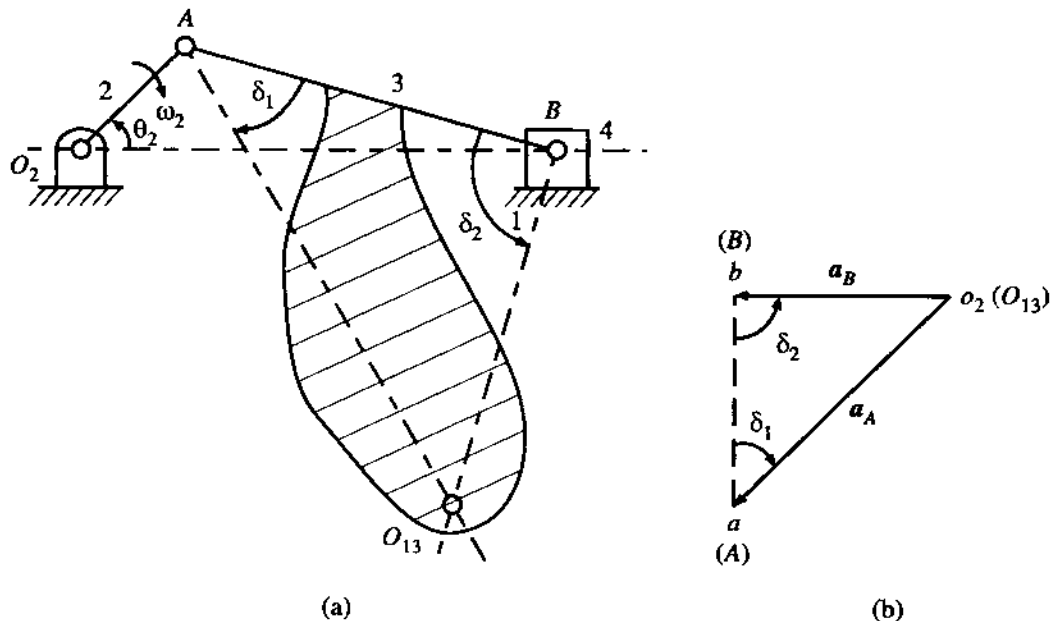


FIGURE 2.24

may note that the point on the connecting rod which has zero velocity at this instant (i.e., the instantaneous centre I_{13}) is located at the intersection of O_2A and a vertical line through B and, therefore, is different from O_{13} .

PROBLEM 2.13

Figure 2.25a shows a Geneva mechanism (used to produce intermittent rotary motion from continuous rotation) with curved slots in the output member 3. The centre of curvature of the slot (at the location of pin P_2) is at C . Given $\omega_2 = 30 \text{ rad/s}$ (CW) and it is constant. Determine ω_3 and α_3 at the instant shown.

SOLUTION

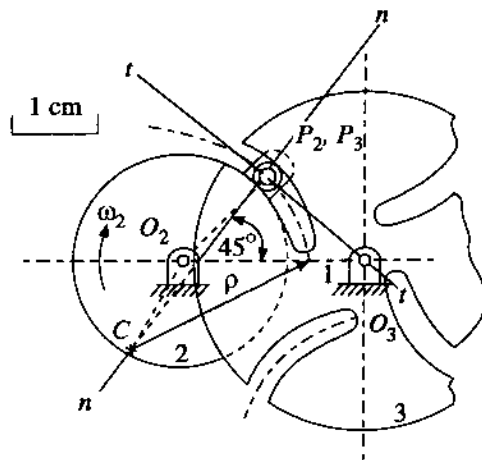
Consider two instantaneously coincident points P_2 and P_3 (Fig. 2.25a). From measurements, $O_2P_2 = 1.6 \text{ cm}$, $O_3P_3 = 1.8 \text{ cm}$, and $\rho = 2.8 \text{ cm}$. The path of P_2 in 3 is the curved slot whose tangent and normal at this instant are along $t-t$ and $n-n$, respectively.

Velocity Analysis (Fig. 2.25b)

From (2.18), we can write

$$\mathbf{V}_{P_2} = \mathbf{V}_{P_3} + \mathbf{V}_{P_{2/3}}, \quad (a)$$

where $\mathbf{V}_{P_2} (= \omega_2 \cdot O_2P_2 = 48 \text{ cm/s})$ is in a direction perpendicular to O_2P_2 and in the sense of ω_2 and is represented by $\mathbf{o}_2\mathbf{p}_2$ in Fig. 2.25b. The direction of \mathbf{V}_{P_3} is perpendicular to O_3P_3 and



(a)

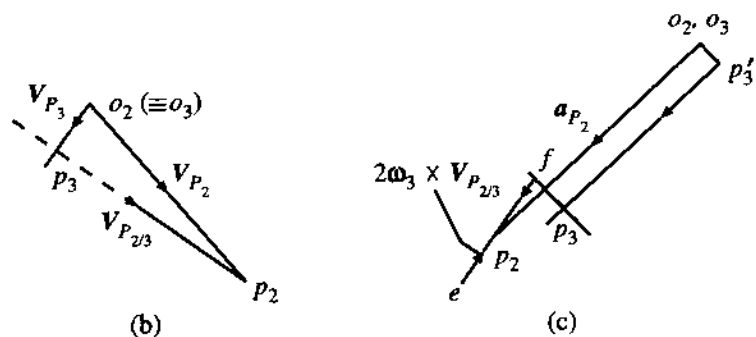


FIGURE 2.25

that of $\mathbf{V}_{P_{2/3}}$ is along $t-t$ (tangent to the curved slot at P_2). Thus, the velocity diagram, shown in Fig. 2.25b, satisfies equation (a). From measurements, we get $o_3p_3 = V_{P_3} = 8 \text{ cm/s} = \omega_3 \cdot O_3P_3$. Therefore, $\omega_3 = 4.44 \text{ rad/s}$ (CCW) (the direction is judged from the direction of \mathbf{V}_{P_3}). Further, $p_3p_2 = V_{P_{2/3}} = 47.8 \text{ cm/s}$.

Acceleration Analysis (Fig. 2.25c)

From (2.21), we can write

$$\begin{aligned}\mathbf{a}_{P_2} &= \mathbf{a}_{P_3} + \mathbf{a}_{P_{2/3}}^n + \mathbf{a}_{P_{2/3}}^t + 2\omega_3 \times \mathbf{V}_{P_{2/3}} \\ &= \mathbf{a}_{P_3}^n + \mathbf{a}_{P_3}^t + \mathbf{a}_{P_{2/3}}^n + \mathbf{a}_{P_{2/3}}^t + 2\omega_3 \times \mathbf{V}_{P_{2/3}}.\end{aligned}\quad (b)$$

First, we should note that there are only two unknowns (at this stage) in equation (b), namely, the magnitudes of $\mathbf{a}_{P_3}^t$ and $\mathbf{a}_{P_{2/3}}^t$. Hence, the acceleration diagram (Fig. 2.25c) can be completed.

In Fig. 2.25c: $\mathbf{o}_2p_2 = \mathbf{a}_{P_2}$ of magnitude $\omega_2^2 \cdot O_2P_2 = 1440 \text{ cm/s}^2$ and direction parallel to P_2O_2 (because $\alpha_2 = 0$), $\mathbf{o}_3p_3 = \mathbf{a}_{P_3}^n$ of magnitude $\omega_3^2 \cdot O_3P_3 = 35.55 \text{ cm/s}^2$ and direction parallel to P_3O_3 , $\mathbf{ep}_2 = 2\omega_3 \times \mathbf{V}_{P_{2/3}}$ of magnitude $2\omega_3 V_{P_{2/3}} = 426.24 \text{ cm/s}^2$, $\mathbf{fe} = \mathbf{a}_{P_{2/3}}^t$ of magnitude $V_{P_{2/3}}^2/\rho = 822.86 \text{ cm/s}^2$ and direction parallel to P_3C ($= n-n$), $\mathbf{p}_3f = \mathbf{a}_{P_{2/3}}^t$ in the direction parallel to $t-t$, $\mathbf{p}_3'p_3 = \mathbf{a}_{P_3}^t$ in the direction perpendicular to O_3P_3 . The point p_3 is determined by the intersection of the last two vectors mentioned above. So finally, from measurement, we get

$$\alpha_3 = \frac{a_{P_3}^t}{O_3P_3} = \frac{1020}{1.8} = 566.7 \text{ rad/s}^2$$

(CCW - the direction is judged from the direction of $\mathbf{a}_{P_3}^t$, i.e., $\mathbf{p}_3'p_3$).

2.8 ACCELERATION ANALYSIS OF COMPLEX MECHANISMS

If the radii of curvature of the paths traversed by the *motion-transfer points*⁵ of all links comprising a mechanism are known, the acceleration analysis of the mechanism can be completed by the direct use of the method already explained in Problems 2.9-2.13. For example, in Problem 2.9, the radius of curvature of the motion-transfer point A is O_2A and that of B is infinity. Sometimes, the concept of acceleration image may have to be used. Under these circumstances, the mechanism is said to be kinematically simple. But if a mechanism has a ternary or higher-order *floating link* (i.e., one which is not connected to the frame), the direct successive application of the acceleration-difference equation of the form $\mathbf{a}_B = \mathbf{a}_A + \mathbf{a}_{BA}$ (where A and B are the motion-transfer points of a link) may fail to complete the acceleration analysis. Such a mechanism is considered to be *kinematically complex*. Figure 2.26 shows two such mechanisms.

In the mechanism shown in Fig. 2.26a, if 2 is the input link, \mathbf{a}_B cannot be determined from \mathbf{a}_A as the radius of path curvature of B is not known. However, if in the same mechanism the input link is 6 or 5, then \mathbf{a}_C and \mathbf{a}_D can be determined. Thereafter, by using the image of BCD , we can obtain \mathbf{a}_B . Such mechanisms as become simple mechanisms by changing the input link are called complex mechanisms with a *low degree of complexity*. This transformation to a simple mechanism, by changing the input link from 2 to 6, is not possible for the mechanism shown in Fig. 2.26b. Such a mechanism is said to have a *high degree of complexity*. If the radii of path curvature of two

⁵The motion-transfer points of a link are the points responsible for transferring motion to other connected links.

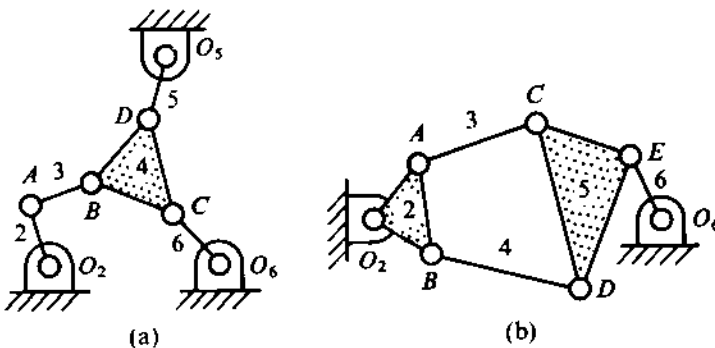


FIGURE 2.26

(or more) motion-transfer points of the floating link are known, the mechanism has a low degree of complexity. Otherwise, the mechanism will have a high degree of complexity. Special methods have to be adopted for the analysis of complex mechanisms; a few of these are discussed in this chapter. Yet another way is to first determine the unknown radius of path curvature geometrically. This can be accomplished by using the famous Euler-Savary equation. This equation and its use for the determination of path curvature and acceleration analysis are not included in this text. The interested reader may refer to any advanced text on kinematics (e.g., Mallik, A.K., Ghosh, A. and Dittrich, G., Kinematic Analysis and Synthesis of Mechanisms, CRC Press, Boca Raton, 1994).

Method of Normal Accelerations

This method is applicable only to mechanisms having a low degree of complexity. It is also useful as a supplement to the auxiliary-point method (discussed later) for certain mechanisms with a high degree of complexity when the latter method alone is not sufficient. The underlying principle of the method is that the acceleration component of a point P on a constrained link, in a direction perpendicular to its velocity (called normal component), is independent of the angular acceleration of the link. Thus, $a_P^n = V_{P/\rho P}^2$, where ρ_P is the instantaneous radius of curvature of the path of point P . The steps to be followed in applying this method are:

1. Transform the mechanism into a simple one by changing the input link.
2. Carry out the velocity analysis with this alternative input link, and determine the true velocities. This step will be clear from Problem 2.14.⁶
3. Draw an *auxiliary acceleration diagram* based on true velocities and zero acceleration of the alternative input link. Determine the normal component of acceleration of the floating point which has a path of unknown radius of curvature.
4. Construct the *true acceleration diagram* with the actual input acceleration, using the information obtained in steps 1-3.

PROBLEM 2.14

In the mechanism shown in Fig. 2.27a, $\omega_2 = 10 \text{ rad/s}$ (CW) (constant). Determine ω_6 and α_6 . Given

$$O_2A = 7.5 \text{ cm}, \quad AB = 5 \text{ cm}, \quad BC = 7.5 \text{ cm},$$

⁶It should be noted that the velocity diagram can be completed without any reference to the actual magnitude of the velocities. Only the scale of the diagram will vary according to the magnitude of the input velocities.

$$O_5C = 6.25 \text{ cm} \text{ (and is vertical)}, \quad CD = 10 \text{ cm},$$

$$BD = 5 \text{ cm}, \quad O_6D = 5 \text{ cm},$$

$$\angle O_2AB = 110^\circ, \quad \angle ABC = 115^\circ, \quad \angle O_6DB = 117^\circ.$$

SOLUTION

With link 2 as the driving link, the mechanism is complex, but with link 6 as driving, the mechanism is transformed into a simple one.

Velocity Analysis

The velocity diagram in Fig. 2.27b is drawn to some scale assuming link 6 to be the input link. When the diagram is completed, its scale is determined by $V_A = \omega_2 \cdot O_2A = 75 \text{ cm/s}$ in the direction obtained in the diagram (the scale could have been negative due to a wrong choice of the sense of V_D and V_C , when V_A from the diagram would have been opposite to the actual sense). Having determined the scale, all velocities can be obtained as

$$V_D = 140 \text{ cm/s}, \quad \omega_6 = \frac{V_D}{O_6D} = 28 \text{ rad/s (CCW)},$$

$$\omega_3 = 25.8 \text{ rad/s (CCW)}, \quad \omega_4 = 18.66 \text{ rad/s (CW)}, \quad \omega_5 = 14.9 \text{ rad/s (CCW)}. \quad \curvearrowright$$

Acceleration Analysis

An auxiliary acceleration diagram (Fig. 2.27c) is drawn with 6 as the input link and taking $\alpha_6 = 0$, based on the actual velocities already obtained. $\overset{\circ}{a}_B$ is obtained from this diagram ($\overset{\circ}{a}_B$ means the *auxiliary acceleration* of the point B).

From $\overset{\circ}{a}_B$ and $\overset{\circ}{a}_D$, $\overset{\circ}{a}_B^n (\perp^r \text{ to } V_B)$ and $\overset{\circ}{a}_D^n (\perp^r \text{ to } V_D)$ are obtained as shown in Fig. 2.27d.

Obviously, in this case, $\overset{\circ}{a}_D^n = \overset{\circ}{a}_D$ as α_6 is taken to be zero.

As $\overset{\circ}{a}_B^n = \overset{\circ}{a}_B$, and $\overset{\circ}{a}_D^n = \overset{\circ}{a}_D$, we can draw the true acceleration diagram with 2 as the input link;

this is shown in Fig. 2.27e where

$$\alpha_2 d = a_D, \quad d'd = a_{DO_6}^t = O_6D \cdot \alpha_6, \quad \alpha_6 = 320 \text{ rad/s}^2 \text{ (CW)}.$$

The completion of the acceleration analysis and the determination of α_3 , α_4 (already shown in Fig. 2.27e), and α_5 are left as an exercise for the reader.

Auxiliary-point Method

The auxiliary-point method is very powerful and is applicable to all low-complexity mechanisms and to most high-complexity mechanisms. In certain cases of high-complexity mechanisms, this method alone may not be sufficient and has to be used in conjunction with the method of normal components.

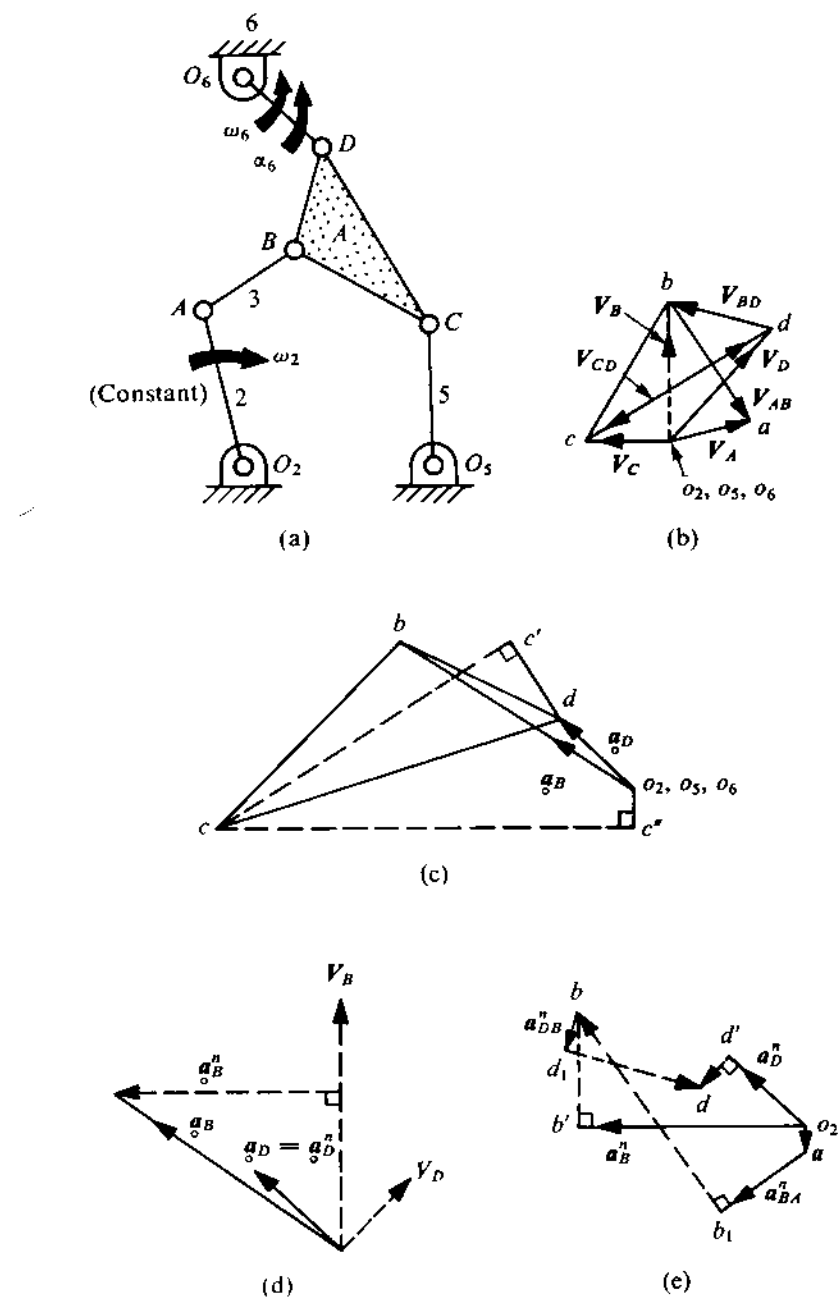


FIGURE 2.27

In this method, the *auxiliary points* are determined on the higher-order floating link at the intersection of *auxiliary lines* drawn through the motion-transfer point of the link in directions along which components of velocities and accelerations can be obtained. Two such auxiliary points are sufficient. The velocity and acceleration components of these two auxiliary points are obtained in two auxiliary directions (along which they lie). Thereby, the vector itself can be obtained. Once the velocities and accelerations of the two auxiliary points have been determined, the analysis can be completed with the help of images of the floating links. These principles will be clear from the solution of Problem 2.15.

PROBLEM 2.15

Solve Problem 2.14 by the auxiliary-point method.

SOLUTION

In Fig. 2.28a, BCD (link 4) is a ternary floating link with B , C , and D as its motion-transfer points. Three auxiliary lines I , II , and III are drawn through B , C , and D in the directions of the connecting links as shown. So, X , Y , and Z are the auxiliary points on the ternary link 4. Two of these are sufficient; let us consider X and Y .

Velocity Analysis

Through the pole o of the velocity diagram (Fig. 2.28b), three lines are drawn parallel to the auxiliary directions. V_A is laid out to some scale (oa). As $V_{BA}^I = 0$ and $V_{XB}^I = 0$, we have

$$V_X^I = V_B^I + V_{XB}^I = V_A^I + V_{BA}^I + V_{XB}^I = V_A^I.$$

Thus, the point x lies on the line through a drawn perpendicular to I . Again,

$$V_D^{II} = 0, \quad V_{XD}^{II} = 0, \quad V_X^{II} = V_D^{II} + V_{XD}^{II} = 0.$$

Therefore, the point x lies on the line through o drawn perpendicular to II . Thus, x is determined. Similarly,

$$V_Y^{III} = 0 \quad (\text{as } V_{YD}^{III} = 0, V_D^{III} = 0), \quad V_Y^{III} = 0 \quad (\text{as } V_C^{III} = 0, V_{YC}^{III} = 0).$$

As the components of V_Y are zero in two different directions, $V_Y = 0$. So, y is at the pole o . Once x and y are determined, the points b , c , and d are obtained by the velocity image of link 4 as all these points are on link 4. So, all the velocities are obtained from this diagram and

$$\omega_3 = \frac{V_{BA}^t}{AB} = \frac{V_{BA}}{AB} = \frac{ab}{AB} = 25.8 \text{ rad/s (CCW)}.$$

Acceleration Analysis (Fig. 2.28c)

Through the acceleration pole o , three lines are drawn parallel to the auxiliary directions I , II , and III . a_A is laid out to scale from which a_A^I is obtained. Then, we can get a_X as follows:

$$\begin{aligned} a_X^I &= a_A^I + a_{BA}^I + a_{XB}^I \quad (\text{all towards } A) \\ &= a_A^I + \omega_3^2 \cdot AB + \omega_4^2 \cdot BX \\ &= oa' + a'b' + b'x' \\ &= ox'. \end{aligned}$$

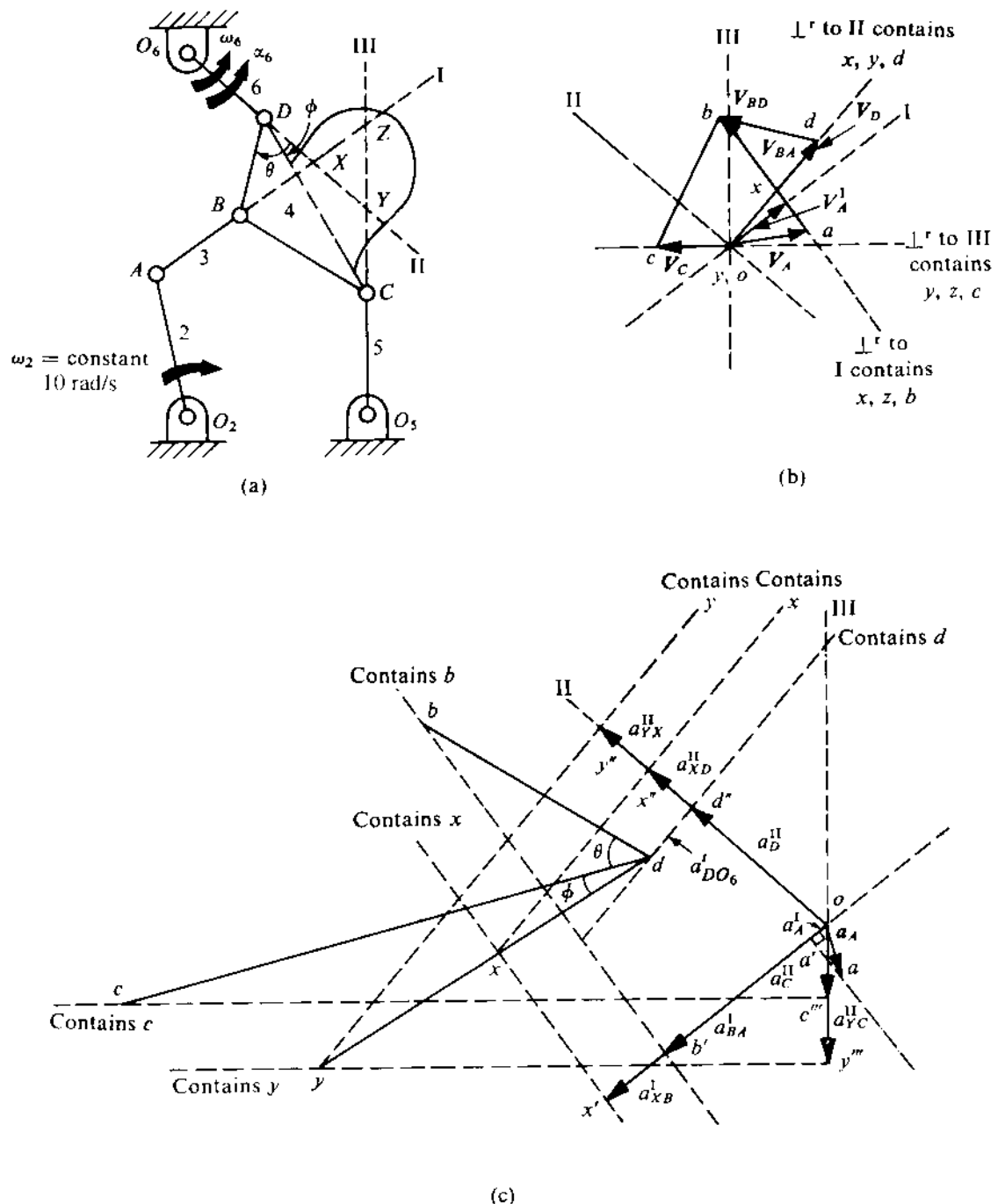


FIGURE 2.28

So, x lies on the line through x' drawn perpendicular to direction I . Similarly,

$$\begin{aligned} a_X^{II} &= a_D^{II} + a_{XD}^{II} \quad (\text{both towards } O_6) \\ &= \omega_6^2 \cdot O_6 D + \omega_4^2 \cdot X D \quad (\text{as } a_D^{II} = a_{DO_6}^n - \omega_6^2 \cdot O_6 D) \\ &= o d'' + d'' x'' \\ &= o x''. \end{aligned}$$

So, x lies on the line through x'' drawn perpendicular to direction II . Thus, the point x is obtained. Similarly, y is obtained from

$$\begin{aligned} a_Y^{II} &= a_X^{II} + a_{YX}^{II} \\ &= o x'' + x'' y'' \quad (= \omega_4^2 \cdot X Y) \\ &= o y'', \end{aligned}$$

$$\begin{aligned} a_Y^{III} &= a_C^{III} + a_{YC}^{III} \quad (\text{both towards } O_5) \\ &= \omega_5^2 \cdot O_5 C + \omega_4^2 \cdot Y C \quad (\text{as } a_C^{III} = a_{CO_5}^n - \omega_5^2 \cdot O_5 C) \\ &= o c''' + c''' y''' \\ &= o y''' \end{aligned}$$

Once both x and y are determined, the points b , c , and d can be obtained from the image of link 4. For example, d , x , and y must be on the same line and in this sequence. d is obtained from the relation $dx/dy = DX/DY$. (It may be checked that d lies on the line through d'' drawn perpendicular to II so that the value of a_D^{II} so determined agrees with that obtained before.)

The procedure for obtaining b and c has been explained in Fig. 2.28c. As $a_B^I = a_A^I + a_{BA}^I - o b'$, b lies on a line through b' drawn \perp^r to I . Similarly, since $a_C^{III} = o c'''$, c lies on a line through c''' drawn \perp^r to III . (Further, check that $bd/BD = cd/CD = bc/BC$.) Since $d''d = a_{DO_6}^t$, we get

$$\alpha_6 = \frac{a_{DO_6}^t}{O_6 D} = 320 \text{ rad/s}^2 \quad (\text{CW}).$$

In Problem 2.15, all the motion-transfer points B , C , and D of the floating link have hinged joints and the auxiliary lines are drawn through them in the directions of the connecting links. However, we may encounter situations in which the floating link may not have hinged joints at all motion-transfer points. One such case is shown in Fig. 2.29, where a higher-order floating link also has one prismatic pair. In this figure, D is the centre of the sliding block and E is on the floating link (motion-transfer point) which is instantaneously coincident with D . The reasons for the choice of the three auxiliary directions I , II , and III will be clear from the following analyses.

Velocity Analysis

\mathbf{V}_A and \mathbf{V}_D are known and \mathbf{V}_C is horizontal. Thus, V_A^{III} , V_D^{II} , and V_C^I ($= 0$) are known. As $V_{ED}^{II} = 0$ and $V_{XE}^{II} = 0$, $V_X^I (= V_D^{II} + V_{ED}^{II} + V_{XE}^{II})$ can be determined. Similarly, $V_X^I = V_C^I + V_{XC}^I = 0 + 0 = 0$. Thus, \mathbf{V}_X can be obtained. Again,

$$V_Z^I = 0, \quad V_Z^{III} = V_A^{III} + V_{BA}^{III} + V_{ZB}^{III} = V_A^{III} \quad (\text{others being zero}).$$

So, \mathbf{V}_Z can also be determined.

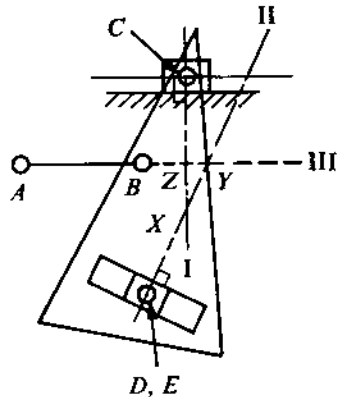


FIGURE 2.29

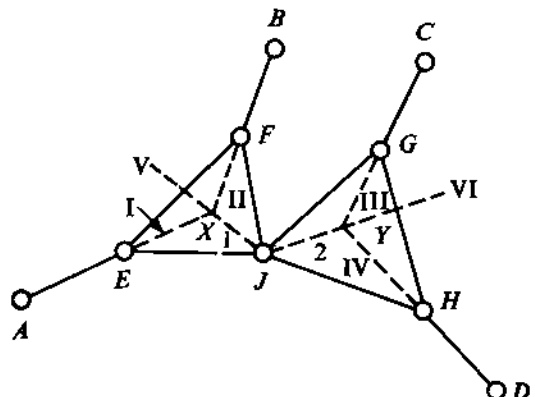


FIGURE 2.30

Acceleration Analysis

α_A , α_D are known and α_C is horizontal. So, a_A^{II} , a_D^{II} , and a_C^I ($= 0$) are known. Then, α_X can be determined as follows:

$a_{ED}^{II} = -\alpha_c = -2\omega_f \times \mathbf{V}_{D/f}$ (where f denotes the floating link), since $\alpha_{D/f}$ is perpendicular to II , i.e., along the slot and $a_{XE}^{II} = \omega_f^2 \cdot XE$ (known).

So, a_X^{II} ($= a_D^{II} + a_{ED}^{II} + a_{XE}^{II}$), a_X^I ($= a_C^I + a_{XC}^I = 0 + \omega_f^2 \cdot XC$), and α_x are obtained.

Similarly,

$$a_Z^I = a_C^I + a_{ZC}^I = 0 + \omega_f^2 \cdot ZC,$$

$$a_Z^{III} = a_A^{III} + a_{BA}^{III} + a_{ZB}^{III} = a_A^{III} + \omega_{AB}^2 \cdot AB + \omega_f^2 \cdot ZB.$$

Thus, α_z can also be obtained.

If two ternary links (say, 1 and 2) of a mechanism are connected physically as shown in Fig. 2.30, the analysis has to be carried out in two steps with the help of six auxiliary directions. An explanation of this follows.

The accelerations of the points A , B , C , and D are known. From α_A and α_B , α_X can be determined as

$$a_X^I = a_A^I + a_{EA}^I + a_{XE}^I = a_A^I + \omega_{AE}^2 \cdot AE + \omega_1^2 \cdot XE,$$

$$a_X^{II} = a_B^{II} + a_{FB}^{II} + a_{XF}^{II} = a_B^{II} + \omega_{BF}^2 \cdot BF + \omega_1^2 \cdot XF.$$

Similarly, α_Y is determined from α_C and α_D . Now, from α_X and α_Y , we can determine α_J as

$$a_J^V = a_X^V + a_{JX}^V = a_X^V + \omega_1^2 \cdot JX,$$

$$a_J^{VI} = a_Y^{VI} + a_{JY}^{VI} = a_Y^{VI} + \omega_2^2 \cdot JY.$$

From α_J and α_X , by the acceleration image of link 1, the accelerations of the points E and F can be determined. Similarly, from α_J and α_Y , the accelerations of the points G and H can be obtained.

In Problem 2.15, we considered a mechanism with a low degree of complexity as shown in Fig. 2.26a. Let us now consider a mechanism, shown in Fig. 2.26b, which has a high degree of complexity.

In Fig. 2.31, three auxiliary lines and two auxiliary points X and Y on link 5 are shown. Let us now consider the following two different cases:

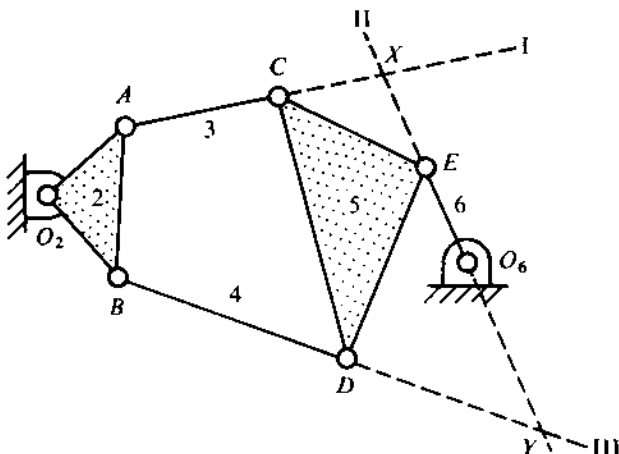


FIGURE 2.31

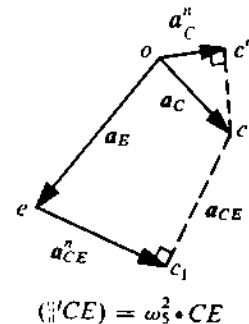


FIGURE 2.32

- (i) Link 2 is the input link when \mathbf{V}_A , \mathbf{V}_B , a_A , and a_B are known. To determine ω_6 and α_6 , the analysis can be carried out as

$$V_X^I = V_A^I + V_{CA}^I + V_{XC}^I = V_A^I,$$

$$V_X^{II} = V_E^I + V_{XE}^{II} = 0,$$

$$V_Y^{II} = V_E^{II} + V_{YE}^{II} = 0,$$

$$V_Y^{III} = V_B^{III} + V_{DB}^{III} + V_{YD}^{III} = V_B^{III},$$

$$a_X^I = a_A^I + a_{CA}^I + a_{XC}^I = a_A^I + \omega_{AC}^2 \cdot AC + \omega_5^2 \cdot XC \text{ (all towards } A\text{),}$$

$$a_X^{II} = a_E^{II} + a_{XE}^{II} = \omega_6^2 \cdot O_6 E + \omega_5^2 \cdot XE \text{ (all towards } O_6\text{),}$$

$$a_Y^{II} = a_E^{II} + a_{YE}^{II} = \omega_6^2 \cdot O_6 E - \omega_5^2 \cdot YE \text{ (as these two are in the opposite sense),}$$

$$a_Y^{III} = a_B^{III} + a_{DB}^{III} + a_{YD}^{III} = a_B^{III} + \omega_4^2 \cdot BD + \omega_5^2 \cdot YD \text{ (all towards } B\text{).}$$

- (ii) Link 6 is the input link when \mathbf{V}_E and a_E are known. To determine ω_2 and α_2 , the velocity analysis is carried out by drawing \mathbf{V}_A and \mathbf{V}_B to some arbitrary scale in the proper directions with magnitudes proportional to O_2A and O_2B , respectively, i.e., $V_A/V_B = O_2A/O_2B$. The rest of the analysis is carried out as in (i) and the scale of the diagram follows from the known value of V_E . So, V_A is known and ω_2 can be found out.

The acceleration analysis is carried out by the method of normal components. An auxiliary acceleration diagram is constructed on the basis of true velocities with the alternative input link 2 having zero acceleration [as explained in (i), because now $\overset{\circ}{a}_A$ and $\overset{\circ}{a}_B$ are known]. From this

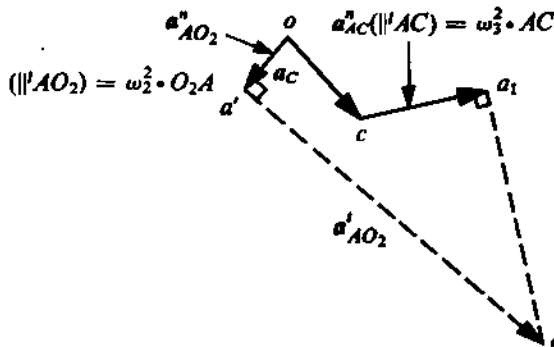


FIGURE 2.33

auxiliary acceleration diagram, the normal components of acceleration a_C^n and a_D^n are obtained. With any one of these known (say, a_C^n), the actual acceleration diagram can be obtained from the actual acceleration a_E as

$$a_C = a_E + a_{CE} = a_E + a_{CE}^n + a_{CE}^t.$$

Since a_C^n is also known, the point c can be obtained as explained in Fig. 2.32. a_A can be obtained from a_C (see Fig. 2.33) as

$$a_A = a_C + a_{AC} = a_C + a_{AC}^n + a_{AC}^t,$$

$$a_A = a_{AO_2} = a_{AO_2}^n + a_{AO_2}^t.$$

So, $\alpha_2 (= a_{AO_2}^t / O_2A)$ can be found out.

Now that the auxiliary-point method has been explained in detail, we should note that, for mechanisms with a low degree of complexity, only one auxiliary point may be sufficient. For example, let us consider Problem 2.15 in which one of the auxiliary points, viz., X , Y , and Z , is sufficient. For carrying out the analysis with X alone once V_X and a_X are known, we can determine V_C and a_C because the direction of V_C also is known (it is horizontal, as explained in Figs. 2.34a and 2.34b). Having obtained the velocities and accelerations of two points (X and C) on the floating links, the diagrams can be completed by the image method. Similarly, for the analysis with Z alone, we should first find V_D and a_D and then apply the image method. In Problem 2.15, two auxiliary points were intentionally used only to explain how this method should be used for mechanisms with a high degree of complexity.

Goodman's Indirect Method

Goodman's indirect approach to the acceleration analysis of a complex mechanism is based on the following two properties of a constrained mechanism:

- (i) The angular velocities and accelerations of the links are linear functions of the respective input quantities.
- (ii) The relative angular velocities and accelerations between different links of a linkage remain unaffected by a kinematic inversion.

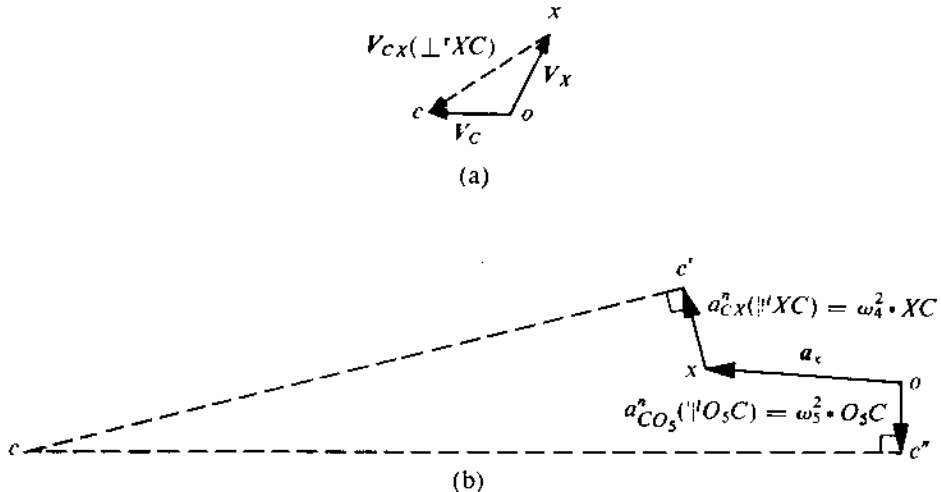


FIGURE 2.34

Basic Relations

Let i denote the input link and l denote any other link. The angular velocity of l at any instant can be expressed in terms of that of i . Thus,

$$\begin{aligned}\omega_l &= \frac{d\theta_l}{dt} = \frac{d\theta_l}{d\theta_i} \cdot \frac{d\theta_i}{dt} \quad (\theta \text{ denotes the rotation}) \\ &= C_l \omega_i \quad (C_l = \frac{d\theta_l}{d\theta_i} = \frac{\omega_l}{\omega_i}).\end{aligned}\quad (2.25)$$

C_l is a geometrical property depending only on the configuration of the mechanism (except at dead-centre locations, when two links are collinear) and is independent of velocities and accelerations. Equation (2.25) is the mathematical statement of the obvious fact that the velocity polygons of a mechanism at any instant with different input velocities are scale drawings of (i.e., they are similar to) one another. The angular acceleration of the link l is

$$\begin{aligned}\alpha_l &= \frac{d^2\theta_l}{dt^2} = \frac{d}{dt}(C_l \omega_i) = \omega_i \frac{dC_l}{dt} + C_l \dot{\omega}_i = \omega_i \frac{d}{d\theta_i} \left(\frac{d\theta_l}{d\theta_i} \right) \frac{d\theta_i}{dt} + C_l \alpha_i \\ &= \omega_i^2 \frac{d^2\theta_l}{d\theta_i^2} + C_l \alpha_i \\ &= C'_l \omega_i^2 + C_l \alpha_i \quad (C'_l = \frac{d^2\theta_l}{d\theta_i^2}).\end{aligned}\quad (2.26)$$

C'_l is also a geometrical property. The first term on the right-hand side of (2.26) represents the acceleration of the link l , the acceleration of the input link being zero and the actual velocity being ω_i . Thus, (2.26) can be written as

$$\alpha_l = \alpha_{\frac{\omega_l}{\omega_i}} + \frac{\omega_l}{\omega_i} \alpha_i, \quad (2.27)$$

where $\alpha_{\frac{\omega_l}{\omega_i}}$ denotes the angular acceleration of the link l obtained from an auxiliary acceleration diagram drawn with true velocities but with zero input acceleration as shown in Fig. 2.27.

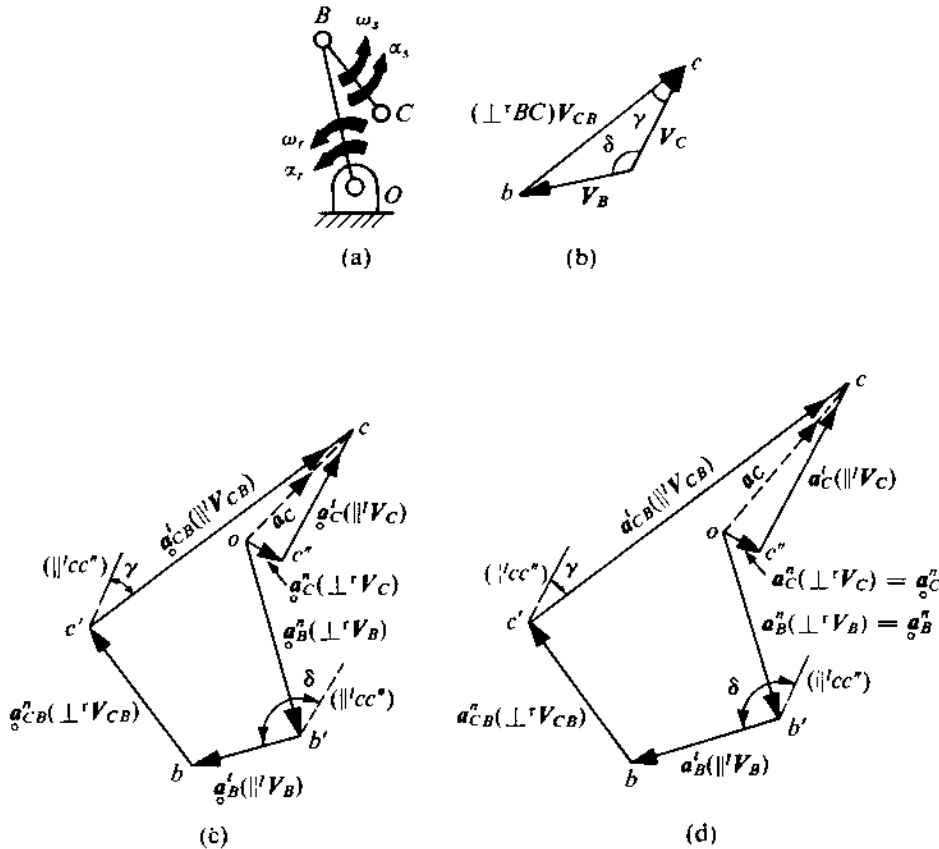


FIGURE 2.35

For a sliding input link, we have

$$\alpha_l = \alpha_{\dot{o}_l} + \frac{\omega_l}{V_i} a_i, \quad (2.28)$$

where V_i and a_i denote the velocity and acceleration of the input link.

Figure 2.35a shows two consecutive links of some mechanism moving with angular velocities and accelerations as indicated. The corresponding velocity diagram is shown in Fig. 2.35b. The auxiliary acceleration diagram with $\alpha_i = 0$ is shown in Fig. 2.35c and the true acceleration diagram with α_i is shown in Fig. 2.35d. Note that the normal components of accelerations (\perp' to the corresponding velocities) remain the same in Figs. 2.35c and 2.35d.

Let us consider the motion of the point C. Without losing any generality, for simplicity of analysis, the point O is taken as fixed. ω_r and ω_s are the angular velocities and α_r and α_s are the angular accelerations of the two links. Since the normal components remain the same in Figs. 2.35c and 2.35d, the difference between a_C^t and $\dot{a}_{\dot{o}_C}^t$ is entirely due to the difference between the tangential

components (\parallel^l to the corresponding velocities). So,

$$\begin{aligned}
 a_C^t - a_{\circ C}^t &= (a_B^t - a_{\circ B}^t) \cos \delta + (a_{CB}^t - a_{\circ CB}^t) \cos \gamma \\
 &= OB(\alpha_r - \alpha_{\circ r}) \cos \delta + BC(\alpha_s - \alpha_{\circ s}) \cos \gamma \\
 &= OB \frac{\omega_i}{\omega_i} \alpha_i \cos \delta + BC \frac{\omega_i}{\omega_i} \alpha_i \cos \gamma \quad [\text{using (2.27)}] \\
 &= (V_B \cos \delta + V_{CB} \cos \gamma) \frac{\alpha_i}{\omega_i} \\
 &= V_C \frac{\alpha_i}{\omega_i} \quad [\text{from the velocity diagram}].
 \end{aligned}$$

Or

$$a_C^t = a_{\circ C}^t + V_C \frac{\alpha_i}{\omega_i}. \quad (2.29)$$

Similarly, for a sliding input link, we have

$$a_C^t = a_{\circ C}^t + V_C \frac{\alpha_i}{V_i}. \quad (2.30)$$

In sliders, the total acceleration is in the direction of the velocity (i.e., the tangential component is the total acceleration). So, for a rotating input link, we can write

$$a_S = a_{\circ S} + \frac{V_S}{\omega_i} \alpha_i, \quad (2.31)$$

and for the sliding input link, we have

$$a_S = a_{\circ S} + \frac{V_S}{V_i} a_i. \quad (2.32)$$

The absolute velocities and accelerations mean those with respect to the fixed link f (i.e., the frame). Thus, (2.27) and (2.28) can be written as

$$\alpha_{if} = \alpha_{\circ if} + \frac{\omega_{if}}{\omega_i} \alpha_{if}, \quad (2.27a)$$

$$\alpha_{if} = \alpha_{\circ if} + \frac{\omega_{if}}{V_i} a_{if}. \quad (2.28a)$$

Applications

The form of equations (2.27a) and (2.28a) is applicable to any inversion of the mechanism where the use of f is no longer restricted to the frame. The subscript i denotes any alternative input link (not necessarily the actual input link) with assumed zero acceleration, on the basis of which the auxiliary acceleration diagram should be drawn.

The indirect approach can be applied to a mechanism with a low degree of complexity in the following manner:

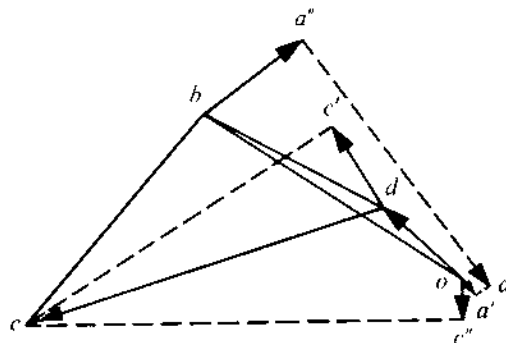


FIGURE 2.36

- (i) Choose an alternative input link to transform the mechanism to a simple one. The auxiliary analysis is carried out with zero acceleration of this alternative input link.
- (ii) Find the actual values by using (2.27) to (2.32).

For mechanisms with a high degree of complexity, a direct kinematic inversion is made to transform the mechanism to a simple one. The auxiliary velocities and accelerations are obtained first. Thereafter, using (2.27a) and (2.28a), the actual values can be determined. The method will be clear from the solution to Problems 2.16-2.18.

It may be noted that in deriving the foregoing equations, the rotational quantities were considered positive in the counter-clockwise directions, and the tangential components of accelerations were taken to be positive if directed in the same sense as that of the corresponding velocities.

Furthermore, it would be seen that the method obviously fails in the case of a mechanism with a high degree of complexity if no kinematic inversion yields a simple mechanism (one such mechanism is shown in Fig. 1.52b).

PROBLEM 2.16

Solve Problem 2.14 by Goodman's indirect approach.

SOLUTION

This mechanism has a low degree of complexity and is transformed to a simple mechanism by considering link 6 as the alternative input link.

Velocity Analysis

The velocity analysis considering 6 as the driver has been carried out completely in Problem 2.14, and the true velocities of all the links have been obtained.

Acceleration Analysis

An auxiliary acceleration diagram, with 6 as the input link, based on $\alpha_6 = 0$ and with true velocities, is drawn in Fig. 2.36. A part of this was also obtained in Fig. 2.27c which has been reproduced here. The steps thereafter to complete the diagram are

$$oa' = \omega_2^2 \cdot O_2 A \quad (\text{towards } O_2 \text{ and towards } O_2),$$

$$ba'' = \omega_3^2 \cdot AB \quad (\parallel^t \text{ to } AB \text{ and towards } B).$$

a is determined by the intersection of $a''a$ (\perp^r to ba'') and $a'a$ (\perp^r to oa'). In this auxiliary acceleration diagram, $\overset{o}{a}a = \overset{o}{a}_A^t = 850 \text{ cm/s}^2$ (positive, because this tangential component is in the direction of V_A) but, as $\omega_2 = \text{constant}$ and $\alpha_2 = 0$, we have $a_A^t = 0$. Using (2.29), we have

$$a_A^t = a_A^t + V_A \frac{\alpha_6}{\omega_6},$$

$$\alpha_6 = -a_A^t \frac{\omega_6}{V_A} = -850 \times \frac{28}{75} = -318 \text{ rad/s}^2,$$

that is, $\alpha_6 = 318 \text{ rad/s}^2$ (CW).

PROBLEM 2.17

For the mechanism shown in Fig. 2.37a, $\omega_2 = 1 \text{ rad/s}$ (CCW) (constant). Determine ω_6 and α_6 .

SOLUTION

Velocity Analysis

With link 2 as the input link, the velocity diagram (Fig. 2.37b) is drawn with V_A represented by ba to some scale (say, $K_V \text{ cm/s per cm}$). Using this diagram, we get

$$ba = 5.5 \text{ cm},$$

$$V_A = AB \cdot \omega_{24} = 5.5 K_V,$$

$$\omega_{24} = \frac{5.5}{6.5} K_V = 0.846 K_V \text{ rad/s (CCW)},$$

$$V_{O_6 O_2} = O_2 O_6 \cdot \omega_{14} = 13 \omega_{14} = o_2 o_6 = 3 K_V,$$

$$\omega_{14} = 0.231 K_V \text{ rad/s (CCW)},$$

$$V_{O_6 E} = O_6 E \cdot \omega_{64} = 5.5 \omega_{64} = e o_6 = 2.65 K_V,$$

$$\omega_{64} = 0.482 K_V \text{ rad/s (CCW)}.$$

Similarly,

$$\omega_{34} = \frac{ac}{AC} = 0.805 K_V = -0.805 K_V \text{ rad/s (CCW)},$$

$$\omega_{54} = \frac{dc}{CD} = 0.533 K_V \text{ rad/s (CCW)}.$$

The problem states that $\omega_2 = \omega_{21} = 1 \text{ rad/s}$ (CCW). Now,

$$\omega_{21} = \omega_{24} - \omega_{14} = (0.846 - 0.231) K_V = 1, \quad K_V = 1.627 \text{ cm/s per cm}.$$

Substituting this value of K_V , we get

$$\omega_{24} = 1.378 \text{ rad/s (CCW)},$$

$$\omega_{14} = 0.376 \text{ rad/s (CCW)},$$

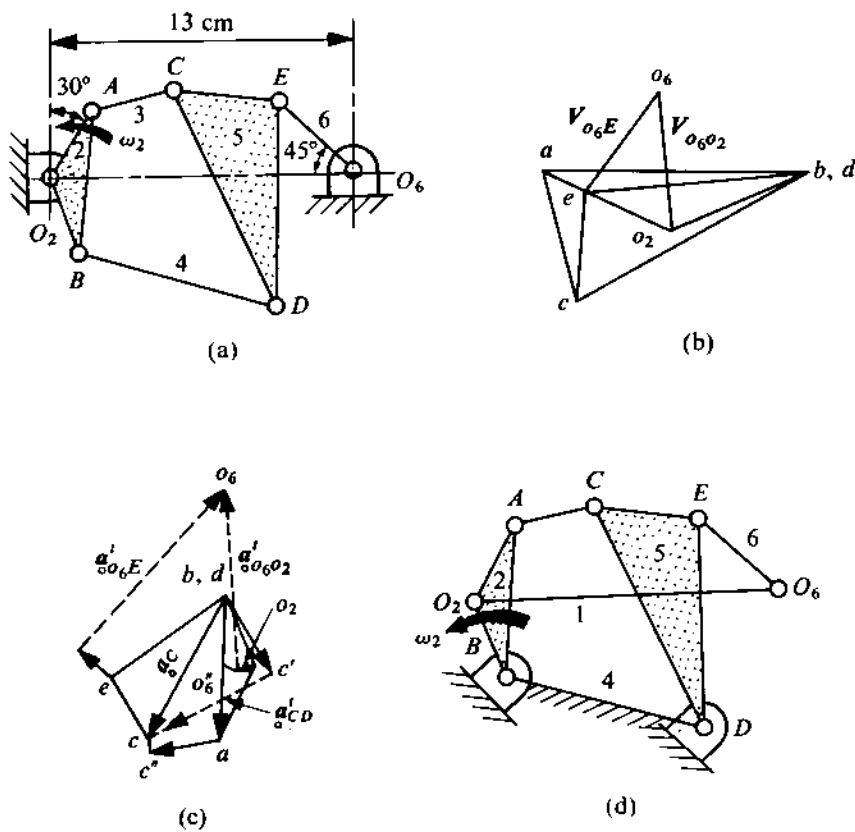


FIGURE 2.37

$$\omega_{64} = 0.783 \text{ rad/s (CCW)},$$

$$\omega_{34} = 1.31 \text{ rad/s (CW)},$$

$$\omega_{54} = 0.866 \text{ rad/s (CCW)}.$$

Finally, $\omega_6 = \omega_{61} = \omega_{64} - \omega_{14} = 0.407 \text{ rad/s (CCW)}$.

Acceleration Analysis

The auxiliary acceleration diagram based on these velocities and on $\alpha_{24} = 0$ is shown in Fig. 2.37c. From this diagram, we get

$$\alpha_{14}^t = \frac{\alpha_{O_6 O_2}^t}{O_2 O_6} = \frac{\alpha_{O_6 O_6}^t}{O_2 O_6} = \frac{15.3}{13} = 1.176 \text{ rad/s}^2 \text{ (CCW)},$$

$$\alpha_{64}^t = \frac{\alpha_{O_6 E}^t}{O_6 E} = \frac{\alpha_{O_6 O_6}^t}{O_6 E} = \frac{18.6}{5.5} = 3.38 \text{ rad/s}^2 \text{ (CCW)},$$

$$\alpha_{54}^t = \frac{\alpha_{CD}^t}{CD} = \frac{c'c}{CD} = \frac{12}{10.5} = 1.142 \text{ rad/s}^2 \text{ (CCW)}.$$

Using (2.27a), we have

$$\alpha_{14} = \alpha_{14}^t + \frac{\omega_{14}}{\omega_{24}} \alpha_{24}, \quad (a)$$

$$\alpha_{64} = \alpha_{64}^t + \frac{\omega_{64}}{\omega_{24}} \alpha_{24}. \quad (b)$$

α_{24} is not yet known. Given $\alpha_2 = \alpha_{21} = 0$, it follows that

$$\alpha_{21} = \alpha_{24} - \alpha_{14} = \alpha_{24} - \alpha_{14}^t - \frac{\omega_{14}}{\omega_{24}} \alpha_{24} = 0,$$

$$\alpha_{24} - \frac{0.376}{1.376} \alpha_{24} - 1.176 = 0,$$

$$\alpha_{24} = \frac{1.176}{0.727} = 1.619 \text{ rad/s (CCW)}.$$

Substituting this value of α_{24} in (a) and (b), we get

$$\alpha_{14} = 1.176 + 0.273 \times 1.619 = 1.618 \text{ rad/s}^2 \text{ (CCW)},$$

$$\alpha_{64} = 3.38 + 0.568 \times 1.619 = 4.30 \text{ rad/s}^2 \text{ (CCW)}.$$

Finally, $\alpha_6 = \alpha_{64} - \alpha_{14} = 2.682 \text{ rad/s}^2 \text{ (CCW)}$. The determination of angular velocities and accelerations of the other links is left as an exercise for the reader.

PROBLEM 2.18

For the mechanism shown in Fig. 2.37a, given $\omega_6 = 0.5 \text{ rad/s}$ and $\alpha_6 = 1.5 \text{ rad/s}^2$, both clockwise, determine ω_2 and α_2 .

SOLUTION

The same kinematic inversion as shown in Fig. 2.37d is used to transform the mechanism to a simple one.

Velocity Analysis

With link 2 as the input link, the velocity diagram shown in Fig. 2.37b can be used here. In this problem, $\omega_6 = \omega_{61} = 0.5 \text{ rad/s}$. Now,

$$\omega_{61} = \omega_{64} - \omega_{14} = 0.482K_V - 0.231K_V = 0.5, \quad K_V = 1.99 \text{ cm/s per cm.}$$

Thus, using the results and the value of K_V obtained in Problem 2.17 ($K_V = 1.627$), we get

$$\omega_{24} = \frac{1.99}{1.627} \times 1.378 = 1.685 \text{ rad/s (CCW)},$$

$$\omega_{14} = 0.461 \text{ rad/s (CCW)},$$

$$\omega_{64} = 0.958 \text{ rad/s (CCW)},$$

$$\omega_{34} = 1.602 \text{ rad/s (CW)},$$

$$\omega_{54} = 1.06 \text{ rad/s (CCW)}.$$

Finally, $\omega_2 = \omega_{21} = \omega_{24} - \omega_{14} = 1.224 \text{ rad/s (CCW)}$.

Acceleration Analysis

The auxiliary acceleration diagram shown in Fig. 2.37c can also be used for this problem if the scale factor is adjusted in the ratio of the square of the velocity scale factors [i.e., all values obtained from the diagram should be multiplied by the factor $(1.99/1.627)^2 = 1.5$]. So, we get

$$\alpha_{14} = 1.76 \text{ rad/s}^2 \text{ (CCW)},$$

$$\alpha_{64} = 5.07 \text{ rad/s}^2 \text{ (CCW)}.$$

It is given that $\alpha_6 = \alpha_{61} = \alpha_{64} - \alpha_{14} = 1.5 \text{ rad/s}^2$ (CCW). Using (2.27a), we get

$$\alpha_{64} = \alpha_{64} + \frac{\omega_{64}}{\omega_{24}} \alpha_{24} = 5.07 + 0.57\alpha_{24},$$

$$\alpha_{14} = \alpha_{14} + \frac{\omega_{14}}{\omega_{24}} \alpha_{24} = 1.76 + 0.208\alpha_{24}.$$

Subtracting α_{14} from α_{64} , we have

$$1.5 = (5.07 - 1.76) + (0.57 - 0.208)\alpha_{24} = 3.31 + 0.362\alpha_{24},$$

$$\alpha_{24} = -5 \text{ rad/s}^2.$$

Using this value of α_{24} , we get $\alpha_{14} = 0.72 \text{ rad/s}^2$. Finally,

$$\alpha_2 = \alpha_{21} = \alpha_{24} - \alpha_{14} = -5.72 \text{ rad/s}^2, \text{ that is, } \alpha_2 = 5.72 \text{ rad/s}^2 \text{ (CW)}.$$

2.9 VELOCITY AND ACCELERATION ANALYSIS (ANALYTICAL)

The analytical method of velocity and acceleration analysis starts from the loop-closure equations which were discussed during displacement analysis. These equations are valid at all times, and therefore successive differentiations of these equations with respect to time establish the relationships between the velocity and acceleration quantities of various links of a mechanism. The most important point to note is that, once the configuration of the mechanism is known (i.e., the displacement analysis is complete), the velocity and acceleration equations are linear in the unknown quantities and, therefore, are very easy to solve. Consequently, when the velocity and acceleration analysis has to be carried out for a large number of configurations, the analytical method turns out to be more advantageous than the graphical method. Moreover, the accuracy obtained by the analytical method is very high and a simple computer program can always be written. At this stage, it may be noted that softwares like KINSYN, ADAMS, LINKAGES.4, etc. are commercially available, which can be used for kinematic analysis and synthesis of simple mechanisms. We shall now derive in detail the angular velocity and acceleration of the coupler and the follower of a 4R linkage when the configuration and the crank motions are prescribed.

Referring back to Fig. 2.4, assume that the configuration of the mechanism has already been determined, i.e., l_1 , l_2 , l_3 , l_4 , and θ_2 are prescribed and θ_3 and θ_4 have been solved. The task is to determine the angular velocity and acceleration of the coupler and the follower ($\dot{\theta}_3$, $\dot{\theta}_4$, $\ddot{\theta}_3$, and $\ddot{\theta}_4$) if those of the crank ($\dot{\theta}_2$, $\ddot{\theta}_2$) are given. Towards this end, differentiate (2.2a) and (2.2b) with respect to time and obtain

$$l_4 \sin \theta_4 \dot{\theta}_4 + l_3 \sin \theta_3 \dot{\theta}_3 - l_2 \sin \theta_2 \dot{\theta}_2 = 0, \quad (2.33a)$$

$$l_4 \cos \theta_4 \dot{\theta}_4 + l_3 \cos \theta_3 \dot{\theta}_3 - l_2 \cos \theta_2 \dot{\theta}_2 = 0. \quad (2.33b)$$

We should note that (2.33a) and (2.33b) are two simultaneous linear equations in the two unknowns, viz., $\dot{\theta}_3$ and $\dot{\theta}_4$, which can be easily solved to yield

$$\dot{\theta}_3 = \frac{l_2 \sin (\theta_2 - \theta_4)}{l_3 \sin (\theta_3 - \theta_4)},$$

$$\dot{\theta}_4 = \frac{l_2 \sin (\theta_2 - \theta_3)}{l_4 \cos (\theta_4 - \theta_3)}.$$

Differentiating (2.33a) and (2.33b) once more with respect to time, we get

$$l_4(\cos \theta_4 \dot{\theta}_4^2 + \sin \theta_4 \ddot{\theta}_4) + l_3(\cos \theta_3 \dot{\theta}_3^2 + \sin \theta_3 \ddot{\theta}_3) = l_2(\cos \theta_2 \dot{\theta}_2^2 + \sin \theta_2 \ddot{\theta}_2), \quad (2.34a)$$

$$l_4(-\sin \theta_4 \dot{\theta}_4^2 + \cos \theta_4 \ddot{\theta}_4) + l_3(-\sin \theta_3 \dot{\theta}_3^2 + \cos \theta_3 \ddot{\theta}_3) = l_2(-\sin \theta_2 \dot{\theta}_2^2 + \cos \theta_2 \ddot{\theta}_2). \quad (2.34b)$$

Once the velocity analysis is complete, (2.34a) and (2.34b) again provide two linear equations in $\ddot{\theta}_3$ and $\ddot{\theta}_4$ which are obtained as

$$\ddot{\theta}_3 = \frac{l_2 \dot{\theta}_2^2 \cos (\theta_2 - \theta_4) + l_2 \ddot{\theta}_2 \sin (\theta_2 - \theta_4) - l_4 \dot{\theta}_4^2 - l_3 \dot{\theta}_3^2 \cos (\theta_3 - \theta_4)}{l_3 \sin (\theta_3 - \theta_4)},$$

$$\ddot{\theta}_4 = \frac{l_2 \dot{\theta}_2^2 \cos (\theta_2 - \theta_3) + l_2 \ddot{\theta}_2 \sin (\theta_2 - \theta_3) - l_3 \dot{\theta}_3^2 - l_4 \dot{\theta}_4^2 \cos (\theta_4 - \theta_3)}{l_4 \sin (\theta_4 - \theta_3)}.$$

The same methodology can be extended to a mechanism having prismatic pairs. The only difference will be that all vectors appearing in the loop-closure equation will not be constant. The vector representing the slider displacement will be time-dependent as illustrated in the next problem.

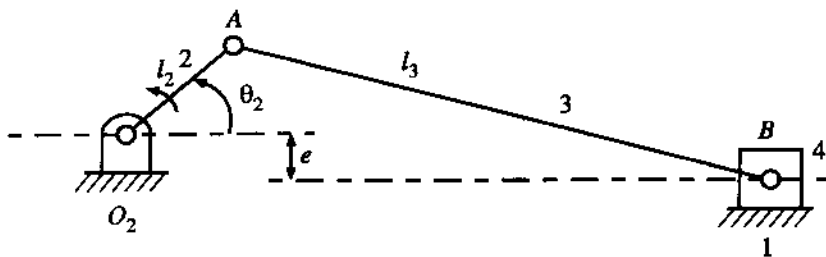


FIGURE 2.38

PROBLEM 2.19

Consider the quick-return mechanism shown in Fig. 2.9a. With prescribed values of l_1 , l_2 , θ_2 , and $\dot{\theta}_2$, determine the angular velocity and angular acceleration of the slotted lever (link 4), i.e., θ_4 and $\ddot{\theta}_4$.

SOLUTION

Equating the real and imaginary parts of (2.8) separately to zero, we obtain

$$s_4 \cos \theta_4 = l_2 \cos \theta_2, \quad (a)$$

$$-l_1 + s_4 \sin \theta_4 = l_2 \sin \theta_2. \quad (b)$$

Differentiating (a) and (b) with respect to time, we get

$$\dot{s}_4 \cos \theta_4 - s_4 \sin \theta_4 \dot{\theta}_4 = -l_2 \sin \theta_2 \dot{\theta}_2, \quad (c)$$

$$\dot{s}_4 \sin \theta_4 + s_4 \cos \theta_4 \dot{\theta}_4 = l_2 \cos \theta_2 \dot{\theta}_2. \quad (d)$$

(Note that s_4 and θ_4 can be determined from (2.10) and (2.11) and are therefore assumed to be known.) Solving (c) and (d), we get

$$\dot{\theta}_4 = \frac{l_2 \dot{\theta}_2}{s_4} \cos (\theta_4 - \theta_2), \quad (e)$$

$$\dot{s}_4 = l_2 \dot{\theta}_2 \sin (\theta_4 - \theta_2). \quad (f)$$

Now differentiating (c) and (d) once more with respect to time, we can obtain $\ddot{\theta}_4$ and \ddot{s}_4 . This is left as an exercise for the reader to complete.

2.10 PROBLEMS

- 2.20 An offset slider-crank mechanism is shown in Fig. 2.38. Assume $l_2 = 10$ cm, $e = 3$ cm, and $l_3 = 35$ cm. If the crank rotates at a uniform angular speed, determine the quick-return ratio of the slider.

- 2.21 Consider the slotted-lever quick-return mechanism shown in Fig. 2.22a. Determine the stroke and quick-return ratio of the cutting tool (i.e., link 6).

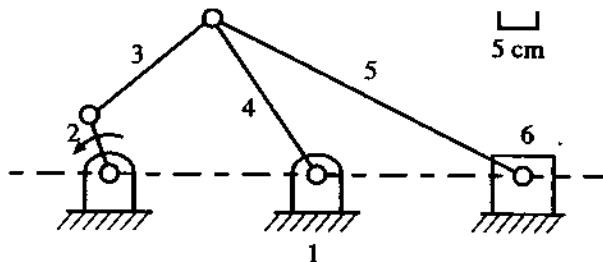


FIGURE 2.39

2.22 Figure 2.39 shows a six-link mechanism in which slider 6 is driven by the oscillating output link of a 4R crank-rocker mechanism and the input crank rotates with a constant angular speed. Determine the total travel of slider 6 and its quick-return ratio.

2.23 Determine the extreme positions and swing angles of links 2 and 4 of a four-bar linkage with the link lengths $l_1 = 3.25$ cm, $l_2 = 3.5$ cm, $l_3 = 6.25$ cm, and $l_4 = 2$ cm.

2.24 An earth-moving machinery is shown in Fig. 2.40 to the scale indicated therein. The bin (i.e., the link JK) is positioned mainly by the hydraulic actuators Z_1 and Z_2 whereas the actuator Z_3 is used mainly to tilt the bin. The ranges of movement of Z_1 and Z_2 are such that $(O_2A)_{\min} = 1100$ mm, $(O_2A)_{\max} = 1800$ mm, $(BC)_{\min} = 1500$ mm, $(BC)_{\max} = 2400$ mm. First draw the kinematic diagram of the mechanism with the vehicle as stationary. Then determine graphically (use of a tracing paper suggested)

- the positions of all the revolute joints corresponding to position II of the bin, indicated in Fig. 2.40,
- the zone in which the hinge K lies when the full ranges of movement of Z_1 and Z_2 are utilized, and
- the maximum value of the tilt angle α , keeping the lip L at the location indicated for position II.

2.25 Figure 2.41 shows a six-link wiper mechanism for large windshields. The wiper blade 5 is the coupler of a parallelogram linkage O_4CDO_6 . The input link 2 rotates at a constant angular speed.

- Determine graphically the field being wiped. (Remember that the coupler points of a parallelogram linkage generate parallel circular arcs, i.e., the coupler undergoes curvilinear translation.)
- It is desired that the wiping field be made symmetrical about the vertical line through O_4 by changing only the angle δ . Obtain the required value of δ .
- A symmetrical (as in (ii)) wiping field of 450 mm width is desired along with equal time for forward and backward motions of the wiper, by changing only δ , O_2A , and AB , keeping all the other dimensions unchanged. Determine the new values of δ , O_2A , and AB .

2.26 Determine all the relative instantaneous centres for the six-link mechanism shown in Fig. 2.42.

2.27 Determine ω_6 in Problem 2.14 by the method of instantaneous centres.

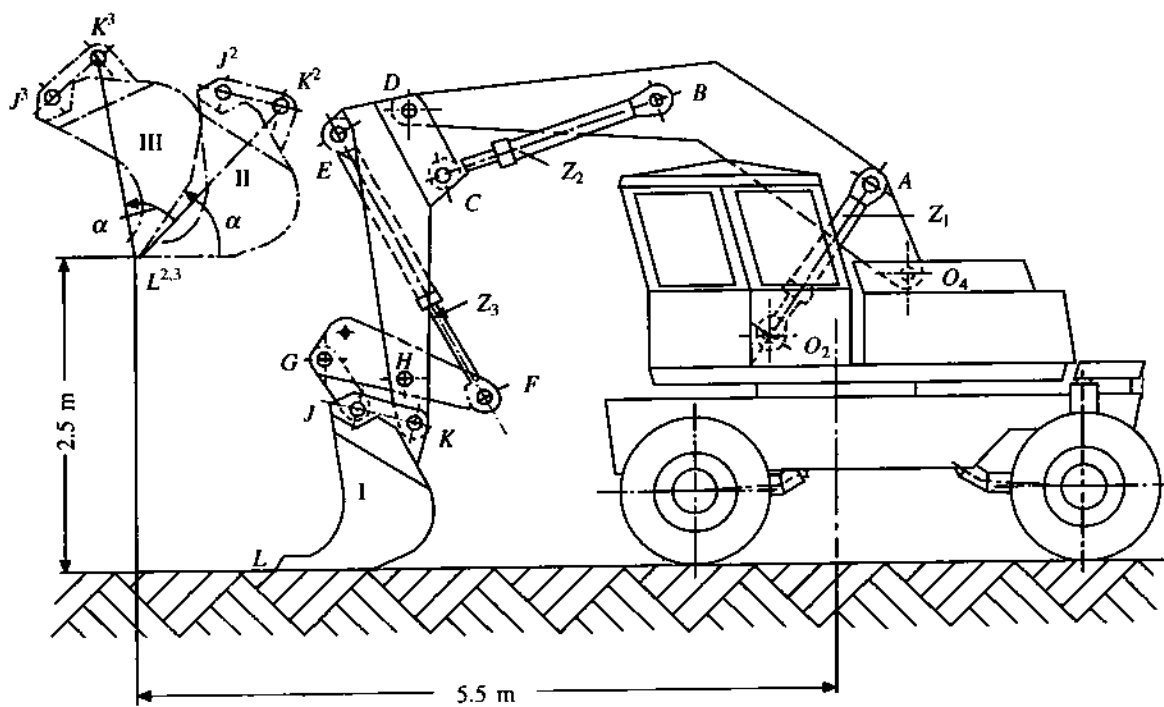


FIGURE 2.40

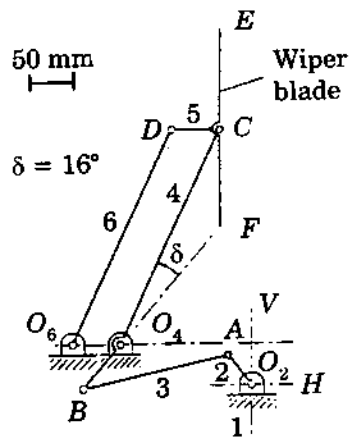


FIGURE 2.41

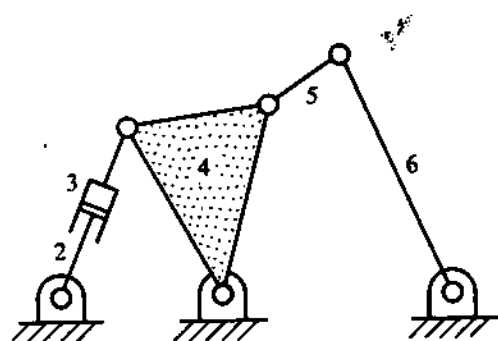


FIGURE 2.42

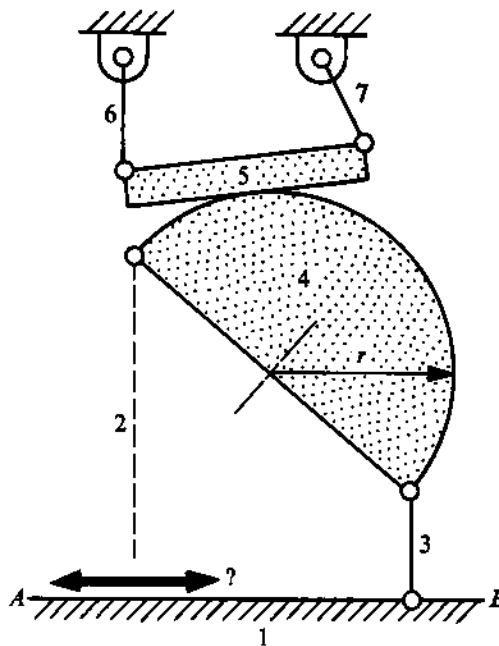


FIGURE 2.43

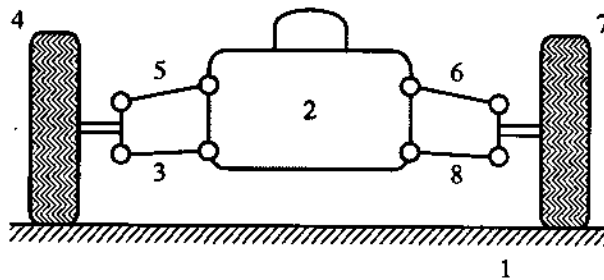


FIGURE 2.44

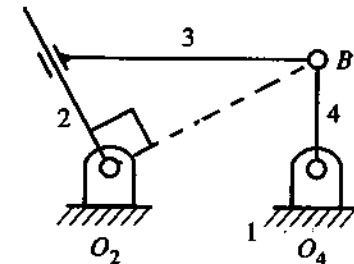


FIGURE 2.45

2.28 Figure 2.43 shows a mechanism where links 4 and 5 are always kept in contact by an external force. It is desired to have a pure rolling contact between 4 and 5 at the instant shown. Determine the required location of the hinge between the fixed link 1 and link 2 on the line AB.

2.29 Figure 2.44 shows schematically a planar approximation of the front suspension of an automobile. The roll centre refers to the point about which the body of the automobile (link 2) seems to rotate with respect to the ground. Assuming no slip between the tyres and the road, locate the roll centre.

2.30 Locate all the relative IC's for the 3R-1P mechanism at the configuration shown in Fig. 2.45. (Notice that subscripts 1 and 4 in the IC's are interchangeable. This implies that, at this instant, $\omega_4 = \omega_1 = 0$, whatever may be the value of ω_2 ($= \omega_3$ because of a prismatic pair between 2 and 3). At this instant, the mechanism cannot be driven by link 4. If it is driven by link 2, then link 4 reverses its motion at this configuration.)

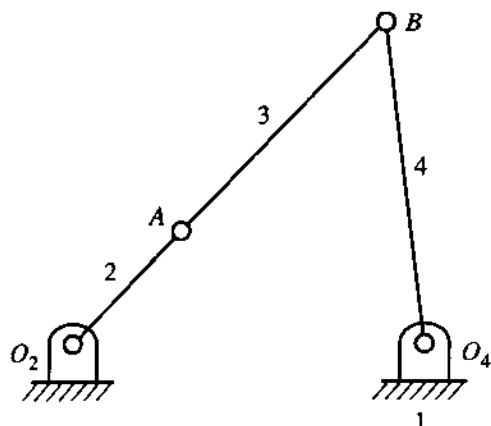


FIGURE 2.46

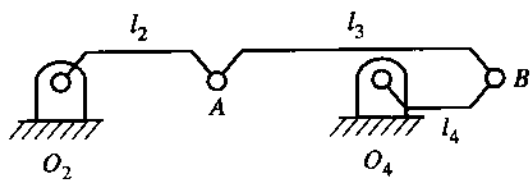


FIGURE 2.47

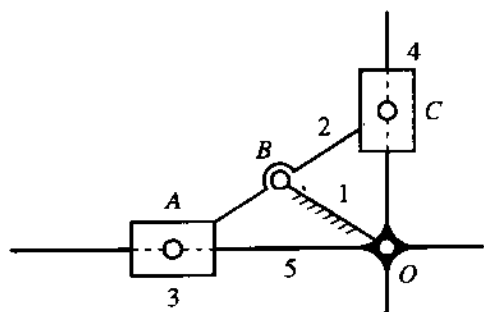


FIGURE 2.48

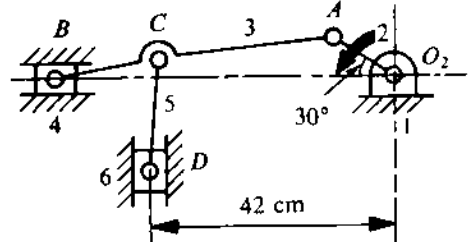


FIGURE 2.49

- 2.31 Verify the dead-centre configuration of the crank-rocker linkage, shown in Fig. 2.46, by locating all the IC's and noticing the interchangeability of subscripts 1 and 4.
- 2.32 Figure 2.47 shows the uncertainty configuration of a four-bar linkage, where $l_2 + l_3 = l_1 + l_4$. Verify that the IC 24 cannot be determined, because, for a given ω_2 , the direction of ω_4 can be either clockwise or counter-clockwise (i.e., uncertain).
- 2.33 Figure 2.48 shows the kinematic diagram of a crossed-slider trammel. In this mechanism, link 5 contains two mutually perpendicular slots in which links 3 and 4 slide. Link 5 is hinged to the fixed link at O and link 2 is hinged to the fixed link at C . Link 2 is also hinged to sliders 3 and 4 at A and B , respectively. It is further given that $OB = AB = BC$. Obtain all the relative instantaneous centres and determine ω_2/ω_5 . Notice that ω_2/ω_5 is independent of the configuration of the mechanism.
- 2.34 In the mechanism shown in Fig. 2.49, the crank O_2A rotates at 20 rpm in the direction indicated. For the given configuration, determine (i) the velocities of sliding at B and D , and (ii) the linear acceleration of D . Given $O_2A = 12$ cm, $AB = 48$ cm, $BC = 18$ cm, and $CD = 18$ cm.
- 2.35 Figure 2.50 shows the mechanism used in a two-cylinder 60° V-engine with an articulated connecting rod. Crank 2 rotates in a clockwise direction at a speed of 2000 rpm. Determine the velocities and accelerations of the sliders at B and D . Given $O_2A = 2$ cm, $AC = 2$ cm, $AB = BC = 6$ cm, and $AC = 5$ cm.

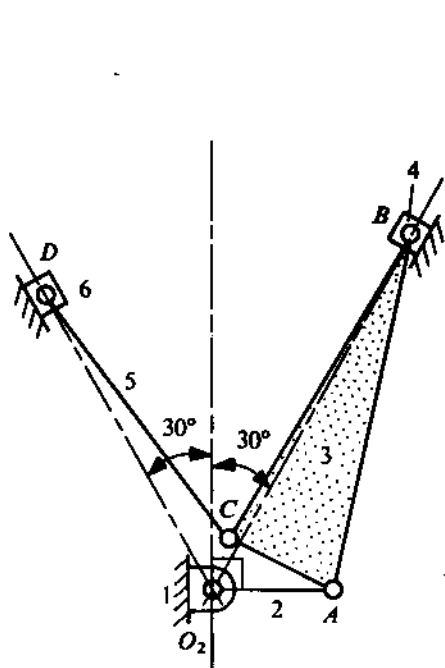


FIGURE 2.50

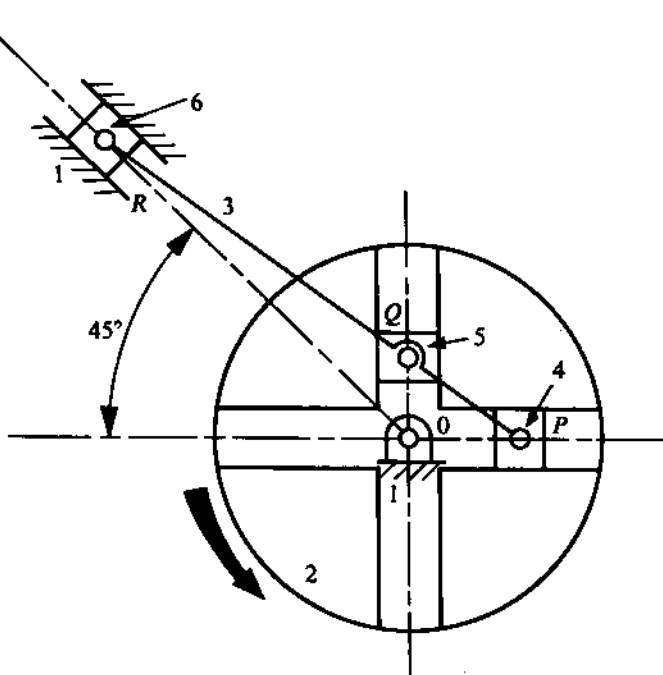


FIGURE 2.51

- 2.36 A slotted disc, labelled 2 in Fig. 2.51, rotates in the anticlockwise direction at 1000 rpm. Blocks 4 and 5 slide in the slots in the disc. The slots are at right angles. Block 6 slides in a fixed slot as indicated. A straight rigid rod, labelled 3, is pinned to the blocks at P , Q , and R so that $PQ = 20$ cm and $PR = 60$ cm. Determine the velocity and acceleration of block 6, using a graphical method.
- 2.37 Link 2 of the Geneva mechanism shown in Fig. 2.52 rotates clockwise at a speed $\omega_2 = 10$ rad/s. Determine the corresponding values of ω_3 and α_3 .
- 2.38 In the Whitworth quick-return mechanism shown in Fig. 2.29, link 2 rotates at a constant speed of 120 rpm in a clockwise direction. Determine the velocity and acceleration of the slider at D .
- 2.39 The guide D in Fig. 2.53 has an upward velocity of 24 cm/s and an acceleration of 48 cm/s². Determine the corresponding values of V_A and a_A . Given $\theta = 30^\circ$ and $AB = BC = 6$ cm.
- 2.40 A small pin P is carried by the slots in links 2 and 4 of the 4R mechanism shown in Fig. 2.54. Determine the velocity and acceleration of the pin at this instant if $\omega_2 = 1$ rad/s (CCW) and $\alpha_2 = 0$.
- 2.41 A circular disc cam with an oscillating follower is shown in Fig. 2.55. If the cam rotates at a constant speed of 1000 rpm, determine the angular velocity and acceleration of the follower. Given $O_2C = 8.5$ cm, $O_2O_3 = 43$ cm, and $\angle O_3O_2C = 30^\circ$.
- 2.42 The kinematic arrangement of a machine is schematically shown in Fig. 2.56. The slotted lever and the crank O_2C are being rotated with angular velocities of 1000 rpm and 100 rpm,

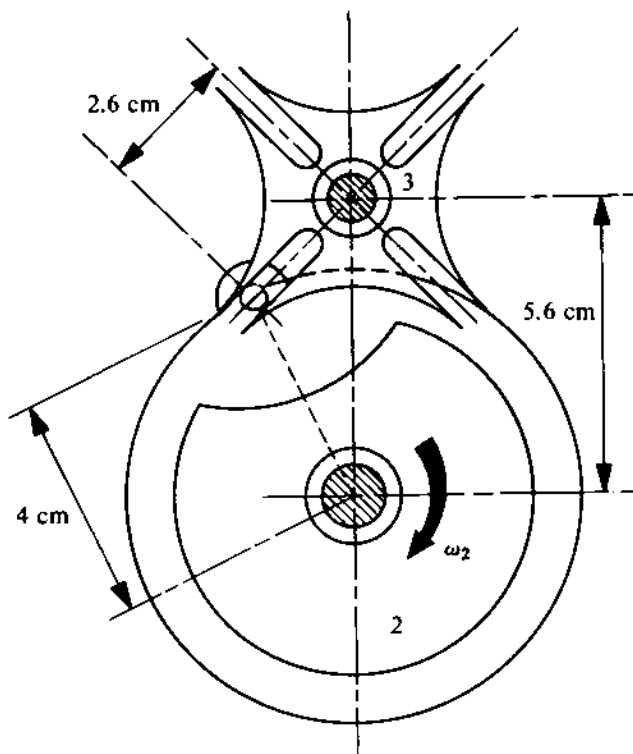


FIGURE 2.52

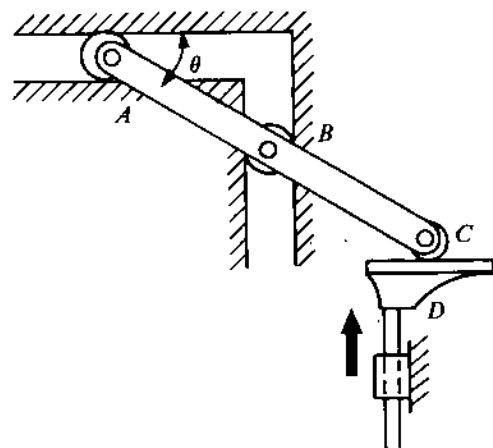


FIGURE 2.53

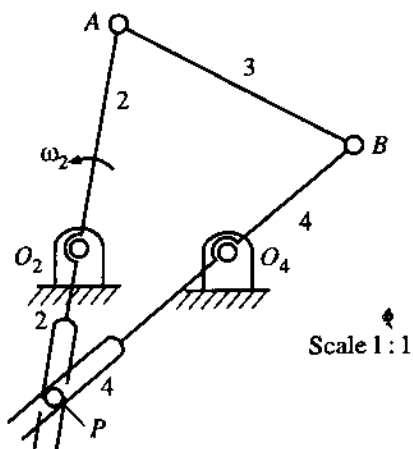


FIGURE 2.54

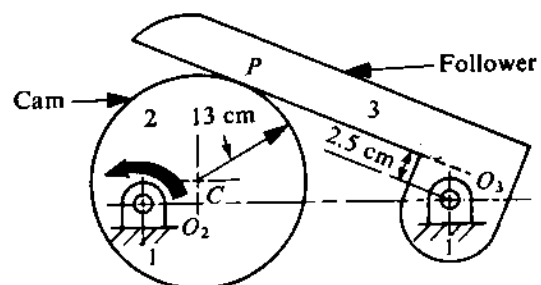
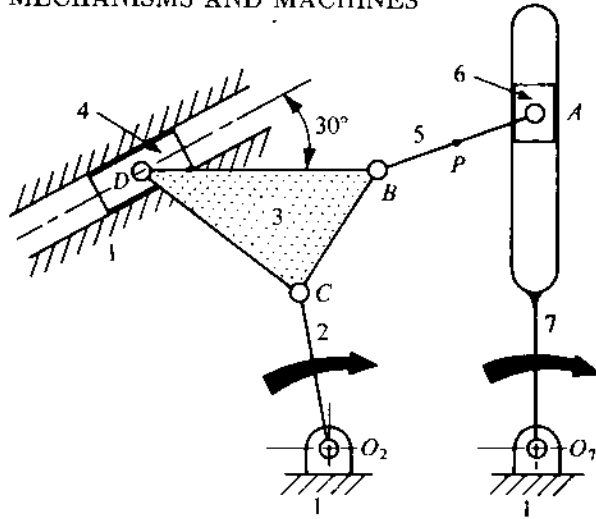


FIGURE 2.55



Scale 1 : 10

FIGURE 2.56

respectively. Use a graphical method to find out the velocity of the midpoint P of the link AB .

- 2.43 Figure 2.57 shows a mechanism in which link 5 rotates at 1 rad/s and the hydraulic cylinder-piston system O_7C expands at a rate of 10 cm/s. Determine the angular velocity of link 2 at this instant, using a graphical method. Given $O_2A = 10$ cm, $AB = 12$ cm, $O_7C = 142$ cm, and $O_5D = 15$ cm.
- 2.44 Solve Problem 2.17 by the auxiliary-point method.
- 2.45 A Watt 'walking-beam' mechanism is shown in Fig. 2.58. Determine the velocity and acceleration of the slider if the crank O_2A rotates with a speed of 1 rad/s in a clockwise direction. Given $O_2A = 2$ cm, $AB = 8.5$ cm, $BC = 7.5$ cm, $CD = 5.25$ cm, and $O_5C = 7$ cm.
- 2.46 In the modified six-link mechanism shown in Fig. 2.59, $\omega_2 = 10$ rad/s (CCW) and is constant. Determine the velocity and acceleration of the slider at C . Given $O_2A = 4$ cm, $O_5B = 5$ cm, and $BC = 24$ cm.
- 2.47 In the Atkinson engine mechanism shown in Fig. 2.60, the velocity and acceleration of the slider at D are given as 40 cm/s and 450 cm/s². Determine ω_2 , α_2 , ω_3 , and α_3 . Take $O_2A = 4.5$ cm, $AB = 12$ cm, $O_4B = 6$ cm, $BC = 2$ cm, $AC = 13$ cm, $CD = 14$ cm.
- 2.48 Figure 2.61 shows a simplified version of the feed-dog drive in a sewing machine. Cam 5 rotates at a constant speed of 200 rpm. Determine the velocity of the point P at the instant shown.
- 2.49 Determine the velocity and acceleration expressions for slider 4 in Fig. 2.38 in terms of t_2 , t_3 , e , and the crank motion (i.e., θ_2 , $\dot{\theta}_2$, and $\ddot{\theta}_2$) by using an analytical method.
- 2.50 An oscillating engine mechanism is shown in Fig. 2.62a. With 2 as the input link, first draw the kinematic diagram shown in Fig. 2.62b to identify the kinematic dimensions. Then obtain the angular velocity and acceleration of the cylinder using an analytical method.

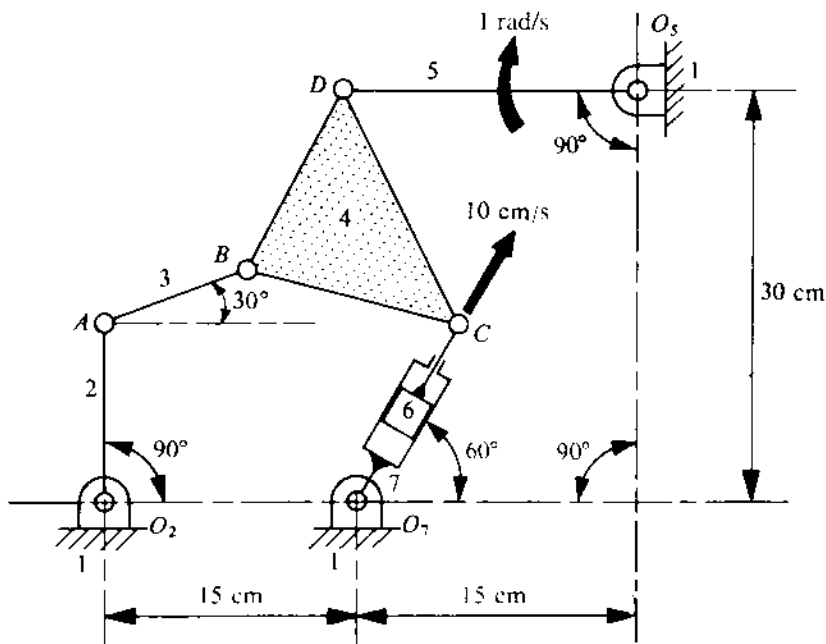


FIGURE 2.57

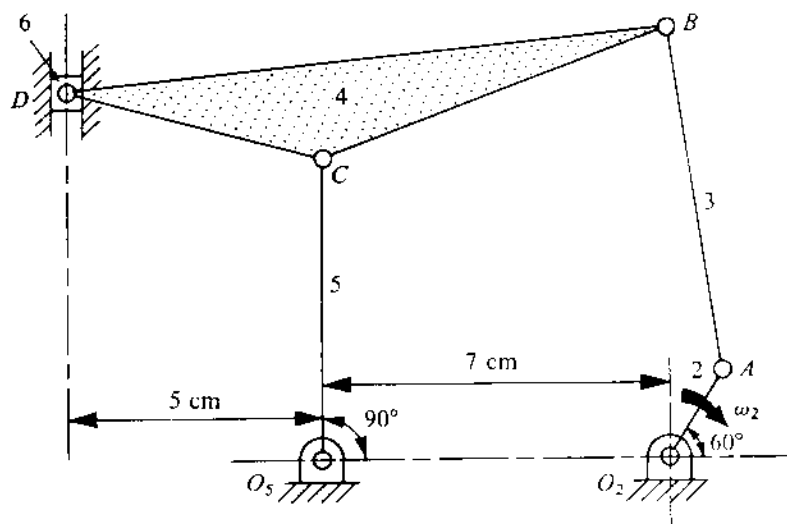


FIGURE 2.58

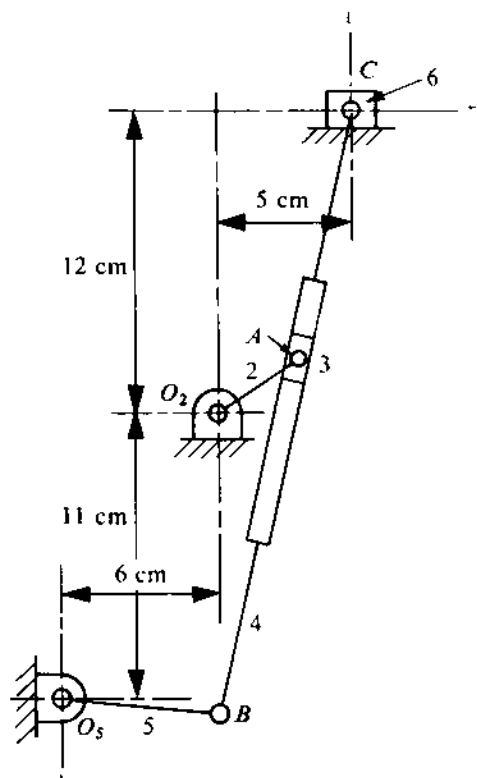


FIGURE 2.59

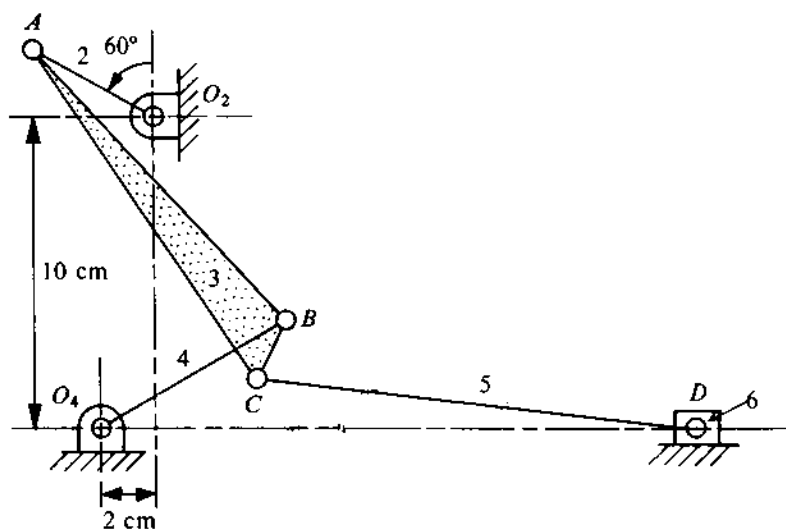


FIGURE 2.60

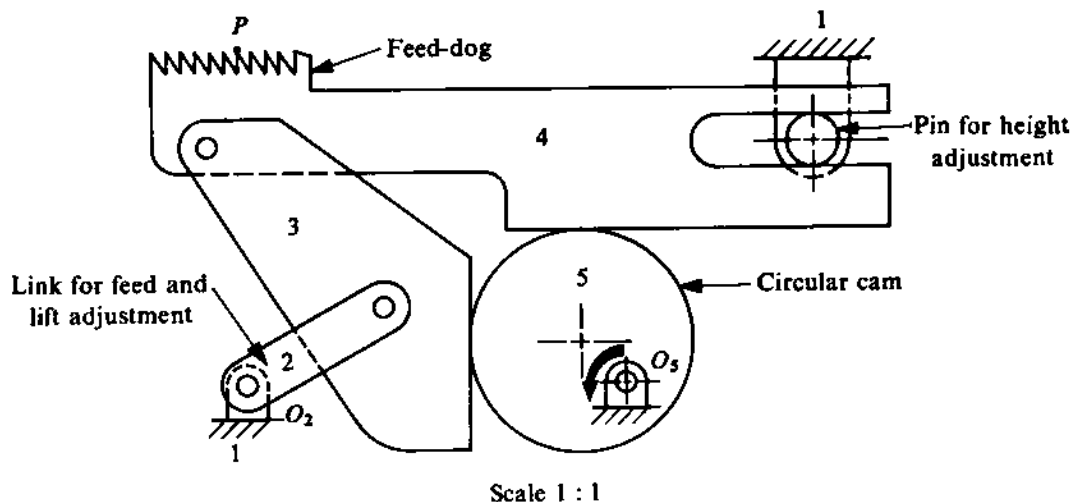
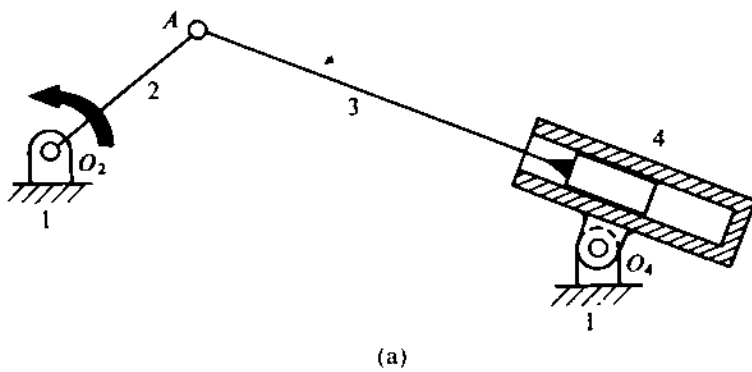
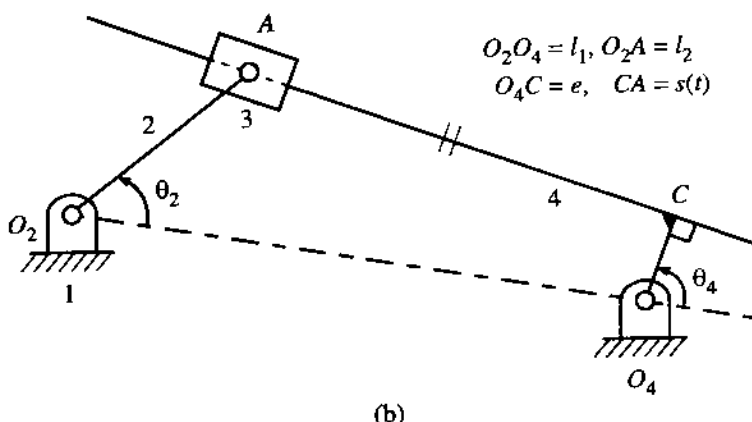


FIGURE 2.61



(a)



(b)

FIGURE 2.62

Chapter 3

DIMENSIONAL SYNTHESIS OF LINKAGES

3.1 INTRODUCTION

Dimensional synthesis deals with the determination of kinematic dimensions (link lengths, offsets, etc.) of the mechanism to satisfy the required (specified) motion characteristics. Just as in kinematic analysis, both graphical and analytical methods are available for dimensional synthesis. The choice of the method depends, to a large extent, on the type of the problem to be solved. Broadly speaking, the problems can be classified under four headings as follows:

- (i) Motion generation - In this class of problem, the linkage has to be so designed that a rigid body (say, the coupler of a 4R linkage) can be guided in a prescribed manner. The guidance may or may not be coordinated with the input movement.
- (ii) Path generation - If a point on the floating link of a mechanism has to be guided along a prescribed path, then such a problem is classified as a path-generation problem. This guidance again may or may not be coordinated with the input movement.
- (iii) Function generation - By function generation we mean that the output and input motion characteristics (e.g., displacement, velocity, and acceleration) have to maintain a specified functional relationship.
- (iv) Dead-centre problems - In this type of a problem, the linkage has to be so designed as to generate the prescribed dead-centre configuration.

In this chapter, we shall discuss both graphical and analytical methods with respect to *kinematic synthesis* of 4R and slider-crank mechanisms.

Approximate and Exact Synthesis

There are two approaches to the first three categories of problems: approximate and exact. By approximate synthesis, we mean that the motion generated by the mechanism fits the desired characteristics only at a finite number of points in the interval or that the path generated intersects the desired path at a finite number of points. By exact synthesis, we mean that the generated function

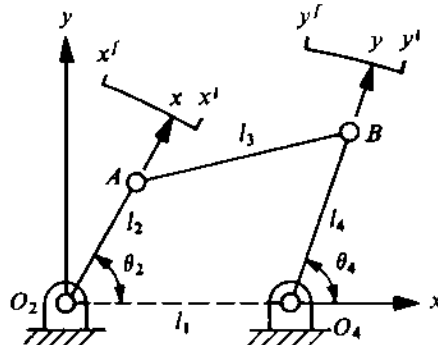


FIGURE 3.1

or path fits the desired function or path at all points in the interval. Exact synthesis is limited to a few arbitrary functions known as *nice functions*, whereas approximate synthesis pertains to almost all functions (of course, within a limited range). Our further discussion will be limited mainly to approximate synthesis.

The points at which the generated and desired functions agree are called *precision points* or *accuracy points*. The number of such points is equal to the number of design parameters at our disposal. This number varies and the difficulties encountered in the solution procedure are more as the number of accuracy points increases.

Before going into the details of the methods of solution, let us discuss how to choose the accuracy points for a given range of movement. The discussion is centred around function generation and essentially the same technique is followed for other categories of problems.

Function Generation by Mechanisms

Let $y = f(x)$ be the function to be generated by a four-bar linkage in the interval $x^i \leq x \leq x^f$. The orientation θ_2 of the driver link (crank) O_2A represents the independent variable x . The orientation θ_4 of the driven link (follower) O_4B represents the dependent variable y (Fig. 3.1). The relation between Δx and $\Delta\theta_2$, and that between Δy and $\Delta\theta_4$ is usually assumed to be linear (though this is not necessarily so). Let θ_2^i and θ_4^i be the initial values of θ_2 and θ_4 representing x^i and y^i [$= f(x^i)$], respectively. On the basis of an assumed linear relationship, we have

$$\frac{\theta_2 - \theta_2^i}{x - x^i} = \text{constant} = r_x = \frac{\theta_2^f - \theta_2^i}{x^f - x^i}, \quad (3.1)$$

$$\frac{\theta_4 - \theta_4^i}{y - y^i} = \text{constant} = r_y = \frac{\theta_4^f - \theta_4^i}{y^f - y^i}, \quad (3.2)$$

where r_x and r_y are called the *scale factors*. The superscripts i and f denote the initial and final values, respectively. Thus, we see that there are seven design parameters. These are θ_2^i , θ_4^i , r_x , and r_y , and the three ratios of link lengths l_1/l_2 , l_1/l_3 , and l_1/l_4 , where l_1 , l_2 , l_3 , and l_4 are the lengths of the four links as indicated in Fig. 3.1. Note that only the ratios of the link lengths, and not their absolute values, determine the relative motion, i.e., the coordination of $\Delta\theta_4$ with $\Delta\theta_2$. Finally, by approximate function generation using a mechanism, after suitably choosing r_x , r_y , θ_2^i , and θ_4^i and the accuracy points, we mean the generation of prescribed (coordinated) pairs of movements for the output and input links. If the number of precision points is N (any positive integer), then the number

of prescribed pairs of coordinated movements (between these N precision points) is obviously $N - 1$. Since we have only five design parameters so far as the linkage is concerned (disregarding the scale factors r_x and r_y), the maximum number of coordinated pairs that can be theoretically handled is five.

Chebyshev's Spacing of Accuracy Points

Let $f(x)$ be the function desired to be generated in an interval $x^i \leq x \leq x^f$, where the superscripts i and f refer to the initial and final values. Let the generated function be $F(x, R_1, R_2, \dots, R_k)$, where R_1 to R_k represent the k design parameters. Let

$$E(x) = f(x) - F(x, R_1, R_2, \dots, R_k). \quad (3.3)$$

It is evident that $E(x)$ will be zero only at the accuracy points, i.e., for $x = x_1, x_2, x_3, \dots, x_k$, where $x_1, x_2, x_3, \dots, x_k$ are the k accuracy points. $E(x)$ is called the *structural error*.¹

The best choice for the spacing of accuracy points will be that which gives the minimum value of $E(x)$ between any two adjacent accuracy points. For this purpose, the accuracy points can be determined only by trial and error, because the errors depend on the nature of $f(x)$ and $F(x, R_1, R_2, R_3, \dots, R_k)$. An exact analysis for $E(x)$ to be minimum is extremely difficult. However, Chebyshev's spacing of accuracy points can always be taken as a first approximation.

It can be proved that if $f(x)$ is a polynomial of the k -th order in x , and if $F(x, R_1, R_2, R_3, \dots, R_k)$ is a polynomial in x of the $(k - 1)$ -th order, then Chebyshev's spacing will minimize $E(x)$ between any two accuracy points. For other forms of $f(x)$ and $F(x, R_1, R_2, R_3, \dots, R_k)$, these functions can be expanded in Taylor series; as a first approximation, terms up to x^k are retained in $f(x)$ and those up to x^{k-1} are retained in $F(x, R_1, R_2, R_3, \dots, R_k)$. The accuracy points according to Chebyshev's spacing are given by²

$$x_l = a + h \cos \frac{(2l - 1)\pi}{2k} \quad (l = 1, 2, 3, \dots, k), \quad (3.4)$$

where

$$a = \frac{x^i + x^f}{2}, \quad h = \frac{x^f - x^i}{2}.$$

In further discussions, we shall always use, unless otherwise specified, Chebyshev's accuracy points obtained from (3.4).

There is a simple geometrical method for obtaining Chebyshev's accuracy points described by (3.4). A circle is drawn with the centre at a distance a from O on the x -axis, and with h as radius as shown in Fig. 3.2a. A regular polygon of side $2k$ is inscribed within this circle so that two sides are perpendicular to the x -axis. The projections of the vertices of this polygon on the x -axis determine the locations of the k accuracy points.

Figures 3.2a and 3.2b show this geometric method for $k = 3$ and $k = 4$, respectively. Semicircles showing only one-half of the inscribed polygons are obviously sufficient. The proof of this geometrical method is very simple and is left as an exercise for the reader.

Besides using precision points, there exists another approach to dimensional synthesis using an analytical method. In this approach, the structural error is not rendered zero at some finite number

¹This structural error is inherent in approximate synthesis. The error caused by a mechanical defect such as clearance at the joints or inaccuracy in length is called *mechanical error*.

²For a detailed proof of (3.4), see Hartenberg, R.S. and Denavit, J., Kinematic Synthesis of Linkages, McGraw-Hill, New York, 1964.

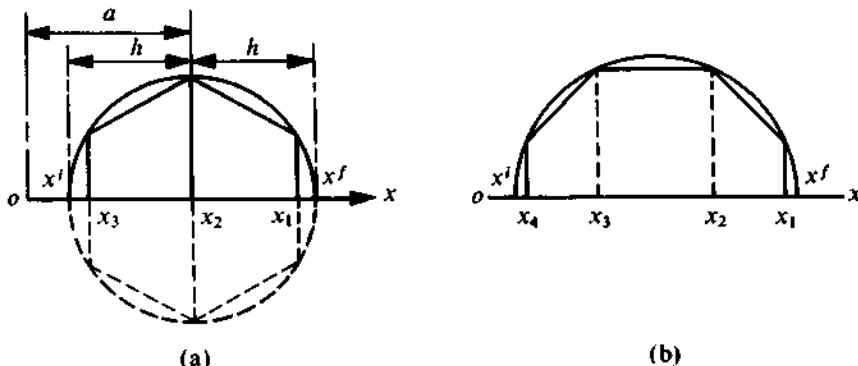


FIGURE 3.2

of accuracy points. Rather the structural error in the entire interval is minimized in an overall sense. For details of this optimization approach, the reader is referred to the second edition of this book.

3.2 GRAPHICAL METHOD (THREE POSITIONS)

The essence of the graphical methods will be brought out by solving problems of motion generation, path generation, and function generation with three accuracy points. Such problems are referred to as three-position synthesis.

Motion Generation

Let a rigid body be guided through three prescribed positions. The task is to design a 4R linkage of which this rigid body will be the coupler link. Referring to Fig. 3.3, the three prescribed positions are I, II, and III. Consider any two arbitrary points A and B on the rigid body. The locations of these two points in the three given configurations are A_1, A_2, A_3 and B_1, B_2, B_3 , respectively. Assuming these two sets of three points as noncollinear, let O_2 be the centre of the circle passing through A_1, A_2 , and A_3 , and O_4 be the centre of the circle passing through B_1, B_2 , and B_3 . Then $O_2A_1B_1O_4$ is obviously the required 4R linkage which takes the coupler A_1B_1 through A_2B_2 and A_3B_3 . It may be pointed out at this stage that if the solution turns out to be a Grashof linkage, then there is no guarantee that all the configurations will be attainable by the same mode of assembly. The details of this aspect will be discussed later in Section 3.6.

In most real-life problems, however, the locations of the ground pivots, i.e., O_2 and O_4 , are specified for various reasons such as convenience of location and constraint in space. In that case, the same problem will be rephrased as: Given positions I, II, and III (say, in terms of the axes $\xi - \eta$ fixed to the coupler) and the locations of O_2 and O_4 , determine the suitable locations of A and B on the coupler. In such a situation, the methodology discussed above can be used after considering a kinematic inversion with the coupler (i.e., the body to be guided) fixed at one of the three positions. In what follows, we explain this by fixing the coupler at its first position. For a better understanding and practice, it is suggested that, after going through the solution, the reader should obtain the same solution by fixing the coupler at any other position (i.e., either II or III).

Referring to Fig. 3.4a, let O_2 and O_4 be the prescribed positions of the ground pivots in the fixed frame OXY . The three prescribed positions of the coupler are indicated by the three configurations of the axes $\xi - \eta$ fixed to the coupler. To locate the hinges on the coupler, in its first (I) position

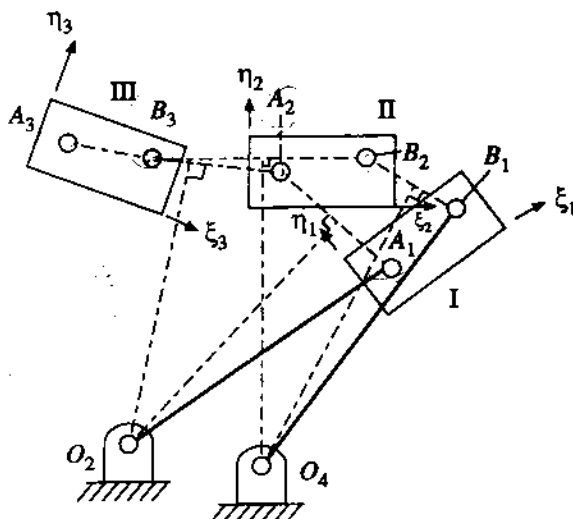


FIGURE 3.3

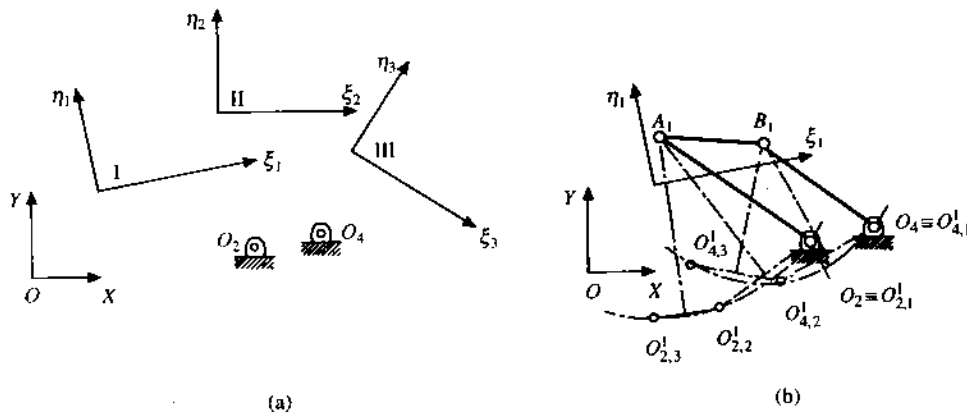


FIGURE 3.4

we invert the required 4R linkage by fixing the coupler in position I. The inverted positions of O_2 and O_4 (signifying the prescribed relative movements) are most conveniently obtained by using a tracing paper³ as now explained.

First, draw the given locations of O_2 and O_4 and the axes $\xi_1 - \eta_1$ (Fig. 3.4b). Then place the tracing paper on Fig. 3.4a and mark the axes $\xi_2 - \eta_2$ and the points O_2 and O_4 on it. Then place the tracing paper on Fig. 3.4b with $\xi_2 - \eta_2$ coinciding with the axes $\xi_1 - \eta_1$. The locations of O_2 and O_4 on the tracing paper are marked in Fig. 3.4b as $O_{2,2}^1$ and $O_{4,2}^1$. These are the inverted positions of O_2 and O_4 signifying the relative movement between I and II if the coupler is held fixed (and the frame is allowed to move). The reader should carefully note the labelling. The superscript (1) refers to the position where the inversion has been done and the second subscript (2) refers to the position which is being inverted. Similarly, marking $\xi_3 - \eta_3$, O_2 , and O_4 on the tracing paper and placing it on Fig. 3.4b so as to make $\xi_3 - \eta_3$ coincide with $\xi_1 - \eta_1$, the inverted positions $O_{2,3}^1$ and $O_{4,3}^1$ are marked on Fig. 3.4b. Since the lengths O_2A and O_4B are constant, the location of the coupler

³The same construction is possible without a tracing paper by using a compass.

hinges (in the first position) A_1 and B_1 are obtained as the centres of the circles passing through $O_{2,1}^1 (\equiv O_2)$, $O_{2,2}^1$, $O_{2,3}^1$ and $O_{4,1}^1 (\equiv O_4)$, $O_{4,2}^1$, $O_{4,3}^1$, respectively.

PROBLEM 3.1

Figure 3.5a shows three positions of a classroom desk which, when not in use, can be folded away (III). Position I indicates the configuration for writing. This desk is the coupler of a 4R linkage (which is driven by the coupler). The convenient locations of the ground pivots are indicated as O_2 and O_4 and another intermediate position is assumed as II. Determine the locations of the hinges A and B on the coupler and hence all the link lengths.

SOLUTION

Identify any two points C and D on the desk whose locations in the three prescribed configurations are marked as (C_1, D_1) , (C_2, D_2) , and (C_3, D_3) , respectively (Fig. 3.5a). Now locate O_2 , O_4 , and the desk (represented by the line C_1D_1) in its first configuration as shown in Fig. 3.5b. Placing a tracing paper on Fig. 3.5a, mark C_2, D_2, O_2 , and O_4 on the tracing paper. Move the tracing paper on Fig. 3.5b so that C_2 and D_2 coincide with C_1 and D_1 , respectively. The points O_2 and O_4 on the tracing paper are located on Fig. 3.5b at $O_{2,2}^1$ and $O_{4,2}^1$ respectively. Similarly, using (C_3, D_3) , O_2 , and O_4 on the tracing paper (from Fig. 3.5a) and placing (C_3, D_3) , on to (C_1, D_1) , in Fig. 3.5b, obtain the inverted positions $O_{2,3}^1$ and $O_{4,3}^1$. Thereafter, A is obtained at the centre of the circle passing through $O_2 (\equiv O_{2,1}^1)$, $O_{2,2}^1$, $O_{2,3}^1$. Likewise, B is obtained at the centre of the circle passing through $O_4 (\equiv O_{4,1}^1)$, $O_{4,2}^1$, $O_{4,3}^1$. From measurement and using the scale indicated in Fig. 3.5a, the link lengths are given as

$$l_1 = O_2O_4 = 9.6 \text{ cm}, \quad l_2 = O_2A = 24.9 \text{ cm},$$

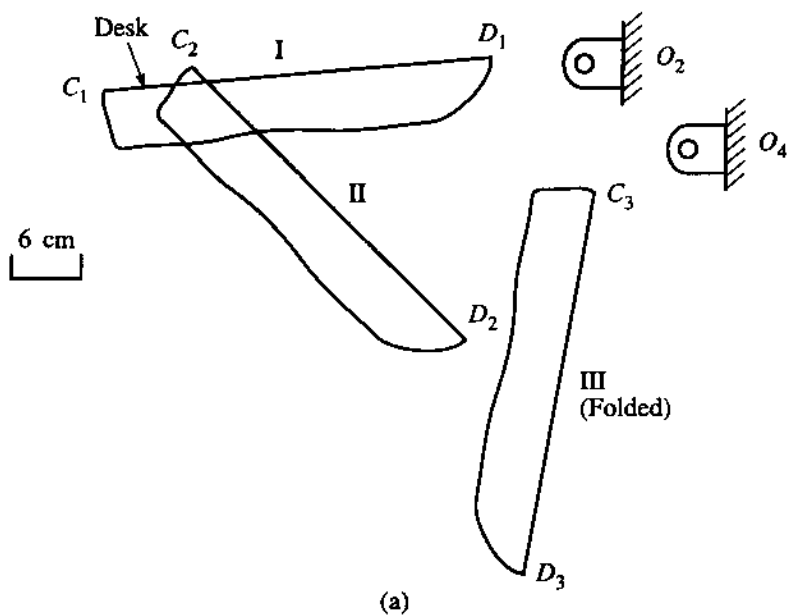
$$l_3 = AB = 6 \text{ cm}, \quad l_4 = O_4B = 25.02 \text{ cm}.$$

Path Generation

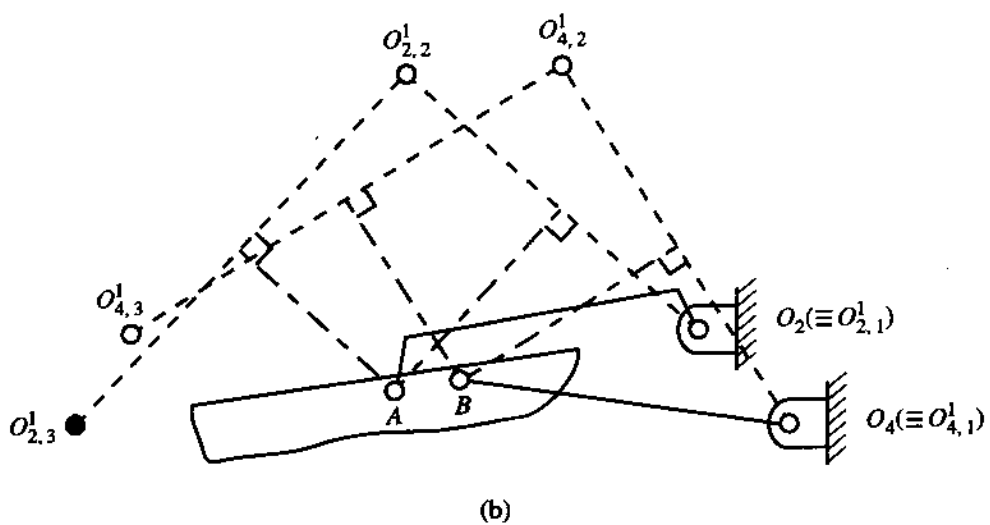
The technique of using kinematic inversion can also be followed for the design of a 4R linkage so that a point chosen on the coupler passes through three prescribed locations. Referring to Fig. 3.6a, let a coupler point C pass through three prescribed positions C_1 , C_2 , and C_3 . The locations of O_2 , O_4 , and B_1 are chosen conveniently as indicated in Fig. 3.6a and the task to obtain A_1 remains so as to achieve the desired objective. Since O_4B and BC are of constant length, the locations B_2 and B_3 are easily obtained using O_4 , C_2 , and C_3 .

Since O_2A is of constant length, we consider an inversion with the coupler fixed at position, say, 1 and obtain the three inverted positions of O_2 as follows.

First, reproduce O_2 , O_4 , B_1 , and C_1 from Fig. 3.6a in Fig. 3.6b. Place a tracing paper on Fig. 3.6a and mark B_2 , C_2 , and O_2 on it. Move the tracing paper on to Fig. 3.6b with B_2 coinciding with B_1 and C_2 with C_1 . Mark the location of O_2 on Fig. 3.6b as $O_{2,2}^1$. Similarly, using the tracing paper once more, obtain $O_{2,3}^1$. The centre of the circle passing through $O_2 (\equiv O_{2,1}^1)$, $O_{2,2}^1$, and $O_{2,3}^1$ is obtained as A_1 and the desired 4R linkage is obtained as $O_2A_1B_1O_4$ with C_1 as the coupler point. It is suggested that, to gain confidence, the reader repeat this problem with an assumed location for A_1 (may be the one just obtained above) and obtain B_1 as the solution (of course using inverted positions of O_4 instead of O_2).



(a)



(b)

FIGURE 3.5

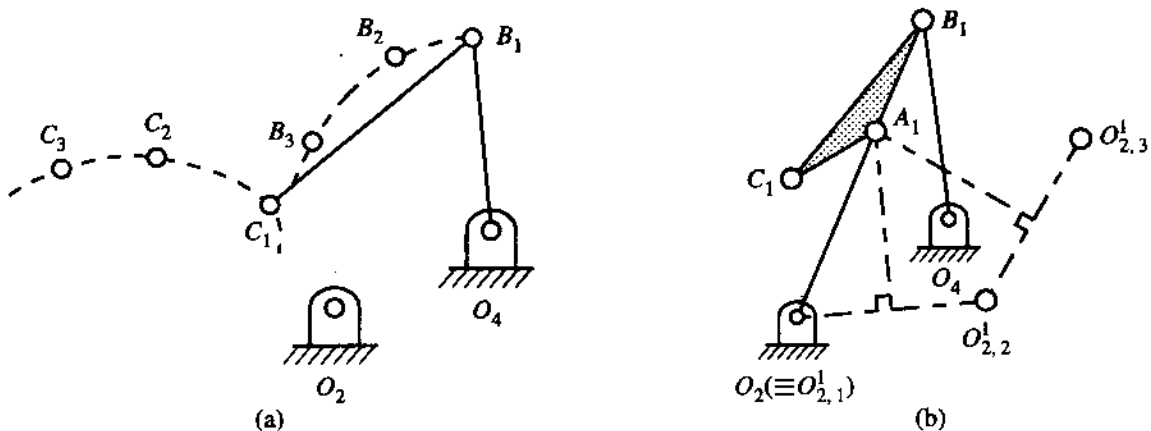


FIGURE 3.6

Function Generation

The method discussed so far for motion and path generation can be easily extended to function generation. Let two specified pairs of coordinated movements of the input and output links be generated. These are indicated in Fig. 3.7a as $(\theta_2^{12}, \theta_4^{12})$ and $(\theta_2^{23}, \theta_4^{23})$. In this notation, in general, $\theta_k^{ij} = \theta_k^j - \theta_k^i$, where $k = 2$ for the input link and $k = 4$ for the output link. To design the required 4R linkage, we assume the locations of O_2 , O_4 , and, say, A_1 (i.e., the crank pin at the first configuration); the task is to obtain B_1 . With the assumed location of A_1 and prescribed values of θ_2^{12} and θ_2^{23} , we can easily locate A_2 and A_3 as shown in Fig. 3.7a. Since the length AB is constant, we consider a kinematic inversion with the follower (output link O_4B) held fixed at its first position and follow the given relative movements. From configuration I to II, if the output link is held fixed, then the fixed link rotates about O_4 through an angle $-\theta_4^{12}$. Therefore, the inverted position of O_2 is obtained as $O_{2,2}^1$ as explained in Fig. 3.7b. The inverted position of A_2 is A_2^1 , where $\angle A_2^1 O_{2,2}^1 O_4 = \theta_2 = \theta_2^1 + \theta_2^{12}$. From congruent triangles, it is easy to prove that A_2^1 can also be obtained by rotating $O_4 A_2$ about O_4 through an angle $-\theta_4^{12}$. Similarly, the inverted position A_3^1 can be obtained by rotating $O_4 A_3$ about O_4 through an angle $-\theta_4^{13}$. Thereafter, B_1 is located at the centre of the circle passing through A_1^1 ($\equiv A_1$), A_2^1 , and A_3^1 and the desired linkage is obtained as $O_2 A_1 B_1 O_4$ at its first configuration. Again, it is instructive to solve the problem by assuming O_2 , O_4 , and B_1 (instead of A_1) and considering an inversion with the input link fixed to obtain A_1 . Furthermore, the reader may convince him(her)self completely by inverting on the second position (assuming either link O_2A or O_4B fixed, depending on whether B_2 or A_2 has been assumed along with the locations of O_2 and O_4).

PROBLEM 3.2

The sketch of a paper-cutting mechanism is shown in Fig. 3.8a, where a 40° CCW rotation of the handle is supposed to produce a 20° CCW rotation of the cutter as indicated in the figure. Determine the required offset e .

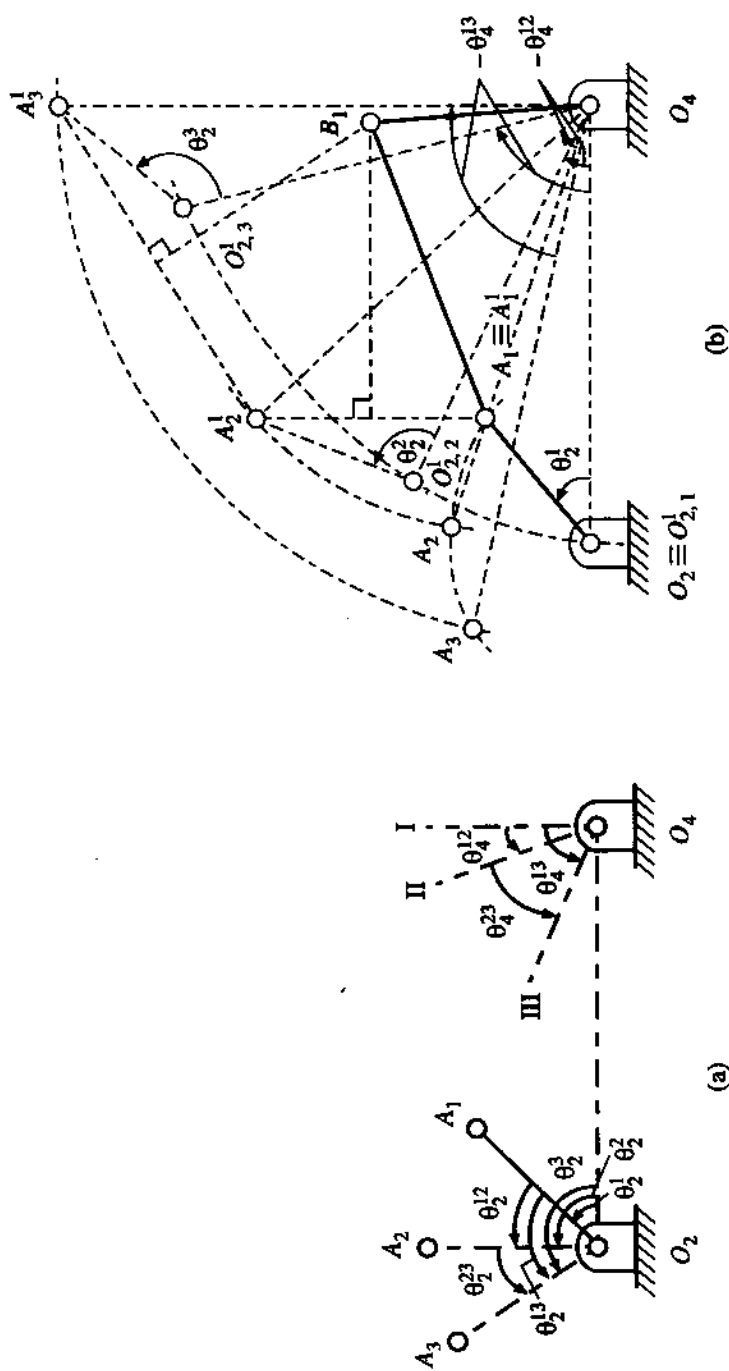


FIGURE 3.7

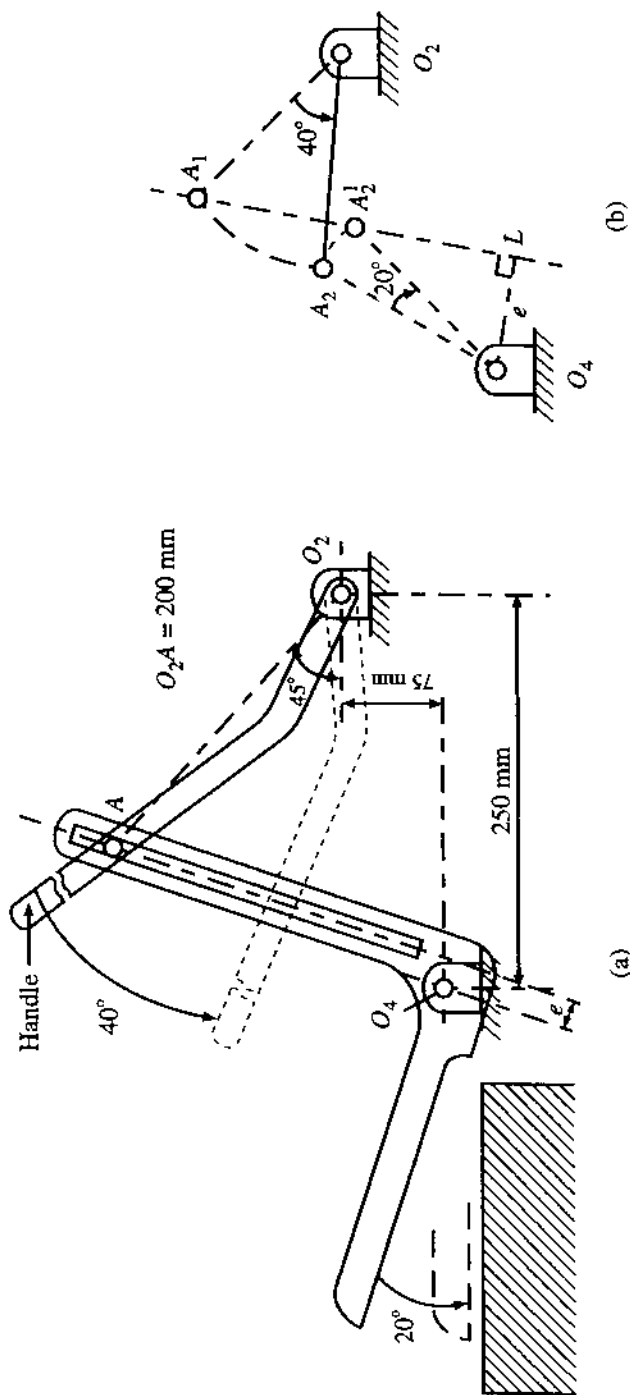


FIGURE 3.8

SOLUTION

Let us consider the initial configuration (solid lines) as I and the final configuration (dashed lines) as II. Since the pin centre is always along the slot axis, we make a kinematic inversion with the cutter held fixed. Then the line joining A_1 and A_2^1 (the inverted position of A_2) defines the slot axis as explained in Fig. 3.8b. Obviously, A_2^1 is obtained by rotating O_4A_2 about O_4 through 20° in the clockwise direction ($\equiv -\theta_4^{12}$). From measurement, using the scale of the diagram, the offset $e = 60$ mm.

By now, it is hoped that the use of kinematic inversion for dimensional synthesis is clear. Therefore, we venture to demonstrate the versatility of this technique by solving a more involved problem.

PROBLEM 3.3

Figure 3.9a shows the scheme of an overhead garage door with only hinge joints (without rails for guidance, i.e., a prismatic pair, difficult to maintain and costly to manufacture). In this six-link mechanism, link 6 is the door-board. The three desired positions of the door-board are indicated in Fig. 3.9b, as I (door closed), II (intermediate), and III (door open). The rotations of link 4 during these positions are desired as $\theta_4^{12} = 12^\circ$ CW and $\theta_4^{23} = 26^\circ$ CW. Obtain the location of the hinge B corresponding to position III and hence the link lengths O_4B and AB . Also determine the link lengths BD , CD , and $\angle DCE$.⁴

SOLUTION

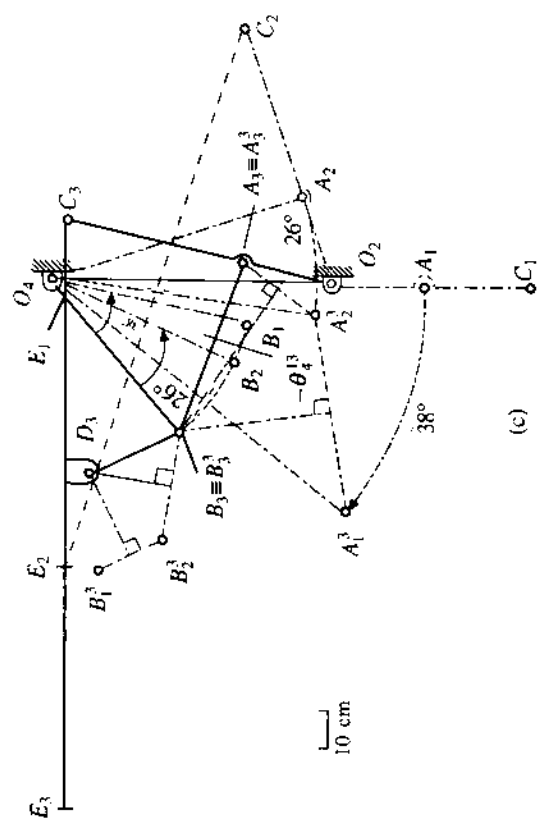
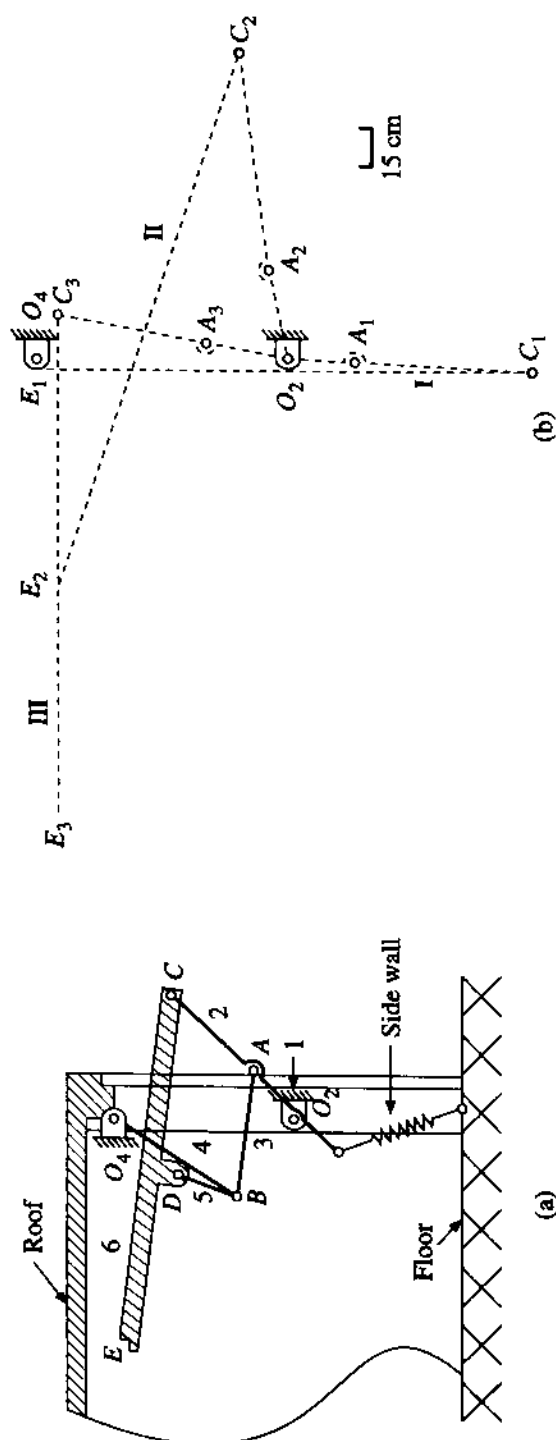
Since the linkage O_2ABO_4 is to be designed at position III, we invert the mechanism by keeping link 4 fixed at this position and obtain the inverted location of A_1 and A_2 as A_1^3 and A_2^3 , respectively. Obviously, $A_3 \equiv A_3^3$. The point A_1^3 is obtained by rotating O_4A_1 about O_4 through an angle $-\theta_4^{31}$ (see function generation), i.e., through $\theta_4^{13} = \theta_4^{12} + \theta_4^{23} = 38^\circ$ CW. This is shown in Fig. 3.9c. Similarly, A_2^3 is located by rotating O_4A_2 about O_4 through an angle $-\theta_4^{32} = \theta_4^{23} = 26^\circ$ CW. Since AB is of constant length, the point B_3 is located at the centre of the circle passing through A_1^3 , A_2^3 , and A_3^3 ($\equiv A_3$). From measurements, using the scale indicated, we get $O_4B = 72$ cm, $AB = 60$ cm.

To obtain the location of the hinge D on link 6, we make a kinematic inversion with link 6 held fixed (say, at position III) and consider the inverted positions of B . Towards this end, first obtain B_2 and B_1 from B_3 with the given rotations of link 4, i.e., by making $\angle B_3O_4B_2 = 26^\circ$ (CCW) and $\angle B_3O_4B_1 = 38^\circ$ (CCW). The inverted location of B_2 is obtained as B_2^3 using a tracing paper in the manner explained below. CE is considered fixed at C_3E_3 . On a tracing paper, mark the points C_2 , E_2 , and B_2 . Then move the tracing paper so that C_2 and E_2 coincide with C_3 and E_3 , respectively. Then the location of B_2 on the tracing paper is marked as B_2^3 in Fig. 3.9c. Similarly, B_1^3 is obtained by marking C_1 , E_1 , and B_1 on it and moving it to make C_1 coincide with C_3 and E_1 with E_3 . Since BD (link 5) is of constant length, D_3 is located at the centre of the circle passing through B_1^3 , B_2^3 , and B_3^3 ($\equiv B_3$). Again, from measurements, we get $BD = 38$ cm, $CD = 84$ cm, and $\angle DCE = 4^\circ$.

Use of Poles and Relative Poles

So far the graphical methods of dimensional synthesis have been discussed directly in the light of kinematic inversion. In what follows, we shall first develop the concept and properties of what are

⁴A simple 4R linkage with door-board as the coupler does not leave much of free space within the garage. That is why a six-link mechanism is required. The students may design a similar mechanism for covered book racks or almirah.



(a)

(b)

(c)

FIGURE 3.9

known as *poles* and *relative poles*. Then it will be demonstrated how the poles and relative poles can be used for dimensional synthesis (say, function generation) of 4R and slider-crank mechanisms. While designing a mechanism, a part may be designed by inversion while another part is designed by using relative poles. The choice of the method is mostly guided by convenience, depending on the prescribed or assumed data. Some worked out examples at the end of the section will use both the approaches.

Four-bar Linkage

Let us consider a finite movement of the coupler of a four-bar linkage from A_1B_1 and A_2B_2 as shown in Fig. 3.10. The normals drawn at the midpoints of A_1A_2 and B_1B_2 intersect at the point P_{12} . This point is the centre for the finite rotation from A_1B_1 to A_2B_2 and is called the *pole* of the rotation θ_3^{12} of the coupler. Obviously, the pole P_{12} depends only on the initial and final positions and is independent of the actual movement of the coupler. If the amount of rotation θ_3^{12} is infinitesimally small, then P_{12} is the well-known instantaneous centre of rotation of the coupler at that instant. From Fig. 3.10, it is clear that

$$\angle A_1P_{12}A_2 = \angle B_1P_{12}B_2 = \theta_3^{12}, \quad \angle A_1P_{12}N_1 = \angle B_1P_{12}N_2 = \theta_3^{12}/2.$$

Using these results, it can easily be seen from Fig. 3.10 that the frame and the coupler (at both positions) subtend equal angles at the pole. In other situations, as shown in Fig. 3.11, the angles subtended at the pole by the frame and the coupler (at both positions) differ by 180° . Similarly, the crank and the follower also subtend angles at the pole which are either equal or differ by 180° . One should be careful while measuring this angle. The directions of the angles (CW or CCW) from A to O_2 and B to O_4 (and not O_4 to B) are important. Similarly, the angle subtended (at P_{12}) by O_2O_4 must correspond to that by AB (and not BA).

In the foregoing discussion of poles of a four-bar linkage, the movement of the coupler was considered from a point P_{12} without establishing any relation between the angular displacements of the crank and the follower. We will now correlate the angular movements of the crank θ_2^{12} and of the follower θ_4^{12} through the coupler motion. To do this, we consider a kinematic inversion as shown in Figs. 3.12a and 3.12b. The motion represented in Fig. 3.12a can be obtained from the inverted mechanism shown in Fig. 3.12b by two separate rotations: (i) rotation of O_2O_4 (about O_2) through an angle $(-\theta_2^{12})$ when the configuration is $O'_4B'_1$, and (ii) rotation of $O'_4B'_1$ (about O'_4) through an angle θ_4^{12} when the configuration is $O'_4B'_2$, as shown in Fig. 3.12c. With the crank acting as the frame, the follower becomes the coupler. Our objective is to find the centre of a single rotation which is equivalent to the resultant of the aforementioned two rotations, (i) and (ii). This centre of equivalent rotation is called the *relative pole* R_{12} . Now, the initial and final positions of the coupler (after inversion) are O_4B_1 and $O'_4B'_2$ as shown in Fig. 3.12c. Using the principle explained earlier, we can determine the relative pole R_{12} as the centre of finite rotation from O_4B_1 to $O'_4B'_2$. From Fig. 3.12c, we have $\phi = \psi + \theta_2^{12}/2$. Again, since ψ is half the angle of resultant rotation, we get $\psi = (\theta_4^{12} - \theta_2^{12})/2$ when $\phi = \theta_4^{12}/2$. As ϕ is in the clockwise direction, we shall write $\phi = -\theta_4^{12}/2$ (all angles being positive when measured in the CCW direction). Thus, R_{12} is the intersection of the lines N_1 and N_2 (Fig. 3.12c); the angles which these lines make with O_2O_4 are $(-\theta_2^{12}/2)$ at O_2 and $(-\theta_4^{12}/2)$ at O_4 , respectively. It can be verified easily that O_2A_1 and O_4B_1 subtend equal angles at the point R_{12} and also that O_2O_4 and A_1B_1 subtend equal angles at R_{12} . This result is very useful for dimensional synthesis by the graphical methods.

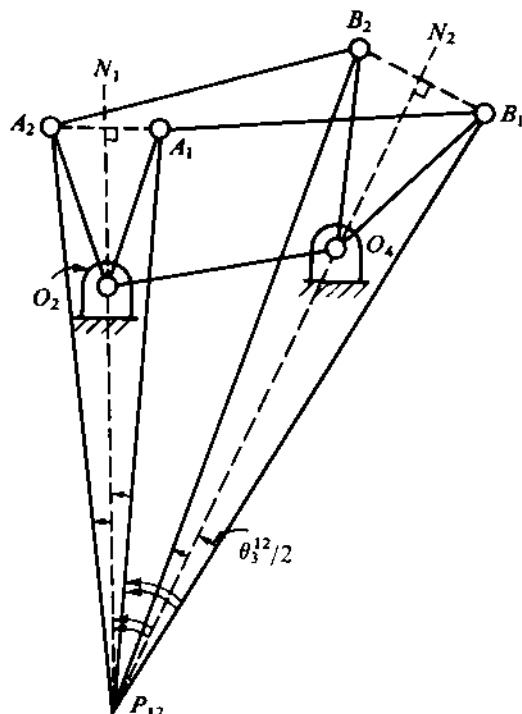


FIGURE 3.10

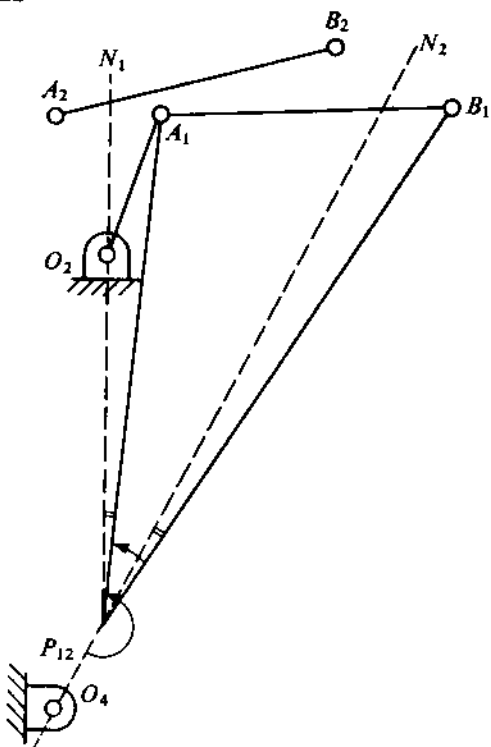


FIGURE 3.11

Slider-crank Mechanism

In Chapter 1, it was shown that the slider-crank mechanism is obtained as a limit of the four-bar linkage where one revolute pair is replaced by a sliding pair. In other words, the hinge O_4 of the follower can be regarded as being at infinity in a direction perpendicular to the line of movement of the slider. Using this concept, the relative poles of a slider-crank mechanism can be easily obtained by extending the method used for a four-bar mechanism. Let the problem be to find the relative pole R_{12} which gives the centre of rotation of the connecting rod for crank rotation of θ^{12} , the corresponding slider movement being s^{12} (Fig. 3.13). A line N_1 is drawn through O_2 at an angle $(-\theta^{12}/2)$ with O_2O_4 . The line N_2 is drawn at a distance $(-s^{12}/2)$ from O_2 and perpendicular to the line of movement of the slider. The point R_{12} is the intersection of the lines N_1 and N_2 . The frame O_2O_4 and the connecting rod subtend equal angles at R_{12} . This information, as in the case of the four-bar linkage, will be used for synthesis of slider-crank mechanisms by the graphical methods.

Synthesis of Four-bar Linkage

We shall first synthesize a four-bar linkage using the relative poles so that the crank (input) rotation θ_2^{12} corresponds to the follower (output) rotation θ_4^{12} (see Fig. 3.14). We choose the frame O_2O_4 arbitrarily (Fig. 3.14). The relative pole R_{12} is determined by the intersection of the lines N_1 and N_2 , which are drawn such that the angles they make with O_2O_4 are $(-\theta_2^{12}/2)$ at O_2 and $(-\theta_4^{12}/2)$ at O_4 , respectively. Then, the point A is taken arbitrarily. The last point B can be taken anywhere on the line $R_{12}Z$ so drawn that $\angle O_2R_{12}O_4 = \angle AR_{12}Z$ (subtended by the frame at R_{12}) = $\angle AR_{12}Z$ (subtended

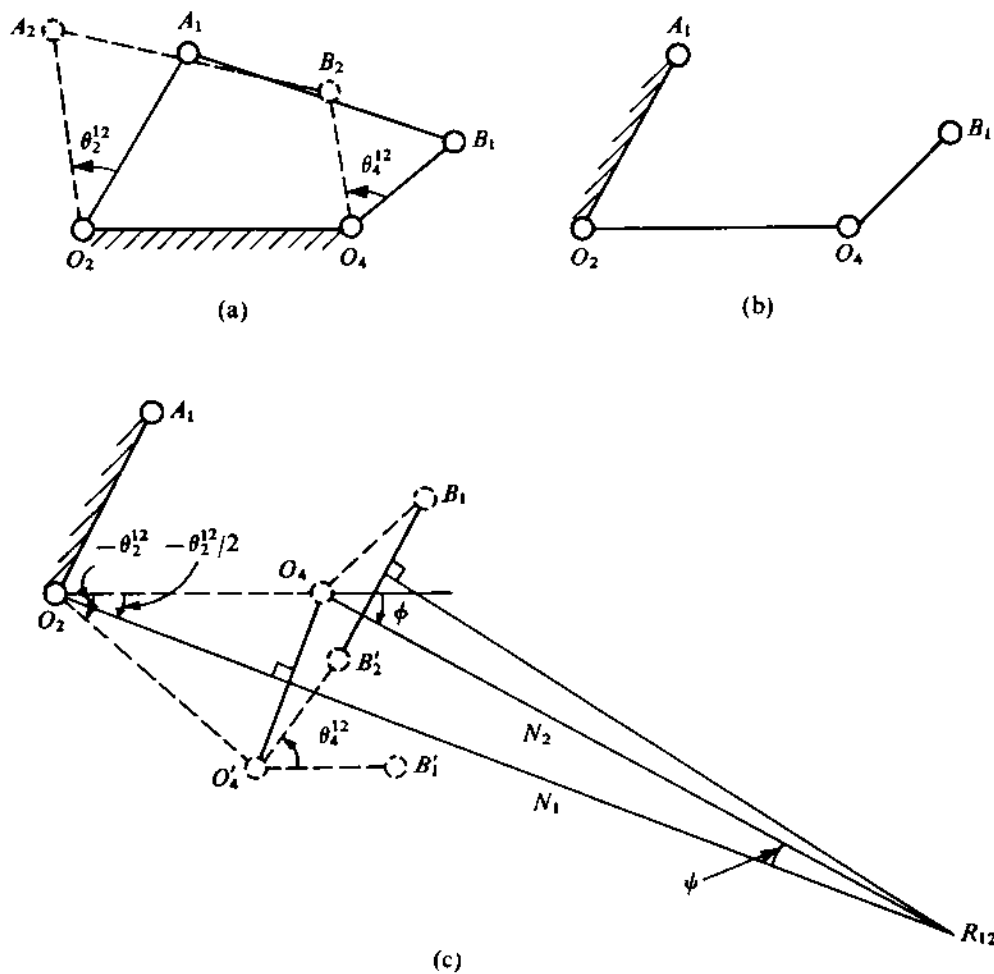


FIGURE 3.12

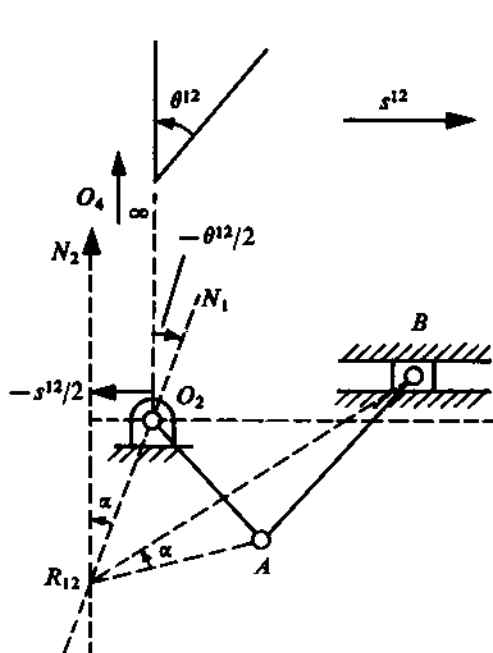


FIGURE 3.13

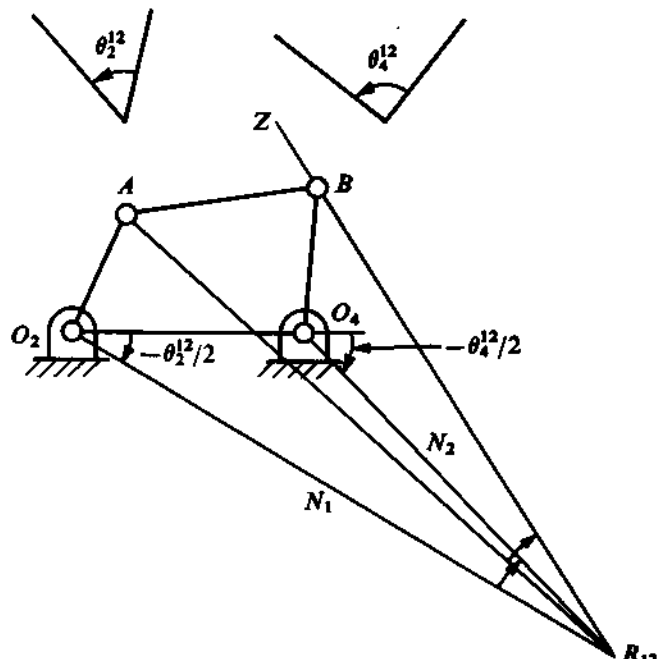


FIGURE 3.14

by the coupler at R_{12}).

The reader is advised to solve Problem 3.2 by using relative poles. It is pointed out that in this problem, the point B is at infinity in a direction perpendicular to the slot. Hence, if the direction of B is determined, the slot axis will be passing through A and perpendicular to the direction in which B lies (at infinity).

Next, we synthesize another four-bar linkage so that the two pairs of the crank and follower rotations are coordinated. Figure 3.15a shows the amount of crank and follower rotations between positions 1, 2, and 3. We shall take $(\theta_2^{12}, \theta_4^{12})$ and $(\theta_2^{13}, \theta_4^{13})$ as the two pairs of coordinated rotations. The relative poles R_{12} and R_{13} are located graphically after assuming the locations of the fixed hinges O_2 and O_4 (see Fig. 3.15b). (If the length of the fixed link is specified, then O_2O_4 should be equal to this length.) The first position and the length of the input link are either assumed or specified. Let the first position be represented by O_2A_1 . As the crank and the follower subtend equal angles at the relative poles, the first position of the follower pin B_1 must lie on the lines $R_{12}Y$ and $R_{13}Z$ so drawn that

$$\angle O_2R_{12}A_1 = \angle O_4R_{12}Y, \quad \angle O_2R_{13}A_1 = \angle O_4R_{13}Z.$$

Thus, $O_2A_1B_1O_4$ is the configuration of the mechanism at the initial position.

We could have obtained the mechanism in its second configuration by choosing A_2 arbitrarily and using the relative poles R_{21} (instead of R_{12}) and R_{23} . The relative pole R_{21} is obtained at the intersection of two lines, one drawn at O_2 at an angle $-\theta_2^{21}/2$ ($\equiv \theta_2^{12}/2$) to O_2O_4 and the other drawn at O_4 at an angle $-\theta_4^{21}/2$ ($\equiv \theta_4^{12}/2$) to O_2O_4 . It is then obvious that R_{21} will be the mirror image of R_{12} with the mirror along O_2O_4 . Now, B_2 will be located using the fact that O_2A_2 and O_4B_2 subtend equal angles at R_{21} and also at R_{23} .

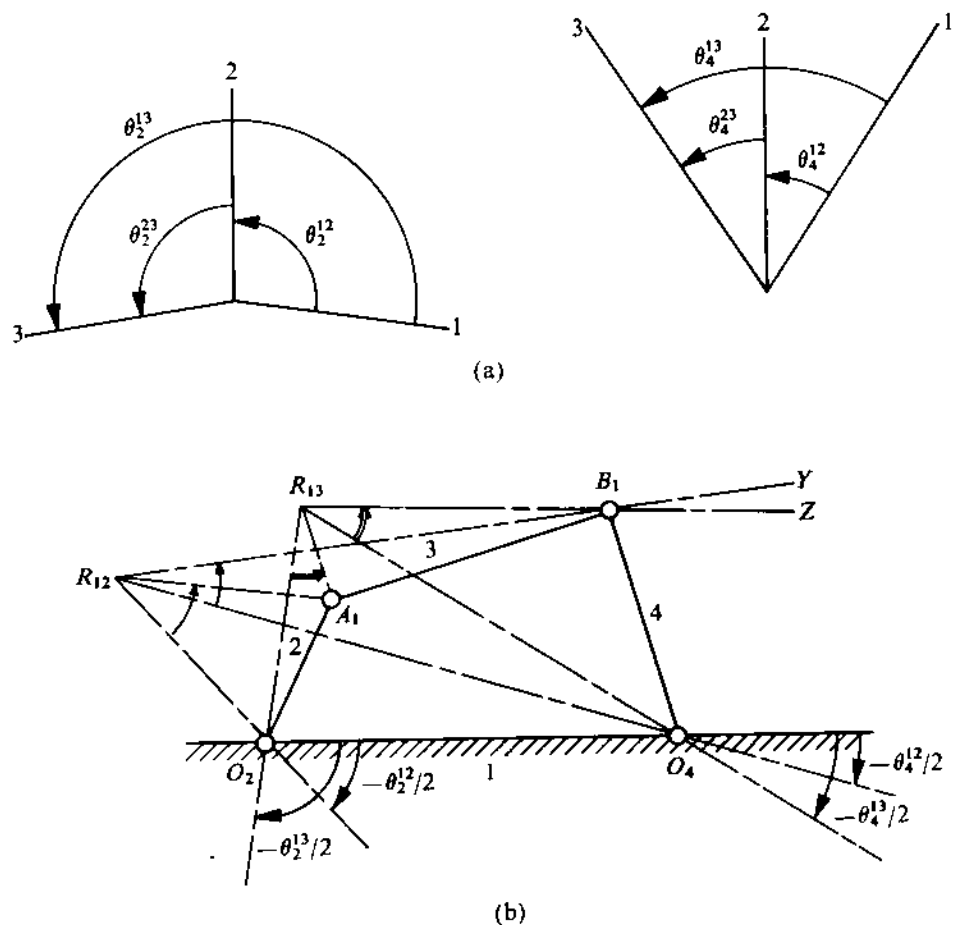


FIGURE 3.15

Synthesis of Slider-crank Mechanism

Since the reader by now is quite familiar with the concept of relative poles, we shall not discuss the situation with only one pair of coordinated movements (θ_2^{12}, s^{12}). Instead, we shall demonstrate the use of relative poles by considering a mechanism with two pairs of coordinated movements (see Fig. 3.16a).

First, O_2 is chosen and a line O_2X is drawn along the line of slider movement. Another line O_2Y is drawn perpendicular to O_2X (Fig. 3.16b). Using the given pairs of coordinated movements, the relative poles R_{12} and R_{13} are located. Then, the crank O_2A_1 is drawn at its first position (specified or assumed). Two lines $R_{12}P$ and $R_{13}Q$ are drawn so that $\angle O_2R_{12}O_4 = \angle A_1R_{12}P$ and $\angle O_2R_{13}O_4 = \angle A_1R_{13}Q$. The point of intersection of these two lines, B_1 , determines the location of the slider at its first position. Thus, the connecting-rod length and the offset required are determined.

Now that the reader is conversant with the graphical methods of dimensional synthesis having three precision points, let us discuss a more involved problem of kinematic design of a mechanism. It is hoped that the solution of this problem provides the flavour of a real-life design which always has more than one solution, depending on the designer's choice.

PROBLEM 3.4

Figure 3.17a shows the kinematic diagram of a fork lift with only revolute joints. It should be noted that the fork (6) is not guided in the vertical direction by a prismatic pair (which is costly to manufacture and maintain). Instead, it is desired that the fork move approximately in the vertical direction over a distance of 1.5 m. It is further stipulated that the vertical movement of the fork be approximately proportional to the rotation of the input link (2). Design the linkage with suitable assumptions using three accuracy points.

SOLUTION

The design can be arrived at in several steps as detailed here. The reader should carefully note the various assumptions and alternatives which are important to reach an acceptable working solution.

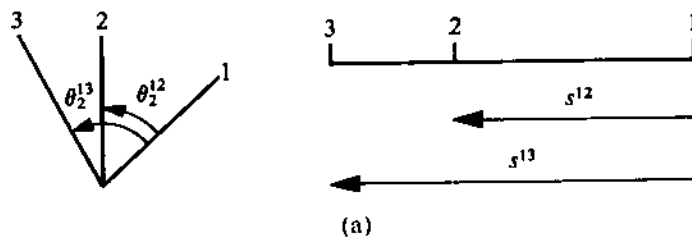
Step 1: First, let us design an imaginary slider-crank mechanism O_2AB (Fig. 3.17b) so that the slider at B moves vertically through a distance of 1.5 m maintaining approximately a proportional relationship with the rotation of the crank O_2A . Let us assume that a 60° CCW rotation of the crank produces a 1.5 m downward movement of the slider.

As shown in Fig. 3.17c, three Chebyshev's accuracy points for the slider positions are determined for a total travel of 1.5 m. The accuracy points are labelled as B_1 , B_2 , and B_3 . The crank rotations corresponding to these accuracy points are determined using the proportionality relation

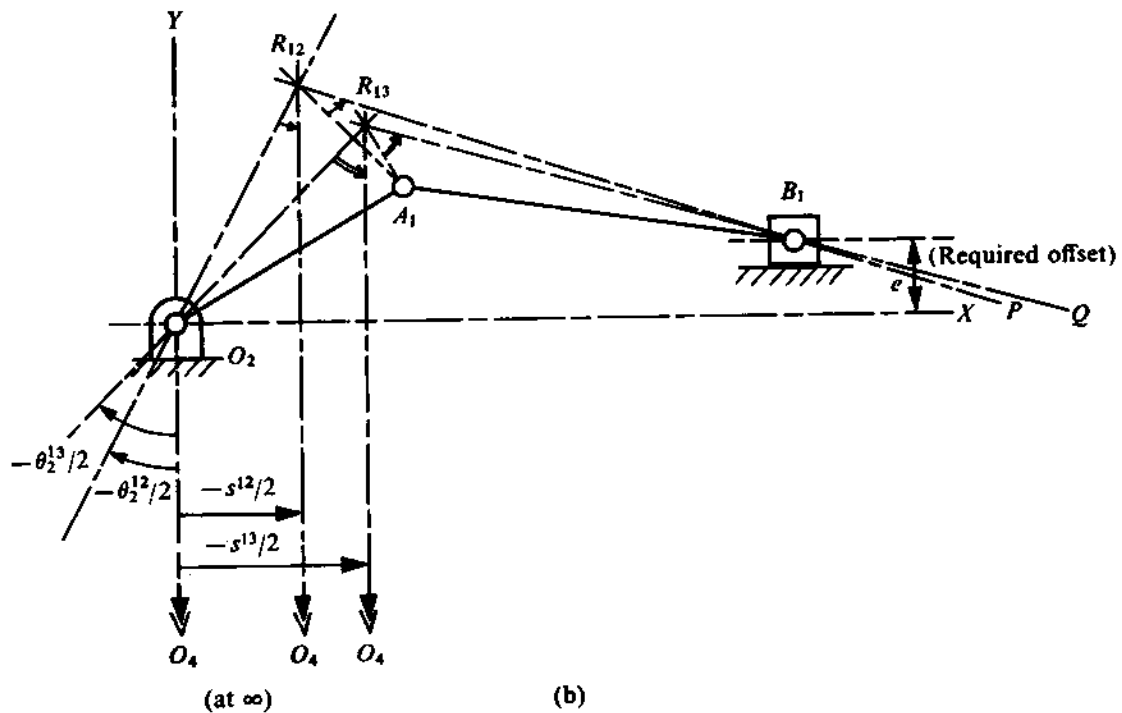
$$\frac{\Delta\theta_2}{\Delta s} = \frac{\theta_2^{12}}{s^{12}} = \frac{\theta_2^{13}}{s^{13}}, \quad (a)$$

where $\Delta\theta_2 = 60^\circ$, $\Delta s = 1.5$ m, $s^{12} = B_1B_2$, $s^{13} = B_1B_3$. From (a), we obtain $\theta_2^{12} = 26^\circ$ (CCW) and $\theta_2^{13} = 52^\circ$ (CCW).

Next, we choose a convenient location for O_2 on the body of the fork-lift truck. Using the relative poles, the slider-crank mechanism is synthesized for two pairs of coordinated movements, viz., (θ_2^{12}, s^{12}) and (θ_2^{13}, s^{13}) , with a convenient location of B_1 , as explained in Fig. 3.17d. The reader may note that, in Fig. 3.16, the location of A_1 was assumed and that of B_1 was



(a)



(b)

FIGURE 3.16

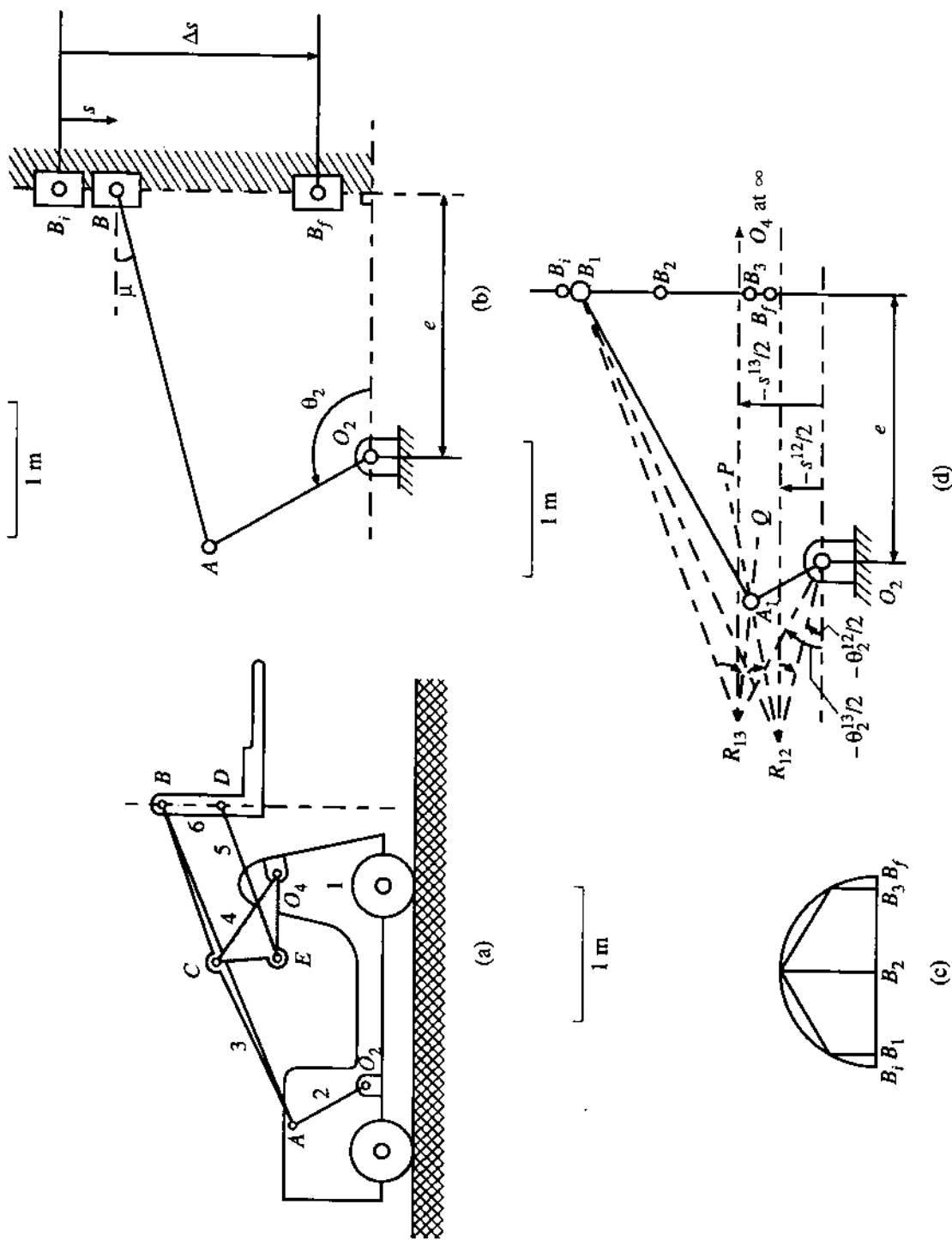


FIGURE 3.17 (cont.)

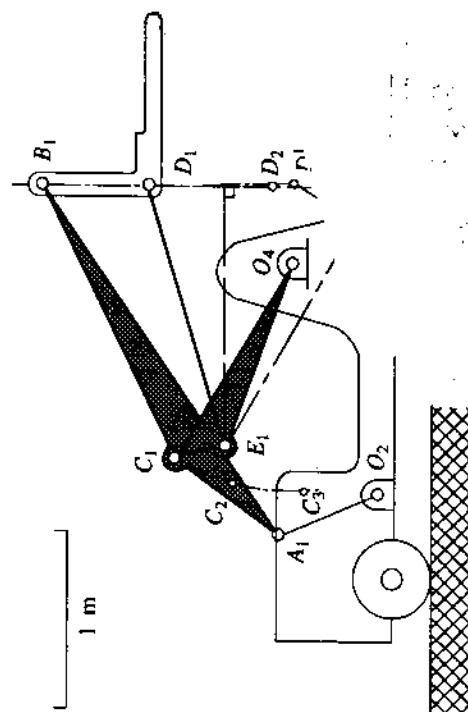
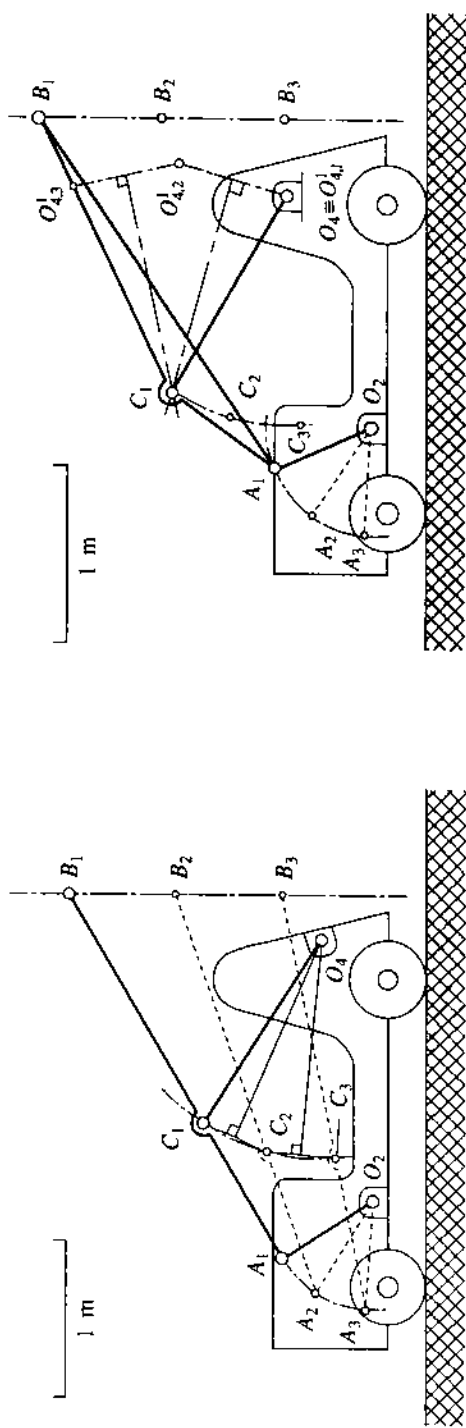
determined. However, here the line and stroke of travel of the fork are conveniently chosen. The mechanism so designed should not only have reasonable link lengths but also ensure a minimum value of the transmission angle μ ($\geq 30^\circ$) during the entire travel. Otherwise, a redesign with changed values of the assumed parameters (such as $\Delta\theta_2$, locations of O_2 and B_1) is warranted.

Step 2: Now the slider at B can be replaced by adding a suitable link O_4C (Fig. 3.17a) so that the point B of the connecting rod (or the coupler of the new 4R linkage O_2ACO_4) still passes through the accuracy points B_1 , B_2 , and B_3 . Of course, the path of B will now deviate from the exact vertical line. So long as the deviation is not too large, it is acceptable.

Different approaches can be adopted towards the design of O_4C . One method is to take C arbitrarily near the midpoint of AB (Fig. 3.17e) and determine its locations C_1 , C_2 , and C_3 corresponding to the three accuracy points. Then O_4 lies at the centre of the circle passing through C_1 , C_2 , and C_3 . It may be emphasized that this choice of C renders link 3 as a slender member. Furthermore, if C is taken too close to A , then O_4 moves close to O_2 and the resulting linkage will have very poor transmission quality. On the other hand, if C is taken too close to B , then obviously O_4 moves very far off (may be too far outside the body of the truck) since, for the point B , the centre of the circle (a straight line) passing through B_1 , B_2 , and B_3 moves to infinity. Again, a few trials may be needed for the location of C to ensure a convenient location of O_4 .

Another approach may be to first choose the location of O_4 conveniently on the body of the truck and determine C_1 so that the coupler point B of the 4R linkage $O_2AC(B)O_4$ passes through B_1 , B_2 , and B_3 , as explained in Fig. 3.17f. Here, a kinematic inversion has been made with the coupler fixed at its first position (A_1B_1) and with a tracing paper the inverted locations $O_{4,1}^1$ ($\equiv O_4$), $O_{4,2}^1$, and $O_{4,3}^1$ have been determined. (Refer to the procedure explained in Fig. 3.6. The only difference is that here A_1 is already known.) Thereafter, the location of C_1 is obtained at the centre of the circle passing through $O_{4,1}^1$, $O_{4,2}^1$, and $O_{4,3}^1$ as explained in Fig. 3.17f. For an acceptable design, C_1 should not be too far away from the line A_1B_1 . Otherwise, a redesign with a different choice of O_4 is recommended. Fortunately, the location of C_1 in Fig. 3.17f is acceptable and we shall proceed with this design in the next step to complete the mechanism.

Step 3: First we determine the locations C_1 , C_2 , and C_3 corresponding to the three accuracy points (Figs. 3.17e and 3.17f). So far, we have made no attempt to keep the fork close to horizontal as it is simply hinged only at B . To make the fork remain horizontal, another point on the fork, say, D (Fig. 3.17a), has to be constrained in a suitable manner. This is achieved by adding link 5 after determining the location of E on link 4 as now explained. Locate the positions D_1 , D_2 , and D_3 corresponding to the three accuracy points (Fig. 3.17g). Now consider a kinematic inversion by keeping link 4 fixed in its first position (i.e., O_4C_1). Mark O_4 , C_2 , and D_2 on a tracing paper. Place the tracing paper on Fig. 3.17g with O_4 and C_2 coinciding with O_4 and C_1 , respectively. The location of D_2 on the tracing paper is marked as D_2^1 on Fig. 3.17g. Similarly, marking O_4 , C_3 , and D_3 on the tracing paper, locate D_3^1 (Fig. 3.17g). The centre of the circle passing through D_1^1 ($\equiv D_1$), D_2^1 , and D_3^1 is at E_1 . The finally designed six-link mechanism is shown in Fig. 3.17g at the configuration corresponding to the first accuracy point.



6

3.3 FOUR-POSITION SYNTHESIS (POINT-POSITION REDUCTION)

The general approach to dimensional synthesis for four positions is beyond the scope of this text. However, some restricted solutions can be easily obtained by extending the method outlined in section 3.2. This method is known as *point-position reduction*. We shall now illustrate this method with respect to both function-generation and path-generation problems.

For function generation with three pairs of coordinated movements, let us add a fourth position V to Fig. 3.7a, as indicated in Fig. 3.18a, as $(\theta_2^{14}, \theta_4^{14})$. Now, with an arbitrary choice of A_1 (as was done in Fig. 3.7b), there is no guarantee that the four inverted positions of A , viz., $A_1^1 (\equiv A_1)$, A_2^1 , A_3^1 , and A_4^1 , will lie on a circle. However, with particular choices of A_1 , we can make two of these four inverted positions coincide. For example, as shown in Fig. 3.18b, let A_1 be chosen as the relative pole R_{12} with an assumed O_2O_4 . The corresponding locations of A_2 , A_3 , and A_4 are then easily obtained since θ_2^{1j} are given for $j = 2, 3, 4$. From the method of construction of the inverted position, explained in Fig. 3.7b, i.e., by rotating O_4A_2 about O_4 through $-\theta_4^{12}$, it is readily seen that A_2^1 coincides with $A_1 (\equiv A_1^1)$ in Fig. 3.18b. This is not at all surprising because the relative movement between links 4 and 2 from position I to II is a pure rotation about R_{12} . In other words, this point does not move during the relative movement from position I to II. Now B_1 can be easily located at the centre of the circle passing through $A_1 (\equiv A_1^1$ and $A_2^1)$, A_3^1 , and A_4^1 as shown in Fig. 3.18b. Thus, the mechanism in its first configuration is obtained as $O_2A_1B_1O_4$. It may be noted that we could also choose A_1 at R_{13} (or R_{14}) when A_3^1 (or A_4^1) would have coincided with A_1 . The reader should also think about choosing A_2 (instead of A_1) at R_{23} or R_{24} . Moreover, it should be pointed out that link 2 of the linkage designed by this point-position reduction method necessarily has to cross the line of frame O_2O_4 , and hence cannot be the rocker of a crank-rocker linkage.

The method of point-position reduction, just explained for function generation with four accuracy points, can also be used for path generation so that a coupler point passes through four prescribed locations. Let a fourth point C_4 be added to Fig. 3.6a, as shown in Fig. 3.19a, and our objective is to synthesize the desired linkage. In Fig. 3.6b, the locations of B_1 , O_2 , and O_4 were chosen arbitrarily. But in that case, again there is no guarantee that the four inverted positions of O_2 will lie on a circle. We can, however, ensure that two of the four inverted positions of O_2 coincide by choosing P_2 as one of the poles (of the coupler movements) P_{12} , P_{13} , etc. In Fig. 3.19b, it is illustrated by choosing O_2 at P_{13} . For given locations of C_1 , C_2 , C_3 , and C_4 , we choose O_4 and B_1 arbitrarily. Since B moves on a circle (k_B) with centre at O_4 and radius O_4B and the length BC is constant, we determine B_2 , B_3 , and B_4 on k_B . The pole P_{13} of the coupler movement from position 1 to 3 is located at the intersection of the midnormals of B_1B_3 and C_1C_3 . The location of O_2 is chosen at P_{13} . Thus, $O_2 \equiv O_{2,1}^1 \equiv O_{2,3}^1$. Marking B_2 , C_2 , and O_2 on a tracing paper and placing it on Fig. 3.19b with B_2 and C_2 coinciding with B_1 and C_1 , respectively, the location of O_2 on the tracing paper is marked as $O_{2,2}^1$ in Fig. 3.19b. Similarly, marking B_4 , C_4 , and O_2 on the tracing paper and placing it on Fig. 3.19b with B_4 and C_4 coinciding with B_1 and C_1 , respectively, we obtain the inverted position $O_{2,4}^1$. The centre of the circle passing through $O_2 (\equiv O_{2,1}^1 \equiv O_{2,3}^1)$, $O_{2,2}^1$, and $O_{2,4}^1$ is the location of A_1 . Thus, the desired mechanism at the first configuration is obtained as $O_2A_1B_1(C_1)O_4$.

Four-bar coupler curves (specially of crank rockers) can be of various shapes and are often used to guide a point along a desired, complicated path. To facilitate their application, a comprehensive

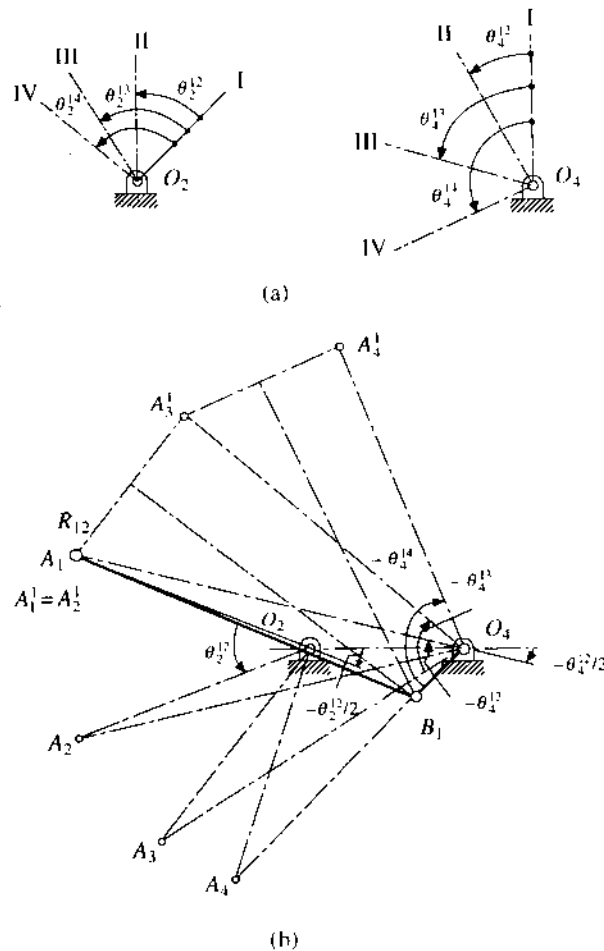


FIGURE 3.18

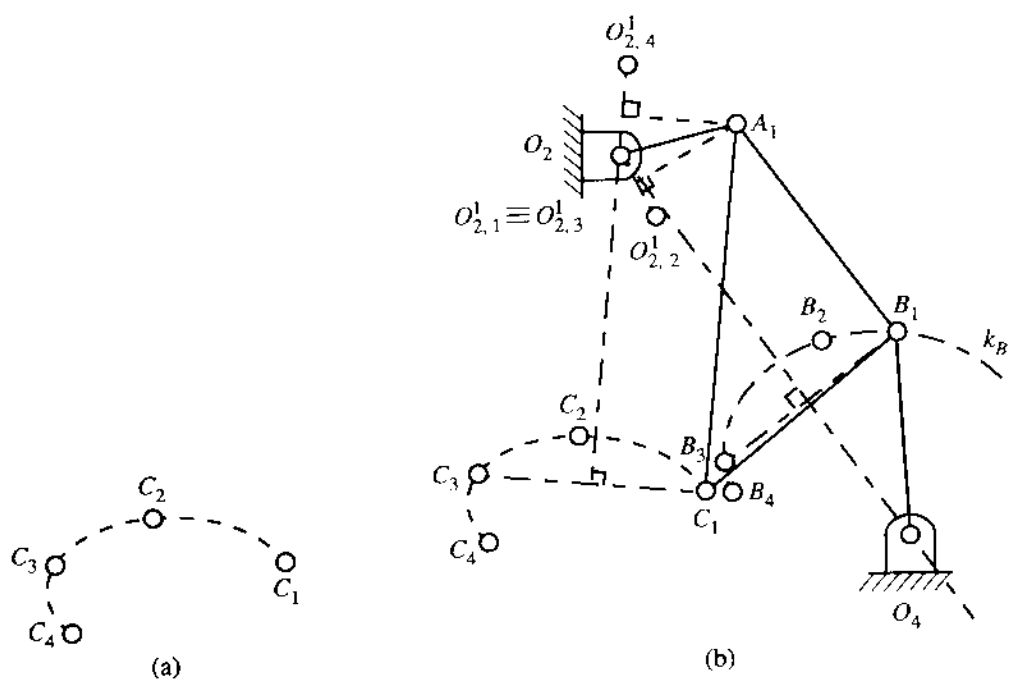


FIGURE 3.19

atlas⁵ (consisting of 7300 coupler curves and indicating the rate of traverse) has been compiled.

3.4 DEAD-CENTRE PROBLEMS

In this section, we shall discuss the graphical methods of synthesizing slider-crank and 4R crank-rocker mechanisms for specified quick-return ratios (with a constant speed of the input link).

Slider-crank Mechanisms

A slider-crank mechanism is to be synthesized for prescribed values of quick-return ratio and slider stroke. The offset may be either specified or assumed. Figure 3.20a shows the extreme (dead-centre) positions 1 and 2 of a slider-crank mechanism with offset e . Obviously, $O_2B_1 = l_3 + l_2$ and $O_2B_2 = l_3 - l_2$ and the quick-return ratio is $\theta_2^{12}/(2\pi - \theta_2^{12})$. To synthesize the mechanism, first B_1 and B_2 are located at a distance s^{12} apart (see Fig. 3.20b). The point C is located on the perpendicular bisector of B_1B_2 such that $\angle B_1CB_2 = 2(\theta_2^{12} - \pi)$. The circle k is constructed with C as the centre and CB_1 as the radius. Then, the line YZ is drawn parallel to B_1B_2 at a distance e , intersecting the circle k at O_2 . The point D is located on the extension of B_1O_2 so that $O_2D = O_2B_2$. Finally, A_1 is obtained as the midpoint of B_1D and the mechanism obtained is $O_2A_1B_1$. The proof of this construction is very simple and is left as an exercise for the reader.

4R Crank-rocker Mechanisms

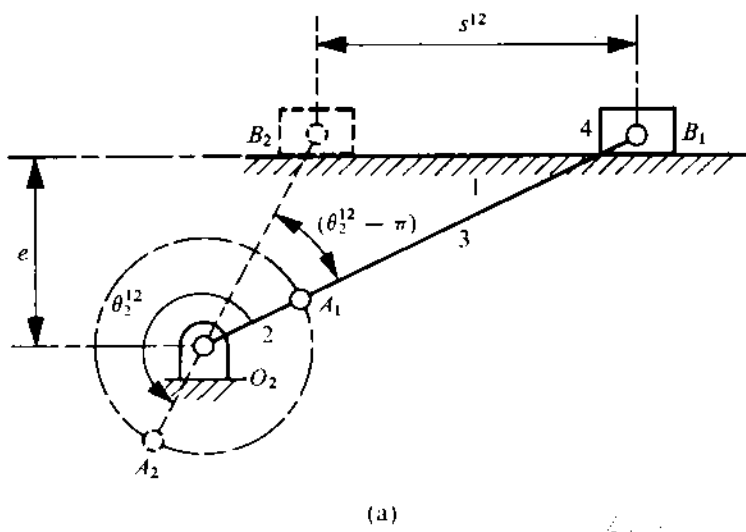
A crank-rocker mechanism is very frequently used in various machines and a systematic method of kinematic synthesis of such a mechanism is very useful from the design standpoint. Figure 3.21a shows the two extreme configurations, labelled 1 and 2, of one such mechanism. As can be seen, if the crank (i.e., link 2) rotates through an angle θ_2^{12} , the rocker (i.e., link 4) swings through an angle θ_4^{12} . Thus, for a constant speed of rotation of the crank, the time taken by the rocker during its forward motion 1 → 2 is more than that during its return motion 2 → 1.

In what follows, we shall synthesize this mechanism with prescribed values of θ_4^{12} and quick-return ratio $\theta_2^{12}/(2\pi - \theta_2^{12})$. The dimension O_2O_4 may be either prescribed or assumed before starting the synthesis. When $\theta_2^{12} < \pi$, the points O_2 and O_4 are first located at the distance specified (or assumed). Then, using the values of θ_2^{12} and θ_4^{12} , the relative pole R_{12} is located as shown in Fig. 3.21b. The perpendicular bisector of O_2R_{12} intersects O_4R_{12} at C_2 . Now, two circles k_1 and k_2 are drawn with C_1 and C_2 as the centres and C_1O_2 and C_2O_2 as the radii, respectively. A line O_4Z is drawn with $\angle O_2O_4Z = \theta_4^{12}$. The arc of the circle k_2 above the line O_4Z can be used for locating B_1 . With B_1 thus located, O_2B_1 intersects k_1 at A_1 . The desired linkage is then given by $O_2A_1B_1O_4$.

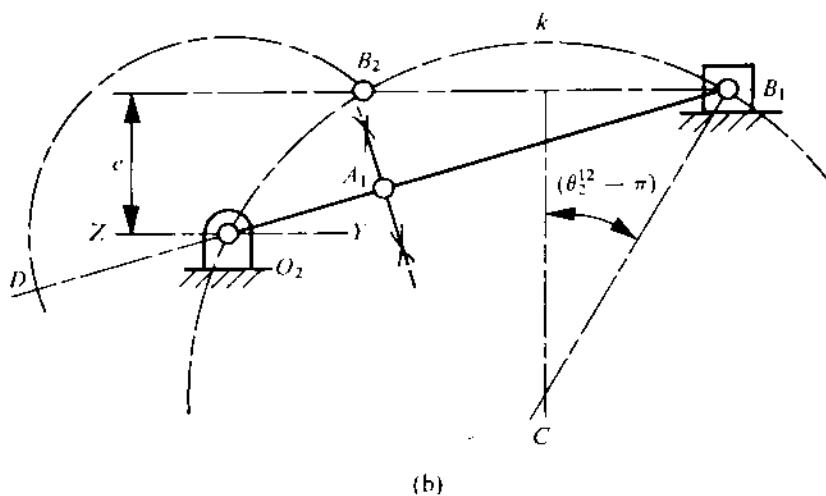
If $\theta_2^{12} > \pi$, the construction is similar to the one we have described, the only difference here being that the circle k_2 would intersect the horizontal line at Q outside the segment O_2O_4 , as indicated in Fig. 3.21c. In this situation, the choice of B_1 is restricted to the arc PQ .

If there is no quick return, i.e., $\theta_2^{12} = \pi$, then the point Q coincides with O_4 . Further, if $\theta_2^{12} = \pi + \theta_2^{14}$, then the midnormal of O_2R_{12} becomes parallel to O_4R_{12} and the radius of the circle k_2 becomes infinity. In other words, the circle k_2 degenerates into the straight line O_2R_{12} . Then the point B_1 can be taken on the line O_2R_{12} above the point P where $O_2P = 2.O_2R_{12}$.

⁵Hrones, J.A. and Nelson, G.L., Analysis of the Four-Bar Linkage, MIT Press, Cambridge, Massachusetts, 1951.



(a)



(b)

FIGURE 3.20

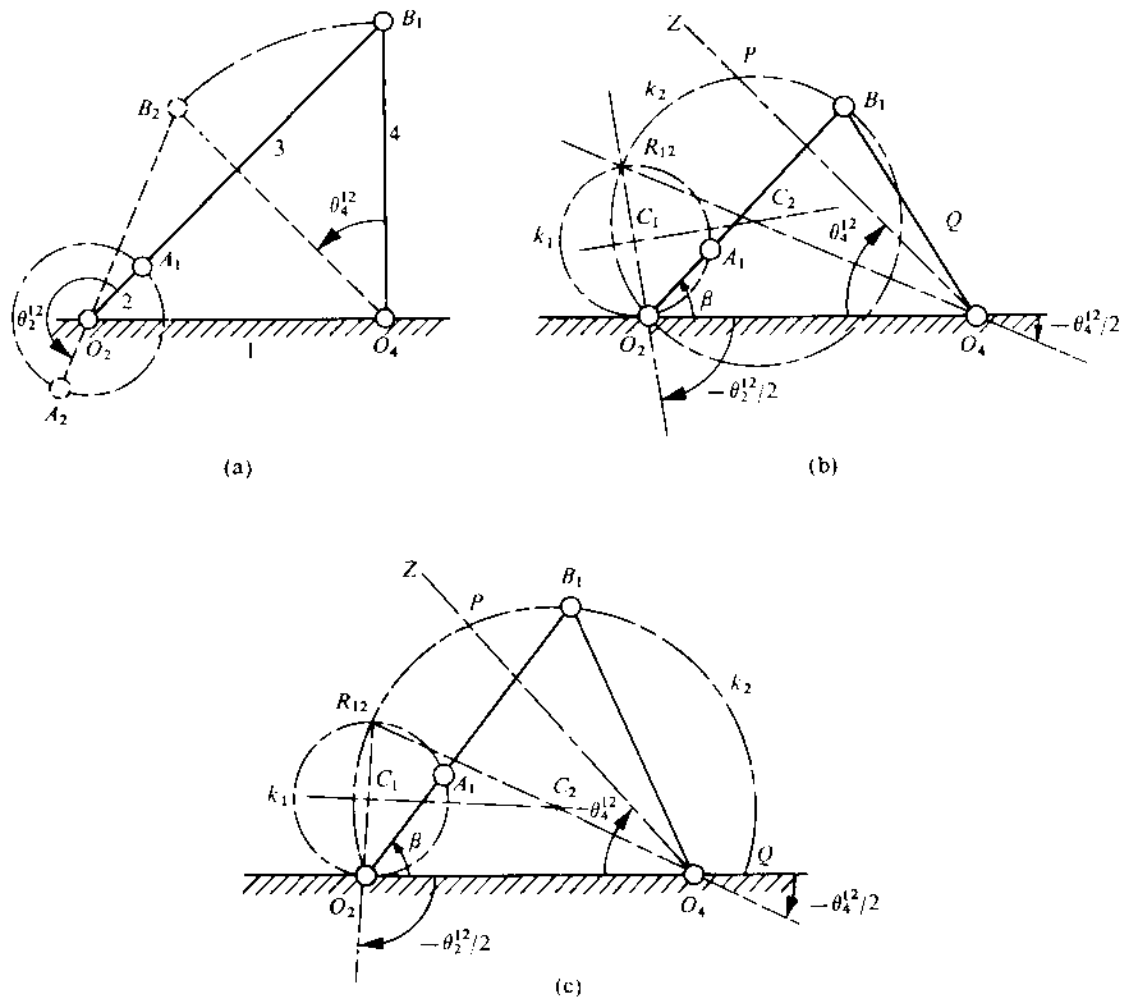


FIGURE 3.21

It should be noted from Figs. 3.21b and 3.21c that this method (known as Alt's construction) does not yield a unique solution, since B_1 can be taken anywhere on the arc PQ . In practice, we would like to obtain the optimum solution which will have the highest value of the minimum transmission angle (μ_{\min}). For given values of θ_2^{12} and θ_4^{12} , the maximum value of the minimum transmission angle (μ_{\min})_{max} and the required value of the angle β (see Figs. 3.21b and 3.21c) which yield this optimum solution, can be obtained from Volmer's nomogram reproduced in Fig. 3.22. For example, if $\theta_2^{12} = 210^\circ$ and $\theta_4^{12} = 60^\circ$, then, from the nomogram, we obtain $(\mu_{\min})_{\max} \approx 33^\circ$ and we need to use $\beta \approx 47^\circ$.

The nomogram does not give any specific value of β , though it provides the value of $(\mu_{\min})_{\max}$ in case there is no quick return (i.e., $\theta_2^{12} = 180^\circ$). This value of $(\mu_{\min})_{\max}$ can then be used in the solution of Problem 2.6 to design the optimum linkage. Finally, as has already been mentioned, if $\theta_2^{12} = \theta_4^{12} + 180^\circ$, then again β has a unique value ($= 90^\circ - \theta_4^{12}/2$). So, the knowledge of β does not yield the optimum solution. It can be shown that the optimum design satisfies the relations

$$l_2 = l_1 \sin (\theta_4^{12}/2), \quad (3.5a)$$

$$(l_1 - l_2)^2 = l_3^2 + l_4^2 - 2l_3l_4 \cos (\mu_{\min})_{\max}, \quad (3.5b)$$

$$l_4^2 = l_1^2 + l_3^2 - l_2^2, \quad (3.5c)$$

where the value of $(\mu_{\min})_{\max}$ can be read from the nomogram.

3.5 ANALYTICAL METHODS

We shall consider here a few important mechanisms to illustrate the different types of dimensional syntheses with various degrees of accuracy.

Four-bar Function Generator with Three Accuracy Points

As discussed in Section 3.1, with three accuracy points, the number of design parameters that can be determined is also three. We take the three length ratios as the design parameters, the remaining four (θ_2^i , θ_4^i , r_x , and r_y) being assumed beforehand. The reason for this choice will be clear later in this section.

The first step is to obtain the three accuracy points (x_1 , x_2 , and x_3) from (3.4), when the corresponding values of y (y_1 , y_2 , and y_3) can be obtained as $y = f(x)$. Then, using (3.1) and (3.2), we get $(\theta_2^1, \theta_2^2, \text{ and } \theta_2^3)$ and $(\theta_4^1, \theta_4^2, \text{ and } \theta_4^3)$, corresponding to the values of x and y , respectively. The problem now reduces to the determination of the link-length ratios such that three related pairs (θ_2^1 and θ_4^1), (θ_2^2 and θ_4^2), and (θ_2^3 and θ_4^3) are satisfied, i.e., when $\theta_2 = \theta_2^1$, θ_4 should be equal to θ_4^1 , and when $\theta_2 = \theta_2^2$, θ_4 should be equal to θ_4^2 , and so on. The procedure is based on the displacement equation, known as *Freudenstein's equation*, which can be derived as follows.

In the coordinate system xy (Fig. 3.1), the coordinates of the point A are $(l_2 \cos \theta_2, l_2 \sin \theta_2)$ and the coordinates of the point B are $[(l_1 + l_4 \cos \theta_4), l_4 \sin \theta_4]$. Now,

$$\begin{aligned} AB^2 &= l_3^2 = (x_A - x_B)^2 + (y_A - y_B)^2 \\ &= (l_2 \cos \theta_2 - l_1 - l_4 \cos \theta_4)^2 + (l_2 \sin \theta_2 - l_4 \sin \theta_4)^2 \\ &= l_1^2 + l_2^2 + l_4^2 + 2l_1l_4 \cos \theta_4 - 2l_1l_2 \cos \theta_2 - 2l_2l_4 (\cos \theta_2 \cos \theta_4 + \sin \theta_2 \sin \theta_4). \end{aligned}$$

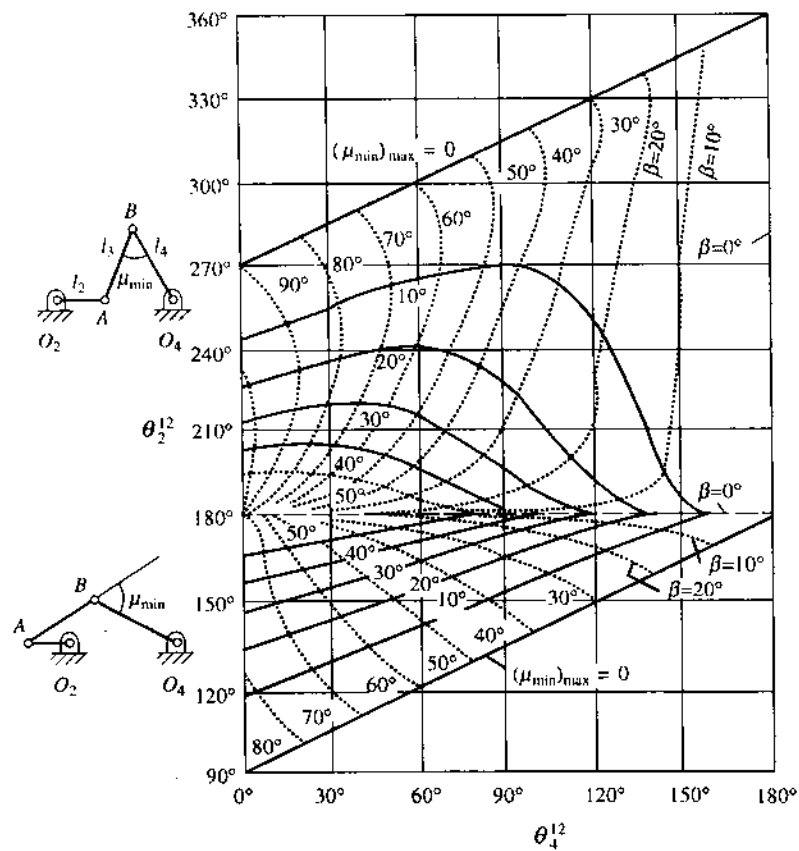


FIGURE 3.22

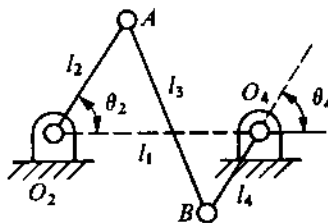


FIGURE 3.23

Rearranging, and dividing throughout by $2l_2l_4$, we get

$$\begin{aligned}\cos(\theta_2 - \theta_4) &= \frac{l_1}{l_2} \cos \theta_4 - \frac{l_1}{l_4} \cos \theta_2 + \frac{l_1^2 + l_2^2 - l_3^2 + l_4^2}{2l_2l_4} \\ &= K_1 \cos \theta_4 - K_2 \cos \theta_2 + K_3,\end{aligned}\quad (3.6)$$

where

$$K_1 = \frac{l_1}{l_2}, \quad K_2 = \frac{l_1}{l_4}, \quad K_3 = \frac{l_1^2 + l_2^2 - l_3^2 + l_4^2}{2l_2l_4}.$$

Substituting the three related pairs $(\theta_2^1$ and θ_4^1), $(\theta_2^2$ and θ_4^2), and $(\theta_2^3$ and θ_4^3) successively in (3.6), we obtain three linear simultaneous equations in K_1 , K_2 , and K_3 . Solving for K_1 , K_2 , and K_3 from these three equations, we get the three length ratios (design parameters). Negative values of l_2 and l_4 are to be interpreted in the vector sense (l_1 and l_3 are always positive). The situation in which l_4 is negative has been shown in Fig. 3.23. From Freudenstein's equation (3.6), it is obvious that if any one of the four assumed parameters (θ_2^i , θ_4^i , r_x , and r_y) is left undetermined (with, of course, one of the link-length ratios assumed instead), then the simultaneous algebraic equations, from which the unknowns are to be obtained, would no longer be linear. The solution would thus be far more complicated. The same reasoning applies to synthesis with four accuracy points, when any one of the four parameters θ_2^i , θ_4^i , r_x , and r_y , over and above the three link-length ratios, is an unknown.

PROBLEM 3.5

Determine the lengths of the links of a four-bar linkage to generate $y = \log_{10} x$ in the interval $1 \leq x \leq 10$. The length of the smallest link is 5 cm. Use three accuracy points with Chebyshev's spacing.

SOLUTION

For $x^i = 1$ and $x^f = 10$, let us first determine the three accuracy points. Using (3.4), we have

$$a = \frac{x^i + x^f}{2} = 5.5, \quad h = \frac{x^f - x^i}{2} = 4.5, \quad k = 3,$$

$$x^1 = 5.5 + 4.5 \cos \frac{\pi}{6} = 9.4, \quad y^1 = \log_{10}(x^1) = 0.974,$$

$$x^2 = 5.5 + 4.5 \cos \frac{\pi}{2} = 5.5, \quad y^2 = \log_{10}(x^2) = 0.741,$$

$$x^3 = 5.5 + 4.5 \cos \frac{5\pi}{6} = 1.6, \quad y^3 = \log_{10} (x^3) = 0.204,$$

$$y^i = \log_{10} (x^i) = 0, \quad y^f = \log_{10} (x^f) = 1.$$

For three accuracy points, we shall have to assume θ_2^i , θ_4^i , r_x , and r_y . Let $\theta_2^i = 45^\circ$ and $\theta_4^i = 135^\circ$. To calculate r_x and r_y , we assume $\theta_2^f = 105^\circ$ and $\theta_4^f = 225^\circ$. Using (3.1) and (3.2), we get

$$r_x = \frac{\theta_2^f - \theta_2^i}{x^f - x^i} = \frac{60}{9}, \quad r_y = \frac{\theta_4^f - \theta_4^i}{y^f - y^i} = \frac{90}{1}.$$

(Actually, r_x and r_y are to be prescribed, and the values of θ_2^f and θ_4^f calculated therefrom. To get reasonable values of θ_2^f and θ_4^f , we obtain r_x and r_y in this indirect manner.)

Let us now find the values of θ_2 and θ_4 corresponding to the accuracy points for these values of r_x and r_y . Using (3.1) and (3.2), for x^1 , we get

$$\frac{\theta_2^1 - \theta_2^i}{x^1 - x^i} = r_x, \quad \theta_2^1 = \theta_2^i + r_x(x^1 - x^i) = 45^\circ + \frac{60}{9} \times 8.4^\circ = 101^\circ,$$

and, for y^1 , we get

$$\frac{\theta_4^1 - \theta_4^i}{y^1 - y^i} = r_y, \quad \theta_4^1 = \theta_4^i + r_y(y^1 - y^i) = 135^\circ + 90 \times 0.974^\circ = 222.7^\circ.$$

So, one related pair of rotations is $(101^\circ, 222.7^\circ)$. Two other related pairs of rotations are similarly determined; these are $(75^\circ, 201.7^\circ)$ for (x^2, y^2) and $(49^\circ, 153.4^\circ)$ for (x^3, y^3) . Substituting (θ_2^1, θ_4^1) in (3.6), we obtain

$$\begin{aligned} \theta_2^1 &= 101^\circ, \quad \theta_4^1 = 222.7^\circ, \\ \cos(101^\circ - 222.7^\circ) &= K_1 \cos(222.7^\circ) - K_2 \cos(101^\circ) + K_3, \\ -0.5255 &= -0.7349K_1 + 0.1908K_2 + K_3. \end{aligned} \quad (1)$$

Similarly, substituting the values of the other two related pairs in (3.6), we get

$$-0.5976 = -0.9291K_1 - 0.2588K_2 + K_3, \quad (1)$$

$$-0.2487 = -0.8942K_1 - 0.6561K_2 + K_3. \quad (1)$$

Solving for K_1 , K_2 , and K_3 from equations (a), (b), and (c), we get

$$K_1 = 2, \quad K_2 = -0.703, \quad K_3 = 1.078.$$

So,

$$\frac{l_1}{l_2} = 2, \quad \frac{l_1}{l_4} = -0.703.$$

Again,

$$K_3 = \frac{l_1^2 + l_2^2 - l_3^2 + l_4^2}{2l_2l_4} = 1.078,$$

$$\frac{l_1^2 + l_1^2/4 - l_3^2 + \frac{1}{0.495}l_1^2}{2(l_1/2)(-\frac{1}{0.703}l_1)} = 1.078,$$

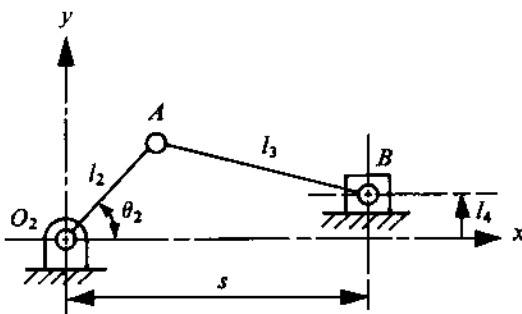


FIGURE 3.24

$$\frac{3.27l_1^2 - l_3^2}{-1.42l_1^2} = 1.078, \quad -2.3 + 0.705 \frac{l_3^2}{l_1^2} = 1.078,$$

$$\frac{l_3^2}{l_1^2} = 4.79, \quad \frac{l_1}{l_3} = 0.457.$$

Noting the values of the three ratios l_1/l_2 , l_1/l_4 , and l_1/l_3 , it is evident that $l_2 < l_1 < l_4 < l_3$ (when only the magnitudes are considered). Therefore, $l_2 = 5$ cm and, correspondingly,

$$l_1 = 10 \text{ cm}, \quad l_3 = 21.85 \text{ cm}, \quad l_4 = 14.20 \text{ cm} \text{ (negative)}.$$

Slider-crank Function Generator with Three Accuracy Points

In the problem of slider-crank mechanisms, the displacement of the slider has to be coordinated with the rotation of the crank O_2A in a prescribed manner (see Fig. 3.24). For example, let us consider the case when the slider displacement has to be proportional to the crank rotation over a given interval, i.e.,

$$s - s^i = C(\theta_2 - \theta_2^i) \quad \text{for } \theta_2^i \leq \theta_2 \leq \theta_2^f, \quad (3.7)$$

where

C = given constant of proportionality,

s = position of the slider,

θ_2 = orientation of the crank,

and the superscript i refers to the initial values.

Referring to Fig. 3.24, we see that there are five design parameters, namely, θ_2^i , s^i , and the three lengths l_2 , l_3 , and l_4 . For three accuracy points, the three design parameters are taken to be the lengths l_2 , l_3 , and l_4 ; the others are assumed beforehand. The reason for this choice is the same as that already stated in the context of four-bar function generator.

The first step is to obtain the Chebyshev accuracy points θ_2^1 , θ_2^2 , and θ_2^3 , using (3.4), with the corresponding values of s determined by means of (3.7). The problem then reduces to the determination of the link lengths l_2 , l_3 , and l_4 , such that three related pairs (θ_2^1, s^1) , (θ_2^2, s^2) , and (θ_2^3, s^3) are satisfied. The procedure is based on the displacement equation derived in a manner similar to that for (3.6). In the xy -coordinate system (Fig. 3.24), the coordinates of the point A are

$(l_2 \cos \theta_2, l_2 \sin \theta_2)$ and the coordinates of the point B are (s, l_4) . Now,

$$\begin{aligned} AB^2 &= l_3^2 = (x_A - x_B)^2 + (y_A - y_B)^2 \\ &= (l_2 \cos \theta_2 - s)^2 + (l_2 \sin \theta_2 - l_4)^2 = l_2^2 + s^2 - 2sl_2 \cos \theta_2 - 2l_4 l_2 \sin \theta_2 + l_4^2. \end{aligned}$$

Or

$$K_1 s \cos \theta_2 + K_2 \sin \theta_2 - K_3 = s^2, \quad (3.8)$$

where $K_1 = 2l_2$, $K_2 = 2l_4$, and $K_3 = l_2^2 - l_3^2 + l_4^2$. Substituting the three related pairs (θ_2^1, s^1) , (θ_2^2, s^2) , and (θ_2^3, s^3) successively in (3.8), we obtain three linear simultaneous equations in K_1 , K_2 , and K_3 . The lengths l_2 , l_3 , and l_4 are obtained after solving for K_1 , K_2 , and K_3 from these equations. As in the four-bar linkage, negative values of l_2 and l_4 should be interpreted in the vector sense (l_3 is always positive).

PROBLEM 3.6

Design a slider-crank mechanism so that the displacement of the slider is proportional to the square of the crank rotation in the interval $45^\circ \leq \theta_2 \leq 135^\circ$. Use the three-point Chebyshev spacing.

SOLUTION

Since $\theta_2^i = 45^\circ$ and $\theta_2^f = 135^\circ$, the superscript f denoting the final value, the desired relationship between s and θ_2 is

$$s - s^i = C(\theta_2 - \theta_2^i)^2, \quad (a)$$

where C is a constant. The value of s^i is assumed to be 10 cm. To determine C , let $s^f = 3$ cm (assumed). Thus, when the values of θ in (a) are expressed in degrees, we get

$$C = \frac{s^f - s^i}{(\theta_2^f - \theta_2^i)^2} = -\frac{7}{90^2}. \quad (b)$$

(Actually the value of C is prescribed to specify relation (a), from which s^f can be calculated. The value of C has been calculated in this indirect manner to get a reasonable value of s^f .) The three accuracy points θ_2^1 , θ_2^2 , and θ_2^3 are determined by means of (3.4) to be

$$\theta_2^1 = 128.7^\circ, \quad \theta_2^2 = 90^\circ, \quad \theta_2^3 = 51.3^\circ.$$

The corresponding values of s are obtained by means of (a), using the value of C obtained from (b). Thus,

$$s^1 = 3.95 \text{ cm}, \quad s^2 = 8.26 \text{ cm}, \quad s^3 = 9.97 \text{ cm}.$$

Now, substituting the related pairs $(128.7^\circ, 3.96 \text{ cm})$, $(90^\circ, 8.26 \text{ cm})$, and $(51.3^\circ, 9.97 \text{ cm})$ in (3.8) we get

$$-2.472K_1 + 0.7804K_2 - K_3 = 15.6, \quad (c)$$

$$K_2 - K_3 = 68.0, \quad (d)$$

$$6.230K_1 + 0.7804K_2 - K_3 = 99.2. \quad (e)$$

Solving for K_1 , K_2 , and K_3 from (c), (d), and (e), we have

$$K_1 = 9.61, \quad K_2 = 130.75, \quad K_3 = 62.75.$$

Thus,

$$l_2 = K_1/2 = 4.805 \text{ cm}, \quad l_4 = K_2/2l_2 = 13.6 \text{ cm},$$

$$l_3^2 = l_2^2 + l_4^2 - K_3 = 145.35, \quad l_3 = 12.05 \text{ cm}.$$

Slider-crank Function Generator with Four Accuracy Points

If in Problem 3.6 four accuracy points are to be satisfied, then s^i (besides l_2 , l_3 , and l_4) is left out as an unassumed design parameter which has to be determined.

The first step for this will be to determine the four accuracy points θ_2^1 , θ_2^2 , θ_2^3 , and θ_2^4 within the range $\theta_2^i \leq \theta_2 \leq \theta_2^f$ using (3.4). From (a) of Problem 3.6,

$$s = s^i + C(\theta_2 - \theta_2^i)^2.$$

Thus, for the accuracy points,

$$s^l = s^i + C(\theta_2^l - \theta_2^i)^2 = s^i + s^{il} \quad \text{for } l = 1, 2, 3, 4,$$

where the values of s^{il} are known since C is given. Now, writing the displacement equation (3.8) corresponding to the accuracy points, we have

$$\begin{aligned} K_1(s^i + s^{il}) \cos \theta_2^l + K_2 \sin \theta_2^l - K_3 &= (s^i + s^{il})^2, \\ 2l_2(s^i + s^{il}) \cos \theta_2^l + 2l_2l_4 \sin \theta_2^l - (l_2^2 - l_3^2 + l_4^2) &= (s^i)^2 + (s^{il})^2 + 2s^i s^{il} \quad \text{for } l = 1, 2, 3, 4, \\ R_1 \cos \theta_2^l + R_2 s^{il} \cos \theta_2^l + R_3 \sin \theta_2^l - R_4 &= R_5 s^{il} + (s^{il})^2 \quad \text{for } l = 1, 2, 3, 4, \end{aligned} \quad (3.9)$$

where

$$R_1 = 2l_2 s^i, \quad R_2 = 2l_2, \quad R_3 = 2l_2 l_4, \quad R_4 = [l_2^2 - l_3^2 + l_4^2 + (s^i)^2], \quad R_5 = 2s^i.$$

With four different values of l , (3.9) gives four equations, but there are five unknown quantities, R_1 to R_5 . It may thus appear that this system of four equations is indeterminate. However, this is not so, as all values of R , by definition, are not independent, i.e.,

$$2R_1 = R_2 R_5, \quad 2R_1 - R_2 R_5 = 0. \quad (3.10)$$

Thus, (3.10), known as the *compatibility equation*, when combined with the four equations (3.9), gives a system of five equations which has five unknowns and is not indeterminate. However, as (3.10) is not linear, this system of five equations cannot be solved easily. The method of solution adopted for this situation is as follows.

Let R_5 be denoted by λ , and (3.10) be expressed as

$$2R_1 - R_2 \lambda = 0. \quad (3.11)$$

The system of equations (3.9) can be rewritten in the form

$$R_1 \cos \theta_2^l + R_2 s^{il} \cos \theta_2^l + R_3 \sin \theta_2^l - R_4 = s^{il} + (s^{il})^2 \quad \text{for } l = 1, 2, 3, 4. \quad (3.12)$$

To express R_1 , R_2 , R_3 , and R_4 in terms of λ , let us consider two systems of linear equations for $l = 1, 2, 3, 4$, namely,

$$P_1 \cos \theta_2^l + P_2 s^{il} \cos \theta_2^l + P_3 \sin \theta_2^l - P_4 = s^{il}, \quad (3.13a)$$

$$Q_1 \cos \theta_2^l + Q_2 s^{il} \cos \theta_2^l + Q_3 \sin \theta_2^l - Q_4 = (s^{il})^2. \quad (3.13b)$$

(3.13a) and (3.13b) can be solved for P_l and Q_l , for $l = 1, 2, 3, 4$, when

$$R_4 = Q_l + \lambda P_l \quad \text{for } l = 1, 2, 3, 4. \quad (3.14)$$

Substituting R_1 and R_2 from (3.14) in (3.11), we have

$$2(Q_1 + \lambda P_1) - (Q_2 + \lambda P_2)\lambda = 0, \quad \lambda^2 P_2 + (Q_2 - 2P_1)\lambda - 2Q_1 = 0. \quad (3.15)$$

λ can be solved from (3.15), which gives R_5 , and substituting the value of λ in (3.14), the values for R_1 , R_2 , R_3 , and R_4 can be obtained. Once R_1 to R_5 are known, all the design parameters l_2 , l_3 , l_4 , and s^i can be determined as

$$l_2 = R_2/2, \quad s^i = R_5/2, \quad l_4 = R_3/R_2, \quad l_3 = [l_2^2 + l_4^2 + (s^i)^2 - R_4]^1/2.$$

Note that s^i can be negative like l_2 and l_4 , and should be interpreted in a similar way. Obviously, considering the discriminant of the quadratic equation (3.15), if

- | | |
|---|--|
| $(Q_2 - 2P_1)^2 + 4P_2 \cdot 2Q_1 > 0,$ | two solutions exist for λ and, consequently,
for the design parameters, |
| $(Q_2 - 2P_1)^2 + 8P_2 Q_1 = 0,$ | a unique solution exists, |
| $(Q_2 - 2P_1)^2 + 8P_2 Q_1 < 0,$ | no solution exists. |

To gain more familiarity with this method, the reader is advised to solve Problem 3.6 with four accuracy points, using the value of C as given by (b) in that problem.

If five accuracy points are to be satisfied, θ_2^i is also to be left out as an unassumed design parameter (besides l_2 , l_3 , l_4 , and s^i). It should be observed that with θ_2^i as an unknown quantity, the problem can no longer be stated as in (3.7) or as in Problem 3.6 by (a). The problem has now to be expressed in the following manner.

The absolute positions of the five accuracy points are not specified, rather the spacing with respect to the first accuracy point (which is left out as a design parameter) is to be specified. Similarly, the displacement of the slider, corresponding to the first accuracy point, is left out as a design parameter. The spacings of other accuracy points from this point are also specified. Thus,

$$\theta_2^l = \theta_2^1 + \phi^{1l} \quad \text{for } l = 1, 2, 3, 4, 5 \quad (3.16)$$

(with ϕ^{1l} having specified values, $\phi^{11} = 0$), and

$$s^l = s^1 + s^{1l} \quad \text{for } l = 1, 2, 3, 4, 5 \quad (3.17)$$

(with s^{1l} having specified values, $s^{11} = 0$). Substituting θ_2^l and s^l from (3.16) and (3.17) in (3.8), for $l = 1$ to 5, we get five equations with five unknowns l_2 , l_3 , l_4 , θ_2^1 , and s^1 . However, the solution is extremely difficult, and is impossible to handle without the help of a digital computer.

Four-bar Linkage for Specified Instantaneous Conditions

The problem to be discussed here is concerned with the design of a four-bar linkage so that, for a given configuration, the angular velocities, accelerations, etc., of the links of a four-bar mechanism can be coordinated. The following simple example will explain the procedure to be adopted for this purpose.

PROBLEM 3.7

The three conditions to be satisfied by a four-bar linkage are

$$\theta_2 = 60^\circ, \quad \theta_4 = 90^\circ,$$

$$\omega_2 = \frac{d\theta_2}{dt} = 3 \text{ rad/s}, \quad \omega_4 = \frac{d\theta_4}{dt} = 2 \text{ rad/s},$$

$$\alpha_2 = \frac{d^2\theta_2}{dt^2} = -1 \text{ rad/s}^2, \quad \alpha_4 = \frac{d^2\theta_4}{dt^2} = 0.$$

Determine the link-length ratios.

SOLUTION

We can use Freudenstein's equation (3.6) for this particular problem as the conditions have been prescribed only for links 2 and 4. To start with, (3.6) is reproduced here for convenience, that is,

$$\cos(\theta_2 - \theta_4) = K_1 \cos \theta_4 - K_2 \cos \theta_2 + K_3. \quad (\text{a})$$

Taking the first and second time derivatives of both sides of (a), we get

$$(\omega_2 - \omega_4) \sin(\theta_2 - \theta_4) = K_1 \omega_4 \sin \theta_4 - K_2 \omega_2 \sin \theta_2, \quad (\text{b})$$

$$\begin{aligned} (\alpha_2 - \alpha_4) \sin(\theta_2 - \theta_4) + (\omega_2 - \omega_4)^2 \cos(\theta_2 - \theta_4) \\ = K_1(\alpha_4 \sin \theta_4 + \omega_4^2 \cos \theta_4) - K_2(\alpha_2 \sin \theta_2 + \omega_2^2 \cos \theta_2). \end{aligned} \quad (\text{c})$$

Then, substituting the prescribed values in (a), (b), and (c), three linear simultaneous equations in K_1 , K_2 , and K_3 are obtained, that is,

$$0.866 = -0.5K_2 + K_3, \quad (\text{d})$$

$$-0.5 = 2K_1 - 2.598K_2, \quad (\text{e})$$

$$1.366 = -3.634K_2. \quad (\text{f})$$

Solving these equations, we get

$$K_1 = -0.738, \quad K_2 = -0.376, \quad K_3 = 0.678.$$

From K_1 , K_2 , and K_3 , the link-length ratios will be

$$\frac{l_1}{l_2} = -0.738, \quad \frac{l_1}{l_4} = -0.376, \quad \frac{l_1}{l_3} = 0.446.$$

Use of Complex Numbers and Dyads

It has already been shown in Chapter 2 how link vectors, expressed in complex exponential notation, can be used for kinematic analysis of planar linkages. A similar approach can also be used for dimensional synthesis. The details of this method, known as Block's method, can be found in the second edition of this text. In what follows, we shall briefly discuss another commonly-used approach through the use of dyads.⁶

A 4R linkage, like the great majority of other planar linkages, can be thought of as a combination of vector pairs called *dyads*. Referring to Fig. 3.25, the four-bar linkage $O_2A_1B_1(C_1)O_4$ can be perceived as two dyads. The left side of the linkage consists of two vectors \mathbf{L} and \mathbf{L}^* whereas the right side consists of another two vectors \mathbf{R} and \mathbf{R}^* . The frame O_2O_4 and the coupler link A_1B_1 can be easily determined by vector addition, once these two dyads are synthesized. The path of

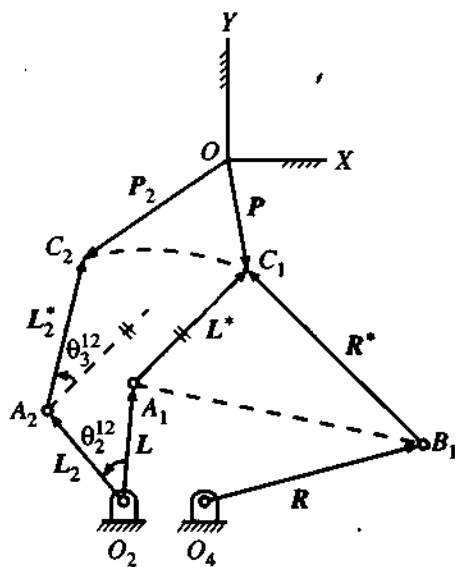


FIGURE 3.25

the coupler point C_1 can be expressed in an arbitrarily chosen coordinate system (XY) through the vector \mathbf{P} .

In Fig. 3.25, two configurations of the left side dyad are shown. The rotation of each vector is measured from its respective starting position, measured positive in the counter-clockwise direction. The complex exponential notation is used for each vector.

Considering the closed loop $O_2A_2C_2O_1C_1A_1O_2$, we can write

$$\mathbf{L}_2 + \mathbf{L}_2^* - \mathbf{P}_2 + \mathbf{P} - \mathbf{L}^* - \mathbf{L} = 0$$

or

$$\mathbf{L}(e^{i\theta_2^{1j}} - 1) + \mathbf{L}^*(e^{i\theta_3^{1j}} - 1) = \mathbf{P}_2 - \mathbf{P}.$$

This equation can be generalized for any j -th ($j = 2, 3, \dots, n$) configuration as

$$\mathbf{L}(e^{i\theta_2^{1j}} - 1) + \mathbf{L}^*(e^{i\theta_3^{1j}} - 1) = \mathbf{P}_j - \mathbf{P} = \delta_j. \quad (3.18)$$

Equation (3.18) is known as the standard-form equation if δ_j and either θ_2^{1j} or θ_3^{1j} are prescribed or assumed. We should note that (3.18) is equivalent to two scalar equations and two scalar unknowns can be solved for each value of j . It will be seen that the standard form is convenient for dimensional synthesis problems like path generation, motion generation, and function generation. The number of scalar equations generated is $2(n - 1)$, where n is the number of accuracy points. So, depending on the number of accuracy points, several parameters are to be assumed in order to obtain a solution. For example, if $n = 4$, i.e., $j = 2, 3, 4$, (3.18) generates 6 scalar equations. So, if θ_3^{1j} , for $j = 2, 3, 4$, are prescribed, then we have 7 unknowns, viz., \mathbf{L} , \mathbf{L}^* (each vector having two scalar unknowns), and θ_2^{1j} for $j = 2, 3, 4$. Therefore, we have to assume only one of these seven to obtain a solution.

⁶For more details on the use of dyads, refer to Erdman, A.G. and Sandor, G.N., Mechanism Design: Analysis and Synthesis, Vol. 1, Prentice-Hall, Englewood Cliffs, New Jersey, 1984.

Since some of the angles are left as unknowns, the resulting equations will be nonlinear. The reader is advised to confirm that, with $n = 5$, no parameter can be freely chosen. For $n = 3$, the resulting equations can always be rendered linear with proper free choices of the parameters.

Considering the right side dyad, we get the standard form

$$\mathbf{R}(e^{i\theta_4^{1j}} - 1) + \mathbf{R}^*(e^{i\theta_3^{1j}} - 1) = \delta_j. \quad (3.19)$$

Let us now explain the use of standard-form equations for different types of three-position problems.

Path Generation

First write (3.18) for $j = 2$ and 3, i.e.,

$$\mathbf{L}(e^{i\theta_2^{12}} - 1) + \mathbf{L}^*(e^{i\theta_3^{12}} - 1) = \delta_2, \quad (3.20a)$$

$$\mathbf{L}(e^{i\theta_2^{13}} - 1) + \mathbf{L}^*(e^{i\theta_3^{13}} - 1) = \delta_3. \quad (3.20b)$$

Note that, for the three given locations of the coupler point, C_1 , C_2 , and C_3 , the right-hand sides of (3.20a) and (3.20b) are known. In all, we have 4 scalar equations; so, only 4 scalar unknowns can be solved. Let these four unknowns be \mathbf{L} and \mathbf{L}^* . Therefore, we can freely choose θ_3^{12} , θ_3^{13} , θ_2^{12} , and θ_2^{13} . Note that the last two free choices imply that the coupler-point movement is also coordinated with the input rotation. To solve for the right dyad using (3.19), we need to assume two more parameters, viz., θ_4^{12} and θ_4^{13} .

Motion Generation

If three positions of the coupler are prescribed as A_1B_1 , A_2B_2 , and A_3B_3 , then we can use A as the coupler point with $\mathbf{L}^* = 0$ and $\mathbf{R}^* = \mathbf{B}_1\mathbf{A}_1$. This problem can also then be solved as a path generation problem.

Function Generation

For function generation, we are interested in coordinating the movements of the input and output links. Therefore, there is no need to consider the coupler point C . Instead, let us consider two positions of a vector triad consisting of three vectors, \mathbf{L} , \mathbf{M} , and \mathbf{R} , as shown in Fig. 3.26. Now, considering the closed loop $O_2A_jB_jO_4B_1A_1O_2$, we can write

$$\mathbf{L}_j + \mathbf{M}_j - \mathbf{R}_j + \mathbf{R} - \mathbf{M} - \mathbf{L} = 0$$

or

$$\mathbf{L}(e^{i\theta_2^{1j}} - 1) + \mathbf{M}^*(e^{i\theta_3^{1j}} - 1) = \mathbf{R}(e^{i\theta_4^{1j}} - 1). \quad (3.21)$$

Choosing \mathbf{R} arbitrarily, (3.21) is now the standard form. The arbitrary choice of \mathbf{R} is justified since it only specifies the scale and orientation of the linkage and the output-input relationship is independent of these. For function generation, the values of θ_3^{1j} 's are assumed. How many of these values are to be assumed and how many to be left as unknowns depend on the number of accuracy points. The reader should satisfy him(her)self that, for more than three accuracy points (i.e., $j = 2, 3, 4$), the resulting equations will be nonlinear since one of θ_3^{1j} has to be left as an unknown parameter. The linkage is designed once \mathbf{L} and \mathbf{M} are determined.

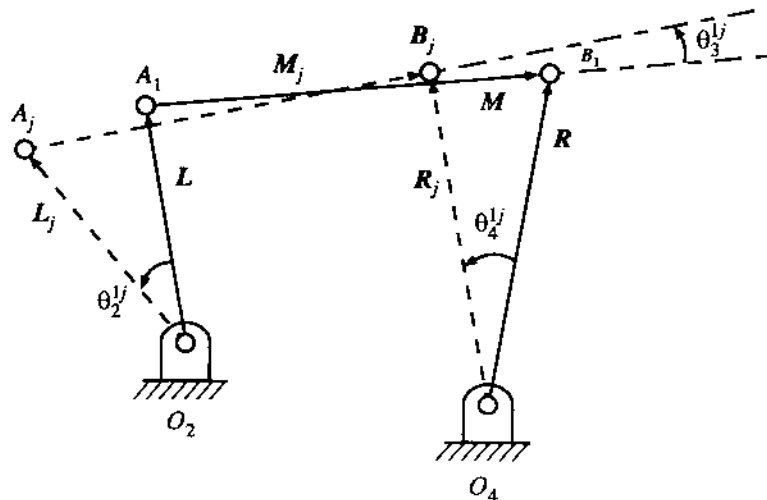


FIGURE 3.26

3.6 BRANCH AND ORDER DEFECTS

We have already discussed both graphical and analytical methods of dimensional synthesis. Irrespective of which method is followed, the designer has to ensure that the linkage serves the desired purpose without any difficulty in practice. Two most common defects, which can arise in practice, known as branch and order defects, are explained here. The methods of dimensional synthesis free of such defects are beyond the scope of this text.

The branch defect may exist if the designed 4R linkage turns out to be a Grashof type. It is already known that a Grashof's linkage has two distinct modes of assembly. It is possible that one particular mode of assembly may not satisfy all the accuracy points. To cover all the accuracy points, the linkage (of given link lengths) has to be dismantled and reassembled in the other mode. Obviously, such a linkage is no good for any practical use.

By order defect it is meant that even if a linkage satisfies all the precision points, say, 1, 2, 3, and 4, there is no guarantee that the accuracy-point configurations will be taken up in that order. The desired configurations may be taken up in sequence 1, 2, 4 and then 3 or 1, 3, 2 and then 4, etc. With three precision points, the desired order can always be achieved with a particular direction of rotation of the input link. By studying the output-input characteristics of 4R linkages (Fig. 2.6), it can be appreciated that even if all the accuracy points are satisfied by a designed linkage, the movements of the input and output links may not be in the directions desired. It is strongly advised, therefore, that a model (say, made of cardboard with R pairs made of drawing-board pins) of the design should be tested to ensure that the designed linkage will work satisfactorily in real life.

3.7 SPECIAL STRAIGHT-LINE MECHANISMS

As already discussed, motion along an exact straight line can always be generated by means of a prismatic pair, but because of the high wear rate of prismatic pairs, a pin-connected mechanism is preferred for achieving the same goal.

The theory concerning pin-connected linkages for generating exact straight lines is based on the geometric relation determined from Fig. 3.27. Let the two points P and Q (Fig. 3.27) be constrained

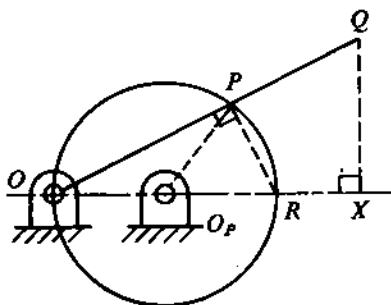


FIGURE 3.27

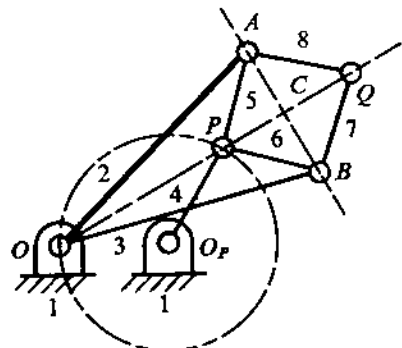


FIGURE 3.28

to move in such a way that P , Q , and a fixed point O are always collinear, satisfying the relation

$$OP \times OQ = \text{constant}.$$

Now, if P moves along a circle passing through O , then Q moves along a straight line drawn perpendicular to the diameter through O of the circle along which P moves. The proof of this statement is as follows. Referring to Fig. 3.27, we see that the triangles OPR and OQX are similar. So,

$$\frac{OP}{OR} = \frac{OX}{OQ},$$

$$OX = \frac{OP \times OQ}{OR} = \text{constant} \quad (\text{since } OP \times OQ = \text{constant}).$$

Thus, Q moves along a straight line perpendicular to OR . Several mechanisms have been invented using this principle; a description of one such follows.

Peaucellier Straight-line Mechanism

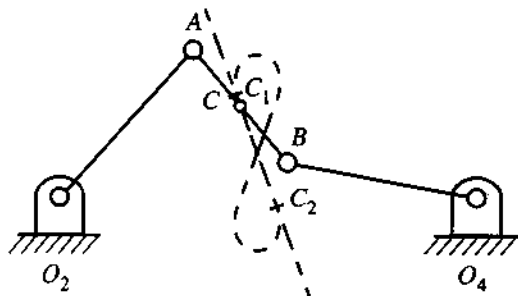
Referring to Fig. 3.28, we see that the rhombus $APBQ$ is connected to the point O by two equal links OA and OB . The point P moves along the circle passing through O . It is easily seen that, whatever the configuration may be, the three points O , P , and Q are always in a straight line. To prove that $OP \times OQ = \text{constant}$, we see, from Fig. 3.28, that

$$\begin{aligned} OP \times OQ &= (OC - PC)(OC + CQ) = OC^2 - PC^2 \\ &= (OA^2 - AC^2) - (AP^2 - AC^2) = OA^2 - AP^2 = \text{constant}. \end{aligned}$$

Thus, as P moves along a circle (centre O_P) passing through O ($OO_P = O_P P$), Q moves along a straight line perpendicular to OO_P .

It is seen that an exact straight-line mechanism is rather complicated, and that the Peaucellier mechanism has eight links. However, simple four-bar linkages have been devised with a suitable choice of the coupler point,⁷ so that it traces an approximate straight line for a small movement of the mechanism. One such linkage was designed as a part of the solution to Problem 3.4. Approximate straight-line generation by a coupler point was an important problem during the early developments of machines when the machining of a prismatic pair was not feasible. Accordingly,

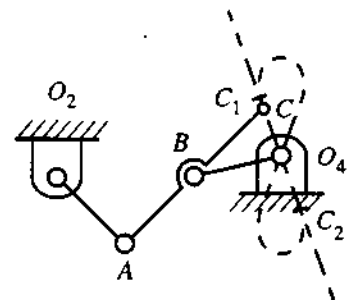
⁷ Actually, the coupler-point curve of a four-bar linkage is a sixth-order curve.



$$O_2A = O_4B, AC = BC$$

$$O_2O_4 : O_2A : AB = 10.77 : 5 : 4$$

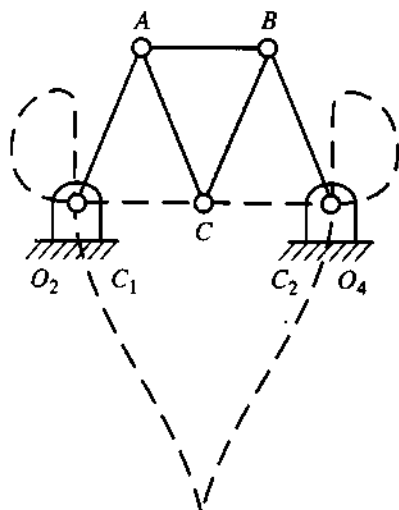
(a) Watt's



$$AB = O_4B = BC$$

$$O_2A : AB : O_2O_4 = 2 : 2.5 : 5.39$$

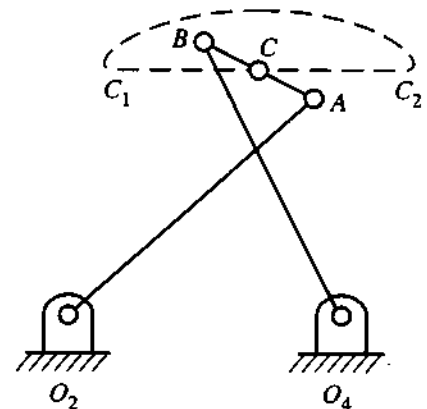
(b) Evans'



$$O_2O_4 = 2AB$$

$$O_2A = AC = BC = O_4B$$

(c) Roberts'



$$AB : O_2O_4 : O_2A : O_4B = 1 : 2 : 2.5 : 2.5$$

(d) Chebyshev's

FIGURE 3.29

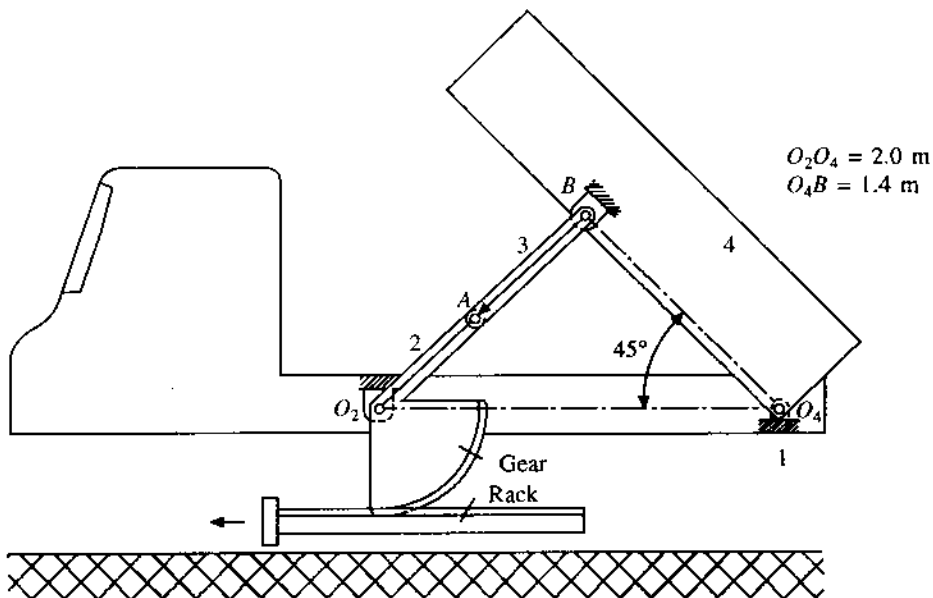


FIGURE 3.30

famous kinematicians, engineers, and mathematicians designed such linkages. A few of these along with the important dimensions and inventor's name are reproduced in Figs. 3.29a-d.

3.8 PROBLEMS

- 3.8 The kinematic scheme of a tipper dumper is shown in Fig. 3.30 where the tipping position corresponds to the outer dead-centre configuration of the four-bar linkage O_2ABO_4 . During transport, the dumper is horizontal, i.e., O_2O_4 and O_4B are collinear. From transport to tipping configuration, the input link O_2A rotates through 90° in the CCW direction. The input movement is provided by the hydraulically-operated rack which, in turn, rotates the gear sector integral with the input link. Determine the required lengths of O_2A and AB with all other dimensions as indicated in the figure.
- 3.9 The kinematic scheme of a level-luffing crane, used for handling cargo in ports, is shown in Fig. 3.31a. For moving cargo approximately in a horizontal direction, it is desired that the coupler point C should pass through three prescribed locations C_1 , C_2 , and C_3 . Determine the required link lengths O_2A and AB . In a real-life design, some trials regarding the assumed locations O_2O_4 and B , and the height h are necessary to arrive at a good design shown in Fig. 3.31b where A lies near the midpoint of BC .
- 3.10 Design a four-bar function generator to obtain the following pairs of coordinated input-output movements: ($\theta_2^{12} = 26^\circ$, $\theta_4^{12} = 54^\circ$) and ($\theta_2^{13} = 52^\circ$, $\theta_4^{13} = 80^\circ$). Assume the frame length $O_2O_4 = 5.1$ cm, $O_2A_1 = 6.4$ cm, and $\angle O_4O_2A_1 = 40^\circ$ (CW) (i.e., $\theta_2^1 = -40^\circ$). Use both methods of inversion and relative poles. As usual, a positive angle means CCW rotation. Also observe the directions of rotation of links 2 and 4 at the three accuracy points.

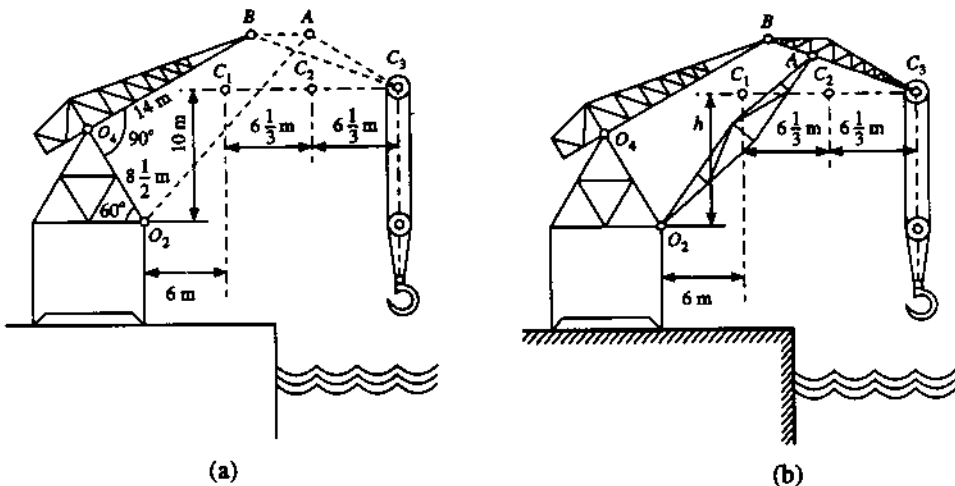


FIGURE 3.31

3.11 Figure 3.32a shows the sketch of a tipper-dumper truck. The locations of the fixed pivots O_2 and O_4 are chosen conveniently on the body of the truck as shown in Fig. 3.32b. Given the transport (I), dumping (III), and an intermediate configuration of the bin, locate A and B on the body of the bin.

3.12 A part of a crank-rocker linkage is shown in Fig. 3.33. It is desired that when the crank O_2A rotates through 90° in the CCW direction, the rocker link O_4B should rotate monotonically in the CCW direction through 45° . Further, the rocker link O_4B should be of minimum length. Determine the required coupler and rocker lengths. Also check that the desired monotonic movements are satisfied in the solution.

3.13 Figure 3.34 shows schematically the mechanism used to open and close the door of a bus. The roller (B) hinged to the door-board moves in a slot in the frame. From the closed to the open position, the roller moves 45 cm to the right and the link O_2A rotates through 90° in the CCW direction. If in the open configuration the pin A_1 is 3 cm away in the horizontal direction (as indicated in the figure) from O_2 , determine the length O_2A_1 . Some other dimensions are also indicated in the figure. Also determine the amount and direction of rotation of the door-board from closed to open position.

3.14 It is required to make the return motion of the slider in the mechanism O_2AB (Fig. 3.35) quicker so that forward time/return time = 1.4. This can be achieved by driving the crank O_2A through a four-bar double-crank mechanism (shown by the dashed lines) and rotating O_6C , instead of O_2A , with a constant angular velocity. The return motion can also be made quicker by providing a suitable offset, keeping the stroke length unchanged. Synthesize a slider-crank mechanism with offset 24 cm and a quick-return ratio 1.4.

3.15 Determine the link lengths of a 4R crank-rocker linkage with a quick-return ratio (assuming uniform crank speed) 1.25 and a swing angle of 50° for the rocker, so that the minimum value of the transmission angle is maximum. Assume a frame length of 100 mm. What are the values of the transmission angle at the dead-centre configurations?

3.16 A four-bar linkage is required to generate the function $y = x^{1.6}$ for $1 \leq x \leq 4$. The crank rotates from an angle of 30° to 120° , whereas the follower rotates from an angle of 60° to 150° .

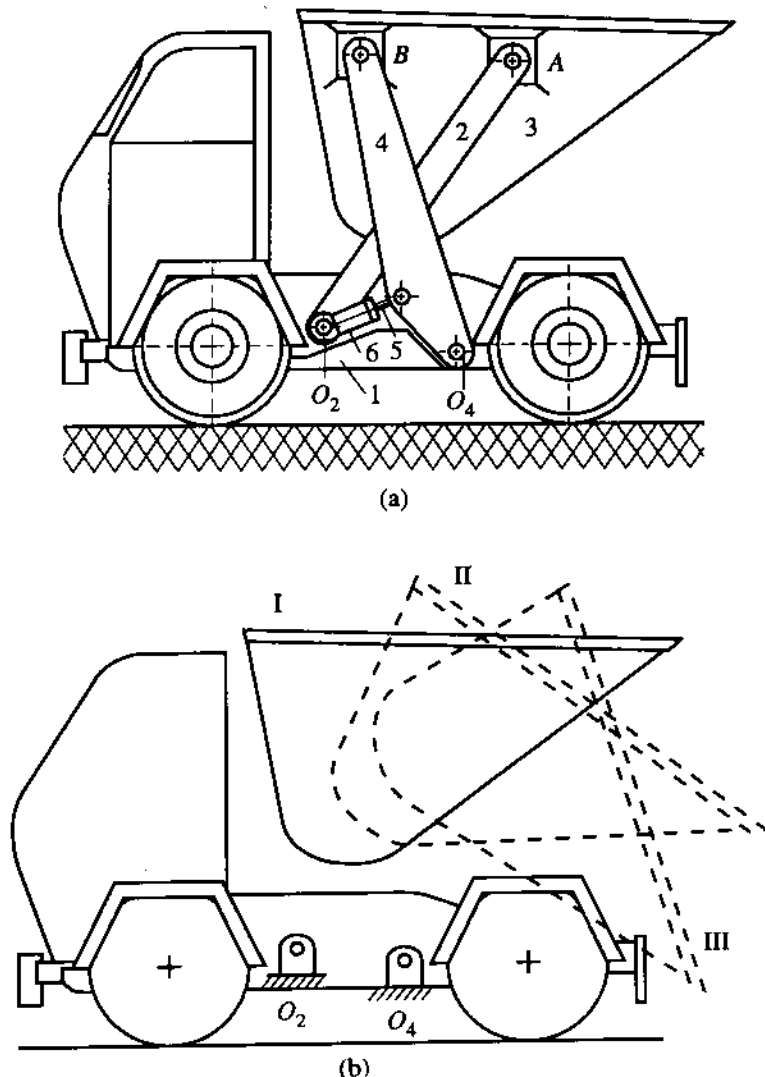


FIGURE 3.32

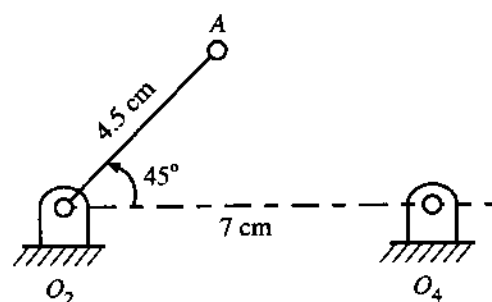


FIGURE 3.33

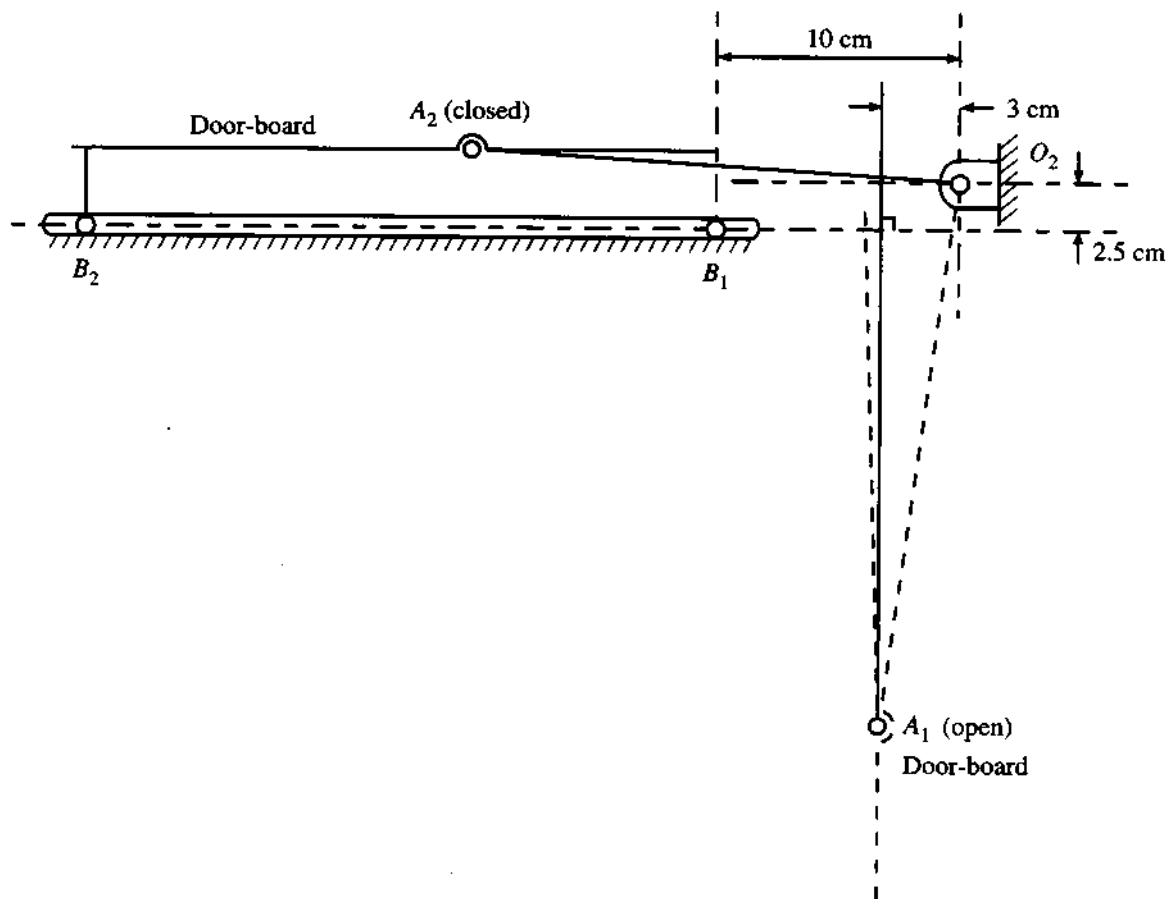


FIGURE 3.34

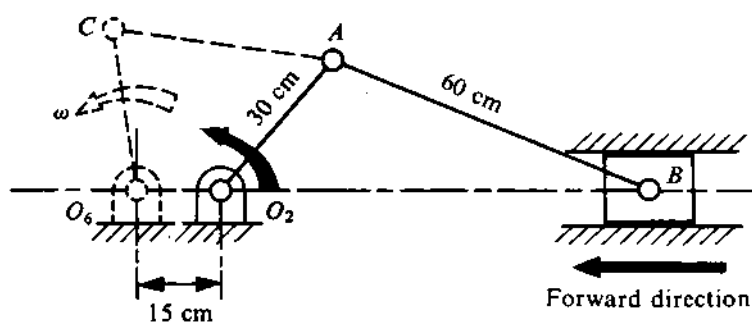


FIGURE 3.35

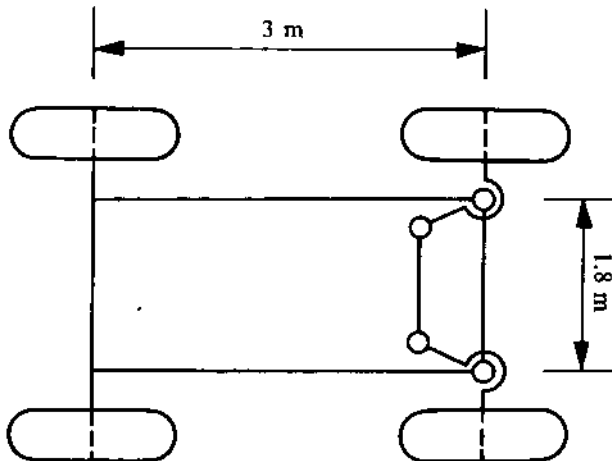


FIGURE 3.36

Given that the length of the largest link is 30 cm, determine the lengths of all the links. Use the three-point Chebyshev spacing.

- 3.17 Design a slider-crank mechanism to satisfy the conditions

$$\theta_2 = 60^\circ, \quad s = 20 \text{ cm}, \quad \dot{\theta}_2 = 5 \text{ rad/s}, \quad \dot{s} = 30 \text{ cm/s}, \quad \ddot{\theta}_2 = 1 \text{ rad/s}^2, \quad \ddot{s} = 60 \text{ cm/s}^2.$$

- 3.18 In a slider-crank mechanism, the rotation of the crank from 60° to 150° (CCW) has to be converted into a 20-cm translation of the slider (from left to right) so that the translation is proportional to the rotation of the crank. Design the mechanism, using four Chebyshev's accuracy points.

- 3.19 Design a four-bar linkage using Freudenstein's equation to generate the following pairs of co-ordinated movements: $(\theta_2^{12} = -54^\circ, \theta_4^{12} = -26^\circ)$, $(\theta_2^{13} = -80^\circ, \theta_4^{13} = -52^\circ)$. Assume the frame length = 5 cm and the first accuracy point $\theta_2^1 = 248^\circ, \theta_4^1 = 220^\circ$. (Notice that two of the accuracy points are taken up by the parallelogram configuration of the designed linkage, whereas the first accuracy point is satisfied by the same link lengths but in the antiparallelogram configuration.)

- 3.20 Synthesize a four-bar steering mechanism for a vehicle with the basic arrangement and dimensions as shown in Fig. 3.36. The minimum radius of curvature of the path traced by the midpoint of the vehicle is 10 m. Why is it necessary for the four-bar mechanism to be symmetrical? How many accuracy points can be considered if the synthesis is done using Freudenstein's equation?

- 3.21 If the output link remains stationary for a part of the cycle when the input link moves continuously, then the mechanism is called a dwell mechanism. Cams are normally used for the design of a dwell mechanism which finds prominent applications in packaging machines. Approximate dwell mechanisms can also be designed by utilizing an approximately circular arc of a four-bar coupler curve as explained in Fig. 3.37. As the input link O_2A of the crank-rocker linkage O_2ABO_4 moves from O_2A_1 to O_2A_2 , the coupler point C moves along the arc C_1C_2 , which is approximately circular, of radius R ($= CD$) with the centre at D . Consequently,

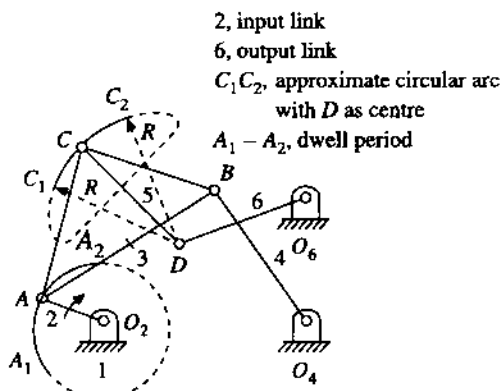


FIGURE 3.37

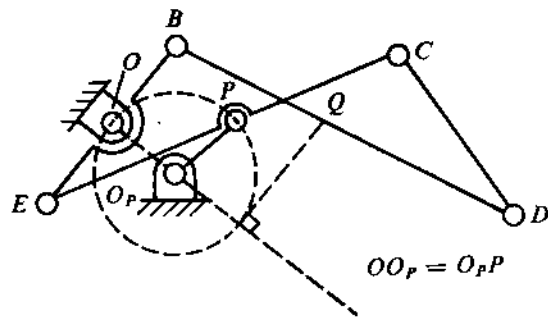


FIGURE 3.38

during this interval, the point D , and hence the output link O_6D , remains (almost) stationary. Taking 4 suitable points on the coupler curve, design this linkage with a swing angle of 30° for the output link 6.

- 3.22 In a strip-chart recorder, the pen driven by the galvanometer moves along a circular arc if it is mounted on a hinged arm. Generally, the amount of rotation of this arm is proportional to the signal the galvanometer receives. This not only necessitates the use of a curvilinear coordinate chart paper but also distorts the signal record. To overcome this problem, design a 4R mechanism to move the pen almost along a straight line, with the pen displacement proportional to the input signal. Assume that the range of rotation of the arm connected to the galvanometer is 90° and that of the pen movement is 10 cm. The movement of the pen can be considered to be reasonably linear if the pen, placed at a suitable coupler point, passes through three Chebyshev's accuracy points on its path.
- 3.23 Hart's chain for generating an exact straight line is shown in Fig. 3.38. The quadrilateral $ECDB$ is an antiparallelogram with $BE = CD$ and $EC = BD$ (BC will always remain parallel to ED). The points O , P , and Q are on a line parallel to BC . Prove that as this mechanism moves, the point Q generates an exact straight line, given $OO_P = O_P P$. The reader should note that Hart's chain consists of only six links as compared to eight for the Peaucellier mechanism.

Chapter 4

DYNAMIC FORCE AND MOTION ANALYSIS OF PLANE MECHANISMS

4.1 INTRODUCTION

For the actual operation of mechanisms and machines, a design based only on kinematic considerations is not sufficient. The links and members must be properly designed to withstand the acting forces without any undue deformation. Otherwise, the proper functioning of the system may not be possible.

The forces associated with the principal function of a machine for doing useful work are normally known. For example, in the slider-crank mechanism of a direct-acting engine, the gas force acting on the piston is known or assumed without any consideration of the motion of the system. The weights of the various members also belong to this group. Apart from such forces, the members of a mechanism also experience inertial forces when subjected to an acceleration. These forces, termed *inertial force*, are set up directly by the motion of the system.

In mechanisms and machines that operate at high speeds, dynamic inertial forces are often greater than static or other applied forces and may play a dominant role in their design.

4.2 MOTION OF A RIGID BODY SUBJECTED TO A SYSTEM OF FORCES

Consider the rigid body shown in Fig. 4.1 to be in motion in the horizontal plane under the action of a system of forces \mathbf{F}_1 and \mathbf{F}_2 . The point G represents the CG of the rigid body. The mass of the body is denoted by m . Both \mathbf{F}_1 and \mathbf{F}_2 act in the plane of motion of the body and their resultant is \mathbf{R} , as shown in Fig. 4.1a. From Newton's laws of motion, we have

$$\sum \mathbf{F} = \mathbf{R} = m\mathbf{a}_G, \quad (4.1)$$

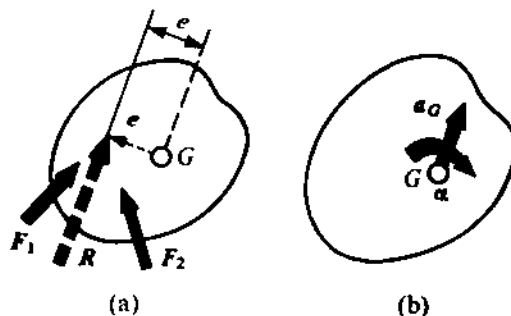


FIGURE 4.1

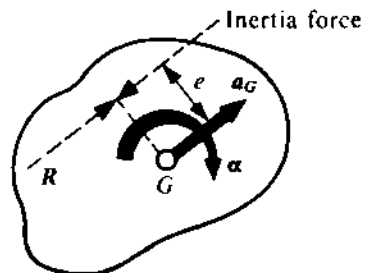


FIGURE 4.2

where a_G is the acceleration of G in a direction parallel to R and in the same sense, as shown in Fig. 4.1b. Furthermore,

$$\sum \mathbf{M} = J\alpha, \quad (4.2)$$

where $\sum \mathbf{M}$ is the sum of the torques and moments of the forces about an axis through G and normal to the plane of motion. J represents the moment of inertia of the body about the same axis and α is the angular acceleration of the body in the plane of motion and in the sense of $\sum \mathbf{M}$. The total torque $\sum \mathbf{M}$ about G can be expressed in terms of R as

$$\sum \mathbf{M} = \mathbf{e} \times \mathbf{R}, \quad (4.3)$$

where e is the vector representing the distance between R and a_G . Therefore, from (4.2) and (4.3), we get

$$e = J\alpha/R. \quad (4.4)$$

In the case of mechanisms, accelerations are usually known from kinematic analysis and the forces and moments producing the accelerations are to be determined.

4.3 PRINCIPLE OF VIRTUAL WORK

The principle of virtual work, in effect, expresses the requirement for the static equilibrium of a system. It states that *if a physical system is in equilibrium and undergoes an infinitesimal displacement consistent with the system constraints, and if this displacement is imagined to take place without any lapse of time, the net work done by the forces during the process is zero.*

4.4 D'ALEMBERT'S PRINCIPLE AND DYNAMIC EQUILIBRIUM

When a body moves with zero acceleration, from Newton's second law it can be concluded that the resultant of the forces acting on the body is zero. In other words, the body is in static equilibrium. For angular motion also, a similar law applies. When a rigid body (Fig. 4.1a) is subjected to a system of forces, the body will be in static equilibrium under the action of the externally applied forces along with a fictitious force $-ma_G$. Similarly, there will be static equilibrium for the combined effect of the externally applied torques about an axis through G perpendicular to the plane of motion and a fictitious couple $(-J\alpha)$. The fictitious force and the fictitious couple are known as *inertia force* and *inertia torque*, respectively. Thus, a dynamic problem can be converted into a static problem. This

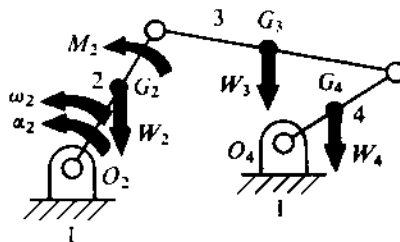


FIGURE 4.3

is commonly known as *D'Alembert's principle*, which states that *the vector sum of all external forces and inertia forces acting on a rigid body is zero*, and that the vector sum of all external moments and inertia torques acting on a rigid body is also separately equal to zero.

Let us consider a rigid body of mass m to be in plane motion. The motion of the body is specified in the following manner. The rectilinear acceleration of the CG (denoted by a point G) is a_G . The angular acceleration about an axis perpendicular to the plane of motion is α^1 (Fig. 4.2). Now, the resultant of the externally applied forces R must act in a direction which is the same as that of a_G , and in the same sense. Again, to produce the angular acceleration α , R must act at such a distance from G that the moment of R about an axis through G perpendicular to the plane of motion is $J\alpha$, where J is the moment of inertia of the body about the same axis. So,

$$Re = J\alpha \quad \text{or} \quad e = J\alpha/R.$$

From D'Alembert's principle, the inertia force of the body due to the prescribed motion should be such that it balances the resultant of the externally applied forces. Thus, the inertia force will act opposite to R along the same line of action.

4.5 DYNAMIC FORCE ANALYSIS (GRAPHICAL METHOD)

It has been shown that by the application of D'Alembert's principle, a dynamic system can be converted into a static system. So, a dynamic problem can be solved by static analysis when inertia forces and moments are taken into account. The analysis can be carried out in two ways, namely,

- (i) by considering the combined action of all the forces simultaneously, and
- (ii) by determining the effect of each force separately and then finding the overall effect at any point by vectorial superposition of the individual effects.

Let us first discuss the former method. When a whole system is in equilibrium, every part of the system must also be in equilibrium. So, every member of a mechanism can be considered to be in equilibrium under the combined effect of all the applied and reactive forces, including its own inertia force. The method will be explained by means of an example. Consider the four-bar mechanism shown in Fig. 4.3. Link 2 rotates with an angular velocity ω_2 and an angular acceleration α_2 , as indicated. A torque M_2 is applied on link 2, and all the links are subjected to their respective gravitational forces W_2 , W_3 , and W_4 (as a matter of fact, each link can be considered to be

¹In plane motion, a vector representing a rotational quantity, e.g., M and α , is perpendicular to the plane of motion. Henceforth, we shall not denote such a quantity by a **boldface** letter, but, instead, will treat it as an algebraic scalar quantity.

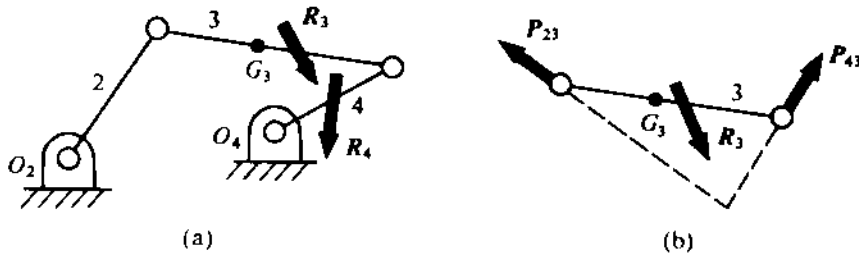


FIGURE 4.4

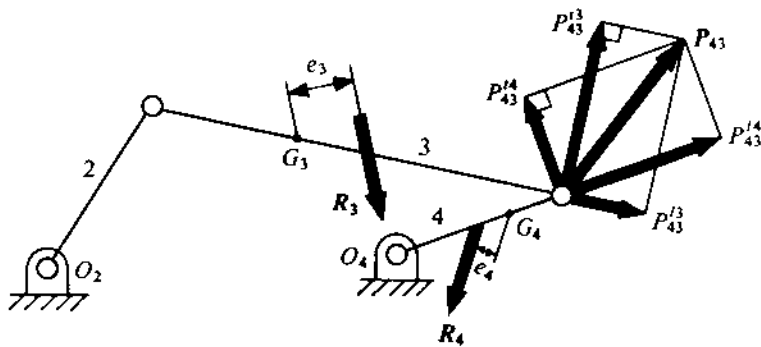


FIGURE 4.5

subjected to an externally applied resultant force and a resultant torque). It is required to determine the magnitude and sense of the applied torque M_2 . The points G_2 , G_3 , and G_4 are the mass centres of links 2, 3, and 4, respectively. The moments of inertia of these links about the axes passing through their corresponding mass centres and perpendicular to the plane of motion are J_2 , J_3 , and J_4 . All other relevant information necessary for kinematic analysis can be assumed.

First, by kinematic analysis, we determine the linear acceleration of the mass centres (\mathbf{a}_{G_2} , \mathbf{a}_{G_3} , and \mathbf{a}_{G_4}) and the angular accelerations (α_3 and α_4), treating α as an algebraic quantity instead of a vector as the acceleration takes place only in the plane of motion. The inertia force \mathbf{F}_j^i and the inertia torque M_j^i in the j -th link are $(-m_j \mathbf{a}_{G_j})$ and $(-J_j \alpha_j)$, respectively (m_j being the mass of the j -th link). So, \mathbf{F}_j^i and M_j can be combined into a force $\mathbf{F}_j^{i'}$, parallel and equal in magnitude to the inertia force but applied at a distance e_j from the mass centre G_j , where $e_j = J_j \alpha_j / (m_j a_{G_j})$ [see (4.4)]. Now, for the j -th link, the externally applied load, its weight (when the plane of motion of the mechanism is vertical), and this shifted inertia force can be combined to give a resultant force \mathbf{R}_j . This method of analysis requires that a simple link should first be located. For the mechanism shown in Fig. 4.4a, the free-body diagram of link 3 is shown in Fig. 4.4b, where \mathbf{R}_3 is balanced by the pin forces \mathbf{P}_{23} and \mathbf{P}_{43} (\mathbf{P}_{ij} denotes the force exerted on the j -th link by the i -th link). As \mathbf{R}_j includes the inertia force and the inertia torque, \mathbf{P}_{23} , \mathbf{P}_{43} , and \mathbf{R}_3 must satisfy the static equilibrium condition according to D'Alembert's principle. \mathbf{P}_{43} may be resolved into longitudinal and transverse components, \mathbf{P}_{43}^l and \mathbf{P}_{43}^t , respectively. \mathbf{P}_{ij}^{lk} and \mathbf{P}_{ij}^{tk} denote the longitudinal and transverse components of \mathbf{P}_{ij} for link k ($= i$ or j). Figure 4.5 shows components of \mathbf{P}_{43} for both links 3 and 4. As link 3 will be in static equilibrium under the action of forces \mathbf{P}_{23} , \mathbf{R}_3 , and \mathbf{P}_{43} , the magnitude and direction of \mathbf{P}_{43}^l can be determined by taking moments about the junction of links 2 and 3 and equating the sum to zero. Similarly, $\mathbf{P}_{34}^{tk} (= -\mathbf{P}_{43}^t)$ can be determined by taking moments of this force and of \mathbf{R}_4 about O_4 . Therefore, the components of \mathbf{P}_{43} in two given directions are known and \mathbf{P}_{43} can thus be determined (Fig. 4.5). When \mathbf{P}_{43} is known, \mathbf{P}_{23} can be very easily

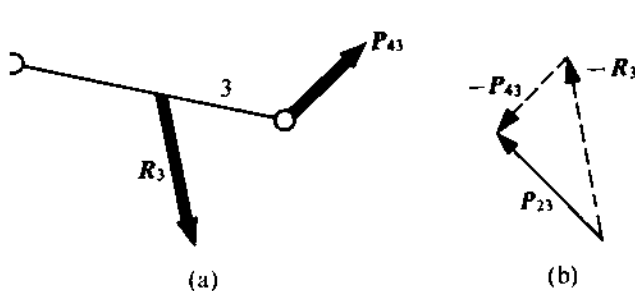


FIGURE 4.6

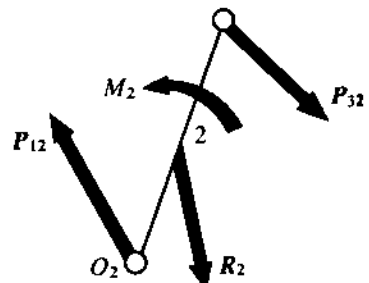


FIGURE 4.7

determined by considering the static equilibrium of link 3 under the action of P_{23} , R_3 , and P_{43} (Fig. 4.6).

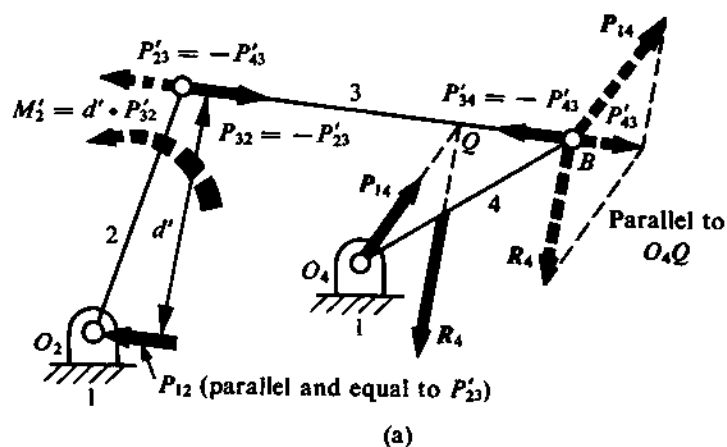
Again, link 2 under the action of R_2 , M_2 (the applied external torque), P_{32} ($= -P_{23}$), and P_{12} must be in static equilibrium (Fig. 4.7). Therefore, taking moments of P_{32} and R_2 about O_2 , we can determine M_2 . In fact, M_2 will be equal and opposite to the resultant moment of P_{32} and R_2 about O_2 . One important point which should always be remembered is that such an analysis will be possible only if we start the analysis from a statically determinate link.

The same problem can also be solved by the second method, i.e., by the method of superposition. Figure 4.8a shows how the forces develop in the joints due to R_4 alone. Link 3 exerts a force P'_{32} on link 2. Therefore, the reaction at the fixed hinge O_2 will be a force which is equal and opposite to P'_{32} , and to keep link 2 in equilibrium, a torque M'_2 ($= d'P'_{32}$, where d' is the distance between P'_{32} and P'_{12}) must be applied as indicated. Similarly, a moment M''_2 , required to keep link 2 in equilibrium under the action of R_3 , can be determined. The method is shown in Fig. 4.8b, which is self-explanatory. Link 2, under the action of R_2 , is shown in Fig. 4.9. It is apparent from the figure that M'''_2 , required to keep link 2 in equilibrium under the action of R_2 , will be $d'''R_2$ (d''' being the distance of R_2 from O_2). As R_2 , R_3 , and R_4 include the inertia effects of the links, the applied torque M_2 on link 2 must keep the whole system in equilibrium. Therefore,

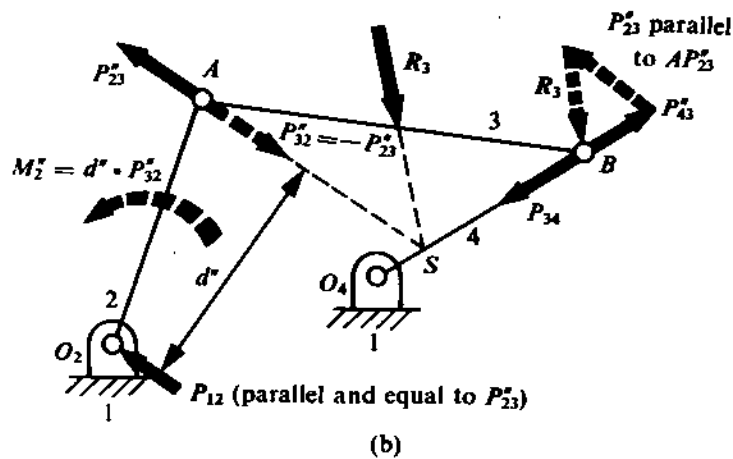
$$M_2 = M'_2 + M''_2 + M'''_2,$$

where M'_2 , M''_2 , and M'''_2 are the torques to be applied on link 2 to keep it in equilibrium under the action of R_4 , R_3 , and R_2 , respectively. In a similar manner, any pin force P_{ij} can also be determined by vectorial superposition of P'_{ij} , P''_{ij} , and P'''_{ij} . It should always be kept in mind that this method of superposition is valid only when the mechanism is free from friction effects. The principle of virtual work can also be applied for the determination of M_2 in the foregoing example. By D'Alembert's principle, the whole mechanism under the action of R_2 , R_3 , R_4 , and M_2 must be in static equilibrium. So, the total virtual work done by all the external forces must be zero. As the points O_2 and O_4 are fixed in space, P_{12} and P_{43} do zero work. The forces R_2 , R_3 , and R_4 act at the points P_2 , P_3 , and P_4 , and the corresponding velocities are \mathbf{V}_{P_2} , \mathbf{V}_{P_3} , and \mathbf{V}_{P_4} , respectively, as shown in Fig. 4.10. Only the components R'_2 , R'_3 , and R'_4 , which are in the direction of the corresponding velocities, will do work. The virtual linear displacements of P_2 , P_3 , and P_4 , and the virtual angular displacements of link 2 will be proportional to the magnitudes of \mathbf{V}_{P_2} , \mathbf{V}_{P_3} , \mathbf{V}_{P_4} , and ω_2 , the directions being the same as those of the velocities. So, the total virtual work done by R_2 , R_3 , R_4 , and M_2 will be proportional to

$$R_2 \cdot \mathbf{V}_{P_2} + R_3 \cdot \mathbf{V}_{P_3} + R_4 \cdot \mathbf{V}_{P_4} + M_2 \omega_2$$



(a)



(b)

FIGURE 4.8

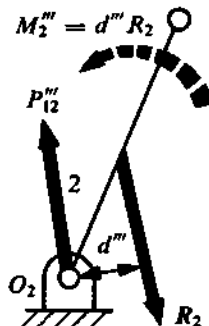


FIGURE 4.9

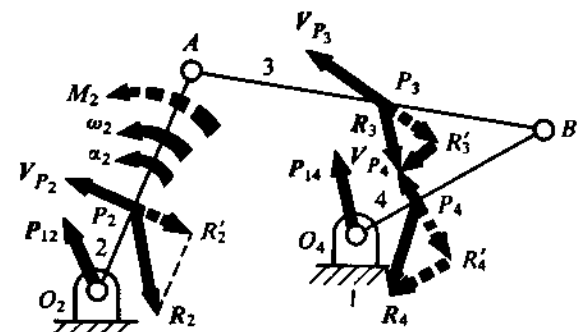


FIGURE 4.10

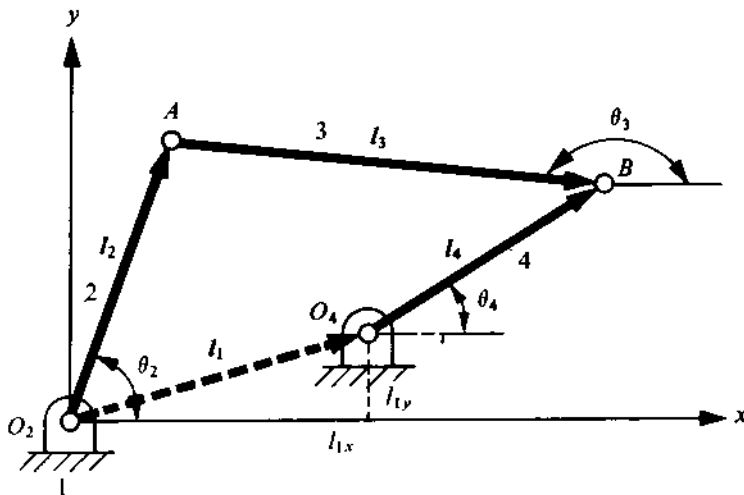


FIGURE 4.11

which must be equal to zero. Therefore,

$$M_2 = -\frac{1}{\omega_2} (\mathbf{R}_2 \cdot \mathbf{V}_{P_2} + \mathbf{R}_3 \cdot \mathbf{V}_{P_3} + \mathbf{R}_4 \cdot \mathbf{V}_{P_4}) = \frac{1}{\omega_2} (V_{P_2} \cdot R'_2 + V_{P_3} \cdot R'_3 + V_{P_4} \cdot R'_4).$$

When M_2 has been determined, all other quantities of interest can be obtained.

4.6 DYNAMIC FORCE ANALYSIS (ANALYTICAL METHOD)

Problems of dynamic force analysis can be solved by representing all vector quantities in terms of i and j (the base vectors). However, this method is tedious as compared to the graphical method. An analytical approach, which is amenable to computer programming, will be discussed here. Systems of considerable complexity can be easily solved by the analytical method with digital computers.

In this method, the displacements, velocities, accelerations, and forces are represented by vectors. Dynamic equilibrium equations for each element are established and then, by combining these equations with kinematic relationships, the final equations for forces are obtained. The method will be explained by an example.

Consider the four-bar mechanism discussed in Section 4.5. The links are represented by vectors as shown in Fig. 4.11, l_j representing the length of the j -th link. From the figure, we see that

$$l_2 + l_3 - l_4 = l_1, \quad (4.5)$$

where

$$\begin{aligned} l_2 &= il_2 \cos \theta_2 + jl_2 \sin \theta_2, \\ l_3 &= -il_3 \cos \theta_3 - jl_3 \sin \theta_3, \\ l_4 &= il_4 \cos \theta_4 + jl_4 \sin \theta_4, \end{aligned} \quad (4.6)$$

i and j being the base vectors in the x - and y -direction, respectively. Substituting (4.6) in (4.5), relationships can be established for θ_2 , θ_3 , and θ_4 by equating the coefficients of i and j from both

sides of (4.5). As the fixed link $\mathbf{l}_1 = i\mathbf{l}_{1x} + j\mathbf{l}_{1y}$, the relationships can be expressed in the form

$$\mathbf{l}_2 \cos \theta_2 - \mathbf{l}_3 \cos \theta_3 - \mathbf{l}_4 \cos \theta_4 = \mathbf{l}_{1x}, \quad \mathbf{l}_2 \sin \theta_2 - \mathbf{l}_3 \sin \theta_3 - \mathbf{l}_4 \sin \theta_4 = \mathbf{l}_{1y}.$$

Since \mathbf{l}_1 is a fixed vector, differentiating both sides of (4.5) with respect to time, we get

$$\dot{\mathbf{l}}_2 + \dot{\mathbf{l}}_3 - \dot{\mathbf{l}}_4 = 0. \quad (4.7)$$

Moreover,

$$\begin{aligned}\dot{\mathbf{l}}_2 &= (-i\mathbf{l}_2 \sin \theta_2 + j\mathbf{l}_2 \cos \theta_2)\dot{\theta}_2, \\ \dot{\mathbf{l}}_3 &= (i\mathbf{l}_3 \sin \theta_3 - j\mathbf{l}_3 \cos \theta_3)\dot{\theta}_3, \\ \dot{\mathbf{l}}_4 &= (-i\mathbf{l}_4 \sin \theta_4 + j\mathbf{l}_4 \cos \theta_4)\dot{\theta}_4.\end{aligned} \quad (4.8)$$

Substituting (4.8) in (4.7), the relationships for $\dot{\theta}_2$, $\dot{\theta}_3$, and $\dot{\theta}_4$ can be expressed in matrix form as

$$\begin{bmatrix} \mathbf{l}_2 \sin \theta_2 & -\mathbf{l}_3 \sin \theta_3 & \mathbf{l}_4 \sin \theta_4 \\ \mathbf{l}_2 \cos \theta_2 & -\mathbf{l}_3 \cos \theta_3 & \mathbf{l}_4 \cos \theta_4 \end{bmatrix} \begin{Bmatrix} \dot{\theta}_2 \\ \dot{\theta}_3 \\ \dot{\theta}_4 \end{Bmatrix} = \{0\}. \quad (4.9)$$

Similarly,

$$\ddot{\mathbf{l}}_2 + \ddot{\mathbf{l}}_3 - \ddot{\mathbf{l}}_4 = 0,$$

and the relationships for $\ddot{\theta}_2$, $\ddot{\theta}_3$, and $\ddot{\theta}_4$ take the form

$$\begin{bmatrix} -\mathbf{l}_2 \sin \theta_2 & \mathbf{l}_3 \sin \theta_3 & -\mathbf{l}_4 \sin \theta_4 \\ \mathbf{l}_2 \cos \theta_2 & -\mathbf{l}_3 \cos \theta_3 & \mathbf{l}_4 \cos \theta_4 \end{bmatrix} \begin{Bmatrix} \ddot{\theta}_2 \\ \ddot{\theta}_3 \\ \ddot{\theta}_4 \end{Bmatrix} = \begin{Bmatrix} \mathbf{l}_2 \cos \theta_2 \cdot \dot{\theta}_2^2 + \mathbf{l}_3 \cos \theta_3 \cdot \dot{\theta}_3^2 - \mathbf{l}_4 \cos \theta_4 \cdot \dot{\theta}_4^2 \\ -\mathbf{l}_2 \sin \theta_2 \cdot \dot{\theta}_2^2 + \mathbf{l}_3 \sin \theta_3 \cdot \dot{\theta}_3^2 - \mathbf{l}_4 \sin \theta_4 \cdot \dot{\theta}_4^2 \end{Bmatrix}. \quad (4.10)$$

The next step will be the formulation of the dynamic equilibrium equations for the j -th link of the mechanism. Any loading on the j -th link can be considered to consist of

$F_{j,x}$ = external force in the x -direction applied at G_j (CG of the j -th link),

$F_{j,y}$ = external force in the y -direction applied at G_j ,

M_j = external moment on the j -th link applied at G_j .

Figure 4.12 shows an exploded view of the mechanism with a free-body diagram of each link, where $\mathbf{l}_j = d_j + f_j$.

For link 2, the dynamic relationships in matrix form will be

$$\begin{Bmatrix} F_{2,x} \\ F_{2,y} \\ M_2 \end{Bmatrix} + \begin{bmatrix} 1 & 0 & 1 & 0 \\ 0 & 1 & 0 & 1 \\ d_2 \sin \theta_2 & -d_2 \cos \theta_2 & -f_2 \sin \theta_2 & f_2 \cos \theta_2 \end{bmatrix} \begin{Bmatrix} P_{O_2,x} \\ P_{O_2,y} \\ P_{A,x} \\ P_{A,y} \end{Bmatrix} = m_2 \begin{Bmatrix} a_{G_2,x} \\ a_{G_2,y} \\ \ddot{\theta}_2 k_2^2 \end{Bmatrix}, \quad (4.11)$$

where $a_{G_2,x}$ and $a_{G_2,y}$ are the x - and y -component of the acceleration of G_2 , and k_2 represents the radius of gyration of link 2 about an axis passing through G_2 and perpendicular to the plane of

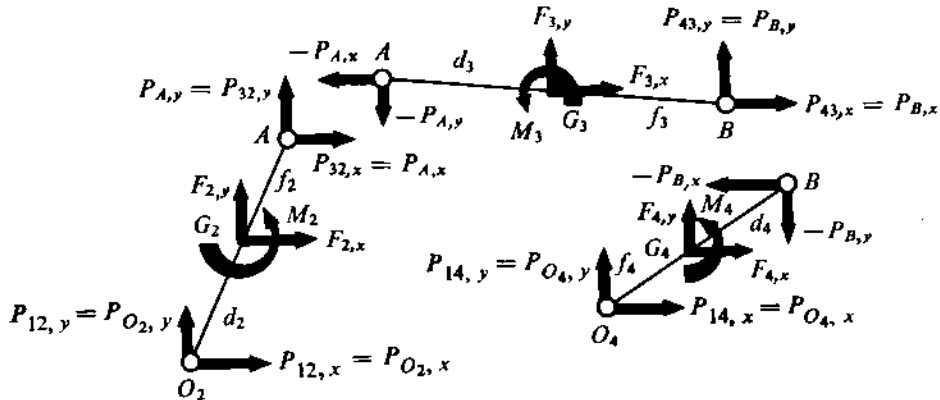


FIGURE 4.12

notion. Similarly, for link 3 and link 4, the dynamic relationships will be

$$\left\{ \begin{array}{l} F_{3,z} \\ F_{3,y} \\ M_3 \end{array} \right\} + \left[\begin{array}{cccc} -1 & 0 & 1 & 0 \\ 0 & -1 & 0 & 1 \\ d_3 \sin \theta_3 & -d_3 \cos \theta_3 & f_3 \sin \theta_3 & -f_3 \cos \theta_3 \end{array} \right] \left\{ \begin{array}{l} P_{A,z} \\ P_{A,y} \\ P_{B,z} \\ P_{B,y} \end{array} \right\} = m_3 \left\{ \begin{array}{l} a_{G_3,z} \\ a_{G_3,y} \\ \ddot{\theta}_3 k_3^2 \end{array} \right\}, \quad (4.12)$$

$$\left\{ \begin{array}{l} F_{4,z} \\ F_{4,y} \\ M_4 \end{array} \right\} + \left[\begin{array}{cccc} -1 & 0 & 1 & 0 \\ 0 & -1 & 0 & 1 \\ d_4 \sin \theta_4 & -d_4 \cos \theta_4 & f_4 \sin \theta_4 & -f_4 \cos \theta_4 \end{array} \right] \left\{ \begin{array}{l} P_{B,z} \\ P_{B,y} \\ P_{O_4,z} \\ P_{O_4,y} \end{array} \right\} = m_4 \left\{ \begin{array}{l} a_{G_4,z} \\ a_{G_4,y} \\ \ddot{\theta}_4 k_4^2 \end{array} \right\}. \quad (4.13)$$

$a_{G_3,z}$, $a_{G_3,y}$, $a_{G_4,z}$, $a_{G_4,y}$, k_3 , and k_4 denote components of acceleration and radii of gyration as already indicated. Now, combining (4.11), (4.12), and (4.13), the dynamic relationship for the complete system will be

$$\{F\} + [Q]\{P\} = \{H\}, \quad (4.14)$$

where

$$\{F\} = \left\{ \begin{array}{l} F_{2,z} \\ F_{2,y} \\ M_2 \\ F_{3,z} \\ F_{3,y} \\ M_3 \\ F_{4,z} \\ F_{4,y} \\ M_4 \end{array} \right\}, \quad \{P\} = \left\{ \begin{array}{l} P_{O_2,z} \\ P_{O_2,y} \\ P_{A,z} \\ P_{A,y} \\ P_{B,z} \\ P_{B,y} \\ P_{O_4,z} \\ P_{O_4,y} \end{array} \right\}, \quad \{H\} = \left\{ \begin{array}{l} m_2 \left\{ \begin{array}{l} a_{G_2,z} \\ a_{G_2,y} \\ \ddot{\theta}_2 k_2^2 \end{array} \right\} \\ m_3 \left\{ \begin{array}{l} a_{G_3,z} \\ a_{G_3,y} \\ \ddot{\theta}_3 k_3^2 \end{array} \right\} \\ m_4 \left\{ \begin{array}{l} a_{G_4,z} \\ a_{G_4,y} \\ \ddot{\theta}_4 k_4^2 \end{array} \right\} \end{array} \right\},$$

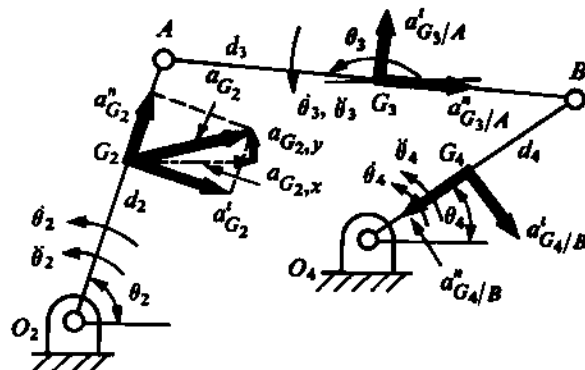


FIGURE 4.13

$$[Q] = \begin{bmatrix} 1 & 0 & 1 & 0 & 0 & 0 & 0 & 0 \\ 0 & 1 & 0 & 1 & 0 & 0 & 0 & 0 \\ d_2 \sin \theta_2 & -d_2 \cos \theta_2 & -f_2 \sin \theta_2 & f_2 \cos \theta_2 & 0 & 0 & 0 & 0 \\ 0 & 0 & -1 & 0 & 1 & 0 & 0 & 0 \\ 0 & 0 & 0 & -1 & 0 & 1 & 0 & 0 \\ 0 & 0 & d_3 \sin \theta_3 & -d_3 \cos \theta_3 & f_3 \sin \theta_3 & -f_3 \cos \theta_3 & 0 & 0 \\ 0 & 0 & 0 & 0 & -1 & 0 & 1 & 0 \\ 0 & 0 & 0 & 0 & 0 & -1 & 0 & 1 \\ 0 & 0 & 0 & 0 & d_4 \sin \theta_4 & -d_4 \cos \theta_4 & f_4 \sin \theta_4 & -f_4 \cos \theta_4 \end{bmatrix}$$

Equation (4.14) represents nine simultaneous equations. So, the eight unknown elements of $\{P\}$ along with the one unknown in $\{F\}$ can be determined when other quantities are known. For example, in the problem solved by the graphical method (Fig. 4.3), all elements in $\{F\}$ except M are known as follows:

$$\begin{aligned} F_{2,z} &= 0, & F_{2,y} &= -W_2, & M_2 &= ?, \\ F_{3,z} &= 0, & F_{3,y} &= -W_3, & M_3 &= 0, \\ F_{4,z} &= 0, & F_{4,y} &= -W_4, & M_4 &= 0. \end{aligned}$$

By solving these nine equations, we can determine M_2 and the eight components of the joint reactions.

In the process of evaluating $\{H\}$, the kinematic relationships (4.7) and (4.8) have to be used. Both (4.7) and (4.8) represent sets of two simultaneous equations with two unknowns (out of three velocities and accelerations, one velocity and one acceleration will be given as input data) and these equations can be solved. When $\dot{\theta}_j$ and $\ddot{\theta}_j$ ($j = 2, 3, 4$) are determined, $\{H\}$ can be calculated.

As shown in Fig. 4.13, a_{G_2} will have two components, one normal ($a_{G_2}^n$) and the other tangentia ($a_{G_2}^t$) to link 2. Thus,

$$\begin{aligned} a_{G_2,z} &= a_{G_2}^n \cos \theta_2 + a_{G_2}^t \sin \theta_2, \\ a_{G_2,v} &= a_{G_2}^n \sin \theta_2 - a_{G_2}^t \cos \theta_2. \end{aligned}$$

Again, $a_{G_2}^n = -d_2 \dot{\theta}_2^2$, $a_{G_2}^t = -d_2 \ddot{\theta}_2$. Thus,

$$a_{G_2,z} = -d_2 \cos \theta_2 \dot{\theta}_2^2 - d_2 \sin \theta_2 \ddot{\theta}_2, \quad a_{G_2,v} = -d_2 \sin \theta_2 \dot{\theta}_2^2 + d_2 \cos \theta_2 \ddot{\theta}_2. \quad (4.15)$$

Since $a_{G_3} = a_A + a_{G_3/A}$, we have

$$a_{G_3,z} = a_{A,z} + a_{G_3/A,z}, \quad a_{G_3,v} = a_{A,v} + a_{G_3/A,v}. \quad (4.16)$$

Substitution of d_2 by l_2 in (4.15) will give $a_{A,x}$ and $a_{A,y}$. Thus,

$$\begin{aligned} a_{A,x} &= -l_2 \cos \theta_2 \dot{\theta}_2^2 - l_2 \sin \theta_2 \ddot{\theta}_2, & a_{A,y} &= -l_2 \sin \theta_2 \dot{\theta}_2^2 + l_2 \cos \theta_2 \ddot{\theta}_2, \\ a_{G_3/A}^n &= -d_3 \dot{\theta}_3^2, & a_{G_3/A}^t &= d_3 \ddot{\theta}_3 \end{aligned} \quad (4.17)$$

which give

$$\begin{aligned} a_{G_3/A,x} &= -a_{G_3/A}^n \cos \theta_3 + a_{G_3/A}^t \sin \theta_3, \\ a_{G_3/A,y} &= -a_{G_3/A}^n \sin \theta_3 - a_{G_3/A}^t \cos \theta_3. \end{aligned} \quad (4.18)$$

From (4.16), (4.17), and (4.18), we get

$$\begin{aligned} a_{G_3,x} &= -l_2 \cos \theta_2 \dot{\theta}_2^2 - l_2 \sin \theta_2 \ddot{\theta}_2 + d_3 \cos \theta_3 \dot{\theta}_3^2 + d_3 \sin \theta_3 \ddot{\theta}_3, \\ a_{G_3,y} &= -l_2 \sin \theta_2 \dot{\theta}_2^2 + l_2 \cos \theta_2 \ddot{\theta}_2 + d_3 \sin \theta_3 \dot{\theta}_3^2 - d_3 \cos \theta_3 \ddot{\theta}_3. \end{aligned} \quad (4.19)$$

By substituting d_3 in place of d_3 we get $a_{B,x}$ and $a_{B,y}$. Therefore,

$$\begin{aligned} a_{B,x} &= -l_2 \cos \theta_2 \dot{\theta}_2^2 + l_3 \cos \theta_3 \dot{\theta}_3^2 - l_2 \sin \theta_2 \ddot{\theta}_2 + l_3 \sin \theta_3 \ddot{\theta}_3, \\ a_{B,y} &= -l_2 \sin \theta_2 \dot{\theta}_2^2 + l_3 \sin \theta_3 \dot{\theta}_3^2 + l_2 \cos \theta_2 \ddot{\theta}_2 - l_3 \cos \theta_3 \ddot{\theta}_3. \end{aligned} \quad (4.20)$$

Again, $a_{G_4,x} = a_{B,x} + a_{G_4/B,x}$, $a_{G_4,y} = a_{B,y} + a_{G_4/B,y}$, and the final expressions for $a_{G_4,x}$ and $a_{G_4,y}$ will be

$$\begin{aligned} a_{G_4,x} &= -l_2 \cos \theta_2 \dot{\theta}_2^2 + l_3 \cos \theta_3 \dot{\theta}_3^2 + d_4 \cos \theta_4 \dot{\theta}_4^2 - l_2 \sin \theta_2 \ddot{\theta}_2 + l_3 \sin \theta_3 \ddot{\theta}_3 + d_4 \sin \theta_4 \ddot{\theta}_4, \\ a_{G_4,y} &= -l_2 \sin \theta_2 \dot{\theta}_2^2 + l_3 \sin \theta_3 \dot{\theta}_3^2 + d_4 \sin \theta_4 \dot{\theta}_4^2 + l_2 \cos \theta_2 \ddot{\theta}_2 - l_3 \cos \theta_3 \ddot{\theta}_3 - d_4 \cos \theta_4 \ddot{\theta}_4. \end{aligned} \quad (4.21)$$

With the help of (4.15), (4.19), and (4.21), we can write $\{H\}$ in the form

$$\{H\} = \{U\} + [\lambda]\{\ddot{\theta}\}, \quad (4.22)$$

where

$$\begin{aligned} \{U\} &= \left\{ \begin{array}{c} m_2 \left\{ \begin{array}{c} -d_2 \cos \theta_2 \dot{\theta}_2^2 \\ -d_2 \sin \theta_2 \dot{\theta}_2^2 \\ 0 \end{array} \right\} \\ m_3 \left\{ \begin{array}{c} (-l_2 \cos \theta_2 \dot{\theta}_2^2 + d_3 \cos \theta_3 \dot{\theta}_3^2) \\ (-l_2 \sin \theta_2 \dot{\theta}_2^2 + d_3 \sin \theta_3 \dot{\theta}_3^2) \\ 0 \end{array} \right\} \\ m_4 \left\{ \begin{array}{c} (-l_2 \cos \theta_2 \dot{\theta}_2^2 + l_3 \cos \theta_3 \dot{\theta}_3^2 + d_4 \cos \theta_4 \dot{\theta}_4^2) \\ (-l_2 \sin \theta_2 \dot{\theta}_2^2 + l_3 \sin \theta_3 \dot{\theta}_3^2 + d_4 \sin \theta_4 \dot{\theta}_4^2) \\ 0 \end{array} \right\} \end{array} \right\}, \\ [\lambda] &= \left[\begin{array}{c} m_2 \left[\begin{array}{ccc} -d_2 \sin \theta_2 & 0 & 0 \\ d_2 \cos \theta_2 & 0 & 0 \\ k_2^2 & 0 & 0 \end{array} \right] \\ m_3 \left[\begin{array}{ccc} -l_2 \sin \theta_2 & d_3 \sin \theta_3 & 0 \\ l_2 \cos \theta_2 & -d_3 \cos \theta_3 & 0 \\ 0 & k_3^2 & 0 \end{array} \right] \\ m_4 \left[\begin{array}{ccc} -l_2 \sin \theta_2 & l_3 \sin \theta_3 & d_4 \sin \theta_4 \\ l_2 \cos \theta_2 & -l_3 \cos \theta_3 & -d_4 \cos \theta_4 \\ 0 & 0 & k_4^2 \end{array} \right] \end{array} \right], \quad \{\ddot{\theta}\} = \left\{ \begin{array}{c} \ddot{\theta}_2 \\ \ddot{\theta}_3 \\ \ddot{\theta}_4 \end{array} \right\} \end{aligned}$$

All the required quantities can now be determined by solving (4.14).

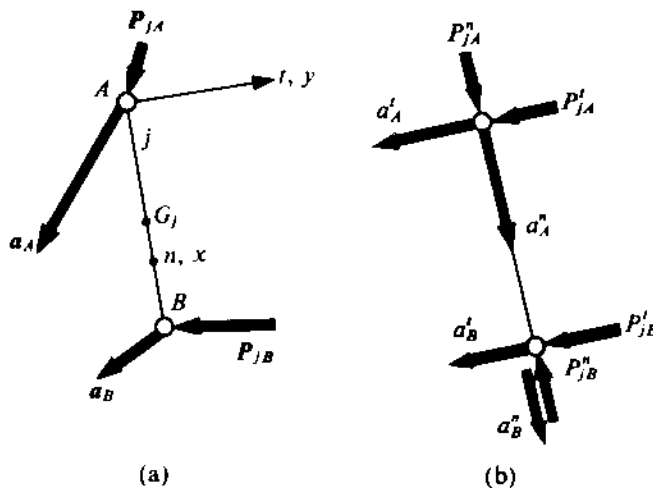


FIGURE 4.14

4.7 STRESSES IN MOVING MEMBERS

For the proper functioning of a mechanism or machine, it is necessary to design the members in such a way that the stresses developed in the members are well within the allowable limits. Computation for the bending moments, shearing forces, and axial forces acting on the individual members of mechanism can be carried out when all the pin forces and slide reactions are determined. Figure 4.14a shows a link j under the action of two pin forces P_{jA} and P_{jB} . The cross-section of the link varies from A to B , the density of the link material being ρ . In Fig. 4.14b, the two forces P_{jA} and P_{jB} , and the accelerations of the points A and B have been resolved into normal and transverse components. The normal and transverse components of the absolute acceleration of a point C on the link at a distance x from A are given by

$$a_C^n = a_A^n + a_{C/A}^n = a_A^n - AC\omega_j^2 = a_A^n - \omega_j^2 x,$$

$$a_C^t = a_A^t + a_{C/A}^t = a_A^t + AC\alpha_j = a_A^t + \alpha_j x,$$

where ω_j and α_j are the angular velocity and acceleration of the j -th link, both being positive in the counter-clockwise direction. So, it is seen that variations of the normal and transverse component of acceleration along the link are linear. Figures 4.15a and 4.15b show the distribution of the normal and tangential components of accelerations. Multiplying these by the local cross-sectional area and density, we obtain the distribution of normal and tangential components of inertia forces. Inertia force components on an element dx of the link are given by the corresponding elemental areas under the inertia-force-component curves. The total stippled areas in Figs. 4.15a and 4.15b represent the total normal and transverse components, respectively, of the inertia force on the link. Considering the externally applied load on the link and the inertia-force distributions, the stresses in the member can be determined.

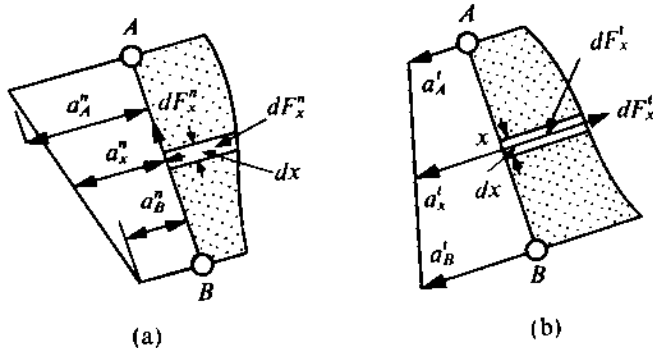


FIGURE 4.15

4.8 DYNAMIC MOTION ANALYSIS

Till now, dynamic analyses required the determination of forces in various members for a prescribed motion of a mechanism. Sometimes, it may be necessary to predict the motion behaviour of a machine (or mechanism) from the mass and moment of inertia of each member of the mechanism, with full details of the impressed force system. This section will be devoted to a discussion of *dynamic motion analysis* of mechanisms and machines with the help of the rate-of-change-of-energy method.

The Rate-of-change-of-energy Method

The rate-of-change-of-energy method² of motion analysis is based on instantaneous energy balance. The time rate of change of the total KE of a mechanism is equal to the power input by the system of external forces acting on it. The total KE of a mechanism can be expressed as

$$T = \frac{1}{2} \sum^r J_0 \omega^2 + \frac{1}{2} \sum^s m V^2 + \frac{1}{2} \sum^f m V_G^2 + \frac{1}{2} \sum^f J_G \omega^2,$$

where r , s , and f refer to rotating, sliding, and floating links; J_0 is the moment of inertia of a rotating link about an axis passing through the hinge; V_G the velocity of the CG of a floating link; and J_G the moment of inertia of the floating link about the axis passing through the CG. The total power input is

$$\sum p = \frac{dT}{dt} = \sum^r J_0 \omega \alpha + \sum^s m V a + \sum^f m V_G (a_G)_t + \sum^f J_G \omega \alpha, \quad (4.23)$$

where $(a_G)_t$ is the tangential component of the acceleration of G , i.e., the component of \mathbf{a}_G in the direction of \mathbf{V}_G . In Chapter 2, it was shown that the angular acceleration of links and the tangential

²For some other methods of dynamic motion analysis, see the second edition of this text.

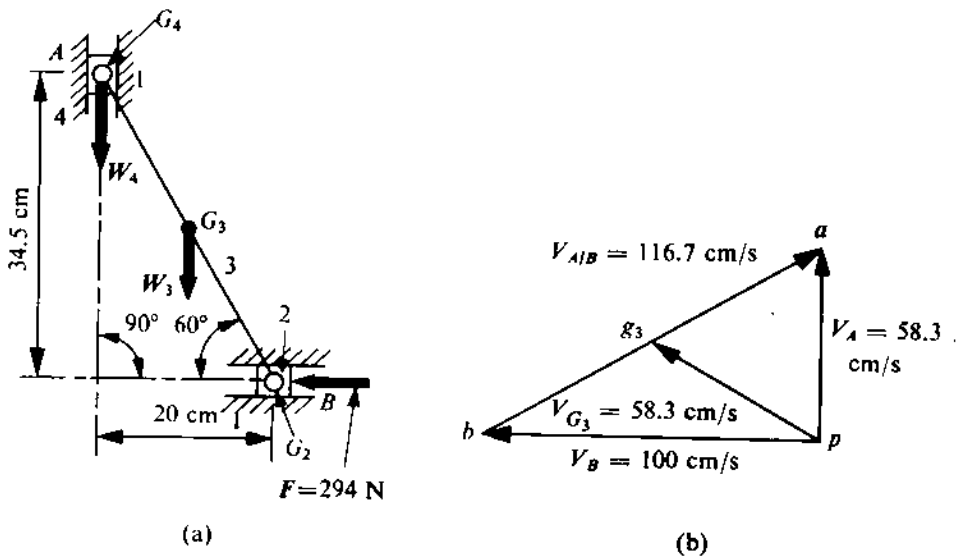


FIGURE 4.16

acceleration of points are linear functions of the input acceleration. Goodman's transformation equations [(2.27) and (2.29)], in the form applicable to mechanisms with a rotating input link, are

$$\alpha_i = \alpha_t + \frac{\omega_i}{\omega_t} \alpha_i,$$

$$(a_G)_t = (a_{\circ G})_t + \frac{V_G}{\omega_t} \alpha_i.$$

The velocity diagram and an auxiliary acceleration diagram, based on actual velocities and an arbitrarily assumed zero input acceleration, can now be constructed. Using the values of velocities and accelerations obtained from these diagrams, we can evaluate the two transformation equations. Substituting α_i and $(a_G)_t$, we get an equation from which α_i , the only unknown, can be calculated.

PROBLEM 4.1

The two ends of a link are constrained to move in guides as shown in Fig. 4.16a. The link is uniform and weighs 196 N. The sliders A and B weigh 98 N each. A force of 294 N is applied to the slider B. If the instantaneous velocity of the slider towards left is 100 cm/s, determine the instantaneous acceleration of the slider A.

SOLUTION

From the velocity diagram shown in Fig. 4.16b, we have, since $V_B = 100$ cm/s, $V_A = V_4 = 58.3$ cm/s, $V_{G_3} = 58.3$ cm/s, $\omega_3 = 2.9$ rad/s (assuming clockwise rotations to be positive). The auxiliary acceleration diagram shown in Fig. 4.17 is constructed on the basis of $V_B = V_2 = 100$ cm/s and $\frac{a}{\omega_B} = \frac{a}{\omega_2} = 0$. This diagram yields $(a_{\circ G_3})_t = 100$ cm/s², $\frac{\alpha}{\omega_3} = -5.62$ rad/s², $\frac{a}{\omega_A} = \frac{a}{\omega_4} = 450$ cm/s². The accelerations and their components for different links, as expressed by Goodman's transformation equations (in this case, the input link happens to be a slider), are

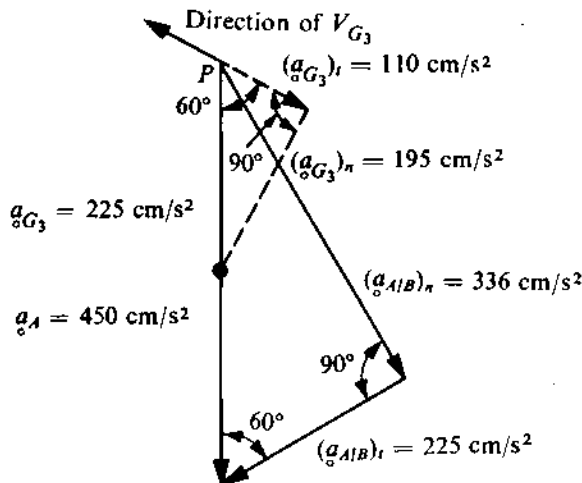


FIGURE 4.17

$$a_2 = \frac{a}{\omega_2} + \frac{V_2}{V_2} \cdot a_2 = a_2 \quad (\text{link 2}),$$

$$\alpha_3 = \frac{\alpha}{\omega_3} + \frac{\omega^2}{V_2} a_2 = -5.62 + 0.05 a_2 \quad (\text{link 3}),$$

$$(a_{G_3})_t = (a_{G_3})_t + \frac{V_{G_3}}{V_2} a_2 = -110 + 0.583 a_2$$

$$a_4 = \frac{a}{\omega_4} + \frac{V_4}{V_2} a_2 = -450 + 0.583 a_2 \quad (\text{link 4}).$$

Accelerations, or components thereof, which are opposite in direction to the velocities of respective points, have been taken to be negative since (4.23) has been derived from the consideration that both velocities and corresponding accelerations act in the same direction. As

$$J_{G_3} = 2650 \text{ kg-m}^2, \quad m_3 = 20 \text{ kg}, \quad m_2 = m_4 = 10 \text{ kg},$$

the corresponding time rates of change of the KE are

$$m_2 V_2 a_{G_2} = 1000 a_2 \quad (\text{link 2}),$$

$$m_3 V_{G_3} (a_{G_3})_t + J_{G_3} \omega_3 \alpha_3 = -171,450 + 1064 a_2 \quad (\text{link 3}),$$

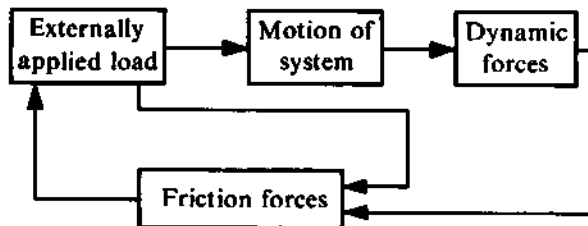
$$m_4 V_4 a_{G_4} = -263,728 + 343 a_2 \quad (\text{link 4}).$$

Substituting the values so obtained for links 2, 3, and 4 in (4.23), we get

$$\frac{dT}{dt} = -435,178 + 2407 a_2 \text{ kg-cm}^2/\text{s}^3.$$

The power input of the force system in the phase considered is

$$\sum \wp = F_2 V_2 + (W_3)_t V_{G_3} + W_4 \cdot V_4 \quad [\text{where } (W_3)_t \text{ is the component of } W_3 \text{ in the direction of } V_{G_3}]$$



$$\begin{aligned}
 &= (294 \times 1) - (98 \times 0.583) - (98 \times 0.583) \\
 &= 180 \text{ W} = 180 \times 10^4 \text{ kg}\cdot\text{cm}^2/\text{s}^3.
 \end{aligned}$$

Since $\sum p = dT/dt$, we get

$$-435,178 + 2407a_2 = 180 \times 10^4$$

or

$$a_2 \approx 930 \text{ cm/s}^2.$$

Therefore,

$$a_4 = -450 + 0.583a_2 = 92 \text{ cm/s}^2.$$

Effects of Friction

Whenever there is relative movement between two mating pairs, frictional forces are developed. Very common examples of such mating pairs are hinged joints and sliders moving in guides. In hinged joints, the friction occurs between the pin and the inside cylindrical surface of the hole in the connected link. The resultant effect is a frictional torque of negligible order as the pin diameter is normally very small. On the other hand, the effect of friction in sliders may be of considerable magnitude.

In general, the dynamic analysis of systems with friction is complex for the reason that the frictional force depends on the resultant reactive forces between the two mating surfaces, which, in turn, depend not only on the static loading but also on the forces developed by the motion of the mechanism. However, the motion of the mechanism is again derivable only when the friction force is known. Thus, a feedback phenomenon complicates the dynamic analysis of the mechanism when we consider the effects of friction (see flowchart). A solution with reasonable accuracy can be obtained, and undue complications avoided, by using a graphical method. A description of one such method follows.

As observed earlier in this section while discussing the rate-of-change-of-energy method and in Problem 4.1, a linear relationship between α_i and the external power input $\sum p$ is obtained by expressing the rate of change of the KE in terms of the known dynamic and kinematic properties of the mechanism and the unknown input acceleration α_i . In general, the rate of change of the KE of the j -th link can be expressed in the form $m_j V_{G_j} (a_{G_j})_t + J_{G_j} \omega_j \alpha_j$, where both $(a_{G_j})_t$ and α_j are obtained with the help of Goodman's equations and the auxiliary acceleration diagram based on zero input acceleration. Thus,

$$(a_{G_j})_t = (a_{\dot{o}_{G_j}})_t + \frac{V_{G_j}}{\omega_i} \alpha_i,$$

$$\alpha_j = \alpha_i + \frac{\omega_j}{\omega_i} \alpha_i.$$

So, the rate of change of the KE of the j -th link takes the form

$$[m_j V_{G_j} (\dot{a}_{G_j})_t + J_{G_j} \omega_j \alpha_{G_j}] + [m_j V_{G_j}^2 / \omega_i + J_{G_j} \omega_j^2 / \omega_i] \alpha_i.$$

Hence, the relationship for the entire mechanism between the rate of change of the total KE and the power input will be

$$\sum_{j=1}^n [m_j V_{G_j} (\dot{a}_{G_j})_t + J_{G_j} \omega_j \alpha_{G_j}] + \alpha_i \sum_{j=1}^n [m_j V_{G_j}^2 / \omega_i + J_{G_j} \omega_j^2 / \omega_i] = \sum p \quad (4.24)$$

when there are n moving links in the mechanism. The simplified form of (4.24) is

$$A + B\alpha_i = \sum p. \quad (4.25)$$

From (4.14), it is seen that at any particular configuration, all the forces acting at the joints, all the externally applied forces and moments, and the accelerations of different moving links have a linear relation with one another. Since the frictional power loss is the summation of the products of respective velocities and frictional forces (which are μ times the respective normal forces at sliding surfaces, μ being the coefficient of friction), it is clear that the frictional power loss will have a linear relationship with the externally applied forces and accelerations of the links. Again, the acceleration of each link depends linearly on the input acceleration α_i . So, it can be concluded that the frictional power loss $\sum p_\mu$ will depend linearly on the input acceleration α_i , and vice versa. Finally, the actual value of α_i is given by the intersection of two straight lines representing the linear relationships

$$\alpha_i = f(\sum p_{wf} + \sum p_\mu), \quad (4.26)$$

$$\alpha_i = f(\sum p), \quad (4.27)$$

where $\sum p_{wf}$ is the power input due to the externally applied force system when the mechanism is assumed to be free from friction. The method is explained by the solution of the problem which follows.

PROBLEM 4.2

Determine the acceleration of slider A of Problem 4.1, assuming the coefficient of friction between the sliders and the guides to be 0.3.

SOLUTION

The relationship equivalent to (4.27) has already been derived in the solution for Problem 4.1, namely,

$$-435,178 + 2407a_2 = \sum p.$$

This gives one of the two lines required and is shown as line 1 in Fig. 4.19. To plot the second straight line representing the relationship expressed by (4.26), let us determine two points on the line. Let a_2 for these two points be 0 cm/s^2 and 200 cm/s^2 . The relevant Goodman transformation equations are

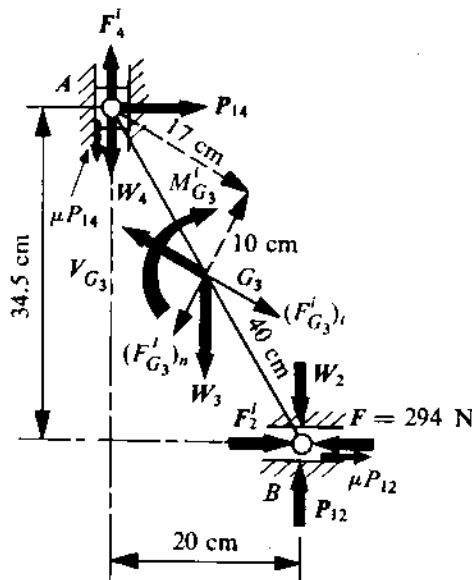


FIGURE 4.18

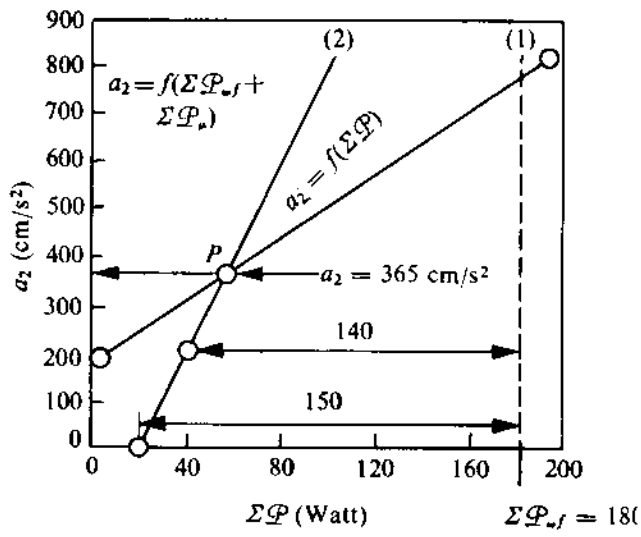


FIGURE 4.19

$$\alpha_3 = -5.6 + 0.05a_2 \quad (\text{link 3}),$$

$$(a_{G_3})_t = -110 + 0.583a_2$$

$$a_4 = -450 + 0.583a_2 \quad (\text{link 4}).$$

From Fig. 4.17, we also obtain $(a_{G_3})_n = (a_{\dot{o}_{G_3}})_n = 195 \text{ cm/s}^2$. Note that the normal component depends on the velocities and not on the input acceleration, i.e., $(a_{G_3})_n = (a_{\dot{o}_{G_3}})_n$. When $a_2 = 0$ we get the values

$$\alpha_3 = -5.6 \text{ rad/s}^2$$

$$(a_{G_3})_t = -110 \text{ cm/s}^2 \quad (\text{link 3}),$$

$$(a_{G_3})_n = 195 \text{ cm/s}^2$$

$$a_4 = -450 \text{ cm/s}^2 \quad (\text{link 4}).$$

Therefore, the inertia torque on link 3 (Fig. 4.18) is $M_{G_3}^i = 149 \text{ N-cm}$. Similarly, other inertia forces will be

$$(F_{G_3}^i)_t = -22 \text{ N}, \quad (F_{G_3}^i)_n = -39 \text{ N}, \quad F_2^i = 0, \quad F_4^i = 45 \text{ N}.$$

Taking moments about A, and considering the equilibrium of link 3, we get

$$M_{G_3}^i + [(F_{G_3}^i)_n \times 17] - [(F_{G_3}^i)_t \times 10] + (W_2 \times 20) - (P_{12} \times 20) - (F_2^i \times 34.5)$$

$$- (\mu P_{12} \times 34.5) + (W_3 \times 10) + (F \times 34.5) = 0$$

or $P_{12} = 452.8 \text{ N}$. Similarly, taking moments about B, and considering the equilibrium of link 3, we get $P_{14} = 84.3 \text{ N}$. Thus, when $a_2 = 0$, we have

$$\sum \wp_\mu = -(\mu P_{12} \cdot V_2) - (\mu P_{14} \cdot V_4) = -1,506,260 \text{ kg-cm}^2/\text{s}^3 \approx 150 \text{ W}.$$

Similarly, when $a_2 = 200 \text{ cm/s}^2$, we get the values

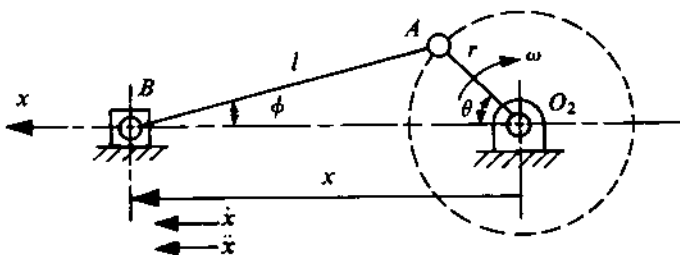


FIGURE 4.20

$$a_2 = 200 \text{ cm/s}^2 \quad (\text{link 2}),$$

$$\alpha_3 = 4.4 \text{ rad/s}^2$$

$$(a_{G_3})_t = 6.6 \text{ cm/s}^2 \quad (\text{link 3}),$$

$$(a_{G_3})_n = (a_{\overset{\circ}{G}_3})_n = 195 \text{ cm/s}^2$$

$$a_4 = -333.4 \text{ cm/s}^2 \quad (\text{link 4}).$$

Correspondingly, we get

$$F_2^i = 20 \text{ N}, \quad M_{G_3}^i = -117.6 \text{ N}\cdot\text{cm}, \quad (F_{G_3}^i)_t = 1.3 \text{ N}, \quad (F_{G_3}^i)_n = -38.7 \text{ N}, \quad F_4^i = 33.3 \text{ N}.$$

Again, substituting these quantities in Fig. 4.18, we get

$$P_{12} = 416.5 \text{ N}, \quad P_{14} = 87.2 \text{ N}, \quad \sum p_\mu = -1,402,380 \text{ kg}\cdot\text{cm}^2/\text{s}^3 \approx 140 \text{ W.}$$

Now, lines 1 and 2 in Fig. 4.19 can be drawn to represent the relationships $a_2 = f(\sum p)$ and $a_2 = f(\sum p_{wf} + \sum p_\mu)$, respectively, and the value of a_2 corresponding to the point of intersection P is the actual value of a_2 .

4.9 DYNAMICS OF SLIDER-CRANK MECHANISM

The slider-crank mechanism is one of the most commonly-used mechanisms for the conversion of rotary motion into rectilinear oscillations or vice versa. In internal-combustion engines, steam engines, etc., the reciprocating motion of the piston is converted into a rotation of the crankshaft, whereas in reciprocating compressors, punching presses, etc., the rotary motion of the crank is converted into a reciprocating motion of the piston or the punch. We will now consider various problems associated with the dynamics of such engine mechanisms. The kinematics has to be studied first, and we shall start with expressions for the displacement, velocity, and acceleration of the slider or of the piston.

Displacement, Velocity, and Acceleration of Piston

In Fig. 4.20, O_2B represents the crank and AB is the connecting rod of a simple slider-crank mechanism used in engines. The point B denotes the position of the piston when the crank has rotated through an angle θ from the outer dead-centre location. At this instant, x denotes the distance of the piston from the crankshaft centre O_2 . Our first objective is to express the displacement of the piston x , its velocity \dot{x} , and its acceleration \ddot{x} as functions of θ , time derivatives of θ , and dimensions of the mechanism. We shall first derive the general relationships (as they are going to be used in Chapter 7) and then we will make suitable assumptions to simplify them as and when required. Let

$$r = \text{crank radius } O_2A,$$

$$l = \text{length of the connecting rod } AB,$$

$$\lambda = r/l \text{ (considerably less than unity in all practical cases),}$$

$$s = \text{stroke of the engine} = 2r, \text{ and}$$

ϕ = angle made by the connecting rod with the line of stroke at the instant considered.
From Fig. 4.20, we have

$$x = l \cos \phi + r \cos \theta, \quad (4.28)$$

$$\begin{aligned} l \sin \phi &= r \sin \theta, \quad \sin \phi = \lambda \sin \theta, \\ \cos \phi &= (1 - \lambda^2 \sin^2 \theta)^{1/2}. \end{aligned} \quad (4.29)$$

Substituting (4.29) in (4.28), we get

$$x = l(1 - \lambda^2 \sin^2 \theta)^{1/2} + r \cos \theta, \quad (4.30)$$

$$\begin{aligned} \frac{x}{r} &= \cos \theta + \frac{1}{\lambda} (1 - \lambda^2 \sin^2 \theta)^{1/2} \\ &= \cos \theta + \frac{1}{\lambda} - \frac{\lambda}{2} \sin^2 \theta - \frac{\lambda^3}{8} \sin^4 \theta - \frac{\lambda^5}{16} \sin^6 \theta - \dots . \end{aligned} \quad (4.31)$$

Now,

$$\sin \theta = \frac{e^{i\theta} - e^{-i\theta}}{2i}, \quad \cos \theta = \frac{e^{i\theta} + e^{-i\theta}}{2}.$$

So,

$$\begin{aligned} \sin^4 \theta &= \frac{(e^{i\theta} - e^{-i\theta})^4}{16} = \frac{1}{16} [(e^{4i\theta} + e^{-4i\theta}) - 4(e^{2i\theta} + e^{-2i\theta}) + 6] \\ &= \frac{\cos 4\theta}{8} - \frac{\cos 2\theta}{2} + \frac{3}{8}. \end{aligned}$$

Similarly,

$$\sin^6 \theta = -\frac{1}{32} \cos 6\theta + \frac{3}{16} \cos 4\theta - \frac{15}{32} \cos 2\theta + \frac{5}{16}$$

Using these values, we can write (4.31) as

$$\begin{aligned}\frac{x}{r} &= \left(\frac{1}{\lambda} - \frac{\lambda}{4} - \frac{3\lambda^3}{64} - \frac{5\lambda^5}{256} - \dots\right) + \cos\theta + \cos 2\theta\left(\frac{\lambda}{4} + \frac{\lambda^3}{16} + \frac{15\lambda^5}{512} + \dots\right) \\ &\quad - \cos 4\theta\left(\frac{\lambda^3}{64} + \frac{3\lambda^5}{256} + \dots\right) + \cos 6\theta\left(\frac{\lambda^5}{512} + \dots\right) - \dots.\end{aligned}\quad (4.32)$$

Differentiating with respect to time, we get

$$\begin{aligned}\frac{\dot{x}}{r} &= \dot{\theta}\left[-\sin\theta - 2\sin 2\theta\left(\frac{\lambda}{4} + \frac{\lambda^3}{16} + \frac{15\lambda^5}{512} + \dots\right) + 4\sin 4\theta\left(\frac{\lambda^3}{64} + \frac{3\lambda^5}{256} + \dots\right)\right. \\ &\quad \left.- 6\sin 6\theta\left(\frac{\lambda^5}{512} + \dots\right) + \dots\right].\end{aligned}\quad (4.33)$$

Differentiating (4.33) again with respect to time, we get

$$\begin{aligned}-\frac{\ddot{x}}{r} &= \dot{\theta}^2\left(\cos\theta + A_2\cos 2\theta - A_4\cos 4\theta + A_6\cos 6\theta - \dots\right) \\ &\quad + \ddot{\theta}\left(\sin\theta + \frac{A_2}{2}\sin 2\theta - \frac{A_4}{4}\sin 4\theta + \frac{A_6}{6}\sin 6\theta - \dots\right),\end{aligned}\quad (4.34)$$

where

$\dot{\theta}$ = angular velocity of the crank,

$\ddot{\theta}$ = angular acceleration of the crank,

$$A_2 = \lambda + \frac{\lambda^3}{4} + \frac{15\lambda^5}{128} + \dots,$$

$$A_4 = \frac{\lambda^3}{4} + \frac{3\lambda^5}{16} + \dots,$$

$$A_6 = \frac{9\lambda^5}{128} + \dots,$$

and so on.

If the engine is running with constant speed (as is approximately the situation when a flywheel is attached to the engine), $\dot{\theta}$ is almost constant (say, ω) and $\ddot{\theta} \approx 0$ throughout the cycle. Assuming $\ddot{\theta} = 0$ and $\dot{\theta} = \omega$, we can rewrite (4.34) as

$$-\frac{\ddot{x}}{r} = \omega^2\left(\cos\theta + A_2\cos 2\theta - A_4\cos 4\theta + A_6\cos 6\theta - \dots\right).$$

When $\lambda \ll 1$, neglecting the terms involving λ^3 or higher powers of λ , we can write

$$\dot{x} = -\omega r\left(\sin\theta + \frac{\lambda}{2}\sin 2\theta\right), \quad (4.35)$$

$$\ddot{x} = -\omega^2 r(\cos\theta + \lambda\cos 2\theta). \quad (4.36)$$

Equations (4.35) and (4.36) will be used throughout this chapter; (4.34) will be useful in Chapter 7.

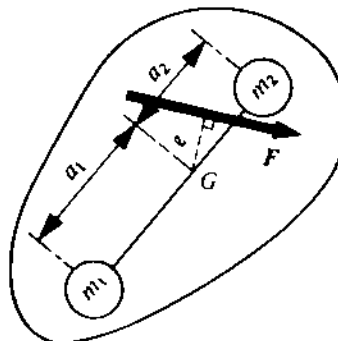


FIGURE 4.21

4.10 TURNING MOMENT ON CRANKSHAFT AND TURNING-MOMENT DIAGRAM

In this section, an expression will be derived for the torque or moment developed at the crankshaft as a function of crank rotation θ . The gas or steam pressure for various values of θ during a cycle can be evaluated from the indicator diagram obtained for the engine during its operation. To simplify the analysis, the connecting rod will be replaced by a dynamically-equivalent massless link, and friction forces neglected everywhere.

Dynamically-equivalent Link

Figure 4.21 shows a rigid body of mass m with CG at the point G . This is subjected to a force F (as shown in the figure) which represents all the external forces and moments acting on the body in the plane of the paper. Due to this force, F , as discussed in Section 4.2, the motion of the body can be described by two quantities, namely,

- (i) the acceleration of the CG (i.e., of the point G)

$$\mathbf{a} = \mathbf{F}/m, \quad (4.37)$$

- (ii) the angular acceleration of the body

$$\alpha = Fe/J, \quad (4.38)$$

where

e = perpendicular distance of F from G , and

J = moment of inertia of the body about an axis, passing through G , perpendicular to the plane of the paper.

The sense of α is the same as that of the moment Fe about the point G .

We want to replace this rigid link by a dynamically-equivalent massless link with two point masses m_1 and m_2 at its ends. By *dynamically equivalent* we mean that this link will have the same

motion as the rigid link when subjected to the same force F , i.e., the CG of this equivalent link will also have the same acceleration a and the same angular acceleration α .

Let a_1 and a_2 , respectively, be the distance of m_1 and m_2 from the point G . It is seen from (4.37) and (4.38) that, if the three conditions

$$m_1 + m_2 = m \quad [\text{as the acceleration of the CG of the equivalent link is } F/(m_1 + m_2) = a], \quad (4.39)$$

$$m_1 a_1 = m_2 a_2, \quad (4.40)$$

$$m_1 a_1^2 + m_2 a_2^2 = J \quad (4.41)$$

are satisfied, the desired dynamic equivalence is achieved.

The second condition [given by (4.40)] indicates that the position of the CG of the equivalent link is also at G , so that the numerator of (4.38) remains the same for any arbitrary direction of F . The third condition [given by (4.41)] signifies that the denominator of (4.38) also remains the same because the moment of inertia of the equivalent system about G (which is its CG once the second condition is satisfied) is $m_1 a_1^2 + m_2 a_2^2$ (m_1 and m_2 being point masses). So, α also remains the same.

Thus, (4.39) to (4.41) must be simultaneously satisfied to achieve complete dynamic equivalence. It is seen that four unknowns, namely, m_1 , m_2 , a_1 , and a_2 , are involved in these three equations. So, any one of these four can be arbitrarily chosen so as to uniquely determine the remaining three. It should also be noted that if two of the quantities (say, a_1 and a_2) are chosen beforehand, then all three equations cannot be satisfied simultaneously.³

Approximate Expression for Turning Moment

In deriving the approximate expression for the turning moment, the connecting rod is replaced by a massless link with two point masses at its ends. As two parameters (a_1 , a_2) of the four unknowns (a_1 , a_2 , m_1 , and m_2) are chosen beforehand, all the three equations (4.39) to (4.41) cannot be satisfied. Let

m_1 = mass at the piston end (known as the *small end*),

m_2 = mass at the crank end (known as the *big end*).

Thus, m_1 has only reciprocating motion and m_2 has only rotary motion. These masses, m_1 and m_2 , are selected so that (4.39) and (4.40) are satisfied, i.e.,

$$m_1 + m_2 = m_c, \quad (4.42)$$

$$m_1 a_1 = m_2 a_2, \quad (4.43)$$

where

m_c = mass of the connecting rod,

a_1 = distance of the CG of the connecting rod from the small end, and

³If, instead of being point masses, m_1 and m_2 are provided with finite moments of inertia, two more quantities, namely, the radii of gyration of m_1 and m_2 , can be suitably adjusted so that all the three conditions are simultaneously satisfied, even when a_1 and a_2 are prescribed.

a_2 = distance of the CG of the connecting rod from the big end.

The expression for the turning moment, obtained with this massless link, will be approximate as (4.41) is not satisfied. The correction needed to this approximate expression will be derived later in this section.

Let us consider a horizontal engine (see Fig. 4.22) in which

p = effective gas pressure on the piston, in N/m^2 , when the crank is at an angle θ from the outer dead-centre position, and

A = area of the piston, in m^2 .

Our aim is to find the turning moment M on the crankshaft at this position. Let

m_{rec} = mass of all the reciprocating parts (such as piston and gudgeon pin) plus the apportioned mass (m_1) of the connecting rod at the small end,

r, l = length of the crank and the connecting rod, respectively,

ϕ = angle made by the connecting rod with the line of stroke,

Q = thrust force on the connecting rod, in N , which will be in the direction of the connecting rod (as it has been replaced by the massless link, and a massless binary link without any external force on it can exert only an axial force to avoid infinite angular acceleration),

ω = angular velocity of the crank, and

$\lambda = r/l$.

Considering the free-body diagram of the piston (Fig. 4.22) along with the inertia force $m_{\text{rec}}\ddot{x}$, where

$$\ddot{x} = -\omega^2 r(\cos \theta + \lambda \cos 2\theta) \quad [\text{from (4.36)}],$$

and $\sum F_x = 0$, we have

$$\begin{aligned} pA + m_{\text{rec}}\ddot{x} &= Q \cos \phi, \\ Q &= \frac{pA - m_{\text{rec}}\omega^2 r(\cos \theta + \lambda \cos 2\theta)}{\cos \phi}. \end{aligned} \quad (4.44)$$

Now, the moment produced by this thrust Q about the axis of rotation is $M = Q.O_2C$, where O_2C is the perpendicular from O_2 to the connecting rod (i.e., to the direction of Q). From Fig. 4.22, we get

$$O_2C = O_2A \sin (\theta + \phi) = r \sin (\theta + \phi).$$

Thus,

$$M = \frac{pA - m_{\text{rec}}\omega^2 r(\cos \theta + \lambda \cos 2\theta)}{\cos \phi} r \sin (\theta + \phi). \quad (4.45)$$

It is to be noted that centrifugal forces due to m_2 and the mass of the crank cannot produce any moment about O_2 (in practice, the crank is so balanced that its CG, along with that of m_2 , lies at

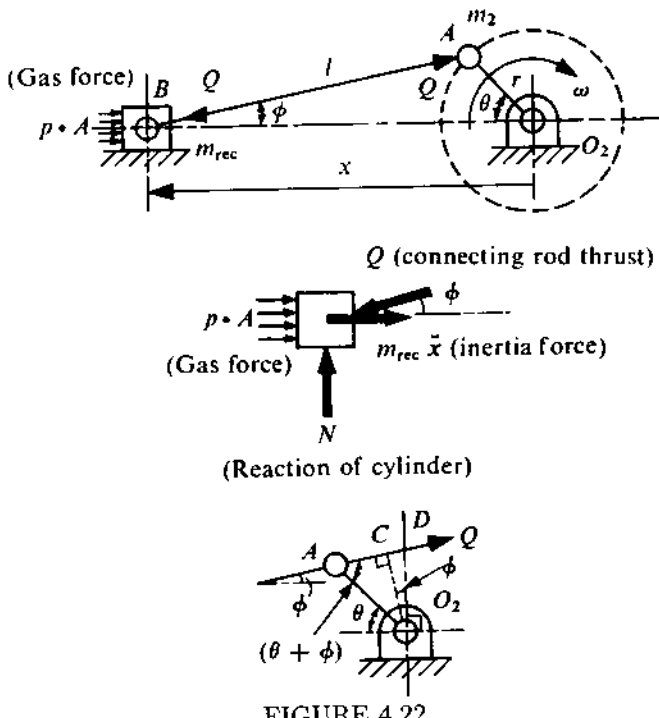


FIGURE 4.22

O_2 ; this will be discussed in Chapter 7). Unless otherwise specified, the mass of the reciprocating parts includes m_1 .

In the case of vertical engines, the weight of the reciprocating parts should be taken into account in (4.44). Thus, when x is measured upwards (i.e., the cylinder is above the crankshaft), for a balanced crank, we have

$$Q = \frac{pA + m_{rec}g - m_{rec}\omega^2 r(\cos \theta + \lambda \cos 2\theta)}{\cos \phi}, \quad (4.44a)$$

$$M = \frac{pA + m_{rec}g - m_{rec}\omega^2 r(\cos \theta + \lambda \cos 2\theta)}{\cos \phi} r \sin (\theta + \phi). \quad (4.44b)$$

The derivation of an alternative expression for M follows. Let O_2D be the perpendicular to the line of stroke at O_2 , intersecting the connecting rod at D . Then, $O_2D = O_2C / \cos \phi$. From (4.45), we have

$$M = [pA - m_{rec}\omega^2 r(\cos \theta + \lambda \cos 2\theta)]O_2D.$$

Using the instantaneous centres of velocity, it can be easily proved that $O_2D = -\dot{x}/\omega$ (the proof of this is left as an exercise for the reader). Using (4.35), we get

$$M = [pA - m_{rec}\omega^2 r(\cos \theta + \lambda \cos 2\theta)]r(\sin \theta + \frac{\lambda}{2} \sin 2\theta). \quad (4.46)$$

Thus, the turning moment M for any value of θ can be obtained approximately from (4.45) or (4.46) if the net gas pressure p is known for the given value of θ .

PROBLEM 4.3

A single-cylinder vertical engine has a bore of 30.5 cm, a stroke 40 cm, and a connecting rod 80 cm long, as shown in Fig. 4.23. The mass of the reciprocating parts is 135 kg. When the piston is at quarter-stroke and is moving downwards, the net pressure on it is 65 N/m². If the speed of the engine is 250 rpm, find the turning moment on the crankshaft at the instant corresponding to the position shown in the figure.

SOLUTION

From the given data, $l = 80$ cm, $s = 2r = 40$ cm, cylinder diameter $d = 30.5$ cm, $r = 20$ cm, $\lambda = r/l = 0.25$, $m_{\text{rec}} = 135$ kg, $p = 65$ N/m², $A = \frac{\pi}{4}d^2 = \frac{\pi}{4}(30.5)^2 = 730$ cm², $N = 250$ rpm, $\omega = \frac{2\pi N}{60} = 26.2$ rad/s. At quarter-stroke, $x = l + r - s/4 = l + r/2 = 90$ cm.

From (4.28) and (4.29), we have

$$x = l \cos \phi + r \cos \theta = 90 \text{ cm}, \quad (\text{a})$$

$$\cos \phi = (1 - \lambda^2 \sin^2 \theta)^{1/2} = (1 - 0.0625 \sin^2 \theta)^{1/2}. \quad (\text{b})$$

The values of θ and ϕ can be found from (a) and (b) or, alternatively, they can be obtained very easily by the graphical procedure shown in Fig. 4.23. Thus,

$$\theta = 55^\circ, \quad \phi = 12^\circ, \quad \cos \theta = 0.574, \quad \cos 2\theta = -0.342, \quad \sin(\theta + \phi) = 0.92, \quad \cos \phi = 0.978.$$

Thus, as it is a vertical engine, from (4.44b), we get

$$\begin{aligned} M &= \frac{65 \times 730 + 135 \times 9.8 - 135 \times 0.2 \times (26.2)^2 (0.574 - 0.25 \times 0.342)}{0.978} \times 0.2 \times 0.92 \text{ N-m} \\ &= 7473 \text{ N-m.} \end{aligned}$$

Correction to the Approximate Expression

As mentioned earlier in this section, some correction has to be applied to equations (4.45) and (4.46) because the moment of inertia of the massless link with end masses (which has replaced the connecting rod) is not the actual moment of inertia about the centroidal axis. Let the moment of inertia of the actual connecting rod about the centroidal axis be $J_c = m_c k^2$, where k is the radius of gyration about the same axis. The moment of inertia of the equivalent link about the centroidal axis is

$$J_e = m_1 a_1^2 + m_2 a_2^2. \quad (4.47)$$

From (4.42) and (4.43), we have

$$m_1 = \frac{m_c a_2}{a_1 + a_2}, \quad m_2 = \frac{m_c a_1}{a_1 + a_2}.$$

Substituting these values in (4.47), we get

$$J_e = m_c a_1 a_2. \quad (4.48)$$

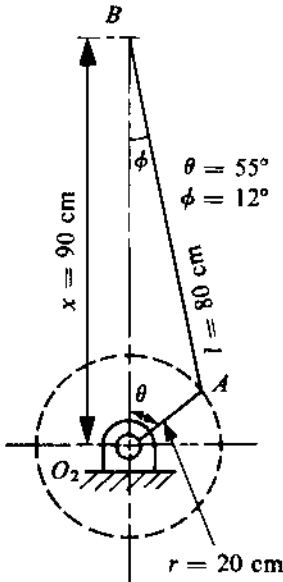


FIGURE 4.23

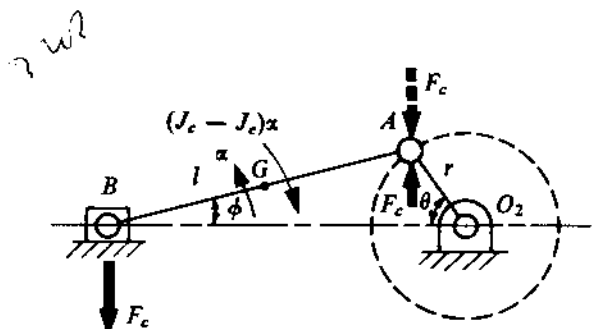


FIGURE 4.24

Thus, the correction in the moment of inertia of the equivalent link is

$$J_c - J_e = m_c(k^2 - a_1 a_2), \quad (4.49)$$

and the correction in the inertia torque of the equivalent link (Fig. 4.24) is

$$(J_c - J_e)\alpha = m_c(k^2 - a_1 a_2)\alpha \quad (4.50)$$

in opposite sense of α , where $\alpha = \ddot{\phi}$ is the angular acceleration of the connecting rod.

The correction in inertia torque given by (4.50) can be replaced by two equal and opposite external correcting forces of magnitude F_c (Fig. 4.24) acting at both ends of the equivalent link. The line of action of the correcting forces is taken vertical so as not to disturb the horizontal equilibrium equation (4.44) already used for obtaining the approximate expression for the turning moment. The magnitude of the force F_c is such that

$$F_c l \cos \phi = m_c(k^2 - a_1 a_2)\alpha,$$

$$F_c = \frac{m_c(k^2 - a_1 a_2)\alpha}{l \cos \phi}. \quad (4.51)$$

The correction in turning moment is equal to the moment of F_c (acting on the crank and shown by the dashed line in Fig. 4.24) about the point O_2 . Thus,

$$M_c = -F_c \cdot r \cos \theta = -\frac{m_c(k^2 - a_1 a_2)\alpha}{l \cos \phi} r \cos \theta. \quad (4.52)$$

The negative sign indicates that the correcting moment is in the counter-clockwise direction [i.e., opposite to the direction of M in (4.45)]. So, the actual turning moment is

$$M_t = M + M_c.$$

In (4.52), $\alpha (= \ddot{\phi})$ can be expressed in Fourier series of θ . From (4.29),

$$\cos \phi = (1 - \lambda^2 \sin^2 \theta)^{1/2} = 1 - \frac{\lambda^2}{2} \sin^2 \theta - \frac{\lambda^4}{8} \sin^4 \theta - \frac{\lambda^6}{16} \sin^6 \theta - \dots$$

Differentiating both sides with respect to time and dividing by $\sin \phi (= \lambda \sin \theta)$, we get

$$\dot{\phi} = \omega (\lambda \cos \theta + \frac{1}{2} \lambda^3 \sin^2 \theta \cos \theta + \frac{3}{8} \lambda^5 \sin^4 \theta \cos \theta + \dots). \quad (4.53)$$

Differentiating again with respect to time, we get

$$\begin{aligned} \frac{\ddot{\phi}}{\lambda} &= -\omega^2 (C_1 \sin \theta - C_3 \sin 3\theta + C_5 \sin 5\theta - \dots) \\ &\quad + \dot{\omega} (C_1 \cos \theta - \frac{1}{3} C_3 \cos 3\theta + \frac{1}{5} C_5 \cos 5\theta - \dots), \end{aligned} \quad (4.54)$$

where

$$\begin{aligned} C_1 &= 1 + \frac{1}{8} \lambda^2 + \frac{3}{64} \lambda^4 + \dots, \\ C_3 &= \frac{3}{8} \lambda^2 + \frac{27}{128} \lambda^4 + \dots, \\ C_5 &= \frac{15}{128} \lambda^4 + \dots. \end{aligned}$$

[Equation (4.54) will be referred to again in Chapter 7.] Neglecting terms of order higher than λ^2 , and assuming ω to be constant, we can write

$$\alpha = \ddot{\phi} = -\omega^2 \lambda \sin \theta. \quad (4.55)$$

Substituting this in (4.52), we get

$$M_c = \frac{m_c(k^2 - a_1 a_2)}{l \cos \phi} \omega^2 \lambda r \sin \theta \cos \theta. \quad (4.56)$$

PROBLEM 4.4

In Problem 4.3, the CG of the connecting rod is 50 cm from the small end and the radius of gyration about the centroidal axis is 30 cm. The mass of the actual reciprocating parts is 90 kg and that of the connecting rod is 120 kg. Determine the actual turning moment for the instant discussed in Problem 4.3.

SOLUTION

The given data is

$$m_c = 120 \text{ kg}, \quad a_1 = 50 \text{ cm}, \quad a_2 = 30 \text{ cm}.$$

So,

$$m_1 = 45 \text{ kg}, \quad m_{\text{rec}} = 90 + 45 = 135 \text{ kg}, \quad m_2 = 75 \text{ kg}.$$

From Problem 4.3, we have

$$k = 30 \text{ cm}, \quad \theta = 55^\circ, \quad \phi = 12^\circ, \quad \sin \theta = 0.82, \quad \cos \phi = 0.978.$$

From (4.55),

$$\alpha = -(26.2)^2 \times 0.25 \times 0.82 = -140.8 \text{ rad/s}^2.$$

From (4.51),

$$F_c = \frac{120(0.09 - 0.15)(-140.8)}{0.8 \times 0.978} = 1295 \text{ N.}$$

From (4.52),

$$M_c = -1295 \times 0.2 \times 0.978 = -252 \text{ N-m.}$$

The approximate turning moment $M = 7473 \text{ N-m}$ (from Problem 4.3). So, the actual turning moment is

$$M_t = (7473 - 252) \text{ N-m} = 7221 \text{ N-m.}$$

Thus, we observe that the error is of the order of only 2% to 3% if the approximate expression is used.

Turning-moment Diagram

Earlier in this section, we obtained the turning moment M as a function of the crank rotation θ [(4.45) and (4.46)]. The diagram showing M as a function of θ for any engine is called the *turning-moment diagram*. The variation of M with θ can be plotted if the net gas pressure p is known for any position of the crank. The values of p for any value of θ can be obtained from the indicator diagram. The following example describes how it can be obtained for a four-stroke internal-combustion engine.

The indicator diagram for a four-stroke-cycle internal-combustion engine in Fig. 4.25a shows the net pressure p plotted against the piston displacement. The net gas force equals pA . Since A is constant, the variation of this force with θ will be the same as that of p . This is shown in Fig. 4.25b. The corresponding variation of the inertia force is also shown in Fig. 4.25b. Using (4.46) and referring to Fig. 4.22, we see that

$$M = (\text{gas force} + \text{inertia force}) \times O_2 D.$$

The resultant of the gas and inertia forces and the dimension $O_2 D$ are shown in Fig. 4.25c for values of θ varying from 0 to 4π . The product of these two quantities, i.e., the turning moment M , is plotted against θ in Fig. 4.25d to give the required diagram. It should be noted that M is zero when either of these two quantities is zero.

It is observed that M is entirely positive during the expansion stroke, entirely negative in the compression stroke, and partly positive and partly negative in the other two strokes. For illustrative problems on this topic, unless otherwise specified, the turning moment in the suction and exhaust strokes is also taken to be entirely negative to simplify their solution. The turning moment of a multicylinder engine can be obtained by the superposition of the turning moments of each cylinder, with the starting point suitably shifted depending on the crank offset.

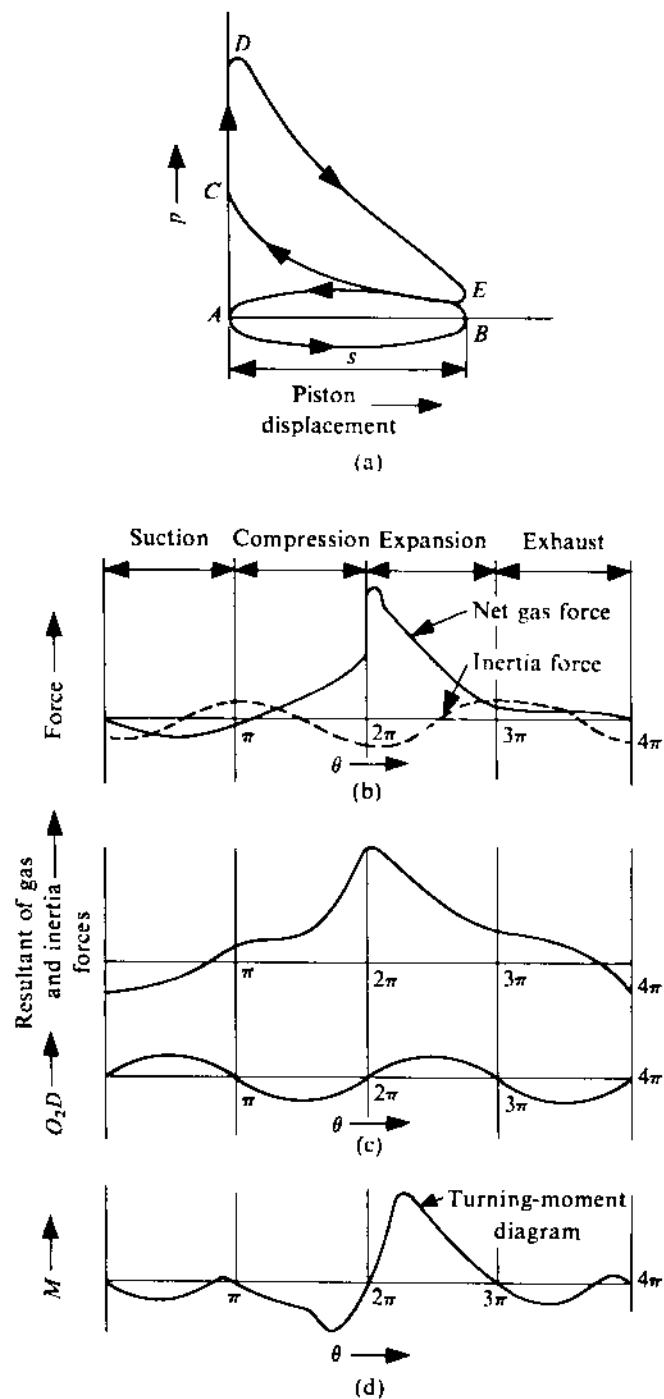


FIGURE 4.25

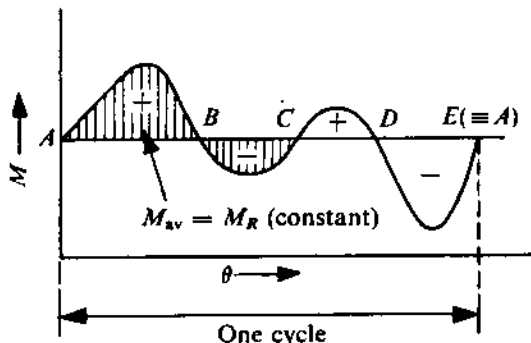


FIGURE 4.26

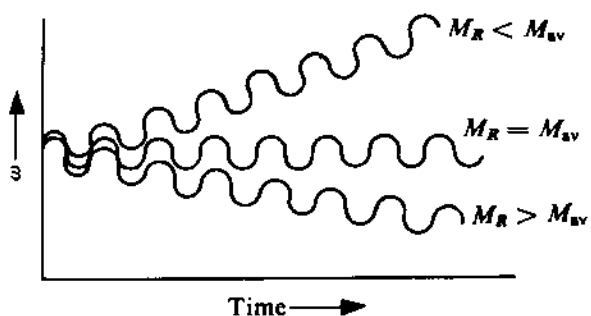


FIGURE 4.27

4.11 FLUCTUATION OF CRANKSHAFT SPEED

For most engines, the load torque or the resisting moment M_R (which opposes the motion of the crankshaft) remains constant over a cycle, whereas the turning moment M varies considerably as shown in Fig. 4.25d. As a result of this, except for certain situations (e.g., when $M = M_R$), there is an unbalanced moment acting on the crankshaft, which either accelerates or decelerates the motion.

Let Fig. 4.26 represent the turning-moment diagram for an engine over one cycle. The area between the turning-moment curve and the θ -axis gives the energy output of the engine in that cycle. This can be expressed mathematically as

$$E = \oint M d\theta. \quad (4.57)$$

Then, the average turning moment in this cycle is

$$M_{av} = \frac{E}{\Theta} = \frac{1}{\Theta} \oint M d\theta = \frac{1}{\Theta} \int_0^\Theta M d\theta, \quad (4.58)$$

where Θ is the rotation in one cycle (it is 2π for two-stroke engines, and 4π for four-stroke engines). The work done in one cycle against the load (resisting moment) M_R (assumed to be constant) is $M_R \cdot \Theta$. If this is equal to E , then there is no net energy input in the crankshaft for the cycle. So, the speed remains the same at the beginning and at the end of the cycle, even though there is variation during the cycle. This condition is referred to as *stable operation*, and is identified mathematically as

$$M_R = \frac{E}{\Theta} = M_{av}. \quad (4.59)$$

If $M_R > M_{av}$, the speed decreases from cycle to cycle (e.g., during the stopping phase). When $M_R < M_{av}$, the speed increases from cycle to cycle (e.g., during the starting phase). The three different states are shown in Fig. 4.27. Unless otherwise specified, we shall assume the condition of stable operation (i.e., almost constant-speed operation with fluctuations during a cycle) with $M_R = M_{av}$. Let us now discuss this case (i.e., $M_R = M_{av}$) with reference to Fig. 4.26. The points A, B, C, D , and $E (\equiv A)$ are the intersections of the M -curve and the M_R -line. Since $M > M_R$ from A to B , the speed of the crankshaft will increase during this period. Thereafter, $M < M_R$ from B to C , and the speed will decrease, and so on. The kinetic energy at B is

$$E_B = E_A + \int_{\theta_A}^{\theta_B} (M - M_R) d\theta = E_A + (\text{hatched area from } A \text{ to } B).$$

Similarly,

$$E_C = E_B + \int_{\theta_B}^{\theta_C} (M - M_R) d\theta = E_B + (\text{hatched area from } B \text{ to } C),$$

and so on.

Thus, we can find the points corresponding to the maximum and minimum kinetic energy levels during the cycle. These points also correspond to the maximum and minimum speeds. The difference in the energy level between these two points is the *maximum fluctuation of kinetic energy* and is denoted by $(\Delta KE)_{\max}$. Mathematically, this can be expressed as

$$(\Delta KE)_{\max} = \int_{\theta_1}^{\theta_2} (M - M_R) d\theta, \quad (4.60)$$

where θ_1 and θ_2 correspond to positions of minimum and maximum speeds.

The *coefficient of fluctuation of energy* in a cycle is defined as

$$k_e = \frac{(\Delta KE)_{\max}}{E}, \quad (4.61)$$

where E is given by (4.57).

The *coefficient of fluctuation of speed* is defined as

$$k_s = \frac{\omega_{\max} - \omega_{\min}}{\omega_{\text{av}}}, \quad (4.62)$$

where ω_{av} is the average angular velocity of the crankshaft. When the fluctuation of speed is not very large, $\omega_{\text{av}} \approx (\omega_{\max} + \omega_{\min})/2$. Table 4.1 gives the normal values of permissible k_s for various systems.⁴

4.12 FLYWHEEL (AN APPROXIMATE ANALYSIS)

In the previous section, we saw that the fluctuation in turning moment results in a fluctuation of the crankshaft speed. The amount of fluctuation in the turning moment, i.e., the fluctuation in kinetic energy of the crankshaft, depends on the nature of the turning-moment diagram. However, the maximum permissible fluctuation in the speed of the crankshaft is determined by the purpose for which the engine is to be used. To keep the maximum fluctuation of speed within a specified limit (i.e., to maintain the prescribed value of k_s) for a given maximum fluctuation of kinetic energy, a flywheel is attached to the crankshaft; in effect, a flywheel provides additional inertia to the crankshaft. It is customary to neglect the inertia of the other rotating parts, being small as compared to that of the flywheel J_f . Thus, using (4.62), we get

$$(\Delta KE)_{\max} = \frac{1}{2} J_f (\omega_{\max}^2 - \omega_{\min}^2) = J_f \omega_{\text{av}}^2 k_s. \quad (4.63)$$

So, for a given value of $(\Delta KE)_{\max}$ and ω_{av} , a value for J_f can be suitably chosen to keep k_s within the specified limit. Equation (4.63) can also be derived by considering that

$$J_f \alpha = M - M_R, \quad (4.64)$$

⁴See Kozesnik, J., Dynamics of Machines, SNTL, Prague, 1962.

TABLE 4.1

Systems	Permissible k_s
Pumps, shears	1/5-1/30
Machine tools, textile and paper machines	1/40-1/50
Spinning frames	1/60-1/100
Generators	1/100-1/300
Automobile engines	1/200-1/300
Aircraft engines	1/1000-1/2000

where α = angular acceleration of the flywheel = $\omega(d\omega/d\theta)$. Thus,

$$J_f \omega \frac{d\omega}{d\theta} = M - M_R.$$

Integrating from θ_1 to θ_2 , we get

$$J_f \int_{\omega_{\min}}^{\omega_{\max}} \omega d\omega = \int_{\theta_1}^{\theta_2} (M - M_R) d\theta.$$

Using (4.60), we have

$$\frac{1}{2} J_f (\omega_{\max}^2 - \omega_{\min}^2) = (\Delta KE)_{\max},$$

$$J_f \omega_{\text{av}}^2 k_s = (\Delta KE)_{\max}.$$

The flywheel acts as a reservoir of energy so that energy can be absorbed during the period when $M > M_R$ and supplied during the period when $M < M_R$, without changing the speed beyond the specified limits.

PROBLEM 4.5

The vertical scale of the turning-moment diagram for a multicylinder engine, shown in Fig. 4.28, is 1 cm = 7000 N·m of torque, and the horizontal scale is 1 cm = 30° of crank rotation. The areas (in cm^2) of the turning-moment diagram above and below the mean resistance line, starting from A in Fig. 4.28 and taken in order, are

$$-0.5, +1.2, -0.95, +1.45, -0.85, +0.71, -1.06.$$

The engine speed is 800 rpm and it is desired that the fluctuation from minimum to maximum speed should not be more than 2% of the average speed. Determine the moment of inertia of the flywheel.

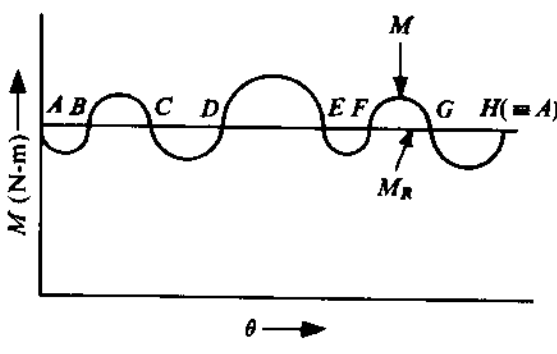


FIGURE 4.28

SOLUTION

An area of 1 cm² of the turning-moment diagram represents

$$7000 \times (\pi/6) = 3670 \text{ J.}$$

A, B, C, D, etc., are the points of intersection between M_R and the turning-moment diagram. Let E_A be the energy level at *A*. Then,

$$\begin{aligned} E_B &= E_A - 0.5, \\ E_C &= E_B + 1.2 = E_A + 0.7, \\ E_D &= E_C - 0.95 = E_A - 0.25, \\ E_E &= E_D + 1.45 = E_A + 1.2, \\ E_F &= E_E - 0.85 = E_A + 0.35, \\ E_G &= E_F + 0.71 = E_A + 1.06, \\ E_H &= E_G - 1.06 = E_A \quad (\text{as it should be at the end of the cycle}). \end{aligned}$$

So, we see that the minimum speed is at *B* and the maximum speed is at *E*. Thus,

$$(\Delta KE)_{\max} = E_E - E_B = (E_A + 1.2) - (E_A - 0.5) = 1.7 \text{ cm}^2 = 1.7 \times 3670 = 6240 \text{ J},$$

$$\omega_{\text{av}} = 800 \frac{2\pi}{60} = 33.8 \text{ rad/s}, \quad k_s = 0.02.$$

From (4.63), we get

$$J_f = \frac{(\Delta KE)_{\max}}{\omega_{\text{av}}^2 k_s} = \frac{6240}{(33.8)^2 \times 0.02} = 44.3 \text{ kg-m}^2.$$

PROBLEM 4.6

The torque exerted on the crankshaft of a two-stroke engine is given by

$$M = 15,000 + 2000 \sin 2\theta - 1800 \cos 2\theta \text{ N-m},$$

where θ is the crank angle measured from the inner dead-centre position. Assuming the resisting torque to be constant, determine

- (i) the power of the engine when turning at 150 rpm,
- (ii) the moment of inertia of the flywheel if the speed variation from the mean speed of 150 rpm is not to exceed $\pm 0.5\%$,
- (iii) the angular acceleration of the flywheel for $\theta = 30^\circ$, and
- (iv) the maximum angle by which this flywheel leads or lags an imaginary flywheel which rotates at a constant speed of 150 rpm.

SOLUTION

- (i) The total angle of crank rotation during a cycle is $\Theta = 2\pi$. From (4.58), we have

$$\begin{aligned} M_{av} &= \frac{1}{2\pi} \int_0^{2\pi} M \cdot d\theta = \frac{1}{2\pi} \int_0^{2\pi} (15,000 + 2000 \sin 2\theta - 1800 \cos 2\theta) d\theta \\ &= 15,000 \text{ N-m} = M_R. \end{aligned}$$

So, the work output per revolution is $15,000 \times 2\pi \text{ J}$, and the time taken for one revolution is $60/150 \text{ s}$. Hence, the work output per second, i.e., the power of the engine, is

$$15,000 \times (2\pi/60) \times 150 \text{ W} = 235.5 \text{ kW.}$$

- (ii) The turning-moment diagram is shown in Fig. 4.29. The values of θ where the turning-moment curve intersects M_R (i.e., θ_1 and θ_2 , where $M_R = M$) are given by

$$2000 \sin 2\theta - 1800 \cos 2\theta = 0,$$

$$\tan 2\theta = 0.9.$$

This gives

$$2\theta_1 = 42^\circ, \quad \theta_1 = 21^\circ, \quad 2\theta_2 = 180^\circ + 42^\circ, \quad \theta_2 = 111^\circ.$$

It is obvious from the diagram that the minimum speed occurs at θ_1 and that it is maximum at θ_2 during the cycle. Thus, from (4.60), we get

$$\begin{aligned} (\Delta KE)_{max} &= \int_{\theta_1}^{\theta_2} (M - M_R) d\theta = \int_{\theta_1}^{\theta_2} (2000 \sin 2\theta - 1800 \cos 2\theta) d\theta \\ &= [900 \sin 2\theta + 1000 \cos 2\theta]_{\theta_1}^{\theta_2} = 2690.2 \text{ J}, \end{aligned}$$

$$k_s = 0.01, \quad \omega_{av} = 150 \frac{2\pi}{60} = 15.7 \text{ rad/s.}$$

Using (4.63),

$$J_f = \frac{2690.2}{(15.7)^2 \times 0.01} = 1090 \text{ kg-m}^2.$$

It is to be noted that for this particular expression of M , $(\Delta KE)_{max}$ will be the same even for a four-stroke engine, i.e., when $\Theta = 4\pi$.

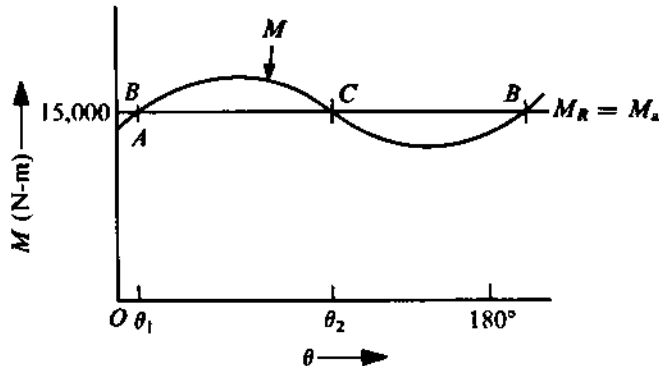


FIGURE 4.29

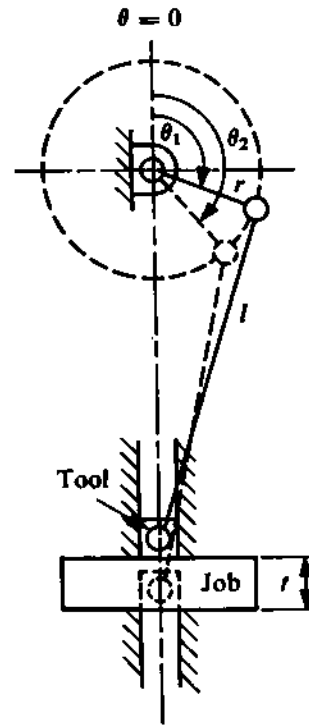


FIGURE 4.30

- (iii) When $\theta = 30^\circ$, $M = 15,000 + 1732 - 900 = 15,832 \text{ N-m}$. So, the angular acceleration of the flywheel, from (4.64), is

$$\alpha = \frac{M - M_R}{J_f} = \frac{832}{1090} = 0.764 \text{ rad/s}^2.$$

- (iv) The equation of motion for the angular oscillation of the flywheel, from (4.64), is

$$J_f \frac{d^2\theta}{dt^2} = M - M_R = 2000 \sin 2\theta - 1800 \cos 2\theta. \quad (a)$$

Without introducing any serious error, we may substitute $\theta = \omega_{av}t$ in the terms on the right-hand side to simplify the differential equation (a), which gives

$$J_f \frac{d^2\theta}{dt^2} = 2000 \sin 2(\omega_{av}t) - 1800 \cos 2(\omega_{av}t).$$

Integrating this equation, we get

$$J_f \frac{d\theta}{dt} = -\frac{1000}{\omega_{av}} \cos 2(\omega_{av}t) - \frac{900}{\omega_{av}} \sin 2(\omega_{av}t) + C_1.$$

Thus,

$$\omega = \frac{d\theta}{dt} = -\frac{1}{J_f \omega_{av}^2} [1000 \cos 2(\omega_{av}t) + 900 \sin 2(\omega_{av}t)] + C_2, \quad (1)$$

where $C_2 = C_1/J_f$, C_1 = constant of integration. In (b), as the terms within the square brackets are harmonic quantities, the average value of ω is C_2 . With $C_2 = \omega_{av}$, integrating (b), we get

$$\theta = (\omega_{av} \cdot t) - \frac{1}{J_f \omega_{av}^2} [500 \sin 2(\omega_{av} \cdot t) - 450 \cos 2(\omega_{av} \cdot t)] + C_3,$$

where C_3 is the constant of integration. Assuming $\theta = 0$ when $t = 0$, we have $C_3 = -450/J_f \omega_{av}^2$. Thus,

$$\theta - (\omega_{av} \cdot t) = \frac{1}{J_f \omega_{av}^2} [450 \cos 2(\omega_{av} \cdot t) - 500 \sin 2(\omega_{av} \cdot t)] - \frac{450}{J_f \omega_{av}^2}.$$

So,

$$[\theta - (\omega_{av} \cdot t)]_{\max} = \frac{10}{J_f \omega_{av}^2} (45^2 + 50^2)^{1/2} - \frac{450}{J_f \omega_{av}^2} = \frac{227}{J_f \omega_{av}^2} \text{ rad} = 0.054^\circ \text{ (leading),}$$

$$[\theta - (\omega_{av} \cdot t)]_{\min} = -\frac{10}{J_f \omega_{av}^2} (45^2 + 50^2)^{1/2} - \frac{450}{J_f \omega_{av}^2} = \frac{1123}{J_f \omega_{av}^2} \text{ rad} = -0.238^\circ \text{ (lagging).}$$

The maximum angle of lag is 0.238° .

4.13 FLYWHEEL IN PUNCHING PRESS

In the previous section, we discussed the function of a flywheel to reduce fluctuations of speed with reference to an engine where the load on the crankshaft is constant whereas the applied torque varies during a cycle. The flywheel can also be used for the same purpose (i.e., to reduce the fluctuations of speed during a cycle so as to be within specified limits) when the driving torque is constant but the load varies during the cycle. This is the case, for example, in a punching press or in a riveting machine.

A punching press is shown schematically in Fig. 4.30. The punching tool is at the position of the slider in the slider-crank mechanism. The crank is driven by a motor which supplies a uniform torque (i.e., the energy is transmitted at almost a steady rate if the speed remains nearly constant). It is seen from Fig. 4.30 that the load acts only during the rotation of the crank from $\theta = \theta_1$ to $\theta = \theta_2$, when the punching takes place, and that the load is zero for the rest of the cycle. Unless $\theta = \theta_2$, when the punching takes place, and that the load is zero for the rest of the cycle. Unless a flywheel is used, the speed of the crankshaft will increase substantially during the rotation from $\theta = \theta_1$ to $\theta = 2\pi (= 0)$, and again from $\theta = 0$ to $\theta = \theta_1$, because there is no load while energy continues to be supplied. On the other hand, there will be a big drop in the speed of the crankshaft during the rotation from $\theta = \theta_1$ to $\theta = \theta_2$ due to the load being much more than the amount of energy supplied. The excess energy available at one stage of the cycle has to be absorbed by the flywheel, and the deficiency of energy at the other stage has to be made up by it so as to keep the speed change within the permissible limits. This is done by suitably choosing the moment of inertia of the flywheel.

Let E be the energy required for one punch. This energy is determined by the size of the hole, and the thickness and properties of the material to be punched. For stable operation (i.e., for the speed to be almost constant), the energy supplied to the crank per revolution should also be equal to E (assuming one punch per revolution).

The energy supplied to the crankshaft from the motor during punching (assuming the power of the motor to remain constant) is approximately $E[(\theta_2 - \theta_1)/(2\pi)]$ if the crank rotates at constant

speed, which is almost so with a flywheel. The balance energy required for punching, i.e., $E[1 - (\theta_2 - \theta_1)/(2\pi)]$, is supplied by the flywheel by the decrease in its kinetic energy when its speed falls from ω_{\max} to ω_{\min} . Thus,

$$(\Delta KE)_{\max} = E(1 - \frac{\theta_2 - \theta_1}{2\pi}) = \frac{1}{2} J_f (\omega_{\max}^2 - \omega_{\min}^2) = J_f \omega_{\text{av}}^2 k_s$$

which is the same as (4.63).

The values of θ_1 and θ_2 can be computed only if the crank radius r , connecting-rod length l , and the relative position of the job (of given thickness t) with respect to the crankshaft axis are given. In the absence of relevant data, taking the velocity of the tool to be constant, we shall assume that

$$\frac{\theta_2 - \theta_1}{2\pi} \approx \frac{t}{2s} = \frac{t}{4r}, \quad (4.65)$$

where s is the stroke of the punch ($= 2r$).

It should be noted, that for the same value of $(\Delta KE)_{\max}$ and k_s , the flywheel size (J_f) can be reduced, for example, if its average speed ω_{av} is increased by using gears.

PROBLEM 4.7

A machine punching 3.8-cm-diameter holes in a 3.2-cm-thick plate does 600 J of work per square cm of sheared area. The punch has a stroke of 10.2 cm and punches 6 holes per minute. The maximum speed of the flywheel at its radius of gyration is 27.5 m/s. Find the mass of the flywheel so that its speed at the same radius does not fall below 24.5 m/s. Also determine the power of the motor driving this machine.

SOLUTION

The sheared area per punch is $A_s = \pi dt$, where

d = diameter of the hole = 3.8 cm,

t = thickness of the job = 3.2 cm.

This gives $A_s = 38.2 \text{ cm}^2$. Thus, the energy required per punch is

$$E = 600 \times 38.2 = 22,920 \text{ J.}$$

Assuming, from (4.65), that

$$\frac{\theta_2 - \theta_1}{2\pi} = \frac{t}{2s} = \frac{3.2}{20.4},$$

equation (4.64) gives

$$\begin{aligned} (\Delta KE)_{\max} &= E(1 - \frac{t}{2s}) = \frac{1}{2} J_f (\omega_{\max}^2 - \omega_{\min}^2), \\ 22,920(1 - \frac{3.2}{20.4}) &= \frac{1}{2} m_f k^2 (\omega_{\max}^2 - \omega_{\min}^2), \end{aligned}$$

where k is the radius of gyration of the flywheel and m_f is its mass. Given that

$$V_{\max} = k\omega_{\max} = 27.5 \text{ m/s},$$

$$V_{\min} = k\omega_{\min} = 24.5 \text{ m/s},$$

we get

$$22,920 \times \frac{17.2}{20.4} = \frac{1}{2}m_f[(27.5)^2 - (24.5)^2] = \frac{1}{2}m_f \times 158,$$

$$m_f = \frac{22,920 \times 34.4}{20.4 \times 158} = 244 \text{ kg.}$$

The energy required per minute is $6 \times 22,920 \text{ J}$. So,

$$\text{motor power} = \frac{6 \times 22,920}{1000 \times 60} \text{ kW} = 2.292 \text{ kW.}$$

4.14 DESIGN OF RIM-TYPE FLYWHEEL

It is seen that the moment of inertia and not the mass of the flywheel is the only criterion for its satisfactory operation. In order to have a large moment of inertia with the least possible material, the flywheel is usually made in the form of a rim, which is connected to the hub by several arms. Neglecting the moment of inertia of the spokes and the hub, the required moment of inertia of the flywheel (obtained by the procedures discussed in Sections 4.12 and 4.13) can be written as

$$J_f = mR_m^2, \quad (4.66)$$

where R_m = mean radius of the rim, and m = mass of the rim.

The maximum value of R_m that can be adopted for a flywheel of a given mass is decided by the maximum value of the hoop stress that the flywheel material can withstand. Let

ρ = density of the flywheel material,

A_c = cross-sectional area of the rim (rectangular), and

σ = allowable tensile stress for the flywheel material.

Referring to Fig. 4.31, the maximum centrifugal force acting radially on a differential element is

$$dF_c = \rho A_c R_m d\theta \omega_{\max}^2 R_m.$$

Taking one-half of the rim as a free body, the total vertical component of the centrifugal force is

$$F_c = (\rho A_c \omega_{\max}^2 R_m^2) 2 \int_0^{\pi/2} \sin \theta d\theta = 2\rho A_c \omega_{\max}^2 R_m^2. \quad (4.67)$$

This has to be balanced by the vertical forces at the ends of the free body, the maximum of which (as shown in Fig. 4.31) is

$$2\sigma A_c. \quad (4.68)$$

(The horizontal component of the centrifugal force is balanced because of symmetry.) Equating (4.67) and (4.68) for the maximum value of R_m , we get

$$2\rho A_c \omega_{\max}^2 R_m^2 = 2\sigma A_c, \quad R_m^2 = \sigma / (\rho \omega_{\max}^2).$$

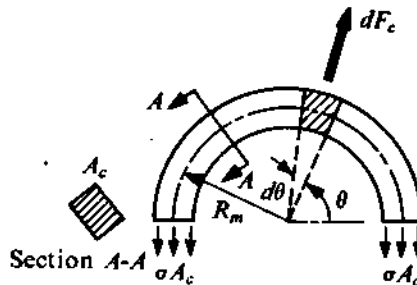


FIGURE 4.31

Thus, the maximum value of R_m is

$$R_m = [\sigma / (\rho \omega_{\max}^2)]^{1/2} \quad (4.69)$$

and, from (4.66), the minimum value of m is

$$m = J_f / [\sigma / (\rho \omega_{\max}^2)] = \rho \omega_{\max}^2 J_f / \sigma. \quad (4.70)$$

From (4.69) and (4.70), we can get the value of A_c . Thus,

$$m = 2\pi \rho R_m A_c,$$

$$A_c = m / (2\pi \rho R_m). \quad (4.71)$$

Choosing a suitable length-to-width ratio for a rectangular cross-section, we can determine the dimensions of the rim from the value of A_c given by (4.71).

4.15 WITTENBAUER'S METHOD OF FLYWHEEL ANALYSIS

So far, we considered the analysis of flywheel systems assuming the moments of inertia of the system (equal to that of the flywheel) to be constant. In fact, this is not so. For example, the moment of inertia of a crank mechanism depends on its configuration which changes periodically when the crank rotates. We will now discuss some interesting points which arise when such considerations are introduced in flywheel analysis.

Let θ be the crank rotation and let the total equivalent moment of inertia of the crank mechanism (which depends on the configuration, i.e., on θ) be denoted by $J(\theta)$. Then, the instantaneous KE of the mechanism is given by

$$T = \frac{1}{2} J(\theta) \left(\frac{d\theta}{dt} \right)^2, \quad (4.72)$$

where T represents the KE. If $x(\theta)$ denotes the position of the piston, the velocity of the piston can be expressed as

$$V = \frac{dx(\theta)}{dt} = \frac{dx(\theta)}{d\theta} \cdot \frac{d\theta}{dt}. \quad (4.73)$$

Now, if the resultant force on the piston exerted by the pressurized gas be $P(\theta)$ (the gas pressure depends on the piston position or on θ) and if $M(\theta)$ be the moment of this force on the crank, then from the principle of virtual work, we get

$$M(\theta) \cdot d\theta = P(\theta) \cdot dx,$$

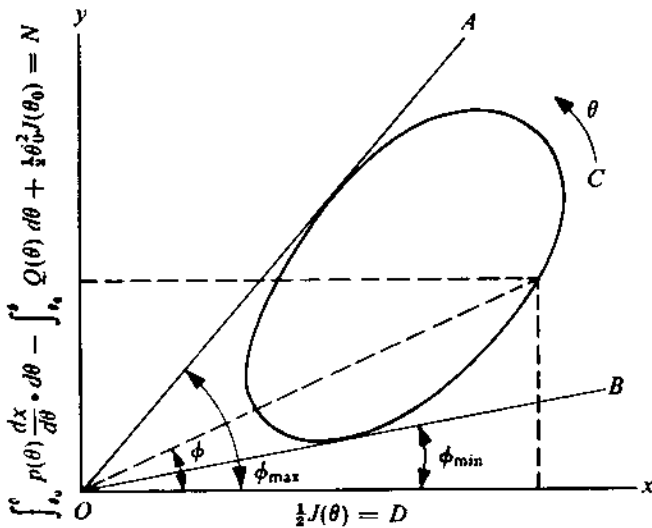


FIGURE 4.32

$$M(\theta) = P(\theta) \cdot \frac{dx}{d\theta} = P(\theta) \cdot \frac{dx}{dt} / \frac{d\theta}{dt}. \quad (4.74)$$

Again, if the resisting moment on the crank exerted by the load be $\{-Q(\theta)\}$, Lagrange's equation for the system can be written as

$$\frac{d}{dt} \left(\frac{\partial T}{\partial \dot{\theta}} \right) - \frac{\partial T}{\partial \theta} = M(\theta) - Q(\theta). \quad (4.75)$$

From (4.72), (4.74), and (4.75), we get

$$\frac{1}{2} \frac{d}{d\theta} [J(\theta) (\frac{d\theta}{dt})^2] = P(\theta) \cdot \frac{dx}{d\theta} - Q(\theta). \quad (4.76)$$

Integrating both sides of (4.76) between the limits (θ, θ_0) and $(\dot{\theta}, \dot{\theta}_0)$, we get

$$\begin{aligned} \frac{1}{2} [J(\theta) \dot{\theta}^2 - J(\theta_0) \dot{\theta}_0^2] &= \int_{\theta_0}^{\theta} P(\theta) \cdot \frac{dx}{d\theta} d\theta - \int_{\theta_0}^{\theta} Q(\theta) d\theta, \\ \dot{\theta}^2 &= \frac{\int_{\theta_0}^{\theta} P(\theta) \cdot \frac{dx}{d\theta} d\theta - \int_{\theta_0}^{\theta} Q(\theta) d\theta + \frac{1}{2} J(\theta_0) \dot{\theta}_0^2}{\frac{1}{2} J(\theta)}. \end{aligned} \quad (4.77)$$

The numerator of the right-hand side of (4.77) is plotted against the denominator in Fig. 4.32. When the engine runs at a steady state, both the numerator and the denominator will be periodic functions with the same time period and a closed curve C is obtained as shown. Again, the tangent of the angle ϕ , made by the radius vector corresponding to a particular value of θ , gives the square of the instantaneous angular velocity [see (4.77)]. The maximum and minimum angular velocities are represented by the lines OA and OB , respectively. Thus,

$$\begin{aligned} \dot{\theta}_{\max} &= (\tan \phi_{\max})^{1/2}, \\ \dot{\theta}_{\min} &= (\tan \phi_{\min})^{1/2}, \\ \dot{\theta} &= (\tan \phi)^{1/2}. \end{aligned} \quad (4.78)$$

It is clear that the shape of the curve C is not altered when the numerator or the denominator, or both, are changed by a quantity or quantities independent of θ . Only the position of the curve is shifted. So, if θ_0 or $\dot{\theta}_0$ varies, or if $J(\theta)$ grows by increasing the moment of inertia of only the rotating parts, the shape of the curve C remains unchanged. Such changes only shift the curve or the origin of the coordinate system with respect to the curve C . By definition,

$$k_s = \frac{\omega_{\max} - \omega_{\min}}{\omega_{\text{av}}} \approx \frac{\dot{\theta}_{\max} - \dot{\theta}_{\min}}{\frac{1}{2}(\dot{\theta}_{\max} + \dot{\theta}_{\min})}.$$

Multiplying both the numerator and the denominator of the right-hand side of this equation by $(\dot{\theta}_{\max} + \dot{\theta}_{\min})$, we get

$$k_s = \frac{2(\dot{\theta}_{\max}^2 - \dot{\theta}_{\min}^2)}{\dot{\theta}_{\max}^2 + \dot{\theta}_{\min}^2 + 2\dot{\theta}_{\max}\dot{\theta}_{\min}}. \quad (4.79)$$

From (4.78) and (4.79), we have

$$k_s = 2 \frac{\tan \phi_{\max} - \tan \phi_{\min}}{\tan \phi_{\max} + \tan \phi_{\min} + 2(\tan \phi_{\max} \tan \phi_{\min})^{1/2}}. \quad (4.80)$$

Normally, the difference between $\tan \phi_{\max}$ and $\tan \phi_{\min}$ will be small. Representing this difference by δ , we can write

$$\delta = \tan \phi_{\max} - \tan \phi_{\min}, \quad \tan \phi_{\min} = \tan \phi_{\max} - \delta.$$

So,

$$\begin{aligned} (\tan \phi_{\max} \tan \phi_{\min})^{1/2} &= [\tan \phi_{\max}(\tan \phi_{\max} - \delta)]^{1/2} = (\tan^2 \phi_{\max} - 2 \tan \phi_{\max} \cdot \frac{\delta}{2})^{1/2} \\ &\approx (\tan^2 \phi_{\max} - 2 \tan \phi_{\max} \cdot \frac{\delta}{2} + \frac{\delta^2}{4})^{1/2} \end{aligned}$$

since $\delta^2/4$ is very small and the addition of this quantity will not cause much change in the value of the expression. So,

$$\begin{aligned} (\tan \phi_{\max} \tan \phi_{\min})^{1/2} &\approx [(\tan \phi_{\max} - \frac{\delta}{2})^2]^{1/2} \\ &= \frac{1}{2}(2 \tan \phi_{\max} - \delta) = \frac{1}{2}[\tan \phi_{\max} + (\tan \phi_{\max} - \delta)] \\ &= \frac{1}{2}(\tan \phi_{\max} + \tan \phi_{\min}). \end{aligned}$$

Therefore, (4.80) takes the form

$$k_s \approx \frac{\tan \phi_{\max} - \tan \phi_{\min}}{\tan \phi_{\max} + \tan \phi_{\min}}. \quad (4.81)$$

Again, by definition, we have

$$k_s = \frac{\omega_{\max} - \omega_{\min}}{\omega_{\text{av}}} = \frac{\omega_{\max} - \omega_{\min}}{\frac{1}{2}(\omega_{\max} + \omega_{\min})}, \quad \frac{1}{2}k_s = \frac{\omega_{\max} - \omega_{\min}}{\omega_{\max} + \omega_{\min}}.$$

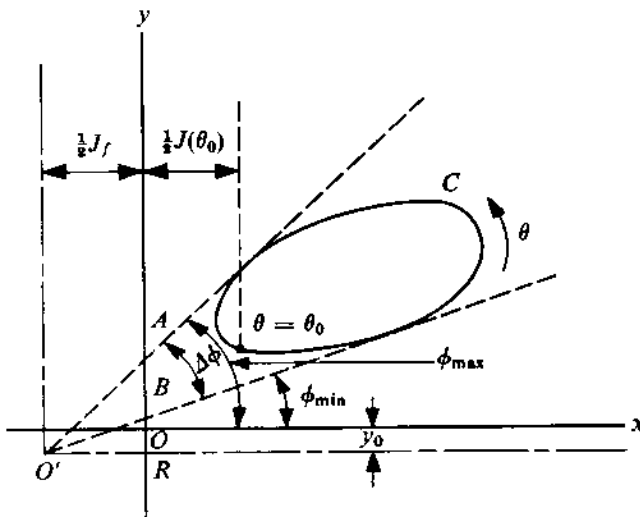


FIGURE 4.33

So,

$$1 + \frac{1}{2} k_s = \frac{2\omega_{\max}}{\omega_{\max} + \omega_{\min}} = \frac{\omega_{\max}}{\omega_{\text{av}}}, \quad 1 - \frac{1}{2} k_s = \frac{2\omega_{\min}}{\omega_{\max} + \omega_{\min}} = \frac{\omega_{\min}}{\omega_{\text{av}}}.$$

Therefore,

$$\begin{aligned} \omega_{\max}^2 &= \tan \phi_{\max} = (1 + \frac{1}{2} k_s)^2 \omega_{\text{av}}^2 \approx (1 + k_s) \omega_{\text{av}}^2, \\ \omega_{\min}^2 &= \tan \phi_{\min} = (1 - \frac{1}{2} k_s)^2 \omega_{\text{av}}^2 \approx (1 - k_s) \omega_{\text{av}}^2. \end{aligned} \quad (4.82)$$

Now, to determine the moment of inertia of the flywheel required to keep the fluctuation of angular velocity within the prescribed limits, first the curve C is plotted for the engine without a flywheel, starting from an arbitrary crank angle θ_0 and taking the rotation to be at an arbitrary average angular velocity $\dot{\theta}_0$ (see Fig. 4.33). The corresponding coordinates on the x - and y -axis are $J(\theta_0)/2$ and $J(\theta_0)\omega_0^2/2$. Since the prescribed average angular velocity and k_s are known, ω_{\max} and ω_{\min} (therefore, ϕ_{\max} and ϕ_{\min}) can be determined from (4.82). The tangents to the curve C are drawn at angles ϕ_{\max} and ϕ_{\min} , as shown in Fig. 4.33. These tangents intersect at O' , the abscissa of which is equal to the value of one-half the moment of inertia of the required flywheel (J_f).

Sometimes, the graphical determination of the point of intersection may not be accurate. In such cases, J_f is calculated by considering the section AB between the intersecting points of the tangents on the y -axis, as shown in Fig. 4.33. From this, we get

$$\begin{aligned} AB &= \frac{1}{2} J_f (\tan \phi_{\max} - \tan \phi_{\min}) \\ &= J_f \omega_{\text{av}}^2 k_s, \end{aligned}$$

$$J_f = \frac{AB}{\omega_{\text{av}}^2 k_s}. \quad (4.83)$$

From Fig. 4.33, it is seen that

$$\Delta\phi = \phi_{\max} - \phi_{\min}.$$

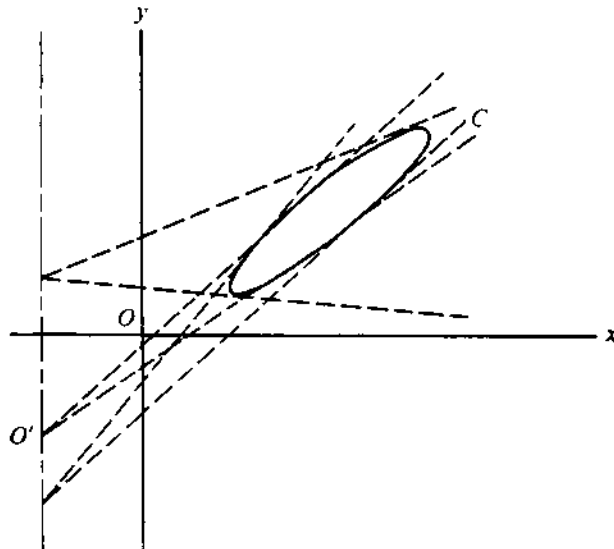


FIGURE 4.34

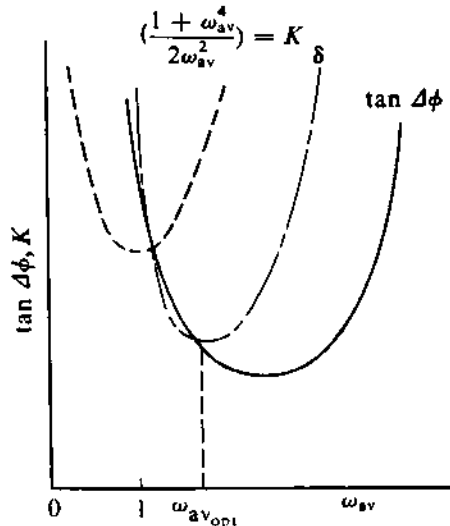


FIGURE 4.35

So,

$$\tan \Delta\phi = \frac{\tan \phi_{\max} - \tan \phi_{\min}}{1 + \tan \phi_{\max} \tan \phi_{\min}}.$$

Substituting $\tan \phi_{\max}$ and $\tan \phi_{\min}$ from (4.82) in this equation, we get

$$\tan \Delta\phi \approx \frac{2k_s \omega_{av}^2}{1 + (1 - k_s^2)\omega_{av}^4}.$$

Neglecting k_s^2 , we have

$$\tan \Delta\phi \approx \left(\frac{2\omega_{av}^2}{1 + \omega_{av}^4} \right) k_s,$$

$$k_s \approx \frac{1 + \omega_{av}^4}{2\omega_{av}^2} \cdot \tan \Delta\phi. \quad (4.84)$$

As explained earlier in this discussion, it is obvious that by changing ω_{av} , the vertical position of C can be changed for a particular system. The angle of inclusion $\Delta\phi$ will also change corresponding (see Fig. 4.34), and for a particular average angular velocity, $\Delta\phi$ becomes minimum. Similarly, the function $(1 + \omega_{av}^4)/(2\omega_{av}^2)$ also attains a minimum value for a particular ω_{av} . Local variations of $\tan \Delta\phi$ and $(1 + \omega_{av}^4)/(2\omega_{av}^2)$ are shown in Fig. 4.35. Both these functions reach minimum values for certain values of ω_{av} and the product of these quantities will also be minimum for a particular value of $\omega_{av}(\omega_{av, opt})$. This is the most suitable speed of an engine when k_s is the least.

Since the ordinates of the curve C represent the instantaneous KE of the system, it is not possible for any part of the curve to go below the x-axis. When the moment of inertia of the system remains independent of the configuration, the curve C becomes a vertical line. Again, when

$$P(\theta) \frac{dx}{d\theta} - Q(\theta) = 0$$

but the moment of inertia is dependent on θ , the curve C becomes a horizontal line.

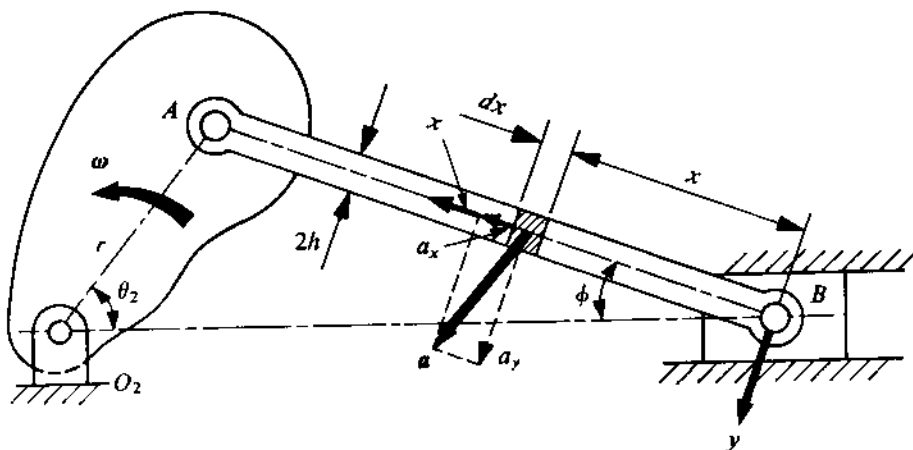


FIGURE 4.36

4.16 DYNAMICS OF MECHANISMS WITH ELASTIC LINKS

Under normal circumstances, the links of a mechanism do not deform much and can be considered to be rigid. However, when the speed of operation of a mechanism becomes quite high, the links are subjected to large inertia forces in addition to the forces due to external loading. It is easy to make out that both these types of forces are dynamic in nature. So, at a high operational speed, such forces can produce large dynamic deformations of the links which in reality are elastic. These deformations generate extra stresses in the links of the mechanism. Therefore, an *elastodynamic analysis* of the mechanism becomes necessary to ensure its safe functioning.⁵ Apart from bringing about extra stresses, the deformation of links leads to some changes in the effective link lengths. In other words, even the kinematic characteristics of the mechanism undergo some changes. As a result, the computation of the dynamic loadings (which depend on the accelerations) of links has to be modified, leading, obviously, to further alterations in the deformation, and so on. The discipline that takes all the foregoing aspects into consideration is known as *kinetoelastodynamics*. In this section, we shall present only the elastodynamic analysis of a simple slider-crank mechanism. To keep our treatment simple, we shall assume that only the connecting rod is elastic. This, to some extent, is justifiable as the rigidity of the crank is generally much more than that of the connecting rod (or coupler).

Figure 4.36 shows a slider-crank mechanism in which only the coupler is assumed to be elastic. Also, the slider is assumed to possess a negligible mass and to move without any external resistance. The crank O_2A is being rotated with a constant angular velocity ω . A coordinate system xy moving with the coupler is chosen. Since the first natural frequency of longitudinal vibration of the coupler is normally very high as compared to the speed of rotation, only the lateral vibration of the coupler is of significance. The equation of motion for the transverse (or lateral) vibration of the coupler is (see Section 11.6)

$$EI \frac{\partial^4 v}{\partial x^4} + \rho A \frac{\partial^2 v}{\partial t^2} = -\rho A a_y, \quad (4.85)$$

⁵For a comprehensive study, see Nath, P.K. and Ghosh, A., Kinetoelastodynamic analysis of mechanisms by finite element method, *Mechanism and Machine Theory*, 15, 179-97, 1980, and Steady state response of mechanisms with elastic links by finite element method, *Mechanism and Machine Theory*, 15, 199-211, 1980. For dynamics of mechanisms with rigid links connected by elastic members (e.g., springs), see the second edition of this text.

where EI is the flexural rigidity of the coupler, ρ is the density of the coupler material, A is the cross-sectional area of the coupler (constant), v is the elastic deflection of the coupler element in the y -direction, and a_y is the y -component of the acceleration of the coupler element (at a distance x) due to the motion of the mechanism. In terms of the nondimensional parameters

$$\bar{t} = \omega t, \quad \bar{x} = \frac{x}{l}, \quad \bar{v} = \frac{v}{l}, \quad q = -\frac{a_y}{\omega^2 l},$$

(4.85) can be written as

$$\frac{\partial^2 \bar{v}}{\partial \bar{t}^2} + k^4 \frac{\partial^4 \bar{v}}{\partial \bar{x}^4} = q, \quad (4.86)$$

where $k^4 = EI/(\rho A \omega^2 l^4)$. The expression for a_y can be written in the form

$$a_y = \omega^2 r \sin(\theta_2 + \phi) + (l - x)\ddot{\phi}. \quad (4.87)$$

Using the series expressions derived in Sections 4.9 and 4.10 and (4.87), q can, finally, be written as

$$q = - \sum_{n=1}^{\infty} (A_n + B_n \bar{x}) \sin n\theta_2,$$

where A_n and B_n are functions of only $r/l (= \lambda)$. Representing $(A_n + B_n \bar{x})$ as a Fourier sine series in \bar{x} , we have

$$q = - \sum_{n=1}^{\infty} \frac{2}{\pi} [(2A_n + B_n) \sum_{p=1}^{\infty} \frac{\sin(2p-1)\pi\bar{x}}{2p-1} - B_n \sum_{p=1}^{\infty} \frac{\sin 2p\pi\bar{x}}{2p}] \sin n\theta_2. \quad (4.88)$$

With this expression for q , the solution of (4.86) can be sought in the form

$$\bar{v} = \sum_{n=1}^{\infty} \sum_{p=1}^{\infty} [\alpha_{np} \sin(2p-1)\pi\bar{x} + \beta_{np} \sin 2p\pi\bar{x}] \sin n\bar{t}. \quad (4.89)$$

Because of the sine series we chose, each term of (4.89), as can be easily seen, can satisfy (4.86) if

$$\alpha_{np} = \frac{-\frac{2}{\pi} \cdot (\frac{2A_n + B_n}{2p-1})}{\pi^4 (2p-1)^4 k^4 - n^2}, \quad \beta_{np} = \frac{\frac{B_n}{\pi p}}{\pi^4 (2p)^4 k^4 - n^2}. \quad (4.90)$$

It should also be noted that each term of the series (4.87) satisfies the boundary conditions of the hinged-hinged coupler. Once the solution for \bar{v} is obtained, the bending stress can be determined as

$$\sigma_b = \pm Eh \frac{\partial^2 \bar{v}}{\partial \bar{x}^2} = \pm \frac{Eh}{l} \frac{\partial^2 \bar{v}}{\partial \bar{x}^2}. \quad (4.91)$$

To realize the effect of the dynamics of the coupler, we can find out the bending stress σ'_b by assuming that the inertia loading $-\rho A a_y$ acts in a static manner [this is equivalent to dropping the second term in the left-hand side of (4.85) – see Problem 4.20]. In what follows, we shall consider a typical numerical example of elastodynamic analysis.

Figure 4.37 shows the coupler of an I -section with dimensions as indicated. The other relevant dimensions are $l = 0.8$ m, $\lambda = 0.333$, $E = 220$ GPa, and $\rho A = 2.4$ kg/m. The figure also shows the variations of both σ_b and σ'_b (denoting the maximum bending stresses at the configuration with $\theta_2 + \phi = 90^\circ$) with the increase in crank speed. Clearly, with the increase in speed, it becomes increasingly important that the elastodynamics of the links (here, the coupler) be considered.

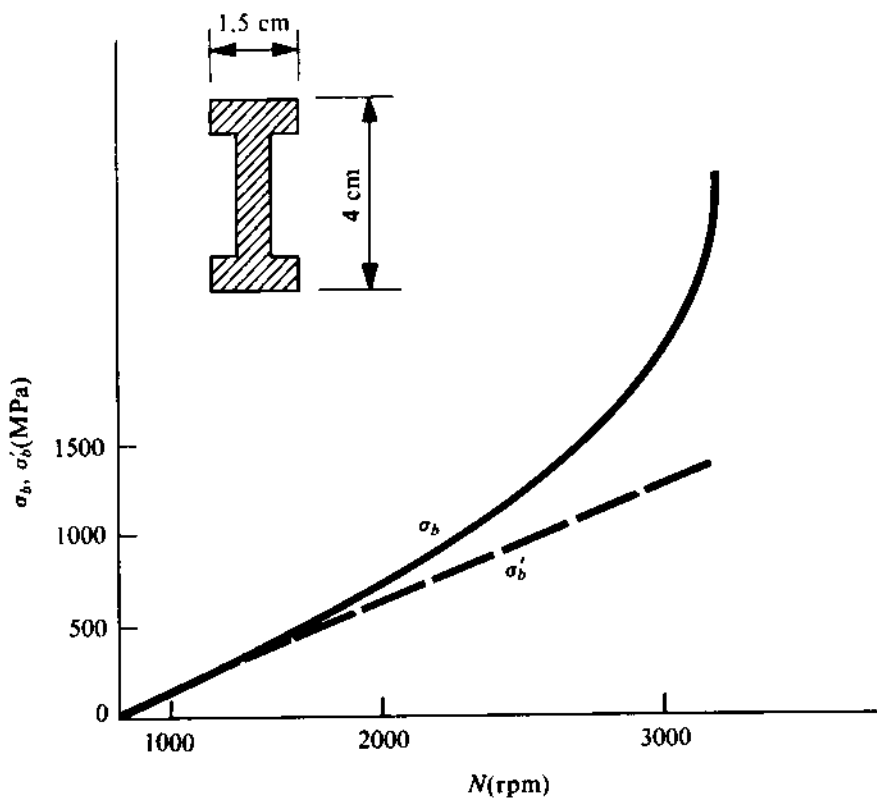


FIGURE 4.37

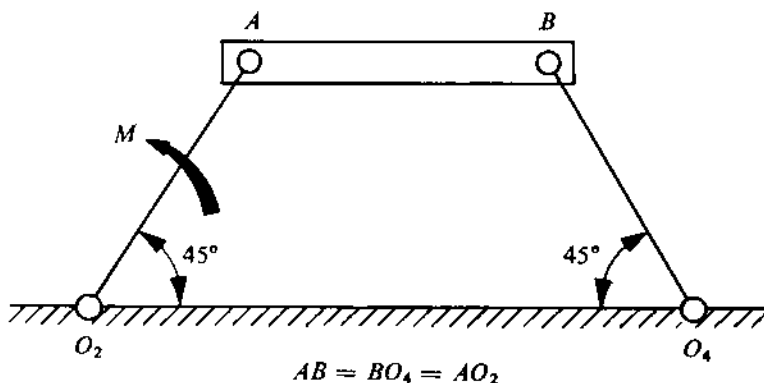


FIGURE 4.38

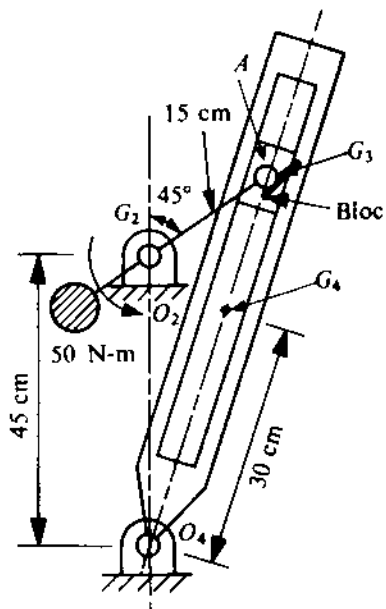


FIGURE 4-3

4.17 PROBLEMS

- 4.8 (i) Figure 4.38 shows a four-bar mechanism in the vertical plane and stationary at the instant indicated. The input and output members O_2A and O_4B are rigid but of a negligible mass. The coupler AB is a rigid, uniform rod of length 50 cm, its total mass being 15 kg. A torque M acts on the crank O_2A , as shown, causing this crank to move with an angular acceleration of 50 rad/s^2 in the direction of M . Determine the magnitude of M .

(ii) What will be the magnitude of M when the input member rotates with an angular velocity of 150 rad/s (CCW) at the same instant as in Problem 4.8(i)?

4.9 A slotted-lever quick-return mechanism is shown in Fig. 4.39. The crank is balanced and its moment of inertia about O_2 is 0.15 kg-m^2 . The moment of inertia of the slotted lever about its CG, G_4 , is 2.5 kg-m^2 , and that of the sliding block about G_3 is 0.01 kg-m^2 . The crank subjected to a torque of 50 N-m and the whole system is stationary. The masses of the block and the slotted lever are 15 kg and 60 kg , respectively. Neglecting gravitational effects and friction, determine the total force on the pin O_4 .

4.10 Figure 4.40 shows Rapson's slide which is used in the steering of ships. The moment of inertia of the slotted lever 2 about G_2 is 10 kg-m^2 . Sliding blocks 3 and 4 are identical; each has a moment of inertia of 0.05 kg-m^2 . The blocks weigh 300 N each, and link 2 weighs 3000 N . The coefficient of friction for each block and guide surface is 0.2 , determine the total pin force at O_2 when block 4 is pulled to the right with a uniform velocity of 10 cm/s .

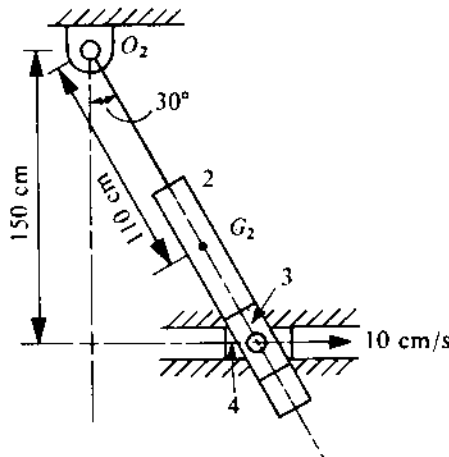


FIGURE 4.40

4.11 Figure 4.41 shows a tipper truck. There are two identical mechanisms on the two sides of the tipper. The tipper mass is 300 kg with its CG at G_3 . Its moment of inertia about the centroidal axis is 350 kg-m^2 . The mass and centroidal moment of inertia of the link O_2A are 50 kg and 15 kg-m^2 , respectively. The CG of this link is at G_2 . The link O_4B is uniform with a mass of 40 kg. The mass of the hydraulic actuator is negligible. The actuator is expanding (i.e., the distance O_4C is increasing) at a rate of 0.5 m/s with an acceleration of 1 m/s^2 . If the internal diameter of the actuator cylinder is 150 mm, determine the pressure of the fluid driving the piston required to achieve the prescribed motion at the instant shown in the figure. Consider the vehicle to be stationary. Given

$$O_2A = 1700 \text{ mm}, AB = 800 \text{ mm}, O_2G_2 = 640 \text{ mm}, AG_2 = 1120 \text{ mm}, AG_3 = 450 \text{ mm},$$

$$BG_3 = 510 \text{ mm}.$$

4.12 (i) Figure 4.42 shows a mechanism where link 2 is driving link 4 with the help of a rigid, uniform coupler of negligible mass. The angular velocity ω_2 at the instant shown is 10 rad/s . If a moment M of magnitude 500 N-m is applied on 2, as shown, determine the acceleration of link 2. The moments of inertia of links 2 and 4 about O_2 and O_4 are 0.5 kg-m^2 and 1.0 kg-m^2 , respectively. Given $O_2O_4 = 25 \text{ cm}$, $AO_2 = 35 \text{ cm}$, and $BO_4 = 50 \text{ cm}$.

(ii) What will be the acceleration of link 2 if the coupler has a mass 2 kg and the mechanism is in a horizontal plane?

4.13 For the mechanism shown in Fig. 4.43, the sliding blocks weigh 45 N each. Both connecting rods are uniform, each being 50.8 cm long. The length of the crank is 15.3 cm and is rigid with a mass 10 kg at its end. All links weigh 172 N/m.

- (i) If a force of 450 N is applied to the slider A as shown in the figure, what will be the acceleration of the slider B at the instant when the force is applied, assuming the mechanism to be initially at rest?
- (ii) Instead of being at rest, if the crank possesses an angular velocity of 300 rad/s in the counter-clockwise direction, what will be the acceleration of the slider B at the instant

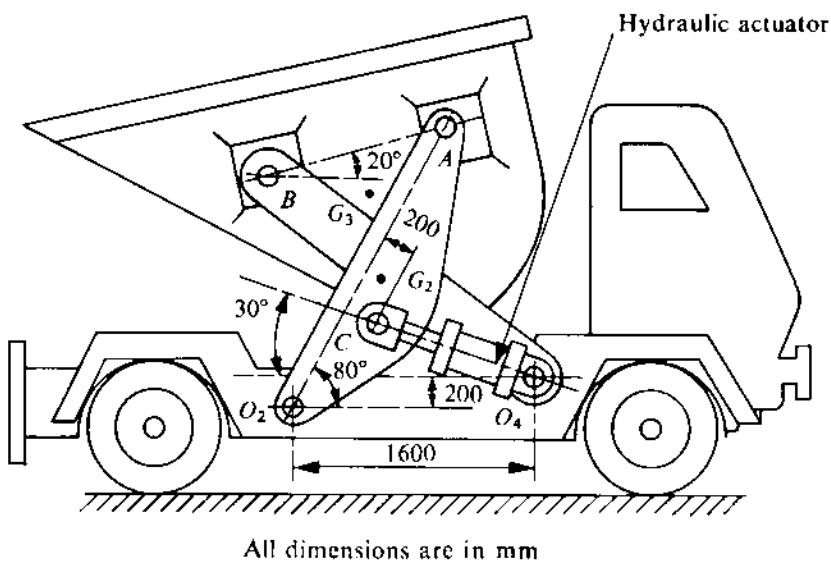


FIGURE 4.41

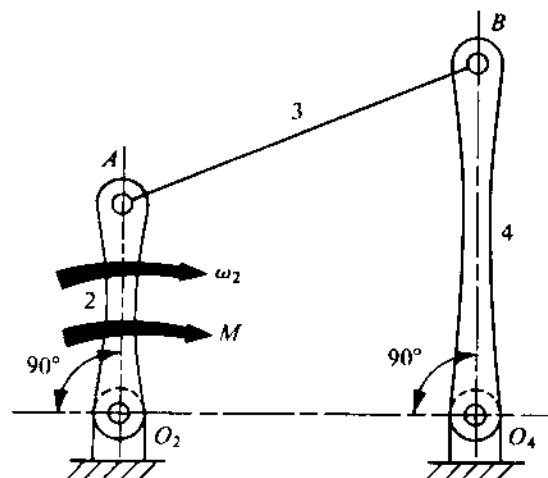


FIGURE 4.42

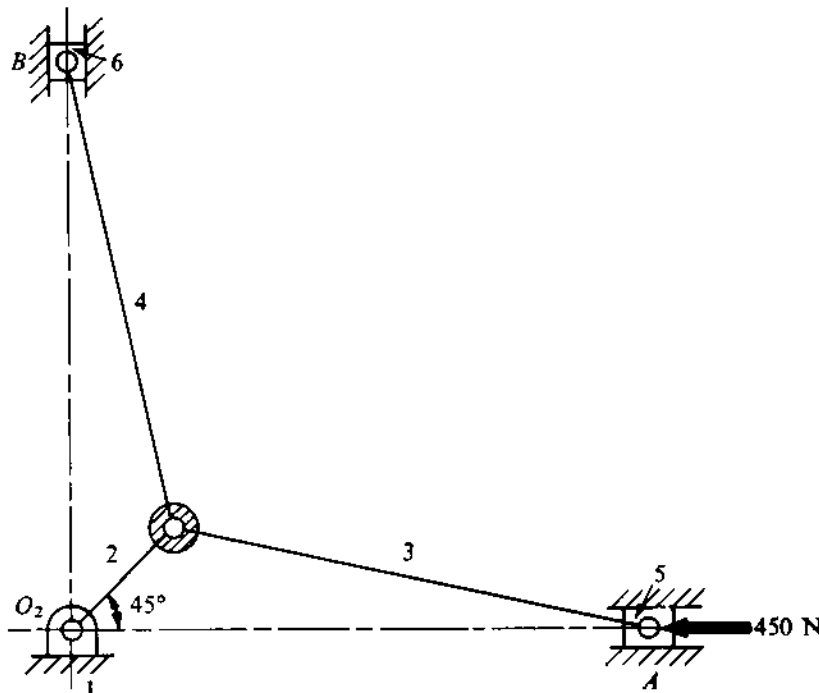


FIGURE 4.43

corresponding to the figure (the crank makes an angle of 45° with OA as shown)? Assume that there is no friction.

4.14 Calculate the angular acceleration of the crank in Problem 4.13 when the coefficient of friction for each slider and guide is 0.3, and the mechanism starts from rest.

4.15 In a slider-crank engine mechanism when the crank angle is θ from the outer dead-centre position, the gas pressure p is suddenly applied on the piston. The mechanism was initially at rest. Prove that the angular acceleration of the crank at the instant when the pressure is applied will be

$$\alpha \approx \frac{pAr \sin(\theta + \phi)}{J_r \cos \phi + m_{rec}r^2(\sin \theta + \frac{\lambda}{2} \sin 2\theta) \sin(\theta + \phi)},$$

where

A = cross-sectional area of the piston,

r = crank length,

$\lambda = r/l$ (l being the length of the connecting rod),

ϕ = angle made by the connecting rod with the line of stroke at this instant,

m_{rec} = mass of the reciprocating parts, and

J_r = moment of inertia of the crank about the axis of rotation.

4.16 The relevant particulars of a double-acting horizontal steam engine are
mass of the reciprocating parts = 125 kg,

crank radius = 40 cm,
 length of the connecting rod = 160 cm,
 steam pressure (assumed constant throughout the stroke) = 70 N/cm²,
 back pressure (assumed constant throughout the stroke) = 2 N/cm²,
 diameter of the piston = 40 cm,
 speed of the engine = 250 rpm.

Determine the power developed and the turning moment when the crank and connecting rod are at right angles.

- 4.17 A horizontal double-acting steam engine running at 250 rpm has a stroke of 30.5 cm. The diameter of the cylinder is 21.5 cm and the connecting rod is 5 cranks long. The mass of the reciprocating parts is 68 kg. Steam is admitted at 56 N/cm² (gauge) for one-third of the stroke after which isothermal expansion takes place ($pv = \text{constant}$, p being the absolute pressure and v the volume). The exhaust pressure is -8.44 N/cm² (gauge). Determine the turning moment when the crank has rotated 120° from the outer dead-centre position. Neglect the difference between the areas of the two sides of the piston and also neglect the side clearance. The atmospheric pressure is 10 N/cm².

- 4.18 Figure 4.44 shows a slider-crank mechanism for an offset engine. Show that the acceleration of the piston towards the crankshaft can be approximately expressed (for a small offset h) as

$$\ddot{x} \approx -\omega^2 r [\cos \theta + \frac{r}{l} \cos 2\theta + \frac{h}{l} \sin \theta].$$

Note that with the proper amount of offset, the overall frictional loss between the cylinder and the piston can be reduced.

- 4.19 The data given for a vertical offset engine are $r = 6.3$ cm, $l = 24.1$ cm, $h = 2$ cm, diameter of the cylinder = 9 cm, speed of the engine = 2400 rpm, and mass of the reciprocating parts = 1.35 kg. Determine the turning moment when the crank has rotated through 60° from the top dead-centre position and the net gas pressure on the piston is 112 N/cm².

- 4.20 In a slider-crank mechanism, the crank and connecting rod are at right angles. Show that the maximum bending moment on the connecting rod due to its angular acceleration is approximately given by

$$M_{\max} \approx \frac{m_c \omega^2 r l}{9\sqrt{3}},$$

where

m_c = mass of the connecting rod (assumed uniform and simply-supported at the ends),

ω = angular velocity of the crank (constant),

r = crank radius, and

l = length of the connecting rod.

- 4.21 A four-stroke engine develops 18.5 kW at 250 rpm. The turning-moment diagram is rectangular for the expansion and compression strokes. The turning moment for the expansion stroke is 2.8 times that of the compression stroke (negative). Assuming constant load, determine the moment of inertia of the flywheel to keep the total fluctuation of the crankshaft speed within 1% of the average speed of 250 rpm.

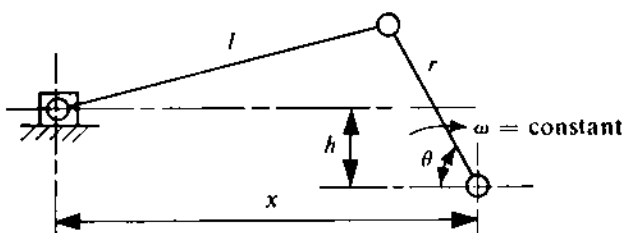


FIGURE 4.44

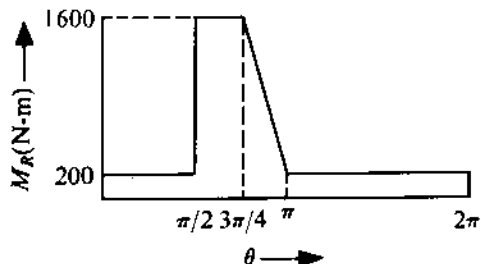


FIGURE 4.45

4.22 The turning-moment diagram for a four-stroke engine may be assumed for the sake of simplicity to be represented by four triangles in each stroke. The areas of these triangles are: expansion stroke 8.5 cm^2 , exhaust stroke 0.8 cm^2 (negative), suction stroke 0.5 cm^2 (negative), and compression stroke 2.1 cm^2 (negative), where 1 cm^2 represents 1400 J of work.

Assuming constant resistance, determine the moment of inertia of the flywheel to keep the speed between 98 rpm and 102 rpm.

Find the size of a rim-type flywheel based on the minimum-material criterion, given that the density of the flywheel material is 8000 kg/m^3 , the allowable tensile stress of the flywheel material is 7.5 MPa , and that the rim cross-section is rectangular, one side being four times the length of the other.

4.23 The resisting torque on the crank of a riveting machine is shown in Fig. 4.45. The duration of the cycle is 2 seconds. The motor driving the machine, however, has a speed of 1500 rpm and it delivers constant torque. The crankshaft of the machine is geared to the motor shaft. Neglecting frictional losses, determine

- (i) the power of the motor, and
- (ii) the moment of inertia of the flywheel mounted on the motor shaft to keep the speed fluctuation within $\pm 2\%$ of the average speed.

4.24 A machine requiring a driving torque of $(2000 + 300 \sin \theta)$ N-m (where θ is the angle of rotation of its shaft measured from some datum) is driven by a directly-coupled two-stroke engine whose turning moment is given by $(2000 + 400 \sin 2\theta)$ N-m. The average speed is 150 rpm. Determine

- (i) the moment of inertia of the flywheel to limit the speed fluctuation to within $\pm 2\%$ of the average speed,
- (ii) the maximum angular acceleration of the flywheel, and
- (iii) the maximum angle by which this flywheel leads or lags an imaginary flywheel which is rotating at a constant speed of 150 rpm.

4.25 The cranks of a three-cylinder two-stroke engine running at 600 rpm are 120° apart. The turning-moment diagram for each cylinder can be represented by a triangle for one stroke with a maximum value of 600 N-m at 60° from the top dead-centre position. The turning moment in the remaining stroke is zero for all the cylinders. Determine

- (i) the power developed by the engine,

- (ii) the coefficient of fluctuation of energy,
- (iii) the coefficient of fluctuation of speed with a flywheel which has a radius of gyration of 0.25 m and a mass of 16 kg.

Chapter 5

KINEMATICS OF SPATIAL CHAINS

5.1 INTRODUCTION

So far we have discussed kinematics and kinetics of planar linkages which consist of only R- and P-pairs. A spatial linkage can have all kinds of lower pairs. Since no single projection can reveal the true motion in a three-dimensional space, graphical methods are not convenient for kinematic analysis and synthesis of spatial linkages. There are quite a few applications of spatial linkages and a very common example is the coupling between misaligned shafts. However, the importance of the subject has increased recently because of the development of robot manipulators. Most common types of robot manipulators are serially connected spatial open kinematic chains. In this chapter, we shall give a brief introduction to an analytical matrix method which forms the basis of kinematic study of both spatial linkages (closed chains) and robotic manipulators.

Degrees of Freedom

A rigid body (link) moving in three dimensions has six degrees of freedom, three of which are translational and the other three rotational. One or more of these is/are curtailed at a kinematic pair; the number of degrees of freedom curtailed depends on the type of kinematic pair (see Chapter 1). The degrees of freedom of a spatial linkage, F , can be easily obtained as

$$F = 6(n - 1) - 5(R + P + H) - 4C - 3(S + P') - f_r, \quad (5.1)$$

where n = number of links; R , P , H , C , S , and P' stand, respectively, for the number of revolute, prismatic, screw (think of helix), cylindric, spherical, and planar pairs present in the linkage; f_r is the number of redundant degrees of freedom. As in the case of a planar linkage, (5.1) also may not give the correct number of degrees of freedom for special dimensions. For example, the Bennett linkage (Fig. 5.1) consisting of only four links and four R-pairs has a single degree of freedom, whereas (5.1) would yield $F = -2$. The Bennett linkage has mobility only with special dimensions. Figure 5.2 shows a four-link R-S-S-R linkage. For this linkage, $f_r = 1$ since link 3 can rotate freely about the axis joining the centres of the two S-pairs without causing any other movement anywhere. Thus,

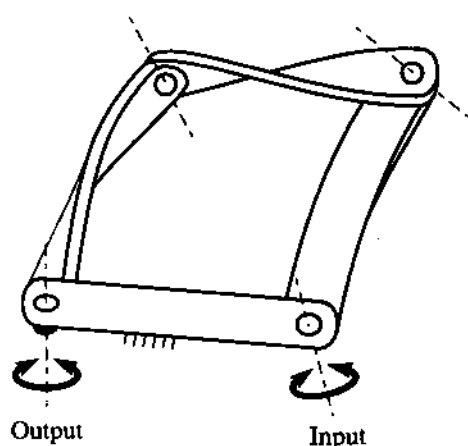


FIGURE 5.1

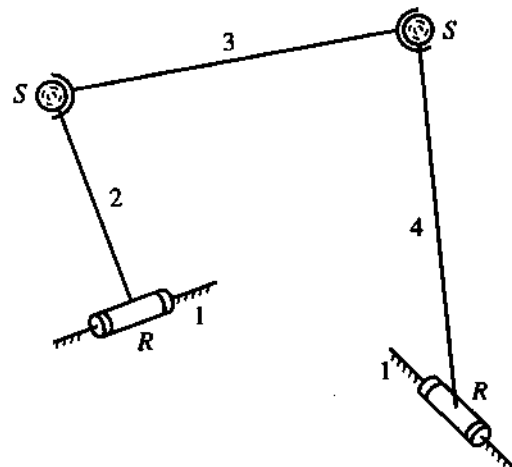


FIGURE 5.2

again from (5.1), we get $F = 1$ for this linkage, implying a unique output movement (say, of link 4) due to a given input movement (say, of link 2).

A simple, closed chain consists of only binary links. For such a chain to produce a single-degree-of-freedom linkage (with one link fixed), the total degrees of freedom of all the kinematic pairs must add up to seven. This statement can be proved as follows. For a simple chain with n links, there are n kinematic pairs. For any i -th kinematic pair, $f_{a_i} + f_{r_i} = 6$, where f_{a_i} is the number of allowed degrees of freedom at the i -th pair and f_{r_i} is the number of degrees of freedom lost at the same pair. Therefore,

$$F = 6(n - 1) - \sum_{i=1}^n f_{r_i} = 6(n - 1) - [6n - \sum_{i=1}^n f_{a_i}].$$

Thus, for $F = 1$, we get $\sum_{i=1}^n f_{a_i} = 7$. For a further discussion on the degrees of freedom and practical applications of spatial linkages, the reader is referred to advanced texts on mechanisms.¹

Simple robotic manipulators, as stated earlier, consist of an open chain of serially connected rigid bodies. At every connection (a kinematic pair), a relative movement is created by an actuator so as to locate and orient the last link (end-effector) suitably. Figures 5.3a-c show the kinematic diagrams of some manipulators having different degrees of freedom. The kinematic study in this case may refer to the determination of the location and orientation of the end-effector when the relative movements at various connections and other relevant geometrical parameters are prescribed. This category of problems is normally called forward kinematics. The inverse problem consists of determining the required joint movements so as to achieve a prescribed location and orientation of the end-effector. The Denavit-Hartenberg (D-H) matrix method, suitable for studying the kinematics of both spatial linkages and robotic arms, will be explained in the sections to follow.

¹For example, Mallik, A.K., Ghosh, A. and Dittrich, G., Kinematic Analysis and Synthesis of Mechanisms, CRC Press, Boca Raton, 1994, and Sandor, G.N. and Erdman, A.G., Advanced Mechanism Design: Analysis and Synthesis, Vol. 2, Prentice-Hall, Englewood Cliffs, New Jersey, 1984.

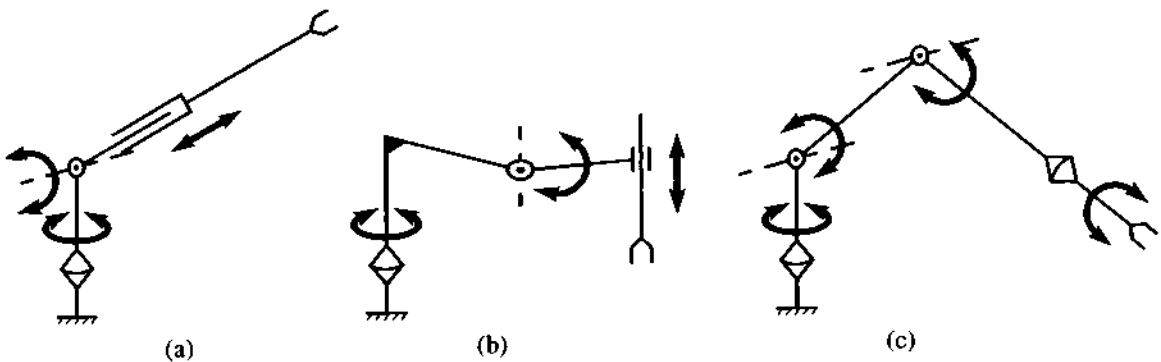


FIGURE 5.3

5.2 MATRIX METHOD

In the matrix method, a cartesian coordinate system is attached to each link following certain conventions. The coordinates of a point in space expressed in two such coordinate systems are related through a 4×4 matrix called the *homogeneous transformation matrix*. The kinematics is studied with the help of the loop-closure equation expressed through these transformation matrices.

Coordinate Transformation

Two cartesian coordinate systems $(XYZ)_1$ and $(XYZ)_2$ with their origins at O_1 and O_2 , respectively, are shown in Fig. 5.4. The coordinates of O_2 in the first system (1) are x'_1 , y'_1 , and z'_1 . Let the coordinates of a point P , expressed in these two systems, be (x_1, y_1, z_1) and (x_2, y_2, z_2) , respectively. These two sets of coordinates are easily seen to be related as

$$\begin{aligned} x_1 &= x'_1 + x_2 \cos(X_2, X_1) + y_2 \cos(Y_2, X_1) + z_2 \cos(Z_2, X_1), \\ y_1 &= y'_1 + x_2 \cos(X_2, Y_1) + y_2 \cos(Y_2, Y_1) + z_2 \cos(Z_2, Y_1), \\ z_1 &= z'_1 + x_2 \cos(X_2, Z_1) + y_2 \cos(Y_2, Z_1) + z_2 \cos(Z_2, Z_1), \end{aligned}$$

where $\cos(.,)$ are the direction cosines of the second set of axes, e.g., $\cos(X_2, X_1)$ is the projection of a unit vector along X_2 on to the X_1 -axis. Adding the identity $1 = 1$ to the above set of three equations, the coordinates of the same point expressed in two sets of axes are related through the matrix equation

$$\begin{Bmatrix} x_1 \\ y_1 \\ z_1 \\ 1 \end{Bmatrix} = \begin{bmatrix} C(X_2, X_1) & C(Y_2, X_1) & C(Z_2, X_1) & x'_1 \\ C(X_2, Y_1) & C(Y_2, Y_1) & C(Z_2, Y_1) & y'_1 \\ C(X_2, Z_1) & C(Y_2, Z_1) & C(Z_2, Z_1) & z'_1 \\ 0 & 0 & 0 & 1 \end{bmatrix} \begin{Bmatrix} x_2 \\ y_2 \\ z_2 \\ 1 \end{Bmatrix} = [A_1] \begin{Bmatrix} x_2 \\ y_2 \\ z_2 \\ 1 \end{Bmatrix}, \quad (5.2)$$

where $C \equiv \cos$.

The 4×4 matrix

$$[A_1] = \begin{bmatrix} C(X_2, X_1) & C(Y_2, X_1) & C(Z_2, X_1) & x'_1 \\ C(X_2, Y_1) & C(Y_2, Y_1) & C(Z_2, Y_1) & y'_1 \\ C(X_2, Z_1) & C(Y_2, Z_1) & C(Z_2, Z_1) & z'_1 \\ 0 & 0 & 0 & 1 \end{bmatrix} \quad (5.3)$$

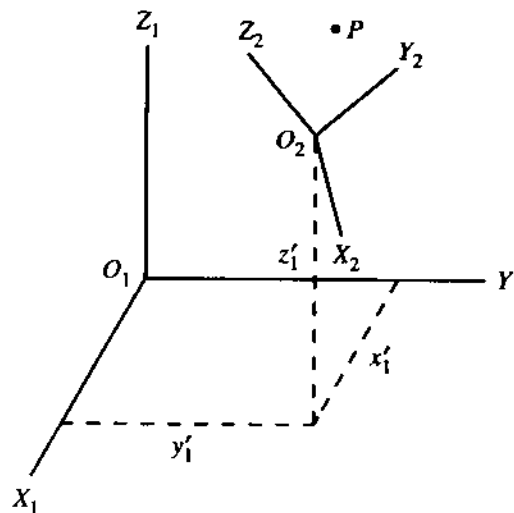


FIGURE 5.4

is called the *homogeneous transformation matrix* which simultaneously accounts for both translation (change of origin) and rotation of a coordinate system. Out of the 12 elements of $[A_1]$, discounting the fourth row, only six are independent. The coordinates of O_2 , i.e., x'_1 , y'_1 , and z'_1 , are independent, and only three of the nine direction cosines can be independent. This is because X_2 , Y_2 , and Z_2 are orthogonal to one another and squares of the direction cosines of a line must add up to 1. Therefore six equations need to be satisfied by these nine direction cosines.

From (5.2), we can write

$$\begin{Bmatrix} x_2 \\ y_2 \\ z_2 \\ 1 \end{Bmatrix} = [A_1]^{-1} \begin{Bmatrix} x_1 \\ y_1 \\ z_1 \\ 1 \end{Bmatrix}, \quad (5.4)$$

where $[A_1]^{-1}$ is given by

$$[A_1]^{-1} = \begin{bmatrix} C(X_2, X_1) & C(X_2, Y_1) & C(X_2, Z_1) & -d_1 \\ C(Y_2, X_1) & C(Y_2, Y_1) & C(Y_2, Z_1) & -d_2 \\ C(Z_2, X_1) & C(Z_2, Y_1) & C(Z_2, Z_1) & -d_3 \\ 0 & 0 & 0 & 1 \end{bmatrix}, \quad (5.5)$$

with

$$d_1 = x'_1 C(X_2, X_1) + y'_1 C(X_2, Y_1) + z'_1 C(X_2, Z_1),$$

$$d_2 = x'_1 C(Y_2, X_1) + y'_1 C(Y_2, Y_1) + z'_1 C(Y_2, Z_1),$$

$$d_3 = x'_1 C(Z_2, X_1) + y'_1 C(Z_2, Y_1) + z'_1 C(Z_2, Z_1).$$

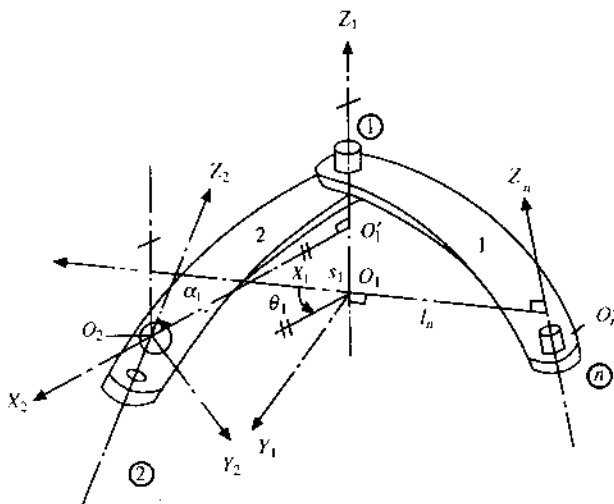


FIGURE 5.5

Since the direction cosines are the projections of a unit vector, we can easily verify that (5.3) and (5.5) can be written, respectively, as

$$[A_1] = \begin{bmatrix} e_{11} & e_{21} & e_{31} & (\vec{O_1 O_2})_1 \\ e_{12} & e_{22} & e_{32} & (\vec{O_1 O_2})_2 \\ e_{13} & e_{23} & e_{33} & (\vec{O_1 O_2})_3 \\ 0 & 0 & 0 & 1 \end{bmatrix}, \quad (5.6)$$

$$[A_1]^{-1} = \begin{bmatrix} e_{11} & e_{12} & e_{13} & -(\vec{O_1 O_2} \cdot e_1) \\ e_{21} & e_{22} & e_{23} & -(\vec{O_1 O_2} \cdot e_2) \\ e_{31} & e_{32} & e_{33} & -(\vec{O_1 O_2} \cdot e_3) \\ 0 & 0 & 0 & 1 \end{bmatrix}, \quad (5.7)$$

where e_1 , e_2 , and e_3 are unit vectors along the axes X_2 , Y_2 , and Z_2 and the second subscripts 1, 2, and 3 refer to the component along X_1 , Y_1 , and Z_1 , respectively. We should note that the elements of the first three rows and columns of $[A_1]^{-1}$ can be obtained by transposing (i.e., interchanging rows and columns) the corresponding part of $[A_1]$.

Link Coordinate System

As stated earlier, to use the matrix method, we need to attach a coordinate system to every link of the mechanism. These coordinate systems are established in a systematic manner following certain conventions which are now explained.

Let us consider two consecutive links 1 and 2 which are connected by a cylindric pair 1 as shown in Fig. 5.5. The pair between links 2 and 3 is numbered 2 and that between the last link and link

1 is numbered n . The axis of each pair is taken as the Z -axis with its positive direction chosen arbitrarily. Thus, the axes Z_n , Z_1 , and Z_2 are obtained. The axis X_1 is along the common normal of Z_n and Z_1 , with its positive direction oriented from Z_n to Z_1 . The axis Y_1 is chosen so as to complete a right-hand coordinate system $X_1Y_1Z_1$ at the origin O_1 (which is the point of intersection of X_1 and Z_1). Similarly, all the coordinate systems (one at each link) are established. With these coordinate systems ($X_iY_iZ_i$'s), the link parameters and pair variables (describing the relative movements between the links connected at that pair) are defined as follows (see Fig. 5.5):

- (i) The link length l_1 is the distance between Z_1 and Z_2 measured along X_2 ($= O'_1O_2$) and is seen to be always positive.
- (ii) The link twist α_1 is the angle through which Z_1 must rotate about positive X_2 -axis in order to be parallel to Z_2 .
- (iii) The pair variable θ_1 is the relative rotation permitted at pair 1 between links 1 and 2. The rotation of X_1 about positive Z_1 needed to make it parallel to X_2 is the measure of θ_1 .
- (iv) The pair variable s_1 is the relative translation permitted at pair 1 between links 1 and 2. The distance of X_2 from X_1 along positive Z_1 is the measure of s_1 . It can be both positive or negative. In Fig. 5.5, $s_1 = O_1O'_1$ and is positive.

It should be noted that if the kinematic pair is a revolute joint, then s_1 is constant and is no longer a pair variable. Similarly, if the kinematic pair is a prismatic joint, then θ_1 is constant and is no longer a pair variable. Moreover, for a prismatic joint, only the direction of Z -axis is important and it can be conveniently located anywhere maintaining its proper direction. For a screw pair the pair variables θ and s are not independent. These two are related through the expression $\Delta\theta/(2\pi) = \Delta s/L$, where L is the lead of the screw. All other lower pairs can be thought of as combinations of R- and/or P-pairs and the methodology we have explained can be used to establish the link coordinate systems. Now we shall derive the homogeneous transformation matrix relating the coordinate systems $(XYZ)_1$ and $(XYZ)_2$ shown in Fig. 5.4. The elements of the matrix $[A]$ will be expressed in terms of link length, link twist, and pair variables.

Homogeneous Transformation Matrix

Two cartesian coordinate systems can always be related through translation and rotation operators. Since the kinematic pairs also allow various translations and rotations, the homogeneous transformation matrix between successive link coordinate systems can be easily derived through translation and rotation operators as now explained.

Let a coordinate system $(XYZ)_1$ undergo the translations Δx , Δy , Δz along the axes X_1 , Y_1 , Z_1 respectively, to produce another coordinate system $(XYZ)_2$ as shown in Fig. 5.6. The coordinates of any point P in these two coordinate systems are simply related as

$$x_1 = x_2 + \Delta x, \quad y_1 = y_2 + \Delta y, \quad \text{and} \quad z_1 = z_2 + \Delta z.$$

Adding the identity $1 = 1$ to these three equations, the two sets of coordinates can be related through matrix notation as

$$\begin{Bmatrix} x \\ y \\ z \\ 1 \end{Bmatrix}_1 = \begin{bmatrix} 1 & 0 & 0 & \Delta x \\ 0 & 1 & 0 & \Delta y \\ 0 & 0 & 1 & \Delta z \\ 0 & 0 & 0 & 1 \end{bmatrix} \begin{Bmatrix} x \\ y \\ z \\ 1 \end{Bmatrix}_2 = [T(\Delta x, \Delta y, \Delta z)] \begin{Bmatrix} x \\ y \\ z \\ 1 \end{Bmatrix}_2. \quad (5.8)$$

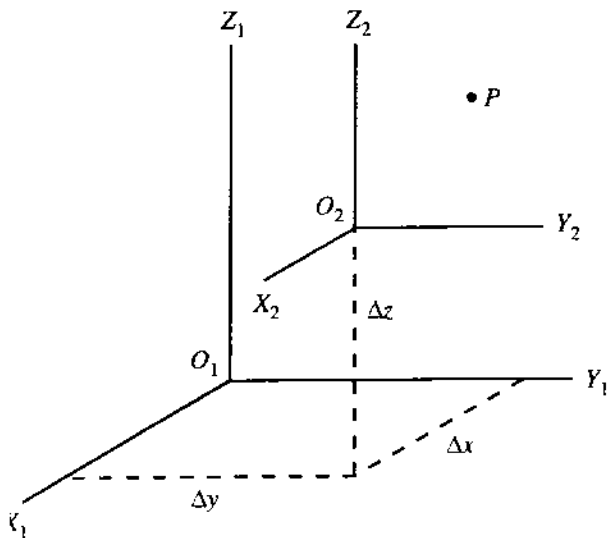


FIGURE 5.6

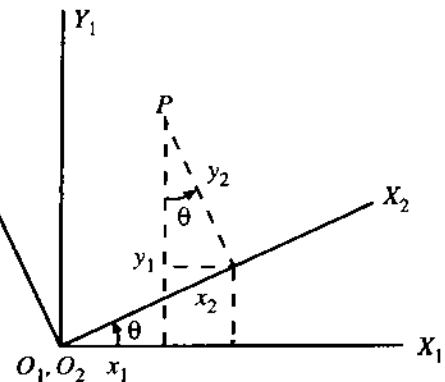


FIGURE 5.7

where $[T(\Delta x, \Delta y, \Delta z)]$ is the translation operator defined as

$$[T(\Delta x, \Delta y, \Delta z)] = \begin{bmatrix} 1 & 0 & 0 & \Delta x \\ 0 & 1 & 0 & \Delta y \\ 0 & 0 & 1 & \Delta z \\ 0 & 0 & 0 & 1 \end{bmatrix}. \quad (5.9)$$

Next, let us consider a rotation operator. Referring to Fig. 5.7, let a coordinate system $(XYZ)_1$ move to $(XYZ)_2$ by rotating about Z_1 through an angle θ . Thus, the origins O_1 and O_2 and the axes Z_1 and Z_2 remain the same. The coordinates of a point P in the two coordinate systems can be related as

$$\begin{aligned} x_1 &= x_2 \cos \theta - y_2 \sin \theta, \\ y_1 &= x_2 \sin \theta + y_2 \cos \theta, \\ z_1 &= z_2. \end{aligned}$$

As usual, in matrix notation these relationships are expressed as

$$\begin{Bmatrix} x \\ y \\ z \\ 1 \end{Bmatrix}_1 = \begin{bmatrix} \cos \theta & -\sin \theta & 0 & 0 \\ \sin \theta & \cos \theta & 0 & 0 \\ 0 & 0 & 1 & 0 \\ 0 & 0 & 0 & 1 \end{bmatrix} \begin{Bmatrix} x \\ y \\ z \\ 1 \end{Bmatrix}_2 = [R(\theta, z)] \begin{Bmatrix} x \\ y \\ z \\ 1 \end{Bmatrix}_2, \quad (5.10)$$

where $[R(\theta, z)]$ is the rotation operator defined as

$$[R(\theta, z)] = \begin{bmatrix} \cos \theta & -\sin \theta & 0 & 0 \\ \sin \theta & \cos \theta & 0 & 0 \\ 0 & 0 & 1 & 0 \\ 0 & 0 & 0 & 1 \end{bmatrix}. \quad (5.11)$$

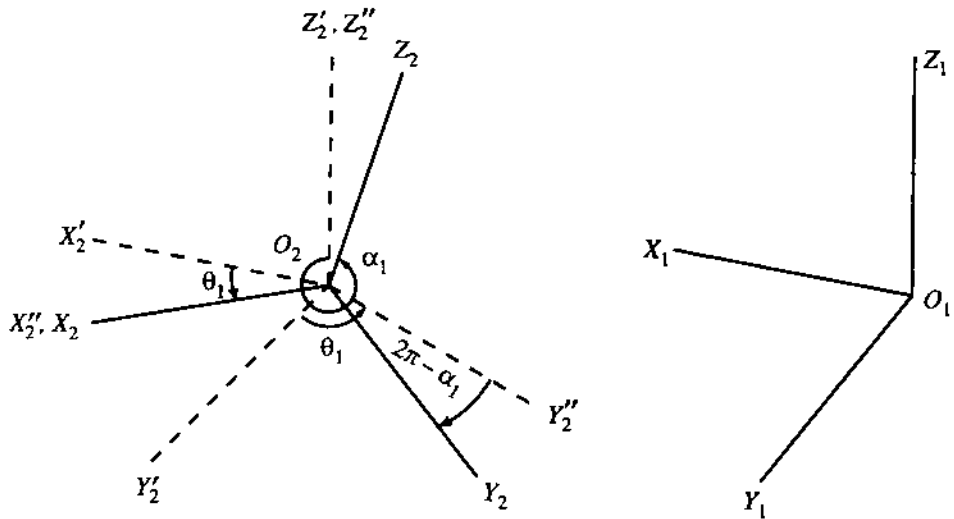


FIGURE 5.8

The reader can verify that the rotation operators signifying the rotations about the axes X_1 and Y_1 can be similarly obtained and are given, respectively, by

$$[R(\theta, x)] = \begin{bmatrix} 1 & 0 & 0 & 0 \\ 0 & \cos \theta & -\sin \theta & 0 \\ 0 & \sin \theta & \cos \theta & 0 \\ 0 & 0 & 0 & 1 \end{bmatrix}, \quad (5.12)$$

$$[R(\theta, y)] = \begin{bmatrix} \cos \theta & 0 & \sin \theta & 0 \\ 0 & 1 & 0 & 0 \\ -\sin \theta & 0 & \cos \theta & 0 \\ 0 & 0 & 0 & 1 \end{bmatrix}. \quad (5.13)$$

The implication of these operators should be clearly understood. These operators signify translations and rotations in the old (1) coordinate system; when premultiplied by these operators, the new coordinates (2) give the old coordinates (1). It should be further pointed out that, unlike the translational operators, the rotational operators are not commutative, i.e., their orders are important. In other words, $[R_i][R_j] \neq [R_j][R_i]$, where R_i and R_j are not about the same axes.

We shall now use the translation and rotation operators to obtain the homogeneous transformation matrix, say, $[A_1]$, correlating the link coordinate systems $(XYZ)_1$ and $(XYZ)_2$ shown in Fig. 5.5. As explained in Fig. 5.8 (also see Fig. 5.5), the system $(XYZ)_1$ can be brought to (XYZ) by the following sequence of movements:

- (i) $[T(l_1 \cos \theta_1, l_1 \sin \theta_1, s_1)]$ moves $(XYZ)_1$ to $(XYZ)'_2$,
- (ii) $[R(\theta_1, z'_2)]$ moves $(XYZ)'_2$ to $(XYZ)''_2$, and
- (iii) $[R(\alpha_1, x''_2)]$ moves $(XYZ)''_2$ to $(XYZ)_2$.

Using (5.9), (5.11), and (5.12), we get

$$[T(l_1 \cos \theta_1, l_1 \sin \theta_1, s_1)] = \begin{bmatrix} 1 & 0 & 0 & l_1 \cos \theta_1 \\ 0 & 1 & 0 & l_1 \sin \theta_1 \\ 0 & 0 & 1 & s_1 \\ 0 & 0 & 0 & 1 \end{bmatrix}, \quad (5.14)$$

$$[R(\theta_1, z'_2)] = \begin{bmatrix} \cos \theta_1 & -\sin \theta_1 & 0 & 0 \\ \sin \theta_1 & \cos \theta_1 & 0 & 0 \\ 0 & 0 & 1 & 0 \\ 0 & 0 & 0 & 1 \end{bmatrix}, \quad (5.15)$$

$$[R(\alpha_1, x''_2)] = \begin{bmatrix} 1 & 0 & 0 & 0 \\ 0 & \cos \alpha_1 & -\sin \alpha_1 & 0 \\ 0 & \sin \alpha_1 & \cos \alpha_1 & 0 \\ 0 & 0 & 0 & 1 \end{bmatrix}. \quad (5.16)$$

If the homogeneous transformation matrix $[A_1]$ correlates $(XYZ)_1$ and $(XYZ)_2$ as

$$\left\{ \begin{array}{c} x \\ y \\ z \\ 1 \end{array} \right\}_1 = [A_1] \left\{ \begin{array}{c} x \\ y \\ z \\ 1 \end{array} \right\}_2, \quad (5.17)$$

then

$$[A_1] = [T(l_1 \cos \theta_1, l_1 \sin \theta_1, s_1)][R(\theta_1, z'_2)][R(\alpha_1, x''_2)]. \quad (5.18)$$

Using (5.14), (5.15), and (5.16) in (5.18), the reader can verify that

$$[A_1] = \begin{bmatrix} \cos \theta_1 & -\cos \alpha_1 \sin \theta_1 & \sin \alpha_1 \sin \theta_1 & l_1 \cos \theta_1 \\ \sin \theta_1 & \cos \alpha_1 \cos \theta_1 & -\sin \alpha_1 \cos \theta_1 & l_1 \sin \theta_1 \\ 0 & \sin \alpha_1 & \cos \alpha_1 & s_1 \\ 0 & 0 & 0 & 1 \end{bmatrix}. \quad (5.19)$$

Thus, finally we get, for the i -th pair,

$$\left\{ \begin{array}{c} x \\ y \\ z \\ 1 \end{array} \right\}_i = [A_i] \left\{ \begin{array}{c} x \\ y \\ z \\ 1 \end{array} \right\}_{i+1}, \quad (5.20)$$

where

$$[A_i] = \begin{bmatrix} \cos \theta_i & -\cos \alpha_i \sin \theta_i & \sin \alpha_i \sin \theta_i & l_i \cos \theta_i \\ \sin \theta_i & \cos \alpha_i \cos \theta_i & -\sin \alpha_i \cos \theta_i & l_i \sin \theta_i \\ 0 & \sin \alpha_i & \cos \alpha_i & s_i \\ 0 & 0 & 0 & 1 \end{bmatrix}. \quad (5.21)$$

It may be emphasized that according to the convention that has been followed, the subscript of the motion variables and link parameters corresponds to the number of the kinematic pair (rather than that of the link as used for planar linkages). If link 1 is the fixed link, then the input and output motion variables will have subscripts 1 and n , respectively, and the length of the fixed link will be l_n (rather than l_1).

5.3 LOOP-CLOSURE EQUATION

The kinematic study of spatial linkages is based on the loop-closure equation. For a simple spatial linkage, let there be only one closed loop consisting of only binary links. Then, if we start from link 1 and follow the loop through links 2, 3, ..., n and return to 1, we can write the loop-closure equations in terms of the matrices $[A]$ as

$$[A_1][A_2][A_3] \dots [A_n] = [I], \quad (5.22)$$

where $[I]$ is a 4×4 identity matrix given by

$$[I] = \begin{bmatrix} 1 & 0 & 0 & 0 \\ 0 & 1 & 0 & 0 \\ 0 & 0 & 1 & 0 \\ 0 & 0 & 0 & 1 \end{bmatrix}. \quad (5.23)$$

Equating element by element of both sides of (5.22), we obtain the relationships between the motion (pair) variables in terms of link parameters. It should be noted that since the fourth row of each matrix $[A]$ is $(0, 0, 0, 1)$, equating the elements of the fourth row of (5.22) leads to the identities $0 \equiv 0$ and $1 \equiv 1$. Of the remaining 12 elements of the matrix $[A]$, not all are independent. Consequently, equating the elements of the matrix equation (5.22) we do not get independent equations. The elements to be equated vary from problem to problem. The resulting equations, in general, are highly nonlinear and can be solved only numerically. In some exceptionally simple situations, the resulting equations can be algebraically manipulated to yield explicit (displacement) equation for a particular motion variable. A few examples of this latter type follow.

PROBLEM 5.1

Figure 5.9 shows a 4R spherical mechanism.² Derive the output (θ_4)-input (θ_1) relationship in terms of the angles α_i 's.

SOLUTION

First, all the Z-axes are established along the axes of the revolute joints with their positive directions chosen arbitrarily. Since all the Z-axes are intersecting, all the link-length parameters, i.e., l_i 's with $i = 1, 2, 3$, and 4, are zero and the positive directions of the X_i -axes with $i = 1, 2, 3$, and 4 are also chosen arbitrarily. With the X_i - and Z_i -axes so determined, we get the link twists α_i 's as indicated in Fig. 5.9. The input variable is θ_1 (Fig. 5.9) which is the required rotation of X_1 about Z_1 for it to coincide with X_2 . The output variable is θ_4 which is the required rotation of X_4 about Z_4 for it to coincide with X_1 (Fig. 5.9). Since all the X_i -axes are intersecting, $s_i = 0$ for $i = 1, 2, 3$, and 4.

²The revolute axes of a spherical mechanism intersect at a point. Each free link has three degrees of freedom (remember that each free link in a planar linkage has also three degrees of freedom). Here, of course, all the three are rotational degrees of freedom. Thus, it is not a generalized spatial linkage in which each free link has six degrees of freedom. In fact, using spherical trigonometry, the counterparts of some well-known features of planar linkages have also been obtained for spherical linkages. For more details, see Chiang, C.H., Kinematics of Spherical Mechanisms Cambridge University Press, Cambridge, 1988.

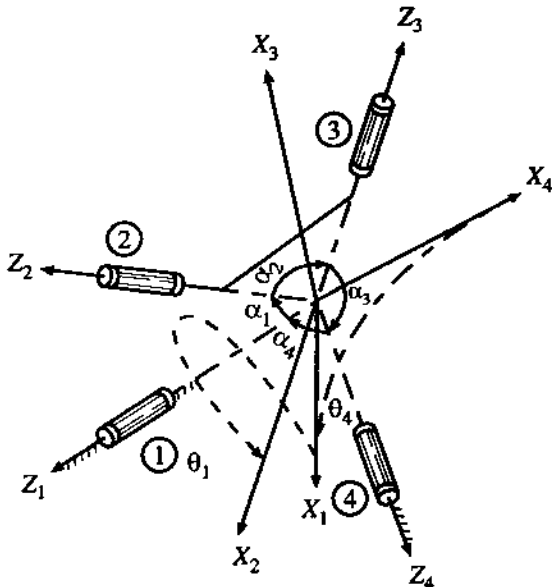


FIGURE 5.9

Now, with $l_i = s_i = 0$, from (5.21), we get, for this mechanism,

$$[A_i] = \begin{bmatrix} C\theta_i & -C\alpha_i S\theta_i & S\alpha_i S\theta_i & 0 \\ S\theta_i & C\alpha_i C\theta_i & -S\alpha_i C\theta_i & 0 \\ 0 & S\alpha_i & C\alpha_i & 0 \\ 0 & 0 & 0 & 1 \end{bmatrix}, \quad (a)$$

where $C \equiv \cos$ and $S \equiv \sin$. Using (5.7), we have

$$[A_i]^{-1} = \begin{bmatrix} C\theta_i & S\theta_i & 0 & 0 \\ -C\alpha_i S\theta_i & C\alpha_i C\theta_i & S\alpha_i & 0 \\ S\alpha_i S\theta_i & -S\alpha_i C\theta_i & C\alpha_i & 0 \\ 0 & 0 & 0 & 1 \end{bmatrix}. \quad (b)$$

(In this particular case, $[A_1]^{-1} = [A_i]^T$.) From (5.22),

$$[A_1][A_2][A_3][A_4] = [I]$$

or

$$[A_3][A_4] = [A_2]^{-1}[A_1]^{-1}. \quad (c)$$

Using (a) and (b) in (c), we get a matrix equation where each side is a 4×4 matrix. Carrying out the algebra and equating the corresponding elements of the third row of both sides of (c), we obtain

$$S\alpha_3 S\theta_4 = S\alpha_2 S\theta_2 C\theta_1 + C\alpha_1 S\alpha_2 C\theta_2 S\theta_1 + S\alpha_1 C\alpha_2 S\theta_1, \quad (d)$$

$$S\alpha_3 C\alpha_4 C\theta_4 + C\alpha_3 S\alpha_4 = S\alpha_2 S\theta_2 C\theta_1 - C\alpha_1 S\alpha_2 C\theta_2 C\theta_1 - S\alpha_1 C\alpha_2 C\theta_1, \quad (e)$$

$$C\alpha_3 C\alpha_4 - S\alpha_3 S\alpha_4 C\theta_4 = C\alpha_1 C\alpha_2 - S\alpha_1 S\alpha_2 C\theta_2. \quad (f)$$

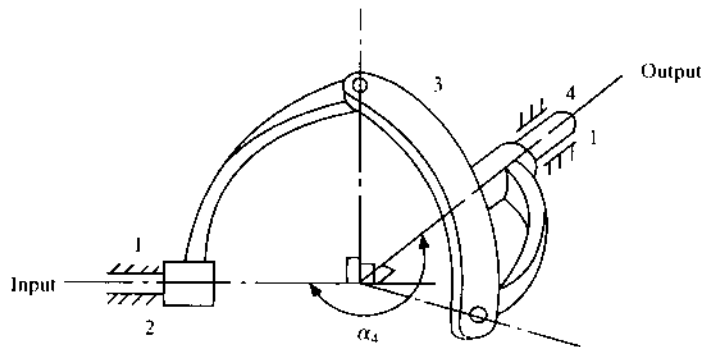


FIGURE 5.10

The elements of the third row were chosen because these elements do not contain θ_3 . To derive the $\theta_4-\theta_1$ relationship, we have to eliminate θ_2 from (d), (e), and (f). Solving for $S\alpha_2C\theta_2$ from (f) and then $S\alpha_2S\theta_2$ from (d) and substituting these in (e), we finally get the output (θ_4)-input (θ_1) relationship as

$$C\alpha_4C\theta_4C\theta_1 - S\theta_4S\theta_1 = \cot\alpha_1 \cot\alpha_3 C\alpha_4 - \frac{C\alpha_2}{S\alpha_1S\alpha_3} - \cot\alpha_1 S\alpha_4C\theta_4 - \cot\alpha_3 S\alpha_4C\theta_1. \quad (g)$$

PROBLEM 5.2

Hooke's joint, shown in Fig. 5.10, is a special case of a 4R spherical mechanism where the shaft angle is α_4 with $\alpha_1 = \alpha_2 = \alpha_3 = \pi/2$. Determine the angular velocity ($\dot{\theta}_4$) and angular acceleration ($\ddot{\theta}_4$) of the output shaft as a function of α_4 , θ_1 and the constant angular velocity of the input shaft $\dot{\theta}_1$.

SOLUTION

With $\alpha_1 = \alpha_2 = \alpha_3 = \pi/2$, from (g) of solution to Problem 5.1, we get

$$\tan\theta_4 = C\alpha_4 \cot\theta_1. \quad (a)$$

Differentiating both sides of (a) with respect to time, we obtain

$$\sec^2\theta_4\dot{\theta}_4 = -C\alpha_4 \operatorname{cosec}^2\theta_1\dot{\theta}_1. \quad (b)$$

Using (a) in (b), we have

$$\dot{\theta}_4 = -\frac{C\alpha_4}{S^2\theta_1 + C^2\alpha_4C^2\theta_1}\dot{\theta}_1. \quad (c)$$

Differentiating both sides of (c) with respect to time, we obtain (with $\ddot{\theta}_1 = 0$)

$$\ddot{\theta}_4 = \frac{C\alpha_4(1 - C^2\alpha_4)S(2\theta_1)}{(S^2\theta_1 + C^2\alpha_4C^2\theta_1)^2}\dot{\theta}_1^2. \quad (d)$$

The reader should note that for a constant angular speed of the driving shaft the speed of the output shaft is not constant but fluctuating. This difficulty can be eliminated if two Hooke's joints are used in series with a proper adjustment of the geometric parameters.

PROBLEM 5.3

Design a 4R spherical mechanism to generate $y = \log_{10} x$ in the interval $1 \leq x \leq 10$. Use three Chebyshev's accuracy points. Assume $\theta_1^i = 45^\circ$, $\theta_4^i = 135^\circ$, $\theta_2^f = 105^\circ$, and $\theta_4^f = 225^\circ$.

SOLUTION

With three accuracy points, we leave out three design parameters α_1 , α_2 , and α_3 as unknowns and assume the value of α_4 ($= \pi/2$, say). As will be seen shortly, the synthesis problem can be handled through a set of three linear equations with this choice of design parameters.

From the solution of Problem 3.5, the three desired coordinate pairs of movements are obtained as $(\theta_1^1 = 101^\circ, \theta_4^1 = 222.7^\circ)$, $(\theta_1^2 = 75^\circ, \theta_4^2 = 201.7^\circ)$, and $(\theta_1^3 = 49^\circ, \theta_4^3 = 153.4^\circ)$.

Now substituting $\alpha_4 = \pi/2$ in (g) of Problem 5.1, the displacement equation (corresponding to the j -th accuracy point) is written as

$$\cot \alpha_1 C\theta_4^j + \cot \alpha_3 C\theta_1^j + \frac{C\alpha_2}{S\alpha_1 S\alpha_3} = S\theta_4^j S\theta_1^j.$$

Rewriting this, we get

$$K_1 \cos \theta_4^j + K_2 \cos \theta_1^j + K_3 = \sin \theta_4^j \sin \theta_1^j, \quad j = 1, 2, 3, \quad (\text{a})$$

where

$$K_1 = \cot \alpha_1, \quad K_2 = \cot \alpha_3, \quad K_3 = \frac{\cos \alpha_2}{\sin \alpha_1 \sin \alpha_3}. \quad (\text{b})$$

Substituting the values of θ_1^j 's and θ_4^j 's in (a), the set of linear equations in K_1 , K_2 , and K_3 we obtain are

$$-0.7349K_1 - 0.1908K_2 + K_3 = -0.6535, \quad (\text{c})$$

$$-0.9291K_1 + 0.2588K_2 + K_3 = -0.3572, \quad (\text{d})$$

$$-0.8942K_1 + 0.6561K_2 + K_3 = 0.3379. \quad (\text{e})$$

Solving (c), (d), and (e), we get

$$K_1 = 2.097, \quad K_2 = 1.565, \quad K_3 = 1.186$$

when, from (b), the design parameters are obtained as³ $\alpha_1 = 25.5^\circ$, $\alpha_3 = 32.58^\circ$, $\alpha_2 = 74.05^\circ$.

5.4 KINEMATICS OF OPEN CHAINS

The study of open kinematic chains has gained considerable importance with the advent of robot technology. Most of the industrial and other robot manipulators are based upon an open kinematic structure with the operational unit (called the end-effector) placed at the end of the open chain. The primary objective of a manipulator is to place the end-effector at a desired location and orient it in a desired manner. This requires the manipulator to possess six degrees of freedom, i.e., there are six independently-driven single-degree-of-freedom joints in the chain. Controlling the joints with cylindrical and spherical pairs is technically very complicated, and therefore only revolute and

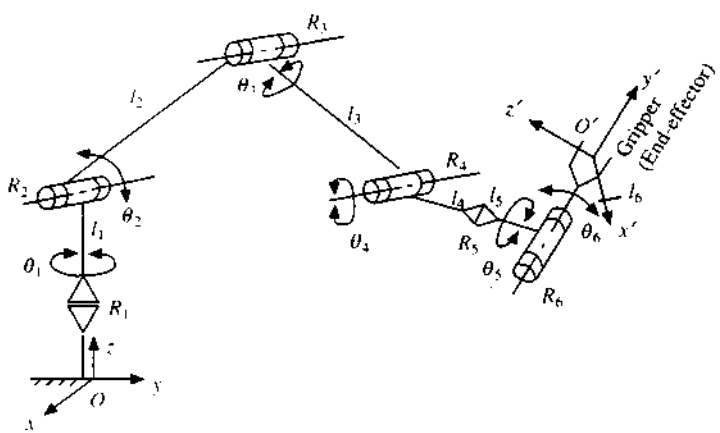


FIGURE 5.11

prismatic pairs are employed for joining consecutive links. Figure 5.11 shows a typical open chain for a six-degree-of-freedom robot having revolute pairs only.

As already mentioned at the beginning of this chapter, there are two basic problems in kinematics of such open chains – (i) to determine the position and orientation of the end link for given joint variables (θ 's in the example shown), known as forward kinematics, and (ii) to determine the joint variables when the position and orientation of the end link (i.e., the end-effector) are prescribed, usually termed as inverse kinematics. In this chapter, our discussion will be limited to displacement analysis only. To mathematically describe the location and orientation of the end-effector, the most convenient approach is to attach a coordinate system to the end-effector (the end link). Then describe this coordinate system (xyz) in the base frame ($x_1y_1z_1$) with the help of a transformation matrix. The elements of the transformation matrix are functions of the link parameters and the joint variables.

Before proceeding, it should be noted that a homogeneous transformation matrix can be considered as a representation of a coordinate system itself. Let a matrix $[A]$ be written as

$$[A] = \begin{bmatrix} x_x & y_x & z_x & p_x \\ x_y & y_y & z_y & p_y \\ x_z & y_z & z_z & p_z \\ 0 & 0 & 0 & 1 \end{bmatrix}. \quad (5.24)$$

Figure 5.12 shows two coordinate systems. The system (1) is the reference coordinate system and the unit vectors

$$x = x_x i + x_y j + x_z k,$$

$$y = y_x i + y_y j + y_z k,$$

$$z = z_x i + z_y j + z_z k$$

³For synthesis of a 4R spherical mechanism to generate symmetric functions like $y = x^2, -1 \leq x \leq 1$, see Hartenberg, R.S. and Denavit, J., Kinematic Synthesis of Linkages, McGraw-Hill, New York, 1964.

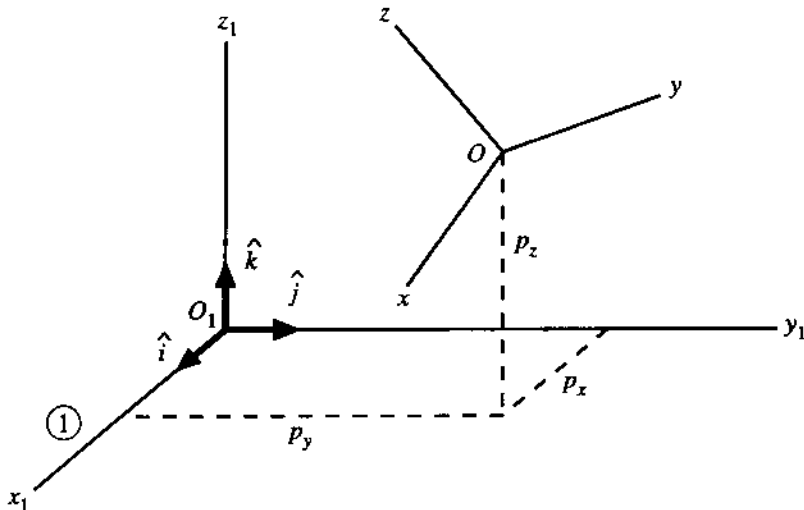


FIGURE 5.12

represent the directions of the axes x , y , and z of the new coordinate system.⁴ The vector

$$\mathbf{p} = p_x \mathbf{i} + p_y \mathbf{j} + p_z \mathbf{k}$$

represents the location of the origin of the new coordinate system, O , with respect to the reference coordinate. The matrix $[A_i]$ given in (5.21) also represents the description of the $(i+1)$ -th coordinate system in the i -th coordinate system.⁵ Now, the position and orientation of the $(n+1)$ -th coordinate system in the base coordinate system can be represented as

$$[T_n] = [A_1][A_2]\dots[A_n]. \quad (5.25)$$

A six-degree-of-freedom manipulator consists of six joints and six moving links. So, the description of the coordinate system embedded in the end-effector in the base coordinate system is given by

$$[T_6] = [A_1][A_2][A_3][A_4][A_5][A_6]. \quad (5.26)$$

The elements of the matrices $[A]$ can be determined in terms of the respective link parameters and the joint variables.

PROBLEM 5.4

Figure 5.13a shows a three-link manipulator. Express the position and orientation of the end link in the base coordinate system as a function of the joint variables and link parameters.

SOLUTION

The origins of the base coordinate system and the second coordinate system (attached to link 2) are chosen at the intersection of the axes of the first and the second revolute pairs. Following the established convention, the joint variables are as tabulated.

⁴In other words, x_x , x_y , and x_z represent the direction cosines of the x -axis with reference to the base frame.

⁵Consider the $(n+1)$ -th coordinate system, embedded in the $(n+1)$ -th link which is connected to the base coordinate system through n kinematic pairs.

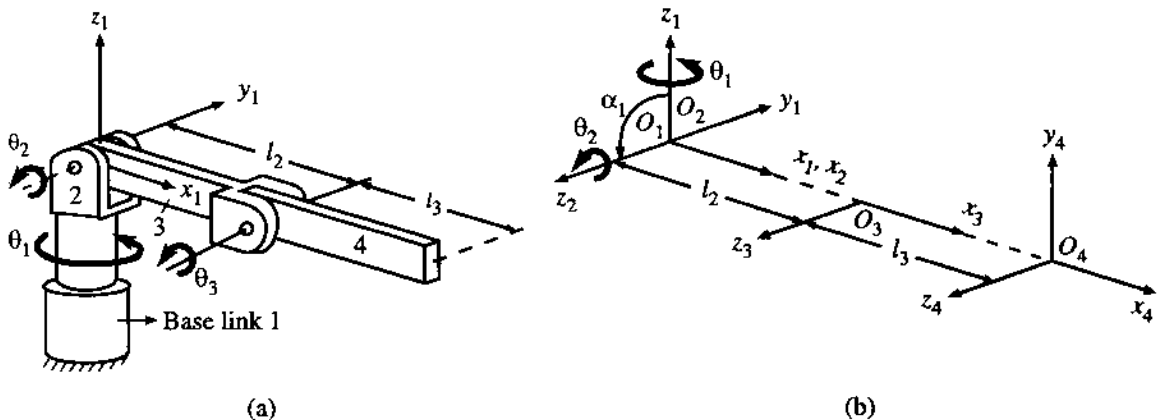


FIGURE 5.13

Link	Pair/ Joint	Pair/ Joint variable	Link parameters			$\cos \alpha$	$\sin \alpha$
			α	l	s		
2	1	θ_1	90°	0	0	0	1
3	2	θ_2	0°	l_2	0	1	0
4	3	θ_3	0°	l_3	0	1	0

The three matrices $[A]$ are then

$$[A_1] = \begin{bmatrix} C_1 & 0 & S_1 & 0 \\ S_1 & 0 & -C_1 & 0 \\ 0 & 1 & 0 & 0 \\ 0 & 0 & 0 & 1 \end{bmatrix},$$

$$[A_2] = \begin{bmatrix} C_2 & -S_2 & 0 & l_2 C_2 \\ S_2 & C_2 & 0 & l_2 S_2 \\ 0 & 0 & 1 & 0 \\ 0 & 0 & 0 & 1 \end{bmatrix},$$

$$[A_3] = \begin{bmatrix} C_3 & -S_3 & 0 & l_3 C_3 \\ S_3 & C_3 & 0 & l_3 S_3 \\ 0 & 0 & 1 & 0 \\ 0 & 0 & 0 & 1 \end{bmatrix},$$

where $C_i \equiv \cos \theta_i$, $S_i \equiv \sin \theta_i$.

The position and orientation of the coordinate system embedded in link 4 can be expressed as

$$[T_3] = [A_1][A_2][A_3] = \begin{bmatrix} C_1 C_{23} & -C_1 S_{23} & S_1 & C_1(l_3 C_{23} + l_2 C_2) \\ S_1 C_{23} & -S_1 S_{23} & -C_1 & S_1(l_3 C_{23} + l_2 C_2) \\ S_{23} & C_{23} & 0 & l_2 C_{23} + l_2 C_2 \\ 0 & 0 & 0 & 1 \end{bmatrix},$$

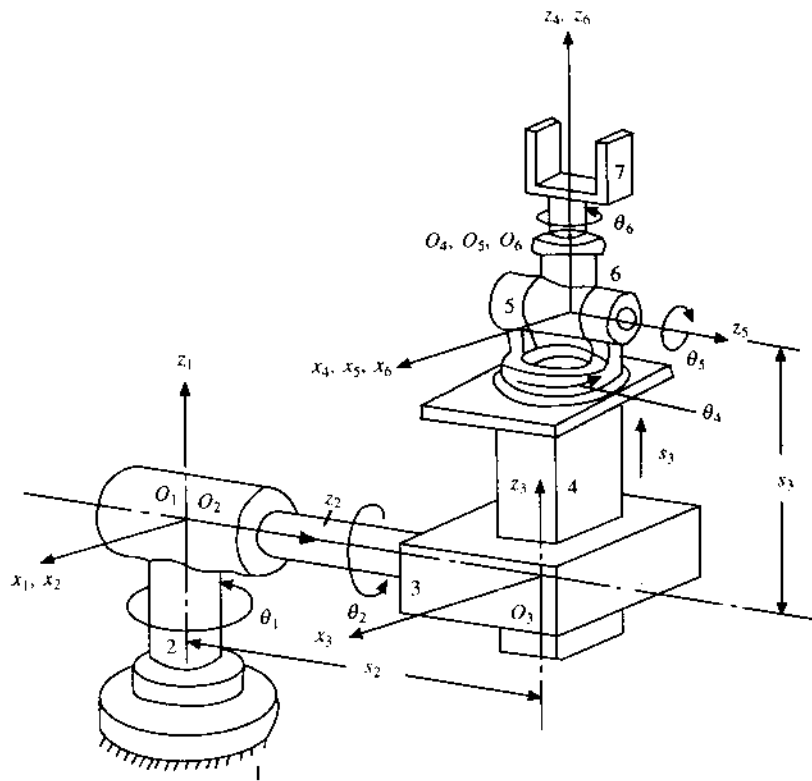


FIGURE 5.14

where $C_{ij} \equiv \cos \theta_i \cos \theta_j$ and so on.

Comparing the elements of $[T_3]$ with those in the RHS of (5.24), the location of the origin O_4 and the directions of the axes x_4 , y_4 , and z_4 are obtained.

PROBLEM 5.5

Figure 5.14 shows a six-degree-of-freedom Stanford manipulator. Express the position and orientation of the end link in terms of the joint variables and link parameters.

SOLUTION

It should be noted that joints 1, 2, 4, 5, and 6 are revolute joints whereas joint 3 is a prismatic one. The intersection of the axes of joints 1 and 2 is chosen as the origins of the base coordinate system $x_1y_1z_1$ and the second coordinate system $x_2y_2z_2$. Again, the intersection of the axes of joints 4, 5, and 6 is taken as the origins O_4 , O_5 , and O_6 . Figure 5.14 indicates the various coordinate systems, and important dimensions as per the convention are given in the table that follows.

Link	Pair/ Joint	Pair/ Joint variable	Link parameters			$\cos \alpha$	$\sin \alpha$
			α	l	s		
2	1	θ_1	-90°	0	0	0	-1
3	2	θ_2	90°	0	s_2	0	1
4	3	s_3	0	0	s_3	1	0
5	4	θ_4	-90°	0	0	0	-1
6	5	θ_5	90°	0	0	0	1
7	6	θ_6	0°	0	0	1	0

The matrices $[A]$ are

$$[A_1] = \begin{bmatrix} C_1 & 0 & -S_1 & 0 \\ S_1 & 0 & C_1 & 0 \\ 0 & -1 & 0 & 0 \\ 0 & 0 & 0 & 1 \end{bmatrix}, [A_2] = \begin{bmatrix} C_2 & 0 & S_2 & 0 \\ S_2 & 0 & -C_2 & 0 \\ 0 & 1 & 0 & s_2 \\ 0 & 0 & 0 & 1 \end{bmatrix}, [A_3] = \begin{bmatrix} 1 & 0 & 0 & 0 \\ 0 & 1 & 0 & 0 \\ 0 & 0 & 1 & s_3 \\ 0 & 0 & 0 & 1 \end{bmatrix},$$

$$[A_4] = \begin{bmatrix} C_4 & 0 & -S_4 & 0 \\ S_4 & 0 & C_4 & 0 \\ 0 & -1 & 0 & 0 \\ 0 & 0 & 0 & 1 \end{bmatrix}, [A_5] = \begin{bmatrix} C_5 & 0 & S_5 & 0 \\ S_5 & 0 & -C_5 & 0 \\ 0 & 1 & 0 & 0 \\ 0 & 0 & 0 & 1 \end{bmatrix}, [A_6] = \begin{bmatrix} C_6 & -S_6 & 0 & 0 \\ S_6 & C_6 & 0 & 0 \\ 0 & 0 & 1 & 0 \\ 0 & 0 & 0 & 1 \end{bmatrix}.$$

The matrix which can represent the last coordinate frame embedded in the gripper link in the base coordinate system is found as the product of these matrices $[A]$. Thus,

$$[T_6] = [A_1][A_2][A_3][A_4][A_5][A_6] = \begin{bmatrix} x_x & y_x & z_x & p_x \\ x_y & y_y & z_y & p_y \\ x_z & y_z & z_z & p_z \\ 0 & 0 & 0 & 0 \end{bmatrix},$$

where

$$x_x = C_1[C_2(C_4C_5C_6 - S_4S_6) - S_2S_5C_6] - S_1(S_4S_5C_6 + C_4S_6),$$

$$x_y = S_1[C_2(C_4C_5C_6 - S_4S_6) - S_2S_5C_6] + C_1(S_4C_5C_6 + C_4S_6),$$

$$x_z = -S_2(C_4C_5C_6 - S_4S_6) - C_2S_5C_6,$$

$$y_x = C_1[-C_2(C_4C_5S_6 + S_4C_6) + S_2S_5S_6] - S_1(-S_4S_6C_5 + C_4C_6),$$

$$y_y = S_1[-C_2(C_4C_5S_6 + S_4C_6) + S_2S_5S_6] + C_1(-S_4C_5S_6 + C_4C_6),$$

$$y_z = S_2(C_4C_5S_6 + S_4C_6) + C_2S_5S_6,$$

$$z_x = C_1(C_2C_4S_5 + S_2C_5) - S_1S_4S_5,$$

$$z_y = S_1(C_2C_4S_5 + S_2C_5) + C_1S_4S_5,$$

$$z_z = -S_2C_4S_5 + C_2C_5,$$

$$p_x = C_1 S_2 s_3 - S_1 s_2,$$

$$p_y = S_1 S_2 s_3 + C_1 s_2,$$

$$p_z = C_2 s_3.$$

An important problem for manipulator position analysis is to determine the required joint variables to achieve a particular specified end-effector position and orientation. In general, this inverse kinematic problem for open chains is more involved than that for closed chains (employed for developing parallel manipulators) and the typically followed approach is now described.

The matrix $[T]$, which represents the end-effector coordinates in the base coordinates, can be expressed as a function of the joint variables. Thus, in general,

$$T_{ij} = T_{ij}(\theta_1, \theta_2, \dots, \theta_n).$$

With $\{\theta_i\}$ prescribed, $[T]$ is easily found as seen in the two preceding examples. In case of inverse kinematics, the T_{ij} 's are prescribed and $\{\theta_i\}$ has to be found out. From (5.26), for a six-degree-of-freedom open chain,

$$[T_6] = [A_1][A_2][A_3][A_4][A_5][A_6].$$

From this equation, the matrix equations obtained are

$$[A_1]^{-1}[T_6] = [A_2][A_3][A_4][A_5][A_6], \quad (5.27a)$$

$$[A_2]^{-1}[A_1]^{-1}[T_6] = [A_3][A_4][A_5][A_6], \quad (5.27b)$$

$$[A_3]^{-1}[A_2]^{-1}[A_1]^{-1}[T_6] = [A_4][A_5][A_6], \quad (5.27c)$$

$$[A_4]^{-1}[A_3]^{-1}[A_2]^{-1}[A_1]^{-1}[T_6] = [A_5][A_6], \quad (5.27d)$$

$$[A_5]^{-1}[A_4]^{-1}[A_3]^{-1}[A_2]^{-1}[A_1]^{-1}[T_6] = [A_6]. \quad (5.27e)$$

The elements of the LHS of (5.27a) contain only one unknown, the first joint variable θ_1 . Now, if we can identify an element of the resultant 4×4 matrix in the RHS of this equation which is either zero or a known quantity, then θ_1 can be determined by equating this term with the corresponding element (containing θ_1) in the LHS of the equation. Once θ_1 is known, the elements of the LHS of (5.27b) will contain only one unknown, i.e., θ_2 , and a similar procedure leads to the determination of θ_2 . The procedure is explained with the help of the example of Stanford manipulator described in Problem 5.5.

PROBLEM 5.6

Determine the joint variables to achieve the end-effector position and orientation of the Stanford manipulator as

$$\begin{bmatrix} x_x & y_x & z_x & p_x \\ x_y & y_y & z_y & p_y \\ x_z & y_z & z_z & p_z \\ 0 & 0 & 0 & 1 \end{bmatrix}.$$

The link parameters are as mentioned in Problem 5.5.

SOLUTION

The LHS of (5.27a) can be written as⁶

$$\begin{bmatrix} C_1 & S_1 & 0 & 0 \\ 0 & 0 & -1 & 0 \\ -S_1 & C_1 & 0 & 0 \\ 0 & 0 & 0 & 1 \end{bmatrix} \begin{bmatrix} x_x & y_x & z_x & p_x \\ x_y & y_y & z_y & p_y \\ x_z & y_z & z_z & p_z \\ 0 & 0 & 0 & 1 \end{bmatrix} = \begin{bmatrix} f_{11}^x & f_{11}^y & f_{11}^z & f_{11}^p \\ f_{12}^x & f_{12}^y & f_{12}^z & f_{12}^p \\ f_{13}^x & f_{13}^y & f_{13}^z & f_{13}^p \\ 0 & 0 & 0 & 1 \end{bmatrix},$$

where

$$f_{11}^x = C_1 x_x + S_1 x_y, \quad f_{12}^x = -x_z, \quad f_{13}^x = -S_1 x_x + C_1 x_y.$$

In general,

$$\begin{aligned} f_{11}^\varsigma &= C_1 \varsigma_x + S_1 \varsigma_y, \\ f_{12}^\varsigma &= -\varsigma_z, \\ f_{13}^\varsigma &= -S_1 \varsigma_x + C_1 \varsigma_y, \end{aligned} \tag{a}$$

where ς stands for x, y, z or p .

When the RHS is expanded and this nomenclature for the LHS is adopted, (5.27a) for the Stanford manipulator takes the form

$$\begin{bmatrix} f_{11}^x & f_{11}^y & f_{11}^z & f_{11}^p \\ f_{12}^x & f_{12}^y & f_{12}^z & f_{12}^p \\ f_{13}^x & f_{13}^y & f_{13}^z & f_{13}^p \\ 0 & 0 & 0 & 1 \end{bmatrix} = \begin{bmatrix} C_2(C_4C_5C_6 - S_4S_6) - S_2S_5C_6 & -C_2(C_4C_5S_6 + S_4C_6) + S_2S_5S_6 & C_2C_4S_5 + S_2C_5 & S_2s_3 \\ S_2(C_4C_5C_6 - S_4S_6) + C_2S_5C_6 & -S_2(C_4C_5S_6 + S_4C_6) - C_2S_5S_6 & S_2C_4S_5 - C_2C_5 & -C_2s_3 \\ S_4C_5C_6 + C_4S_6 & -S_4C_5S_6 + C_4C_6 & S_4S_5 & s_2 \\ 0 & 0 & 0 & 1 \end{bmatrix} \tag{b}$$

The joint variables in this case are $\theta_1, \theta_2, s_3, \theta_4, \theta_5$, and θ_6 . Now, comparing the two sides of equation (b), we get

$$f_{13}^p = s_2.$$

Using (a) in this relation, we get

$$-S_1 p_x + C_1 p_y = s_2. \tag{c}$$

Let $p_x = r \sin \phi$ and $p_y = r \cos \phi$, so that $r = \sqrt{(p_x^2 + p_y^2)}$ and $\phi = \tan^{-1}(p_x/p_y)$. Using this substitution in (c), we obtain

$$\cos \phi \cos \theta_1 - \sin \phi \sin \theta_1 = s_2/r.$$

It should be kept in mind that the geometry of this particular manipulator is such that $0 < s_2/r \leq 1$. Hence,

$$\cos(\theta_1 + \phi) = s_2/r,$$

where $0 < \phi - \theta_1 < \pi$ and

$$\sin(\phi - \theta_1) = \pm[1 - (s_2/r)^2]^{1/2}.$$

⁶Note that $[A_1]^{-1} = [A_1]^T$.

The +ve sign is valid for the right-hand shoulder configuration and the -ve sign is for the left-hand one. Finally,

$$\theta_1 = \tan^{-1} \left(\frac{\pm \sqrt{r^2 - s_2^2}}{s_2} \right) - \tan^{-1} \left(\frac{p_x}{p_y} \right). \quad (\text{d})$$

Once θ_1 is determined, all the elements on the LHS of (5.27a) are known. Next, we look for elements on the RHS of the same equation, which are functions of only one joint variable. We find that

$$f_{11}^p = S_2 s_3, \quad f_{12}^p = -C_2 s_3.$$

These equations, when expanded, take the form

$$\cos \theta_1 \cdot p_x + \sin \theta_1 \cdot p_y = \sin \theta_2 \cdot s_3, \quad -p_z = -\cos \theta_2 \cdot s_3.$$

Since s_3 is always kept greater than zero, we get

$$\theta_2 = \tan^{-1} \left(\frac{p_x \cos \theta_1 + p_y \sin \theta_1}{p_z} \right). \quad (\text{e})$$

Next, we consider (5.27b) which can be written as

$$\begin{bmatrix} f_{21}^x & f_{21}^y & f_{21}^z & f_{21}^p \\ f_{22}^x & f_{22}^y & f_{22}^z & f_{22}^p \\ f_{23}^x & f_{23}^y & f_{23}^z & f_{23}^p \\ 0 & 0 & 0 & 1 \end{bmatrix} = \begin{bmatrix} C_4 C_5 C_6 - S_4 S_6 & -C_4 C_5 S_6 - S_4 C_6 & C_4 S_5 & 0 \\ S_4 C_5 C_6 + C_4 S_6 & -S_4 C_5 S_6 + C_4 C_6 & S_4 S_5 & 0 \\ S_5 S_6 & S_5 S_6 & C_5 & s_3 \\ 0 & 0 & 0 & 1 \end{bmatrix},$$

where

$$f_{21}^x = C_2(C_1 \varsigma_x + S_1 \varsigma_y) - S_2 \varsigma_z,$$

$$f_{22}^x = -S_1 \varsigma_x + C_1 \varsigma_y,$$

$$f_{23}^x = S_2(C_1 \varsigma_x + S_1 \varsigma_y) + C_2 \varsigma_z$$

(ς stands for x, y, z or p).

Equating the elements 34 on both sides, we get

$$f_{23}^p = s_3$$

or

$$s_3 = \sin \theta_2(p_x \cos \theta_1 + p_y \sin \theta_1) + p_z \cos \theta_2. \quad (\text{f})$$

An examination of both sides of the matrix equation yields the equations

$$f_{21}^z = C_4 S_5, \quad f_{22}^z = S_4 S_5.$$

Using these equations, we get

$$\theta_4 = \tan^{-1} \left\{ \frac{-z_x \sin \theta_1 + z_y \cos \theta_1}{\cos \theta_2(z_x \cos \theta_1 + z_y \sin \theta_1) - z_z \sin \theta_2} \right\} \quad \text{if } \theta_5 > 0, \quad (\text{g})$$

THEORY OF MECHANISMS AND MACHINES

$$\theta_4 = \pi + \tan^{-1} \left\{ \frac{-z_x \sin \theta_1 + z_y \cos \theta_1}{\cos \theta_2(z_x \cos \theta_1 + z_y \sin \theta_1) - z_z \sin \theta_2} \right\} \quad \text{if } \theta_5 < 0.$$

This corresponds to two configurations of the manipulator. When $\theta_5 = 0$, the manipulator becomes degenerate with the axes of joints 4 and 6 aligned and only the sum $(\theta_4 + \theta_6)$ is significant. So, if $\theta_5 = 0$, any value for θ_4 can be assumed (in practice, the current value of θ_4 is assumed). It can be shown that (5.27c) does not provide any new information. Equation (5.27d) can be written in the expanded form as

$$\begin{bmatrix} f_{41}^x & f_{41}^y & f_{41}^z & f_{41}^p \\ f_{42}^x & f_{42}^y & f_{42}^z & f_{42}^p \\ f_{43}^x & f_{43}^y & f_{43}^z & f_{43}^p \\ 0 & 0 & 0 & 0 \end{bmatrix} = \begin{bmatrix} C_5 C_6 & -C_5 S_6 & S_5 & 0 \\ S_5 C_6 & -S_5 S_6 & -C_5 & 0 \\ S_6 & C_6 & 0 & 0 \\ 0 & 0 & 0 & 1 \end{bmatrix},$$

where

$$f_{41}^x = C_4 \{C_2(\zeta_x C_1 + \zeta_y S_1) - \zeta_z S_2\} + S_4(-\zeta_x S_1 + \zeta_y C_1),$$

$$f_{42}^x = -S_2(\zeta_x C_1 + \zeta_y S_1) - \zeta_z C_2,$$

$$f_{43}^x = -S_4 \{C_2(\zeta_x C_1 + \zeta_y S_1) - \zeta_z S_2\} + C_4(-\zeta_x S_1 + \zeta_y C_1).$$

Using the 13 and 23 elements, we get

$$\theta_5 = \tan^{-1} \left[\frac{\cos \theta_4 \{\cos \theta_2(z_x \cos \theta_1 + z_y \sin \theta_1) - z_z \sin \theta_2\} + \sin \theta_4(-z_x \sin \theta_1 + z_y \cos \theta_1)}{\sin \theta_2(z_x \cos \theta_1 + z_y \sin \theta_1) + z_z \cos \theta_2} \right]. \quad (\text{h})$$

To determine θ_6 , the 11 and 12 elements are used, resulting in

$$\theta_6 = \tan^{-1} \left[\frac{-\sin \theta_4 \{\cos \theta_2(x_x \cos \theta_1 + x_y \sin \theta_1) - x_z \sin \theta_2\} + \cos \theta_4(-x_x \sin \theta_1 + x_y \cos \theta_1)}{-\sin \theta_4 \{\cos \theta_2(y_x \cos \theta_1 + y_y \sin \theta_1) - y_z \sin \theta_2\} + \cos \theta_4(-y_x \sin \theta_1 + y_y \cos \theta_2)} \right]. \quad (\text{i})$$

This procedure can be used for all types of open chain linkages or serial manipulators for reverse kinematic analysis.

5.5 PROBLEMS

- 5.7 If a spatial linkage consists of only binary links connected by R-pairs, then what must be the number of links and R-pairs to yield a single degree of freedom without any special geometric condition?
- 5.8 A four-link R-S-P-P linkage used in a swash-plate-driven pump is shown in Fig. 5.15. Determine the effective degree of freedom. *Hint:* Look for any redundant degree of freedom.
- 5.9 Set up the link coordinate systems for the Bennett linkage shown in Fig. 5.1.
- 5.10 For a Hooke's joint with a shaft angle α_4 , if the input shaft rotates at a constant speed, determine the ratio of the maximum to minimum speed of the output shaft.
- 5.11 Synthesize a 4R spherical mechanism to generate $y = \sin x$, $0 \leq x \leq \pi/2$, with three Chebyshev's accuracy points. Assume $\alpha_4 = 90^\circ$, $\theta_1^i = 45^\circ$, $\theta_4^i = -45^\circ$, $\Delta\theta_1^i = 60^\circ$, and $\Delta\theta_4 = 90^\circ$.

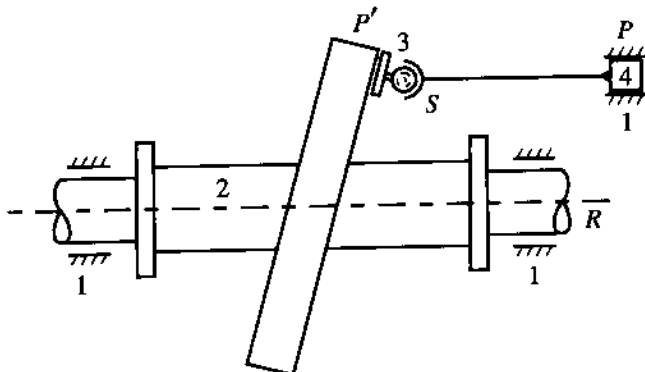


FIGURE 5.15

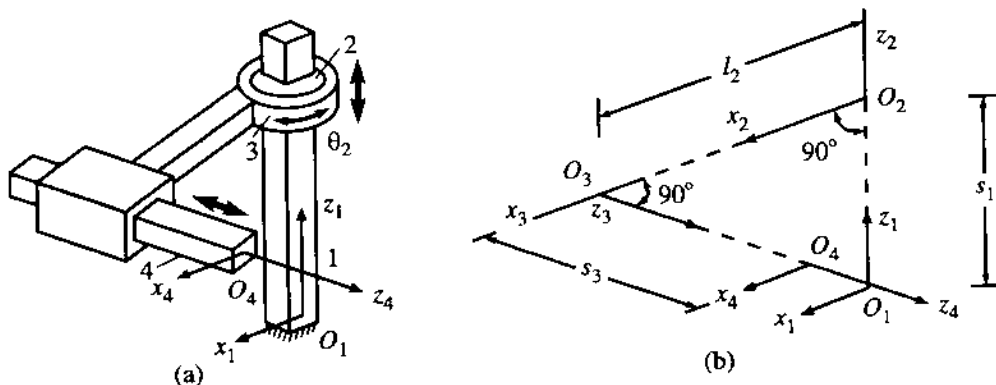


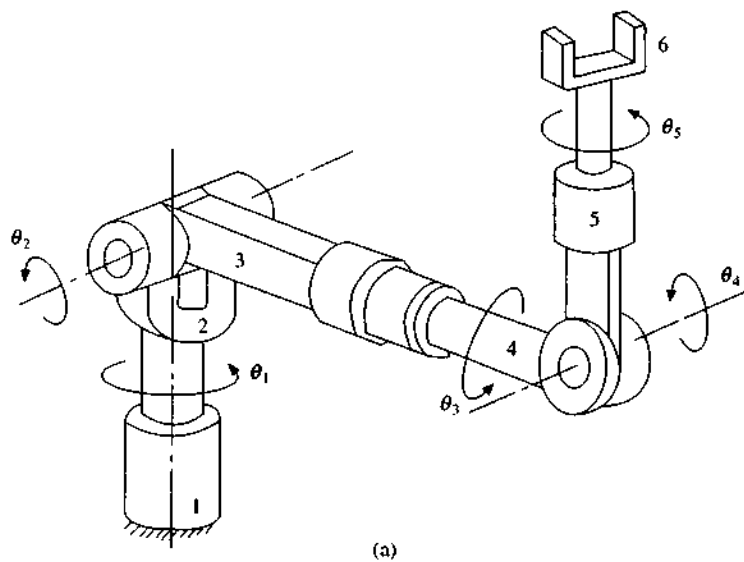
FIGURE 5.16

5.12 Figure 5.16a shows a three-degree-of-freedom arm and Fig. 5.16b shows the coordinate systems attached to various links. Express the end link coordinate system in the base coordinate system in terms of the link parameters and the joint variables s_1 , θ_2 , and s_3 .

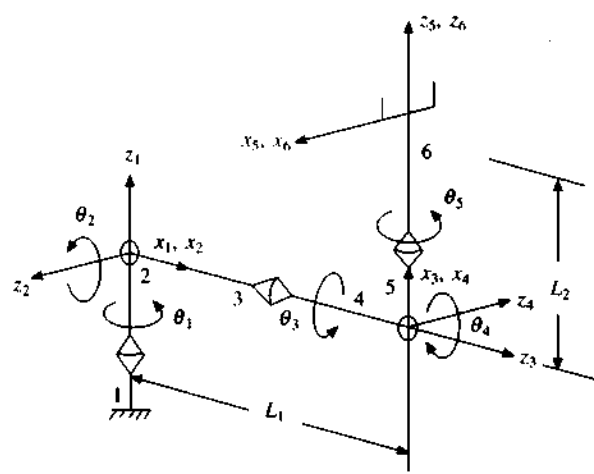
5.13 Figure 5.17a shows a five-degree-of-freedom manipulator and Fig. 5.17b shows the kinematic structure along with the various coordinate systems. Express the sixth coordinate system (attached to the end link 6) in the base coordinate system in terms of the various link parameters and joint variables. [Note that it may not be always possible to transform one coordinate system into the next with the convention followed in deriving the homogeneous transformation matrix. In such cases, derive the transformation matrix separately.]

5.14 Carry out an inverse kinematic analysis of the three-degree-of-freedom arm described in Problem 5.12.

5.15 Figure 5.18 shows a PUMA manipulator arm. Carry out an inverse kinematic analysis to determine the joint variables in terms of the end coordinate position and orientation, the link parameters, and the joint variables.



(a)



(b)

FIGURE 5.17

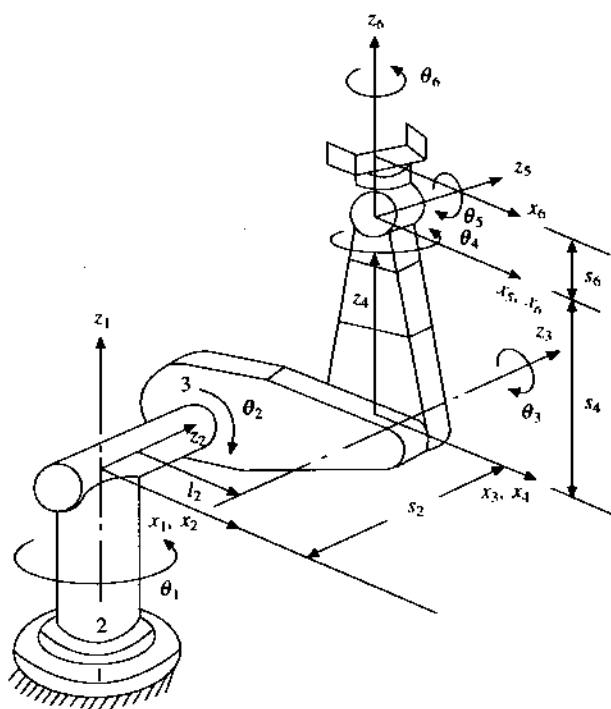


FIGURE 5.18

Chapter 6

GOVERNOR MECHANISMS

3.1 INTRODUCTION

If the efficiency of an engine is plotted against the speed of the engine, a curve similar to that shown in Fig. 6.1 is obtained. As can be observed, there exists an optimum speed N_{opt} for which the efficiency of the engine is maximum. So, for an efficient operation, it is desirable that, irrespective of the load, the speed of the engine should remain close to N_{opt} . To achieve this, engines are provided with a regulatory control or *governor*. The function of a governor is to automatically regulate the power input to the engine as demanded by the variation of load so that the engine speed is maintained at or near the optimum value. The speed-load characteristic of an engine without a governor droops sharply; the governor tends to make it flatter. This point will be explained in detail in Section 6.7.

In addition to engines, there are many situations where it is essential to maintain a desired speed, not necessarily for an efficient operation. Such a speed can be kept constant by dissipating excess power. To do this, again, a governor mechanism can be used. However, the input power available should always be more than that required. Moreover, since excess power is dissipated, such a mechanism is suitable only for a small machine where power consumption is not of much importance. Later in this chapter, we shall discuss a few mechanisms of this type.

The purpose for which a governor is used in an engine should be carefully distinguished from that served by a flywheel. The latter reduces the fluctuations of speed during a cycle above and

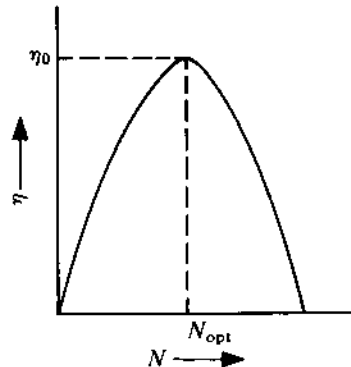


FIGURE 6.1

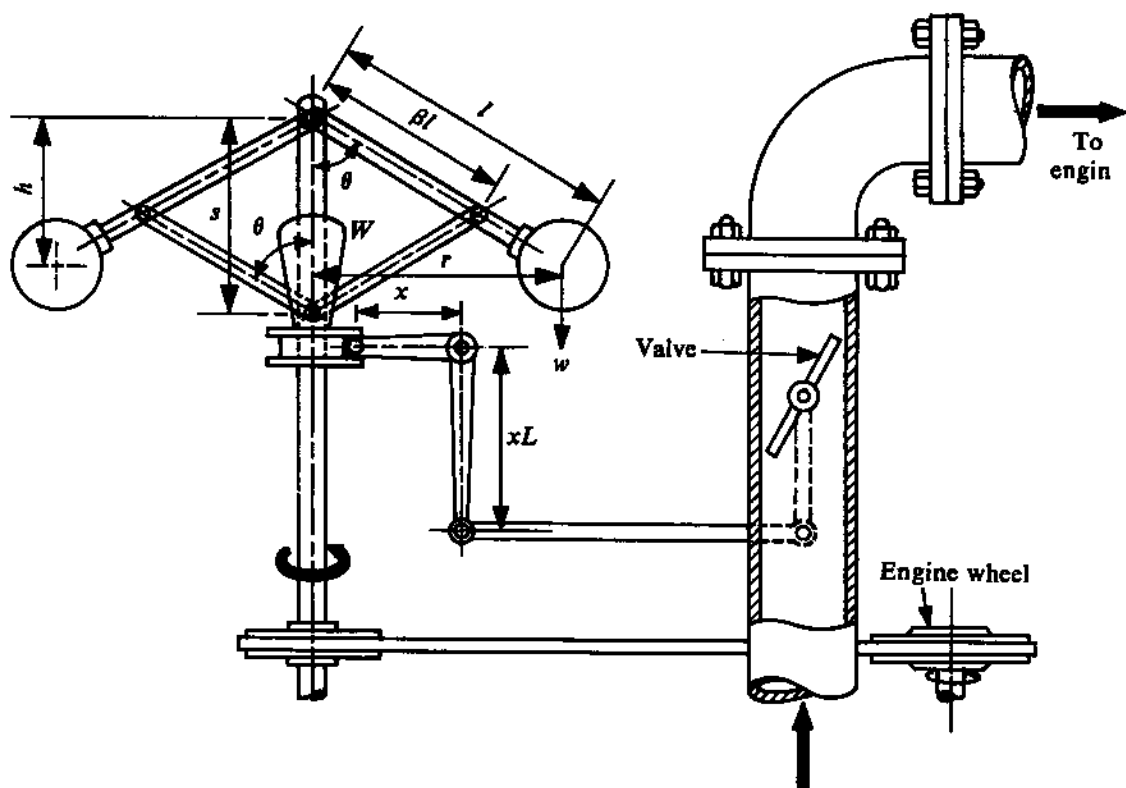


FIGURE 6.2

below the mean value (for constant load). Speed fluctuations are inevitable because of variations in the turning moment. However, the flywheel does not exercise any control over the mean speed of the engine. The governor, on the other hand, has no influence over cyclic speed fluctuations, but it controls the mean speed over a long period during which the load on the engine may vary.

The governor is one of the simplest examples of a mechanical feedback control system. Figure 6.2 shows a governor mechanism in which the governor spindle is directly coupled to the engine shaft. If the load on the engine decreases, the engine speed tends to increase, as a result of which the governor balls try to fly outwards. This causes an upward movement of the sleeve, which is magnified by the lever arrangement as shown in the figure. The magnified movement operates a valve at the other end of the lever to reduce the opening which controls the quality or quantity of fuel supplied to the engine. Thus, the power input is adjusted to the new load on the engine.

It is obviously desirable that the input should be correctly adjusted as soon as the load changes so that no variation in speed can take place. To ensure that the input is automatically regulated, the change in mean speed due to a change in load is used. That is, the mean speed must change for the governor to operate. A sensitive governor can do this with as small a change in speed as possible.

6.2 TYPES OF GOVERNORS

Governors may be classified on the basis of their operating principles. The types most commonly used are (i) centrifugal governors, and (ii) inertia and flywheel governors. In a governor of type (i), the change in the centrifugal forces of the rotating masses due to a change in the speed of the engine is utilized for the movement of the governor sleeve (as shown in Fig. 6.2). Such a governor may be (a) gravity-controlled or (b) spring-controlled. In a gravity-controlled governor, the movement of the governor balls is regulated by the force of gravity, whereas in a spring-controlled governor, this regulation is provided by means of springs.

In a governor of type (ii), the inertia forces caused by the angular acceleration of the engine shaft (or of the flywheel) by the change in speed are utilized for the movement of the governor balls. Thus, the movement of the balls is decided by the rate of change of speed (rather than the change in speed itself, as in a centrifugal governor), with the result that such a governor is more sensitive than a centrifugal governor. Nevertheless, a centrifugal governor is more commonly used because of the simplicity of its operation.

6.3 CHARACTERISTICS OF CENTRIFUGAL GOVERNORS

A centrifugal governor should have the following qualities for satisfactory performance:

- (i) When its sleeve reaches its lowest position, the engine should develop maximum power.
- (ii) Its sleeve should at once reach the topmost position when the load on the engine is suddenly removed.
- (iii) Its sleeve should float at some intermediate position under normal operating conditions.
- (iv) Its response to a change in speed should be fast.
- (v) It should have sufficient power so that it can exert the required force at the sleeve to operate the control mechanism.

The definitions of some terms used for describing these qualities of a governor follow.

Controlling Force

In a centrifugal governor, the resultant of all the external forces which control the movement of the ball can be regarded as a single inward radial force acting at the centre of the ball. The variation of this force F with the radius of rotation of the ball can be studied under static conditions by measuring the outward radial force on the ball which is necessary to keep the ball in equilibrium at various configurations (i.e., for different values of r). The force F is known as the *controlling force* and is a function of a single variable r . Thus,

$$F = F(r). \quad (6.1)$$

Figure 6.3 shows a typical plot of the controlling-force characteristic (curve AB). The controlling force is derived from purely statical considerations without reference to the speed of rotation.

Now, let us suppose that the governor ball rotates at a speed ω . The centripetal force needed for maintaining the radius of rotation r is given by $m\omega^2 r$, where m is the mass of each ball. The plot of this force against r for a given speed ω will obviously be a straight line passing through

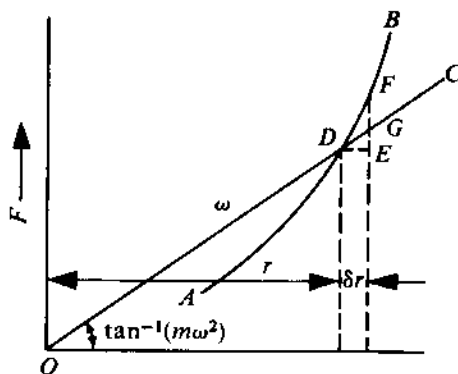


FIGURE 6.3

the origin as shown by the line OC in Fig. 6.3. So, the equilibrium radius for this speed ω will be determined by the intersection of the curve AB with the line AC (at the point D). For this value of r , the controlling force will be equal to the centripetal force. Mathematically, we can express this equilibrium condition as

$$F(r) = m\omega^2 r. \quad (6.2)$$

Stability

If the governor ball is displaced from its equilibrium position for a particular speed without any change in the speed of rotation, and thereafter if it tends to return to its original equilibrium position, then the governor is said to be *stable*. To determine the condition necessary for stability, let the speed of the governor be ω at the equilibrium position given by the point D (Fig. 6.3). If the speed remains the same, and if the radius changes to $r + \delta r$, the increment in the controlling force EF will be $(dF/dr)\delta r$, and the corresponding increment in the centripetal force EG will be $EG = m\omega^2\delta r$. The restoring force FG on the ball is

$$FG = EF - EG = (dF/dr - m\omega^2)\delta r.$$

This should be greater than zero for the equilibrium position to be regained. Thus, for stable operation, we get $dF/dr > m\omega^2$. Using (6.2), we get

$$dF/dr > F/r. \quad (6.3)$$

In other words, the condition for the stability of a governor is that *the slope of the curve for the controlling force should be more than that of the line representing the centripetal force at the speed considered*.

Sensitivity

If a governor operates between the speed limits ω_1 and ω_2 , then *sensitivity* is defined as the ratio of the mean speed to the difference between the maximum and minimum speeds. Thus,

$$\text{sensitivity} = \frac{\omega_{\text{mean}}}{\omega_2 - \omega_1} = \frac{\omega_2 + \omega_1}{2(\omega_2 - \omega_1)}. \quad (6.4)$$

Isochronism

If a governor is at equilibrium only for a particular speed, it is called an *isochronous* governor, for which $\omega_1 = \omega_2 = \omega$. Thus, from (6.4), we can say that an isochronous governor is infinitely sensitive. The controlling-force curve for an isochronous governor coincides with the centripetal-force line corresponding to isochronous speed. Therefore, in this case, we have

$$dF/dr = m\omega^2. \quad (6.5)$$

Comparing (6.5) with (6.3), we see that isochronism (or sensitiveness) can be achieved only at the expense of stability.

Capacity

The magnitude of the controlling force is a measure of the force that can be exerted at the sleeve to operate the control mechanism. The area under the controlling-force curve (i.e., between the curve and the r -axis, see Fig. 6.3) for the limits of operation r_{\min} and r_{\max} represents the work done by the governor against all external forces (since the controlling force is the resultant of all external forces). This also represents the energy released by the governor ball when the speed falls from its maximum to its minimum value, i.e., as r varies from r_{\max} to r_{\min} . Thus, the total *energy capacity* of the governor is

$$E = 2 \int_{r_{\min}}^{r_{\max}} F dr = 2 \int_{r_{\min}}^{r_{\max}} F(r) dr \quad (6.6)$$

is there are two rotating balls.

3.4 GRAVITY-CONTROLLED CENTRIFUGAL GOVERNORS

Three commonly-used gravity-controlled centrifugal governors are shown in Fig. 6.4. The simplest (but obsolete) type is *Watt's pendulum governor* shown in Fig. 6.4a. The *Porter governor* shown in Fig. 6.4b differs from Watt's governor only in the extra sleeve weight, which gives it more sensitiveness than Watt's governor. The poor sensitiveness of Watt's governor, particularly at a high speed, limits its field of application. In the Proell governor (Fig. 6.4c), the balls, instead of being placed at the junction of the arms, are carried on extensions rigidly fixed to the lower arms. This increases the sensitiveness of the governor (of course, with the consequent loss in stability). We shall first consider the characteristics of a Porter governor. The characteristics of Watt's governor can then easily be derived by taking the sleeve mass M to be zero.

Porter Governor

As shown in Fig. 6.5, let both arms of the governor be of length l and hinged at a distance e from the axis of rotation of the governor. One-half of the governor is shown in the figure. Let

m = mass of the rotating ball,

M = mass on the sleeve,

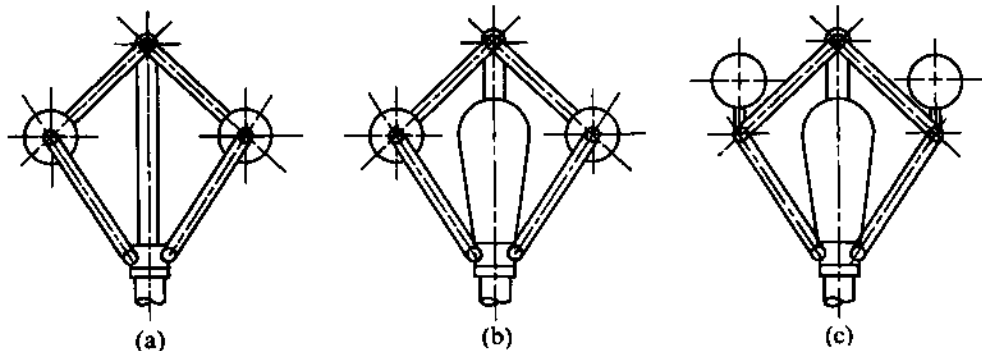


FIGURE 6.4

θ = inclination of the arms with the vertical when the radius of rotation of the governor ball is r

T_u, T_l = tension in the upper, lower arms, respectively, and

F = controlling force (i.e., the resultant of T_u, T_l , and mg).

The friction force at the sleeve is neglected for the time being.

Taking moments about I (the instantaneous centre of rotation of the lower link at this position of all the forces acting on the ball, we get

$$F \cdot BC = mg \cdot IC + T_l \cdot IB \sin 2\theta, \quad (6.7)$$

$$F = mg \tan \theta + T_l \frac{2 \sin \theta \cos \theta}{\cos \theta}. \quad (6.8)$$

Considering the vertical equilibrium of forces on the sleeve, we have

$$2T_l \cos \theta = Mg. \quad (6.9)$$

Substituting T_l from (6.9) in (6.8), we obtain

$$F = (m + M)g \tan \theta \quad (6.10)$$

$$= (m + M) \frac{AC}{BC} g = (m + M) \frac{(r - e)}{[l^2 - (r - e)^2]^{1/2}} g. \quad (6.11)$$

For equilibrium, we also have $F = m\omega^2 r$. Thus, the equilibrium radius r at a speed ω is given by

$$m\omega^2 r = \frac{(m + M)(r - e)}{[l^2 - (r - e)^2]^{1/2}} g,$$

$$\omega^2 = g \left(1 + \frac{M}{m}\right) \frac{(1 - e/r)}{[l^2 - (r - e)^2]^{1/2}}. \quad (6.12)$$

The controlling-force curve given by (6.11) is shown as AB in Fig. 6.6 ($F = 0$ at $r = e$, $F \rightarrow \infty$ at $r = l + e$). From the nature of this curve, it is obvious that the governor is stable throughout its range of operation. This is because the slope of this curve will be more than that of any intersecting line passing through the origin (the slope of the curve being measured at the point of intersection

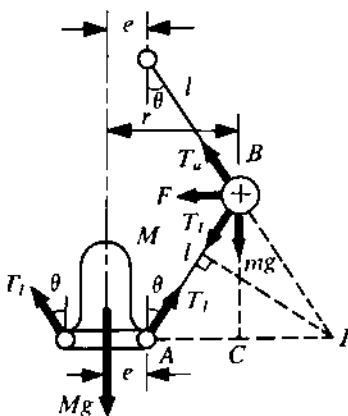


FIGURE 6.5

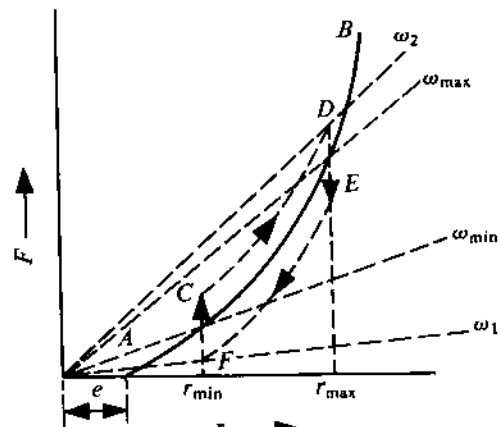


FIGURE 6.6

Let

r_{\min} = minimum radius of operation when the equilibrium speed is ω_{\min} ,

r_{\max} = maximum radius of operation when the equilibrium speed is ω_{\max} .

The energy capacity of the governor, from (6.6), is

$$E = 2 \int_{r_{\min}}^{r_{\max}} F dr = 2 \int_{\theta_{\min}}^{\theta_{\max}} (m + M)g \tan \theta \cdot l d\theta \cos \theta$$

(since $dr = l d\theta \cos \theta$). Thus,

$$E = 2(m + M)lg \int_{\theta_{\min}}^{\theta_{\max}} \sin \theta d\theta = (m + M)2l(\cos \theta_{\min} - \cos \theta_{\max})g. \quad (6.13)$$

Now, the total vertical movement of the ball is $l(\cos \theta_{\min} - \cos \theta_{\max})$ and the total movement of the sleeve is $2l(\cos \theta_{\min} - \cos \theta_{\max})$. So,

$$E = (m + M)g \times (\text{movement of the sleeve}). \quad (6.14)$$

Let us now consider the effect of frictional resistance. The friction force at the sleeve f is assumed to be constant and to always oppose the motion of the sleeve. Thus, in all the preceding equations, the sleeve weight Mg should be replaced by $(Mg + f)$ for rising speed and by $(Mg - f)$ for falling speed (as the friction force will act upwards).

The controlling-force curve with friction is represented by the loop $CDEF$ in Fig. 6.6; the curve for rising speed is CD and that for falling speed, EF . Now, the minimum speed of operation is given by ω_1 and the maximum by ω_2 (Fig. 6.6). As $\omega_1 < \omega_{\min}$ (without friction) and $\omega_2 > \omega_{\max}$ (without friction), the sensitiveness of the governor decreases with friction (note that ω_{mean} remains almost the same with and without friction). At a given value of r , the lower speed limit ω_l [from (6.12)] is given by

$$\omega_l^2 = \frac{g[1 + (M - f/g)/m](1 - e/r)}{[l^2 - (r - e)^2]^{1/2}} \quad (6.15)$$

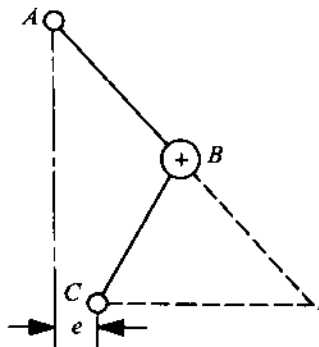


FIGURE 6.7

and the upper speed limit ω_u is given by

$$\omega_u^2 = \frac{g[1 + (M + f/g)/m](1 - e/r)}{[l^2 - (r - e)^2]^{1/2}}. \quad (6.16')$$

From (6.12), (6.15), and (6.16), we get

$$(\omega_u^2 - \omega_l^2)/\omega^2 = 2f/(M + m)g, \quad (6.17)$$

where ω refers to the speed at the same value of r without considering friction. With the approximation $(\omega_u + \omega_l)/2 \approx \omega$, from (6.17), we get

$$(\omega_u - \omega_l)/\omega = f/(M + m)g. \quad (6.18)$$

The ratio given by (6.18) is known as the *coefficient of insensitiveness or detention by friction*.

Another arrangement of a Porter governor is shown in Fig. 6.7, where the upper arm is hinged on the axis of rotation and the lower arm is connected to the sleeve at a distance e from the axis of rotation. The characteristics can be derived in this case also by taking moments about I of all the forces acting on the ball.

PROBLEM 6.1

The arms of a Porter governor are 17.8 cm long and are hinged at a distance of 3.8 cm from the axis of rotation. The mass of the balls is 1.15 kg each and the mass on the sleeve is 20 kg. The governor begins to rise at 280 rpm when the links are at an angle of 30° to the vertical. Assuming the friction force to be constant, determine the higher and lower speeds when the angle of inclination of the arms to the vertical is 45° . Find also the detention by friction at the second position.

SOLUTION

Referring to Fig. 6.5, we have $e = .038$ m, $l = .178$ m, $m = 1.15$ kg, and $M = 20$ kg. Let f (in N) be the constant friction force at the sleeve. For $\theta = 30^\circ$,

$$r = l \sin \theta + e = .127 \text{ m},$$

$$\omega_u = 280(\pi/30) = 29.3 \text{ rad/s.}$$

From (6.16), we get

$$(29.3)^2 = \frac{9.8[1 + (20 + f/9.8)/1.15](1 - .038/.127)}{[(.178)^2 - (.127 - .038)^2]^{1/2}} \quad \text{or} \quad f = 10.29 \text{ N.}$$

For $\theta = 45^\circ$,

$$r = l \sin \theta + e = 0.164 \text{ m.}$$

From (6.15), we have

$$\omega_l^2 = \frac{9.8[1 + (20 - 10.29/9.8)/1.15](1 - .038/.164)}{[(.178)^2 - (.164 - .038)^2]^{1/2}} = 1050 \text{ (rad/s)}^2,$$

$$\omega_l = 32.4 \text{ rad/s, } N_l = 309 \text{ rpm.}$$

Similarly, from (6.16), we get

$$\omega_u^2 = 1156 \text{ (rad/s)}^2 \quad \text{or} \quad \omega_u = 34 \text{ rad/s,}$$

$$N_u = 326.5 \text{ rpm.}$$

Again, from (6.12), we get

$$\omega^2 = 1105 \text{ (rad/s)}^2 \quad \text{or} \quad \omega = 33.2 \text{ rad/s}$$

Thus, the detention by friction is $(\omega_u - \omega_l)/\omega = 0.0482$.

Proell Governor

A typical Proell governor is shown in Fig. 6.8. Here, the upper arm is hinged on the axis of rotation and the lower arm is connected to the sleeve at a distance e from the axis of rotation. The governor ball is not placed at the joint of the upper and lower links. Instead, it is carried on a rigid extension of the lower link as shown in Fig. 6.8 (angle $BB'C$ remains constant).

Taking moments about I (the instantaneous centre of rotation of the lower link) of all forces acting on the ball, it can be shown that

$$F.BD = mg.ID + \frac{Mg}{2}.IC \quad (\text{neglecting friction}),$$

$$F = mg \cdot \frac{ID}{BD} + \frac{Mg}{2} \cdot \frac{IC}{BD} \quad (6.19)$$

$$= m\omega^2 r \quad (\text{at equilibrium speed}). \quad (6.20)$$

PROBLEM 6.2

Proell governor has arms 30.5 cm long. The upper arms are hinged on the axis of rotation, whereas the lower arms are pivoted at a distance of 3.8 cm from the axis of rotation. The extension of the lower arms to which the balls are attached is 10.2 cm long. Each ball has a mass of 4.8 kg and the mass on the sleeve is 54.5 kg. At the minimum radius of rotation of 16.5 cm, the extensions are parallel to the governor axis. Determine the equilibrium speeds at radii 16.5 cm and 21.6 cm.

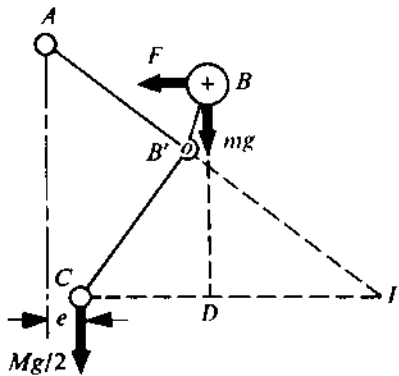


FIGURE 6.8

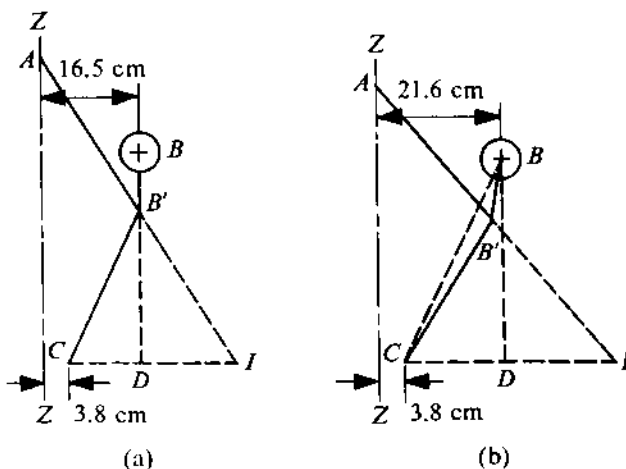


FIGURE 6.9

SOLUTION

It is given that $m = 4.8 \text{ kg}$ and $M = 54.5 \text{ kg}$. Referring to Fig. 6.9a, for the minimum radius $r = 16.5 \text{ cm}$, by measurements we get $ID = 17.2 \text{ cm}$, $IC = 29.8 \text{ cm}$, and $BD = 37.6 \text{ cm}$. (The procedure for locating the points *A*, *B*, *B'*, *C*, and *D* is to first draw the governor axis *ZZ*. Then, take the ball centre *B* anywhere at a distance of 16.5 cm from *ZZ*, and draw *BB'* parallel to the governor axis, so that $BB' = 10.2 \text{ cm}$. Next, draw a line parallel to the governor axis at a distance of 3.8 cm from it. With *B'* as the centre, draw an arc of radius 30.5 cm to intersect this line at *C* and the governor axis at *A*.)

From (6.20), we get

$$m\omega^2 r = mg \cdot \frac{ID}{BD} + \frac{Mg}{2} \frac{IC}{BD} = (4.8 \times \frac{17.2}{37.6} + \frac{54.5}{2} \times \frac{29.8}{37.6}) \times 9.8,$$

$$4.8 \times .165\omega^2 = 225.84$$

or

$$\omega^2 = 286(\text{rad/s})^2 \quad \text{or} \quad \omega = 16.9 \text{ rad/s}, \quad N = 161.5 \text{ rpm}.$$

Referring to Fig. 6.9b, for radius $r = 21.6 \text{ cm}$, by measurements we get $ID = 20.2 \text{ cm}$, $IC = 38.8 \text{ cm}$, and $BD = 35.4 \text{ cm}$. (The procedure for locating the relevant points is similar to the one already described. We get the distance BC from Fig. 6.9a; this does not change as the extensions are connected rigidly to the lower arm. The governor axis *ZZ* is drawn as before, and two lines parallel to it are drawn at a distance of 21.6 cm and 3.8 cm. The point *B* is taken on the first line and, with BC already known, the point *C* is located on the second line. Now, $BB' = 10.2 \text{ cm}$ and $B'C = 30.5 \text{ cm}$. So, we can get the point *B'* and then fix the point *A* on the governor axis with $AB' = 30.5 \text{ cm}$.)

From (6.20), we get

$$m\omega^2 r = mg \cdot \frac{ID}{BD} + \frac{Mg}{2} \frac{IC}{BD} = (4.8 \times \frac{20.2}{35.4} + \frac{54.5}{2} \times \frac{38.8}{35.4}) \times 9.8,$$

$$4.8 \times .216\omega^2 = 319.48$$

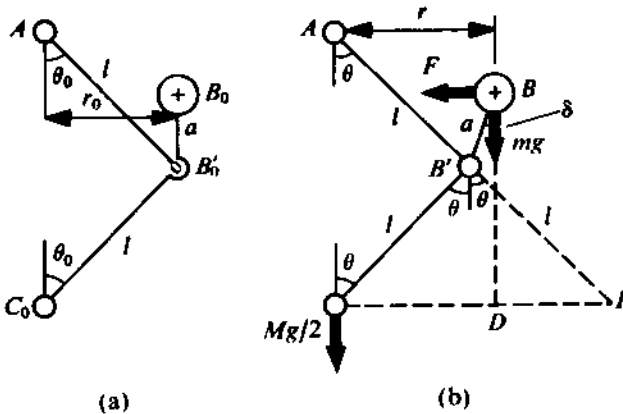


FIGURE 6.10

or

$$\omega^2 = 324 \text{ (rad/s)}^2 \quad \text{or} \quad \omega = 18 \text{ rad/s}, \quad N = 171.5 \text{ rpm.}$$

From (6.19), we can obtain F for different positions of the governor ball (i.e., for different values of δ). This controlling-force curve will show smaller values of dF/dr than those for a Porter governor of the same dimensions (with the ball placed at B'). Thus, this governor has more sensitiveness as compared to a Porter governor. Consequently, there may be chances of instability in a Proell governor which were absent in a Porter governor. This is illustrated by the example which follows.

PROBLEM 6.3

Let the upper and lower arms of a Proell governor be of equal length l , and assume that the arms are pivoted on the axis of rotation as shown in Fig. 6.10. The extensions of the lower arms, to which the governor balls of mass m are attached, are of a length a . The central mass on the sleeve is M . At the minimum radius of rotation r_0 , the extensions are parallel to the governor axis (Fig. 6.10a), and the arms are inclined at an angle θ_0 to the axis of the governor. Determine the minimum value of r_0 to make the governor stable throughout its range of operation. Given $l = 15 \text{ cm}$, $a = 5 \text{ cm}$, $m = 1 \text{ kg}$, $M = 10 \text{ kg}$, and $\theta_0 = 30^\circ$.

SOLUTION

Figure 6.10b shows the configuration of this governor for any radius r when the arms are inclined to the governor axis at an angle θ , the inclination of the extensions to the vertical being δ . Let us now obtain the controlling-force curve for this governor.

From Fig. 6.10a, $\angle B_0B'_0C_0 = \pi - \theta_0$, and Fig. 6.10b, $\angle BB'C = \pi - \theta + \delta$. As the extension is rigidly connected to the lower link, we have

$$\angle B_0B'_0C_0 = \angle BB'C, \quad \pi - \theta_0 = \pi - \theta + \delta \quad \text{or} \quad \delta = \theta - \theta_0.$$

Thus, from Fig. 6.10b, we get

$$r = l \sin \theta + a \sin \delta = l \sin \theta + a \sin (\theta - \theta_0), \quad (a)$$

$$\text{minimum radius } r_0 = l \sin \theta_0. \quad (b)$$

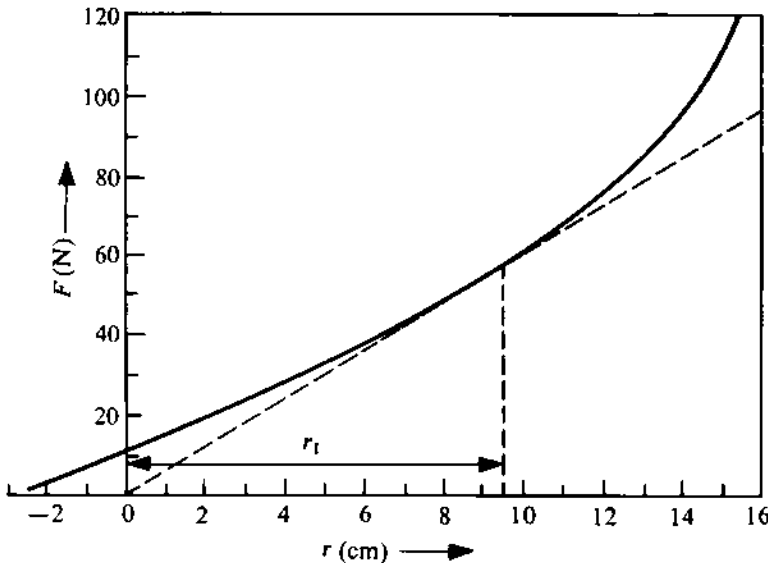


FIGURE 6.11

Taking moments about I , from (6.19), we get

$$\begin{aligned}
 F &= mg \cdot \frac{ID}{BD} + \frac{Mg}{2} \cdot \frac{IC}{BD} = \frac{m(l \sin \theta - a \sin \delta) + \frac{M}{2} \cdot 2l \sin \theta}{l \cos \theta + a \cos \delta} g \\
 &= \frac{m[l \sin \theta - a \sin(\theta - \theta_0)] + M \cdot l \sin \theta}{l \cos \theta + a \cos(\theta - \theta_0)} g. \tag{c}
 \end{aligned}$$

From (b), we get $r_0 = 7.5$ cm, and from (a) and (c), the values obtained are as given in Table 6.1.

TABLE 6.1

θ (degrees)	0	10	20	30	40	50	60
r (cm)	-2.5	0.89	4.26	7.5	10.52	13.21	15.5
F (N)	1.27	15.2	29.5	45.1	62.72	84.77	116.62

The values of F and r , as given in this table, are plotted in Fig. 6.11. A tangent to the curve is drawn from the origin. The radius at the point of tangency is $r_1 = 9.5$ cm (from Fig. 6.11). So for $r < r_1$, $dF/dr < F/r$, and the governor is unstable, whereas, for $r > r_1$, $dF/dr > F/r$, and the governor is stable. As $r_1 > r_0$, we see that the governor is unstable for the zone from the minimum radius r_0 to a radius r_1 .

Let us now find out the minimum inclination θ_0 to make the governor stable throughout its range of operation, for which it is necessary that the governor be stable at the minimum radius. In this case, the condition for stability can be stated as

$$\left. \frac{dF}{dr} \right|_{r=r_0} > \left. \frac{F}{r} \right|_{r=r_0},$$

$$\left. \frac{dF}{dr} \right|_{\theta=\theta_0} > \left. \frac{F}{r} \right|_{\theta=\theta_0}$$

From (a), we get

$$\frac{dr}{d\theta} = l \cos \theta + a \cos (\theta - \theta_0)$$

and from (c), we obtain

$$\begin{aligned} \frac{dF}{d\theta} &= [l \cos \theta + a \cos (\theta - \theta_0)] \{ M.l \cos \theta + m[l \cos \theta - a \cos (\theta - \theta_0)] \} g \\ &\quad + [l \sin \theta + a \sin (\theta - \theta_0)] \times \frac{\{ M.l \sin \theta + m[l \sin \theta - a \sin (\theta - \theta_0)] \}}{[l \cos \theta + a \cos (\theta - \theta_0)]^2} g. \end{aligned}$$

Since $dF/dr = (dF/d\theta)/(dr/d\theta)$, the foregoing equations give

$$\left. \frac{dF}{dr} \right|_{\theta=\theta_0} = \frac{(M+m)l^2 + Mal \cos \theta_0 - ma^2}{(a + l \cos \theta_0)^3} g.$$

Now, from (a) and (c), we have

$$\left. \frac{F}{r} \right|_{\theta=\theta_0} = \frac{(M+m)g}{a + l \cos \theta_0}.$$

Hence, the condition for stability is

$$(M+m)l^2 + Mal \cos \theta_0 - ma^2 > (M+m)(l \cos \theta_0 + a)^2.$$

On simplification, we get

$$(M+m)l^2 \cos^2 \theta_0 + (M+2m)al \cos \theta_0 + a^2(M+2m) - l^2(M+m) < 0.$$

Let $\alpha = a/l$, $\beta = (M+2m)/(M+m)$. Then,

$$\cos^2 \theta_0 + \alpha \beta \cos \theta_0 + (\alpha^2 \beta - 1) < 0. \quad (d)$$

Let

$$\cos^2 \gamma + \alpha \beta \cos \gamma + (\alpha^2 \beta - 1) = 0. \quad (e)$$

With reasonable values of α and β , the only real root of (e) is

$$\cos \gamma = \frac{-\alpha \beta + (\alpha^2 \beta^2 - 4\alpha^2 \beta + 4)^{1/2}}{2}.$$

Thus, for stability, from (d) and (e), we get

$$\cos \theta_0 < \cos \gamma,$$

$$\theta_0 > \gamma, \quad \theta_0 > \cos^{-1} \left\{ \frac{1}{2} [-\alpha \beta + (\alpha^2 \beta^2 - 4\alpha^2 \beta + 4)^{1/2}] \right\}.$$

For this example, $\alpha = 1/3$ and $\beta = 12/11$. So, $\theta_0 > 39.5^\circ$. Therefore, $r_0 \geq 10.38$ cm or $(r_0)_{\min} = 10.38$ cm.

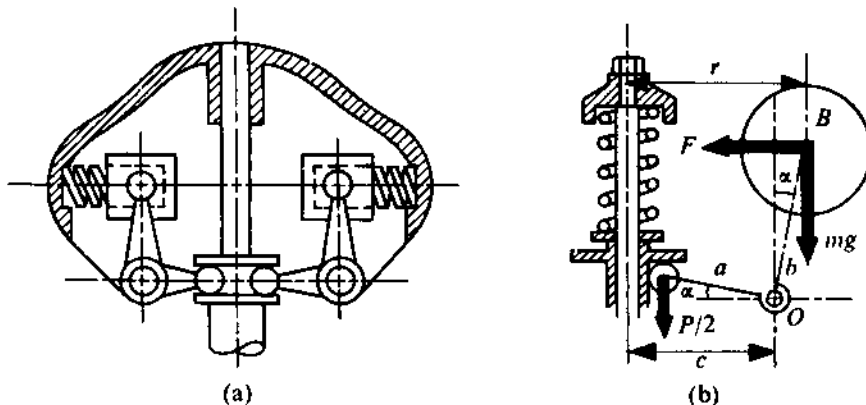


FIGURE 6.12

6.5 SPRING-CONTROLLED CENTRIFUGAL GOVERNORS

Two commonly-used spring-controlled centrifugal governors are shown in Fig. 6.12. The simpler one shown in Fig. 6.12a is called the *Hartung governor*, in which the controlling springs are directly connected to the rotating balls. For the *Hartnell governor* shown in Fig. 6.12b, the controlling spring is connected to the sleeve. In both cases, the movement of the balls is transmitted to the sleeve by means of a bell-crank lever (with arms at right angles), as shown in the figure.

Hartung Governor

Figure 6.13 shows the free-body diagram of a bell-crank lever when the radius of rotation of the ball centre is r . Let

k = stiffness of the spring,

P = spring force at radius r ,

M = mass at the sleeve,

m = mass of the ball,

F = controlling force (at the centre of the ball),

c = radius at which the spring force is zero, i.e., when the spring attains its free length,

b = length of the arm to which the ball is connected,

a = length of the arm connected to the sleeve, and

α = inclination of the arms as shown in Fig. 6.13.

We shall neglect the friction and the moment of the weight mg about the pivot point O .

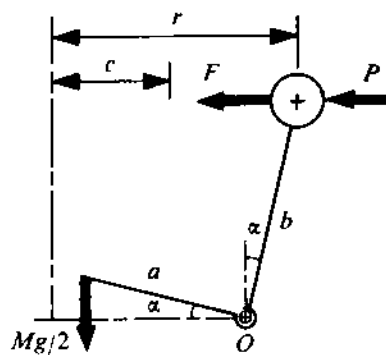


FIGURE 6.13

Taking moments of all the external forces about O , we have

$$F.b \cos \alpha = P.b \cos \alpha + (Mg/2)a \cos \alpha, \quad F = P + Mga/(2b).$$

Further, we see that $P = k(r - c)$ as $(r - c)$ is the compression of the spring. Thus,

$$F = k(r - c) + \frac{Mga}{2b} = k[r - (c - \frac{Mga}{2bk})]. \quad (6.21)$$

So, the controlling-force curve is a straight line with a slope k and an intercept $\{c - (Mga)/(2bk)\}$ on the r -axis (Fig. 6.14). From this curve, the governor is seen to be stable everywhere. The equilibrium speed ω at radius r is given by

$$\begin{aligned} m\omega^2 r &= k[r - (c - \frac{Mga}{2bk})], \\ \omega^2 &= \frac{k}{rm}[r - (c - \frac{Mga}{2bk})]. \end{aligned} \quad (6.22)$$

By adjusting the initial compression of the spring, if c is made equal to $Mga/(2bk)$, the controlling-force curve (the straight line) passes through the origin and the governor becomes isochronous. To determine the isochronous speed, we have $dF/dr = F/r$ and $k = m\omega^2$. Thus, the isochronous speed is

$$\omega_s = (k/m)^{1/2} \quad (6.23)$$

and the condition for isochronism is

$$c = Mga/(2k). \quad (6.24)$$

If a Hartung governor is made isochronous without considering friction as in the foregoing analysis, it can be readily shown that with friction such a governor is stable only for falling speed. The proof of this is left as an exercise for the reader.

Hartnell Governor

Figure 6.15 shows the free-body diagram of the bell-crank lever when the radius of rotation of the ball is r . Let

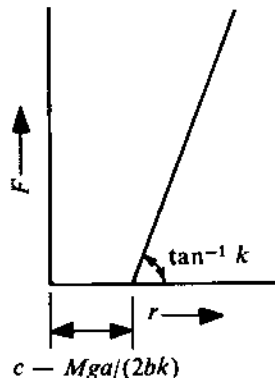


FIGURE 6.14

k = stiffness of the spring,

P = total force at the sleeve due to the weight of the sleeve and the spring,

m = mass of the ball,

F = controlling force of the ball,

p = distance of the pivot O from the axis of rotation,

b = length of the arm to which the ball is connected,

a = length of the arm connected to the sleeve, and

α = inclination of the arms as indicated in Fig. 6.15.

For the present, we shall neglect the friction at the sleeve.

Taking moments about the pivot O , we have

$$\begin{aligned} F \cdot b \cos \alpha &= \frac{P}{2} a \cos \alpha - mg \cdot b \sin \alpha, \\ F &= \frac{Pa}{2b} - mg \tan \alpha. \end{aligned} \quad (6.25)$$

Further, we see that $P = P_0 + ka \sin \alpha$, where P_0 is the value of P with $\alpha = 0$, and

$$\sin \alpha = (r - p)/b. \quad (6.26)$$

Using this value of P in (6.25), we get

$$F = \frac{P_0 a}{2b} + \frac{ka^2}{2b^2}(r - p) - mg \tan \alpha. \quad (6.27)$$

The equilibrium speed ω at any radius r is given by

$$m\omega^2 r = \frac{P_0 a}{2b} + \frac{ka^2}{2b^2}(r - p) - mg \tan \alpha, \quad (6.28)$$

where α is found from (6.26) and P_0 depends on the initial compression of the spring (by initial compression, we do not necessarily mean the compression for $\alpha = 0$; it is the compression of the spring at the lowest position of the sleeve).

To start with, let us neglect the moment of the weight of the ball, i.e., the last term in (6.27), so that

$$F = \frac{P_0 a}{2b} + \frac{ka^2}{2b^2}(r - p). \quad (6.29)$$

So, the controlling-force curve is a straight line CD with a slope of $ka^2/(2b^2)$, passing through the point $A [p, P_0 a/(2b)]$ as shown in Fig. 6.16.

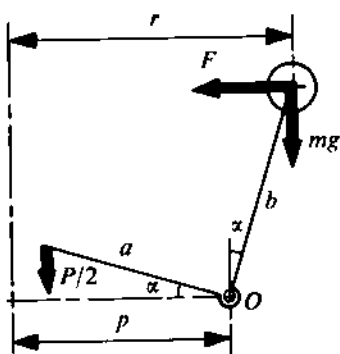


FIGURE 6.15

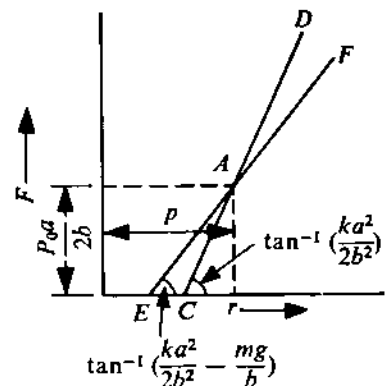


FIGURE 6.16

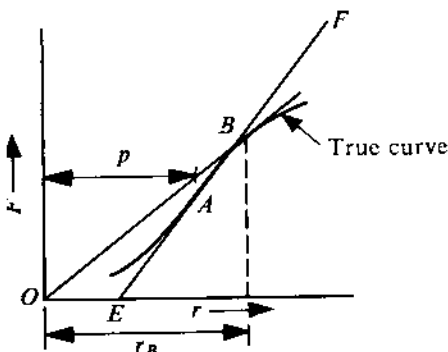


FIGURE 6.17

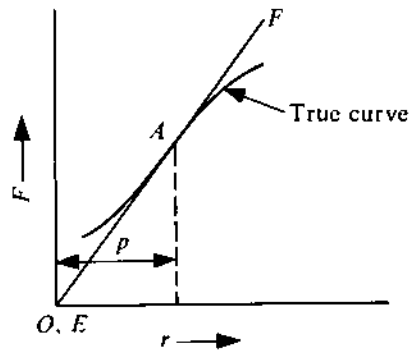


FIGURE 6.18

As a second approximation, we can use $\sin \alpha = \tan \alpha$ which is valid for small values of α . Then, from (6.26) and (6.27), we get

$$F = \frac{P_0 a}{2b} + \left(\frac{ka^2}{2b^2} - \frac{mg}{b} \right) (r - p). \quad (6.30)$$

This curve is also a straight line EF passing through the point A , with a slope of $[ka^2/(2b^2) - mg/b]$, as shown in Fig. 6.16. The true curve given by (6.27) also passes through A and is tangential to the line EF at the point A (because, for $\alpha = 0$, the values of F and dF/dr are the same in both cases). The nature of the true curve is shown in Fig. 6.17. If the tangent to this curve, drawn from the origin, meets the curve at B , then the radius r_B corresponding to the point B gives the limit for the stability of operation. For $r > r_B$, the governor becomes unstable as seen from Fig. 6.17 (dF/dr becomes less than F/r).

If, by the proper choice of parameters, the straight line EF is made to pass through the origin O , then the governor becomes locally isochronous at A (Fig. 6.18) and is unstable anywhere else. The condition for isochronism at A is

$$dF/dr = F/r \text{ at } A,$$

$$\frac{ka^2}{2b^2} - \frac{mg}{b} = m\omega_0^2, \quad (6.31)$$

where ω_0 is the isochronous speed.

For the analysis with friction, the force at the sleeve should be replaced by $(P \pm f)$, where f is the friction force. The plus sign applies to rising speed and the minus sign to falling speed.

PROBLEM 6.4

The total sleeve movement in a spring-controlled Hartnell governor is 3 cm. The mass of the rotating balls is 1.35 kg each. At the midposition of the sleeve, the sleeve arm, which is 6.25 cm long, is horizontal. The ball arm has a length of 7.5 cm. At the midposition of the sleeve, the balls rotate at a radius of 10 cm.

Due to maladjustment of the spring, the equilibrium governor speed at the topmost position of the sleeve is 420 rpm and that corresponding to the lowest position of the sleeve is 435 rpm.

Determine (i) the stiffness and initial compression of the spring, and (ii) the required initial compression of the spring to give an equilibrium speed at the topmost position which is 12 rpm more than that at the lowest position. Neglect the moment due to the weight of the ball.

SOLUTION

Given $a = 6.25$ cm, $b = 7.5$ cm, $r_{\text{mid}} = 10$ cm, and $m = 1.35$ kg. So,

$$r_b = 10 - \frac{3}{2} = 8.5 \text{ cm}, \quad \omega_b = 435 \times (\pi/30) = 45.6 \text{ rad/s},$$

$$r_t = 10 + \frac{3}{2} = 11.5 \text{ cm}, \quad \omega_t = 420 \times (\pi/30) = 44 \text{ rad/s},$$

where the subscripts b and t denote the bottom and top positions, respectively.

(i) From (6.25), neglecting the moment due to the weight of the ball, we have $F = Pa/(2b)$. Using this for the bottom and top positions, we get

$$F_b = m\omega_b^2 r_b = P_b a / (2b), \quad (a)$$

$$F_t = m\omega_t^2 r_t = P_t a / (2b). \quad (b)$$

So,

$$P_b = 1.35 \times \frac{(45.6)^2 \times .085 \times .15}{.0625} = 572.3 \text{ N},$$

$$P_t = 1.35 \times \frac{(44)^2 \times .115 \times .15}{.0625} = 721.3 \text{ N}.$$

Thus, the spring stiffness is

$$k = \frac{P_t - P_b}{\text{sleeve movement}} = \frac{149}{3} = 49.67 \text{ N/cm},$$

and the initial compression of the spring is

$$\frac{P_b}{k} = \frac{572.3}{49.67} = 11.57 \text{ cm}.$$

(ii) It is given that

$$N_t = N_b + 12, \quad \omega_t = \omega_b + 12 \times (\pi/30) = \omega_b + 1.257.$$

From equation (a), we get

$$m(\omega_b)^2 r_b = \frac{P_b a}{2b},$$

$$P_b = 1.35 \times \frac{.085 \times .15}{.0625} \omega_b^2 = 0.28\omega_b^2.$$

Similarly,

$$P_t = 1.35 \times \frac{.115 \times .15}{.0625} \omega_t^2 = 0.37\omega_t^2.$$

Now,

$$P_t = P_b + 3k = P_b + 149$$

or

$$0.37\omega_t^2 = 0.28\omega_b^2 + 149,$$

$$0.37(\omega_b + 1.257)^2 = 0.28\omega_b^2 + 149$$

or

$$\omega_b = 35.8 \text{ rad/s (taking the positive value).}$$

So,

$$P_b = 0.28(35.8)^2 \text{ N} = 358.9 \text{ N},$$

and the initial compression is

$$\frac{P_b}{k} = \frac{358.9}{49.67} = 7.22 \text{ cm.}$$

6.6 HUNTING OF CENTRIFUGAL GOVERNORS

Whenever there is a change in the mean speed, centrifugal governors develop a tendency to oscillate around the desired new mean position. This is because of the fact that when there is a change in the load on the engine, with a consequent change in engine speed, the governor balls and the sleeve seek a new position to restore the original speed. However, due to inertia, they overshoot the mark and thereafter again move towards the desired position in the opposite direction with the same result. The process is then repeated, and oscillations are set up. If the frequency of fluctuations in engine speed happens to coincide with the natural frequency of oscillations of the governor, then, due to resonance, the amplitude of oscillations becomes very high, with the result that the governor tends to intensify the speed variation instead of controlling it. Such a situation is known as *hunting*.

The problem of hunting becomes more acute when the sensitiveness of a governor is high, i.e., when a change in speed causes a large sleeve movement. For example, an isochronous governor (i.e., one that is infinitely sensitive) will oscillate between the highest and the lowest positions if the speed deviates from the isochronous speed.

Let us calculate the natural period of oscillation of the governor ball considering a Hartnell governor. Let

r = radius of the governor ball at a steady speed, and

δr = change in r at the same speed.

Considering the oscillation of the governor ball in the radial direction, $\delta r = x$ is the amount of displacement from the equilibrium position. So, the equation of motion for the oscillation of the governor ball can be written as

$$m_{eq}\ddot{x} + (dF/dr - m\omega^2)\delta r = 0, \quad (6.32)$$

where

$$\begin{aligned} \frac{dF}{dr}\delta r - m\omega^2\delta r &= \text{change in the controlling force} - \text{change in the centripetal force} \\ &= \text{restoring force}, \end{aligned}$$

m = mass of the governor ball, and

m_{eq} = equivalent mass of the governor ball for acceleration in the radial direction.

From (6.32), we have

$$m_{eq}\ddot{x} + (dF/dr - m\omega^2)x = 0.$$

So, the natural period of oscillation is

$$\tau = 2\pi \left[\frac{m_{eq}}{dF/dr - m\omega^2} \right]^{1/2}. \quad (6.33)$$

For an isochronous governor, $dF/dr = m\omega^2$ [from (6.5)] and the time period becomes infinite.

For a Hartnell governor, to find m_{eq} , we use the fact that the kinetic energy of the ball remains the same. If V is the actual velocity of the ball, then $\dot{x} = V \cos \alpha$ (see Fig. 6.15). Now,

$$\begin{aligned} \frac{1}{2}m_{eq}\dot{x}^2 &= \frac{1}{2}mV^2, \\ m_{eq} &= m \sec^2 \alpha. \end{aligned} \quad (6.34)$$

From (6.26), we get

$$\begin{aligned} \cos \alpha \frac{d\alpha}{dr} &= \frac{1}{b}, \\ \frac{d\alpha}{dr} &= \frac{1}{b} \sec \alpha. \end{aligned} \quad (6.35)$$

From (6.27), we get

$$\frac{dF}{dr} = \frac{ka^2}{2b^2} - mg \sec^2 \alpha \frac{d\alpha}{dr}.$$

Using (6.35), we find this equation becomes

$$\frac{dF}{dr} = \frac{ka^2}{2b^2} - \frac{mg}{b} \sec^3 \alpha. \quad (6.36)$$

Substituting the values obtained from (6.34) and (6.36) in (6.33), for a Hartnell governor, we get

$$\tau = \frac{2\pi \sec \alpha}{[ka^2/(2b^2m) - \frac{g}{b} \sec^3 \alpha - \omega^2]^{1/2}}. \quad (6.37)$$

3.7 APPROXIMATE ANALYSIS OF SPEED-LOAD CHARACTERISTICS OF AN ENGINE

In Section 6.1, we mentioned that the speed-load characteristic of an engine becomes flatter when a governor is used. We shall illustrate this by considering a Porter governor. Let

T = load torque on the engine in N-m,

N = speed (in rpm) of the engine with load T ,

η (efficiency of the engine) = $f(N)$ as given by Fig. 6.1, and

P_i = power input to the engine in W.

Then, without the governor, we have

$$P_i \text{ (constant)} = \frac{2\pi}{60} \frac{NT}{\eta}. \quad (6.38)$$

Assuming the η - N curve (Fig. 6.1) to be a parabola, we can write

$$\eta = f(N) = \eta_0 [1 - (1 - \frac{N}{N_0})^2], \quad (6.39)$$

where

η_0 = maximum efficiency, and

N_0 = optimum speed when efficiency is maximum (i.e., for η_0).

If T_0 is the load at speed N_0 , then

$$P_i = \frac{2\pi}{60} \frac{N_0 T_0}{\eta_0}. \quad (6.40)$$

Using (6.38) and (6.39), we get

$$NT = \frac{60}{2\pi} \eta_0 P_i \left(\frac{2N}{N_0} - \frac{N^2}{N_0^2} \right)$$

or

$$T = \frac{60}{2\pi} \eta_0 P_i \left(\frac{2}{N_0} - \frac{N}{N_0^2} \right). \quad (6.41)$$

Thus, the N - T characteristic is a straight line AB as shown in Fig. 6.19. The slope of this line, from (6.41), is

$$\begin{aligned} \frac{dN}{dT} &= -\frac{N_0^2}{\eta_0 P_i} \times \frac{2\pi}{60} \\ &= -N_0/T_0 \quad [\text{from (6.40)}]. \end{aligned} \quad (6.42)$$

Let us now assume that the same engine is fitted with a Porter governor shown in Fig. 6.2 and that the power input to the engine at speed N_0 is given by (6.40) for $N = N_0$ when $T = T_0$, i.e.,

$$P_i^0 = \frac{2\pi N_0 T_0}{60\eta_0}. \quad (6.40a)$$

However, this is no longer constant and is controlled by the governor as the load (i.e., the speed) changes. Referring to Fig. 6.2 and (6.10), the controlling force is

$$F = g(m + M) \tan \theta,$$

$$m\omega^2 r = g(m + M)r/h,$$

$$h = (1 + \frac{M}{m}) \frac{g}{\omega^2} = (1 + \frac{M}{m}) \frac{g}{(4\pi^2/3600)N^2} \quad [\text{as } \omega = \frac{2\pi N}{60}]$$

$$= \frac{K}{N^2} \quad [K = \frac{900g}{\pi^2} (1 + \frac{M}{m})].$$

Hence,

$$dh = -\frac{2K}{N^3} dN. \quad (6.43)$$

From Fig. 6.2, the sleeve movement corresponding to this is

$$ds = 2\beta dh = -4K\beta \frac{dN}{N^3}. \quad (6.44)$$

So, the movement at the other end of the lever, i.e., at the control valve, is $L ds$, where L = ratio of leverage. Let the change in the input power be proportional to this movement and the constant of proportionality be α . Then,

$$dP_i = \alpha L ds = -4K\beta\alpha L \frac{dN}{N^3} = -\gamma \frac{dN}{N^3} \quad [\gamma (= 4K\beta\alpha L) \text{ is constant}].$$

Integrating this equation, we get

$$\int_{P_i^0}^{P_i} dP_i = -\gamma \int_{N_0}^N \frac{dN}{N^3},$$

$$P_i - P_i^0 = \frac{\gamma}{2} \left(\frac{1}{N^2} - \frac{1}{N_0^2} \right),$$

$$P_i = P_i^0 + \frac{\gamma}{2} \left(\frac{1}{N^2} - \frac{1}{N_0^2} \right),$$

$$\frac{2\pi NT}{60\eta} = P_i^0 + \frac{\gamma}{2} \left(\frac{1}{N^2} - \frac{1}{N_0^2} \right).$$

Using (6.39), we get

$$\frac{2\pi}{60\eta_0} \left[\frac{NT}{\frac{2N}{N_0} - \frac{N^2}{N_0^2}} \right] = P_i^0 + \frac{\gamma}{2} \left(\frac{1}{N^2} - \frac{1}{N_0^2} \right),$$

$$\frac{2\pi}{60\eta_0} T = \left(\frac{2}{N_0} - \frac{N}{N_0^2} \right) [P_i^0 + \frac{\gamma}{2} \left(\frac{1}{N^2} - \frac{1}{N_0^2} \right)].$$

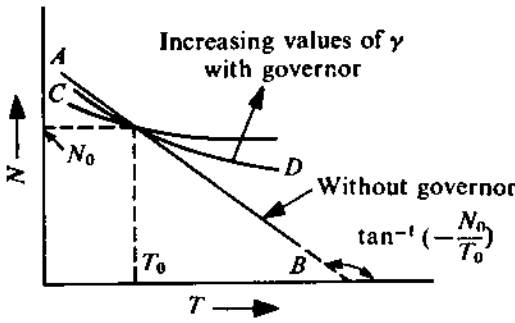


FIGURE 6.19

Differentiating both sides of this equation with respect to T , we get

$$\frac{2\pi}{60\eta_0} = -\left(\frac{2}{N_0} - \frac{N}{N_0^2}\right)\frac{\gamma}{N^3} \frac{dN}{dT} + [P_i^0 + \frac{\gamma}{2}(\frac{1}{N^2} - \frac{1}{N_0^2})]\left(-\frac{1}{N_0^2} \frac{dN}{dT}\right).$$

Let us find the slope dN/dT at $N = N_0$. We can do this as

$$\frac{2\pi}{60\eta_0} = -\frac{\gamma}{N_0^4} \left(\frac{dN}{dT}\right)_{N=N_0} - P_i^0 \frac{1}{N_0^2} \left(\frac{dN}{dT}\right)_{N=N_0}.$$

Using (6.40a), we get

$$\begin{aligned} -\frac{2\pi}{60\eta_0} &= \left(\frac{dN}{dT}\right)_{N=N_0} \left[\frac{2\pi T_0}{60\eta_0 N_0} + \frac{\gamma}{N_0^4} \right], \\ \left(\frac{dN}{dT}\right)_{N=N_0} &= -\frac{2\pi/(60\eta_0)}{\frac{2\pi T_0}{60\eta_0 N_0} + \frac{\gamma}{N_0^4}} = -\frac{N_0}{T_0 + \frac{60\eta_0}{2\pi} \frac{\gamma}{N_0^3}}. \end{aligned} \quad (6.45)$$

Comparing (6.45) with (6.42), we see that, with the governor, the N - T characteristic becomes flatter as shown by the curve CD in Fig. 6.19. By increasing the value of γ (i.e., of K , α , or L), the slope of the curve will reduce. Thus, with the change in load T , the speed N does not vary as much from the optimum speed N_0 as it would have without the governor.

6.8 INERTIA GOVERNORS

Figure 6.20a shows a schematic representation of an inertia governor. As depicted, the relative movement of the governor balls is controlled by the action of a spring. The arm connecting the balls is hinged at A on the flywheel connected to the shaft. The relative position of the ball arm with respect to the flywheel is represented by θ which depends on the angular velocity ω as well as on the instantaneous angular acceleration α of the shaft. The relative movement of the ball arm is used to control the power input to an engine. The dependence of the relative movement ϕ (Fig. 6.20b) on the angular acceleration α can be obtained as follows.

The inertia forces on the governor balls, each of mass m , are obtained from

$$a_x = a_A + a_{x/A},$$

$$a_y = a_A + a_{y/A}.$$

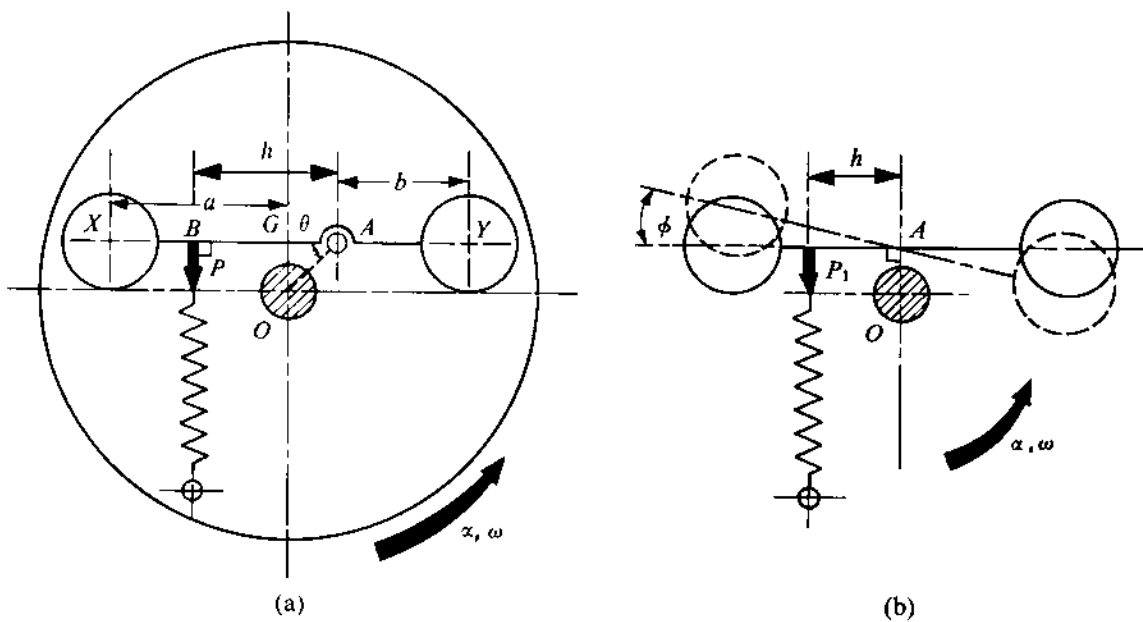


FIGURE 6.20

Now, taking moments of all the forces acting on the rigid rod \$XY\$ about the hinge point \$A\$, the equilibrium equation we get is

$$\begin{aligned} m\ddot{\Omega}.AX^2 + m\alpha.OA.AX \cos\theta - m\omega^2.OA.AX \sin\theta + m\omega^2.OA.AY \sin\theta \\ + m\ddot{\Omega}.AY^2 - m\alpha.OA.AY \cos\theta + (P_0 + k.AB\phi).AB = 0, \end{aligned} \quad (6.46)$$

where

\$P_0\$ = spring force when \$\phi\$ is equal to zero (considered to be the starting position),

\$k\$ = stiffness of the spring,

\$\Omega\$ (angular velocity of the rod \$XY\$) = \$\dot{\theta}\$ - \$\omega\$, and

\$\theta\$ = \$\theta_0\$ + \$\phi\$ (\$\theta_0\$ is the starting equilibrium position when the shaft is rotating at a constant speed \$\omega\$), \$\phi\$ being small.

Equation (6.46) can be written with \$\theta_0 = \pi/2\$ (assumed) as

$$J_A\ddot{\phi} + [kh^2 - mae(a - b)]\phi = J_A\alpha + m\omega^2e(a - b) - P_0h, \quad (6.47)$$

where

$$J_A = m(a^2 + b^2), \quad AX = a, \quad AY = b, \quad OA = e, \quad AB = h.$$

Thus, the differential equation we get for ϕ is

$$\ddot{\phi} + \mu\phi = \nu \quad (6.48)$$

with

$$\begin{aligned}\mu &= \frac{kh^2 - mae(a - b)}{J_A}, \\ \nu &= \frac{J_A\alpha + m(\omega_0 + \alpha t)^2 e(a - b) - P_0 h}{J_A},\end{aligned}$$

where ω_0 is the initial design speed and α is constant. Solving (6.48), we obtain

$$\phi = C_1 \sin \sqrt{\mu}t + C_2 \cos \sqrt{\mu}t + \frac{\nu}{\mu} - \frac{2m\alpha^2 e(a - b)}{J_A \mu^2}. \quad (6.49)$$

The adjustments are such that when the shaft rotates at the design speed ω_0 , $\theta = \theta_0 = \pi/2$. So, $m\omega_0^2 e(a - b) = P_0 h$. Thus,

$$\nu = \alpha + \frac{m\alpha^2 e(a - b)t^2}{J_A} + \frac{2m\omega_0 \alpha e(a - b)t}{J_A}. \quad (6.50)$$

Using the initial conditions

$$\phi = \dot{\phi} = 0 \quad (\text{at } t = 0),$$

we have

$$\begin{aligned}C_2 &= \frac{2m\alpha^2 e(a - b)}{J_A \mu^2} - \frac{\alpha}{\mu}, \\ C_1 &= -\frac{2m\omega_0 \alpha e(a - b)}{J_A \mu^{3/2}}.\end{aligned}$$

PROBLEM 6.5

For an inertia governor, $e = 2.5$ cm, $h = 5$ cm, $a = 7$ cm, $b = 2$ cm, $k = 7$ N/cm, and $m = 0.34$ kg. Assuming an initial running speed of 300 rpm, determine the values of ϕ during the period the speed increases up to 390 rpm at the rate of 50 rad/s^2 .

SOLUTION

Let us determine the values of ϕ at intervals of $\pi/100$ s. Using the given data (converting cm into m), we have

$$\begin{aligned}J_A &= m(a^2 + b^2) = 18.02 \text{ kg-cm}^2 = 18.02 \times 10^{-4} \text{ kg-m}^2, \\ \mu &= \frac{700 \times 0.05^2 - 0.34 \times 50 \times 0.025 \times (0.07 - 0.02)}{18.02 \times 10^{-4}} \approx 960 \text{ s}^{-2}.\end{aligned}$$

Using (6.50) and (6.49), the values of ν and ϕ can be obtained. The final expression for ϕ then becomes

$$\phi = -0.025 \sin 31t - 0.0487 \cos 31t + 0.05 + 0.0772t + 0.615t^2 - 0.0013,$$

and the values of ϕ at intervals of $\pi/100$ s are as shown in Table 6.2.

TABLE 6.2

Time (s)	Shaft (rpm)	ϕ (degrees)
0	300	0
$\pi/100$	315	1.46
$\pi/50$	330	5.4
$3\pi/100$	345	9.68
$\pi/25$	360	11.92
$\pi/20$	375	11.54
$3\pi/50$	390	10.47

6.9 OTHER GOVERNOR MECHANISMS

As already stated, a governor mechanism can also control the speed by dissipating the excess kinetic energy. Such a system is simple since the input energy does not require to be restrained, and can be very conveniently used for a small machine. One very common example of this governor is the hand-wound gramophone. To understand its principle of operation, let us consider the system shown in Fig. 6.21. Here, the shaft, driven by a torque T , rotates with a speed ω . The flymass A also rotates in a horizontal plane with the same speed. The centrifugal force F_c acts in the radially-outward direction and the flymass is prevented from having any radial movement by the brake-drum reaction force N . Thus, $N = F_c = mr\omega^2$, where m is the mass of A . Let the resistive torque acting on the shaft T_R be proportional to ω^2 or $T_R = \lambda\omega^2$, where λ is the constant of proportionality. Now, to see the effectiveness of the governing mechanism, let us find out $(d\omega/dT)$ with and without the governor. When the system operates steadily under the effect of the driving torque T without the governor,

$$T = T_R = \lambda\omega^2$$

or

$$\left(\frac{d\omega}{dT}\right)_{\text{without governor}} = \frac{1}{2(\lambda T)^{1/2}}. \quad (6.51)$$

If the governor mechanism is used, the condition of steady operation gives

$$T = T_R + T_f,$$

where T_f (frictional torque) = $F_f \cdot R = \mu N R = \mu m r \omega^2 R$. Thus,

$$T = (\lambda + \mu m r R)\omega^2$$

or

$$\left(\frac{d\omega}{dT}\right)_{\text{with governor}} = \frac{1}{2[(\lambda + \mu m r R)T]^{1/2}}. \quad (6.52)$$

Comparing (6.51) and (6.52), we find that, in the presence of the governor, the variation of speed is less sensitive to that of the input torque.

The principle of energy dissipation can be applied more effectively if suitable springs are used. Two common mechanisms with springs are shown in Fig. 6.22. It should be noted that in such a system the driving torque should always be more than $\lambda\omega_0^2$, where ω_0 is the desired running speed of the system.

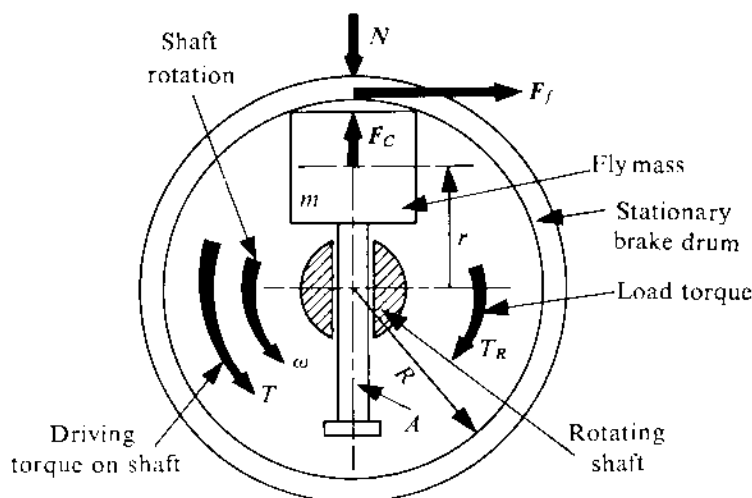


FIGURE 6.21

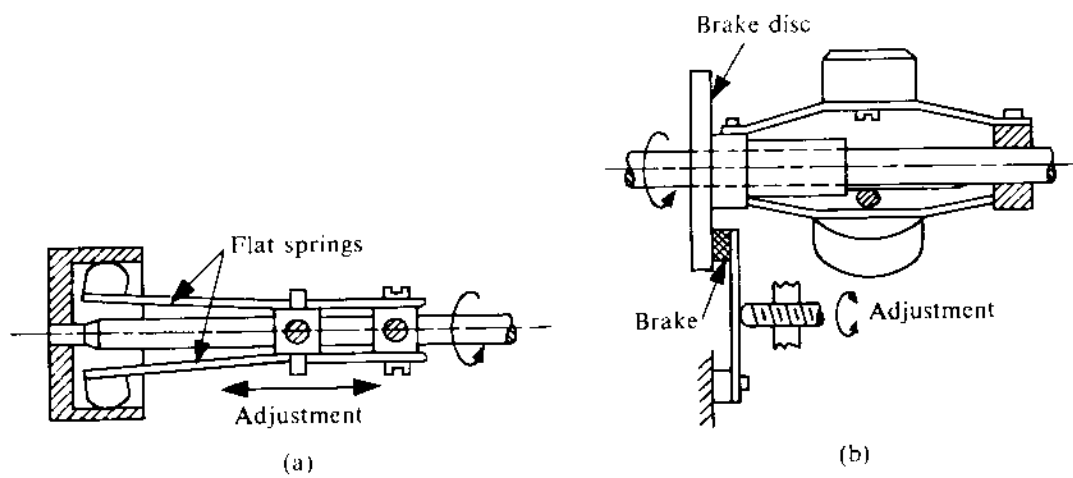


FIGURE 6.22

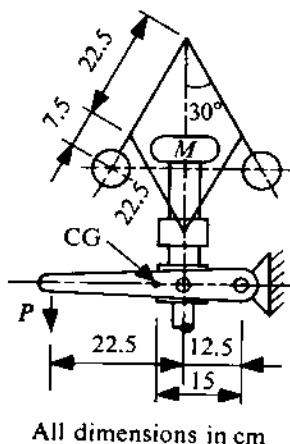


FIGURE 6.23

6.10 PROBLEMS

- 6.6 A Porter governor is shown in Fig. 6.23. The sleeve operates a lever of mass 2.5 kg. This lever has to exert a pull of 30 N at its other end to operate the control mechanism. The mass of each rotating ball is 3.5 kg. The mass of the sleeve itself is 1.25 kg. The friction force at the sleeve has a constant value of 20 N. Determine the central mass on the sleeve so that the sleeve moves up from this position at a speed of 180 rpm. Also find the speed at which the sleeve starts moving down from this position.
- 6.7 All the links of a Proell governor are 25.5 cm long and are pivoted on the axis of rotation. The mass of each governor ball is 4.6 kg and the balls are attached to the extensions of the lower links which are 6.4 cm long. These extensions are parallel to the governor axis when the radius of rotation of the balls is 15.2 cm. Determine the equilibrium speed at this configuration with a central mass of 36.4 kg on the sleeve.
- 6.8 In Problem 6.7, find the alteration required in the central load to produce $d\omega/dr = 0.35 \text{ rad/cm}^2$ at the given configuration. Also determine the equilibrium speed after this alteration.
- 6.9 In a Hartung governor, each of the rotating balls has a mass of 9 kg and each spring has a stiffness of 270 N/cm. The length of each spring is 11.4 cm when the radius of rotation of the balls is 6.9 cm, and the equilibrium speed is 360 rpm. Neglecting the mass of the sleeve, determine the free length of each spring and also investigate whether the governor is isochronous and stable.
- 6.10 Each of the rotating balls of a Hartung governor has a mass of 3.2 kg. The minimum and maximum radii of rotation of the governor balls are 11.4 cm and 14 cm, respectively. Each spring has a stiffness of 87.78 N/cm and an initial compression of 5.1 cm. The mass of the sleeve is negligible. Determine the equilibrium speed of the governor at the mean position when the radius is 12.70 cm. Also find the required spring stiffness and the initial compression to make the governor isochronous at this speed.
- 6.11 The sleeve arm and the ball arm of a Hartnell governor are 9 cm and 10 cm long, respectively. At the mean position of the sleeve, the radius at which the balls rotate is 12 cm when the equilibrium speed is 300 rpm. Each rotating ball has a mass of 2 kg and the sleeve movement

is ± 2 cm from the mean position. The minimum speed is 96% of the mean speed. Determine (i) the stiffness of the spring, and (ii) the maximum speed of the governor. Neglect the frictional resistance.

- 6.12 For the stationary position of a Hartnell governor, the 3-cm-long sleeve arm is horizontal. The ball arm is 6 cm long and the fulcrum of the lever is 5 cm from the governor axis. The sleeve begins to rise at 250 rpm and moves up by 1.5 cm at 260 rpm. Each rotating ball has a mass of 1 kg. Neglecting friction, determine (i) the stiffness of the spring, (ii) the initial spring force P_0 , and (iii) the speed and radius at which the governor becomes unstable. Also plot the controlling-force curve.
- 6.13 The arms of a Hartnell governor are of equal length. At midposition of the sleeve, the ball arm is vertical and the radius at which the ball rotates is 8.25 cm when the equilibrium speed, neglecting friction, is 450 rpm. On changing the speed by 1%, the governor is able to overcome the friction at this position. The friction force is assumed to have a constant value of 30 N at the sleeve. The sleeve moves ± 1.6 cm from the mean position. The minimum speed of the governor (including friction) is 428 rpm. The mass of the sleeve is 3.5 kg. Determine (i) the magnitude of the rotating masses, (ii) the spring stiffness, and (iii) the initial compression of the spring.
- 6.14 Solve Problem 6.5 when each of a and b is 7 cm, the other data remaining unchanged. Also, comment on the initial value of the spring force P_0 .

Chapter 7

BALANCING OF INERTIA FORCES AND MOMENTS IN MACHINES

7.1 INTRODUCTION

In Chapter 4, we observed that the inertia force and the inertia moment of a body are, respectively, equal and opposite to the resultants of all the external forces and moments. Thus, when a machine has accelerating parts, the resultants of inertia forces and moments of all such accelerating parts represent the forces and the moments transmitted to the frame or foundation of the machine. By "frame", we mean only that surrounding structure of the machine which can supply the external forces and moments. If the direction and/or magnitude of these accelerations vary with time (as they generally do), the foundation is subjected to *dynamic forces* and *moments*. Besides being very harmful in reducing the life of the supports, these dynamic forces and moments set up vibrations which result in a noisy operation. So, for longer life and smoother operation of the machine, there is a need to balance these inertia forces and moments. There are two aspects of this balancing problem, namely, (i) the evaluation and analysis of inertia forces and moments, and (ii) the determination of convenient methods of balancing these quantities.

We shall first discuss the balancing of rotating machines and then consider the balancing of internal-combustion engines which have both reciprocating and rotating masses. Finally, we shall study the balancing of general mechanisms.

7.2 BALANCING OF ROTATING MASSES

If the centre of mass of a rotating machine (such as an alternator) does not lie on the axis of rotation, the inertia force is given by

$$F_i = m\omega^2 e, \quad (7.1)$$

where

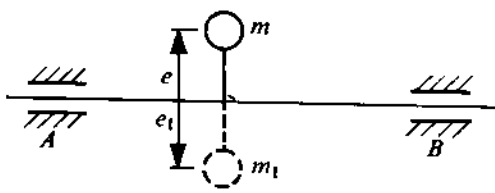


FIGURE 7.1

m = mass of the machine,

ω = angular speed of the machine, and

e = eccentricity, i.e., the distance from the centre of mass to the axis of rotation.¹

Though the magnitude of this force is constant, its direction changes continuously as the machine rotates. Thus, even with a small value of e , a considerable dynamic force is exerted on each bearing at a high speed (since the force varies as the square of the speed). Before discussing the balancing of rotors, we shall analyze the case of discrete unbalanced masses on a rotating shaft (e.g., a disc which is eccentric with respect to the axis of rotation). The theory we shall thus develop can then be readily extended to unbalanced rotors. *Static forces*, such as weights, will be neglected in the analysis, and only the inertia forces (centrifugal forces) of unbalanced masses will be considered.

Internal and External Balancing

Let a shaft carry an unbalanced mass m , with the centre of mass located at a distance e from the axis of rotation (Fig. 7.1). The shaft can be completely balanced by adding a mass m_1 at a distance e_1 from the axis of rotation, diametrically opposite to m , so that

$$m\omega^2 e = m_1\omega^2 e_1 \quad (\text{where } \omega = \text{speed of rotation of the shaft}),$$

$$me = m_1e_1. \quad (7.2)$$

In this case, the dynamic reactions at the bearings (say, at A and B) will be zero, i.e., $R_A = 0 = R_B$. The shaft will also be free from any dynamic bending stress. This situation is referred to as *internal balancing*.

Alternatively, the dynamic reactions R_A and R_B can be reduced to zero (see Fig. 7.2) by adding two balancing masses m_1 and m_2 at distances e_1 and e_2 , respectively, from the shaft, in the same axial plane as m but on the opposite side of the axis of rotation. With this arrangement, we get

$$me = m_1e_1 + m_2e_2, \quad (7.3)$$

$$mea = m_1e_1a_1 + m_2e_2a_2, \quad (7.4)$$

where a , a_1 , and a_2 represent the distance of the masses m , m_1 , and m_2 , respectively, from A . This situation is referred to as *external balancing* where the entire length of the shaft is not free from

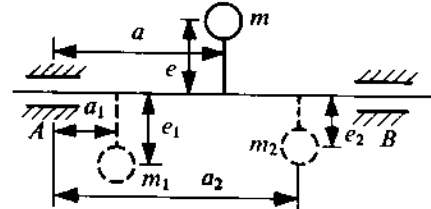


FIGURE 7.2

¹The term eccentricity is used here to represent a scalar quantity. However, in a problem of rotating mass, this term can also be used in the sense of a distance vector. In such a case, the direction of the resulting centrifugal force corresponds to that of the eccentricity vector.

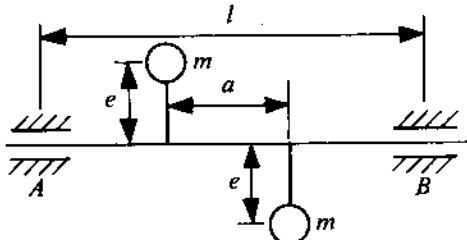


FIGURE 7.3

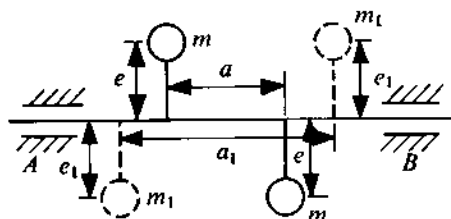


FIGURE 7.4

dynamic bending stresses. In practice, a balancing mass can rarely be placed exactly opposite the unbalanced mass to achieve internal balancing. For this reason, the term "balancing" will generally be used to denote "external balancing".

Static and Dynamic Balancing

If a shaft carries a number of unbalanced masses such that the centre of mass of the system lies on the axis of rotation, the system is said to be *statically balanced*. Such a system may, nevertheless, exert dynamic forces at the supports when it is rotated. To explain this, let us consider the statically-balanced system shown in Fig. 7.3. Two equal masses m , each with an eccentricity e , are placed on opposite sides of the axis in the same axial plane. The axial distance between them is a . The dynamic reactions at the supports will be

$$R_B = -R_A = m(\omega^2 ea/l), \quad (7.5)$$

where ω = speed of rotation, and l = distance between the supports. Since $R_A + R_B = 0$, we can refer to this situation as one in which there is no *total dynamic reaction* at the supports. In this case, the unbalanced dynamic forces result in a pure couple ($= m\omega^2 ea$).

Now, suppose we add a pair of equal masses m_1 in the same axial plane as m , each with the same eccentricity e_1 , such that they are on opposite sides of the axis and the distance between them is a_1 , as shown in Fig. 7.4. For this arrangement, if the relation

$$mea = m_1e_1a_1 \quad (7.6)$$

is satisfied in such a manner that the couple due to the masses m_1 is opposite to that due to the masses m , then the dynamic reactions at the supports are

$$R_A = R_B = 0, \quad (7.7)$$

and the system is said to be *dynamically balanced*. It is obvious that a dynamically-balanced system is also statically balanced, but the reverse is not true. Thus, to ensure complete external balance in a rotating system, the following two conditions must be fulfilled:

- (i) The centre of mass of the system should lie on the axis of rotation when the resultant of all the inertia forces during rotation will be zero. This is the condition for static balance.
- (ii) The resultant couple due to all the inertia forces during rotation must be zero.

These two conditions together will give complete dynamic balance.

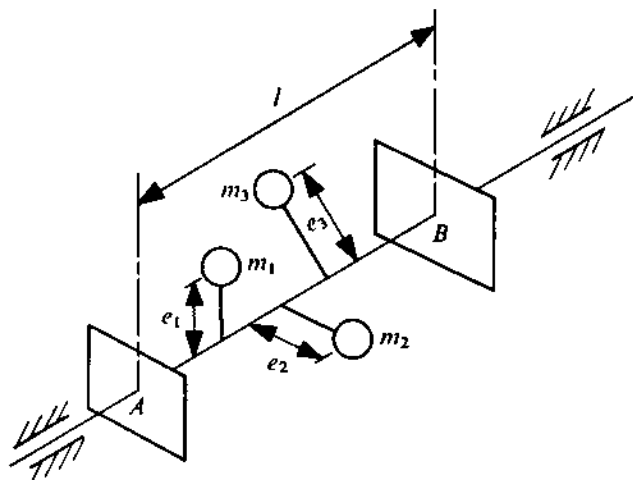


FIGURE 7.5

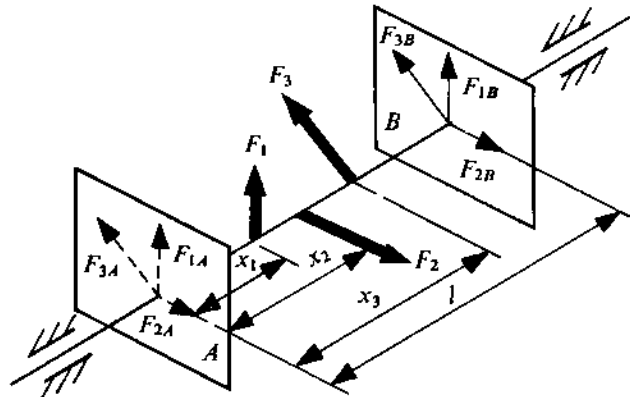


FIGURE 7.6

7.3 TWO-PLANE BALANCING

If a shaft carries a series of unbalanced masses in different axial planes, then two balancing masses in any two arbitrarily chosen planes are sufficient for complete dynamic balancing of the system. Figure 7.5 shows a shaft carrying three unbalanced masses m_1 , m_2 , and m_3 with eccentricities e_1 , e_2 , and e_3 , respectively, in three different axial planes. Let A and B be the positions of two arbitrarily chosen balancing planes at a distance l from each other. In Fig. 7.6, the unbalanced masses have been replaced by their respective inertia forces F_1 , F_2 , and F_3 along the respective eccentricities such that

$$F_1 = m_1 \omega^2 e_1, \quad F_2 = m_2 \omega^2 e_2, \quad F_3 = m_3 \omega^2 e_3,$$

ω being the speed of rotation. Let x_1 , x_2 , and x_3 denote the axial distances of these forces from the plane A .

Now, the force F_1 can be completely replaced by two equivalent forces F_{1A} and F_{1B} in the plane

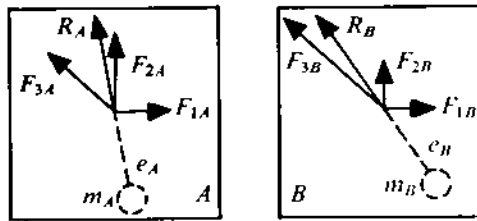


FIGURE 7.7

1 and B , respectively, acting in the direction of F_1 , where

$$F_{1A} = F_1 \left(1 - \frac{x_1}{l}\right), \quad F_{1B} = F_1 \frac{x_1}{l}. \quad (7.8a)$$

Similarly, F_2 and F_3 can be replaced by

$$F_{2A} = F_2 \left(1 - \frac{x_2}{l}\right), \quad F_{2B} = F_2 \frac{x_2}{l}, \quad (7.8b)$$

$$F_{3A} = F_3 \left(1 - \frac{x_3}{l}\right), \quad F_{3B} = F_3 \frac{x_3}{l}. \quad (7.8c)$$

Thus, the unbalanced forces F_1 , F_2 , and F_3 can be replaced by a set of three forces in each of the planes A and B . Let R_A be the resultant of F_{1A} , F_{2A} , and F_{3A} , and let R_B be the resultant of F_{1B} , F_{2B} , and F_{3B} (Fig. 7.7). These two forces R_A and R_B can be completely balanced by two balancing masses m_A and m_B in the planes A and B , respectively. They should be placed so as to act in directions opposite to R_A and R_B , with eccentricities e_A and e_B , such that

$$m_A \omega^2 e_A = R_A, \quad m_B \omega^2 e_B = R_B. \quad (7.9)$$

Thus, two masses in two balancing planes are sufficient for complete dynamic balancing.

It should be noted that balancing is independent of the rotational speed ω as the term ω^2 is common to all the unbalanced and balancing forces. This implies that a system balanced for one speed of rotation remains balanced for any other speed. It should also be observed that the product of mass and the corresponding eccentricity appears in the expressions for all forces. Henceforth, this product me will be referred to as *unbalance*, and the term ω^2 will be omitted everywhere.

7.4 DETERMINATION OF BALANCING MASSES

If a shaft carries n unbalances in different axial planes, the two balancing masses with prescribed eccentricities in two chosen balancing planes can be determined by both graphical and analytical methods. (Actually, the product of each mass and its eccentricity is obtained.) The choice of a suitable method depends on the problem. Figure 7.8a shows n unbalances ($m_1 e_1, m_2 e_2, m_3 e_3, \dots, m_n e_n$) on a shaft, in different axial planes 1, 2, 3, ..., n , designated by angles $\theta_1, \theta_2, \theta_3, \dots, \theta_n$, respectively (Fig. 7.8b), and measured conveniently in the same direction from an arbitrary reference plane. The balancing planes are designated 0 and $(n + 1)$. The axial locations of planes 1, 2, 3, ..., n are denoted by the distance from one of these reference planes (say, 0), shown to be $x_1, x_2, x_3, \dots, x_{n+1}$ in Fig. 7.8a. The axial distances will be considered positive when measured to the right. The problem is to determine $m_0 e_0$ and $m_{n+1} e_{n+1}$ (in planes 0 and $n + 1$, respectively) along with θ_0 and θ_{n+1} (to indicate the inclination of the axial planes containing $m_0 e_0$ and $m_{n+1} e_{n+1}$) to produce dynamic balance in the system. The following two conditions are to be satisfied:

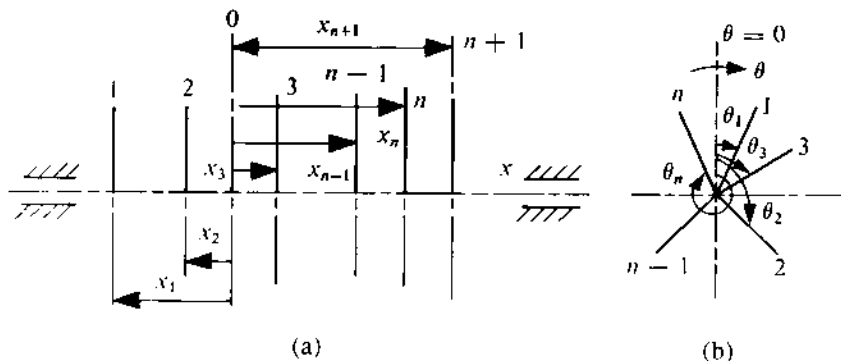


FIGURE 7.8

- (i) The resultant of the inertia forces of all $(n + 2)$ masses should be zero.
- (ii) The resultant couple (i.e., the moment about any point) of the inertia forces of all $(n + 2)$ masses should be zero.

The term ω^2 will be omitted, and the inertia forces will be represented by $m_i e_i$ (in the direction of e_i). Only the relative angular positions of the masses are important and the values of θ can be measured from any convenient reference line (here it is taken to be vertical). If the moments of forces are taken about the location of plane 0, the two aforementioned conditions can be written as

- (i) The vector sum of the forces is zero. Thus,

$$\sum_{i=0}^{n+1} m_i e_i = 0.$$

- (ii) The vector sum of the moments is zero. Thus,

$$\sum_{i=0}^{n+1} m_i e_i x_i = 0.$$

Obviously, $x_0 = 0$, and some values of x may be negative. The couple vectors $m_i e_i x_i$ are at 90° to the corresponding force vectors. The direction of the couple vectors will be obtained by rotating the corresponding force vectors in a clockwise direction (through 90°) for positive values of x , and in the counter-clockwise direction (through 90°) for negative values of x . Since only relative positions are important, as a convention, we shall consider all the couple vectors after rotation through 90° in the counter-clockwise direction. Thus, the couple vectors will be either in the direction of the forces i.e., in the direction of the unbalances (for positive values of x) or in the direction opposite thereto (for negative values of x). This concept will be further clarified by the discussion which follows.

Graphical Method

The procedure for the graphical method is as follows:

- (i) The unbalances $m_i e_i$ for $i = 1, \dots, n$ are drawn at proper relative angular positions $\theta_1, \dots, \theta_n$, respectively, as shown in Fig. 7.8b.

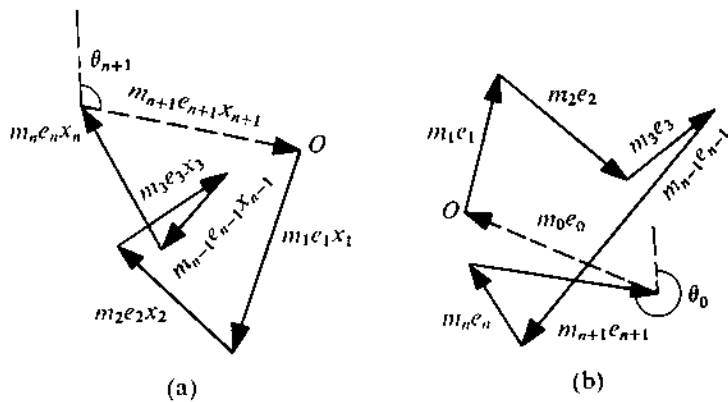


FIGURE 7.9

- (ii) The couple polygon with sides $m_i e_i x_i$ for $i = 1, \dots, n$ is drawn to some scale as shown in Fig. 7.9a. The couple vectors are either in the direction of e_i (for positive values of x_i) or in the direction opposite thereto (for negative values of x_i) as already explained. Since $x_0 = 0$, the closing side of the polygon (shown by the dashed line in Fig. 7.9a) represents $m_{n+1} e_{n+1} x_{n+1}$. As x_{n+1} is known, we can now find $m_{n+1} e_{n+1}$. The direction of this balancing mass, θ_{n+1} , can also be determined, because the vector $m_{n+1} e_{n+1} x_{n+1}$ will be either in the direction θ_{n+1} (if x_{n+1} is positive) or in the opposite direction (if x_{n+1} is negative).
- (iii) Now the force polygon with sides $m_i e_i$ for $i = 1, \dots, (n + 1)$ is drawn to some scale as shown in Fig. 7.9b. The closing side represents $m_0 e_0$ (shown by the dashed line) which gives both the magnitude of $m_0 e_0$ and its direction θ_0 .

Analytical Method

The foregoing problem of determining the two balancing masses can also be solved in the same way as by the graphical method but without drawing any diagrams. To do this, the forces and the couples are resolved along two mutually perpendicular directions, $\theta = 0$ and $\theta = 90^\circ$, and their values are as shown in Table 7.1 (as before, all couple vectors are assumed to be in the direction of the corresponding force vectors for positive values of x).

For complete external balancing, the summation of each of the last four columns of the table should be zero. From the couple vector columns, we get

$$m_{n+1} e_{n+1} x_{n+1} \cos \theta_{n+1} = - \sum_{i=1}^n m_i e_i x_i \cos \theta_i = A_1 \quad (\text{known}), \quad (7.10)$$

$$m_{n+1} e_{n+1} x_{n+1} \sin \theta_{n+1} = - \sum_{i=1}^n m_i e_i x_i \sin \theta_i = A_2 \quad (\text{known}). \quad (7.11)$$

Squaring (7.10) and (7.11) and adding, we get

$$(m_{n+1} e_{n+1} x_{n+1})^2 = A_1^2 + A_2^2, \quad m_{n+1} e_{n+1} x_{n+1} = (A_1^2 + A_2^2)^{1/2}.$$

Thus,

$$m_{n+1} e_{n+1} = (A_1^2 + A_2^2)^{1/2} / x_{n+1}. \quad (7.12)$$

Dividing (7.11) by (7.10), we have

$$\tan \theta_{n+1} = A_2/A_1 \quad (7.12)$$

which gives θ_{n+1} .

TABLE 7.1

Plane	Pro- duct	Distance from reference plane (vertical in this problem)	Angle with reference line	Couple vector		Force vector	
				Vertical component	Horizontal component	Vertical component	Horizontal component
0	$m_0 e_0$	$x_0 = 0$	θ_0	0	0	$m_0 e_0 \cos \theta_0$	$m_0 e_0 \sin \theta_0$
1	$m_1 e_1$	x_1	θ_1	$m_1 e_1 x_1 \cos \theta_1$	$m_1 e_1 x_1 \sin \theta_1$	$m_1 e_1 \cos \theta_1$	$m_1 e_1 \sin \theta_1$
2	$m_2 e_2$	x_2	θ_2	$m_2 e_2 x_2 \cos \theta_2$	$m_2 e_2 x_2 \sin \theta_2$	$m_2 e_2 \cos \theta_2$	$m_2 e_2 \sin \theta_2$
3	$m_3 e_3$	x_3	θ_3	$m_3 e_3 x_3 \cos \theta_3$	$m_3 e_3 x_3 \sin \theta_3$	$m_3 e_3 \cos \theta_3$	$m_3 e_3 \sin \theta_3$
⋮	⋮	⋮	⋮	⋮	⋮	⋮	⋮
n	$m_n e_n$	x_n	θ_n	$m_n e_n x_n \cos \theta_n$	$m_n e_n x_n \sin \theta_n$	$m_n e_n \cos \theta_n$	$m_n e_n \sin \theta_n$
$n+1$	$m_{n+1} e_{n+1}$	x_{n+1}	θ_{n+1}	$m_{n+1} e_{n+1} x_{n+1}$ $\times e_{n+1}$	$m_{n+1} e_{n+1} x_{n+1}$ $\times \cos \theta_{n+1}$	$m_{n+1} e_{n+1}$	$m_{n+1} e_{n+1}$ $\times \sin \theta_{n+1}$

Now, to determine $m_0 e_0$ and θ_0 , we equate the summations of each of the force vector column of Table 7.1 to zero. Thus,

$$m_0 e_0 \cos \theta_0 = - \sum_{i=1}^{n+1} m_i e_i \cos \theta_i = B_1 \quad (\text{known}), \quad (7.13)$$

$$m_0 e_0 \sin \theta_0 = - \sum_{i=1}^{n+1} m_i e_i \sin \theta_i = B_2 \quad (\text{known}). \quad (7.14)$$

Squaring (7.13) and (7.14) and adding, we get

$$(m_0 e_0)^2 = B_1^2 + B_2^2, \\ m_0 e_0 = (B_1^2 + B_2^2)^{1/2}. \quad (7.15)$$

Dividing (7.15) by (7.14), we have

$$\tan \theta_0 = B_2/B_1. \quad (7.16)$$

Thus, θ_0 also is obtained. [Note that to get the correct values of θ_0 and θ_{n+1} from (7.17) and (7.13) we should take care of the signs (+ or -) of the quantities B_1 , B_2 , A_1 , and A_2 since two solutions for θ_0 and θ_{n+1} are obtained from (7.17) and (7.13), respectively.]

PROBLEM 7.1

A shaft carries four masses in parallel planes A , B , C , and D , in this order, along it. The mass at B and C are 18 kg and 12.5 kg, respectively, and each has an eccentricity of 6 cm. The mass at A and D have an eccentricity of 8 cm. The angle between the masses at B and C is 100° , at

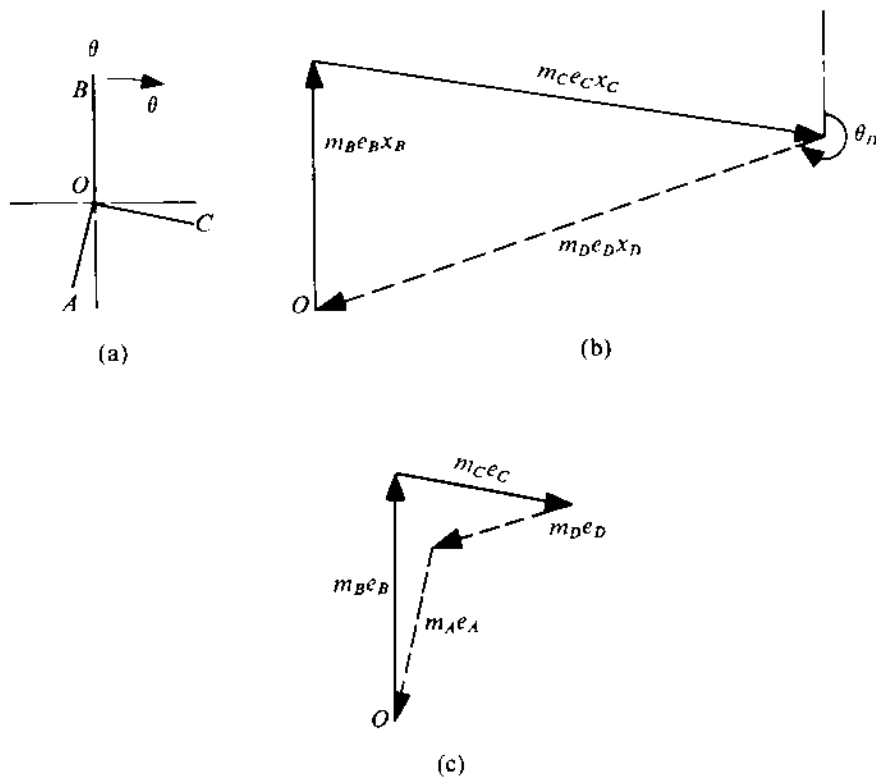


FIGURE 7.10

hat between the masses at B and A is 190° (both angles being measured in the same direction). The axial distance between the planes A and B is 10 cm and that between B and C is 20 cm. If the shaft is in complete dynamic balance, determine

- the masses at A and D ,
- the distance between the planes C and D , and
- the angular position of the mass at D .

SOLUTION

Graphical Method

As the mass at the plane A is unknown, we take the plane A as our reference for fixing the axial locations of the other planes. For locating angular positions, we take the plane B as the reference plane. First, the masses are drawn at relative angular positions as shown in Fig. 7.10a, so that

$$\theta_B = 0, \quad \theta_C = 100^\circ, \quad \theta_A = 190^\circ \quad (\theta_D \text{ is not known}).$$

With A as the reference plane for couple vectors, we have

$$x_A = 0, \quad x_B = 10 \text{ cm}, \quad x_C = 30 \text{ cm} \quad (x_D \text{ is not known}),$$

$$m_B = 18 \text{ kg}, \quad m_C = 12.5 \text{ kg} \quad (m_A \text{ and } m_D \text{ are not known}),$$

$$e_A = 8 \text{ cm}, \quad e_B = 6 \text{ cm}, \quad e_C = 6 \text{ cm}, \quad e_D = 8 \text{ cm}.$$

The couple polygon is shown in Fig. 7.10b, wherefrom by measurements we get $\theta_D = 253^\circ$ (i.e., the angle between the masses at B and D) and $m_D e_D x_D = 2312 \text{ kg-cm}^2$ or $m_D x_D = 289 \text{ kg-cm}$. The force polygon is shown in Fig. 7.10c. From measurements, we get

$$m_D e_D = 63.5 \text{ kg-cm}, \quad m_A e_A = 78 \text{ kg-cm}, \quad m_D = 7.94 \text{ kg}, \quad m_A = 9.75 \text{ kg}.$$

Thus, $x_D = 289/7.94 = 36.4 \text{ cm}$ (i.e., the distance of the plane D from the plane A). So, the distance of the plane D from the plane C = $(36.4 - 30) = 6.4 \text{ cm}$.

Analytical Method

As already explained, the forces and couples are resolved in two mutually perpendicular planes (as done in Table 7.2). Summing up the last four columns of the table and equating each to zero we get

$$m_D x_D \cos \theta_D = -86.17, \quad (a)$$

$$m_D x_D \sin \theta_D = -276.5, \quad (b)$$

$$8m_D \cos \theta_D - 7.88m_A = -94.98, \quad (c)$$

$$8m_D \sin \theta_D - 1.39m_A = -73.73. \quad (d)$$

TABLE 7.2

Plane	Mass m (kg)	Eccen- tricity e (cm)	Distance from reference plane A x (cm)	Angle with reference line B θ (degrees)	Couple vector		Force vector	
					Vertical component $me \cos \theta$	Horizontal component $me \sin \theta$	Vertical component $me \cos \theta$	Horizontal component $me \sin \theta$
A	m_A	8	0	190	0	0	$-7.88m_A$	$-1.39m_A$
B	18	6	10	0	1080	0	108	0
C	12.5	6	30	100	-390.6	2212	-13.02	73.73
D	m_D	8	x_D	θ_D	$8m_D x_D$ $\times \cos \theta_D$	$8m_D x_D$ $\times \sin \theta_D$	$8m_D$ $\times \cos \theta_D$	$8m_D$ $\times \sin \theta_D$

From (a) and (b), $\tan \theta_D = 3.21$. Since x_D is known to be positive, both $\sin \theta_D$ and $\cos \theta_D$ are negative. So, $\theta_D = 252.7^\circ$ (this is the angle between the masses at D and B). Thus, we get

$$\cos \theta_D = -0.2975, \quad \sin \theta_D = -0.955.$$

Substituting these values in (c) and (d), we have

$$-2.38m_D - 7.88m_A = -94.98, \quad (e)$$

$$-7.64m_D - 1.39m_A = -73.73. \quad (f)$$

Solving (e) and (f) simultaneously, we get

$$m_A = 9.67 \text{ kg}, \quad m_D = 7.89 \text{ kg}.$$

Then, using these values of m_D and $\cos \theta_D$ in (a), $x_D = 36.57 \text{ cm}$, and the distance of D from C ($x_D - 30$) = 6.57 cm.

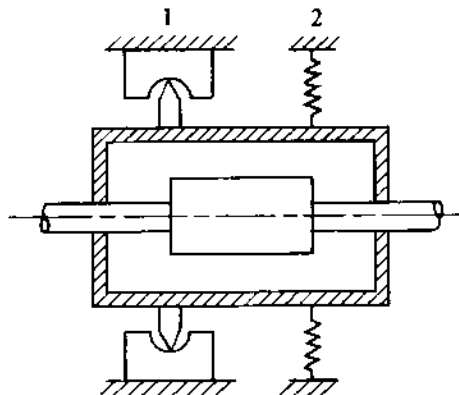


FIGURE 7.11

.5 BALANCING OF ROTORS

It was observed in Section 7.3 that two balancing masses in any two conveniently chosen transverse planes (balancing planes) are sufficient to produce complete dynamic balance in any rotating system. Conversely, the complete unbalance of a rotor can be represented by two unbalances in these two planes. This basic principle is utilized in various balancing machines with which rotors are balanced. In practice, it may not be feasible to add balancing masses. In such situations, balancing can be achieved by the removal of masses from the reference planes (from positions diametrically opposite to those of balancing masses). In this section, we will consider the operation of a few balancing machines in common use.

Pivoted-carriage Balancing Machine

The rotor to be balanced is mounted on half-bearings in a light but stiff carriage. This carriage is pivoted near one end and rests on a spring at the other (Fig. 7.11). Two balancing planes 1 and 2 are chosen on the rotor, and the rotor unbalance is assumed to be represented by unbalances only in these two planes. First, the rotor is mounted with plane 1 on the pivot so that the unbalance in plane 1 will have no effect on the motion of the carriage. On the rotor being rotated in this position, the carriage will oscillate due to the unbalance in plane 2. A trial mass (at a known radius) is then attached in plane 2 and the amplitude of oscillation of the carriage is noted. This procedure is repeated with the same trial mass at different angular positions. A plot of the observed amplitude against the angular position of the trial mass shows the optimum angular position for which the oscillation amplitude is minimum. The magnitude of the trial mass is varied at this position, and the exact amount of balance mass, which reduces the amplitude of oscillation to almost zero, is determined by trial and error. A similar procedure is followed to determine the required balance mass in plane 1, the rotor being mounted with plane 2 on the pivot. Normally, this procedure requires far too many test runs, but there is a method² by which four test runs for each plane are sufficient for determining the balancing masses. However, the machine is unsuitable for small imbalances as the large inertia of the carriage fails to provide measurable amplitudes of oscillation at moderate speeds.

²Discussed later in this section.

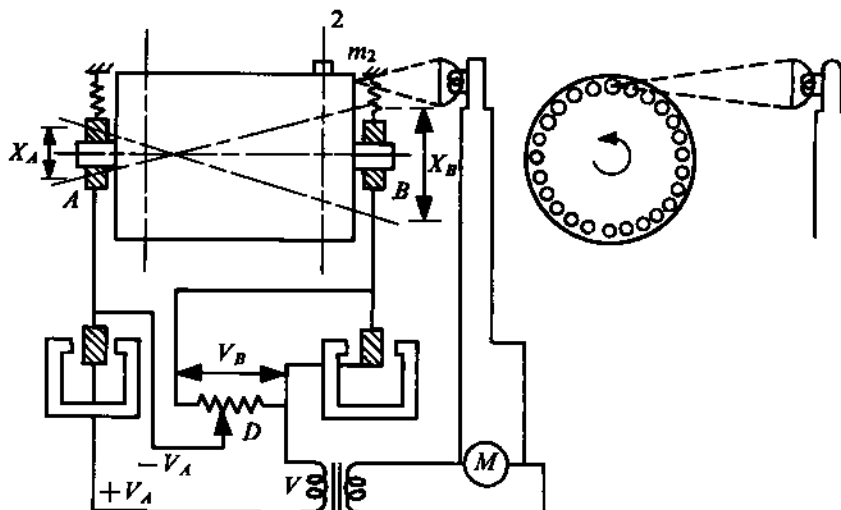


FIGURE 7.12

Gisholt-type Balancing Machine

In the Gisholt-type balancing machine, the rotor is mounted on spring-supported bearings (Fig. 7.12), thus eliminating the disadvantage of large inertia of the carriage in the pivoted-carriage machine. To separate out the effects of the two reference planes, we use, instead of the pivot, two electrical circuits, one for each plane. The operation of this machine can be explained as follows with reference to Fig. 7.12.

Let planes 1 and 2 be the two balancing planes of the rotor. Assuming the rotor to be perfectly balanced, we add an unbalance m_2 in plane 2. When rotated, this will result in vertical oscillation of the rotor axis. Since plane 2 is closer to the support B , it is obvious that the oscillations at B will be more than at the support A . The ratio of the amplitudes of oscillation at B and A is dependent entirely on the distance of plane 2 from the supports A and B . This ratio is independent of the magnitude of the unbalance. The voltages V_B and V_A produced in the two electrical pick-ups (being proportional to the velocities of oscillation) will also be in the same ratio. The voltage divider at D is set so that a portion of V_B , equal to V_A , is applied opposite to V_A , the resultant voltage V being thus reduced to zero. As a result of this, the electrical circuit shown in Fig. 7.12 becomes insensitive to any unbalance in plane 2.

In the actual test run of an unbalanced rotor, the voltage V (or the reading on meter M) corresponds to the amount of unbalance present only in plane 1. The magnitude of the unbalance in plane 1 can thus be determined. The angular position of the unbalance is determined by applying the resultant voltage V to a stroboscope which flashes for a microsecond (on the vertical line of the rotor periphery) whenever the voltage applied to it changes from negative to positive. The voltage corresponds to the direction of the pick-up coil velocity, and the stroboscope will flash when the vertical displacement is maximum (say, in the upward direction). If damping is neglected, the maximum displacement and unbalance will be in the same direction. Thus, the stroboscope will flash in the direction of the unbalance. The rotor periphery is stamped with numbers, and if the speed of rotation is more than 600 rpm, due to the persistence of vision, the number corresponding to the angular position of the unbalance in plane 1 will appear to be steady, and is determined in this manner.

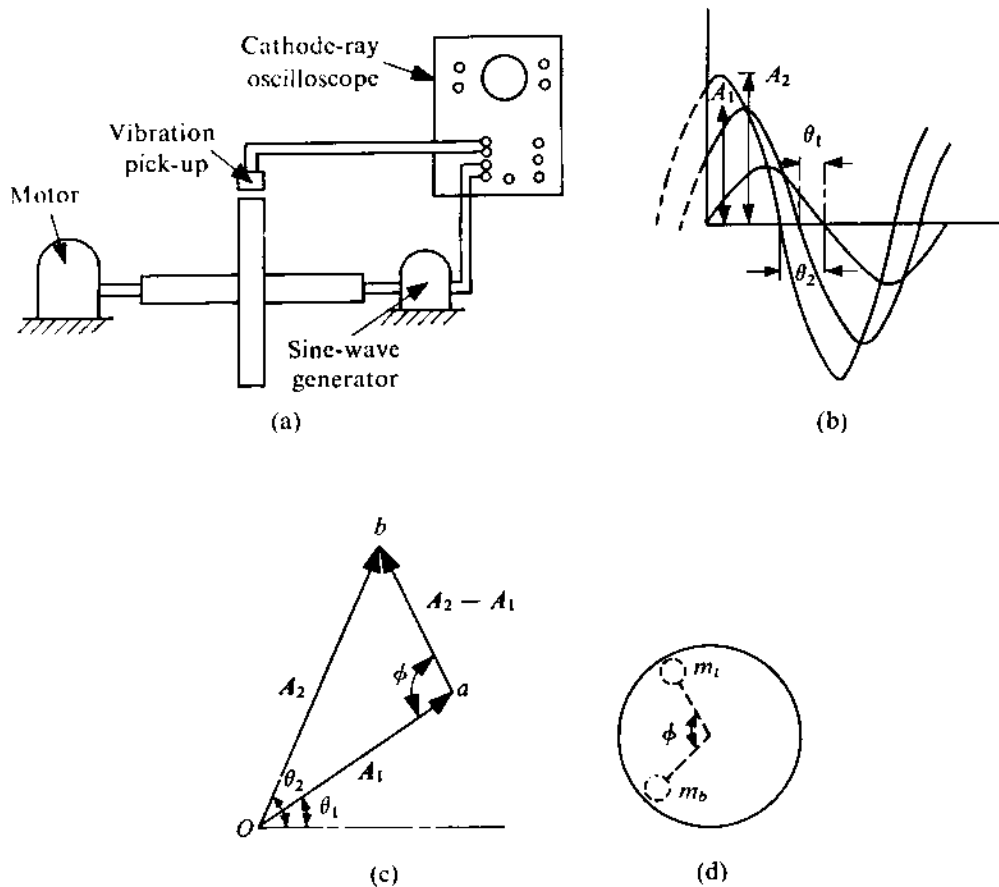


FIGURE 7.13

To determine the amount and direction of the unbalance in plane 2, a similar circuit is used which is made insensitive to any unbalance present in plane 1.

Field Balancing

In a very large rotor, such as the one in a turbine and a generator, the balancing has to be done under normal operating conditions on its own bearings. Being very heavy, such a rotor cannot be mounted on a balancing machine. Furthermore, a rotor that may be perfectly balanced on its own, can get unbalanced during operation due to one of several causes, e.g., the flexibility of the shaft and bearing or a misalignment in the bearing. There are many methods of field balancing of a rotor. One such method, developed by E.L. Thearle, will be discussed in this section. For a better understanding of the method, we shall first consider the balancing of a thin disc and then take up that of a rotor. Another reason we shall consider a thin disc first is that there exists a class of rotors (e.g., industrial fans and blowers) in which the rotating blades contain most of the mass. Such a rotor can be treated as a single-plane rotor, i.e., a thin disc.

Balancing of a Thin Disc

For balancing a thin disc (Fig. 7.13a), a vibration pick-up is used to measure the oscillations of the unbalanced rotating disc³ in one direction (say, vertical), and the output is displayed on the screen of a double-beam cathode-ray oscilloscope. A sine-wave generator is connected to the disc and the generated sine wave is fed to the second beam of the same oscilloscope. This sine wave acts as a reference for measuring the phase. An explanation of this follows.

To start with, the disc is rotated at a speed that is sufficient to produce a measurable amplitude of oscillation. Let A_1 be the amplitude of the oscillation and θ_1 be its phase difference with reference to the generated sine wave (Fig. 7.13b). This oscillation is represented by the vector oa (\mathbf{A}_1) in Fig. 7.13c, which represents the effect of the unbalance present in the disc.

Next, a trial mass m_t (Fig. 7.13d) is attached to the disc at a known angular position and at a known radius (say, at the radius where the balance mass can be attached). The disc is rotated at the same speed as that for the first run. Let the amplitude of this oscillation be A_2 and let the phase difference be θ_2 (Fig. 7.13b). This is represented by the vector ob (\mathbf{A}_2) in Fig. 7.13c. The difference, $ob - oa = ab$, represents the effect of only the trial mass m_t . So, to balance the rotor i.e., to nullify the effect of oa , we should add the balancing mass m_b at the same radius as that of the trial mass m_t , such that

$$m_b = m_t \frac{oa}{ab}, \quad (7.18)$$

and it is located at an angle ϕ , counter-clockwise (as shown in Fig. 7.13c), from the position of the trial mass. Expressing these results in vector notations, the magnitude and position (both known) of the trial mass m_t can be written as

$$m_t = m_t \exp(i\phi_{m_t}), \quad (7.19)$$

where ϕ_{m_t} is measured counter-clockwise from some datum. Let the balance mass be expressed as

$$m_b = \delta m_t, \quad (7.20)$$

where δ is a vector operator which changes both the magnitude and the direction of a vector. If

$$\delta = \delta \exp(i\theta_\delta), \quad (7.21)$$

$$m_b = m_b \exp(i\phi_{m_b}), \quad (7.22)$$

then

$$m_b = \delta m_t, \quad \phi_{m_b} = \phi_{m_t} + \theta_\delta. \quad (7.23)$$

(It should be noted that any vector can be expressed in terms of another through a vector operator. The effect of the trial mass m_t is given by ab (Fig. 7.13c). Then, for complete balancing, we have

$$\delta(ab) = -oa, \quad \delta(\mathbf{A}_2 - \mathbf{A}_1) = -\mathbf{A}_1,$$

$$\delta = -\frac{\mathbf{A}_1}{\mathbf{A}_2 - \mathbf{A}_1} = \frac{\mathbf{A}_1}{\mathbf{A}_1 - \mathbf{A}_2}. \quad (7.24)$$

As $\mathbf{A}_1 (= A_1 e^{i\theta_1})$ and $\mathbf{A}_2 (= A_2 e^{i\theta_2})$ are known, we can obtain δ from (7.24), and m_b from (7.20). Comparing (7.20) and (7.18), we see that

$$\delta = oa/ab, \quad \theta_\delta = \phi.$$

³In fact, the oscillation can be measured at any convenient location, e.g., at any of the bearings.

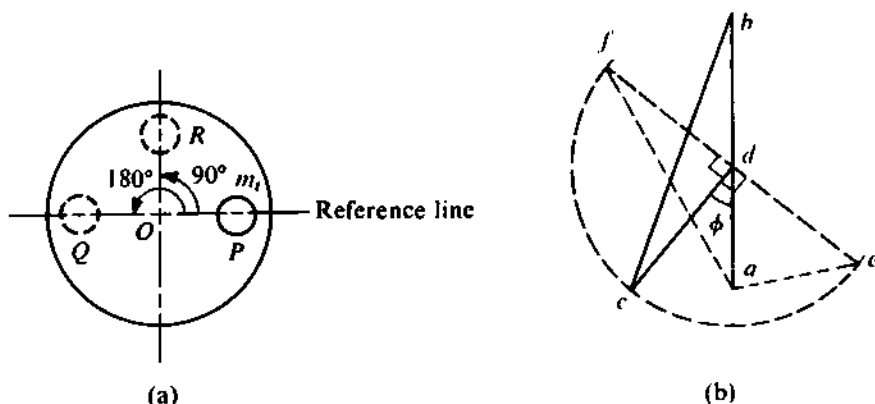


FIGURE 7.14

The advantage of using the vector notation will be clear when we discuss the balancing of rotors. (In a vector equation, by division, we mean the division of magnitudes and subtraction of angles; likewise, by multiplication, we mean the multiplication of magnitudes and addition of angles. Subtraction and addition of vectors can be easily carried out by a graphical method.)

The position of the required balance mass has been shown in Fig. 7.13d. Once this is known, the same balancing effect can obviously be brought about in several ways.

If we employ a phase meter, the use of a sine-wave generator can be avoided. Alternatively, a stroboscope driven by the pick-up output can also be used. In the field, it may be sometimes difficult to either couple a sine-wave generator or use a phase meter. Under such circumstances, the balancing mass required for a single-plane rotor can be determined by measuring only the vibration amplitudes. However, to do this, two additional test runs, using the same trial mass, are required as we shall now explain.

Referring to Fig. 7.14a, let the following four readings be taken for the vibration amplitudes (with the same speed of rotation):

<i>Amplitude</i>	<i>Test condition</i>
A_1	Without any trial mass
A_2	m_t at $P (= 0^\circ)$
A_3	m_t at $Q (= 180^\circ)$
A_4	m_t at $R (= 90^\circ)$

For the last three runs, the radial distance of the trial mass is kept unchanged as indicated in the figure.

Draw a triangle abc with sides $ab (= A_1)$, $ac (= A_2)$, and $bc (= A_3)$ as shown in Fig. 7.14b. Let d be the midpoint of ab . In this figure, dc represents the effect of only the trial mass at P . Hence, the magnitude of the required balancing mass to be placed at the same radius as that of the trial mass is obtained as

$$m_b = m_t \frac{ad}{dc}$$

The balancing mass should be located at an angle ϕ from the reference line, where $\phi = \angle adc$. This angle should be measured in the counter-clockwise or clockwise direction depending on whether the

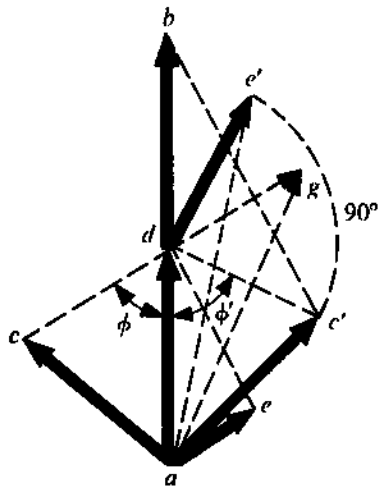


FIGURE 7.15

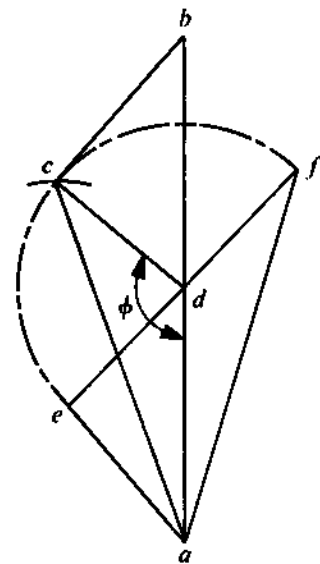


FIGURE 7.16

magnitude of A_4 is given by ae or af . The points e and f are obtained by rotating dc about the point d through 90° in the counter-clockwise and clockwise directions, respectively.

The proof of the foregoing construction is as follows. Let ad and ac represent A_1 and A_2 respectively (see Fig. 7.15). If this diagram is correct, dc must represent the effect of m_t at P . Then, dg ($= -dc$) should represent the effect of m_t at the position Q , i.e., ag should represent A_3 . Now, extend ad up to b so that $ad = db$. Since the diagonals of a parallelogram bisect each other the points a , g , b , and c must be the corner points of a parallelogram. Thus, bc must be equal to the magnitude of A_3 . With $de = dc$ and $\angle cde = 90^\circ$, de represents the effect of m_t at the position R . So, ae must represent A_4 . Thus, to nullify the effect of original unbalance, i.e., A_1 ($= ad$), the balancing mass must be rotated through ϕ (as shown in Fig. 7.15) from the position P .

With the same values of A_1 , A_2 , and A_3 , it is obvious that another triangle, namely, abc (Fig. 7.15), can be drawn, where $ab = 2A_1$, $ac' = A_2$, and $bc' = A_3$. In this figure, e' corresponds to e in Fig. 7.14b.

Of the two constructions, namely, abc and abc' , the correct one can be determined by comparing the magnitude of A_4 with ae and ae' . If abc' is correct, then the balancing mass should be placed at an angle ϕ' in the clockwise direction from the reference line. Geometrically, it is easy to show that the magnitudes of ϕ and ϕ' are the same and ae' (in Fig. 7.15) is equal to af (in Fig. 7.14b).

PROBLEM 7.2

During the field balancing of a cooling tower fan, the measurements taken are $A_1 = 0.7$ mm, $A_2 = 1.06$ mm, $A_3 = 0.5$ mm, and $A_4 = 1.18$ mm. The trial mass used is 250 gm. Determine the necessary balancing mass (to be placed at the same radius as the trial mass) and its angular location with respect to the position of the trial mass during the second run (i.e., when the vibration amplitude is 1.06 mm).

SOLUTION

Following the construction explained in Fig. 7.14b, we draw Fig. 7.16 with the given data. From this latter figure, we get $dc = 0.46$ mm and $\phi = 139^\circ$. So, the magnitude of the balancing mass is

$$m_b = m_t \cdot \frac{ad}{dc} = 250 \cdot \frac{0.7}{0.46} = 380.4 \text{ gm.}$$

Since af is approximately equal to A_4 (and $ae \ll A_4$), the angular location of the balancing mass is 139° in the clockwise direction from that of the trial mass during the second run.

Balancing of Rotors

The method described for balancing a thin disc can be readily extended for balancing of rotors if we consider the two balancing planes to be discs. Let the two balancing planes of a rotor, as shown in Fig. 7.17a, be designated *near end* and *far end*.

The rotor is first rotated at a speed which will give measurable amplitudes at both the near and far ends. These amplitudes are denoted by the vectors N_1 and F_1 , respectively (Fig. 7.17b), and their phases with respect to some datum are also known. Thus, N_1 and F_1 represent the effect of the unbalance of the rotor at near and far ends, respectively.

Next, a trial mass m_{tn} is attached to the near end, at a known angular position and at a known radius. The magnitude and position of this trial mass at the near end can be written vectorially as

$$m_{tn} = m_{tn} \exp(i\phi_{m_{tn}}), \quad (7.25)$$

where ϕ is measured in the counter-clockwise direction from some datum. The rotor is run at the same speed as in the first test. The amplitudes at the near and far ends are measured, along with respective phases. Let these be represented by the vectors N_2 and F_2 , respectively, in Fig. 7.17b. Thus, these vectors N_2 and F_2 represent the effect of the unbalance of the rotor itself plus that of m_{tn} , so that

$$N_2 - N_1 = \text{effect of } m_{tn} \text{ at the near end}, \quad (7.26)$$

$$F_2 - F_1 = \text{effect of } m_{tn} \text{ at the far end.}$$

In the third run, m_{tn} is removed from the near end and another trial mass m_{tf} is placed at the far end at some known radial and angular position. Let

$$m_{tf} = m_{tf} \exp(i\phi_{m_{tf}}). \quad (7.27)$$

The rotor is run at the same speed as in the two previous tests. Let the vectors N_3 and F_3 represent the amplitudes and phases of the oscillations at the near and far ends, respectively (Fig. 7.17c). Thus, these vectors N_3 and F_3 represent the effect of the unbalance of the rotor itself plus that of m_{tf} and, as before, we have

$$N_3 - N_1 = \text{effect of } m_{tf} \text{ at the near end}, \quad (7.28)$$

$$F_3 - F_1 = \text{effect of } m_{tf} \text{ at the far end.}$$

Let the two balance masses required at the near and far ends be m_{bn} and m_{bf} , placed at the same radii as m_{tn} and m_{tf} , respectively. If

$$m_{bn} = \alpha m_{tn}, \quad (7.29)$$

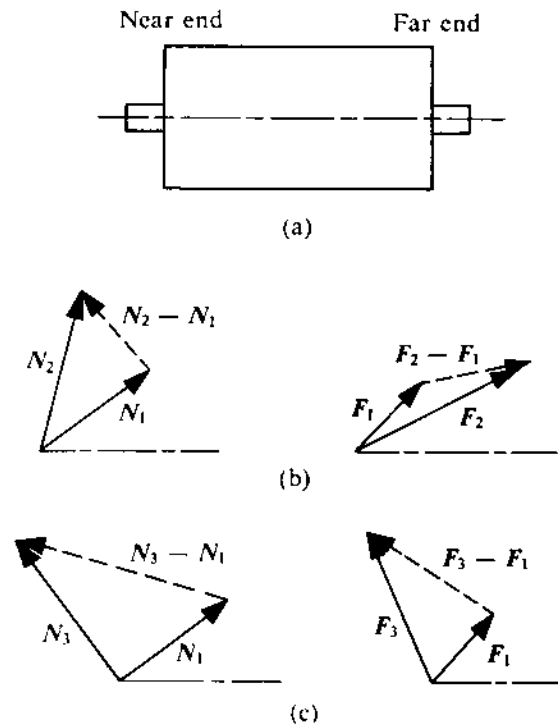


FIGURE 7.17

$$m_{bf} = \beta m_{tf}, \quad (7.30)$$

where $\alpha = \alpha \exp(i\theta_\alpha)$ and $\beta = \beta \exp(i\theta_\beta)$, then the balance mass at the near end is $m_{bn} = \alpha m_{tn}$ and should be placed at an angle θ_α from the position of m_{tn} . Similarly, the balance mass at the far end is $m_{bf} = \beta m_{tf}$, and should be placed at an angle θ_β from the position of m_{tf} . The problem thus reduces to the determination of two vectors α and β .

For complete balancing of the rotor, the total effect of m_{bn} and m_{bf} at the near end should be $-N_1$ and that at the far end it should be $-F_1$. Thus, from (7.26), (7.28), (7.29), and (7.30), we can write

$$\alpha(N_2 - N_1) + \beta(N_3 - N_1) = -N_1, \quad (7.31)$$

$$\alpha(F_2 - F_1) + \beta(F_3 - F_1) = -F_1. \quad (7.32)$$

Solving for α and β , simultaneously, from (7.31) and (7.32), we get

$$\alpha = \frac{F_1(N_3 - N_1) - N_1(F_3 - F_1)}{(N_2 - N_1)(F_3 - F_1) - (N_3 - N_1)(F_2 - F_1)}, \quad (7.33)$$

$$\beta = \frac{N_1(F_2 - F_1) - F_1(N_2 - N_1)}{(N_2 - N_1)(F_3 - F_1) - (N_3 - N_1)(F_2 - F_1)}. \quad (7.34)$$

PROBLEM 7.3

For balancing an alternator rotor by the field-balancing technique, the experimental results obtained are listed in Table 7.3. Determine the correct balance masses that should be placed at these ends (a

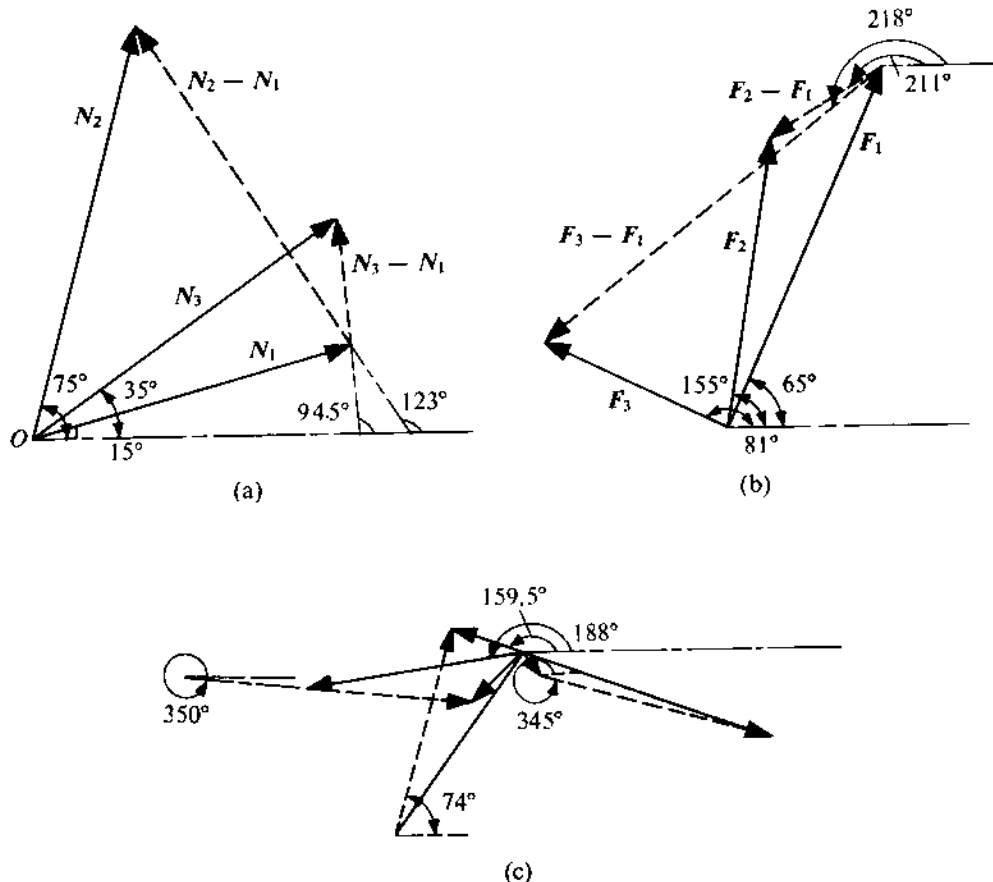


FIGURE 7.18

the same radii as those of the corresponding trial masses), and the angular positions of the balance masses with respect to the corresponding trial masses, for complete dynamic balancing of the rotor.

TABLE 7.3

Trial	Trial mass (kg)	N		F	
		Near-end amplitude (cm)	Near-end phase angle (degrees)	Far-end amplitude (cm)	Far-end phase angle (degrees)
1	0	3.5×10^{-4}	15°	4.2×10^{-4}	65°
2	2 (at near end)	4.5×10^{-4}	75°	3.1×10^{-4}	81°
3	2 (at far end)	4.0×10^{-4}	35°	2.2×10^{-4}	155°

SOLUTION

Figure 7.18a shows the vectors N_1 , N_2 , and N_3 drawn to some scale and Fig. 7.18b shows F_1 , F_2 , and F_3 drawn to the same scale. From these figures, we obtain the vectors $(N_2 - N_1)$, $(N_3 - N_1)$, and F_3 drawn to the same scale.

$(F_2 - F_1)$, and $(F_3 - F_1)$, which are shown by the dashed lines in Figs. 7.18a and 7.18b. From measurements of amplitudes and phases of all the vectors, we can write

$$(N_2 - N_1) = 4.1 \times 10^{-4} e^{i(123^\circ)}, \quad (N_3 - N_1) = 1.4 \times 10^{-4} e^{i(94.5^\circ)},$$

$$(F_2 - F_1) = 1.5 \times 10^{-4} e^{i(211^\circ)}, \quad (F_3 - F_1) = 4.75 \times 10^{-4} e^{i(218^\circ)}.$$

From the experimental results, we get

$$N_1 = 3.5 \times 10^{-4} e^{i(15^\circ)}, \quad F_1 = 4.2 \times 10^{-4} e^{i(65^\circ)}.$$

From (7.33) and (7.34), we have

$$\alpha = \frac{5.88e^{i(159.5^\circ)} - 16.625e^{i(233^\circ)}}{19.475e^{i(341^\circ)} - 2.1e^{i(305.5^\circ)}},$$

$$\beta = \frac{5.25e^{i(226^\circ)} - 17.22e^{i(188^\circ)}}{19.475e^{i(341^\circ)} - 2.1e^{i(305.5^\circ)}}.$$

The numerators and denominators of α and β are obtained graphically as explained in Fig. 7.18c (The scale used for Fig. 7.18c is different from that for Figs. 7.18a and 7.18b.) From measurements we get

$$\alpha = \frac{1.59e^{i(74^\circ)}}{1.77e^{i(345^\circ)}} = 0.902e^{i(-271^\circ)},$$

$$\beta = \frac{1.36e^{i(350^\circ)}}{1.77e^{i(345^\circ)}} = 0.768e^{i(5^\circ)}.$$

Thus, the balance mass at the near end should be $0.902 \times 2 = 1.804$ kg (at the same radius as the trial mass at that end) and at an angle 271° clockwise (i.e., 89° counter-clockwise) from the position of the trial mass at that end.

The balance mass at the far end should be $0.768 \times 2 = 1.536$ kg (at the same radius as the trial mass at that end) and at an angle 5° counter-clockwise from the position of the trial mass at that end.

Balancing of Flexible Rotors

The principles of balancing a rotor we have so far discussed are based on the assumption that the rotor is rigid. This assumption is valid so long as the speed of operation is well below the first critical speed of the rotor. However, there may be a situation where the rotor runs at a speed above its critical speed. For example, an alternator in a power station operates at a speed well above its critical speed. In fact, the operating speed (governed by the frequency) of such an alternator is fixed, whereas its critical speed reduces continuously with increase in its generating capacity. If the alternator has to produce a large power, it has to accommodate additional conductors. This can be accomplished only by increasing the rotor length since the rotor diameter is restricted by the centrifugal stress.

Table 7.4 shows how the flexibility of an alternator increases with its capacity. From this table we can see that as the capacity increases from 60 MW to 500 MW the first critical speed falls approximately by a factor of 2.

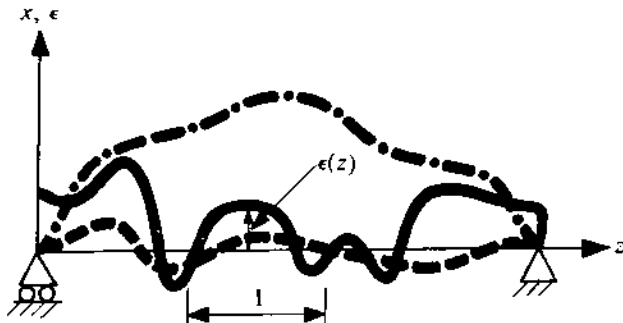


FIGURE 7.19

TABLE 7.4

Capacity (MW)	60	120	200	350	500
Rotor weight (tons)	23	32	42	59	74
Bearing centre distance (m)	6.35	7.37	8.00	9.14	11.68
Midspan static deflection (mm)	0.46	0.48	0.56	0.76	2.29

The balancing of a rotor running at a speed above its critical speed cannot be achieved by only two balancing masses in two arbitrarily chosen planes as established earlier. In such a rotor, the concept to be used is entirely different. In a rigid rotor, the objective of putting the balancing masses is to neutralize the unbalanced forces and moments developed due to the rotor unbalance. In a flexible rotor, on the other hand, the purpose of attaching the balancing masses is to modify the dynamic deflection characteristics of the rotor. The technique to do this is known as the *modal balancing technique*. The dynamic deflection, x , of a rotor at various points along the longitudinal axis z is written as

$$x(z) = C_1\phi_1(z) + C_2\phi_2(z) + \dots + C_n\phi_n(z) + \dots,$$

where $\phi_i(z)$ represents the i -th mode of the rotor and C_i the contribution of the i -th mode to the total deflection. If the operating speed ω lies in the range $\omega_n < \omega < \omega_{n+1}$, where ω_n is the n -th critical speed of the rotor, then the balancing masses are added with a view to making the coefficients C_1, C_2, \dots, C_n zero. If the number of coefficients to be reduced to zero is N , it can then be shown that N sets of balancing masses are required. We shall now explain the principle underlying the modal balancing technique without going into the mathematical details.

For simplicity, let us assume that the mass centre distribution, $\epsilon(z)$, of the rotor lies in one diametral plane (see Fig. 7.19). Then, the deflection curve at a low speed of the rotor (this curve is very close to the static deflection curve corresponding to the centrifugal force distribution) would be as shown by the dashed line in the figure. However, if the rotor runs at a speed close to ω_1 , the deflection curve (shown by the chain line) will then closely resemble the first mode shape of the rotor. To eliminate the contribution from the first mode, the balancing masses should be placed in region I, as indicated.

Now, with the balancing masses attached, if the rotor runs at a speed close to ω_1 , the deflection curve appears as shown by the solid line in Fig. 7.20. When the rotor speed is increased to a value

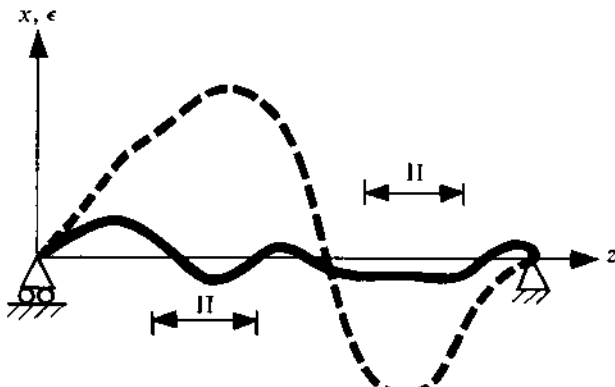


FIGURE 7.20

close to ω_2 , the deflection curve (with a predominant contribution from the second mode) would be as shown by the dashed line. It is obvious that the balancing masses necessary to eliminate the second mode (without re-exciting the first mode) should be placed in regions II. Thus, to eliminate each mode, one set of balancing masses is required. The amount and angular locations of the balancing masses can be determined through a series of experiments very similar to those discussed in the section on field balancing.

The dynamic bearing reactions, left over after the modal balancing has been done, can be further reduced by adding two more balancing masses. These two masses are determined by balancing the rotor at a low speed, i.e., by considering the rotor to be rigid.⁴

Balancing of Rotors with Variable Mass

There exists another class of rotors which need special attention so far as their balancing is concerned. The mass and geometrical characteristics of such a rotor are not definite and may change. A common example of this type of a rotor is the one found in many washing machines. In a washing machine the objects to be cleaned, which form a part of the rotor, neither have a fixed quantity nor do they possess definite geometric shapes. The balancing of such a rotor running at a low speed can be achieved using special means where the requisite balancing mass is self-adjusted.⁵

7.6 BALANCING OF INTERNAL-COMBUSTION ENGINES (APPROXIMATE ANALYSIS)

An internal-combustion engine has both rotating and reciprocating parts. In what follows, we shall discuss the unbalanced (inertia) forces and moments resulting from the acceleration of these parts. Since steam engines (locomotives) have more or less become out of date, we shall not consider their balancing problems. Instead, we shall analyze a single-cylinder internal combustion engine. In so doing, we shall first take up the unbalanced forces and moments and then discuss the proper design

⁴For further details, see Mallik, A.K., Principles of Vibration Control, Affiliated East-West Press (P) Ltd., New Delhi, 1990.

⁵For more details on a few such mechanisms, see Mallik, A.K., Principles of Vibration Control, Affiliated East-West Press (P) Ltd., New Delhi, 1990.

procedure for balancing. Subsequently, we shall consider the balancing of multicylinder engines, e.g., in-line engines, V-twin engines, and radial engines.

Before we rigorously analyze a single-cylinder engine, let us see how only the inertia forces and moments are left unbalanced and transmitted to the foundation of such an engine. For this, we shall assume that

- (i) the replacement of the connecting rod by two masses at its ends maintains complete dynamic equivalence,
- (ii) the crank is so designed that the combined centre of mass of the crank and the apportioned connecting-rod mass (m_2) at the crank pin lies on the axis of rotation, and
- (iii) the engine speed is constant.

When considering multicylinder engines, we shall apply these assumptions to each constituent cylinder.

Single-cylinder Engines

Let us consider a horizontal single-cylinder engine. For approximately analyzing the unbalanced forces and moments, the connecting rod is replaced by two masses m_1 and m_2 at the ends of a massless rod (as in Section 4.10). Thus, m_1 is an entirely reciprocating mass as it moves with the piston, and m_2 is subject to pure rotation along with the crank. As before, let

m_{rec} = total mass (including m_1) of the reciprocating parts (i.e., the piston and the gudgeon pin),

Q = thrust in the connecting rod acting along the direction of the connecting rod, and

$\lambda = r/l$ (where l is the length of the connecting rod and r is the crank radius).

The forces and moments acting on the mechanism and on the foundation are indicated in Fig. 7.21a(i); forces acting on both the machine members and the frame are shown. In this figure,

pA = gas force,

T_R = load torque on the crank (the surrounding structure supplies this load torque and in turn is subjected to the reaction to it),

N = normal thrust between the cylinder and the piston, and

R_H, R_V = horizontal and vertical reactions at the crankshaft bearing.

Considering the forces at the gudgeon pin, i.e., at B [Fig. 7.21a(ii)], we get

$$Q \sin \phi = N, \quad (7.35)$$

$$Q \cos \phi = pA + m_{\text{rec}}\ddot{x}. \quad (7.36)$$

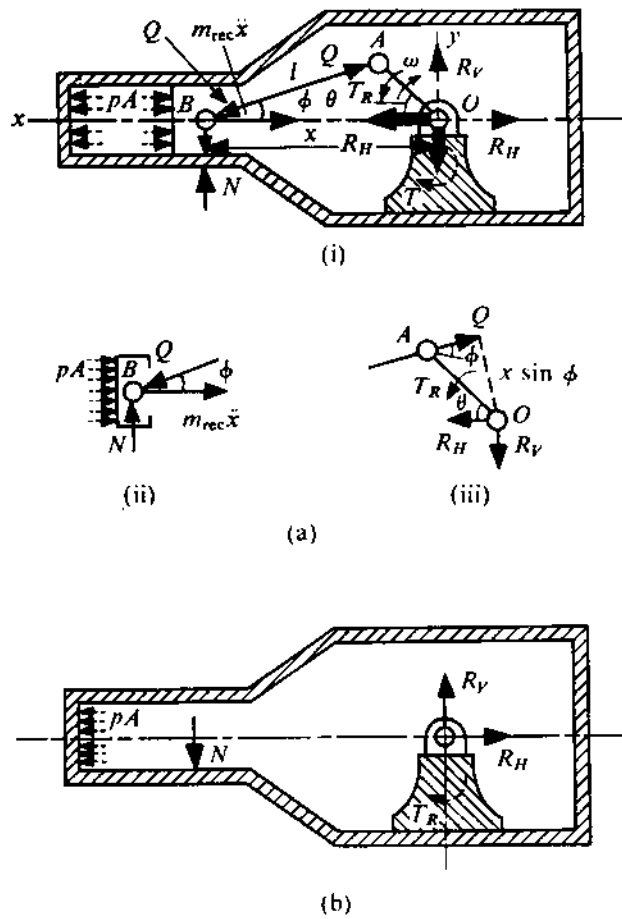


FIGURE 7.21

The crank rotates at a constant speed ω . Taking moments of all the forces on the crank about the point O [Fig. 7.21a(iii)], we get

$$Qx \sin \phi = T_R. \quad (7.37)$$

Balancing the forces on the crank, we get

$$R_H = Q \cos \phi, \quad (7.38)$$

$$R_V = Q \sin \phi. \quad (7.39)$$

Figure 7.21b shows all the forces and the moments on the frame. Thus, using (7.35) to (7.39), the net forces and the moments on the frame are

$$F_x = pA - R_H = -m_{rec}\ddot{x}, \quad (7.40)$$

$$F_y = R_V - N = 0, \quad (7.41)$$

$$M_z = Nx - T_R = 0. \quad (7.42)$$

So, with this approximate analysis and assuming a balanced crank, we see that the only force transmitted to the foundation is in the line of the stroke, namely,

$$F_x = m_{rec}\omega^2 r(\cos \theta + A_2 \cos 2\theta - A_4 \cos 4\theta + \dots) \quad (7.43)$$

[substituting \ddot{x} from (4.34) in (7.40) and neglecting the unsteady part]. Here, the friction forces have not been shown. These forces, being internal, always cancel each other and will in no way affect our subsequent conclusions. This unbalanced force F_x is dynamic in nature as its magnitude changes with θ (i.e., it changes with time as the crank rotates). This force (known as the longitudinal shaking force) tends to vibrate the frame in the x -direction. The coefficients of the terms $\cos j\theta$ (where $j = 1, 2, 4, \dots$) in (7.43) are known as the *unbalanced forces of j -th order*. Thus, the first-order unbalanced force is

$$F_x^1 = m_{rec}\omega^2 r, \quad (7.44)$$

and the second-order unbalanced force is

$$F_x^2 = m_{rec}\omega^2 r A_2. \quad (7.45)$$

These are the magnitudes of the primary and secondary unbalanced forces, respectively, where the *primary unbalanced force* is

$$F_x^P = m_{rec}\omega^2 r \cos \theta, \quad (7.46)$$

and the *secondary unbalanced force* is

$$F_x^S = m_{rec}\omega^2 r A_2 \cos 2\theta. \quad (7.47)$$

Except in a very high-speed engine, forces up to the second order are of importance, those of higher order being of negligible magnitude. If the connecting-rod-to-crank-length ratio (l/r) is considerably greater than unity, then $\lambda = r/l \ll 1$, when $A_2 \approx \lambda$ (see Section 4.9). Thus, the secondary force⁶ can be written as

$$F_x^S = \lambda m_{rec}\omega^2 r \cos 2\theta. \quad (7.48)$$

It should be noted that these results for the horizontal engine will also hold good for a vertical engine.

⁶The terms "primary force" and "secondary force" are used in place of "primary unbalanced inertia force" and "secondary unbalanced inertia force", respectively.

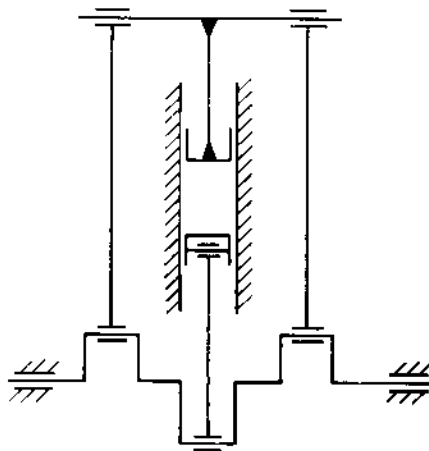


FIGURE 7.22

PROBLEM 7.4

A vertical single-cylinder opposed-piston engine is shown in Fig. 7.22. The lower piston is connected to the centre crank, whereas the upper piston operates the two outer cranks which are at 180° to the centre crank. The stroke of the lower piston is 50 cm. The mass of the reciprocating parts is 150 kg for the lower piston and 225 kg for the upper piston. Find the stroke of the upper piston so that the primary force is balanced.

If the central connecting rod is 100 cm long and each outer connecting rod is 200 cm long, determine the maximum value of the secondary unbalanced force and the corresponding crank positions. The engine speed is 180 rpm (assume a balanced crank).

SOLUTION

Referring to Fig. 7.22, if θ is the orientation of the central crank, then that of the outer cranks will be $\theta + \pi$. For primary balance, we have

$$F_{zl}^P + F_{zu}^P = 0, \quad (a)$$

where l and u refer to the lower and upper pistons, respectively. From the data given, we see that

$$(m_{rec})_l = 150 \text{ kg}, \quad (m_{rec})_u = 225 \text{ kg}, \quad s_l = 50 \text{ cm},$$

$$r_l = s_l/2 = 25 \text{ cm}, \quad \lambda_l = 25/100 = 0.25, \quad \omega = 180 \times (\pi/30) = 18.84 \text{ rad/s.}$$

From (7.46), we have

$$F_{zl}^P = (m_{rec})_l \omega^2 r_l \cos \theta, \quad F_{zu}^P = (m_{rec})_u \omega^2 r_u \cos(\theta + \pi).$$

Substituting these values in equation (a), we get

$$(m_{rec})_l r_l = (m_{rec})_u r_u, \quad r_u = r_l (m_{rec})_l / (m_{rec})_u = 25 \times \frac{150}{225} = 16.7 \text{ cm.}$$

So, the stroke of the upper piston $s_u = 2r_u = 33.4 \text{ cm}$. Thus, $\lambda_u = 16.7/200 = 0.0835$.

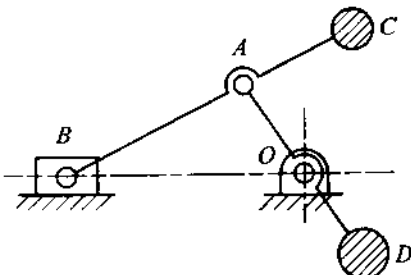


FIGURE 7.23

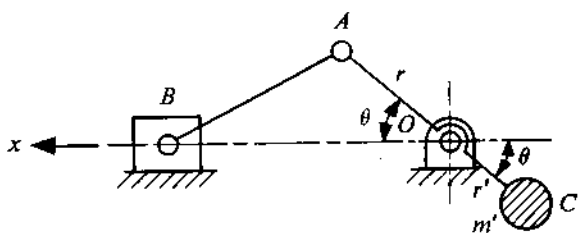


FIGURE 7.24

The secondary unbalanced force is given by

$$\begin{aligned} F_x^S &= F_{xI}^S + F_{xu}^S \\ &= \lambda_I(m_{rec})_I \omega^2 r_I \cos 2\theta + \lambda_u(m_{rec})_u \omega^2 r_u \cos 2(\theta + \pi) \\ &= \omega^2 \cos 2\theta [\lambda_I r_I (m_{rec})_I + \lambda_u r_u (m_{rec})_u]. \end{aligned}$$

Therefore, the maximum value of the secondary unbalanced force is

$$\begin{aligned} (F_x^S)_{max} &= \omega^2 [\lambda_I r_I (m_{rec})_I + \lambda_u r_u (m_{rec})_u] \\ &= (18.84)^2 [0.25 \times .25 \times 150 + 0.0835 \times .167 \times 225] \\ &= 4370.8 \text{ N} \end{aligned}$$

and this maximum occurs when

$$\cos 2\theta = \pm 1,$$

$$2\theta = 0, \pi, 2\pi, 3\pi, 4\pi, \dots, \quad \theta = 0, \frac{\pi}{2}, \pi, \frac{3\pi}{2}, 2\pi, \dots$$

i.e., whenever the crank is either horizontal or vertical.

The complete balancing of unbalanced forces in a single-cylinder engine is extremely difficult because of the practical difficulties in constructing it. However, a scheme to achieve this is shown in Fig. 7.23. Here, the connecting rod is extended beyond the crank pin A and a suitable mass is attached at C so that the combined CG of the reciprocating masses, the extension of the connecting rod, and the mass at C is at A . Then, the crank is extended beyond O and a mass is attached at D in order to bring the resultant CG of the whole system at O . Thus, the CG of the whole system is stationary at O and no inertia forces (i.e., the forces causing unbalance) will be generated. The reader can now easily realize the serious constructional difficulties involved in incorporating the modifications we have explained.⁷

In view of the constructional difficulties we have outlined, attempts can be made to achieve a partial balancing following the method we shall now discuss. Let the crank be extended beyond O and a mass m' be attached at a radius r' (Fig. 7.24) so that $m'r' = m_{rec}r$. As can be seen, the component, along the line of reciprocation, of the centrifugal force of m' will always neutralize the primary unbalanced force. However, it should be noted that, in this process, an inertia force $m'r'\omega^2 \sin \theta$ is generated in the direction perpendicular to the line of reciprocation. Therefore, a compromise is made so that only a part of the original primary force is balanced and an unbalanced force equal

⁷The inertia moment still remains unbalanced (see Section 7.7).

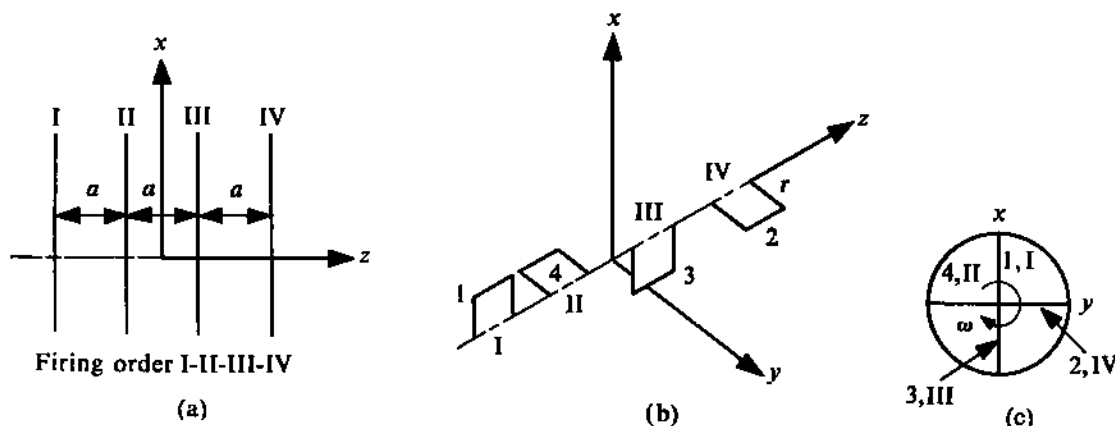


FIGURE 7.25

to this part is created in the direction perpendicular to the line of reciprocity. Depending on the stiffness characteristics of the supporting structure, the application of the method we have given may lead to a satisfactory balancing of the engine. Thus, for a partial balancing, $m'r' = \chi m_{recr}$, where $0 < \chi < 1$.

In-line Engines

The cylinder centrelines of an in-line engine are parallel and lie on the same plane. In such an engine, a common crankshaft is driven by all the connecting rods. Let the spacing (a) between the adjacent centrelines be uniform. Also, assume that the angular interval between the adjacent cranks (sequenced in the order of firing) is uniform. This angular interval depends on the operating cycle and the number of cylinders. For a two-stroke cycle, this interval is $2\pi/n$, and for a four-stroke cycle, it is $4\pi/n$, where n is the number of cylinders.

To study the inertia forces and moments of an in-line engine, we shall first set up a right-handed coordinate system xyz , where the x -axis is parallel to the line of reciprocation and the z -axis is along the axis of rotation of the common crankshaft with the origin at the midpoint of the engine. Figure 7.25 shows a four-cylinder in-line engine operating on a two-stroke cycle. In Figs. 7.25a and 7.25b, it should be noted that, starting from the left end, the cylinders are sequentially numbered as I-II-III-IV. The cranks (see Fig. 7.25c) are, however, numbered in the order of firing, i.e., as 1-4-3-2. Such a diagram is commonly known as a crank diagram. The firing order of the engine is I-II-III-IV. The firing order is always specified in terms of the cylinder numbers. The cranks, on the other hand, are always numbered in the order of firing, e.g., 1, n , $n - 1$, ..., 2, 1, ... for an n -cylinder engine. Figure 7.26 shows two other crank arrangements, each with a different firing order, of the two-stroke-cycle, four-cylinder engine given in Fig. 7.25. It should be noted that the crank numbering 1-4-3-2 is not altered in the crank diagram when the firing order changes. This method of numbering the cranks is very convenient for expressing their angle of inclination to the x -axis (measured along the direction of crank rotation). Thus, for the K -th crank,

$$\theta_K = \theta + (K - 1)(2\pi/n) \quad (\text{for a two-stroke engine}),$$

$\theta_K = \theta + (K - 1)(4\pi/n)$ (for a four-stroke engine),

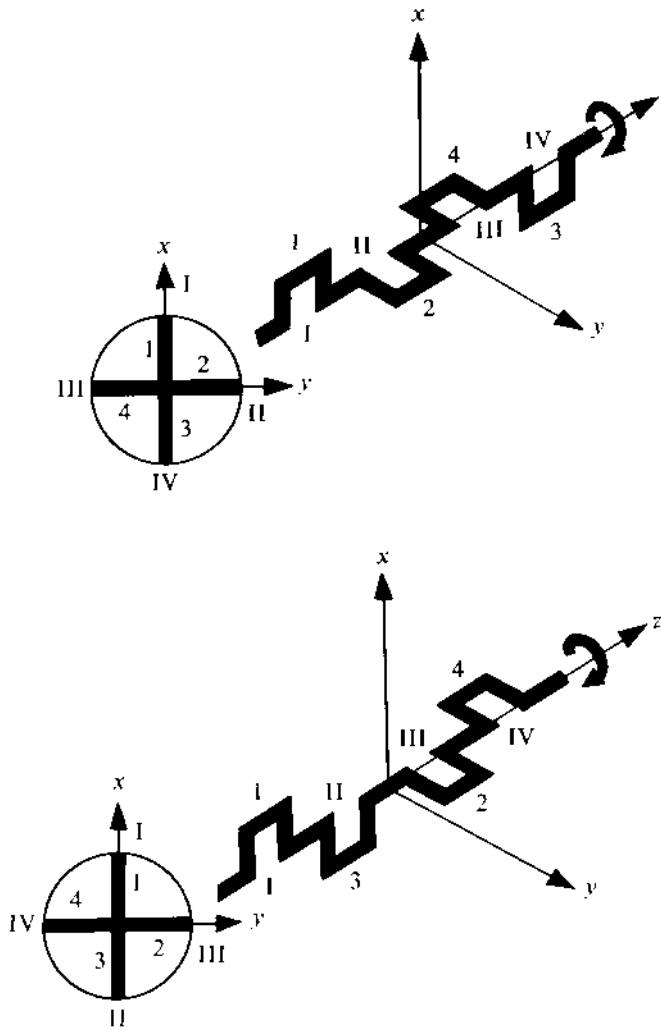


FIGURE 7.26

where θ represents the angle of crank 1 (always belonging to cylinder 1) from the x -axis. In each cylinder, the only effect of the unbalance is the inertia force parallel to the x -direction.

Thus, in the entire engine, the resultant effect consists of (i) an unbalanced force in the x -direction, and (ii) a moment about the y -axis (commonly referred to as the pitching moment). The magnitudes of these quantities and their dependence on the firing order have to be determined. As we shall subsequently see, only the pitching moment depends on the firing order. Therefore, if the firing order is suitably chosen, the state of balancing of an engine may improve. This method is known as *passive balancing*. The balancing can also be achieved by the addition of external masses. This technique is called *active balancing*. For a discussion on the methods of active balancing, see Section 7.8. As in rotary balancing, so too in engine balancing, both the graphical and analytical procedures can be used. Of these, we shall first take up the graphical procedure.

Referring to (7.46), we find that the primary unbalanced force in each cylinder *can be thought of*

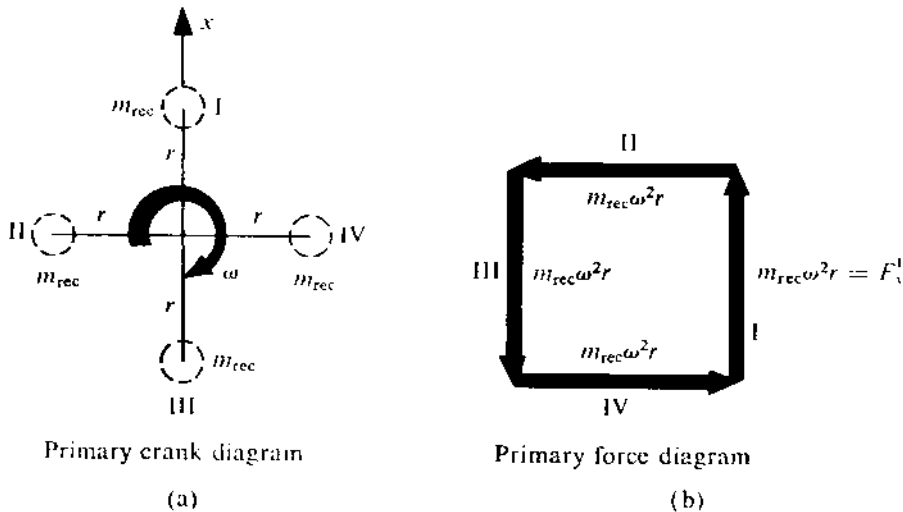


FIGURE 7.27

as the x -component of the centrifugal force that would have developed if m_{rec} were placed at the crank pin corresponding to the cylinder. So, the resultant primary force can be determined by taking the x -component of the resultant centrifugal force vector. The maximum value of this primary force, as we can easily see, will be equal to the resultant centrifugal force. Thus, the problem reduces to that of balancing a series of discrete rotating masses. Consider the two-stroke-cycle, four-cylinder engine along with the crank diagram and other details shown in Fig. 7.25. By (hypothetically) putting m_{rec} at each crank pin (see Fig. 7.27a), the resultant centrifugal force diagram will be as in Fig. 7.27b. This force vector diagram rotates with the cranks, but as the resultant magnitude is zero, the resultant primary force also is zero.

Rewriting (7.47), we find the secondary force of each cylinder is

$$F_x^S = \frac{m_{rec}}{4} (2\omega)^2 \cdot r A_2 \cos 2\theta.$$

This, then, can be considered as the x -component of the centrifugal force developed by a mass ($A_2 m_{rec}/4$) placed at the end of a hypothetical crank of radius r but rotating at a speed 2ω . To investigate the secondary unbalanced force of the engine, we draw the *secondary crank diagram* as done in Fig. 7.28a. Here, the secondary crank of each cylinder is so positioned that the angle it makes with the x -axis is twice the angle made by the primary crank corresponding to it. All angles are measured in the direction of rotation of the crankshaft. The secondary force diagram corresponding to Fig. 7.28a is shown in Fig. 7.28b. As we can make out from this figure, the engine is balanced so far as the secondary force is concerned.

Following the same procedure as we adopted in Section 7.4 for drawing a couple (moment) polygon, we can draw the primary couple polygon, taking xy as the reference plane. The primary

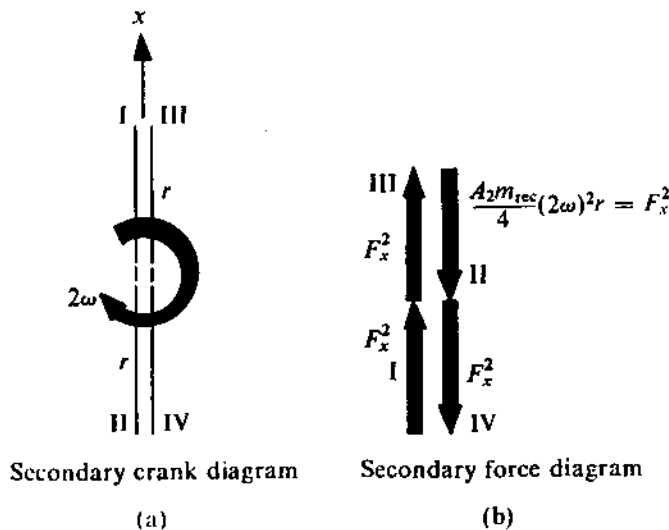


FIGURE 7.28

pitching moment polygon is shown in Fig. 7.29a. The resultant primary moment AB has a maximum value $2\sqrt{2}m_{rec}\omega^2ra$. However, at the instant crank 1 is along the x -direction, the primary moment is given by the projection of AB along the x -axis (according to the convention followed in this construction). The instantaneous moment then has a value $-2m_{rec}\omega^2ra$. Since the moment polygon rotates with the cranks, the maximum primary moment, i.e., $\pm 2\sqrt{2}m_{rec}\omega^2ra$, occurs when crank 1 is at 225° and 45° , respectively, with the x -axis.

Similarly, using the secondary crank diagram, the secondary moment polygon can be drawn as in Fig. 7.29b. The maximum values of the secondary moment are $\pm 2A_2m_{rec}\omega^2ra$ and these occur when the *secondary crank 1* is at 180° and 0° , respectively, with the x -axis. This implies that the maximum secondary moment occurs alternately with the positive and negative values when crank 1 is at 90° , 180° , 270° , and 0° with the x -axis.

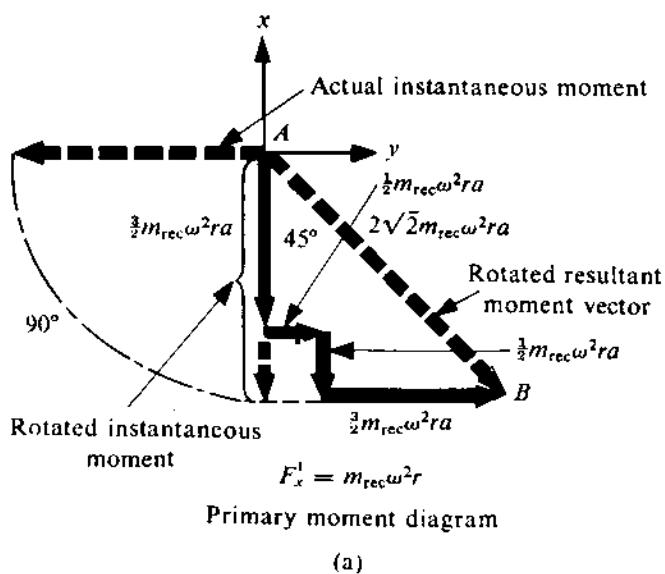
PROBLEM 7.5

Investigate the state of primary and secondary balancing of a four-stroke-cycle four-cylinder engine with a firing order I-II-III-IV. What will be the change in this state when the firing order is altered to I-II-IV-III?

SOLUTION

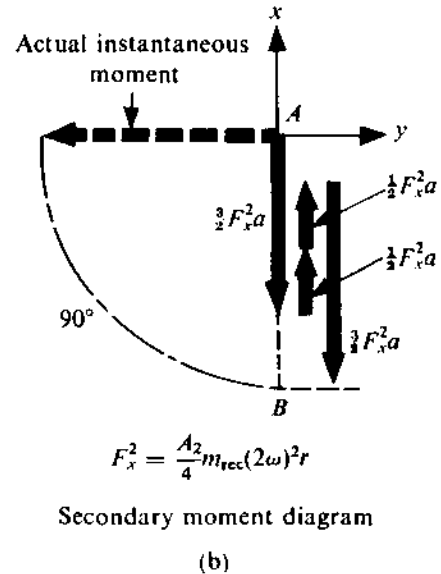
In a four-stroke-cycle four-cylinder in-line engine, the angular interval between the consecutive firing cranks is $4\pi/4 (= \pi)$. First, let us construct the primary crank diagram (Fig. 7.30a). Here, it is identical with the crank arrangement in the given engine. The primary force polygon corresponding to it is as shown in Fig. 7.30b, and the primary force is found to be balanced. The primary moment polygon (Fig. 7.30c) is drawn following the usual conventions, and the maximum values of the primary moment are found to be $\pm 2m_{rec}\omega^2ra$. These values occur when crank 1 is at 180° and 0° , respectively.

The secondary crank diagram is drawn as in Fig. 7.31a. As we can see, the maximum values of the resulting unbalanced secondary force are $\pm 4A_2m_{rec}\omega^2r$ (Fig. 7.31b), and these occur when



Primary moment diagram

(a)



Secondary moment diagram

(b)

FIGURE 7.29

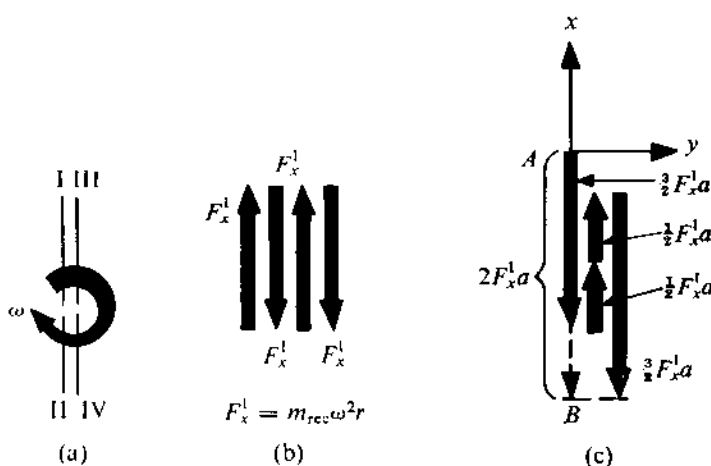


FIGURE 7.30

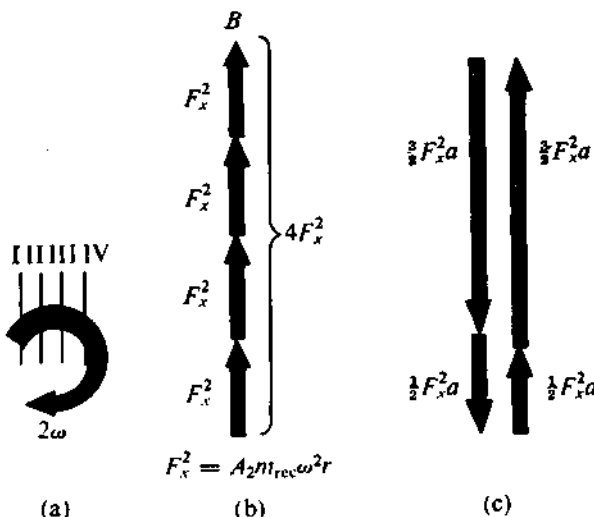


FIGURE 7.31

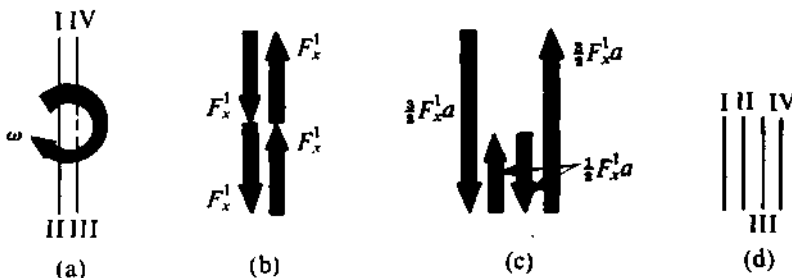


FIGURE 7.32

crank 1 is at 0° and 90° , respectively. After the secondary moment polygon (Fig. 7.31c) is drawn, it is found to be closed, implying the secondary moment is zero.

When the firing order is altered to I-II-IV-III, the corresponding primary crank, force, and moment diagrams would be as in Figs. 7.32a, 7.32b, and 7.32c, respectively. As we can notice, the engine has complete primary balancing. The secondary crank diagram (Fig. 7.32d) is identical with that in Fig. 7.31a. So, the state of secondary balancing remains unchanged.

Thus, we find that the change in the firing order improves the state of balancing because the primary moment gets balanced.

An analytical procedure, similar to that in Section 7.4 for rotary balancing, can also be used for an in-line engine. The problem that follows illustrates this.

PROBLEM 7.6

The firing order of a two-stroke-cycle six-cylinder diesel engine is I-V-III-VI-II-IV. The adjacent cylinder centrelines are 75 cm apart. Each cylinder has a connecting rod 120 cm long and a stroke of 45 cm. The mass of the reciprocating parts in each cylinder is 200 kg. Determine the magnitudes of the primary and secondary unbalanced forces and moments when the engine runs at a constant speed of 250 rpm.

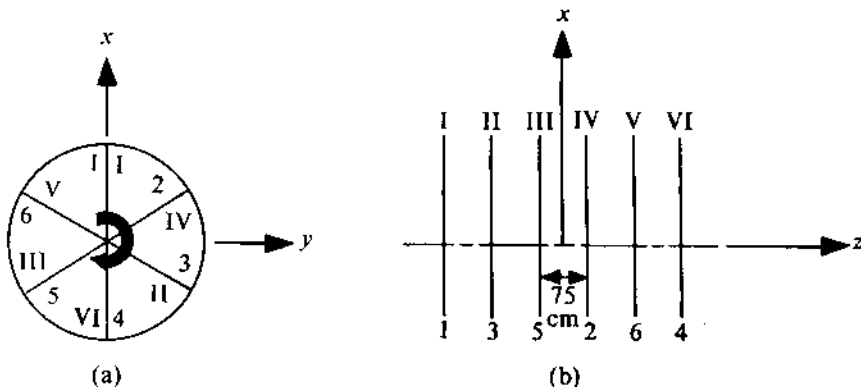


FIGURE 7.33

SOLUTION

As mentioned at the beginning of this section, we shall assume that the cranks are so designed that the rotary unbalance has been taken care of. With the given data, the angular interval between adjacent firing cranks = $2\pi/6$ rad = 60° , $r = 45/2$ cm = 0.225 m, and $A_2 \approx \lambda = r/l = 0.225/1.2 = 0.188$. Then, the crank diagram and cylinder arrangement will be as shown in Fig. 7.33. In this figure, 1, 2, 3, ... refer to the crank numbers, whereas I, II, III, ... refer to the cylinder numbers. To study the state of primary unbalance, we shall, using the given particulars, prepare the data as in Table 7.5. The term $m_{rec}\omega^2 r$, since it is common to all force and moment expressions, has been excluded from the table.

As the total of each of the two force columns (Table 7.5) is zero, the primary force is balanced independent of the crank positions, i.e., the engine is balanced so far as the primary force is concerned. The magnitude of the primary moment will be

$$m_{rec}\omega^2 r [(-1.2985)^2 + (-2.25)^2]^{1/2} = 200 \times \left(\frac{250 \times 2\pi}{60}\right)^2 \times 0.225 \times 2.5978 \text{ N-m} \\ = 80,123 \text{ N-m.}$$

TABLE 7.5

Crank number K	Distance from origin z_K (in)		Angle θ_K (degrees)	Force		Moment (rotated through 90°)	
	y -component $\sin \theta_K$	x -component $\cos \theta_K$		y -component $z_K \sin \theta_K$	x -component $z_K \cos \theta_K$		
1	-1.875	0	0	0	1	0	-1.875
2	0.375	60	0.866	0.5	0.325	0.1875	0.1875
3	-1.125	120	0.866	-0.5	-0.97425	0.5625	0.5625
4	1.875	180	0	-1	0	-1.875	-1.875
5	-0.375	240	-0.866	-0.5	0.325	0.1875	0.1875
6	1.125	300	-0.866	0.5	-0.97425	0.5625	0.5625
Total				0	0	-1.2985	-2.25

The inclination of this rotated moment vector with the x -axis at the instant considered (i.e., $\theta_1 = 0$)

is given by

$$\psi = \tan^{-1} \left(\frac{\sum z_K \sin \theta_K}{\sum z_K \cos \theta_K} \right) = \tan^{-1} \left(\frac{-1.2985}{-2.25} \right) = 30^\circ \text{ or } 210^\circ.$$

As both the components of the moment are negative, $\psi = 210^\circ$ is the correct solution. When the rotated moment vector is along the x -axis, the real moment vector is along the y -axis. Since the instantaneous moment is given by the y -component of the real moment vector, the instantaneous value is maximum when the rotated moment vector is along the x -axis. Thus, the unbalanced moment is maximum when $\theta_1 = 360^\circ - 210^\circ = 150^\circ$. Obviously, after the cranks are further rotated by 180° , the maximum unbalanced moment will be negative. Figure 7.34 illustrates the explanation we have given.

To investigate the state of secondary unbalance, we shall use Table 7.6. As before, the term $A_2 m_{\text{rec}} (2\omega)^2 r$ is dropped from the table. It is obvious from this table that the engine possesses complete secondary balancing.

TABLE 7.6

Crank number K	Distance from origin z_K (m)	Angle $2\theta_K$ (degrees)	Force		Moment	
			y -component $\sin 2\theta_K$	x -component $\cos 2\theta_K$	y -component $z_K \sin 2\theta_K$	x -component $z_K \cos 2\theta_K$
1	-1.875	0	0	1	0	-1.875
2	0.375	120	0.866	-0.5	0.325	-0.1875
3	-1.125	240	-0.866	-0.5	0.97425	0.5625
4	1.875	0	0	1	0	1.875
5	-0.375	120	0.866	-0.5	-0.325	0.1875
6	1.125	240	-0.866	-0.5	-0.97425	-0.5625
Total			0	0	0	0

V-twin Engines

A V-twin engine consists of two identical cylinders lying in the xy -plane such that the angle between their centrelines ox_1 and ox_2 (known as the V-angle) is 2α and it is bisected by the x -axis (Fig. 7.35). Also, it has two identical connecting rods attached to a single crank (OA). The rotation of the crank measured from the x_1 -, x -, and x_2 -axis is given by θ_1 , θ , and θ_2 , respectively, where $\theta_1 = \theta - \alpha$ and $\theta_2 = \theta + \alpha$. The reciprocating unbalanced forces (only up to the second order) of the two cylinders along their respective lines of reciprocation can be written as

$$F_{x_1} = m_{\text{rec}} \omega^2 r [\cos \theta_1 + A_2 \cos 2\theta_1], \quad (7.49a)$$

$$F_{x_2} = m_{\text{rec}} \omega^2 r [\cos \theta_2 + A_2 \cos 2\theta_2]. \quad (7.49b)$$

Hence, the resultant unbalanced forces are

$$F_x = (F_{x_1} + F_{x_2}) \cos \alpha, \quad F_y = (F_{x_1} - F_{x_2}) \sin \alpha.$$

Substituting for F_{x_1} , F_{x_2} , θ_1 , and θ_2 in these expressions, we get

$$F_x = m_{\text{rec}} \omega^2 r [\cos (\theta - \alpha) + \cos (\theta + \alpha) + A_2 \{ \cos 2(\theta - \alpha) + \cos 2(\theta + \alpha) \}] \cos \alpha.$$

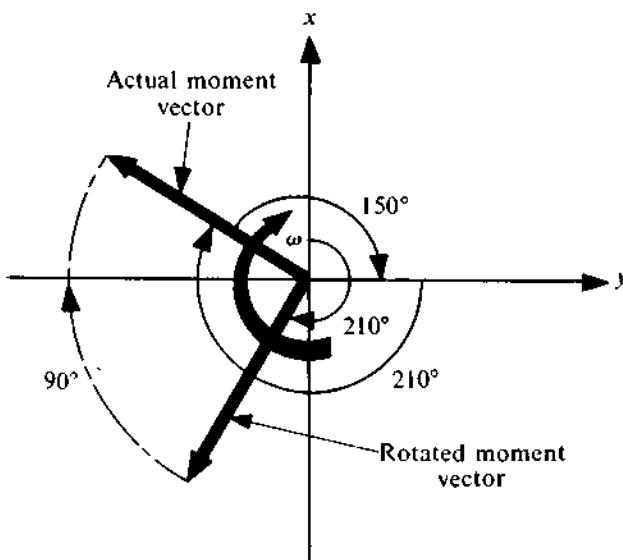


FIGURE 7.34

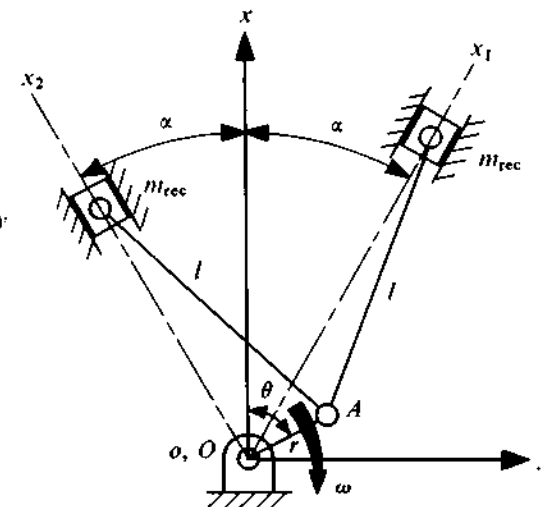


FIGURE 7.35

$$F_y = m_{\text{rec}} \omega^2 r [\cos(\theta - \alpha) - \cos(\theta + \alpha) + A_2 \{\cos 2(\theta - \alpha) - \cos 2(\theta + \alpha)\}] \sin \alpha.$$

On simplification, we have

$$F_x = 2m_{\text{rec}} \omega^2 r \cos \alpha (\cos \alpha \cos \theta + A_2 \cos 2\alpha \cos 2\theta), \quad (7.50a)$$

$$F_y = 2m_{\text{rec}} \omega^2 r \sin \alpha (\sin \alpha \sin \theta + A_2 \sin 2\alpha \sin 2\theta). \quad (7.50b)$$

Separating the primary and secondary parts, we can express the resultant forces as

$$F^P \text{ (primary force)} = (F_x^{P^2} + F_y^{P^2})^{1/2} = 2m_{\text{rec}} \omega^2 r [\cos^2 \theta \cos^4 \alpha + \sin^2 \theta \sin^4 \alpha]^{1/2}, \quad (7.51a)$$

$$\begin{aligned} F^S \text{ (secondary force)} = (F_x^{S^2} + F_y^{S^2})^{1/2} &= 2m_{\text{rec}} \omega^2 r A_2 [\cos^2 2\theta \cos^2 \alpha \cos^2 2\alpha \\ &+ \sin^2 2\theta \sin^2 \alpha \sin^2 2\alpha]^{1/2}. \end{aligned} \quad (7.51b)$$

PROBLEM 7.7

Determine the maximum and minimum values of the primary and secondary forces for a 90° V-twin engine. Also, indicate the crank positions corresponding to these values. Given m_{rec} per cylinder = 2 kg, stroke = 12 cm, connecting-rod length = 20 cm, and engine speed = 2000 rpm.

SOLUTION

From the given data,

$$r = 6 \text{ cm} = 0.06 \text{ m}, \quad l = 0.2 \text{ m}, \quad \alpha = 45^\circ,$$

$$\omega = \frac{2000 \times 2\pi}{60} = 209.44 \text{ rad/s}, \quad A_2 \approx \lambda = \frac{r}{l} = 0.3.$$

Substituting these values in (7.51a) and (7.51b), we get

$$\begin{aligned} F^P &= 2 \times 2 \times 209.44^2 \times 0.06 \times [\cos^2 \theta \cdot \frac{1}{4} + \sin^2 \theta \cdot \frac{1}{4}]^{1/2} \text{ N} \\ &= 5263.8 \text{ N}, \end{aligned}$$

$$\begin{aligned} F^S &= 2 \times 2 \times 209.44^2 \times 0.06 \times 0.3 \times [\cos^2 2\theta \times \frac{1}{2} \times 0 + \sin^2 2\theta \times \frac{1}{2} \times 1]^{1/2} \text{ N} \\ &= 2233.2 \sin 2\theta \text{ N}. \end{aligned}$$

The magnitude of the primary force is constant and the force can be considered as a vector in the direction **OA** rotating with the crank. Thus, to balance this force, a suitable mass opposite to the crank has to be added. This can be done very easily.

So far as the secondary force is concerned, it is observed that the *x*-component is always equal to zero. Thus, the secondary force acts along the *y*-axis and fluctuates harmonically with an angular frequency twice the speed of crank rotation. The secondary unbalanced force is zero when $\theta = 0^\circ, 180^\circ, 270^\circ$. It attains the maximum positive and negative values $\pm 2233.2 \text{ N}$ alternately when $\theta = 45^\circ, 135^\circ, 225^\circ, 315^\circ$.

PROBLEM 7.8

The reciprocating mass per cylinder in a 60° V-twin engine is 1.2 kg. The stroke and the connecting rod length are 10 cm and 25 cm, respectively. If the engine runs at 2000 rpm, determine the maximum and minimum values of the primary and secondary forces. Also, find out the crank positions corresponding to these values.

SOLUTION

Using the given data, we have

$$r = 5 \text{ cm} = 0.05 \text{ m}, \quad l = 0.25 \text{ m}, \quad \alpha = 30^\circ,$$

$$\omega = \frac{2000 \times 2\pi}{60} = 209.44 \text{ rad/s}, \quad A_2 \approx \lambda = \frac{r}{l} = 0.2.$$

Substituting these values in (7.51a) and (7.51b), we get

$$\begin{aligned} F^P &= 2 \times 1.2 \times 209.44^2 \times 0.05 \times (\cos^2 \theta \times 0.866^4 + \sin^2 \theta \times 0.5^4)^{1/2} \text{ N} \\ &= 5263.8 \times (0.562 \cos^2 \theta + 0.0625 \sin^2 \theta)^{1/2} \text{ N}, \end{aligned}$$

$$\begin{aligned} F^S &= 2 \times 1.2 \times 209.44^2 \times 0.05 \times 0.2(\cos^2 2\theta \times 0.866^2 \times 0.5^2 + \sin^2 2\theta \times 0.5^2 \times 0.866^2)^{1/2} \text{ N} \\ &= 455.9 \text{ N}. \end{aligned}$$

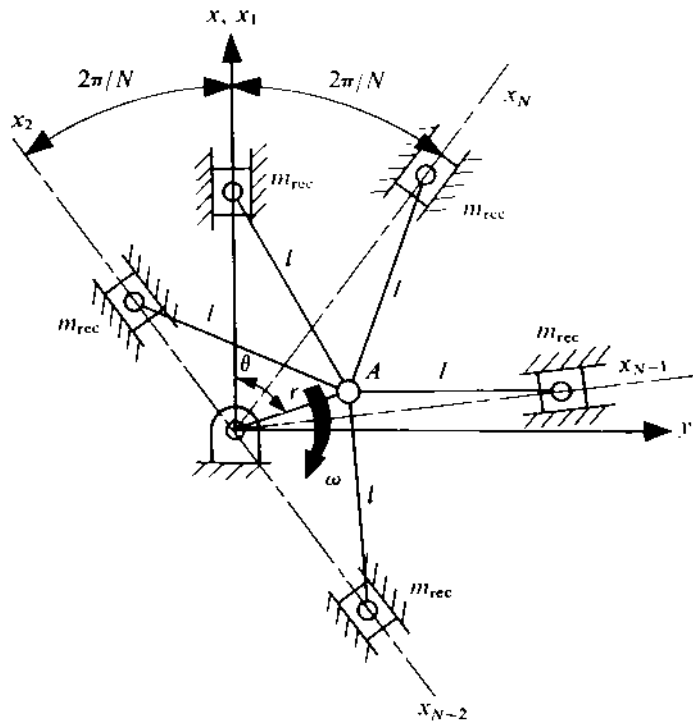


FIGURE 7.36

Thus, the secondary force is constant in magnitude and acts at an angle 2θ from the x -axis. The primary force is minimum when $\theta = 90^\circ, 270^\circ$ and maximum when $\theta = 0^\circ, 180^\circ$ as we shall now see. Rewriting F^P as

$$F^P = 5263.8 \times (0.4995 \cos^2 \theta + 0.0625)^{1/2},$$

we see it reaches the maximum magnitude when $\cos \theta = \pm 1$, i.e., $\theta = 0^\circ, 180^\circ$. Similarly, for $\theta = 90^\circ, 270^\circ$, F^P is minimum. The maximum and minimum values of F^P can be found out to be 3946.1 N and 1316 N, respectively.

Radial Engines

In a radial engine, N identical cylinders are placed in one plane, with their centrelines at a uniform angular interval $\alpha (= 2\pi/N)$. One connecting rod from each cylinder is attached to a single common crank. As shown in Fig. 7.36, the x -axis is taken along the centreline of the first cylinder. We shall consider the engines with $N > 2$. Since a radial engine generally runs at a high speed, we shall when analyzing it, have to consider the forces of an order higher than the secondary. The analysis can be carried out using both the graphical and analytical methods. In the graphical procedure, the concept of direct and reverse cranks is used, and therefore this technique is sometimes also referred to as the method of direct and reverse cranks. As usual, we shall first take up the graphical method.

When analyzing the engine graphically, the reciprocating unbalanced force along the line of reciprocation is replaced by two masses, placed at a distance r from O , rotating in opposite directions with the same speed. These masses are so arranged that, while rotating, both coincide only on the cylinder centreline. Figure 7.37a shows a single-cylinder engine with crank radius r , connecting-rod

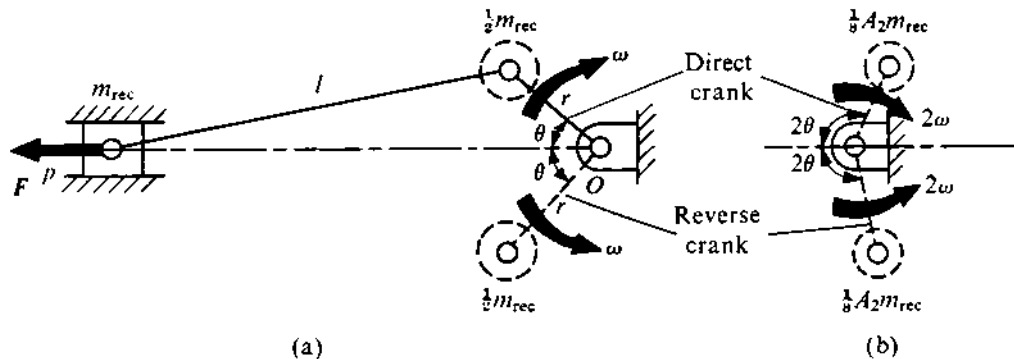


FIGURE 7.37

length l , and reciprocating mass m_{rec} . The primary force of this engine, for a crank speed ω , is given by

$$F^P = m_{rec}\omega^2 r \cos \theta.$$

A force identical to this force is generated by the two rotating masses, each $\frac{1}{2}m_{rec}$ (Fig. 7.37a). The crank rotating in the direction of the engine rotation is called the *direct crank*, and the other crank, the *reverse crank*. The secondary force is generated by the two rotating masses, each $\frac{1}{8}A_2m_{rec}$, attached to the secondary direct and reverse cranks, as shown in Fig. 7.37b. We can similarly generate the forces of an order higher than the secondary. It should be noted that each of the coefficients A_4, A_8, A_{12}, \dots (i.e., those with a subscript divisible by 4) in these forces has a negative sign [see (4.34)]. In our analysis, we shall disregard the negative sign, and therefore the direction of the net unbalanced forces of orders $j = 4, 8, 12, \dots$ will be opposite to that we obtain.

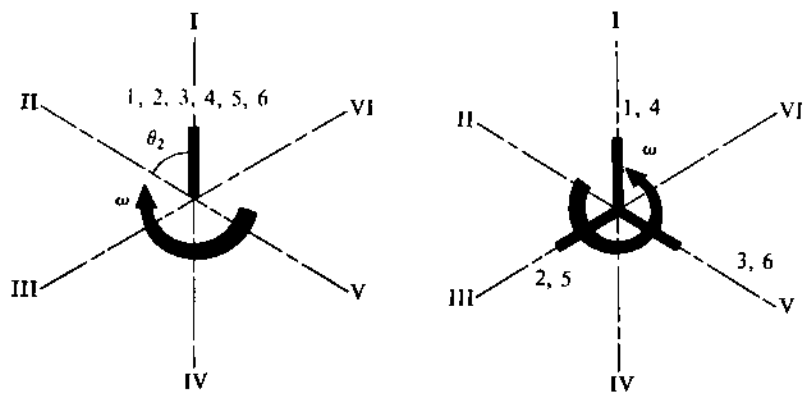
In a radial engine, the unbalanced force of each order (in each cylinder) is replaced by masses attached to the direct and reverse cranks corresponding to the order. As all the direct cranks rotate in the forward direction with the same speed, the relative positions of the generated centrifugal force vectors remain unchanged. The same is true of the reverse cranks. The resultant unbalanced force of the engine can then be obtained by a vectorial summation of the centrifugal force vectors. In the problems that follow, we shall illustrate this.

PROBLEM 7.9

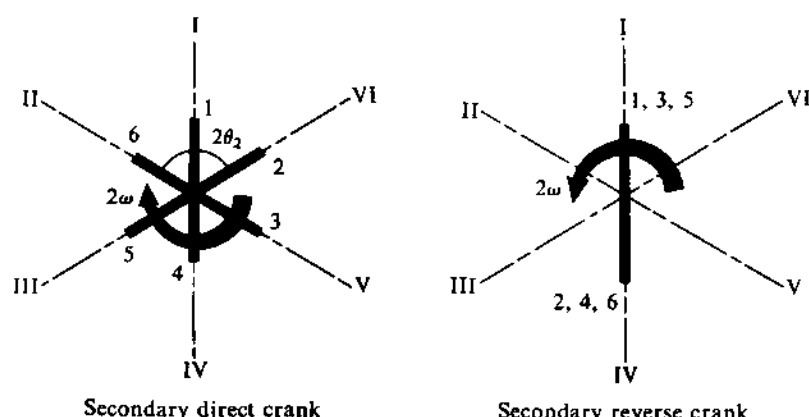
Investigate the state of unbalance (up to the fourth order) of a two-stroke radial engine with six cylinders.

SOLUTION

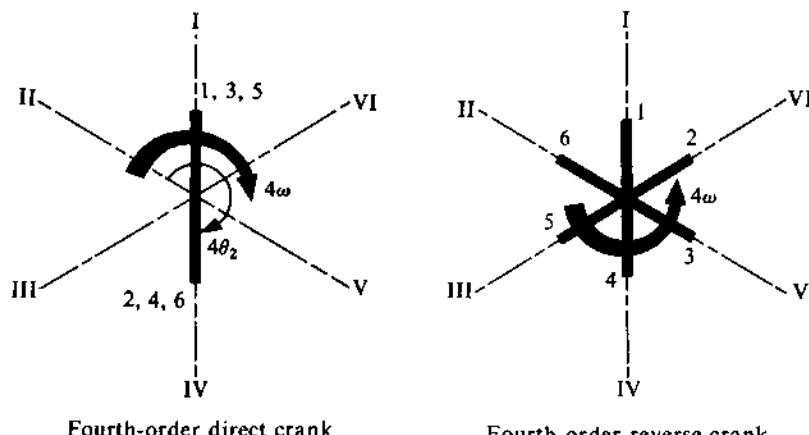
For convenience, let us draw the direct and reverse cranks separately for the primary, secondary, and fourth-order forces at the instant $\theta = 0$ (Fig. 7.38). It is obvious that the direct primary crank of all the cylinders is the actual common crank itself. The reverse primary crank of each cylinder is given by the mirror image of the direct primary crank, with the mirror placed along the cylinder centreline. The secondary direct crank of each cylinder has to be placed at an angle twice that between the direct primary crank and the cylinder centreline. This angle is measured from the cylinder centreline in the direction of engine rotation. Thus, if θ_2 is the inclination of the direct primary crank with the centreline of engine 2, then the inclinations of the second- and fourth-order direct cranks will be $2\theta_2$ and $4\theta_2$, respectively (Fig. 7.38). The secondary reverse cranks are drawn



(a)



(b)



(c)

FIGURE 7.38

in a manner similar to that followed for drawing the primary reverse cranks. Since the combined effect of the centrifugal forces due to the masses placed at the end of the direct and reverse cranks is the resultant unbalanced force, an examination of Fig. 7.38 leads to the following conclusions:

- (i) The primary unbalanced force is given by a centrifugal force, along the crank, of a magnitude $6 \times \frac{1}{2}m_{\text{rec}}\omega^2r$. This can obviously be balanced by a rotating mass.
- (ii) The secondary and fourth-order forces are completely balanced.

It can be shown that for an even number of cylinders all inertia forces of an order higher than the primary are balanced. The reader is advised to verify that in a four-stroke-cycle radial engine with an even number of cylinders only the alternate cylinders will be fired if the firing takes place at equal intervals.

PROBLEM 7.10

A four-stroke-cycle five-cylinder radial engine runs at 3000 rpm. The reciprocating mass per cylinder is 2 kg, the crank radius and the connecting-rod length being 5 cm and 25 cm, respectively. Investigate the state of unbalance of the engine.

SOLUTION

Let us first determine A_2 , A_4 , A_6 from the given data. From (4.34),

$$A_2 \approx \lambda + \frac{\lambda^3}{4} + \frac{15\lambda^4}{128} + \dots,$$

$$A_4 \approx \frac{\lambda^3}{4} + \frac{3\lambda^5}{16} + \dots,$$

$$A_6 \approx \frac{9\lambda^5}{28} + \dots,$$

where $\lambda = r/l = 0.2$. Using this value of λ , we have

$$A_2 = 0.2 + 0.002 + 0.00004 + \dots \approx 0.202,$$

$$A_4 = 0.002 + 0.00006 + \dots \approx 0.002,$$

$$A_6 = 0.0001 + \dots \approx 0.$$

From these values, we see that it is sufficient to consider the inertia forces only up to the fourth order. Let us now draw the direct and reverse cranks for the primary, secondary, and fourth-order forces as in Fig. 7.39. Then, a study of the direct and reverse cranks reveals the following:

- (i) The primary force is unbalanced and can be represented by a force of magnitude $5 \times \frac{1}{2}m_{\text{rec}}\omega^2r$ rotating along with the actual crank. This unbalanced force can be balanced by a rotating mass.
- (ii) The secondary forces are balanced.
- (iii) The fourth-order force is unbalanced and has a constant magnitude $\frac{5}{2}(m_{\text{rec}}A_4/16)(4\omega)^2r$. Its line of action coincides with the fourth-order reverse crank which rotates at a speed of 4ω in a direction opposite to that of the actual crank. This force is directed towards the crankshaft

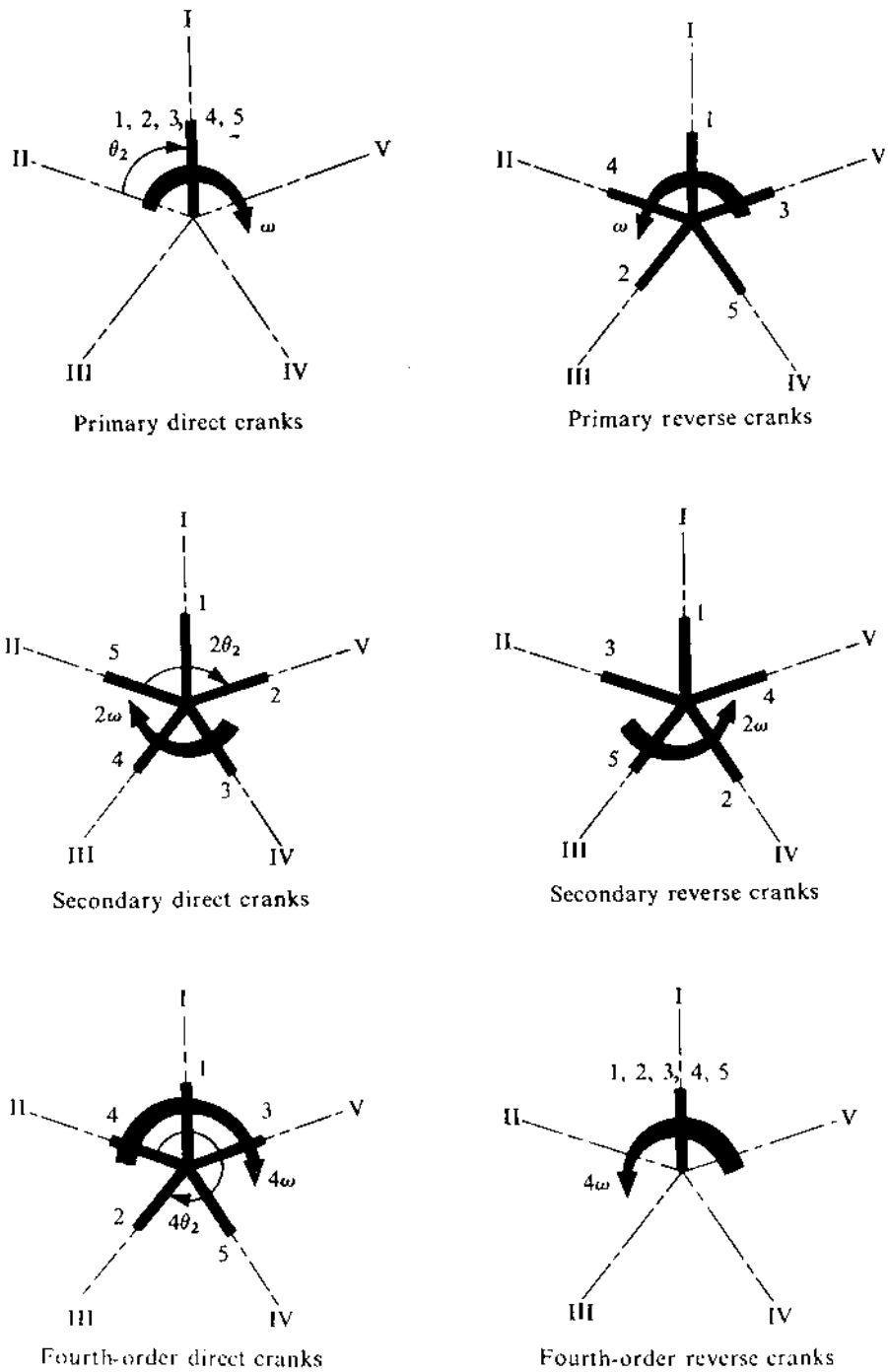


FIGURE 7.39

(opposite to the centrifugal force of this reverse crank) as the order of the force is divisible by 4. As can be seen, when the actual crank coincides with any cylinder centreline, the line of action of this unbalanced force also coincides with that centreline.

Using the given data, we have

$$r = 0.05 \text{ m}, \quad m_{\text{rec}} = 2 \text{ kg}, \quad \omega = \frac{3000 \times 2\pi}{60} = 314.16 \text{ rad/s.}$$

Thus, the magnitude of the primary unbalanced force is

$$5 \times \frac{1}{2} m_{\text{rec}} \omega^2 r = 24,674 \text{ N,}$$

and that of the fourth-order unbalanced force is

$$5 \times \frac{1}{2} \frac{m_{\text{rec}} A_4}{16} (4\omega)^2 r = 49.35 \text{ N.}$$

We shall now discuss the analytical procedure. This method helps to find the important general characteristics of a radial engine. Referring to Fig. 7.36, we find the inertia force of the K -th cylinder can be written as

$$F_{x_K} = m_{\text{rec}} \omega^2 r (\cos \theta_K + A_2 \cos 2\theta_K - A_4 \cos 4\theta_K + \dots),$$

where $\theta_K = \theta + (K-1)(2\pi/N)$. Resolving F_{x_K} along the x - and y -direction and summing up these components for each cylinder, we can express the resultant inertia force components as

$$F_x = \sum_{K=1}^N F_{x_K} \cos (K-1) \frac{2\pi}{N}, \quad (7.52a)$$

$$F_y = - \sum_{K=1}^N F_{x_K} \sin (K-1) \frac{2\pi}{N}. \quad (7.52b)$$

Let us now separately consider the inertia forces of different orders. The primary force components can be written as

$$F_x^P = m_{\text{rec}} \omega^2 r \sum_{K=1}^N \cos [\theta + (K-1) \frac{2\pi}{N}] \cos (K-1) \frac{2\pi}{N}, \quad (7.53a)$$

$$F_y^P = -m_{\text{rec}} \omega^2 r \sum_{K=1}^N \cos [\theta + (K-1) \frac{2\pi}{N}] \sin (K-1) \frac{2\pi}{N}. \quad (7.53b)$$

To simplify these expressions, we shall use the trigonometrical results

$$\sum_{K=1}^N \cos [\alpha + (K-1)\beta] = \frac{\sin \frac{N\beta}{2} \cos (\alpha + \frac{N-1}{2}\beta)}{\sin \frac{\beta}{2}}, \quad (7.54a)$$

$$\sum_{K=1}^N \sin [\alpha + (K-1)\beta] = \frac{\sin \frac{N\beta}{2} \sin (\alpha + \frac{N-1}{2}\beta)}{\sin \frac{\beta}{2}}, \quad (7.54b)$$

where $\beta \neq 2\pi, 4\pi, 6\pi, \dots$. If $\beta = 2\pi, 4\pi, 6\pi, \dots$, then

$$\sum_{K=1}^N \cos [\alpha + (K-1)\beta] = N \cos \alpha, \quad (7.54c)$$

$$\sum_{K=1}^N \sin [\alpha + (K-1)\beta] = N \sin \alpha. \quad (7.54d)$$

Using (7.54) in (7.53), we can write

$$\begin{aligned} F_x^P &= \frac{N}{2} m_{rec} \omega^2 r \cos \theta + \frac{m_{rec} \omega^2 r}{2 \sin \frac{2\pi}{N}} \sin N \cdot \frac{2\pi}{N} \cdot \cos [\theta + (N-1) \frac{2\pi}{N}] \\ &= \frac{N}{2} m_{rec} \omega^2 r \cos \theta \quad (\text{as } N > 2) \end{aligned} \quad (7.55a)$$

and, similarly,

$$F_y^P = \frac{N}{2} m_{rec} \omega^2 r \sin \theta \quad (\text{as } N > 2). \quad (7.55b)$$

Thus, we see that the resultant primary force is of a magnitude $(N/2)m_{rec}\omega^2r$ and acts along the engine crank.

Considering the force of order j in an analogous manner, we get

$$\begin{aligned} F_x^j &= \pm A_j m_{rec} \omega^2 r \sum_{K=1}^N \cos [j\theta + j(K-1) \frac{2\pi}{N}] \cos (K-1) \frac{2\pi}{N} \quad \text{for } j = \begin{cases} 2, 6, 10, \dots \\ 4, 8, 12, \dots \end{cases} \\ &= \pm \frac{1}{2} A_j m_{rec} \omega^2 r \sum_{K=1}^N [\cos \{j\theta + (K-1)(j+1) \frac{2\pi}{N}\} \\ &\quad + \cos \{j\theta + (K-1)(j-1) \frac{2\pi}{N}\}] \quad \text{for } j = \begin{cases} 2, 6, 10, \dots \\ 4, 8, 12, \dots \end{cases} \end{aligned} \quad (7.56a)$$

$$\begin{aligned} F_y^j &= \mp A_j m_{rec} \omega^2 r \sum_{K=1}^N \cos [j\theta + j(K-1) \frac{2\pi}{N}] \sin (K-1) \frac{2\pi}{N} \quad \text{for } j = \begin{cases} 2, 6, 10, \dots \\ 4, 8, 12, \dots \end{cases} \\ &= \pm \frac{1}{2} A_j m_{rec} \omega^2 r \sum_{K=1}^N [\sin \{j\theta + (K-1)(j+1) \frac{2\pi}{N}\} \\ &\quad - \sin \{j\theta + (K-1)(j-1) \frac{2\pi}{N}\}] \quad \text{for } j = \begin{cases} 2, 6, 10, \dots \\ 4, 8, 12, \dots \end{cases} \end{aligned} \quad (7.56b)$$

Using (7.54) in (7.56), the results we obtain are as follows. When $j = 2, 6, 10, \dots$, then

$$\begin{aligned} F_x^j &= 0 && \text{if } j \pm 1 \neq N, 2N, 3N, \dots, \\ F_x^j &= \frac{N}{2} A_j m_{rec} \omega^2 r \cos j\theta && \text{if } j \pm 1 = N, 2N, 3N, \dots, \\ F_y^j &= 0 && \text{if } j \pm 1 \neq N, 2N, 3N, \dots, \\ F_y^j &= \mp \frac{N}{2} A_j m_{rec} \omega^2 r \sin j\theta && \text{if } j \pm 1 = N, 2N, 3N, \dots. \end{aligned} \quad (7.57)$$

For $j = 4, 8, 12, \dots$, the signs of F_x^j and F_y^j obtained from (7.57) should be reversed. A careful study of (7.57) in respect of forces of an order higher than primary leads to the following conclusions:

- (i) For an even number of cylinders, all forces are balanced as $(j \pm 1)$ can never be equal to N or its integral multiples because j is even.
- (ii) For an odd number of cylinders [as is usually the case for reasons already mentioned (see the discussion following Problem 7.9)], the lowest order unbalanced force is $(N - 1)$.

Table 7.7 indicates the state of balancing for various cylinder numbers.

TABLE 7.7

Number of cylinders	Order of force	P	2	4	6	8	10	12	14	16	18	20
3		U	U	U	B	U	U	B	U	U	B	U
4		U	B	B	B	B	B	B	B	B	B	B
5		U	B	U	U	B	B	B	U	U	B	B
6		U	B	B	B	B	B	B	B	B	B	B
7		U	B	B	U	U	B	B	B	B	B	U
8		U	B	B	B	B	B	B	B	B	B	B
9		U	B	B	B	U	U	B	B	B	B	B
10		U	B	B	B	B	B	B	B	B	B	B

B, balanced; U, unbalanced.

7.7 BALANCING OF INTERNAL-COMBUSTION ENGINES (GENERALIZED APPROACH)

In our analyses in Section 7.6, we made three assumptions (see the beginning of Section 7.6), namely, (i), (ii), and (iii). In this section, we shall analyze only the single-cylinder engines without making these assumptions. For other types of engines, viz., in-line, V-, W-, and radial engines with special features like nonuniform cylinder spacing, see the second edition of this text.

Single-cylinder Engines

Figure 7.40 shows a fixed coordinate system xyz in which the z -axis passes through the crank centre O and is perpendicular to the plane of rotation of the crank OA (i.e., the z -axis is along the angular velocity vector of the crank). Thus, the coordinates of the point O are $(0, 0, a)$, where a is the distance of O from the origin of the coordinate system. The point A is at the location of the gudgeon pin which is at a distance x from the crank centre O at that instant. Let

θ = rotation of the crank from the dead-centre position,

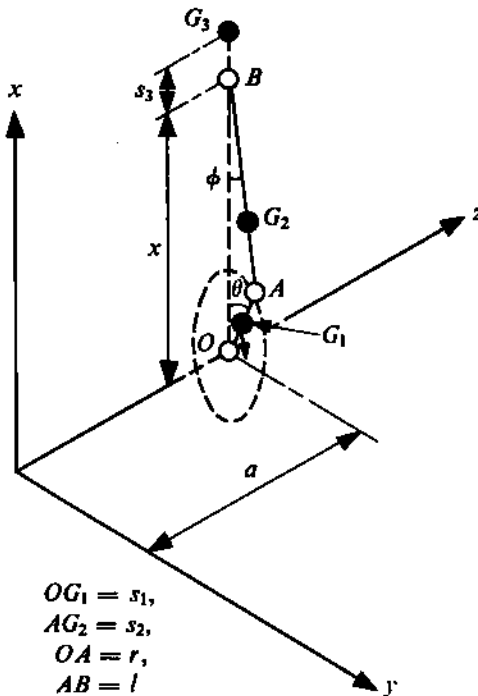


FIGURE 7.40

ϕ = inclination of the connecting rod to the line of stroke,

r = crank radius OA ,

l = length of the connecting rod AB ,

$\lambda = r/l$,

m_c = mass of the crank with CG of the crank at the point G_1 which is at a distance s_1 from the point O ,

m_{cr} = mass of the connecting rod, its CG being at the point G_2 , which is at a distance s_2 from the point A , and

m_{re} = mass of the reciprocating parts with CG at the point G_3 which is at a distance s_3 from the point B and on the line of stroke.

We shall determine the following inertia forces and moments of the mechanism:

F_x = longitudinal inertia force (in the line of stroke),

F_y = transverse inertia force (normal to the line of stroke and in the plane of crank rotation),

$F_z = 0$ (obviously),

M_x (moment about the x -axis) = yawing moment,

M_y (moment about the y -axis) = pitching moment, and

M_z (moment about the z -axis) = rolling moment.

For calculating the inertia forces, the connecting rod is replaced by two concentrated masses at its ends so that the total mass and the position of the CG remain unchanged (see Chapter 4). Thus the masses m_2 and m_1 at A and B , respectively, are

$$m_2 = (1 - s_2/l)m_{cr}, \quad m_1 = (s_2/l)m_{cr}. \quad (7.58)$$

The x - and y -component of the acceleration of the point G_1 (i.e., of mass m_C) and of the point A (i.e., of mass m_2) are

$$\begin{aligned} f_{G_1}^x &= -s_1\dot{\theta}^2 \cos \theta - s\ddot{\theta} \sin \theta, & f_{G_1}^y &= -s_1\dot{\theta}^2 \sin \theta + s\ddot{\theta} \cos \theta, \\ f_A^x &= -r\dot{\theta}^2 \cos \theta - r\ddot{\theta} \sin \theta, & f_A^y &= -r\dot{\theta}^2 \sin \theta + r\ddot{\theta} \cos \theta. \end{aligned} \quad (7.59)$$

The acceleration components of the point B (i.e., of mass m_1) and G_3 (i.e., of mass m_{re}) are

$$f_{G_3}^x = f_B^x = \ddot{x}, \quad f_{G_3}^y = f_B^y = 0, \quad (7.60)$$

where \ddot{x} is the acceleration of the piston from (4.34). Thus, the inertia forces F_x and F_y are obtained from

$$F_x = -m_C f_{G_1}^x - m_2 f_A^x - (m_{re} + m_1)\ddot{x}, \quad F_y = -m_C f_{G_1}^y - m_1 f_A^y.$$

Using (7.58), (7.59), and (7.60), we get

$$F_x = m_C(s_1\dot{\theta}^2 \cos \theta + s_1\ddot{\theta} \sin \theta) + m_{cr}(1 - \frac{s_2}{l})(r\dot{\theta}^2 \cos \theta + r\ddot{\theta} \sin \theta) - (m_{re} + \frac{s_2}{l}m_{cr})\ddot{x}, \quad (7.61)$$

$$F_y = m_C(s_1\dot{\theta}^2 \sin \theta - s_1\ddot{\theta} \cos \theta) + (1 - \frac{s_2}{l})m_{cr}(r\dot{\theta}^2 \sin \theta - r\ddot{\theta} \cos \theta). \quad (7.62)$$

Substituting

$$\omega = \dot{\theta} \quad (\text{angular velocity of the crank}),$$

$$\dot{\omega} = \ddot{\theta} \quad (\text{angular acceleration of the crank}),$$

$$Q = r[m_{re} + (s_2/l)m_{cr}], \quad Q' = [s_1m_C + (1 - s_2/l)r m_{cr}], \quad (7.63)$$

we get

$$F_x = Q'(\omega^2 \cos \theta + \dot{\omega} \sin \theta) - Q(\ddot{x}/r), \quad F_y = Q'(\omega^2 \sin \theta - \dot{\omega} \cos \theta). \quad (7.64)$$

Q and Q' are called the *reduced first moments* of the mechanism. [It should be noted that $Q/r = m_{rec}$ as defined in (7.40).] The inertia moments about the x - and y -axis are easily obtained to be

$$M_x = -F_y a, \quad M_y = F_x a. \quad (7.65)$$

To determine the rolling moment M_z , we have to calculate the angular momentum of the connecting rod. In this case, the equivalent massless link with end masses, representing the connecting rod, must have the same moment of inertia about the axis at G_2 as the connecting rod. So, as discussed in Chapter 4, we assume the end masses m_1 and m_2 (which can no longer be assumed to be point masses) to have the radii of gyration k_1 about the axis at A and k_2 about the axis at B , respectively. Now, applying the parallel-axis theorem, we have

$$m_{cr}k_{cr}^2 = (k_2^2 + s_2^2)m_2 + [k_1^2 + (l - s_2)^2]m_1,$$

where k_{cr} is the radius of gyration of the connecting rod about the axis at G_2 . Thus, using (7.58), we get

$$m_1k_1^2 + m_2k_2^2 = m_{cr}k_{cr}^2 - m_2s_2^2 - m_1(l - s_2)^2 = [k_{cr}^2 - s_2(l - s_2)]m_{cr}. \quad (7.66)$$

We can now determine the total angular momentum of the mechanism about the z -axis. It consists of three parts, namely,

- (i) the angular momentum of the crank ($= m_C k_C^2$, where k_C is the radius of gyration of the crank about O),
- (ii) the angular momentum of the masses m_1 and m_2 which is $(m_1 k_1^2 + m_2 k_2^2)(-\dot{\phi})$, where $\dot{\phi}$ is the angular velocity of the connecting rod (from Fig. 7.40, this is positive when the $\dot{\phi}$ -vector is in the direction of negative z -axis),
- (iii) the angular momentum of the masses m_1 and m_2 about O (as the velocity vector of mass m_1 passes through O , the corresponding angular momentum will be zero; for the mass m_2 , this will be equal to $m_2 \omega r^2$).

Thus, the total angular momentum will be

$$H_z = [\omega(k_C^2 m_C + r^2 m_2) - \dot{\phi}(m_1 k_1^2 + m_2 k_2^2)].$$

Using (7.66) and (7.58), we get

$$H_z = \{\omega[k_C^2 m_C + r^2(1 - s_2/l)m_{\text{cr}}] - \dot{\phi}[k_{\text{cr}}^2 - s_2(l - s_2)]m_{\text{cr}}\} = R'\omega + (R/\lambda)\dot{\phi},$$

where

$$R = \lambda m_{\text{cr}}[s_2(l - s_2) - k_{\text{cr}}^2], \quad R' = [m_C k_C^2 + r^2(1 - \frac{s_2}{l})m_{\text{cr}}]. \quad (7.67)$$

R and R' are called the *reduced moments of inertia* of the mechanism. Thus, the rolling moment is

$$M_z = -\frac{dH_z}{dt} = -R'\ddot{\omega} - R\frac{\ddot{\phi}}{\lambda}. \quad (7.68)$$

Using (4.34) for \ddot{x}/r and (4.54) for $\ddot{\phi}/\lambda$, we find the expressions for the inertia forces and moments of a single-cylinder engine, from (7.64), (7.65), and (7.68), will be

$$\begin{aligned} F_x &= \omega^2[(Q + Q')\cos\theta + Q(A_2 \cos 2\theta - A_4 \cos 4\theta + A_6 \cos 6\theta - \dots)] \\ &\quad + \dot{\omega}[(Q + Q')\sin\theta + Q(\frac{A_2}{2} \sin 2\theta - \frac{A_4}{4} \sin 4\theta + \frac{A_6}{6} \sin 6\theta - \dots)], \end{aligned} \quad (7.69)$$

$$F_y = \omega^2 Q' \sin\theta - \dot{\omega} Q' \cos\theta, \quad (7.70)$$

$$\begin{aligned} M_z &= \omega^2 R(C_1 \sin\theta - C_3 \sin 3\theta + C_5 \sin 5\theta - \dots) - R'\ddot{\omega} \\ &\quad - \dot{\omega} R(C_1 \cos\theta - \frac{C_3}{3} \cos 3\theta + \frac{C_5}{5} \cos 5\theta - \dots), \end{aligned} \quad (7.71)$$

$$M_x = -F_y a, \quad (7.72)$$

$$M_y = F_x a. \quad (7.73)$$

The coefficients of the terms $\cos j\theta$ and $\sin j\theta$ in (7.69) to (7.73) are called forces and moments of the j -th order. The magnitude of the forces and moments reduces as the value of j increases (since the harmonic coefficients A_j and C_j decrease with j). The terms containing ω^2 are known as *steady components* of the forces or moments and those with $\dot{\omega}$ are known as the *unsteady components*. In normal operation, the value of $\dot{\omega}$ is very low, and unsteady forces and moments are only a small percentage of the steady components.

An examination of (7.69) to (7.71) reveals that the unsteady forces and moments [except $(-\dot{\omega}R')$] can be obtained from the corresponding steady terms by using $\dot{\omega}$ in place of ω^2 , and by integrating all cosine and sine functions of the steady terms with respect to θ , i.e., instead of

$$\omega^2, \quad \cos\theta, \quad \sin\theta, \quad \cos j\theta, \quad \sin j\theta, \quad \cos(j\theta + \psi), \dots$$

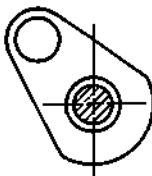


FIGURE 7.41

in steady terms, we use

$$\omega, \quad \sin \theta, \quad -\cos \theta, \quad \frac{\sin j\theta}{j}, \quad \frac{-\cos j\theta}{j}, \quad \frac{\sin (j\theta + \psi)}{j}, \dots$$

in unsteady terms. This fact will simplify representation of inertia forces and moments. Hereafter, we shall explicitly state only the steady components and denote the unsteady terms (which can be obtained from the former as explained) by $((\dot{\omega}))$. Thus, (7.69) to (7.71) can be rewritten as

$$F_x = \omega^2[(Q + Q') \cos \theta + Q(A_2 \cos 2\theta - A_4 \cos 4\theta + \dots)] + ((\dot{\omega})), \quad (7.69a)$$

$$F_y = \omega^2 Q' \sin \theta + ((\dot{\omega})), \quad (7.70a)$$

$$M_z = \omega^2 R(C_1 \sin \theta - C_3 \sin 3\theta + \dots) + ((\dot{\omega})) - \dot{\omega} R'. \quad (7.71a)$$

For complete balancing of the transverse force F_y , the value of Q' should be zero. Thus, from (7.63), we get

$$m_{C1}s_1 + (1 - s_2/l)m_{Cr}r = 0. \quad (7.74)$$

This condition can be easily satisfied by making s_1 negative, i.e., by extending the crank web backwards past the crankshaft axis as shown in Fig. 7.41. This condition was assumed to be satisfied in the approximate analysis for a single-cylinder engine given in Section 7.6 by taking a balanced crank along with m_2 .

From (7.69), the complete balancing of the longitudinal force F_x requires that $Q + Q' = 0$ and $Q = 0$, that is, $Q = Q' = 0$. Thus, from (7.63), we get

$$m_{re}l + s_2 m_{cr} = 0, \quad m_{C1}s_1 + (1 - s_2/l)m_{Cr}r = 0. \quad (7.75)$$

The second condition here is the same as (7.74) and can be easily satisfied as already explained. However, to satisfy the first condition of (7.75), it is necessary that $s_2 < 0$, i.e., the connecting rod has to be extended beyond the crank pin, but this involves serious constructional difficulties as already discussed (see Fig. 7.23). So, we look for only partial balancing; this can be done in several ways depending on other factors such as the rigidity of the foundation in various directions. The brief discussion which follows will throw some more light on this aspect.

It has already been stated that the first-order quantities, being of greater magnitude, are more important than the higher-order quantities. If we satisfy $Q + Q' = 0$ and thereby, from (7.63), ensure that

$$r(m_{re} + m_{cr}) + s_1 m_{C1} = 0, \quad (7.76)$$

then the first-order longitudinal forces are balanced. Even with this, $Q' \neq 0$ (as $Q \neq 0$), and the transverse force will remain unbalanced. Thus, both longitudinal and transverse forces will be only partially balanced.

In practice, a compromise is attempted by satisfying

$$\chi Q + Q' = 0 \quad (0 \leq \chi \leq 1). \quad (7.77)$$

The condition $\chi = 0$ results in complete balancing of the transverse force, and the condition $\chi = 1$ results in complete balancing of the first-order longitudinal force. Normally, the value of χ adopted in practical cases is $1/2$.

Unless it is otherwise specified, we shall assume $Q' = 0$, i.e., we shall assume a balanced crank, so as to eliminate the transverse force completely. A reduction in the longitudinal and transverse forces will lower the pitching and yawing moments, respectively. From (7.73), it is seen that complete balancing of the rolling moment requires

$$R = 0, \quad R' = 0.$$

Using (7.67), these conditions imply

$$s_2(l - s_2) = k_{cr}^2, \quad m_c k_c^2 + r^2(1 - s_2/l)m_{cr} = 0. \quad (7.78a)$$

These two conditions can never be satisfied simultaneously; the requirement of the second condition is that $s_2 > l$, and if this be so, the first condition cannot be met. Consequently, complete balancing of the rolling moment in a single-cylinder engine cannot be achieved, not even theoretically.

It has already been indicated that the unsteady component for normal operation is not very large. So, an attempt can be made to balance only the steady component of M_z , which requires $R = 0$. From (7.67),

$$k_{cr}^2 = s_2(l - s_2). \quad (7.78b)$$

This condition can be very easily satisfied if a uniformly tapered (or cylindrical) connecting rod, with symmetric bearings at the ends, is extended a small amount beyond one or both bearings.⁸ Condition (7.78b) implies that the period of oscillation of the connecting rod will be the same whether it is suspended at the crank-pin bearing or at the gudgeon-pin bearing.

7.8 MANCHESTER TECHNIQUE OF ENGINE BALANCING

In Section 7.6, we saw how countermasses on the crank can improve the state of balancing of a single-cylinder engine. Yet another method of active balancing to remove inertia forces of a given order is to rotate the eccentric masses. In this section, we shall illustrate this method through examples.

To balance the first-order inertia forces of a single-cylinder engine, we first make $Q' = 0$ by putting countermasses on the crank web. Then, only the first-order longitudinal force (primary), i.e.,

$$F_x^P = Q(\omega^2 \cos \theta + \dot{\omega} \sin \theta), \quad (7.79)$$

will remain to be balanced. This can be achieved with two eccentric masses m_{eP} (as shown in Fig. 7.42) rotating in opposite directions at the same speed as that of the crank.⁹ Due to symmetry, the component along the y -axis of the inertia forces of the two eccentric masses together will always be zero and the component along the x -axis will be

$$F_x^{eP} = -2m_{eP}(\omega^2 \cos \theta + \dot{\omega} \sin \theta), \quad (7.80)$$

⁸Biezeno, C.B. and Grammel, R.E., Engineering Dynamics, Vol. IV, Blackie, London, 1954.

⁹It should be noted that the angular acceleration of the eccentric masses will be proportional to that of the crank, depending on the speed ratio.

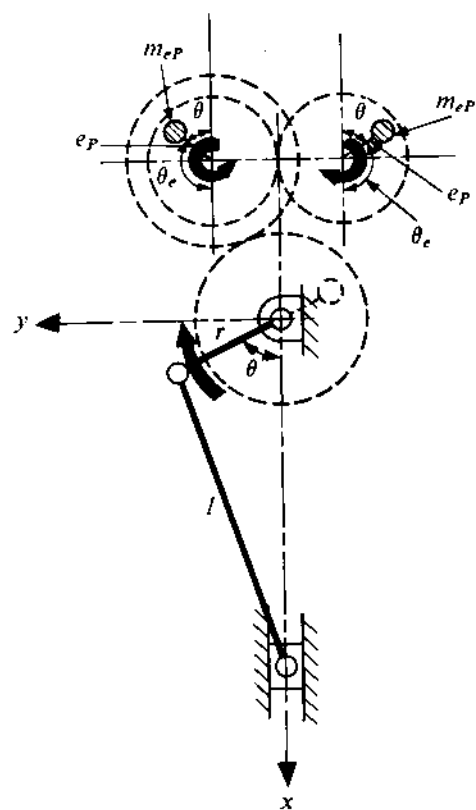


FIGURE 7.42

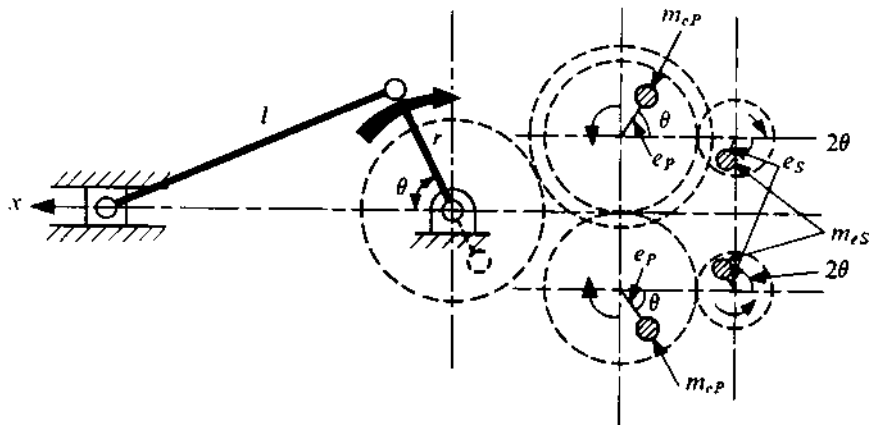


FIGURE 7.43

where θ is the crank angle and e_P is the eccentricity. From (7.79) and (7.80), it is obvious that these eccentric masses completely balance the first-order forces if

$$2m_{eP}e_P = Q,$$

$$m_{eP}e_P = \frac{r}{2}(m_{re} + \frac{s_2}{l}m_{cr}) = \frac{r}{2}m_{rec}. \quad (7.81)$$

It should be noted from Fig. 7.42 that when $\theta = 0$, both eccentric masses are at an angle $\theta_{e0} = 180^\circ$ to the x -axis.

Similarly, to balance out the secondary forces, two more rotating eccentric masses m_{eS} are necessary, both rotating at a speed 2ω but in a direction opposite to each other. The inertia forces of these along the x -axis will be

$$F_x^{eS} = -2(2)^2 m_{eS} e_S (\omega^2 \cos 2\theta + \frac{\dot{\omega}}{2} \sin 2\theta),$$

where e_S is the eccentricity. Thus, if

$$8m_{eS}e_S = A_2 Q,$$

$$m_{eS}e_S = \frac{A_2 r}{8} m_{rec}, \quad (7.82)$$

then the second-order forces will be completely balanced. Thus, the arrangement, shown in Fig. 7.43, will balance both the primary and secondary forces. Here also, $\theta_{e0} = 180^\circ$.

Extending the foregoing analysis to balance the j -th order forces, we get

$$m_{ej}e_j = \frac{1}{2j^2} A_j r m_{rec} \quad (j = 2, 4, 6, \dots). \quad (7.83)$$

$$\omega_e = \pm j\omega, \quad \dot{\omega}_e = \pm j\dot{\omega}, \quad \theta_{e0} = j(\pi/2)$$

The details of the analysis leading to this result are left as an exercise for the reader.

Another application of this method of balancing with rotating eccentric masses is to the 90° V-engine. In such an engine, as has been shown in Problem 7.7, the primary force can be balanced by using large countermasses on the crank. Considering the secondary force, with $2\alpha = 90^\circ$, we get, from (7.50a) and (7.50b),

$$F_x^S = 0,$$

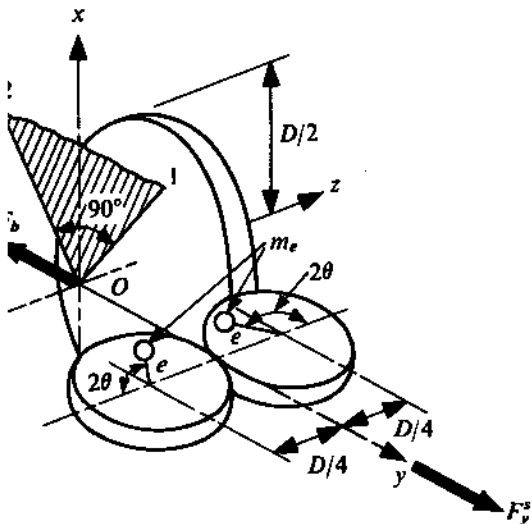


FIGURE 7.44

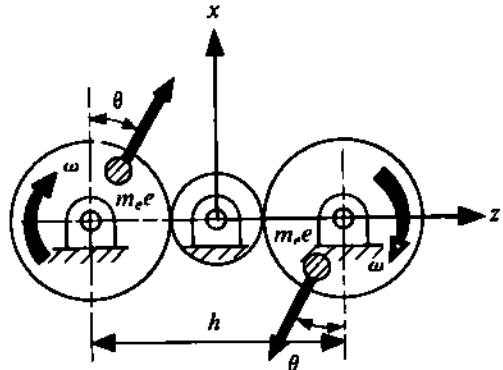


FIGURE 7.45

$$F_y^S = \omega^2 2m_{rec} r \frac{1}{\sqrt{2}} A_2 \sin 2\theta + ((\dot{\omega})) \quad (\text{including the unsteady part}). \quad (7.84)$$

Now, two eccentric masses (m_e) rotating in opposite directions at a speed 2ω (see Fig. 7.44) will produce the inertia force

$$F_y = -\{2.(2)^2 m_e e [\omega^2 \sin 2\theta - \frac{\dot{\omega}}{2} \cos 2\theta]\}, \quad (7.85)$$

where e is the eccentricity. Thus, complete balancing of F^S is possible if [from (7.84) and (7.85)]

$$\begin{aligned} 8.m_e e &= A_2 \sqrt{2} m_{rec} r, \\ m_e e &= \frac{r}{4\sqrt{2}} A_2 m_{rec}. \end{aligned} \quad (7.86)$$

It should be noted that, for $\theta = 0$, the position of one of the eccentric masses is along the z -axis and that of the other is opposite thereto.

The examples we have given show how rotating eccentric masses can generate the inertia forces along the line of reciprocation to nullify the unbalanced forces. A similar principle can be used to generate an inertia couple to neutralize the unbalanced couple. Figure 7.45 shows a scheme to generate a couple (about the y -axis) $-m_e e \omega^2 h \cos \theta$ to neutralize the unbalanced couple. Obviously, the magnitude, speed of rotation, and relative phases of the eccentric masses depend on the order of the unbalanced couple.

7.9 BALANCING OF PLANAR LINKAGES

So far, we have discussed balancing of inertia forces in rotors and slider-crank mechanisms. Balancing of inertia forces in mechanisms other than these is not simple. For example, the problem of balancing of planar linkages is still being investigated and satisfactory solutions have been obtained only in a few individual situations after elaborate analysis. In what follows, we shall consider a few

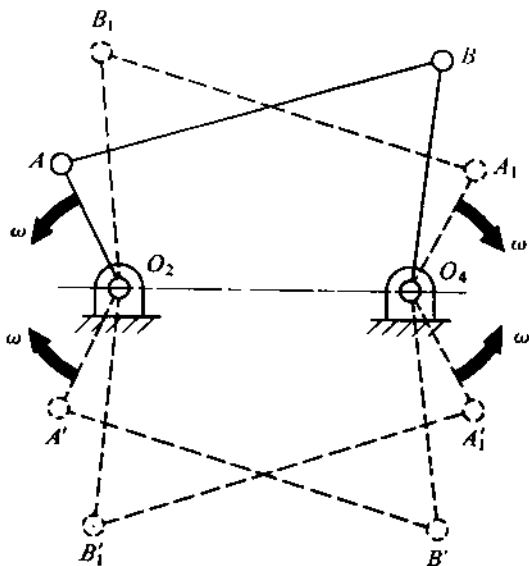


FIGURE 7.46

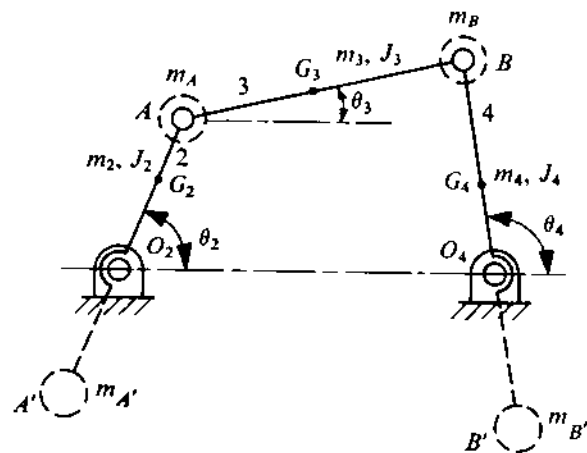


FIGURE 7.47

simple problems related to four-bar mechanisms and, in the process, highlight the basic principles and difficulties involved in balancing mechanisms, in general. For more details, see the relevant literature.¹⁰

In a four-bar mechanism, two of the moving members are in pure rotation, whereas the coupler has a complicated motion. As a result, both the inertia forces and couples are transmitted to the frame. There are two ways of neutralizing the resultant unbalanced force and couple. As we shall subsequently see, the unbalanced force can be easily eliminated, but the complete elimination of the unbalanced couple poses serious problems. Though this unbalanced couple can be eliminated by active balancing, this method leads to a considerable increase in the hinge reactions, overall mass, and input torque required. In what follows, we shall give one possible solution of complete balancing. Consider the balancing of the linkage O_2ABO_4 (Fig. 7.46). Adding its mirror image $O_2A'B'O_4$, we find that the resulting system generates only an unbalanced force along the fixed link O_2O_4 . This can be neutralized by adding two more linkages $O_2B_1A_1O_4$ and its image $O_2B'_1A'_1O_4$ (Fig. 7.46). Thus, this system of four identical four-bar linkages leaves no unbalanced force or couple.

It is obvious that the solution we have given is only of academic interest and cannot be realized in practice. So, we present a passive balancing technique which is applicable to a real-life situation. This technique requires that the links be redesigned so that the unbalance effects are minimized. Figure 7.47 shows a four-bar mechanism O_2ABO_4 , where the CG of the coupler G_3 lies on the line AB . As we have already seen, the coupler can be replaced by two end masses m_A and m_B , where

$$m_A = (BG_3/AB)m_3, \quad m_B = (AG_3/AB)m_3.$$

Comparing the coupler with the connecting rod of a slider-crank mechanism and referring to (7.78), we find that we can also eliminate the inertia moment (equivalent to the rolling moment already discussed) due to the angular acceleration $\ddot{\theta}_3$ of the coupler by properly redesigning the coupler.

¹⁰ Berkof, R.S., Lowen, G.G. and Tepper, F.R., Balancing of linkages, *Shock and Vibration Digest*, 9, 3-10, 1977, and Wiederrick, J.L. and Roth, B., Momentum balancing of four-bar linkages, *Journal of Engineering for Industry*, Trans. ASME, 98, 1289-1295, 1976.

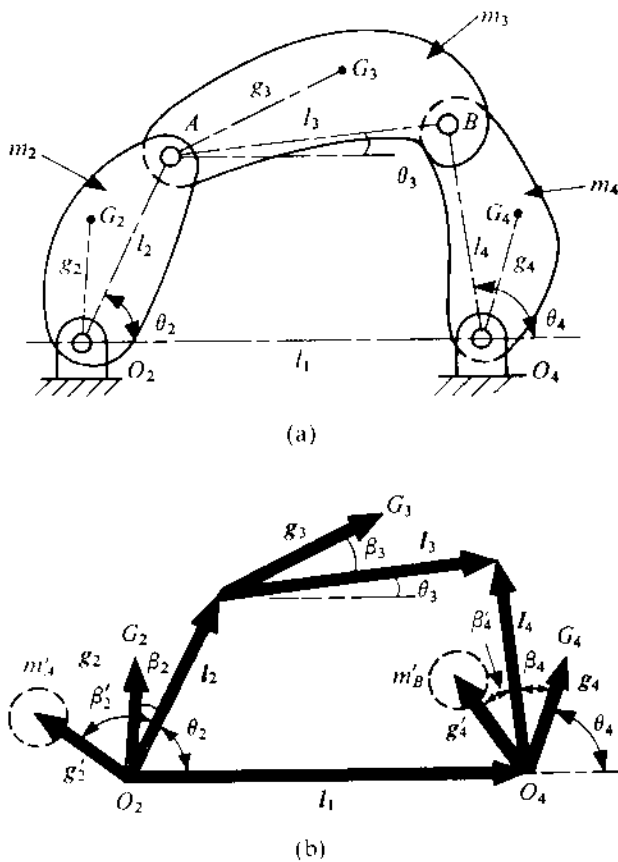


FIGURE 7.48

Thus, we are left with purely rotating masses \$m_A, m_B, m_2\$, and \$m_4\$. So far as the unbalanced forces are concerned, these can be easily balanced by countermasses \$m'_A\$ and \$m'_B\$ if the following conditions are satisfied:

$$m_2 \cdot O_2 G_2 + m_A \cdot O_2 A = m'_A \cdot O_2 A',$$

$$m_4 \cdot O_4 G_4 + m_B \cdot O_4 B = m'_B \cdot O_4 B'.$$

Hence, the only unbalance effect is the couple due to the angular accelerations (if any) of links 2 and 4. The magnitude of the final unbalanced couple is

$$(m_A \cdot O_2 A^2 + m'_A \cdot O_2 A'^2 + J_2 + m_2 O_2 G_2^2) \ddot{\theta}_2 - (m_B \cdot O_4 B^2 + m'_B \cdot O_4 B'^2 + J_4 + m_4 O_4 G_4^2) \ddot{\theta}_4$$

which may be more than that of the unbalanced couple in the original linkage. Therefore, in practice, a compromise is often attempted so that both the force and couple are partially balanced.

The problem of redesigning the links becomes involved when the CG of the links does not lie on the respective link vectors. Such a situation is shown in Fig. 7.48a. The link vectors and the CG vectors are indicated in Fig. 7.48b. Let us determine the two countermasses fixed one each to links 2 and 4 so that the total inertia force becomes zero. Let the countermasses be attached at \$g'_2\$ and

\mathbf{g}'_4 . Then, the condition for force balance can be written as

$$m_2 \mathbf{g}_2 + m_3 (\mathbf{l}_2 + \mathbf{g}_3) + m_4 \mathbf{g}_4 + m'_A \mathbf{g}'_2 + m'_B \mathbf{g}'_4 = \text{constant}, \quad (7.87)$$

implying that the resultant CG of the entire system remains stationary in space. Attaching the unit vectors i_1, i_2, i_3 , and i_4 along $\mathbf{l}_1, \mathbf{l}_2, \mathbf{l}_3$, and \mathbf{l}_4 , respectively, we can write (in complex notation)

$$\begin{aligned} \mathbf{g}_2 &= i_2 g_2 \exp(i\beta_2), \quad \mathbf{l}_2 + \mathbf{g}_3 = i_2 \mathbf{l}_2 + i_3 g_3 \exp(i\beta_3), \\ \mathbf{g}_4 &= i_4 g_4 \exp(i\beta_4), \quad \mathbf{g}'_2 = i_2 g'_2 \exp(i\beta'_2), \quad \mathbf{g}'_4 = i_4 g'_4 \exp(i\beta'_4). \end{aligned} \quad (7.88)$$

Substituting (7.88) in (7.87), we obtain

$$\begin{aligned} i_2 m_2 g_2 \exp(i\beta_2) + m_3 [i_2 l_2 + i_3 g_3 \exp(i\beta_3)] + i_4 m_4 g_4 \exp(i\beta_4) + i_2 m'_A g'_2 \exp(i\beta'_2) \\ + i_4 m'_B g'_4 \exp(i\beta'_4) = \text{constant}. \end{aligned} \quad (7.89)$$

Now, writing the loop closure equation

$$i_2 l_2 + i_3 l_3 = i_1 l_1 + i_4 l_4 \quad (7.90)$$

and eliminating i_3 from (7.89) and (7.90), we get

$$C_2 i_2 + C_4 i_4 + C_0 = \text{constant}, \quad (7.91)$$

where C_0 includes the constant unit vector i_1 . For (7.91) to be valid,

$$\begin{aligned} C_2 &= m_2 g_2 l_3 \exp(i\beta_2) - m_3 g_3 l_2 \exp(i\beta_3) + m'_A g'_2 l_3 \exp(i\beta'_2) + m_3 l_2 l_3 = 0, \\ C_4 &= m_3 g_3 l_4 \exp(i\beta_3) + m_4 g_4 l_3 \exp(i\beta_4) + m'_B g'_4 l_3 \exp(i\beta'_4) = 0. \end{aligned} \quad (7.92)$$

As C_2 and C_4 are complex, (7.92) yield four real equations which can be easily solved to determine the four unknowns, namely, $m'_A g'_2, \beta'_2$ and $m'_B g'_4, \beta'_4$.

PROBLEM 7.11

The data pertaining to the four-bar linkage shown in Fig. 7.48 is

$$\begin{aligned} l_2 &= 5 \text{ cm}, \quad l_3 = 15 \text{ cm}, \quad l_4 = 7.5 \text{ cm}, \\ \beta_2 &= 0^\circ, \quad g_2 = 2.5 \text{ cm}, \quad \beta_3 = 15^\circ, \quad g_3 = 8 \text{ cm}, \quad \beta_4 = 0^\circ, \quad g_4 = 3.75 \text{ cm}, \\ m_2 &= 0.05 \text{ kg}, \quad m_3 = 0.125 \text{ kg}, \quad m_4 = 0.06 \text{ kg}. \end{aligned}$$

Determine the positions and the magnitudes of the balancing masses to eliminate the inertia force

SOLUTION

Using the given data in (7.92) and writing $e^{i\phi} = \cos \phi + i \sin \phi$, we get

$$0.05 \times 2.5 \times 15 - 0.125 \times 8 \times 5(\cos 15^\circ + i \sin 15^\circ)$$

$$+ m'_A g'_2 (\cos \beta'_2 + i \sin \beta'_2) \times 15 + 0.125 \times 5 \times 15 = 0,$$

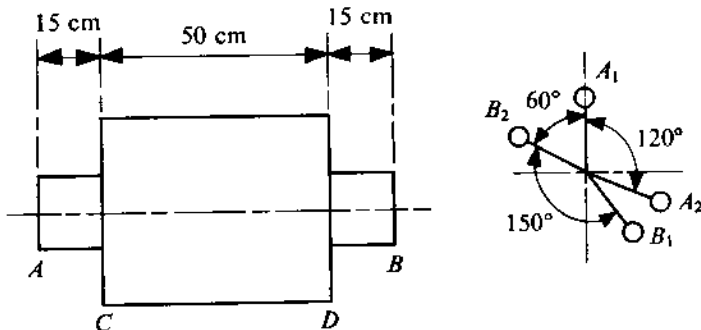


FIGURE 7.49

$$0.125 \times 8 \times 7.5(\cos 15^\circ + i \sin 15^\circ) + 0.06 \times 3.75 \times 15 + m'_B g'_4 (\cos \beta'_4 + i \sin \beta'_4) \times 15 = 0.$$

Separating the real and imaginary parts of these equations, the four equations we obtain are

$$15m'_A g'_2 \cos \beta'_2 = -1.875 + 4.83 - 9.375 = -6.42,$$

$$15m'_A g'_2 \sin \beta'_2 = 1.294,$$

$$15m'_B g'_4 \cos \beta'_4 = -7.244 - 3.375 = -10.619,$$

$$15m'_B g'_4 \sin \beta'_4 = -1.941.$$

Solving, we get

$$m'_A g'_2 = 0.436 \text{ kg-cm}, \quad \beta'_2 = 168.6^\circ,$$

$$m'_B g'_4 = 0.72 \text{ kg-cm}, \quad \beta'_4 = 190.36^\circ.$$

7.10 PROBLEMS

- 7.12 The bearings of a shaft at *A* and *B* are 5 metres apart. The shaft carries three eccentric masses *C*, *D*, and *E* which are 160 kg, 170 kg, and 85 kg, respectively. The respective eccentricity of each mass, measured from the axis of rotation, is 0.5 cm, 0.3 cm, and 0.6 cm, and the distance from *A* is 1.3 m, 3 m, and 4 m. Determine the angular position of each mass with respect to *C* so that no dynamic force is exerted at *B*, and also find the dynamic force at *A* for this arrangement when the shaft runs at 100 rpm.
- 7.13 In Problem 7.12, let the masses be arranged so as to give static balance to the system. With this angular arrangement, determine the dynamic reaction at *A* and *B* for a speed of 100 rpm.
- 7.14 A rotor is balanced by attaching two 2-kg trial masses in each of the planes *A* and *B* (Fig. 7.49) at a radius of 15 cm. Complete dynamic balance is obtained with the angular positions shown in Fig. 7.49. Determine the position and mass of the material to be removed from each of the planes *C* and *D* at a radius of 10 cm in order to balance the rotor when the trial masses are removed.
- 7.15 A shaft, rotating at a uniform speed, carries two discs *A* and *B* of masses 5 kg and 4 kg, respectively. The CG of each disc is 2.5 mm from the axis of rotation, and the angle between

the radii containing the centres of gravity is 90° . The shaft has bearings at C and D , between A and B , such that $AC = 300$ mm, $AD = 900$ mm, and $AB = 1200$ mm. It is desired to make the dynamic forces on the bearings equal and opposite, and to have a minimum value for a given speed by means of a mass in the plane E at a radius of 25 mm. Determine

- (i) the magnitude of the mass to be attached at E and its angular position with respect to that at A ,
- (ii) the distance of the plane E from the plane through A , and
- (iii) the dynamic force on the bearing with the attached mass in the plane E for a speed of 250 rpm.

7.16 A rough casting of a rotor, with a mass of 200 kg, is mounted on centres 110 cm apart for machining. The rotor is statically balanced by attaching two masses, one each in the planes A (9 kg) and B (12 kg), which are on opposite sides of the plane containing the mass centre of the rotor, at a distance of 50 cm and 35 cm, respectively, from it. The angle between the CG of the plane A and that of the plane B is 90° . The distance of each mass from the axis of rotation is 37 cm (for the plane A) and 44 cm (for the plane B).

Determine the distance of the CG of the rotor from the axis of rotation, and its angular position with respect to the mass in the plane A . Also find the forces on the bearings when the rotor (with the masses attached in the planes A and B) runs at a speed of 100 rpm.

7.17 During the field balancing of a large cooling tower fan, the vibration amplitudes measured are 0.5 mm (without any trial mass), 0.8 mm (with a trial mass of 0.5 kg placed at a radius of 2 m), and 0.8 mm (with the trial mass of 0.5 kg now placed at a diametrically opposite point). Determine the magnitude of the required balancing mass to be placed at the same radius of 2 m. Comment on the possible angular positions.

7.18 A 4-m-diameter industrial fan with four symmetrical blades is being balanced. A trial mass of 1 kg is placed at a radius of 1.75 m and at each of the three different locations A , B , and C (Fig. 7.50). The amplitudes of vibration (when the fan rotates at 700 rpm) are found to be 1 mm (without a trial mass), 1.7 mm (with a trial mass at A), 2.6 mm (with a trial mass at B), and approximately 1.2 mm (with a trial mass at C).

- (i) Determine the magnitude and angular position of the required balancing mass if it is assumed to be attached at a radius of 1 m.
- (ii) If the balancing masses can be placed only along the centreline of a blade and their distance from the fan axis has not to exceed 1.5 m, suggest a scheme for balancing the fan, causing minimum increase in the fan mass.

7.19 For balancing a huge rotor while in operation, the usual technique of field balancing is used. The measurements of the three test runs are given in Table 7.8. Determine the magnitude of the balance masses at the near and far ends. Also find the angular locations of these balance masses with respect to the corresponding trial masses. It may be assumed that the balance masses are placed at radii twice those of the corresponding trial masses.

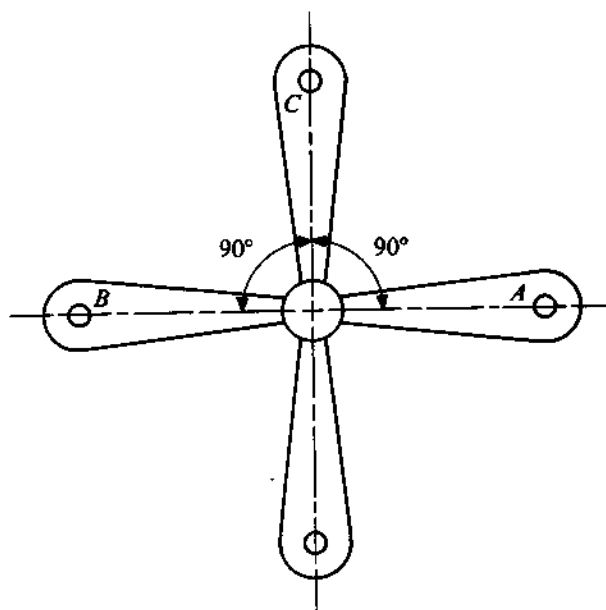


FIGURE 7.50

TABLE 7.8

Trial	Trial mass (kg)	<i>N</i>		<i>F</i>	
		Near-end amplitude (cm)	Near-end phase angle (degrees)	Far-end amplitude (cm)	Far-end phase angle (degrees)
1	0	4.2×10^{-4}	30°	3.5×10^{-4}	60°
2	3 (at the near end)	4.0×10^{-4}	60°	2.5×10^{-4}	97°
3	5 (at the far end)	4.5×10^{-4}	45°	3.0×10^{-4}	140°

7.20 Solve Problem 7.6 if the firing order for the cylinders is I-IV-V-II-III-VI.

7.21 Figure 7.51 shows the crank-cylinder arrangement of a four-stroke four-cylinder opposed in-line engine. Find out the possible firing orders and investigate the state of balancing of the engine.

7.22 Determine the firing orders of a four-stroke six-cylinder in-line engine for which the engine is completely balanced up to the second order. Use the graphical approach.

7.23 The following particulars refer to an eight-cylinder two-stroke diesel engine:

reciprocating mass per cylinder = 25 kg,

crank radius = 10 cm,

axial pitch of the cylinders = 20 cm,

speed (constant) = 300 rpm,

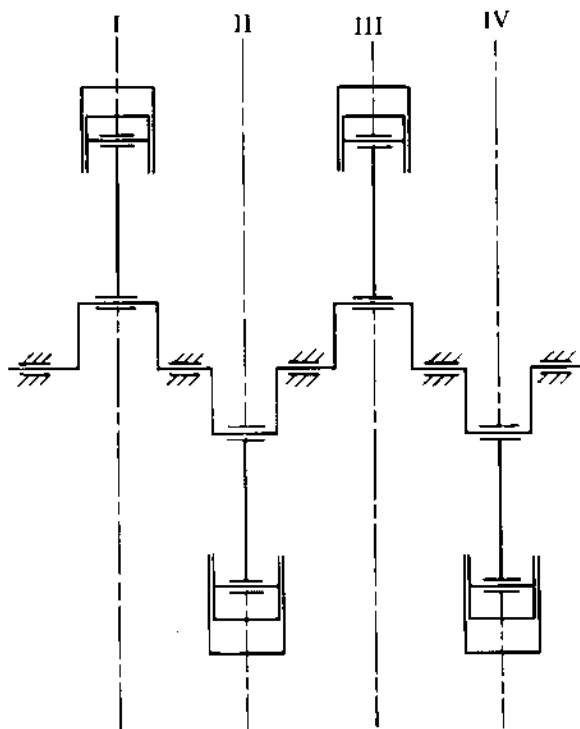


FIGURE 7.51

harmonic coefficients $A_2 = 0.22$, $A_4 = 0.0025$, $A_6 = 0.000035$,
firing order I-II-III-IV-V-VI-VII-VIII.

Compute the unbalanced effects up to the sixth order.

- 7.24 In a four-cylinder two-stroke symmetrical engine, the pair of outside cylinders *A* and *D* and the pair of inside cylinders *B* and *C* are symmetrical about the centreline of the engine (the cylinder centres are not uniformly spaced). The angular interval between the cranks of *A* and *D* is the same as that between the cranks of *A* and *C*. The reciprocating masses of *A* and *D* are 600 kg and those of *B* and *C* are 900 kg. The distance between the centres of *A* and *D* is 6 metres. It is desired that the primary and secondary forces and the primary pitching moments should vanish. (The origin of the coordinate system is at the centre of the engine. Determine the distance between the cylinders *B* and *C* and the angular interval (which is non-uniform) between the cranks. The firing order is *A-D-B-C*.

Also determine the maximum value of the secondary pitching moment when the crank is rotating at a constant speed of 150 rpm, given that the crank radius is 0.5 m and the connecting rod length is 2 m.

- 7.25 The internal-combustion engine shown in Fig. 7.52 has three cylinders at an interval of 120° . The cylinders open in a common combustion chamber. The mass of the reciprocating part of each cylinder is 2 kg, the stroke of each piston is 8 cm, and the length of each connecting rod is 15 cm. Show that the primary and secondary forces are balanced when $\theta_1 = \theta_2 = \theta_3$. Obtain the aforementioned components if $\theta_3 = \theta_1 + 15^\circ = \theta_2 + 15^\circ$ when the engine speed is 1200 rpm.

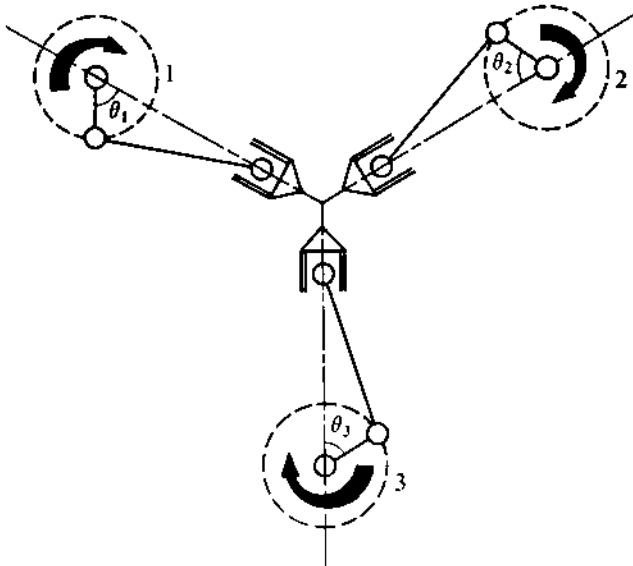


FIGURE 7.52

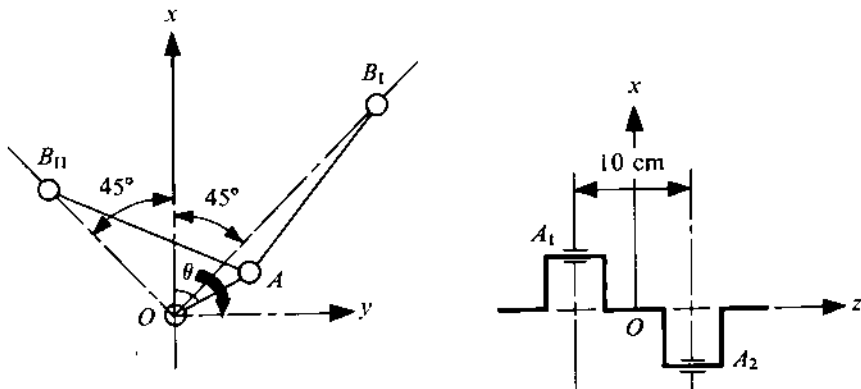


FIGURE 7.53

- 7.26 In a four-cylinder engine, the centrelines of the two pairs of cylinders form a V-angle of 90° . There are two cranks at 180° ; the distance between them is 10 cm. Each crank is connected to one pair of cylinders. The mass of the reciprocating parts of each cylinder is 2 kg, the crank radius for each crank is 5 cm, and each connecting rod is 20 cm long. For the coordinate system shown in Fig. 7.53, calculate the maximum primary and secondary components of the resultant unbalanced forces and moments when the engine is running at 1200 rpm.

- 7.27 The arrangement of a 12-cylinder engine shown in Fig. 7.54 is equivalent to four W-engines. The cranks of these four W-engines are at 180° as shown in the figure. Show that the primary component of the resultant unbalanced force (F^P) is balanced. Compute the maximum and minimum values of the secondary component of the resultant unbalanced force (F^S) and the corresponding crank positions with the following data: mass of reciprocating parts of each cylinder = 3 kg, crank radius = 7.5 cm, connecting-rod length = 30 cm, engine speed = 1200 rpm.

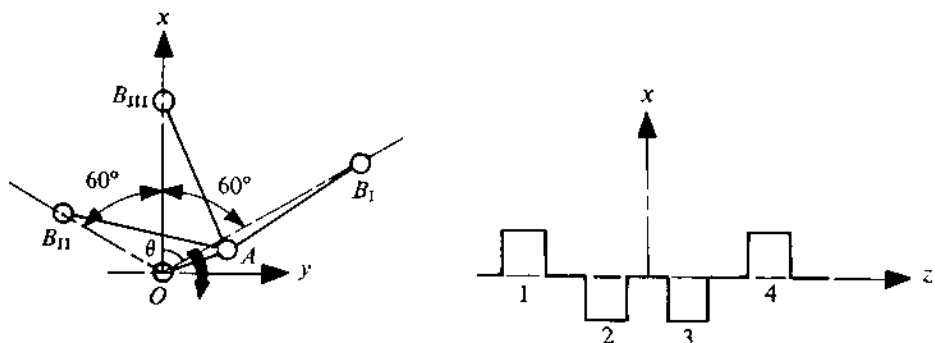


FIGURE 7.54

- 7.28 Four arrangements of opposed-piston engines (with coordinate systems) are shown in Fig. 7.55. Obtain expressions for F_x , F_y , and M_z for each of these arrangements.
- 7.29 In a slider-crank mechanism, the connecting rod is 120 cm long and its CG lies in its centreline at a distance of 80 cm from the small end. Determine the required radius of gyration of the connecting rod so that the rolling moment is zero at a constant crank speed.
- 7.30 The data given for a four-bar linkage is $m_2 = 0.3 \text{ kg}$, $m_3 = 0.3 \text{ kg}$, $m_4 = 0.25 \text{ kg}$, $l_2 = 2 \text{ cm}$, $l_3 = 30 \text{ cm}$, $l_4 = 25 \text{ cm}$, $g_2 = 6 \text{ cm}$, $g_3 = 15 \text{ cm}$, $g_4 = 12 \text{ cm}$, $\beta_2 = 0^\circ$, $\beta_3 = 20^\circ$, and $\beta_4 = -10^\circ$. Determine the magnitudes and the angular locations of the balancing masses to neutralize the unbalanced forces.

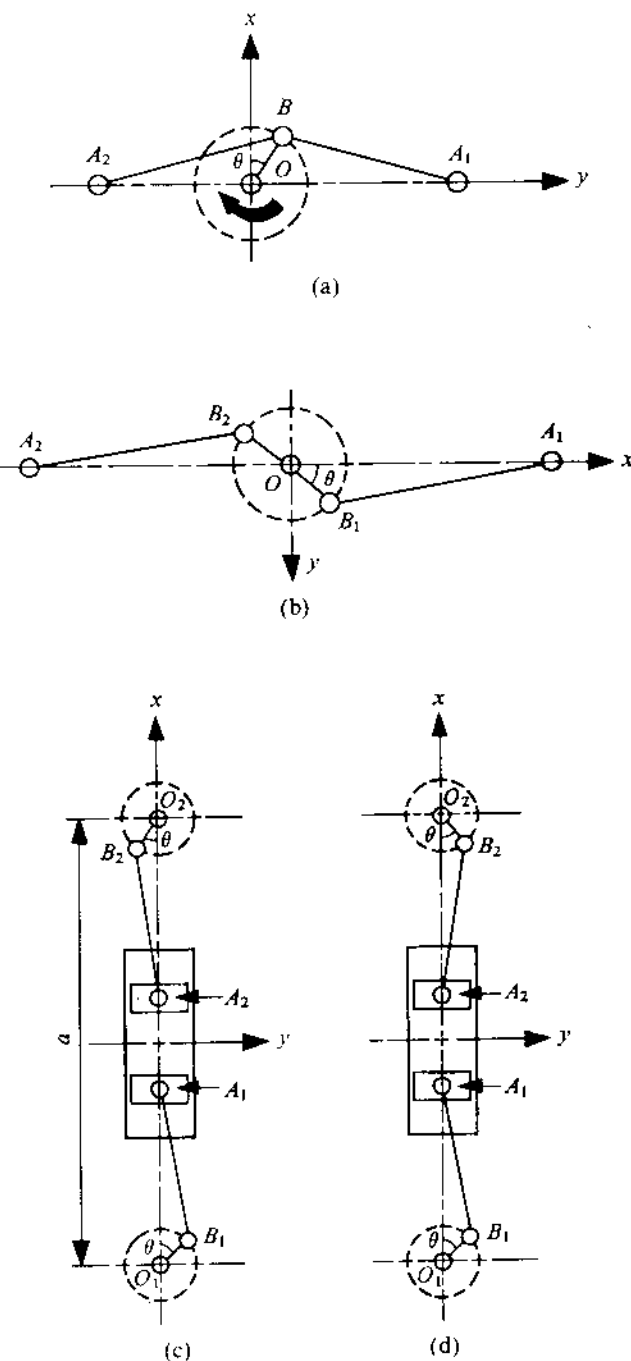


FIGURE 7.55

Chapter 8

CAMS

3.1 INTRODUCTION

So far, we have studied the mechanisms consisting of only the lower pairs. In this chapter, we shall discuss the synthesis, analysis, and dynamics of a higher-pair mechanism. Such a mechanism, known as a cam mechanism, is one of those used most commonly. In it, the driving member is called the cam, and the driven member is referred to as the follower. Cam mechanisms can generate complex, coordinated movements. Such mechanisms are relatively compact and easy to design.

3.2 CLASSIFICATION OF FOLLOWERS AND CAMS

A follower is classified either according to its motion or the nature of its surface in contact with the cam. The former class has three categories, namely,

- (i) the *radial-translating follower*, where the follower translates along a line passing through the axis of rotation of the cam,
- (ii) the *offset-translating follower*, where the direction of translation of the follower is offset from the axis of rotation of the cam in the desired direction, depending on the direction of rotation of the cam, and
- (iii) the *oscillating follower*, where the follower oscillates about a hinge point as the cam rotates.

A follower classified according to the nature of its surface in contact with the cam has four categories. These are:

- (i) the *knife-edge follower*,
- (ii) the *flat-face follower*,
- (iii) the *roller follower*, and
- (iv) the *spherical-face follower*.

A cam is classified according to its shape. A *plate cam* (also known as the *disc* or *radial cam*) is used most commonly, and we shall limit our discussion to this type. The *wedge* and *cylindrical cams* also find application in many situations.

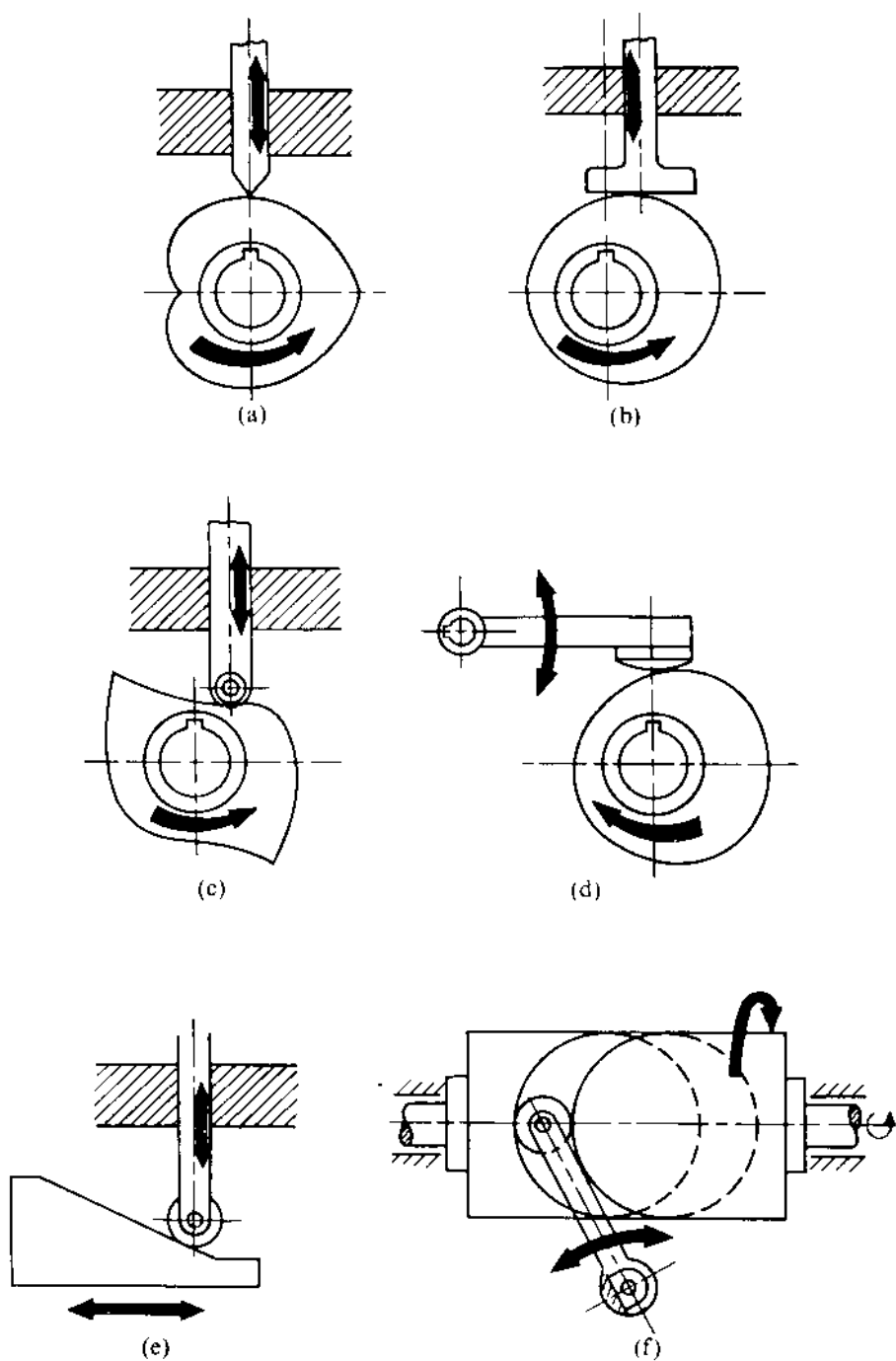


FIGURE 8.1 (cont.)

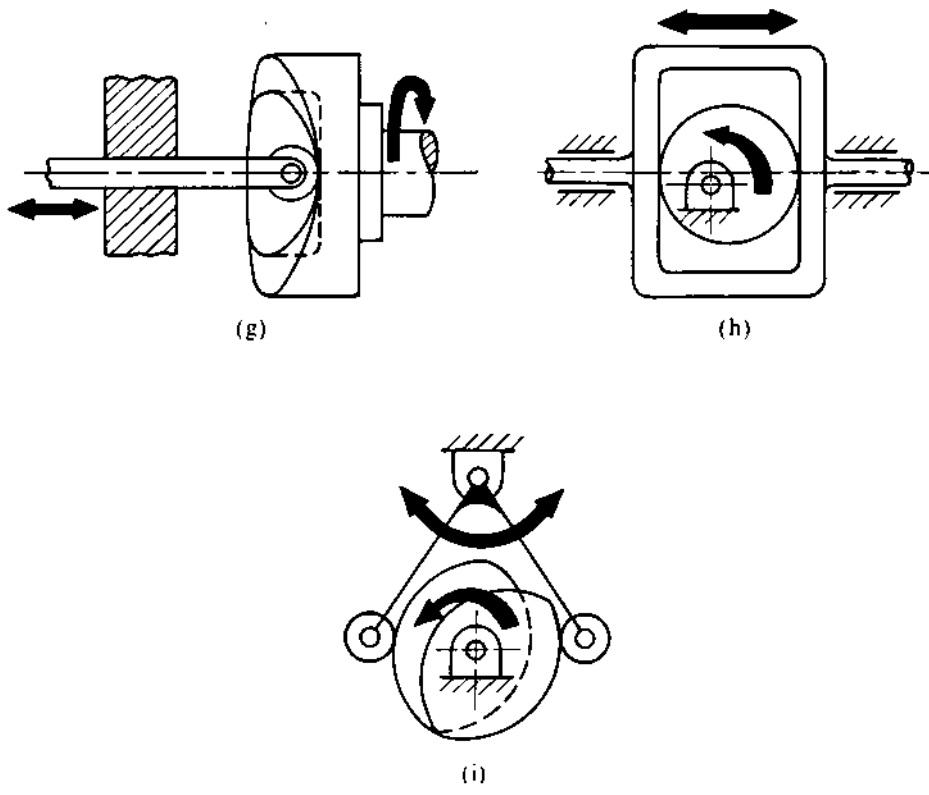


FIGURE 8.1

Figures 8.1a-d, respectively, show categories (i)-(iv) of followers we have mentioned. The knife-edge follower, though simple from the point of view of analysis, is rarely used because the wear rate is high. The flat-face follower exerts at its bearings a side thrust which is less than that for the knife-edge and roller followers. This implies reduced friction force and less chances of jamming in the bearings. This side thrust can be further reduced by properly offsetting the follower from the axis of rotation of the cam. (Compare this with the case of the offset engine in Problem 4.18.) The sliding wear in the case of a flat-face translating follower is reduced by offsetting the follower in a direction perpendicular to the plane of cam rotation so that the follower rotates about the axis of its translation. The flat-face follower is used in automobiles, where space is limited. The use of roller followers in such situations is restricted by the minimum size of the pin to be used to connect the roller with the follower. Roller followers are rather common in larger stationary gas or oil engines.

Figures 8.1e and 8.1f and 8.1g show the wedge and two types of cylindrical cams, respectively.

In all the cam-follower mechanisms we have stated, the contact between the cam and the follower is ensured by a spring. But in another type of cams, known as *positive-acting* cams, no spring is necessary to bring about the contact, as illustrated in Figs. 8.1h and 8.1i.

3.3 RADIAL CAM NOMENCLATURE

Figure 8.2 shows a radial cam with a radial-translating roller follower. With reference to this diagram, let us define the various terms we will very frequently use to describe the geometry of a

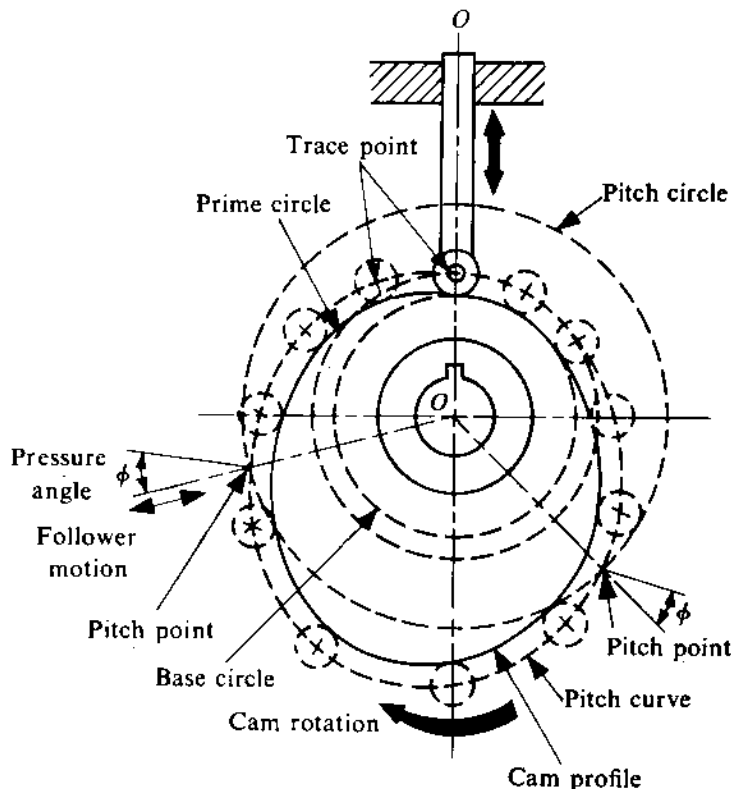


FIGURE 8.2

radial cam.

Base Circle

The base circle is the smallest circle (with its centre at the cam centre) that can be drawn tangent to the cam profile. The base circle decides the overall size of a cam and is, therefore, a fundamental feature of the cam.

Trace Point

A trace point is a theoretical point on the follower, its motion describing the movement of the follower. For a knife-edge follower, the trace point is at the knife-edge.¹ For a roller follower, the trace point is at the roller centre, and for a flat-face follower, it is at the point of contact between the follower and the cam surface when the contact is along the base circle of the cam. It should be noted that the trace point is not necessarily the point of contact for all other positions of the cam.

¹ As only plane motion is being considered, the projection of the cam-follower system on the plane of motion is sufficient for complete description. So, the projection of the contact line (i.e., the knife-edge) will be a point.

Pitch Curve

If we apply the principle of inversion, i.e., if we hold the cam fixed and rotate the follower in a direction opposite to that of the cam, then the curve generated by the locus of the trace point is called the pitch curve. Obviously, for a knife-edge follower, the pitch curve and the cam profile are identical.

Pressure Angle

The angle between the direction of the follower movement and the normal to the pitch curve at any point is referred to as the pressure angle. During a complete rotation, the pressure angle varies from its maximum to its minimum value. The greater the pressure angle, the higher will be the side thrust, and consequently the chances of the translating follower jamming in its guide will increase.

The pressure angle should be as small as possible within the limits of design. In case of low-speed cam mechanisms with oscillating followers, the highest permissible value of the pressure angle is 45° , whereas it should not exceed 30° in case of cam mechanisms with translating followers. The pressure angle can be reduced (for a given motion requirement) by increasing the cam size. However, a bigger cam requires more space and is more prone to unbalance at high speeds. Another way to control the pressure angle is by adjusting the offset.

Pitch Point

A pitch point corresponds to the point of maximum pressure angle, and a circle drawn with its centre at the cam centre, to pass through the pitch point, is known as the *pitch circle*.

Prime Circle

The prime circle is the smallest circle that can be drawn (with its centre at the cam centre) so as to be tangential to the pitch curve. Obviously, for a roller follower, the radius of the prime circle will be equal to the radius of the base circle plus that of the roller.

3.4 DESCRIPTION OF FOLLOWER MOVEMENT

The cam is assumed to rotate with constant speed and the movement of the follower during a complete revolution of the cam is described by a *displacement diagram*, in which follower displacement, i.e., the movement of the trace point, is plotted against the cam rotation θ . Figure 8.3 shows a typical displacement diagram. The maximum follower displacement is referred to as the *lift L* of the follower. It is seen that, in general, the displacement diagram consists of four parts, namely, (i) the *rise* (which is the movement of the follower away from the cam centre), (ii) the *dwell* (when there is no movement of the follower), (iii) the *return* (which is now the movement of the follower towards the cam centre), and (iv) the *dwell*.

Unless otherwise specified, it is always assumed that there is a dwell before and after the rise. The inflection points of the displacement diagram (corresponding to the maximum and minimum velocities of the follower) correspond to the pitch points. In the case of oscillating followers, the follower displacement is measured along the arc on which the trace point moves.

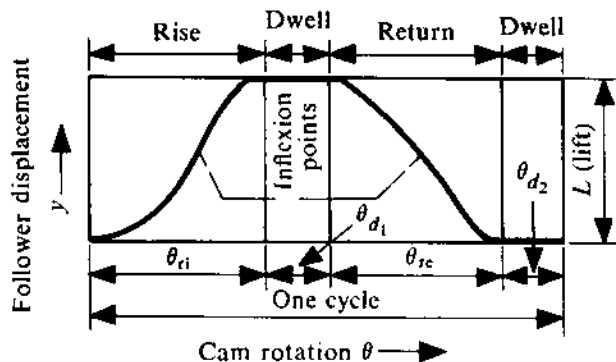


FIGURE 8.3

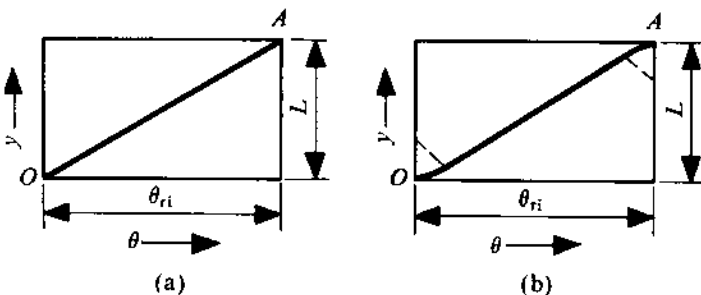


FIGURE 8.4

Construction of Displacement Diagrams

The rise and return of the follower can take place in many different ways. In this section, we shall discuss the graphical methods of constructing the displacement diagrams for the basic follower movements, namely,

- (i) uniform motion and its modifications,
- (ii) simple harmonic motion,
- (iii) uniform acceleration motion (or parabolic motion) and its modifications, and
- (iv) cycloidal motion.

The method will be demonstrated for the rise portion of the diagram. A similar procedure can be adopted for the return movement. Let

L = lift of the follower, and

θ_{ri} = angle of cam rotation for the rise phase.

Uniform Motion

By uniform motion, we mean that the velocity of the follower is constant. Since the follower displacement is from $y = 0$ to $y = L$ when the cam rotates from $\theta = 0$ to $\theta = \theta_{ri}$, it will be apparent that the straight line joining the two points ($\theta = 0, y = 0$) and ($\theta = \theta_{ri}, y = L$) represents the displacement

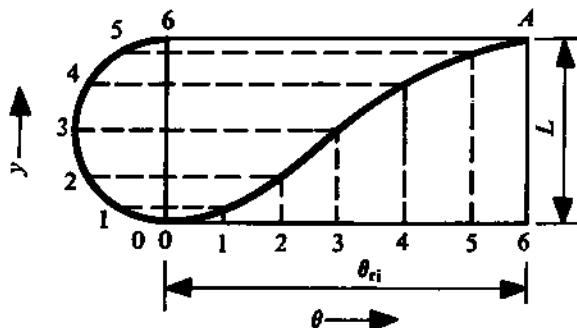


FIGURE 8.5

agram for uniform motion (Fig. 8.4a). As there is an instantaneous change from zero velocity at the beginning of the rise and a change to zero velocity at the end of the rise, the acceleration of the follower at these instants will attain a very high value. To avoid this, the straight line of the displacement diagram is connected tangentially to the dwell at both ends of the rise by means of smooth curves of any convenient radius, as shown in Fig. 8.4b. The bulk of the displacement takes place at uniform velocity, which is represented by the straight line in the diagram.

Simple Harmonic Motion

The displacement diagram for *simple harmonic motion* can be obtained as explained in Fig. 8.5. The line representing the angle θ_{ri} is divided into a convenient number of equal lengths (six divisions are shown in Fig. 8.5). A semicircle of diameter L is drawn as shown and divided into the same number of circular arcs of equal length. Horizontal lines are drawn from the points so obtained on the semicircle, to meet the corresponding vertical lines through the points on the length θ_{ri} . For simple harmonic motion, we always have finite velocity, acceleration, jerk, and higher-order derivatives of displacement.

Parabolic or Uniform Acceleration Motion

With dwell at the beginning and at the end of the rise, when lift of the follower has to take place in a given time, it is easy to show that the maximum acceleration will be the least if the first half of the rise takes place at a *constant acceleration* and the remaining displacement is at a constant deceleration (of the same magnitude). This fact makes parabolic motion very suitable for high-speed cams as it minimizes the maximum inertia force. The method of constructing the displacement diagram is explained in Fig. 8.6. As in Fig. 8.5, six equal divisions are marked on the line representing the angle θ . For locating the corresponding six vertical divisions, we make use of the fact that, at constant acceleration, the displacement is proportional to the square of time (i.e., it is proportional to the square of the cam rotation as the cam rotates at constant speed) for the first half. This is also true for the second half of the diagram if the origin is shifted to the end of the rise.

For cams operating valves of internal-combustion engines, the modified uniform acceleration motion is used for the follower. It is desired that the valves should open and close quickly, at the same time maintain the aforementioned advantage of parabolic motion. In this modified parabolic motion, the acceleration f_1 during the first part of the rise is more than the deceleration f_2 during the rest of the rise. Let

$$f_1 = K f_2 \quad (K > 1). \quad (8.1)$$

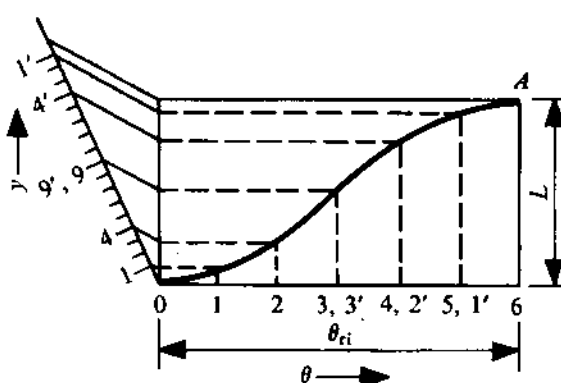


FIGURE 8.6

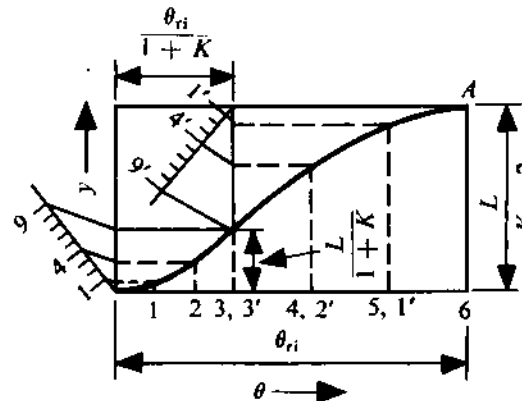


FIGURE 8.7

Then, it is easy to prove that

$$\theta_{ri} = \theta_a + K\theta_a, \quad (8.2)$$

where

$\theta_a = \theta_{ri}/(1 + K)$ = angle of cam rotation when the acceleration is f_1 , and

$K\theta_a$ = angle of cam rotation with deceleration f_2 .

The lift L is given by

$$L = L_1 + KL_1, \quad (8.3)$$

where

L_1 = rise with acceleration $f_1 = L/(1 + K)$, and

KL_1 = rise with deceleration f_2 .

The construction of the displacement diagram for this motion is similar to that shown in Fig. 8.6 and is explained in Fig. 8.7, taking three divisions in each part of the rise, with an assumed value of K . For uniform acceleration, $K = 1$. A similar curve is used for the return phase.

Cycloidal Motion

Cycloidal motion is obtained by rolling a circle of radius $L/(2\pi)$ on the ordinate of the displacement diagram. A point P on the circle, rolling on the ordinate, describes a cycloid. A convenient graphic method of constructing the displacement diagram is shown in Fig. 8.8. A circle of radius $L/(2\pi)$ drawn with centre at the end A of the displacement diagram. This circle is divided into the same number of equal divisions (six divisions, obtained by the radial lines to points 1, 2, ..., 6, are shown in Fig. 8.8) as the abscissa of the diagram representing the cam rotation θ_{ri} . The projections of points 1, ..., 6 on the circumference are taken on the vertical diameter, represented by points 1', ..., 6'. Lines parallel to OA are drawn therefrom as shown. The displacement diagram is obtained

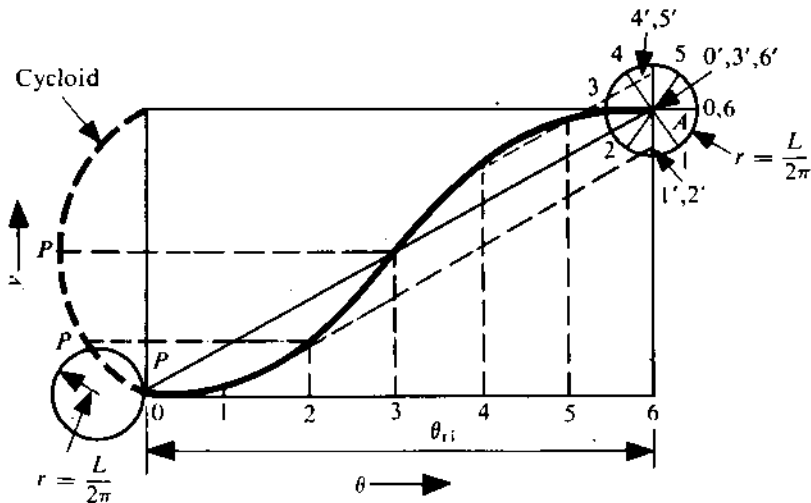


FIGURE 8.8

from the intersection of the vertical lines through the points on the abscissa and the corresponding lines parallel to OA .

3.5 ANALYSIS OF FOLLOWER MOTION

The displacement diagrams, discussed in Section 8.4, give the follower movement y for any rotation θ of the cam. The displacement y can also be expressed as a function of θ . Conversely, if the displacement y is given as a function of θ , we can draw the displacement diagram and thereby obtain the cam profile. Once y is expressed as a function of θ , the velocity, acceleration, jerk, etc., of the follower can be obtained by successive differentiation.

Basic Follower Motions

The basic follower motions, discussed in Section 8.4, will now be expressed as functions of θ . The detailed derivation is given here only for parabolic motion.

During the accelerating period of parabolic motion, let

$$y = C\theta^2, \quad 0 \leq \theta \leq \theta_{ri}/2, \quad (8.4)$$

where C is a constant. Since $y = L/2$ when $\theta = \theta_{ri}/2$, we get

$$\begin{aligned} C &= 2L/\theta_{ri}^2, \\ y &= 2L(\theta/\theta_{ri})^2. \end{aligned} \quad (8.5)$$

So, the velocity of the follower is

$$\dot{y} = \frac{4L}{\theta_{ri}^2} \theta \omega, \quad (8.6)$$

where $\dot{\theta} = \omega$ (angular velocity of the cam) = constant. The maximum velocity of the follower (at $\theta = \theta_{ri}/2$) is

$$\dot{y}_{max} = 2L\omega/\theta_{ri}, \quad (8.7)$$

and the acceleration of the follower is

$$\ddot{y} = \frac{4L}{\theta_{ri}^2} \omega^2 = \text{constant.} \quad (8.8)$$

During the retardation period of the rise, let

$$y = C_1 + C_2\theta + C_3\theta^2, \quad \theta_{ri}/2 \leq \theta \leq \theta_{ri}. \quad (8.9)$$

To obtain the three constants C_1 , C_2 , and C_3 , we make use of three conditions, namely,

$$\theta = \theta_{ri}, \quad y = L,$$

$$\theta = \theta_{ri}, \quad \dot{y} = 0 \text{ (assuming a dwell at the end of the rise),}$$

$$\theta = \theta_{ri}/2, \quad \dot{y} = 2L\omega/\theta_{ri} \text{ [from (8.7), maintaining the velocity continuity at } \theta = \theta_{ri}/2].$$

Thus,

$$C_1 = -L, \quad C_2 = 4L/\theta_{ri}, \quad C_3 = -2L/\theta_{ri}^2$$

when

$$y = L[1 - 2(1 - \theta/\theta_{ri})^2]. \quad (8.10)$$

So, the velocity of the follower is

$$\dot{y} = \frac{4L\omega}{\theta_{ri}} \left(1 - \frac{\theta}{\theta_{ri}}\right), \quad (8.11)$$

and the acceleration of the follower is

$$\ddot{y} = -4L\omega^2/\theta_{ri}^2. \quad (8.12)$$

The rate of change of acceleration, i.e., \ddot{y} , is called *jerk* and is a useful index of the quality of the motion. Assuming dwell at the beginning and the end of the rise, it can be noted that

$$\begin{aligned} \text{jerk} &\rightarrow \infty \text{ at } \theta = 0 \\ &\rightarrow -\infty \text{ at } \theta = \theta_{ri}/2 \\ &\rightarrow \infty \text{ at } \theta = \theta_{ri}. \end{aligned}$$

Using (8.5), (8.6), (8.8), and (8.10) to (8.12), we can plot the displacement, velocity, acceleration and jerk of the follower during the rise.

The equations for other types of basic follower motions are as follows:

(i) For uniform motion,

$$y = L \frac{\theta}{\theta_{ri}}, \quad 0 \leq \theta \leq \theta_{ri}. \quad (8.13)$$

(ii) For simple harmonic motion,

$$y = \frac{L}{2} \left(1 - \cos \frac{\pi\theta}{\theta_{ri}}\right), \quad 0 \leq \theta \leq \theta_{ri}. \quad (8.14)$$

(iii) For cycloidal motion,

$$y = L \left(\frac{\theta}{\theta_{ri}} - \frac{1}{2\pi} \sin \frac{2\pi\theta}{\theta_{ri}}\right), \quad 0 \leq \theta \leq \theta_{ri}. \quad (8.15)$$

A plot of the displacement, velocity, acceleration, and jerk of the follower for each basic follower motion can be obtained from these equations. This is left as an exercise for the reader.

Advanced Cam Curves

In most situations, the basic follower motions discussed so far are inadequate for smooth operation. This is particularly so for high-speed operation. One method of rectifying this deficiency is to combine several portions of these basic curves to obtain the displacement diagram. While doing this, the velocities and accelerations should be matched at the junction points. Another method is to represent the basic follower motions by polynomial curves.² Such curves are called *advanced cam curves* and can be used to approximately satisfy any requirement, but this involves many computational difficulties. For our further discussion, the displacement y will be taken to be a polynomial in θ , that is,

$$y = C_0 + C_1\theta + C_2\theta^2 + C_3\theta^3 + \dots + C_n\theta^n. \quad (8.16)$$

The number of terms to be taken is equal to the number of conditions to be satisfied. For example, to satisfy the six boundary conditions, namely,

$$y = 0, \quad \dot{y} = 0, \quad \ddot{y} = 0 \quad \text{at } \theta = 0,$$

$$y = L, \quad \dot{y} = 0, \quad \ddot{y} = 0 \quad \text{at } \theta = \theta_{ri},$$

we can use terms up to C_5 . Thus, we get

$$y = C_0 + C_1\theta + C_2\theta^2 + C_3\theta^3 + C_4\theta^4 + C_5\theta^5.$$

Using these conditions, we get six linear simultaneous equations, from which the six constants C_0, C_1, \dots, C_5 may be obtained, and finally we get

$$y = 10L\left(\frac{\theta}{\theta_{ri}}\right)^3 - 15L\left(\frac{\theta}{\theta_{ri}}\right)^4 + 6L\left(\frac{\theta}{\theta_{ri}}\right)^5. \quad (8.17)$$

This curve is referred to as a 3-4-5 curve since terms of only these orders finally appear in the polynomial.

8.6 DETERMINATION OF BASIC DIMENSIONS

To determine the shape of the cam profile for generating a prescribed motion of the follower, it is necessary to have information about some basic dimensions, viz., the base circle radius and the offset. However, in most cases, these parameters are not specified by the customer and have to be found out by the designer based on certain requirements on the quality of motion transmission. Certain conditions have also to be satisfied by the cam surface curvature in order to limit the contact stresses. This section presents the procedures followed for determining the basic dimensions in a few commonly-used cam-follower configurations.³

²For detailed analysis, see Rothbart, H.A., *Cams - Design, Dynamics and Accuracy*, Wiley, New York, 1956, and Mallik, A.K., Ghosh, A. and Dittrich, G., *Kinematic Analysis and Synthesis of Mechanisms*, CRC Press, Boca Raton, 1994.

³For a more detailed treatment, see Mallik, A.K., Ghosh, A. and Dittrich, G., *Kinematic Analysis and Synthesis of Mechanisms*, CRC Press, Boca Raton, 1994.

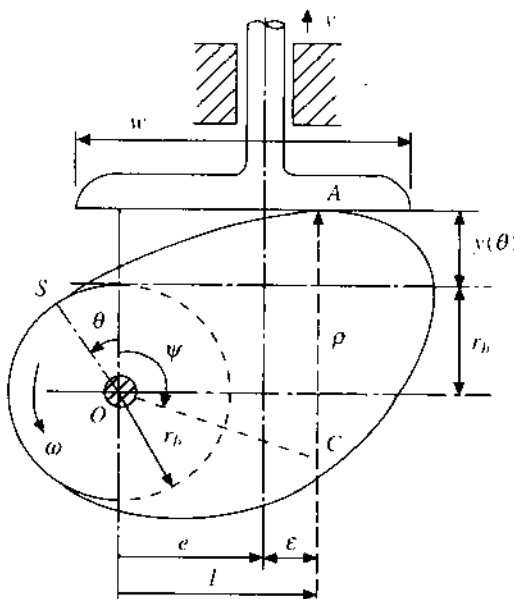


FIGURE 8.9

Translating Flat-face Follower

A typical cam mechanism with an offset-translating flat-face follower is shown in Fig. 8.9. The base circle, with a radius r_b , touches the cam profile at the point S and, so, the follower starts lifting when it touches the cam at S . At the instant shown in the figure, the cam has rotated by an angle θ in the CCW direction from the position corresponding to the beginning of the rise. The flat face touches the cam at A where the profile has a radius of curvature ρ with the centre at C . The offset is e towards the right. The force exerted (in the direction of follower motion) by the cam on the follower acts at A and the eccentricity of this driving effort is given by ϵ as indicated in the figure. As explained in Section 1.8, the velocity and acceleration of the follower at the instant will remain unchanged if the actual cam is replaced by a cam having a circular profile with a radius of curvature ρ and the centre at C . It should be further noted that with this cam (in place of the actual cam at the instant) both ρ and OC remain invariant. Since both the points S and C are fixed on the body of the cam,

$$\theta + \psi = \text{constant}$$

or

$$d\theta = -d\psi \quad \text{or} \quad \dot{\theta} = -\dot{\psi}. \quad (8.18)$$

From the figure,

$$\rho = r_b + y(\theta) - OC \cos \psi, \quad (8.19)$$

where $y(\theta)$ represents the rise of the follower from its lowermost position (i.e., when it touches the base circle). Differentiating both sides of (8.19),⁴ we obtain

$$y'(\theta)\dot{\theta} = -OC \sin \psi \cdot \dot{\psi}.$$

⁴Prime ('') denotes differentiation with respect to θ .

Using (8.18) in this equation, we have

$$y'(\theta) = OC \sin \psi. \quad (8.20)$$

Differentiating (8.20) once more with respect to time and again using (8.18), we get

$$y''(\theta) = -OC \cos \psi. \quad (8.21)$$

Now, using this equation in (8.19), the expression for the radius of curvature of the cam profile becomes

$$\rho = r_b + y(\theta) + y''(\theta). \quad (8.22)$$

If ρ_{\min} be the minimum permitted radius of curvature from the contact stress point of view, then the minimum permissible base circle radius becomes

$$r_b \min = \rho_{\min} - [y(\theta) + y''(\theta)]_{\min}. \quad (8.23)$$

The minimum value of $[y(\theta) + y''(\theta)]$ can be found out from the prescribed follower motion. It should be further noted that at no point can the cam profile be concave when a flat-face follower is used.

The eccentricity of the driving effort, ϵ , cannot be also allowed to exceed some limiting value beyond which the follower rod may get jammed in the prismatic guide. From Fig. 8.9,

$$OC \sin \psi = e + \epsilon = l.$$

Using (8.20) in this relation, we get

$$l = e + \epsilon = y'(\theta). \quad (8.24)$$

If ϵ_{\max} be the maximum permissible eccentricity of the driving effort, then the minimum required offset

$$e_{\min} = [y'(\theta)]_{\max} - \epsilon_{\max} \quad \text{when } y'(\theta) > 0. \quad (8.25)$$

There is no driving effort during return (i.e., $y'(\theta) < 0$) and the spring force ensures the desired movement of the follower. The minimum required width of the follower face can be determined from (8.24) as

$$w_{\min} = [y'(\theta)]_{\max} + |[y'(\theta)]_{\min}| + 2 \times \text{allowance on each side.} \quad (8.26)$$

PROBLEM 8.1

The follower movement in a cam-follower mechanism with a translating flat-face follower is given by

$$y(\theta) = 60(1 - \cos \theta) \text{ mm}, \quad 0 \leq \theta \leq 2\pi.$$

The limit on the contact stress requires that the minimum radius of curvature of the cam profile should not be less than 100 mm anywhere and during the rise period the driving effort should not have an eccentricity more than 40 mm. Determine the minimum permissible base circle radius and the minimum required offset.

SOLUTION

From the prescribed displacement function, we get

$$y'(\theta) = 60 \sin \theta \text{ mm}, \quad 0 \leq \theta \leq 2\pi, \quad (\text{a})$$

$$y''(\theta) = 60 \cos \theta \text{ mm}, \quad 0 \leq \theta \leq 2\pi. \quad (\text{b})$$

Therefore,

$$y(\theta) + y''(\theta) = 60 \text{ mm}, \quad 0 \leq \theta \leq 2\pi.$$

This result, when used in (8.22), yields the expression for the radius of curvature of the cam profile as

$$\rho = r_b + 60 \text{ mm}, \quad 0 \leq \theta \leq 2\pi. \quad (\text{c})$$

This implies that the cam profile is a circle with a constant radius of curvature. From (8.23) and (c), we get

$$r_b \min = (100 - 60) \text{ mm} = 40 \text{ mm}.$$

From (a) we know that

$$[y'(\theta)]_{\max} = 60 \text{ mm}. \quad (\text{d})$$

As the maximum allowable eccentricity of the driving effort is prescribed to be 40 mm, (8.25) and (d) yield

$$e_{\min} = (60 - 40) \text{ mm} = 20 \text{ mm}.$$

PROBLEM 8.2

What should be the minimum width of the follower in the previous problem if an allowance of 2 mm is desirable on both sides?

SOLUTION

From (a), we get

$$[y'(\theta)]_{\max} = 60 \text{ mm},$$

$$|[y'(\theta)]_{\min}| = 60 \text{ mm}.$$

Hence, using these results in (8.26), we get

$$w_{\min} = 60 \text{ mm} + 60 \text{ mm} + 2 \times 2 \text{ mm} = 124 \text{ mm}.$$

PROBLEM 8.3

In a cam mechanism with a flat-face translating follower, the total rise of the follower is 30 mm and the cam rotates through 180° during the rise period. During the first 90° of cam rotation, the follower rises with constant acceleration and it decelerates uniformly during the second half of the rise period. The return of the follower is a simple harmonic motion during which the cam rotates through another 180° . (a) If the minimum radius of curvature of the cam profile is not to be less than 40 mm during the rise, determine the minimum required radius of the base circle. (b) Find out the minimum required width of the follower face with a 2.5 mm allowance on each side. (c) What should be the minimum amount of offset if the maximum eccentricity of the driving effort during rise is not to exceed 15 mm?

OLUTION

Using (8.5), (8.10), and (8.14), the displacement functions during the rise and return can be expressed as

$$\begin{aligned}y(\theta) &= 60(\theta/\pi)^2 \text{ mm}, \quad 0 \leq \theta \leq \pi/2, \\y(\theta) &= 30[1 - 2(1 - \theta/\pi)^2] \text{ mm}, \quad \frac{\pi}{2} \leq \theta \leq \pi, \\y(\theta) &= 15[1 - \cos \theta] \text{ mm}, \quad \pi \leq \theta \leq 2\pi.\end{aligned}$$

The first and the second derivatives with respect to θ are

$$\begin{aligned}y'(\theta) &= 120\theta/\pi^2 \text{ mm}, \quad 0 \leq \theta \leq \pi/2, \\y'(\theta) &= \frac{120}{\pi}(1 - \frac{\theta}{\pi}) \text{ mm}, \quad \frac{\pi}{2} \leq \theta \leq \pi, \\y'(\theta) &= 15 \sin \theta \text{ mm}, \quad \pi \leq \theta \leq 2\pi, \\y''(\theta) &= 120/\pi^2 \text{ mm}, \quad 0 \leq \theta \leq \pi/2, \\y''(\theta) &= -120/\pi^2 \text{ mm}, \quad \frac{\pi}{2} \leq \theta \leq \pi, \\y''(\theta) &= 15 \cos \theta \text{ mm}, \quad \pi \leq \theta \leq 2\pi.\end{aligned}$$

(a) For the rise period, the expressions for the cam profile curvature are

$$\begin{aligned}\rho &= r_b + 60(\theta/\pi)^2 + 120/\pi^2, \quad 0 \leq \theta \leq \pi/2, \\&\rho = r_b + 30[1 - 2(1 - \theta/\pi)^2] - 120/\pi^2, \quad \pi/2 \leq \theta \leq \pi.\end{aligned}$$

The minimum value of ρ during the whole rise period is found to be (at $\theta = \pi/2$)

$$\rho = r_b + (15 - 120/\pi^2) \text{ mm}.$$

Hence,

$$\begin{aligned}r_{b\min} &= \rho_{\min} - (15 - 120/\pi^2) \text{ mm} \\&= (40 - 15 + 12.16) \text{ mm} = 37.16 \text{ mm}.\end{aligned}$$

(b) Considering the whole cycle,

$$\begin{aligned}[y'(\theta)]_{\max} &= 60/\pi \text{ mm} \quad (\text{when } \theta = \pi/2), \\[y'(\theta)]_{\min} &= -15 \text{ mm} \quad (\text{when } \theta = 3\pi/2).\end{aligned}$$

Using (8.26), we get

$$w_{\min} = (60/\pi + |-15| + 5) \text{ mm} = 39.1 \text{ mm}.$$

(c) During rise, the maximum value of $y'(\theta)$

$$[y'(\theta)]_{\max} = 60/\pi \text{ mm} \quad (\text{when } \theta = \pi/2).$$

The maximum eccentricity during rise

$$\epsilon_{\max} = 15 \text{ mm}.$$

Hence, from (8.25),

$$e_{\min} = (60/\pi - 15) \text{ mm} = 4.1 \text{ mm}.$$

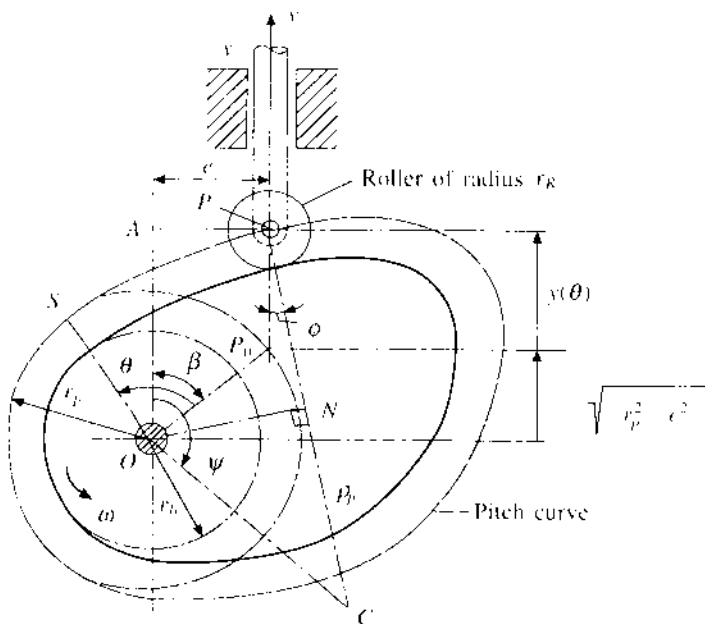


FIGURE 8.10

Translating Roller Follower

A cam-follower mechanism with an offset-translating roller follower is shown in Fig. 8.10. In this case, the force acting on the follower always passes through the roller centre P (which is also the trace point). Neglecting the effect of friction on the roller, the force will be normal to the cam profile at the point of contact and, hence, will pass through the centre of curvature C . The tendency of jamming of the follower in its guide, in this case, depends on the angle of the driving force with the direction of follower motion, termed as the pressure angle. This angle (ϕ in the figure) should not exceed a permissible limit for a proper functioning of the system. Furthermore, to limit the contact stress, the radius of curvature of the cam profile should never be less than a minimum value. It is also obvious that at no point can the cam profile be permitted to be concave with a radius of curvature less than that of the roller.

The point of intersection, P_0 , of the path of the trace point and the prime circle indicates the lowest position of the follower. The rising motion of the follower starts when the point S coincides with P_0 . The radius of curvature of the pitch curve PC , at the instant considered, is denoted by ρ_p as shown in the figure. So, if ρ be the corresponding radius of curvature of the cam profile, then

$$\rho = \rho_p - r_R, \quad (8.27)$$

where r_R is the roller radius. If ON be the normal dropped on the line PC from O , then, from Fig. 8.10,

$$\begin{aligned} ON &= OA \sin \phi + AP \cos \phi \\ &= [\sqrt{r_p^2 - e^2} + y(\theta)] \sin \phi + e \cos \phi, \end{aligned} \quad (8.28)$$

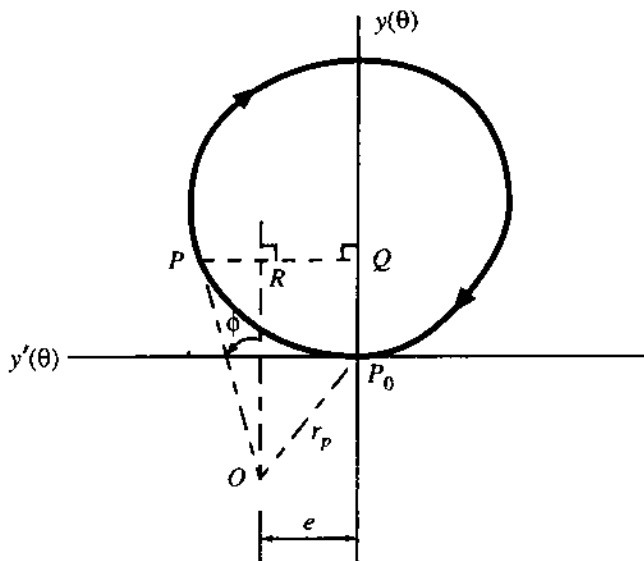


FIGURE 8.11

where θ is the cam rotation from the position when the rising motion of the follower starts. Since the component of the velocity of the point P along the normal CP has to be equal⁵ to the velocity of the point N (which is along CP and is equal to $\omega \cdot ON$),

$$v \cos \phi = \frac{dy(\theta)}{dt} \cdot \cos \phi = \omega \cdot ON$$

or

$$y'(\theta) \cdot \cos \phi = ON \quad (\text{because } \dot{\theta} = \omega). \quad (8.29)$$

Substituting the expression for ON from (8.28) in this equation and rearranging, we get the relation

$$\tan \phi = \frac{y'(\theta) - e}{y(\theta) + \sqrt{r_p^2 - e^2}}. \quad (8.30)$$

This equation can be represented graphically as in Fig. 8.11. A plot of $y'(\theta)$ vs. $y(\theta)$ (corresponding to a prescribed displacement function) for a complete cycle of cam rotation is shown. The direction of the arrow should be noted. The values of $y(\theta)$ and $y'(\theta)$ corresponding to a typical position indicated by the point P completely specify the cam-follower configuration. If the point O is so selected that its distance from the point P_0 (the origin of the plot coordinates) is r_p and it is at a distance e from the $y(\theta)$ -axis towards the left, then

$$\tan \angle POR = \frac{PR}{OR} = \frac{PQ - RQ}{OR} = \frac{y'(\theta) - e}{y(\theta) + \sqrt{r_p^2 - e^2}}.$$

⁵This is because the points P and N are connected by two rigid bodies whose common normal at the point of contact passes through P and N .

Comparing this equation with (8.30), it is obvious that

$$\angle POR = \phi,$$

i.e., the inclination of the line OP from the $y(\theta)$ -axis represents the corresponding pressure angle. According to the convention followed, e is positive with CCW rotation of the cam when the point O lies towards the left of the $y(\theta)$ -axis in this diagram. If the extreme values of the pressure angle are prescribed, it is possible to determine the minimum required prime circle radius and the corresponding offset.

The radius of curvature of the cam profile can be also found out in the following manner. Referring to Fig. 8.10,

$$\rho_p \cos \phi = y(\theta) + \sqrt{r_p^2 - e^2} - OC \cos \psi, \quad (8.31)$$

where $\psi = \angle AOC$, and

$$\rho_p \sin \phi = OC \sin \psi - e.$$

Differentiating this equation with respect to θ (and again considering the actual cam to be instantaneously replaced by a circular cam with C as the centre and CP as the radius), we get

$$\rho_p \cos \phi \cdot \frac{d\phi}{d\theta} = OC \cos \psi \cdot \frac{d\psi}{d\theta}.$$

But since the lines OS and OC are rigidly attached to the cam, $d\theta = -d\psi$ and this equation becomes

$$\rho_p \cos \phi \cdot \phi' = -OC \cos \psi$$

or

$$OC = -\rho_p \cos \phi \cdot \phi' / \cos \psi.$$

Substituting OC in (8.31) by the RHS of this equation, we get

$$\rho_p \cos \phi = y(\theta) + \sqrt{r_p^2 - e^2} + \rho_p \cos \phi \cdot \phi'$$

or

$$\rho_p = \frac{y(\theta) + \sqrt{r_p^2 - e^2}}{(1 - \phi') \cos \phi}. \quad (8.32)$$

Next, differentiating both sides of (8.30) with respect to θ and rearranging the terms, after some manipulations, we get

$$\phi' = \frac{y''(\theta) - y' \tan \phi}{y(\theta) + \sqrt{r_p^2 - e^2}} \cdot \cos^2 \phi. \quad (8.33)$$

Again,

$$\sec^2 \phi = 1 + \tan^2 \phi = 1 + \left[\frac{y'(\theta) - e}{y(\theta) + \sqrt{r_p^2 - e^2}} \right]^2. \quad (8.34)$$

Using (8.30), (8.33), and (8.34), (8.32) yields

$$\rho_p = \frac{[\{\sqrt{r_p^2 - e^2} + y(\theta)\}^2 + \{e - y'(\theta)\}^2]^{3/2}}{[\sqrt{r_p^2 - e^2} + y(\theta)]^2 + [e - y'(\theta)][e - 2y'(\theta)] - [\sqrt{r_p^2 - e^2} + y(\theta)]y''(\theta)}. \quad (8.35)$$

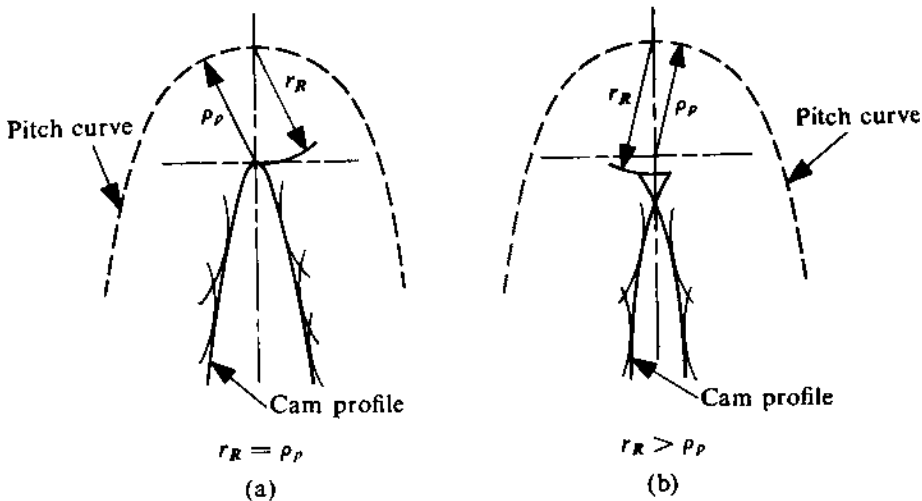


FIGURE 8.12

Once ρ_p is determined, (8.27) yields the radius of curvature of the cam profile as

$$\rho = \rho_p - r_R.$$

Once the required offset, e , is determined, ρ can be evaluated. It should be checked whether at any point ρ becomes less than the minimum permissible value based on the contact stress. Even if no restriction is imposed on ρ from the point of view of the contact stress, cusp formation should be avoided. Cusp is formed when at a point $\rho_p = r_R$ as indicated in Fig. 8.12a. Figure 8.12b shows what happens if $\rho_p < r_R$.

PROBLEM 8.4

Figure 8.13 shows the $y'(\theta)$ - $y(\theta)$ plot for a cam mechanism with a translating roller follower. If there is no offset provided to the translation axis, find out the maximum magnitudes of the pressure angle during the rise and during the return. The radii of the base circle and the roller are 35 mm and 10 mm, respectively.

SOLUTION

From the given data, $r_p = 35 \text{ mm} + 10 \text{ mm} = 45 \text{ mm}$ and $e = 0$. Following the construction indicated in Fig. 8.11, the point O is located, in Fig. 8.14, 45 mm below the point P_0 (the origin of the $y(\theta)$ - $y'(\theta)$ plot) on the $-y'(\theta)$ -axis. If a line OR is drawn through O touching the rise part of the $y(\theta)$ - $y'(\theta)$ diagram (i.e., when $y'(\theta) > 0$), its inclination from the $y(\theta)$ -axis indicates the maximum possible pressure angle during the rise when the follower has moved up by 22.5 mm. This angle is measured to be 24.3° . Similarly, during the return, the maximum pressure angle is equal to 19° and occurs when the follower is at a height of 15.3 mm from the lowermost position. However, the reader should note that the pressure angle is not always important during the return as during this part of the motion the follower is driven back by a spring, and is not driven by the cam.

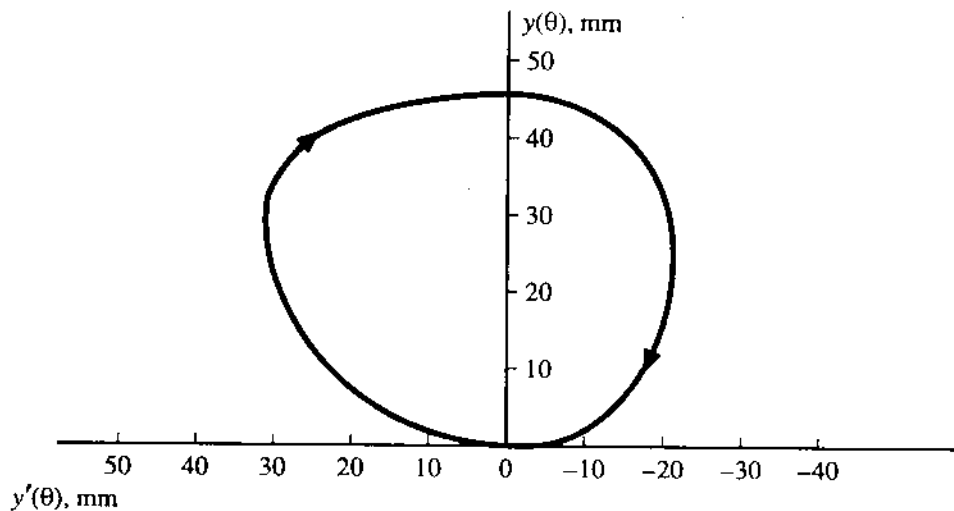


FIGURE 8.13

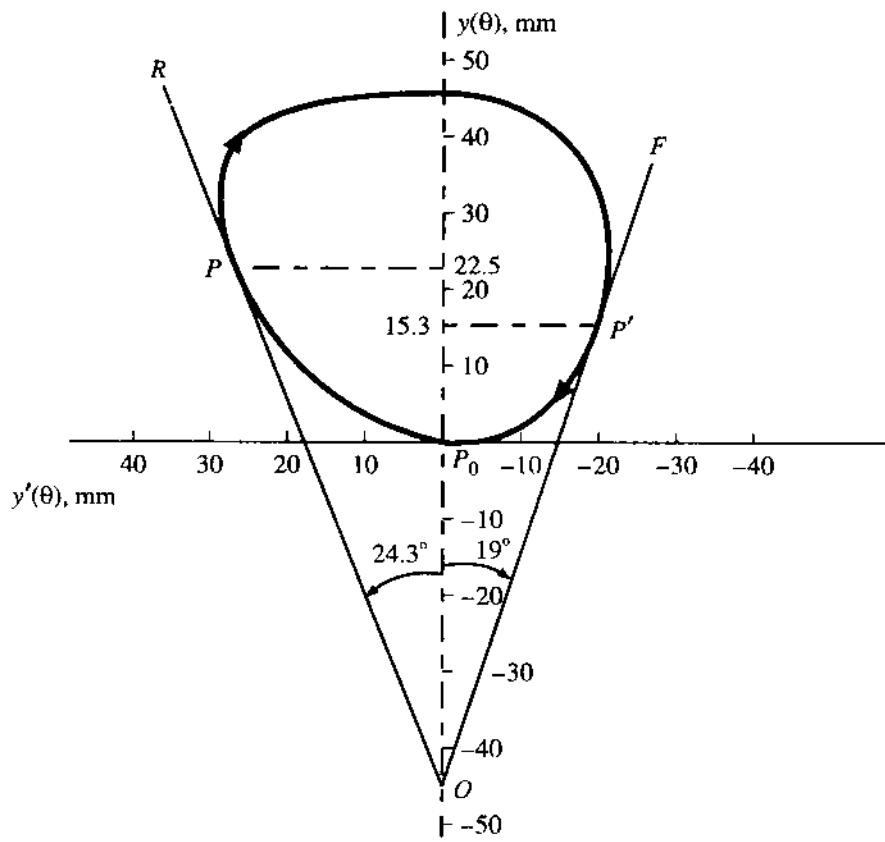


FIGURE 8.14

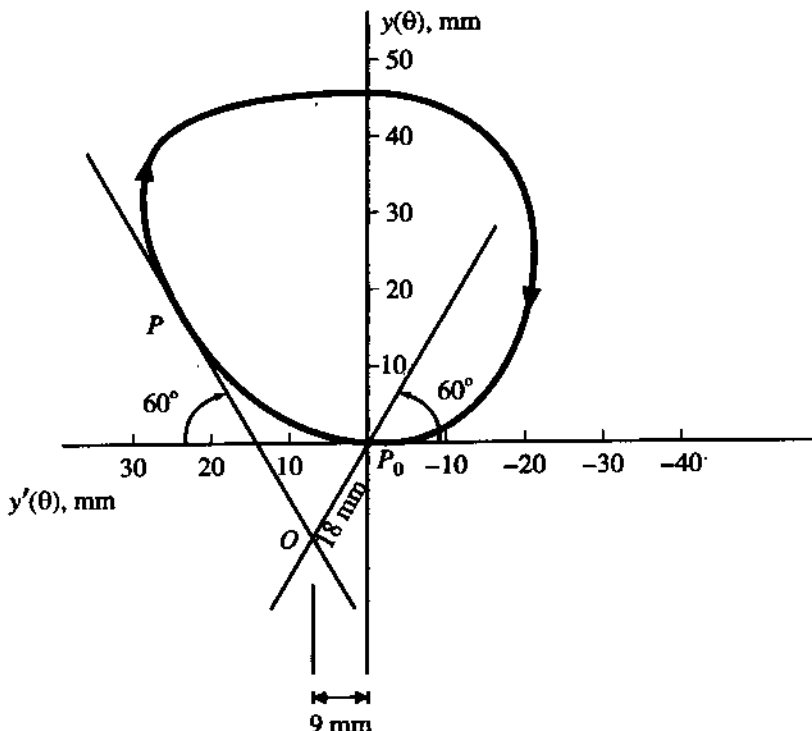


FIGURE 8.15

PROBLEM 8.5

If the displacement function of the follower of a cam-translating roller follower mechanism be the same as that of the mechanism in Problem 8.4, and if the maximum magnitude of the pressure angle during the rise period is not to exceed 30° , find out the minimum base circle radius and the corresponding offset. Assume the roller radius to be 10 mm.

SOLUTION

Since the displacement function is the same as that in Problem 8.4, the $y'(\theta)$ - $y(\theta)$ plot will be identical. In Fig. 8.15, the $y'(\theta)$ - $y(\theta)$ plot is reproduced. The rise period of the plot is represented by the portion of the diagram for which $y'(\theta) > 0$, i.e., the portion which lies to the left of the $y(\theta)$ -axis. The minimum prime circle size will correspond to the situation when the two extreme tangents to the rise part of the plot make 30° with the $y(\theta)$ -axis or 60° with the $y'(\theta)$ -axis. Two such lines have been drawn in Fig. 8.15 and they intersect at O . By measurement it is found that $r_p \text{ min} = 18 \text{ mm}$ and the corresponding offset of the follower axis is 9 mm to the right of the cam axis when it rotates in the CCW direction. Since the roller radius is 10 mm, the minimum base circle radius is $(18 - 10) \text{ mm} = 8 \text{ mm}$.

It should be noted that if the maximum allowable pressure angle exceeds 45° , the minimum prime circle radius has to be found out by dropping a normal to the tangent OP .

PROBLEM 8.6

The displacement function of a cam mechanism with a translating roller follower during rise is

$$y(\theta) = \begin{cases} 10(\theta/\pi)^2 \text{ cm} & 0 \leq \theta \leq \pi/2 \\ 5 - 10(1 - \theta/\pi)^2 \text{ cm} & \pi/2 \leq \theta \leq \pi \end{cases}$$

The radius of the roller is 7.5 mm and the magnitude of the pressure angle during rise should not exceed 30°. Determine the minimum permissible base circle radius and the necessary offset. With these values of the offset and the base circle, what will be the expression for the radius of curvature of the cam profile during the first part of the rise? The cam rotates in the CCW direction.

SOLUTION

Differentiating the displacement function with respect to the cam rotation θ , we obtain

$$y'(\theta) = \begin{cases} (20/\pi^2)\theta \text{ cm} & 0 \leq \theta \leq \pi/2 \\ \frac{20}{\pi}(1 - \theta/\pi) \text{ cm} & \pi/2 \leq \theta \leq \pi \end{cases}$$

Figure 8.16 shows the $y(\theta)$ - $y'(\theta)$ plot during rise. Drawing two lines at 60° with the $y'(\theta)$ -axis as shown, the optimal position of O is determined. The minimum value of the prime circle radius and the corresponding offset (to the right of the cam centre) are found to be 18 mm and 9 mm respectively. Hence the minimum permissible base circle radius is

$$r_b \min = r_p \min - r_R = (18 - 7.5) \text{ mm} = 10.5 \text{ mm}.$$

Substituting the values of r_b and e and the expressions for $y(\theta)$ and $y'(\theta)$ in (8.35), we get the expression for the radius of curvature of the pitch curve during the first part of the rise period as

$$\rho_p = \frac{(a^2 + b^2)^{3/2}}{a^2 - b(2b - 9) - 200a/\pi^2} \text{ mm}, \quad 0 \leq \theta \leq \pi/2,$$

where $a = \{15.6 + 100(\theta/\pi)^2\}$ and $b = (9 - 200\theta/\pi^2)$.

The expression for the radius of curvature of the cam profile during this phase is

$$\rho = \rho_p - r_R.$$

8.7 SYNTHESIS OF CAM PROFILE (GRAPHICAL APPROACH)

The basic approach to laying out the cam profile involves the principle of inversion. The cam is held stationary and the fixed link is rotated at the cam speed in a direction opposite to that of the cam; this maintains the same relative motion between the cam and the follower. The movement of the trace point corresponding to this rotation is obtained from the displacement diagram. Thus, the trace points are obtained for all positions of the cam, called *station points*, and the curve drawn through these trace points is the pitch curve. Once the trace points are obtained, we can draw the follower positions corresponding to these station points. The cam profile is given by the envelope of the follower surfaces at these positions. The following two examples will clarify the principle. We shall discuss only roller and flat-face followers because, for a knife-edge follower, the pitch curve itself represents the cam profile.⁶

⁶To maintain clarity of the diagrams, we have used only fourteen station points in each problem, but in practice, to obtain an accurate cam profile, a large scale drawing with many more station points should be prepared.

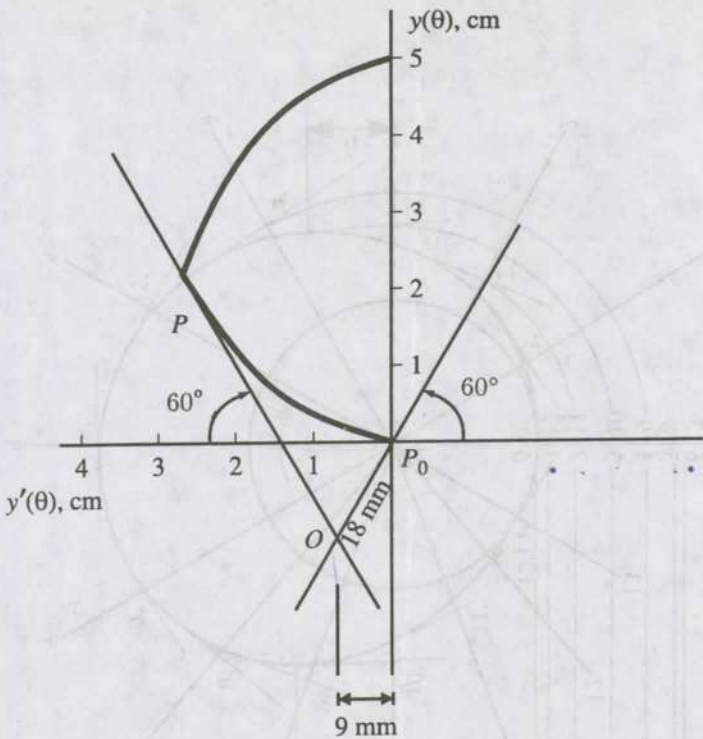


FIGURE 8.16

PROBLEM 8.7

A radial-translating flat-face follower has a lift of 3 cm. The rise takes place with simple harmonic motion for 180° of cam rotation. Then, there is a dwell for 30° and the return motion (also simple harmonic) is for 120° . The balance 30° of cam rotation is dwell. The base circle radius of the cam is 3 cm. Obtain the cam profile and the minimum length of the follower face with a clearance of 0.3 cm at both ends. The cam rotates in the counter-clockwise direction.

SOLUTION

We have first to draw the displacement diagram as shown in Fig. 8.17a. Using six divisions for θ_{ri} and θ_{re} , each interval between the station points 0 and 6 (during the rise) corresponds to 30° of cam rotation, and each interval between the station points 7 and 13 (during the return) corresponds to 20° of cam rotation. Each dwell corresponds to 30° of cam rotation. The displacement diagram is obtained as explained in Fig. 8.5.

The cam centre O in Fig. 8.17b is chosen in a manner such that the projections can be taken directly from the displacement diagram to locate the position of the trace points on the line of translation corresponding to the station points 0 to 13.

As the cam is rotating in the CCW direction, the follower axis is rotated in the CW direction. Thus, the radial lines marked 1, 2, 3, ..., 13, drawn through O (at equal angular intervals, as in the displacement diagram), represent the follower axes corresponding to station points 1 to 13.

Now, corresponding to each station point, the distance of the trace point is known from the cam

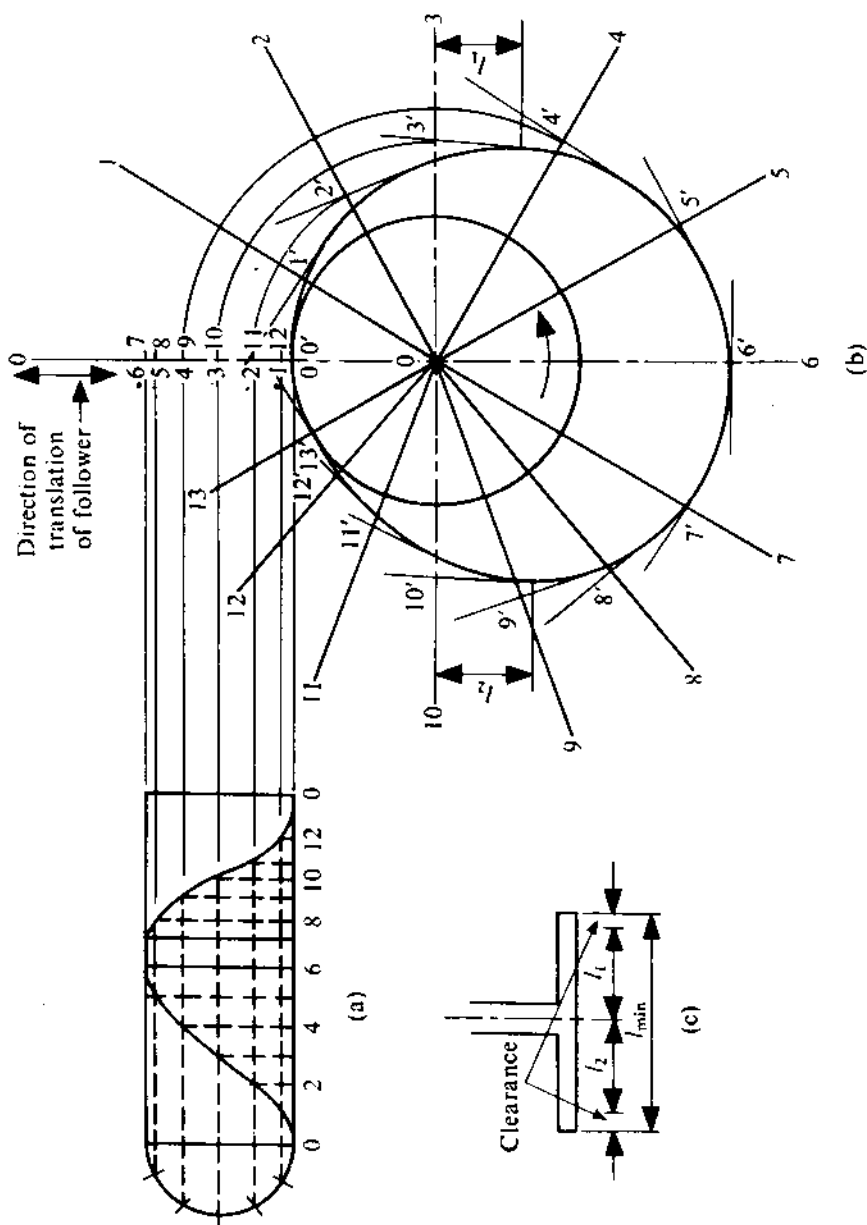


FIGURE 8.17

centre O , which is transferred to each moving axis of the follower. The new trace point locations so obtained are designated $1'$, $2'$, $3'$, $4'$, ..., $13'$. As the trace points are obtained, the follower face (which is perpendicular to the follower axis) corresponding to each station point can be drawn. Then, the curve drawn tangential to all these lines (representing the follower face) will give the cam profile.

By inspection, it will be seen from Fig. 8.17 that the point of contact is the trace point at station point 0; for other positions, the point of contact and the trace point are different. The point of contact shifts towards the right of the trace point as the station point proceeds from 0 to 1, and then from 1 to 2, and so on. The point of contact is farthest to the right of the trace point at the station point 3. After this, the point of contact moves to the left and reaches farthest to the left of the trace point at the station point 10. Let

l_1 = distance of the point of contact from the trace point when it is farthest to the right (this occurs at the station point 3 in the present case, and from measurements we get $l_1 = 1.32$ cm), and

l_2 = distance of the point of contact from the trace point when it is farthest to the left (this occurs at the station point 10 in the present case, and from measurements we get $l_2 = 2.06$ cm).

So, the minimum length required for the follower flat face (Fig. 8.17c) is

$$\begin{aligned} l_{\min} &= l_1 + l_2 + 2 \quad (\text{clearance}) \\ &= (1.72 + 2.06 + 2 \times 0.3) = 4.38 \text{ cm.} \end{aligned}$$

It should be noted that the first step is to obtain the trace point corresponding to each station point. The curve passing through these points is the pitch curve and represents the cam profile in the case of a knife-edge follower. For a roller follower, as the trace point is the roller centre, rollers should be drawn at every station point after locating the trace point (i.e., the roller centre) and then a curve drawn tangential to the rollers to give the cam profile. Some of the construction lines have been omitted from Fig. 8.17 to avoid confusion.

PROBLEM 8.8

A translating roller follower is offset to the left of the cam centre by 1.5 cm. The cam has a base circle radius of 3 cm and the follower has a lift of 4 cm. The cam rotates in the clockwise direction. The follower has a 150° parabolic motion for both the rise and return phases. The duration of the dwell before and after the rise is 30° . Assume the roller radius to be 0.5 cm, and determine the required cam profile.

SOLUTION

The displacement diagram is drawn in Fig. 8.18a with six divisions for both rise and return, each interval being 25° .

In this problem, the follower axis will always be at a distance e (the amount of offset) from the cam centre (Fig. 8.18b). Thus, if the cam is held fixed, the follower axis will be tangential to the offset circle (with centre at the cam centre and a radius equal to e). The first step is to divide this offset circle into the same number of equal angular intervals as in the displacement diagram, and to locate points $0, 1, \dots, 13$ corresponding to the station points on the follower axis. Then, the trace

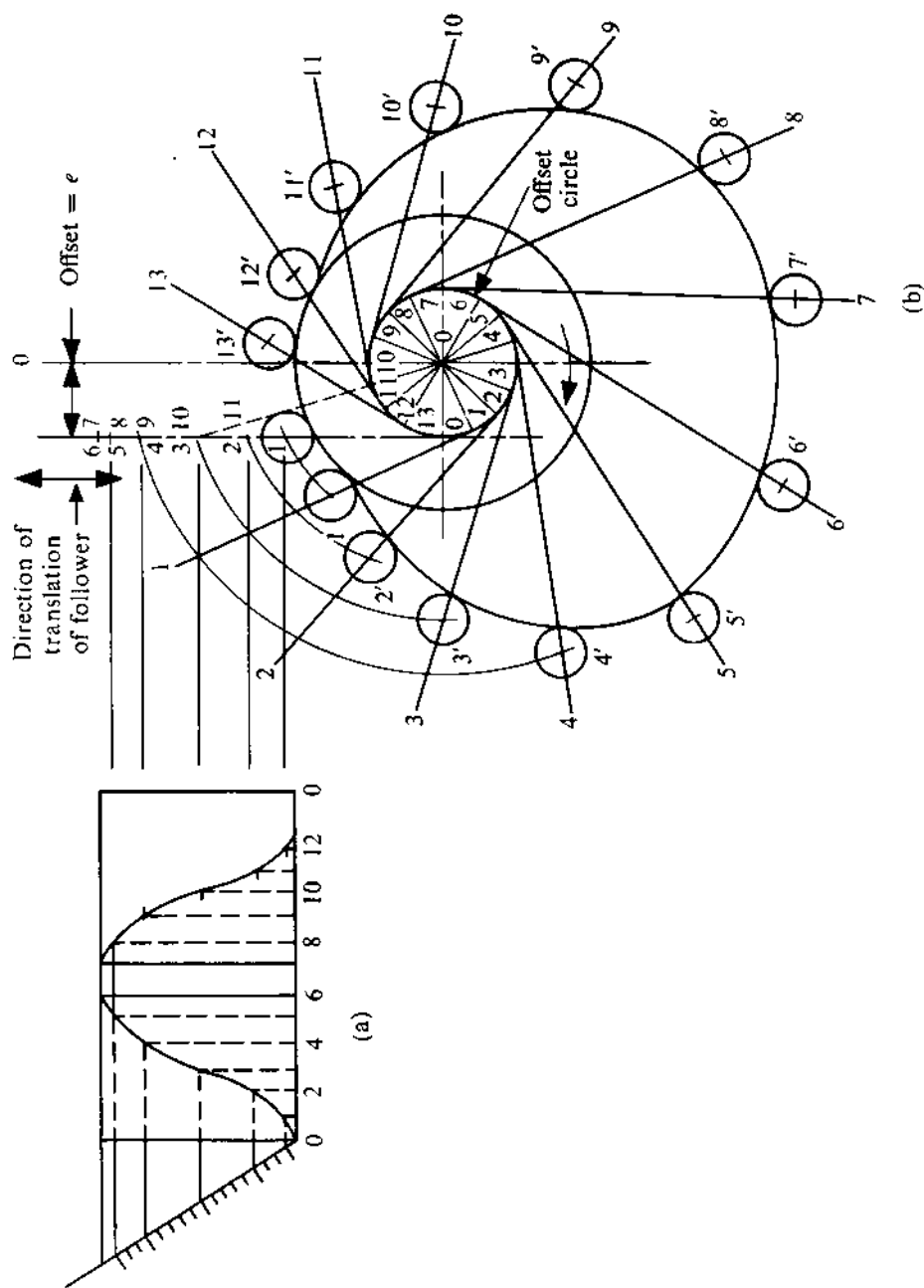


FIGURE 8.18

oints are located on these lines, shown as $1'$, $2'$, $3'$, $4'$, ..., $13'$, as their distances from the cam centre O are known. The rollers are drawn with each of these trace points as centre, and the cam profile is obtained by drawing a curve tangential to the circles representing the rollers.

PROBLEM 8.9

Figure 8.19a shows an oscillating roller follower. The displacement diagram is shown in Fig. 8.19b. The hinge point of oscillation of the follower is C , and the cam centre is at O . The base circle radius of the cam and the radius of the roller are prescribed. It is desired that the follower should oscillate through an angle α when the cam rotates. The oscillation of the follower takes place with modified uniform motion, during both the rise and return phases, as the cam rotates through 150° in each period. The dwell is for 30° at the end of the rise and also at the end of the return. Obtain the cam profile.

SOLUTION

The lift in the displacement diagram is given by $L = R\alpha$, where R is the radius of oscillation of the trace point (i.e., the roller centre). The displacement diagram is completed first, and both the rise and return portions are divided into six equal parts.

The locations of the trace points, corresponding to the station points $0, 1, \dots, 13$, are marked on the arc of oscillation, and designated $0, 1, \dots, 13$. To reduce the error in measuring along the arc, the points should be located successively by measuring the displacements from 0 to 1 , 1 to 2 , to 3 , and so on. Since the displacements are to be measured along the arc, the accuracy will be greater as the number of divisions increases.

Now, holding the cam fixed, the centre of oscillation is rotated in a direction opposite to the rotation of the cam, maintaining a fixed distance from the cam centre O . Thus, C_1, C_2, \dots, C_{13} are the centres of oscillation corresponding to the station points $1, 2, \dots, 13$. Then, the trace points $1', 2', \dots, 13'$ can be located using the fact $C_11' = C_22' = \dots = C_{13}13' = R$. This is explained in Fig. 8.19b for the trace points $1'$, $2'$, and $3'$.

Once the trace points are located, circles are drawn to represent the rollers and the cam profile is obtained as the tangent to all these circles.

3.8 SYNTHESIS OF CAM PROFILE (ANALYTICAL APPROACH)

Though the graphical methods of cam profile synthesis are simple and can lead to quick solutions, the accuracy achieved is low and as such they may not be acceptable in many cases. Furthermore, the easy access to computers has made the analytical procedures more attractive. Not only is the accuracy achieved much higher, it is also very easy to change the design by altering the basic parameters, which is essential to arrive at the optimal design.

If the displacement of the follower y is expressed as a function of the cam rotation θ , i.e., $y = f(\theta)$, then the cam profile can be analytically obtained and expressed in the polar coordinates (r_c, θ_c) in the form of parametric equations, where θ_c is measured from a reference line on the cam and r_c is the corresponding radial distance of the point on the cam from the origin. The basic principle is just the same as that we discussed in the previous section for the graphical approach. In this section, a generalized approach, applied to different configurations, is presented.

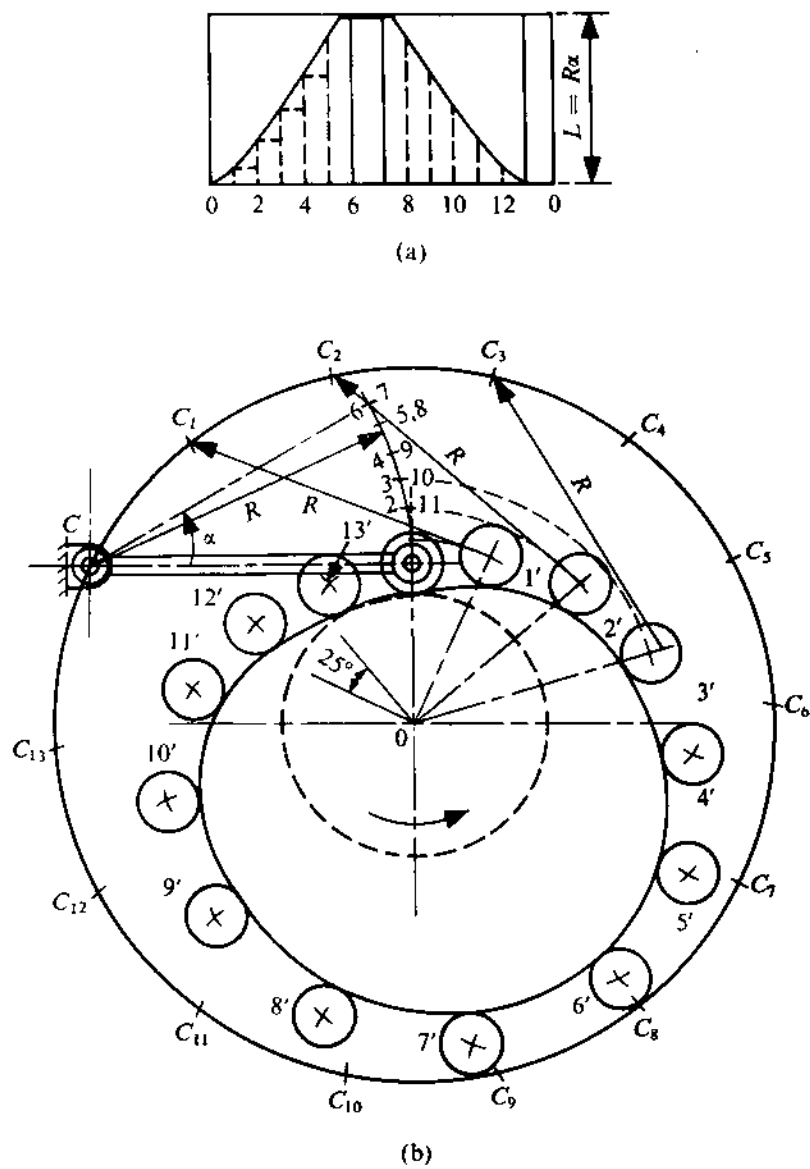


FIGURE 8.19

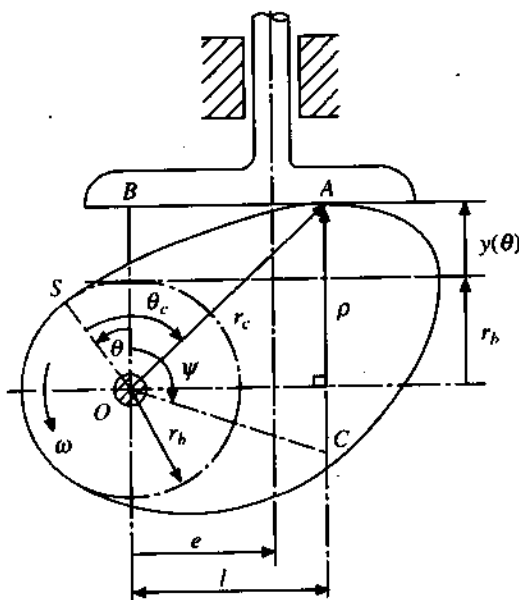


FIGURE 8.20

Flat-face Translating Follower

A cam mechanism with a flat-face translating follower is shown in Fig. 8.20 in which the axis of follower translation is offset from the cam centre O . This figure is very similar to Fig. 8.9. The only difference is that in Fig. 8.20 θ_c and r_c are indicated. Since the line OS is a fixed line on the cam, this can be taken as a reference for measuring θ_c . So, the values of θ_c and the length of the corresponding radius vector r_c (OA) define the cam profile. The simplest way to get the cam profile is to express θ_c and r_c as functions of the cam rotation θ . From Fig. 8.20,

$$\begin{aligned}\theta_c - \theta &= \tan^{-1} (AB/OB) \\ &= \tan^{-1} [l/\{r_b + y(\theta)\}].\end{aligned}$$

Using (8.24), this relation gives

$$\theta_c = \theta + \tan^{-1} [y'(\theta)/\{r_b + y(\theta)\}]. \quad (8.36a)$$

Again, from Fig. 8.20,

$$r_c = (AB^2 + OB^2)^{1/2}$$

or

$$r_c = [\{y'(\theta)\}^2 + \{r_b + y(\theta)\}^2]^{1/2}. \quad (8.36b)$$

The pair of equations (8.36a) and (8.36b) represents the parametric equations of the cam profile. By changing θ from 0° to 360° , the polar coordinates of the points on the cam profile can be found out.

PROBLEM 8.10

In a cam-follower mechanism, the flat-face translating follower rises with cycloidal motion. The total lift is 75 mm and it takes 180° rotation of the cam (CCW). The maximum allowed eccentricity of the driving effort is 25 mm, and to avoid excessive contact stress, the minimum permissible radius of curvature of the cam profile during rise is 60 mm. Synthesize the rise part of the cam profile. What is the minimum offset required?

SOLUTION

The displacement function for the cam (during the rise period) can be found out using (8.15) along with the given data. Thus,

$$y(\theta) = 75 \left(\frac{\theta}{\pi} - \frac{1}{2\pi} \sin 2\theta \right) \text{ mm}, \quad 0 \leq \theta \leq \pi. \quad (\text{a})$$

Differentiating both sides of (a) with respect to θ , we get

$$y'(\theta) = \frac{75}{\pi} (1 - \cos 2\theta) \text{ mm}, \quad 0 \leq \theta \leq \pi, \quad (\text{b})$$

and, after one more differentiation,

$$y''(\theta) = \frac{150}{\pi} \sin 2\theta \text{ mm}, \quad 0 \leq \theta \leq \pi. \quad (\text{c})$$

From (b),

$$[y'(\theta)]_{\max} = \frac{150}{\pi} \text{ mm} = 47.75 \text{ mm}.$$

Using this value in (8.25), we get the minimum required offset as

$$e_{\min} = (47.75 - 25) \text{ mm} = 22.75 \text{ mm}.$$

The minimum base circle radius can be found out using (a) and (c) in (8.23) along with the given data. Thus,

$$r_b \min = 60 - [75(\frac{\theta}{\pi} - \frac{1}{2\pi} \sin 2\theta) + \frac{150}{\pi} \sin 2\theta]_{\min} \text{ mm}.$$

It can be easily shown that, in the interval $0 \leq \theta \leq \pi$, the minimum value of the expression within the square brackets is zero. Hence,

$$r_b = r_b \min = 60 \text{ mm}.$$

With $r_b = 60$ mm, the parametric equation of the cam profile in polar form can be determined from (8.36a) and (8.36b). Then,

$$\theta_c = \theta + \tan^{-1} \left[\frac{75}{\pi} (1 - \cos 2\theta) / \{60 + \frac{75}{\pi} (\theta - \frac{1}{2} \sin 2\theta)\} \right],$$

$$r_c = \left[\left\{ \frac{75}{\pi} (1 - \cos 2\theta) \right\}^2 + \left\{ 60 + \frac{75}{\pi} (\theta - \frac{1}{2} \sin 2\theta) \right\}^2 \right]^{1/2} \text{ mm}.$$

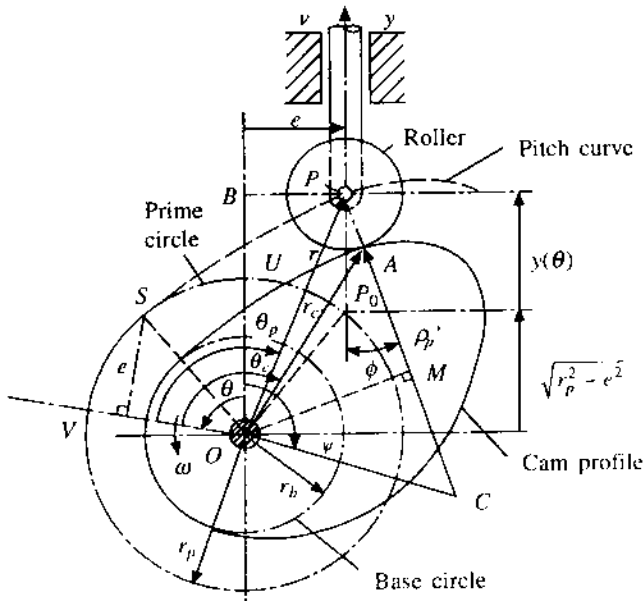


FIGURE 8.21

Translating Roller Follower

Figure 8.21 shows a cam mechanism with an offset-translating follower. In this case, the roller centre P is the trace point. The lowest position of P , represented by P_0 , is at the intersection of the line of translation and the prime circle. The corresponding point on the pitch curve is S . The point U on the prime circle (corresponding to the start of the rise period) rotates to V as the cam rotates through an angle θ and the follower rises by $y(\theta)$, as shown in the figure. So, $\angle UOV = \theta = \angle P_0OS$. The line OV is taken as the reference and the parametric equations of the pitch curve are given by r ($= OP$) and θ_p ($= \angle VOP$) expressed as functions of θ . Thus,

$$\theta_p = \theta + \tan^{-1} (PB/OB)$$

or

$$\theta_p = \theta + \tan^{-1} [e / \{\sqrt{r_p^2 - e^2} + y(\theta)\}]. \quad (8.37a)$$

Again,

$$r = (OB^2 + PB^2)^{1/2}$$

or

$$r = [\{\sqrt{r_p^2 - e^2} + y(\theta)\}^2 + e^2]^{1/2}. \quad (8.37b)$$

The corresponding point on the cam profile is the point A , where the roller touches the cam. The parametric equation of the cam profile can be expressed as

$$\theta_c = \theta + \tan^{-1} [(e + r_R \sin \phi) / \{(r_p^2 - e^2)^{1/2} + y(\theta) - r_R \cos \phi\}], \quad (8.38)$$

$$r_c = [\{(r_p^2 - e^2)^{1/2} + y(\theta) - r_R \cos \phi\}^2 + (e + r_R \sin \phi)^2]^{1/2}, \quad (8.39)$$

where ϕ is determined from (8.30).

PROBLEM 8.11

Synthesize the rise part of the profile of the cam described in Problem 8.6.

SOLUTION

Keeping the conditions and data the same, we have $r_R = 7.5$ mm, $r_b = 10.5$ mm, $r_p = 18$ mm, and $e = 9$ mm. Using these in (8.38a) and (8.38b), the equations for the rise part of the cam profile in parametric form can be expressed as follows.

For $0 \leq \theta \leq \pi/2$,

$$\theta_c = \theta + \tan^{-1} [(9 + 7.5 \sin \phi)/\{15.6 + 100(\theta/\pi)^2 - 7.5 \cos \phi\}], \quad (a)$$

$$r_c = [\{15.6 + 100(\theta/\pi)^2 - 7.5 \cos \phi\}^2 + (9 + 7.5 \sin \phi)^2]^{1/2}, \quad (b)$$

where $\phi = \tan^{-1} [((200\theta/\pi^2) - 9)/\{100(\theta/\pi)^2 + 15.6\}]$.

For $\pi/2 \leq \theta \leq \pi$,

$$\theta_c = \theta + \tan^{-1} [(9 + 7.5 \sin \phi)/\{65.6 - 100(1 - \theta/\pi)^2 - 7.5 \cos \phi\}], \quad (c)$$

$$r_c = [\{65.6 - 100(1 - \theta/\pi)^2 - 7.5 \cos \phi\}^2 + (9 + 7.5 \sin \phi)^2]^{1/2}, \quad (d)$$

where $\phi = \tan^{-1} [((200/\pi)(1 - \theta/\pi) - 9)/\{65.6 - 100(1 - \theta/\pi)^2\}]$.

Varying θ from 0 to π , the values of θ_c and corresponding r_c can be calculated using either (a) and (b) or (c) and (d), depending on the value of θ .

Oscillating Flat-face Follower

The kinematic view of a cam mechanism with an oscillating flat-face follower is shown in Fig. 8.22. The flat face of the oscillating follower is at a distance e from the follower hinge Q whose x - and y -coordinate are a and b , respectively. The cam centre is chosen as the origin of the coordinate system. The point of tangency of the flat face with the cam profile is at A at the instant shown in the figure. At this instant, the follower face makes an angle ψ with the reference line which is chosen to be parallel to the x -axis. The position of the follower face at the beginning of the rise period is indicated by the dashed line making an angle ψ_b with the reference line. The point of tangency at this instant is A_0 as shown, which moves to S when the cam rotates through an angle θ . Correspondingly, the point U (intersection of the cam profile and the y -axis at the beginning of the rise period) moves to V as indicated. Thus, when the cam rotates through an angle θ , the oscillating follower rotates through an angle $\delta(\theta)$ from its lowest position and

$$\psi = \psi_b + \delta(\theta), \quad (8.39)$$

where $\delta(\theta)$ is the displacement function of an oscillating follower. It is simple to show that

$$\psi_b = \sin^{-1} [(e + r_b)/(a^2 + b^2)^{1/2}] - \tan^{-1} (b/a). \quad (8.40)$$

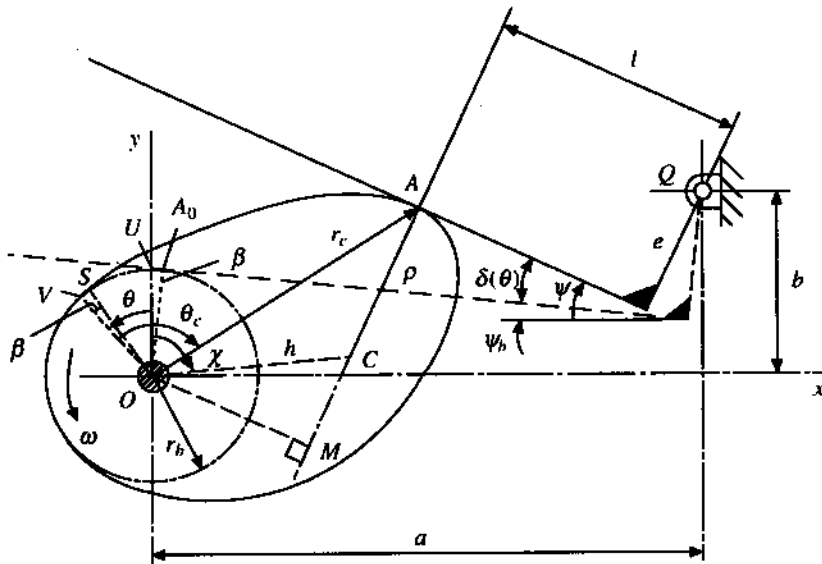


FIGURE 8.22

Since the components of the velocities of two coincident points at \$A\$ (one on the cam and the other being on the follower) along the common normal at \$A\$ are the same, we can write

$$\dot{\psi} \cdot l = \omega \cdot OM, \quad (8.41)$$

where \$OM\$ is the perpendicular dropped on the common normal. From (8.39), \$\dot{\psi} = \delta'(\theta) \cdot \omega\$ and using this in (8.41), we get

$$OM = \delta'(\theta) \cdot l. \quad (8.42)$$

From Fig. 8.22,

$$OM = a \cos \psi - b \sin \psi - l$$

and using this in (8.42), we get

$$l = (a \cos \psi - b \sin \psi) / \{1 + \delta'(\theta)\}. \quad (8.43)$$

The coordinates of the point \$A\$ can be expressed as

$$x_A = a - l \cos \psi - e \sin \psi, \quad (8.44a)$$

$$y_A = b + l \sin \psi - e \cos \psi. \quad (8.44b)$$

Finally, the polar equation of the cam profile in parametric form can be expressed as

$$\theta_c = \theta + \tan^{-1} (x_A / y_A), \quad (8.45a)$$

$$r_c = (x_A^2 + y_A^2)^{1/2}. \quad (8.45b)$$

The centre of curvature of the cam corresponding to the point \$A\$ is at \$C\$ on the common normal \$AM\$ at a distance \$\rho\$ from \$A\$. Taking \$OC = h\$, from the figure, we can write

$$a - e \sin \psi - l \cos \psi - \rho \sin \psi - h \sin \chi = 0,$$

$$b - e \cos \psi + l \sin \psi - \rho \cos \psi - h \cos \chi = 0, \quad (8.46b)$$

where $\angle UOC = \chi$. Differentiating (8.46b) with respect to θ and considering ρ and h as constants (assuming the real cam to be replaced by an instantaneously equivalent circular cam), we get

$$e \sin \psi \cdot \psi' + l \cos \psi \cdot \psi' + l' \sin \psi + \rho \sin \psi \cdot \psi' - h \sin \chi = 0$$

because $\chi' = -1$. Therefore,

$$h \sin \chi = (e \sin \psi + l \cos \psi + \rho \sin \psi) \cdot \psi' + l' \sin \psi. \quad (8.47)$$

Again, differentiating (8.43) with respect to θ , we get (after some algebraic manipulations)

$$l' = -\{(a \sin \psi + b \cos \psi) \cdot \psi' + l \delta''(\theta)\} / \{1 + \delta'(\theta)\}. \quad (8.48)$$

Substituting l from (8.43), $h \sin \chi$ from (8.47), and l' from (8.48) in (8.46a), we can get an expression for the radius of curvature of the cam profile in the form (after some manipulations)

$$\rho = a \sin \psi + b \cos \psi + (a \cos \psi - b \sin \psi) \cdot \psi'' / (1 + \psi')^3. \quad (8.49)$$

PROBLEM 8.12

Derive the equation of the cam profile (rise part) of a mechanism with an oscillating flat-face follower so that the rotational displacement function of the follower is simple harmonic during the rise period. The angular rotation of the follower is 45° and it takes place when the cam rotates through 180° . Following the convention used in Fig. 8.22, the data are given as follows: $r_b = 40$ mm, $a = 200$ mm, $b = 60$ mm, $e = 40$ mm. Also determine the radius of curvature of the cam at the middle of the rise period.

SOLUTION

First, ψ_b is determined using (8.40). Substituting the data, we get

$$\begin{aligned} \psi_b &= \sin^{-1} [80/(200^2 + 60^2)^{1/2}] - \tan^{-1} (60/200) \\ &= (0.393 - 0.291) \text{ rad} \\ &= 0.102 \text{ rad} \end{aligned}$$

or

$$\psi = 0.102 + \delta(\theta) \text{ rad.} \quad (a)$$

The angular displacement function is prescribed to be simple harmonic with a rise of 45° ($\equiv \pi/4$ rad) when the cam rotates through 180° ($\equiv \pi$ rad). Hence, following (8.14),

$$\delta(\theta) = (\pi/8)(1 - \cos \theta) \text{ rad.} \quad (b)$$

Next, using (8.43), the expression for l is found out as

$$l = [200 \cos \{0.102 + (\pi/8)(1 - \cos \theta)\} - 60 \sin \{0.102 + (\pi/8)(1 - \cos \theta)\}] / \{1 + (\pi/8) \sin \theta\}. \quad (c)$$

The coordinates of the point of contact are

$$= 200 - \left[[200 \cos \{0.102 + (\pi/8)(1 - \cos \theta)\} - 60 \sin \{0.102 + (\pi/8)(1 - \cos \theta)\}] / \{1 + (\pi/8) \sin \theta\} \right]$$

$$\times \cos \{0.102 + (\pi/8)(1 - \cos \theta)\} - 40 \sin \{0.102 + (\pi/8)(1 - \cos \theta)\}, \quad (d)$$

$$A = 60 + \left[[200 \cos \{0.102 + (\pi/8)(1 - \cos \theta)\} - 60 \sin \{0.102 + (\pi/8)(1 - \cos \theta)\}] / \{1 + (\pi/8) \sin \theta\} \right] \\ \times \sin \{0.102 + (\pi/8)(1 - \cos \theta)\} - 40 \cos \{0.102 + (\pi/8)(1 - \cos \theta)\}. \quad (e)$$

Finally,

$$\theta_c = \theta + \tan^{-1}(x_A/y_A),$$

$$r_c = (x_A^2 + y_A^2)^{1/2}.$$

If $\theta = 0$ is taken as the beginning of the rise period, then the middle of the rise period implies $\theta = \pi/2$. To estimate the radius of curvature corresponding to this position, we can use (8.49) after determining the values of ψ , ψ' , and ψ'' corresponding to this position. From (a) and (b),

$$\psi = 0.102 + (\pi/8)(1 - \cos \theta) \text{ rad.} \quad (f)$$

Differentiating with respect to θ once and twice, we get ψ' and ψ'' , respectively. Thus,

$$\psi' = (\pi/8) \sin \theta, \quad (g)$$

$$\psi'' = (\pi/8) \cos \theta. \quad (h)$$

Hence, for $\theta = \pi/2$,

$$\psi = 0.495 \text{ rad}, \quad \psi' = 0.393, \quad \psi'' = 0.$$

Using these in (8.49), we get

$$\begin{aligned} \rho &= (200 \sin 0.495 + 60 \cos 0.495 + 0) \text{ mm} \\ &= 147.8 \text{ mm.} \end{aligned}$$

Oscillating Roller Follower

The approach followed to determine the cam profile of a mechanism with an oscillating roller follower is similar to that used in the previous case. Figure 8.23 shows the kinematic features of a cam-follower mechanism with an oscillating roller follower. The lowest position of the follower, making an angle δ_b with the reference line, corresponds to the situation in which the trace point (the roller centre) lies on the prime circle at P_0 . In the position shown, the cam has rotated through an angle θ from the beginning of the rise period. As in the previous case,

$$\psi = \psi_b + \delta(\theta).$$

The x - and y -coordinate of the follower hinge are a and b , respectively, and the coordinates of the trace point P at the instant shown are

$$x_P = a - l \cos \psi, \quad (8.50a)$$

$$y_P = b + l \sin \psi. \quad (8.50b)$$

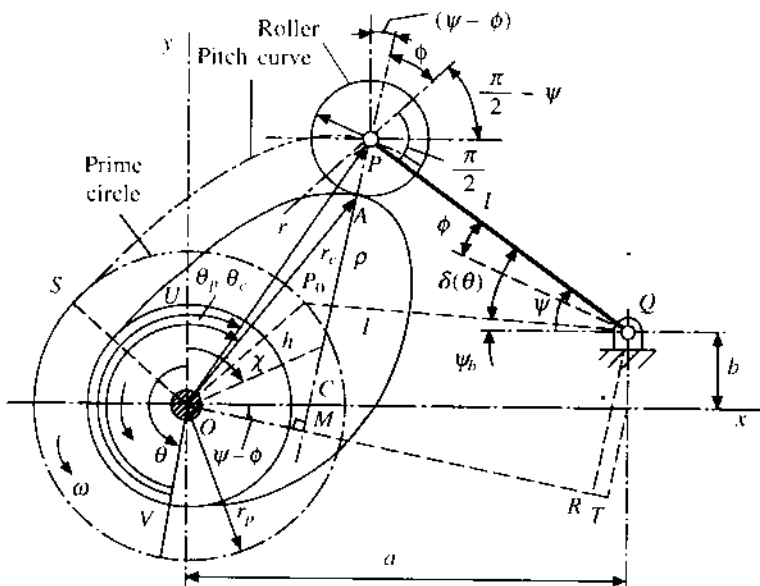


FIGURE 8.23

Since the components of the velocities of the points A (on the cam) and P (the roller centre along the common normal are the same,

$$l\dot{\psi} \cos \phi = OM \cdot \omega$$

or

$$l\dot{\psi}' \cos \phi = OM. \quad (8.51)$$

Again, from the figure,

$$OM = OT - RT - MR$$

or

$$OM = a \cos(\psi - \phi) - b \sin(\psi - \phi) - l \cos \phi.$$

Using this in (8.51), we get

$$l\dot{\psi}' \cos \phi = a \cos(\psi - \phi) - b \sin(\psi - \phi) - l \cos \phi.$$

Rearranging the terms in this relation, we finally get

$$\tan \phi = \{l(1 + \dot{\psi}') - (a \cos \psi - b \sin \psi)\} / (a \sin \psi + b \cos \psi). \quad (8.52)$$

Once ϕ is determined, the coordinates of A can be found out as

$$x_A = x_P - r_R \sin(\psi - \phi), \quad (8.53a)$$

$$y_A = y_P - r_R \cos(\psi - \phi). \quad (8.53b)$$

The polar equations of the cam profile in parametric form become

$$\theta_c = \theta + \tan^{-1} (x_A/y_A), \quad (8.54a)$$

$$r_c = (x_A^2 + y_A^2)^{1/2}. \quad (8.54b)$$

The basic principle for determining the radius of curvature is the same as that followed in the previous cases. From Fig. 8.23, we get

$$a - l \cos \psi - \rho_P \sin (\psi - \phi) - h \sin \chi = 0, \quad (8.55a)$$

where $\rho_P = CP$. We also get

$$b + l \sin \psi - \rho_P \cos (\psi - \phi) - h \cos \chi = 0. \quad (8.55b)$$

Differentiating (8.55b) with respect to θ and using $\chi' = -1$, we obtain

$$h \sin \chi = l \cos \psi \cdot \psi' + \rho_P \sin (\psi - \phi) \cdot (\psi' - \phi').$$

Substituting $h \sin \chi$ from this equation into (8.55a), we get

$$a - l \cos \psi - \rho_P \sin (\psi - \phi) - l \cos \psi \cdot \psi' - \rho_P \sin (\psi - \phi) \cdot (\psi' - \phi') = 0.$$

Rearranging the terms in this equation, we get

$$\rho_P = \{a - l \cos \psi(1 + \psi')\} / \{\sin (\psi - \phi)(1 + \psi' - \phi')\}. \quad (8.56)$$

The radius of curvature of the cam profile

$$\rho = \rho_P - r_R. \quad (8.57)$$

PROBLEM 8.13

In a cam-follower mechanism with an oscillating roller follower, the displacement function of the follower is

$$\delta(\theta) = \frac{\pi}{4} \left[\frac{\theta}{\pi} - \frac{1}{2\pi} \sin 2\theta \right], \quad 0 \leq \theta \leq \pi.$$

The other data using the convention followed are as follows: $a = 200$ mm, $b = 50$ mm, $l = 150$ mm. It is further given that at the lowermost position the follower is parallel to the x -axis. Derive the equation for the rise part of the pitch curve.

SOLUTION

Since it is given that $\psi_b = 0$, it can be easily shown that

$$(a - l)^2 + b^2 = r_p^2. \quad (a)$$

Substituting the values in this equation, we get

$$r_p = 70.7 \text{ mm}.$$

Again,

$$\psi = \delta(\theta) = (\pi/4)[\theta/\pi - (1/2\pi)\sin 2\theta], \quad 0 \leq \theta \leq \pi.$$

From (8.50a) and (8.50b), the coordinates of the points on the pitch curve are

$$x_P = 200 - 150 \cos [(\pi/4)\{\theta/\pi - (1/2\pi)\sin 2\theta\}], \quad (b)$$

$$y_P = 50 + 150 \sin [(\pi/4)\{\theta/\pi - (1/2\pi)\sin 2\theta\}]. \quad (c)$$

If r and θ_P be, respectively, the radius vector and the angle made by it with the reference line OV (Fig. 8.23), then the polar equation of the rise part of the pitch curve in parametric form will be

$$\theta_P = \theta + \tan^{-1}(x_P/y_P), \quad (d)$$

$$r = (x_P^2 + y_P^2)^{1/2}, \quad (e)$$

where x_P and y_P (as functions of θ) are given by (b) and (c), respectively.

8.9 CAMS WITH SPECIFIED CONTOURS

For the mass production of cams, an iterative design approach is taken rather than the synthesis approach discussed in Section 8.7. A trial cam is designed with a combination of simple curves such as straight lines, circular arcs, and involutes. These curves are simple from the manufacturing point of view. The follower movement is analyzed with this trial cam and modifications are introduced in the cam surface till satisfactory follower movement is obtained. Once this is achieved, the master cam thus produced is copied for mass production.

The motion of the follower on two such cams with specified contours is discussed in this section.

Tangent Cam with Radial-translating Roller Follower

The cam profile shown in Fig. 8.24a consists of two straight lines AB and EF (say, of length l) which are tangential to the base circle. The portions BU and EV are circular arcs, each of radius r_2 , with centres at G and D , respectively. The portion UV is also a circular arc with the cam centre as its centre. Thus, when the contact is along UV , the follower will have dwell. The follower movement will be symmetric as the cam profile is symmetric. We will consider the motion of the follower during the rise in two parts, namely,

- (i) when the contact is along the straight flank AB , i.e., $0 \leq \theta \leq \alpha$, θ being the rotation of the cam, and
- (ii) when the contact is along the nose BU , i.e., $\alpha \leq \theta \leq \beta$.

The pitch curve is shown by the dashed line in Fig. 8.24a. The prime circle radius

$$OC = r_p = r_b + r_R,$$

where r_b = base circle radius, and r_R = radius of the roller follower. From Fig. 8.24, we see that

$$\tan \alpha = \frac{CK}{OC} = \frac{AB}{OC} = \frac{l}{r_p} = \frac{l}{r_b + r_R},$$

$$\tan \beta = \frac{GR}{OR} = \frac{AB}{OA - AR} = \frac{l}{r_b - r_2}.$$

The angles α and β can be obtained from these equations.

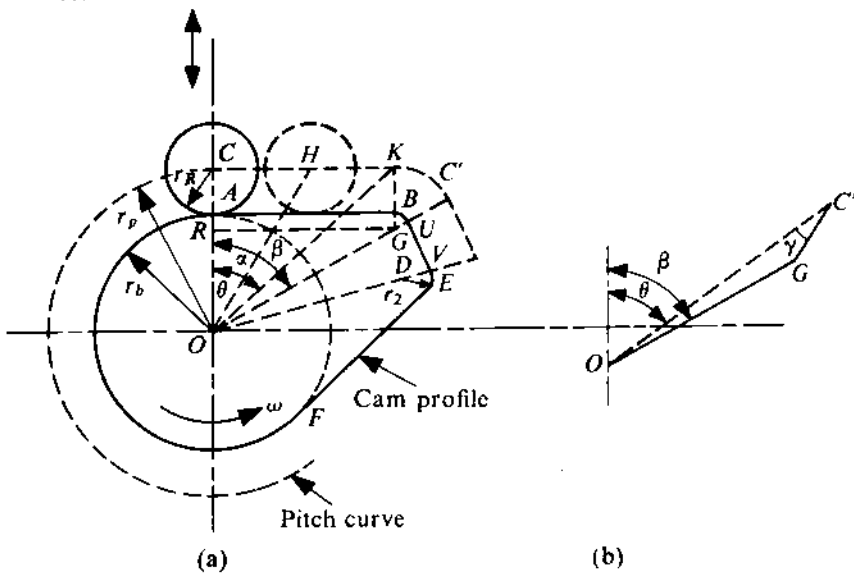
Direction of follower movement


FIGURE 8.24

Displacement Equation for $0 \leq \theta \leq \alpha$

The rise of the follower is

$$y = OH - OC = OC(\sec \theta - 1) = r_p(\sec \theta - 1). \quad (8.58)$$

The velocity of the follower is

$$\begin{aligned} \dot{y} &= \frac{dy}{dt} = \frac{dy}{d\theta} \omega \quad (\text{where } \omega = \text{angular velocity of the cam}) \\ &= \omega \cdot r_p \sec \theta \tan \theta. \end{aligned} \quad (8.59)$$

The acceleration, jerk, etc., of the follower can be similarly obtained.

Displacement Equation for $\alpha \leq \theta \leq \beta$

The distance of the roller centre C' from the point G remains constant during contact along the nose. So, the motion is equivalent to a slider-crank mechanism with OG as the crank and GC' as the connecting rod (Fig. 8.24b). The rise of the follower is

$$\begin{aligned} y &= OC' - OC = OG \cos(\beta - \theta) + GC' \cos \gamma - r_p \\ &= (r_b - r_2) \sec \beta \cos(\beta - \theta) + (r_2 + r_R) \cos \gamma - r_p, \end{aligned} \quad (8.60)$$

where

$$\sin \gamma = \frac{OG \sin(\beta - \theta)}{GC'}. \quad (8.61)$$

The lift of the follower is obtained by putting $\gamma = 0$ and $\theta = \beta$ in (8.60), that is,

$$L = (r_b - r_2) \sec \beta + (r_2 + r_R) - r_p = (r_b - r_2) \sec \beta + r_2 - r_b. \quad (8.62)$$

The velocity of the follower is $\dot{y} = \omega(dy/d\theta)$. Using (8.60), we get

$$\dot{y} = \omega[(r_b - r_2) \sec \beta \sin(\beta - \theta) - GC' \sin \gamma(d\gamma/d\theta)]. \quad (8.63)$$

Differentiating (8.61) with respect to θ , we get

$$\cos \gamma \frac{d\gamma}{d\theta} = -\frac{OG}{GC'} \cos(\beta - \theta).$$

Again, using (8.61) to replace $\cos \gamma$ in this equation, we get

$$\frac{d\gamma}{d\theta} = -\frac{OG}{GC'} \frac{\cos(\beta - \theta)}{[1 - (OG^2/GC'^2) \sin^2(\beta - \theta)]^{1/2}}.$$

Now, from (8.63) and this equation, we have

$$\dot{y} = \omega[(r_b - r_2) \sec \beta \sin(\beta - \theta) + \frac{OG^2}{GC'} \frac{\sin(\beta - \theta) \cos(\beta - \theta)}{[1 - (OG^2/GC'^2) \sin^2(\beta - \theta)]^{1/2}}], \quad (8.64)$$

where $OG = (r_b - r_2) \sec \beta$ and $GC' = r_2 + r_R$.

Circular-arc Cam with Radial-translating Flat-face Follower

The cam profile shown in Fig. 8.25a consists of circular arcs of radii r_b (base circle radius), r_1 , and r_2 (nose radius). α is the angle of cam rotation during the rise. Here also, the displacement equation will be derived in two parts, namely,

- (i) when the contact is along the circular arc of radius r_1 (centre at P), i.e., when $0 \leq \theta \leq \beta$, and
- (ii) when the contact is along the circular arc of radius r_2 (centre at Q), i.e., when $\beta \leq \theta \leq \alpha$.

Displacement Equation for $0 \leq \theta \leq \beta$

From Fig. 8.25a, we see that the rise of the follower is

$$\begin{aligned} y &= OB - OA = DE - OA = PE - PD - OA = PA - OP \cos \theta - OA \\ &= OP(1 - \cos \theta) = (r_1 - r_b)(1 - \cos \theta). \end{aligned} \quad (8.65)$$

The velocity of the follower is

$$\dot{y} = \omega(r_1 - r_b) \sin \theta. \quad (8.66)$$

Displacement Equation for $\beta \leq \theta \leq \alpha$

From Fig. 8.25b, the rise of the follower is

$$\begin{aligned} y &= OB - OA = GD - OA = GQ + QD - OA \\ &= GQ + OQ \cos(\alpha - \theta) - OA = (r_2 - r_b) + OQ \cos(\alpha - \theta). \end{aligned} \quad (8.67)$$

The lift will be given by

$$L = (r_2 - r_b) + OQ \quad (\text{when } \theta = \alpha). \quad (8.68)$$

The velocity of the follower, from (8.67), is

$$\dot{y} = \omega OQ \sin(\alpha - \theta). \quad (8.69)$$

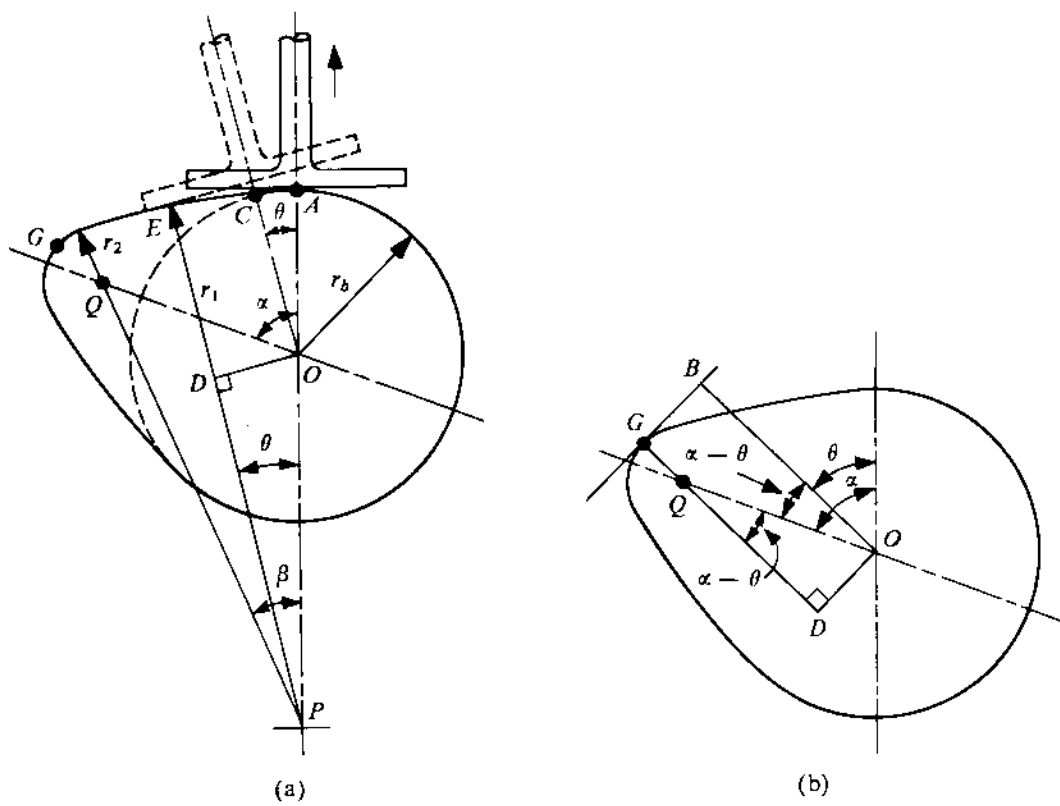


FIGURE 8.25

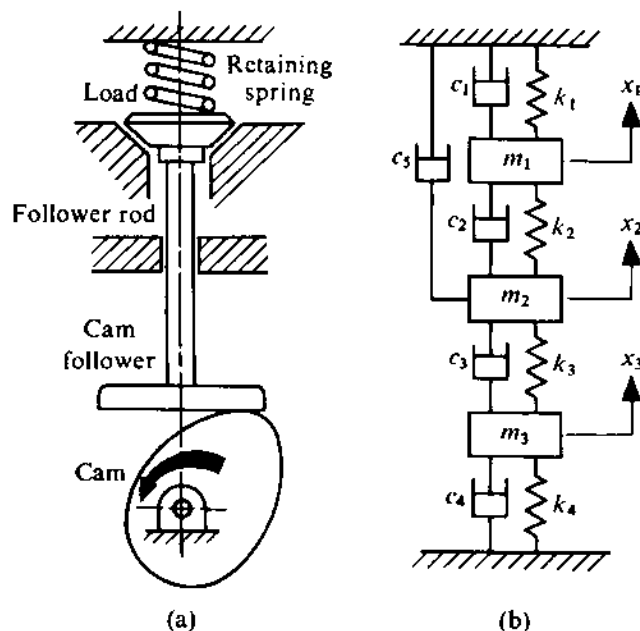


FIGURE 8.26

8.10 DYNAMIC ANALYSIS OF CAMS

For high-speed cam mechanisms, kinematic analysis alone may not be sufficient to ensure the faithful reproduction of the follower motion. Although ideally the elements of a cam mechanism are considered to be rigid, in fact they are not so. Depending on flexibility and mass distribution, the follower train possesses a definite dynamic response characteristic, which may play a very predominant role in high-speed cams. In this section, we shall discuss problems involving the dynamic analysis of cam mechanisms.

As the mathematical treatment of an actual system is extremely complicated, mathematical modelling of the whole mechanism is necessary. So, we will first formulate a simple mathematical model of a cam-follower system. Figure 8.26a shows a typical cam-follower system which consists of (i) bearings, (ii) cam shaft, (iii) cam, (iv) cam follower, (v) follower rod, (vi) load, and (vii) retaining spring. A fairly accurate mathematical model of this system of elastic components is shown in Fig. 8.26b, in which \$m_1\$ is the inertia of the load, moving against a spring of stiffness \$k_1\$. The motion of the load is represented by \$x_1\$. The inertia of the follower train is represented by \$m_2\$ and the elasticity is represented by \$k_2\$ and \$k_3\$. The cam mounted on the cam shaft is represented by \$m_3\$ supported on a spring of stiffness \$k_4\$.

In spite of this idealization of the actual system, the solution is not very easy. Therefore, further simplification of the mathematical model is necessary. Generally, the rigidity of the cam shaft is much higher than that of the other components of the mechanism. Assuming the cam shaft to be absolutely rigid, the system will be replaced by one which has two degrees of freedom as shown in Fig. 8.27a, where the motion machined into the cam surface is represented by \$y\$. Reducing the load and the entire follower train into a single mass \$m\$, the system can be further simplified so that it has a single degree of freedom as shown in Fig. 8.27b. Neglecting the damping involved, we get a simple system as shown in Fig. 8.27c. For preliminary analysis, this system is very convenient. But

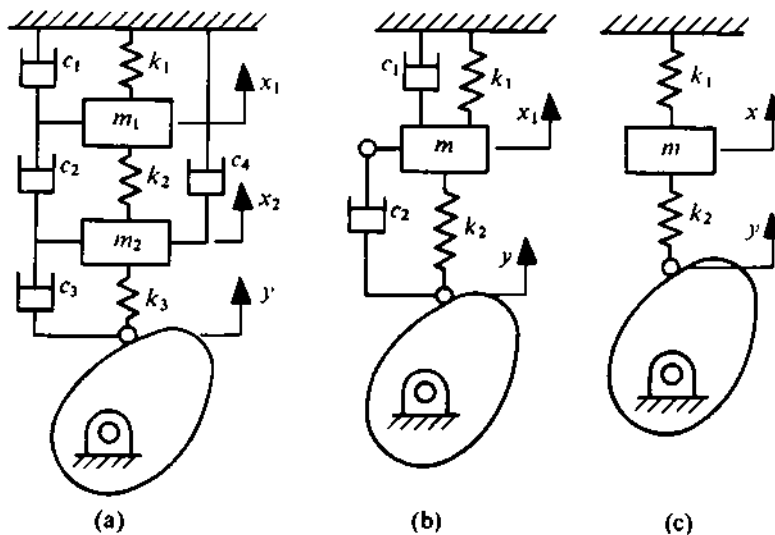


FIGURE 8.27

When the preliminary design is over, the analysis of the damped system is necessary.

Now, the objective of the dynamic analysis of the cam system is to determine the response x when y is known as a function of time. Both analytical and numerical methods are presented here for the simple undamped system shown in Fig. 8.27c.

Response of Undamped Cam Mechanism (Analytical Method)

The free-body diagrams of the springs and the mass are shown in Fig. 8.28. Considering the inertia force of the mass ($-m\ddot{x}$) along with the other forces on the mass, the dynamic equilibrium equation becomes

$$\begin{aligned} m\ddot{x} + k_1x - k_2(y - x) &= 0, \\ \ddot{x} + \left(\frac{k_1 + k_2}{m}\right)x &= \frac{k_2}{m}y(t). \end{aligned} \quad (8.70)$$

When $y(t)$ is known, the solution of (8.70) can be obtained. The form of the general solution will be

$$x(t) = A \cos \omega_n t + B \sin \omega_n t + (\text{particular integral}), \quad (8.71)$$

here $\omega_n = [(k_1 + k_2)/m]^{1/2}$, and the particular integral depends on the function $y(t)$. A and B are constants to be determined from the starting conditions. As a specific case, let us consider a cam profile which gives a uniform rise for an angle of rotation θ_{ri} followed by a dwell. The total lift or rise is L and the cam rotates with a constant angular velocity ω . Then, at any instant of time t , when $\theta = 0$, we have

$$y(t) = \frac{L}{\theta_{ri}}\theta = \frac{L}{\theta_{ri}}\omega t. \quad (8.72)$$

The particular integral in this case will be

$$\frac{k_2 L \omega t}{m \theta_{ri} \omega_n^2} = \frac{k_2 y}{m \omega_n^2}.$$

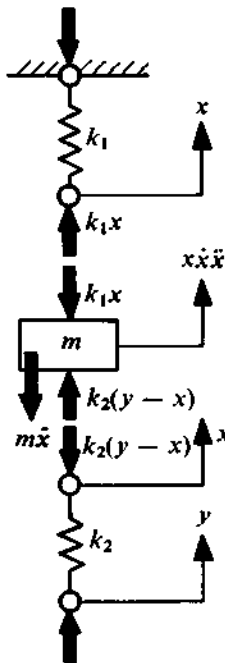


FIGURE 8.28

So, from (8.71), the general solution for $x(t)$ will be

$$x(t) = A \cos \omega_n t + B \sin \omega_n t + \frac{k_2 y}{m \omega_n^2}. \quad (8.73)$$

This particular integral is called the *follower command*. Now, with the initial conditions $t = 0$ and $x = \dot{x} = 0$, the final solution becomes

$$x(t) = \frac{k_2}{m \omega_n^2} \left(y - \frac{\dot{y}}{\omega_n} \sin \omega_n t \right), \quad \dot{x}(t) = \frac{k_2}{m \omega_n^2} \left(\dot{y} - \ddot{y} \cos \omega_n t \right), \quad (8.74)$$

where $\dot{y} = L\omega/\theta_{ri} = \text{constant}$. Replacing ω_n/ω in (8.74) by λ and since $t = \theta/\omega$, we get

$$x(\theta) = \frac{k_2 L}{\lambda m \omega_n^2 \theta_{ri}} (\lambda \theta - \sin \lambda \theta), \quad \dot{x}(\theta) = \frac{k_2 L}{\lambda m \omega_n \theta_{ri}} (1 - \cos \lambda \theta). \quad (8.75)$$

When $\theta = \theta_{ri}$, i.e., at the end of the rise, we get

$$x_{\theta_{ri}} = \frac{k_2 L}{\lambda m \omega_n^2 \theta_{ri}} (\lambda \theta_{ri} - \sin \lambda \theta_{ri}), \quad \dot{x}_{\theta_{ri}} = \frac{k_2 L}{\lambda m \omega_n \theta_{ri}} (1 - \cos \lambda \theta_{ri}). \quad (8.76)$$

During the dwell, y remains constant and equal to L . So, the solution of (8.70) for this phase will be

$$x(t') = A' \cos \omega_n t' + B' \sin \omega_n t' + \frac{k_2 L}{m \omega_n^2}, \quad (8.77)$$

where time t' is counted from the start of the dwell. The initial conditions for $t' = 0$ will be

$$x = x_{\theta_{ri}} = \frac{k_2 L}{\lambda m \omega_n^2 \theta_{ri}} (\lambda \theta_{ri} - \sin \lambda \theta_{ri}), \quad \dot{x} = \dot{x}_{\theta_{ri}} = \frac{k_2 L}{\lambda m \omega_n \theta_{ri}} (1 - \cos \lambda \theta_{ri}).$$

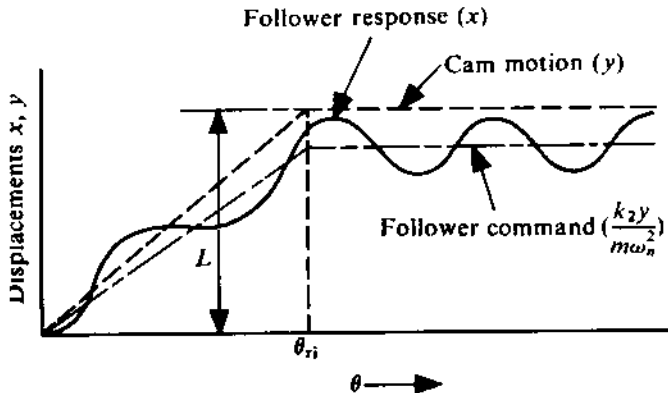


FIGURE 8.29

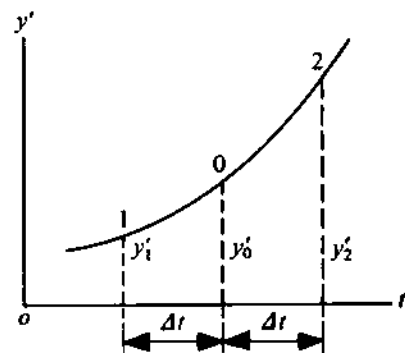


FIGURE 8.30

The corresponding expressions for A' and B' will be

$$A' = \frac{k_2 L}{\lambda m \omega_n^2 \theta_{ri}} (\lambda \theta_{ri} - \sin \lambda \theta_{ri}) - \frac{k_2 L}{m \omega_n^2}, \quad B' = \frac{k_2 L}{\lambda m \omega_n^2 \theta_{ri}} (1 - \cos \lambda \theta_{ri}).$$

Thus, the solution for the dwell period will be

$$x = \left[\frac{k_2 L}{\lambda m \omega_n^2 \theta_{ri}} (\lambda \theta_{ri} - \sin \lambda \theta_{ri}) - \frac{k_2 L}{m \omega_n^2} \right] \cos \omega_n t' + \frac{k_2 L}{\lambda m \omega_n^2 \theta_{ri}} (1 - \cos \lambda \theta_{ri}) \sin \omega_n t' + \frac{k_2 L}{m \omega_n^2}. \quad (8.78)$$

The response of the follower, the cam motion y , and the follower command are shown in Fig. 8.29. The follower command is different from the cam motion because of the finite elasticity of the follower train. When the model has only a single degree of freedom, the follower command is

$$y'(t) = \frac{k_2}{m \omega_n^2} y(t) = \frac{k_2}{k_1 + k_2} y(t). \quad (8.79)$$

From this expression for the follower command, it is seen that the greater the follower-train stiffness k_2 , the smaller will be the difference between the cam motion and the follower command. When $k_2 \gg k_1$, the follower command $y'(t)$ approaches $y(t)$.

Cam-follower Response (Numerical Method)

In some situations, a numerical method for the determination of cam-follower response may be useful, particularly when the geometry is complicated or a high degree of accuracy is required, as such a method is amenable to computer programming. The method developed by R. C. Johnson is described here.

A portion of the follower-command curve is shown in Fig. 8.30. Considering the three points 1, 0, and 2 on this curve, and taking the time interval to be Δt as shown, the rate of change of the follower command at point 0 will be

$$\dot{y}'_0 = \frac{y'_2 - y'_1}{2 \Delta t}. \quad (8.80)$$

When the cam rotates with a constant angular velocity ω , the cam rotation $\Delta\theta$ during the period Δt will be $\omega \Delta t$. Thus, $\Delta t = \Delta\theta/\omega$ and, from (8.80), we get

$$\dot{y}_0 = \frac{\omega}{\Delta\theta} \left(\frac{y'_2 - y'_1}{2} \right). \quad (8.81)$$

Similarly, if P and Q are the midpoints of each time interval Δt , the rate of change of follower command at these points will be

$$\dot{y}'_P = \frac{y'_0 - y'_1}{\Delta t}, \quad \dot{y}'_Q = \frac{y'_2 - y'_0}{\Delta t}.$$

Therefore, at 0, we get

$$\ddot{y}'_0 = \frac{\dot{y}'_Q - \dot{y}'_P}{\Delta t} = \frac{\frac{y'_2 - y'_0}{\Delta t} - \frac{y'_0 - y'_1}{\Delta t}}{\Delta t} = \frac{1}{\Delta t^2} (y'_1 + y'_2 - 2y'_0).$$

Since $\Delta t = \Delta\theta/\omega$, we finally get

$$\ddot{y}'_0 = \left(\frac{\omega}{\Delta\theta}\right)^2 (y'_1 + y'_2 - 2y'_0). \quad (8.82)$$

Similar equations can be written for x . Thus,

$$\dot{x}_0 = \frac{\omega}{\Delta\theta} \left(\frac{x_2 - x_1}{2}\right), \quad (8.83)$$

$$\ddot{x}_0 = \left(\frac{\omega}{\Delta\theta}\right)^2 (x_1 + x_2 - 2x_0). \quad (8.84)$$

Now, the dynamic equilibrium equation of the cam-follower system can be written in the finite-difference form by substituting the expressions for x , \ddot{x} , and y at station 0 in (8.70). For station 0, the equation is

$$\ddot{x}_0 = -\left(\frac{k_1 + k_2}{m}\right)x_0 + \frac{k_2}{m}y_0. \quad (8.85)$$

From (8.79), we get

$$y = \frac{k_1 + k_2}{k_2}y'.$$

So, (8.85) takes the form

$$\ddot{x}_0 = -\left(\frac{k_1 + k_2}{m}\right)x_0 + \left(\frac{k_1 + k_2}{m}\right)y'_0 = \left(\frac{k_1 + k_2}{m}\right)(y'_0 - x_0). \quad (8.86)$$

Substituting the expression for \ddot{x}_0 from (8.84) in (8.86), we get

$$\begin{aligned} \frac{\omega^2}{\Delta\theta^2}(x_1 + x_2 - 2x_0) &= \left(\frac{k_1 + k_2}{m}\right)(y'_0 - x_0), \\ x_2 &= \frac{\Delta\theta^2(k_1 + k_2)(y'_0 - x_0)}{m\omega^2} + 2x_0 - x_1. \end{aligned} \quad (8.87)$$

This equation gives the value of x_2 when x_1 and x_0 are known and y'_0 , $\Delta\theta$, m , ω , k_1 , and k_2 are prescribed. When x_2 is determined, this value is used as the value of x_0 in the next step. Similarly, the value of x_0 is used as x_1 and the new value of x_2 is calculated. The process is repeated to determine the follower response. For every step, a proper value of y'_0 should be used for the calculation. The procedure is explained by the solution of Problem 8.14.

PROBLEM 8.14

A dwell-rise-dwell cam has a 3-cm rise with uniform velocity for 120° of cam rotation. The follower is assembled with a retaining spring with sufficient precompression, the stiffness of the spring being 40 N/cm. The equivalent mass and stiffness of the follower train are 0.27 kg and 700 N/cm, respectively. Determine the follower response when the cam rotates with a speed of 3500 rpm.

SOLUTION

To start with, the step $\Delta\theta$ should be selected such that the time required for the cam to rotate through this angle is less than that for the system to undergo one complete cycle of free oscillation. Rather, one complete cycle of vibration should be represented by a sufficiently large number of these steps.

As $k_1 = 40,000$ N/m and $k_2 = 700,000$ N/m, the natural frequency of the system is

$$\omega_n = \left(\frac{k_1 + k_2}{m} \right)^{1/2} = \left(\frac{740,000}{0.27} \right)^{1/2} \text{ rad/s} \approx 1660 \text{ rad/s.}$$

The angular velocity of the cam is

$$\omega = \frac{2\pi \times 3500}{60} \approx 367 \text{ rad/s.}$$

Therefore,

$$\lambda = \frac{\omega_n}{\omega} = \frac{1660}{367} \approx 4.25.$$

So, for one complete cycle of system oscillation, the cam rotates through an angle $\theta_n = 360^\circ / 4.25 \approx 84.8^\circ$.

The value of $\Delta\theta$ is selected so that there may be seven or eight steps for one complete cycle of oscillation. If $\Delta\theta$ is assumed to be 10° ($= \pi/18$), equation (8.87) will take the form

$$x_2 = \frac{(\pi/18)^2 \times 740,000}{367^2 \times 0.27} (y'_0 - x_0) + 2x_0 - x_1 \approx 0.62(y'_0 - x_0) + (2x_0 - x_1).$$

Now, if the follower command y' is expressed in terms of the given cam motion y , we get

$$\begin{aligned} y' &= \frac{k_2}{k_1 + k_2} y = 0.946y \\ &= 0.946 \left(\frac{3}{120} \right) \theta \quad (\text{assuming } \theta = 0 \text{ when the rise starts}). \end{aligned}$$

The step-by-step calculation to determine x is shown in Table 8.1. As the quantity $(x_1 + x_2 - 2x_0)$ is a measure of the acceleration of the mass, this has also been tabulated. For the first step in this table, $x = 0$, $y = 0$, and $y' = 0$ when $\theta = 0$. In the second step also, $x = 0$. Thereafter, x is calculated from the relation

$$x_2 = 0.62(y'_0 - x_0) + (2x_0 - x_1),$$

i.e., the values of x for any step are obtained by adding the fifth and sixth columns of the previous step. The sixth column in any step is the difference between twice the value of x in that step and the value of x in the previous step. Similarly, the seventh column for any step is obtained as the difference between twice the value of x in that step and the sum of the values of x in the preceding and succeeding steps.

It should be remembered that y' remains unchanged after the cam has rotated through 120° . The results are shown in Fig. 8.31.

TABLE 8.1

θ (degrees)	y' (cm)	x (cm)	$y'_0 - x_0$ (cm)	$0.62(y'_0 - x_0)$ (cm)	$2x_0 - x_1$ (cm)	$x_1 + x_2 - 2x_0$ (cm)
1	2	3	4	5	6	7
0	0	0	0	0	0	0
10	0.237	0	0.237	0.147	0	0.147
20	0.474	0.147	0.327	0.203	0.294	0.203
30	0.711	0.497	0.214	0.137	0.847	0.137
40	0.948	0.984	-0.036	-0.022	1.471	-0.022
50	1.185	1.449	-0.264	-0.164	1.914	-0.164
60	1.422	1.750	-0.328	-0.203	2.051	-0.203
70	1.659	1.848	-0.189	-0.117	1.946	-0.117
80	1.896	1.829	0.067	0.041	1.810	0.041
90	2.133	1.851	0.282	0.175	1.873	0.175
100	2.360	2.048	0.312	0.193	2.245	0.193
110	2.597	2.438	0.159	0.099	2.828	0.099
120	2.834	2.927	-0.093	-0.058	3.416	-0.058
130	2.834	3.358	-0.524	-0.325	3.789	-0.325
140	2.834	3.464	-0.630	-0.391	3.570	-0.391
150	2.834	3.179	-0.345	-0.214	2.894	-0.214
160	2.834	2.680	0.154	0.095	2.181	0.095
170	2.834	2.276	0.558	0.346	1.872	0.346
180	2.834	2.218				

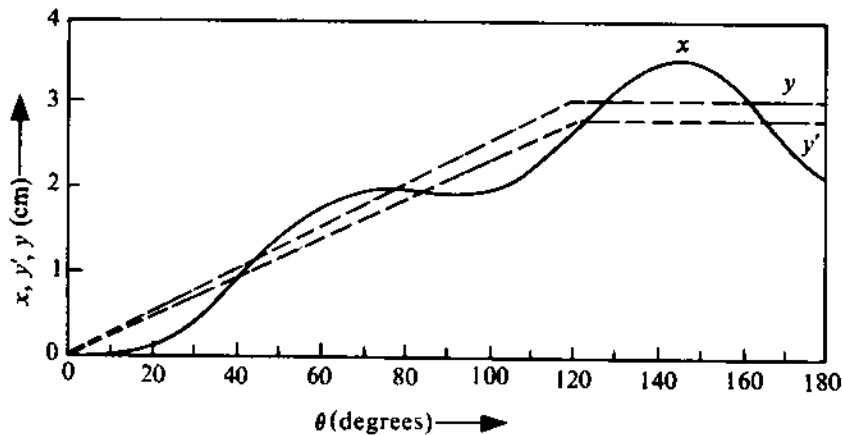


FIGURE 8.31

Cam Synthesis (Numerical Method)

We have just seen how the numerical method can be used for determining the follower response when the cam profile and cam speed are given. The same principle can be adopted for arriving at the cam shape which will produce a prescribed follower response for a particular cam speed.

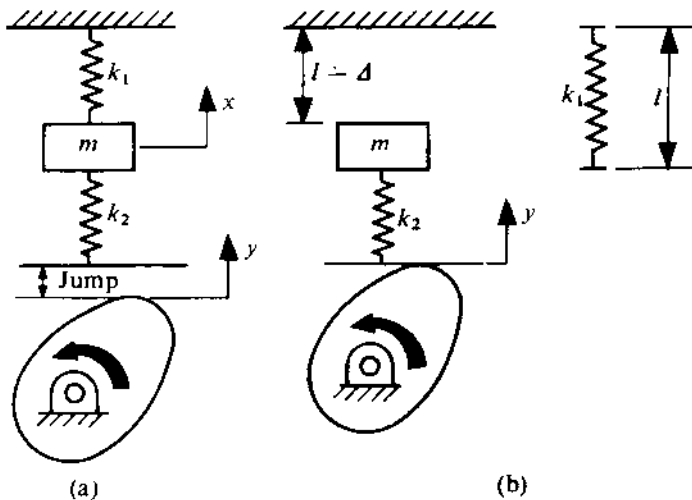


FIGURE 8.32

Equation (8.87) can be rewritten in the form

$$y'_0 = x_0 + \frac{m}{k_2} \left(\frac{\omega}{\Delta\theta} \right)^2 (x_1 + x_2 - 2x_0).$$

We also have

$$y = \left(\frac{k_1 + k_2}{k_2} \right) y'_0.$$

Hence, we finally get

$$y_0 = \frac{k_1 + k_2}{k_2} [x_0 + \frac{m}{k_2} \left(\frac{\omega}{\Delta\theta} \right)^2 (x_1 + x_2 - 2x_0)]. \quad (8.88)$$

When the follower motion is specified, we can find x_1 , x_0 , and x_2 for every station. Using (8.88), the corresponding value of y can be calculated. It should be remembered that both (8.87) and (8.88) will not hold good when the follower loses its contact with the cam surface, i.e., when the follower jumps. During the jump period, the spring k_2 will be ineffective, and (8.87) and (8.88) should be modified accordingly.

Jump and Cross-over Shock

It has been mentioned previously that the follower is kept pressed against the cam surface by means of a retaining spring. Under certain conditions, the follower may lose this contact with the cam. This phenomenon is called the *jump*. For the duration of the jump, i.e., when the follower is not in contact with the cam surface, only the retaining spring is active and the natural frequency of the system changes. Figure 8.32a shows a model of a cam-follower system with a single degree of freedom. The spring k_2 loses contact with the cam and is carried with the mass during the jump. This change in the natural frequency should be taken into account when (8.87) is derived for the numerical procedure.

We shall now find the condition for which the jump occurs. It is obvious that whenever the distance of the mass from the cam (i.e., from the relevant point which transmits motion to the follower, depending on the type of follower) is more than the natural length of the spring k_2 , the

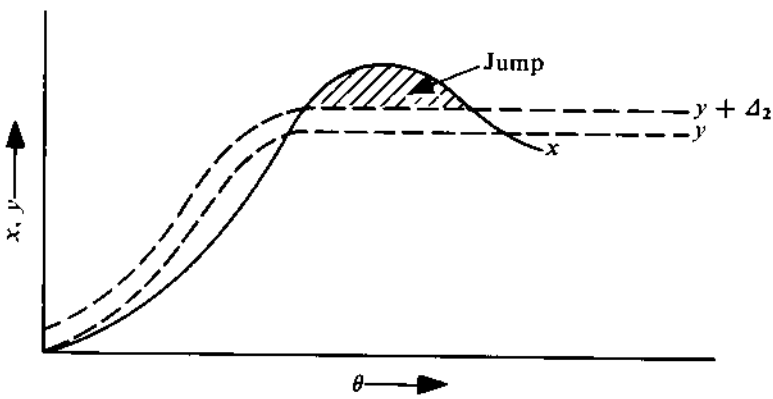


FIGURE 8.33

contact will be lost and jump will occur. In other words, the jump will take place whenever the compression of the spring k_2 is zero. Let us consider the case shown in Fig. 8.32b where the retaining spring (of natural length l) is assembled in a space ($l - \Delta$). This space is available when the spring k_2 is under no compression. So, after assembly, both springs will be under compression and the compressive forces on both springs must be the same (neglecting the weight of m). If the compression in the spring k_2 is Δ_2 , then the compressive force will be $k_2\Delta_2$. Again, as the original space available for the retaining spring was $(l - \Delta)$, after assembly, the length of the retaining spring will be $(l - \Delta + \Delta_2)$. So, the amount of compression for the retaining spring will be $(\Delta - \Delta_2)$ with a corresponding compressive force $k_1(\Delta - \Delta_2)$. Since the forces in the spring have to be equal, we get

$$k_1(\Delta - \Delta_2) = k_2\Delta_2,$$

$$\Delta_2 = \frac{k_1}{k_1 + k_2}\Delta. \quad (8.89)$$

Now, Δ_2 is the precompression of the spring k_2 , i.e., when both x and y are zero. So, the jump will occur when

$$x > y + \frac{k_1}{k_1 + k_2}\Delta. \quad (8.90)$$

The follower response is shown in Fig. 8.33. To investigate the jump, the curve showing the variation in $(y + \Delta_2)$ with time should also be plotted. Whenever x becomes more than $y + \Delta_2$, a jump will occur as shown in the figure by the hatched area.

In case of positive-acting cams, jump does not occur but *cross-over shocks* are felt whenever the acceleration changes direction. If there is any backlash, it will be accompanied by an *impact* when the contact point changes from one side to the other. The impact can be reduced by eliminating the effect of backlash with the proper amount of preloading.

8.11 SPATIAL CAM-FOLLOWER MECHANISMS

In the case of a spatial cam-follower mechanism, the motions of the points on the follower and the cam do not lie on parallel planes. Though there exists a wide variety of such mechanisms, one of the most commonly-used spatial cam mechanisms is the cylindrical cam-follower mechanism. As the cylindrical surfaces can be easily developed onto a flat surface, the design and fabrication of such cams are relatively simpler.

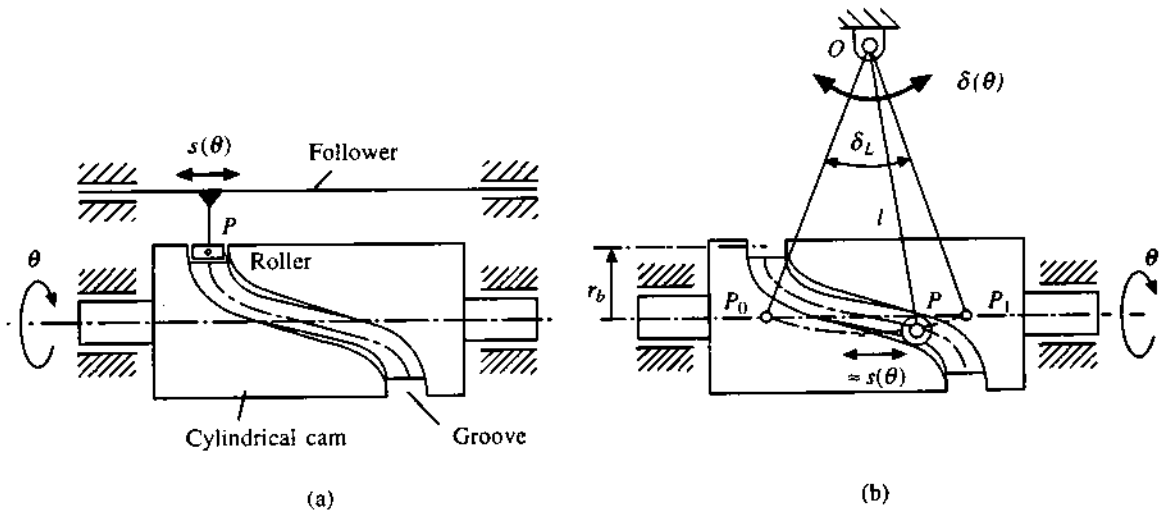


FIGURE 8.34

Figures 8.34a and 8.34b show a cylindrical cam-follower mechanism with translating and oscillating roller followers, respectively. In both the cases, the information about the required motion of the follower is encoded on the cylindrical surface of the cam in the form of a groove of uniform width and depth to accommodate the roller. The width of the groove is equal to the roller diameter. In case of the translating follower, the trace point P (the centre of the roller) moves in a straight line as shown in Fig. 8.34a and its displacement $s(\theta)$ is a function of the cam rotation θ . When the system has an oscillating roller follower (Fig. 8.34b), the trace point P moves in a circular arc. To achieve the best result, the configuration is so designed that the extreme positions of the trace point, P_0 and P_1 , lie on the tangent between the cylindrical cam surface and the plane in which the follower moves. The radius of the cylinder passing through the middle of the groove, r_b , is considered equivalent to the base circle radius of a disc cam system. The trace point is also taken on the middle of the roller axis so that P_0 and P_1 lie on the imaginary cylindrical surface with radius r_b . All analyses and calculations are done with reference to this base cylinder. In most cases, the circular path of the trace point does not deviate much from the line P_0P_1 as the follower link length, l , is generally much larger than the distance P_0P_1 and, therefore, it is possible to derive approximate relations assuming the displacement to be a straight line and approximately represented by $s(\theta)$ as indicated in the figure.

Pressure Angle and Minimum Base Cylinder Radius

A simple relation can be derived to estimate the minimum required base cylinder radius so that the pressure angle does not exceed a prescribed maximum value. The analysis is exact in case of translating followers and it is approximate in case of oscillating followers.

When the base cylinder is developed, the centreline of the groove lying on the base cylinder develops into a plane curve as shown in Fig. 8.35. The displacement of the trace point $s(\theta)$ is indicated against $r_b\theta$. At any instant, the velocity of the trace point P is along the $s(\theta)$ -axis and the force, F , exerted by the groove on the roller is normal to the developed groove centreline (assuming negligible friction). In case of translating follower, $s(\theta)$ is the exact displacement. If the follower is

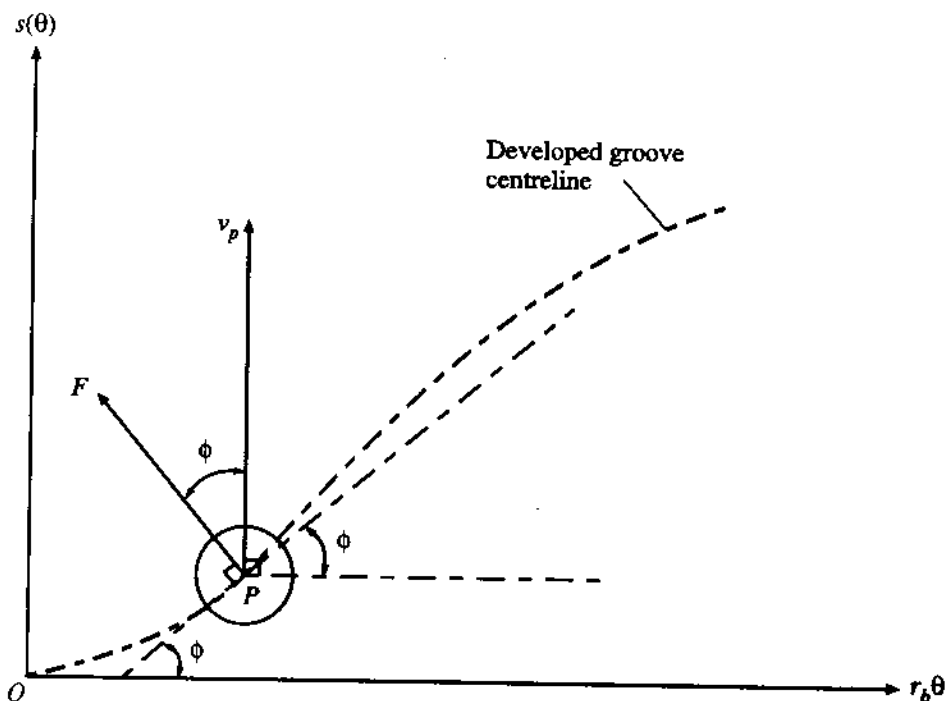


FIGURE 8.35

an oscillating one, then $s(\theta) \approx l\delta(\theta)$. From the figure, it is easy to see that

$$\frac{ds(\theta)}{d(r_b\theta)} = \tan \phi$$

or

$$\frac{1}{r_b} \frac{ds}{d\theta} = \frac{s'}{r_b} = \tan \phi. \quad (8.91)$$

Thus, ϕ is maximum when s' is maximum. Hence, the minimum required base cylinder radius $r_b \text{min}$ can be expressed as

$$r_b \text{min} = \frac{|s'|_{\max}}{\tan \phi_{\max}} \quad (\text{in case of translating followers}), \quad (8.92a)$$

$$r_b \text{min} \approx \frac{|s'|_{\max}}{\tan \phi_{\max}} \quad (\text{in case of oscillating followers}), \quad (8.92b)$$

where ϕ_{\max} is the maximum allowable pressure angle.

PROBLEM 8.15

The oscillating roller follower of a cylindrical cam-follower mechanism swings through 25° with simple harmonic motion during the rise period. The total rise is accomplished in a 120° rotation of the cam. If the pressure angle is not to exceed 35° during rise, find out the minimum required base cylinder radius. The follower is 80 mm long.

SOLUTION

The approximate displacement function of the trace point can be expressed as

$$\begin{aligned}s(\theta) &= l\delta(\theta) \\ &\approx 80 \cdot \frac{1}{2} \left(\frac{25\pi}{180} \right) [1 - \cos \{\pi\theta/(120\pi/180)\}] \text{ mm}\end{aligned}$$

or

$$s(\theta) = 17.45(1 - \cos 1.5\theta) \text{ mm.} \quad (\text{a})$$

Differentiating (a) with respect to θ , we get

$$\begin{aligned}s'(\theta) &= 17.45 \times \sin 1.5\theta \text{ mm} \\ &= 26.18 \sin 1.5\theta \text{ mm, } 0 \leq \theta \leq 2\pi/3.\end{aligned} \quad (\text{b})$$

From (b), the maximum value of s' is 26.18 mm when $\theta = \pi/3$. The maximum permissible value of the pressure angle $\phi_{\max} = 35^\circ$, i.e., $\tan \phi_{\max} = 0.7$. Using these values in (8.92b), we get

$$\begin{aligned}r_b \min &= (26.18/0.7) \text{ mm} \\ &= 37.39 \text{ mm.}\end{aligned}$$

Synthesis of Cylindrical Cams

In the case of a cylindrical cam (with the base cylinder radius either prescribed or determined), the synthesis involves laying out the groove centreline on the developed base cylinder. The width of the groove at all locations is equal to the roller diameter. First the base cylinder is developed as shown in Fig. 8.36. It should be noted that the length of the cylinder L is not relevant except for the fact that it should be more than the total lift of the follower plus the roller diameter. In the case of a translating follower, the groove centreline is simply the displacement diagram with a suitably chosen origin. The groove boundaries are parallel to this displacement diagram at a distance of r_R (roller radius) on both sides. The whole construction has been shown in the self-explanatory diagram (Fig. 8.36).

In the case of an oscillating follower, the locus (a line parallel to the $2\pi r_b$ side of the developed cylinder) of the hinge point O is determined so that it bisects the follower swing angle δ_L as shown in Fig. 8.37. Next, the locations of O corresponding to the station points are determined as shown. The locations of the trace point can be found out by rotating the follower (in the required direction) by $\delta(\theta)$ which corresponds to the displacement for that station point. Figure 8.37 shows this for station point 3. Once the locations of the trace points are determined and the roller radius is known, the groove can be laid out.

The analytical determination of the groove centreline is also quite simple in the case of a cylindrical cam mechanism. When a translating follower is used, the parametric equation of the trace point for any cam rotation θ can be found out in terms of the x - and y -coordinate as (the x -axis is along the $r_b\theta$ -direction and the y -axis is along the $s(\theta)$ -direction)

$$x_P(\theta) = r_b\theta, \quad (8.93a)$$

$$y_P(\theta) = s(\theta). \quad (8.93b)$$

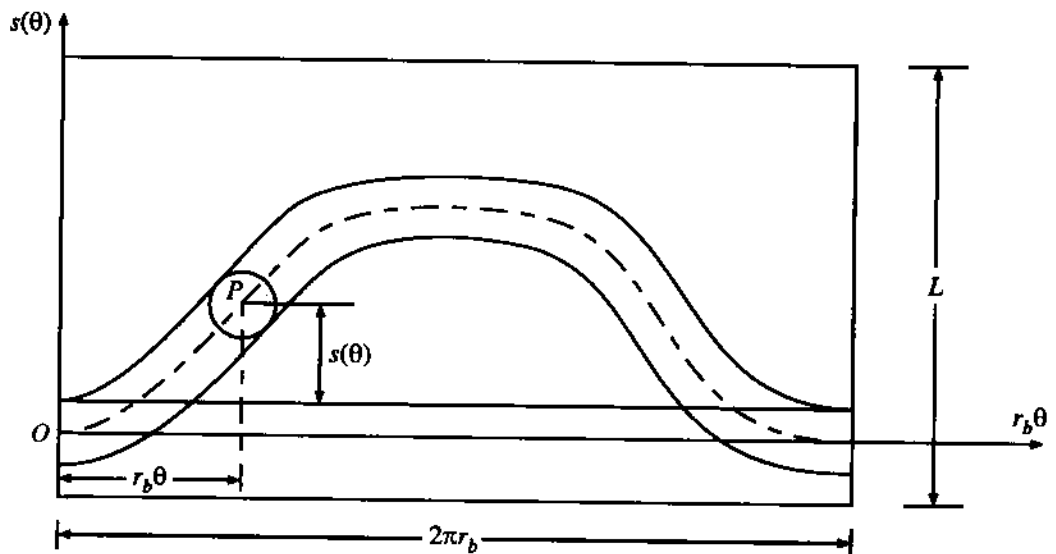


FIGURE 8.36

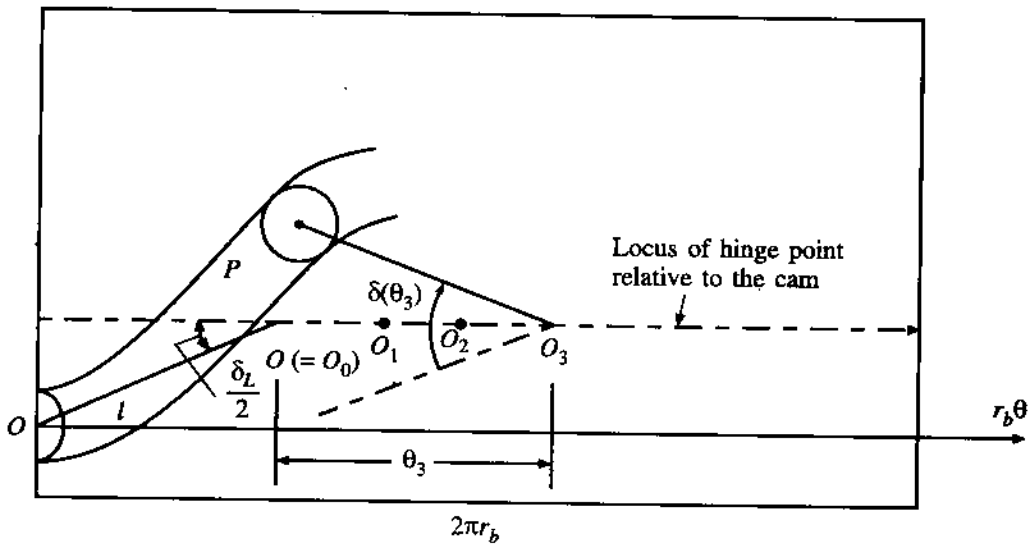


FIGURE 8.37

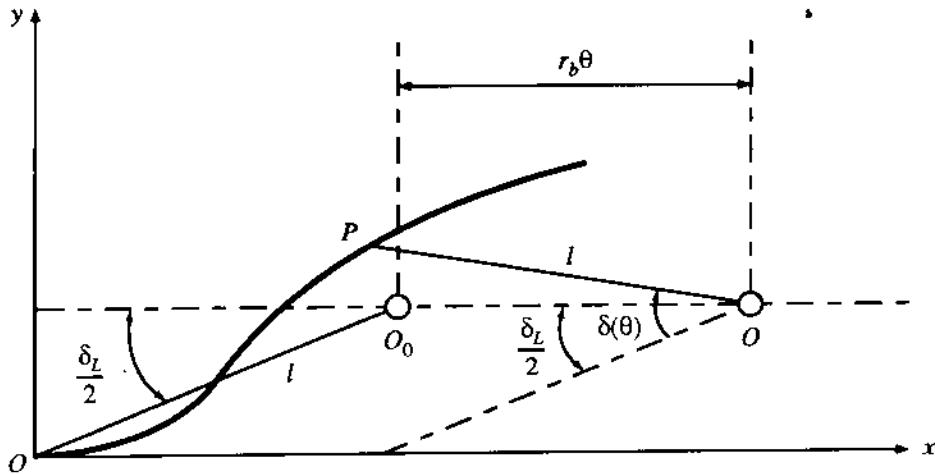


FIGURE 8.38

In the case of an oscillating follower, the coordinates of the trace point for any cam rotation θ can be determined in the following manner.

From Fig. 8.38, the coordinates of the point O are

$$x_O = l \cos(\delta_L/2) + r_b \theta,$$

$$y_O = l \sin(\delta_L/2).$$

Now, the angle made by the follower link OP at the instant is equal to $[\delta(\theta) - \delta_L/2]$. Using this, the coordinates of the trace point P can be expressed as

$$x_P(\theta) = x_O - l \cos[\delta(\theta) - \delta_L/2],$$

$$y_P(\theta) = y_O + l \sin[\delta(\theta) - \delta_L/2].$$

Substituting x_O and y_O in these relations, the parametric equation of the groove centreline can be expressed in the form

$$x_P(\theta) = l \cos(\delta_L/2) + r_b \theta - l \cos[\delta(\theta) - \delta_L/2], \quad (8.94a)$$

$$y_P(\theta) = l \sin(\delta_L/2) + l \sin[\delta(\theta) - \delta_L/2]. \quad (8.94b)$$

PROBLEM 8.16

During the rise, the oscillating follower of a cylindrical cam mechanism swings through 30° with a cycloidal motion when the cam rotates through 90° . The base cylinder radius and the follower link length are 45 mm and 80 mm, respectively. Find out the equation of the rise part of the groove centreline on the developed cylinder surface.

SOLUTION

As per the prescribed conditions, the displacement function of the follower can be expressed as

$$\delta(\theta) = (\delta_L/2)[(2\theta/\pi) - (1/2\pi)\sin 4\theta] \text{ rad}, \quad (a)$$

where $\delta_L = \pi/12$ rad. Now, using (8.94a) and (8.94b) along with the values for r_b and l , the coordinates of the groove centreline in parametric form can be expressed in the form

$$x_P(\theta) = 77.27 + 45\theta - 80 \cos [0.131(0.637\theta - 0.159 \sin 4\theta) - 0.131] \text{ mm},$$

$$y_P(\theta) = 20.71 + 80 \sin [0.131(0.637\theta - 0.159 \sin 4\theta) - 0.131] \text{ mm}.$$

Rearranging, these equations become

$$x_P(\theta) = 77.27 + 45\theta - 80 \cos [0.131(0.637\theta - 0.159 \sin 4\theta - 1)] \text{ mm},$$

$$y_P(\theta) = 20.71 + 80 \sin [0.131(0.637\theta - 0.159 \sin 4\theta - 1)] \text{ mm},$$

where θ is in radians and the range of θ is given by $0 \leq \theta \leq \pi/2$.

8.12 PROBLEMS

- 8.17 In a disc cam-follower mechanism, the follower rises with constant acceleration for 25 mm and then rises with constant deceleration for the next 25 mm, the total lift being 50 mm. The velocities at the beginning and at the end of the rise period are zero and the cam rotates through 120° during the rise period. Find out the displacement function during the rise.
- 8.18 In a cam-follower mechanism with a translating flat-face follower, the follower rises by 40 mm with a cycloidal motion, the corresponding cam rotation being 180° . (a) If the radius of curvature of the cam profile is not to be less than 120 mm during the rise period, what should be the minimum required base circle radius? (b) Determine the minimum required offset if the eccentricity of the driving effort is not to exceed 20 mm.
- 8.19 Find out the minimum necessary width of the follower in Problem 8.18 keeping an allowance of 3 mm on both sides.
- 8.20 The displacement of the flat-face translating follower of a cam-follower mechanism is as follows: (i) rise by 50 mm with simple harmonic motion for a cam rotation of 0° to 120° , (ii) a dwell for a cam rotation of 30° , (iii) return to the original location with simple harmonic motion for a cam rotation of 210° .
 (a) If the maximum allowable radius of curvature of the cam profile is not to exceed 60 mm, find out the minimum required base circle radius of the cam. (b) If the maximum eccentricity of the driving effort is not to exceed 40 mm, determine the required offset.
- 8.21 If a translating roller follower is used in the mechanism of the previous problem (8.20) and the same motion characteristics of the follower are desired, what are the minimum prime circle radius and the required offset if the magnitude of the pressure angle is not to exceed 25° during the complete cycle?
- 8.22 If the roller radius is 8 mm and all other data remain the same as those in Problem 8.20, determine the radius of curvature of the cam profile at a position corresponding to the middle of the rise period.

- 8.23 A flat-face radial follower has a lift of 4 cm. The follower rises the first 1 cm at a constant acceleration for 60° of cam rotation and then rises 2 cm at a constant velocity for the next 60° of cam rotation, and finally rises the remaining 1 cm at a constant retardation for another 60° of cam rotation. After a dwell for 45° of cam rotation, the follower returns with simple harmonic motion for the next 90° of cam rotation followed by a dwell. Determine the minimum base circle radius of the cam, and the minimum length of the follower face.
- 8.24 For the displacement diagram shown in Fig. 8.17a, determine the optimum offset with a roller follower. If the maximum pressure angle is 25° , what is the minimum radius of the prime circle?
- 8.25 A flat-face follower is offset to the left by 1.2 cm. The base circle radius of the cam is 2.5 cm. The desired displacement of the follower y for any cam rotation θ is listed in Table 8.2. Lay out the cam profile and determine the length of the follower face (by trial from the drawing) with 0.3-cm clearance on either side. The cam rotates in the clockwise direction.
- 8.26 A roller follower is offset to the right by 1.2 cm. The lift of the follower is 4 cm. The base circle radius of the cam is 2.5 cm, and the roller radius is 1 cm. The cam rotates in the counter-clockwise direction. Lay out the cam profile if (i) the rise is for 150° of cam rotation, the first 60° being at constant acceleration and the rest at constant deceleration, (ii) the dwell is for 30° , (iii) the return is for 150° of cam rotation, the first 90° being at constant retardation and the rest at constant acceleration, and (iv) the second dwell is for 30° . Also find the maximum pressure angle during the rise and return.
- 8.27 Lay out the cam profile in Fig. 8.39 so that the roller follower oscillates through an angle of 30° as indicated in the figure. The follower rises for 150° of cam rotation in simple harmonic motion. The dwell is for 30° of cam rotation, the return for 150° of cam rotation with cycloidal motion, and the second dwell for 30° of cam rotation.
- 8.28 The oscillating flat-face follower shown in Fig. 8.40 is to rise through an angle of 20° with modified uniform motion in 180° of cam rotation. This is followed by a dwell for 30° and return with modified uniform motion for 150° of cam rotation. Lay out the cam profile and find the length of the follower face with 0.3-cm clearance on each side.

TABLE 8.2

Cam rotation θ (degrees)	Follower displacement y (cm)	Cam rotation θ (degrees)	Follower displacement y (cm)
0	0.00	180	3.75
30	0.25	210	3.50
60	0.92	240	2.83
90	1.87	270	1.87
120	2.83	300	0.92
150	3.50	330	0.25

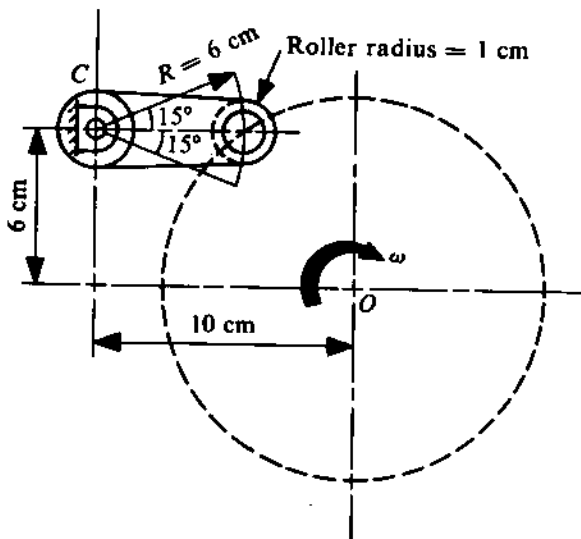


FIGURE 8.39

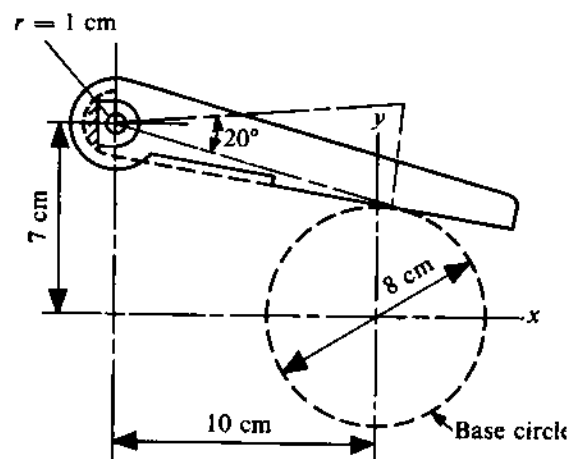


FIGURE 8.40

- 8.29 A follower rises through a distance L with cycloidal motion for $0 \leq \theta \leq \theta_{ri}$, where θ is the cam rotation. Determine the value of θ for which the acceleration of the follower is maximum. Find the velocity and jerk for $\theta = \theta_{ri}/2$. The cam rotates at a constant speed ω .
- 8.30 The boundary conditions of a polynomial-curve cam are

$$y = 0, \quad \dot{y} = 0 \quad \text{at } \theta = 0,$$

$$y = L, \quad \dot{y} = 0 \quad \text{at } \theta = \theta_{ri}.$$

Determine the displacement, velocity, acceleration, and jerk equations.

- 8.31 A plate cam drives an offset flat-face follower with simple harmonic motion for a rise of 5 cm. The follower moves out and returns in one revolution without any dwell. The base circle radius is 2.5 cm, and the offset is 1 cm. Find the parametric equations of the cam profile.
- 8.32 Synthesize the rise part of a cam with a translating roller follower with the following information: (i) the rise is simple harmonic with a total lift of 3 cm when the cam rotates through 100°, (ii) the base circle radius is 8 cm, (iii) the offset is 1.5 cm to the right of the cam centre with the cam rotating in the CCW direction, and (iv) the roller radius is equal to 0.75 cm.
- 8.33 Obtain the equation of the profile of the cam described in Problem 8.20.
- 8.34 An oscillating flat-face follower swings through 30° during the rise period with simple harmonic motion when the cam rotates through 120°. The distance of the follower face from the hinge is 1.5 cm (below the hinge) and the hinge coordinates (with the cam centre as the origin and x- and y-axis in the horizontal and vertical directions) are $x = 20$ cm, $y = 10$ cm. The base circle radius of the cam is 8 cm. Determine the parametric equation of the rise part of the cam profile and plot it taking 10° interval.
- 8.35 For a tangent cam with a radial roller follower, the lift is 1.2 cm, the base circle radius 2.5 cm, the nose radius 0.6 cm, and the radius of the roller 1.3 cm. The total angle of cam rotation

from the start of the rise to the end of the return is 120° . The cam rotates at a constant speed of 1000 rpm. Obtain the displacement and draw the displacement and velocity diagrams for the follower during the rise.

- 8.36 For a circular-arc cam with a radial flat-face follower, the base circle radius is 3 cm and the nose radius is 0.3 cm. The lift of the follower is 1.2 cm and the cam rotation during the rise is 55° . The cam rotates at a constant speed of 1000 rpm. Derive the displacement equation and draw the displacement and velocity diagrams for the follower during the rise.
- 8.37 A dwell-rise-dwell cam has a rise of 2.5 cm with a cycloidal motion in 150° of cam rotation. The follower is assembled with a 400-N/cm retaining spring which has sufficient preload to prevent jumping. The follower train has an equivalent mass of 250 gm and an equivalent stiffness of 7000 N/cm. Determine the follower response for a cam speed of 3500 rpm.
- 8.38 If the preloading in both the spring and the follower train is 1000 N, determine the minimum cam speed required for a jump to occur. If the cam speed is 1.5 times this minimum speed, determine the duration of the jump when it first occurs.
- 8.39 The stiffness of the retaining spring of a cam-follower system is 600 N/cm. The equivalent mass and stiffness of the follower train are 500 gm and 8000 N/cm, respectively. The base circle diameter of the cam is 5 cm and a flat-face follower is used. The cam rotates at 5000 rpm and it is desired that the follower motion should be harmonic with an amplitude of 1/2 cm, completing one cycle during one complete cam rotation. The preload is sufficient to prevent jumping. Determine the required cam profile.
- 8.40 The oscillating roller follower of a cylindrical cam mechanism swings through 30° with constant acceleration and then with constant deceleration (both of the same magnitude) when the cam rotates through 120° . If the follower link length is 10 cm, find out the minimum base cylinder radius if the pressure angle during rise is not to exceed 35° . Determine the parametric equation of the groove centreline (on the developed base cylinder) using this minimum base cylinder radius.
- 8.41 Repeat Problem 8.40 considering the rise to be simple harmonic, all other conditions remaining the same.
- 8.42 If the displacement function during rise of the oscillating roller follower in a cylindrical cam mechanism be
- $$\delta(\theta) = \frac{5\pi}{6} \left(\frac{3\theta}{\pi}\right)^3 - \frac{5\pi}{4} \left(\frac{3\theta}{\pi}\right)^4 + \frac{\pi}{2} \left(\frac{3\theta}{\pi}\right)^5, \quad 0 \leq \theta \leq \pi/3,$$
- and the maximum pressure angle during rise be 30° when a follower link of 10 cm length is used, derive the equation for the rise part of the groove centreline for the smallest possible cam.

Chapter 9

GEARS

9.1 INTRODUCTION

A gear is a toothed element commonly used for transmitting rotary motion from one shaft to another. It is a higher-pair mechanism and is one of the earliest to be studied. Gears are of various types; a brief description of several types (listing their uses) is given in Section 9.6. As the theory of gearing is vast and cannot be covered in a single chapter, we shall not discuss the details of gear geometry here. (For the geometry and dimensions of various standard tooth profiles, see the available tables and handbooks.¹) Instead, we shall briefly introduce the kinematics of gears and their use in mechanism trains.

Before we consider the kinematics of gears, we shall define the terms used for describing the shape, size, and geometry of a gear tooth. The definitions given here are with respect to a straight spur gear, a part of which is shown in Fig. 9.1. A spur gear is used for connecting parallel shafts, and the teeth in it may be straight (parallel to the axis of rotation) or helical. For parallel shafts, all the quantities are defined with reference to the projection taken on a plane perpendicular to the axis of rotation. Therefore, a cylindrical gear is normally called a circular gear.

¹For example, Dudley, D.W., Gear Handbook, McGraw-Hill, New York, 1962.

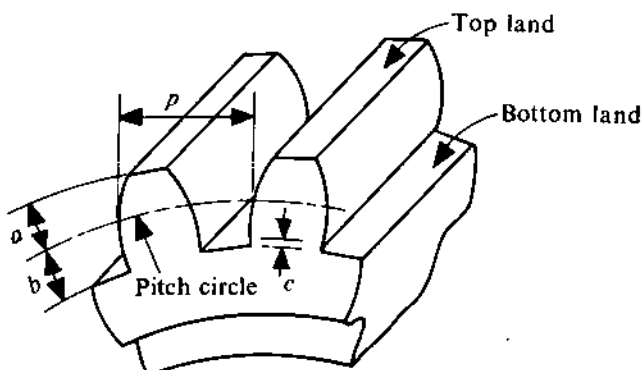


FIGURE 9.1

Pinion

The smaller of two mating gears is referred to as the *pinion*. The larger gear is termed the *wheel*.

Pitch Curve

The *pitch curve* of a gear is the theoretical curve along which the gear rolls (without slipping) on the corresponding pitch curve of the other gear, for transmitting equivalent motion. Obviously, at the point of contact of the pitch curves (called the *pitch point*), the relative velocity between the mating gears is zero. So, these pitch curves are the loci of the relative instantaneous centres (called *centrodes* or *polodes*) between the mating gears. From the definition, it follows that the ratio of the angular velocities of two mating gears is proportional to the ratio of the radius vectors of the pitch curves at the point of contact. So, if a constant angular velocity ratio is to be maintained, the pitch curves become circles (if the distance between the centres of the gears remains constant) and are known as *pitch circles*. All calculations are usually based on pitch circles.

Rack

If the pitch curve is a straight line, i.e., if the radius of the pitch circle is infinite, then the gear is called a *rack*; obviously, it will transmit only translating motion.

Circular Pitch

The distance measured along the pitch circle from one point of a tooth to the corresponding point of the adjacent tooth is called the *circular pitch* p . Thus,

$$p = \pi d_p / N, \quad (9.1)$$

where N is the number of teeth, and d_p is the diameter of the pitch circle.

Diametral Pitch

The number of teeth per unit length of the pitch circle diameter is termed the *diametral pitch* P . So,

$$P = N/d_p. \quad (9.2)$$

From (9.1) and (9.2), we get $p \cdot P = \pi$.

Module

The inverse of the diametral pitch is referred to as the *module* m . From (9.2), we have

$$m = d_p/N. \quad (9.3)$$

Addendum

The radial distance between the pitch circle and the top land of the gear is called the *addendum* a .

Dedendum

The radial distance between the pitch circle and the bottom land of the gear is called the *dedendum*.

Clearance

The amount by which the dedendum of a gear exceeds the addendum of the mating gear is known as the *clearance c*.

3.2 GEARING ACTION, FUNDAMENTAL LAW OF GEARING, AND INVOLUTE SPUR GEARS

When two parallel shafts are connected to each other by a pair of toothed wheels (gears), the number of teeth from each gear passing through the engagement zone in a given period of time is equal. If his number be N for a period of 1 second and the numbers of teeth on the two gears 1 and 2 be N_1 and N_2 , respectively, then gears 1 and 2 make (N/N_1) and (N/N_2) revolutions, respectively. Hence, the average angular velocities of these two gears can be written as

$$(\omega_1)_{av} = \frac{2\pi N}{N_1},$$

$$(\omega_2)_{av} = \frac{2\pi N}{N_2}.$$

The ratio of these average angular velocities is

$$(\omega_1)_{av}/(\omega_2)_{av} = -(N_2/N_1) = \text{constant.}$$

However, the ratio of the instantaneous angular speeds in general is not a constant and takes the form

$$\omega_1/\omega_2 = -(N_2/N_1) + P(t),$$

where $P(t)$ is a periodic function of time with zero average. This relation suggests that, for a given constant driving speed, the rotation of the driven gear is not uniform and has a periodic motion superimposed on a uniform rotation. This results in harmful effects, and proper gearing action requires the tooth profile to be so chosen that, for a constant driving speed, the driven shaft also rotates uniformly. Thus, proper gearing action implies

$$\omega_1/\omega_2 = -(N_2/N_1) = \text{constant.}$$

When the distance between the gear centres is constant, many tooth profiles satisfying this condition are possible. Of all possible curves, the involute² is advantageous in that the angular velocity ratio will be constant even if the distance between the centres varies. In what follows, we shall explain this.

²Recall that an "involute" is the locus of a point on a straight line that rolls without sliding on a curve, in the plane of the curve.

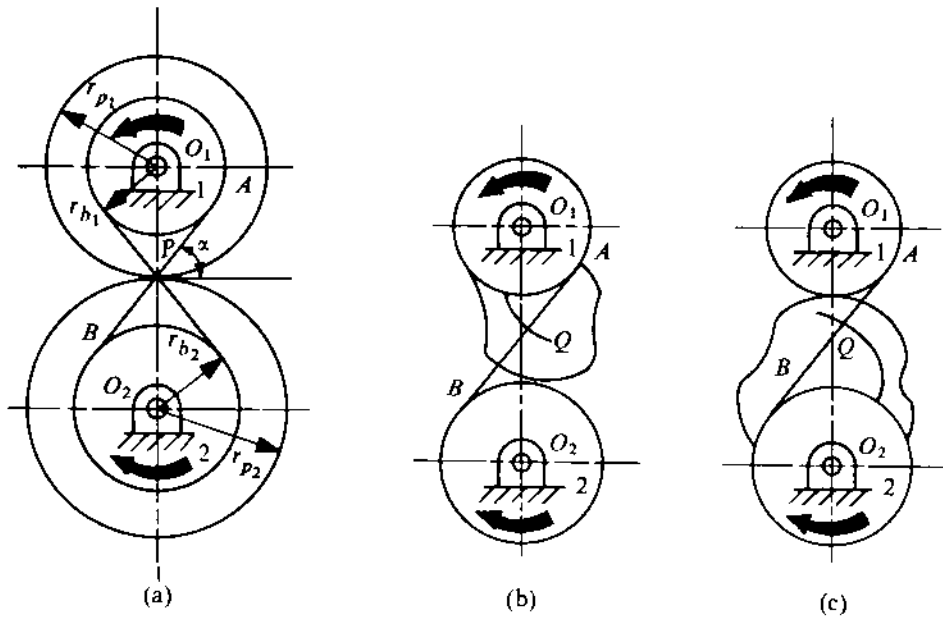


FIGURE 9.2

As already noted, with a constant distance between the centres, the pitch curves are circles for a constant angular velocity ratio. Figure 9.2a shows two circular discs of radii r_{p_1} and r_{p_2} which roll on each other without slipping and thus maintain a constant angular velocity ratio given by

$$\omega_1/\omega_2 = r_{p_2}/r_{p_1}. \quad (9.4)$$

These friction discs actually represent the pitch circle of a gear for transmitting equivalent motion. The same motion can be transmitted by two pulleys and a crossed belt (which is always maintained taut) as shown in Fig. 9.2a. From the geometry of Fig. 9.2a, we get

$$\omega_1/\omega_2 = r_{b_2}/r_{b_1} = r_{p_2}/r_{p_1}, \quad (9.5)$$

where r_{b_1} and r_{b_2} are the radii of the two pulleys. It is obvious that (9.5) holds good even if the distance between the centres of the pulleys is changed.

Now, let us see how the equivalent motion between two shafts can be transmitted without the belt and pulley. For convenience, let us imagine that a plate is attached to pulley 1 (as shown in Fig. 9.2b) and a scribe is attached to the belt at the point Q . As pulley 2 turns, the scribe traces a straight line in space. However, in relation to pulley 1, the scribe traces an involute on the plate attached to pulley 1. The same involute could also be generated by the point Q if the belt were cut at this point and unwrapped from pulley 1 (keeping the belt taut). A similar involute will be traced by Q on a plate attached to pulley 2, as shown in Fig. 9.2c. Now, if the plates are machined along the involutes and the belt is removed, the involute on one pulley can be used to drive the other (the involutes will roll on each other) and produce the same relative motion between the shafts as that with the belt. The angular velocity ratio will still be constant and equal to r_{p_2}/r_{p_1} . This is because, by the method of construction, the common normal AB to the involutes at the point of contact Q (called the *line of action*) meets the line of centres O_1O_2 at the (fixed) pitch point P . This is the condition required for maintaining a constant angular velocity ratio and is known as the

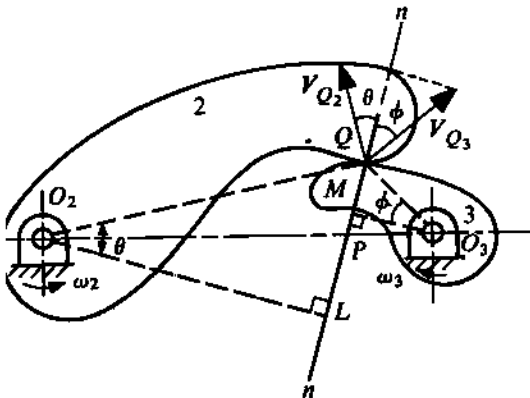


FIGURE 9.3

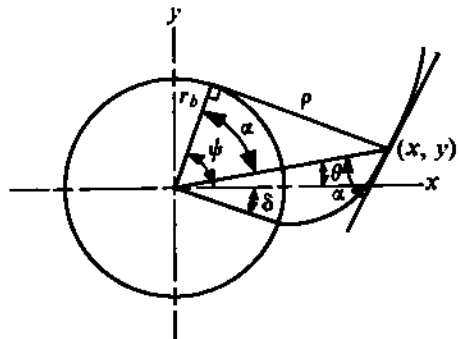


FIGURE 9.4

fundamental law of gearing. To prove this, consider two bodies in relative motion in direct contact with each other (Fig. 9.3). The velocity of the point of contact Q in body 2 is $V_{Q_2} = \omega_2 \cdot O_2 Q$, ($\perp^r O_2 Q$), and that in body 3 is $V_{Q_3} = \omega_3 \cdot O_3 Q$, ($\perp^r O_3 Q$). nn is the common normal to the bodies at Q , intersecting the line of centres at P . $O_2 L$ and $O_3 M$ are perpendicular to nn . Now,

$$\begin{aligned}\frac{\omega_2}{\omega_3} &= \frac{V_{Q_2}}{V_{Q_3}} \cdot \frac{O_3 Q}{O_2 Q} = \frac{V_{Q_2} \cos \theta}{V_{Q_3} \cos \phi} \cdot \frac{O_3 Q \cos \phi}{O_2 Q \cos \theta} \\ &= \frac{O_3 Q \cos \phi}{O_2 Q \cos \theta} = \frac{O_3 M}{O_2 L} = \frac{O_3 P}{O_2 P} \quad (\text{from similar triangles}).\end{aligned}$$

As the bodies are rolling on each other, the relative velocity along nn should be zero, i.e., $V_{Q_2} \cos \theta = V_{Q_3} \cos \phi$. Thus, for ω_2/ω_3 to be constant, P must be a fixed point on $O_2 O_3$.

The above result can be also derived by using the concept of instantaneous centre of velocity. By inspection, the points O_2 and O_3 are the instantaneous centres 12 and 13, respectively. According to the Aronhold-Kennedy theorem, the relative instantaneous centre 23 must be so located that 12, 13, and 23 are collinear. As 23 has to lie on the line $n-n$, P is the instantaneous centre 23 and the ratio of the angular velocities ω_2/ω_3 is given by $O_3 P/O_2 P$.

As already stated, the transmission of a constant angular velocity ratio is also possible using profiles other than the involute. In involute profiles, the additional advantage is that even if the centre distance of the gears is changed the angular velocity ratio will remain unchanged though some different portions of the same involutes will be brought into contact.

The circles corresponding to the pulleys, which are used for generating the involutes, are called *base circles*. Comparing (9.4) and (9.5), we observe that the pitch circle radius of a gear is not a unique property and depends on the distance between the centres of the mating gears. Thus, an intermediate gear in a gear train may have a different pitch circle for the mating gears of equal size. [Note that $(r_{p_1}/r_{p_2}) = (r_{b_1}/r_{b_2}) = \text{constant}$, and that $(r_{p_1} + r_{p_2}) = \text{distance between gear centres}$.]

Another major advantage of an involute tooth profile is that the common normal to the mating tooth curves at the point of contact makes a constant angle with the common tangent to the pitch circles passing through the pitch point. This angle is called the *pressure angle*. If this angle remains constant, then the direction of the bearing reactions also remains unchanged. Thus, under a steady condition, the bearings are free from any dynamic reaction, leading to a quieter and vibration-free operation. In Section 9.4, we shall further elaborate on this. Yet another advantage of an involute profile is that the meshing rack will have a straight tooth profile perpendicular to the line of action.

Such a straight-sided rack cutter is used for generating the involute tooth profile on a gear. Thus from the point of view of production also, involute teeth are easy to generate. In view of the advantages we have highlighted, the involute tooth profile is widely used.

9.3 PROPERTIES OF THE INVOLUTE OF A CIRCLE

We have seen that, by definition, an involute is the curve drawn by a point on a taut string as the string is unwrapped from the surface of a cylinder. The radius of the cylinder is known as the *base circle radius* of the involute. The properties of the involute that can be easily derived from the geometry of the curve shown in Fig. 9.4 are

$$\begin{aligned}\rho &= r_b(\psi + \delta) = \text{length of the string unwrapped} \\ &= r_b \tan \alpha.\end{aligned}\quad (9.6)$$

From this, we get

$$\psi + \delta = \tan \alpha, \quad (9.7)$$

$$\begin{aligned}x &= r_b \cos \psi + \rho \sin \psi \\ &= r_b[\cos \psi + (\psi + \delta) \sin \psi],\end{aligned}\quad (9.8)$$

$$y = r_b[\sin \psi - (\psi + \delta) \cos \psi], \quad (9.9)$$

$$\begin{aligned}\theta + \alpha &= \psi = \tan \alpha - \delta, \\ \theta &= \tan \alpha - \alpha - \delta = \text{inv } (\alpha) - \delta,\end{aligned}\quad (9.10)$$

where $\text{inv } (\alpha) = \tan \alpha - \alpha$. There are standard tables from which α can be obtained if $\text{inv } (\alpha)$ is known.

9.4 CHARACTERISTICS OF INVOLUTE ACTION

This section is devoted to a quantitative analysis of some important aspects relating to involute gears.

Contact Ratio

To transmit rotational motion continuously, there must be at least one pair of teeth in contact at all times. In the actual case, certain amount of overlap exists between the actions of two consecutive pairs of teeth. The term *contact ratio* is used to provide a quantitative measure of the amount of this overlap. Figure 9.5a shows a pair of teeth at the beginning and end of contact. So, at the point *E* (on the line of action, i.e., the common tangent to the base circles of the two gears), the contact begins and at *F* the contact ends. The points *S* and *T* are the points on a tooth of gear 2 (on its base circle) at the start and end of contact, respectively. Since *E* and *F* are two points on two involutes with the same base circle, the length *EF* (called the *length of action*) will be equal to *ST*. Now, the ratio (*ST*/base pitch) is a measure of the contact ratio, m_c . So,

$$\begin{aligned}m_c &= ST/\text{base pitch} = EF/\text{base pitch} \\ &= EF/p_b.\end{aligned}$$

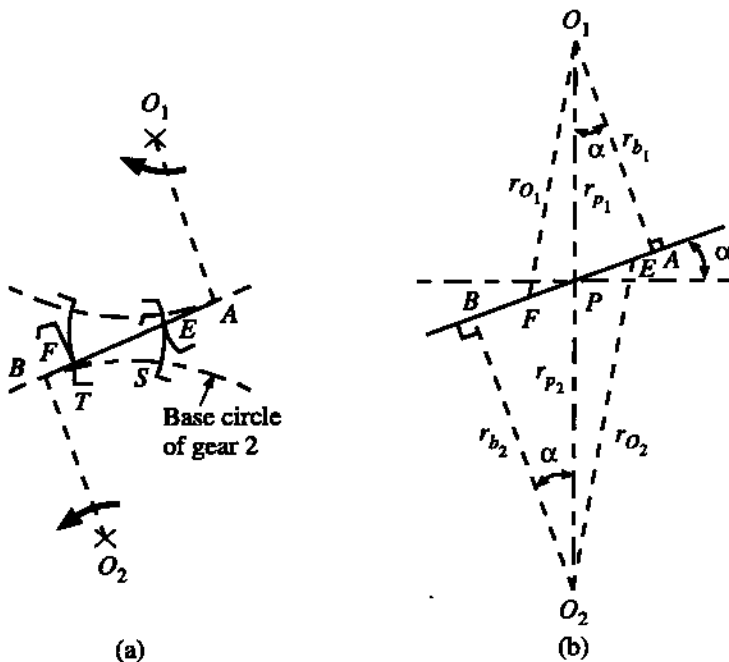


FIGURE 9.5

The base pitch of gear 2 can be expressed as $2\pi r_{b_2}/N_2$, where r_{b_2} is the base circle radius of gear 2 and N_2 is the number of teeth on this gear. Figure 9.5b shows the essential dimensions of the two gears in contact. From this figure, the length of action

$$\begin{aligned} EF &= (EF + AE) + (EF + BF) - (AE + BF + EF) \\ &= AF + BE - AB. \end{aligned}$$

r_{O_1} and r_{O_2} are the outer circle (same as the addendum circle) radii, then this relation yields

$$EF = (r_{O_1}^2 - r_{b_1}^2)^{1/2} + (r_{O_2}^2 - r_{b_2}^2)^{1/2} - C \sin \alpha, \quad (9.11)$$

here $C = r_{p_1} + r_{p_2}$ (= centre distance) and r_{b_1} is the base circle radius of gear 1, r_{p_1} and r_{p_2} being the pitch circle radii with α as the pressure angle. So, the expression for contact ratio becomes

$$m_c = \frac{EF}{2\pi r_{b_2}/N_2} = \frac{(r_{O_1}^2 - r_{b_1}^2)^{1/2} + (r_{O_2}^2 - r_{b_2}^2)^{1/2} - C \sin \alpha}{2\pi r_{b_2}/N_2}. \quad (9.12)$$

Normally, the contact ratio is not a whole number. If the ratio is 1.3, it means that there are alternately one pair and two pairs of teeth in contact and the time average is 1.3. In practice, a value of 1.4 is recommended for m_c for smooth and good performance. It can be seen from Fig. 9.5 that by increasing the addendum the length of the path of contact EF can be increased, resulting in a larger value of the contact ratio. But increasing the addendum can lead to some problems as will be seen in the next subsection.

PROBLEM 9.1

The pitch circle radii of two involute spur gears in mesh are 51.5 mm and 64.2 mm. The outer circle radii are 57.5 mm and 71.2 mm, respectively, the operating pressure angle being 20° . Determine

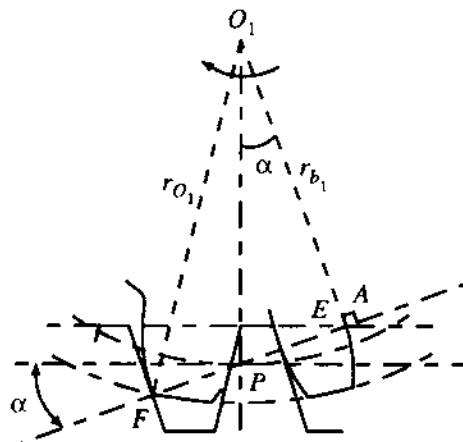


FIGURE 9.6

(i) the length of the path of contact, and (ii) the contact ratio if the number of teeth on the large gear is 20.

SOLUTION

From the given data, $r_{p_1} = 51.5$ mm, $r_{p_2} = 64.2$ mm, $r_{O_1} = 57.5$ mm, $r_{O_2} = 71.2$ mm, and $\alpha = 20^\circ$. From Fig. 9.5b, we can see that

$$r_b = r_p \cos \alpha.$$

Using this, $r_{b_1} = 51.5 \cos 20^\circ = 48.39$ mm, $r_{b_2} = 64.2 \cos 20^\circ = 60.33$ mm, and $C = r_{p_1} + r_{p_2} = 115.7$ mm. Substituting the values in (9.11), the length of path of contact is found out as

$$\begin{aligned} EF &= [(57.5^2 - 48.39^2)^{1/2} + (71.2^2 - 60.33^2)^{1/2} - 115.7 \sin 20^\circ] \\ &= 29.3 \text{ mm.} \end{aligned}$$

The contact ratio is found out by substituting the values in (9.12) as

$$m_c = \frac{EF}{2\pi r_{b_2}/N_2} = \frac{29.3}{2\pi \times 60.33/20} = 1.55.$$

The length of the path of contact and the contact ratio for the case where a pinion is in mesh with a rack can be determined in a similar way. Figure 9.6 shows a pinion in mesh with a rack. The base circle and the outer circle radii are r_{b_1} and r_{O_1} , respectively, and the addendum of the rack is a_r . The pitch circle for the rack is a straight line passing through P and the line of action passes through P making an angle α with the pitch line. The line of action touches the base circle radius at the pinion at A . E and F are the points of contact at the start and end of the engagement between a pair of teeth. From the figure, the length of the path of contact is found as

$$\begin{aligned} EF &= EP + PF \\ &= a_r / \sin \alpha + (AF - AP). \end{aligned}$$

But $AF = (r_{O_1}^2 - r_{b_1}^2)^{1/2}$ and $AP = r_{b_1} \tan \alpha$. Using these in the foregoing relation, we get

$$EF = \frac{a_r}{\sin \alpha} + (r_{O_1}^2 - r_{b_1}^2)^{1/2} - r_{b_1} \tan \alpha. \quad (9.13)$$

he base pitch of the pinion

$$p_{b_1} = \frac{2\pi r_{b_1}}{N_1}$$

nd the contact ratio

$$m_c = \frac{EF}{p_{b_1}} = \frac{N_1}{2\pi r_{b_1}} \left[\frac{a_r}{\sin \alpha} + (r_{O_1}^2 - r_{b_1}^2)^{1/2} - r_{b_1} \tan \alpha \right]. \quad (9.14)$$

'ROBLEM 9.2

pinion of 62 mm pitch circle radius is in mesh with a rack, the operating pressure angle being 20° . The module is 4 mm and the rack and pinion addendum is 4 mm, determine the contact ratio.

OLUTION

rom the given data, $N_1 = 2r_{p_1}/m = 31$, $a_r = 4$ mm, $r_{O_1} = (62 + 4)$ mm = 66 mm, and $r_{b_1} = \frac{r_{O_1}}{\cos 20^\circ} = 58.26$ mm. Substituting these values in (9.14), the contact ratio can be determined as

$$\begin{aligned} m_c &= \frac{31}{2\pi \times 58.26} \left[\frac{4}{\sin 20^\circ} + (66^2 - 58.26^2)^{1/2} - 58.26 \tan 20^\circ \right] \\ &= 1.82. \end{aligned}$$

nterference and Undercutting

We have already seen that, by definition, an involute curve is the locus of the end of a taut string as it is unwrapped from the outside surface of a cylinder. It is not possible to unwrap a string from the inside of a cylinder. So, the involute profile does not exist inside the base circle. From (9.8) and (9.9), it can be seen that $x^2 + y^2 \geq r_b^2$, which also confirms that the involute curve does not exist inside the base circle. Referring to Fig. 9.2b, if the generating point Q is moved beyond the base circle of gear 1, the involute profile of gear 2 will continue to be generated, but there is no involute profile of gear 1 to meet it. On the base circle, the direction of the involute is radial. So, theoretically, the portion of the tooth profile which lies inside the base circle is assumed to be radial. The extended part of the involute profile of gear 2 will be found to interfere with this imaginary radial portion of gear 1. To avoid this interference, it will be necessary to cut out a portion of this radial part of the tooth in gear 1 (Fig. 9.7a). This undercutting results in a clearance between the mating teeth and weakens the undercut tooth.

To avoid interference without undercutting, the addendum circles of both the pinion and the gear should intersect the common tangent AB to the base circles within the points of tangency A and B (Fig. 9.7b). When the addenda are equal, obviously, then the interference will always occur first at the pinion base circle. The situation where the interference just starts is indicated in Fig. 9.7b. The number of teeth on the pinion (for a given speed ratio) for this situation can be determined as now explained.

The addendum length $a = O_2A - O_2P$. From ΔO_2AP , we can write, with α as the pressure angle,

$$\begin{aligned} O_2A^2 &= O_2P^2 + AP^2 - 2O_2P \cdot AP \cos(\pi/2 + \alpha) = O_2P^2 + AP^2 + 2O_2P \cdot AP \sin \alpha \\ &= O_2P^2 + O_1P^2 \sin^2 \alpha + 2O_2P \cdot O_1P \sin^2 \alpha \\ &= O_2P^2 [1 + (O_1P/O_2P)(O_1P/O_2P + 2) \sin^2 \alpha]. \end{aligned}$$

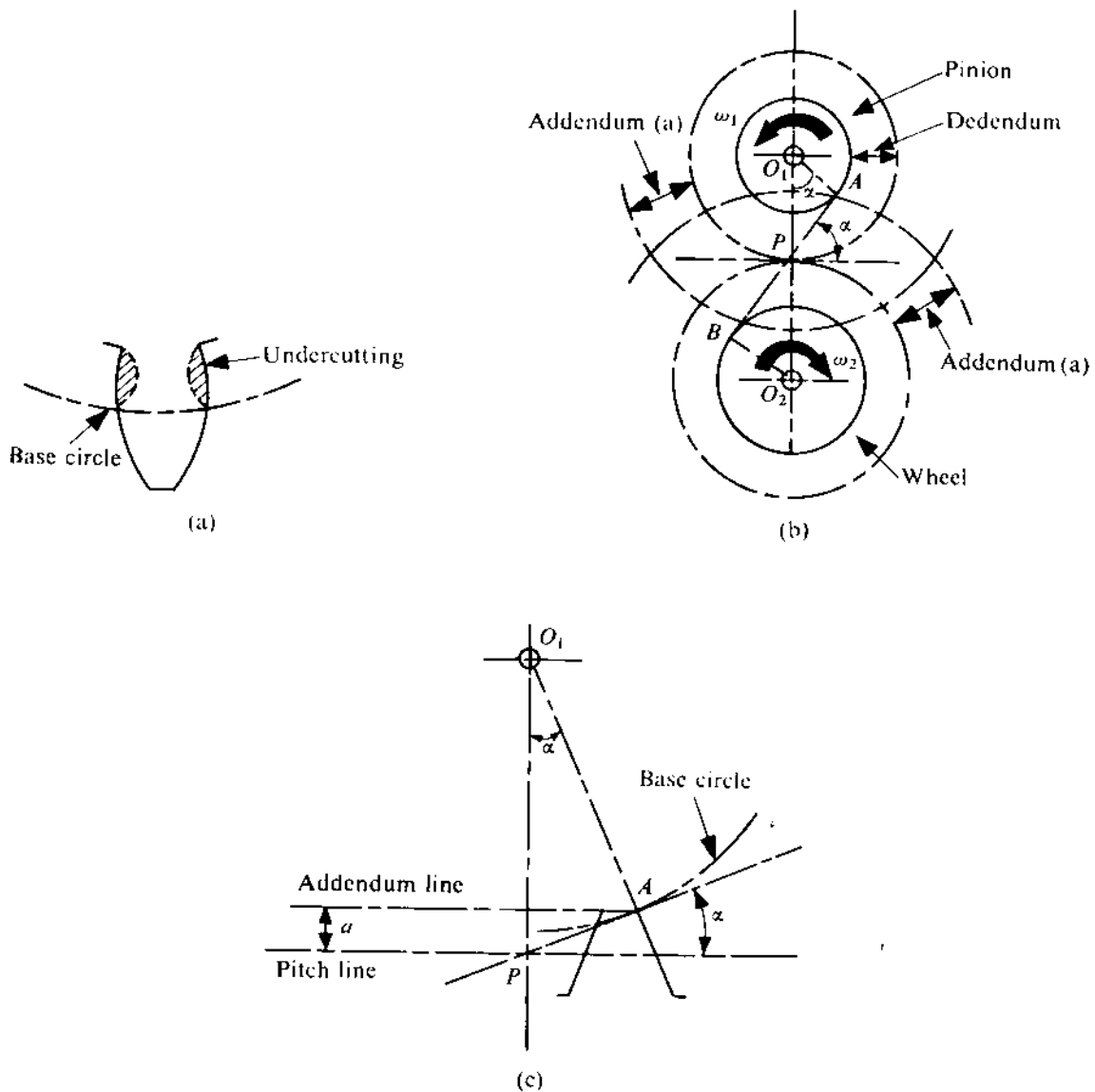


FIGURE 9.7

hus,

$$a = O_2 P [\{ 1 + (O_1 P / O_2 P) (O_1 P / O_2 P + 2) \sin^2 \alpha \}^{1/2} - 1].$$

or a given speed ratio $\omega_2 / \omega_1 = \lambda$, a can be expressed as

$$a = O_2 P [\{ 1 + \lambda(\lambda + 2) \sin^2 \alpha \}^{1/2} - 1]. \quad (9.15)$$

ormally, an addendum is expressed as a fraction f of a module m . So, let

$$a = fm = f \cdot 2O_2 P / N_2. \quad (9.16)$$

sing (9.16) in (9.15), we get

$$2f = N_2 [\{ 1 + \lambda(\lambda + 2) \sin^2 \alpha \}^{1/2} - 1] = (N_1 / \lambda) [\{ 1 + \lambda(\lambda + 2) \sin^2 \alpha \}^{1/2} - 1].$$

o,

$$N_1 = \frac{2f\lambda}{[1 + \lambda(\lambda + 2) \sin^2 \alpha]^{1/2} - 1}. \quad (9.17)$$

This is the minimum number of teeth on the pinion when the interference just starts. For a pinion meshing with a rack, the situation where the interference just starts is shown in Fig. 9.7c. From geometry,

$$a = AP \sin \alpha = O_1 P \sin^2 \alpha.$$

With $a = fm = f \cdot 2O_1 P / N_1$, we get

$$N_1 = 2f / \sin^2 \alpha. \quad (9.18)$$

PROBLEM 9.3

A pair of spur gears has 16 teeth and 18 teeth, a module 12.5 mm, an addendum 12.5 mm, and a pressure angle 14.5°. Prove that the gears have interference. Determine the minimum number of teeth and the velocity ratio to avoid interference.

SOLUTION

From the given data, $a = 12.5$ mm = m . So, $f = 1$. The speed ratio $\lambda = 16/18$. Since the pressure angle α is equal to 14.5°, $\sin \alpha = 0.25038$. Using (9.17), we get

$$N_{1\min} = \frac{2 \times 1 \times (16/18)}{\{1 + \frac{16}{18}(\frac{16}{18} + 2) \times 0.25038^2\}^{1/2} - 1} = 22.94 \approx 23.$$

Since $N_{1\min}$ is greater than the actual number of teeth in the pinion (given to be 16), interference will occur.

With $N_1 = 23$, the minimum number of teeth $N_{2\min}$ on the wheel required to maintain the speed ratio as close to 16/18 as possible will be $(18/16) \times 23 \approx 26$. Hence, the speed ratio = 23/26 = 0.885, whereas the given speed ratio = 16/18 = 0.889. If the speed ratio has to be maintained exactly at 16/18, we should then have $N_1 = 24$ and $N_2 = 27$.

PROBLEM 9.4

Find out the minimum number of teeth a pinion meshing with a rack having a 20° pressure angle and an addendum equal to the module should have to avoid interference.

SOLUTION

Since the addendum is equal to the module, $f = 1$. With $\alpha = 20^\circ$, the minimum number of teeth on the pinion can be found, using (9.18), as

$$N_{1\min} = (2 \times 1) / \sin^2 20^\circ = 17.1 \approx 18.$$

There are several methods of avoiding undercutting with a small number of teeth on the pinion. One such is by using a tooth profile which is a combination of involute and cycloidal curves. (A cycloidal profile also maintains conjugate action, i.e., the angular velocity ratio is uniform.)

Standardization of Involute Gears

The previous two subsections make the importance of a proper selection of addendum amply clear. Such a selection has to be done to achieve the required contact ratio but without causing any interference. This, along with the need to ensure interchangeability, has led to the standardization of involute gears.

In the past, an operating pressure angle of $14\frac{1}{2}^\circ$ had been common. This was due to the fact that most gears used to be cast in the earlier days and $\sin 14\frac{1}{2}^\circ$ being approximately equal to $1/4$ layout of pattern was very convenient. Currently, a pressure angle of 20° is used as fewer teeth can be cut without undercutting. Due to the tendency towards larger pressure angle, sometimes $22\frac{1}{2}^\circ$ or even 25° is recommended, especially in aerospace engineering. The addendum and dedendum are also standardized by relating them to the module, following the British system, as

$$\text{addendum } (a) = \text{module } (m),$$

$$\text{dedendum } (b) = 1.25 \text{ module } (m).$$

9.5 SYNTHESIS OF CONJUGATE TOOTH PROFILES FOR CIRCULAR SPUR GEARS

It has been shown in Section 9.2 that proper gearing action is obtained when the common normal to the mating tooth surfaces passes through a fixed point on the line of centres. This action (satisfying the fundamental law of gearing) is often termed as *conjugate action* and the profiles satisfying this condition are called *conjugate profiles*.³ It has been shown that involutes fulfil the requirement of conjugate action. However, in general, if any profile is prescribed, its conjugate profile can be found out. In this section, we present the graphical and analytical procedures for determining the conjugate of a prescribed arbitrary profile.

Graphical Approach

The main advantage of the graphical approach is that the mathematical equation of the prescribed profile is not required. Figure 9.8 shows two bodies 1 and 2, hinged to the frame at O_1 and O_2 respectively. If $S_1 T_1$ is the prescribed profile on body 1, it is desired to determine the conjugate profile on body 2. The conjugate action requires that the common normal to the contacting surface at the point of contact should pass through a fixed point P on the line of centres. To determine

³For noncircular spur gears, see the second edition of this text.

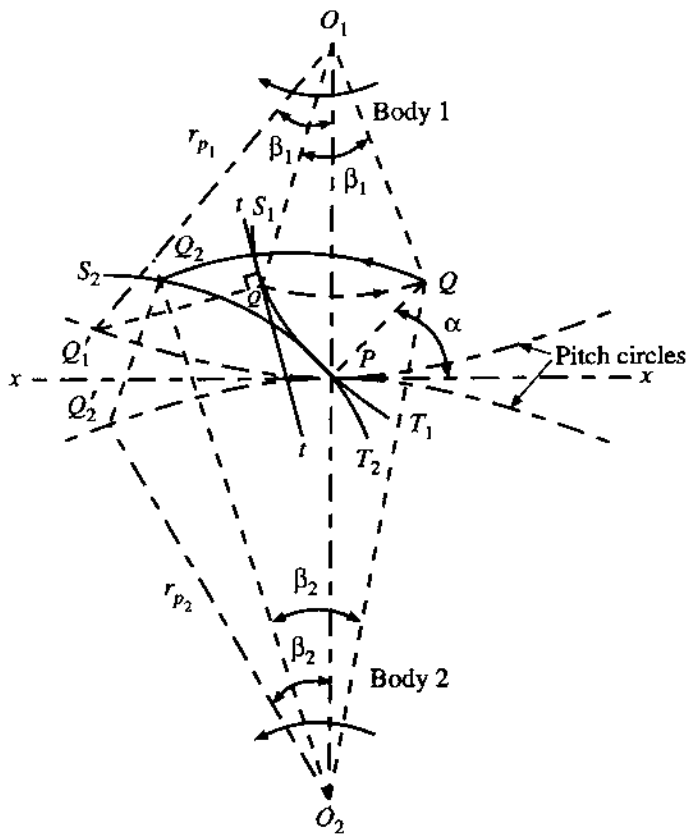


FIGURE 9.8

the conjugate profile of S_1T_1 , we will take a point Q_1 on this profile and find out the corresponding point Q_2 of the conjugate profile. Repeating this for a large number of points on S_1T_1 , the conjugate profile S_2T_2 can be determined.

A tangent $t-t$ is first drawn to the prescribed profile at Q_1 , and a line perpendicular to this tangent is drawn through Q_1 that intersects the circular arc with O_1 as the centre and $O_1P (= r_{p_1})$ as the radius at Q'_1 . Q_1 takes the position Q when body 1 is rotated back to bring Q'_1 to P . A circular arc is drawn through Q_1 with O_1 as the centre and Q is marked on this arc so that $PQ = Q'_1Q_1$. The point Q indicates the location of the contact point in space when the point Q_1 on the profile S_1T_1 touches its conjugate. The point on body 2 at Q takes the position Q_2 when body 2 rotates through an amount corresponding to the rotation of body 1 which brings Q to Q_1 . Since the pitch circles roll over each other, arc PQ'_1 = arc PQ'_2 . So,

$$r_{p_1}\beta_1 = r_{p_2}\beta_2.$$

We first draw a circular arc through Q with O_2 as the centre and then mark Q_2 on this arc so that $PQ = Q'_2Q$. This instantaneous value of the pressure angle (when the point of contact is at Q) α is given by $\angle xPQ$ as shown in the figure.

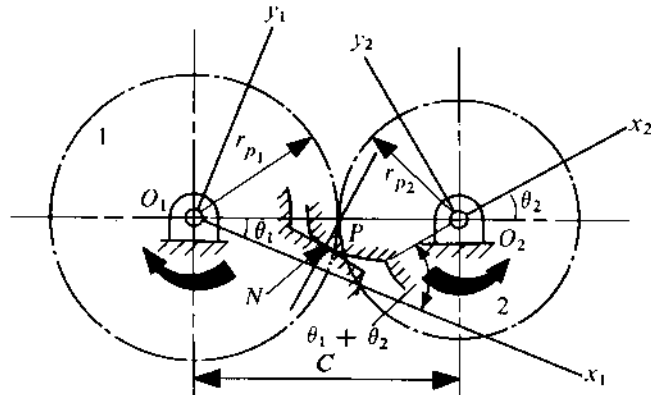


FIGURE 9.9

Analytical Approach

The pitch circles of two mating gears are shown in Fig. 9.9. P is the pitch point; as noted earlier this is also the instantaneous centre of rotation of the two gears. The coordinate systems x_1y_1 and x_2y_2 are fixed for gears 1 and 2, respectively. The profile of the tooth on gear 1 in the system x_1y_1 is

$$y_1 = f_1(x_1). \quad (9.19)$$

It is convenient to choose the x_1 -axis so as to pass through the centreline of the given tooth. The problem is to find the profile of the mating tooth,

$$y_2 = f_2(x_2), \quad (9.20)$$

so that constant angular velocity ratio is maintained.

As the pitch circles roll on each other without slipping, we have $r_{p_1}\theta_1 = r_{p_2}\theta_2$, where θ_1 and θ_2 are the inclinations of the line of centres in the two coordinate systems as shown in Fig. 9.9. So,

$$\theta_1 + \theta_2 = (1 + r_{p_1}/r_{p_2})\theta_1 = \gamma\theta_1, \quad (9.21)$$

where $\gamma = 1 + r_{p_1}/r_{p_2}$. Let $C (= r_{p_1} + r_{p_2})$ be the distance between gear centres. The angle between the coordinate axes x_2 and x_1 (as also between the y_2 - and y_1 -axis) is $(\theta_1 + \theta_2)$ or $\gamma\theta_1$ [from (9.21)]. The coordinates of the point O_2 in the system x_1y_1 are $(C \cos \theta_1, C \sin \theta_1)$. So, the equations of transformations between the coordinate systems will become

$$x_2 = (x_1 - C \cos \theta_1) \cos (\gamma\theta_1) + (y_1 - C \sin \theta_1) \sin (\gamma\theta_1), \quad (9.22)$$

$$y_2 = -(x_1 - C \cos \theta_1) \sin (\gamma\theta_1) + (y_1 - C \sin \theta_1) \cos (\gamma\theta_1). \quad (9.23)$$

N is the point of contact of the two tooth profiles. For the angular velocity ratio to be constant, the common normal to the profiles at N must pass through the point P . As (9.19) is given the slope of the line PN , $[-1/f'_1(x_1)]$, can be determined. The coordinates of the point P are $(r_{p_1} \cos \theta_1, r_{p_1} \sin \theta_1)$. Thus, the equation for the line PN is

$$y_1 - r_{p_1} \sin \theta_1 = -\frac{1}{f'_1(x_1)}(x_1 - r_{p_1} \cos \theta_1). \quad (9.24)$$

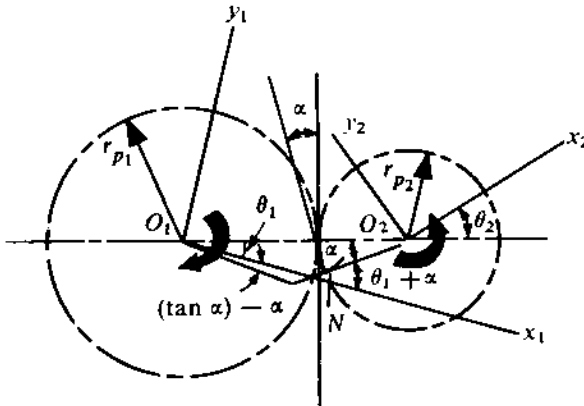


FIGURE 9.10

The coordinates of the point of contact N in the system x_1y_1 can be obtained by the simultaneous solution of (9.19) and (9.24). Using the transformation equations (9.22) and (9.23), we obtain the tooth profile (x_2, y_2) for the mating gear. The equation of the tooth profile is obtained in parametric form, with θ_1 as the parameter. The coordinates of the point of contact N , expressed in terms of a fixed coordinate system, yield the equation of the line of action. Generally, (9.19) is also given in the parametric form

$$x_1 = x_1(\theta_1), \quad y_1 = y_1(\theta_1), \quad (9.25)$$

and the mating gear tooth profile is obtained in the form

$$x_2 = x_2(\theta_1), \quad y_2 = y_2(\theta_1). \quad (9.26)$$

The solution obtained so far is not unique; there are, in fact, many profiles of the form $y_1 = f_1(x_1)$ and $y_2 = f_2(x_2)$ which will ensure a constant angular velocity ratio.

To illustrate this, let us now impose another restriction, namely, the bearing reactions should be constant for constant torque (this will tend to reduce noise and vibrations). To satisfy this condition, the line PN , normal to the mating tooth curves at the point of contact N , must make a constant angle α (known as *pressure angle*) with the perpendicular to the line of centres O_1O_2 (Fig. 9.10). Note that the torque $T_1 = F_c \cos \alpha \cdot r_{p_1}$, where F_c is the contact force at the tooth. The components of the bearing reaction are $F_c \cos \alpha$ and $F_c \sin \alpha$.

From Fig. 9.10, it is seen that the tangent to the tooth profile at N (the point of contact) makes an angle α with the line of centres O_1O_2 (as the normal makes an angle α with the line perpendicular to O_1O_2). Thus, the slope of the tooth profile at N is

$$\begin{aligned} y'_1 &= dy_1/dx_1 = f'_1(x_1) \\ &= \tan(\theta_1 + \alpha). \end{aligned} \quad (9.27)$$

Let the profile of tooth on gear 1 be of the same form as that given by (9.25). Using (9.27), we can write (9.24) as

$$y_1 = r_{p_1} \sin \theta_1 - (x_1 - r_{p_1} \cos \theta_1)/\tan(\theta_1 + \alpha). \quad (9.28)$$

Differentiating, we get

$$\begin{aligned} dy_1 &= r_{p_1} \cos \theta_1 d\theta_1 - \cot(\theta_1 + \alpha) dx_1 - \cot(\theta_1 + \alpha) r_{p_1} \sin \theta_1 d\theta_1 \\ &\quad + (x_1 - r_{p_1} \cos \theta_1) \operatorname{cosec}^2(\theta_1 + \alpha) d\theta_1. \end{aligned}$$

Again using (9.27), we get

$$\begin{aligned}\tan(\theta_1 + \alpha) dx_1 &= r_{p_1} \cos \theta_1 d\theta_1 - \cot(\theta_1 + \alpha) dx_1 - \cot(\theta_1 + \alpha) r_{p_1} \sin \theta_1 d\theta_1 \\ &\quad + (x_1 - r_{p_1} \cos \theta_1) \operatorname{cosec}^2(\theta_1 + \alpha) d\theta_1\end{aligned}$$

which, on simplification, gives

$$\frac{dx_1}{d\theta_1} - x_1 \cot(\theta_1 + \alpha) = -r_{p_1} \cos \alpha \frac{\cos^2(\theta_1 + \alpha)}{\sin(\theta_1 + \alpha)}. \quad (9.29)$$

This is the linear differential equation for the point of contact N . Multiplying both sides by

$$\exp \left[\int -\cot(\theta_1 + \alpha) d\theta_1 \right] = \exp[-\log \sin(\theta_1 + \alpha)] = \operatorname{cosec}(\theta_1 + \alpha),$$

we get

$$\begin{aligned}\frac{d}{d\theta_1} [\operatorname{cosec}(\theta_1 + \alpha) x_1] &= -r_{p_1} \cos \alpha \cot^2(\theta_1 + \alpha), \\ x_1 \frac{1}{\sin(\theta_1 + \alpha)} &= r_{p_1} \cos \alpha \left[\frac{\cos(\theta_1 + \alpha)}{\sin(\theta_1 + \alpha)} + (\theta_1 + \alpha) \right] + V.\end{aligned}$$

If the constant of integration V is taken as $(\tan \alpha - \alpha)r_{p_1} \cos \alpha$, then

$$x_1 = r_{p_1} \cos \alpha [(\theta_1 + \tan \alpha) \sin(\theta_1 + \alpha) + \cos(\theta_1 + \alpha)]. \quad (9.30)$$

Substituting (9.30) in (9.28), we have

$$\begin{aligned}y_1 &= r_{p_1} \sin \theta_1 - r_{p_1} \{ \cos \alpha [(\theta_1 + \tan \alpha) \sin(\theta_1 + \alpha) + \cos(\theta_1 + \alpha)] - \cos \theta_1 \} / \tan(\theta_1 + \alpha) \\ &= r_{p_1} [\sin \theta_1 - (\theta_1 + \tan \alpha) \cos \alpha \sin(\theta_1 + \alpha) + \cos \alpha \cos(\theta_1 + \alpha) \\ &\quad - \cos \theta_1] / \tan(\theta_1 + \alpha).\end{aligned}$$

On simplification, we get

$$y_1 = r_{p_1} \cos \alpha [\sin(\theta_1 + \alpha) - (\theta_1 + \tan \alpha) \cos(\theta_1 + \alpha)]. \quad (9.31)$$

Equations (9.30) and (9.31) define the tooth profile of gear 1. Comparing these two equations with (9.8) and (9.9), we see that this profile is an involute with

$$r_{b_1} = r_{p_1} \cos \alpha, \quad (9.32)$$

$$\psi = \theta_1 + \alpha, \quad (9.33)$$

$$\psi + \delta = \theta_1 + \tan \alpha, \quad \delta = \tan \alpha - \alpha = \operatorname{inv}(\alpha).$$

So, for the particular constant of integration chosen, the involute starts at an angle $(\tan \alpha - \alpha)$ below the x_1 -axis. Putting $\theta_1 = 0$, we get $x_1 = r_{p_1}$ and $y_1 = 0$. Thus, the curve cuts the pitch circle at the x_1 -axis.

Having obtained x_1 and y_1 , the profile of the mating tooth can be determined from the transformation equations (9.22) and (9.23), using (9.21) and the relation $C = r_{p_1} + r_{p_2}$. Thus,

$$x_2 = -r_{p_2} \cos \alpha [(-\theta_2 + \tan \alpha) \sin(-\theta_2 + \alpha) + \cos(-\theta_2 + \alpha)], \quad (9.34)$$

$$y_2 = r_{p_2} \cos \alpha [(-\theta_2 + \tan \alpha) \cos (-\theta_2 + \alpha) + \sin (-\theta_2 + \alpha)]. \quad (9.35)$$

Therefore, the mating profile is also an involute with a base circle (of radius $r_{p_2} \cos \alpha$) which is tangent to the line of action PN , and we see that the involute profile is the unique curve for a spur gear tooth that will maintain a constant pressure angle (implying that the bearing reaction constant load will be constant). This advantage is in addition to the advantage mentioned in section 9.2.

PROBLEM 9.5

Let the profile of a tooth on a 25-cm 12-tooth pinion be trapezoidal with an included angle of 30° (see Fig. 9.11). Determine the tooth profile of the mating gear which has 24 teeth. The addendum and dedendum of the given tooth are 1.25 cm and 1.60 cm, respectively.

SOLUTION

The coordinate axis x_1 is taken to be through the centre of the given trapezoidal tooth. As there are 12 teeth on the pinion, $\angle P_1 O_1 P_2 = 360^\circ / (2 \times 12) = 15^\circ$. The coordinates of the point D are $(D, 0)$, where

$$x_D = O_1 D = O_1 P_1 \cos 7.5^\circ + D P_1 \cos 15^\circ, \quad D P_1 / \sin 7.5^\circ = O_1 P_1 / \sin 15^\circ.$$

Therefore,

$$x_D = O_1 P_1 (\cos 7.5^\circ + \sin 7.5^\circ \cot 15^\circ) = r_{p_1} (1.478) = \frac{25}{2} \times 1.478 = 18.5 \text{ cm}.$$

Furthermore,

$$C = r_{p_1} + r_{p_2} = 12.5 + 25 = 37.5 \text{ cm}, \quad \theta_2 = \theta_1 / 2, \quad \gamma = 1 + r_{p_1} / r_{p_2} = 1.5.$$

Thus, (9.19) for the given tooth profile becomes

$$y_1 - y_D = -\tan 15^\circ (x_1 - x_D),$$

$$y_1 = -0.268(x_1 - 18.5) = 4.96 - 0.268x_1. \quad (a)$$

Thus, $f'_1(x_1) = -0.268$. Equation (9.24) for the line of action can now be written as

$$y_1 - 12.5 \sin \theta_1 = 3.73(x_1 - 12.5 \cos \theta_1). \quad (b)$$

The simultaneous solution of (a) and (b) gives the coordinates of the point of contact N . These are

$$x_1 = 1.24 + 11.65 \cos \theta_1 - 3.125 \sin \theta_1, \quad y_1 = 4.628 - 3.13 \cos \theta_1 + 0.837 \sin \theta_1.$$

Now, using (9.22) and (9.23), we get

$$\begin{aligned} x_2 &= (1.24 - 25.85 \cos \theta_1 - 3.125 \sin \theta_1) \cos (1.5\theta_1) \\ &\quad + (4.628 - 3.13 \cos \theta_1 - 36.663 \sin \theta_1) \sin (1.5\theta_1), \end{aligned}$$

$$\begin{aligned} y_2 &= -(1.24 - 25.85 \cos \theta_1 - 3.125 \sin \theta_1) \sin (1.5\theta_1) \\ &\quad + (4.628 - 3.13 \cos \theta_1 - 36.663 \sin \theta_1) \cos (1.5\theta_1). \end{aligned}$$

By using different values of θ_1 in these equations for x_2 and y_2 , we can get the profile of the mating tooth.

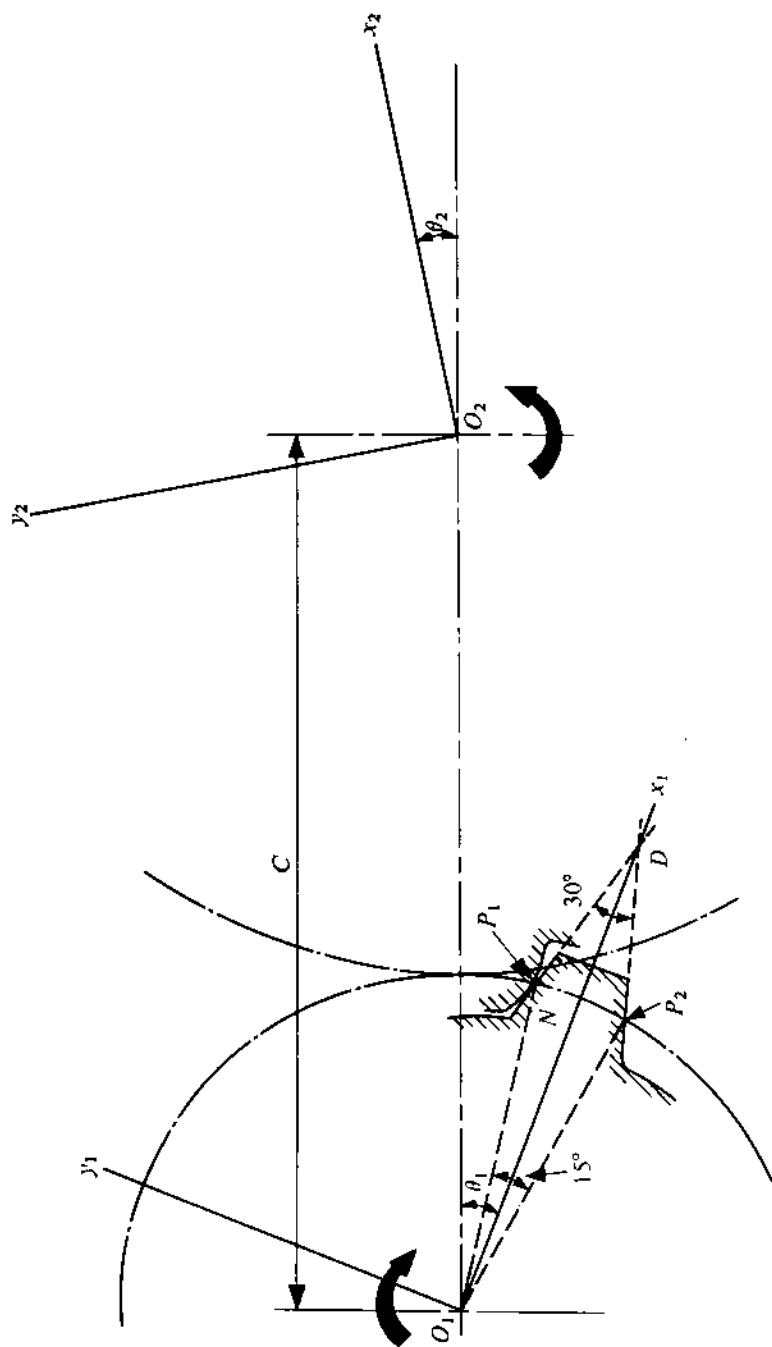


FIGURE 9.11

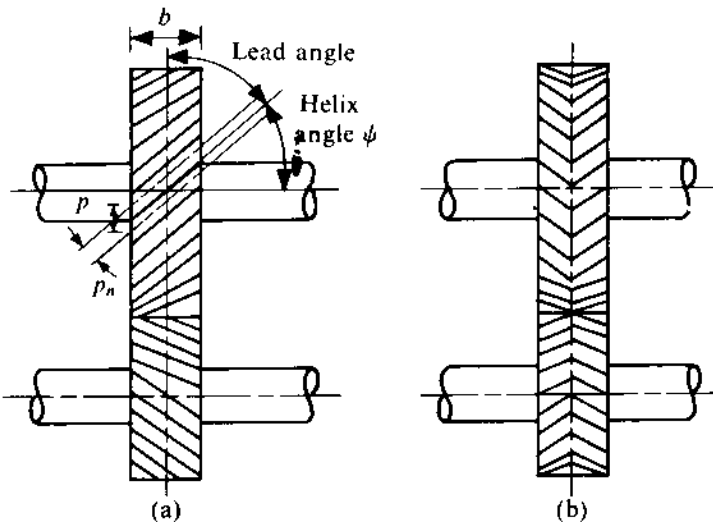


FIGURE 9.12

9.6 HELICAL, SPIRAL, BEVEL, AND WORM GEARS

In this section, we shall briefly discuss helical, spiral, bevel, and worm gears which are often used instead of spur gears to meet some particular requirement.

Helical Gears

The use of spur gears is most common when two parallel shafts are to be connected. However, to reduce noise and to improve the smoothness of operation, helical gears are preferred. The teeth of such gears form part of a helix (Fig. 9.12a), and the normal force between the teeth is inclined to the axis of rotation, resulting in an axial thrust. This can be obviated by the use of double helical gearing (called herring bone gears) where each gear has both left- and right-handed helices (Fig. 9.12b). Note that in both Figs. 9.12a and 9.12b the mating helices should be in opposite directions. While discussing straight spur gears, we saw that the tooth surface is generated by a line parallel to the axis of rotation (line aa in Fig. 9.13a). In a helical gear, the tooth surface is generated by the line aa shown in Fig. 9.13b, which is inclined to the axis of rotation at an angle ψ_b , called the *base helix angle*. The surface generated is called an *involute helicoid*. The smoothness of operation results from the fact that the engagement between the teeth is gradual; it starts from one end and the length of the contact line increases gradually as it proceeds.

The helix angle ψ is measured at the pitch circle as shown in Fig. 9.12a. The circular pitch, measured in the plane normal to the teeth, is

$$p_n = p \cos \psi, \quad (9.36)$$

where p is the circular pitch measured in the plane of rotation. As the normal diametral pitch $P_n = \pi/p_n$, we can write

$$P_n = P / \cos \psi, \quad (9.37)$$

where P is the diametral pitch in the plane of rotation. The angle $(90^\circ - \psi)$ is known as the *lead angle*.

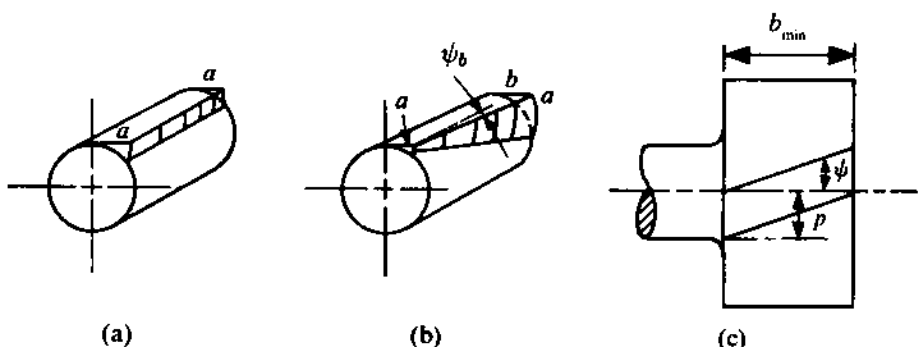


FIGURE 9.13

The minimum face width b of a helical gear can be found out since as soon as a tooth leaves its contact the tooth succeeding it must come into engagement. Thus, from Fig. 9.13c,

$$b_{\min} = p / \tan \psi. \quad (9.38)$$

The American Gear Manufacturers' Association recommends that b_{\min} so calculated should be increased by 15%. Thus,

$$b_{\min} = 1.15p / \tan \psi. \quad (9.39)$$

Spiral Gears

Spiral gears or crossed-helical gears are used for connecting inclined shafts which do not intersect. As the contact between the mating teeth is always at a point, these gears are suitable only for transmitting a small amount of power. The distance between the gear centres is given by the shortest distance between the axes of rotation. A pair of spiral gears is shown in Fig. 9.14. When viewed along the line connecting the gear centres, the shaft angle θ is the angle by which the axis of rotation of one gear has to be rotated to make it parallel to that of the other when the two shafts rotate in opposite directions. Note that crossed-helical gears are no different from helical gears unless mounted on shafts. For gears with the same hand helix, the angle between the shafts (Fig. 9.14) is

$$\theta = \alpha + \beta, \quad (9.40)$$

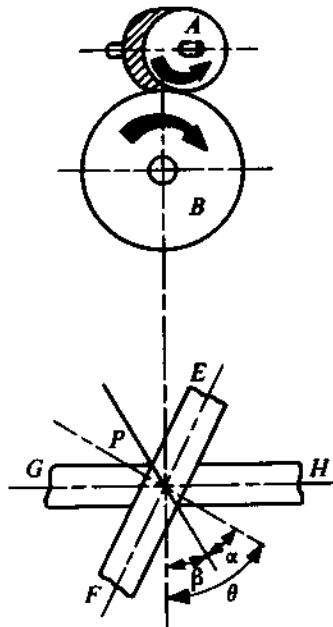
where α and β are the helix angles of the gears. When the hands of the gears are opposite,

$$\theta = \alpha - \beta. \quad (9.41)$$

The proof of (9.41) is left as an exercise for the reader.

PROBLEM 9.6

Two inclined shafts are connected by a pair of spiral gears. The angle between the shafts is 15° and one of the spiral gears is right-handed with a helix angle of 25° . Determine the hand and the helix angle of the other gear.



α, β = helix angles
 θ = shaft angle

FIGURE 9.14

SOLUTION

When the hands in a pair of spiral gears are the same, the angle between the shafts is the sum of the helix angles of the two gears. Since the shaft angle is less than the helix angle of the right-handed spiral gear, the hands of the two gears must be opposite. Thus, the other spiral gear of the pair must be left-handed, and its helix angle is $25^\circ - 15^\circ = 10^\circ$.

Bevel Gears

Bevel gears are used for connecting two shafts whose axes are intersecting. The pitch surfaces in this case are truncated cones, one of which rolls over the other (Fig. 9.15a). The standard practice is to specify the pitch diameter at the larger end of the pitch surface (Fig. 9.15b). The angles γ_1 and γ_2 are known as *pitch angles* and $\theta (= \gamma_1 + \gamma_2)$ is called the *shaft angle*. If the teeth on the bevel gears are parallel to the lines generating the pitch cones, then they are called straight-bevel gears. If the pitch angle of any one of the two bevel gears is 90° , then it is known as a *crown* or *face gear*. The pitch surface of a face gear is obviously a cylinder. (Note the similarity of a rack in spur gearing to a face gear in bevel gearing.) To reduce noise, helical teeth can also be used on bevel gears; these are known as *spiral-bevel gears*. Sometimes, gears very similar to bevel gears are used with the shafts offset. These are called *hypoid gears* as their pitch surfaces are hyperboloids of revolution.

Worm and Worm Gears

If a tooth of a helical gear makes complete revolutions on the pitch cylinder, the resulting gear is known as a *worm*. The mating gear is called *worm gear* or *worm wheel*. A single-threaded worm and

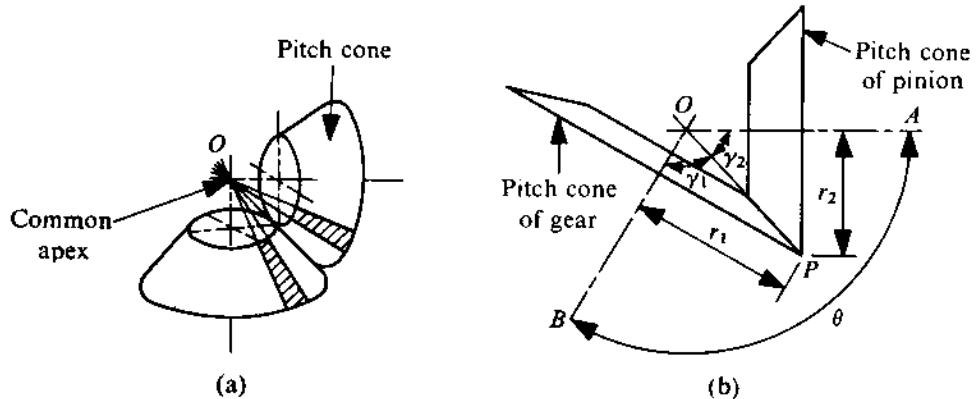


FIGURE 9.15

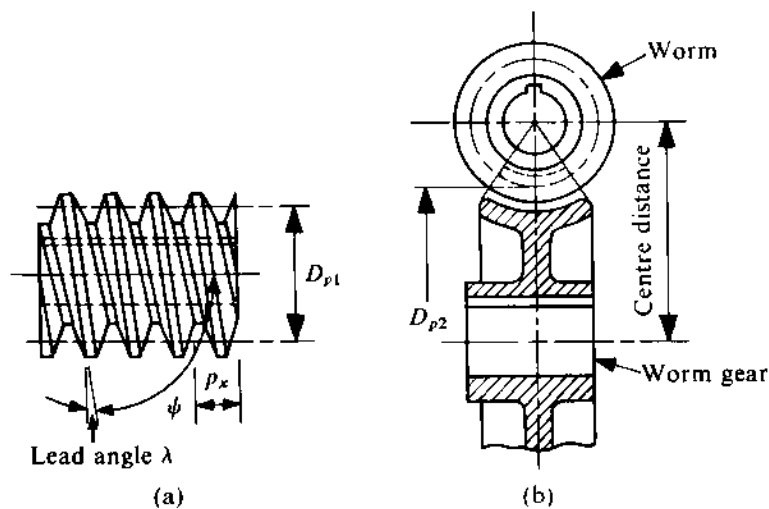


FIGURE 9.16

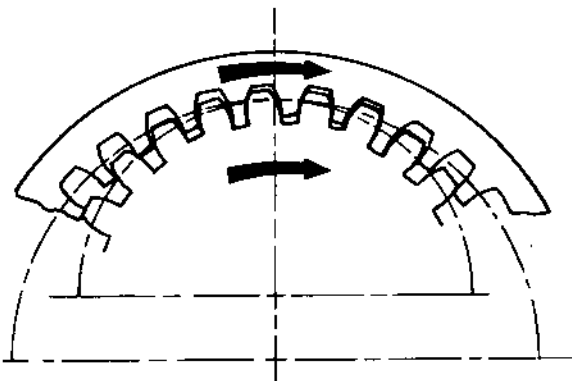


FIGURE 9.17

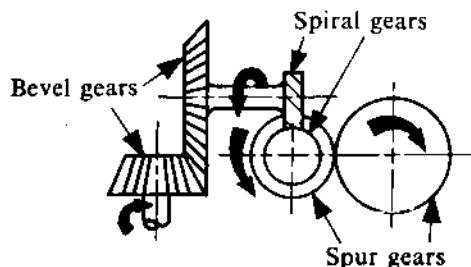


FIGURE 9.18

worm wheel, with axes at 90° , are shown in Figs. 9.16a and 9.16b, respectively. The driver is the worm and it is used for obtaining a high reduction in speed. The contact between the mating teeth along a line and is different from that in spiral gearing where the contact is at a point. Thus, it can be used for transmitting greater loads. A new quantity *lead* has to be defined in the case of a worm for calculating the speed ratio. The *lead* l is the axial movement of a point on the helix of a worm when it makes one revolution. Thus,

$$l = p_x N_1, \quad (9.42)$$

$$\omega_1 / \omega_2 = N_2 / N_1, \quad (9.43)$$

where p_x is the axial pitch of the worm, N_1 is the number of threads on the worm, N_2 is the number of teeth on the wheel, and ω_1 and ω_2 are the angular velocities of the worm and the wheel, respectively.

If the shafts are at right angles to each other (which is most common), $p_x = p$, where p is the circular pitch of the worm wheel. The lead angle of the worm will be equal to the helix angle of the worm wheel. So, with the shafts at right angles to each other,

$$\omega_1 / \omega_2 = \pi D_{p2} / l, \quad (9.44)$$

where D_{p2} is the pitch diameter of the worm wheel.

All the examples given so far refer to external gearing, but there can be internal gearing also as shown in Fig. 9.17. The direction of rotation of internally-mating gears is the same, as indicated in Fig. 9.17.

7 GEAR TRAINS

A combination of gears that is used for transmitting motion from one shaft to another is known as a *gear train*; it may include various types of gears. One such gear train of bevel, spiral, and spur gears is shown in Fig. 9.18. We shall consider two types of gear trains. In one type, referred to as a *simple train*, the axes of rotation of the gears are fixed in space as in the train shown in Fig. 9.18. In the other type, known as an *epicyclic gear train*, the gears revolve about axes that are not fixed in space. The term "epicyclic" comes from the fact that points on gears with moving axes of rotation will describe epicycloid paths. The second type will be discussed in detail later in this section.

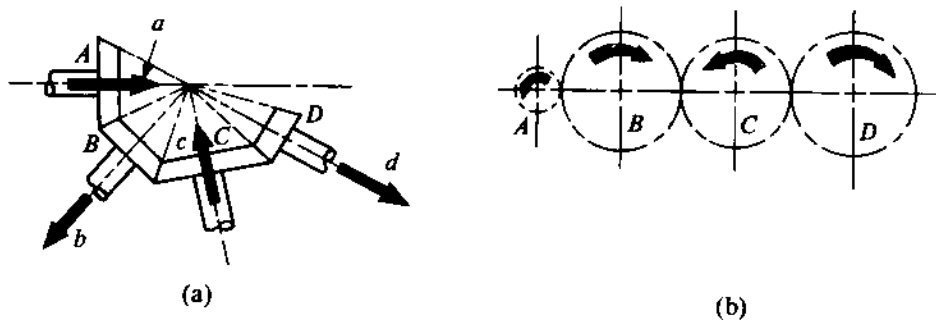


FIGURE 9.19

In a simple gear train, each shaft carries only one gear. If any one of the intermediate shaft (i.e., a shaft other than the input and output shafts) carries more than one gear, then the train is said to be a *compound gear train*.

Figure 9.19a shows a simple gear train consisting of four gears A , B , C , and D . Let the speed of rotation (rpm) be n_A , n_B , n_C , and n_D , respectively, and let the number of teeth in each gear be N_A , N_B , N_C , and N_D . Then,

$$n_A/n_B = N_B/N_A, \quad n_B/n_C = N_C/N_B, \quad n_C/n_D = N_D/N_C, \quad (9.45)$$

$$n_A/n_D = N_D/N_A. \quad (9.46)$$

The number of teeth on intermediate gears is not significant in respect of the speed ratio between two gears. The direction of the rotation is indicated in the figure (viewed from the same direction). For the simple train (consisting of only bevel gears) shown in Fig. 9.19b, equations (9.45) and (9.46) will apply, and the direction of rotation is represented by the vectors a , b , c , and d along respective axes (using the right-hand-screw notation for the sense). For gears with parallel axes of rotation the proper sign should be used for the right-hand side of (9.45) or (9.46), depending on the direction of rotation. So,

$$n_A/n_B = -N_B/N_A, \quad n_B/n_C = -N_C/N_B, \quad n_C/n_D = -N_D/N_C, \quad (9.45a)$$

$$n_A/n_D = -N_D/N_A. \quad (9.46a)$$

In a compound gear train, the number of teeth on the intermediate gears will influence the speed ratio. Consider the compound gear train shown in Fig. 9.20. Here, $n_B = n_C$ as the gears are mounted on the same shaft. Now,

$$n_A/n_B = -N_B/N_A, \quad n_C/n_D = -N_D/N_C, \quad n_B/n_D = -N_D/N_C,$$

$$\frac{n_A}{n_D} = \frac{N_B N_D}{N_A N_C} = \text{train value from } D \text{ to } A. \quad (9.47)$$

It is not difficult to visualize the motion of the gears in a simple or a compound gear train and it is easy to find the speed ratio. However, in epicyclic gear trains, it is sometimes difficult to see how the gears will operate as some of them rotate about axes which also are in motion. That is why we use methods for analyzing epicyclic gear trains which are rather mechanical, without trying to visualize the actual motion of the gears. Two such methods are discussed in this section. These are (i) the tabulation method, and (ii) the algebraic method.

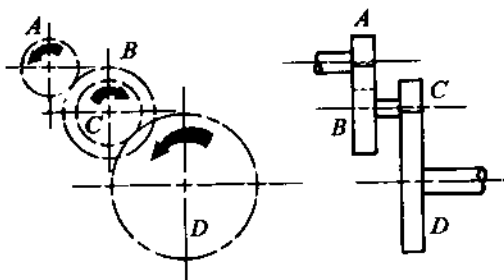


FIGURE 9.20

The basic principle of these methods is that the relative motion between a pair of mating gears is always the same (being equal to the inverse ratio of the number of teeth on the gears) whether the axes of rotation are fixed or moving. Figure 9.21 shows a simple epicyclic gear train where the gear A can rotate about an arm which itself rotates about the axis of the gear B . Before explaining this principle, let us consider the epicyclic gear train in Fig. 9.21, and show that it has two degrees of freedom. The number of links n is four, namely, the fixed link, gear B , arm, and gear A . The number of higher pairs h is 1. From equation (1.6), the number of simple hinges is

$$j = j_1 + 2j_2 + \dots = 1 + 2 \cdot 1 = 3 \quad (j_1 = 1 \text{ at } Q, j_2 = 1 \text{ at } O).$$

So, from (1.7a), the number of degrees of freedom is

$$F = 3(n - 1) - 2j - h = 9 - 6 - 1 = 2.$$

Thus, to have one output speed, two of the other speeds must be specified, i.e., we must have two inputs. Alternatively, one input will give rise to two outputs.

To explain the principle of relative motion in an epicyclic train, let us consider one of the inputs n_B of the train, shown in Fig. 9.21, to be zero (i.e., the gear B is fixed) and the other input n_{arm} as given. Under such circumstances, the fixed gear B is called the *sun* gear, A is termed the *planet* gear, and the arm is said to be the *planet carrier*. Such trains are referred to as *planetary gear trains*.

Let the arm be given a clockwise rotation θ (Fig. 9.21), thereby bringing the initial point of contact on A to T . Obviously,

$$\text{arc } RT = \text{arc } RP, \quad \frac{\phi}{\theta} = \frac{D_B}{D_A} = \frac{N_B}{N_A},$$

where D_A and D_B are the respective pitch diameters of the gears A and B . Thus,

$$\text{relative rotation of } B \text{ with respect to the arm} = \theta \quad (\text{CCW}),$$

$$\text{relative rotation of } A \text{ with respect to the arm} = \phi = \frac{N_B}{N_A} \theta \quad (\text{CW}).$$

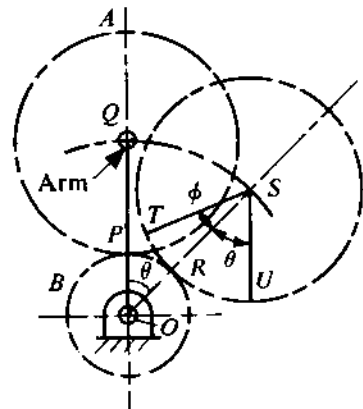


FIGURE 9.21

(Note that the absolute rotations of gears are obtained after adding the rotation of the arm to these values.) So, we can write

$$\frac{n_B - n_{\text{arm}}}{n_A - n_{\text{arm}}} = \frac{\theta}{\phi} = -\frac{N_A}{N_B} = \text{train value from } A \text{ to } B. \quad (9.48)$$

Equation (9.48) forms the basis of the algebraic method of analyzing epicyclic gear trains. In general, the right-hand side of (9.48) should be replaced by the train value from A to B if there is any intermediate compound gear train. The method will be explained by the solved problems that follow.

There are three steps in the tabular method of analyzing the train:

- (i) Lock all gears to the arm and give the arm x turns. Tabulate the resulting number of turns of each gear.
- (ii) Fix the arm and give y turns to one of the gears. Tabulate the resulting number of turns of the arm and of each gear.
- (iii) Add the results from steps (i) and (ii) to obtain the resultant number of turns of the arm and of all the gears.

Now, as two inputs are given, two equations are obtained for solving x and y . Once x and y are known, the revolutions of all the other elements can be determined, as these have already been expressed in terms of x and y in step (iii).

The analysis of a few epicyclic trains by both methods is given in Problems 9.7, 9.8, and 9.9. We shall always assume CCW rotation to be positive and CW rotation to be negative. If the number of teeth on a gear in a gear train is not given, it should be calculated on the assumption that all gears are of the same pitch.

PROBLEM 9.7

The gear B of the planetary gear train shown in Fig. 9.22 is fixed. The arm A carries a planet gear C . The arm A , and the gears D and E are free to turn on the shaft. The number of teeth on each gear is indicated in the figure. The gears B , D , and E are cut from gear blanks of the same diameter. Determine the number of turns of the gears D and E if the arm A is given one counter-clockwise rotation.

SOLUTION

Algebraic Method

Using (9.48), we have

$$\begin{aligned} \frac{n_B - n_{\text{arm}}}{n_E - n_{\text{arm}}} &= \text{train value from } E \text{ to } B \\ &= \frac{51}{20} \times \frac{20}{50} = \frac{51}{50}. \end{aligned}$$

Since $n_B = 0$ and $n_{\text{arm}} = 1$, we get

$$-\frac{1}{n_E - 1} = \frac{51}{50}, \quad 1 - n_E = \frac{50}{51}, \quad n_E = \frac{1}{51} \quad (\text{CCW}).$$

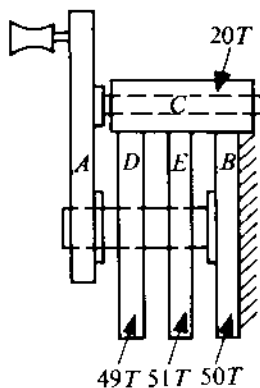


FIGURE 9.22

Similarly,

$$\begin{aligned} \frac{n_B - n_{\text{arm}}}{n_D - n_{\text{arm}}} &= \text{train value from } D \text{ to } B \\ &= \frac{49}{20} \times \frac{20}{50} = \frac{49}{50}, \\ 1 - n_D &= \frac{50}{49}, \quad n_D = -\frac{1}{49} = \frac{1}{49} \quad (\text{CW}). \end{aligned}$$

Tabular Method

Using the tabular method, we obtain the details as in Table 9.1. It is given that $x = 1$ and $x + y = 0$. So, $x = 1$ and $y = -1$. Therefore,

$$n_D = 1 - \frac{50}{49} = -\frac{1}{49},$$

$$n_E = \frac{1}{49} \quad (\text{CW}),$$

$$n_E = 1 - \frac{50}{51} = \frac{1}{51},$$

$$n_E = \frac{1}{51} \quad (\text{CCW}).$$

This train is known as *Ferguson's paradox*. The results indicate that, as the arm rotates, the gears D and E rotate very slowly in opposite directions.

PROBLEM 9.8

In the gear train shown in Fig. 9.23, the wheel C is fixed, the gear B is connected to the input shaft, and the gear F is connected to the output shaft. The arm A , carrying the compound wheels D and E , turns freely on the output shaft. If the input speed is 1000 rpm (CCW) when seen from the right, determine the speed of the output shaft. The number of teeth on each gear is indicated in the figure.

TABLE 9.1

Condition	Arm A	Rotations of Gears		
		B	D	E
Gears locked		x	x	x
Arm fixed	0	y	$\frac{50}{49}y$	$\frac{50}{51}y$
Resultant	x	$x + y$	$x + \frac{50}{49}y$	$x + \frac{50}{51}y$

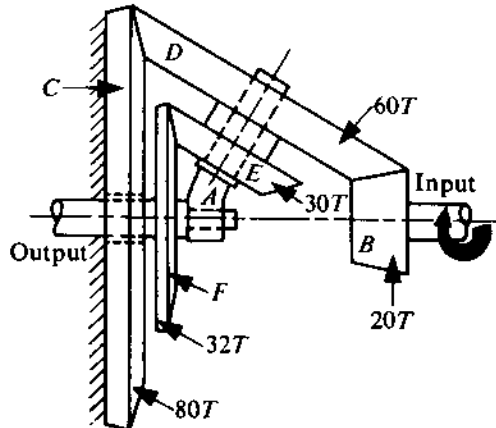


FIGURE 9.23

SOLUTION*Algebraic Method*

It is given that $n_C = 0$ and $n_B = 1000$. Applying (9.48), we get

$$\frac{n_C - n_{\text{arm}}}{n_B - n_{\text{arm}}} = \text{train value from } B \text{ to } C$$

$$= -\frac{20}{60} \times \frac{60}{80} = -\frac{1}{4}.$$

The negative sign is judged from the sense of rotation of B and C connected by D. Thus,

$$\frac{-n_{\text{arm}}}{1000 - n_{\text{arm}}} = -\frac{1}{4}, \quad 4n_{\text{arm}} = 1000 - n_{\text{arm}}, \quad n_{\text{arm}} = 200.$$

Again using (9.48), we get

$$\frac{n_F - n_{\text{arm}}}{n_B - n_{\text{arm}}} = \text{train value from } B \text{ to } F$$

TABLE 9.2

Condition	Arm <i>A</i>	Rotations of		
		<i>B</i>	<i>C</i>	<i>F</i>
Gears locked	<i>x</i>	<i>x</i>	<i>x</i>	<i>x</i>
Arm fixed	0	<i>y</i>	$-\frac{20}{80}y$	$-\frac{20}{60} \times \frac{30}{32}y$
Resultant	<i>x</i>	$x + y$	$x - \frac{20}{80}y$	$x - \frac{20}{60} \times \frac{30}{32}y$

$$= -\left(\frac{20}{60} \times \frac{30}{32}\right) = -\frac{5}{16}.$$

Considering the train $B - (D - E) - F$, we have

$$\frac{n_F - 200}{800} = -\frac{5}{16}, \quad 3200 - 16n_F = 4000, \quad n_F = -50.$$

So, the output speed is 50 rpm (CW) if viewed from the right.

Tabular Method

The details we get using the tabular method are listed in Table 9.2. It is given that

$$x + y = 1000 = n_B,$$

$$n_C = x - \frac{20}{80}y = 0.$$

Solving these equations, we get $y = \frac{4}{5} \times 1000 = 800$ and $x = 200$. Thus, the output speed is $n_F = x - \frac{5}{16}y = 200 - 250 = -50$ rpm, that is, 50 rpm (CW) if viewed from the right.

PROBLEM 9.9

In the gear train shown in Fig. 9.24, *A* is the driving shaft which rotates at 270 rpm in the counter-clockwise direction (viewed from the left). The casing (which is an annular wheel) is fixed. The gears *E* and *H* are keyed to the vertical shaft on which *F* is free to rotate. The compound gears *K* and *L* are rigidly connected to the pin carried by *F*. The number of teeth on each gear is indicated in the figure. Determine the speed of the output shaft.

SOLUTION

The gears *D* and *G* are not part of the epicyclic gear train, so we consider the rest of the train and calculate the speed of *D* from that of *E*, and the speed of *G* from that of *F*. The number of teeth on the annular wheel *C* is

$$N_C = N_H + N_K + N_L$$

TABLE 9.3

Condition	Arm (Gear F)	Rotations of Gears*		
		E and H	K and L	C
Gears locked	y	y	y	y
Arm fixed	0	x	$-\frac{40}{20}x$	$-\frac{40}{20} \times \frac{30}{90}x$
Resultant	y	$x + y$	$y - \frac{40}{20}x$	$y - \frac{40}{20} \times \frac{30}{90}x$

*The gears L and C rotate in the same direction.

since $r_C = r_H + r_K + r_L$, and assuming the pitch to be same for all the gears. Thus, $N_C = 40 + 20 + 30 = 90$. The epicyclic train, consisting of the arm (pin) and gears E , F , H , K , L , and C , is solved by the tabular method as shown in Table 9.3.

It is given that $n_C = 0$ and $n_D = 270$ rpm. So,

$$n_E = \frac{40}{30}n_D = \frac{40}{30} \times 270 = 360 \text{ rpm (CCW)} \quad (\text{when viewed from the top}),$$

$$n_F = x + y = 360, \quad n_C = y - \frac{2}{3}x = 0.$$

Solving these equations, we get $x = 216$ rpm, $y = 144$ rpm. Therefore,

$$n_F = y = 144 \text{ rpm (CCW)} \quad (\text{when viewed from the top}),$$

$$n_G = \frac{N_F}{N_G}n_F = \frac{50}{80} \times 144 = 90 \text{ rpm (CCW)} \quad (\text{when viewed from the right}).$$

Thus, the output shaft rotates at 90 rpm in a direction opposite to that of the input shaft. The solution to this problem by the algebraic method is left as an exercise for the reader.

The fact that an epicyclic gear train has two degrees of freedom has application in the rear-axle differential of an automobile (Fig. 9.25). The purpose of the rear-axle differential is to permit the wheels to rotate at different speeds when the automobile is taking a turn. When the automobile moves along a straight track, there is no relative motion between the gear C (called the planet gear) and the gears D and E (which are connected to the wheel shafts). The two planet gears act just as keys to transmit motion from the ring gear B to the gears D and E . The speed at which the gears B , D , and E rotate is the same. While taking a turn, the planet gears rotate about their own axes and the train becomes an epicyclic one, giving two output speeds (for the gears D and E) with one input speed (for the gear B). Using any of the methods explained earlier, it can be shown that the speed of B is always the arithmetic mean of the speed at which the gears D and E rotate.

9.8 TORQUES IN EPICYCLIC GEAR TRAINS

If all members of an epicyclic gear train rotate at a constant angular velocity (i.e., without any acceleration), then the sum of the three external torques (two inputs and one output, or vice versa)

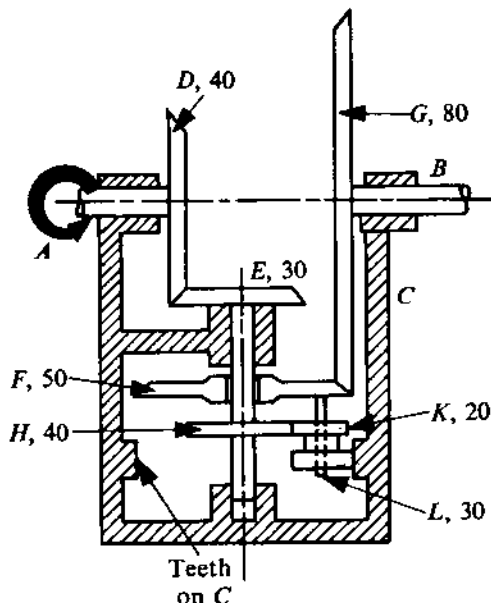


FIGURE 9.24

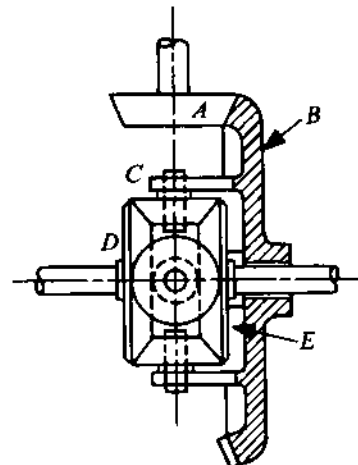


FIGURE 9.25

must be zero. Thus,

$$M_1 + M_2 + M_3 = 0. \quad (9.49)$$

If there is no friction loss, the power input must be equal to the power output. Mathematically, this can be expressed as

$$M_1\omega_1 + M_2\omega_2 + M_3\omega_3 = 0, \quad (9.50)$$

where ω_1 , ω_2 , and ω_3 are the angular velocities of corresponding members.

In a planetary gear train, the angular velocity of one member (called the sun gear) is zero. If

$$\omega_3 = 0, \quad (9.51)$$

then M_3 is known as the *holding torque*, which is the torque required to hold that gear fixed. Let M_1 refer to the input torque and M_2 be the output torque. Then, (9.49) to (9.51) can be used to determine the output torque and the holding torque if the input torque is given.

PROBLEM 9.10

In Problem 9.8, let the input power be 7.5 kW. Find the output torque and the holding torque to keep the wheel C fixed.

SOLUTION

The input torque is

$$M_1 = \frac{7.5 \times 10^3 \times 60}{2\pi n_1}.$$

With $n_1 = 1000$ rpm, we get $M_1 = 71.66$ N-m. If the output torque is M_2 , since $\omega_3 = 0$, and $n_2 = -50$ rpm, (9.50) gives

$$M_2 = -M_1 \frac{\omega_1}{\omega_2} = -71.66 \times \frac{1000}{-50} = 1433 \text{ N-m.}$$

From (9.49), the holding torque is

$$M_3 = -(M_1 + M_2) = -1504.66 \text{ N-m.}$$

9.9 PROBLEMS

9.11 Solve Problem 9.5 if the given tooth profile is rectangular instead of trapezoidal.

9.12 The tooth of the pinion is a pin of circular cross-section (as used in alarm clocks) of radius a with centre on the pitch circle of radius r_{p_1} . Show that the equation of the mating tooth profile is given by

$$x_2 = r_{p_1} \cos(C\theta_1/r_{p_2}) + a \sin\left(\frac{1}{2} + \frac{r_{p_1}}{r_{p_2}}\right)\theta_1 - C \cos\left(\frac{r_{p_1}}{r_{p_2}}\theta_1\right),$$

$$y_2 = -r_{p_1} \sin(C\theta_1/r_{p_2}) + a \cos\left(\frac{1}{2} + \frac{r_{p_1}}{r_{p_2}}\right)\theta_1 + C \sin\left(\frac{r_{p_1}}{r_{p_2}}\theta_1\right),$$

where

r_{p_2} = pitch circle radius of the gear,

C = distance between the centres of the gears, and

θ_1 = angle made by the line of centres with the x_1 -axis (passing through the centre of the pinion and the centre of the circular tooth).

9.13 When two equal gears mesh without interference, show that the minimum number of teeth N of these gears must satisfy the relation

$$3N^2 \sin^2 \alpha - 4fN - 4f^2 = 0.$$

9.14 Two identical involute spur gears are in mesh. The module is 4 mm and each gear has 22 teeth. If the operating pressure angle is 20° , determine the minimum value of addendum needed to ensure continuous transmission of motion.

9.15 Two involute spur gears of module 3 mm and with 18 and 26 teeth operate at a pressure angle of 20° . Find out the maximum addendum for the gears so that no interference occurs. Assume the addendum for the gears to be equal.

9.16 Speed is intended to be reduced from 1800 rpm in a single stage using two standard involute spur gears with 20° pressure angle. If the pinion has 14 teeth, determine the lowest possible speed of the driven shaft without causing any interference.

9.17 The teeth of a 18-tooth pinion have a rectangular profile. The pitch circle radius of the pinion is 250 mm. The addendum and the dedendum of the given tooth are 16 mm and 20 mm, respectively. Determine the tooth profile of a mating gear with 30 teeth.

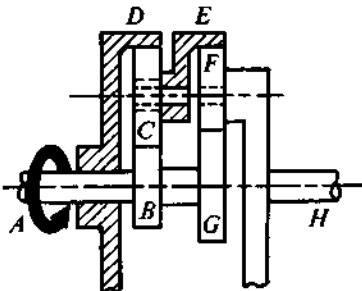


FIGURE 9.26

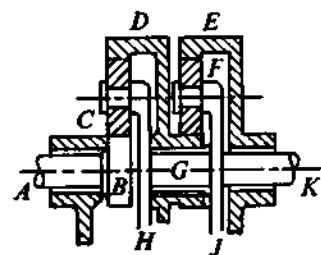


FIGURE 9.27

- 9.18 In the epicyclic gear train shown in Fig. 9.26, the wheels *B* and *G* are integral with the driving shaft *A*. The internal gear *D* is fixed, and the gear *C* rotates about a pin carried by the internal gear *E*. The gear *F* is carried by an arm which is keyed to the output shaft *H*. The number of teeth on each gear is

$$N_B = 20, \quad N_D = 80, \quad N_G = 24, \quad N_E = 80.$$

Determine the speed of the output shaft and the direction in which it rotates when the shaft *A* rotates at a speed of 1000 rpm in the counter-clockwise direction (viewed from the left), and the input power is 11 kW. Also determine the output torque and the torque required to keep the gear *D* fixed. *Hint:* Consider the two epicyclic trains separately having two different arms (i) keyed to *H*, (ii) carried by *E*.

- 9.19 The number of teeth on each gear of the automobile differential shown in Fig. 9.25 is

$$N_A = 12, \quad N_B = 56, \quad N_C = 12, \quad N_D = N_E = 16.$$

If the drive shaft rotates the gear *A* at 1000 rpm, find the speed of the right wheel when it is jacked-up, with the left wheel resting on the road surface.

- 9.20 A vehicle, with the differential shown in Fig. 9.25, takes a turn to the left so that the right wheel becomes the outer wheel. The speed of the vehicle is 45 km per hour, and the radius of the turn is 30 m (at the centre of the differential). The distance between the centres of the wheels is 1.65 m and the tyres are 40 cm in diameter. Calculate the speed of rotation of the wheels and of the ring gear *B*.

- 9.21 In the epicyclic gear train shown in Fig. 9.27, the input shaft *A* rotates at 1200 rpm CCW (viewed from the left). The internal wheel *E* is fixed, the gear *B* is keyed to the input shaft, and the planet carriers *H* and *J* are fixed with the output shaft *K*. The internal gear *D* and gear *G* form a compound gear which revolves about the axis of *A* and *K*. The planet *C* is carried by *H* and the planet *F* is carried by *J*. The number of teeth on the gears is $N_B = 24$, $N_D = 68$, $N_G = 30$, and $N_E = 64$. Determine the speed of the output shaft *K*, and the output torque and the holding torque on *E* if the input power is 3.7 kW.

- 9.22 In the gear train shown in Fig. 9.28, the sun gear *S* rotates at 500 rpm, and the planet carrier (arm *A*) rotates at 100 rpm in the same direction. Determine the number of teeth on each gear and the speed of the planet gear *P* if the diametral pitch of all the gears is 3 (teeth/cm) and the diameter of the fixed gear *F* (internal) is to be as close to 25 cm as possible.

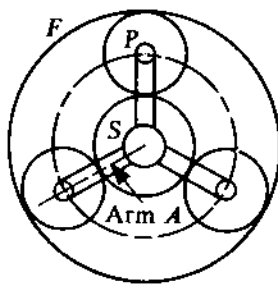


FIGURE 9.28

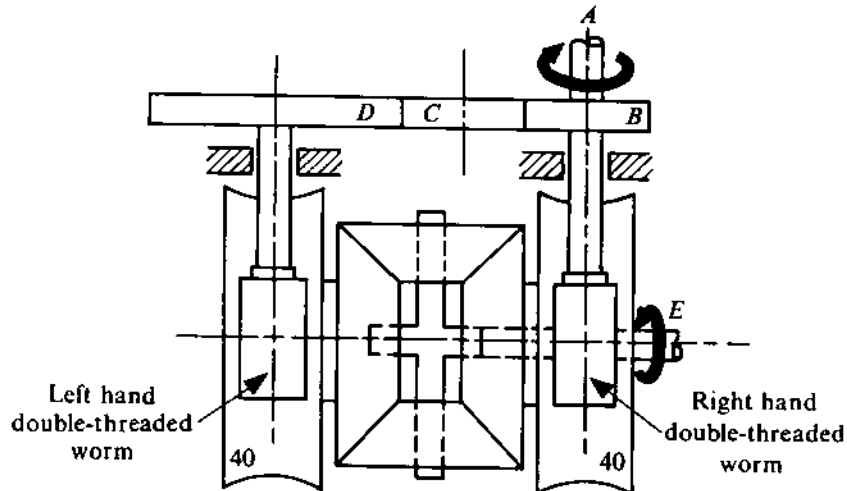


FIGURE 9.29

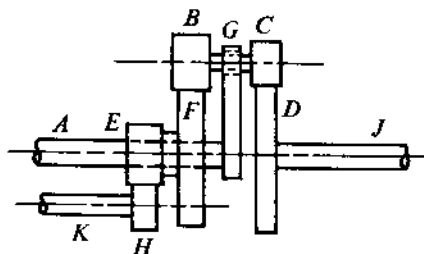


FIGURE 9.30

9.23 In the gear train shown in Fig. 9.29, the shaft A rotates at 500 rpm in the direction indicated. Determine N_B/N_D if the shaft E rotates at 5 rpm as shown. What would be the value of N_B/N_D if the rotation of the shaft E at 5 rpm is reversed? The number of teeth on each gear is indicated in the figure.

9.24 In the epicyclic gear train shown in Fig. 9.30, the compound wheels E and F rotate freely on the shaft A which carries the planet carrier G . The planets B and C are compound gears. The number of teeth on each gear is

$$N_E = 30, \quad N_H = 15, \quad N_B = 20, \quad N_C = 18, \quad N_D = 68.$$

The shafts A and K rotate in the same direction at 250 rpm and 100 rpm, respectively. Determine the speed of the shaft J . Hint: The gear H should not be considered as a part of the epicyclic train; the speed of H will determine that of E .

Chapter 10

GYROSCOPIC ACTION IN MACHINES

10.1 INTRODUCTION

The earliest observations and studies on gyroscopic phenomena were carried out during Newton's time (1642-1727). These were made in the context of the motion of our planet which, in effect, is a massive gyroscope. The credit for the mathematical foundation of the principles of gyroscopic motion goes to Euler (1707-1783). He derived a set of dynamical equations relating applied moment, inertia, angular acceleration, and angular velocity. In many machines, the rotating components are forced to turn about axes other than their own axes of rotation, and gyroscopic effects are thus set up. This chapter deals with the dynamics of gyroscopic action and some practical cases where gyroscopic effects play a dominant role.

10.2 MOTION OF A RIGID BODY IN THREE DIMENSIONS

Consider a rigid body which is free to move, as shown in Fig. 10.1. P represents a particle of the rigid body, with a mass δm . The total mass of the body is m . The coordinate axes are fixed in space, and the coordinates of the particle P at any instant of time are x , y , and z . The components of the velocity and acceleration of P are $(\dot{x}, \dot{y}, \dot{z})$ and $(\ddot{x}, \ddot{y}, \ddot{z})$, respectively. If $G(x_G, y_G, z_G)$ is the CG of the body, then, by definition, we get

$$\begin{aligned}\sum x\delta m &= mx_G, \\ \sum y\delta m &= my_G, \\ \sum z\delta m &= mz_G,\end{aligned}\tag{10.1}$$

the summation being taken over all the particles constituting the body. The component of force acting on the particle P in the x -direction at any instant is given by

$$\delta F_x = \ddot{x}\delta m.$$

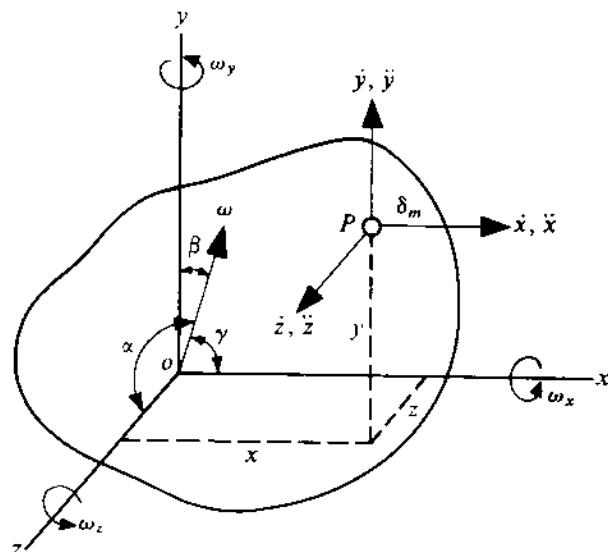


FIGURE 10.1

Similarly,

$$\delta F_y = \dot{y}\delta m,$$

$$\delta F_z = \dot{z}\delta m.$$

Therefore, the components of the resultant force acting on the whole body, obtained by summing δF_x , δF_y , and δF_z for all particles, are given by

$$F_x = \sum \delta F_x = \sum \ddot{x}\delta m = \frac{d^2}{dt^2} \sum x\delta m = \frac{d^2}{dt^2}(x_G m),$$

$$F_x = m\ddot{x}_G, \quad F_y = m\dot{y}_G, \quad F_z = m\dot{z}_G. \quad (10.2)$$

The resultant force acting on the body will be $F = \sqrt{(F_x^2 + F_y^2 + F_z^2)}$. The angular momentum of the particle P about the x -axis is given by the relation $\delta H_x = -(\delta m\dot{y})z + (\delta m\dot{z})y$ (considering the right-hand-screw rule for the sign convention). We can now obtain the total angular momentum of the body about the x -axis, and similarly, get the total angular momentum about the other two axes. Thus,

$$H_x = \sum \delta H_x = \sum \delta m(y\dot{z} - z\dot{y}),$$

$$H_y = \sum \delta H_y = \sum \delta m(z\dot{x} - x\dot{z}), \quad (10.3)$$

$$H_z = \sum \delta H_z = \sum \delta m(x\dot{y} - y\dot{x}).$$

The moment of the externally applied force about the x -axis is

$$M_x = \sum (\delta m y \ddot{z} - \delta m z \ddot{y}) = \frac{d}{dt} \sum \delta m(y\dot{z} - z\dot{y}).$$

The moment about the x -, y -, and z -axis can thus be expressed as

$$M_x = \frac{dH_x}{dt}, \quad M_y = \frac{dH_y}{dt}, \quad M_z = \frac{dH_z}{dt}. \quad (10.4)$$

10.3 RIGID BODIES IN SPHERIC MOTION

If one point in a moving rigid body remains fixed in space, then all other particles of the body are constrained to move on spherical surfaces. This is because the distance of any particle from the fixed point remains unchanged. Hence, this type of motion is called *spheric motion*.

Let the fixed point of the body correspond to the origin o (Fig. 10.1). Then, if the angular velocity of the body at any instant is ω (which is represented by a vector passing through the point o) and the inclination of the angular velocity vector to the x -, y -, and z -axis is α , β , and γ , respectively, the components of the angular velocity are given by

$$\omega_x = \omega \cos \alpha, \quad \omega_y = \omega \cos \beta, \quad \omega_z = \omega \cos \gamma, \quad (10.5)$$

the positive direction being clockwise when looking outwards from o . The velocity components of the particle P , expressed in terms of the angular velocity components, will be

$$\dot{x} = -y\omega_z + z\omega_y, \quad \dot{y} = -z\omega_x + x\omega_z, \quad \dot{z} = -x\omega_y + y\omega_x. \quad (10.6)$$

Using (10.3) and (10.6), the angular momentum H_x takes the form

$$H_x = \sum \delta m(y\dot{z} - z\dot{y}) = \sum \delta m[z^2\omega_x - xz\omega_z - xy\omega_y + y^2\omega_x].$$

As $\delta m \rightarrow 0$, we get

$$\begin{aligned} H_x &= \int [(z^2 + y^2)\omega_x - xz\omega_z - xy\omega_y] dm \\ &= \omega_x \int (z^2 + y^2) dm - \omega_y \int xy dm - \omega_z \int xz dm. \end{aligned}$$

By definition, the moments and the products of inertia are

$$J_{xx} = \int (y^2 + z^2) dm, \quad J_{xy} = \int xy dm, \quad J_{xz} = \int xz dm.$$

We can now obtain the angular momentum about the x -axis, and similarly, get the angular momentum about the other two axes. Thus,

$$\begin{aligned} H_x &= J_{xx}\omega_x - J_{xy}\omega_y - J_{xz}\omega_z, \\ H_y &= J_{yy}\omega_y - J_{yz}\omega_z - J_{yx}\omega_x, \\ H_z &= J_{zz}\omega_z - J_{zx}\omega_x - J_{zy}\omega_y. \end{aligned} \quad (10.7)$$

Principal Axes

If the xy -plane be a plane of symmetry (i.e., for every particle P , there exists an image particle P' , as shown in Fig. 10.2), then there will be two axes u and v in the xy -plane such that $J_{uv} = 0$. Moreover, as the xy -plane is a plane of symmetry, $J_{uu} = J_{vv} = 0$. For this condition, the z -axis

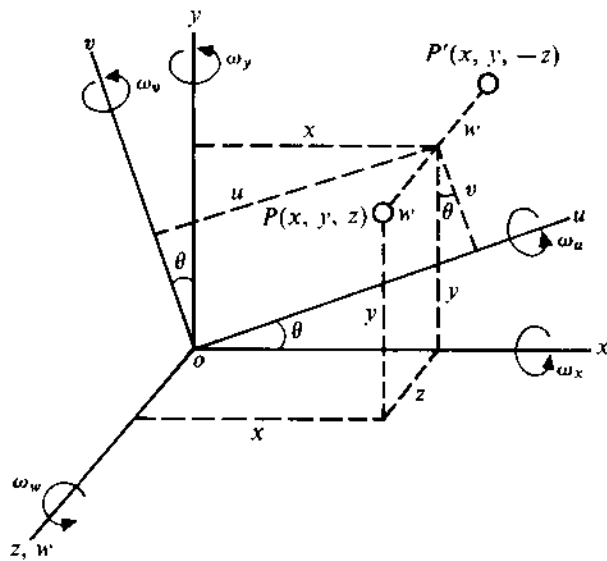


FIGURE 10.2

(or \$w\$-axis) is a *principal axis*, and the other principal axes \$u\$ and \$v\$ can be determined. If \$N\$ is the projection of the point \$P\$ (or \$P'\$) on the \$xy\$-plane, then

$$u = x \cos \theta + y \sin \theta, \quad v = y \cos \theta - x \sin \theta.$$

Now,

$$\begin{aligned} J_{uv} &= \int uv \, dm = \int (x \cos \theta + y \sin \theta)(y \cos \theta - x \sin \theta) \, dm \\ &= \sin \theta \cos \theta \int (y^2 - x^2) \, dm + (\cos^2 \theta - \sin^2 \theta) \int xy \, dm \\ &= \frac{1}{2} \sin 2\theta \int \{(y^2 + w^2) - (x^2 + w^2)\} \, dm + \cos 2\theta J_{xy} \\ &= \frac{1}{2} \sin 2\theta (J_{xx} - J_{yy}) + \cos 2\theta J_{xy}. \end{aligned}$$

If \$u\$ and \$v\$ are the principal axes, then \$J_{uv}\$ should vanish and we will get the equation for \$\theta\$. Thus,

$$\tan 2\theta = \left(\frac{2J_{xy}}{J_{yy} - J_{xx}} \right). \quad (10.8)$$

\$J_{uu}\$ can now be calculated and \$J_{vv}\$ obtained similarly. Thus,

$$\begin{aligned} J_{uu} &= \int (v^2 + w^2) \, dm = \int [(y \cos \theta - x \sin \theta)^2 + w^2] \, dm \\ &= \cos^2 \theta \int (y^2 + w^2) \, dm + \sin^2 \theta \int (x^2 + w^2) \, dm - 2 \sin \theta \cos \theta \int xy \, dm \end{aligned}$$

$$\begin{aligned}
 &= J_{xx} \cos^2 \theta + J_{yy} \sin^2 \theta - J_{xy} \sin 2\theta, \\
 J_{vv} &= J_{xx} \sin^2 \theta + J_{yy} \cos^2 \theta + J_{xy} \sin 2\theta.
 \end{aligned} \tag{10.9}$$

Angular Velocity and Momentum about the Principal Axes

When the principal axes have been determined and the components of angular velocity ω_x , ω_y , and ω_z are known, ω_u , ω_v , and ω_w can be readily evaluated. Thus,

$$\omega_u = \omega_x \cos \theta + \omega_y \sin \theta, \quad \omega_v = \omega_y \cos \theta - \omega_x \sin \theta, \quad \omega_w = \omega_z. \tag{10.10}$$

From (10.7), the components of angular momentum are

$$H_u = J_{uu}\omega_u, \quad H_v = J_{vv}\omega_v, \quad H_w = J_{ww}\omega_w \tag{10.11}$$

Since $J_{uv} = J_{vw} = J_{wu} = 0$. The resultant angular momentum will be

$$H = \sqrt{(H_u^2 + H_v^2 + H_w^2)} = \sqrt{(J_{uu}^2\omega_u^2 + J_{vv}^2\omega_v^2 + J_{ww}^2\omega_w^2)}. \tag{10.12}$$

Moreover,

$$\omega = \sqrt{(\omega_u^2 + \omega_v^2 + \omega_w^2)}. \tag{10.13}$$

Comparing (10.12) and (10.13), it is seen that the resultant angular velocity and angular momentum vectors are not in the same direction since

$$\omega_u : \omega_v : \omega_w \neq H_u : H_v : H_w.$$

Only when $J_{uu} = J_{vv} = J_{ww}$, will ω and H (the angular velocity vector and the angular momentum vector) act in the same direction.

10.4 EULER'S EQUATION OF MOTION

Figure 10.3 shows the resultant angular momentum H of a rigid body in motion with the point o fixed in space. The coordinate system xyz is also fixed, and the components of angular momentum are H_x , H_y , and H_z . At the instant shown, the coordinate system $\xi\eta\zeta$, which is rigidly connected with the moving body, is coincident with xyz as indicated in Fig. 10.3. This coordinate system rotates with the body, the components of angular velocity being ω_ξ , ω_η , and ω_ζ . Now, a change in the components of the angular momentum will be due to (i) an absolute change in magnitude of H or (ii) a rotation of the H -vector. The changes in these components in time δt are shown in Fig. 10.3. The total change in the x -, y -, and z -direction (or ξ -, η -, and ζ -direction), from Fig. 10.3, is

$$\delta H_\xi + H_\zeta \omega_\eta \delta t - H_\eta \omega_\zeta \delta t \quad (\text{in the } \xi\text{-direction}),$$

$$\delta H_\eta + H_\xi \omega_\zeta \delta t - H_\zeta \omega_\xi \delta t \quad (\text{in the } \eta\text{-direction}),$$

$$\delta H_\zeta + H_\eta \omega_\xi \delta t - H_\xi \omega_\eta \delta t \quad (\text{in the } \zeta\text{-direction}).$$

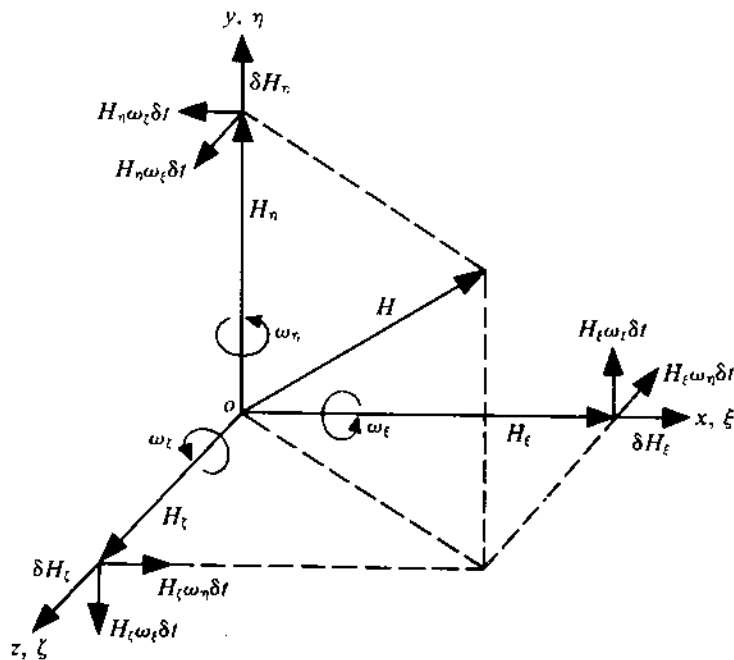


FIGURE 10.3

So, the rate of change of angular momentum in the x -, y -, and z -direction [which is equal to the corresponding component of the externally applied torque, according to equation (10.4)] is given by

$$\begin{aligned}\frac{dH_\xi}{dt} - H_\eta\omega_\zeta + H_\zeta\omega_\eta &= M_\xi, \\ \frac{dH_\eta}{dt} - H_\zeta\omega_\xi + H_\xi\omega_\eta &= M_\eta, \\ \frac{dH_\zeta}{dt} - H_\xi\omega_\eta + H_\eta\omega_\xi &= M_\zeta.\end{aligned}\quad (10.14)$$

These equations are known as *Euler's equations of motion*.

Euler's Modified Equation

In the derivation of (10.14), we assumed that the set of body axes ξ , η , and ζ are rigidly connected to the body in motion. It should be noted at this stage that this assumption is made in order to make the moments and products of inertia integrals invariant with time. If we choose a set of axes other than the body-fixed coordinate system, these integrals will then become functions of time and introduce an undesirable complexity in the angular momentum relationships. However, a notable exception occurs when a symmetric body spins about its axis of symmetry. Here, the moments of inertia integrals are not affected by the angular position of the body about its spin axis. In such a situation, it is advantageous to select another coordinate system $\xi'\eta'\zeta'$ such that the axes rotate about the fixed point o with an angular velocity which is different from that of the rigid body. The axes ξ' , η' , and ζ' are made to rotate with the frame supporting the body, and the resultant angular momentum vector \mathbf{H} is locked with the system $\xi'\eta'\zeta'$ and rotates along with it. If the components of

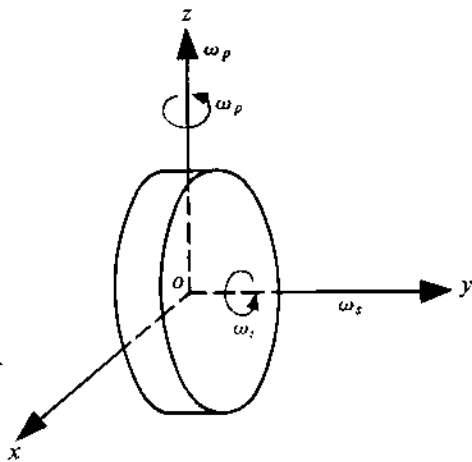


FIGURE 10.4

angular momentum are $H_{\xi'}$, $H_{\eta'}$, $H_{\zeta'}$ ($\omega_{\xi'}$, $\omega_{\eta'}$, $\omega_{\zeta'}$ being the corresponding components of angular velocity), then we get

$$\begin{aligned}\frac{dH_{\xi'}}{dt} - H_{\eta'}\omega_{\zeta'} + H_{\zeta'}\omega_{\eta'} &= M_{\xi'}, \\ \frac{dH_{\eta'}}{dt} - H_{\zeta'}\omega_{\xi'} + H_{\xi'}\omega_{\zeta'} &= M_{\eta'}, \\ \frac{dH_{\zeta'}}{dt} - H_{\xi'}\omega_{\eta'} + H_{\eta'}\omega_{\xi'} &= M_{\zeta'}.\end{aligned}\quad (10.15)$$

These equations are known as Euler's modified equations.

If ξ' is the axis of spin, then it can be shown that the angular momentum component $H_{\xi'}$ can be written as

$$H_{\xi'} = J_{\xi'\xi'}(\omega_{\xi'} + \omega_s),$$

where ω_s is the spin velocity. The other two angular momentum components can be expressed as

$$H_{\eta'} = J_{\eta'\eta'}\omega_{\eta'},$$

$$H_{\zeta'} = J_{\zeta'\zeta'}\omega_{\zeta'}.$$

10.5 SIMPLE PRECESSION OF A SYMMETRICAL ROTOR

Let us consider the rigid wheel shown in Fig. 10.4, which rotates at a constant angular velocity ω_s about the y -axis. The y -axis is termed the *axis of spin* and ω_s is known as the *spin velocity*. Now, if the axis of spin is rotated in the xy -plane with a uniform velocity ω_p about the z -axis, this is called simple *precessional motion*. The z -axis is termed the *axis of precession* and ω_p is known as the *precessional velocity*. Our objective is to determine the required external torque to produce motion of this type.

Let us consider a coordinate system $\xi'\eta'\zeta'$, which rotates about the z -axis with a velocity ω_p , and is coincident with the system xyz at any instant. Then,

$$\omega_{\xi'} = \omega_{\eta'} = 0,$$

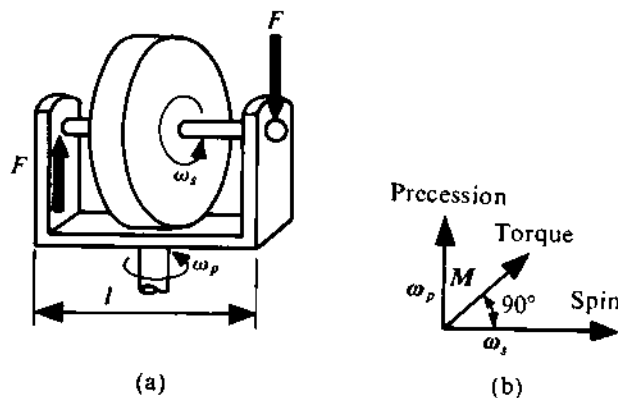


FIGURE 10.5

$$\omega_{\zeta'} = \omega_p.$$

The axes x , y , and z are the principal axes (as each of these is placed symmetrically with respect to the body at the instant being considered). Therefore, the corresponding components of angular momentum of the rotor are

$$H_x = H_{\xi'} = 0, \quad H_y = H_{\eta'} = J_{yy}\omega_s, \quad H_z = H_{\zeta'} = J_{zz}\omega_p.$$

Substituting these values in (10.15), we get

$$M_{\xi'} = -J_{yy}\omega_s\omega_p, \quad M_{\eta'} = 0, \quad M_{\zeta'} = 0.$$

So, a torque of magnitude $J_{yy}\omega_s\omega_p$ has to be applied on the rotor about the x -axis in a counter-clockwise direction when viewed outwards from o . An actual system describing such a motion is shown in Fig. 10.5a. In this case, a force F will be automatically developed on the bearings of the rotor shaft in the directions indicated, if the assembly is given a rotation ω_p about the vertical axis. If the moment of inertia of the rotor about the shaft axis is J , and if the spin velocity is ω_s , then

$$F = J\omega_s\omega_p/l.$$

In other words, the reaction at the bearings will be $(-F)$ if such a spinning rotor is given a precessional motion. This force is commonly termed the *gyroscopic reaction*.

In all such cases of simple precession, the relative orientation of the spin vector, the precession vector, and the torque vector can be easily determined as indicated in Fig. 10.5b. It is shown there that if the spin vector is rotated about the precession vector in the direction of precession through 90° , the new position of the spin vector will indicate the direction of the torque vector.

PROBLEM 10.1

The rotor of a turbojet engine has a mass 200 kg and a radius of gyration 25 cm. The engine rotates at a speed of 10,000 rpm in the clockwise direction if viewed from the front of the aeroplane. The plane while flying at 1000 km/hr turns with a radius of 2 km to the right. Compute the gyroscopic moment the rotor exerts on the plane structure. Also, determine whether the nose of the plane tends to rise or fall when the plane turns.

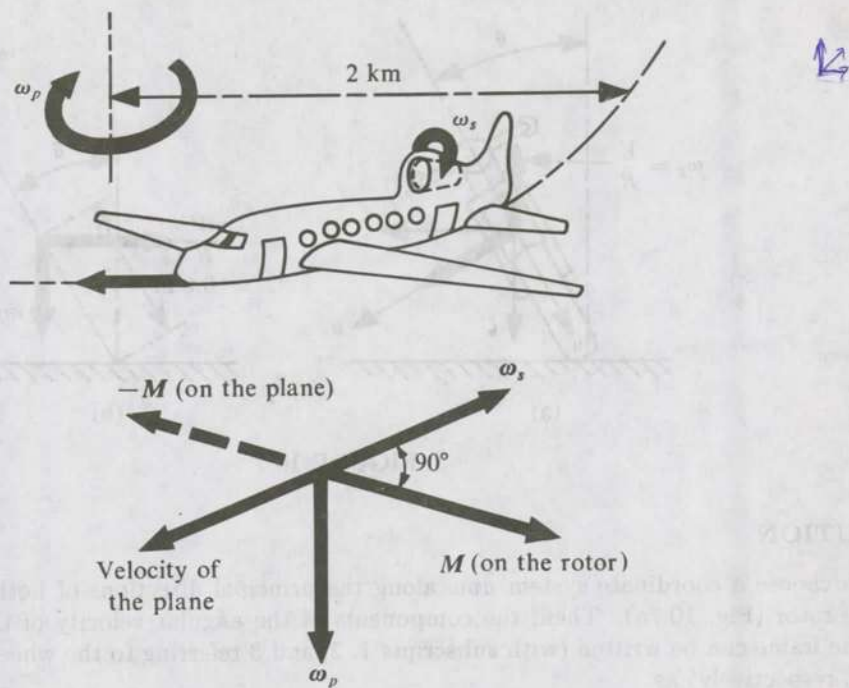


FIGURE 10.6

SOLUTION

The moment of inertia of the rotor is

$$J = 200 \times (0.25)^2 = 12.5 \text{ kg-m}^2.$$

The spin velocity is

$$\omega_s = (10,000 \times 2\pi)/60 = 1047.2 \text{ rad/s.}$$

The precessional velocity is

$$\omega_p = 1000/(2 \times 60 \times 60) = 0.139 \text{ rad/s.}$$

As ω_p and ω_s are at 90° (see Fig. 10.6), the magnitude of the gyroscopic moment is

$$M = J\omega_s\omega_p = 12.5 \times 1047.2 \times 0.139 = 1819.5 \text{ N-m.}$$

Referring again to Fig. 10.6, we find that the action of the moment M on the plane is such that it tends to raise the nose upwards.

PROBLEM 10.2

The total mass of a motorcycle with its rider is 200 kg and the resultant centre of mass is 0.6 m above the road level (when the machine is upright). The moment of inertia of each wheel of the motorcycle is 1 kg-m^2 . The engine rotates at a speed six times that of and in the same sense as the wheels. The moment of inertia of the rotating parts of the engine is 0.15 kg-m^2 . The diameter of the wheels is 0.6 m. Determine the angle of heel if the unit is travelling at a speed 60 km/hr along a curved road with a radius of 30 m.

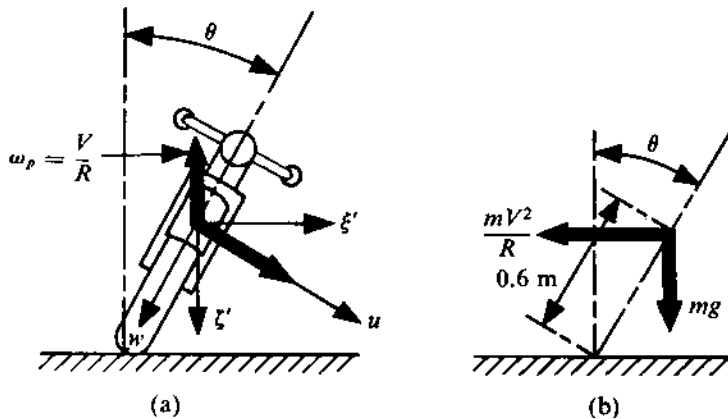


FIGURE 10.7

SOLUTION

Let us choose a coordinate system uvw along the principal directions of both the wheels and the engine rotor (Fig. 10.7a). Then, the components of the angular velocity of the wheels, the rotor and the frame can be written (with subscripts 1, 2, and 3 referring to the wheels, the rotor, and the frame, respectively) as

$$\omega_{1u} = \frac{V}{r} - \frac{V}{R} \sin \theta, \quad \omega_{2u} = \frac{6V}{r} - \frac{V}{R} \sin \theta, \quad \omega_{3u} = -\frac{V}{R} \sin \theta,$$

$$\omega_{1v} = 0, \quad \omega_{2v} = 0, \quad \omega_{3v} = 0, \quad \omega_{1w} = \omega_{2w} = \omega_{3w} = -(V/R) \cos \theta,$$

where V is the speed of the vehicle, R is the radius of the curved path, r is the radius of each wheel and θ is the angle of heel. The components of the angular momentum of the unit as a whole are

$$H_u = J_{1u}\omega_{1u} + J_{2u}\omega_{2u} + J_{3u}\omega_{3u},$$

$$H_v = 0,$$

$$H_w = J_{1w}\omega_{1w} + J_{2w}\omega_{2w} + J_{3w}\omega_{3w},$$

where the J 's refer to the moments of inertia. As $R = 100r$ and J_1 , J_2 , and J_3 are of the same order of magnitude, the components of H can be approximated, neglecting the term V/R , as

$$H_u \approx J_{1u}\omega_{1u} + J_{2u}\omega_{2u} \\ = 1 \times \left(\frac{60 \times 1000}{0.3 \times 60 \times 60} \right) + 0.15 \times \left(\frac{6 \times 60 \times 1000}{0.3 \times 60 \times 60} \right) = 105.56 \text{ kg-m}^2/\text{s},$$

$$H_v = 0,$$

$$H_w \approx 0.$$

Now, fixing the coordinate system $\xi'\eta'\zeta'$ to the motorcycle frame (as done in Fig. 10.7a), we can express the angular momentum and angular velocity components as

$$H_\xi' = H_u \cos \theta = 105.56 \cos \theta, \quad H_\eta' = 0, \quad H_\zeta' = H_u \sin \theta = 105.56 \sin \theta,$$

$$\omega_\xi' = 0, \quad \omega_\eta' = 0, \quad \omega_\zeta' = -\frac{V}{R} = -\frac{60 \times 1000}{30 \times 60 \times 60} = -0.56 \text{ rad/s}.$$

sing (10.15) and noting that all angular velocities are constant, we obtain

$$M_{\xi'} = -H_{\eta'}\omega_{\zeta'} + H_{\zeta'}\omega_{\eta'} = 0,$$

$$M_{\eta'} = -H_{\zeta'}\omega_{\xi'} + H_{\xi'}\omega_{\zeta'} = -59.11 \cos \theta \text{ N-m},$$

$$M_{\zeta'} = -H_{\xi'}\omega_{\eta'} + H_{\eta'}\omega_{\xi'} = 0.$$

Considering that the ground force at the tyre-road junction balances the weight and the centrifugal force (see Fig. 10.7b), we have

$$M_{\eta'} = (mv^2/R) \times 0.6 \cos \theta - mg \times 0.6 \sin \theta = -59.11 \cos \theta$$

$$\tan \theta = \frac{0.6mv^2/R + 59.11}{0.6mg} = \frac{1170.2}{1177.2} = 0.99$$

$$\theta \approx 45^\circ.$$

PROBLEM 10.3

For the turbine rotor of a ship, mass = 20,000 kg, radius of gyration = 0.75 m, and speed = 2000 rpm clockwise when viewed from the front of the ship). The ship pitches harmonically with an amplitude of 10° and a time period of 20 s. The turbine is supported on bearings 5 m apart. Determine the maximum reaction at the front bearing and the direction of this reaction force when the front of the ship is rising. The CG of the rotor may be assumed to be at the midspan between the bearings.

SOLUTION

The gyroscopic moment on the rotor will be maximum when the angular velocity of pitching ω_p is maximum. With a harmonic motion, the instantaneous pitch angle is

$$\theta_p = \Theta_0 \sin(2\pi t/T),$$

where Θ_0 is the amplitude and T is the time period. So,

$$\omega_p = \dot{\theta}_p = \frac{2\pi}{T} \Theta_0 \cos \frac{2\pi t}{T}.$$

The maximum value of ω_p will be

$$\omega_{p\max} = 2\pi\Theta_0/T.$$

When the front of the ship is rising, the direction of ω_s , ω_p , and M will be as shown in Fig. 10.8. The magnitude of M_{\max} is found out to be

$$M_{\max} = 20,000 \times 0.75^2 \times (2000 \times 2\pi/60) \times 0.054 = 127,235 \text{ N-m.}$$

The front bearing reaction (horizontal) on the rotor shaft is

$$R = M_{\max}/5 = 25,446 \text{ N.}$$

The vertical bearing reaction is

$$\frac{1}{2}mg = \frac{1}{2} \times 20,000 \times 9.8 = 98,000 \text{ N.}$$

So, the maximum resultant front bearing reaction on the rotor shaft is given by

$$(25,446^2 + 98,000^2)^{1/2} = 101,250 \text{ N.}$$

The direction of the reaction force is also shown in Fig. 10.8.

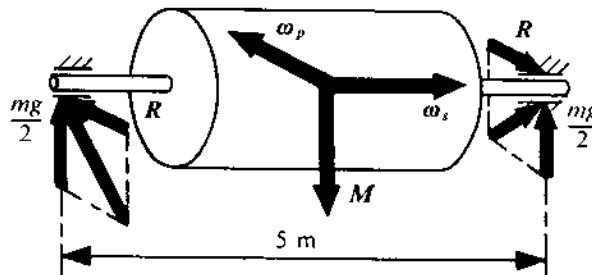
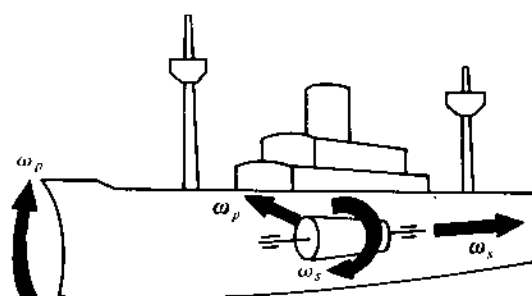


FIGURE 10.8

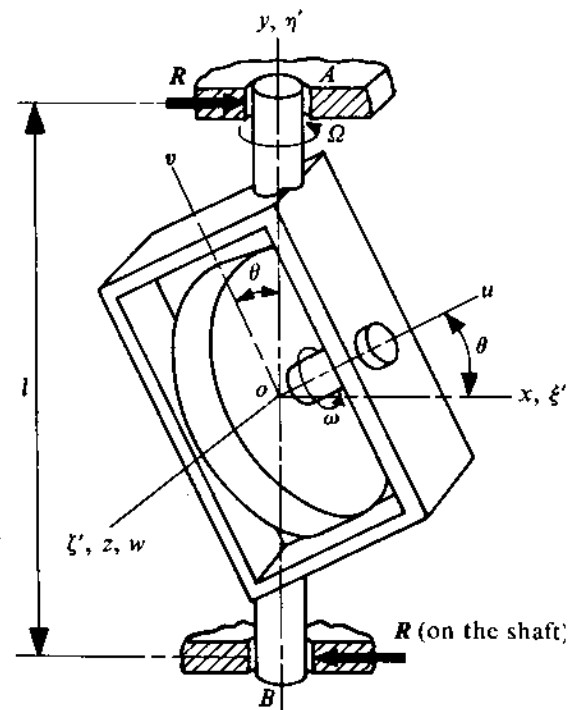


FIGURE 10.9

PROBLEM 10.4

A rotor spinning with a constant angular velocity ω about its axis is mounted on an inclined frame as shown in Fig. 10.9. The frame itself is capable of rotation about the vertical y -axis. The distance between the bearings A and B is l . The axes u , v , and w are the principal axes for the rotor and frame, the corresponding components of moments of inertia of the rotor and frame being J_{r_u} , J_{r_v} , J_{r_w} , J_{f_u} , J_{f_v} , and J_{f_w} , respectively. If the axis of spin is inclined to the horizontal plane at an angle θ , and if the frame rotates with a constant angular velocity Ω about the vertical axis, determine the magnitude and direction of the bearing reactions at A and B .

SOLUTION

The components of the angular velocities of the rotor and frame about the principal axes are

$$\begin{aligned}\omega_{r_u} &= \omega + \Omega \sin \theta, \\ \omega_{r_v} &= \Omega \cos \theta, \quad \omega_{r_w} = 0, \\ \omega_{f_u} &= \Omega \sin \theta, \quad \omega_{f_v} = \Omega \cos \theta, \\ \omega_{f_w} &= 0.\end{aligned}$$

So, the corresponding components of the total angular momentum of the whole system are

$$\begin{aligned}H_u &= J_{r_u} \omega_{r_u} + J_{f_u} \omega_{f_u} = J_{r_u} \omega + (J_{r_u} + J_{f_u}) \Omega \sin \theta, \\ H_v &= J_{r_v} \omega_{r_v} + J_{f_v} \omega_{f_v} = (J_{r_v} + J_{f_v}) \Omega \cos \theta, \\ H_w &= J_{r_w} \omega_{r_w} + J_{f_w} \omega_{f_w} = 0.\end{aligned}$$

ow, the components of the total angular momentum in the system $\xi'\eta'\zeta'$ can be calculated. This stem $\xi'\eta'\zeta'$ is fixed with the frame and rotates with it. At the instant under consideration, the stem $\xi'\eta'\zeta'$ is coincident with the system xyz which is fixed in space. Thus,

$$H_{\xi'} = H_u \cos \theta - H_v \sin \theta = J_{r_u} \omega \cos \theta + \frac{1}{2} \Omega \sin 2\theta [(J_{r_u} + J_{f_u}) - (J_{r_v} + J_{f_v})],$$

$$H_{\eta'} = H_u \sin \theta + H_v \cos \theta = (J_{r_u} + J_{f_u}) \Omega \sin^2 \theta + J_{r_u} \omega \sin \theta + (J_{r_v} + J_{f_v}) \Omega \cos^2 \theta,$$

$$H_{\zeta'} = H_w = 0.$$

Furthermore,

$$\omega_{\xi'} = 0, \quad \omega_{\eta'} = \Omega, \quad \omega_{\zeta'} = 0.$$

he torque to be applied for producing the prescribed motion can be determined directly from Euler's modified equation (10.15). Substituting therein values of the various quantities, we get

$$M_{\xi'} = M_x = 0,$$

$$M_{\eta'} = M_y = 0,$$

$$M_{\zeta'} = M_z = -H_{\xi'} \omega_{\eta'} = -J_{r_u} \omega \Omega \cos \theta - \frac{1}{2} \Omega^2 \sin 2\theta [(J_{r_u} + J_{f_u}) - (J_{r_v} + J_{f_v})].$$

ence, the reactions on the bearings A and B will be horizontal and parallel to the ζ' -axis. At A , i.e bearing reaction acts from left to right, and at B , the reaction is in the opposite direction. The magnitude R of the reaction is obtained from

$$Rl = |M_z| = J_{r_u} \omega \Omega \cos \theta + \frac{1}{2} \Omega^2 \sin 2\theta [(J_{r_u} + J_{f_u}) - (J_{r_v} + J_{f_v})].$$

0.6 GYRODYNAMICS

his section covers the analysis of different types of gyroscopic motion. We will consider uniform and nonuniform motion for both symmetrical and unsymmetrical rotors.

Free Motion of a Symmetrical Gyroscope

et us consider the symmetrical gyroscope shown in Fig. 10.10a, which rotates freely with an angular velocity ω about the point coincident with the mass centre of the gyroscope (to avoid any moment exerted by the gravitational force). The moment of inertia of the gyroscope about the axis of spin or about the axis of the gyroscope in the present case) is J and is called the *axial moment of inertia*. The moment of inertia of the gyroscope about any axis perpendicular to the spin axis and passing through the mass centre is termed the *equatorial moment of inertia* and is denoted by J_1 . If we fix coordinate system $\xi\eta\zeta$ to the gyroscope with the origin O at the CG, and if the ζ -axis is the axis of spin, then, by definition, we have

$$J_{\xi} = J_{\eta} = J_1, \quad J_{\zeta} = J.$$

Let us assume that the gyroscope rotates with constant angular velocity ω about the ζ -axis (see Fig. 10.10b), which is inclined to the fixed vertical z -axis at an angle θ . At the same time,

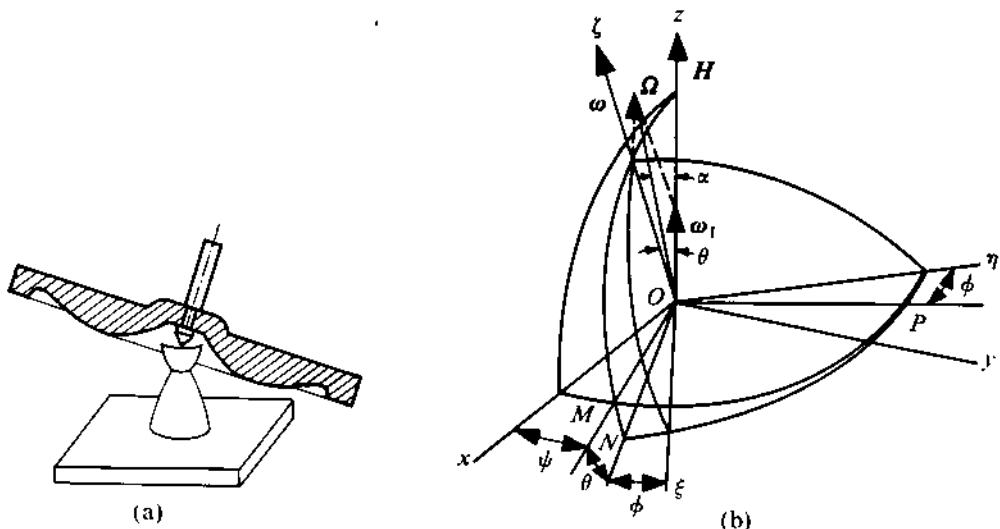


FIGURE 10.10

the $z\zeta$ -plane rotates with a constant angular velocity ω_1 about the z -axis. (In Fig. 10.10b, the transformation from the system xyz to the system $\xi\eta\zeta$ is effected in several stages. First, the x -axis and y -axis are rotated about the z -axis through an angle ψ to the new positions OM and OI respectively. Then, OM and the z -axis are rotated about OP through an angle θ and we get OI and the ζ -axis. Finally, OP and ON are rotated about the ζ -axis through an angle ϕ and the system $\xi\eta\zeta$ is obtained.) So, at any instant of time t , we have

$$\psi = \omega_1 t, \quad \phi = \omega t \quad (10.16)$$

if it is assumed that, at $t = 0$, the planes xz and $\xi\zeta$ are coincident. The components of the angular velocity of the gyroscope about the axes ξ , η , and ζ can be expressed in terms of ω , ω_1 , θ , and ϕ . Thus, we get

$$\omega_\xi = -\omega_1 \sin \theta \cos \phi = -\omega_1 \sin \theta \cos \omega t,$$

$$\omega_\eta = \omega_1 \sin \theta \sin \phi = \omega_1 \sin \theta \sin \omega t, \quad (10.17)$$

$$\omega_\zeta = \omega + \omega_1 \cos \theta.$$

Figure 10.11 shows how to arrive at the components of ω_1 in the ξ - and η -direction. To obtain Euler's equations of motion (10.14) for this case, we substitute therein values of H_ξ , H_η , and H_ζ namely,

$$H_\xi = J_\xi \omega_\xi = J_1 \omega_\xi, \quad H_\eta = J_\eta \omega_\eta = J_1 \omega_\eta, \quad H_\zeta = J_\zeta \omega_\zeta = J \omega_\zeta.$$

Thus, we get

$$J_1 \frac{d\omega_\xi}{dt} - (J_1 - J) \omega_\zeta \omega_\eta = 0, \quad J_1 \frac{d\omega_\eta}{dt} - (J - J_1) \omega_\zeta \omega_\xi = 0, \quad J \frac{d\omega_\zeta}{dt} = 0. \quad (10.18)$$

We find that the third equation is satisfied since ω_ζ is constant. To satisfy the two other equations we have to satisfy the relationships for θ , ω , ω_1 , J , and J_1 , namely,

$$J_1 \frac{d}{dt} (-\omega_1 \sin \theta \cos \omega t) - (J_1 - J)(\omega + \omega_1 \cos \theta)(\omega_1 \sin \theta \sin \omega t) = 0,$$

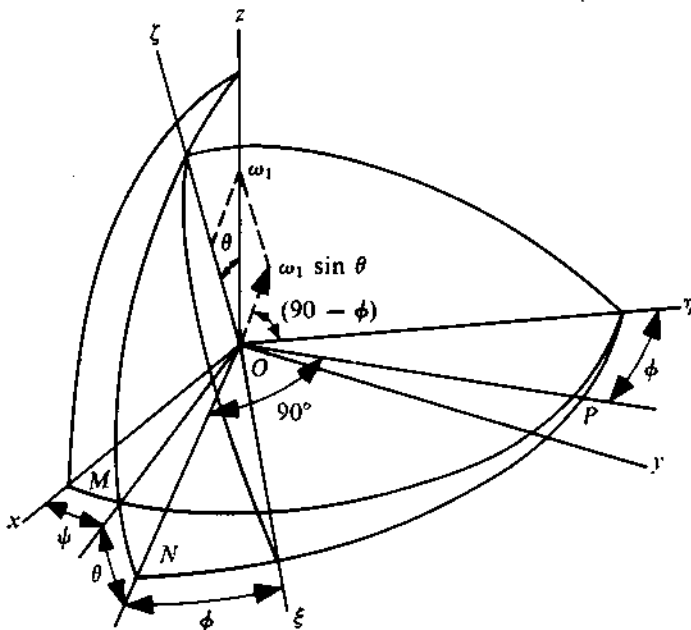


FIGURE 10.11

$$J_1 \frac{d}{dt} (\omega_1 \sin \theta \sin \omega t) - (J - J_1)(\omega + \omega_1 \cos \theta)(-\omega_1 \sin \theta \cos \omega t) = 0.$$

Both these conditions reduce to a single condition, that is,

$$J\omega + (J - J_1)\omega_1 \cos \theta = 0,$$

$$\omega_1 = \frac{J\omega}{(J_1 - J)\cos \theta}. \quad (10.19)$$

Therefore, we can conclude that if (10.19) is satisfied, Euler's equations of motion are also satisfied. In other words, the gyroscope will execute the motion described previously, for the particular value of ω_1 given by (10.19). This velocity ω_1 is called the *velocity of precession*, and the motion which a free symmetrical gyroscope executes is known as *regular precession*.

Now, the resultant angular velocity of the gyroscope (see Fig. 10.10b) can be resolved into two components, along $O\xi$ and ON . These are $(\omega + \omega_1 \cos \theta)$ and $(-\omega_1 \sin \theta)$, respectively. Since both $O\xi$ and ON are principal axes for a symmetrical gyroscope, using (10.19), we can express the corresponding components of angular momentum as

$$H_\xi = J(\omega + \omega_1 \cos \theta) = J_1 \omega_1 \cos \theta, \quad H_N = -J_1 \omega_1 \sin \theta. \quad (10.20)$$

Again, it is obvious that the vector \mathbf{H} must lie in the plane containing H_ξ and H_N . So, from (10.20), it is seen that the magnitude of \mathbf{H} will be $J_1 \omega_1$ and \mathbf{H} will act along the z -axis [i.e., it is fixed with respect to the system xyz (Fig. 10.10b)]. Since no external torque is applied, it is expected that \mathbf{H} will remain fixed in space. So, during regular precession of a symmetrical gyroscope, the resultant angular momentum \mathbf{H} remains constant both in magnitude and direction and can be expressed as

$$\mathbf{H} = J_1 \boldsymbol{\omega}_1. \quad (10.21)$$

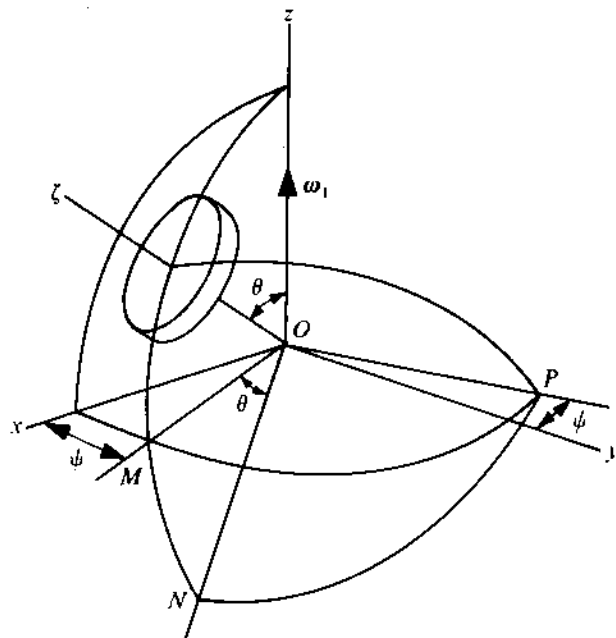


FIGURE 10.12

Gyroscopic Moment of a Symmetrical Gyroscope in Regular Precession

In the preceding discussion, we considered the motion of a symmetrical gyroscope when there is no external moment. However, the motion of a gyroscope may sometimes be different from that for the condition of no external moment. In such cases, it is necessary to apply some external moment to the gyroscope. In practice, bearing forces are automatically developed, and as a consequence of this, the bearing supports are subjected to reactive forces, producing a moment on the supporting frame which is equal and opposite to the moment acting on the gyroscope. This moment, which acts on the support during the prescribed motion of the gyroscope, is known as *gyroscopic moment*.

Let us consider the symmetrical gyroscope shown in Fig. 10.12 to be rotating about the vertical z -axis at a constant speed ω_1 . The gyroscopic axis ζ makes a constant angle θ with the z -axis, and the gyroscope spins about the ζ -axis with a constant angular velocity ω . Considering Euler's modified equation (10.15) and the moving trihedron $ONP\zeta$ (rotating at an angular speed ω_1 about the z -axis), the equation of motion can be obtained. Substituting the values of the components of angular momentum and angular velocity, the required components of the moments can be determined. We know that

$$\dot{\psi} = \omega_1,$$

$$\omega'_N = -\omega_1 \sin \theta, \quad \omega'_P = 0, \quad \omega'_\zeta = \omega_1 \cos \theta, \quad (10.22)$$

$$\omega_N = -\omega_1 \sin \theta, \quad \omega_P = 0, \quad \omega_\zeta = \omega + \omega_1 \cos \theta,$$

where the components ω'_N , ω'_P , and ω'_ζ refer to the frame $ONP\zeta$ and ω_N , ω_P , and ω_ζ represent the corresponding components of the angular velocity of the gyroscope itself. Since ON , OP , and $O\zeta$

are the principal axes, the components of angular momentum can be expressed as

$$H_N = J_1 \omega_N = -J_1 \omega_1 \sin \theta, \quad H_P = J_1 \omega_P = 0, \quad H_\zeta = J \omega_\zeta = J(\omega + \omega_1 \cos \theta). \quad (10.23)$$

From (10.15), (10.22), and (10.23), we get

$$M_N = 0, \quad M_P = J \omega \omega_1 \sin \theta + (J - J_1) \omega_1^2 \sin \theta \cos \theta, \quad M_\zeta = 0. \quad (10.24)$$

So, the only nonzero component of the gyroscopic moment is given by

$$M_P^G = -M_P = -[J \omega + (J - J_1) \omega_1 \cos \theta] \omega_1 \sin \theta. \quad (10.25)$$

We can verify this result by putting $M_P = 0$. Then, the condition to be satisfied is

$$\omega_1 = J \omega / [(J_1 - J) \cos \theta]$$

which agrees with the result obtained for the free motion of a symmetrical gyroscope.

Gyroscopic Moment of a Symmetrical Gyroscope in General Motion

For the general case, the position of the trihedron $ONP\zeta$ is defined by ψ and θ . The components of angular velocity can be expressed as

$$\omega'_N = -\dot{\psi} \sin \theta, \quad \omega'_P = \dot{\theta}, \quad \omega'_\zeta = \dot{\psi} \cos \theta. \quad (10.26)$$

The corresponding components of angular velocity of the gyroscope are

$$\omega_N = -\dot{\psi} \sin \theta, \quad \omega_P = \dot{\theta}, \quad \omega_\zeta = \dot{\phi} + \dot{\psi} \cos \theta. \quad (10.27)$$

Therefore, the components of angular momentum of the gyroscope are

$$H_N = -J_1 \dot{\psi} \sin \theta, \quad H_P = J_1 \dot{\theta}, \quad H_\zeta = J(\dot{\phi} + \dot{\psi} \cos \theta). \quad (10.28)$$

From (10.15), (10.26), and (10.28), we get

$$M_N = -J_1 \frac{d}{dt} (\dot{\psi} \sin \theta) + J \ddot{\theta} (\dot{\phi} + \dot{\psi} \cos \theta) - J_1 \dot{\theta} \dot{\psi} \cos \theta, \quad (10.29)$$

$$M_P = J_1 \ddot{\theta} + \dot{\psi} \sin \theta [J \dot{\phi} + (J - J_1) \dot{\psi} \cos \theta], \quad M_\zeta = J \frac{d}{dt} (\dot{\phi} + \dot{\psi} \cos \theta).$$

Under normal circumstances, $\dot{\phi}$ is much greater than $\dot{\psi}$ and $\dot{\theta}$. Therefore, (10.29) can be reduced to the approximate form

$$M_N = -M_N^G \approx J \dot{\psi} \dot{\phi} \sin \theta, \quad M_P = -M_P^G \approx J \dot{\theta} \dot{\phi}, \quad M_\zeta = -M_\zeta^G \approx J \ddot{\phi}. \quad (10.30)$$

General Motion of an Unsymmetrical Gyroscope

For a symmetrical gyroscope, the calculation of the components of angular momentum is easy because ON and OP remain the principal axes of the gyroscope, irrespective of the instantaneous position with respect to the system $PN\zeta$. The moments of inertia about OP and ON do not depend on ϕ because of the symmetry of the gyroscope. When the gyroscope is not symmetrical, OP and ON are no longer the principal axes of the gyroscope, and the corresponding components of angular

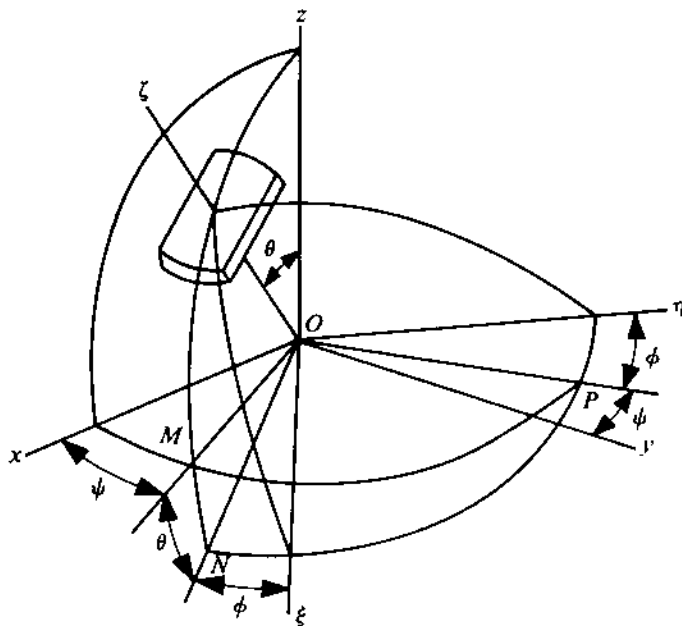


FIGURE 10.13

momentum are not given by the direct product of the moment of inertia and the angular velocity components. Such an unsymmetrical gyroscope in motion is shown in Fig. 10.13. However, ξ and η (which are taken to be fixed with the rotating gyroscope) can be chosen in a manner such that they represent the principal axes. It should be remembered that $O\zeta$ is still the principal axis of the rotor. Therefore, H_ξ and H_η can be expressed as

$$H_\xi = J_\xi \omega_\xi, \quad H_\eta = J_\eta \omega_\eta. \quad (10.31)$$

Using (10.27), ω_ξ and ω_η can be expressed in terms of θ , ϕ , $\dot{\theta}$, and $\dot{\psi}$. Thus,

$$\omega_\xi = \omega_P \sin \phi + \omega_N \cos \phi = -\dot{\psi} \sin \theta \cos \phi + \dot{\theta} \sin \phi,$$

$$\omega_\eta = \omega_P \cos \phi - \omega_N \sin \phi = \dot{\psi} \sin \theta \sin \phi + \dot{\theta} \cos \phi, \quad (10.32)$$

$$\omega_\zeta = \dot{\phi} + \dot{\psi} \cos \theta.$$

Hence, the components of angular momentum H_ξ , H_η , and H_ζ take the form

$$H_\xi = J_\xi \omega_\xi = J_\xi (-\dot{\psi} \sin \theta \cos \phi + \dot{\theta} \sin \phi),$$

$$H_\eta = J_\eta \omega_\eta = J_\eta (\dot{\psi} \sin \theta \sin \phi + \dot{\theta} \cos \phi), \quad (10.33)$$

$$H_\zeta = J_\zeta \omega_\zeta = J_\zeta (\dot{\phi} + \dot{\psi} \cos \theta).$$

H_N , H_P , and H_ζ can now be expressed in terms of H_ξ , H_η , and H_ζ as

$$H_N = H_\xi \cos \phi - H_\eta \sin \phi, \quad H_P = H_\eta \cos \phi + H_\xi \sin \phi, \quad H_\zeta = H_\zeta.$$

Substituting H_ξ , H_η , and H_ζ from (10.33) in these equations, we get

$$H_N = -J_\eta \sin \phi (\dot{\psi} \sin \theta \sin \phi + \dot{\theta} \cos \phi) - J_\xi \cos \phi (\dot{\psi} \sin \theta \cos \phi - \dot{\theta} \sin \phi),$$

$$H_P = J_\eta \cos \phi (\dot{\psi} \sin \theta \sin \phi + \dot{\theta} \cos \phi) - J_\xi \sin \phi (\dot{\psi} \sin \theta \cos \phi - \dot{\theta} \sin \phi), \quad (10.34)$$

$$H_\zeta = J_\zeta (\dot{\phi} + \dot{\psi} \cos \theta).$$

Further, the angular velocity components of the trihedron $OPN\zeta$ are [see equation (10.26)]

$$\omega'_N = -\dot{\psi} \sin \theta, \quad \omega'_P = \dot{\theta}, \quad \omega'_\zeta = \dot{\psi} \cos \theta. \quad (10.35)$$

From (10.15), (10.34), and (10.35) we get the expressions for the components of applied torque. Assuming $\dot{\phi}$ to be much greater than $\dot{\psi}$ and $\dot{\theta}$, which is valid in normal cases, these expressions take the form

$$M_N \approx (J_\xi - J_\eta) \dot{\phi} (\dot{\theta} \cos 2\phi + \dot{\psi} \sin \theta \sin 2\phi) + J_\zeta \dot{\phi} \dot{\theta} = -M_N^G,$$

$$M_P \approx (J_\xi - J_\eta) \dot{\phi} (\dot{\theta} \sin 2\phi - \dot{\psi} \sin \theta \cos 2\phi) + J_\zeta \dot{\psi} \dot{\phi} \sin \theta = -M_P^G, \quad (10.36)$$

$$M_\zeta = 0 = -M_\zeta^G.$$

In the case of regular precession, $\dot{\theta} = 0$ and we get

$$-M_N^G = M_N = (J_\xi - J_\eta) \dot{\phi} \dot{\psi} \sin \theta \sin 2\phi,$$

$$-M_P^G = M_P = (J_\eta - J_\xi) \dot{\phi} \dot{\psi} \sin \theta \cos 2\phi + J_\zeta \dot{\psi} \dot{\phi} \sin \theta, \quad (10.37)$$

$$-M_\zeta^G = M_\zeta = 0.$$

So, it is seen that, for unsymmetrical gyroscopes, the gyroscopic moment contains harmonic functions of time having twice the frequency of the spin. Thus, systems with high-speed unsymmetrical rotors under precessional motion are subjected to gyroscopic moments of very high frequency. This may be dangerous in many cases and should be taken care of when designing such a system.

PROBLEM 10.5

A propeller plane is flying at 600 km/hour along a circular path in the horizontal plane. The radius of the path is 5 km. Each propeller rotates at 1800 rpm and can be considered to be a 2-m-long uniform rod of mass 40 kg. Calculate the gyroscopic moment. The propellers rotate in the counter-clockwise direction when viewed from the front.

SOLUTION

We have first to find the precessional velocity ω_1 . This is the same as the angular velocity of the plane. As the plane moves along a circle with a radius of 5 km, and has a velocity of 600 km/hour, the angular velocity of the plane will be

$$\omega_1 = V_{\text{plane}}/R_{\text{path}} = 600/(5 \times 60 \times 60) = \frac{1}{30} \text{ rad/s.}$$

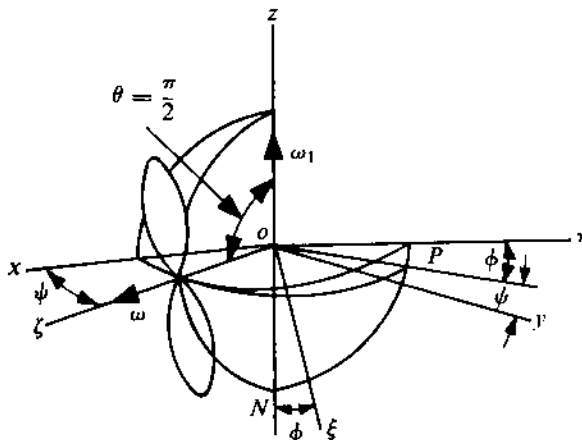


FIGURE 10.14

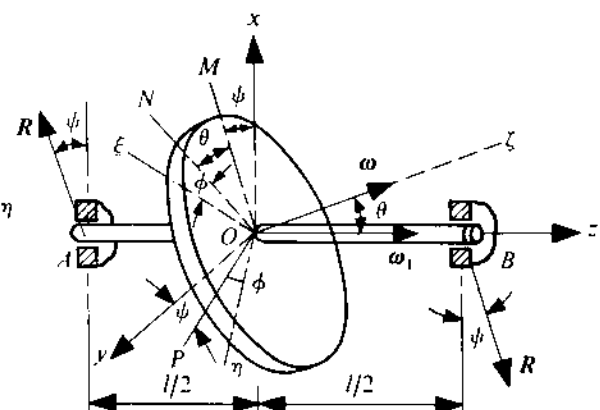


FIGURE 10.15

Let us assume ω_1 to be in the counter-clockwise direction. The gyroscopic motion is evident from Fig. 10.14. For the given data, we find that

$$\begin{aligned} J_\xi &\approx 0, \\ J_\eta &\approx \frac{1}{12} \times 40 \times 2^2 \text{ kg-m}^2 \\ &= 13.3 \text{ kg-m}^2, \\ J_\zeta &\approx 13.3 \text{ kg-m}^2. \end{aligned}$$

It should be remembered that, although to explain the motion we have shown the propeller to be at some distance from the origin o , actually the propeller centre and the origin are at the same point. Moreover, we know that

$$\omega = (1800/60) \times 2\pi = 188.4 \text{ rad/s.}$$

The motion is of the regular precession type with $\theta = 90^\circ$, $\dot{\phi} = \omega = 188.4 \text{ rad/s}$, and $\dot{\psi} = \omega_1 = \frac{1}{30} \text{ rad/s}$. Hence, from (10.37), we get

$$\begin{aligned} M_P^G &= -(J_\eta - J_\xi)188.4 \times \frac{1}{30} \cos(2 \times 188.4t) - J_\zeta 188.4 \times \frac{1}{30} \\ &= -83.524(\cos 377.8t + 1) \text{ N-m}, \end{aligned}$$

$$M_N^G = 83.524 \sin 377.8t \text{ N-m},$$

$$M_\zeta^G = 0.$$

The negative sign indicates the counter-clockwise direction of the torque when viewed outwards from o .

10.7 GYROSCOPIC EFFECTS IN MACHINES

Gyroscopic effects are present in all systems that involve forced precessional motion of spinning rotors. In some systems, this motion is readily detectable, whereas in others it is not so apparent.

Precessional motion is set up because of the kinematic requirements of a system. Although gyroscopic effects are generally not desirable, sometimes their presence is utilized with advantage in fulfilling the objective of the system. In this section, we will consider a few situations in which gyroscopic effects may play a dominant role in the operation of the system.

Rotating Shaft with Inclined Disc

Sometimes, a system may have a disc mounted on a rotating shaft, in a manner such that the axis of the shaft is not perpendicular to the plane of the disc. This may be due to an error in mounting the disc on the shaft, or it may be deliberately provided as in the case of Swash-plate pumps. Anyhow, our problem is to analyze the gyroscopic effect in such a system. Consider the circular disc and rotating shaft shown in Fig. 10.15. The disc is inclined at an angle θ to the true position, and the angular velocity of the shaft is ω_1 . Let J and J_1 , respectively, be the axial and equatorial moments of inertia of the disc. The CG of the disc coincides with the point O . Then, adopting the notations used heretofore, we get

$$\begin{aligned}\omega'_N &= -\omega_1 \sin \theta, & \omega'_P &= 0, & \omega'_\zeta &= \omega_1 \cos \theta, \\ \omega_N &= -\omega_1 \sin \theta, & \omega_P &= 0, & \omega_\zeta &= \omega_1 \cos \theta.\end{aligned}\quad (10.38)$$

Thus, the components of angular momentum are

$$H_N = J_1 \omega_N = -J_1 \omega_1 \sin \theta, \quad H_P = J_1 \omega_P = 0, \quad H_\zeta = J \omega_\zeta = J \omega_1 \cos \theta. \quad (10.39)$$

From (10.15), (10.38), and (10.39), the components of gyroscopic moment will be

$$\begin{aligned}M_N^G &= -\left(\frac{dH_N}{dt} + H_\zeta \omega'_P - H_P \omega'_\zeta\right) = 0, \\ M_P^G &= -\left(\frac{dH_P}{dt} + H_N \omega'_\zeta - H_\zeta \omega'_N\right) = J_1 \omega_1^2 \sin \theta \cos \theta - J \omega_1^2 \sin \theta \cos \theta \\ &= (J_1 - J) \omega_1^2 \sin \theta \cos \theta, \\ M_\zeta^G &= -\left(\frac{dH_\zeta}{dt} + H_P \omega'_N - H_N \omega'_P\right) = 0.\end{aligned}\quad (10.40)$$

From (10.40), it is seen that only one component of the gyroscopic moment remains, and its magnitude does not change with time. However, as the N -axis rotates with an angular velocity ω_1 , the gyroscopic moment vector will also rotate with the same velocity. The effect of the gyroscopic moment is manifest in the equal and opposite reactions at the bearings A and B (see Fig. 10.15), the magnitude R being

$$|R| = \frac{1}{l} [(J_1 - J) \omega_1^2 \sin \theta \cos \theta].$$

These reactions in a direction perpendicular to the axis of the rotating shaft will be contained in the plane passing through the axis of the rotating shaft and perpendicular to ON .

Rotors in Vehicles

As already seen, gyroscopic effects may be considerable when a vehicle, carrying rotating bodies with large angular momentum, changes its course. Turbine rotors in ships, wheels and flywheels

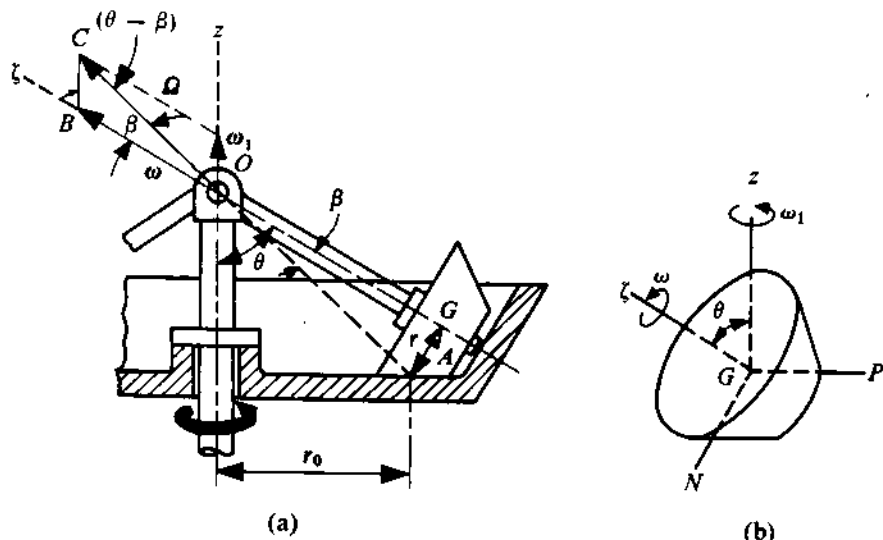


FIGURE 10.16

in automobiles, rotors in helicopters, propellers and gas turbine rotors in aircrafts are examples of rotating bodies. In ships, the pitching motion will introduce additional alternating variation in the bearing reactions because of the periodic gyroscopic moment.

Grinding Mills

As stated earlier in this section, gyroscopic effects may sometimes be useful in fulfilling the objectives of a system. Towards this end, gyroscopic effects may even be deliberately introduced in the system. A good example is that of a grinding mill in which gyroscopic effects increase the crushing force. One such mill is shown in Fig. 10.16a. Conical rollers (represented by *G* in Fig. 10.16a, and shown separately in Fig. 10.16b) are placed symmetrically in a pan and are free to rotate on shafts which are hinged to the central driving shaft. When the driving shaft rotates, the rollers move around the pan and crush the material placed within it. The crushing takes place not only due to the weight of the rollers but also because of the extra crushing force which is developed by gyroscopic action.

The angular velocity of the roller on the shaft is ω and the shaft rotates about the vertical axis with a velocity ω_1 as shown in Fig. 10.16a. The resultant velocity vector Ω of the roller can be obtained by the vectorial summation of ω and ω_1 . In Fig. 10.16a, the point *A* indicates the intersection of Ω and the line of contact between the pan floor and the roller. At this point, the roller will have zero relative velocity with respect to the pan floor and the position of *A* will depend on the frictional characteristics of the roller and the pan. Considering the triangle *OBC*, we get

$$\frac{OB}{\sin(\theta - \beta)} = \frac{BC}{\sin \beta},$$

$$\frac{OB}{BC} = \frac{\omega}{\omega_1} = \frac{\sin(\theta - \beta)}{\sin \beta}. \quad (10.41)$$

Moreover, as the relative velocity between the roller and the pan floor at *A* is zero, we get

$$\frac{\omega}{\omega_1} = \frac{r_0}{r}, \quad (10.42)$$

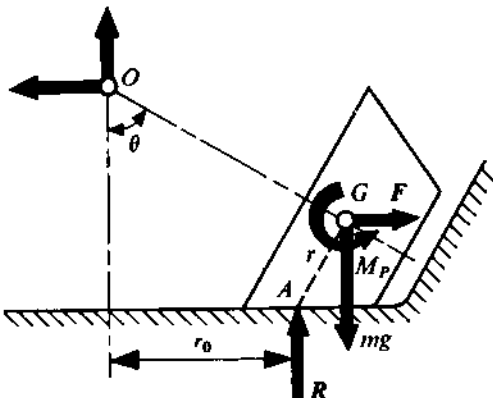


FIGURE 10.17

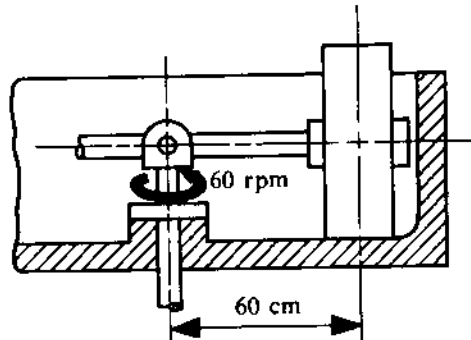


FIGURE 10.18

where r is the radius of the roller at the cross-section containing the point A .

The forces and moments acting on the system are shown in Fig. 10.17, where mg is the weight of the roller and F is the centrifugal force. It is assumed that the cross-section containing the point A also contains the CG of the roller G and that the resultant crushing force R acts at the point A . These assumptions will not cause much error. The nonvanishing component of the moment M_P , which is necessary to produce the required precessional motion, will be caused by this system of forces. Both mg and F will act through the CG of the roller G . Comparing Fig. 10.16b and Fig. 10.10b, the components of the moment [given by (10.24)] will be

$$M_P = J\omega\omega_1 \sin \theta + (J - J_1)\omega_1^2 \sin \theta \cos \theta, \quad M_N = M_C = 0.$$

Using (10.42), M_P can be expressed in the form

$$M_P = J\omega^2 \cdot \frac{r_0}{r} \sin \theta + (J - J_1)\omega_1^2 \sin \theta \cos \theta = [(J - J_1) \cos \theta + J \cdot \frac{r_0}{r}] \omega_1^2 \sin \theta, \quad (10.43)$$

where J and J_1 , respectively, are the axial and equatorial moments of inertia of the roller. Taking moments about O (Fig. 10.17), and considering the total moment to be equal to M_P (which is the moment required to produce the precessional motion), we get

$$M_P = F(r_0 + r \cos \theta) \cot \theta - mg(r_0 + r \cos \theta) + R \cdot r_0.$$

Rearranging this equation and combining it with (10.43), we get

$$\frac{R}{mg} = \left(1 + \frac{r}{r_0} \cos \theta\right) + \frac{\omega_1^2 \sin \theta}{mgr_0} \left[(J - J_1) \cos \theta + J \frac{r_0}{r}\right] - \frac{F \cot \theta}{mg} \left(1 + \frac{r}{r_0} \cos \theta\right). \quad (10.44)$$

It is obvious from this expression that, for suitable values of θ , R/mg can be more than unity. For example, if $\theta = \pi/2$, we get

$$\frac{R}{mg} = 1 + \frac{J\omega_1^2}{mgr} > 1.$$

PROBLEM 10.6

Figure 10.18 shows a crusher in which each roller is of mass 100 kg and the driving shaft rotates at 60 rpm. The rollers are cylindrical, and the radius of each roller is 45 cm. The axial moment of inertia of each roller is 15 kg-m^2 . Determine the total crushing force.

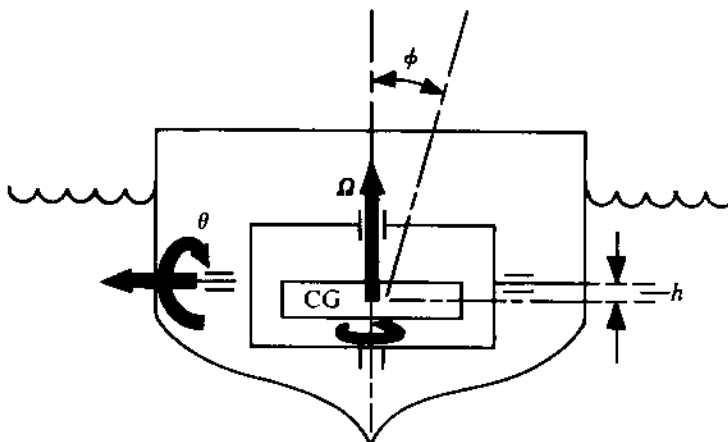


FIGURE 10.19

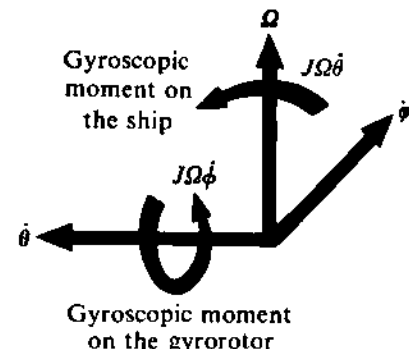


FIGURE 10.20

SOLUTION

The crusher under consideration is a special case of Fig. 10.16a, with $\theta = 90^\circ$, $r = 45 \text{ cm}$, and $r_0 = 60 \text{ cm}$. It is given that ω_1 is $2\pi \text{ rad/s}$. Substituting these values in (10.44), we get

$$R/980 = 1 + (4\pi^2/980)(1500/45) \approx 2.34, \quad R \approx 2293 \text{ N.}$$

So, it is seen that the crushing force is 134% greater than the weight of the roller. This increase is purely due to gyroscopic action in the system.

Gyroscopic Stabilization

A spinning body tends to maintain the orientation of its spin axis in space. This is true also of a bullet fired from a rifle. Therefore, for a given exit velocity, the range of a rifle is more than that of a shotgun. The reason this is so is that an external torque in a suitable direction is required to change the orientation of the spin axis. This principle has extensively been applied in guidance of missiles and rockets, navigation and direction finding, and stabilization of a rocking body. Here, we shall present one such application, namely, reduction of the rolling of ships and yachts.

Figure 10.19 shows the cross-section of a ship with a massive gyrorotor spinning with an angular velocity Ω about the vertical axis. The CG of the rotor is at a distance h below the axis of the outer gimbal, as shown. The placement of the CG of the rotor below the gimbal axis is necessary so that, under normal working conditions (without rolling), the moment due to the rotor weight exerts a restoring couple so far as the θ -motion is concerned. The gyroscopic moments on the ship and the gyrorotor are shown in Fig. 10.20. In this figure, we have shown only those moments that we shall need to derive the equations of motion.

Let mg be the weight of the entire gyrosystem, J_s the moment of inertia of the ship about the roll axis, J and J_1 the polar and equatorial moments of inertia of the gyrorotor, respectively, k_r the equivalent stiffness of the ship against the rolling motion (i.e., ϕ -motion), $M_s \cos \omega t$ the external disturbing torque (due to waves, wind, and such other factors) causing rolling, and c the viscous damping coefficient (of the gyrosystem) resisting the θ -motion. Then, the equations of motion of the ship and the gyrorotor (including the gyroscopic effect) can be written as

$$J_s \ddot{\phi} + k_r \phi + J \Omega \dot{\theta} = M_s \cos \omega t, \quad (10.45)$$

$$J_1 \ddot{\theta} = -c\dot{\theta} - mgh\theta - (-J\Omega\dot{\phi})$$

$$J_1 \ddot{\theta} + c\dot{\theta} + mgh\theta - J\Omega\dot{\phi} = 0. \quad (10.46)$$

Assuming steady-state solutions of the form

$$\phi = \phi_0 \cos(\omega t - \alpha), \quad (10.47a)$$

$$\theta = \theta_0 \cos(\omega t - \beta), \quad (10.47b)$$

and using these in (10.45) and (10.46), we get the amplitude of rolling ϕ_0 as

$$\frac{\phi_0}{M_s/k_r} = \frac{\{(1 - r_g^2)^2 + (2\zeta r_g)^2\}^{1/2}}{\{[(1 - r_g^2)(1 - r^2) - r^2\mu]^2 + (2\zeta r_g)^2(1 - r^2)^2\}^{1/2}}, \quad (10.48)$$

where

$$r_g = \frac{\omega}{(mgh/J_1)^{1/2}}, \quad r = \frac{\omega}{(k_r/J_s)^{1/2}}, \quad \zeta = c/[2(mghJ_1)^{1/2}], \quad \mu = (J\Omega)^2/(mghJ_s).$$

It can be shown that, for a given value of μ , the maximum amplitude of ϕ over a wide range of frequency (ω) is minimum with an optimum value of ζ . In other words, if the value of ζ is more or less than this optimum value ζ_{opt} , the maximum amplitude increases. However, with typical values of other parameters and $\zeta = \zeta_{opt}$, the amplitude of θ -motion becomes very large. So, to keep the oscillation of the outer gimbal within reasonable limits, in practice, ζ is maintained at a value higher than ζ_{opt} .

From (10.48), we see that, for $r = 1$ (i.e., at the natural frequency of rolling),

$$\frac{\phi_0}{M_s/k_r} = \frac{1}{\mu} [(1 - r_g^2)^2 + (2\zeta r_g)^2]^{1/2}. \quad (10.49)$$

This implies that, for $r = 1$, the rolling amplitude is inversely proportional to the square of the spin angular momentum of the gyrorotor. The overall effect of adding a gyrorotor is that the moment of inertia of the ship increases. A significant increase in inertia can be achieved by a relatively small increase in the mass of the ship if the gyrorotor has a high spin rate.

10.8 PROBLEMS

- 10.7 A thin disc of radius r and mass m is mounted on a light rigid rod of length $2a$ which is freely hinged at O , the other end A of the rod being supported by a light string (Fig. 10.21). The disc spins with an angular velocity ω as shown and the whole assembly rotates about a vertical axis through O with an angular velocity Ω . Determine the tension in the string. What will be the string tension if the system rotates with a velocity Ω in the opposite direction?

- 10.8 A small aeroplane while taking off retracts its landing gear in the manner shown in Fig. 10.22. Each wheel of the plane has a mass 30 kg, a radius of gyration 30 cm, and a diameter 90 cm. The take-off speed is 200 km/hr and the landing gear is retracted with an angular velocity of 0.5 rad/s. Determine the direction and magnitude of the gyroscopic moment on each wheel bearing.

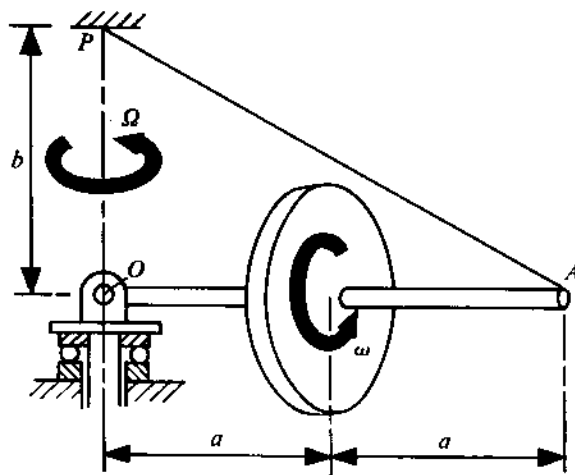


FIGURE 10.21

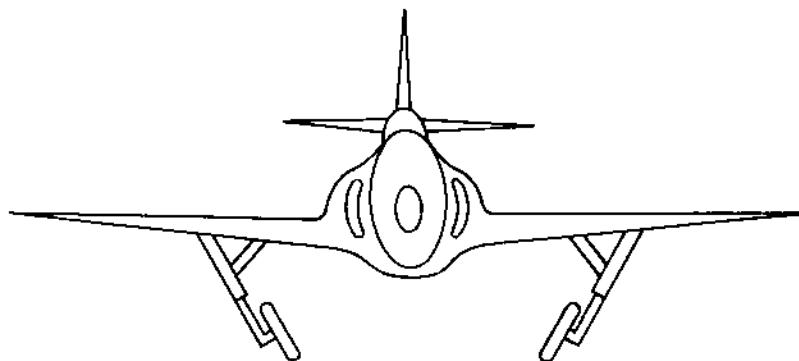


FIGURE 10.22

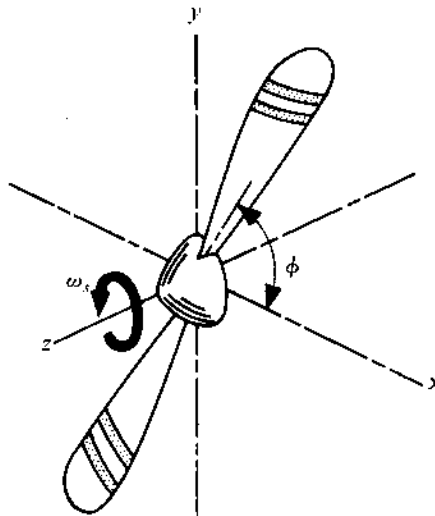


FIGURE 10.23

- 10.9 A trolley car with a total mass of 2700 kg runs on rails 1 m apart with a speed of 30 km/hr. The track is curved with a radius of 40 m towards the right of the driver. The car has four wheels each of diameter 70 cm and the total moment of inertia of each pair of wheels and the axle is 15 kg-m^2 . The car is driven by a motor running in the direction opposite to that of the wheels at a speed five times the speed of rotation of the wheels. The motor and the gear pinion have a moment of inertia 10 kg-m^2 . The rails are at the same level and the height of the CG of the car is 1 m above the rail level. Determine the vertical force exerted by each wheel on the rails.
- 10.10 A two-blade propeller (Fig. 10.23) rotates with a constant speed ω_s about its axis which is horizontal. The aeroplane is taking a horizontal left-hand turn with a velocity V along a circle of radius R . Each propeller blade can be assumed to be a uniform thin rod of length l and mass m . Show that the instantaneous resultant bending and torsional moments on the propeller shaft can be expressed as

$$M_b = \frac{4}{3} ml^2 \omega_s \left(\frac{V}{R} \right) \sin \phi,$$

$$M_t = \frac{1}{3} ml^2 \left(\frac{V}{R} \right)^2 \sin 2\phi.$$

Hint: Do not use (10.37) where (V/R) was assumed to be small as compared to ω_s .

- 10.11 Use (10.15), (10.34), and (10.35) to solve Problem 10.5 without making the assumptions that are implicit in the solution to Problem 10.5. Compare the magnitudes of the three components of the gyroscopic moment so obtained with those arrived at in Problem 10.5.

Chapter 11

VIBRATIONS IN MECHANICAL SYSTEMS

1.1 INTRODUCTION

In our study so far, we have encountered many situations where the machine members are subjected to time-varying disturbances in the form of, for example, forces and moments. As a result, these members undergo oscillatory movements, also known as vibrations. The response of a flexible body to a dynamic excitation (i.e., disturbance) has characteristics different from those of its response to a static (i.e., steadily applied) disturbance. For example, in static loading, the stress in a bar under simple tension always decreases with increase in cross-section, but when the applied load is dynamic, the maximum stress may decrease even with a decrease in cross-section. For a periodically-varying load, the induced stress may be very high (leading, sometimes, to a permanent damage) even when the maximum value of the load is quite low. This happens only for certain values of the time period. Thus, it is apparent that a comprehensive study of vibrations in a mechanical system is necessary to successfully design the system.

1.2 BASIC FEATURES OF VIBRATORY SYSTEMS

For a mathematical analysis of the vibration in a mechanical system, it is necessary that an appropriate idealized model be prepared to represent the system. For this, it is necessary to classify the systems and the excitations and to develop a few concepts. In what follows, we shall attempt this.

Basic Elements and Lumping of Parameters

Every vibratory system must possess inertial and restoring elements. Such a system also has mechanisms responsible for dissipating the energy. These mechanisms are idealized as a damper. For conveniently carrying out the mathematical formulation, the inertial properties are represented by lumped masses for rectilinear motion and by lumped moments of inertia for angular motion. Similarly, the restoring elements are represented by massless linear or torsional springs, depending on the nature of motion. The energy dissipation is taken care of by including in the formulation massless dampers comprised of rigid elements. The lumping of parameters (i.e., inertia, stiffness, and

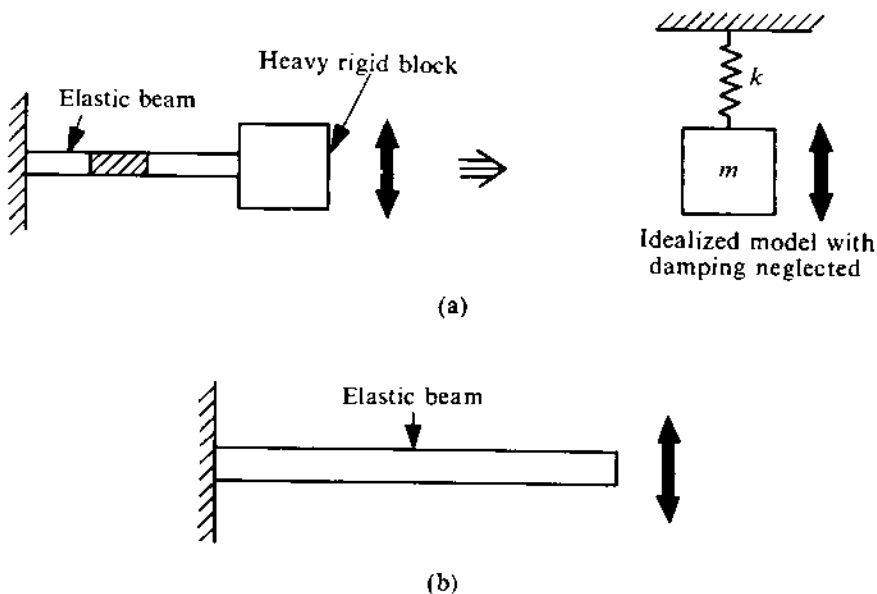


FIGURE 11.1

damping) depends on the distribution of these quantities in the system and is accordingly done. For example, consider the system shown in Fig. 11.1a. If the mass of the beam is small as compared to that of the end block, the lumping of parameters, as indicated, is justified. On the other hand, if the system shown in Fig. 11.1b, no such lumping is meaningful.

Degrees of Freedom

A vibratory system is often classified on the basis of the degrees of freedom it has. The minimum number of independent coordinates required to describe the motion of a system is called the degree of freedom. Figures 11.2a, 11.2b, and 11.2c show three systems having one degree of freedom, two degrees of freedom, and an infinite degrees of freedom, respectively. In Fig. 11.2c, the deflected shape during the transverse vibration of the beam can be completely specified only by a continuous function $x = x(z)$. In other words, for every point z , a coordinate is necessary to describe the motion of the beam. It should be remembered that all bodies possess some flexibility, and therefore a real-life system has an infinite degrees of freedom. Such a system can be converted into a system having a finite degrees of freedom by lumping the inertial parameter (mass). Further, in a mathematical model of a system, the actual number of degrees of freedom to be used is decided on the basis of the predominant directions of excitation and motion. Consider, for example, the system shown in Fig. 11.1a. It has an infinite degrees of freedom. But, after the lumping of mass, it will have only six degrees of freedom (i.e., degrees of freedom of a rigid body). Moreover, the dimensions of the beam are such that the predominant oscillation of the block can take place only in the vertical direction. Thus, the final idealized system will be as shown in Fig. 11.1a.

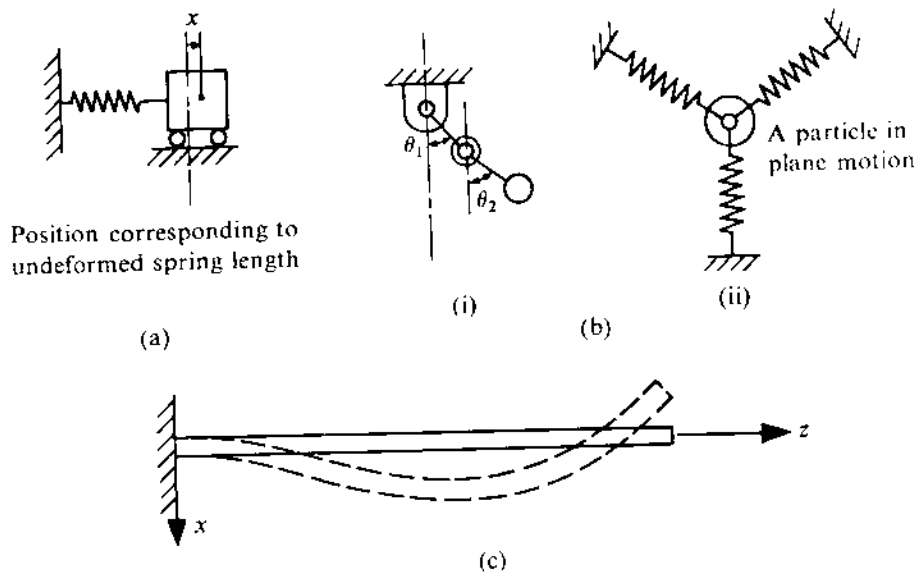


FIGURE 11.2

Linearization of System Elements

The three basic elements, discussed already, give rise to three different types of forces, viz., inertial, restoring, and damping forces. These forces are functions of acceleration, displacement, and velocity of oscillation, respectively. In Newtonian mechanics, the inertia force is always linear, as shown in Fig. 11.3. However, the other two forces, in general, may be nonlinear. But, for small oscillations, these two forces can also be approximated as linear forces. In this chapter, we shall deal only with linear systems. It should, however, be noted that the occurrence of certain phenomena in a real-life system cannot be explained by the linear theory.

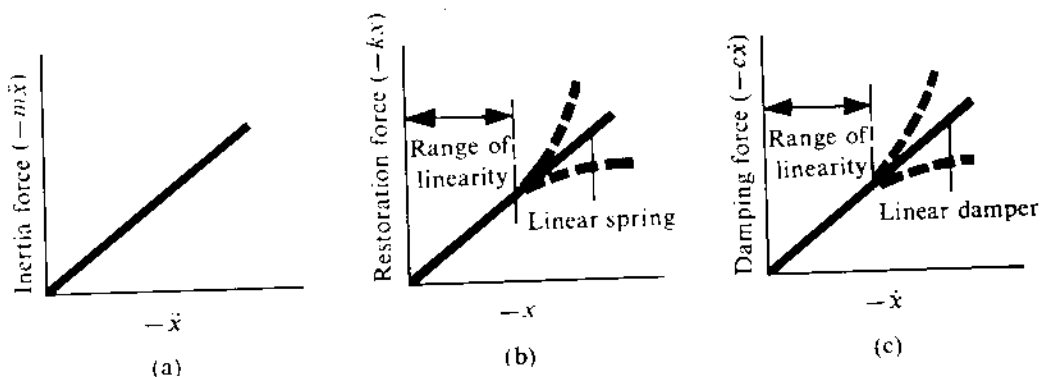


FIGURE 11.3

Types of Vibrations

A mechanical system may be subjected to various types of dynamic disturbances. The vibrations that are thus produced are classified as follows:

- (i) Free vibrations: These are set up when the system is disturbed from its equilibrium position and is allowed to oscillate on its own.
- (ii) Forced vibrations: These are generated when the system is subjected to an external disturbance independent of the resulting motion. The external disturbance may be (a) harmonic or (b) periodic or (c) an arbitrary function of time.
- (iii) Self-excited vibrations: These are brought about when the system is subjected to an external disturbance dependent on the resulting motion.
- (iv) Parametrically-excited vibrations: These result from the dependence of system parameters on time.
- (v) Random vibrations: In each of the vibration types (i) to (iv), it is possible to describe the excitation and the system parameters by suitable deterministic functions. However, there may be a situation where only a statistical description of these quantities is possible. The vibrations in such a situation are called random vibrations.

We shall limit our discussion to the first two types of vibrations.

11.3 SINGLE-DEGREE-OF-FREEDOM SYSTEMS

For a clear understanding of the basic features of a vibration problem, it is important that we study the single-degree-of-freedom systems in detail. This is because, as we shall subsequently see, to analyze a given system with more than one degree of freedom, the system is ultimately converted into single-degree-of-freedom systems, the number of such systems being equal to the degrees of freedom of the given system. In this section, we shall discuss the free and forced vibrations of both the undamped and damped systems.

Undamped Free Vibration

Figure 11.4a shows a single-degree-of-freedom system executing free oscillations. When the displacement of the mass (from the equilibrium position) is x , the corresponding free-body diagram would be as shown (Fig. 11.4a). From Newton's second law, the equation of motion can be written as $m\ddot{x} = -kx$ or

$$m\ddot{x} + kx = 0. \quad (11.1)$$

The general solution of this equation is

$$x(t) = A \sin \omega_n t + B \cos \omega_n t, \quad (11.2)$$

where $\omega_n = (k/m)^{1/2}$. This equation can also be written in the form

$$x(t) = X \cos (\omega_n t + \phi). \quad (11.3)$$

The arbitrary constants A and B in (11.2) or X and ϕ in (11.3) can be determined from the initial conditions, i.e., from the disturbance initiating the vibration. Thus, the free vibration is always

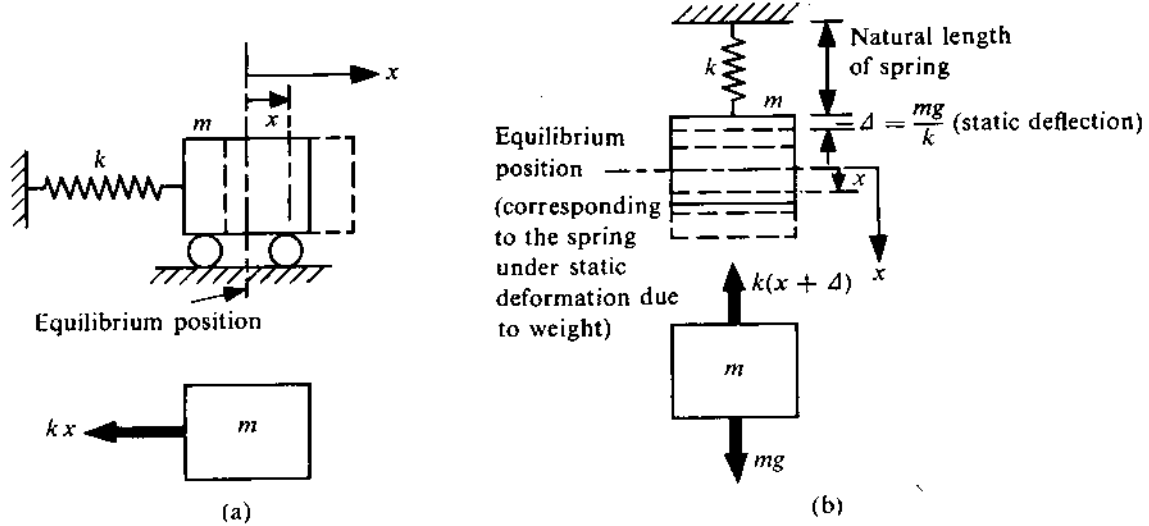


FIGURE 11.4

a simple harmonic function of time with a frequency ω_n . This frequency is called the *natural frequency* of the system. It should be noted that ω_n is a property of the system and does not depend on the disturbance. When expressed in radians per second, it is generally called the *circular natural frequency*. When expressed in cycles per second, it can be written as $f_n = \omega_n/(2\pi)$ Hz. The time period of natural oscillation corresponding to this frequency is $\tau_n = 2\pi/\omega_n$ s.

In the system we have described, the mass moves on a horizontal surface and the equilibrium position corresponds to the natural length of the spring. Now, if we consider the system in Fig. 11.4b, we shall see that the mass is always under the action of gravity. So, the equilibrium position no longer corresponds to the natural length of the spring. Instead, it is given by the position for which the spring has an extension $\Delta = mg/k$. If the vibratory displacement, x , is measured from this static equilibrium position, the corresponding free-body diagram would be as shown (Fig. 11.4b). Thus, the equation of motion is

$$m\ddot{x} = mg - k(x + \Delta) = -kx$$

or

$$m\ddot{x} + kx = 0.$$

Hence, the equation of motion in terms of x , measured in the manner stated, is the same as that for the horizontal system.

For a conservative system, in particular a system with constraint forces, the equation of motion can be more easily derived using the principle of energy conservation. Let us do this for the system shown in Fig. 11.4b. When the displacement is x , the KE of the system is

$$T = \frac{1}{2}m\dot{x}^2.$$

At this instant, the total PE of the system is

$$\begin{aligned} V &= \text{PE due to gravity + strain energy of the spring} \\ &= -mgx + \frac{1}{2}k(x + \Delta)^2 = \frac{1}{2}kx^2 + \frac{1}{2}k\Delta^2. \end{aligned}$$

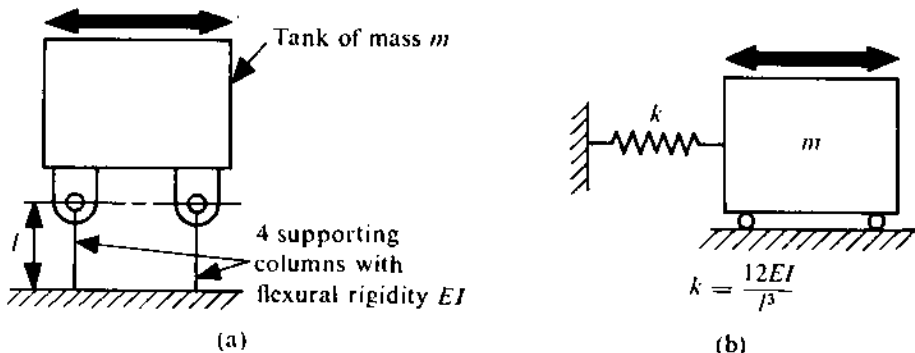


FIGURE 11.5

The datum for the gravitational PE is taken to be the equilibrium position. As the system is conservative, $T + V = \text{constant}$ or

$$\frac{d}{dt}(T + V) = 0. \quad (11.4)$$

Substituting for T and V in this equation, we get $(m\ddot{x} + kx)\dot{x} = 0$. As $\dot{x} \neq 0$ at all instants of time, the equation of motion is obtained as

$$m\ddot{x} + kx = 0.$$

The values of stiffness parameters of some commonly-used structural restoring elements are given in Table 11.1. We shall use these values in our subsequent study.

PROBLEM 11.1

A tank of mass m is supported by four vertical columns of length l and flexural rigidity (for bending in the plane of the paper) EI as shown in Fig. 11.5a. The columns are hinged to the tank and clamped at the base. Determine the natural frequency of oscillation of the system, neglecting the mass of the columns.

SOLUTION

An examination of the system reveals that the predominant vibration can take place only in the direction indicated. Referring to Table 11.1, we find the equivalent stiffness of each column at the hinge is $3EI/l^3$. Thus, the total stiffness of the equivalent spring in the model (Fig. 11.5b) is $12EI/l^3$. Hence, the natural frequency of the system is given by $\omega_n = [12EI/(ml^3)]^{1/2}$.

PROBLEM 11.2

Figure 11.6 shows a V-tube of constant cross-sectional area A filled with a liquid of density ρ . The length of the fluid column in each arm is l and each arm is inclined to the vertical at an angle α . If the equilibrium configuration is disturbed by displacing the free surface of the liquid in one arm, what will be the frequency of the resulting oscillation?

SOLUTION

Let us use the energy method to determine the equation of motion. If the free surface A' is at a depth x below the original position A , then the PE can be evaluated as follows. We can imagine

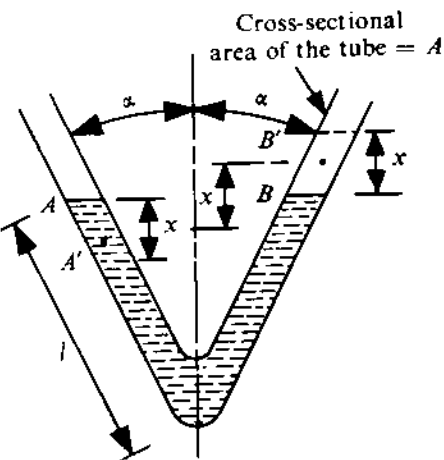


FIGURE 11.6

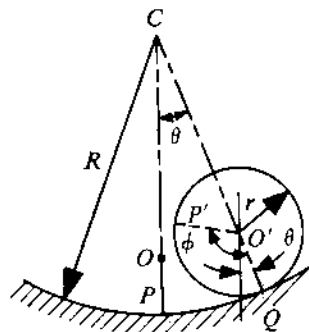


FIGURE 11.7

that the only change from the equilibrium configuration is that the column AA' shifts to BB' when the CG of the former column goes up by x (see Fig. 11.6). Then,

$$V = \rho A \frac{x}{\cos \alpha} g \cdot x = \rho A g \frac{x^2}{\cos \alpha}, \quad (a)$$

where $\rho Ax/\cos \alpha$ is the mass of AA' . Clearly, the magnitude of velocity everywhere in the liquid is $\dot{x}/\cos \alpha$. Therefore, the KE of the system is

$$T = \frac{1}{2} \rho A \cdot 2l \left(\frac{\dot{x}}{\cos \alpha} \right)^2 = \rho Al \frac{\dot{x}^2}{\cos^2 \alpha}. \quad (b)$$

From (11.4),

$$\frac{d}{dt} \left[\frac{\rho Al}{\cos^2 \alpha} \cdot \dot{x}^2 + \frac{\rho Ag}{\cos \alpha} \cdot x^2 \right] = 0$$

or

$$\frac{\rho Al}{\cos^2 \alpha} \ddot{x} + \frac{\rho Ag}{\cos \alpha} x = 0$$

or

$$\ddot{x} + \frac{g \cos \alpha}{l} x = 0.$$

So, the natural frequency of oscillation is $\omega_n = (g \cos \alpha / l)^{1/2}$.

PROBLEM 11.3

A uniform solid cylinder of radius r and mass m rolls without slipping on a cylindrical cavity of radius R . Determine the natural frequency of oscillation of the cylinder about its lowest position (Fig. 11.7).

SOLUTION

If we derive the equation of motion directly from the free-body diagram of a rolling cylinder, we will have to take into account the constraining forces, namely, the normal reaction and the friction force at the point of contact. In our situation, since both these forces do not do any work, the system is conservative, and we can use the energy method to obtain the equation of motion without bringing in these forces.

Let us consider the displaced position of the cylinder shown in Fig. 11.7. As there is no slip, $\text{arc } QP = \text{arc } QP'$, where $O'P'$ is the new position of the vertical radius OP (at the equilibrium configuration). Thus, $r\dot{\phi} = R\dot{\theta}$ or

$$r\dot{\phi} = R\dot{\theta}. \quad (\text{a})$$

Obviously, the rotation of the cylinder from its original position where $O'P'$ was OP is given by $(\phi - \theta)$. So, the instantaneous angular velocity is $(\dot{\phi} - \dot{\theta})$. Hence, the KE is

$$T = T_{\text{rotational}} + T_{\text{translational}} = \frac{1}{2}J_{O'}(\dot{\phi} - \dot{\theta})^2 + \frac{1}{2}mv_{O'}^2, \quad (\text{b})$$

where $J_{O'} = \frac{1}{2}mr^2$ and $v_{O'} = (R - r)\dot{\theta}$. Finally, using (a) in (b), we get

$$T = \frac{3}{4}m(R - r)^2\dot{\theta}^2. \quad (\text{c})$$

The potential energy can be easily found out as

$$V = mg(R - r)(1 - \cos \theta). \quad (\text{d})$$

Since we are considering only small oscillations, θ is small. So,

$$\cos \theta \approx 1 - \theta^2/2.$$

(It should be noted that the assumption $\cos \theta \approx 1$ does not lead to any solution as it implies no change in the potential energy with θ .) Using this approximation in (d), we obtain

$$V = \frac{1}{2}mg(R - r)\theta^2. \quad (\text{e})$$

Now, using (c) and (e) in (11.4), we get

$$\frac{d}{dt} \left[\frac{3}{4}m(R - r)^2\dot{\theta}^2 + \frac{1}{2}mg(R - r)\theta^2 \right] = 0$$

or

$$\ddot{\theta} + \frac{2}{3} \left(\frac{g}{R - r} \right) \theta = 0.$$

Hence, the natural frequency is $\omega_n = [2g/(3(R - r))]^{1/2}$.

PROBLEM 11.4

The radius of gyration of an irregular body can be easily experimentally determined using a trifilar suspension. Figure 11.8a shows such a suspension. It consists of a disc suspended by three inextensible light strings, each of length l . These strings are attached to the disc symmetrically at a

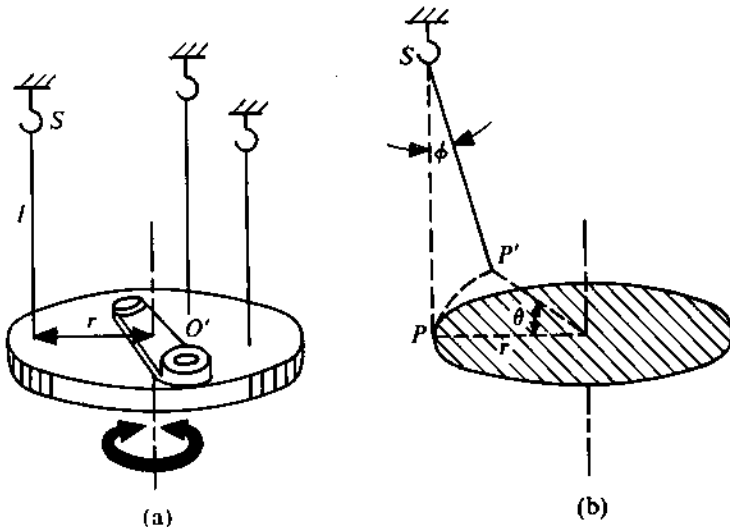


FIGURE 11.8

distance r from the centre O . The natural frequency of small angular oscillation, of the disc and a component of mass m_c placed on the disc, about the vertical axis passing through O is measured to be f_n . Determine the radius of gyration of this component. The radius of gyration and mass of the disc are given to be k_d and m_d , respectively. It is ensured that no relative movement between the component and the disc is possible.

SOLUTION

For a rotation θ of the disc, the strings are inclined to the vertical by an angle ϕ (Fig. 11.8b). So, the lift of the disc is given by $l(1 - \cos \phi) \approx \frac{1}{2}l\phi^2$. Further, $r\theta = l\phi$. So,

$$V = (m_d + m_c) \cdot \frac{1}{2}l \left(\frac{r\theta}{l}\right)^2 g = \frac{1}{2}(m_d + m_c) \cdot \frac{r^2}{l} \cdot \theta^2 g. \quad (a)$$

The KE of the system is

$$T = \frac{1}{2}(m_d k_d^2 + m_c k_c^2) \dot{\theta}^2. \quad (b)$$

Applying the principle of conservation of energy, we have

$$\frac{d}{dt} \left[\frac{1}{2}(m_d k_d^2 + m_c k_c^2) \dot{\theta}^2 + \frac{1}{2}g(m_d + m_c) \frac{r^2}{l} \cdot \theta^2 \right] = 0$$

or

$$\ddot{\theta} + \frac{g(m_d + m_c)r^2}{(m_d k_d^2 + m_c k_c^2)l} \cdot \theta = 0.$$

So, the circular natural frequency is

$$\omega_n = \left[\frac{g(m_d + m_c)r^2}{(m_d k_d^2 + m_c k_c^2)l} \right]^{1/2} = 2\pi f_n.$$

Thus,

$$k_c = \left\{ \frac{1}{m_c} \left[\frac{g(m_d + m_c)r^2}{4\pi^2 f_n^2 l} - m_d k_d^2 \right] \right\}^{1/2}.$$

PROBLEM 11.5

Figure 11.9a shows a rotating cantilever leaf spring with flexural rigidity EI carrying a mass m at its end. Neglecting the mass of the spring, determine the natural frequency of oscillation of the system. The angular speed of the shaft is Ω .

SOLUTION

As the oscillation is taking place in a rotating system (i.e., in a noninertial frame of reference), Newton's second law can be applied only after introducing the proper inertia forces – in this case, a centrifugal force $m\Omega^2(r + l)$. Figure 11.9b shows the free-body diagram of m when the mass is displaced upwards by an amount x . Here, S indicates the tension in the spring and the vertical force $3EIx/l^3$ represents the restoring force exerted by the spring. For equilibrium in the horizontal direction, $S \cos \theta = m\Omega^2(r + l)$. As θ is small,

$$S \approx m\Omega^2(r + l). \quad (a)$$

(It should be noted that here, unlike in Problem 11.3, we have approximated $\cos \theta$ to 1. The reader is advised to justify this approximation.) In the x -direction, the equation of motion is

$$m\ddot{x} = -\frac{3EI}{l^3}x - S \sin \theta. \quad (b)$$

Now, a reasonable assumption has to be made to correlate θ to x . We shall do this by using the relationship that is valid for a concentrated load at the free end of the cantilever leaf spring (see Fig. 11.9c). Since, from the beam theory,

$$x = \frac{Fl^3}{3EI}, \quad \theta = \frac{Fl^2}{2EI},$$

we get $\theta = 3x/(2l)$. Using this relation in (b) and substituting S from (a), the final equation of motion we get is

$$\ddot{x} + \frac{1}{m} \left(\frac{3EI}{l^3} + \frac{3}{2}m\Omega^2 \cdot \frac{l+r}{l} \right)x = 0.$$

Hence,

$$\omega_n = \left\{ \frac{3EI}{ml^3} + \frac{3\Omega^2(l+r)}{2l} \right\}^{1/2}.$$

It may be noted that the rotation (Ω) adds to the stiffness of the leaf spring.

PROBLEM 11.6

A uniform plank of mass m is resting over two rollers rotating in the opposite directions as shown in Fig. 11.10a. The distance between the roller axes is $2a$ and the rollers are spinning at a high speed. The coefficient of friction between the plank and the rollers is μ . Show that the plank will oscillate when its CG is displaced from the midpoint between the rollers. Also, determine the frequency of this oscillation. Further, investigate the motion of the plank when the directions of rotation of both the rollers are reversed.

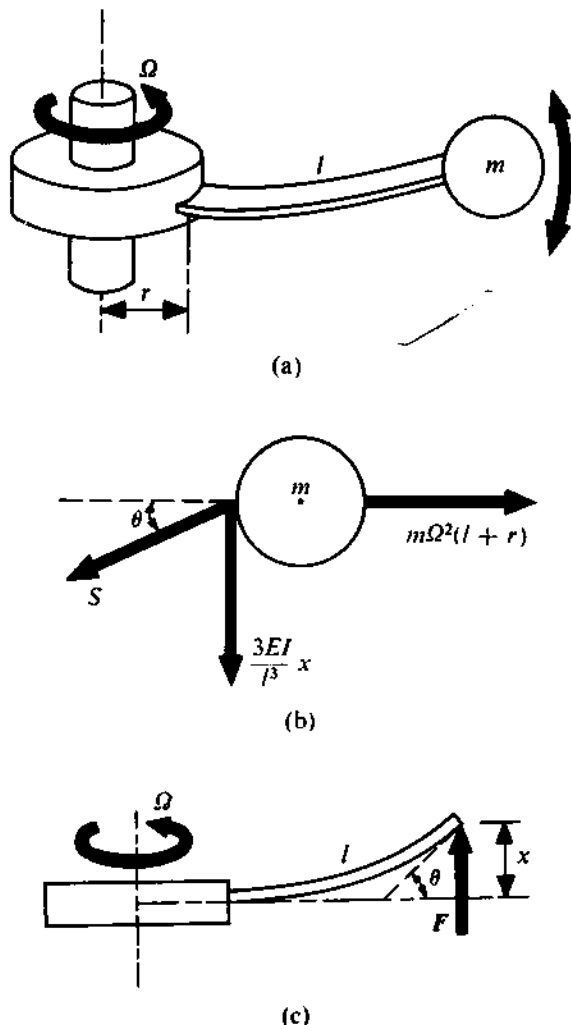


FIGURE 11.9

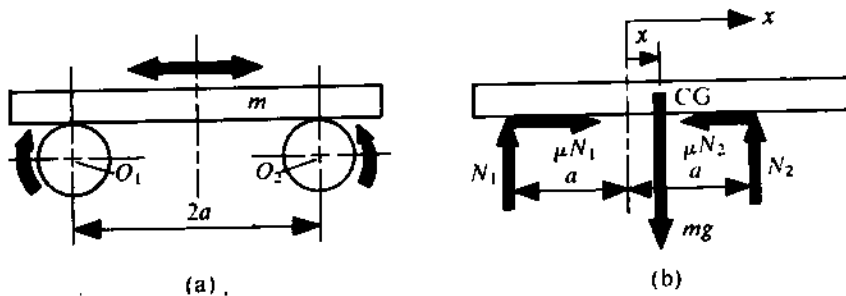


FIGURE 11.10

SOLUTION

Since the rollers are rotating at a high speed, we can assume continuous slip and the friction force on the plank (acting inwards) has reached the limiting value. When the CG of the plank is at a distance x from its equilibrium position (the midpoint), the normal reactions N_1 and N_2 acting on it will (see the free-body diagram shown in Fig. 11.10b) be

$$N_1 = mg \cdot \frac{a - x}{2a}, \quad N_2 = mg \cdot \frac{a + x}{2a}. \quad (\text{a})$$

The equation of motion of the plank in the x -direction is given by

$$m\ddot{x} = -\mu(N_2 - N_1)$$

or

$$m\ddot{x} + (\mu mg/a)x = 0$$

or

$$\ddot{x} + (\mu g/a)x = 0. \quad (\text{b})$$

Comparing (b) with (11.1), we find that this motion is identical with the free oscillation of a single-degree-of-freedom (SDF) system. The frequency of oscillation is

$$\omega_n = (\mu g/a)^{1/2}. \quad (\text{c})$$

The possibility here of a free oscillation of the system in the absence of any restoring element may surprise the reader. The fact is that the situation we are considering is an example of a self-excited oscillation where the exciting force is generated by the motion of the system.

When the directions of rotation of the rollers are reversed, the directions of the friction forces change and the resulting equation of motion becomes $\ddot{x} - (\mu g/a)x = 0$. Obviously, the solution of this equation will yield x as an exponential function of time and no oscillation will take place.

Equation (c) is sometimes used to measure the coefficient of friction μ . Since the frequency of oscillation f can be easily measured, μ is expressed as

$$\mu = \omega^2 a/g = 4\pi^2 f^2 a/g.$$

By varying the roller speed, the variation of μ with sliding velocity can be investigated.

Equivalent Inertia and Stiffness

In the problems we have so far discussed, we had only one inertial element. However, there may be a system where more than one inertial element has to be connected so as to give only one degree of freedom to the system. In such a system, an equivalent inertia (related to the chosen coordinate) can be derived. This is done by maintaining the total KE of the system the same. Similarly, an equivalent stiffness can be obtained by keeping the total PE of the system unchanged. We shall illustrate these principles in the problems that follow.

PROBLEM 11.7

Figure 11.11a shows an SDF system consisting of a gear of radius r and moment of inertia J , a rack of mass m , a linear spring of stiffness k , and a torsional spring with stiffness K . Obtain the equivalent inertia and stiffness (i) with θ as the chosen coordinate, and (ii) with x as the chosen coordinate.

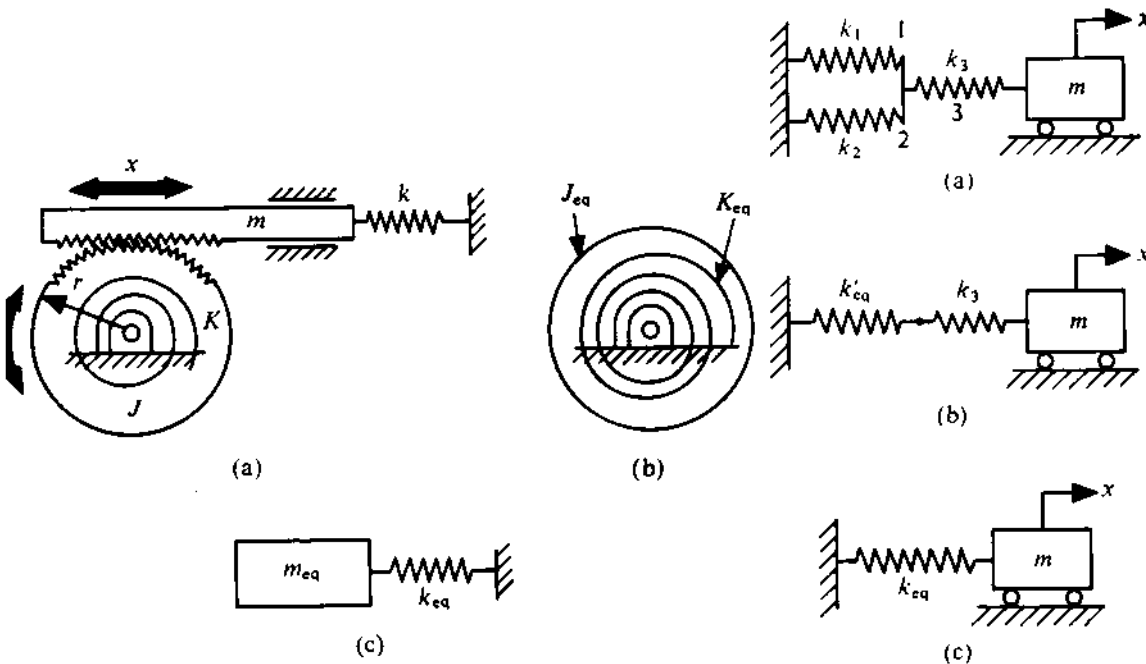


FIGURE 11.11

FIGURE 11.12

SOLUTION

(i) The total KE of the system is

$$T = \frac{1}{2}J\dot{\theta}^2 + \frac{1}{2}m\dot{x}^2 = \frac{1}{2}(J + mr^2)\dot{\theta}^2 = \frac{1}{2}J_{eq}\dot{\theta}^2$$

since, from the geometry of motion, $x = r\theta$. Similarly, the total PE of the system is

$$V = \frac{1}{2}K\theta^2 + \frac{1}{2}kx^2 = \frac{1}{2}(K + kr^2)\theta^2 = \frac{1}{2}K_{eq}\theta^2.$$

The equivalent system is shown in Fig. 11.11b where $J_{eq} = J + mr^2$ and $K_{eq} = K + kr^2$.

(ii) The equivalent system is shown in Fig. 11.11c. In terms of the coordinate x ,

$$T = \frac{1}{2}J\dot{\theta}^2 + \frac{1}{2}m\dot{x}^2 = \frac{1}{2}(J/r^2 + m)\dot{x}^2 = \frac{1}{2}m_{eq}\dot{x}^2,$$

$$V = \frac{1}{2}(K/r^2 + k)x^2 = \frac{1}{2}k_{eq}x^2.$$

So, $m_{eq} = J/r^2 + m$ and $k_{eq} = K/r^2 + k$. It should be noted that $\omega_n = (K_{eq}/J_{eq})^{1/2} = (k_{eq}/m_{eq})^{1/2}$ is independent of the choice of the coordinate for the equivalent system.

PROBLEM 11.8

A mass m is connected to the wall by three springs as shown in Fig. 11.12a. Determine the natural frequency of the system.

SOLUTION

First, we shall attempt to determine the equivalent system (Fig. 11.12c) with a spring of stiffness k'_{eq} . Let the amount of elongation of springs 1, 2, and 3 be x_1 , x_2 , and x_3 , respectively. From geometry,

$$x_1 = x_2, \quad x = x_1 + x_3. \quad (\text{e})$$

The total PE of the system is

$$V = \frac{1}{2}(k_1 + k_2)x_1^2 + \frac{1}{2}k_3x_3^2 = \frac{1}{2}k'_{\text{eq}}x_1^2 + \frac{1}{2}k_3x_3^2. \quad (\text{f})$$

As can be seen, if the springs are parallel (i.e., have the same deformation), the resultant stiffness given by the sum of the stiffnesses of the individual springs. This is shown in Fig. 11.12b. We also see that k'_{eq} and k_3 are in series (i.e., transmitting the same force). Therefore, $k'_{\text{eq}}x_1 = k_3x_3$ or

$$x_3 = x_1(k'_{\text{eq}}/k_3). \quad (\text{g})$$

From the second equation in (a), we have

$$x = x_1 + x_3 = x_1(1 + k'_{\text{eq}}/k_3). \quad (\text{h})$$

Using (c) in (b), we get

$$V = \frac{1}{2}k'_{\text{eq}}x_1^2 + \frac{1}{2}k_3 \left(x_1 \frac{k'_{\text{eq}}}{k_3} \right)^2.$$

Using (d) in this equation, we finally get

$$V = \frac{1}{2} \left(k'_{\text{eq}} + \frac{k'^2_{\text{eq}}}{k_3} \right) \cdot \frac{x^2}{(1 + k'_{\text{eq}}/k_3)^2} = \frac{1}{2} \left(\frac{1}{1/k'_{\text{eq}} + 1/k_3} \right) x^2 = \frac{1}{2}k_{\text{eq}}x^2.$$

So, when the springs are in series, the reciprocal of the equivalent stiffness is equal to the sum of the reciprocals of the stiffnesses of the individual springs.

The final equivalent system (Fig. 11.12c) has a natural frequency

$$\omega_n = \left(\frac{k_{\text{eq}}}{m} \right)^{1/2} = \left[\frac{1}{\{1/(k_1 + k_2) + 1/k_3\}m} \right]^{1/2}.$$

The conclusions about the resultant stiffnesses of springs in series or parallel can be easily extended to a system with more than two springs. The generalized conclusions are

$$k_{\text{resultant}} = \sum_{i=1}^n k_i \quad \text{for } n \text{ springs in parallel (having the same deformation)} \quad (11.5)$$

$$= \frac{1}{\sum_{i=1}^n \frac{1}{k_i}} \quad \text{for } n \text{ springs in series (transmitting the same force).} \quad (11.5')$$

The concept of equivalent inertia can be used to take into consideration the inertia of a restoring (spring) element. For this, it is necessary to assume a *dynamic deformation pattern* of such an element. The example that follows illustrates the use of this concept.

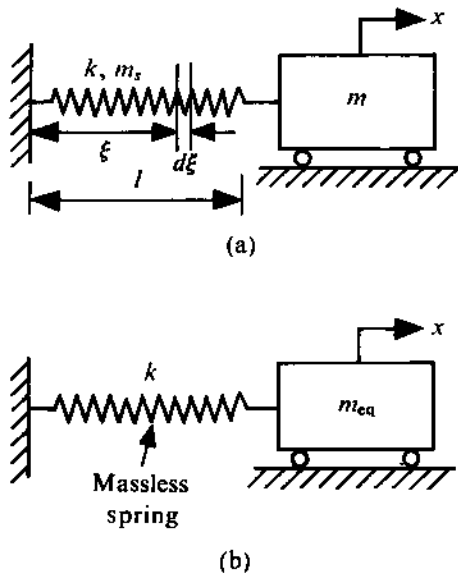


FIGURE 11.13

PROBLEM 11.9

Figure 11.13a shows a spring mass system with a uniform spring of mass m_s , and unstretched length l . Determine the natural frequency of the system, taking into account the mass of the spring.

SOLUTION

First, we shall try to find out the equivalent ideal model. This is shown in Fig. 11.13b. To determine m_{eq} , we keep the kinetic energy of the given and the equivalent systems the same. To calculate the contribution of the spring to the KE, a suitable dynamic deformation pattern of the spring has to be assumed. The natural frequency obtained by making such an assumption, as we shall subsequently see, is quite accurate. In the situation we are considering, the left end of the spring does not move, whereas its right end is displaced through a distance x . Let us assume that the displacement varies linearly along the length of the spring. Thus, the displacement of an element $d\xi$ (Fig. 11.13a) is $x\xi/l$ when the velocity of this element is $\dot{x}\xi/l$. So, the KE of the element is

$$dT_s = \frac{1}{2} \cdot \frac{m_s}{l} \cdot d\xi \cdot (\dot{x} \frac{\xi}{l})^2.$$

For the entire spring, the KE is

$$T_s = \frac{1}{2} \cdot \frac{m_s \dot{x}^2}{l^3} \int_0^l \xi^2 d\xi = \frac{1}{2} \cdot \left(\frac{1}{3} m_s\right) \dot{x}^2.$$

So, the total KE of the system is

$$T = \frac{1}{2} m \dot{x}^2 + \frac{1}{2} \cdot \frac{1}{3} m_s \dot{x}^2 = \frac{1}{2} m_{eq} \dot{x}^2$$

or

$$m_{eq} = m + \frac{1}{3} m_s.$$

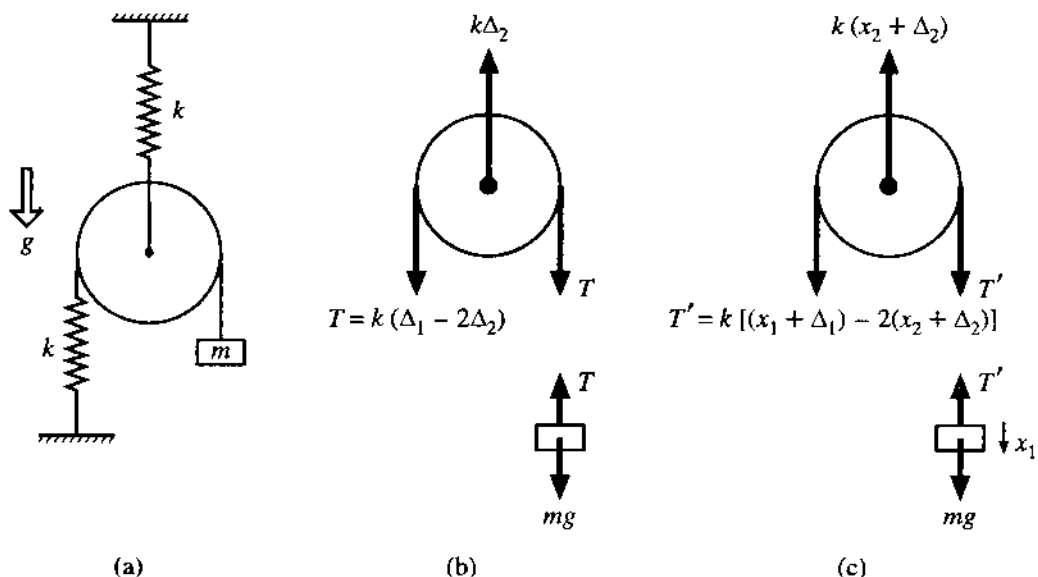


FIGURE 11.14

Hence, the natural frequency of the system is

$$\omega_n = (k/m_{\text{eq}})^{1/2} = [k/(m + \frac{1}{3}m_s)]^{1/2}.$$

PROBLEM 11.10

The system shown in Fig. 11.14a is constrained to move in the vertical direction. Assuming the pulley to be massless and frictionless, determine the natural frequency of oscillation. The amplitude of oscillation is small enough to ensure that the string connected to the mass m always remains taut.

SOLUTION

Let Δ_1 and Δ_2 be the static deflections due to gravity of the mass m and the pulley, respectively. The stretches of the upper and lower springs then are Δ_2 and $(\Delta_1 - 2\Delta_2)$, respectively. From the free-body diagrams, shown in Fig. 11.14b, we can write

$$k\Delta_2 = 2T = 2k(\Delta_1 - 2\Delta_2), \quad (\text{a})$$

$$T = mg. \quad (\text{b})$$

From (a) and (b), we obtain

$$\Delta_1 = 5mg/k, \quad \Delta_2 = 2mg/k. \quad (\text{c})$$

If x_1 and x_2 be the further downward deflections, from the static equilibrium positions, of the mass m and the pulley, respectively, then the stretch of the lower spring is $x_1 + \Delta_1 - 2(x_2 + \Delta_2)$. From the free-body diagrams, shown in Fig. 11.14c, we can write

$$m\ddot{x}_1 = mg - T', \quad (d)$$

$$k(x_2 + \Delta_2) = 2T' = 2k[(x_1 + \Delta_1) - 2(x_2 + \Delta_2)]. \quad (\text{e})$$

From (e), we get

$$2(x_1 + \Delta_1) = 5(x_2 + \Delta_2), \quad (\text{f})$$

$$\begin{aligned} T' &= k[(x_1 + \Delta_1) - 2(x_2 + \Delta_2)] \\ &= \frac{k}{5}(x_1 + \Delta_1) \quad (\text{using (f)}). \end{aligned} \quad (\text{g})$$

Using (g) and (c) in (d), we obtain

$$m\ddot{x}_1 = -\frac{k}{5}x_1$$

when the natural frequency of oscillation $\omega_n = \sqrt{\frac{k}{5m}}$. It is seen again that for linear oscillations with constant system parameters, the force of gravity has no role except to shift the static equilibrium position around which the vibration occurs.

Damping

As already stated, a real-life system has mechanisms responsible for dissipating the energy, thus causing a free vibration to damp out. The rate of decay of a free vibration is a measure of the damping in a system. The major sources of damping depend on both the system and the environment. The most common sources are

- (i) dry friction between moving surfaces,
- (ii) drag between a moving body and its fluid environment,
- (iii) internal friction within a material, and
- (iv) radiation of energy into the environment.

The damping resulting from source (i) is better known as the *coulomb damping*. Here, a resisting force of constant magnitude acts opposite to the relative motion.

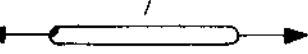
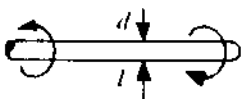
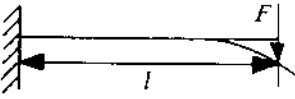
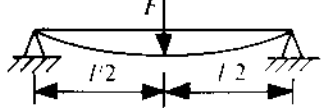
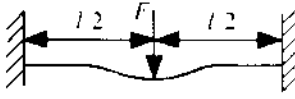
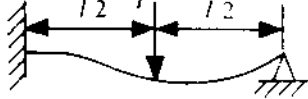
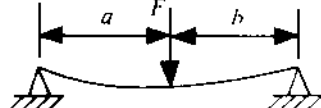
In the damping generated by source (ii), the drag is viscous in nature. Therefore, this damping is known as *viscous damping*. When the relative velocity is not very high (i.e., the Reynolds number is within the laminar range), the drag force is proportional to the relative velocity. This type of damping is widely used to control the vibrations. An ideal element to represent viscous damping (a dashpot) is shown in Fig. 11.15a where a piston with a number of small holes moves in a cylinder filled with a viscous oil. In a mathematical model, an idealized viscous dashpot is represented as shown in Fig. 11.15b. If the relative velocity between the cylinder and the piston is \dot{x} , obviously, then, the rate of fluid flow through the holes is proportional to \dot{x} . The associated pressure drop across the piston will be $R\dot{x}$, where R is the combined fluid resistance of the holes. Hence, the force acting on the piston is proportional to \dot{x} . So, the force F_d associated with the *relative velocity* \dot{x} can be expressed as

$$F_d = c\dot{x}, \quad (11.6)$$

where the constant of proportionality c is called the viscous damping coefficient.

It has been established that a vibrating body, even when it is completely isolated from the surrounding, dissipates energy, resulting in the decay of its free vibration. The reason the body dissipates energy is that its KE gets converted into heat, thus raising its temperature. Such a

TABLE 11.1

Spring element	Equivalent stiffness
	$K^* = EI/l$
flexural rigidity = EI length = l 	$k = EA/l$
cross-sectional area = A	
	$K = \pi Gd^4/(32l)$
shear modulus = G	
	$k = Gd^4/(64nR^3)$
number of coils = n	
	$k = 3EI/l^3$
	$k = 48EI/l^3$
	$k = 192EI/l^3$
	$k = 768EI/(7l^3)$
	$k = 3EIl/(a^2b^2)$

* K represents rotational stiffness.

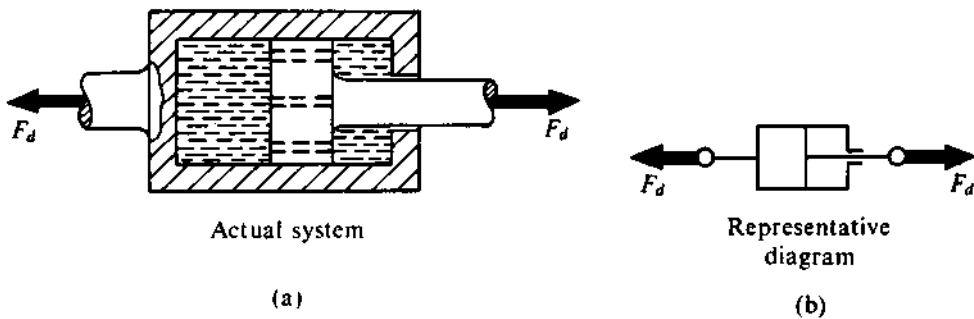


FIGURE 11.15

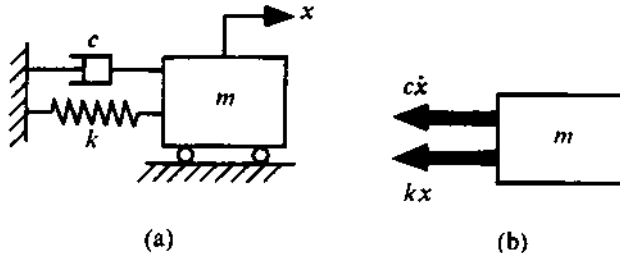


FIGURE 11.16

body has various mechanisms within its material responsible for the dissipation of energy. These mechanisms constitute the *internal friction*.

A body vibrating in a fluid medium, e.g., a submerged structure and an aeroplane, can generate waves which propagate and, in the process, carry away the vibrational energy. This loss of energy manifests itself as radiation damping.

Free Vibration with Viscous Damping

Since the characteristic of viscous damping is linear, this form of damping is most convenient for mathematical analysis. Let us consider the free vibration of a viscously-damped system shown in Fig. 11.16a. It may be noted that the spring and the dashpot here are parallel. This arrangement is known as Voigt's model and is the simplest for representing a real-life system. Considering the free-body diagram of the mass (Fig. 11.16b), we can write the equation of motion as

$$m\ddot{x} + c\dot{x} + kx = 0. \quad (11.7)$$

Assuming that its solution is of the form $x = e^{st}$, we get

$$ms^2 + cs + k = 0.$$

Solving this equation, we obtain

$$s_{1,2} = -\frac{c}{2m} \pm \left(\frac{c^2}{4m^2} - \frac{k}{m} \right)^{1/2}. \quad (11.8)$$

From (11.8), it is clear that the system can be in one of three different situations, namely:

- (i) $c > 2\sqrt{km}$ (i.e., overdamped): Here, both s_1 and s_2 are real and the general solution of (11.7) can be written as

$$x = Ae^{s_1 t} + Be^{s_2 t}, \quad (11.9)$$

where s_1 and s_2 are given by (11.8) and the constants A and B are to be determined from the initial conditions. It is obvious that the two terms in (11.9) decay exponentially since both s_1 and s_2 are negative. Thus, the system does not execute any oscillatory motion. Such a motion is called *aperiodic*.

- (ii) $c = 2\sqrt{km}$ (i.e., critically damped): With this amount of damping,

$$s_1 = s_2 = -c/(2m),$$

and the general solution of (11.7) is of the form

$$x = (A + Bt)e^{-ct/(2m)}. \quad (11.10)$$

This value of damping is known as *critical damping* (c_c). In a system, the damping is in fact expressed as a fraction of critical damping. The nondimensional ratio $\zeta = c/c_c$ is known as the *damping factor*. Using this terminology, we see that $\zeta > 1$ in (i), and $\zeta = 1$ in the situation here.

From (11.10), it is clear that critical damping also gives rise to aperiodic motion.

- (iii) $c < 2\sqrt{km}$ (i.e., underdamped): When the damping is below critical,

$$s_{1,2} = -\frac{c}{2m} \pm i\left(\frac{k}{m} - \frac{c^2}{4m^2}\right)^{1/2} = -[\zeta \mp i(1 - \zeta^2)^{1/2}]\omega_n.$$

The general solution of (11.7) then is

$$\begin{aligned} x &= \exp(-\zeta\omega_n t)\{A_1 \exp[i\sqrt{(1 - \zeta^2)\omega_n t}] + B_1 \exp[-i\sqrt{(1 - \zeta^2)\omega_n t}]\} \\ &= \exp(-\zeta\omega_n t)[A \cos((1 - \zeta^2)^{1/2}\omega_n t) + B \sin((1 - \zeta^2)^{1/2}\omega_n t)] \end{aligned} \quad (11.11a)$$

$$= X \exp(-\zeta\omega_n t) \cos[(1 - \zeta^2)^{1/2}\omega_n t + \phi]. \quad (11.11b)$$

As usual, the constants A , B or X , ϕ are determined from the initial conditions.

Now, let us rewrite the general solution for the overdamped situation in terms of ζ in the form

$$x(t) = A \exp\{[-\zeta + \sqrt{(\zeta^2 - 1)}]\omega_n t\} + B \exp\{[-\zeta - \sqrt{(\zeta^2 - 1)}]\omega_n t\}.$$

When the initial conditions are $x = x(0)$, $\dot{x} = \dot{x}(0)$ at $t = 0$, the foregoing form of the general solution can be written as

$$\begin{aligned} x(t) &= \frac{\dot{x}(0) + [\zeta + (\zeta^2 - 1)^{1/2}]\omega_n x(0)}{2\omega_n(\zeta^2 - 1)^{1/2}} \exp\{[-\zeta + \sqrt{(\zeta^2 - 1)}]\omega_n t\} \\ &\quad + \frac{-\dot{x}(0) - [\zeta - (\zeta^2 - 1)^{1/2}]\omega_n x(0)}{2\omega_n(\zeta^2 - 1)^{1/2}} \exp\{[-\zeta - \sqrt{(\zeta^2 - 1)}]\omega_n t\}. \end{aligned} \quad (11.12)$$

In (11.12), since both the terms on the right-hand side are exponentially decaying to zero as $t \rightarrow \infty$, $x(t)$ will asymptotically become zero as $t \rightarrow \infty$. However, depending on the values of $x(0)$ and $\dot{x}(0)$,

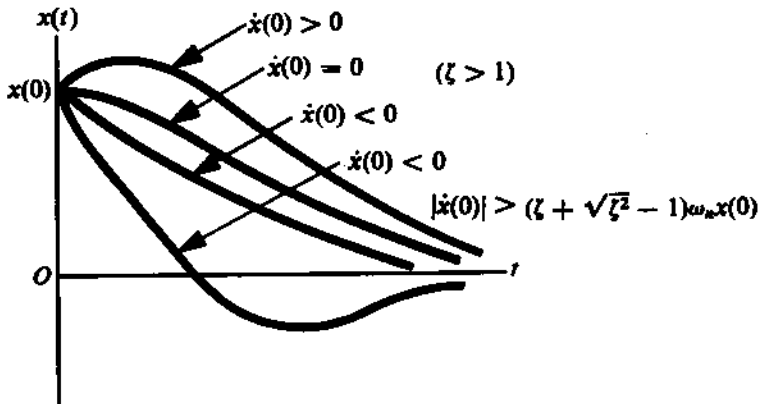


FIGURE 11.17

the mass can pass through its equilibrium position only once. This will never happen when both $x(0)$ and $\dot{x}(0)$ have the same sign. In what follows, we shall prove this.

Let us find out those values of t for which the right-hand side of (11.12) will become zero. Equating the right-hand side to zero, we get

$$\begin{aligned} & \frac{\dot{x}(0) + [\zeta + (\zeta^2 - 1)^{1/2}]\omega_n x(0)}{2\omega_n(\zeta^2 - 1)^{1/2}} \exp \{[-\zeta + \sqrt{(\zeta^2 - 1)}\omega_n t\}] \\ & + \frac{-\dot{x}(0) - [\zeta - (\zeta^2 - 1)^{1/2}]\omega_n x(0)}{2\omega_n(\zeta^2 - 1)^{1/2}} \exp \{[-\zeta - \sqrt{(\zeta^2 - 1)}\omega_n t\}] = 0 \end{aligned}$$

or

$$\begin{aligned} & \exp(-\zeta\omega_n t) \left[\frac{\dot{x}(0) + [\zeta + (\zeta^2 - 1)^{1/2}]\omega_n x(0)}{2\omega_n(\zeta^2 - 1)^{1/2}} \exp \{\sqrt{(\zeta^2 - 1)}\omega_n t\} \right. \\ & \left. - \frac{\dot{x}(0) + [\zeta - (\zeta^2 - 1)^{1/2}]\omega_n x(0)}{2\omega_n(\zeta^2 - 1)^{1/2}} \exp \{-\sqrt{(\zeta^2 - 1)}\omega_n t\} \right] = 0. \end{aligned}$$

As can be seen, one root of this equation is $t \rightarrow \infty$ as already discussed. The other root of the equation will be given by the solution of

$$\exp[2\sqrt{(\zeta^2 - 1)}\omega_n t] = \frac{\dot{x}(0) + [\zeta - (\zeta^2 - 1)^{1/2}]\omega_n x(0)}{\dot{x}(0) + [\zeta + (\zeta^2 - 1)^{1/2}]\omega_n x(0)}$$

Obviously, for $\zeta > 1$, this equation will have no positive root for t unless the right-hand side of the equation is greater than 1. This implies that no overshooting is possible when $\dot{x}(0)$ and $x(0)$ are of the same sign. When these quantities have opposite signs and $|\dot{x}(0)| > |[\zeta + (\zeta^2 - 1)^{1/2}]\omega_n x(0)|$, one positive root for t is possible. In other words, the mass will cross its equilibrium position only once. Figure 11.17 illustrates the displacement as a function of time for various initial velocities.

When the system is critically damped, the general solution of (11.7) in terms of the initial disturbances can be written as

$$x(t) = \exp(-\omega_n t)[\{\dot{x}(0) + \omega_n x(0)\}t + x(0)]. \quad (11.13)$$

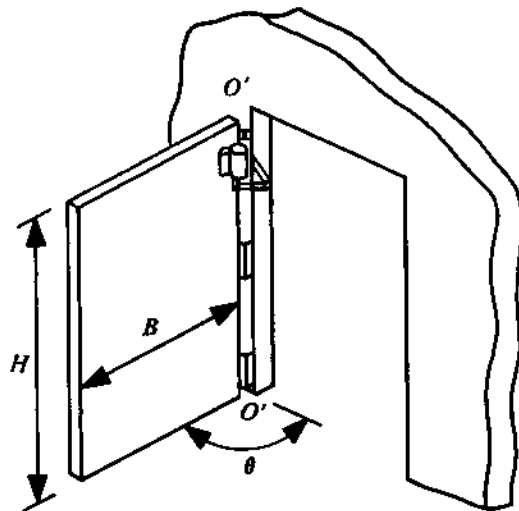


FIGURE 11.18

Here too, the mass may cross its equilibrium position only once, depending on the initial conditions. From (11.13), x becomes zero when $t \rightarrow \infty$ and

$$t = \frac{-x(0)}{\dot{x}(0) + \omega_n x(0)}. \quad (11.14)$$

Obviously, for t to be positive, the necessary conditions are $|\dot{x}(0)| > |\omega_n x(0)|$ and $\dot{x}(0)$ should have a sign opposite to that of $x(0)$. The nature of variation of x with time is similar to that shown in Fig. 11.17. The reader is advised to satisfy himself that in a critically damped system the mass tends to regain its equilibrium condition (i.e., $x = \dot{x} = 0$) in the shortest possible time.

A system where oscillation is unwanted is provided with critical damping. A door closer and gun recoil are examples of such a system.

PROBLEM 11.11

Figure 11.18 shows a door frame and a door with a door closer. The door closer exerts a critical amount of damping torque 24 N-m-s/rad and it is provided with a torsional spring which exerts a resisting torque proportional to the door opening angle θ . The door is swung open by 60° . Determine the maximum angular velocity with which the door can be swung back so as not to hit the frame. The uniform rectangular door has a mass 48 kg , a height 2 m , and a width 1 m .

SOLUTION

Let us assume the door is thin. Then, its moment of inertia about the hinge axis is

$$J_0 = mB^2/3 = (48 \times 1^2)/3 = 16 \text{ kg-m}^2.$$

The equation of motion of the door is

$$J_0\ddot{\theta} + C\dot{\theta} + K\theta = 0.$$

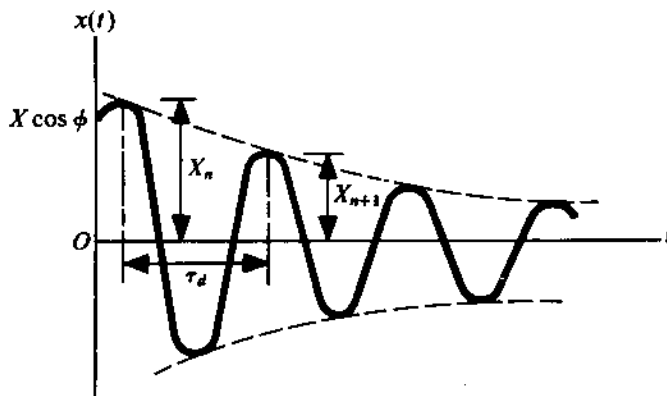


FIGURE 11.19

Comparing this with (11.7), we find that the critical damping coefficient here is $C_c = 2(KJ_0)^{1/2} = 24 \text{ N-m-s/rad}$. Since $J_0 = 16 \text{ kg-m}^2$, K comes out as 9 N-m/rad . So, the natural frequency is $\omega_n = (K/J_0)^{1/2} = 3/4 \text{ rad/s}$. From (11.14), we find that the maximum velocity of the door for it not to hit the frame is

$$\dot{\theta}(0) = -\omega_n \theta(0) = -(3/4) \times (\pi/3) = -\pi/4 \text{ rad/s.}$$

If $\dot{\theta}(0)$ is negative with $|\dot{\theta}(0)| > \pi/4 \text{ rad/s}$, the door will hit the frame.

When $\zeta < 1$, a system will execute an oscillatory motion as is evident from (11.11b). The nature of this motion is seen to be harmonic with an exponentially decaying amplitude. Figure 11.19 shows a record of such a damped oscillatory motion. The frequency of this oscillation, $\omega_n(1 - \zeta^2)^{1/2}$, is called the *damped natural frequency*. Such a record of free vibration decay is useful for evaluating the damping of a system. Considering any two successive peaks (Fig. 11.19), we can write

$$X_n = X \exp(-\zeta \omega_n t) \cos[(1 - \zeta^2)^{1/2} \omega_n t + \phi],$$

$$X_{n+1} = X \exp[-\zeta \omega_n (t + \tau_d)] \cos[(1 - \zeta^2)^{1/2} \omega_n (t + \tau_d) + \phi],$$

where τ_d is the *damped time period* and is given by $\tau_d = 2\pi/[\omega_n(1 - \zeta^2)^{1/2}]$. So,

$$X_n/X_{n+1} = \exp[2\pi\zeta/(1 - \zeta^2)^{1/2}]$$

or

$$\ln(X_n/X_{n+1}) = 2\pi\zeta/(1 - \zeta^2)^{1/2} = \delta, \quad (11.15)$$

where δ is called the *logarithmic decrement*. It may be noted that δ is a system property and is independent of n . In a lightly damped system, if two successive amplitudes are used for evaluating δ , the result may have a significant amount of error. This is because the difference between X_n and X_{n+1} is very small, and consequently the measurement error will be more. The error can be avoided by a simple modification of the expression for δ . Let the interval between two peaks be p cycles. Then, (11.15) can be modified as

$$\ln(X_n/X_{n+p}) = 2\pi p \zeta / (1 - \zeta^2)^{1/2} = p\delta$$

or

$$\delta = (1/p) \ln(X_n/X_{n+p}). \quad (11.16)$$

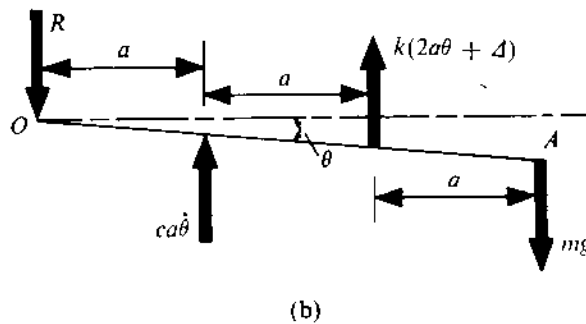
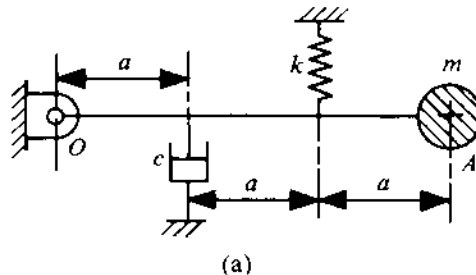


FIGURE 11.20

We can also express δ and ζ in terms of the ratio of the energy dissipated in a cycle to the maximum energy in the cycle (obviously, at the beginning of the cycle), as follows. Let the amplitudes at the beginning and the end of a cycle be X_1 and X_2 . Obviously, the maximum energy in the cycle is $E_1 = \frac{1}{2}kX_1^2$. The energy dissipated during the cycle is

$$\Delta E = E_1 - E_2 = \frac{1}{2}k(X_1^2 - X_2^2).$$

So, $\Delta E/E_1 = 1 - (X_2/X_1)^2$. From (11.15), this equation can be written as

$$\Delta E/E_1 = 1 - e^{-2\delta} \approx 1 - (1 - 2\delta + \dots) \quad \text{for small values of } \delta$$

or $\delta = 1/2(\Delta E/E_1)$. Again from (11.15), $\delta \approx 2\pi\zeta$ for small values of ζ (even when ζ is as high as 0.3, this approximation leads to an error of only 4.6%). Thus,

$$\zeta \approx \delta/(2\pi) \approx \Delta E/(4\pi E_1).$$

PROBLEM 11.12

Figure 11.20a shows an SDF system where a massless rigid bar OA is hinged at O and carries a mass m at its other end A . A spring and a dashpot are attached to the bar vertically as depicted. Determine the critical damping coefficient.

SOLUTION

The free-body diagram of the bar after it has rotated through an angle θ from the initial horizontal position is shown in Fig. 11.20b. At the horizontal position, the spring had stretched by an amount

Δ to balance the gravitational effect. Thus, taking moment about O for the static equilibrium position, we have

$$2ak\Delta = 3amg. \quad (\text{a})$$

Considering Fig. 11.20b and again taking moment about O , we get

$$m.(3a)^2\ddot{\theta} = mg.3a - k(2a\theta + \Delta) \times 2a - c.a\dot{\theta}.a.$$

Using (a) in this equation, we find the equation of motion is

$$9a^2m\ddot{\theta} + ca^2\dot{\theta} + 4a^2k\theta = 0$$

or

$$9m\ddot{\theta} + c\dot{\theta} + 4k\theta = 0. \quad (\text{b})$$

Seeking a solution in the form $\theta = e^{st}$, the equation for s we obtain is

$$9ms^2 + cs + 4k = 0$$

or

$$s = \frac{-c \pm (c^2 - 144km)^{1/2}}{18m}.$$

Hence, the critical damping coefficient is $c_c = 12(km)^{1/2}$.

Free Vibration with Coulomb Damping

Figure 11.21a schematically represents an SDF system with coulomb damping, where f indicates the constant friction force opposing the velocity. It is obvious that the direction of f changes with that of \dot{x} . The equation of motion can be written in two parts, namely,

$$m\ddot{x} + kx - f = 0 \quad (\dot{x} < 0), \quad (11.17\text{a})$$

$$m\ddot{x} + kx + f = 0 \quad (\dot{x} > 0). \quad (11.17\text{b})$$

We need to separately solve each of these equations for the half-cycle corresponding to it. Now, let us consider free motion of the system with the initial conditions $x = X_1$, $\dot{x} = 0$ at $t = 0$. As $\dot{x} < 0$ during the first half-cycle of the ensuing motion, we get, solving (11.17a),

$$x = A \sin (k/m)^{1/2}t + B \cos (k/m)^{1/2}t + f/k. \quad (11.18\text{a})$$

Substituting the initial conditions in (11.18a), we get $A = 0$ and $B = X_1 - f/k$. So, the final solution becomes

$$x = (X_1 - f/k) \cos (k/m)^{1/2}t + f/k. \quad (11.18\text{b})$$

Differentiating (11.18b), we have

$$\dot{x} = -(k/m)^{1/2}(X_1 - f/k) \sin (k/m)^{1/2}t.$$

This becomes zero when $(k/m)^{1/2}t = \pi$ with

$$x \Big|_{t=\pi/\omega_n} = -(X_1 - 2f/k).$$

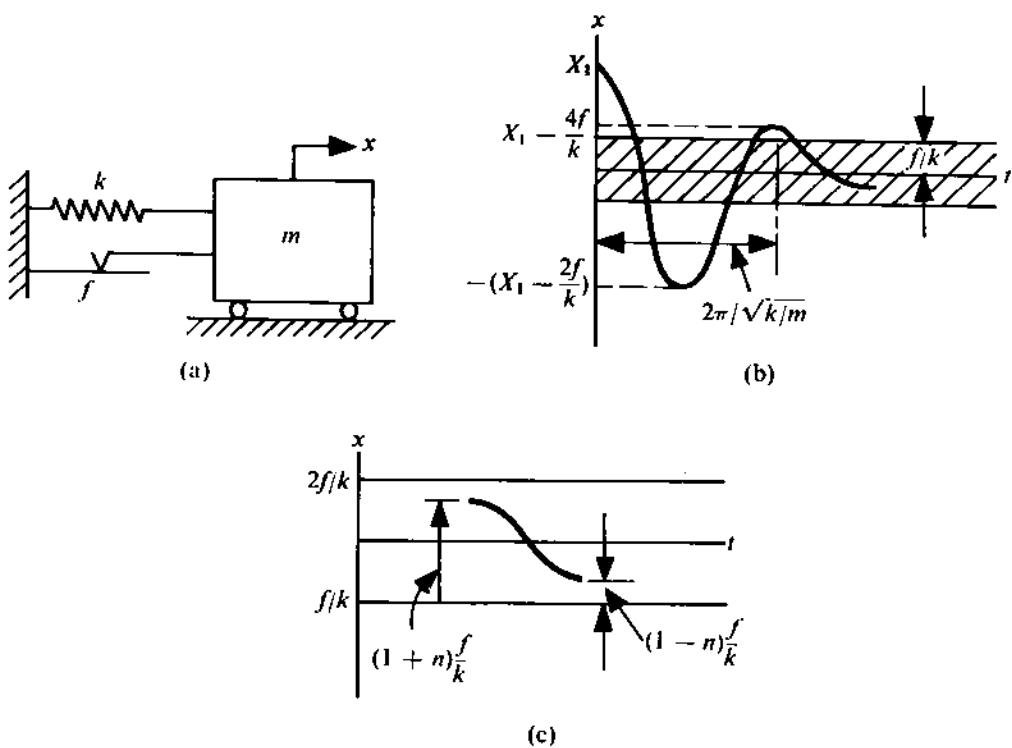


FIGURE 11.21

or the next half-cycle, we obtain, solving (11.17b),

$$x = A_1 \sin(k/m)^{1/2}t + B_1 \cos(k/m)^{1/2}t - f/k. \quad (11.19a)$$

The condition at the end of the first half-cycle becomes the initial condition for the next half-cycle. Thus,

$$x = -(X_1 - 2f/k), \quad \dot{x} = 0 \quad \text{at } t = \pi/\omega_n.$$

Sing this in (11.19a), we get $A_1 = 0$ and $B_1 = X_1 - 3f/k$. Hence,

$$\begin{aligned} x &= (X_1 - \frac{3f}{k}) \cos(k/m)^{1/2}t - \frac{f}{k}, \\ \dot{x} &= -(k/m)^{1/2}(X_1 - \frac{3f}{k}) \sin(k/m)^{1/2}t. \end{aligned} \quad (11.19b)$$

The mass will again come to a stop when $(k/m)^{1/2}t = 2\pi$ with

$$x \Big|_{t=2\pi/\omega_n} = X_1 - 4f/k. \quad (11.20)$$

So, we see that the motion is harmonic with a frequency $(k/m)^{1/2}$ and the amplitude decreases by constant amount $4f/k$ per cycle.

The motion continues until it is arrested by the friction. This happens when the mass stops at distance less than $\pm f/k$ from its equilibrium position. Thus, whenever a peak falls in the shaded region (Fig. 11.21b), the system comes to rest. However, it may so happen that, in the beginning of the preceding half-cycle, the amplitude is more than f/k but less than $2f/k$. In such a situation, the decay will of course not be equal to $2f/k$. If the starting amplitude is $(1+n)f/k$, where $n < 1$, the mass will stop on the same side of the equilibrium position at a distance $(1-n)f/k$ after an interval of π/ω_n (Fig. 11.21c).

The decay rate with coulomb damping can also be easily derived by considering the energy, as now explained. At the beginning of a cycle, the total energy is $E_1 = \frac{1}{2}kX_1^2$. At the end of the first half-cycle, the total energy is $E'_1 = \frac{1}{2}kX'_1$, where $-X'_1$ is the distance from the equilibrium position. So, the total distance travelled by the mass during this interval is $(X_1 + X'_1)$. The energy lost due to this displacement is $f(X_1 + X'_1)$. Hence,

$$f(X_1 + X'_1) = \frac{1}{2}k(X_1^2 - X'^2_1)$$

$$X_1 - X'_1 = 2f/k.$$

In the next half-cycle also, the amplitude decays by the same amount. For the situation depicted in Fig. 11.21c, we get from the energy consideration

$$f(X_1 - X'_1) = \frac{1}{2}k(X_1^2 - X'^2_1)$$

$$X_1 + X'_1 = 2f/k.$$

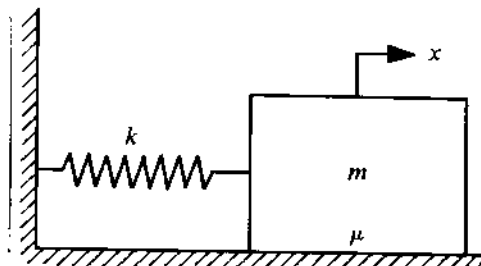


FIGURE 11.22

PROBLEM 11.13

A block of mass 1 kg moves over a flat surface, the coefficient of friction being 0.3. A spring of stiffness 150 N/m connects the block to a wall as shown in Fig. 11.22. The block is pulled through a distance of 5 cm away from the wall and is released with a velocity of 60 cm/s towards the wall. Find out the period for which the block will oscillate before coming to rest and also the position of the block when it comes to rest.

SOLUTION

Since, initially, the block moves with $\dot{x} < 0$, we can use (11.18a). Thus,

$$x = A \sin \omega_n t + B \cos \omega_n t + f/k, \quad (a)$$

where $f = \mu mg$. Now, $\omega_n = (150/1)^{1/2} = 12.25$ rad/s. At $t = 0$, $x = 0.05$ m and $\dot{x} = -0.6$ m/s. Substituting these initial values in (a), we obtain

$$\begin{aligned} x &= -0.049 \sin 12.25t + 0.03 \cos 12.25t + 0.0196 \text{ m}, \\ \dot{x} &= -0.6 \cos 12.25t - 0.368 \sin 12.25t \text{ m/s}. \end{aligned} \quad (b)$$

The mass will reach the end of its travel when $\dot{x} = 0$, i.e., when

$$\tan 12.25t = -1.63$$

or

$$t = 0.173 \text{ s.}$$

At this instant, x can be found out by substituting this value of t in (b). Thus,

$$x = -0.0384 \text{ m.} \quad (c)$$

In every succeeding half-cycle, the amplitude reduces by $2\mu mg/k = 0.0392$ m. But since the value of $|x|$ given by (c) is less than 0.0392 m, the amplitude at the end of the next half-cycle cannot be obtained by subtracting $2f/k$ from this value of x . In fact, the block will stop after one half-cycle at a position which is determined as follows (see Fig. 11.21c). We have

$$x_{\text{starting}} = -0.0384 \text{ m}$$

and

$$x_{\text{starting}} + x_{\text{final}} = -0.0392 \text{ m}$$

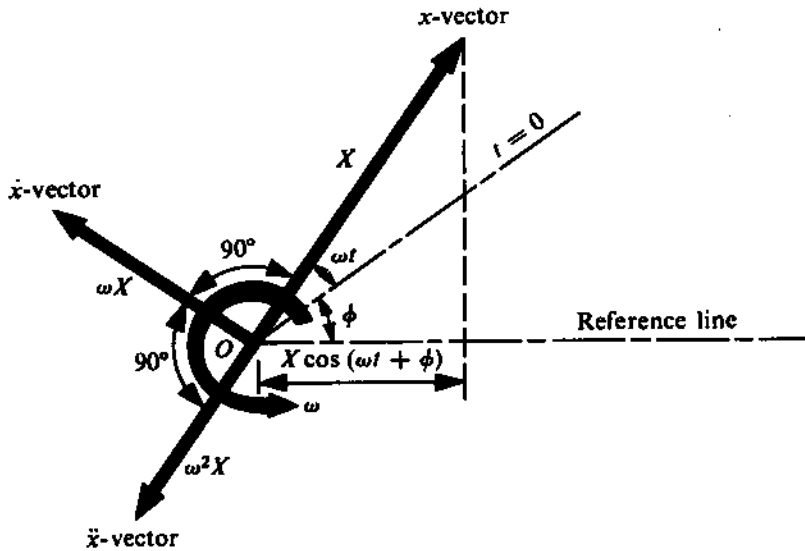


FIGURE 11.23

$$x_{\text{final}} = -0.0008 \text{ m.}$$

As the last half-cycle takes $\pi/\omega_n = 0.256$ s, the total duration of oscillation is $(0.173 + 0.256)$ s = .429 s.

Harmonic Quantities as Rotating Vectors and Phase-plane Representation

A harmonic function of time can be conveniently represented by a rotating vector. The speed of rotation is given by the circular frequency ω and the length of the vector represents the amplitude. Figure 11.23 shows a vector of length X rotating with an angular speed ω , its initial position being at an angle ϕ from the reference line. The projection of the vector on the reference line, $X \cos(\omega t + \phi)$, represents the instantaneous value of the harmonic quantity. Similarly, $X \sin(\omega t + \phi)$ represents the instantaneous value of the harmonic quantity when the projection of the vector is taken on a line perpendicular to the reference line. The reader is advised to verify that the differentiation of a harmonic quantity x gives rise to a new vector of magnitude ωX leading the x -vector by 90° . The \dot{x} -vector also rotates with a speed ω . Each successive differentiation leads the vector by 90° with an amplification of the magnitude by a factor ω (Fig. 11.23).

Referring to (11.3), we find that the velocity of free undamped oscillation can be expressed as

$$\dot{x} = -\omega_n X \sin(\omega_n t + \phi). \quad (11.21)$$

From (11.3) and (11.21), it is readily seen that during a free oscillation

$$x^2 + (\dot{x}/\omega_n)^2 = X^2. \quad (11.22)$$

Thus, the motion during a free undamped oscillation is represented by a circle (Fig. 11.24a) on a coordinate system x and \dot{x}/ω_n (known as *phase plane* since a point in this plane represents the phase of motion). The points on this circle represent the state of motion during a cycle. Obviously, the

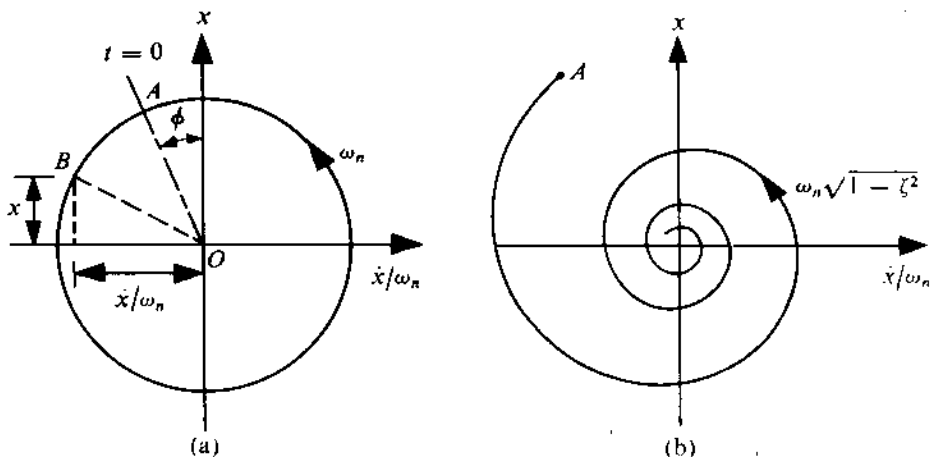


FIGURE 11.24

radius of this circle is equal to the amplitude of oscillation. The arrowhead to denote the motion should be such that, for a positive velocity, x must increase. In Fig. 11.24a, the motion has to be CCW. The point A represents the initial state, whereas B with $\angle AOB = \omega_n t$ represents the state at a time t .

For a viscously-damped system (with $\zeta < 1$), a representation similar to the one we have described gives rise to logarithmic spirals, instead of circles, as shown in Fig. 11.24b.¹

When a system is provided with coulomb damping, the motion is again simple harmonic in each half-cycle as seen from (11.18b) and (11.19b). However, for phase-plane representation, we can rewrite these as

$$(x - f/k) = (X_1 - f/k) \cos \omega_n t \quad \text{for } \dot{x} < 0,$$

$$(x + f/k) = (X_1 - 3f/k) \cos \omega_n t \quad \text{for } \dot{x} > 0.$$

Thus, it is obvious that, for each half-cycle, the phase-plane diagram is given by a semicircle with the centre at O_1 ($x = f/k$) for $\dot{x} < 0$ and at O_2 ($x = -f/k$) for $\dot{x} > 0$ (Fig. 11.25). From this diagram, it is clear that if the motion starts from A , then the system comes to rest after one and a half cycles at D .

PROBLEM 11.14

Use a phase-plane diagram to solve Problem 11.13.

SOLUTION

The circular frequency can be calculated as $\omega_n = (k/m)^{1/2} = 150^{1/2} = 12.25 \text{ rad/s}$. Next, the friction force f can be found out as $f = \mu mg = 0.3 \times 9.8 \text{ N} = 2.94 \text{ N}$. Therefore,

$$f/k = 2.94/150 \text{ m} = 0.0196 \text{ m.}$$

Let us now start drawing the phase-plane diagram (Fig. 11.26). The point A , i.e., the starting point has the coordinates

$$x = 0.05 \text{ m},$$

¹For more details, see Jacobsen, L.S. and Ayre, R.S., Engineering Vibrations, McGraw-Hill, New York, 1958.

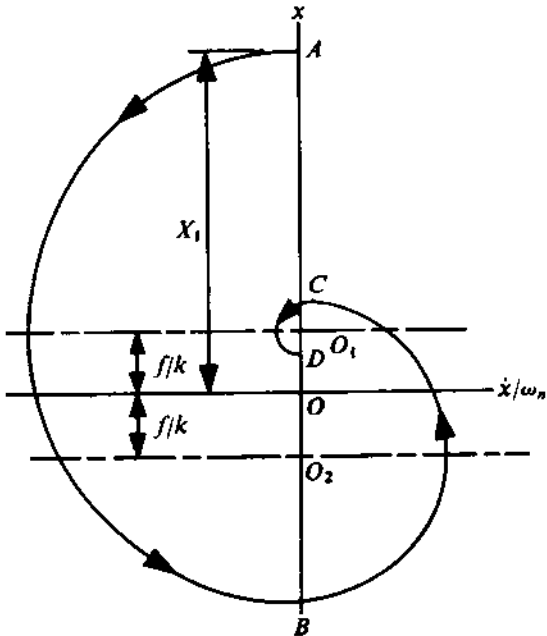


FIGURE 11.25

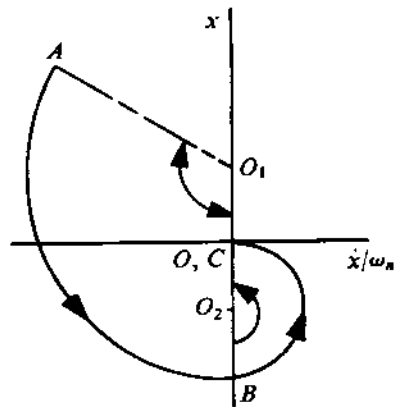


FIGURE 11.26

$$\dot{x}/\omega_n = (-0.6/12.25) \text{ m} = -0.049 \text{ m.}$$

We draw a circular arc with O_1 as the centre and O_1A as the radius. It intersects the x -axis at B . Since now onwards $\dot{x} > 0$, we have to draw a circle with O_2 as the centre and O_2B as the radius. The semicircle intersects the x -axis at C , very near O . No further oscillation takes place. Therefore, the total time is

$$(\angle AO_1B + \angle BO_2C)/\omega_n = (121.5^\circ + 180^\circ) \times (\pi/180)/12.25 = 0.4296 \text{ s.}$$

Undamped Vibration with Harmonic Excitation

It is important to study the systems where the vibration is generated by harmonic disturbances. The reasons for doing so are as follows:

- (i) A machine is often subjected to harmonic forces (or displacements), as noted in Chapter 7.
- (ii) When the excitation is periodic, the response of a linear system can be obtained from the results of harmonic excitation using the Fourier series.
- (iii) The response of arbitrary and random excitations can be determined using the Fourier transformation.
- (iv) The most fundamental and important features of forced vibration can be easily understood by analyzing a harmonically excited system.
- (v) It is easy to carry out experiments with harmonic excitation.

Let us consider an undamped SDF system (Fig. 11.27) subjected to a harmonic force $F_0 \cos \omega t$. The equation of motion is

$$m\ddot{x} + kx = F_0 \cos \omega t, \quad (11.23)$$

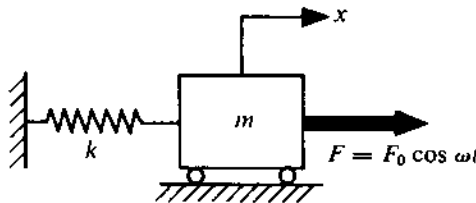


FIGURE 11.27

where \$\omega\$ and \$F_0\$ are the frequency and the amplitude of excitation, respectively. The solution of (11.23) consists of two parts. The complementary function obtained with the right-hand side of (11.23) zero represents the free oscillation. The particular integral represents the forced vibration due to the excitation. The general form of the solution, when \$\omega \neq \omega_n\$, is

$$x = A \sin \omega_n t + B \cos \omega_n t + \frac{F_0/k}{1 - (\omega/\omega_n)^2} \cos \omega t. \quad (11.24)$$

If the forcing frequency \$\omega\$ coincides with the natural frequency \$\omega_n [= (k/m)^{1/2}]\$, the general solution then is of the form

$$x = A \sin \omega_n t + B \cos \omega_n t + \frac{F_0 t}{2m\omega_n} \sin \omega_n t. \quad (11.25)$$

The constants \$A\$ and \$B\$ are found out from the initial conditions. Let us assume that, to start with the system was in relaxed state, i.e., at \$t = 0\$, \$x = 0\$, and \$\dot{x} = 0\$. Using this in (11.24), we get

$$A = 0, \quad B = -\frac{F_0/k}{1 - r^2},$$

where \$r\$ is the nondimensional frequency ratio \$\omega/\omega_n\$. So,

$$x = \frac{F_0/k}{1 - r^2} (\cos \omega t - \cos \omega_n t) \quad (11.26)$$

$$= 2\left(\frac{F_0/k}{1 - r^2}\right) \sin \frac{(\omega_n + \omega)t}{2} \sin \frac{(\omega_n - \omega)t}{2}. \quad (11.27)$$

Figure 11.28 shows a graphical representation of (11.27). As can be seen, the maximum possible value of \$x\$ is limited to \$(2F_0/k)/|1 - r^2|\$ and the oscillation beats (i.e., grows and decays alternately) with a frequency \$|\omega_n - \omega|\$.

As \$\omega\$ approaches \$\omega_n\$, the beat period and the maximum possible value of \$x\$ both tend to infinity. At \$\omega = \omega_n\$, this is demonstrated by (11.25). Figure 11.29 shows the growth of vibration with time for \$\omega = \omega_n\$. As can be noticed, the oscillation grows with time without any limit. This phenomenon is called *resonance*. Therefore, a knowledge of the natural frequency of a system is essential to avoid resonance during its operation.

When analyzing an undamped system with forced vibration, we should keep in mind that it is not possible to make a system with zero damping. So, even when a system may, for all practical purposes, be considered undamped, the free vibration part of the solution [given by (11.24)] will eventually die out and the steady-state response will be given by the particular integral. This is shown in Fig. 11.30. Thus, the steady response is given by

$$x = \frac{F_0/k}{1 - r^2} \cos \omega t \quad (r \neq 1). \quad (11.28a)$$

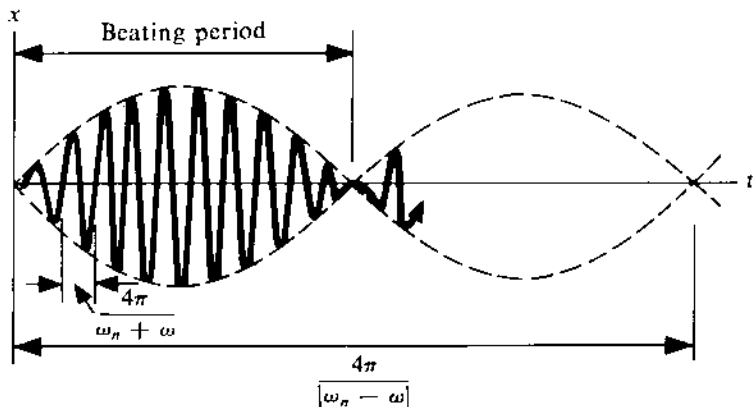


FIGURE 11.28

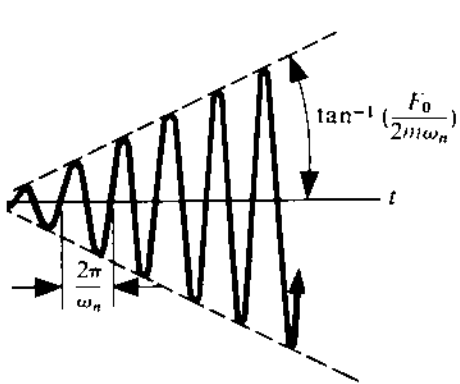


FIGURE 11.29

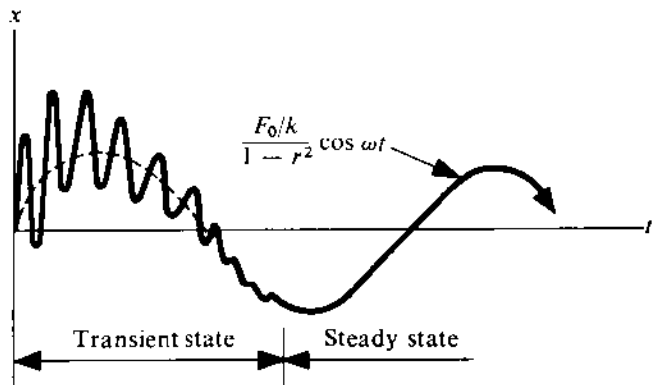


FIGURE 11.30

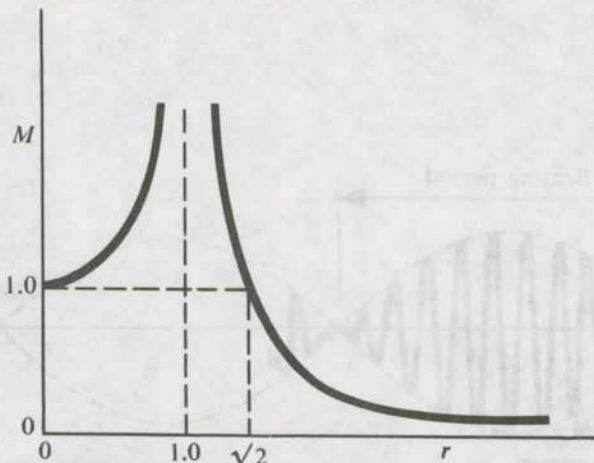


FIGURE 11.31

This equation implies (i) the frequency of response is the same as that of excitation, and (ii) the response of the system is either in phase (when $r < 1$) or out of phase (when $r > 1$) with the excitation. This is because, with $r > 1$, (11.28a) can be rewritten as

$$x = \frac{F_0/k}{r^2 - 1} \cos(\omega t - \pi). \quad (11.28)$$

It is further seen that due to the dynamic nature of the force, the maximum displacement (i.e., the amplitude) is $|1/(1 - r^2)|$ times that when the force F_0 is applied statically. The nondimension factor $X/(F_0/k)$ is called the *magnification factor* M , where X is the amplitude of response. Thus

$$M = \left| \frac{1}{1 - r^2} \right|. \quad (11.29)$$

The nature of variation of M with r is shown in Fig. 11.31. It is interesting to observe that, for $\omega > \sqrt{2}\omega_n$, the dynamic deflection is less than the static deflection.

PROBLEM 11.15

A disc with a moment of inertia $J = 0.53 \text{ kg-m}^2$ is attached to one end of a shaft whose other end is fixed. The length, l , and diameter, d , of the shaft are 300 mm and 30 mm, respectively. If the shear modulus of the shaft material is $G = 8 \times 10^4 \text{ MPa}$, determine the maximum shear stress developed in the shaft when the disc is subjected to a torque $300 \cos 314t \text{ N-m}$. If the diameter of the shaft increased to 35 mm, determine the maximum shear stress.

SOLUTION

The torsional stiffness of the shaft (from Table 11.1) is

$$K = \frac{\pi G d^4}{32l} = \frac{\pi \times 8 \times 10^{10} \times 0.03^4}{32 \times 0.3} = 21,206 \text{ N-m/rad.}$$

The natural frequency of the system is

$$\omega_n = (K/J)^{1/2} = (21,206/0.53)^{1/2} = 200 \text{ rad/s.}$$

o, the frequency ratio is

$$r = \omega/\omega_n = 314/200 = 1.57.$$

Using (11.29) and this value of r , we find the magnification factor is

$$M = \left| \frac{1}{1 - 1.57^2} \right| = 0.68.$$

With a torque of 300 N-m, the static twist is

$$\Theta_s = \frac{32Tl}{\pi Gd^4} = \frac{32 \times 300 \times 0.3}{\pi \times 8 \times 10^{10} \times 0.03^4} = 0.0141 \text{ rad.}$$

o, the amplitude of the twist under the dynamic load is

$$\Theta = M\Theta_s = 0.68 \times 0.0141 = 0.0096 \text{ rad.}$$

hence, the maximum shear stress is

$$\tau = \frac{Gd\Theta}{2l} = \frac{8 \times 10^{10} \times 0.03 \times 0.0096}{2 \times 0.3} = 0.384 \times 10^8 \text{ N/m}^2 = 38.4 \text{ MPa.}$$

When the diameter is increased to 35 mm, the foregoing calculations are repeated. The values obtained are

$$K = 39,287 \text{ N-m/rad}, \quad \omega_n = 272 \text{ rad/s}, \quad r = 1.15, \quad M = 3.1,$$

$$\Theta_s = 0.0076 \text{ rad}, \quad \Theta = 0.0236 \text{ rad}, \quad \tau = 110 \text{ MPa.}$$

In Problem 11.15, as we can note, the maximum shear stress drastically increases when the shaft diameter is increased. This is quite surprising at the first glance. Therefore, when designing a machine member to be subjected to dynamic loads, care has to be taken. The common thumb rule of increasing the dimensions to make it safer may not hold good when the loading is dynamic.

Viscously Damped Vibration with Harmonic Excitation

The analysis of the undamped system we have given can be easily extended to a system with viscous damping (Fig. 11.32). The equation of motion here is

$$m\ddot{x} + c\dot{x} + kx = F_0 \cos \omega t. \quad (11.30)$$

This equation can also be written in the form

$$\ddot{x} + 2\zeta\omega_n\dot{x} + \omega_n^2x = (F_0/m) \cos \omega t. \quad (11.31)$$

Since the free vibration represented by the complementary function dies out due to the presence of damping, the steady-state solution, given by the particular integral, can be expressed as

$$x = X \cos (\omega t - \phi), \quad (11.32a)$$

where

$$X = \frac{F_0/k}{[(1 - r^2)^2 + (2\zeta r)^2]^{1/2}}, \quad (11.32b)$$

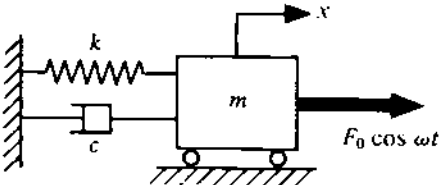


FIGURE 11.32

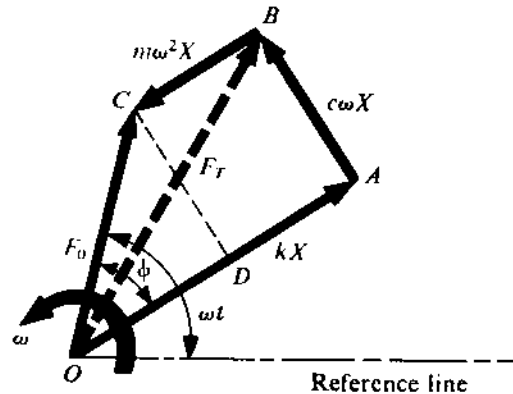


FIGURE 11.33

$$\phi = \tan^{-1} \left(\frac{2\zeta r}{1 - r^2} \right). \quad (11.32c)$$

The steady-state solution (11.32) can also be easily derived using the rotating-vector approach. Since the steady-state response is harmonic with the same frequency as that of the excitation, let

$$x = X \cos(\omega t - \phi),$$

where X is the amplitude and ϕ the phase lag from the excitation. As both x and F are harmonic quantities with the same frequency ω , (11.30) can be represented by the rotating-vector diagram shown in Fig. 11.33. The terms on the left-hand side of (11.30) correspond to OA , AB , and BC respectively, when OC must represent the right-hand side. From the diagram,

$$OC = (OD^2 + DC^2)^{1/2} = [(OA - BC)^2 + AB^2]^{1/2}$$

or

$$F_0 = X[(k - m\omega^2)^2 + (c\omega)^2]^{1/2}$$

or

$$F_0/k = X[(1 - \frac{\omega^2}{k/m})^2 + (\frac{c\omega}{k})^2]^{1/2}.$$

Finally, we get

$$X = \frac{F_0/k}{[(1 - r^2)^2 + (2\zeta r)^2]^{1/2}}.$$

From Fig. 11.33, we also get the phase difference between the excitation and response vectors as $\angle COA$. It is readily seen that

$$\tan \phi = \frac{CD}{OD} = \frac{AB}{OA - BC} = \frac{c\omega}{k - m\omega^2} = \frac{2\zeta r}{1 - r^2}.$$

For the forced vibration of a viscously-damped system, the magnification factor is

$$M = \frac{X}{F_0/k} = \frac{1}{[(1 - r^2)^2 + (2\zeta r)^2]^{1/2}}. \quad (11.33)$$

The variation of M and ϕ with r for different values of ζ is shown in Figs. 11.34a and 11.34b, respectively. In what follows, we shall discuss the various interesting features these diagrams reveal.

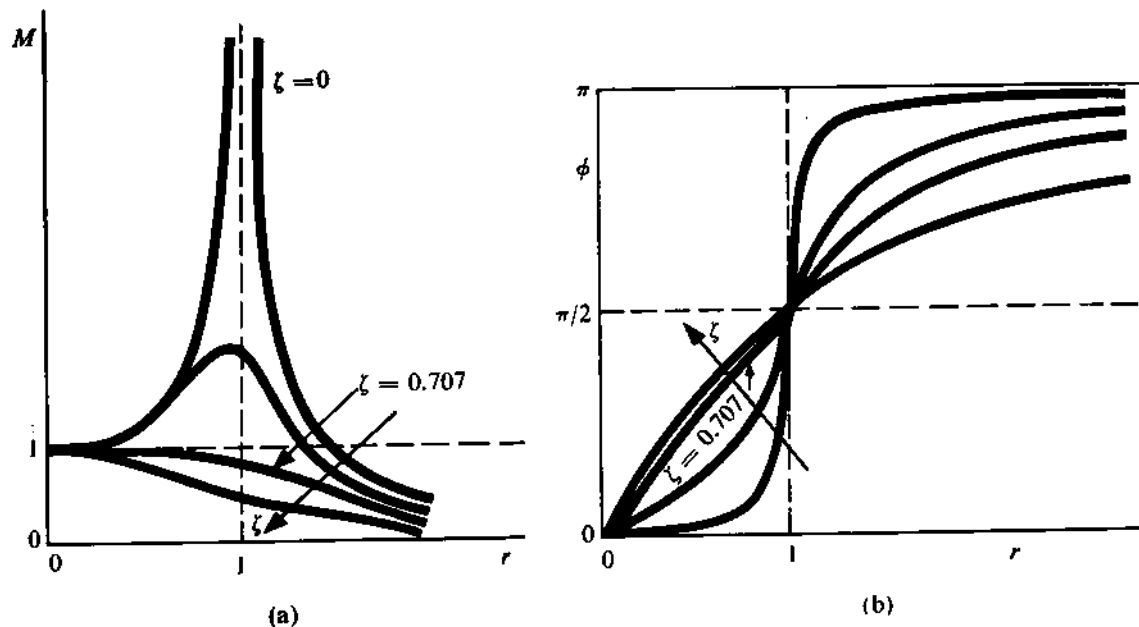


FIGURE 11.34

The phase difference ϕ is equal to 90° when $\omega = \omega_n$ for all values of ζ . At resonance (i.e., $\omega = \omega_n$), the spring force $-kx$ neutralizes the inertia force $-m\ddot{x}$ (i.e., $OA = BC$) according to the definition of ω_n . So, OC is parallel to AB , implying $\phi = 90^\circ$.

The frequency at which the magnification factor M is maximum decreases with increase in damping. This frequency is referred to as the *peak frequency* (ω_p). Its value can be obtained by differentiating (11.33) and setting it equal to zero as

$$\omega_p = (1 - 2\zeta^2)^{1/2} \omega_n. \quad (11.34)$$

For typical values of ζ , the difference between ω_p and ω_n in a real-life system is negligible. From (11.34), we find that $\omega_p = 0$ when $\zeta = 1/\sqrt{2}$. Therefore, for this and higher values of damping, the dynamic deflection is always less than the static one.

From (11.33), we see that at a very low frequency ratio, i.e., $r \ll 1$, $M \approx 1$. This means that X will be low only if k is increased. Thus, the low-frequency regime is controlled mainly by the stiffness of the system. Similarly, when $r \gg 1$, $M \approx 1/r^2$ or $X \approx F_0/(m\omega^2)$. Hence, the response in the high-frequency region is controlled mainly by the inertia of the system. If $r \approx 1$ (i.e., when the vibration becomes excessive), $M \approx 1/(2\zeta)$ or $X \approx F_0/(c\omega)$. So, the damping in the system effectively controls the response near resonance.

Another important feature Fig. 11.34 reveals is that, when $\zeta = 0.707$, the phase difference ϕ varies almost linearly with r up to 1.5.

As we will explain now, the frequency-response diagram showing the response amplitude against the excitation frequency (keeping the excitation amplitude unchanged) is also used for measuring the damping in the system. This method is applicable for small values of ζ , as is most often the case. Figure 11.35 shows a typical frequency-response diagram for small values of ζ where $\omega_p \approx \omega_n$. Two frequencies, namely, ω_1 and ω_2 , are located (on either side of ω_n) for which the response amplitude is $0.707X_{\text{res}}$, X_{res} being the peak (\approx resonance) amplitude. The frequencies ω_1 and ω_2 are called the

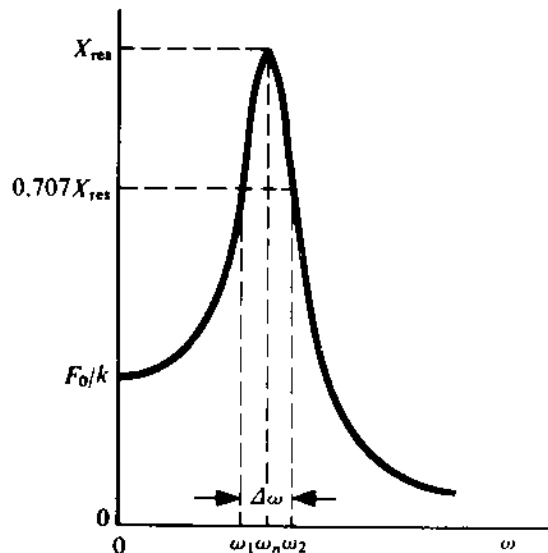


FIGURE 11.35

half-power points and $\Delta\omega (= \omega_2 - \omega_1)$ is referred to as the *half-power band width*. In what follows, we shall show that

$$\zeta \approx (\omega_2 - \omega_1)/(2\omega_n). \quad (11.35)$$

Substituting $r = 1$ in (11.33), we get

$$\frac{X_{\text{res}}}{F_0/k} = \frac{1}{2\zeta}. \quad (11.36)$$

The frequency ratios r_1 and r_2 corresponding to the half-power points are given by

$$\frac{X_{\text{res}}/\sqrt{2}}{F_0/k} = \frac{1}{[(1 - r^2)^2 + (2\zeta r)^2]^{1/2}}. \quad (11.37)$$

From (11.36) and (11.37), we get

$$8\zeta^2 = (1 - r^2)^2 + (2\zeta r)^2.$$

Solving this quadratic equation in r^2 , we obtain

$$r_{2,1}^2 = 1 - 2\zeta^2 \pm 2\zeta(1 + \zeta^2)^{1/2}.$$

Neglecting the terms of the order ζ^2 , we have $r_{2,1}^2 \approx 1 \pm 2\zeta$. Finally,

$$\begin{aligned} r_2 &\approx (1 + 2\zeta)^{1/2} &\approx 1 + \zeta, \\ r_1 &\approx (1 - 2\zeta)^{1/2} &\approx 1 - \zeta. \end{aligned} \quad (11.38)$$

Hence,

$$r_2 - r_1 = (\omega_2 - \omega_1)/\omega_n = 2\zeta.$$

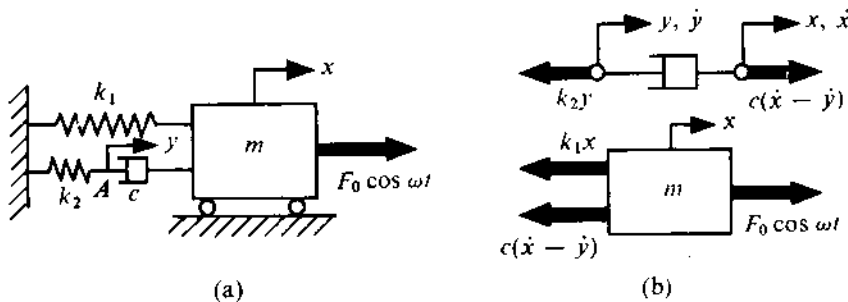


FIGURE 11.36

Systems with Elastically Mounted Dashpots

Sometimes, the dashpot in a system may be elastically mounted as shown in Fig. 11.36a. Here, both the ends of the dashpot are moving. From the free-body diagram of the mass (Fig. 11.36b), we get

$$m\ddot{x} + k_1x + c(\dot{x} - \dot{y}) = F_0 \cos \omega t = F(t), \quad (11.39)$$

where y denotes the extension of the spring k_2 . Now, considering the forces transmitted through the dashpot and the spring k_2 , we have

$$k_2y = c(\dot{x} - \dot{y}). \quad (11.40)$$

Using (11.40) in (11.39), we get

$$m\ddot{x} + k_1x + k_2y = F_0 \cos \omega t = F(t).$$

So,

$$\dot{y} = \frac{1}{k_2} [\dot{F}(t) - m\ddot{x} - k_1\dot{x}].$$

Substituting this in (11.39), we obtain

$$m\ddot{x} + k_1x + c\dot{x} - \frac{c}{k_2} [\dot{F}(t) - m\ddot{x} - k_1\dot{x}] = F(t).$$

Rearranging, we get

$$\frac{cm}{k_2} \ddot{x} + m\ddot{x} + c(1 + \frac{k_1}{k_2})\dot{x} + k_1x = \frac{c}{k_2} \dot{F}(t) + F(t). \quad (11.41)$$

Again, assuming that the steady-state solution of (11.41) has the form $x = X \cos(\omega t - \phi)$, we can draw the rotating-vector diagram (Fig. 11.37a) to represent (11.41). From this diagram, we can write

$$OA^2 = F_0^2 \left(1 + \frac{c^2 \omega^2}{k_2^2}\right) = X^2 \left[\left(k_1 - m\omega^2\right)^2 + \left\{c\omega \left(1 + \frac{k_1}{k_2}\right) - \frac{cm\omega^3}{k_2}\right\}^2\right].$$

Finally,

$$M = \frac{X}{F_0/k_1} = \left[\frac{1 + (2\lambda\zeta r)^2}{(1 - r^2)^2 + (2\zeta r)^2 (1 + \lambda - \lambda r^2)^2} \right]^{1/2}, \quad (11.42)$$

where $r = \omega/(k_1/m)^{1/2}$, $\zeta = c/[2(k_1 m)^{1/2}]$, and $\lambda = k_1/k_2$. Obviously, when $k_2 \rightarrow \infty$ or $\lambda \rightarrow 0$, (11.42) reduces to (11.33). The reader is advised to check the limiting forms of (11.42) for $\zeta = 0$.

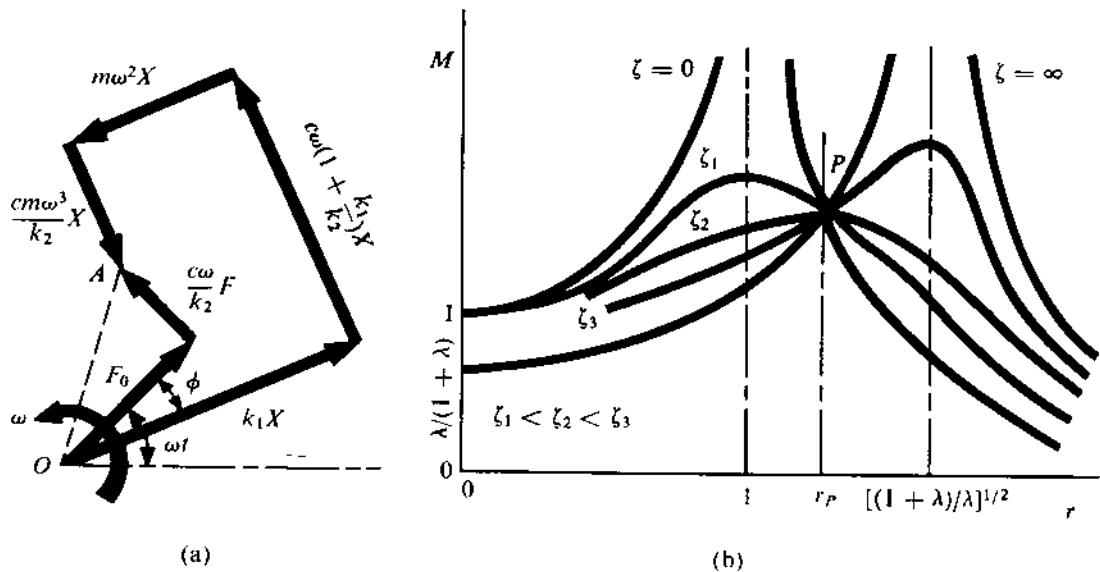


FIGURE 11.37

and $\zeta = \infty$, and verify the nature of $(M-r)$ curves shown in Fig. 11.37b. These curves are seen to intersect at P and the corresponding frequency ratio r_P can be found out as follows. Equating $M_{\zeta=0}$ and $M_{\zeta=\infty}$, we get

$$\pm \frac{1}{1-r_P^2} = \frac{\lambda}{1+\lambda-\lambda r_P^2}.$$

We have to take the negative sign since, for $\zeta = 0$ with $r_P > 1$, $M = -1/(1-r_P^2)$. Thus,

$$r_P = [(1+2\lambda)/(2\lambda)]^{1/2}. \quad (11.43)$$

Since at this frequency ratio the system is insensitive to the value of ζ , it is expected that the curves for all values of ζ will pass through P . In fact, this is really so and can be proved by considering the right-hand side of (11.42). This is left as an exercise for the reader. The value of ζ for which the maximum of the curve lies at P provides the optimum value of damping to keep the level of vibration minimum in the entire range of frequency. This optimum value of damping can be found out analytically.²

Systems with Base Excitation

We have so far analyzed the response of systems excited by the harmonic forces. However, a large number of systems are excited by the dynamic movement of supports. One such system is shown in Fig. 11.38a. From the free-body diagram (Fig. 11.38b), we find the equation of motion is

$$m\ddot{x} + c(\dot{x} - \dot{y}) + k(x - y) = 0$$

or

$$m\ddot{x} + c\dot{x} + kx = cy + ky, \quad (11.44)$$

²A standard method to do this is given in Snowdon, J.C., Vibration and Shock in Damped Mechanical Systems, Wiley, New York, 1968.

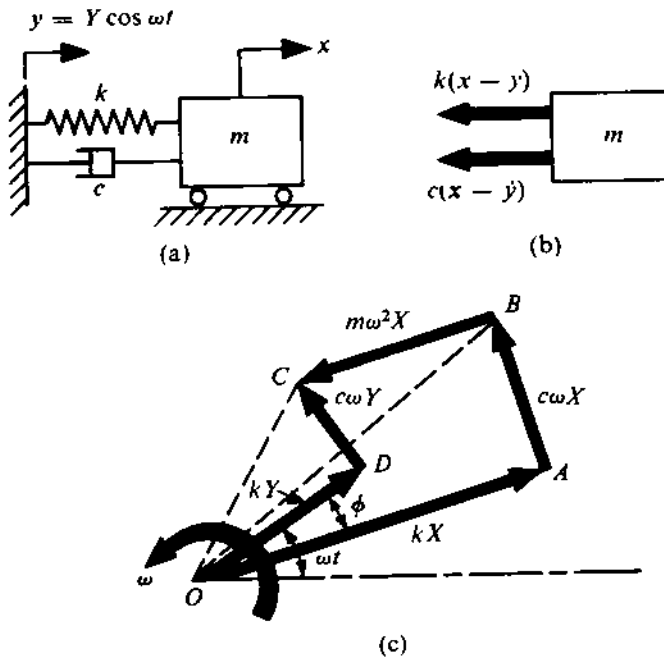


FIGURE 11.38

where $y = Y \cos \omega t$. Let us assume that the steady-state solution of (11.44) has the form $x = X \cos(\omega t - \phi)$. The rotating-vector diagram, representing (11.44), is shown in Fig. 11.38c. This diagram yields

$$(OA - BC)^2 + AB^2 = OD^2 + DC^2$$

or

$$X^2[(k - m\omega^2)^2 + c^2\omega^2] = Y^2(k^2 + c^2\omega^2)$$

or

$$X = Y \left[\frac{k^2 + c^2\omega^2}{(k - m\omega^2)^2 + c^2\omega^2} \right]^{1/2}.$$

Finally,

$$X = Y \left[\frac{1 + (2\zeta r)^2}{(1 - r^2)^2 + (2\zeta r)^2} \right]^{1/2}. \quad (11.45)$$

Again, the phase difference ϕ between the motions of the support and the mass can be computed as follows. We know that

$$\tan(\angle COD) = c\omega/k = \tan(\angle AOB)$$

or

$$\angle COD = \angle AOB.$$

Let $\angle BOD = \beta$. Then,

$$\angle COB = \angle COD - \beta = \angle AOB - \beta = \angle AOD = \phi.$$

Now,

$$\angle AOC = \angle AOD + \angle DOB + \angle BOC = \phi + \beta + \phi = 2\phi + \beta.$$

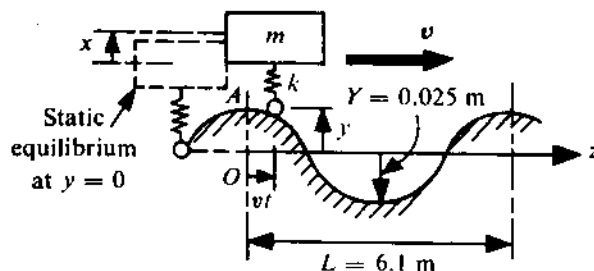


FIGURE 11.39

Again,

$$\tan(\angle AOC) = \tan(2\phi + \beta) = \frac{c\omega}{k - m\omega^2} = \frac{2\zeta r}{1 - r^2}.$$

Rewriting, we get

$$\tan[\phi + (\phi + \beta)] = \frac{2\zeta r}{1 - r^2}$$

or

$$\frac{\tan \phi + \tan(\phi + \beta)}{1 - \tan \phi \tan(\phi + \beta)} = \frac{2\zeta r}{1 - r^2}. \quad (11.46)$$

Since $\angle COD = \phi + \beta$,

$$\tan(\phi + \beta) = c\omega/k = 2\zeta r.$$

Using this relation in (11.46), we obtain

$$\tan \phi = \frac{2\zeta r^3}{1 - r^2 + (2\zeta r)^2}. \quad (11.47)$$

PROBLEM 11.16

A vehicle with a rider has a total mass of 450 kg and travels along a rough road at 96 km/hr. An idealized and simplified model of the vehicle is shown in Fig. 11.39. The road is assumed to be represented by a harmonic curve with an amplitude $Y = 0.025$ m and a wavelength $L = 6.1$ m. Determine (i) the spring stiffness k so that resonance occurs under the conditions specified, and (ii) the required spring stiffness so that a steady-state amplitude of 0.6 cm is obtained at the given speed and also if the rider would leave his seat under this condition. Neglect the effect of damping.

SOLUTION

With the origin at O , the motion of the wheel in the vertical direction can be written as $y = Y \cos(2\pi vt/L)$, where v is the velocity of the vehicle and, at $t = 0$, it was at A . The equation of motion of the vehicle in terms of x and y explained in Fig. 11.39 is

$$m\ddot{x} + k(x - y) = 0$$

or

$$m\ddot{x} + kx = kY \cos \omega t \quad (11.48)$$

with $\omega = 2\pi v/L$.

i) For resonance, $\omega = \omega_n$ or

$$2\pi v/L = (k/m)^{1/2}$$

or

$$k = 4\pi^2 mv^2/L^2 = 34 \times 10^4 \text{ N/m.}$$

ii) Comparing (a) with (11.44), we can obtain the solution from (11.45) by substituting in it $\zeta = 0$. Thus,

$$X = \pm Y[1/(1 - r^2)].$$

Y and X are given to be 0.025 m and 0.006 m, respectively. Since X is less than Y , only the negative sign will yield a sensible result.³ So,

$$r^2 = 1 + Y/X = 5.17$$

or

$$r = 2.275.$$

Hence,

$$\frac{\omega}{\omega_n} = 2.275$$

or

$$\omega_n = (\frac{k}{m})^{1/2} = \frac{2\pi v}{L \times 2.275}$$

or

$$k = 6.57 \times 10^4 \text{ N/m.}$$

The rider will leave his seat if at any stage the downward acceleration of the vehicle is more than . In the steady state, the maximum acceleration (both in the downward and upward directions) is given by

$$\omega^2 X = (4\pi^2 v^2/L^2).X = 4.6 \text{ m/s}^2 < g.$$

Hence, the rider will not leave his seat.

Transmissibility and Vibration Isolation

When unbalanced dynamic forces are present in a machine, then, as we know, these forces are transmitted to the foundation. Similarly, as we have just seen, if the foundation or the support has an oscillatory motion, then this is also transmitted into the machine or the system. If the support and the machine are connected rigidly, then the entire force or motion, as the case may be, is transmitted. On the other hand, if this connection is made through resilient elements (and/or dashpots), the transmission characteristics can be favourably controlled. Therefore, the term *transmissibility* (TR) can be defined as

$$TR = X/Y \quad \text{in support motion (Fig. 11.38a)} \quad (11.48a)$$

$$= F_{T_0}/F_0 \quad \text{in force excitation (Fig. 11.32),} \quad (11.48b)$$

where F_{T_0} is the amplitude of the force transmitted to the support.

³Equation (a) can also be compared with (11.23). The reader is advised to verify that, with the given values of X and Y , the forcing frequency ω is greater than ω_n , resulting in a phase difference of 180° between x and y .

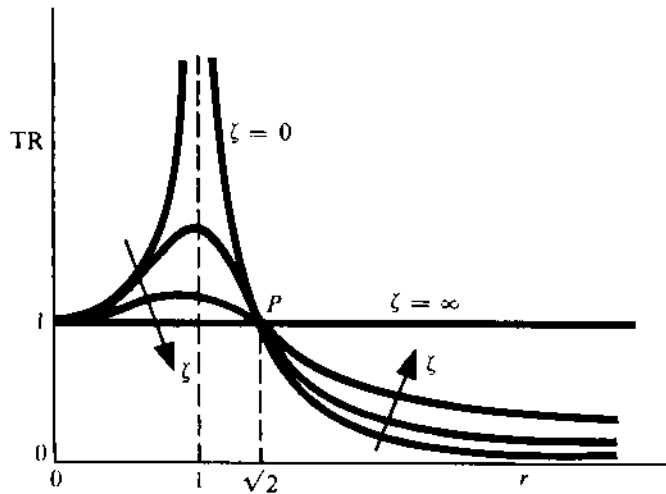


FIGURE 11.40

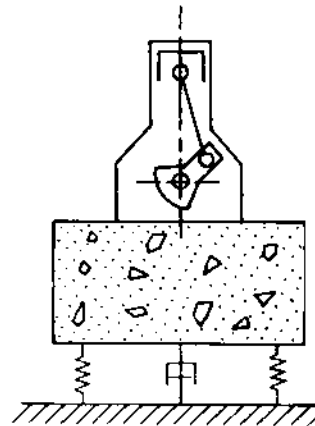


FIGURE 11.4

Referring to Fig. 11.33, we note that F_{T_0} , the resultant of the spring and dashpot forces, is given by OB . So,

$$F_{T_0} = X(k^2 + c^2\omega^2)^{1/2} = kX[1 + (2\zeta r)^2]^{1/2}. \quad (11.49)$$

Substituting for X from (11.32b) in (11.49), we get

$$TR = \left[\frac{1 + (2\zeta r)^2}{(1 - r^2)^2 + (2\zeta r)^2} \right]^{1/2}. \quad (11.50)$$

In support motion (or base excitation), the transmissibility X/Y is obtained from (11.45) and found to be the same as that given by (11.50).

The nature of variation of TR with frequency for different values of ζ is shown in Fig. 11.40. It should be noted that TR is always equal to unity at $r = 0, \sqrt{2}$. Further, at a low-frequency ratio ($r < \sqrt{2}$), it is always more than unity. However, it can be made less than unity by so choosing the resilient element that ω_n is low enough to make $r > \sqrt{2}$. For an effective isolation of vibration, r normally kept ≥ 5 . In a vertical system, it is difficult to get a still lower value of ω_n since such a low value of k gives rise to an unduly large static deflection. Further, a very low value of k may generate too large a vibration in the system even when the transmitted force to the support is reduced.

PROBLEM 11.17

An engine is mounted on a concrete block which is isolated from the floor, as shown in Fig. 11.4. The unbalanced force of the engine at n rpm is given (assuming the connecting rod to be very long as compared to the crank radius) by

$$F(t) = 100\left(\frac{n}{1000}\right)^2 \cos \frac{2\pi nt}{60} \text{ N.}$$

At 1000 rpm, it is found that the force transmitted to the floor has an amplitude of 100 N. Determine the amplitude of the transmitted force at 1500 rpm when the damper is disconnected.

SOLUTION

At 1000 rpm, the amplitude of the unbalanced force is $F_0 = 100$ N. Hence,

$$\text{TR}_{n=1000} = \frac{F_{T_0}}{F_0} = \frac{100}{100} = 1.$$

So, the corresponding frequency ratio must be equal to $\sqrt{2}$. Therefore,

$$\omega_n = \frac{\omega}{\sqrt{2}} = \frac{2\pi \times 1000}{60 \times \sqrt{2}} \text{ rad/s.} \quad (\text{a})$$

At 1500 rpm,

$$F_0 = 100 \times 1.5^2 \text{ N} = 225 \text{ N} \quad (\text{b})$$

and the corresponding frequency ratio [using (a)] is

$$r' = \frac{\omega}{\omega_n} = \frac{2\pi \times 1500}{60} \times \frac{60 \times \sqrt{2}}{2\pi \times 1000} = 1.5\sqrt{2}.$$

So, $r'^2 = 4.5$. Using (11.50) with $\zeta = 0$ (as the damper is disconnected) and substituting in it the value of r'^2 , we get

$$\text{TR}_{n=1500} = \frac{1}{1 - 4.5} = 1/3.5 = \frac{F_{T_0}}{F_0}. \quad (\text{c})$$

Hence, using (b) and (c), we obtain $F_{T_0} = (225/3.5)$ N = 64.29 N.

Whirling of Shafts

A rotating shaft tends to bow out with a large amplitude at a certain speed of rotation. This phenomenon is known as the whirling of the shaft. The speed at which it occurs is called the critical speed. There are various mechanisms responsible for this phenomenon. For a comprehensive treatment on it, see Chapter 12. For now, we shall study a simple model of the phenomenon when it is caused by an unbalance in the rotor.

Figure 11.42a shows an unbalanced disc mounted at the midspan of the shaft with negligible inertia and rotating with a speed ω . It is assumed that the plane A containing the bearing axis (z) and the bent shaft also rotates at the same speed ω . This particular situation is referred to as the synchronous whirl. The plane xOy is a horizontal plane fixed in space, where O is the point of intersection of the bearing axis and the disc. The geometric centre of the disc at the instant shown is at O' , whereas its centre of mass is at G (Fig. 11.42b) at a distance e from O' . In a synchronous whirl, each of the lines OO' and $O'G$ has the same angular velocity ω , and so the relative configuration of O , O' , and G remains the same.

Let, at $t = 0$, $O'G$ be coincident with the x -axis. The transverse stiffness of the shaft at its midpoint O' is represented by k . The free-body diagram of the disc is shown in Fig. 11.42c. The shaft exerts a force $k.OO'$ in the direction O' . The viscous drag force due to the atmosphere is distributed over the disc surface; its resultant is assumed to pass through O' and magnitude is considered to be proportional to the velocity of the point O' . Obviously, this drag force $c.\omega.OO'$ will act in a direction opposite to that of the velocity of O' , i.e., $V_{O'}$.

If the distance OO' is denoted by ρ , then the coordinates of G can be obtained as

$$x_G = x_{O'} + e \cos \omega t = \rho \cos \theta + e \cos \omega t; \quad (11.51a)$$

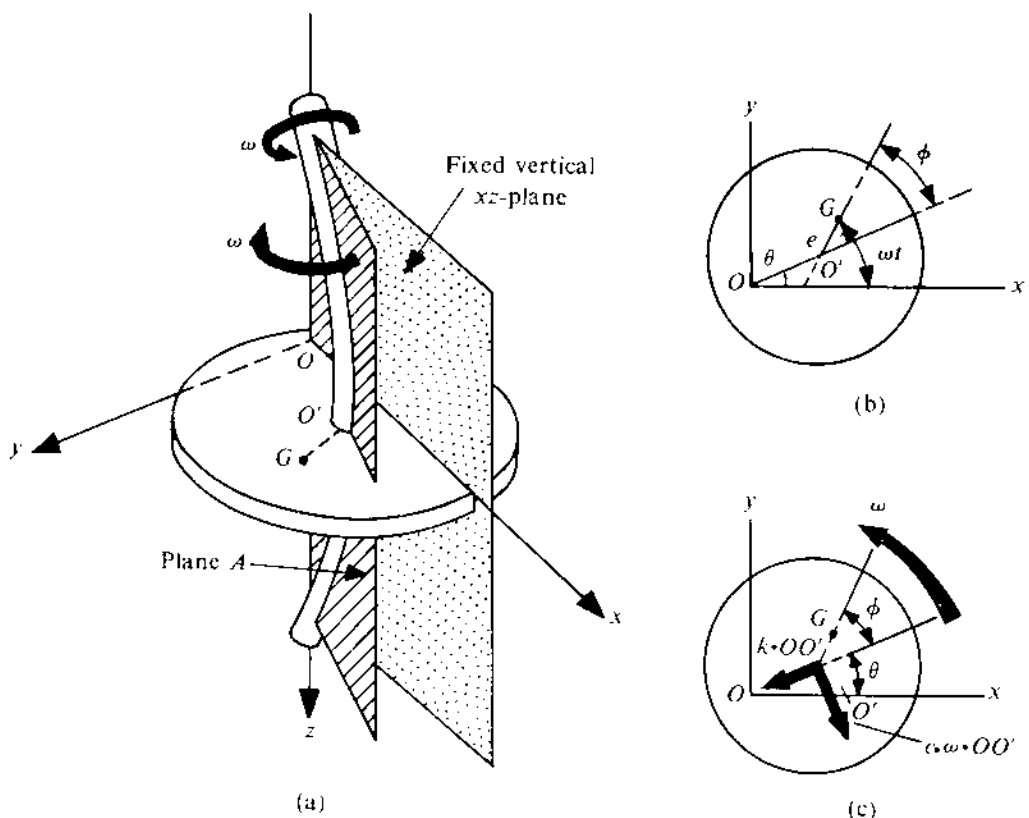


FIGURE 11.42

$$y_G = y_{O'} + e \sin \omega t = \rho \sin \theta + e \sin \omega t. \quad (11.51b)$$

The equations of motion of the disc in the x - and y -direction can be written as

$$m\ddot{x}_G = -k\rho \cos \theta + c\omega\rho \sin \theta = -kx_{O'} - c\dot{x}_{O'} \quad (\text{as } \omega = \dot{\theta}),$$

$$m\ddot{y}_G = -k\rho \sin \theta - c\omega\rho \cos \theta = -ky_{O'} - c\dot{y}_{O'} \quad (\text{as } \omega = \dot{\theta}),$$

where m is the mass of the disc. Using (11.51) in these equations, we get

$$m\ddot{x}_{O'} + c\dot{x}_{O'} + kx_{O'} = m\omega^2 e \cos \omega t, \quad (11.52a)$$

$$m\ddot{y}_{O'} + c\dot{y}_{O'} + ky_{O'} = m\omega^2 e \sin \omega t. \quad (11.52b)$$

The steady-state solutions of (11.52), obtained from (11.32), are

$$x_{O'} = \frac{m\omega^2 e / k}{[(1 - r^2)^2 + (2\zeta r)^2]^{1/2}} \cos(\omega t - \phi), \quad (11.53a)$$

$$y_{O'} = \frac{m\omega^2 e / k}{[(1 - r^2)^2 + (2\zeta r)^2]^{1/2}} \sin(\omega t - \phi), \quad (11.53b)$$

where $\phi = \tan^{-1} [2\zeta r / (1 - r^2)]$. It should be noted that the phase difference is the same for each of $x_{O'}(t)$ and $y_{O'}(t)$. From (11.53), we get

$$\rho = (x_{O'}^2 + y_{O'}^2)^{1/2} = \frac{m\omega^2 e / k}{[(1 - r^2)^2 + (2\zeta r)^2]^{1/2}}. \quad (11.54)$$

Thus, for small damping, the deflection of the shaft at the midpoint ρ is large when $r \approx 1$, i.e., $\omega \approx (k/m)^{1/2}$. This implies that if the shaft speed ω coincides with the natural frequency of transverse oscillation of the shaft-disc system, the shaft whirls with a large deflection. This speed ω is referred to as the critical speed ω_{cr} .

The foregoing discussion was with reference to the steady-state motion of the system. Let us now see how the shaft deflection grows at ω_{cr} to reach the steady state. It is assumed that ζ is small enough so that ζ^2 can be neglected in comparison to ζ and 1. Moreover, initially, O' has the velocity zero and coincides with O .

The general solutions of (11.52a) and (11.52b) can be written [the complementary function being of the form given by (11.11b)] as

$$x_{O'} = X \exp(-\zeta\omega_n t) \cos[(1 - \zeta^2)^{1/2}\omega_n t - \psi] + \frac{m\omega_{cr}^2 e / k}{[(1 - r^2)^2 + (2\zeta r)^2]^{1/2}} \cos(\omega_{cr} t - \phi),$$

$$y_{O'} = Y \exp(-\zeta\omega_n t) \sin[(1 - \zeta^2)^{1/2}\omega_n t - \psi'] + \frac{m\omega_{cr}^2 e / k}{[(1 - r^2)^2 + (2\zeta r)^2]^{1/2}} \sin(\omega_{cr} t - \phi).$$

Here, the constants X , Y , ψ , and ψ' have to be determined from the initial conditions, viz., at $t = 0$, $x_{O'} = y_{O'} = \dot{x}_{O'} = \dot{y}_{O'} = 0$. Also, $\omega = \omega_{cr} = \omega_n$ (i.e., $r = 1$) and, as we have already shown, for $r = 1$, ϕ is always equal to $\pi/2$. Therefore, putting $r = 1$, $\phi = \pi/2$, and $(1 - \zeta^2) \approx 1$, we can rewrite the two foregoing equations as

$$x_{O'} \approx X \exp(-\zeta\omega_n t) \cos(\omega_n t - \psi) + \frac{e}{2\zeta} \sin(\omega_n t), \quad (11.55a)$$

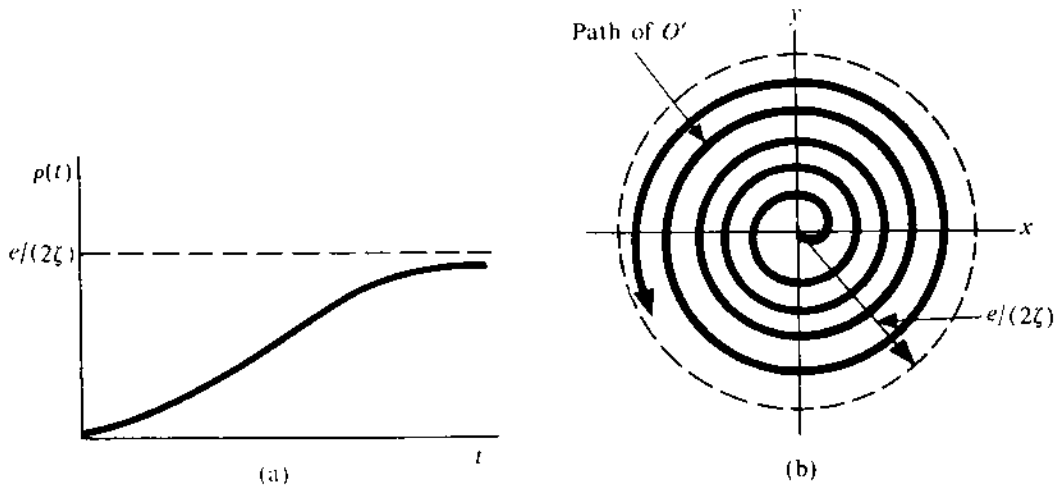


FIGURE 11.43

$$y_{O'} \approx Y \exp(-\zeta \omega_n t) \sin(\omega_n t - \psi') - \frac{e}{2\zeta} \cos(\omega_n t). \quad (11.55b)$$

Using the initial conditions, we get

$$X = -e/(2\zeta), \quad \psi = \pi/2, \quad Y = e(1 + \zeta^2)^{1/2}/(2\zeta), \quad \psi' = \tan^{-1}(-1/\zeta).$$

Thus, the final form of the solutions is

$$x_{O'} \approx \frac{e}{2\zeta} [1 - \exp(-\zeta \omega_n t)] \sin \omega_n t, \quad (11.56a)$$

$$\begin{aligned} y_{O'} &\approx \frac{e}{2} \exp(-\zeta \omega_n t) \sin \omega_n t + \frac{e}{2\zeta} \exp(-\zeta \omega_n t) \cos \omega_n t - \frac{e}{2\zeta} \cos \omega_n t \\ &\approx -\frac{e}{2\zeta} [1 - \exp(-\zeta \omega_n t)] \cos \omega_n t. \end{aligned} \quad (11.56b)$$

Squaring and adding both sides of each of these equations, the growth of the shaft deflection $\rho(t)$ shown in Fig. 11.43a, we get is

$$\rho(t) = \frac{e}{2\zeta} [1 - \exp(-\zeta \omega_n t)]. \quad (11.57)$$

The path of O' in the xy -plane is indicated in Fig. 11.43b. The entire analysis of a vertical shaft we have given is applicable to a horizontal shaft if the gravitational force is neglected.

PROBLEM 11.18

A uniform shaft of diameter 15 mm and length 1000 mm is mounted on two long bearings. A heavy disc with a mass of 25 kg is mounted on the shaft at the midspan. The effective damping factor can be taken as 0.005. The eccentricity of the centre of mass of the disc is 0.5 mm. Determine the steady-state deflection of the shaft at the critical speed. Also estimate the time taken for the shaft deflection to reach 90% and 10% of the steady-state value. The modulus of elasticity of the shaft material is 210 GPa and the shaft inertia can be neglected.

SOLUTION

Since the supporting bearings are long, the slope of the shaft at its ends is zero. So, the corresponding transverse stiffness, obtained from Table 11.1, is

$$k = 192EI/l^3,$$

here $I = \pi d^4/64$, $E = 210 \times 10^9$ N/m², $l = 1$ m, and $d = 0.015$ m. Substituting these values in this expression, we get $k = 100,197$ N/m. Hence,

$$\omega_n = (k/m)^{1/2} = (100,197/25)^{1/2} = 63.3 \text{ rad/s.}$$

The steady-state amplitude can be found by putting $t = \infty$ in (11.57) [or from (11.54) with $r = 1$ for our problem]. Thus,

$$\rho = \frac{e}{2\zeta} = \frac{0.5}{2 \times 0.005} = 50 \text{ mm.}$$

With $\rho(t) = 0.9\rho = 45$ mm, we get, from (11.57),

$$45 = 50[1 - \exp(-0.005 \times 63.3 \times t)].$$

Solving this equation, we obtain $t = 7.28$ s. When $\rho(t) = 0.1\rho = 5$ mm, the corresponding time would be

$$5 = 50[1 - \exp(-0.005 \times 63.3 \times t)]$$

$$t = 0.33 \text{ s.}$$

In many situations, the shaft rotates at a speed higher than the critical speed. As we can see from the foregoing example, at the critical speed it takes time for the shaft to build up a large deflection. So, if the critical speed is crossed quickly, an undue large deflection can be avoided. When $\omega \gg \omega_{cr}$, the steady-state deflection approaches e as seen from (11.54).

Equivalent Viscous Damping

In all our analyses of a harmonically excited system, we assumed that the damping is purely viscous. But, in practice, the contributions from solid friction and material damping may be quite significant. In such a situation, the concept of equivalent viscous damping can be applied to simplify the analysis. This concept is based on the principle that the energy dissipated per cycle is the same. To see this, let us first determine the amount of energy dissipated per cycle, with a viscous damping coefficient and harmonic motion of amplitude X and frequency ω .

The energy dissipated per cycle for the system shown in Fig. 11.32 is

$$E_d = \oint c\dot{x} dx = \oint c\dot{x} \frac{dx}{dt} dt = \oint c\dot{x}^2 dt,$$

where $x = X \cos(\omega t - \phi)$. So,

$$E_d = \int_0^{2\pi/\omega} c\dot{x}^2 dt = \int_0^{2\pi/\omega} c\omega^2 X^2 \sin^2(\omega t - \phi) dt.$$

Finally,

$$E_d = \pi c \omega X^2. \quad (11.5)$$

The energy input by the exciting force per cycle can be expressed as

$$E_i = \oint F(t) dx = \int_0^{2\pi/\omega} F(t) \cdot \dot{x} dt = \int_0^{2\pi/\omega} -F_0 \cos \omega t \cdot \omega X \sin(\omega t - \phi) dt.$$

Finally,

$$E_i = \pi F_0 X \sin \phi. \quad (11.5)$$

The reader is advised to verify that, at steady state, $E_i = E_d$ when the expressions for X and from (11.32) are substituted in (11.58) and (11.59).

So, a damping other than viscous can be represented by an equivalent viscous damping coefficient if E_d is known. The equivalent damping coefficient is

$$c_{eq} = E_d / (\pi \omega X^2). \quad (11.6)$$

PROBLEM 11.19

The system shown in Fig. 11.21a is being excited by a harmonic force $F_0 \cos \omega t$. Use the concept of equivalent viscous damping to determine the amplitude of oscillation.

SOLUTION

Let us assume the response to be harmonic and of the form $x = X \cos(\omega t - \phi)$. With this motion (and f as the friction force),

$$E_d = f \cdot 4X = \pi c_{eq} \omega X^2$$

or

$$c_{eq} = 4f / (\pi \omega X). \quad (11.7)$$

Now, replacing the coulomb damping by a dashpot with the damping coefficient given by (a), we can find the equivalent damping factor as

$$\zeta_{eq} = \frac{c_{eq}}{c_c} = \frac{4f}{\pi \omega X} \cdot \frac{1}{2(km)^{1/2}} = \frac{2f}{\pi X m \omega_n \omega}.$$

Substituting this in (11.32b), we obtain

$$X = \frac{F_0/k}{[(1 - r^2)^2 + (\frac{4f}{\pi k X})^2]^{1/2}}.$$

Solving this equation, we get

$$X = \pm \frac{\frac{F_0}{k} [1 - (\frac{4f}{\pi F_0})^2]^{1/2}}{1 - r^2}. \quad (11.8)$$

The positive sign is taken when $r < 1$, and the negative sign, when $r > 1$. Further, even with viscous damping, we see that (b) indicates an infinite steady-state amplitude at $r = 1$. So, with coulomb damping, at resonance the steady state is never attained.

However, it should be remembered that the form of harmonic response we assumed is not applicable to the situation we have considered. As we can see from (b), X is imaginary or zero, implying

no movement when $F_0 \leq 4f/\pi$. But it is obvious that the motion can take place if $F_0 > f$ (but $< 4f/\pi$).

For most structural materials, the energy dissipated per cycle due to mechanical hysteresis (i.e. internal friction) has been experimentally found to be

$$E_d = \alpha X^2, \quad (11.61)$$

where α is the material constant. In such a material,

$$c_{eq} = \alpha/(\pi\omega) = h/\omega, \quad (11.62)$$

where h is known as the *hysteretic damping coefficient*. Unlike coulomb damping, c_{eq} here is independent of the amplitude of motion.

Representation of Harmonic Quantities by Complex Notation

As already explained, a harmonic quantity can be represented by a rotating vector. Also, the instantaneous value is given by the projection of this vector on the reference line. A harmonic quantity can also be represented analytically by using the complex notation.

A harmonic quantity of the form $x = X \cos(\omega t - \phi)$ can also be written in the form $\text{Re} [X e^{i\omega t}]$,⁴ where Re indicates the real part and X is a complex number of the form $\tilde{X} = X_R + iX_I$. It is readily seen that

$$X = |\tilde{X}| = (X_R^2 + X_I^2)^{1/2}, \quad (11.63)$$

$$\phi = \tan^{-1} (-X_I/X_R). \quad (11.64)$$

The complex amplitude X takes care of both the amplitude and phase.

A mathematical analysis involving harmonic quantities can be carried out by representing the quantities in complex notation. However, it should be remembered that a physical quantity, e.g., force and displacement, is real, and so *the final result of such an analysis is given by the real part of the complex quantity corresponding to the physical quantity*.

For harmonic excitation, the force may be represented by $\tilde{F} e^{i\omega t}$ and the steady-state response corresponding to it by $\tilde{x} e^{i\omega t}$.

Considering the system shown in Fig. 11.32, we can write the equation of motion, i.e., (11.30), in terms of the complex quantities \tilde{x} and $\tilde{F}(t)$ as

$$\tilde{m}\ddot{\tilde{x}} + \tilde{c}\dot{\tilde{x}} + \tilde{k}\tilde{x} = \tilde{F}(t).$$

Using the foregoing complex notation for \tilde{x} and $\tilde{F}(t)$, i.e., substituting \tilde{x} by $\tilde{X} e^{i\omega t}$ (for steady-state response) and $\tilde{F}(t)$ by $\tilde{F}_0 e^{i\omega t}$, we get

$$[(k - m\omega^2) + ic\omega] \tilde{X} = \tilde{F}_0 \quad (11.65)$$

⁴A complex quantity is represented by placing a tilde (~) below the character representing it and the real part corresponding to it is the physical quantity.

or

$$\tilde{X} = \frac{\tilde{F}_0/k}{(1 - r^2) + 2i\zeta r}. \quad (11.66)$$

The nondimensional deflection

$$\frac{\tilde{x}}{\tilde{F}(t)/k} = \frac{\tilde{X}}{\tilde{F}_0/k} = H(\omega) \quad (11.67a)$$

is known as the *complex frequency response* function and is given by

$$\tilde{H}(\omega) = \frac{1}{(1 - r^2) + 2i\zeta r}. \quad (11.67b)$$

The magnification factor M is obviously given by

$$M = |\tilde{H}(\omega)| = \frac{1}{[(1 - r^2)^2 + (2\zeta r)^2]^{1/2}}.$$

Let us now analyze the steady-state motion of an SDF system with hysteretic damping under harmonic excitation using complex notation and standard symbols. The equation of motion with hysteretic damping can be written, using (11.62), as

$$\tilde{m}\ddot{\tilde{x}} + \frac{h}{\omega}\dot{\tilde{x}} + k\tilde{x} = \tilde{F}_0 e^{i\omega t}.$$

Seeking a solution in the form

$$\tilde{x} = \tilde{X} e^{i\omega t}, \quad (11.68)$$

we get

$$\tilde{m}\ddot{\tilde{x}} + (ih + k)\tilde{x} = \tilde{F}_0 e^{i\omega t}$$

or

$$\tilde{m}\ddot{\tilde{x}} + k(1 + i\eta)\tilde{x} = \tilde{F}_0 e^{i\omega t}, \quad (11.69)$$

where η ($= h/k$) is called the *loss factor* of the system. As can be seen, structural damping can be taken care of by expressing the stiffness in complex notation as

$$\tilde{k} = k(1 + i\eta). \quad (11.70)$$

It should be noted that this can be done only when the motion is harmonic. Using (11.68) and (11.70) in (11.69), we obtain

$$\tilde{X} = \frac{\tilde{F}_0}{\tilde{k} - m\omega^2}$$

or

$$|\tilde{X}| = \frac{|F_0|/k}{[(1 - r^2)^2 + \eta^2]^{1/2}}. \quad (11.71)$$

It is left to the reader to verify that

$$\eta = E_d/(2\pi E_t), \quad (11.72)$$

where E_d represents the energy dissipation per cycle and E_1 is the maximum total energy of the system during a cycle. Applying the definition of η given by (11.72) to viscous damping, we get

$$\eta = 2\zeta r. \quad (11.73)$$

The reader is advised to obtain the magnification factor M from (11.71) and compare this with that given by (11.33) (for the viscously-damped system) in view of (11.73). Further, it is evident from (11.71) that the peak frequency (see (11.34)) for the hysteretically damped system is ω_n for all values of η .

Periodic Excitation

The response of a single-degree-of-freedom system to a periodic (nonharmonic) excitation can be readily obtained by using the complex frequency response function $\tilde{H}(\omega)$ of the system and the Fourier series.

Let $F(t)$ be a periodic excitation acting on the system shown in Fig. 11.32. The time period of $F(t)$ is T , and we define $\omega_0 = 2\pi/T$. Using the complex Fourier series representation, we can write⁵

$$F(t) = \sum_{p=-\infty}^{\infty} \tilde{A}_p e^{ip\omega_0 t}, \quad (11.74)$$

where

$$\tilde{A}_p = \frac{1}{T} \int_{-T/2}^{T/2} F(t) e^{-ip\omega_0 t} dt. \quad (11.75)$$

It should be noted that the p -th term on the right-hand side of (11.74) represents a harmonic force of frequency $p\omega_0$ in complex notation. Thus,

$$\tilde{F}_p = \tilde{A}_p e^{ip\omega_0 t}.$$

So,

$$\tilde{x}_p = \tilde{A}_p. \quad (11.76)$$

The response due to this component can be obtained, using (11.67a), as

$$\tilde{x}_p = \frac{1}{k} \tilde{A}_p \tilde{H}_p,$$

where $\tilde{H}_p = H(p\omega_0)$. Hence, the total response in complex form is

$$\tilde{x} = \sum_{p=-\infty}^{\infty} \tilde{x}_p e^{ip\omega_0 t} = \frac{1}{k} \sum_{p=-\infty}^{\infty} \tilde{A}_p \tilde{H}_p e^{ip\omega_0 t}. \quad (11.77)$$

The actual response is given by $x = \operatorname{Re}(\tilde{x})$.

PROBLEM 11.20

Determine the steady response of the SDF system shown in Fig. 11.32 to a periodic excitation of the form shown in Fig. 11.44.

⁵Pipes, L.A. and Harvill, L.R., Applied Mathematics for Engineers and Physicists, McGraw-Hill, New York, 1970.

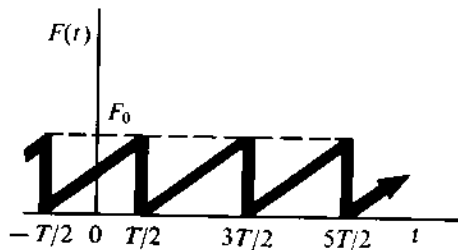


FIGURE 11.44

SOLUTION

For one cycle (with a period T), the exciting force can be represented as

$$F(t) = F_0 \cdot \left(\frac{t + T/2}{T} \right), \quad -\frac{T}{2} < t < +\frac{T}{2}.$$

From (11.75),

$$\tilde{A}_p = \frac{1}{T} \int_{-T/2}^{T/2} F_0 \left(\frac{t + T/2}{T} \right) e^{-ip\omega_0 t} dt,$$

where $\omega_0 = 2\pi/T$. Carrying out the integration, we get

$$\tilde{A}_p = \frac{iF_0}{2p\pi} (-1)^p \quad (p \neq 0), \quad \tilde{A}_0 = F_0/2.$$

Using (11.67b) in (11.77) and noting that $r_p = p\omega_0/\omega_n$, we obtain

$$\tilde{x} = \frac{1}{k} \sum_{p=-\infty, p \neq 0}^{\infty} \frac{iF_0(-1)^p}{2p\pi} \cdot \frac{e^{ip\omega_0 t}}{1 - (p\omega_0/\omega_n)^2 + 2i\zeta p\omega_0/\omega_n} + \frac{F_0}{2k},$$

where $\omega_n = (k/m)^{1/2}$. The actual response is found by taking the real part of \tilde{x} . Thus,

$$x(t) = \frac{F_0}{2k} - \frac{1}{k} \sum_{p=-\infty, p \neq 0}^{\infty} \frac{F_0(-1)^p}{2\pi p} \left[\frac{(1 - r_p^2) \sin p\omega_0 t - 2\zeta r_p \cos p\omega_0 t}{(1 - r_p^2)^2 + (2\zeta r_p)^2} \right],$$

where $r_p = p\omega_0/\omega_n$.

Arbitrary Excitation (Analytical Approach)

In an arbitrary excitation without any periodicity, the time period T can be considered to be infinite. Thus,

$$\omega_0 = 2\pi/T = \Delta\omega_p \quad (11.78)$$

tends to $d\omega$, an infinitesimal quantity. Now, since we do not have any discrete frequencies for the Fourier components, the Fourier series (11.74) converges to an integral as

$$F(t) = \sum_{p=-\infty}^{\infty} \frac{1}{T} \cdot (T \tilde{A}_p) e^{ip\omega_0 t} = \frac{1}{2\pi} \sum_{p=-\infty}^{\infty} \tilde{A}_p e^{ip\omega_0 t} \cdot \Delta\omega_p \quad [\text{using (11.78)}].$$

Now, when $T \rightarrow \infty$,

$$F(t) = \frac{1}{2\pi} \int_{-\infty}^{\infty} \lim_{T \rightarrow \infty} (T A_p) e^{i\omega t} d\omega, \quad (11.79)$$

where $p\omega_0 = \omega$. From (11.75),

$$\lim_{T \rightarrow \infty} (T A_p) = \int_{-\infty}^{\infty} F(t) e^{-i\omega t} dt. \quad (11.80)$$

Now, from (11.79) and (11.80), we define the Fourier transform pair

$$F(t) = \frac{1}{2\pi} \int_{-\infty}^{\infty} \tilde{F}(\omega) e^{i\omega t} d\omega, \quad (11.81a)$$

$$\tilde{F}(\omega) = \int_{-\infty}^{\infty} F(t) e^{-i\omega t} dt. \quad (11.81b)$$

Proceeding in a similar manner and converting (11.77) into an integral, we get⁶

$$\tilde{x} = \frac{1}{k} \cdot \frac{1}{2\pi} \int_{-\infty}^{\infty} \tilde{F}(\omega) H(\omega) e^{i\omega t} d\omega. \quad (11.82)$$

Thus, with arbitrary excitation $F(t)$, we have to first find out $\tilde{F}(\omega)$ from (11.81b). Then, knowing $H(\omega)$ for the given system, we can determine the response \tilde{x} , using (11.82).

Using the definition of Fourier transform given by (11.81), it is obvious from (11.82) that the Fourier transform of the response is

$$\tilde{x}(\omega) = \frac{1}{k} \tilde{F}(\omega) H(\omega). \quad (11.83)$$

This approach, using the change of variable from t to ω , is known as the *frequency domain* analysis.

PROBLEM 11.21

The undamped SDF system shown in Fig. 11.27 is excited by an impulse \hat{F} . Determine its response.

⁶Another heuristic approach to establish (11.82) is as follows. From (11.81a),

$$F(t) = \int dF(t) = \int_{-\infty}^{\infty} \frac{1}{2\pi} \tilde{F}(\omega) d\omega \cdot e^{i\omega t}.$$

So, for the elemental force $dF(t)$, which is harmonic with an amplitude $[1/(2\pi)]\tilde{F}(\omega) d\omega$, the response is given by (11.67a) as

$$\tilde{dx} = \frac{1}{2\pi} \frac{\tilde{F}(\omega) d\omega}{k} \cdot \tilde{H}(\omega) e^{i\omega t}.$$

Finally,

$$\tilde{x} = \int \tilde{dx} = \frac{1}{k} \cdot \frac{1}{2\pi} \int_{-\infty}^{\infty} \tilde{F}(\omega) \tilde{H}(\omega) e^{i\omega t} d\omega.$$

SOLUTION

An impulsive force acts for a very short interval of time and the variation of the force $F(t)$ during this interval cannot be prescribed. However, the time integral of the force is defined as the impulse. Thus,

$$\hat{F} = \int_{-\infty}^{\infty} F(t) dt. \quad (\text{a})$$

In such a situation, the force can be expressed as a function of time only through the use of *delta function*, $\delta(t)$. This function has special properties and those that are useful are

$$\delta(t - \tau) = 0 \quad \text{for } t \neq \tau, \quad (\text{b})$$

$$\int_{-\infty}^{\infty} \delta(t - \tau) dt = 1, \quad (\text{c})$$

$$\int_{-\infty}^{\infty} F(t)\delta(t - \tau) dt = F(\tau). \quad (\text{d})$$

It should be noted from (c) that the dimension of the delta function is the reciprocal of that of delta function's variable (here, time). Now, $F(t)$ can be written as

$$F(t) = \hat{F}\delta(t).$$

This satisfies (a). So, using (d) and (11.81b), we get

$$\underset{\sim}{F}(\omega) = \hat{F}. \quad (\text{e})$$

Again, $\underset{\sim}{H}(\omega)$ for the given system is

$$\underset{\sim}{H}(\omega) = \frac{1}{1 - r^2} = \frac{\omega_n^2}{\omega_n^2 - \omega^2}. \quad (\text{f})$$

Now, substituting $\underset{\sim}{F}(\omega)$ and $\underset{\sim}{H}(\omega)$ from (e) and (f), respectively, in (11.82), we get

$$\begin{aligned} \underset{\sim}{x} &= \frac{1}{k} \cdot \frac{1}{2\pi} \int_{-\infty}^{\infty} \hat{F} \cdot \frac{\omega_n^2}{\omega_n^2 - \omega^2} \cdot e^{i\omega t} d\omega \\ &= \frac{\hat{F}\omega_n^2}{2\pi k} \int_{-\infty}^{\infty} \frac{e^{i\omega t}}{\omega_n^2 - \omega^2} d\omega. \end{aligned} \quad (\text{g})$$

The complex integral on the right-hand side of (g) can be evaluated by using the Cauchy integral formula⁷ as

$$\int_{-\infty}^{\infty} \frac{e^{i\omega t}}{\omega_n^2 - \omega^2} d\omega = 2\pi i \left(\frac{-i \sin \omega_n t}{\omega_n} \right). \quad (\text{h})$$

Finally, from (h) and (g),

$$\underset{\sim}{x} = \frac{\hat{F}\omega_n}{k} \sin \omega_n t$$

⁷Churchill, R.V., Complex Variables and Applications, McGraw-Hill, New York, 1960.

or

$$\tilde{x} = \frac{\hat{F}}{m\omega_n} \sin \omega_n t. \quad (i)$$

Since the right-hand side of this equation is entirely real,

$$x = \operatorname{Re}(\tilde{x}) = \frac{\hat{F}}{m\omega_n} \sin \omega_n t.$$

The foregoing problem can also be solved directly in the time domain as now explained. We can consider the input \hat{F} as an initial velocity, \hat{F}/m , given to the body without causing any displacement. Thus, the problem is converted into a free vibration problem with the initial conditions

$$x = 0, \quad \dot{x} = \hat{F}/m \quad \text{at } t = 0.$$

Using these conditions in the general solution (11.2), we get $B = 0$ and $A = \hat{F}/(m\omega_n)$. So,

$$x = \frac{\hat{F}}{m\omega_n} \sin \omega_n t. \quad (11.84)$$

Let us now write the response of a system to a unit impulse (i.e., $\hat{F} = 1$ in consistent units) applied at $t = \tau$ as $g(t - \tau)$. For example, in the undamped system we have just considered,

$$\begin{aligned} g(t - \tau) &= \frac{1}{m\omega_n} \sin \omega_n(t - \tau) \quad (t > \tau) \\ &= 0 \quad (t < \tau). \end{aligned} \quad (11.85)$$

The function $g(t - \tau)$ is known as the *impulsive response* of a system and can be used for evaluating its response to any arbitrary excitation. The procedure to do this is as follows.

Consider the arbitrary excitation $F(t)$ shown in Fig. 11.45. We can think of the effect of this excitation as that due to a series of impulses. One such impulse, $F(\tau) d\tau$, applied at $t = \tau$, is represented by the hatched portion in the figure. The response at the instant t' due to this impulse only is given by $F(\tau) g(t' - \tau)$. So, the total response at this instant can be obtained by summing up the effects of all such impulses applied up to t' . Thus,

$$x(t') = \int_0^{t'} F(\tau) g(t' - \tau) d\tau.$$

Replacing t' by t , we get

$$x(t) = \int_0^t F(\tau) g(t - \tau) d\tau. \quad (11.86)$$

Sometimes, the integral here may be difficult to evaluate. In such a situation, a simple transformation of the variable $(t - \tau) = \xi$ may be helpful. This leads to

$$x(t) = \int_0^t F(t - \xi) g(\xi) d\xi.$$

Since ξ is a dummy variable, we can replace it by τ . Then,

$$x(t) = \int_0^t F(t - \tau) g(\tau) d\tau. \quad (11.87)$$

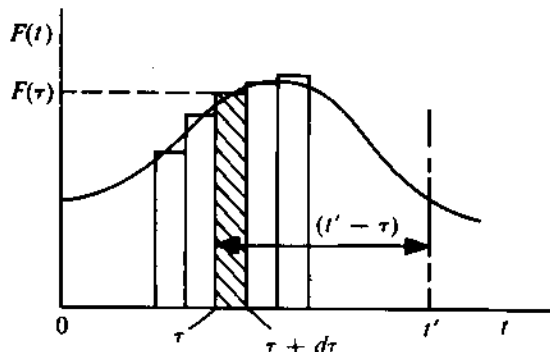


FIGURE 11.45

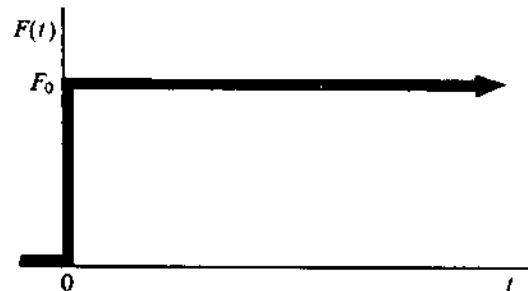


FIGURE 11.46

It may appear to the reader that the frequency domain approach is not necessary, particularly when the solution can be obtained by following the time domain approach using the concept of impulsive response. The reason we have applied the former approach is that, for a real-life system, it is much easier to experimentally determine $\tilde{H}(\omega)$ than $\tilde{g}(t)$. The reader should verify that $\tilde{g}(t)$ and $\tilde{H}(\omega)/k$ form a Fourier transform pair defined by (11.81).

PROBLEM 11.22

Determine the response of the undamped SDF system shown in Fig. 11.27 to the step excitation depicted in Fig. 11.46.

SOLUTION

The exciting force $F(t)$ can be expressed as

$$\begin{aligned} F(t) &= F_0 \quad \text{for } t > 0 \\ &= 0 \quad \text{for } t < 0. \end{aligned} \tag{a}$$

From (11.85), the impulsive response of the system is

$$g(t) = \frac{1}{m\omega_n} \sin \omega_n t \quad (\text{since } \tau = 0). \tag{b}$$

In order to use (11.87), we can write, from (a),

$$\begin{aligned} F(t - \tau) &= F_0 \quad \text{for } (t - \tau) > 0 \\ &= 0 \quad \text{for } (t - \tau) < 0. \end{aligned} \tag{c}$$

Using (b) and (c) in (11.87), we get

$$x(t) = \int_{0+}^t F(t - \tau) \frac{\sin \omega_n \tau}{m\omega_n} d\tau = \int_{0+}^t F_0 \cdot \frac{\sin \omega_n \tau}{m\omega_n} d\tau = \frac{F_0}{m\omega_n^2} - \cos \omega_n \tau \Big|_{0+}^t$$

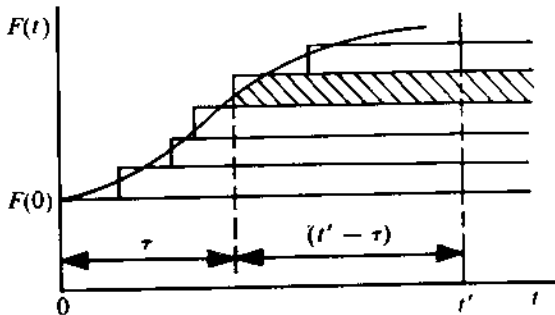


FIGURE 11.47

$$= \frac{F_0}{k}(1 - \cos \omega_n t) \quad \text{for } t > 0. \quad (\text{d})$$

From the foregoing problem, we see that the response, to a unit step input, $u(t - \tau)$, at $t = \tau$ can be expressed as $x(t)$ so that

$$\begin{aligned} x(t) &= \frac{1}{k}[1 - \cos \omega_n(t - \tau)] \quad (t > \tau) \\ &= 0 \quad (t < \tau). \end{aligned} \quad (11.88)$$

For a system, let the response to such a unit step input be $h(t - \tau)$. This is called the *indicial response* of the system and can also be used to determine the response of the system to an arbitrary excitation. To do this, let an arbitrary excitation $F(t)$ be thought of as composed of a series of infinitesimal step inputs (Fig. 11.47). The step input applied at a time τ is of magnitude $\dot{F}(\tau) \cdot d\tau$, where $\dot{F}(\tau) = \partial F / \partial t$ at $t = \tau$. The response at t' to this step input is given by $F(\tau) \cdot d\tau \cdot h(t' - \tau)$. The total response at t' can be written as

$$x(t') = F(0)h(t') + \int_0^{t'} \dot{F}(\tau)h(t' - \tau) d\tau.$$

Introducing t in place of t' , we find this expression becomes

$$x(t) = F(0)h(t) + \int_0^t \dot{F}(\tau)h(t - \tau) d\tau. \quad (11.89)$$

The reader is advised to verify that

$$\begin{aligned} \frac{du(t)}{dt} &= \delta(t), \\ \frac{dh(t)}{dt} &= g(t). \end{aligned} \quad (11.90)$$

PROBLEM 11.23

A shaft (Fig. 11.48a) of torsional stiffness K carries a disc with moment of inertia J_2 at one end and is driven by a clutch with moment of inertia J_1 at its other end. The starting torque on the clutch varies with t as shown in Fig. 11.48b. The build-up time t_0 is much smaller as compared to the natural time period of oscillation. Determine the maximum torque transmitted by the shaft.

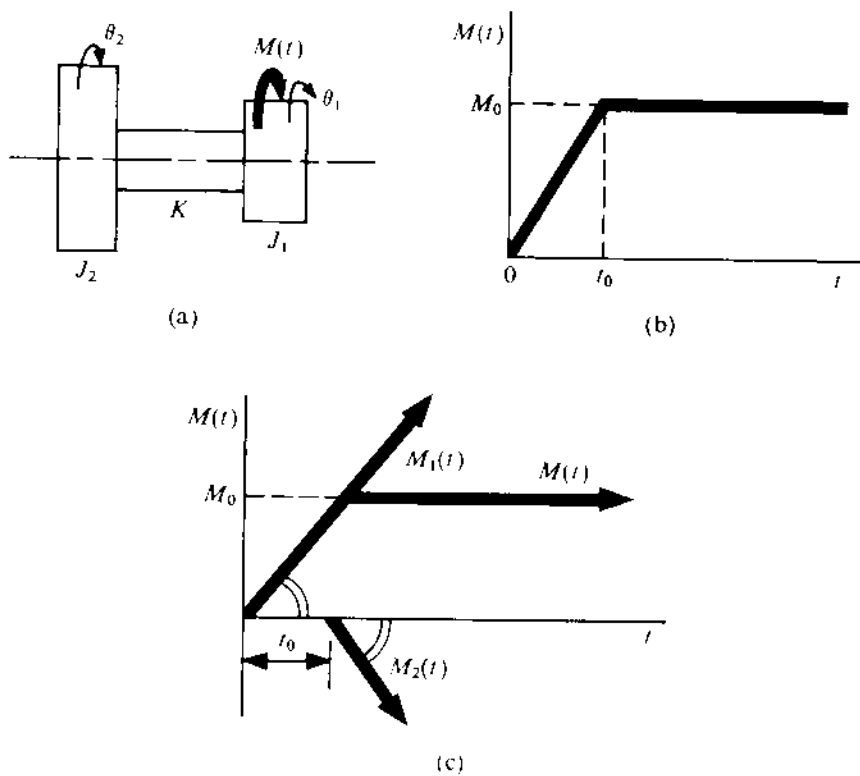


FIGURE 11.48

SOLUTION

With θ_1 and θ_2 as the rotation of the clutch and the disc, respectively, the equations of motion can be written as

$$J_1 \ddot{\theta}_1 + K(\theta_1 - \theta_2) = M(t),$$

$$J_2 \ddot{\theta}_2 - K(\theta_1 - \theta_2) = 0.$$

The amount of twist in the shaft is $\psi = \theta_1 - \theta_2$. Using these equations of motion, we get

$$\ddot{\psi} + \omega_n^2 \psi = M(t)/J_1, \quad (\text{a})$$

here

$$\omega_n = \left[\frac{K(J_1 + J_2)}{J_1 J_2} \right]^{1/2}. \quad (\text{b})$$

The impulsive response function for the system can be written, from (11.85) with $\tau = 0$, as

$$\begin{aligned} g(t) &= \frac{1}{J_1 \omega_n} \sin \omega_n t \quad (t > 0) \\ &= 0 \quad (t < 0). \end{aligned} \quad (\text{c})$$

or the interval $t < t_0$,

$$M(t) = M_0 \cdot (t/t_0)$$

Then, from (11.87),

$$\psi(t) = \frac{M_0}{t_0} \int_0^t (t - \tau) \cdot \frac{1}{J_1 \omega_n} \sin \omega_n \tau d\tau \quad (t < t_0).$$

So, in this interval of time,

$$\psi(t) = \frac{M_0}{J_1 \omega_n^3 t_0} (\omega_n t - \sin \omega_n t). \quad (\text{d})$$

When $t > t_0$, the applied torque $M(t)$ can be written as (Fig. 11.48c)

$$M(t) = M_1(t) + M_2(t) = M_0 \cdot \frac{t}{t_0} - M_0 \cdot \frac{t - t_0}{t_0}. \quad (\text{e})$$

The response during this interval can then be written as

$$\psi(t) = \psi_1(t) + \psi_2(t) = \psi_1(t) - \psi_1(t - t_0),$$

where $\psi_1(t)$ is given by (d). Thus, finally, for $t > t_0$,

$$\begin{aligned} \psi(t) &= \frac{M_0}{J_1 \omega_n^3 t_0} [\omega_n t - \sin \omega_n t - \omega_n (t - t_0) + \sin \omega_n (t - t_0)] \\ &= \frac{M_0}{J_1 \omega_n^3 t_0} [\omega_n t_0 - 2 \cos \omega_n (t - \frac{t_0}{2}) \sin \omega_n \frac{t_0}{2}]. \end{aligned} \quad (\text{f})$$

We now have to decide whether the maximum twist, $\psi(t)_{\max}$, occurs for $t < t_0$ or $t > t_0$. As $t_0 \ll \pi/\omega_n$, we see from (d) that $\psi(t)$ is maximum when $t = t_0$ [actually, $\psi(t)$ increases monotonically from $t = 0$ to t_0]. At $t = t_0$,

$$\psi(t_0) = \frac{M_0}{J_1 \omega_n^3 t_0} (\omega_n t_0 - \sin \omega_n t_0). \quad (g)$$

The maximum twist, $\psi(t)\max$, for $t > t_0$ obviously occurs when $\cos \omega_n(t - t_0/2) = -1$. Thus,

$$\psi(t)\max = \frac{M_0}{J_1 \omega_n^3 t_0} (\omega_n t_0 + 2 \sin \omega_n t_0/2). \quad (h)$$

Comparing (g) and (h), we see that the maximum twist (during the entire time $0 \leq t \leq \infty$) occur for $t > t_0$. So, rewriting (h), we have

$$\psi(t)\max = \frac{M_0}{J_1 \omega_n^2} [1 + \frac{\sin(\omega_n t_0/2)}{\omega_n t_0/2}]. \quad (i)$$

Hence, the maximum torque transmitted by the shaft, M_{\max} , can be expressed as

$$M_{\max} = K \psi(t)\max = \frac{K M_0}{J_1 \omega_n^2} [1 + \frac{\sin(\omega_n t_0/2)}{\omega_n t_0/2}].$$

Using (b) in this equation, we obtain

$$M_{\max} = \frac{M_0 J_2}{J_1 + J_2} [1 + \frac{\sin(\omega_n t_0/2)}{\omega_n t_0/2}]. \quad (j)$$

Now, we see that if the torque M_0 is applied instantaneously (i.e., at $t_0 = 0$), then

$$M_{\max} = \frac{2 J_2}{J_1 + J_2} \cdot M_0.$$

Arbitrary Excitation (Graphical Approach)

The phase-plane technique can be conveniently used for determining the response of a system to an arbitrary excitation. The exciting force can be considered to be composed of steps as shown in Fig. 11.45. However, when following the graphical approach, only a finite number of steps are used to represent this force as shown in Fig. 11.49. The more the number of steps, the higher the accuracy of the result. This method can also be used for a viscously-damped system. But since it involves the construction of logarithmic spirals, the time taken to solve a problem is more. However, for a system with coulomb damping, the method is quite quick and simple.

We shall now use the method to determine the response of a spring mass system to the arbitrary exciting force shown in Fig. 11.49. Due to the step input F_1 , the ensuing motion, as seen from equation (d) of Problem 11.22, is a free harmonic oscillation about a new equilibrium position $x = F_1/k$.

PROBLEM 11.24

Determine the response of an SDF system with coulomb damping to the excitation shown in Fig. 11.50. Given $m = 0.406$ kg, $k = 100$ N/m, and $f = 1$ N.

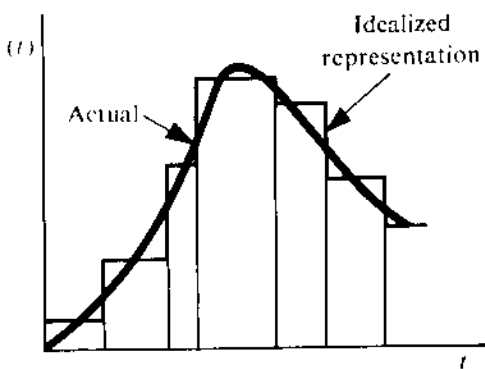


FIGURE 11.49

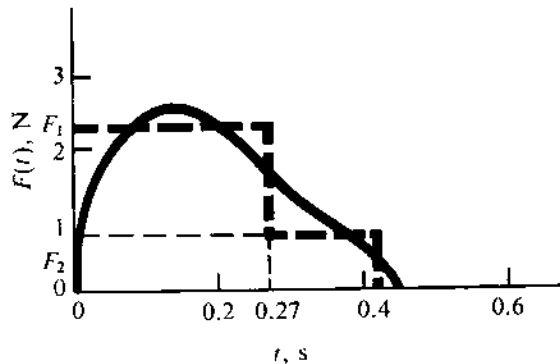


FIGURE 11.50

SOLUTION

First, we find out the natural frequency of the system as $\omega_n = (k/m)^{1/2} = 15.7 \text{ rad/s}$. In Fig. 11.50, the actual excitation (shown by the solid line) is approximated by the step inputs (shown by the dashed lines). This figure also represents F/k versus t on a suitable scale. We shall use this diagram to determine the equilibrium positions for different time intervals and the effect of the friction force, the direction of which depends on \dot{x} . The phase-plane diagram (Fig. 11.51a) is drawn as follows:

- As the mass starts moving with $\dot{x} > 0$, the point O_1 , representing the equilibrium position, is located with

$$OO_1 = \frac{F_1 - f}{k} = \frac{2.3 - 1}{100} \text{ m} = 13 \text{ mm}.$$

The semicircle OA is drawn with O_1 as its centre. The time taken to reach the point A is $\pi/\omega_n = 0.2 \text{ s}$.

- Beyond the point A , \dot{x} tends to become negative when the centre of the phase-plane circle moves to O'_1 (not shown in Fig. 11.51a), where

$$OO'_1 = \frac{F_1 + f}{k} = 33 \text{ mm}.$$

But with O'_1 as the centre and O'_1A as the radius, the phase-plane circle cannot be drawn in the CCW direction to make \dot{x} negative. This implies that the mass stays at rest at the location A' ($\equiv A$) until the step input F_2 becomes operative (i.e., till $t = 0.27 \text{ s}$). During $0.2 \text{ s} < t < 0.27 \text{ s}$, the spring force kx remains less than $F_1 + f$.

- At $t = 0.27 \text{ s}$, the equilibrium position is at O_2 , where

$$OO_2 = \frac{F_2 + f}{k} = \frac{0.8 + 1}{100} = 18 \text{ mm}.$$

The phase-plane plot for the time interval up to $t = 0.42 \text{ s}$ is drawn as AB with $\angle AO_2B = \omega_n(0.42 - 0.27) = 2.355 \text{ rad} = 135^\circ$.

- At $t = 0.42 \text{ s}$, the equilibrium position moves to O_3 , where

$$OO_3 = f/k = 10 \text{ mm},$$

and the system comes to a stop at C .

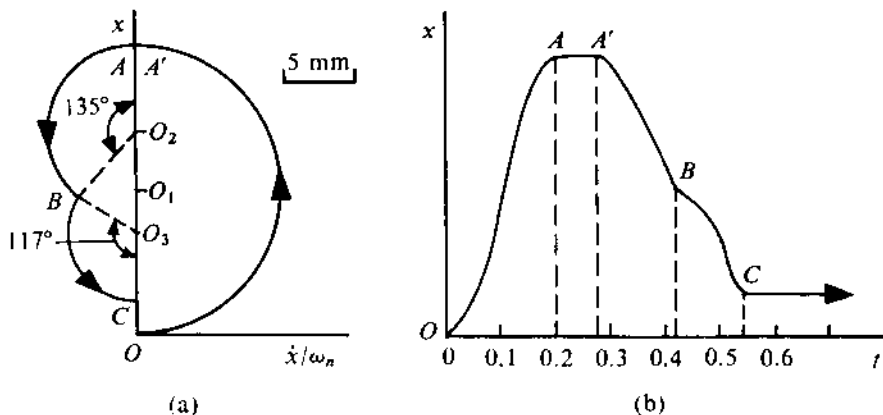


FIGURE 11.51

The displacement-time diagram [which is approximate since we have approximated $F(t)$ by step inputs] corresponding to Fig. 11.51a is as shown in Fig. 11.51b.

11.4 SYSTEMS WITH TWO DEGREES OF FREEDOM

The vibration characteristics of a system with more than one degree of freedom basically differ from those of the SDF systems we have so far discussed. Before we analyze the multidegree-of-freedom systems, we shall identify these basic differences and discuss them with reference to a two-degree-of-freedom system. From now onwards, we shall consider only the undamped systems.

Free Vibration of a Two-degree-of-freedom System

In an SDF system, an arbitrary initial disturbance gives rise to a harmonic oscillation with the same frequency as the natural frequency of the system. This is, however, *not true* of a multidegree-of-freedom system. In such a system, we can make each coordinate (representing the motion of the system) execute a harmonic motion with the same frequency only with certain special initial disturbances. The number of such motions is equal to the number of degrees of freedom of a system. The frequencies of these motions are called the natural frequencies. During a free vibration at these frequencies, all the coordinates pass through their respective equilibrium positions simultaneously. This implies that the possible phase differences between the various coordinates are either zero or π . Therefore, definite relationships exist among the amplitudes of the various coordinates. Each of these definite ratios obviously defines a configuration which, like a natural frequency, is also a system property. Such a configuration, known as a *normal mode*, is defined by the *ratios* of the amplitude of the coordinates.

Let us explain the foregoing aspects with the help of the two-degree-of-freedom system shown in Fig. 11.52a. During a normal mode vibration, the coordinates x_1 and x_2 have the same frequency and a phase difference zero or π . Hence, with ω as the natural frequency, we can write

$$x_1 = X_1 \cos \omega t, \quad x_2 = X_2 \cos \omega t. \quad (11.91)$$

The phase difference π is indicated by assigning opposite signs to X_1 and X_2 . The equations of motion for the two masses can be written as

$$m\ddot{x}_1 + 2kx_1 - kx_2 = 0, \quad m\ddot{x}_2 + 2kx_2 - kx_1 = 0. \quad (11.92)$$

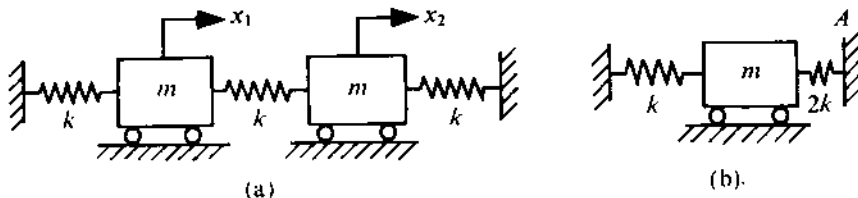


FIGURE 11.52

Substituting (11.91) in (11.92), we get

$$(2k - m\omega^2)X_1 - kX_2 = 0, \quad -kX_1 + (2k - m\omega^2)X_2 = 0. \quad (11.93)$$

For a nontrivial solution of X_1 and X_2 , the determination of the coefficients of the set of homogeneous equations (11.93) must be zero. Thus, we have

$$(2k - m\omega^2)^2 - k^2 = 0 \quad \text{or} \quad m^2\omega^4 - 4km\omega^2 + 3k^2 = 0.$$

Solving this equation, known as the *characteristic equation*, we obtain

$$\omega_1^2 = k/m, \quad \omega_2^2 = 3k/m, \quad (11.94)$$

where ω_1 and ω_2 are the two natural frequencies of the system. The lowest natural frequency in a system is normally known as the *fundamental frequency* of the system.

Substituting the values of ω from (11.94) in any one of (11.93), we get

$$X_1/X_2 = 1 \quad \text{for } \omega = \omega_1, \quad (11.95)$$

$$X_1/X_2 = -1 \quad \text{for } \omega = \omega_2.$$

These two equations define the two normal modes of the system. In the first mode, since $x_1 = x_2$, the intermediate spring does not deform and, obviously, the natural frequency of the system is given by $(k/m)^{1/2}$. In the second mode, since $x_1 = -x_2$, we can see that the midpoint A of the intermediate spring (Fig. 11.52a) does not move. So, the system can be thought of as composed of two identical systems (Fig. 11.52b) with the natural frequency $(3k/m)^{1/2}$. This point A is referred to as a *node*. It can be shown that an N -th order mode (for a multidegree-of-freedom system) has $(N - 1)$ nodes. Let the normal modes of a two-degree-of-freedom (2DOF) system be given by

$$X_1^{(1)}/X_2^{(1)} = \lambda^{(1)}, \quad X_1^{(2)}/X_2^{(2)} = \lambda^{(2)}.$$

Then, the general solution with an arbitrary initial disturbance can be expressed as a linear combination of the two normal modes as

$$x_1 = \lambda^{(1)}X_2^{(1)} \cos(\omega_1 t + \phi_1) + \lambda^{(2)}X_2^{(2)} \cos(\omega_2 t + \phi_2), \quad (11.96)$$

$$x_2 = X_2^{(1)} \cos(\omega_1 t + \phi_1) + X_2^{(2)} \cos(\omega_2 t + \phi_2).$$

The four unknown constants $X_2^{(1)}$, $X_2^{(2)}$, ϕ_1 , and ϕ_2 can be found out from the initial conditions, viz., $x_1(0)$, $x_2(0)$, $\dot{x}_1(0)$, and $\dot{x}_2(0)$.

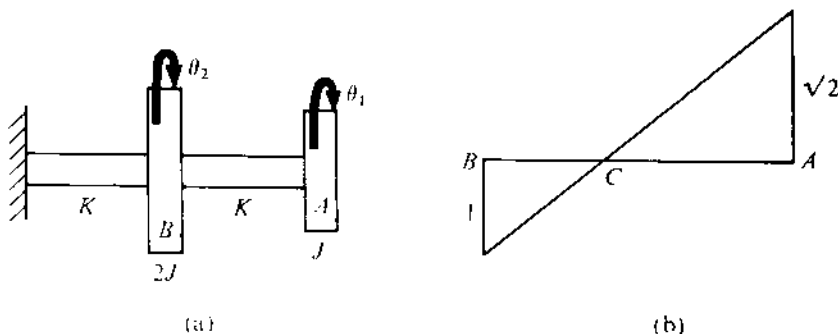


FIGURE 11.53

PROBLEM 11.25

Figure 11.53a shows a system consisting of two discs connected in series to a fixed wall through two shafts. The moments of inertia of the discs are J and $2J$, the torsional stiffness of the shafts being K as indicated. The outer disc is given a rotation ψ while holding the other disc fixed. Then the system is released from rest. Determine the subsequent motion of the two discs.

SOLUTION

The equations of angular motion of the discs can be written as

$$J\ddot{\theta}_1 + K(\theta_1 - \theta_2) = 0, \quad 2J\ddot{\theta}_2 + K\theta_2 - K(\theta_1 - \theta_2) = 0. \quad (\text{a})$$

Assume that the two normal mode oscillations have the form

$$\theta_1 = \Theta_1 \cos \omega t, \quad \theta_2 = \Theta_2 \cos \omega t, \quad (\text{b})$$

where ω represents the natural frequencies. From (a) and (b), the characteristic equation for the frequency we get is

$$2(K - \omega^2 J)(K - \omega^2 J) - K^2 = 0$$

or

$$2J^2\omega^4 - 4KJ\omega^2 + K^2 = 0 \quad (\text{c})$$

or

$$\omega_1^2 = (1 - \frac{1}{\sqrt{2}})\frac{K}{J}, \quad \omega_2^2 = (1 + \frac{1}{\sqrt{2}})\frac{K}{J}. \quad (\text{d})$$

Using (d), the normal modes we obtain are

$$\lambda^{(1)} = \frac{\Theta_1^{(1)}}{\Theta_2^{(1)}} = \sqrt{2}, \quad \lambda^{(2)} = \frac{\Theta_1^{(2)}}{\Theta_2^{(2)}} = -\sqrt{2}. \quad (\text{e})$$

The node in the second mode is at C (Fig. 11.53b), where $AC/BC = \sqrt{2}$. The given initial conditions are

$$\theta_1(0) = \psi, \quad \dot{\theta}_1(0) = 0, \quad \theta_2(0) = 0, \quad \dot{\theta}_2(0) = 0. \quad (\text{f})$$

With this initial disturbance, we can write, from (11.96), the disc motions as

$$\begin{aligned}\theta_1(t) &= \lambda^{(1)}\Theta_2^{(1)} \cos(\omega_1 t + \phi_1) + \lambda^{(2)}\Theta_2^{(2)} \cos(\omega_2 t + \phi_2), \\ \theta_2(t) &= \Theta_2^{(1)} \cos(\omega_1 t + \phi_1) + \Theta_2^{(2)} \cos(\omega_2 t + \phi_2).\end{aligned}\quad (g)$$

Using (e) and (f) in (g), we can obtain four equations in terms of the four unknown quantities $\Theta_2^{(1)}$, $\Theta_2^{(2)}$, ϕ_1 , and ϕ_2 . Solving these, we get

$$\phi_1 = \phi_2 = 0, \quad \Theta_2^{(1)} = \frac{\psi}{2\sqrt{2}}, \quad \Theta_2^{(2)} = -\frac{\psi}{2\sqrt{2}}.$$

So, the subsequent motions can be expressed as

$$\begin{aligned}\theta_1(t) &= \frac{1}{2}\psi[\cos\{(1 - \frac{1}{\sqrt{2}})\frac{K}{J}\}^{1/2}t + \cos\{(1 + \frac{1}{\sqrt{2}})\frac{K}{J}\}^{1/2}t], \\ \theta_2(t) &= \frac{1}{2\sqrt{2}}\psi[\cos\{(1 - \frac{1}{\sqrt{2}})\frac{K}{J}\}^{1/2}t - \cos\{(1 + \frac{1}{\sqrt{2}})\frac{K}{J}\}^{1/2}t].\end{aligned}$$

Sometimes, depending on the situation, one of the natural frequencies may turn out to be zero. This implies a rigid-body motion instead of oscillation. In such a situation, the number of oscillatory degrees of freedom is reduced by one from that of the coordinates used. The reader is advised to determine the natural frequencies of the system shown in Fig. 11.48a using θ_1 and θ_2 as the coordinates and verify this statement. A system with one of its natural frequencies zero is referred to as a *semidefinite system*.

Forced Vibration with Harmonic Excitation

Let the mass m_1 in the 2DOF system shown in Fig. 11.54 be excited by a harmonic force $F = F_0 \cos \omega t$. As in the undamped SDF systems, so too here, we shall consider the steady-state motion since the transient part always dies out even if the damping is very small. The equations of motion are given by

$$\begin{aligned}m_1\ddot{x}_1 + k_1x_1 + k_2(x_1 - x_2) &= F_0 \cos \omega t, \\ m_2\ddot{x}_2 - k_2(x_1 - x_2) &= 0.\end{aligned}\quad (11.97)$$

The steady-state solutions are given by

$$x_1 = X_1 \cos \omega t, \quad x_2 = X_2 \cos \omega t. \quad (11.98)$$

Using (11.98) in (11.97), the equations in X_1 and X_2 we get are

$$\begin{aligned}(k_1 + k_2 - m_1\omega^2)X_1 - k_2X_2 &= F_0, \\ -k_2X_1 + (k_2 - m_2\omega^2)X_2 &= 0.\end{aligned}$$

Solving these equations, we obtain

$$X_1 = \frac{F_0(k_2 - m_2\omega^2)}{(k_1 + k_2 - m_1\omega^2)(k_2 - m_2\omega^2) - k_2^2}, \quad (11.99a)$$

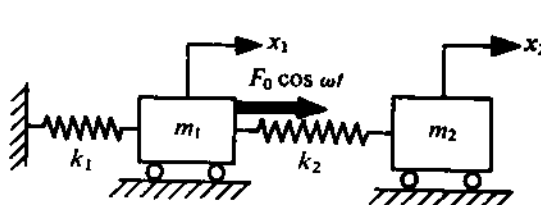


FIGURE 11.54

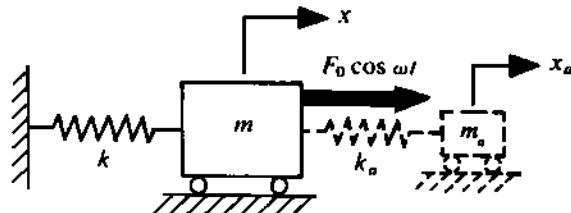


FIGURE 11.55

$$X_2 = \frac{F_0 k_2}{(k_1 + k_2 - m_1 \omega^2)(k_2 - m_2 \omega^2) - k_2^2}. \quad (11.99b)$$

It is seen that by setting the denominator (of each of X_1 and X_2) equal to zero, we can get the characteristic equation of the system. Since the roots of this equation are the natural frequencies ω_1 and ω_2 , the denominator can, obviously, be factorized in the form

$$(k_1 + k_2 - m_1 \omega^2)(k_2 - m_2 \omega^2) - k_2^2 = m_1 m_2 (\omega^2 - \omega_1^2)(\omega^2 - \omega_2^2).$$

So, if the forcing frequency ω coincides with any of the two natural frequencies of the system, both the masses will undergo resonance even though the excitation is applied only to m_1 .

Undamped Vibration Absorbers (Neutralizers)

An examination of (11.99a) reveals that X_1 becomes zero when $k_2 = m_2 \omega^2$. This leads to a very useful method of vibration control of an SDF system. Let us consider an undamped SDF system consisting of m and k subjected to a harmonic force $F_0 \cos \omega t$. The resulting vibration will be large when $\omega \approx \omega_{n_p}$, where ω_{n_p} is the natural frequency of the system, i.e., $\omega_{n_p} = (k/m)^{1/2}$. We shall refer to this system as the primary system. This large vibration can be very effectively neutralized by the addition of an auxiliary system (m_a, k_a) as shown in Fig. 11.55. The primary and auxiliary systems together constitute a 2DOF system. Thus, from (11.99), we can write

$$X = \frac{F_0 (k_a - m_a \omega^2)}{(k + k_a - m \omega^2)(k_a - m_a \omega^2) - k_a^2}, \quad (11.100a)$$

$$X_a = \frac{F_0 k_a}{(k + k_a - m \omega^2)(k_a - m_a \omega^2) - k_a^2}, \quad (11.100b)$$

where X and X_a are the steady-state amplitudes of the primary and auxiliary masses, respectively. If the parameters of the auxiliary system are so chosen that $\omega^2 = k_a/m_a$ (i.e., $\omega_{n_a} = \omega$), the primary mass will not oscillate as can be seen from (11.100a). Under this condition,

$$X_a = -F_0/k_a. \quad (11.101)$$

In other words, the auxiliary spring exerts a force on m equal to $k_a(x_a - x) = -F_0 \cos \omega t$ (as $x = 0$), thus neutralizing the exciting force. Therefore, for vibration neutralization, the natural frequency of the auxiliary system should coincide with the exciting frequency, i.e.,

$$\omega = \omega_{n_a} = (k_a/m_a)^{1/2}. \quad (11.102)$$

The values of the absorber parameters are arrived at by considering the exciting frequency and the maximum permissible amplitude of the auxiliary mass. Hence, (11.101) and (11.102) can be used in designing an auxiliary system.

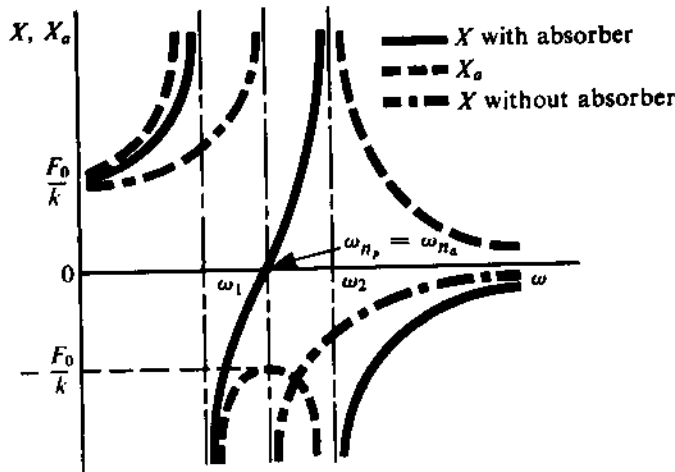


FIGURE 11.56

The vibration neutralization process we have described is effective only if the exciting frequency remains constant and the absorber is tuned to this frequency [see (11.102)]. Let us now study the effect of a tuned absorber on the response in a nonsynchronous operation (when the excitation frequency varies over a wide range). Obviously, the absorber would normally be tuned to the natural frequency of the primary system since the excitation with this frequency results in maximum vibration. So, we study this typical situation, i.e., when $\omega_{n_p} = \omega_{n_a}$. The plots of X and X_a versus the excitation frequency ω are shown in Fig. 11.56 where ω_1 and ω_2 are the natural frequencies of the resulting 2DOF system. As can be seen, if ω_1 and ω_2 are close to ω_{n_p} , a small variation in ω makes X very large which may be even more than that without the absorber. Therefore, the interval between ω_1 and ω_2 should be as wide as possible. This interval depends only on the mass ratio $\nu = m_a/m$ as we now show.

Considering the denominator of (11.100), we find ω_1 and ω_2 are given by the roots of

$$(k + k_a - m\omega^2)(k_a - m_a\omega^2) - k_a^2 = 0$$

$$\omega^4 - \left(\frac{k_a}{m_a} + \frac{k}{m} + \frac{k_a}{m}\right)\omega^2 + \frac{kk_a}{mm_a} = 0$$

$$\left(\frac{\omega}{\omega_{n_p}}\right)^4 - (2 + \nu)\left(\frac{\omega}{\omega_{n_a}}\right)^2 + 1 = 0 \quad (11.103)$$

since $k/m = \omega_{n_p}^2 = \omega_{n_a}^2 = k_a/m_a$. Putting $\omega/\omega_{n_a} = \chi$, we get, from (11.103),

$$\chi_1^2 + \chi_2^2 = 2 + \nu, \quad \chi_1^2 \cdot \chi_2^2 = 1, \quad \text{i.e.,} \quad \chi_1 \chi_2 = 1. \quad (11.104)$$

Thus, finally,

$$\chi_1 = \frac{1}{2}[(4 + \nu)^{1/2} + \sqrt{\nu}], \quad \chi_2 = \frac{1}{2}[(4 + \nu)^{1/2} - \sqrt{\nu}]. \quad (11.105)$$

So, the interval

$$\omega_2 - \omega_1 = \omega_{n_a} \sqrt{\nu}. \quad (11.106)$$

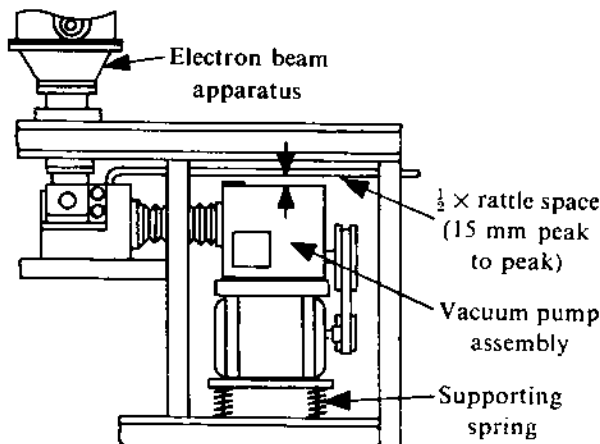


FIGURE 11.57

PROBLEM 11.26

The vacuum pump of an electron beam set-up is schematically shown in Fig. 11.57. The pump mounted on springs and a vertical unbalanced harmonic force $F_0 \cos \omega t$ is generated, where ω is the rotational speed of the pump motor. The magnitude of F_0 is 50 N and the pump body is found to resonate at the normal working speed of the pump which is 1500 rpm. To minimize the vibration, it is proposed to attach an auxiliary system (absorber) to the pump body, as indicated in the figure. The absorber, tuned to ω , has to be designed with the following constraints:

- The resulting natural frequencies of the combined system should lie outside the range 1350-165 cycles/min to take care of the possible variation in the pump speed.
- The available rattle space for the absorber mass is such that m_a should not move more than 15 mm at the normal working speed.

First, a trial absorber mass of 0.1 kg, tuned to ω , is attached. This results in two natural frequencies, namely, 1400 cycles/min and 1607 cycles/min. Determine k_a and m_a of the absorber.

SOLUTION

With the tuned absorber,

$$\omega_{n_a} = \omega_{n_p} = \omega = (1500 \times 2\pi)/60 = 157 \text{ rad/s.}$$

For the trial absorber,

$$\chi_{1t} = 1400/1500 = 0.933, \quad \chi_{2t} = 1/\chi_{1t} = 1.071.$$

Using (11.106), we get

$$\nu_t = (\chi_{2t} - \chi_{1t})^2 = 0.019. \quad (a)$$

Let the first natural frequency ω_1 with the designed absorber be 1350 cycles/min. Then,

$$\chi_{1d} = \omega_1/\omega_{n_a} = 1350/1500 = 0.9$$

nd the second natural frequency ω_2 comes out as

$$\omega_2 = \chi_{2d} \cdot \omega_{n_a} = \frac{1}{\chi_{1d}} \cdot \omega_{n_a} = 1667 \text{ cycles/min.}$$

hus, the frequency constraint is satisfied. (The reader can check that if the second natural frequency taken to be 1650 cycles/min, then the first natural frequency comes out as 1363 cycles/min. So, this case, the first constraint would not have been satisfied.) Now, using (11.106), we obtain

$$\nu_d = (\chi_{2d} - \chi_{1d})^2 = 0.0446. \quad (b)$$

viding (b) by (a), we get

$$\frac{\nu_d}{\nu_t} = 2.347$$

$$\frac{m_{a_d}}{m_{a_t}} = 2.347$$

$$m_{a_d} = 0.1 \times 2.347 = 0.2347 \text{ kg.}$$

ith $\omega_{n_a} = 157 \text{ rad/s}$, we can find k_{a_d} as

$$k_{a_d} = \omega_{n_a}^2 \cdot m_{a_d} = 5785 \text{ N/m.}$$

o, the amplitude of the absorber motion [using (11.101)] is

$$|X_{a_d}| = F_0/k_{a_d} = (50/5785) \times 100 = 8.64 \text{ mm.}$$

ence, the required rattle space comes out as $2 \times 8.64 \text{ mm} = 17.28 \text{ mm}$. Since this is more than the llowed value, i.e., 15 mm, the design is not acceptable.

So, let us start with the second constraint. If $|X_{a_d}|$ has to be $15/2 \text{ mm}$, the required absorber tiffness is

$$k_{a_d} = F_0/|X_{a_d}| = 50 \times 2/15 \text{ N/mm} = 6666.7 \text{ N/m.}$$

With $\omega_{n_a} = 157 \text{ rad/s}$, the required absorber mass is $m_{a_d} = 0.27 \text{ kg}$. So,

$$\nu_d = (0.27/0.2347) \times 0.0446 = 0.051.$$

Using (11.105) and this value of ν_d , we get $\chi_{1d} = 0.893$, $\chi_{2d} = 1.119$. Thus, ω_1 and ω_2 come out as 340 cycles/min and 1679 cycles/min, respectively. Hence, the first constraint is satisfied.

For further interesting applications of vibration absorbers, the reader should see Mallik, A.K., 'Principles of Vibration Control', Affiliated East-West Press (P) Ltd., New Delhi, 1990.

1.5 SYSTEMS WITH MULTIDEGREES OF FREEDOM

There is no difference between the vibration characteristics of a 2DOF system and a multidegree-of-freedom system. However, for compactness of notation and ease of numerical computation, matrix methods are used for studying the multidegree-of-freedom systems. As we shall subsequently discover, a system with N degrees of freedom has N natural frequencies and normal modes.

Natural Frequencies and Normal Modes

Let us consider the 2DOF system shown in Fig. 11.54. The equations of motion of this system during free vibration can be written, from (11.97) with the right-hand side as zero, as

$$m_1 \ddot{x}_1 + (k_1 + k_2)x_1 - k_2x_2 = 0,$$

$$m_2 \ddot{x}_2 - k_2x_1 + k_2x_2 = 0.$$

In matrix form, these equations can be expressed as

$$[M]\{\ddot{x}\} + [K]\{x\} = 0, \quad (11.107)$$

where $[M]$ and $[K]$ are called the mass and stiffness matrices, respectively, and $\{x\}$ is the displacement vector (i.e., a column matrix). These are given by

$$[M] = \begin{bmatrix} m_1 & 0 \\ 0 & m_2 \end{bmatrix},$$

$$[K] = \begin{bmatrix} k_1 + k_2 & -k_2 \\ -k_2 & k_2 \end{bmatrix},$$

$$\{x\} = \begin{Bmatrix} x_1 \\ x_2 \end{Bmatrix}.$$

The matrices $[M]$ and $[K]$ here are seen to be symmetric. For a multidegree-of-freedom system also the equations of free vibration can be written in the form given by (11.107). Obviously, the order of $[M]$, $[K]$, and $\{x\}$ for an N -degree-of-freedom system will be $N \times N$, $N \times N$, and $N \times 1$, respectively. For most vibratory systems, with any choice of the coordinates, $[M]$ and $[K]$ can be always rendered symmetric. For example, if the equations of motion are derived through the Lagrangian formulation these matrices automatically turn out to be symmetric. If the Newtonian formulation is used, with a certain choice of the coordinates, $[M]$ and $[K]$ may not be symmetric initially. However, a suitable addition and subtraction of the equations will finally make $[M]$ and $[K]$ symmetric. So, in our subsequent discussions, we shall always assume that $[M]$ and $[K]$ are symmetric.

For a normal mode vibration of an N -degree-of-freedom system, we can write

$$\{x\} = \{X\} \cos \omega t. \quad (11.108)$$

Substituting (11.108) in (11.107), we get

$$-\omega^2 [M]\{X\} + [K]\{X\} = 0 \quad (11.109)$$

or

$$-\omega^2 \{X\} + [M]^{-1}[K]\{X\} = 0$$

or

$$[A]\{X\} = \omega^2 \{X\}, \quad (11.110)$$

where $[A] = [M]^{-1}[K]$ is known as the *dynamic matrix* of the system. Rewriting (11.110) in the form

$$([A] - \omega^2 [I])\{X\} = 0, \quad (11.111)$$

we can see that, for a nontrivial solution of $\{X\}$, the determinant

$$|[A] - \omega^2[I]| = 0. \quad (11.112)$$

This is the characteristic equation. Solving (11.112), we can obtain N roots for ω^2 .⁸ Using each of these roots in (11.110), we can determine the corresponding $N - 1$ ratios among the N amplitudes $\{X\}$. These ratios define the normal modes corresponding to the roots.⁹ There exists a very useful special property of the normal modes, which we shall now discuss.

If $\{X\}^{(i)}$ and $\{X\}^{(j)}$ are the i -th and j -th normal modes, then, writing (11.109) for each of these two modes, we get

$$\omega_i^2 [M] \{X\}^{(i)} = [K] \{X\}^{(i)},$$

$$\omega_j^2 [M] \{X\}^{(j)} = [K] \{X\}^{(j)}.$$

Premultiplying the first equation by $\{X\}^{(j)T}$ and the second one by $\{X\}^{(i)T}$ and then subtracting the second from the first, we obtain

$$(\omega_i^2 - \omega_j^2) \{X\}^{(j)T} [M] \{X\}^{(i)} = 0 \quad (11.113)$$

since

$$\{X\}^{(j)T} [M] \{X\}^{(i)} = \{X\}^{(i)T} [M] \{X\}^{(j)},$$

$$\{X\}^{(j)T} [K] \{X\}^{(i)} = \{X\}^{(i)T} [K] \{X\}^{(j)}$$

when $[M]$ and $[K]$ are symmetric. Since $\omega_i \neq \omega_j$, from (11.113),

$$\{X\}^{(j)T} [M] \{X\}^{(i)} = 0 \quad (i \neq j). \quad (11.114a)$$

It is evident, in view of (11.114a), that

$$\{X\}^{(j)T} [K] \{X\}^{(i)} = 0 \quad (i \neq j). \quad (11.114b)$$

Relations (11.114) are known as the *orthogonality of normal modes*. Let us define

$$\{X\}^{(i)T} [M] \{X\}^{(i)} = M^{(i)},$$

$$\{X\}^{(i)T} [K] \{X\}^{(i)} = K^{(i)}.$$

These are called the *generalized mass* and the *generalized stiffness* of the i -th mode.

Forced Vibration (Modal Analysis)

Using the orthogonal property of normal modes, we can convert a forced vibration problem of an N -degree-of-freedom system into that of N single-degree-of-freedom systems. Thereafter, applying the methods elaborated in Section 11.3, we can solve this resulting problem. Here, we shall discuss only this conversion technique.

⁸When N is large, the roots (all real and positive) of (11.112) can be computed using a numerical method.

⁹To determine the normal modes of a large system, several numerical methods have been developed and can be found in any standard graduate text.

To start with, we define the *modal matrix* $[\tilde{P}]$ as

$$[\tilde{P}] = [\{X\}^{(1)} \{X\}^{(2)} \dots \{X\}^{(N)}], \quad (11.115)$$

where each column of $[\tilde{P}]$ represents the normal modes. Each normal mode defines only the ratios of amplitudes. To get unique values for the amplitudes, the modes are normalized as

$$\{X\}^{(i)T} [M] \{X\}^{(i)} = M^{(i)} = 1 \quad \text{for all } i \quad (11.116)$$

and, consequently, $K^{(i)} = \omega_i^2$. Using the normalized normal modes given by (11.116), we define the modal matrix $[P]$ corresponding to these modes as the *weighted modal matrix* and denote it by $[P]$. The equations of motion for forced vibration can be written in matrix form as

$$[M]\{\ddot{x}\} + [K]\{x\} = \{F(t)\}. \quad (11.117)$$

We now use the transformation of coordinates

$$\{x\} = [P]\{y\}, \quad (11.118)$$

where $[P]$ is the *weighted modal matrix* and $\{y\}$ represents the new set of coordinates, known as the *principal coordinates*. Substituting (11.118) in (11.117), we get

$$[M][P]\{\ddot{y}\} + [K][P]\{y\} = \{F(t)\}.$$

Premultiplying this equation by $[P]^T$, we obtain

$$[P]^T[M][P]\{\ddot{y}\} + [P]^T[K][P]\{y\} = [P]^T\{F(t)\}.$$

Using the orthogonality property and (11.116), we find this equation becomes

$$[I]\{\ddot{y}\} + \text{diag}[\omega_i^2]\{y\} = [P]^T\{F(t)\}, \quad (11.119)$$

where $\text{diag}[\omega_i^2]$ is a diagonal matrix with ω_i^2 as the elements. This matrix equation represents the equations

$$\ddot{y}_i + \omega_i^2 y_i = Q_i(t), \quad i = 1, 2, \dots, N, \quad (11.120)$$

where $Q_i(t)$ are the elements of the column matrix on the right-hand side of (11.119). Equations (11.120) can be solved in a manner similar to that used for solving the equation for the SDF system. After $y_i(t)$ is obtained for all i 's, the system response $\{x\}$ can be determined, using (11.118). So, in order to solve a forced vibration problem of a multidegree-of-freedom system by modal analysis, first the free vibration problems corresponding to it have to be solved.

PROBLEM 11.27

A three-degree-of-freedom system is shown in Fig. 11.58. The magnitude of the exciting force F_0 is equal to 50 N and the exciting frequency Ω is 20 rad/s. The system parameters are $k_1 = k_2 = 1000$ N/m, $k_3 = 2000$ N/m, $m_1 = m_2 = 1$ kg, and $m_3 = 2$ kg. Determine the steady-state response of m_1 , m_2 , and m_3 , using the modal matrix approach.

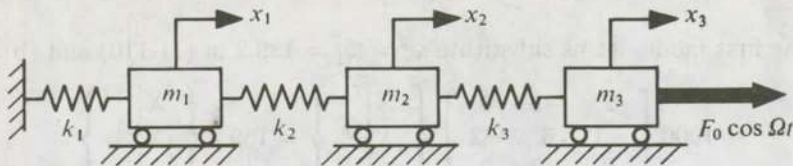


FIGURE 11.58

SOLUTION

The equations of motion of the three masses can be written in the form

$$\begin{aligned} m_1 \ddot{x}_1 + k_1 x_1 + k_2(x_1 - x_2) &= 0, \quad \rightarrow m_1 \ddot{x}_1 + k_1 x_1 + k_2(x_2 - x_1) = 0, \\ m_2 \ddot{x}_2 + k_2(x_2 - x_1) + k_3(x_2 - x_3) &= 0, \\ m_3 \ddot{x}_3 + k_3(x_3 - x_2) &= F_0 \cos \Omega t. \end{aligned}$$

In matrix form, these equations become

$$\begin{bmatrix} m_1 & 0 & 0 \\ 0 & m_2 & 0 \\ 0 & 0 & m_3 \end{bmatrix} \begin{Bmatrix} \ddot{x}_1 \\ \ddot{x}_2 \\ \ddot{x}_3 \end{Bmatrix} + \begin{bmatrix} k_1 + k_2 & -k_2 & 0 \\ -k_2 & k_2 + k_3 & -k_3 \\ 0 & -k_3 & k_3 \end{bmatrix} \begin{Bmatrix} x_1 \\ x_2 \\ x_3 \end{Bmatrix} = \begin{Bmatrix} 0 \\ 0 \\ F_0 \cos \Omega t \end{Bmatrix} \quad (a)$$

Using the given data, we obtain

$$\begin{aligned} [M] &= \begin{bmatrix} 1 & 0 & 0 \\ 0 & 1 & 0 \\ 0 & 0 & 2 \end{bmatrix} \text{ kg}, \\ [K] &= 1000 \begin{bmatrix} 2 & -1 & 0 \\ -1 & 3 & -2 \\ 0 & -2 & 2 \end{bmatrix} \text{ N/m}. \end{aligned}$$

or,

$$[M]^{-1} = \begin{bmatrix} 1 & 0 & 0 \\ 0 & 1 & 0 \\ 0 & 0 & \frac{1}{2} \end{bmatrix} \text{ kg}^{-1}.$$

Hence,

$$[A] = [M]^{-1}[K] = 1000 \begin{bmatrix} 2 & -1 & 0 \\ -1 & 3 & -2 \\ 0 & -1 & 1 \end{bmatrix} \text{ s}^{-2}. \quad (b)$$

The corresponding characteristic equation will be

$$\begin{vmatrix} (2000 - \omega^2) & -1000 & 0 \\ -1000 & (3000 - \omega^2) & -2000 \\ 0 & -1000 & (1000 - \omega^2) \end{vmatrix} = 0.$$

The solution of this equation yields

$$\omega_1^2 = 139.2 \text{ (rad/s)}^2, \quad \omega_2^2 = 1745.8 \text{ (rad/s)}^2, \quad \omega_3^2 = 4115.2 \text{ (rad/s)}^2.$$

To determine the first mode, let us substitute $\omega^2 = \omega_1^2 = 139.2$ in (11.110) and (b) for [A]. Then,

$$1000 \begin{bmatrix} 2 & -1 & 0 \\ -1 & 3 & -2 \\ 0 & -2 & 2 \end{bmatrix} \begin{Bmatrix} X_1^{(1)} \\ X_2^{(1)} \\ X_3^{(1)} \end{Bmatrix} = 139.2 \begin{Bmatrix} X_1^{(1)} \\ X_2^{(1)} \\ X_3^{(1)} \end{Bmatrix}. \quad (c)$$

To normalize the mode, we use (11.116). Then,

$$[X_1^{(1)} \ X_2^{(1)} \ X_3^{(1)}] \begin{bmatrix} 1 & 0 & 0 \\ 0 & 1 & 0 \\ 0 & 0 & 2 \end{bmatrix} \begin{Bmatrix} X_1^{(1)} \\ X_2^{(1)} \\ X_3^{(1)} \end{Bmatrix} = M^{(1)} = 1. \quad (d)$$

Using any two equations of (c) along with (d), we find the normalized first mode to be

$$\begin{Bmatrix} 0.269 \\ 0.501 \\ 0.582 \end{Bmatrix}$$

Similarly, the other normalized modes can be found out, and the weighted modal matrix becomes

$$[P] = \begin{bmatrix} 0.269 & 0.878 & 0.395 \\ 0.501 & 0.223 & -0.836 \\ 0.582 & -0.299 & 0.269 \end{bmatrix}.$$

Now, if we define the principal coordinates y as given by (11.118), the transformed excitation matrix corresponding to the weighted modal matrix becomes

$$\begin{Bmatrix} Q_1(t) \\ Q_2(t) \\ Q_3(t) \end{Bmatrix} = \begin{bmatrix} 0.269 & 0.501 & 0.582 \\ 0.878 & 0.223 & -0.299 \\ 0.395 & -0.836 & 0.269 \end{bmatrix} \begin{Bmatrix} 0 \\ 0 \\ 50 \cos 20t \end{Bmatrix} N$$

or

$$Q_1(t) = 29.1 \cos 20t \text{ N},$$

$$Q_2(t) = -14.95 \cos 20t \text{ N},$$

$$Q_3(t) = 13.45 \cos 20t \text{ N}.$$

The set of equations of motion in terms of the principal coordinates is

$$\ddot{y}_1(t) + 139.2y_1(t) = 29.1 \cos 20t,$$

$$\ddot{y}_2(t) + 1745.8y_2(t) = -14.95 \cos 20t,$$

$$\ddot{y}_3(t) + 4115.2y_3(t) = 13.45 \cos 20t.$$

The steady-state solutions of these equations are given by

$$y_1(t) = -0.112 \cos 20t \text{ m},$$

$$y_2(t) = -0.011 \cos 20t \text{ m},$$

$$y_3(t) = 0.004 \cos 20t \text{ m}.$$

Hence, the steady-state system response $\{x\}$ is given by (11.118) as

$$\begin{Bmatrix} x_1(t) \\ x_2(t) \\ x_3(t) \end{Bmatrix} = \begin{Bmatrix} -0.038 \\ -0.062 \\ -0.063 \end{Bmatrix} \cos 20t \text{ m}.$$

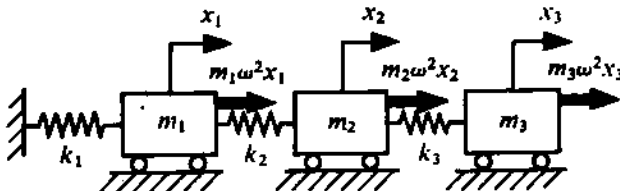


FIGURE 11.59

Dunkerley's Method

Quite often, the knowledge of only the first natural frequency of a multidegree-of-freedom system is useful to the designer. This can be conveniently computed by Dunkerley's method which, of course, gives only an approximate value.

During the free vibration of a multidegree-of-freedom system in a normal mode (i.e., $x_i = A_i \cos \omega t$), we apply D'Alembert's principle to convert the problem into a static one. Consider the three-degree-of-freedom system along with the inertia forces shown in Fig. 11.59. The displacements of the masses can be written as

$$x_1 = a_{11}m_1\omega^2x_1 + a_{12}m_2\omega^2x_2 + a_{13}m_3\omega^2x_3,$$

$$x_2 = a_{21}m_1\omega^2x_1 + a_{22}m_2\omega^2x_2 + a_{23}m_3\omega^2x_3,$$

$$x_3 = a_{31}m_1\omega^2x_1 + a_{32}m_2\omega^2x_2 + a_{33}m_3\omega^2x_3,$$

where a_{ij} is the displacement of the i -th mass due to a unit static force applied to the j -th mass. The a_{ij} 's are known as the *influence coefficients*. In matrix form, the foregoing set of equations becomes

$$\begin{bmatrix} m_1a_{11} - 1/\omega^2 & m_2a_{12} & m_3a_{13} \\ m_1a_{21} & m_2a_{22} - 1/\omega^2 & m_3a_{23} \\ m_1a_{31} & m_2a_{32} & m_3a_{33} - 1/\omega^2 \end{bmatrix} \begin{Bmatrix} x_1 \\ x_2 \\ x_3 \end{Bmatrix} = 0. \quad (11.121)$$

The condition for a nontrivial solution leads to the equation

$$\begin{vmatrix} m_1a_{11} - 1/\omega^2 & m_2a_{12} & m_3a_{13} \\ m_1a_{21} & m_2a_{22} - 1/\omega^2 & m_3a_{23} \\ m_1a_{31} & m_2a_{32} & m_3a_{33} - 1/\omega^2 \end{vmatrix} = 0. \quad (11.122)$$

The expansion of the left-hand side of (11.122) yields

$$(1/\omega^2)^3 - (a_{11}m_1 + a_{22}m_2 + a_{33}m_3)(1/\omega^2)^2 + \dots = 0.$$

For an N -degree-of-freedom system, this equation takes the form

$$(1/\omega^2)^N - (a_{11}m_1 + a_{22}m_2 + \dots + a_{NN}m_N)(1/\omega^2)^{N-1} + \dots = 0. \quad (11.123)$$

The roots of this equation are $1/\omega_1^2, 1/\omega_2^2, \dots, 1/\omega_N^2$, their sum (i.e., of the reciprocals of the square of the natural frequencies) is

$$1/\omega_1^2 + 1/\omega_2^2 + \dots + 1/\omega_N^2 = a_{11}m_1 + a_{22}m_2 + \dots + a_{NN}m_N.$$

Since, in general, $\omega_1 \ll \omega_2 \ll \omega_3 \ll \dots \ll \omega_N$,

$$1/\omega_1^2 \approx a_{11}m_1 + a_{22}m_2 + \dots + a_{NN}m_N. \quad (11.124)$$

It is obvious from the definition that a_{ii} represents the reciprocal of the *system stiffness* at the i -th station. So, $a_{ii}m_i = 1/\omega_{ii}^2$, where ω_{ii} is the natural frequency of the single-degree-of-freedom system obtained by assuming that all masses except the i -th one are zero. Hence, (11.124) can be written as

$$1/\omega_1^2 \approx 1/\omega_{11}^2 + 1/\omega_{22}^2 + \dots + 1/\omega_{NN}^2. \quad (11.125)$$

This equation is known as *Dunkerley's equation*. The reader is advised to check that the matrix formed by the influence coefficients a_{ii} , commonly known as the *flexibility matrix*, is nothing but the inverse of the stiffness matrix $[K]$.

PROBLEM 11.28

Determine the first natural frequency of the system shown in Fig. 11.58.

SOLUTION

Let us first find out the natural frequencies $\omega_{11}, \omega_{22}, \omega_{33}$. A simple inspection of the system yield

$$a_{11} = 1/k_1 = 10^{-3} \text{ m/N},$$

$$a_{22} = 1/k_1 + 1/k_2 = 2 \times 10^{-3} \text{ m/N},$$

$$a_{33} = 1/k_1 + 1/k_2 + 1/k_3 = 2.5 \times 10^{-3} \text{ m/N}.$$

Thus,

$$1/\omega_{11}^2 = a_{11}m_1 = 10^{-3} \text{ s}^2/\text{rad}^2,$$

$$1/\omega_{22}^2 = a_{22}m_2 = 2 \times 10^{-3} \text{ s}^2/\text{rad}^2,$$

$$1/\omega_{33}^2 = a_{33}m_3 = 5 \times 10^{-3} \text{ s}^2/\text{rad}^2.$$

Using Dunkerley's equation along with these values, we get

$$1/\omega_1^2 \approx 8 \times 10^{-3} \text{ s}^2/\text{rad}^2$$

or

$$\omega_1 \approx 11.18 \text{ rad/s}.$$

In Problem 11.27, the exact value of ω_1 was found to be $(139.2)^{1/2} \text{ rad/s} = 11.8 \text{ rad/s}$.

As is obvious from the derivation of (11.124), the value of ω_1 obtained by Dunkerley's method will always be lower than the exact value.

PROBLEM 11.29

Dunkerley's equation can also be used to determine the first natural frequency of a complicated structure. To do this, a rotating eccentric mass of known magnitude is used to resonate the structure along with the shaker mass. Determine the first natural frequency of the transverse vibration in the vertical direction of the nonuniform cantilever beam shown in Fig. 11.60a using the results of the following test runs. A small shaker with rotating eccentric masses is rigidly mounted on the beam as shown in Fig. 11.60b. The total mass of the shaker is 1 kg and the resulting system is four times more likely to resonate when the eccentric masses rotate at 2115 rpm. Next, an additional mass of 0.5 kg is clamped to the shaker body (Fig. 11.60b). This lowers the resonance to 1870 rpm.

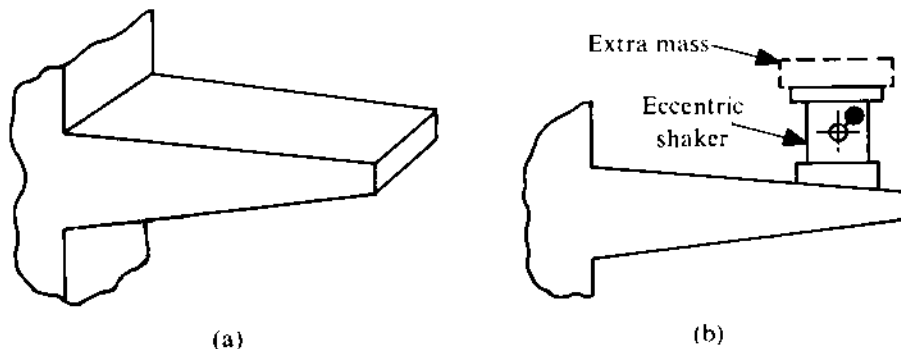


FIGURE 11.60

SOLUTION

If ω_{11} is the first natural frequency of the beam, then Dunkerley's equation can be rewritten in the form

$$1/\omega_1^2 \approx 1/\omega_{11}^2 + a_{22}m_2, \quad (a)$$

where ω_1 is the natural frequency of the combined system, m_2 is the total shaker mass, and a_{22} is the influence coefficient at the shaker location. Using equation (a) for the two test runs, we get

$$(30/\pi)^2(1/2115^2) \approx 1/\omega_{11}^2 + a_{22} \times 1,$$

$$(30/\pi)^2(1/1870^2) \approx 1/\omega_{11}^2 + a_{22} \times 1.5.$$

Solving these equations, we obtain

$$1/\omega_{11}^2 = [0.054/(10^6 \times 0.5)](30/\pi)^2$$

3

$$\omega_{11} = 318.65 \text{ rad/s.}$$

so, the first natural frequency of the beam is $\omega_{11}/(2\pi) = 50.74$ Hz.

Holzer's Method (Transfer Matrix)

If a system can be represented by a series of lumped inertias with intermediate elastic connecting elements, the transfer matrix approach is very suitable for determining the natural frequencies. When applied to a torsional system, this approach is commonly referred to as Holzer's method. When each inertial element of a system possesses only one degree of freedom, the associated problem is called a Holzer-type problem. Two such systems are shown in Fig. 11.61.

In the transfer matrix approach, a station point is associated with each lumped inertia. The displacement (or rotation) and the internal constraining force (or torque) at each such station are related to those at the adjacent stations through a 2×2 matrix known as the *transfer matrix*. The column matrix consisting of the displacement and the internal force is called the *state vector*. As we shall show, the transfer matrix is obtained as the product of two matrices, namely, the *point matrix* (defining the dynamic properties) and the *field matrix* (defining the elastic property), associated with the station.

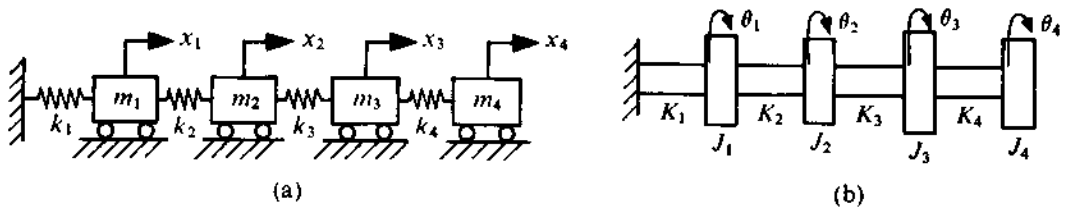


FIGURE 11.61

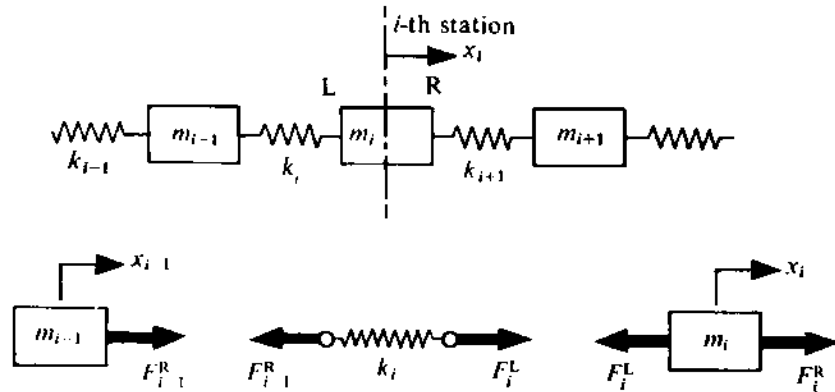


FIGURE 11.62

When determining the natural frequencies of a system, it is assumed that each inertial element undergoes a harmonic motion with the same frequency. Then, using the transfer matrices, calculations are made, proceeding from one end to the other end of the system. Finally, the natural frequencies are given by those values that satisfy the boundary conditions.

Let us now find out the point matrix, the field matrix, and the transfer matrix associated with the i -th station of a rectilinear system shown in Fig. 11.61a. Figure 11.62 shows three consecutive masses of the system, together with the free-body diagrams of the i -th spring and the i -th mass. Here, x and F refer to the displacement and the force, respectively, and the superscripts L and R denote the left side and the right side of the i -th station. From the free-body diagram of m_i , we get

$$m_i \ddot{x}_i = F_i^R - F_i^L.$$

Assuming harmonic motion with a frequency ω , we find this equation becomes

$$F_i^R = F_i^L - \omega^2 m_i x_i. \quad (11.126a)$$

Again, obviously,

$$x_i^R = x_i^L = x_i. \quad (11.126b)$$

Equations (11.126) can be written in matrix form as

$$\begin{Bmatrix} x \\ F \end{Bmatrix}_i^R = \begin{bmatrix} 1 & 0 \\ -\omega^2 m_i & 1 \end{bmatrix}_i \begin{Bmatrix} x \\ F \end{Bmatrix}_i^L \quad (11.127a)$$

or

$$\{S\}_i^R = [\pi]_i \{S\}_i^L, \quad (11.127b)$$

where $\{S\}$ and $[\pi]$ represent the state vector and the point matrix, respectively.

Now, considering the free-body diagram of the i -th spring, we can write

$$F_i^L = F_{i-1}^R.$$

Again, obviously,

$$x_i^L - x_{i-1}^R = F_{i-1}^R/k_i.$$

These equations, when represented in matrix form, become

$$\begin{Bmatrix} x \\ F \end{Bmatrix}_i^L = \begin{bmatrix} 1 & 1/k \\ 0 & 1 \end{bmatrix}_i \begin{Bmatrix} x \\ F \end{Bmatrix}_{i-1}^R \quad (11.128a)$$

$$\{S\}_i^L = [\phi]_i \{S\}_{i-1}^R, \quad (11.128b)$$

where $[\phi]$ represents the field matrix. Using (11.128) in (11.127), we get

$$\{S\}_i^R = [\pi]_i [\phi]_i \{S\}_{i-1}^R$$

$$\{S\}_i^R = [T]_i \{S\}_{i-1}^R, \quad (11.129)$$

where the transfer matrix for the i -th station, $[T]_i$, is given by

$$[T]_i = [\pi]_i [\phi]_i = \begin{bmatrix} 1 & 1/k \\ -\omega^2 m & 1 - \omega^2 m/k \end{bmatrix}_i. \quad (11.130)$$

Similarly, for a torsional system, we have

$$\{S\}_i = \begin{Bmatrix} \theta \\ M \end{Bmatrix}_i, \quad [\pi]_i = \begin{bmatrix} 1 & 0 \\ -\omega^2 J & 1 \end{bmatrix}_i, \quad [\phi]_i = \begin{bmatrix} 1 & 1/K \\ 0 & 1 \end{bmatrix}_i, \quad [T]_i = \begin{bmatrix} 1 & 1/K \\ -\omega^2 J & 1 - \omega^2 J/K \end{bmatrix}_i. \quad (11.131)$$

state vector is a function of time. For assumed harmonic motion, however, the part $\cos \omega t$ may not always be written.

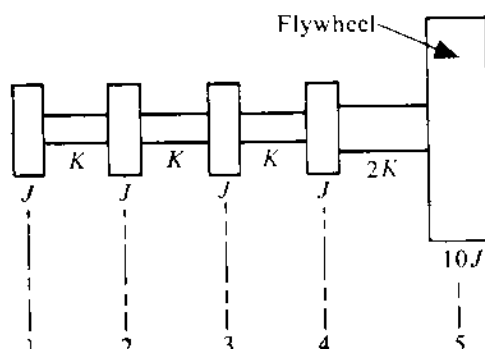
PROBLEM 11.30

The crankshaft of a four-cylinder IC engine can be idealized by a lumped-parameter model shown in Fig. 11.63a. Determine the first two natural frequencies of torsional oscillation when $K = 2 \times 10^5$ N-m/rad and $J = 0.1$ kg-m².

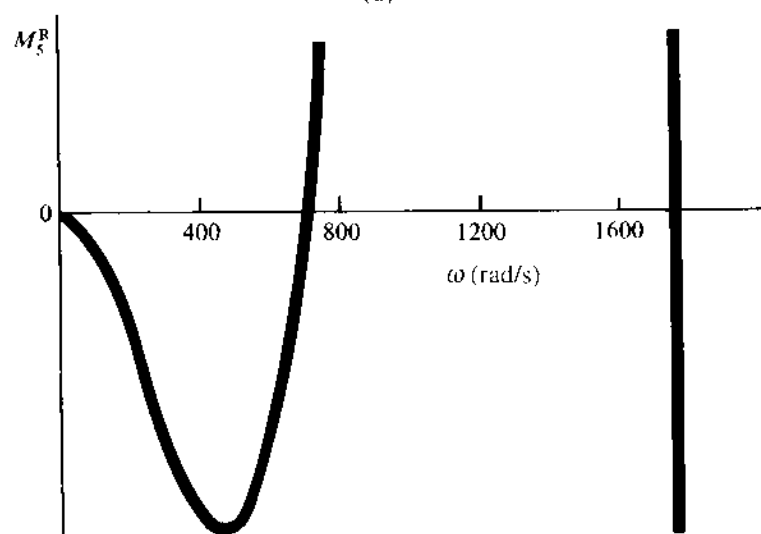
SOLUTION

Referring to Fig. 11.63, let us assume $\theta_1 = 1$ rad. As the ends of the crankshaft are free, $M_1^L = M_5^R = 0$. Hence, we can start with the state vector

$$\{S\}_1^L = \begin{Bmatrix} 1 \\ 0 \end{Bmatrix}.$$



(a)



(b)

FIGURE 11.63

Using the point matrix for station 1, we have

$$\{S\}_1^R = [\pi]_1 \{S\}_1^L.$$

Then, using the transfer matrices of all the stations, we obtain

$$\{S\}_5^R = [T]_5 [T]_4 [T]_3 [T]_2 [\pi]_1 \{S\}_1^L.$$

We can calculate M_5^R by using this equation and assuming a value for ω . The natural frequencies can then be determined from the condition $M_5^R = 0$. So, to facilitate the process, we plot M_5^R against ω (Fig. 11.63b). The details of the calculations are not presented here. The zero crossings of this curve indicate the natural frequencies. We have shown the plot of M_5^R versus ω up to the second zero crossing (Fig. 11.63b). The first two natural frequencies thus obtained are $\omega_1 = 694$ rad/s and $\omega_2 = 1768$ rad/s.

The transfer matrix method can also be very conveniently applied to determine the steady-state response to a *harmonic excitation*. In this case, the frequency of the response is the same as that of the excitation, and the state vector at the exciting station is matched with the given conditions. If there are more than one harmonic excitation of different frequencies, only one excitation should be considered at a time. A linear superposition of the responses so obtained then gives the final result.

PROBLEM 11.31

Solve Problem 11.27 using the Holzer (or transfer matrix) method.

SOLUTION

Referring to Fig. 11.58, we have

$$\left\{ \begin{array}{c} x \\ F \end{array} \right\}_3^R = [T]_3 [T]_2 [\pi]_1 \left\{ \begin{array}{c} x \\ F \end{array} \right\}_1^L = [T]_3 [T]_2 [\pi]_1 \left\{ \begin{array}{c} x \\ kx \end{array} \right\}_1^L.$$

We can determine $[\pi]_1$, $[T]_2$, and $[T]_3$ for $\omega = 20$ rad/s, and $\{S\}_3^R$ can be found out as

$$\{S\}_3^R = \left[\begin{array}{cc} 1 & \frac{1}{2000} \\ -800 & \frac{1200}{2000} \end{array} \right] \left[\begin{array}{cc} 1 & \frac{1}{1000} \\ -400 & \frac{600}{1000} \end{array} \right] \left[\begin{array}{cc} 1 & 0 \\ -400 & 1 \end{array} \right] \left\{ \begin{array}{c} x_1 \\ 1000x_1 \end{array} \right\}$$

or

$$\left\{ \begin{array}{c} x \\ F \end{array} \right\}_3^R = \left\{ \begin{array}{c} 1.580x_1 \\ -1304x_1 \end{array} \right\}.$$

Since $F_3^R = 50 \cos 20t$ N,

$$x_1 = -(50/1304) \cos 20t \text{ m} = -0.0383 \cos 20t \text{ m},$$

$$x_3 = 1.580x_1 = -0.0605 \cos 20t \text{ m}.$$

To determine x_2 , we proceed as

$$\{S\}_2^R = [T]_2 \{S\}_1^R = [T]_2 [\pi]_1 \{S\}_1^L$$

or

$$\begin{Bmatrix} x \\ F \end{Bmatrix}_2^R = \begin{bmatrix} 1 & \frac{1}{1000} \\ -400 & \frac{600}{1000} \end{bmatrix} \begin{bmatrix} 1 & 0 \\ -400 & 1 \end{bmatrix} \begin{Bmatrix} -0.0383 \\ -38.3 \end{Bmatrix} \cos 20t = \begin{Bmatrix} -0.061 \\ 1.52 \end{Bmatrix} \cos 20t.$$

Hence, $x_2 = -0.061 \cos 20t$ m. The results obtained here agree well with those arrived at in Problem 11.27.

The transfer matrix $[T]_i$ given by (11.130) and by the last matrix in (11.131) transforms the state vector $\{S\}_{i-1}^R$ to $\{S\}_i^R$ as shown in (11.129). Premultiplying (11.129) by $[T]_i^{-1}$, we get

$$\{S\}_{i-1}^R = [T]_i^{-1} \{S\}_i^R, \quad (11.132)$$

where

$$[T]_i^{-1} = \begin{bmatrix} 1 - \omega^2 m/k & -1/k \\ \omega^2 m & 1 \end{bmatrix}_i \quad (11.133a)$$

in a translatory system and

$$[T]_i^{-1} = \begin{bmatrix} 1 - \omega^2 J/k & -1/K \\ \omega^2 J & 1 \end{bmatrix}_i \quad (11.133b)$$

in a torsional system.

When the excitation is applied at an intermediate station, the state vectors at both the end of the system have to be assumed. Then, the resulting state vectors on either side of the point of excitation are matched considering the externally applied force. In the problem that follows, we shall illustrate this.

PROBLEM 11.32

Determine the steady-state response of the system shown in Fig. 11.64a. Given $k_1 = k_2 = 1000$ N/m, $k_3 = 3000$ N/m, $m_1 = m_2 = 1$ kg, $m_3 = 2$ kg, $F_0 = 50$ N, and $\omega = 20$ rad/s.

SOLUTION

For steady-state motion, let us assume that the state vectors at C and D (Fig. 11.64b) are given by

$$\{S\}_C = \{S\}_0^R = \begin{Bmatrix} 0 \\ F_C \end{Bmatrix} \cos 20t, \quad (e)$$

$$\{S\}_D = \{S\}_3^R = \begin{Bmatrix} X_D \\ 0 \end{Bmatrix} \cos 20t. \quad (f)$$

Using the transfer matrices, we obtain

$$\{S\}_A = \{S\}_{2+}^R = [T]_2 [T]_1 \{S\}_0^R, \quad (g)$$

$$\{S\}_B = \{S\}_{2+}^R = [T]_3^{-1} \{S\}_3^R. \quad (h)$$

As is apparent from Fig. 11.64b,

$$x_A = x_B, \quad (i)$$

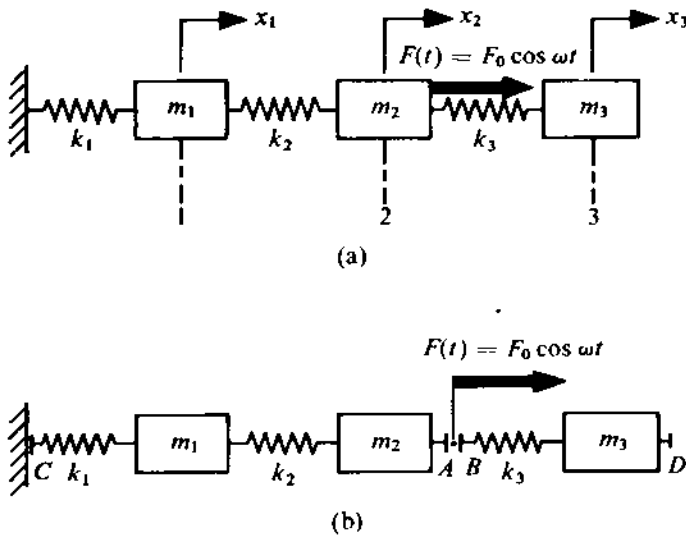


FIGURE 11.64

$$-F_A + F_B + F(t) = 0.$$

(f)

Using the given numerical values in (11.130) and (11.133), we have

$$\begin{aligned} \{S\}_A &= \begin{bmatrix} 1 & \frac{1}{1000} \\ -400 & \frac{600}{1000} \end{bmatrix} \begin{bmatrix} 1 & \frac{1}{1000} \\ -400 & \frac{600}{1000} \end{bmatrix} \begin{Bmatrix} 0 \\ F_C \end{Bmatrix} \cos 20t, \\ \{S\}_B &= \begin{bmatrix} \frac{2200}{3000} & -\frac{1}{3000} \\ 800 & 1 \end{bmatrix} \begin{Bmatrix} X_D \\ 0 \end{Bmatrix} \cos 20t. \end{aligned}$$

From these two equations, we get

$$\begin{aligned} \{S\}_A &= \left\{ \begin{array}{c} x \\ F \end{array} \right\}_{2-}^R = \left\{ \begin{array}{c} 0.0016F_C \\ -0.04F_C \end{array} \right\} \cos 20t, \\ \{S\}_B &= \left\{ \begin{array}{c} x \\ F \end{array} \right\}_{2+}^R = \left\{ \begin{array}{c} 0.733X_D \\ 800X_D \end{array} \right\} \cos 20t. \end{aligned}$$

Using (e) and (f), we obtain

$$0.0016F_C = 0.733X_D,$$

$$0.04F_C + 800X_D + 50 = 0.$$

Solving these equations, we have

$$F_C = -27.95 \text{ N},$$

$$X_D = -0.061 \text{ m}$$

or

$$x_D = X_D \cos 20t = -0.061 \cos 20t \text{ m.}$$

Since $x_D = x_3$, using (d), we get

$$x_2 = (11/15)x_D = -0.0447 \cos 20t \text{ m.}$$

Again, as $F_C = k_1 X_1$, we find

$$x_1 = -0.02795 \cos 20t \text{ m.}$$

11.6 CONTINUOUS SYSTEMS

Earlier in this chapter, we stated that a system with distributed mass and stiffness, i.e., a continuous system, possesses an infinite degrees of freedom. In such a system, obviously, the number of natural frequencies and modes will also be infinite. Most structural and machine elements, e.g., bars, beams, shafts, plates, shells, and membranes, fall in the category of continuous systems. In this section, we shall consider the undamped free vibration of uniform one-dimensional structures such as bars, shafts, and beams. In such structures, the vibratory displacement is a function of time and only one spatial coordinate. We shall restrict our discussion to determining only the natural frequencies.

The equation of motion of a continuous system is not an ordinary differential equation because the vibratory displacement is a function of two variables. It is derived by considering the motion of an element of the system and the force deformation relationship applicable to the system. Then, assuming the motion to be a harmonic function of time (in a normal mode), the natural frequencies are obtained by satisfying the prescribed boundary conditions. In what follows, we shall illustrate this methodology for various structures.

Longitudinal Vibration of Bars

Figure 11.65a shows a uniform bar of length L and cross-sectional area A undergoing a longitudinal vibration. Let us consider $PQRS$, an element of length dz at z , as shown. At any instant t , the longitudinal displacement of the plane PQ is denoted by $w(z, t)$. Obviously, the same for the plane RS can be written as $w(z, t) + (\partial w / \partial z).dz$. The free-body diagram of the element is shown in Fig. 11.65b, where $\sigma_z(z, t)$ denotes the stress at the section PQ . From Newton's second law applied to this element, we get

$$\rho A.dz \cdot \frac{\partial^2 w}{\partial t^2} = A \cdot \frac{\partial \sigma_z}{\partial z} dz, \quad (11.134)$$

where ρ is the density of the material. Due to the deformation of $PQRS$ to $P'Q'R'S'$, the longitudinal strain is given by

$$\epsilon_z = \frac{(w + \frac{\partial w}{\partial z}.dz) - w}{dz} = \frac{\partial w}{\partial z}.$$

So, from Hooke's law,

$$\sigma_z = E\epsilon_z = E(\partial w / \partial z), \quad (11.135)$$

where E is the modulus of elasticity. Substituting (11.135) in (11.134), we get

$$\frac{\partial^2 w}{\partial t^2} = c^2 \cdot \frac{\partial^2 w}{\partial z^2}, \quad (11.136)$$

where $c = (E/\rho)^{1/2}$ is the velocity of sound (longitudinal wave) in the bar. This equation is the *longitudinal wave equation*. Since our objective is to determine the natural frequencies, we shall consider the normal mode vibration in the form

$$w(z, t) = W(z) \cdot \cos \omega t, \quad (11.137)$$

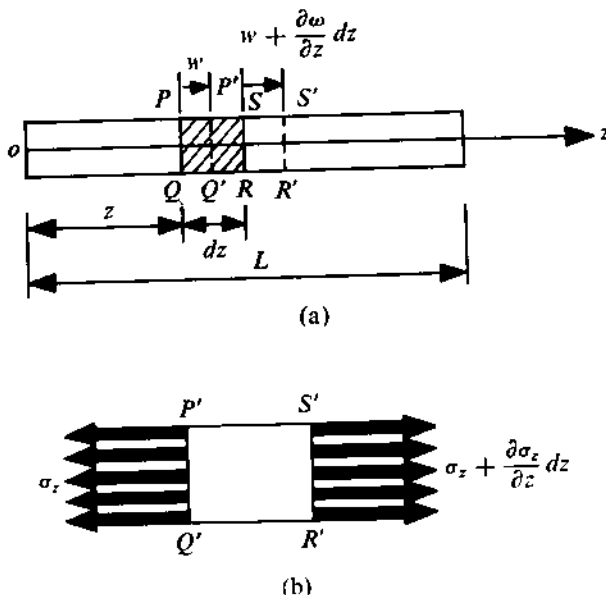


FIGURE 11.65

where $W(z)$ gives the mode shape. Substituting w from (11.137) in (11.136) and rearranging, we get

$$\frac{d^2W(z)}{dz^2} + \left(\frac{\omega}{c}\right)^2 W(z) = 0. \quad (11.138)$$

The general solution of (11.138) is

$$W(z) = C_1 \cos(\omega/c)z + C_2 \sin(\omega/c)z. \quad (11.139)$$

The values of ω for which the boundary conditions on $w(z, t)$ are satisfied by $W(z)$ are the natural frequencies. Let us consider the following boundary conditions.

- (i) Both ends free: At the free ends, the longitudinal strain, and consequently the stress, is zero. Thus, from (11.135),

$$\frac{\partial w(z, t)}{\partial z} = 0 \quad \text{at } z = 0, z = L \text{ for all } t.$$

This can be satisfied only if

$$\frac{dW(z)}{dz} = 0 \quad \text{at } z = 0, z = L. \quad (11.140)$$

Using (11.140) in (11.139), we get

$$C_2 \cdot \frac{\omega}{c} = 0, \quad \frac{\omega}{c} (-C_1 \sin \frac{\omega L}{c} + C_2 \cos \frac{\omega L}{c}) = 0.$$

For a nontrivial solution of these equations,

$$\sin(\omega L/c) = 0. \quad (11.141)$$

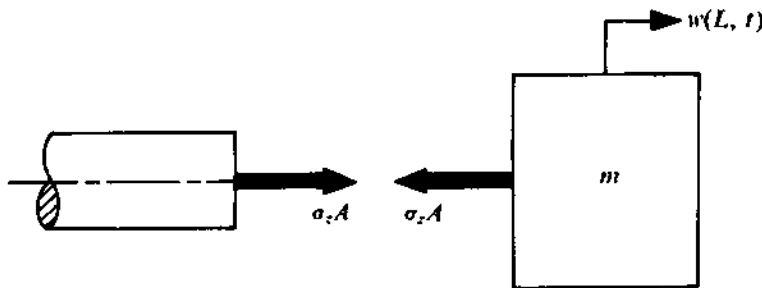


FIGURE 11.66

Since the values of ω satisfying (11.141) represent the natural frequencies ω_i , we can finally write¹⁰

$$\omega_i = i\pi c/L \quad (i = 1, 2, 3, \dots). \quad (11.142)$$

- (ii) One end fixed and the other end free: Let the end at $z = 0$ be fixed. The boundary conditions then are

$$W(0) = 0, \quad \left. \frac{dW(z)}{dz} \right|_{z=L} = 0.$$

Using these conditions in (11.139), we get

$$C_1 = 0, \quad \frac{\omega}{c} \left(-C_1 \sin \frac{\omega L}{c} + C_2 \cos \frac{\omega L}{c} \right) = 0.$$

For a nontrivial solution of these equations, $\cos(\omega L/c) = 0$ or

$$\omega_i = \frac{(2i-1)\pi c}{2L} \quad (i = 1, 2, 3, \dots). \quad (11.143)$$

- (iii) Both ends fixed: The reader is advised to verify that the natural frequencies here are given by

$$\omega_i = i\pi c/L \quad (i = 1, 2, 3, \dots). \quad (11.144)$$

PROBLEM 11.33

A uniform bar of length L and cross-sectional area A is fixed at its left end. A rigid block of mass m is clamped to its right end. If the density and modulus of elasticity are ρ and E , respectively, determine the natural frequencies of longitudinal oscillation.

SOLUTION

The boundary conditions here can be framed as follows. At the left end (i.e., $z = 0$),

$$W(0) = 0 \quad \text{or} \quad C_1 = 0. \quad (\text{a})$$

¹⁰Since the number of possible values of ω is infinite, the general solution for $w(z, t)$ for arbitrary initial conditions can be rewritten as

$$w(z, t) = \sum_{i=1}^{\infty} (A_i \cos \omega_i t + B_i \sin \omega_i t) \sin \frac{\omega_i}{c} z.$$

The infinite number of arbitrary constants A_i 's and B_i 's can be determined from the initial conditions.

To obtain the other boundary condition, let us consider Fig. 11.66. Applying Newton's second law to the mass m , we get

$$m \frac{d^2 w(L, t)}{dt^2} = -\sigma_z(L, t).A \quad \text{for all } t.$$

For a harmonic motion, this equation can be written as

$$-m\omega^2 w(L, t) = -E \frac{\partial w(z, t)}{\partial z} \Big|_{z=L} .A.$$

Using (11.137), we find that this relation becomes

$$-m\omega^2 W(L) = -EA \cdot \frac{dW}{dz} \Big|_{z=L} .$$
(b)

Now, from (11.139) and (b), we get

$$m\omega^2(C_1 \cos \frac{\omega L}{c} + C_2 \sin \frac{\omega L}{c}) = EA \frac{\omega}{c}(-C_1 \sin \frac{\omega L}{c} + C_2 \cos \frac{\omega L}{c}).$$
(c)

For the nontrivial solutions of (a) and (c),

$$m\omega^2 \sin \frac{\omega L}{c} - EA \frac{\omega}{c} \cos \frac{\omega L}{c} = 0$$

or

$$\frac{\omega L}{c} \tan \frac{\omega L}{c} = \frac{\rho AL}{m} = \frac{m_{\text{bar}}}{m}.$$

This transcendental equation can be solved either graphically or by using a standard mathematical table.

Torsional Vibration of Shafts

Let us consider the uniform circular shaft of length L and radius r shown in Fig. 11.67a. During torsional oscillation, the line PS takes the position PS' at an instant t . If the twist at the section z is $\theta(z, t)$, the twist at the other end of the element of length dz at z is $\theta(z, t) + (\partial\theta/\partial z).dz$. The free-body diagram of the element is shown in Fig. 11.67b. The equation of motion of the element is

$$\frac{1}{2}(\pi r^2 dz \rho).r^2 \cdot \frac{\partial^2 \theta}{\partial t^2} = \frac{\partial M}{\partial z}.dz.$$
(11.145)

From the elementary theory of torsion of circular shafts,

$$M = GI_p(\partial\theta/\partial z),$$

where G is the shear modulus and I_p is the polar second moment of area of the shaft cross-section ($= \pi r^4/2$). Using this relation in (11.145) and rearranging, we find that the equation of motion in the final form is

$$\frac{\partial^2 \theta}{\partial t^2} = c_t^2 (\partial^2 \theta / \partial z^2),$$
(11.146)

where $c_t = (G/\rho)^{1/2}$ is the speed of torsional wave in the shaft.

Comparing (11.146) and (11.136), we see that the results of torsional oscillation can be found out from those of longitudinal oscillation by replacing w by θ and c by c_t .

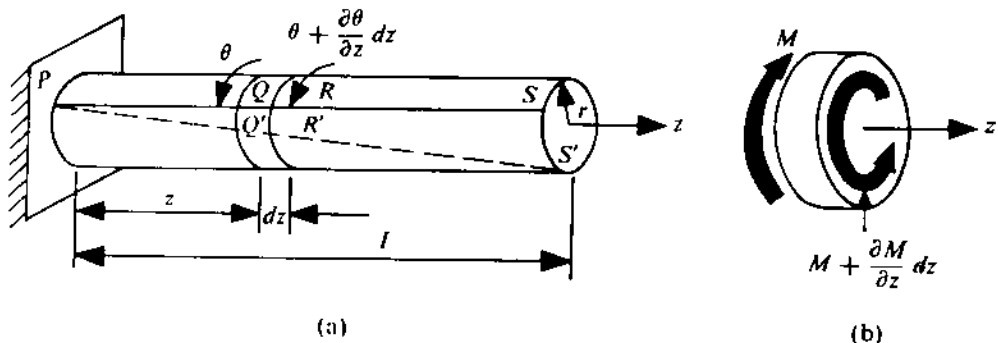


FIGURE 11.67

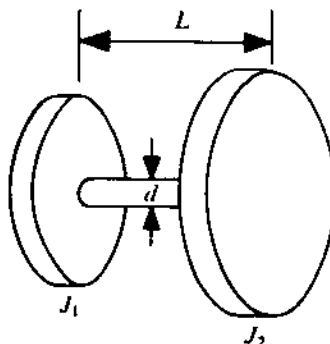


FIGURE 11.68

PROBLEM 11.34

Figure 11.68 shows two circular discs of moments of inertia J_1 and J_2 connected by a uniform circular shaft of length L and diameter d . If the shear modulus and the density of the shaft material are G and ρ , respectively, determine the natural frequencies of the system.

SOLUTION

The general solution of (11.146) can (during a normal mode oscillation) be written in the form $\theta(z, t) = \Theta(z) \cos \omega t$ which, when substituted in (11.146), yields

$$\Theta(z) = C_1 \cos(\omega/c_t)z + C_2 \sin(\omega/c_t)z. \quad (a)$$

The boundary conditions can be obtained in a manner similar to that followed in Problem 11.33. Thus,

$$J_1 \omega^2 \Theta(0) = -G I_p \frac{d\Theta}{dz} \Big|_{z=0}, \quad (b)$$

$$J_2 \omega^2 \Theta(L) = G I_p \frac{d\Theta}{dz} \Big|_{z=L} \quad (c)$$

Using (a) in (b) and (c), we get

$$C_1 \omega^2 J_1 = -C_2 (\omega/c_t) G I_p, \quad (d)$$

$$J_2\omega^2(C_1 \cos \frac{\omega L}{c_t} + C_2 \sin \frac{\omega L}{c_t}) = GI_p \cdot \frac{\omega}{c_t}(-C_1 \sin \frac{\omega L}{c_t} + C_2 \cos \frac{\omega L}{c_t}). \quad (\text{e})$$

For the nontrivial solutions of (d) and (e) to exist,

$$\begin{vmatrix} \omega^2 J_1 & GI_p \frac{\omega}{c_t} \\ (J_2\omega^2 \cos \frac{\omega L}{c_t} + GI_p \cdot \frac{\omega}{c_t} \sin \frac{\omega L}{c_t}) & (J_2\omega^2 \sin \frac{\omega L}{c_t} - GI_p \cdot \frac{\omega}{c_t} \cos \frac{\omega L}{c_t}) \end{vmatrix} = 0. \quad (\text{f})$$

Expanding and simplifying the left-hand side of this equation, the frequency equation we obtain is

$$\tan \frac{\omega L}{c_t} = (p+q) \frac{\omega L}{c_t} / \{pq(\frac{\omega L}{c_t})^2 - 1\}, \quad (\text{g})$$

where $p = J_1/(\rho L I_p)$ and $q = J_2/(\rho L I_p)$. The frequency equation can be solved either graphically or by using a numerical method.

Let us consider an extreme situation when the shaft inertia is negligible in comparison to the disc inertias. This reduces the system to a semidefinite 2DOF system whose natural frequency we found out in Problem 11.23 as

$$\omega_n = [K(J_1 + J_2)/(J_1 J_2)]^{1/2},$$

where $K = GI_p/L$. This result can also be obtained from (g) by letting p and q tend to infinity. With this extreme condition, we can rewrite (g) as

$$(\omega L/c_t) \tan (\omega L/c_t) \approx 1/q + 1/p. \quad (\text{h})$$

Since the right-hand side of this equation is very small, $\omega L/c_t$ is also small when

$$\tan (\omega L/c_t) \approx \omega L/c_t. \quad (\text{i})$$

Thus, from (h) and (i), $(\omega L/c_t)^2 \approx \rho L I_p [(J_1 + J_2)/(J_1 J_2)]$ or

$$\omega^2 \approx \frac{GI_p}{L} \left(\frac{J_1 + J_2}{J_1 J_2} \right)$$

or

$$\omega \approx \left[\frac{K(J_1 + J_2)}{J_1 J_2} \right]^{1/2}.$$

Transverse Vibration of Beams

As in bars and shafts, so too in beams, we shall assume that the deflection is small. In addition, we shall neglect the rotation of the beam elements during oscillation. We shall consider the deflections only due to the bending moment. Figure 11.69a shows the coordinate axes and the deformation of an element $PQRS$ (of length dz) at z . The free-body diagram of this element at an instant t , together with the sign convention for the bending moment M and the shear force V , is given in Fig. 11.69b. Applying Newton's second law to the element, we find that the equation of motion in the x -direction can be written as

$$\rho A dz \cdot \frac{\partial^2 x(z, t)}{\partial t^2} = \frac{\partial V}{\partial z} \cdot dz. \quad (11.147)$$

Moreover, since we are neglecting the rotational motion of the element, the total moment about the

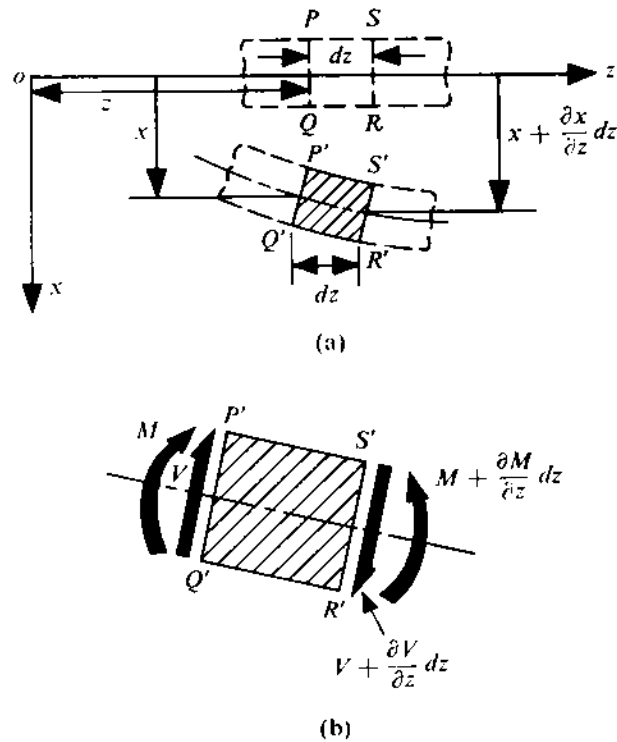


FIGURE 11.69

y-axis must be zero. Thus, $(\partial M / \partial z) \cdot dz = V \cdot dz$ or

$$V = \frac{\partial M}{\partial z}. \quad (11.148)$$

Further, from the elementary beam theory, we get (with the sign convention used)

$$M = -EI(\partial^2 x / \partial z^2), \quad (11.149)$$

where *I* is the second moment of beam cross-section about its neutral axis. Using (11.148) in (11.147) in conjunction with (11.149), the final equation of motion we obtain is

$$\frac{\partial^2 x}{\partial t^2} = -[EI/(\rho A)](\partial^4 x / \partial z^4). \quad (11.150)$$

Assuming a normal mode vibration in the form $x(z, t) = X(z) \cos \omega t$, we can rewrite the foregoing equation as

$$\frac{d^4 X}{dz^4} - \beta^4 X = 0, \quad (11.151)$$

where $\beta^4 = \omega^2 \rho A / (EI)$ or

$$\omega = \beta^2 [EI/(\rho A)]^{1/2}. \quad (11.152)$$

The general solution of (11.151) can be written as

$$X = C_1 \cosh \beta z + C_2 \sinh \beta z + C_3 \cos \beta z + C_4 \sin \beta z. \quad (11.153)$$

The values of β can be obtained when the boundary conditions of the beam are prescribed. Once the β 's are known, the natural frequencies can be computed from (11.152). Let us consider the following common types of boundary conditions:

- (i) Both ends simply-supported: In this situation, the deflections and the bending moments at the support cross-sections must be equal to zero. Thus, at such ends,

$$x = 0, \quad M = 0 \quad \text{for all } t.$$

This implies $X = 0$ and $d^2X/dz^2 = 0$ at the simply-supported ends. Therefore, the boundary conditions can be written as

$$X(0) = 0, \quad \left. \frac{d^2X}{dz^2} \right|_{z=0} = 0, \quad X(L) = 0, \quad \left. \frac{d^2X}{dz^2} \right|_{z=L} = 0.$$

Substituting these conditions in (11.153), we get, for the nontrivial solutions, $\sin \beta L = 0$ or

$$\beta_i = i\pi/L \quad (i = 1, 2, 3, \dots). \quad (11.154)$$

Hence, using (11.152) in (11.154), we find the natural frequencies come out as

$$\omega_i = \frac{i^2\pi^2}{L^2} \left(\frac{EI}{\rho A} \right)^{1/2} \quad (i = 1, 2, 3, \dots).$$

- (ii) One end fixed and the other end free (cantilever): When one end of the beam is clamped, both x and $\partial x/\partial z$ should be zero for all t . This yields, at the clamped end,

$$X = 0, \quad dX/dz = 0.$$

For the free end of the beam, the bending moment and the shear force are zero which yield $\partial^2x/\partial z^2 = \partial^3x/\partial z^3 = 0$ for all t [see (11.148) and (11.149)]. Thus, for such an end,

$$d^2X/dz^2 = 0, \quad d^3X/dz^3 = 0.$$

Therefore, the boundary conditions can be written as

$$X(0) = 0, \quad \left. \frac{dX}{dz} \right|_{z=0} = 0, \quad \left. \frac{d^2X}{dz^2} \right|_{z=L} = 0, \quad \left. \frac{d^3X}{dz^3} \right|_{z=L} = 0.$$

Using these conditions in (11.153) and considering the nontrivial solutions, the frequency equation we get has the form

$$\cos \beta L \cosh \beta L = -1. \quad (11.155)$$

The first three roots of this equation are

$$\beta_1 L = 1.876, \quad \beta_2 L = 4.733, \quad \beta_3 L = 7.855.$$

For $i > 3$, the roots of (11.155) can be approximated as

$$\beta_i L \approx \left(i - \frac{1}{2} \right) \pi. \quad (11.156)$$

- (iii) Both ends fixed: Proceeding in a manner similar to that in (i) and (ii), the frequency equation we obtain is

$$\cos \beta L \cosh \beta L = 1. \quad (11.157)$$

The first three roots and the asymptotic solutions of (11.157) are

$$\beta_1 L = 4.733, \quad \beta_2 L = 7.855, \quad \beta_3 L = 11, \quad \beta_i L \approx \left(i + \frac{1}{2} \right) \pi, \quad i > 3. \quad (11.158)$$

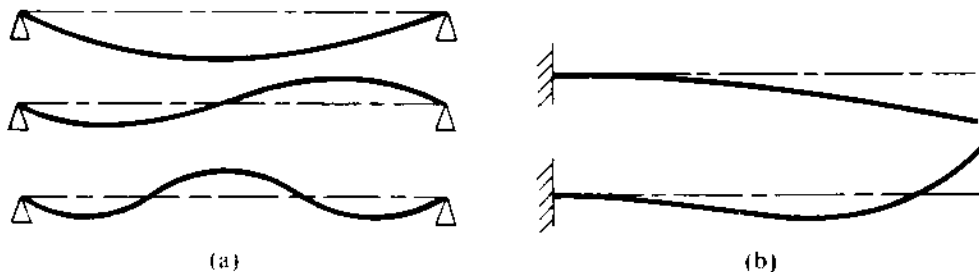


FIGURE 11.70

(iv) One end fixed and the other end simply-supported: Here, the frequency equation is given by

$$\tan \beta L = \tanh \beta L. \quad (11.159)$$

The first three roots and the asymptotic solutions of (11.159) are

$$\beta_1 L = 3.924, \quad \beta_2 L = 7.071, \quad \beta_3 L = 10.198, \quad \beta_i L \approx (i + \frac{1}{4})\pi, \quad i > 3. \quad (11.160)$$

Normal Modes

In a simply-supported beam, the i -th normal mode is obtained as

$$X^{(i)} = C_4^{(i)} \sin \beta_i z.$$

Using (11.154) in this equation, we get

$$X^{(i)} = C_4^{(i)} \sin (i\pi z/L). \quad (11.161)$$

The first three normal modes of a simply-supported beam are shown in Fig. 11.70a.

For boundary conditions of a beam other than the one simply-supported at both ends, the mode shapes cannot be expressed by a simple trigonometric function, and they include the hyperbolic functions as well. The approximate nature of the first and the second modes of a cantilever beam is shown in Fig. 11.70b.

PROBLEM 11.35

Figure 11.71 shows a uniform beam of length L and flexural rigidity EI . One end of the beam is clamped, whereas its other end is supported on a spring of stiffness k . Determine the frequency equation.

SOLUTION

The boundary conditions at the left end can directly be written as

$$X(0) = 0, \quad \left. \frac{dX}{dz} \right|_{z=0} = 0.$$

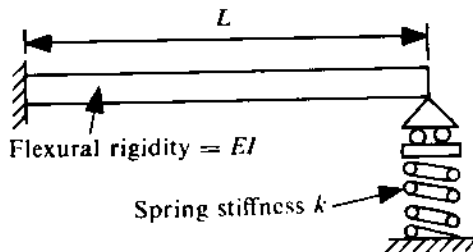


FIGURE 11.71

at $z = L$, the moment is zero but the shear force is $-kX(L)$. The reader is advised to check the sign of the shear force. Thus, the boundary conditions can be written as

$$\frac{d^2X}{dz^2} \Big|_{z=L} = 0, \quad \frac{d^3X}{dz^3} \Big|_{z=L} = \frac{k}{EI} X(L).$$

Substituting these conditions in (11.153), we get

$$C_1 + C_3 = 0,$$

$$C_2 + C_4 = 0,$$

$$C_1 \cosh \beta L + C_2 \sinh \beta L - C_3 \cos \beta L - C_4 \sin \beta L = 0,$$

$$C_1 \sinh \beta L + C_2 \cosh \beta L + C_3 \sin \beta L - C_4 \cos \beta L$$

$$= \frac{k}{EI\beta^3} (C_1 \cosh \beta L + C_2 \sinh \beta L + C_3 \cos \beta L + C_4 \sin \beta L).$$

For the nontrivial solution of these equations,

$$\begin{vmatrix} 1 & 0 & 1 & 0 \\ 0 & 1 & 0 & 1 \\ \cosh \beta L & \sinh \beta L & -\cos \beta L & -\sin \beta L \\ (\sinh \beta L - \alpha \cosh \beta L) & (\cosh \beta L - \alpha \sinh \beta L) & (\sin \beta L - \alpha \cos \beta L) & (-\cos \beta L - \alpha \sin \beta L) \end{vmatrix} = 0,$$

where $\alpha = k/(EI\beta^3)$. This equation can be finally reduced to the form

$$1 + \cosh \beta L \cos \beta L + \alpha(\sin \beta L \cosh \beta L - \cos \beta L \sinh \beta L) = 0.$$

We can easily verify the limiting cases. When $k = 0 = \alpha$, the system is reduced to a cantilever beam and the frequency equation is given by (11.155). On the other hand, when k is very large, the end with the spring can be considered to be simply-supported and the corresponding frequency equation is given by (11.159).

11.7 APPROXIMATE METHODS

Quite often, free vibration of a continuous system is not amenable to a closed-form analytical treatment outlined in Section 11.6. For example, if a bar, shaft, or beam is of nonuniform cross-section, the frequency equation cannot be derived in most situations. In such an instance, an approximate method can be very helpful in estimating the natural frequencies with a high accuracy. However,

a knowledge of the fundamental frequency is more important when designing a mechanical system. For this, a number of powerful approximate methods are available. Of these, we shall discuss on a few commonly-used ones with reference to the vibrations of a beam. Of course, these methods can also be readily applied to other types of problems. We shall also briefly discuss a method that determines not only the fundamental frequency but also the higher natural frequencies.

Rayleigh's Method

Let us consider a nonuniform beam of cross-sectional area $A(z)$ and length L . The normal mode vibration of such a beam can be represented by $X(z) \cos \omega t$. In the absence of any knowledge about $X(z)$, the normal mode is assumed to be $X_a(z)$. With this assumed mode shape, the maximum T of the beam during vibration can be written as

$$T_{\max} = \frac{1}{2}\omega^2 \int_0^L \rho A(z) X_a^2(z) dz. \quad (11.16)$$

Again, the maximum strain energy stored in the beam during this vibration can be expressed as¹¹

$$U_{\max} = \frac{1}{2} \int_0^L EI(z) \left(\frac{d^2 X_a}{dz^2} \right)^2 dz. \quad (11.16)$$

If the assumed mode shape $X_a(z)$ is correct, then, during vibration without damping, $T_{\max} = U_{\max}$ or

$$\omega^2 = \frac{\int_0^L EI(z) \left(\frac{d^2 X_a}{dz^2} \right)^2 dz}{\int_0^L \rho A(z) X_a^2 dz} \quad (11.16)$$

gives the natural frequency *corresponding* to the mode shape. If the assumed mode $X_a(z)$ is not exactly correct, then the right-hand side of (11.164) is called *Rayleigh's quotient*, R . This quotient has the following interesting and useful properties (stated without proof):

- (i) R is stationary at the normal modes with a minimum at the first mode.
- (ii) If $X_a(z)$ is not correct (but satisfies the boundary conditions) and its deviation from the correct mode shape is of the order of ϵ , then R deviates from the square of the natural frequency corresponding to $X_a(z)$ by an order of ϵ^2 , i.e., if $X_a(z) - X(z) = O(\epsilon)$, then $|R - \omega^2| = O(\epsilon^2)$.

These properties of R are used in various approximate methods.

In Rayleigh's method, the first mode shape is so assumed that it satisfies as many boundary conditions as possible. Normally, the boundary conditions are classified into two groups, viz., (i) geometric, and (ii) natural (or force). The first category includes conditions on deflection and slope, whereas the second category includes those on prescribed shear force and bending moment. It is essential for the chosen mode to satisfy the geometric boundary conditions. Obviously, the accuracy of the result will be more if the natural (or force) boundary conditions are also satisfied. It is clear from the second property of R that, with any reasonable choice of the mode shape, R provides the natural frequency quite accurately. This method is used for determining only the first natural frequency as it is difficult to make a reasonable guess about the mode corresponding to a higher frequency. The first mode shape can be assumed to be given by the static deflection curve which is very easy to determine or guess. Again, the first property of R indicates that the first natural frequency, obtained with any assumed mode shape, will always be higher than the exact value.

¹¹For a bar or shaft, the corresponding expression for strain energy has to be used. The rest of the procedure remains the same.

PROBLEM 11.36

Determine the natural frequencies and normal modes of the system shown in Fig. 11.52a using Rayleigh's principle.

SOLUTION

Let the normal modes be $x_1 = X_1 \cos \omega t$ and $x_2 = X_2 \cos \omega t$ with $\lambda = X_2/X_1$. The maximum potential energy

$$U_{\max} = \frac{1}{2}kX_1^2 + \frac{1}{2}kX_2^2 + \frac{1}{2}k(X_2 - X_1)^2 = \frac{k}{2}X_1^2[1 + \lambda^2 + (\lambda - 1)^2].$$

Thus, Rayleigh's quotient

$$R = \frac{\frac{k}{2}X_1^2[1 + \lambda^2 + (\lambda - 1)^2]}{\frac{1}{2}mX_1^2 + \frac{1}{2}mX_2^2} = \frac{k}{m} \frac{1 + \lambda^2 + (\lambda - 1)^2}{1 + \lambda^2}. \quad (a)$$

From Rayleigh's principle, $\frac{\partial R}{\partial \lambda} = 0$, i.e.,

$$(1 + \lambda^2)[2\lambda + 2(\lambda - 1)] - [1 + \lambda^2 + (\lambda - 1)^2]2\lambda = 0$$

or

$$\lambda^2 = 1$$

or

$$\lambda = \pm 1.$$

Substituting these values of λ in (a), we get

$$R_{\min} \text{ (at } \lambda = 1) = k/m,$$

$$R_{\max} \text{ (at } \lambda = -1) = 3k/m.$$

Thus, the first natural frequency $\omega_1 = \sqrt{\frac{k}{m}}$ with $\frac{X_2}{X_1} = 1$ and the second natural frequency $\omega_2 = \sqrt{\frac{3k}{m}}$ with $\frac{X_2}{X_1} = -1$. The reader is advised to calculate the approximate value of ω_1 with an assumed mode $\lambda = 1.5$, i.e., with a 50% error in the assumed mode shape.

PROBLEM 11.37

Determine the first natural frequency of a uniform, simply-supported beam by Rayleigh's method assuming the mode shapes

$$X_a(z) = \frac{C}{L}(L - z)z, \quad (a)$$

$$X_a(z) = \frac{C}{L^3}(L^3z - 2Lz^3 + z^4), \quad (b)$$

$$X_a(z) = CL \sin(\pi z/L), \quad (c)$$

where C is a nondimensional constant.

SOLUTION

Substituting the given expressions for $X_a(z)$ in (11.164), we get the results

$$\omega_1 = 10.9545 [EI/(\rho AL^4)]^{1/2}, \quad (a)$$

$$\omega_1 = 9.8766 [EI/(\rho AL^4)]^{1/2}, \quad (b)$$

$$\omega_1 = 9.8696 [EI/(\rho AL^4)]^{1/2}. \quad (c)$$

It should be noted that in (a) only the geometric boundary conditions have been satisfied, and in (b) all the boundary conditions have been satisfied. Further, (c) represents the actual mode shape. The percentage errors for (a) and (b) are 11 and 0.07, respectively.

PROBLEM 11.38

Determine the first natural frequency of the tapered cantilever beam shown in Fig. 11.72.

SOLUTION

Let us assume the mode shape $X_a(z) = C(1 - z/L)^2$, where C is a constant with the dimension of length. This assumed mode satisfies all the boundary conditions. (It should be noted that at $z = 0, I = 0$.) Substituting in (11.164) the expression for $X_a(z)$, $I(z) = Bz^3H^3/(12L^3)$, and $A(z) = BzH/L$, we get

$$\omega_1 = 2.74 \frac{H}{L^2} \left(\frac{E}{3\rho} \right)^{1/2} = 1.582 \frac{H}{L^2} \left(\frac{E}{\rho} \right)^{1/2}.$$

It is possible here to work out the exact natural frequency. The value of ω_1 we have found is 3% higher than the exact value.

Obviously, in the absence of a knowledge of the exact value of ω_1 (which is quite often the situation), various mode shapes $X_a(z)$ can be assumed. The lowest value of ω_1 that is thus obtained is closest to the exact result.

Rayleigh's Method with Grammel's Modification

The accuracy of the result obtained by Rayleigh's method can be improved if the method is modified as follows. Let the maximum intensity of the distributed inertial loading be $\rho A(z)\omega^2 X_a(z)$. Also, let $M(z)$ be the bending moment due to this distributed loading. Then, the strain energy U_{\max} can be written as

$$U_{\max} = \int_0^L \frac{M^2(z) dz}{2EI(z)}. \quad (11.165)$$

Equating U_{\max} with T_{\max} given by (11.162), we have

$$\omega^2 = \frac{\int_0^L \frac{M^2(z) dz}{EI(z)}}{\int_0^L \rho A(z) X_a^2(z) dz}. \quad (11.166)$$

The reason the result gets improved is that no differentiation of the assumed mode is required. But, of course, this modified method involves more numerical computations.

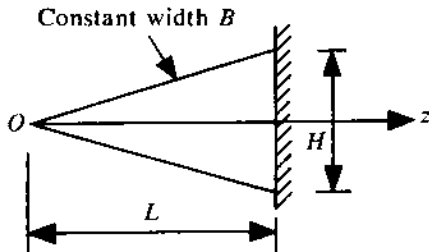


FIGURE 11.72

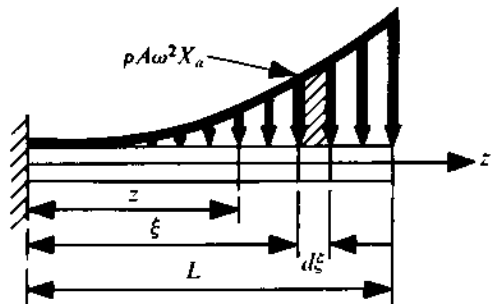


FIGURE 11.73

PROBLEM 11.39

Determine the first natural frequency of a uniform cantilever beam of length L and flexural rigidity EI . The cross-sectional area of the beam is A and the density of the beam material is ρ . Use both Rayleigh's method and modified Rayleigh's method assuming the mode shape to be $X_a(z) = Cz^2$ with $z = 0$ as the fixed end. Compare the results so obtained with the exact first natural frequency.

SOLUTION

It should be noted that the assumed mode satisfies the geometric conditions. Using the given expression for $X_a(z)$ in (11.164), we have

$$\omega_1^2 = 20EI/(\rho AL^4). \quad (\text{a})$$

Now, let us follow modified Rayleigh's approach. The bending moment at z can be found out (see Fig. 11.73) as

$$M(z) = -\rho A \omega^2 \int_z^L X_a(\xi)(\xi - z) d\xi. \quad (\text{b})$$

Using the assumed mode shape $X_a(z) = Cz^2$ in (b), we get

$$M(z) = -\frac{C\rho A \omega^2}{12}(z^4 - 4zL^3 + 3L^4). \quad (\text{c})$$

Now, substituting this expression in (11.166), we obtain

$$\omega_1^2 = 12.46EI/(\rho AL^4). \quad (\text{d})$$

The exact value can be found out by using (11.152) with $\beta_1 = 1.876/L$. This gives

$$\omega_1^2 = 12.387EI/(\rho AL^4). \quad (\text{e})$$

So, the drastic improvement in the result arrived at using the modification will be obvious if we compare (a) and (d) with (e).

Rayleigh-Ritz Method

The first property of Rayleigh's quotient, R , is utilized in the Rayleigh-Ritz method. Here, the assumed displacement function is written in the form

$$X_a(z) = \sum_{i=1}^N C_i X_i(z), \quad (11.167)$$

where the $X_i(z)$'s satisfy the boundary conditions. As already mentioned, the assumed mode must satisfy the geometric boundary conditions, and if it satisfies all the boundary conditions, a better result is obtained. Substituting (11.167) in (11.164), we find Rayleigh's quotient assumes the form

$$R = R(C_1, C_2, C_3, \dots, C_N). \quad (11.168)$$

The constants C_i 's should be such that they make R a minimum, i.e.,

$$\frac{\partial R}{\partial C_i} = 0 \quad (i = 1, 2, \dots, N). \quad (11.169)$$

To get the nontrivial solutions of C_i 's from (11.169), the coefficient determinant is set equal to zero. This gives the frequency equation (of order ω^{2N}). Rewriting (11.164) as

$$R = \frac{\int_0^L EI(z) \left(\frac{d^2 X_a}{dz^2} \right)^2 dz}{\int_0^L \rho A(z) X_a^2 dz}, \quad (11.170)$$

(11.169) yields

$$\left[\int_0^L \rho A(z) X_a^2 dz \right] \left[\frac{\partial}{\partial C_i} \int_0^L EI(z) \left(\frac{d^2 X_a}{dz^2} \right)^2 dz \right] - \left[\int_0^L EI(z) \left(\frac{d^2 X_a}{dz^2} \right)^2 dz \right] \left[\frac{\partial}{\partial C_i} \int_0^L \rho A(z) X_a^2 dz \right] = 0. \quad (11.171)$$

Using (11.164) in (11.171), we get

$$\frac{\partial}{\partial C_i} \int_0^L [EI(z) \left(\frac{d^2 X_a}{dz^2} \right)^2 - \omega^2 \rho A(z) X_a^2] dz = 0 \quad (i = 1, 2, 3, \dots). \quad (11.172)$$

This equation is another form of (11.169).

If N terms are used in (11.167), the first $(N - 1)$ natural frequencies can be determined quite accurately.

PROBLEM 11.40

Determine the first two natural frequencies of the tapered cantilever beam shown in Fig. 11.72 using the Rayleigh-Ritz method.

SOLUTION

We have to use at least a two-term series for $X_a(z)$ in (11.167). But it is obvious that with such a series the second natural frequency will not come out very accurately. Let us assume

$$X_1(z) = (1 - \frac{z}{L})^2,$$

$$X_2(z) = \frac{z}{L}(1 - \frac{z}{L})^2.$$

Substituting these expressions in (11.167) and using the resulting expression for $X_a(z)$ in the left-hand side of (11.172), we get

$$\frac{\partial}{\partial C_i} \left[\left\{ (C_1 - 2C_2)^2 + \frac{24}{5} C_2 (C_1 - 2C_2) + 6C_2^2 \right\} \frac{H^2 E}{12L^3} - \omega^2 \rho H L \left(\frac{C_1^2}{30} + \frac{2C_1 C_2}{105} + \frac{C_2^2}{280} \right) \right] = 0 \quad (i = 1, 2).$$

Differentiating this equation and simplifying, the two equations in C_1 and C_2 we obtain are

$$\left(\frac{EH^2}{12\rho L^4} - \frac{\omega^2}{30}\right)C_1 + \left(\frac{EH^2}{30\rho L^4} - \frac{\omega^2}{105}\right)C_2 = 0,$$

$$\left(\frac{EH^2}{30\rho L^4} - \frac{\omega^2}{105}\right)C_1 + \left(\frac{EH^2}{30\rho L^4} - \frac{\omega^2}{280}\right)C_2 = 0.$$

For the nontrivial solution of these equations,

$$\begin{vmatrix} \left(\frac{EH^2}{12\rho L^4} - \frac{\omega^2}{30}\right) & \left(\frac{EH^2}{30\rho L^4} - \frac{\omega^2}{105}\right) \\ \left(\frac{EH^2}{30\rho L^4} - \frac{\omega^2}{105}\right) & \left(\frac{EH^2}{30\rho L^4} - \frac{\omega^2}{280}\right) \end{vmatrix} = 0$$

or

$$0.2835\omega^4 - 7.7381\lambda\omega^2 + 16.6667\lambda^2 = 0,$$

where $\lambda = EH^2/(\rho L^4)$. Solving this quadratic equation in ω^2 , the two natural frequencies we get are

$$\omega_1 = 1.535 \frac{H}{L^2} \left(\frac{E}{\rho}\right)^{1/2},$$

$$\omega_2 = 4.994 \frac{H}{L^2} \left(\frac{E}{\rho}\right)^{1/2}.$$

The improvement in the accuracy of ω_1 can be seen by comparing it with the result obtained in Problem 11.38. The error here is only 0.1%.

11.8 VIBRATION MEASURING INSTRUMENTS

The vibratory response of a system can be expressed in terms of various parameters, e.g., displacement, velocity, acceleration, and induced stress. The choice of the quantity depends on the objective and the field of application. For example, the vibration in a vehicle is normally expressed in terms of the acceleration which is related to the passenger comfort. On the other hand, if the fatigue failure of an element is of primary importance, it should then be expressed in terms of the dynamic stresses. To measure a parameter, a pick-up (transducer) is used. This instrument generates a voltage proportional to the magnitude of the parameter. In this section, we shall briefly discuss some of the commonly-used transducers.

Frequency Measurement

Very often, a direct measurement of the predominant frequencies of vibration is useful for detecting the source of vibration and for properly designing a system. To do this, a simple instrument, based on the principle of resonance and known as the reed frequency meter, is used. This basic principle can be readily understood from Fig. 11.74. The length of the cantilever portion of the vibrating reed can be varied by rotating the control knob. If the frequency of the vibrating surface coincides with the natural frequency of the reed, resonance of the reed takes place. This is detected visually and the reading from the frequency scale (which is calibrated) is directly obtained. This instrument can measure a frequency ranging from 2 Hz to 250 Hz. When a frequency in the range 2-10 Hz has to be measured, a standard mass is attached to the tip of the reed. Since the natural frequency of a cantilever is proportional to $1/L^2$, the sensitivity of this instrument is low at a high frequency.

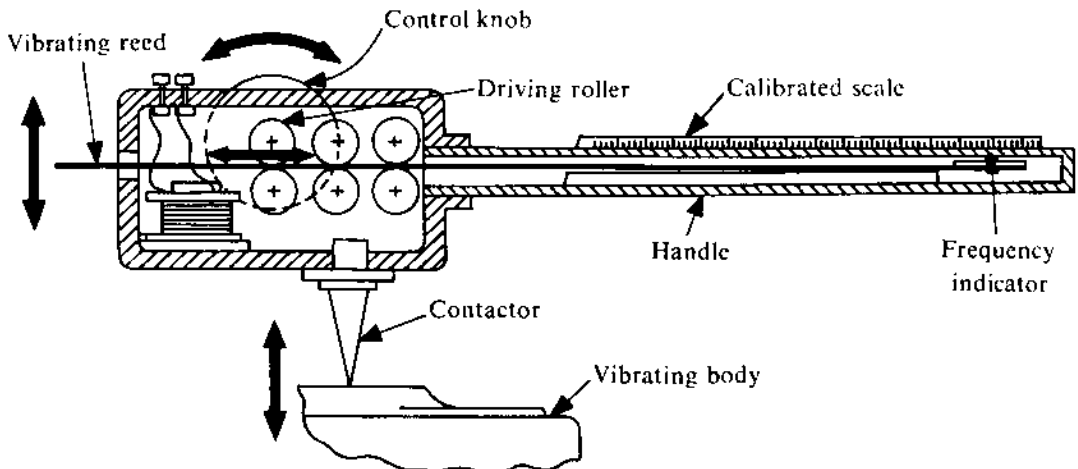


FIGURE 11.74

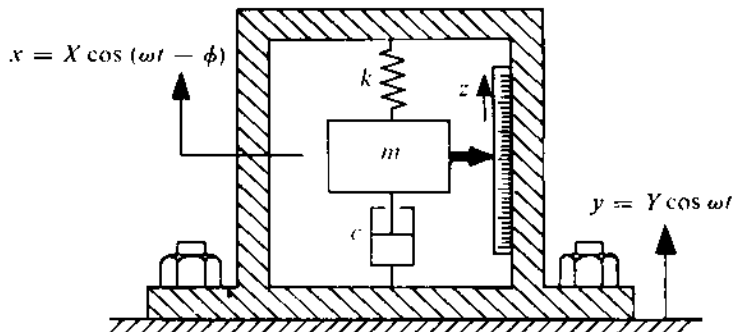


FIGURE 11.75

Vibration Pick-ups

The vibration pick-ups can be classified into two broad groups, viz., (i) contacting-type, and (ii) noncontacting-type. Obviously, a pick-up belonging to the first category can be used for a system whose characteristics remain unaffected when the pick-up is attached to it. There is no limit on the amount of movement of the vibratory system that can be measured by such a pick-up. On the other hand, a noncontacting transducer should be used for a very light and flexible system having a small movement. Each of categories (i) and (ii) can be further classified as passive and active. In a passive pick-up, no separate power source is necessary for the operation, whereas in an active pick-up, a separate power source has to be used.

A contacting-type transducer can be so designed that it generates an electrical signal proportional either to the velocity or the acceleration of oscillation. The signal so generated can be integrated to give the displacement. The theory underlying the design of this type of pick-up can be easily understood from the analysis of an SDF system with base excitation.

Figure 11.75 schematically represents a contacting-type pick-up as an SDF system connected to a surface whose motion y has to be measured. Comparing this figure with Fig. 11.38, we see that the equation of motion of the pick-up mass is given by (11.44), where x represents its absolute motion. Defining the relative movement of m with respect to the pick-up body (i.e., to the vibrating surface)

as $z = x - y$, we can rewrite (11.44) as

$$m\ddot{z} + c\dot{z} + kz = -m\ddot{y}. \quad (11.173)$$

Assuming the steady-state solution

$$z = Z \cos(\omega t - \psi) \quad (11.174)$$

and substituting for y ($= Y \cos \omega t$) in (11.173), we get

$$Z = \frac{r^2 Y}{[(1 - r^2)^2 + (2\zeta r)^2]^{1/2}}, \quad (11.175)$$

$$\psi = \tan^{-1} \left(\frac{2\zeta r}{1 - r^2} \right), \quad (11.176)$$

where $r = \omega/\omega_n = \omega/(k/m)^{1/2}$ and $\zeta = c/[2(km)^{1/2}]$. Thus, if the pick-up system is so designed that $r \gg 1$, then

$$Z \approx Y \quad (11.177)$$

since only the term r^4 in the denominator of the right-hand side of (11.175) need be considered. With $r \gg 1$,

$$\psi \approx \pi. \quad (11.178)$$

Hence, the relative movement z represents the motion of the vibrating surface y with a phase difference of 180° . However, in a real-life pick-up, z is not measured mechanically as has been suggested in Fig. 11.75. In fact, it is measured by having a magnet fixed to the container (representing the scale) and a coil connected to m . Due to the relative movement between the coil and the magnet, a voltage is induced across the coil. This voltage is proportional to the relative velocity \dot{z} ($\approx -\dot{y}$). Thus, if the natural frequency ω_n of the pick-up is much lower than that of the vibration to be measured, the pick-up acts as a velocity transducer. The graphical representation of (11.175) has been given in Fig. 11.76. It is evident from this figure that the range of frequency for which y can be approximated by z is maximum when $\zeta = 0.707$. In a real-life pick-up, ζ is kept nearer this value and the transducer can be used in the frequency range $\omega > 2.5\omega_n$. A pick-up with a low natural frequency (2-5 Hz) is commonly known as a seismometer. One obvious drawback of such a transducer is its big size (required to allow the relative movement \approx actual movement).

If a pick-up is designed such that $r \ll 1$, it can then be used to generate a signal proportional to the acceleration of the vibrating surface as now explained. Rewriting (11.175) as

$$\omega_n^2 Z = \frac{\omega^2 Y}{[(1 - r^2)^2 + (2\zeta r)^2]^{1/2}} \quad (11.179a)$$

for $r \ll 1$, we get

$$Z \approx \omega^2 Y / \omega_n^2. \quad (11.179b)$$

Thus, the relative movement is proportional to the acceleration of the surface since ω_n is constant for a given pick-up. So, to use the pick-up as an accelerometer, two conditions have to be satisfied, viz., (i) its natural frequency ω_n should be very high, and (ii) it should generate a signal proportional to the relative displacement z . A piezoelectric crystal satisfies both these requirements because it is very stiff (i.e., has a high ω_n) and produces a signal proportional to its deformation. Figure 11.77 schematically shows the construction of a piezoelectric accelerometer. The typical values of the natural frequency of such a pick-up are in the MHz range. (This pick-up can be used to measure a

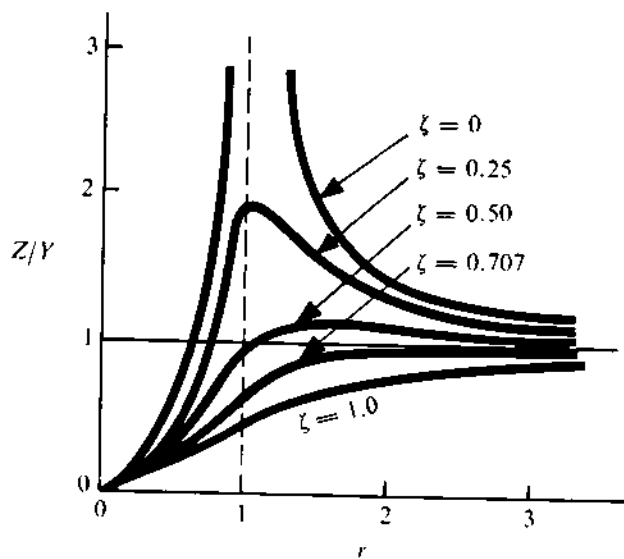


FIGURE 11.76

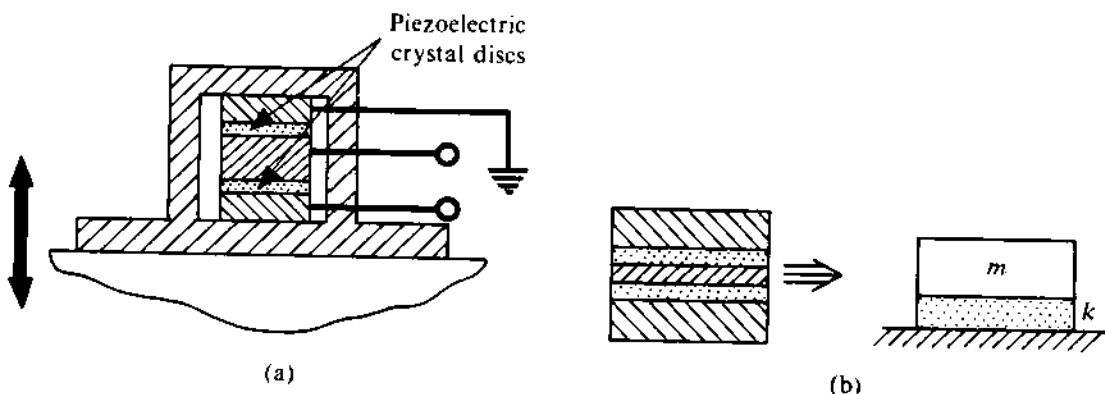


FIGURE 11.77

frequency up to a few kHz.) Further, from (11.179b), it should be noted that for such a high value of ω_n , Z is extremely small. However, a piezoelectric crystal is capable of generating a measurable signal even for such a small deformation. We shall discuss the sensitivity of this type of pick-up later in this section.

Let us now plot $\omega_n^2 Z/\text{acceleration amplitude } (\omega^2 Y)$, and ψ against r (Fig. 11.78) for various values of ζ . As can be seen, the range of operating frequency for the accelerometer we have described is maximum, again, when $\zeta = 0.707$. There is another important aspect of this value of the damping factor, namely, the phase difference (see Fig. 11.78b) varies linearly with the exciting frequency ω (since ω_n is constant for a given pick-up). Let an accelerometer be used for measuring a periodic (nonharmonic) motion $y(t)$ with a time period $2\pi/\omega_0$, where

$$y(t) = \sum_{p=1}^{\infty} A_p \cos p\omega_0 t.$$

For each Fourier component of $y(t)$, the corresponding signal generated will be of the form

$$S_p(t) \propto (p\omega_0)^2 A_p \cos(p\omega_0 t - \psi_p),$$

where $\psi_p \propto p\omega_0$ (if $\zeta = 0.707$). Thus, the resultant signal is

$$S(t) \propto \sum_{p=1}^{\infty} (p\omega_0)^2 A_p \cos p\omega_0(t - \lambda),$$

where $\lambda = \psi_p/(p\omega_0)$. Again, from the expression for $y(t)$, we see that

$$\ddot{y}(t) = - \sum_{p=1}^{\infty} (p\omega_0)^2 A_p \cos p\omega_0 t.$$

Comparing the expressions for $\ddot{y}(t)$ and $S(t)$, we find that the form of $\ddot{y}(t)$ is faithfully represented (without distortion) by $S(t)$.

Let us now estimate the order of sensitivity of the two-disc accelerometer shown in Fig. 11.77a. If the diameter and the thickness of the piezoelectric discs are d and t , respectively, then the stiffness of each disc is given by $k_d = E\pi d^2/(8t)$, where E is the modulus of elasticity of the piezoelectric material. With two discs in series (as shown), the resultant stiffness of the system (Fig. 11.77b) is

$$k = k_d/2 = E\pi d^2/(16t). \quad (11.180)$$

If the total effective mass of the system is m , then the force transmitted through the piezodiscs is

$$F = m\ddot{y} \quad (\text{since the relative movement } z \text{ tends to zero with } r \gg 1). \quad (11.181)$$

So, the total charge produced by the two discs is

$$q = 2\chi F, \quad (11.182)$$

where χ is the piezoelectric constant of the material. The capacitance of a pick-up having two discs in parallel (electrically) is

$$C = \epsilon\pi d^2/(2t), \quad (11.183)$$

where ϵ is the dielectric constant of the piezoelectric material. The charge sensitivity of the pick-up, s_c , is given by

$$s_c = q/\ddot{y}. \quad (11.184)$$

The open circuit voltage is

$$e_o = q/C. \quad (11.185)$$

So, the voltage sensitivity, s_v , of the pick-up can be found out as

$$s_v = e_o/\ddot{y} = q/(C\ddot{y}) = s_c/C. \quad (11.186)$$

PROBLEM 11.41

A seismic vibration pick-up for measuring velocity has a natural frequency of 5 Hz and a damping factor $\zeta = 0.6$. Determine the lowest frequency vibration it can measure if the allowable error is 2%. If the allowable error is 5%, then what is the lowest frequency?

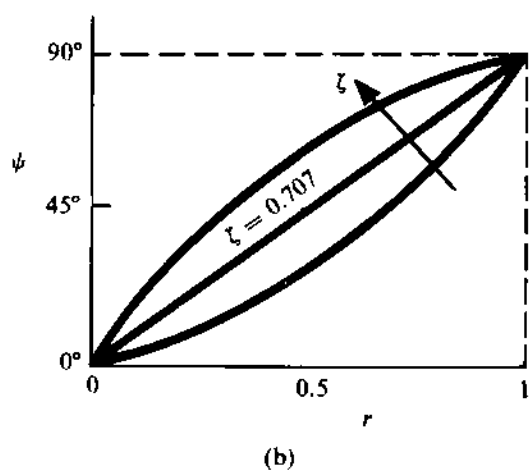
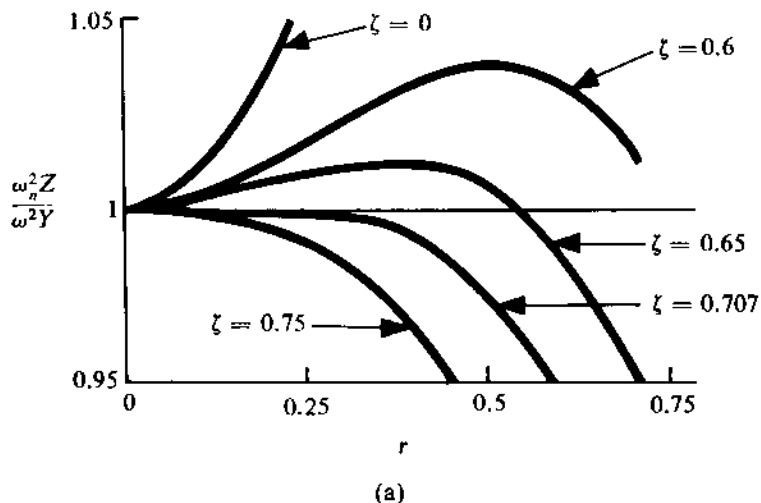


FIGURE 11.78

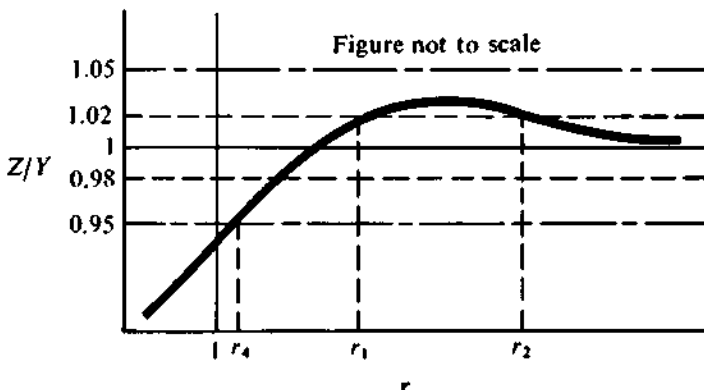


FIGURE 11.79

SOLUTION

A careful examination of Fig. 11.77 or (11.175) reveals that, for $\zeta < 0.707$, Z approaches Y from above with increasing r . For $\zeta = 0.6$ and with 2% error, one possibility is $Z/Y = 1.02$, the other being $Z/Y = 0.98$. We examine these two cases separately.

From (11.175) with $Z/Y = 1.02$, we get

$$\frac{r^2}{[(1-r^2)^2 + (1.2r)^2]^{1/2}} = 1.02.$$

Solving this equation, we obtain two roots, r_1 and r_2 (see Fig. 11.79). The values of r_1 and r_2 are 1.43 and 3.52, respectively. From Fig. 11.79, it is obvious that the error between r_1 and r_2 is more than 2%. So, the lowest frequency of vibration that can be measured, ensuring the error to be less than 2%, is $f_n r_2 = 5 \times 3.52 = 17.6$ Hz.

If the error is 5%, then it can be seen that $Z/Y = 1.05$ does not yield any real value for r^2 . This indicates that Z/Y can never reach 1.05 as shown in Fig. 11.79. Therefore, we solve for the situation $Z/Y = 0.95$. Substituting this value in (11.175), we get

$$\frac{r^2}{[(1-r^2)^2 + (1.2r)^2]^{1/2}} = 0.95.$$

The solution of this equation yields only one real value of r ($= r_4$ in Fig. 11.79) equal to 1.185. Thus, the required minimum frequency of vibration is given by $f_n r = 5 \times 1.185 = 5.925$ Hz.

PROBLEM 11.42

For a two-disc piezoelectric pick-up, the constants and dimensions are $E = 10^{11}$ N/m², $\chi = 10^{-10}$ C/N, $\epsilon = 10^{-8}$ F/m, $d = 6$ mm, and $t = 0.5$ mm. Determine the voltage sensitivity of the pick-up in mV/g if the effective mass is 2 gm.

SOLUTION

Using (11.181)-(11.186), we get

$$s_v = \frac{4\chi mt}{\epsilon \pi d^2}.$$

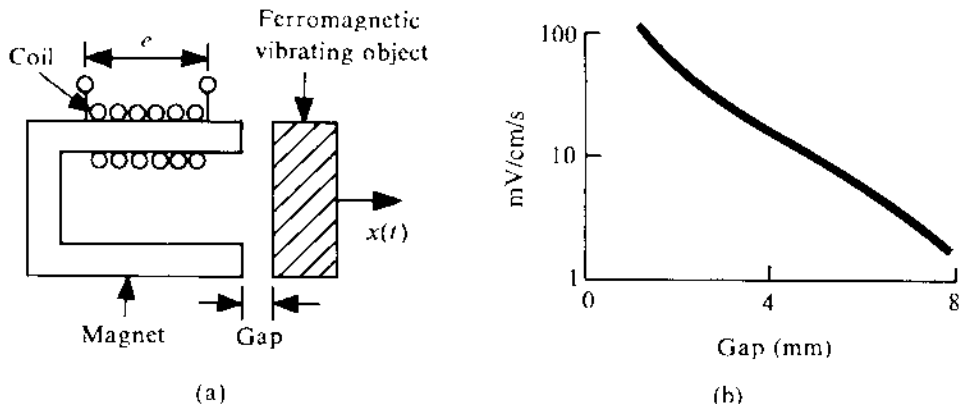


FIGURE 11.80

Substituting in it the given values, we obtain

$$s_v = \frac{4 \times 10^{-10} \times 2 \times 10^{-3} \times 0.5 \times 10^{-3}}{10^{-8} \times \pi \times (6 \times 10^{-3})^2} = 0.000354 \text{ V/m/s}^2.$$

Converting the unit to mV/g, we have $s_v = 3.47 \text{ mV/g}$. The natural frequency of this pick-up can be calculated and is found to be of the order of 10^5 Hz . If a damping factor of the order of 0.707 is provided, the frequency up to which the pick-up can be used with 1% error can be obtained from (11.179a). This is found to be the order of 35 kHz . However, there is also a limit to the lowest frequency, which is imposed by the circuit used to amplify the piezoelectric signal. This is normally around 2-5 Hz.

Electromagnetic Pick-up

The electromagnetic pick-up is schematically shown in Fig. 11.80a. The changing air gap between the vibrating surface and the pick-up changes the magnetic reluctance of the path. As a result, the magnetic flux cutting across the coil changes, thus generating a voltage. Since this voltage, e , is proportional to the rate of change of flux, ϕ , and the number of coils, N ,

$$e = -N(d\phi/dt) = -N(d\phi/dx)\dot{x}.$$

For a given range of the gap, $d\phi/dx$ remains essentially constant, so the generated voltage is proportional to the velocity of oscillation. Normally, the gap is maintained within 3-5 mm and should be several times the amplitude of vibration. A typical plot of the voltage induced per unit velocity (in cm/s) versus the gap is shown in Fig. 11.80b. As the sensitivity changes with the gap, the characteristic of the pick-up is, obviously, nonlinear. This introduces a distortion in the output signal. The typical frequency range of operation of such a transducer is 0-2 kHz. A severe limitation of application of this transducer is that the vibrating object has to be ferromagnetic. Of course, for a nonferromagnetic object, this problem can be overcome by attaching a small piece of ferromagnetic substance to the object. This solves the problem partially as the sensitivity of the pick-up gets reduced. Obviously, this is a passive-type pick-up.

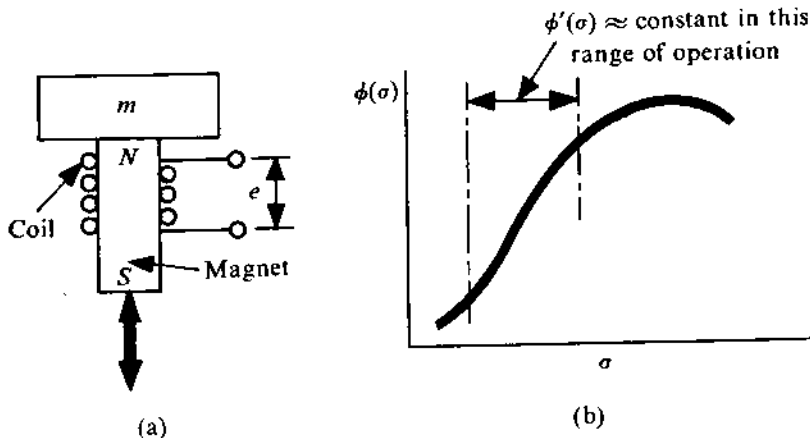


FIGURE 11.81

Magnetostriuctive Pick-up

The phenomenon of magnetostriction is used to develop a contacting passive pick-up where a voltage proportional to the third time derivative of displacement (i.e., jerk) is generated. Figure 11.81a illustrates the principle of such a pick-up. The stress (due to the inertia force of m) σ induced in the magnet changes the intensity of magnetization or the flux density, ϕ , across the coil. Thus, the rate of change of flux is

$$\frac{d\phi}{dt} = \frac{d}{dt}[\phi(\sigma)].$$

ence $\sigma = m\ddot{x}/A$, A being the cross-sectional area of the magnet, the voltage generated is

$$e \propto d\phi/dt \propto (d\phi/d\sigma) \cdot (d\sigma/dt) \propto \phi'(\sigma). \quad \square$$

A typical plot of $\phi(\sigma)$ is shown in Fig. 11.81b for permalloy. For Ni, $\phi'(\sigma)$ is negative.

Capacitance Pick-up

The capacitance pick-up is of noncontacting active type. It generates an output proportional to the displacement of oscillation. In it, one plate of the capacitor is the vibrating object, the other being the probe kept at some distance from the vibrating surface. The change in capacitance due to a variation in the air gap is utilized in an RC circuit to indicate the amount of the vibratory displacement. The size of the probe to be used depends on the range of amplitude to be measured. The range of amplitude covered by such a pick-up is 0.025-10 mm.

Mutual Inductance Pick-up

The mutual inductance pick-up is very useful for a nonmagnetic metallic vibratory surface. The principle of this noncontacting active pick-up is explained in Fig. 11.82. If the mutual inductance between the primary and secondary coils is L_m , then the voltage induced across the secondary will be $e = L_m \omega i_p$, where i_p is a high-frequency primary coil current and ω is the frequency of i_p . The mutual inductance L_m changes due to a variation in the air gap (between the vibrating surface and the pick-up). This changes the field due to eddy current in the metal body. This field opposes the field set up by the primary coil. The output voltage is modulated by the oscillatory motion and

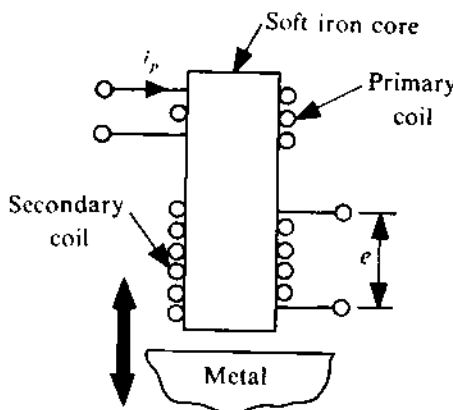


FIGURE 11.82

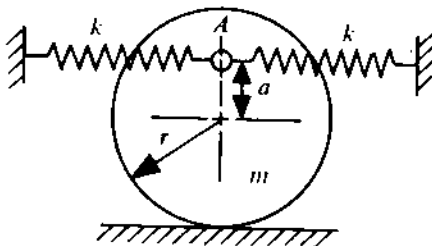


FIGURE 11.83

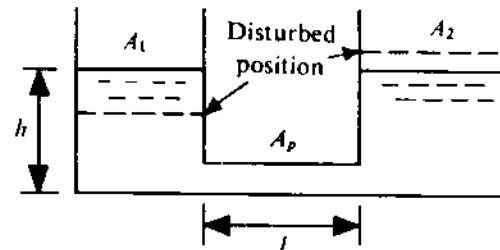


FIGURE 11.84

the demodulated output is proportional to the displacement. Such a pick-up can be used for a very wide range of frequency.

11.9 PROBLEMS

- 11.43 A mass, when suspended by a helical spring, has a natural frequency 125 cycles/min. Now the spring is cut into two equal halves and the same mass is suspended by both the halves in parallel. What will be the natural frequency of the new system?
- 11.44 Determine the natural frequency of the system shown in Fig. 11.83. The point A (where the ends of the springs are attached to the cylinder) is at a distance a vertically above the centre. The cylinder rolls without slip.
- 11.45 Two cylindrical tanks of cross-sectional areas A_1 and A_2 are connected by a pipe of length l and cross-sectional area A_p , as shown in Fig. 11.84. If h is the equilibrium height of the liquid surface, determine the natural frequency of oscillation of the fluid when disturbed.
- 11.46 Determine the natural frequency of oscillation of the system shown in Fig. 11.85. Here, J is the moment of inertia of the integral pulley about its axis of rotation.
- 11.47 What will be the natural frequency of rocking motion of the rectangular block shown in Fig. 11.86? What happens when $R < H/2$? Assume no slip condition.
- 11.48 Figure 11.87 shows a uniform helicopter blade, of a length l and a mass m , hinged to the rotating hub at a distance r from the axis. Determine the natural frequency of indicated angular oscillation. Assume Ω to be so high that the gravitational field can be neglected.

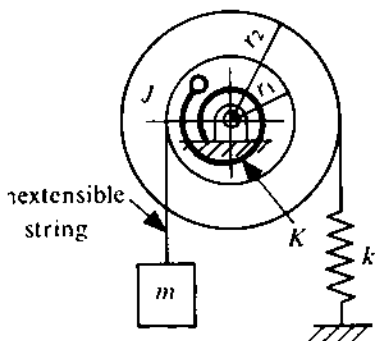


FIGURE 11.85

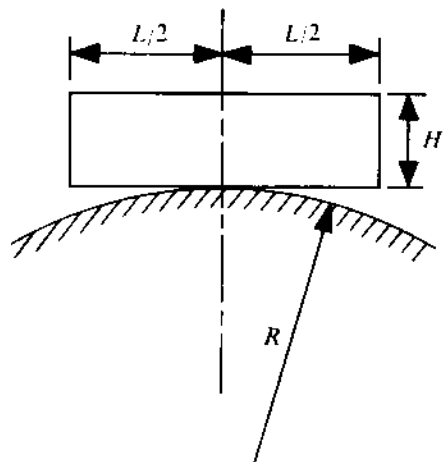


FIGURE 11.86

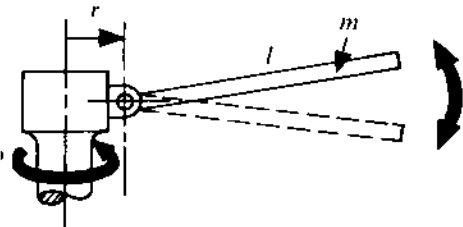


FIGURE 11.87

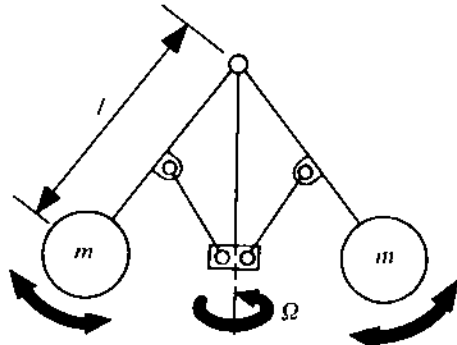


FIGURE 11.88

11.49 Figure 11.88 shows the Watt governor in which the rigid links, carrying balls of mass m , are of length l . Determine the natural frequency of pendulum oscillation of this mechanism when the shaft speed Ω is (i) greater than $(g/l)^{1/2}$, (ii) less than $(g/l)^{1/2}$. Comment on the situation $\Omega = (g/l)^{1/2}$. Neglect the mass of the links and the sleeve.

11.50 The system shown in Fig. 11.89 is constrained to move in the vertical direction. Assuming the pulley to be massless and frictionless, determine the natural frequency of oscillation. The amplitude of oscillation is small and the string around the pulley always remains taut.

11.51 A heavy door along with a door-closing system is shown in Fig. 11.90. The moment of inertia of the door panel about the hinge axis is 20 kg-m^2 and the stiffness of the torsional spring is 25 N-m/rad . Find out the most suitable value of the damping coefficient C . Neglect the effect of inclination of the dashpot axis when the door is open.

11.52 The recoil system for a large gun is so designed that the barrel moves against a spring. At the end of the recoil, a dashpot gets engaged which makes the barrel return to its initial position in minimum time but without any oscillation. The mass of the barrel is 700 kg and the recoil velocity at the instant of firing is 25 m/s . If the recoil distance is 1.5 m , determine the spring constant and the damping coefficient of the dashpot.

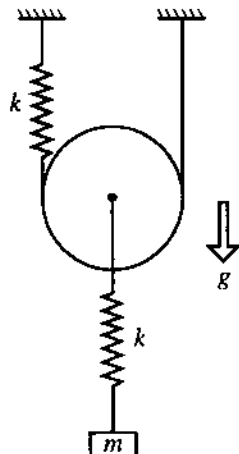


FIGURE 11.89

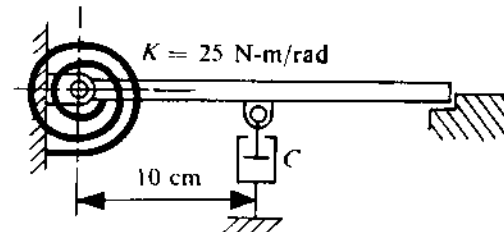


FIGURE 11.90

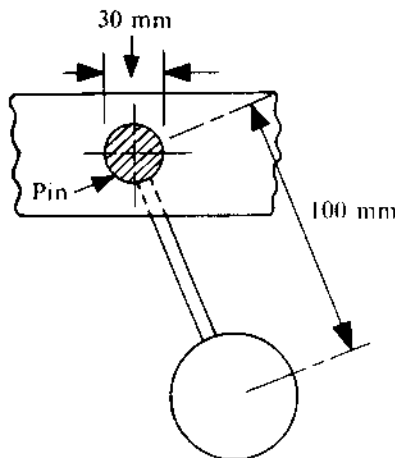


FIGURE 11.91

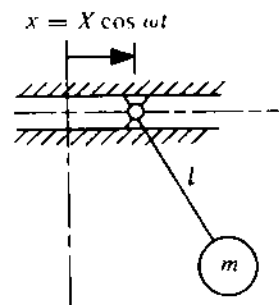


FIGURE 11.92

11.53 A pendulum is supported by a pin of diameter 30 mm as shown in Fig. 11.91. The effective length of the pendulum is 100 mm and the mass of the pendulum is 0.2 kg. If the pin support is dry and the coefficient of friction between the pin and the hole surface is 0.3, how long will the pendulum oscillate when the pendulum is hit at the bottom position to impart a velocity of 0.05 m/s? At what angle from the vertical will the pendulum stop oscillating?

11.54 The hinge point of a simple pendulum oscillates horizontally with an amplitude X and frequency ω as shown in Fig. 11.92. Assuming the amplitude of oscillation to be small, derive the equation of motion and find out the steady-state amplitude of angular oscillation of the pendulum when $\omega = \frac{1}{2}(g/l)^{1/2}$. If $\omega = 3(g/l)^{1/2}$, which point of the pendulum rod does not move during the steady-state motion?

11.55 The coupling shaft of a motor-generator set has a diameter = 8.4 cm and length = 35.6 cm with $G = 8 \times 10^4$ MPa. The moments of inertia of the rotors of the generator and the motor are 69.2 kg-m^2 and 17.3 kg-m^2 , respectively. The torque delivered by the motor varies from zero to twice the full-load torque with a frequency 50 Hz. The rated capacity of the set

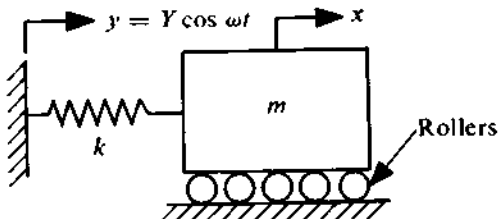


FIGURE 11.93

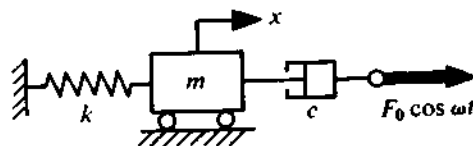


FIGURE 11.94

150 kW at 725 rpm. The load torque of the generator is constant. Determine the maximum shear stress induced in the shaft. What will be the stress when the diameter is reduced to 6.25 cm? Neglect the inertia of the shaft.

- 11.56 A rectangular block of mass m is supported on n identical rollers, each with a mass and radius m_R and r , respectively. The block is connected to an oscillating body through a spring of stiffness k (Fig. 11.93) and negligible inertia. No slipping of the rollers either with respect to the base or with respect to the bottom of the block is allowed. Find out the expression for the amplitude of steady-state oscillation of the block.

- 11.57 Set up the equation of motion for the system shown in Fig. 11.94 and find out the steady-state solution.

- 11.58 A viscously-damped single-degree-of-freedom system is excited by a force $\lambda \omega \cos \omega t$. The nondimensional amplitude is defined as $X / (\omega_n \lambda / k)$, where X is the amplitude, ω_n is the natural frequency, and k is the stiffness. Determine the frequency ratios in terms of the damping factor, ζ , for which the nondimensional amplitude is unity.

- 11.59 For a viscously-damped SDF system excited by a harmonic force of amplitude F_0 , show that the energy input per cycle (i) at resonance is $\pi F_0 X_{\text{res}}$, where X_{res} is the resonance amplitude, (ii) at the peak frequency ω_p is $\pi F_0 X_{\text{res}} (1 - 2\zeta^2)^{1/2} / (1 - \zeta^2)$, and (iii) is maximum $\pi F_0 X_{\text{res}} / (1 - \zeta^2)^{1/2}$. Assume ζ to be small.

- 11.60 A steel shaft of diameter 25 mm is supported by two short bearings 1.25 m apart. The shaft carries a disc of mass 25 kg at its midpoint, the mass centre of the disc being 0.5 mm from the axis of the shaft. The shaft material has a modulus of elasticity 210 GPa. If the mass of the shaft is neglected and no damping force acts, determine the range of the shaft speed in which the bending stress in the shaft would exceed 70 MPa.

- 11.61 In a single-cylinder reciprocating engine supported on springs and dashpots, the

total mass = 400 kg,

mass of the reciprocating parts = 15 kg,

static deflection of springs due to the system's weight = 50 mm,

stroke = 200 mm,

ratio of consecutive amplitudes in free vibration of the system = 1 : 0.42.

The connecting rod is long enough to generate a near-harmonic motion of the reciprocating parts. Determine (i) the amplitude of engine vibration at 250 rpm, and (ii) the force transmitted to the ground at this speed.

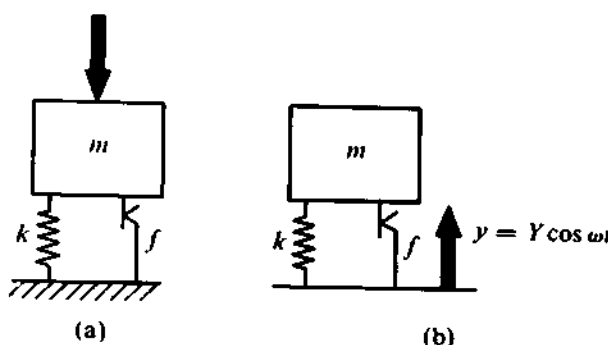


FIGURE 11.95

- 11.62 Figures 11.95a and 11.95b show a mass supported by a spring and a coulomb damper. In Fig. 11.95a, the mass is excited by a harmonic force, whereas in Fig. 11.95b, it is excited by vibrating the base.

Show that the equivalent damping factors in Figs. 11.95a and 11.95b, respectively, will be

$$\zeta_{\text{eq}}^2 = \frac{[2f/(\pi F_0)]^2(1-r^2)^2}{r^2[1-\{4f/(\pi F_0)\}^2]},$$

$$\zeta_{\text{eq}}^2 = \left(\frac{2f}{\pi k Y}\right)^2 (1 - r^2)^2 / [r^2 \{r^4 - (\frac{4f}{\pi k Y})^2\}],$$

where F_0 is the force amplitude, r is the frequency ratio, f is the friction force in the damper, k is the spring stiffness, and Y is the amplitude of base motion.

Further, show that the transmissibility in Fig. 11.95b can be expressed as

$$\begin{aligned} \text{TR} &= \left[\frac{1 + [4f/(\pi kY)]^2(1 - 2/r^2)}{(1 - r^2)^2} \right]^{1/2} \quad \text{for } r^2 > 4f/(\pi kY) \\ &= 1 \quad \text{for } r^2 < 4f/(\pi kY) \end{aligned}$$

Also determine the value of f so that the transmissibility is always less than or equal to 0.5.

- 11.63 Determine the steady-state response (under harmonic excitation) of an SDF system with hysteretic damping and complex stiffness $k = k \exp(i2\alpha)$.

- 11.64 For a damped SDF system, the maximum magnification factor 5 was seen to occur at $\omega = \omega_n$. Determine the magnification factor at $\omega = \sqrt{2}\omega_n$.

- 11.65 A simple spring mass system is excited by a periodic force with a period T and of the form

$$\begin{aligned} F(t) &= F_0 \quad (0 < t < T/2) \\ &\equiv -F_0 \quad (T/2 < t < T) \end{aligned}$$

Determine the response of the system. What happens when $2\pi p/T$ is equal to the circular natural frequency of the system (for $n = 1, 2, 3, \dots$)?

- 11.66 Solve Problem 11.21 when the system is viscously damped and the damping factor is 6.

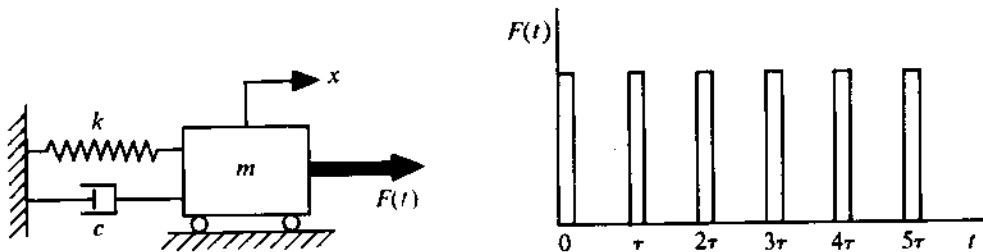


FIGURE 11.96

- 11.67 Obtain the impulsive response function for a viscously-damped SDF system and show that $H(\omega)/k$ is the Fourier transform of this response.
- 11.68 A simple SDF spring-mass-damper system is excited by a series of blows, each having an impulse \hat{F} as depicted in Fig. 11.96. Show that the response of the system at any time t can be written in the form
- $$x(t) = \sum_{i=0}^{\infty} \hat{F} \frac{\exp[-\zeta\omega_n(t-i\tau)]}{m\omega_n(1-\zeta^2)^{1/2}} \cdot \sin(1-\zeta^2)^{1/2}\omega_n(t-i\tau)u(t-i\tau).$$
- 11.69 An undamped spring mass system is acted upon by a step force input of magnitude F_0 for an interval $0 < t < t_0$. The force F is equal to zero for $t > t_0$. Determine the steady-state amplitude of the residual motion (i.e., $t \gg t_0$).
- 11.70 A vibrating system consisting of a mass m , a spring with stiffness k , and a coulomb damper with a friction force f is acted upon by a transient force which can be approximated by three steps as
- $$\begin{aligned} F(t) &= 3600 \text{ N} & (0 < t < 0.05 \text{ s}) \\ &= -1350 \text{ N} & (0.05 < t < 0.11 \text{ s}) \\ &= 900 \text{ N} & (0.11 < t < 0.15 \text{ s}). \end{aligned}$$
- If $m = 40 \text{ kg}$, $k = 750 \text{ N/cm}$, and $f = 800 \text{ N}$, determine the motion of the mass until it comes to rest. The mass is at rest initially.
- 11.71 A lift contains a spring (k) mass (m) system with one end of the spring attached to the floor of the lift. The lift while moving downward with a constant speed v_0 applies the brake at $t = 0$ so that its speed decreases linearly to zero after an interval t_0 . Determine the displacement of the mass m for $0 \leq t \leq t_0$.
- 11.72 A pendulum is hinged at the centre of a cylinder with mass m_1 and radius R (Fig. 11.97). The pendulum mass is m_2 and the length of the rod is l . The cylinder does not slip. Determine the equations of motion for free (small) oscillation of this system and find out the natural frequencies of the system.
- 11.73 A stepped shaft carries two discs, of moments of inertia J_1 and J_2 , at its ends. The end of the shaft connected to J_1 has a diameter d_1 . This diameter d_1 is over a length l_1 and the rest of the shaft has a diameter d_2 over a length l_2 . The shaft inertia is negligible. Determine the natural frequencies and normal modes of torsional oscillation of the system. Also determine the distance of the nodes from J_2 . The shear modulus of the shaft material is G .

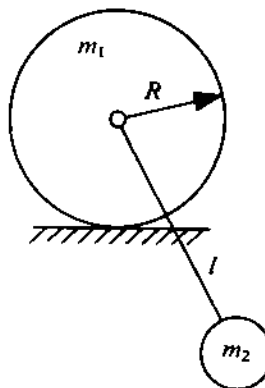


FIGURE 11.97

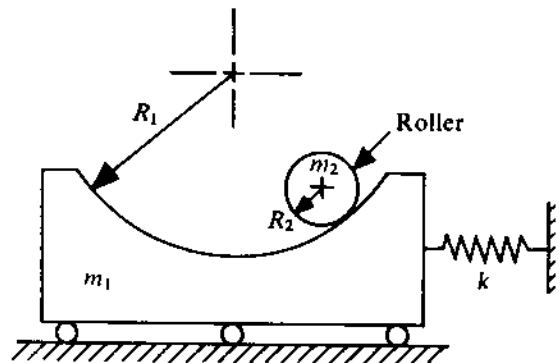


FIGURE 11.9

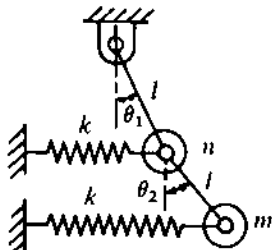


FIGURE 11.99

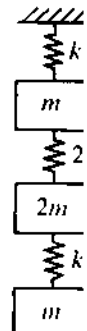


FIGURE 11.10

11.74 Find out the equations of motion and the natural frequencies for small oscillation of the system shown in Fig. 11.98.

11.75 Determine the natural frequencies and the normal modes of the system shown in Fig. 11.9 for small oscillation.

11.76 A section of a pipeline carrying a fluid from a compressor is found to resonate when the compressor speed is 232 rpm. A trial absorber of mass 1 kg, tuned to this frequency, resulted in two natural frequencies 198 cycles per minute and 272 cycles per minute. Determine the absorber mass and stiffness if the natural frequencies have to lie outside the range 160-32 cycles per minute.

11.77 A steel shaft with a diameter 30 mm and a length 2 m is supported at the ends by two short bearings. Two heavy identical pulleys (each with a mass of 200 kg) are mounted at the quarter span and midspan. If the modulus of elasticity of the shaft material is 210 GPa, determine the lowest critical speed of the system.

11.78 Find out the first natural frequency of the system shown in Fig. 11.100 using Dunkerley's method.

11.79 Find out all the natural frequencies of the system shown in Fig. 11.100 using the transfer matrix (Holzer) method.

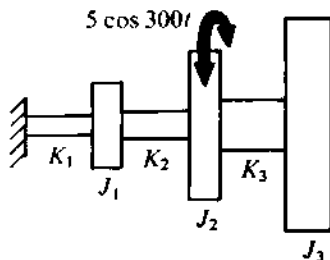


FIGURE 11.101

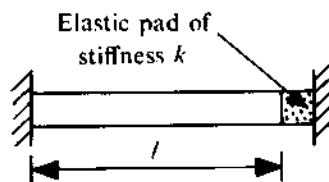


FIGURE 11.102

11.80 A torsional system is shown in Fig. 11.101 and a harmonic torque $5 \cos 300t$ N-m acts on the middle disc, as indicated. Determine the amplitudes of angular oscillation of the three discs. Given $K_1 = 10^5$ N-m/rad, $K_2 = 2 \times 10^5$ N-m/rad, $K_3 = 8 \times 10^5$ N-m/rad, $J_1 = 1 \text{ kg}\cdot\text{m}^2$, $J_2 = 2 \text{ kg}\cdot\text{m}^2$, and $J_3 = 10 \text{ kg}\cdot\text{m}^2$.

11.81 One end of a uniform bar of length l is fixed to a rigid wall, whereas the other end is resting against an elastic pad of negligible mass but with a stiffness k (Fig. 11.102). Determine the frequency equation of the bar. The modulus of elasticity and the density of the bar material are E and ρ , respectively.

11.82 A rigid block of mass $5m$ is mounted on the tip of a uniform cantilever beam with a flexural rigidity EI . The length and the mass of the beam are l and m , respectively.

- Determine the frequency equation of the system and find out the first natural frequency.
- Estimate the first natural frequency of the system using Dunkerley's principle. Hint: Use (11.156) to determine the first natural frequency of the cantilever beam without the end mass. Then, follow the approach adopted in solving Problem 11.29.
- Again estimate the first natural frequency of the system using Rayleigh's method. Choose $X_a(z) = C[1 - \cos(\pi z/l)]$.

Compare the results obtained in (i), (ii), (iii) and comment.

11.83 Solve Problem 11.35 by Rayleigh's method. Use the mode shape given in Problem 11.82 (iii).

11.84 Solve Problem 11.75 using Rayleigh's principle.

11.85 A uniform beam of length l and mass m with flexural rigidity EI is supported on two identical springs, each with stiffness k (Fig. 11.103). Assuming $X_a(z) = C[\sin(\pi z/l) + b]$, show that, using Rayleigh's method, the natural frequency is obtained as

$$\omega_1^2 = \frac{4k}{m} \left[\left(\frac{\pi^4 EI}{8kl^3} + \frac{b^2}{2} \right) / (0.5 + \frac{4b}{\pi} + b^2) \right].$$

Also show that, using the first property of Rayleigh's quotient,

$$b = -\frac{\pi}{4} \left(\frac{1}{2} - \frac{\pi^4 EI}{4kl^3} \right) \pm \left\{ \left[\frac{\pi}{2} \left(\frac{1}{2} - \frac{\pi^4 EI}{4kl^3} \right) \right]^2 + \frac{\pi^4 EI}{4kl^3} \right\}^{1/2}.$$

Of the above two values, one which minimizes ω_1 should be taken.

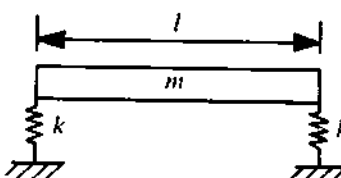


FIGURE 11.103

- 11.86 Determine the first natural frequency by Rayleigh's method of a simply-supported tapered beam with its height varying linearly from h_1 in one end to h_2 in the other. Use the first mode of a uniform simply-supported beam.
- 11.87 Find out the first two natural frequencies of the tapered beam of Problem 11.86 using the Rayleigh-Ritz method.
- 11.88 In Problem 11.48, determine the first natural frequency by Rayleigh's method in case the blade is fixed (not hinged) to the hub. Obviously, in this case, the oscillation under consideration is transverse and not angular. Use the assumed mode, in the form of a polynomial in z , satisfying all the boundary conditions.
- 11.89 A piezoelectric pick-up has a natural frequency 25 kHz and a damping factor 0.6. Determine the maximum frequency of vibration for which the pick-up can be used with an error less than 2%. Solve this problem also if the damping factor is 0.75.
- 11.90 A two-disc piezoelectric pick-up with the properties $E = 10^{11}$ N/m², $\chi = 10^{-10}$ C/N, and $\epsilon = 10^{-8}$ F/m has a natural frequency 25 kHz. Determine the open circuit voltage sensitivity of the pick-up.

Chapter 12

DYNAMICS OF ROTATING SHAFTS

12.1 INTRODUCTION

In many engineering systems, we have to design rotating members which are capable of smooth operation under various conditions of speed and load. In some systems, specially for machinery with members rotating at high speeds, it is extremely difficult to ensure stable and smooth operation. Although this subject is still in the developing stage, nevertheless, because of its importance, it is necessary for designers to have some understanding of the behaviour of rotating members. A simple mathematical treatment of rotating shafts has already been given in Chapter 11. Many phenomena cannot be explained by this simple theory and require more detailed analyses which are presented in this chapter.

It will be helpful if we first discuss the nature of motion of a rotating shaft. When a shaft with a rigid rotor rotates, the rotor-shaft system can exhibit the following types of motion for various speeds and loading conditions:

- (i) Synchronous precession, in which the precession rate (or angular velocity) of the rotor is equal to the angular velocity of the shaft. In this type of motion, the bent shaft (the shaft gets bent by the centrifugal force resulting from the unbalance in the rotating system) rotates along with the rotor as a rigid body.
- (ii) Nonsynchronous precession, in which the angular velocity of the plane containing the shaft axis differs from the angular velocity of the shaft.

Apart from this, there are two aspects of the rotating-shaft problem, namely, (i) forced vibrations due to unbalance, and (ii) stability of a balanced rotating shaft.

Let us consider a shaft with a single rigid disc mounted at the middle as shown in Fig. 12.1. The coordinate system xyz is fixed in space. The flexural displacement of the centre of any cross-section of the shaft is represented by the x - and y -coordinate of the centre. Due to bending, the cross-section of the shaft at any point will be rotated by ϕ_x and ϕ_y about the central axes of the cross-section, parallel to the x - and y -axis, respectively. The movement of the CG of the disc is represented by two vectors, one denoting the deflection of the geometric centre C of the shaft cross-section at the

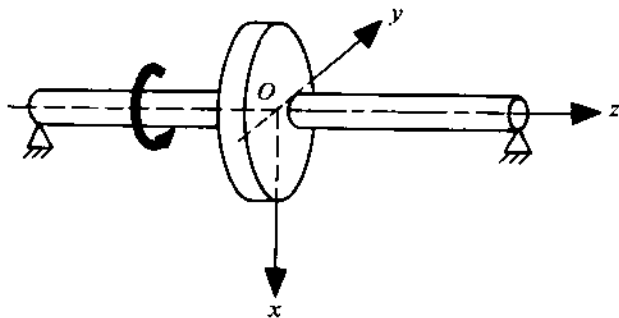


FIGURE 12.1

central plane of the disc, and the other, the position of the CG of the disc G with respect to the geometric centre (see Fig. 12.2a). So, the position of G is given by

$$\rho = OC + CG$$

or, in the complex form, we can write

$$\rho = x + iy = \delta \exp(i\psi) + e \exp(i\theta), \quad (12.1)$$

where ρ denotes the position of G , δ denotes the elastic deflection of the shaft, and e represents the unbalance in mounting the disc. In general, the shaft centre may describe an elliptic path and the shaft will rotate with an angular velocity $\omega (= \dot{\theta})$. From Fig. 12.2b, it is further seen that $\delta = OQ + QC$, where OQ and QC are two vectors rotating in opposite directions with the same angular velocity λ ; their respective magnitudes are Γ_1 and Γ_2 . The position of the CG can thus be expressed as

$$\rho = \Gamma_1 \exp(i\lambda t) + \Gamma_2 \exp(-i\lambda t) + e \exp(i\omega t). \quad (12.2)$$

The motion represented by the sum of three vectors is most general and can take care of all types of motions involved in rotating shafts. If one of the quantities, Γ_1 or Γ_2 , is zero, the motion of G will comprise the circular motion of the shaft centre C and the circular motion of the unbalance vector CG . The movement of C is commonly known as the *precession of the shaft* and λ represents the *speed of precession*. When Γ_2 is zero, the direction of precession and that of the shaft rotation θ are the same, and the precession is said to be *straight*. Similarly, when Γ_1 is zero, the precession is *reversed*. When $\Gamma_1 \neq \Gamma_2 \neq 0$, the precession is straight if $\Gamma_1 > \Gamma_2$, and is reversed if $\Gamma_1 < \Gamma_2$. When the speed of precession λ and $\omega (= \dot{\theta})$ are the same, the precession is termed *synchronous*.

To represent only the deformation of the shaft, we can select a coordinate system which rotates along with the shaft and takes care of shaft rotation. Any movement in this coordinate system is then due only to the elastic deformation of the shaft. Let us consider the coordinate system $\xi\eta$ (Fig. 12.3) when ξ is always parallel to the unbalance vector and the coordinate system $\xi\eta$ rotates with the system with an angular velocity $\dot{\theta} (= \omega)$. Then,

$$\begin{aligned} x &= \xi \cos \theta - \eta \sin \theta = \xi \cos \omega t - \eta \sin \omega t, \\ y &= \xi \sin \theta + \eta \cos \theta = \xi \sin \omega t + \eta \cos \omega t. \end{aligned}$$

Expressing the deformation in the complex form, we get

$$\begin{aligned} \rho &= x + iy = \zeta \exp(i\omega t) = (\xi + i\eta) \exp(i\omega t) \\ &= \Gamma_1 \exp(i\lambda t) + \Gamma_2 \exp(-i\lambda t) + e \exp(i\omega t). \end{aligned}$$

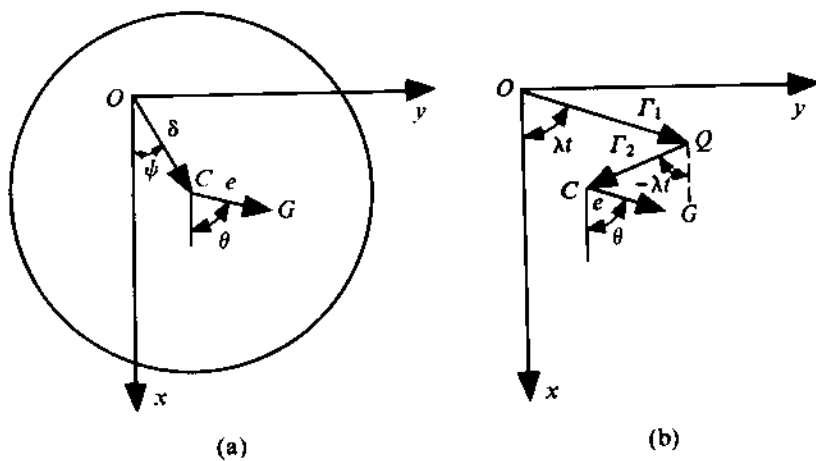


FIGURE 12.2

So,

$$\zeta = \Gamma_1 \exp(i(\lambda - \omega)t) + \Gamma_2 \exp(-i(\lambda + \omega)t) + e. \quad (12.3)$$

12.2 SHAFT WITH AN UNBALANCED DISC AT THE MIDSPAN

The most simple shaft-rotor system consists of a disc mounted on a shaft at the central position (Fig. 12.1). We will analyze this system first. The most general displacement of such a system is shown in Fig. 12.4. n_x and n_y are unit vectors in the x - and y -direction, respectively, and n_r and n_ψ are the unit vectors in the radial and tangential directions, as shown. The weight mg of the rotor acts downwards at G . To derive the equations of motion for the system, it is necessary to first identify the generalized coordinates. For the system under consideration, there are three degrees of freedom, namely, (i) the position of CG with respect to $OC(\beta)$, (ii) the precession angle ψ , and (iii) the shaft deflection δ . In Fig. 12.4, β represents the phase angle between OC and CG . Let (x_C, y_C) be the position coordinates of the rotor centre C . Now, in order to write Lagrange's equations of motion, it is necessary to determine the KE (T) and PE (V) of the system, and the generalized forces acting on the system.

Kinetic Energy

Neglecting the mass of the shaft, the KE of the system will be

$$T = \frac{1}{2}mv_G^2 + \frac{1}{2}J_G\omega^2, \quad (12.4)$$

where v_G is the absolute speed of the mass centre G , and J_G is the moment of inertia of the rotor about an axis perpendicular to the plane of the disc and passing through the CG. Now,

$$v_G = v_C + v_{GC}, \quad (12.5)$$

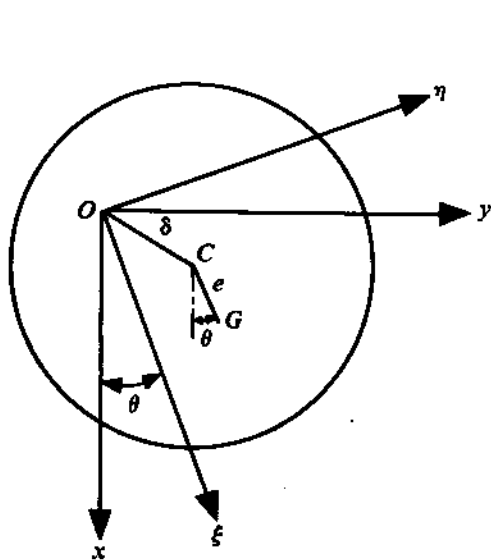


FIGURE 12.3

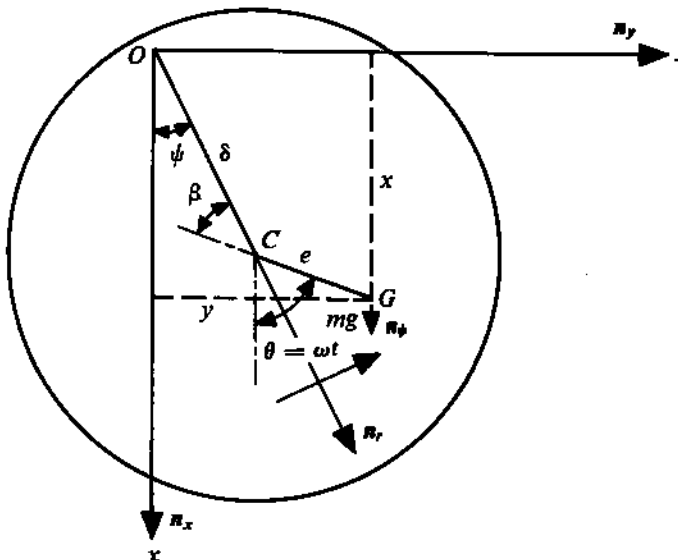


FIGURE 12.4

where v_{GC} is the velocity of G with respect to C . From Fig. 12.4, it is clear that the r - and ψ -component of v_C are $\dot{\delta}$ and $\dot{\delta}\psi$, respectively. Similarly, it is easy to show that the r - and ψ -component of v_{GC} are $(-\epsilon\omega \sin \beta)$ and $(\epsilon\omega \cos \beta)$, respectively. So,

$$\begin{aligned} v_G &= (\dot{\delta}n_r + \dot{\delta}\psi n_\psi) + [(-\epsilon\omega \sin \beta)n_r + (\epsilon\omega \cos \beta)n_\psi] \\ &= (\dot{\delta} - \epsilon\omega \sin \beta)n_r + (\dot{\delta}\psi + \epsilon\omega \cos \beta)n_\psi. \end{aligned}$$

Hence,

$$v_G^2 = (\dot{\delta} - \epsilon\omega \sin \beta)^2 + (\dot{\delta}\psi + \epsilon\omega \cos \beta)^2. \quad (12.6)$$

Now, from (12.4) and (12.6), the KE can be expressed as

$$T = \frac{1}{2} \{ m[(\dot{\delta} - \epsilon\omega \sin \beta)^2 + (\dot{\delta}\psi + \epsilon\omega \cos \beta)^2] + J_G \omega^2 \}. \quad (12.7)$$

Potential Energy

If we assume the shaft to be horizontal, the gravitational field will contribute towards the potential energy of the system. When the shaft rotates in a vertical position, the gravitational effect need not be considered. For more generality, let us consider a horizontal shaft. Neglecting the external forces on the system, the total potential energy of the system consists of the strain energy involved in the shaft deformation and the gravitational potential energy. If the gravitational PE at the level of O is considered to be zero, then the PE of the system can be expressed as

$$V = \frac{1}{2} k \delta^2 - mg[\delta \cos \psi + e \cos(\psi + \beta)], \quad (12.8)$$

where k represents the flexural stiffness of the shaft corresponding to the disc position.

Generalized Forces

As the external forces applied on the system (except the weight of the disc) were not taken into account so far, it is necessary to represent them in terms of the generalized forces corresponding to the generalized coordinates. These forces are (i) the resultant damping force acting at C exerted by the surrounding medium, and (ii) the driving torque M applied on the shaft. If we assume the surrounding medium to be viscous, then the components of the resultant damping force at C will be proportional to the corresponding components of the velocity of the point C . Hence,

$$\mathbf{F}_C = -[\gamma\dot{\delta}\mathbf{n}_r + \gamma\dot{\psi}\mathbf{n}_\psi]. \quad (12.9)$$

The negative sign on the right-hand side of (12.9) results from the fact that the damping force acts in a direction opposite to that of the velocity. γ is the damping coefficient for the system.¹ The generalized force Q_j corresponding to a particular generalized coordinate q_j can be expressed in terms of the applied forces, that is,

$$Q_j = \sum_i \mathbf{F}_i \cdot \frac{\partial \mathbf{v}_i}{\partial q_j},$$

where \mathbf{F}_i is the externally applied force and \mathbf{v}_i is the velocity of the point where the external force (or moment) is applied. Thus,

$$Q_\delta = -[\gamma\dot{\delta}\mathbf{n}_r + \gamma\dot{\psi}\mathbf{n}_\psi] \cdot \frac{\partial(\dot{\delta}\mathbf{n}_r + \dot{\psi}\mathbf{n}_\psi)}{\partial \dot{\delta}} + M\mathbf{n}_z \cdot \frac{\partial(\omega\mathbf{n}_z)}{\partial \dot{\delta}},$$

where \mathbf{n}_z is the unit vector in the z -direction (see Fig. 12.1). Further, we have

$$Q_\beta = -[\gamma\dot{\delta}\mathbf{n}_r + \gamma\dot{\psi}\mathbf{n}_\psi] \cdot \frac{\partial(\dot{\delta}\mathbf{n}_r + \dot{\psi}\mathbf{n}_\psi)}{\partial \dot{\beta}} + M\mathbf{n}_z \cdot \frac{\partial(\omega\mathbf{n}_z)}{\partial \dot{\beta}},$$

$$Q_\psi = -[\gamma\dot{\delta}\mathbf{n}_r + \gamma\dot{\psi}\mathbf{n}_\psi] \cdot \frac{\partial(\dot{\delta}\mathbf{n}_r + \dot{\psi}\mathbf{n}_\psi)}{\partial \dot{\psi}} + M\mathbf{n}_z \cdot \frac{\partial(\omega\mathbf{n}_z)}{\partial \dot{\psi}}.$$

Noting that $\omega = \dot{\beta} + \dot{\psi}$, we finally get

$$Q_\delta = -\gamma\dot{\delta}, \quad Q_\beta = M, \quad Q_\psi = -\gamma\dot{\delta}^2 + M. \quad (12.10)$$

Lagrange's Equation of Motion

Now we are in a position to write Lagrange's equation for the generalized coordinates δ , β , and ψ . In general, we have

$$\frac{d}{dt} \left(\frac{\partial L}{\partial \dot{q}_j} \right) - \frac{\partial L}{\partial q_j} = Q_j, \quad (12.11)$$

where $L = T - V$. From (12.7) and (12.8), we get

$$\begin{aligned} L &= \frac{1}{2} \{ m[(\dot{\delta} - e\omega \sin \beta)^2 + (\dot{\delta}\dot{\psi} + e\omega \cos \beta)^2] + J_G \omega^2 \} - \frac{1}{2} k\delta^2 \\ &\quad + mg[\delta \cos \psi + e \cos(\psi + \beta)]. \end{aligned} \quad (12.12)$$

So, from (12.10), (12.11), and (12.12), the equations of motion (assuming ω to be constant) will be as follows:

¹In Chapter 11, the symbol used for viscous damping coefficient was c . To avoid confusion with the disc centre C , the symbol used in this chapter is γ .

(i) For δ ,

$$m\ddot{\delta} + \gamma\dot{\delta} + (k - m\psi^2)\delta = em\omega^2 \cos \beta + mg \cos \psi.$$

(ii) For β ,

$$e[(\delta\ddot{\psi} + 2\delta\dot{\psi}) \cos \beta - (\ddot{\delta} - \delta\dot{\psi}^2) \sin \beta] = M/m - eg \sin(\beta + \psi).$$

(iii) For ψ ,

$$\begin{aligned} \delta^2\ddot{\psi} + [2\delta + (\gamma/m)\delta]\delta\dot{\psi} + e\{(\delta\ddot{\psi} + 2\delta\dot{\psi}) \cos \beta - [\ddot{\delta} + \delta(\omega^2 - \psi^2)] \sin \beta\} \\ = M/m - g[\delta \sin \psi + e \sin(\psi + \beta)]. \end{aligned}$$

Eliminating M/m from (ii) and (iii), these equations can be written in the form

$$\begin{aligned} \ddot{\delta} + (\gamma/m)\dot{\delta} + (k/m - \psi^2)\delta &= em\omega^2 \cos \beta + g \cos \psi, \\ \delta\ddot{\psi} + [2\dot{\delta} + (\gamma/m)\delta]\dot{\psi} &= e\omega^2 \sin \beta - g \sin \psi. \end{aligned} \quad (12.13)$$

The rotor motion can now be analyzed with the help of (12.13). We will discuss the different cases separately.

Synchronous Precession

For synchronous precession,² the precessional velocity and rotor velocity are the same. So, $\dot{\psi} = \omega$ and $\ddot{\beta} = 0$. For such motion, the governing equations can be obtained from (12.13) by substituting ω for $\dot{\psi}$. Thus,

$$\begin{aligned} \ddot{\delta} + (\gamma/m)\dot{\delta} + (k/m - \omega^2)\delta &= em\omega^2 \cos \beta + g \cos \psi, \\ \omega[2\dot{\delta} + (\gamma/m)\delta] &= e\omega^2 \sin \beta - g \sin \psi. \end{aligned} \quad (12.14)$$

Assuming steady-state motion, which is obtained when δ is constant and the effect of gravity is neglected ($g = 0$), these equations are further simplified and we get

$$(k/m - \omega^2)\delta = em\omega^2 \cos \beta, \quad (\gamma/m)\delta\omega = e\omega^2 \sin \beta. \quad (12.15)$$

Squaring both sides of (12.15) and adding, we get

$$\begin{aligned} \delta^2[(k/m - \omega^2)^2 + ((\gamma/m)\omega)^2] &= e^2\omega^4, \\ \delta &= e/\{[1 - (k/m)/\omega^2]^2 + [(\gamma/m)/\omega]^2\}^{1/2}. \end{aligned} \quad (12.16)$$

Equations (12.15) also yield

$$\tan \beta = -\left[\frac{(\gamma/m)/\omega}{1 - (k/m)/\omega^2}\right]. \quad (12.17)$$

From (12.16), it is seen that, for the undamped case (i.e., when $\gamma = 0$), the steady-state rotor deflection tends to infinity when ω approaches $\sqrt{(k/m)}$. This particular speed is called the *critical speed* ω_{cr} of the shaft-rotor system. Equation (12.17) gives the steady-state value of β . Figures 12.5a and 12.5b show how δ and β vary with the ratio ω/ω_{cr} .

²The situation discussed in Chapter 11 is a special case of this phenomenon.

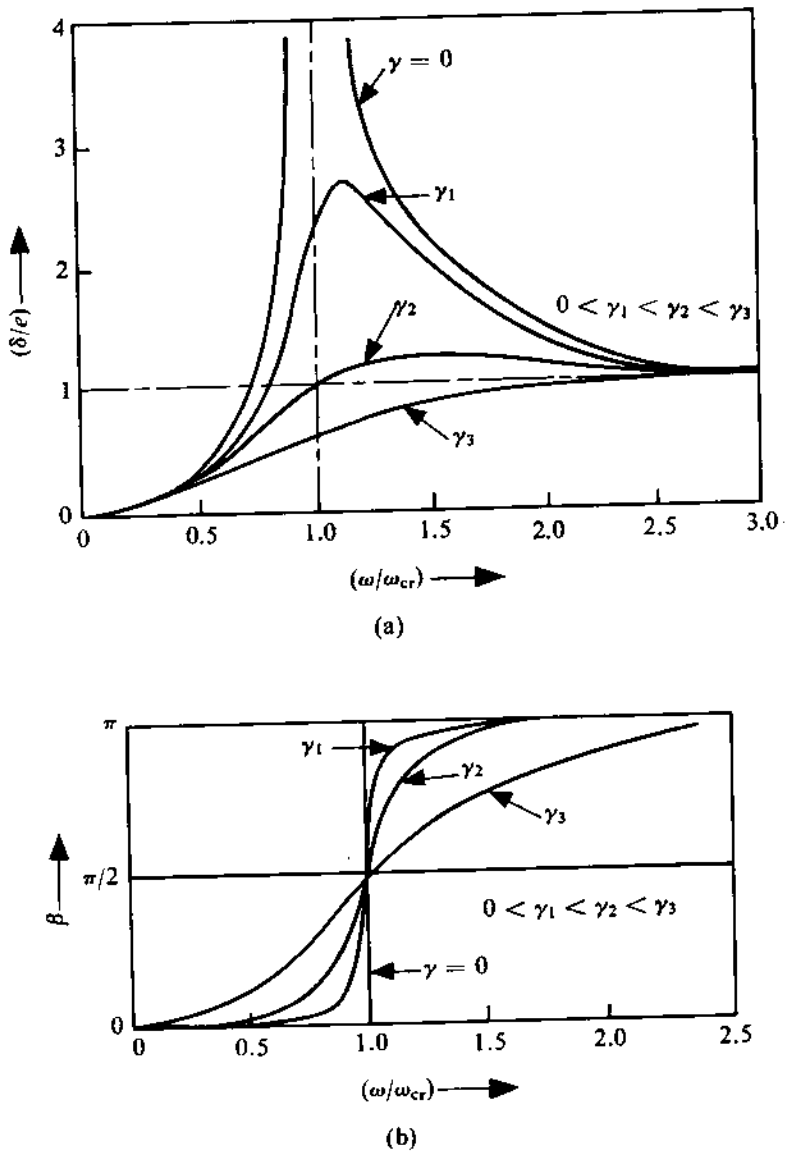


FIGURE 12.5

Nonsynchronous Precession

For the general case, $\dot{\beta}$ will not be zero. Let us assume that

$$\dot{\beta} = n\omega, \quad \dot{\beta} + \dot{\psi} = \omega = \text{constant}. \quad (12.18)$$

Then, $\dot{\psi} = \omega - \dot{\beta} = \omega(1 - n)$. From (12.18), we get $\beta = nwt + \beta_0$, where β_0 is the value of β at time $t = 0$. Neglecting the effect of gravity, (12.13) becomes

$$\ddot{\delta} + \frac{\gamma}{m}\dot{\delta} + [\frac{k}{m} - (1 - n)^2\omega^2]\delta = e\omega^2 \cos(nwt + \beta_0), \quad (12.19)$$

$$(2\dot{\delta} + \frac{\gamma}{m}\delta)(1 - n)\omega = e\omega^2 \sin(nwt + \beta_0). \quad (12.20)$$

Equation (12.20) can be reduced to the form

$$\dot{\delta} + \frac{\gamma}{2m}\delta = \frac{e\omega}{2(1 - n)} \sin(nwt + \beta_0)$$

and the solution to this equation will be

$$\delta = C_1 \exp(-\frac{\gamma}{2m}t) - \frac{e\omega}{2(1 - n)[(\frac{\gamma}{2m})^2 + n^2\omega^2]^{1/2}} \cos(nwt + \beta_0 - \tan^{-1}\frac{\gamma}{2mn\omega}).$$

Assuming δ to be δ_0 at $t = 0$, this equation can be written as

$$\begin{aligned} \delta &= \{\delta_0 + \frac{e\omega}{2(1 - n)[(\frac{\gamma}{2m})^2 + n^2\omega^2]^{1/2}} \cos(\beta_0 - \tan^{-1}\frac{\gamma}{2mn\omega})\} \\ &\quad \times \exp(-\frac{\gamma}{2m}t) - \frac{e\omega}{2(1 - n)[(\frac{\gamma}{2m})^2 + n^2\omega^2]^{1/2}} \cos(nwt + \beta_0 - \tan^{-1}\frac{\gamma}{2mn\omega}). \end{aligned} \quad (12.21)$$

Substituting this expression for δ in (12.19), we get

$$\begin{aligned} &\exp(-\frac{\gamma}{2m}t)\{[\delta_0 + \chi \cos(\beta_0 - \tan^{-1}\frac{\gamma}{2mn\omega})][\frac{k}{m} - (1 - n)^2\omega^2 - \frac{\gamma^2}{4m^2}] \\ &\quad + \chi \cos(\beta - \tan^{-1}\frac{\gamma}{2mn\omega})[n^2\omega^2 - \frac{k}{m} + (1 - n)^2\omega^2] \\ &\quad + \chi \frac{\gamma}{m}n\omega \sin(\beta - \tan^{-1}\frac{\gamma}{2mn\omega}) - e\omega^2 \cos\beta = 0, \end{aligned} \quad (12.22)$$

where

$$\chi = \frac{e\omega}{2(1 - n)[(\frac{\gamma}{2m})^2 + n^2\omega^2]^{1/2}}.$$

When the damping in the system is small, we have

$$(\frac{\gamma}{2m})^2 \ll n^2\omega^2, \quad (12.23)$$

$$\chi \approx \frac{e}{2n(1 - n)}.$$

In such cases, (12.22) becomes

$$\exp(-\frac{\gamma}{2m}t)\{[\frac{k}{m} - (1 - n)^2\omega^2][\delta_0 + \frac{e}{2n(1 - n)} \cos\beta_0]\} + \frac{e}{2n(1 - n)}[(2n - 1)^2\omega^2 - \frac{k}{m}] \cos\beta = 0. \quad (12.24)$$

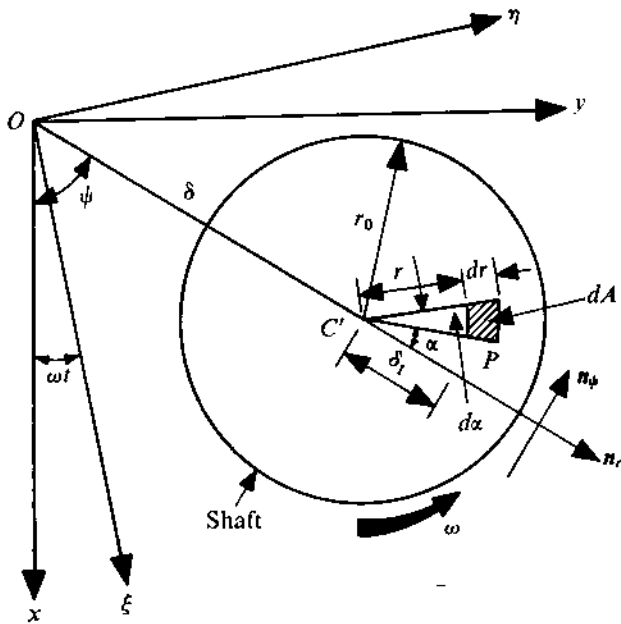


FIGURE 12.6

Since $\gamma/(2m)$ is very small, the terms containing $\gamma/(2m)$ can be neglected. Now, (12.24) is always satisfied when

$$k/m - (1-n)^2\omega^2 = 0, \quad (2n-1)^2\omega^2 - k/m = 0,$$

and these two conditions are satisfied if $n = 2/3$ and $\omega = 3\omega_{cr}$. Hence, a solution will exist when $n = 2/3$, that is, when

$$\dot{\psi} = \omega(1-n) = \omega/3 = \omega_{cr}.$$

Therefore, if the rotor angular velocity is three times the critical speed ω_{cr} , precession with a speed equal to ω_{cr} is possible.

Again, for the case when the transient motion dies out, the necessary condition to be satisfied is

$$\frac{e}{2n(1-n)}[(2n-1)^2\omega^2 - \frac{k}{m}] \cos \beta = 0, \\ (2n-1)^2 - (k/m)/\omega^2 = 0. \quad (12.25)$$

When the speed of the rotor is much higher than the first critical speed, we have $(k/m)/\omega^2 \ll 1$ and (12.25) becomes $n \approx \frac{1}{2}$, and $\dot{\psi} = \omega(1-n) = \omega/2$. Hence, half-frequency precession is possible when the rotor speed is much larger than the first critical speed and damping in the system is small. It is of interest to note that the possibility of this motion cannot be shown if damping is neglected.

12.3 EFFECT OF INTERNAL FRICTION

In previous sections, we considered the frictional forces exerted on the system by external agencies, and their effect on the system was demonstrated. It is seen that external friction always has a damping effect. However, another kind of friction is present in such cases; it arises from the hysteresis

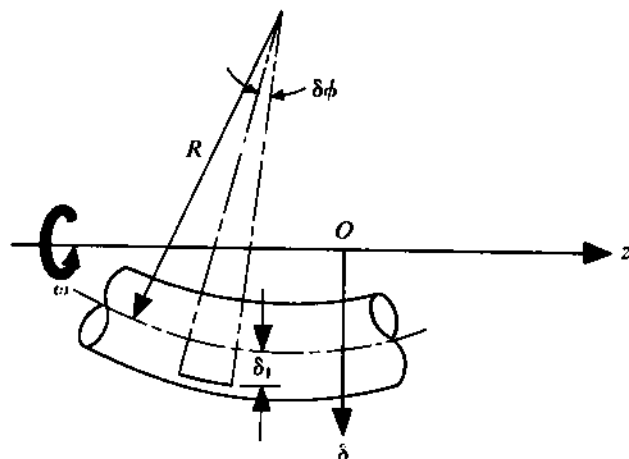


FIGURE 12.7

loss in the rotating shaft itself. It has been observed that under certain conditions this kind of frictional effect (commonly known as internal friction) can increase the amplitude. To analyze the effect of internal friction in a rotating shaft with a symmetrically mounted disc, let us consider Fig. 12.6. To estimate the internal friction of a rotating shaft, it will be necessary to obtain the relationship which the fibre stress has with the corresponding strain and strain rate. When a shaft rotates in a bent condition, it is obvious that all fibres will undergo a cyclic change in the state of stress which causes the hysteresis loss. A suitable stress-strain relationship is

$$\sigma_z = E\epsilon_z + \mu_i \frac{d\epsilon_z}{dt}, \quad (12.26)$$

where σ_z = fibre stress, ϵ_z = fibre strain, μ_i = internal friction factor, and E = modulus of elasticity. Now, the longitudinal strain ϵ_z in the shaft fibre can be obtained from simple beam theory. Figure 12.7 shows the bent shaft at any instant. The neutral plane passes through the central axis of the shaft and the strain ϵ_z at a distance δ_1 from this plane can be expressed as

$$\epsilon_z = \frac{(R + \delta_1)\delta\phi - R\delta\phi}{R\delta\phi} = \frac{\delta_1}{R}.$$

Since $1/R = \partial^2\delta(z, t)/\partial z^2$, we have

$$\epsilon_z = \delta_1 \frac{\partial^2\delta(z, t)}{\partial z^2}. \quad (12.27)$$

So, the strain at any point P in the circular shaft will be given by

$$\epsilon_z = r \cos \alpha \cdot \frac{\partial^2\delta(z, t)}{\partial z^2}.$$

Putting

$$\epsilon_0 = r_0 \frac{\partial^2\delta(z, t)}{\partial z^2} \quad (12.28)$$

in this equation, we get

$$\epsilon_z = \epsilon_0(r/r_0) \cos \alpha.$$

Now, the rate of strain will depend on the rate of deformation. For a particular bent condition, the rate of change of α , i.e., the position of an element with respect to the plane of bending of the shaft, and the rate of change of bending will control the strain rate. Thus,

$$\frac{\partial \epsilon_z}{\partial t} = -\epsilon_0 \left(\frac{r}{r_0} \right) \sin \alpha \dot{\alpha} + \dot{\epsilon}_0 \left(\frac{r}{r_0} \right) \cos \alpha. \quad (12.29)$$

From (12.26), (12.28), and (12.29), we get

$$\begin{aligned} \sigma_z &= E \epsilon_0 \left(\frac{r}{r_0} \right) \cos \alpha + \mu_i \left[-\epsilon_0 \left(\frac{r}{r_0} \right) \sin \alpha \dot{\alpha} + \dot{\epsilon}_0 \left(\frac{r}{r_0} \right) \cos \alpha \right] \\ &= \epsilon_0 \left(\frac{r}{r_0} \right) [E \cos \alpha - \mu_i \sin \alpha \dot{\alpha}] + \mu_i \left(\frac{r}{r_0} \right) \cos \alpha \dot{\epsilon}_0. \end{aligned} \quad (12.30)$$

The components of the bending moment M_r and M_ψ at any cross-section are given by

$$M_r = \int_A \int \sigma_z r \cos \alpha \, dA, \quad M_\psi = \int_A \int \sigma_z r \sin \alpha \, dA. \quad (12.31)$$

From Fig. 12.6, the area of the element can be expressed as

$$dA = r \, d\alpha \, dr. \quad (12.32)$$

Substituting σ_z and dA in (12.31), we can evaluate M_r and M_ψ . Thus,

$$\begin{aligned} M_r &= \int_0^{2\pi} \int_0^{r_0} \epsilon_0 \frac{r^3}{r_0} [E \cos \alpha - \mu_i \sin \alpha \dot{\alpha}] \cos \alpha \, dr \, d\alpha + \int_0^{2\pi} \int_0^{r_0} \mu_i \frac{r^3}{r_0} (\cos^2 \alpha) \dot{\epsilon}_0 \, dr \, d\alpha, \\ M_\psi &= \int_0^{2\pi} \int_0^{r_0} \epsilon_0 \frac{r^3}{r_0} [E \cos \alpha - \mu_i \sin \alpha \dot{\alpha}] \sin \alpha \, dr \, d\alpha + \int_0^{2\pi} \int_0^{r_0} \mu_i \epsilon_0 \frac{r^3}{r_0} \cos \alpha \sin \alpha \, dr \, d\alpha. \end{aligned}$$

Evaluating the integrals, we get

$$M_r = \frac{1}{r_0} (\epsilon_0 E + \mu_i \dot{\epsilon}_0) \int_0^{2\pi} \int_0^{r_0} (r \cos \alpha)^2 r \, dr \, d\alpha = \frac{I}{r} (\epsilon_0 E + \mu_i \dot{\epsilon}_0), \quad (12.33)$$

$$M_\psi = -(\epsilon_0 / r_0) \mu_i I \dot{\alpha},$$

where I is the second moment of area of the shaft cross-section about the diameter. From simple beam theory, we know that

$$p_r(z) = -\partial^2 M_r / \partial z^2, \quad (12.34)$$

where $p_r(z)$ is the load per unit length acting on the beam in the radial direction. From (12.28), (12.33), and (12.34), we get

$$p_r(z) = -[EI \frac{\partial^4 \delta(z, t)}{\partial z^4} + \mu_i I \frac{\partial^4 \dot{\delta}(z, t)}{\partial z^4}]. \quad (12.35)$$

Similarly,

$$p_\psi(z) = -\frac{\partial^2 M_\psi}{\partial z^2} = \alpha \mu_i I \frac{\partial^4 \delta(z, t)}{\partial z^4}. \quad (12.36)$$

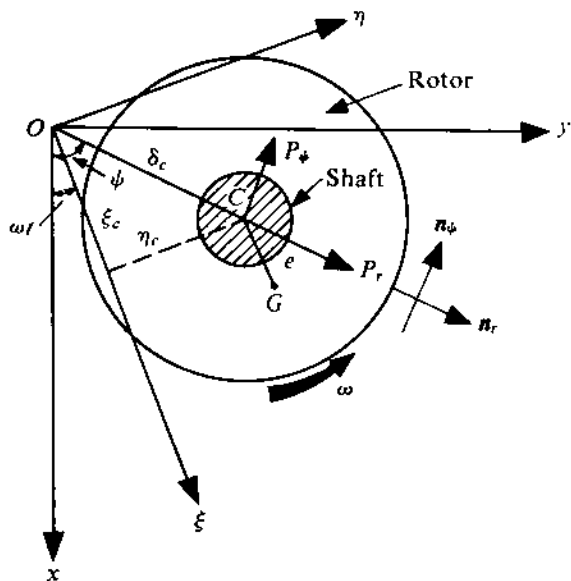


FIGURE 12.8

Since the rotational speed of the shaft is ω and the speed of precession is $\dot{\psi}$, from Fig. 12.6, we get

$$\dot{\alpha} = \omega - \dot{\psi}. \quad (12.37)$$

So, the force p_ψ possesses damping characteristics when the precessional speed $\dot{\psi}$ is more than the shaft speed ω . Now, without introducing much error, we can assume the shaft deflection in the present case to be

$$\delta(z, t) = \delta_C(t) \cos(\pi z/L), \quad (12.38)$$

where $\delta_C(t)$ denotes the deflection of the rotor centre C . The total radial and tangential components of the force can be determined by integrating p_r and p_ψ over the length of the shaft. Thus,

$$\begin{aligned} P_r &= \int_{-L/2}^{L/2} p_r(z) dz = -2(\frac{\pi}{L})^3 [EI\ddot{\delta}_C + \mu_i I \dot{\delta}_C], \\ P_\psi &= \int_{-L/2}^{L/2} p_\psi(z) dz = 2(\frac{\pi}{L})^3 \mu_i I \delta_C (\omega - \dot{\psi}). \end{aligned} \quad (12.39)$$

Let us consider the coordinate system $\xi\eta$ which is rotating with a speed ω . So, any movement of the point C indicates deformation of the shaft, since the rigid-body rotation is already taken care of (see Fig. 12.8). Let the position of C be denoted by ζ_C , where $\zeta_C = \xi_C + i\eta_C$. The position of C with respect to the system xy is denoted by ρ_C and

$$\rho_C = \zeta_C e^{i\omega t}. \quad (12.40)$$

From (12.39), the radial and tangential components of force developed because of internal friction are

$$F_r = -2(\pi/L)^3 \mu_i I \dot{\delta}_C,$$

$$F_\psi = 2(\pi/L)^3 \mu_i I \delta_C (\omega - \dot{\psi})$$

$$F_r = -\gamma_i \dot{\delta}_C, \quad F_\psi = \gamma_i \delta_C (\omega - \dot{\psi}), \quad (12.41)$$

where $\gamma_i = 2(\pi/L)^3 \mu_i I$. γ_i can be termed the coefficient of internal friction. The resultant force can be represented by

$$\mathbf{F} = F_r \mathbf{n}_r + F_\psi \mathbf{n}_\psi = -\gamma_i \dot{\delta}_C \mathbf{n}_r + \gamma_i \delta_C (\omega - \dot{\psi}) \mathbf{n}_\psi.$$

As \mathbf{n}_r and \mathbf{n}_ψ are unit vectors, these can be expressed in the complex variable form in terms of the components ξ and η . Thus,

$$\begin{aligned}\mathbf{n}_r &= \cos(\psi - \omega t) + i \sin(\psi - \omega t), \\ \mathbf{n}_\psi &= -\sin(\psi - \omega t) + i \cos(\psi - \omega t).\end{aligned}$$

So,

$$\begin{aligned}\mathbf{F} &= -\gamma_i \dot{\delta}_C [\cos(\psi - \omega t) + i \sin(\psi - \omega t)] + \gamma_i \delta_C (\omega - \dot{\psi}) [-\sin(\psi - \omega t) + i \cos(\psi - \omega t)] \\ &= \gamma_i \{-\dot{\delta}_C \cos(\psi - \omega t) - \delta_C (\omega - \dot{\psi}) \sin(\psi - \omega t) + i[-\dot{\delta}_C \sin(\psi - \omega t) \\ &\quad + \delta_C (\omega - \dot{\psi}) \cos(\psi - \omega t)]\}.\end{aligned}$$

Finally, since $\xi_C = \delta_C \cos(\psi - \omega t)$ and $\eta_C = \delta_C \sin(\psi - \omega t)$, we have

$$\mathbf{F} = \gamma_i \left\{ \frac{d}{dt} [-\dot{\delta}_C \cos(\psi - \omega t)] + i \frac{d}{dt} [-\dot{\delta}_C \sin(\psi - \omega t)] \right\} = -\gamma_i (\dot{\xi}_C + i \dot{\eta}_C) = -\gamma_i \dot{\zeta}_C. \quad (12.42)$$

This force \mathbf{F} acts at C . Since the eccentricity e is very small, we can take the force \mathbf{F} to be acting at G along with a couple of very small magnitude. If we assume the coordinates of G in the xy -system to be x and y , and those of C to be x_C and y_C , the equations of motion (in the x - and y -direction) of the rigid rotor mounted on the elastic shaft (of negligible mass) will be

$$m\ddot{x} + k(x - e \cos \omega t) = 0, \quad m\ddot{y} + k(y - e \sin \omega t) = 0,$$

where $k(x - e \cos \omega t)$ and $k(y - e \sin \omega t)$ represent the x - and y -component of the restoring force applied on the rotor by the shaft. When there is no damping, these equations can be written in the form

$$m\ddot{x} + kx = ke \cos \omega t, \quad m\ddot{y} + ky = ke \sin \omega t,$$

and in the complex variable form, we obtain

$$\begin{aligned}m\ddot{x} + mi\ddot{y} + kx + kiy &= ke(\cos \omega t + i \sin \omega t), \\ m \frac{d^2}{dt^2} (x + iy) + k(x + iy) &= ek \cdot \exp(i\omega t), \\ m\ddot{\rho} + k\rho &= ek \cdot \exp(i\omega t),\end{aligned} \quad (12.43)$$

where $\rho = x + iy$. Representing the position of G in the system $\xi\eta$ in the complex variable form, we get $\zeta = \xi + i\eta$, where ξ and η are the coordinates of G in the moving system $\xi\eta$. Therefore,

$$\rho = \zeta \exp(i\omega t). \quad (12.44a)$$

From this equation, we get the relationships

$$\dot{\rho} = (\dot{\zeta} + i\omega\zeta) \exp(i\omega t), \quad (12.44b)$$

$$\ddot{\rho} = (\ddot{\zeta} + 2i\omega\dot{\zeta} - \omega^2\zeta) \exp(i\omega t). \quad (12.44c)$$

Substituting these values in (12.43), we get

$$m(\ddot{\zeta} + 2i\omega\dot{\zeta} - \omega^2\zeta) \exp(i\omega t) + k\zeta \exp(i\omega t) = ek \exp(i\omega t),$$

$$\ddot{\zeta} + 2i\omega\dot{\zeta} + \left(\frac{k}{m} - \omega^2\right)\zeta = e \frac{k}{m}. \quad (12.45)$$

This is the equation of vibration of a rotating shaft in the coordinate system $\xi\eta$ in the absence of any damping. If internal friction is considered, a damping force $\gamma_i\dot{\zeta}$ (approximately) acting at G resisting the deformation will appear in this equation of motion. Thus, when internal friction is present, the equation of vibrational motion will be

$$\ddot{\zeta} + \left(\frac{\gamma_i}{m} + 2i\omega\right)\dot{\zeta} + \left(\frac{k}{m} - \omega^2\right)\zeta = e \frac{k}{m}. \quad (12.46)$$

This equation can be again transformed into the stationary coordinate system with the help of the substitutions

$$\zeta = \rho \exp(i\omega t), \quad \dot{\zeta} = (\dot{\rho} - i\omega\rho) \exp(-i\omega t), \quad \ddot{\zeta} = (\ddot{\rho} - 2i\omega\dot{\rho} - \omega^2\rho) \exp(-i\omega t).$$

The final form of the equation of motion will be

$$\ddot{\rho} + \frac{\gamma_i}{m}\dot{\rho} + \left(\frac{k}{m} - i\omega\frac{\gamma_i}{m}\right)\rho = \frac{ek}{m} \exp(i\omega t). \quad (12.47)$$

The general solution of (12.47) is

$$\rho = A_1 \exp(i\Lambda_1 t) + A_2 \exp(i\Lambda_2 t) + \frac{e}{1 - \omega^2/(k/m)} \exp(i\omega t). \quad (12.48)$$

The last term in (12.48) represents the forced vibration caused by the disc unbalance and describes the bent line of the shaft which rotates with the velocity of the shaft about the line of supports. So for this motion, there is no change in the state of stress in the shaft and internal friction neither comes into the picture nor limits the shaft deflection when ω^2 approaches k/m or ω_{cr}^2 . To study the effect of internal friction, we shall shift our attention to the first two terms in the solution. The frequencies Λ_1 and Λ_2 are the roots of the characteristic equation of (12.47), which is

$$\Lambda^2 - i\frac{\gamma_i}{m}\Lambda - \left(\frac{k}{m} - i\omega\frac{\gamma_i}{m}\right) = 0.$$

Therefore,

$$\Lambda = \frac{i\frac{\gamma_i}{m} \pm \left[-\left(\frac{\gamma_i}{m}\right)^2 + 4\left(\frac{k}{m} - i\omega\frac{\gamma_i}{m}\right)\right]^{1/2}}{2}. \quad (12.49)$$

To separate the real and imaginary parts of Λ , let us assume

$$\Lambda = \lambda + i\nu, \quad (12.50)$$

where both λ and ν are real. From (12.49) and (12.50), we get

$$\lambda + i\nu = i\frac{\gamma_i}{2m} \pm \left\{ \left[\frac{k}{m} - \left(\frac{\gamma_i}{2m} \right)^2 \right] - i\omega\frac{\gamma_i}{m} \right\}^{1/2}$$

or

$$i(\nu - \frac{\gamma_i}{2m}) + \lambda = \pm \{[\frac{k}{m} - (\frac{\gamma_i}{2m})^2] - i\omega \frac{\gamma_i}{m}\}^{1/2}.$$

Squaring both sides of this equation, we get

$$-(\nu - \frac{\gamma_i}{2m})^2 + \lambda^2 + i2\lambda(\nu - \frac{\gamma_i}{2m}) = [\frac{k}{m} - (\frac{\gamma_i}{2m})^2] - i\omega \frac{\gamma_i}{m}.$$

Equating the real and imaginary parts of the two sides, we obtain

$$-(\nu - \frac{\gamma_i}{2m})^2 + \lambda^2 = \frac{k}{m} - (\frac{\gamma_i}{2m})^2, \quad 2\lambda(\nu - \frac{\gamma_i}{2m}) = -\omega \frac{\gamma_i}{m}. \quad (12.51)$$

From the second equation of (12.51), we get

$$(\nu - \frac{\gamma_i}{2m}) = -\omega \frac{\gamma_i}{2m} \frac{1}{\lambda}.$$

Substituting this in the first equation of (12.51), we get

$$\lambda^2 - \frac{\omega^2 \gamma_i^2}{4m^2} \frac{1}{\lambda^2} - [\frac{k}{m} - (\frac{\gamma_i}{2m})^2] = 0, \quad \lambda^4 - [\frac{k}{m} - (\frac{\gamma_i}{2m})^2]\lambda^2 - \omega^2(\frac{\gamma_i}{2m})^2 = 0.$$

Solving this quadratic equation, we get

$$\begin{aligned} \lambda^2 &= \frac{1}{2} \{ [\frac{k}{m} - (\frac{\gamma_i}{2m})^2] \pm \sqrt{[\frac{k}{m} - (\frac{\gamma_i}{2m})^2]^2 + \omega^2(\frac{\gamma_i}{m})^2} \}, \\ \lambda &= \pm \sqrt{\frac{1}{2} \{ [\frac{k}{m} - (\frac{\gamma_i}{2m})^2] + \sqrt{[\frac{k}{m} - (\frac{\gamma_i}{2m})^2]^2 + \omega^2(\frac{\gamma_i}{m})^2} \}}. \end{aligned} \quad (12.52)$$

A negative sign for the second term in the equation for λ^2 is not possible as it will result in λ becoming imaginary. Substituting this value of λ in the first equation of (12.51), we get

$$\begin{aligned} (\nu - \frac{\gamma_i}{2m})^2 &= \frac{1}{2} \{ -[\frac{k}{m} - (\frac{\gamma_i}{2m})^2] \mp \sqrt{[\frac{k}{m} - (\frac{\gamma_i}{2m})^2]^2 + \omega^2(\frac{\gamma_i}{m})^2} \}, \\ \nu_{1,2} &= \frac{\gamma_i}{2m} \pm \sqrt{\frac{1}{2} \{ -[\frac{k}{m} - (\frac{\gamma_i}{2m})^2] + \sqrt{[\frac{k}{m} - (\frac{\gamma_i}{2m})^2]^2 + \omega^2(\frac{\gamma_i}{m})^2} \}}. \end{aligned} \quad (12.53)$$

Here also, a negative sign for the second term of $[\nu - \gamma_i/(2m)]^2$ is not possible as this will result in $\nu_{1,2}$ becoming imaginary. Now, when the imaginary part of the complex frequency Λ is negative, the natural vibration superimposed on the forced vibration will be unstable. So, for stability of the system, $\nu_{1,2}$ must be positive. In other words,

$$\frac{\gamma_i}{2m} > \sqrt{\frac{1}{2} \{ -[\frac{k}{m} - (\frac{\gamma_i}{2m})^2] + \sqrt{[\frac{k}{m} - (\frac{\gamma_i}{2m})^2]^2 + \omega^2(\frac{\gamma_i}{m})^2} \}}.$$

Squaring both sides of this inequality, we have

$$(\frac{\gamma_i}{2m})^2 > \frac{1}{2} \{ -[\frac{k}{m} - (\frac{\gamma_i}{2m})^2] + \sqrt{[\frac{k}{m} - (\frac{\gamma_i}{2m})^2]^2 + \omega^2(\frac{\gamma_i}{m})^2} \},$$

$$\begin{aligned}\frac{k}{m} + \left(\frac{\gamma_i}{2m}\right)^2 &> \sqrt{\left[\frac{k}{m} - \left(\frac{\gamma_i}{2m}\right)^2\right]^2 + \omega^2\left(\frac{\gamma_i}{m}\right)^2}, \\ \left(\frac{k}{m} + \left(\frac{\gamma_i}{2m}\right)^2\right)^2 &> \left[\frac{k}{m} - \left(\frac{\gamma_i}{2m}\right)^2\right]^2 + \omega^2\left(\frac{\gamma_i}{m}\right)^2, \\ k/m &> \omega^2, \quad \omega < \omega_{cr}.\end{aligned}$$

Hence, for shaft speeds greater than ω_{cr} , the vibration will be unstable due to the presence of internal friction.

12.4 EFFECT OF EXTERNAL FRICTION

External friction always has a tendency to stabilize the system. It has been shown that internal friction induces instability whenever the shaft speed exceeds the first critical speed. However, the presence of external friction will try to suppress any such instability and a wider range of stable shaft speed is thus possible.

The frictional force exerted by the external agencies can be considered to be acting at G (Fig. 12.8) and the magnitude of this resistive force can be assumed to be proportional to the velocity of G . If the coefficient of this external friction is γ , then (12.47) will be slightly modified, so that

$$\ddot{\rho} + \frac{\gamma_i + \gamma}{m} \dot{\rho} + \left(\frac{k}{m} - i\omega \frac{\gamma_i}{m}\right)\rho = \frac{ek}{m} e^{i\omega t}. \quad (12.54)$$

The corresponding characteristic equation will be

$$\Lambda^2 - i\left(\frac{\gamma_i + \gamma}{m}\right)\Lambda - \left(\frac{k}{m} - i\omega \frac{\gamma_i}{m}\right) = 0$$

and the corresponding criterion for stability (obtained by means of a method similar to that described in Section 12.3) will be $\omega < (1 + \gamma/\gamma_i)\omega_{cr}$, indicating thereby a wider range of stability. When $\gamma \gg \gamma_i$, we get $\omega_{lim} \gg \omega_{cr}$.

12.5 GYROSCOPIC EFFECT ON CRITICAL SPEED

The analysis in the preceding sections was for a disc which is symmetrically mounted on a shaft. As the disc is mounted at the centre, the axis of spin of the disc will always be parallel to the line of supports (Fig. 12.9a). However, when the disc is not mounted at the centre, the shaft deflection causes a change in the orientation of the disc plane (Fig. 12.9b). It has been shown in Chapter 10 that any such phenomenon will be accompanied by a gyroscopic effect which will always tend to bring the shaft axis into coincidence with the axis of rotation, resulting in an increase in the effective stiffness of the shaft and a higher critical speed.

Figure 12.10 shows a simple shaft-rotor system subjected to external forces and moments. For simplicity, the unbalance in mounting the disc is neglected and the critical speed can be determined from the equilibrium of the shaft under the action of various forces and moments. Let δ be the deflection of the shaft at the position of the disc and ϕ be the slope of the shaft axis at this position C . A centrifugal force $m\omega^2\delta$ and a gyroscopic moment $J_1\omega^2\phi$ (which tends to restore the plane of the disc to its original position as shown in Fig. 12.10) will act on the shaft at the position of the

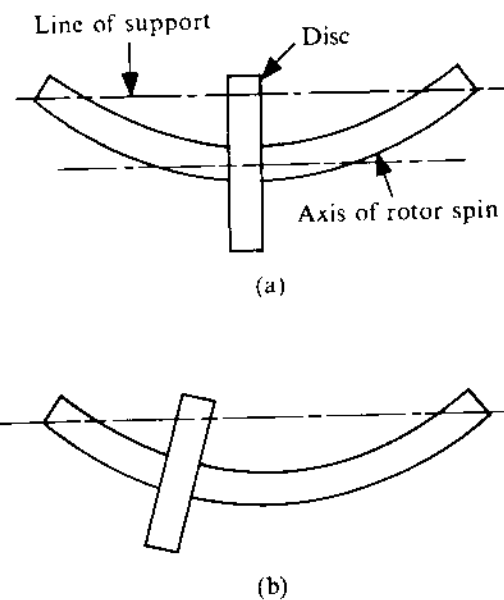


FIGURE 12.9

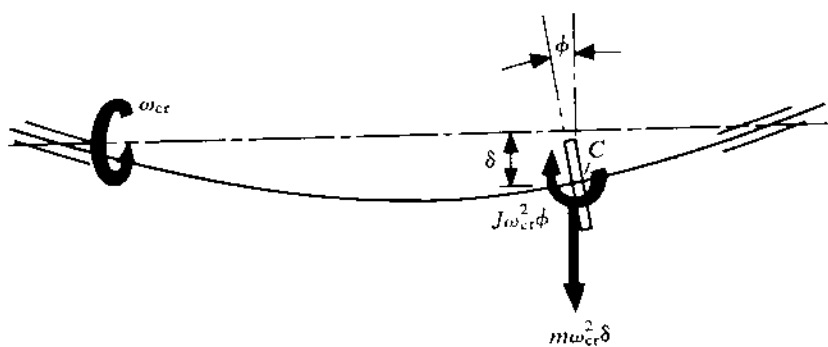


FIGURE 12.10

disc when ϕ is small (see Section 10.6). Then, the deflection of the shaft δ and the slope of the shaft axis at this point ϕ will be given by

$$\delta = m\omega^2 \delta a_{\delta\delta} - J_1 \omega^2 \phi a_{\delta\phi}, \quad \phi = m\omega^2 \delta a_{\phi\delta} - J_1 \omega^2 \phi a_{\phi\phi}, \quad (12.55)$$

where

$a_{\delta\delta}$ = deflection of the shaft at the disc position C due to a unit radial deflecting force acting at C ,

$a_{\delta\phi}$ = deflection of the shaft at C due to a unit moment acting at C , the direction of the moment being opposite to that of the gyroscopic couple,

$a_{\phi\delta}$ = slope of the shaft axis at C due to a unit load at C ,

$a_{\phi\phi}$ = slope of the shaft axis at C due to a unit moment acting at C ,

m = mass of the disc, and

J_1 = moment of inertia of the disc about a diameter.

Rearranging (12.55), we get

$$(1 - m\omega^2 a_{\delta\delta})\delta + J_1 \omega^2 a_{\delta\phi}\phi = 0, \quad -m\omega^2 a_{\phi\delta}\delta + (1 + J_1 \omega^2 a_{\phi\phi})\phi = 0.$$

A nonzero solution for δ and ϕ is possible only when the determinant

$$\begin{vmatrix} (1 - m\omega^2 a_{\delta\delta}) & J_1 \omega^2 a_{\delta\phi} \\ -m\omega^2 a_{\phi\delta} & (1 + J_1 \omega^2 a_{\phi\phi}) \end{vmatrix}$$

vanishes. Expanding the determinant, we get

$$\omega^4 + \frac{ma_{\delta\delta} - J_1 a_{\phi\phi}}{mJ_1(a_{\phi\phi}a_{\delta\delta} - a_{\phi\delta}a_{\delta\phi})}\omega^2 - \frac{1}{mJ_1(a_{\phi\phi}a_{\delta\delta} - a_{\phi\delta}a_{\delta\phi})} = 0. \quad (12.56)$$

Solving this equation, we get only one positive value of ω^2 from which the critical value of the shaft speed can be calculated. Thus,

$$\omega_{cr} = \sqrt{\frac{1}{2mJ_1\Delta}[J_1 a_{\phi\phi} - ma_{\delta\delta} + \sqrt{(ma_{\delta\delta} + J_1 a_{\phi\phi})^2 - 4mJ_1 a_{\phi\delta} a_{\delta\phi}}]},$$

where $\Delta = (a_{\phi\phi}a_{\delta\delta} - a_{\phi\delta}a_{\delta\phi})$. At any other shaft speed, both δ and ϕ will be zero, i.e., the shaft will not deflect.

12.6 EFFECT OF THE GRAVITATIONAL FIELD (SECONDARY CRITICAL SPEED)

In horizontal shafts with heavy discs, the rotation becomes nonuniform because of the unidirectional gravitational pull. It is obvious that the frequency of nonuniformity (superimposed on the average uniform rotation) will be equal to the average speed of rotation. If the coordinates of the rotor-mass centre G are represented by x and y (see Fig. 12.4), and the rotation of the shaft rotor by

(Fig. 12.4), then x , y , and θ can be considered to be the generalized coordinates of the system. Disregarding the driving torque, Lagrange's equations for such a system (without any damping) will be

$$m\ddot{x} + kx = ke \cos \theta + mg,$$

$$m\ddot{y} + ky = ke \sin \theta, \quad (12.57)$$

$$J_G \ddot{\theta} + ke(x \sin \theta - y \cos \theta) = -mge \sin \theta,$$

where J_G is the moment of inertia of the disc about an axis through G . The derivation is simple and is left as an exercise for the reader. Let us assume that, in the first approximation, $\theta = \omega t$. Then, considering the free vibration to be damped out, the steady-state solutions for the first two equations of (12.57) will be

$$x = \frac{ke}{k - m\omega^2} \cos \omega t + \frac{mg}{k}, \quad y = \frac{ke}{k - m\omega^2} \sin \omega t. \quad (12.58)$$

Substituting x and y from (12.58) in the third equation of (12.57), we get

$$\begin{aligned} J_G \ddot{\theta} + mge \sin \theta &= -mge \sin \theta, \\ \ddot{\theta} &= -\frac{2mge}{J_G} \sin \theta. \end{aligned} \quad (12.59)$$

Solving this, the expression for θ will be

$$\theta = \frac{2mge}{J_G \omega^2} \sin \omega t + C_1 t + C_2. \quad (12.60)$$

When solving (12.59), it is assumed that $\theta = \omega t$ for the right-hand side of the equation. To fix the initial condition, let us assume that $\theta = 0$ at $t = 0$. Then, from (12.60), we get $C_2 = 0$. Now, since the second approximation in θ [given by equation (12.60)] should tally with our first approximation, C_1 should be equal to ω as e is normally very small. Thus, we get

$$\theta = \omega t + \frac{2mge}{J_G \omega^2} \sin \omega t. \quad (12.61)$$

Substituting this value of θ in the second equation of (12.57), we get a differential equation in y . Thus,

$$\begin{aligned} m\ddot{y} + ky &= ke \sin [\omega t + \frac{2mge}{J_G \omega^2} \sin \omega t] \\ &= ke \{ \sin \omega t \cdot \cos [\frac{2mge}{J_G \omega^2} \sin \omega t] + \cos \omega t \cdot \sin [\frac{2mge}{J_G \omega^2} \sin \omega t] \}. \end{aligned} \quad (12.62)$$

Since e is normally very small, we have

$$\cos [\frac{2mge}{J_G \omega^2} \sin \omega t] \rightarrow 1, \quad \sin [\frac{2mge}{J_G \omega^2} \sin \omega t] \rightarrow \frac{2mge}{J_G \omega^2} \sin \omega t.$$

So, (12.62) reduces to the form

$$m\ddot{y} + ky \approx ke(\sin \omega t + \frac{mge}{J_G \omega^2} \sin 2\omega t).$$

Therefore, steady-state motion of the rotor CG in the y -direction will be

$$y = \frac{ke}{k - m\omega^2} \sin \omega t + \frac{kmge^2}{J_G \omega^2(k - 4m\omega^2)} \sin 2\omega t. \quad (12.63)$$

From (12.63), it is seen that the rotor CG will have a very large deflection when either

$$\omega = (k/m)^{1/2} = \omega_{cr}$$

or

$$\omega = \frac{1}{2}(k/m)^{1/2} = \frac{1}{2}\omega_{cr}.$$

So, it is evident that, for heavy shaft-rotor systems which are very lightly damped, resonance is also possible when the speed is half the critical speed. This is known as the *secondary critical speed*.

12.7 EFFECT OF BEARING STIFFNESS

So far, we have assumed that the supports of a shaft do not have any flexibility and also that they do not provide any damping. In fact, the bearings of a shaft are not infinitely rigid and have some damping capacity. In this section, we will discuss the effect of support stiffness on the critical speed of a shaft.

Let us consider a shaft which is supported by identical bearings of finite rigidity, and a disc mounted on the shaft at the central position. Let the stiffnesses of the bearings in the two principal directions be k_1 and k_2 . In practice, it is observed that the rigidity characteristics of the bearings of a system are not isotropic and depend on the direction of the deformation. Other considerations such as the mass of the bearings and damping, will be omitted to simplify the analysis. Due to the flexibility of the bearings, the line of supports will not remain stationary and the point of intersection of the line of supports with the principal plane S (i.e., the plane perpendicular to the line of supports and to the disc) at any instant is shown in Fig. 12.11. As before, the points $C(x_C, y_C)$ and $G(x, y)$ represent the shaft-disc centre and the CG of the disc, respectively. The displacement of the line of supports can be obtained by calculating the deflection of the bearings due to the force exerted at the ends of the shaft. If the principal directions coincide with the x - and y -direction, and if the corresponding total stiffnesses in respective directions (taking both bearings together) are k_1 and k_2 , the resultant stiffness of the shaft at the point where the disc has been mounted, in the x - and y -direction, can be found by considering the shaft to be a spring of stiffness k in series with the equivalent spring with stiffness k_1 or k_2 depending on the direction. In the x -direction, the overall effective stiffness of the point of mounting the disc will be equal to the resultant stiffness of two springs with stiffnesses k_1 and k in series and that in the y -direction will be the resultant stiffness of two springs with stiffnesses k_2 and k in series. So, the resultant stiffnesses in the x - and y -direction will be

$$k_{xx} = \frac{kk_1}{k + k_1}, \quad k_{yy} = \frac{kk_2}{k + k_2}. \quad (12.64)$$

The total potential and kinetic energies of the system (disregarding the driving torque) can now be determined to be

$$V = \frac{1}{2}k_{xx}(x - e \cos \omega t)^2 + \frac{1}{2}k_{yy}(y - e \sin \omega t)^2,$$

$$T = \frac{1}{2}m\dot{x}^2 + \frac{1}{2}m\dot{y}^2 + \frac{1}{2}J_G\dot{\theta}^2.$$

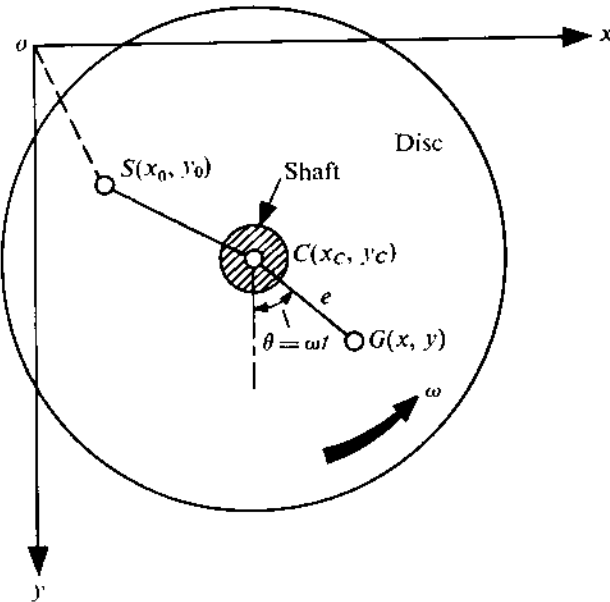


FIGURE 12.11

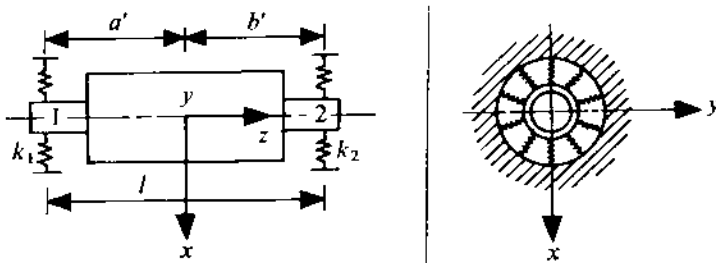


FIGURE 12.12

Lagrange's equations of motion for the x - and y -direction will be

$$m\ddot{x} + k_{xx}x = k_{xx}e \cos \omega t, \quad m\ddot{y} + k_{yy}y = k_{yy}e \sin \omega t.$$

Substituting the values for k_{xx} and k_{yy} in these equations, we get

$$m\ddot{x} + \frac{kk_1}{k+k_1}x = \frac{kk_1e}{k+k_1} \cos \omega t, \quad m\ddot{y} + \frac{kk_2}{k+k_2}y = \frac{kk_2e}{k+k_2} \sin \omega t. \quad (12.65)$$

From (12.65), it is obvious that resonance will occur when the speed of the shaft is $\{kk_1/[m(k+k_1)]\}^{1/2}$ or $\{kk_2/[m(k+k_2)]\}^{1/2}$. Therefore, the flexibility of the bearing and its variation with direction cause the critical speed of the shaft to split into two lower values. The real problem of a rotating shaft on elastic bearings is extremely complicated; the foregoing analysis only gives some idea of the behaviour of such a system.

Sometimes, a somewhat similar problem arises (though the basic characteristic is different) when rigid rotors are supported on elastic bearings. Because of the comparatively greater rigidity of the rotor, the deflection will be only due to the deflection of the supporting bearings. A problem of this type, with some idealizations to simplify the analysis, will be discussed here. The first idealization

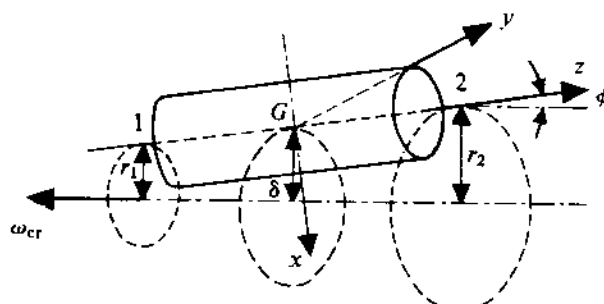


FIGURE 12.13

is that the bearings are assumed to have different but isotropic rigidity characteristics (i.e., the characteristics are independent of the direction). Let the stiffnesses of the bearings be k_1 and k_2 (see Fig. 12.12). Secondly, the rotor is assumed to be balanced and the moments of inertia of the rotor about x , y , and z are J_x , J_y , and J_z , respectively, the coordinate system xyz being fixed with the rotor. When the shaft rotates, the bearings will deflect and each end of the shaft will describe a circle as shown in Fig. 12.13. The axis of a rigid rotor will always remain straight and it will describe the surface of a cone. In the critical condition, the system will be in neutral equilibrium under the action of the centrifugal force and bearing reactions, regardless of the magnitude of the deflection.

If the deflection of the shaft at its ends 1 and 2 is r_1 and r_2 , respectively, then, from Fig. 12.13, it is seen that $r_1 = r$ and $r_2 = r + \phi l$, where ϕ is the inclination of the rotor axis with the original line of supports, and l is the distance between ends 1 and 2. Since the rotor is rigid, the radial displacement of the CG of the rotor G will be $(r + \phi a')$. Hence, we get the relationship

$$m\omega_{cr}^2(r + \phi a') = k_1 r + k_2(r + \phi l), \quad (12.66)$$

where $k_1 r$ and $k_2(r + \phi l)$ are the support reactions. When in motion, the rotor is subjected to a moment due to the support reactions. Now, as the motion is considered to be synchronous, i.e., the rotor speed and the precessional-motion speed are the same, it can be assumed (by suitably selecting the directions of the x - and y -axis) that the deflection vector δ of the point G always lies in the xz -plane (Fig. 12.13). Since the bearing reaction forces are parallel to δ , the only possible nonzero component of the moment due to the bearing reactive forces is M_y , where

$$M_y \approx k_1 r a' - k_2(r + \phi l) b' \quad (12.67)$$

(assuming the angle of deflection ϕ to be small). As the coordinate system xyz is fixed with the rotor, Euler's equation of motion will be

$$J_y \dot{\omega}_y + (J_z - J_x) \omega_z \omega_x = M_y, \quad (12.68)$$

where ω_x , ω_y , and ω_z are respectively the x -, y -, and z -component of ω_{cr} . From Fig. 12.13, it is clear that $\omega_x = \omega_{cr} \sin \phi$, $\omega_y = 0$, and $\omega_z = \omega_{cr} \cos \phi$. Assuming ϕ to be small, we get

$$\omega_x = \omega_{cr} \phi, \quad \omega_y = 0, \quad \omega_z = \omega_{cr}. \quad (12.69)$$

Substituting these values in (12.68), we obtain

$$M_y = (J_z - J_x) \omega_{cr}^2 \phi. \quad (12.70)$$

uating M_y from (12.67) and (12.70), we get

$$(J_z - J_x)\omega_{cr}^2\phi = k_1ra' - k_2(r + \phi l)b',$$

$$(k_1a' - k_2b')r - [k_2b'l + (J_z - J_x)\omega_{cr}^2]\phi = 0. \quad (12.71)$$

Again, equation (12.66) can be written in the form

$$(k_1 + k_2 - m\omega_{cr}^2)r + (k_2l - m\omega_{cr}^2a')\phi = 0. \quad (12.72)$$

, the nonzero solution for r and ϕ will be possible from (12.71) and (12.72) only when

$$\begin{vmatrix} (k_1a' - k_2b') & -[k_2b'l + (J_z - J_x)\omega_{cr}^2] \\ (k_1 + k_2 - m\omega_{cr}^2) & (k_2l - m\omega_{cr}^2a') \end{vmatrix} = 0,$$

and since $a' + b' = l$, the condition to be satisfied is

$$\omega_{cr}^4 + \left[\frac{k_1a'^2 + k_2b'^2}{J_z - J_x} - \frac{k_1 + k_2}{m} \right] \omega_{cr}^2 + \frac{k_1k_2l^2}{m(J_z - J_x)} = 0. \quad (12.73)$$

The value of ω_{cr} can be determined by solving (12.73).

2.8 EFFECT OF VARIABLE SHAFT STIFFNESS

In the foregoing analyses, we have assumed that the shaft has a uniform stiffness in all directions. Sometimes, the shaft may not have a circular cross-section and its moment of inertia may be dependent on the direction of the axis of bending. Such a situation is commonly created by the presence of keyways. Rotating disc-shaft systems of this type will be considered here.

Figure 12.14 shows the cross-section of the central portion of the shaft at any instant. It will be assumed that the disc is mounted at the middle of the shaft and that gyroscopic action is absent. The axes ξ and η of a coordinate system rotating with the shaft are chosen so as to be parallel to the principal directions about which the second moment of area of the shaft cross-section is maximum and minimum. As the coordinate system rotates with the shaft, the shaft rigidity with respect to this coordinate system does not change with time. Let the stiffnesses in the ξ' - and η' -direction be k_1 and k_2 , respectively, where the ξ' - and η' -axis are parallel to ξ and η , respectively, and pass through the centre C of the shaft (see Fig. 12.14). For the sake of simplicity, the damping effects will be neglected, and the restoring force exerted by the bent shaft on the disc can be expressed as $i(k_1\xi_C + ik_2\eta_C)e^{i\omega t}$. Furthermore,

$$\xi_C = \xi - e \cos \theta_0, \quad \eta_C = \eta - e \sin \theta_0, \quad \rho = x + iy = \zeta e^{i\omega t} = (\xi + i\eta) e^{i\omega t}.$$

Now, taking the restoring force and gravitational pull into account, the equilibrium equation will be

$$m(\ddot{\zeta} + 2i\omega\dot{\zeta} - \omega^2\zeta)e^{i\omega t} + [k_1(\xi - e \cos \theta_0) + ik_2(\eta - e \sin \theta_0)]e^{i\omega t} = mg. \quad (12.74)$$

Substituting $\zeta = \xi + i\eta$ in (12.74), we get

$$m(\ddot{\xi} - 2\omega\dot{\eta} - \omega^2\xi)e^{i\omega t} + im(\ddot{\eta} + 2\omega\xi - \omega^2\eta)e^{i\omega t} + k_1(\xi - e \cos \theta_0)e^{i\omega t} + ik_2(\eta - e \sin \theta_0)e^{i\omega t} = mg,$$

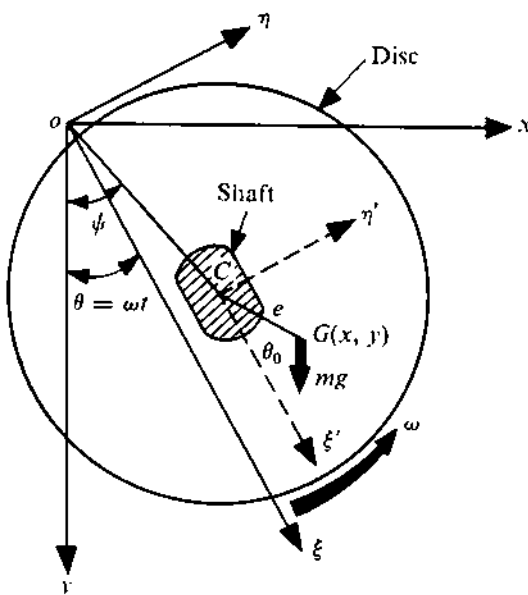


FIGURE 12.14

$$[m(\ddot{\xi} - 2\omega\dot{\eta} - \omega^2\xi) + k_1(\xi - e \cos \theta_0)] + i[m(\ddot{\eta} + 2\omega\dot{\xi} - \omega^2\eta) + k_2(\eta - e \sin \theta_0)] \\ = e^{-i\omega t}mg = mg \cos \omega t - img \sin \omega t.$$

Equating the real and imaginary parts of the two sides of this equation, we obtain

$$\ddot{\xi} - 2\omega\dot{\eta} + (k_1/m - \omega^2)\xi = (k_1/m)e \cos \theta_0 + g \cos \omega t, \quad (12.75)$$

$$\ddot{\eta} + 2\omega\dot{\xi} + (k_2/m - \omega^2)\eta = (k_2/m)e \sin \theta_0 - g \sin \omega t.$$

These equations represent the elastic vibration of the shaft-rotor system. To investigate the stability of such a system (apart from the resonance which may occur at some values of ω), we have to investigate the free-vibration component of the motion. Therefore, we shall examine the homogeneous equations obtained by setting the right-hand sides of the set of equations (12.75) equal to zero. Assuming that the solutions will have the form

$$\xi = C_1 e^{\Lambda t}, \quad \eta = C_2 e^{\Lambda t},$$

we get

$$(\Lambda^2 + k_1/m - \omega^2)C_1 - 2\omega\Lambda C_2 = 0, \quad 2\omega\Lambda C_1 + (\Lambda^2 + k_2/m - \omega^2)C_2 = 0.$$

Hence, the characteristic equation will be

$$\Lambda^4 + (k_1/m + k_2/m + 2\omega^2)\Lambda^2 + (k_1/m - \omega^2)(k_2/m - \omega^2) = 0.$$

This characteristic equation has four roots, namely,

$$\Lambda_{1, 2, 3, 4} = \pm \left[-\left(\frac{k_1/m + k_2/m + 2\omega^2}{2} \right) \pm \left\{ \left(\frac{k_1/m + k_2/m + 2\omega^2}{2} \right)^2 - \left(\frac{k_1}{m} - \omega^2 \right) \left(\frac{k_2}{m} - \omega^2 \right) \right\}^{1/2} \right]^{1/2}.$$

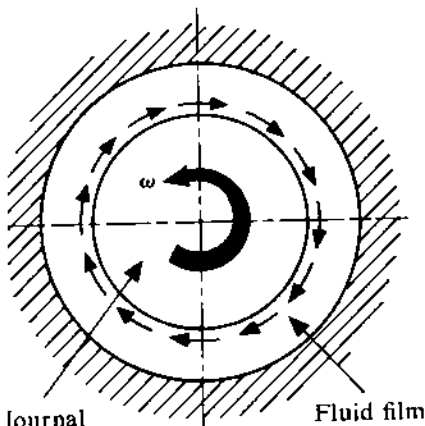


FIGURE 12.15

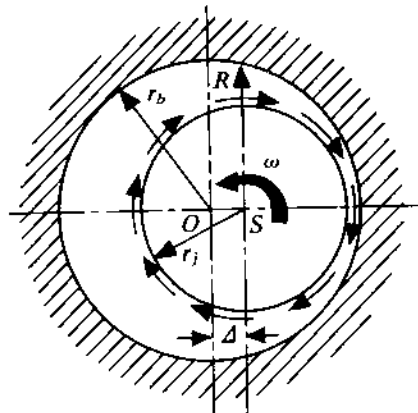


FIGURE 12.16

xamining the right-hand side, it is found that when

$$[(\frac{k_1/m + k_2/m + 2\omega^2}{2})^2 - (\frac{k_1}{m} - \omega^2)(\frac{k_2}{m} - \omega^2)]^{1/2} > (\frac{k_1/m + k_2/m + 2\omega^2}{2})$$

$$(k_1/m - \omega^2)(k_2/m - \omega^2) < 0, \quad (12.76)$$

is possible for Λ to have positive real values for which the free-vibration component will diverge to infinity. When $k_1 > k_2$, condition (12.76) is satisfied if the value of ω lies within the range

$$(k_1/m)^{1/2} < \omega < (k_2/m)^{1/2}.$$

Therefore, the free vibration of such a shaft-rotor system will be unstable for the whole range of ω between $\sqrt{(k_1/m)}$ and $\sqrt{(k_2/m)}$.

12.9 EFFECT OF OIL FILM IN BEARINGS

When a rotating shaft is supported by journal bearings, the oil film affects the motion of the shaft and may cause dangerous critical situations. We shall consider a highly simplified model to show the effect of oil film on the motion of a shaft-rotor system. It will be assumed that the bearings are identical in respect of their hydrodynamic characteristics.

When a journal rotates in a bearing and the annular space between the bearing and the journal (see Fig. 12.15) is filled with a viscous fluid, the frictional force exerted by the annular fluid film on the journal surface will be in a direction opposite to that in which the journal rotates. The magnitude of this force at a particular point will depend on the difference between the linear velocity of the journal surface and the average fluid-film velocity at the corresponding plane. The greater the difference between these velocities, the larger will be the magnitude of the frictional force. When the journal rotates at the central position, the frictional force over the journal surface will be uniform, as shown in Fig. 12.15. Now, let us consider the case when the journal has shifted a distance Δ from the central position due to the application of some force (Fig. 12.16). At this position, the annular gap varies in width, and consequently the average velocity of the fluid film also varies. If the rate of flow

is Q , the condition for continuity of flow requires that $Q = hv_{av}$ or

$$v_{av} = Q/h, \quad (12.7)$$

where v_{av} is the average film velocity at any section and h is the thickness of the fluid film at the corresponding section. Therefore, the relative velocity between the journal surface and the average flow of the fluid at any section will be

$$v_{rel} = \omega r_j - v_{av} = \omega r_j - Q/h, \quad (12.7)$$

where r_j is the radius of the journal and ω is the angular speed of the shaft. For this condition the frictional force on the journal surface will vary along the circumference, with the result that the journal will be subjected to a resistive torque and a resultant force R in a direction perpendicular to that of the shift (see Fig. 12.16).

To estimate the magnitude of R , let us consider Fig. 12.17. The journal centre S has shifted to the right by an amount Δ . The magnitude of the force on element $r_j d\alpha$ will be $dF = fr_j d\alpha$, where f is the frictional force on the journal per unit length at P . As this elemental force acts in a direction normal to the radius SP , the vertical component of the force will be

$$dR = -fr_j \cos \alpha d\alpha. \quad (12.7)$$

To determine f , let us find the relative velocity between the journal surface and the average fluid flow at P . From the triangle OST in Fig. 12.17, it is seen that

$$\frac{OT}{\sin(\pi - \alpha)} = \frac{OS}{\sin \beta} = \frac{ST}{\sin(\alpha - \beta)}, \quad \frac{r_b}{\sin \alpha} = \frac{\Delta}{\sin \beta} = \frac{r_j + h}{\sin(\alpha - \beta)},$$

where r_b is the radius of the bearing. So, $\sin \beta = (\Delta/r_b) \sin \alpha$. Furthermore, we get

$$r_j + h = \frac{r_b}{\sin \alpha} \sin(\alpha - \beta) = \frac{r_b}{\sin \alpha} [\sin \alpha \cos \beta - \cos \alpha \sin \beta].$$

Assuming Δ/r_b to be small, we get

$$h = (r_b - r_j) - \Delta \cos \alpha. \quad (12.80)$$

From (12.78) and (12.80), the value of v_{rel} will be

$$v_{rel} = \omega r_j - \frac{Q}{(r_b - r_j) - \Delta \cos \alpha}.$$

Since the intensity of friction force on the journal surface is proportional to v_{rel} , f can be expressed as

$$f = \mu v_{rel} = \mu(\omega r_j - \frac{Q}{r_b - r_j} \cdot \frac{1}{1 - a \cos \alpha}), \quad (12.81)$$

where $a = \Delta/(r_b - r_j)$. Hence, from (12.79) and (12.81), we get

$$\begin{aligned} R &= \int dR = -\mu r_j \int_0^{2\pi} \cos \alpha (\omega r_j - \frac{Q}{r_b - r_j} \cdot \frac{1}{1 - a \cos \alpha}) d\alpha \\ &= -\mu \omega r_j^2 \int_0^{2\pi} \cos \alpha d\alpha + \frac{\mu Q r_j}{r_b - r_j} \int_0^{2\pi} \frac{\cos \alpha d\alpha}{1 - a \cos \alpha}. \end{aligned}$$

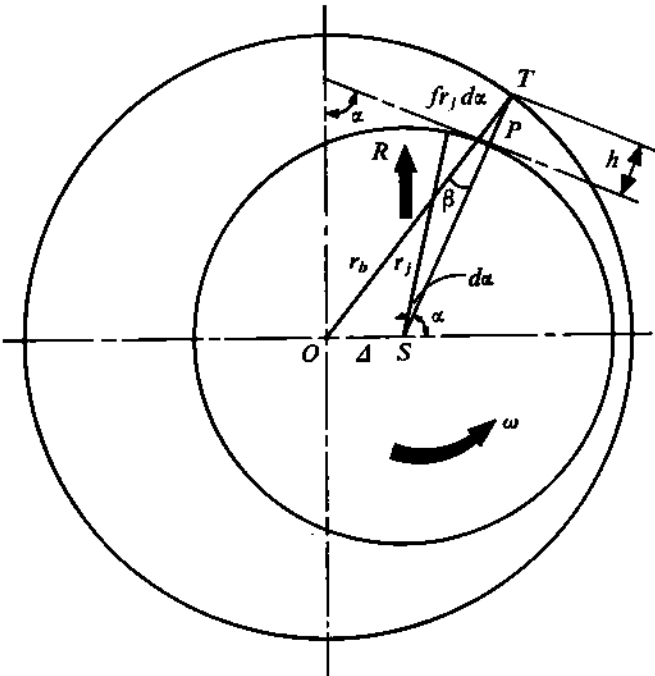


FIGURE 12.17

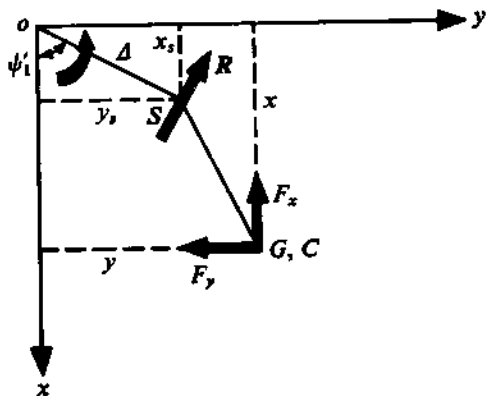


FIGURE 12.18

Now,

$$\int_0^{2\pi} \cos \alpha \, d\alpha = 0,$$

$$\begin{aligned} \int_0^{2\pi} \frac{\cos \alpha \, d\alpha}{1 - a \cos \alpha} &= \frac{1}{a} \int_0^{2\pi} \frac{a \cos \alpha \, d\alpha}{1 - a \cos \alpha} = \frac{1}{a} \int_0^{2\pi} \left(\frac{1}{1 - a \cos \alpha} - 1 \right) d\alpha \\ &= \frac{1}{a} \left\{ \left[\frac{4}{\sqrt{(1-a^2)}} \tan^{-1} \left[\frac{\sqrt{(1+a)}}{\sqrt{(1-a)}} \tan \frac{\alpha}{2} \right] \right]_0^\pi - 2\pi \right\} \\ &= \frac{2\pi}{a} \left[\frac{1}{\sqrt{(1-a^2)}} - 1 \right] \approx 2\pi a, \end{aligned}$$

neglecting higher-order terms in a (since a is normally much less than unity). Therefore, we finally get

$$R \approx \frac{2\pi\mu Q r_j}{(r_b - r_j)^2} \Delta \approx \tau \Delta. \quad (12.82)$$

So, it is found that the resultant force on the journal will be proportional to the shift and will act in a direction perpendicular to that of the shift. Actually, the force R causes the centre of journal S to rotate about the bearing centre O in the direction of rotation of the journal.

To determine the effect of this force and of damping, let us consider the shaft-rotor system as shown in Fig. 12.18. The point G represents the instantaneous position of the CG of the disc and S is the centre of the journal. For this analysis, it is assumed that the unbalance is negligible so

that the mass centre of the disc and the centre of the shaft coincide. The shift Δ sets up a force F which is given by $R = \tau\Delta$. From Fig. 12.18, it is obvious that

$$R_x = -\tau\Delta \sin \psi' = -\tau y_s, \quad R_y = \tau\Delta \cos \psi' = \tau x_s. \quad (12.83)$$

The components of the viscous drag force at G will be proportional to the corresponding component of velocity of the point G , that is, $F_x = \gamma\dot{x}$ and $F_y = \gamma\dot{y}$. Now, neglecting the mass of the shaft, the equations of motion of the shaft-disc system will be

$$m\ddot{x} = -\gamma\dot{x} - \tau y_s, \quad m\ddot{y} = -\gamma\dot{y} + \tau x_s. \quad (12.84)$$

Again, considering the dynamic equilibrium of only the disc, we get

$$m\ddot{x} = -\gamma\dot{x} - k(x - x_s), \quad m\ddot{y} = -\gamma\dot{y} - k(y - y_s). \quad (12.85)$$

Equating the right-hand sides of (12.84) and (12.85), x_s and y_s can be expressed in the form

$$x_s = x - (\tau/k)y_s, \quad y_s = (\tau/k)x_s + y$$

or

$$x_s = \frac{k^2}{k^2 + \tau^2}x - \frac{k\tau}{k^2 + \tau^2}y,$$

$$y_s = \frac{k\tau}{k^2 + \tau^2}x + \frac{k^2}{k^2 + \tau^2}y.$$

Substituting these values of x_s and y_s in (12.84), we get the equations of motion in terms of x and y to be

$$m\ddot{x} + \gamma\dot{x} + \frac{k\tau^2}{k^2 + \tau^2}x + \frac{k^2\tau}{k^2 + \tau^2}y = 0,$$

$$m\ddot{y} + \gamma\dot{y} + \frac{k\tau^2}{k^2 + \tau^2}y - \frac{k^2\tau}{k^2 + \tau^2}x = 0$$

or

$$\ddot{x} + \frac{\gamma}{m(k^2 + \tau^2)}\dot{x} + \frac{k^2\tau}{m(k^2 + \tau^2)}x + \frac{k^2\tau}{m(k^2 + \tau^2)}y = 0, \quad \ddot{y} + \frac{\gamma}{m}\dot{y} + \frac{k\tau^2}{m(k^2 + \tau^2)}y - \frac{k^2\tau}{m(k^2 + \tau^2)}x = 0. \quad (12.86)$$

Assuming the solutions for (12.86) to be of the form $x = Xe^{\Lambda t}$, $y = Ye^{\Lambda t}$, we get

$$[\Lambda^2 + \frac{\gamma}{m}\Lambda + \frac{k\tau^2}{m(k^2 + \tau^2)}]X + \frac{k^2\tau}{m(k^2 + \tau^2)}Y = 0,$$

$$-\frac{k^2\tau}{m(k^2 + \tau^2)}X + [\Lambda^2 + \frac{\gamma}{m}\Lambda + \frac{k\tau^2}{m(k^2 + \tau^2)}]Y = 0.$$

For a nonzero solution to exist, the condition

$$[\Lambda^2 + \frac{\gamma}{m}\Lambda + \frac{k\tau^2}{m(k^2 + \tau^2)}]^2 + [\frac{k^2\tau}{m(k^2 + \tau^2)}]^2 = 0 \quad (12.87)$$

nust be satisfied. In general, the root Λ will be complex and of the form $\Lambda = \lambda + i\nu$, λ and ν both being real. The system, when disturbed, will have stable motion only if λ is negative. Equation (12.87) can be written in the form

$$\Lambda^2 + \frac{\gamma}{m}\Lambda + \frac{k\tau}{m(k^2 + \tau^2)}(\tau \mp ik) = 0$$

and solving this, we get

$$\Lambda = -\frac{\gamma}{2m} \pm \sqrt{\frac{\gamma^2}{4m^2} - \frac{k\tau}{m(k^2 + \tau^2)}(\tau \mp ik)}$$

or

$$\begin{aligned} \Lambda = -\frac{\gamma}{2m} &\pm \sqrt{\frac{1}{2}\left\{\sqrt{\left[\frac{k\tau^2}{m(k^2 + \tau^2)} - \frac{\gamma^2}{4m^2}\right]^2 + \left[\frac{k^2\tau}{m(k^2 + \tau^2)}\right]^2} - \frac{k\tau^2}{m(k^2 + \tau^2)} + \frac{\gamma^2}{4m^2}\right\}} \\ &\pm i\sqrt{\frac{1}{2}\left\{\sqrt{\left[\frac{k\tau^2}{m(k^2 + \tau^2)} - \frac{\gamma^2}{4m^2}\right]^2 + \left[\frac{k^2\tau}{m(k^2 + \tau^2)}\right]^2} + \frac{k\tau^2}{m(k^2 + \tau^2)} - \frac{\gamma^2}{4m^2}\right\}}. \end{aligned}$$

The real parts of $\Lambda_1, 2, 3, 4$ are

$$\lambda_{1, 2} = -\frac{\gamma}{2m} \pm \sqrt{\frac{1}{2}\left\{\sqrt{\left[\frac{k\tau^2}{m(k^2 + \tau^2)} - \frac{\gamma^2}{4m^2}\right]^2 + \left[\frac{k^2\tau}{m(k^2 + \tau^2)}\right]^2} - \frac{k\tau^2}{m(k^2 + \tau^2)} + \frac{\gamma^2}{4m^2}\right\}}.$$

So, the system will be stable when both λ_1 and λ_2 are negative, that is, when

$$\frac{\gamma}{2m} > \sqrt{\frac{1}{2}\left\{\sqrt{\left[\frac{k\tau^2}{m(k^2 + \tau^2)} - \frac{\gamma^2}{4m^2}\right]^2 + \left[\frac{k^2\tau}{m(k^2 + \tau^2)}\right]^2} - \frac{k\tau^2}{m(k^2 + \tau^2)} + \frac{\gamma^2}{4m^2}\right\}},$$

i.e., $\gamma > k[km/(k^2 + \tau^2)]^{1/2}$. Thus, it is found that in the absence of any damping such a system will always be unstable. Again, as experiments have shown that $\tau \propto \omega$, the critical value of γ depends on ω . A lower damping capacity will be required to stabilize the system at higher shaft speeds, and vice versa. It is also seen that systems with heavier discs tend to be more unstable.

PROBLEM 12.1

A uniform circular shaft, supported by two short bearings, carries a circular disc at the free end of the overhang as shown in Fig. 12.19. The supported portion of the shaft has a length l and the length of the overhang is $l/2$. The diameter and mass of the disc are d and m , respectively. Find the critical speed of the system and compare the answer with the critical speed of the same system when the gyroscopic effects are neglected. Assume $d = l/2$.

SOLUTION

From (12.56), it is seen that the critical speed is obtained by solving the equation

$$\omega_{cr}^4 + \frac{ma_{\delta\delta} - Ja_{\phi\phi}}{mJ_1(a_{\phi\phi}a_{\delta\delta} - a_{\phi\delta}a_{\delta\phi})}\omega_{cr}^2 - \frac{1}{mJ_1(a_{\phi\phi}a_{\delta\delta} - a_{\phi\delta}a_{\delta\phi})} = 0.$$

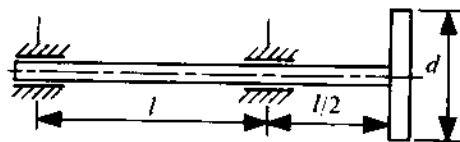


FIGURE 12.19

For the given system, the values of the influence coefficients will be

$$a_{\delta\delta} = 0.125 \frac{l^3}{EI}, \quad a_{\delta\phi} = a_{\phi\delta} = 0.292 \frac{l^2}{EI}, \quad a_{\phi\phi} = 0.833 \frac{l}{EI},$$

where E is the modulus of elasticity of the shaft material and I is the second moment of area of the shaft cross-section about its diameter. The moment of inertia of the disc about its diameter will be given by the equation

$$J_1 = \frac{1}{4}m(d/2)^2 = md^2/16.$$

Substituting these values in the equation for critical speed, we get

$$\omega_{cr}^4 + 377 \frac{EI}{kl^3} \omega_{cr}^2 - 3440 \left(\frac{EI}{ml^3} \right)^2 \approx 0, \quad \omega_{cr} \approx 3.0 \left(\frac{EI}{ml^3} \right)^{1/2}.$$

If the gyroscopic effects are neglected, the critical speed will be

$$\omega_{cr} \approx 2.83 \left(\frac{EI}{ml^3} \right)^{1/2}.$$

The higher critical speed is due to the increased stiffness caused by the gyroscopic action.

PROBLEM 12.2

A circular disc has a diameter of 30 cm, and is mounted on a shaft of rectangular cross-section which is supported on short bearings 80 cm apart. The cross-section of the shaft is 5 cm by 2.5 cm and the material of all the components is mild steel. Determine the range of instability for the system.

SOLUTION

From Section 12.8, it is seen that the system will be unstable when the angular speed lies between $\sqrt{k_1/m}$ and $\sqrt{k_2/m}$. k_1 and k_2 are the principal stiffnesses and m is the mass of the disc. For the problem under consideration, the limits of speed for instability are found to be 420 rad/s and 210 rad/s, respectively.

12.10 ROTATING SHAFTS WITH SEVERAL DISCS

When several discs are mounted on a rotating shaft, the gyroscopic effects will always be present because all the discs will not maintain the original plane of rotation when the shaft deflects. In analyzing these problems, the magnitude of unbalance in the discs is considered to be very small and the mass centres of the several discs are assumed to coincide with the corresponding shaft centres. The dynamic equilibrium equations are written for each disc, separately for linear motions

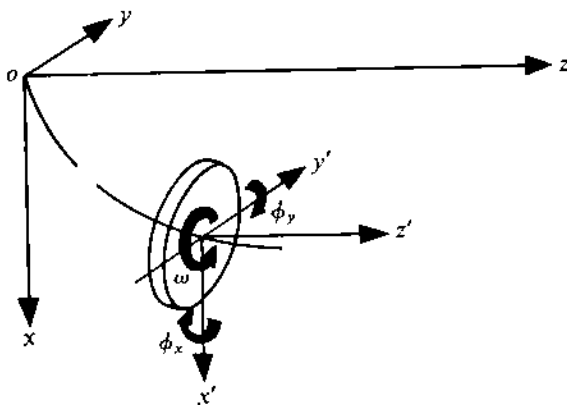


FIGURE 12.20

in the x - and y -direction and angular motions in the xz - and yz -plane (see Fig. 12.20). The equations of motion for the x - and y -direction will be

$$m\ddot{x} + F_x = 0, \quad m\ddot{y} + F_y = 0, \quad (12.88)$$

where m is the mass of the disc, and F_x and F_y are the components of resultant force on the disc in the x - and y -direction, respectively. Representing the components of angular rotation by ϕ_x and ϕ_y , the equations of angular motion will be

$$J_1\ddot{\phi}_x - J\omega\dot{\phi}_y + M_x = 0, \quad J_1\ddot{\phi}_y + J\omega\dot{\phi}_x + M_y = 0, \quad (12.89)$$

where J_1 and J are the equatorial and polar moments of inertia of the disc, ω is the rotational speed of the shaft about its own axis, and M_x and M_y are the components of the moment exerted by the shaft on the disc. $J\omega$ is the angular momentum of the disc and $-J\omega\dot{\phi}_y$ and $J\omega\dot{\phi}_x$ are the components of the gyroscopic moment on the disc when the deflections are assumed to be small. It should be remembered that this is not a case of synchronous precession. The magnitude of total gyroscopic moment for synchronous precession is $(-J_1\omega^2\phi)$, ϕ being the inclination of the shaft with the line of supports. To express M_x , M_y , F_x , and F_y in terms of the shaft deflections and rotations, we use influence coefficients which are defined as

- $a_{\mu\nu}$ = force on the disc μ due to a unit deflection of the shaft at the disc ν ,
- $b_{\mu\nu}$ = force on the disc μ due to a unit rotation of the shaft at the disc ν or moment on the disc μ due to a unit deflection of the shaft at the disc ν , and
- $c_{\mu\nu}$ = moment on the disc μ due to a unit rotation of the shaft at the disc ν .

Therefore, the components of the force and moment on the disc μ can be expressed as

$$F_{\mu_x} = \sum_{\nu=1}^N a_{\mu\nu}x_{\nu} + \sum_{\nu=1}^N b_{\mu\nu}\phi_{y_{\nu}}, \quad F_{\mu_y} = \sum_{\nu=1}^N a_{\mu\nu}y_{\nu} + \sum_{\nu=1}^N b_{\mu\nu}\phi_{x_{\nu}},$$

$$M_{\mu_x} = \sum_{\nu=1}^N c_{\mu\nu}\phi_{x_{\nu}} + \sum_{\nu=1}^N b_{\mu\nu}x_{\nu}, \quad M_{\mu_y} = \sum_{\nu=1}^N c_{\mu\nu}\phi_{y_{\nu}} + \sum_{\nu=1}^N b_{\mu\nu}y_{\nu},$$

where N is the number of discs mounted on the shaft. Using these expressions, the equations of motion can be expressed as

$$\begin{aligned} M_\mu \ddot{x}_\mu + \sum_{\nu=1}^N a_{\mu\nu} x_\nu + \sum_{\nu=1}^N b_{\mu\nu} \phi_{y_\nu} &= 0, \\ J_{1_\mu} \ddot{\phi}_{x_\mu} + J_\mu \omega^2 \dot{\phi}_{x_\mu} + \sum_{\nu=1}^N b_{\mu\nu} x_\nu + \sum_{\nu=1}^N c_{\mu\nu} \phi_{y_\nu} &= 0, \end{aligned} \quad (12.90a)$$

$$\begin{aligned} M_\mu \ddot{y}_\mu + \sum_{\nu=1}^N a_{\mu\nu} y_\nu + \sum_{\nu=1}^N b_{\mu\nu} \phi_{x_\nu} &= 0, \\ J_{1_\mu} \ddot{\phi}_{x_\mu} - J_\mu \omega^2 \dot{\phi}_{y_\mu} + \sum_{\nu=1}^N b_{\mu\nu} y_\nu + \sum_{\nu=1}^N c_{\mu\nu} \phi_{x_\nu} &= 0. \end{aligned} \quad (12.90b)$$

Multiplying (12.90b) by i and adding (12.90a), we get

$$\begin{aligned} M_\mu \ddot{\rho}_\mu + \sum_{\nu=1}^N a_{\mu\nu} \rho_\nu + \sum_{\nu=1}^N b_{\mu\nu} \phi_\nu &= 0, \\ J_{1_\mu} \ddot{\phi}_\mu - i J_\mu \omega \dot{\phi}_\mu + \sum_{\nu=1}^N b_{\mu\nu} \rho_\nu + \sum_{\nu=1}^N c_{\mu\nu} \phi_\nu &= 0, \end{aligned} \quad (12.91)$$

where $\rho = x + iy$ and $\phi = \phi_y + i\phi_x$. Assuming solutions of the form

$$\rho_\mu = \rho_\mu \exp(i\Lambda t), \quad \phi_\mu = \Phi_\mu \exp(i\Lambda t),$$

the equation for the condition that there is nonzero solution will be

$$\left| \begin{array}{ccccccccc} (-m_1 \Lambda^2 + a_{11}) & a_{12} & \dots & a_{1N} & b_{11} & b_{12} & \dots & b_{1N} \\ a_{21} & (-m_2 \Lambda^2 + a_{22}) & \dots & a_{2N} & b_{21} & b_{22} & \dots & b_{2N} \\ \vdots & \vdots & \ddots & \vdots & \vdots & \vdots & \ddots & \vdots \\ a_{N1} & a_{N2} & \dots & (-m_N \Lambda^2 + a_{NN}) & b_{N1} & b_{N2} & \dots & b_{NN} \\ b_{11} & b_{12} & \dots & b_{1N} & (-J_{11} \Lambda^2 + J_1 \omega \Lambda + c_{11}) & c_{12} & \dots & c_{1N} \\ b_{21} & b_{22} & \dots & b_{2N} & c_{21} & (-J_{12} \Lambda^2 + J_2 \omega \Lambda + c_{22}) & \dots & c_{2N} \\ \vdots & \vdots & \ddots & \vdots & \vdots & \vdots & \ddots & \vdots \\ b_{N1} & b_{N2} & \dots & b_{NN} & c_{N1} & c_{N2} & \dots & (-J_{1N} \Lambda^2 + J_N \omega \Lambda + c_{NN}) \end{array} \right| = 0. \quad (12.92)$$

We can determine the values of Λ by solving (12.92). It is obvious that these values will depend on ω .

For forward synchronous precession, the magnitude of the resisting gyroscopic moment can be expressed as $M_\mu = J_{1_\mu} \omega^2 \phi$, where both moment and rotation are considered to be in the plane containing the bent shaft and the original line of supports. The centrifugal force acting on the disc μ will be $m_\mu \delta_\mu \omega^2$. Using the influence coefficients defined earlier, the total deflection at the station μ due to all the centrifugal forces and gyroscopic moments acting at different stations can be expressed in the form

$$\delta_\mu = \omega^2 \sum_{\nu=1}^N a_{\mu\nu} m_\nu \delta_\nu - \omega^2 \sum_{\nu=1}^N b_{\mu\nu} J_{1_\nu} \phi_\nu. \quad (12.93a)$$

Similarly, the slope of the shaft (or inclination of the disc) at the station μ will be

$$\phi_\mu = \omega^2 \sum_{\nu=1}^N b_{\mu\nu} m_\nu \delta_\nu - \omega^2 \sum_{\nu=1}^N c_{\mu\nu} J_{1,\nu} \phi_\nu. \quad (12.93b)$$

Writing (12.93a) and (12.93b) for $\mu = 1, 2, \dots, N$, we can obtain $2N$ homogeneous equations in δ and ϕ . For a nonzero solution of these equations, the condition to be satisfied is

$$\begin{vmatrix} (a_{11}m_1 - \frac{1}{\omega^2}) & a_{12}m_2 & \dots & a_{1N}m_N & -b_{11}J_{11} & -b_{12}J_{12} & \dots & -b_{1N}J_{1N} \\ a_{21}m_1 & (a_{22}m_2 - \frac{1}{\omega^2}) & \dots & a_{2N}m_N & -b_{21}J_{11} & -b_{22}J_{12} & \dots & -b_{2N}J_{1N} \\ \vdots & \vdots & \ddots & \vdots & \vdots & \vdots & \ddots & \vdots \\ a_{N1}m_1 & a_{N2}m_2 & \dots & (a_{NN}m_N - \frac{1}{\omega^2}) & b_{N1}J_{11} & -b_{N2}J_{12} & \dots & -b_{NN}J_{1N} \\ -b_{11}m_1 & -b_{12}m_2 & \dots & -b_{1N}m_N & (c_{11}J_{11} + \frac{1}{\omega^2}) & c_{12}J_{12} & \dots & c_{1N}J_{1N} \\ -b_{21}m_1 & -b_{22}m_2 & \dots & -b_{2N}m_N & c_{21}J_{11} & (c_{22}J_{12} + \frac{1}{\omega^2}) & \dots & c_{2N}J_{1N} \\ \vdots & \vdots & \ddots & \vdots & \vdots & \vdots & \ddots & \vdots \\ -b_{N1}m_1 & -b_{N2}m_2 & \dots & -b_{NN}m_N & c_{N1}J_{11} & c_{N2}J_{12} & \dots & (c_{NN}J_{1N} + \frac{1}{\omega^2}) \end{vmatrix} = 0. \quad (12.94)$$

Neglecting the gyroscopic effects, we get the following N -th order equation in $1/\omega^2$ which was obtained in Chapter 11 while deriving Dunkerley's equation:

$$(\frac{1}{\omega^2})^N - (\frac{1}{\omega^2})^{N-1} \sum_{\mu=1}^N a_{\mu\mu} m_\mu + (\frac{1}{\omega^2})^{N-2} [] + \dots = 0. \quad (12.95)$$

Following the same logic, we get the approximate expression for the fundamental critical speeds of a shaft with N discs (for forward synchronous precession) as

$$\frac{1}{\omega_1^2} \approx \sum_{\mu=1}^N a_{\mu\mu} m_\mu \approx \frac{1}{\omega_{11}^2} + \frac{1}{\omega_{22}^2} + \dots + \frac{1}{\omega_{NN}^2}, \quad (12.96)$$

where $\omega_{11}, \omega_{22}, \dots, \omega_{NN}$ are the critical speeds with the first, second, \dots , N -th discs considered individually.

12.11 WHIRLING OF SHAFTS WITH DISTRIBUTED MASS

In the discussion so far, the mass of the shaft has not been considered for calculating the critical speed. When a system consists of only a rotating flexible shaft or of a flexible shaft with a light disc, the effect of the shaft mass cannot be ignored. In this section, we will consider the critical speeds of only the rotating flexible shafts. The analysis can be extended to include discs and shafts of considerable mass.

The equation of motion for transverse vibrations will first be derived for a rotating shaft taking into account the rotary inertia and gyroscopic action of the elements. Figure 12.21a shows the free-body diagram of an element of the shaft (at a distance z from the origin) corresponding to the deflection of the shaft in the x -direction. From the force balance in the x -direction, we get

$$Q_x + (\partial Q_x / \partial z) dz - Q_x + f_x dz = 0, \quad . \quad (12.97)$$

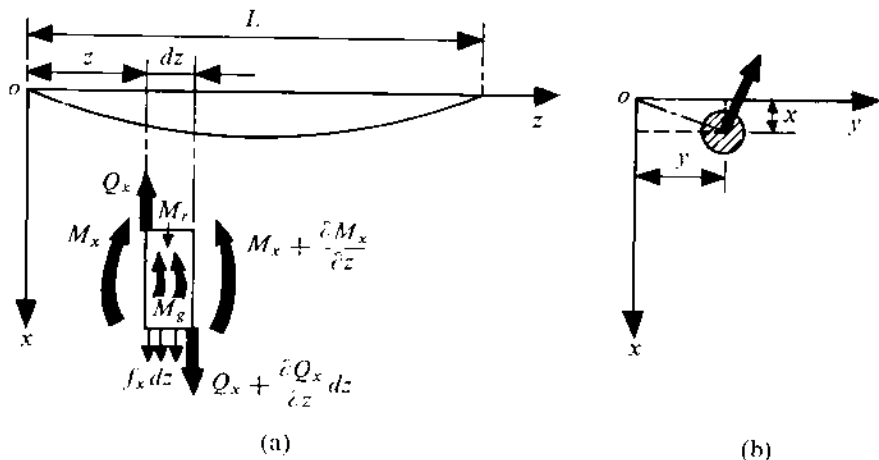


FIGURE 12.21

where f_x is the transverse inertia force per unit length. If m is the mass per unit length of the shaft, then $f_x = -m(\partial^2 x / \partial t^2)$. So, (12.97) becomes

$$\partial Q_x / \partial z = m(\partial^2 x / \partial t^2). \quad (12.98)$$

Again, considering the moment balance of the element in the xz -plane, we get

$$M_r + (\partial M_r / \partial z) dz = M_x - Q_x dz + M_r + M_g = 0,$$

where

$$M_r \text{ (rotary inertia of the element)} = mr^2 dz \frac{\partial^2}{\partial t^2} \left(\frac{\partial x}{\partial z} \right),$$

$$M_g \text{ (gyroscopic moment)} = 2mr^2 dz \omega \frac{\partial}{\partial t} \left(\frac{\partial y}{\partial z} \right),$$

$mr^2 dz$ = moment of inertia of the element about a diameter, and

r = radius of gyration.

So, the equation of moment balance finally becomes

$$EI \frac{\partial^3 x}{\partial z^3} + Q_x = mr^2 \frac{\partial}{\partial z} \left(\frac{\partial^2 x}{\partial t^2} \right) + 2mr^2 \omega \frac{\partial}{\partial z} \left(\frac{\partial y}{\partial t} \right) \quad (12.99)$$

since $M_x = -EI(\partial^2 x / \partial z^2)$. Differentiating (12.99) with respect to z and substituting the value of $\partial Q_x / \partial z$ from (12.98), we get

$$EI \frac{\partial^4 x}{\partial z^4} - mr^2 \left(\frac{\partial^4 x}{\partial z^2 \partial t^2} + 2\omega \frac{\partial^3 y}{\partial z^2 \partial t} \right) + m \frac{\partial^2 x}{\partial t^2} = 0. \quad (12.100)$$

Similarly, for the components of motion in the yz -plane, we get

$$EI \frac{\partial^4 y}{\partial z^4} - mr^2 \left(\frac{\partial^4 y}{\partial z^2 \partial t^2} - 2\omega \frac{\partial^3 x}{\partial z^2 \partial t} \right) + m \frac{\partial^2 y}{\partial t^2} = 0. \quad (12.101)$$

Multiplying (12.101) by i and adding (12.100), the two equations can be combined in the form

$$EI \frac{\partial^4 \rho}{\partial z^4} - mr^2 \left(\frac{\partial^4}{\partial z^2 \partial t^2} - 2i\omega \frac{\partial^3}{\partial z^2 \partial t} \right) \rho + m \frac{\partial^2 \rho}{\partial t^2} = 0, \quad (12.102)$$

where $\rho = x + iy$. Assuming a particular solution (a harmonic function of both z and t) of the form

$$\rho = \varphi \exp(iz\sqrt{\tau}/L) \exp(i\lambda t), \quad (12.103)$$

where $\sqrt{\tau}$ and λ are real numbers, and substituting in (12.102), we obtain the frequency equation

$$\frac{EI}{m} \frac{\tau^2}{L^4} - \frac{r^2}{L^2} (\lambda^2 - 2\omega\lambda)\tau - \lambda^2 = 0. \quad (12.104)$$

In (12.104), τ defines the mode of deflection of the shaft and depends on the boundary conditions. When the shaft is supported by two short bearings which can be considered to be simple supports, the shaft deflection can be expressed as

$$\rho = \varphi \sin \frac{\sqrt{\tau}}{L} z e^{i\lambda t} = \varphi \sin \frac{\pi n z}{L} e^{i\lambda t}, \quad (12.105)$$

where $n = 1, 2, 3, \dots$. Substituting $\sqrt{\tau} = \pi n$, the frequency equation becomes

$$(1 + \frac{\pi^2 n^2 r^2}{L^2})\lambda^2 - 2\frac{\pi^2 n^2 r^2}{L^2}\omega\lambda - \frac{EI}{m} \frac{\pi^4 n^4}{L^4} = 0 \quad (12.106)$$

which gives

$$\lambda_{1,2} = \left(\frac{\pi^2 n^2 r^2}{L^2} \right) \frac{\omega \pm [\omega^2 + (1 + \frac{\pi^2 n^2 r^2}{L^2}) \frac{EI}{mr^2}]^{1/2}}{1 + \pi^2 n^2 r^2 / L^2}. \quad (12.107)$$

The positive value of λ corresponds to the forward precession and the negative value to the reverse precession. These values of λ give the natural frequencies of the rotating shaft and it is clear that when any one of these values coincides with the speed of shaft rotation ω , a critical state will be reached. So, when ω is equal to λ , the speed will be critical. Therefore,

$$\omega_{cr_n} = \frac{\pi^2 n^2}{L^2} \left(\frac{EI/m}{1 - \pi^2 n^2 r^2 / L^2} \right)^{1/2}. \quad (12.108)$$

Equation (12.108) shows that, when $n > L/(pr)$, the value of ω_{cr_n} becomes imaginary. In other words, there is no critical speed for that particular mode of shaft deflection. When $n = 1$, there is no critical speed if $(L/r) > \pi$. This suppression of the critical state is due to the gyroscopic action. Similarly, the critical speed of reverse precession can be obtained by putting $\lambda = -\omega$ in (12.107). Denoting these critical speeds by ω'_{cr_n} , we get

$$\omega'_{cr_n} = \frac{\pi^2 n^2}{L^2} \left(\frac{EI/m}{1 + 3\pi^2 n^2 r^2 / L^2} \right)^{1/2}. \quad (12.109)$$

It is clear from (12.109) that there is an infinite number of critical speeds of reverse precession. When the shaft cannot be considered to be simply-supported, the deflection is assumed to be of the form

$$\rho = \varphi \exp(z\sqrt{\tau}/L) \exp(i\lambda t)$$

and the corresponding frequency equation becomes

$$\frac{EI}{m} \frac{\tau^2}{L^4} + \frac{r^2}{L^2} (\lambda^2 - 2\omega\lambda)\tau - \lambda^2 = 0. \quad (12.110)$$

Solving this quadratic equation in τ , we get

$$\tau = -\frac{mr^2 L^2}{2EI} (\lambda^2 - 2\omega\lambda) \pm L^2 \left\{ \left[\frac{mr^2}{2EI} (\lambda^2 - 2\omega\lambda) \right]^2 + \frac{m}{EI} \lambda^2 \right\}^{1/2}. \quad (12.111)$$

One root τ_1 will be positive and the other ($-\tau_2$) will be negative. So, the general form of the solution for ρ will be

$$\rho = (A \cosh \frac{\sqrt{\tau_1}}{L} z + B \sinh \frac{\sqrt{\tau_1}}{L} z + C \cos \frac{\sqrt{\tau_2}}{L} z + D \sin \frac{\sqrt{\tau_2}}{L} z) e^{i\lambda t}. \quad (12.112)$$

From (12.110), we find that

$$\tau_1 - \tau_2 = -\frac{mr^2 L^2}{EI} (\lambda^2 - 2\omega\lambda), \quad \tau_1 \tau_2 = \frac{mL^4}{EI} \lambda^2. \quad (12.113)$$

To get an approximate solution, we assume the ratio of precessional speed λ to shaft speed ω to be $\sigma = \omega/\lambda$. Eliminating λ^2 from (12.113), we get the relation

$$\tau_1 - \tau_2 = -\tau_1 \tau_2 (r^2/L^2)(1 - 2\sigma). \quad (12.114)$$

Now, using the conditions of the end supports, another equation with τ_1 and τ_2 can be obtained from (12.112). With the help of this equation and (12.114), τ_1 and τ_2 can be calculated for a given value of σ .

As an example, let us consider a shaft which is supported at the left end by a long bearing, whereas at the right end it is supported on a short bearing. So,

$$\rho(0) = \left. \frac{\partial \rho}{\partial z} \right|_{z=0} = \rho(L) = \left. \frac{\partial^2 \rho}{\partial z^2} \right|_{z=L} = 0. \quad (12.115)$$

From (12.112) and (12.115), we get

$$\sqrt{\tau_2} \tanh \sqrt{\tau_1} = \sqrt{\tau_1} \tan \sqrt{\tau_2}. \quad (12.116)$$

Since direct solutions of (12.114) and (12.116) are not possible, we adopt another procedure to determine the roots of τ . From (12.114), we get

$$\tau_1 = \frac{\tau_2}{1 + \tau_2(r^2/L^2)(1 - 2\sigma)} \quad (12.117)$$

and substituting this value in (12.116), we get

$$\begin{aligned} \sqrt{\tau_2} \tanh \frac{\sqrt{\tau_2}}{[1 + \tau_2(r^2/L^2)(1 - 2\sigma)]^{1/2}} &= \frac{\sqrt{\tau_2}}{[1 + \tau_2(r^2/L^2)(1 - 2\sigma)]^{1/2}} \tan \sqrt{\tau_2}, \\ \frac{\tan \sqrt{\tau_2}}{\sqrt{\tau_2}} &= \frac{\tanh [\tau_2 / \{1 + \tau_2(r^2/L^2)(1 - 2\sigma)\}]^{1/2}}{[\tau_2 / \{1 + \tau_2(r^2/L^2)(1 - 2\sigma)\}]^{1/2}}. \end{aligned} \quad (12.118)$$

This equation can be solved graphically for a given value of σ . τ_2 having been determined, τ_1 can be calculated from (12.117). For critical speeds of forward and reverse precession, $\sigma = 1$ and $\sigma = -1$, respectively. For these values of σ , (12.117) becomes

$$\tau_{1n} = \frac{\tau_{2n}}{1 - \tau_{2n}(r^2/L^2)}, \quad \tau'_{1n} = \frac{\tau'_{2n}}{1 + 3\tau'_{2n}(r^2/L^2)} \quad (12.119)$$

and correspondingly, (12.118) becomes

$$\begin{aligned} \frac{\tan \sqrt{\tau}_{2n}}{\sqrt{\tau}_{2n}} &= \frac{\tanh [\tau_{2n}/\{1 - \tau_{2n}(r^2/L^2)\}]^{1/2}}{[\tau_{2n}/\{1 - \tau_{2n}(r^2/L^2)\}]^{1/2}}, \\ \frac{\tan \sqrt{\tau}'_{2n}}{\sqrt{\tau}'_{2n}} &= \frac{\tanh [\tau'_{2n}/\{1 + 3\tau'_{2n}(r^2/L^2)\}]^{1/2}}{[\tau'_{2n}/\{1 + 3\tau'_{2n}(r^2/L^2)\}]^{1/2}}. \end{aligned}$$

When τ_{1n} , τ_{2n} , τ'_{1n} , and τ'_{2n} are known, the corresponding critical speeds of forward and reverse precession [from the second equation of (12.113)] will be

$$\omega_{crn} = \frac{\sqrt{(\tau_{1n}\tau_{2n})}}{L^2} \left(\frac{EI}{m}\right)^{1/2}, \quad \omega'_{crn} = \frac{\sqrt{(\tau'_{1n}\tau'_{2n})}}{L^2} \left(\frac{EI}{m}\right)^{1/2}.$$

For forward precession, (12.119) indicates that τ_{1n} will be negative for sufficiently large value of τ_{2n} and the critical speed will be imaginary. Therefore, it is clear that there will be a finite number of possible critical speeds of forward precession.

PROBLEM 12.3

A uniform mild steel shaft of diameter 2.5 cm is supported by two long bearings at the two ends. The length of the shaft between the two bearings is 90 cm. Determine the first critical speed of forward precession.

SOLUTION

The shaft can be considered to be clamped at the ends. The deflection pattern is given by the equation

$$\rho = [A \cosh \frac{\sqrt{\tau}_1}{L} z + B \sinh \frac{\sqrt{\tau}_1}{L} z + C \cos \frac{\sqrt{\tau}_2}{L} z + D \sin \frac{\sqrt{\tau}_2}{L} z] e^{i\lambda t}.$$

The boundary conditions are

$$\rho(0) = \left. \frac{\partial \rho}{\partial z} \right|_{z=0} = \rho(L) = \left. \frac{\partial \rho}{\partial z} \right|_{z=L} = 0 \quad \text{for all values of } t.$$

Substituting the first condition in the foregoing equation, we get $A + C = 0$ and $C = -A$, and from the second condition, we get $B\sqrt{\tau}_1 + D\sqrt{\tau}_2 = 0$ and $D = -B(\tau_1/\tau_2)^{1/2}$. From the third and fourth conditions, we get

$$A \cosh \sqrt{\tau}_1 + B \sinh \sqrt{\tau}_1 + C \cos \sqrt{\tau}_2 + D \sin \sqrt{\tau}_2 = 0,$$

$$A\sqrt{\tau}_1 \sinh \sqrt{\tau}_1 + B\sqrt{\tau}_1 \cosh \sqrt{\tau}_1 - C\sqrt{\tau}_2 \sin \sqrt{\tau}_2 + D\sqrt{\tau}_2 \cos \sqrt{\tau}_2 = 0.$$

Since $C = -A$ and $D = -B(\tau_1/\tau_2)^{1/2} = -\alpha B$, we get

$$\begin{aligned} & (\cosh \sqrt{\tau_1} - \cos \sqrt{\tau_2})A + (\sinh \sqrt{\tau_1} - \alpha \sin \sqrt{\tau_2})B = 0, \\ & [\sinh \sqrt{\tau_1} + (1/\alpha) \sin \sqrt{\tau_2}]A + (\cosh \sqrt{\tau_1} - \cos \sqrt{\tau_2})B = 0. \end{aligned}$$

For a nonzero solution to exist, the condition to be satisfied is

$$2(1 - \cosh \sqrt{\tau_1} \cos \sqrt{\tau_2}) = (\alpha - 1/\alpha) \sinh \sqrt{\tau_1} \sin \sqrt{\tau_2}.$$

The relationship between τ_1 and τ_2 for forward precession [from (12.119)] will be

$$\tau_1 = \frac{\tau_2}{1 - \tau_2(r^2/L^2)}.$$

Now, r = radius of gyration of the shaft cross-section about a diameter = 1.55 mm. So,

$$\tau_1 = \frac{\tau_2}{1 - \tau_2(0.15)^2/90}.$$

For the first critical speed, $\tau_2(0.15)^2/90 \ll 1$ and $\tau_{11} \approx \tau_{21}$. Therefore,

$$\begin{aligned} & 2(1 - \cosh \sqrt{\tau_{11}} \cos \sqrt{\tau_{11}}) \approx 0, \\ & \cosh \sqrt{\tau_{11}} \cos \sqrt{\tau_{11}} \approx 1. \end{aligned}$$

The roots of this equation are $\tau_{11} = 0, 4.73, 7.853, 10.996, \dots$. So, $\tau_{11} = 4.73$ corresponds to the first critical speed of forward precession. Finally, we get

$$\omega_{\text{crit}} = \frac{4.73}{(90)^2} \left[\frac{2.11 \times 10^6 \times \pi \times (2.54)^4 / 64}{\frac{\pi}{4} \times (2.54)^2 \times \frac{0.28}{2.2 \times (2.54)^3 \times 2.54 \times 3.26}} \right]^{1/2} \approx 186 \text{ rad/s.}$$

FURTHER READING

- Arnold, R.N. and Maunder, L., Gyrodynamics and Its Engineering Applications, Academic Press, New York, 1961.
- Arthobolevskii, I.I., Theory of Mechanisms (in Russian), Nauka, Moscow, 1965.
- Beggs, J.S., Mechanism, McGraw-Hill, New York, 1955.
- Bevan, T., The Theory of Machines, Longmans Green, London, 1962.
- Biezeno, C.B. and Grammel, R.E., Engineering Dynamics, Vol. IV, Blackie, London, 1954.
- Buckingham, E., Analytical Mechanics of Gears, Dover, New York, 1949.
- Den Hartog, J.P., Mechanical Vibrations, McGraw-Hill, New York, 1956.
- Dijksman, E.A., Motion Geometry of Mechanisms, Cambridge University Press, London, 1976.
- Dimentberg, F.M., Flexural Vibration of Rotating Shafts, Butterworths, London, 1961.
- Dittrich, G. and Braune, R., Theory of Mechanisms through Examples (in German), R. Oldenbourg Verlag, Munich, 1978.
- Dizioglu, B., Theory of Machines, Vols. 1-4 (in German), Friedr. Vieweg and Sohn, Braunschweig, 1966.
- Dudley, D.W., Gear Handbook, McGraw-Hill, New York, 1962.
- Erdman, A.G. and Sandor, G.N., Mechanism Design: Analysis and Synthesis, Vol. 1 (Second Edition), Prentice-Hall, Englewood Cliffs, New Jersey, 1991.
- Green, W.G., Theory of Machines, Blackie, Bombay, 1961.
- Gunter, E.I., Dynamic Stability of Rotor-Bearing Systems, NASA SP-113, Washington, 1966.
- Hain, K., Applied Kinematics, McGraw-Hill, New York, 1967.
- Hartenberg, R.S. and Denavit, J., Kinematic Synthesis of Linkages, McGraw-Hill, New York, 1964.
- Hirschhorn, J., Kinematics and Dynamics of Plane Mechanisms, McGraw-Hill, New York, 1962.
- Holowenko, A.R., Dynamics of Machinery, Wiley, New York, 1955.
- Hrones, J.A. and Nelson, G.L., Analysis of the Four-Bar Linkage, MIT Press, Cambridge, Massachusetts, 1951.
- Hunt, K.H., Kinematic Geometry of Mechanisms, Oxford University Press, Oxford, 1978.
- Jacobsen, L.S. and Ayre, R.S., Engineering Vibrations, McGraw-Hill, New York, 1958.

- Kobrinskii, A.E., Dynamics of Mechanisms with Elastic Connections and Impact Systems. Iliffe, London, 1969.
- Kozesnik, J., Dynamics of Machines, SNTL, Prague, 1962.
- Litvin, F.L., Theory of Toothed Gearing (in Russian), Science Publishers, Moscow, 1968.
- Mabie, H.H. and Ocvirk, F.W., Mechanisms and Dynamics of Machinery, Wiley, New York, 1975.
- Macduff, J.N. and Curreri, J.R., Vibration Control, McGraw-Hill, New York, 1958.
- Mallik, A.K., Principles of Vibration Control, Affiliated East-West Press (P) Ltd., New Delhi, 1990.
- Mallik, A.K., Ghosh, A. and Dittrich, G., Kinematic Analysis and Synthesis of Mechanisms, CRC Press, Boca Raton, 1994.
- Martin, G.H., Kinematics and Dynamics of Machines, McGraw-Hill, New York, 1982.
- McLarnan, C.W., Four Bar Linkage Function Generators (Bulletin 197), Engineering Experiment Station, Ohio State University, Columbia, 1966.
- Meirovitch, L., Elements of Vibration Analysis, McGraw-Hill, New York, 1975.
- Norton, R.L., Design of Machinery, McGraw-Hill, New York, 1992.
- Panovko, Y., Elements of the Applied Theory of Elastic Vibration, Mir Publishers, Moscow, 1971.
- Paul, B., Kinematics and Dynamics of Planar Machinery, Prentice-Hall, Englewood Cliffs, New Jersey, 1979.
- Rosenauer, N. and Willis, A.H., Kinematics of Mechanisms, Dover, New York, 1967.
- Rothbart, H.A., Cams – Design, Dynamics and Accuracy, Wiley, New York, 1956.
- Shigley, J.E. and Uicker (Jr.), J.J., Theory of Machines and Mechanisms, McGraw-Hill, New York, 1980.
- Snowdon, J.C., Vibration and Shock in Damped Mechanical Systems, Wiley, New York, 1968.
- Suh, C.H. and Radcliffe, C.W., Kinematics and Mechanisms Design, Wiley, New York, 1978.
- Tao, D.C., Applied Linkage Synthesis, Addison-Wesley, Reading, Massachusetts, 1964.
- Tao, D.C., Fundamentals of Applied Kinematics, Addison-Wesley, Reading, Massachusetts, 1967.
- Thomson, W.T., Theory of Vibration with Applications, Prentice-Hall, Englewood Cliffs, New Jersey, 1973.
- Timoshenko, S.P. and Young, D.H., Advanced Dynamics, McGraw-Hill, New York, 1948.
- Timoshenko, S.P. and Young, D.H., Vibration Problems in Engineering, Van Nostrand, Princeton, 1955.

ANSWERS TO SELECTED PROBLEMS

CHAPTER 1

1.11 Degrees of freedom: Fig. 3.28 = 1, Fig. 1.52a = 2, Fig. 1.52b = 1, Fig. 1.52c = 1

1.14 (a), (d), (e), (g), (h), (i), (j) 1.15 $F = 1$

CHAPTER 2

2.20 $q_{rr} = 1.04$ 2.21 $q_{rr} = 1.57$ 2.22 4.65 cm, $q_{rr} = 1.182$ 2.23 $\theta_2^* = 205^\circ$, $\theta_4^* = 245^\circ$
2.24 (iii) $\alpha_{max} = 46^\circ$ 2.25 (ii) $\delta = 20^\circ$, (iii) $\delta = 5^\circ$, $O_2A = 54.7$ mm, $AB = 159.1$ mm
2.33 $\omega_2/\omega_5 = 2$ 2.34 (i) $V_B = 15$ cm/s (towards left), $V_D = 14.25$ cm/s (downward),
(ii) $a_D = 21.5$ cm/s² (upward) 2.35 $V_B = 420$ cm/s (downward), $V_D = 390$ cm/s (downward),
 $a_B = 9700$ cm/s² (downward), $a_D = 10,700$ cm/s² (downward) 2.36 $V_6 = 18$ cm/s (upward),
 $a_6 = 2100$ m/s² (upward) 2.37 $\omega_3 = 6.15$ rad/s (CCW), $\alpha_3 = 3.27$ rad/s² (CW) 2.38 V_D
= 33 cm/s (towards right), $a_D = 294$ cm/s² (towards right) 2.39 $V_A = 6.93$ cm/s (towards
left), $a_A = 23.1$ cm/s² (towards right) 2.41 $\omega_3 = 15.94$ rad/s (CW), $\alpha_3 = 2778$ rad/s² (CCW)
2.42 $V_P = 6040$ cm/s 2.45 $V_D = 0.89$ cm/s (upward), $a_D = 0.79$ cm/s² (upward)
2.46 $V_C = 60$ cm/s (towards left), $a_C = 2$ cm/s² (towards right) 2.48 $V_P = 2.218$ m/s

CHAPTER 3

3.8 $O_2A = 0.8$ m, $AB = 0.6$ m 3.9 $O_2A = 17.3$ m, $AB = 3.7$ m 3.10 $A_1B_1 = 1.9$ cm,
 $O_4B_1 = 2.9$ cm 3.12 $l_3 = 5.0$ cm, $l_4 = 7.1$ cm 3.15 $l_1 = 100$ mm, $l_2 = 37$ mm, $l_3 =$
84.5 mm, $l_4 = 93$ mm, $\mu_1 = 84^\circ$, $\mu_2 = 53^\circ$ 3.17 $l_2 = -6.5$ cm, $l_3 = 23.38$ cm, $e = -8.2$ cm
3.19 $l_1 = l_3 = 5.1$ cm, $l_2 = l_4 = 17.06$ cm

CHAPTER 4

4.8 (i) 125 N-m, (ii) 142,100 N-m 4.9 50.8 N 4.10 2850 N 4.11 20.4×10^3 N/m²
4.12 (i) 514 rad/s² (CW), (ii) 504 rad/s² (CW) 4.16 914.4 kW, 34,927 N-m 4.17 1642.5 N-m
4.19 318.3 N-m 4.21 1691.5 kg-m² 4.22 2315.5 kg-m², 2.86 m, 2.2 cm, 8.8 cm
4.23 (i) 1.45 kW, (ii) 1.27 kg-m² 4.24 (i) 76.6 kg-m², (ii) 8.12 rad/s², (iii) 0.018 rad
4.25 (i) 28.26 kW, (ii) 2.78%, (iii) 1.99%

CHAPTER 5

$$5.6 \quad 7 \quad 5.7 \quad F = 1 \quad 5.9 \quad \sec^2 \alpha_4$$

CHAPTER 6

- 6.6** 26.14 kg, 170.8 rpm **6.7** 18.04 rad/s **6.8** Addition of 39.6 kg, 25.3 rad/s
6.9 14.67 cm, not isochronous, stable **6.10** 355.2 rpm, 44.23 N/cm, 11.4 cm
6.11 (i) 65.5 N/cm. (ii) 308 rpm **6.12** (i) 66.63 N/cm, (ii) 137 N **6.13** (i) 4.07 kg,
(ii) 199.6 N/cm, (iii) 5.73 cm

CHAPTER 7

- 7.12** $\theta_D = 76.6^\circ$, $\theta_E = 226.8^\circ$, $R_A = 63.9$ N **7.13** $R_A = 39.2$ N = $-R_B$
7.14 $m_C = 4.35$ kg, $\theta_C = 240^\circ$ (CW from A_1), $m_D = 2.84$ kg, $\theta_D = 50^\circ$ (CW from A)
7.15 (i) $m_E = 0.64$ kg, $\theta_E = 218.66^\circ$ (CW from A), (ii) 468.5 mm, (iii) 10.73 N
7.16 3.12 cm, 237.76° (CW from A), 247.7 N **7.17** 0.40 kg, 90° (CW or CCW)
7.18 (i) 0.89 kg, 60° (CCW), (ii) $m_A = 0.297$ kg, $m_C = 0.514$ kg
7.19 Near end, 3.39 kg at 72.2° CCW from the near-end trial mass; far end, 1.39 kg at 295° CCW
from the far-end trial mass
7.20 Forces balanced, primary couple balanced, secondary couple = 30,049 N-m
7.21 (I, II)-(III, IV), (I, III)-(II, IV), (I, IV)-(II, III), forces balanced, moments unbalanced
7.22 I-II-III-VI-V-IV, I-II-IV-VI-V-III, I-V-III-VI-II-IV, I-V-IV-VI-II-III, I-III-II-VI-IV-V, I-IV-II-
VI-III-V, I-III-V-VI-IV-II, I-IV-V-VI-III-II
7.23 Forces balanced; moments: first order, 5154 N-m; second order, 614.5 N-m; fourth order,
4.94 N-m; sixth order, 0.01 N-m
7.24 2.45 m, $A-C-B-D = 0^\circ-95.26^\circ-204.76^\circ-300^\circ$, 160,099 N-m
7.25 Primary, 329.5 N; secondary, 174.2 N
7.26 Primary force, balanced; secondary force, 1115.3 N; primary moment, 157.75 N-m; secondary
moment, balanced **7.27** Maximum, 5324 N; minimum, 1774.7 N
7.29 0.566 m **7.30** $m'_A g'_2 = 5.09$ kg-cm, $\beta'_2 = 168.36^\circ$, $m'_B g'_4 = 6.52$ kg-cm, $\beta'_4 = 186.7^\circ$

CHAPTER 8

- 8.17** $y = 100(3\theta/2\pi)^2$, $0 \leq \theta \leq \frac{\pi}{2}$; $y = 50[1 - 2(1 - 3\theta/2\pi)^2]$, $\frac{\pi}{3} \leq \theta \leq \frac{2\pi}{2}$
8.18 (a) 120 mm, (b) 5.46 mm **8.19** 56.93 mm
8.23 4 cm, 5.92 cm **8.24** 0.35 cm (to the left), 2.8 cm
8.29 $\theta_{ri}/4$, $2L\omega/\theta_{ri}$, $-4\pi^2 L\omega^3/\theta_{ri}^3$ **8.30** $y = L\{3(\theta/\theta_{ri})^2 - 2(\theta/\theta_{ri})^3\}$
8.31 $x = 5 \sin \theta - 1$, $y = 5 \cos \theta - 2.5$, 5 cm, $(y + 2.5)^2 + (x + 1)^2 = 25$
8.35

$$y = 3.8(\sec \theta - 1) \text{ cm} \quad \text{for } 0 \leq \theta \leq 32.8^\circ,$$

$$y = \{3.1 \cos(52.2^\circ - \theta) + 1.9 \cos \gamma - 3.8\} \text{ cm} \quad \text{for } 32.8^\circ \leq \theta \leq 52.2^\circ,$$

where $\gamma = \sin^{-1}\{1.63 \sin(52.2^\circ - \theta)\}$

8.36

$$y = 8.55(1 - \cos \theta) \text{ cm} \quad \text{for } 0 \leq \theta \leq 16.5^\circ,$$

$$y = \{3.9 \cos(55^\circ - \theta) - 2.7\} \text{ cm} \quad \text{for } 16.5^\circ \leq \theta \leq 55^\circ$$

8.40 7.14 cm,

$$x_p(\theta) = 9.66 + 7.14\theta - 10 \cos\left[\frac{3\theta^2}{4\pi} - \frac{\pi}{12}\right],$$

$$y_p(\theta) = 2.59 + 10 \sin\left(\frac{3\theta^2}{4\pi} - \frac{\pi}{12}\right), \quad 0 \leq \theta \leq \pi/3$$

$$x_p(\theta) = 9.66 + 7.14\theta - 10 \cos\left[\frac{\pi}{6}\{1 - 2(1 - \frac{3\theta}{2\pi})^2\} - \frac{\pi}{12}\right],$$

$$y_p(\theta) = 2.59 + 10 \sin\left[\frac{\pi}{6}\{1 - 2(1 - \frac{3\theta}{2\pi})^2\} - \frac{\pi}{12}\right], \quad \frac{\pi}{3} \leq \theta \leq \frac{2\pi}{3}$$

8.41 5.61 cm,

$$x_p(\theta) = 9.66 + 5.61\theta - 10 \cos\left[\frac{\pi}{12}(1 - \cos\frac{3\theta}{2}) - \frac{\pi}{12}\right],$$

$$y_p(\theta) = 2.59 + 10 \sin\left[\frac{\pi}{12}(1 - \cos\frac{3\theta}{2}) - \frac{\pi}{12}\right], \quad 0 \leq \theta \leq \pi/3$$

CHAPTER 9**9.11**

$$x_2 = (x_1 - 37.5 \cos \theta_1) \cos 1.5\theta_1 + (1.63 - 37.5 \sin \theta_1) \sin 1.5\theta_1,$$

$$y_2 = -(x_1 - 37.5 \cos \theta_1) \sin 1.5\theta_1 + (1.63 - 37.5 \sin \theta_1) \cos 1.5\theta_1$$

9.14 2.35 mm **9.15** 4.04 mm **9.16** 963.7 rpm**9.18** (5000/13) rpm in the same direction as that of the input shaft, 168.1 N-m**9.19** 428.6 rpm **9.20** 613.6 rpm, 581 rpm, 597.3 rpm**9.21** 237.9 rpm opposite to that of *A*, 148.6 N-m, 178.1 N-m**9.22** 166.7 rpm opposite to that of arm *A* **9.23** 7/5, 3/5**9.24** 12.06 rpm opposite to that of shaft *A***CHAPTER 10****10.7** $T = (mga - \frac{1}{2}mr^2\omega\Omega)(b^2 + 4a^2)^{1/2}/(2ab)$, $T = (mga + \frac{1}{2}mr^2\omega\Omega)(b^2 + 4a^2)^{1/2}/(2ab)$ **10.8** 26.53 N-m (magnitude) **10.9** 8692.6 N (inner wheel), 17,794.4 N (outer wheel)**10.11** $83.7(1 - \cos 376.8t)$ N-m, $83.7 \sin 376.8t$ N-m, $-0.74 \sin 376.8t$ N-m**CHAPTER 11****11.43** 250 Hz **11.44** $[4k/(3m)]^{1/2}(1 + a/r)$ **11.45** $\{g(1 + A_1/A_2)/[h\{1 + A_1/A_2 + lA_1/(hA_p)\}]\}^{1/2}$ **11.46** $[(kr_2^2 + K)/(J + mr_1^2)]^{1/2}$ **11.47** $[g(R - H/2)/(L^2/12 + H^2/3)]^{1/2}$ **11.48** $[3\Omega^2\{r/(2l) + 1/3\}]^{1/2}$ **11.49** (i) $\Omega[1 - \{g/(\Omega^2 l)\}^2]^{1/2}$, (ii) $(g/l - \Omega^2)^{1/2}$ **11.50** $(4k/5m)^{1/2}$ **11.51** 4472.14 N-m-s/rad **11.52** 194,444.4 N/m, 23.3×10^3 N-s/m **11.53** 0.085 s, 0.0226 rad**11.54** $X/(3l)$, $8l/9$ from hinge **11.55** 11.08×10^7 N/m², 5.204×10^7 N/m²

11.56 $X = |Y/(1 - r_1^2)|$ with $r_1 = \omega/[k/(m + 3nm_R/8)]^{1/2}$ **11.57** $F_0 \cos \omega t / (1 - \omega^2 m/k)$
11.58 $\frac{1}{\sqrt{2}} \{3 - 4\zeta^2 \pm [(4\zeta^2 - 3)^2 - 4]^{1/2}\}^{1/2}$ **11.60** 58.8 rad/s to 67.98 rad/s

11.61 (i) 51.45×10^{-4} m, (ii) 453.7 N **11.62** $(1/2)\pi k Y$

11.63 Amplitude = $F_0/[k^2 + (m\omega^2)^2 - 2m\omega^2 k \cos 2\alpha]^{1/2}$, phase difference =
 $\tan^{-1}\{\frac{1}{2} \sin 2\alpha / (k \cos 2\alpha - m\omega^2)\}$ **11.64** 0.9806

11.65 $[4F_0/(\pi k)] \sum_{p=1, 3, 5, \dots}^{\infty} \sin p\omega_0 t / [p\{1 - (p\omega_0/\omega_n)^2\}]$ ($\omega_0 = 2\pi/T$)

11.66 $\{\hat{F}/[m(1 - \zeta^2)^{1/2}\omega_n]\} \exp(-\zeta\omega_n t) \sin[(1 - \zeta^2)^{1/2}\omega_n t]$ **11.69** $[2F_0 \sin(\omega_n t_0/2)]/k$

11.71 $x = \frac{v_0}{\omega_n t_0} (1 - \cos \omega_n t) + v_0 t (1 - \frac{t}{2t_0})$ where $\omega_n = (k/m)^{1/2}$

11.72 0, $[g\{1 + 2m_2/(3m_1)\}/l]^{1/2}$

11.73

$$\omega_1 = 0, \quad \left\{ \begin{array}{c} 1 \\ 1 \end{array} \right\},$$

$$\omega_2 = [\frac{K_1 K_2}{K_1 + K_2} (\frac{1}{J_1} + \frac{1}{J_2})]^{1/2}, \quad \left\{ \begin{array}{c} 1 \\ -J_1/J_2 \end{array} \right\} \quad (K_1 = \frac{\pi G d_1^4}{32 l_1}, K_2 = \frac{\pi G d_2^4}{32 l_2})$$

$$J_1(K_1 + K_2)l_2 / \{K_1(J_1 + J_2)\}$$

11.75

$$\omega_1 = [k/m + \sqrt{2}g/\{l(\sqrt{2} + 1)\}]^{1/2}, \quad \left\{ \begin{array}{c} 1 \\ \sqrt{2} \end{array} \right\},$$

$$\omega_2 = [k/m + \sqrt{2}g/\{l(\sqrt{2} - 1)\}]^{1/2}, \quad \left\{ \begin{array}{c} 1 \\ -\sqrt{2} \end{array} \right\}$$

11.76 5.6245 kg, 3319.85 N/m **11.77** 121 rpm **11.78** $0.39(k/m)^{1/2}$

11.79 $0.425\sqrt{k/m}$, $1.192\sqrt{k/m}$, $1.97\sqrt{k/m}$ **11.80** 0.677×10^{-6} rad, 0.711×10^{-6} rad,
 -5.69×10^{-6} rad **11.81** $\tan(\omega l/c) + AE\omega l/(kltc) = 0$ with $c = (E/\rho)^{1/2}$

11.82 (i) $1 + \cosh \beta l \cos \beta l - 5\beta l(\cosh \beta l \sin \beta l - \cos \beta l \sinh \beta l) = 0$, $\omega_1 = 0.7569[EI/(ml^3)]^{1/2}$,
(ii) $\omega_1 = 0.7565[EI/(ml^3)]^{1/2}$, (iii) $\omega_1 = 1.505[EI/(ml^3)]^{1/2}$

11.83 $[(\pi^4 EI + 8kt^3)/(3ml^3)]^{1/2}$

11.86 $[\pi^4 E \{h_1^3 + 1.5h_1^2(h_2 - h_1) + h_1(\pi^2 - 3)(h_2 - h_1)^2/(2\pi^2)$
 $+ (\pi^2 - 3)(h_2 - h_1)^3/(4\pi^2)\} / \{6\rho l^4(h_1 + h_2)\}]^{1/2}$

11.88 $[12.46EI/(ml^3) + \Omega^2(4.45r + 0.9743l)/l]^{1/2}$ **11.89** 7115 Hz, 8419 Hz

11.90 10.13 mV/m-s²

INDEX

- Acceleration
angular, 66, 188
Coriolis, 69
diagram, 79
image, 73
- Accuracy point, 120
- Addendum, 402
- Alt's construction, 147
- Aronhold-Kennedy theorem, 72, 75, 405
- Auxiliary
acceleration diagram, 90, 99, 180
lines, 92
point, 92
- Balancing
active, 305
dynamic, 279
external, 278
field, 289
internal, 278
machine, 287
Gisholt-type, 288
pivoted-carriage, 287
masses, 281
analytical method of determining, 283
graphical method of determining, 282
modal, technique, 297
of flexible rotor, 296
of in-line engine, 304
of internal-combustion engine, 277, 298, 321
Lanchester technique for, 326
of planar linkage, 329
of radial engine, 314
of rotors with variable mass, 298
of single-cylinder engine, 299
generalized approach to, 321
of thin disc, 290
of V-twin engine, 311
partial, 325
passive, 305
- planes, 281
static, 279
- Base circle, 344, 405
- Branch defect, 158
- Cam
basic dimensions of, 351
circular-arc, 380
cross-over shock in, 390
curves, advanced, 351
cylindrical, 343, 390
design, 362
analytical, 367
optimal, 361, 370
dynamic analysis of, 382
numerical method for, 385
- plate, 341
positive-acting, 343
profile, equation of, 367
side thrust in, 343
spatial, 390
synthesis, 362
by graphical method, 362
by numerical method, 388
- tangent, 378
wedge, 341
- Centrode, 402
- Chebyshev's accuracy point, 121
- Clearance, 403
- Coefficient
of fluctuation of energy, 198
of fluctuation of speed, 198
- Coordinate transformation, 223
- Coupler point, 124, 159
- Crank
diagram, 304
primary, 307
secondary, 306
direct, 315
reverse, 315

- Critical speed**, 507, 589
 effect of bearing stiffness on, 600
 effect of oil film in bearings on, 605
 effect of variable shaft stiffness on, 603
 gyroscopic effect on, 596
 of shaft with distributed mass, 613
 of shaft with several discs, 610
 secondary, 598
- D'Alembert's principle**, 168
- Damping**, 479
 coulomb, 479
 critical, 482
 factor, 482
 hysteretic, 513
 optimum, 502
 viscous, 479
 equivalent, 511
- Dead-centre problems**, 119, 144
- Dedendum**, 403
- Degree of freedom**, 4, 24, 221, 464
- Displacement**
 analysis, 45
 diagram, 345
- Dunkerley's equation**, 540
- Dunkerley's method**, 539
- Dwell**, 345
- Dyads**, 155
- Dynamic**
 equilibrium, 168
 equation, 174
 motion analysis, 179
 effects of friction in, 182
 rate-of-change-of-energy method of, 179
- Dynamics**, 2
- End effector**, 233
- Energy balance, instantaneous**, 179
- Equivalent**
 dynamically, link, 188
 inertia, 474
 stiffness, 474
- Euler's equation**, 439
 modified, 440
- Feedback control**, 248
- Ferguson's paradox**, 427
- Firing order**, 304
- Fluctuation**
 of crankshaft speed, 197
 of energy, 198
- Flywheel analysis**, 198
 Wittenbauer's method of, 206
- Follower**
 cam, 343
 command, 384
 flat-face, 341
 jump, 389
 knife-edge, 341
 motion analysis, 349
 offset-translating, 341
 oscillating, 341
 preloading, 390
 radial-translating, 341
 roller, 341
 spherical-face, 341
 velocity, 349
- Force**
 analysis, dynamic, 169
 analytical method for, 173
 graphical method for, 169
 bearing, 442
 controlling, 249
 dynamic, 277
 inertia, 167, 277
 restoring, 249, 465
 static, 167
- Frequency**
 domain analysis, 517
 fundamental, 527
 measurement, 563
 natural, 467
 circular, 467
 damped, 485
 peak, 499
 ratio, 494
 response, complex, 514
- Freudenstein's equation**, 147
- Friction**
 external, 596
 internal, 481, 589
- Function generation**, 119, 126
- Fundamental law of gearing**, 403, 405
- Gear**, 401
 bevel, 419, 421
 contact ratio, 406
 crown (or face), 421

- differential, 430
helical, 419
hypoid, 421
involute, 403
line of action of, 404
planetary, 425
spiral-bevel, 421
spur, 401
sun, 425
- Gear train, 423
compound, 424
epicyclic, 424
torque in, 430
planetary, 425
simple, 424
- Generalized
mass, 535
stiffness, 535
- Goodman's transformation equation, 99, 180
- Governor
capacity of, 251
centrifugal, 249
gravity-controlled, 249, 251
spring-controlled, 249, 260
coefficient of insensitiveness of, 254
detention by friction of, 254
effect of friction on, 253
flywheel, 249
Hartnell, 260, 261
Hartung, 260
hunting, 265
inertia, 249, 269
instability of, 257
isochronous, 251, 261
mechanisms, 272
Porter, 251
Proell, 255
sensitivity, 250
speed-torque characteristics with and without, 267
stability of, 250
- Grashof's criterion, 33
- Grübler's criterion, 24
- Gyroscope
symmetrical, 447, 450, 451
unsymmetrical, 451
- Gyroscopic
action, 435
effects in machines, 454
moment, 450, 451
reaction, 442
- stabilization, 458
- Half-power band width, 500
Harmonic analysis, 186
Helicoid surface, involute, 419
Helix angle, 419
Hinge
higher-order, 25
simple, 24
- Holzer's method, 541
- Hooke's joint, 7, 232
- Hysteresis, 589
- Inflexion point, 345
- Instantaneous centre, 71
of relative velocity, 72
of velocity, 71
- Interference, 409
- Involute, 404
properties of, 406
- Kinematic
analysis, 45
analytical method for, 51, 106
auxiliary-point method for, 90
Goodman's indirect method for, 97
graphical method for, 45, 75
instantaneous centres method for, 75
method of normal accelerations for, 89
of complex mechanisms, 88
of open chain, 233
- chain, 7
classification of, 7
closed, 7
constrained, 9
simple, 9
- diagram, 9
- element, 4
- inversion, 12
- pair, 4
- synthesis, 2
analytical methods for, 147
approximate and exact, 119
by point-position reduction, 141
dimensional, 119
four-position, 141
graphical methods for, 122
number, 2, 24
of cam, 362, 367

- three-position, 122, 147
- type, 2
- Kinematics, 2**
 - forward, 222
 - inverse, 222
 - of spatial chains, 221
- Kinetics, 2**
- Kutzbach equation, 24

- Lead angle, 419
- Lift, 345
- Link, 7**
 - binary, 7
 - coordinate system, 225
 - diagram, 73
 - floating, 89
 - length ratio, 149
 - singular, 7
 - Stephenson's, 30
 - ternary, 9
- Linkage**
 - Bennett, 221
 - deltoid, 36
 - equivalent, 17
 - four-bar, 21, 131
 - parallelogram, 36
- Logarithmic decrement, 485
- Loop-closure equation, 51, 106, 230
- Loss factor, 514

- Machine, 3
- Magnification factor, 496
- Manipulator, 221
 - PUMA, 243
 - Stanford, 237
- Matrix
 - Denavit-Hartenberg, 222
 - dynamic, 534
 - field, 542
 - flexibility, 540
 - homogeneous transformation, 226
 - mass, 534
 - method, 223
 - modal, 536
 - weighted, 536
 - point, 541
 - stiffness, 534
 - transfer, 541
- Mechanism, 3
 - cam-follower, 343

- Chebyshev's, 161
- complex, 88
- crank-rocker, 33
- double-crank (drag-link), 33
- double-rocker, 33
- elliptic trammel, 14
- Evan's, 161
- Galloway, 36
- high degree of complexity of, 88
- low degree of complexity of, 88
- Peaucellier, 159
- plagiograph, 62
- plane, 7
- quick-return, 46
- Robert's, 161
- scotch yoke, 14
- slider-crank, 3, 22
- space, 7, 221
- straight-line, 158
- Watt's, 161
- Whitworth quick-return, 46, 77
- Mobility, 24**
- Modal analysis, 535
- Module, 402
- Moment**
 - dynamic, 277
 - inertia, 277, 322
 - pitching, 305, 322
 - reduced first, 323
 - rolling, 322
 - turning, 188, 189
 - turning, correction to, 192
 - yawing, 322
- Moment of inertia
 - equivalent, 474
 - reduced, 324
- Motion**
 - cycloidal, 348
 - generation, 119, 122
 - parabolic, 347
 - simple harmonic, 347
 - spheric, 439
 - transfer point, 88
 - uniform, 346
- Movability, 33

- Normal mode, 526
 - of beam, 556
 - orthogonality of, 535

Oldham's coupling, 14

Operator

rotation, 227

translation, 227

Optimum

offset, 358

speed, 210, 247

Order defect, 158

Pair

cylindrical, 5

force-closed, 4

form-closed, 4

higher, 5

lower, 4

planar, 5

prismatic, 4

revolute, 4

 disguise of, 9

 limit of, 9

screw, 5

spheric, 5

variables, 4

wrapping, 5

Path generation, 119, 124

Phase-plane diagram, 491

Pinion, 402

Pitch

angle, 422

circle, 402

circular, 402

curve, 402

diametral, 402

point, 402

Pole, 129

relative, 129

 of four-bar linkage, 131

 of slider-crank mechanism, 132

Polode, 402

Polygon

couple, 283

force, 283

Precession

axis of, 441

nonsynchronous, 581, 588

of shaft, 582

reversed, 582

simple, 441

straight, 582

synchronous, 581

velocity of, 441

Pressure angle, 345

 critical value of, 345

Prime circle, 345

Principal

axes, 437

coordinate, 536

Rack, 402

Rayleigh's method, 558

 with Grammel's modification, 561

Rayleigh's quotient, 559

Rayleigh-Ritz method, 562

Reed frequency meter, 564

Resonance, 494

Response

 impulsive, 519

 indicial, 521

Return, 345

Rise, 345

Semidefinite system, 529

Speed

 -load characteristic, 267

 mean, 198

 optimum, 210, 247

Spin

 axis, 441

 velocity, 441

Stability of rotating shaft, 581, 596, 605

State vector, 541

Static equilibrium, 168

Statics, 2

Station point, 362

Stresses in moving member, 178

Structure, 9

Tooth profile

 conjugate, 412

 synthesis, 412

Trace point, 344

Transmissibility, 505

Transmission angle, 64

Turning-moment diagram, 195

Unbalance, amount of, 281

Unbalanced force

 lowest order, 321

- primary, 301
secondary, 301
- Undercutting**
of cam, 359
of gear, 409
- Velocity**
diagram, 79
image, 73
- Vibration**
aperiodic, 481
forced, 466
with harmonic excitation, 493, 497, 529
free (natural), 466
free, with coulomb damping, 487
free, with viscous damping, 481
isolation, 505
of bar, 548
of beam, 553
of continuous system, 548
of multidegree-of-freedom system, 533
of shaft, 551
of single-degree-of-freedom system, 466
of two-degree-of-freedom system, 526
measuring instrument, 563
- parametrically-excited, 466
pick-up, 564
- capacitance, 571
electromagnetic, 570
magnetostriuctive, 571
mutual inductance, 572
piezoelectric, 565
- random, 466
self-excited, 466
undamped, 530
absorber (neutralizer), 530
free, 466
with harmonic excitation, 493
viscously damped, with harmonic excitation, 497
with arbitrary excitation, 516
with base excitation, 502
with elastically mounted dashpot, 501
with periodic excitation, 515
- Virtual work**, 168
- Voigt's model**, 481
- Volmer's nomogram**, 147
- Whirling of shaft**, 507
- Worm**, 421

